

FOURTH EDITION

# Basic Transport Phenomena in Biomedical Engineering

Ronald L. Fournier



CRC Press  
Taylor & Francis Group

# Basic Transport Phenomena in Biomedical Engineering

Fourth Edition



Taylor & Francis

Taylor & Francis Group

<http://taylorandfrancis.com>

# Basic Transport Phenomena in Biomedical Engineering

Fourth Edition

Ronald L. Fournier, PhD, PE

Department of Bioengineering  
The University of Toledo



CRC Press

Taylor & Francis Group

Boca Raton London New York

---

CRC Press is an imprint of the  
Taylor & Francis Group, an **informa** business

MATLAB® is a trademark of The MathWorks, Inc. and is used with permission. The MathWorks does not warrant the accuracy of the text or exercises in this book. This book's use or discussion of MATLAB® software or related products does not constitute endorsement or sponsorship by The MathWorks of a particular pedagogical approach or particular use of the MATLAB® software.

CRC Press  
Taylor & Francis Group  
6000 Broken Sound Parkway NW, Suite 300  
Boca Raton, FL 33487-2742

© 2018 by Taylor & Francis Group, LLC  
CRC Press is an imprint of Taylor & Francis Group, an Informa business

No claim to original U.S. Government works

Printed on acid-free paper

International Standard Book Number-13: 978-1-1387-4953-5 (Paperback)  
International Standard Book Number-13: 978-1-4987-6871-9 (Hardback)

This book contains information obtained from authentic and highly regarded sources. Reasonable efforts have been made to publish reliable data and information, but the author and publisher cannot assume responsibility for the validity of all materials or the consequences of their use. The authors and publishers have attempted to trace the copyright holders of all material reproduced in this publication and apologize to copyright holders if permission to publish in this form has not been obtained. If any copyright material has not been acknowledged please write and let us know so we may rectify in any future reprint.

Except as permitted under U.S. Copyright Law, no part of this book may be reprinted, reproduced, transmitted, or utilized in any form by any electronic, mechanical, or other means, now known or hereafter invented, including photocopying, microfilming, and recording, or in any information storage or retrieval system, without written permission from the publishers.

For permission to photocopy or use material electronically from this work, please access [www.copyright.com](http://www.copyright.com) (<http://www.copyright.com/>) or contact the Copyright Clearance Center, Inc. (CCC), 222 Rosewood Drive, Danvers, MA 01923, 978-750-8400. CCC is a not-for-profit organization that provides licenses and registration for a variety of users. For organizations that have been granted a photocopy license by the CCC, a separate system of payment has been arranged.

**Trademark Notice:** Product or corporate names may be trademarks or registered trademarks, and are used only for identification and explanation without intent to infringe.

---

**Library of Congress Cataloging-in-Publication Data**

---

Names: Fournier, Ronald L., author.  
Title: Basic transport phenomena in biomedical engineering / Ronald L. Fournier.  
Description: Fourth edition. | Boca Raton : Taylor & Francis, 2017.  
Identifiers: LCCN 2017006894| ISBN 9781498768719 (hardback : alk. paper) | ISBN 9781315120478 (ebook)  
Subjects: | MESH: Biological Transport | Body Fluids--metabolism | Cell Membrane--metabolism | Tissue Engineering  
Classification: LCC R857.B52 | NLM QU 120 | DDC 571.6/4--dc23  
LC record available at <https://lccn.loc.gov/2017006894>

---

Visit the Taylor & Francis Web site at  
<http://www.taylorandfrancis.com>

and the CRC Press Web site at  
<http://www.crcpress.com>

*To Sophie and Ben...*



Taylor & Francis

Taylor & Francis Group

<http://taylorandfrancis.com>

# Contents

<b>Preface . . . . .</b>	<b>xvii</b>
<b>Notation . . . . .</b>	<b>.xix</b>
<b>Author . . . . .</b>	<b>xxix</b>
<b>1 Introduction . . . . .</b>	<b>1</b>
1.1 <i>Review of units and dimensions</i>	1
1.1.1 <i>Units</i>	1
1.1.2 <i>Fundamental dimensions</i>	1
1.1.2.1 <i>Mass and weight</i>	3
1.1.2.2 <i>Temperature</i>	4
1.1.2.3 <i>Mole</i>	5
1.1.3 <i>Derived dimensional quantities</i>	5
1.1.3.1 <i>Pressure</i>	6
1.1.3.2 <i>Volume</i>	7
1.1.3.3 <i>Equations of state</i>	7
1.2 <i>Dimensional equation</i>	8
1.3 <i>Conservation of mass</i>	9
1.3.1 <i>Law of conservation</i>	9
1.3.2 <i>Chemical reactions</i>	11
1.3.3 <i>The extent of a chemical reaction</i>	13
1.3.4 <i>Material balances</i>	15
1.4 <i>Tips for solving engineering problems</i>	18
1.5 <i>Useful numerical methods</i>	19
<i>Problems</i>	33
<b>2 A review of thermodynamic concepts . . . . .</b>	<b>35</b>
2.1 <i>The first law of thermodynamics</i>	35
2.1.1 <i>Closed systems</i>	35
2.1.2 <i>Steady flow processes</i>	36
2.2 <i>The second law of thermodynamics</i>	38
2.2.1 <i>Reversible processes</i>	38

---

2.3	<i>Properties</i>	39
2.3.1	<i>Heat capacity</i>	40
2.3.2	<i>Calculating the change in entropy</i>	41
2.3.2.1	<i>Entropy change of an ideal gas</i>	41
2.3.3	<i>The Gibbs and Helmholtz free energy</i>	43
2.3.3.1	<i>Gibbs free energy</i>	43
2.3.3.2	<i>Helmholtz free energy</i>	43
2.4	<i>The fundamental property relations</i>	43
2.4.1	<i>Exact differentials</i>	44
2.5	<i>Single phase open systems</i>	46
2.5.1	<i>Partial molar properties</i>	47
2.5.1.1	<i>Binary systems</i>	48
2.5.1.2	<i>Property changes of mixing</i>	49
2.5.1.3	<i>Ideal gas</i>	49
2.5.1.4	<i>Gibbs free energy of an ideal gas mixture</i>	51
2.5.2	<i>Pure component fugacity</i>	52
2.5.2.1	<i>Calculating the pure component fugacity</i>	53
2.5.3	<i>Fugacity of a component in a mixture</i>	55
2.5.4	<i>The ideal solution</i>	56
2.6	<i>Phase equilibrium</i>	58
2.6.1	<i>Pure component phase equilibrium</i>	59
2.6.1.1	<i>Fugacity of a pure component as a compressed liquid</i>	62
2.6.2	<i>Excess properties</i>	62
2.6.3	<i>Applications of equilibrium thermodynamics</i>	66
2.6.3.1	<i>Solubility of a solid in a liquid solvent</i>	66
2.6.3.2	<i>Depression of the freezing point of a solvent by a solute</i>	71
2.6.3.3	<i>Equilibrium between a solid and a gas phase</i>	73
2.6.3.4	<i>Solubility of a gas in a liquid</i>	74
2.6.3.5	<i>Osmotic pressure</i>	78
2.6.3.6	<i>Distribution of a solute between two liquid phases</i>	81
2.6.3.7	<i>Single-stage solute extraction</i>	83
2.6.3.8	<i>Multistage solute extraction</i>	84
2.6.3.9	<i>Vapor-liquid equilibrium</i>	87
2.6.3.10	<i>Flammability limits</i>	91
2.6.3.11	<i>Thermodynamics of surfaces</i>	94
2.6.3.12	<i>Equilibrium dialysis</i>	97
2.6.3.13	<i>The Gibbs-Donnan effect</i>	102
2.6.3.14	<i>Donnan potential</i>	108
2.6.3.15	<i>Chemical equilibrium in ideal aqueous solutions</i>	109
	<i>Problems</i>	115
<b>3</b>	<b>Physical properties of the body fluids and the cell membrane . . .</b>	<b>125</b>
3.1	<i>Body fluids</i>	125
3.2	<i>Fluid compositions</i>	126
3.3	<i>Capillary plasma protein retention</i>	127

---

3.4	<i>Osmotic pressure</i>	129
3.4.1	<i>Osmolarity</i>	129
3.4.2	<i>Calculating the osmotic pressure</i>	130
3.4.3	<i>Other factors that may affect the osmotic pressure</i>	131
3.5	<i>Filtration flow across a membrane</i>	132
3.5.1	<i>Predicting the hydraulic conductance</i>	133
3.5.1.1	<i>Rectangular pores</i>	135
3.6	<i>Net capillary filtration rate</i>	136
3.6.1	<i>A comparison of the blood flow into the capillary with the capillary filtration flow rate</i>	138
3.7	<i>Lymphatic system</i>	138
3.8	<i>Solute transport across the capillary endothelium</i>	139
3.9	<i>The cell membrane</i>	140
3.9.1	<i>Action potentials</i>	143
3.10	<i>Ion pumps maintain nonequilibrium state of the cell</i>	146
	<i>Problems</i>	147
<b>4</b>	<b>The physical and flow properties of blood and other fluids . . . . .</b>	<b>153</b>
4.1	<i>Physical properties of blood</i>	153
4.2	<i>Cellular components</i>	153
4.3	<i>Rheology</i>	154
4.4	<i>The capillary viscometer and laminar flow in tubes</i>	158
4.4.1	<i>Hagen–Poiseuille equation for laminar flow of a Newtonian liquid in a cylindrical tube</i>	159
4.4.1.1	<i>Laminar flow of a Newtonian fluid through a tube of very short length</i>	162
4.4.2	<i>Hagen–Poiseuille equation for laminar flow of a Newtonian liquid in tubes of noncircular cross section</i>	162
4.5	<i>The Rabinowitsch equation for the flow of a non-Newtonian fluid in a cylindrical tube</i>	163
4.6	<i>Other useful flow relationships</i>	164
4.7	<i>The rheology of blood and the Casson equation</i>	166
4.7.1	<i>The Casson equation</i>	166
4.7.2	<i>Using the Casson equation</i>	167
4.7.3	<i>The velocity profile for tube flow of a Casson fluid</i>	168
4.7.4	<i>Tube flow of blood at low shear rates</i>	170
4.8	<i>The effect of tube diameter at high shear rates</i>	170
4.8.1	<i>The Fahraeus effect</i>	170
4.8.2	<i>The Fahraeus–Lindqvist effect</i>	171
4.8.3	<i>Marginal zone theory</i>	173
4.8.3.1	<i>Using the marginal zone theory</i>	175
4.9	<i>Boundary layer theory</i>	177
4.9.1	<i>The flow near a wall that is set in motion</i>	177
4.9.2	<i>Laminar flow of a fluid along a flat plate</i>	182
4.9.2.1	<i>Approximate solution for laminar boundary flow over a flat plate</i>	183

---

4.10 Generalized mechanical energy balance equation	188
4.10.1 The hydraulic diameter	191
4.11 Capillary rise and capillary action	200
4.11.1 Equilibrium capillary rise	200
4.11.2 Dynamics of capillary action	202
Problems	205
<b>5 Mass transfer fundamentals . . . . .</b>	<b>221</b>
5.1 Description of solute mass transfer	221
5.2 Important definitions used in solute mass transfer	221
5.2.1 Binary diffusion	223
5.2.2 Fick's first law	223
5.2.3 Simplifications of Fick's first law	224
5.2.3.1 The case of forced convection	224
5.2.3.2 The case of a stagnant or quiescent fluid	224
5.2.3.3 The case of dilute solutions	225
5.2.3.4 Equimolar counterdiffusion	225
5.2.4 Boundary conditions for diffusion problems	225
5.2.4.1 Concentration is known at the boundary	225
5.2.4.2 Zero solute flux at the boundary	226
5.2.4.3 Convective transport at the boundary	226
5.2.4.4 Chemical reaction at the boundary	226
5.3 Estimating the diffusivity	228
5.3.1 Stokes-Einstein equation	229
5.4 Fick's second law	232
5.5 Some solutions to Fick's second law	234
5.5.1 Solution for the concentration profile for diffusion from a flat plate into a semi-infinite stagnant medium	234
5.5.1.1 Calculation of the solute flux at the surface of the plate	236
5.5.2 Solution for the concentration profile for diffusion from a planar source into an infinite stagnant medium	236
5.5.3 Solution for the concentration profile for diffusion from a point source into an infinite planar stagnant medium	238
5.6 The mass transfer coefficient	240
5.6.1 The Sherwood number	241
5.7 Diffusion from a flat plate into a semi-infinite stagnant medium	241
5.7.1 Film theory	242
5.8 Mass transfer from the surface of a sphere into an infinite quiescent medium	243
5.8.1 Mass transfer between the surface of a sphere and a flowing fluid	247
5.9 Solute transport by convection and diffusion	247
5.9.1 Solute mass transfer from a gas into a falling liquid film: short contact time solution	248
5.9.1.1 A general solution for gas absorption into a laminar falling liquid film	254

---

5.9.2	<i>Mass transfer from a rotating disk</i>	256
5.9.3	<i>Mass transfer in laminar boundary layer flow over a flat plate</i>	262
5.9.4	<i>Mass transfer between the wall of a cylindrical tube and a fluid in laminar flow</i>	268
5.9.4.1	<i>Overall solute mass balance for the short contact time solution</i>	273
5.10	<i>The general case of mass transfer between the wall of a cylindrical tube and a flowing fluid</i>	275
5.10.1	<i>Derivation of the log mean concentration difference</i>	276
5.10.2	<i>Mass transfer in a tube of arbitrary cross section</i>	277
5.11	<i>A summary of useful mass transfer coefficient correlations</i>	278
5.11.1	<i>Mass transfer for undeveloped laminar flow in a cylindrical tube</i>	278
	<i>Problems</i>	282
<b>6</b>	<b>Mass transfer in heterogeneous materials . . . . .</b>	<b>289</b>
6.1	<i>Solute diffusion within heterogeneous media</i>	289
6.1.1	<i>Solute transport across thin porous membranes</i>	289
6.1.1.1	<i>Steric exclusion and hindered diffusion</i>	290
6.1.1.2	<i>Solute diffusion in a single pore of a thin planar membrane</i>	291
6.1.1.3	<i>Solute diffusion across a thin planar membrane</i>	292
6.1.1.4	<i>The Renkin equation</i>	293
6.1.1.5	<i>Solute membrane permeability</i>	295
6.1.1.6	<i>Capillary wall solute permeability</i>	295
6.1.1.7	<i>Membrane permeability and the overall mass transfer coefficient</i>	296
6.1.2	<i>Diffusion of a solute from within a porous polymeric material</i>	298
6.1.2.1	<i>A solution valid for short contact times</i>	301
6.1.2.2	<i>A solution valid for long contact times</i>	304
6.1.3	<i>Diffusion in blood and tissue</i>	304
6.1.3.1	<i>Diffusion in the interstitial fluid and other gel-like materials</i>	305
6.1.4	<i>Solute transport across gel membranes</i>	306
6.2	<i>The irreversible thermodynamics of membrane transport</i>	307
6.2.1	<i>Finding <math>L_p</math>, <math>P_m</math>, and <math>\sigma</math></i>	310
6.2.1.1	<i>Estimating the reflection coefficient</i>	311
6.2.2	<i>Multicomponent membrane transport</i>	312
6.2.3	<i>Membrane Peclet number</i>	312
6.3	<i>Solute transport by filtration and diffusion across the capillary wall</i>	313
6.4	<i>Transport of a solute between a capillary and the surrounding tissue space</i>	317
6.4.1	<i>The Krogh tissue cylinder</i>	318
6.4.2	<i>A model of the Krogh tissue cylinder</i>	319
6.4.2.1	<i>The critical radius</i>	321
6.4.2.2	<i>A comparison of convection and diffusion effects</i>	323

6.4.3	<i>The Renkin-Crone equation</i>	324
6.4.3.1	<i>Determining the value of <math>P_mS</math></i>	326
6.4.4	<i>Solute transport in vascular beds: The well-mixed assumption</i>	328
6.5	<i>Solute transport by filtration flow across a membrane</i>	329
6.5.1	<i>The change in the bulk flow of a fluid flowing within a hollow fiber with filtration</i>	333
6.5.2	<i>Describing the change in the bulk concentration of a solute in a fluid flowing in a hollow fiber with filtration</i>	334
	<i>Problems</i>	339
<b>7</b>	<b>Oxygen transport in biological systems. . . . .</b>	<b>349</b>
7.1	<i>The diffusion of oxygen in multicellular systems</i>	349
7.1.1	<i><math>pO_2</math> and Henry's constant</i>	349
7.1.2	<i>Oxygen transport to a spherical volume of cells</i>	350
7.2	<i>Hemoglobin</i>	354
7.3	<i>The oxygen-hemoglobin dissociation curve</i>	355
7.4	<i>Oxygen levels in blood</i>	356
7.5	<i>The Hill equation</i>	356
7.6	<i>Other factors that can affect the oxygen-hemoglobin dissociation curve</i>	358
7.7	<i>Tissue oxygenation</i>	359
7.7.1	<i>Nominal tissue oxygen consumption rate</i>	360
7.7.2	<i>Calculating the venous <math>pO_2</math> for a given oxygen demand</i>	361
7.8	<i>Oxygen transport in blood oxygenators, bioartificial organs, and tissue engineered constructs</i>	363
7.8.1	<i>Oxygen mass balance for a blood oxygenator</i>	363
7.8.2	<i>Oxygen transport in planar bioartificial organs</i>	364
7.8.3	<i>Oxygen transport in planar tissue engineered constructs</i>	367
7.8.3.1	<i>In vitro culture of planar tissue engineered constructs</i>	368
7.8.3.2	<i>Maximum thickness of planar tissue engineered constructs</i>	370
7.9	<i>Oxygen transport in perfusion bioreactors</i>	372
7.9.1	<i>A model of convective and diffusive transport of oxygen through a planar layer of cells</i>	373
7.9.2	<i>A microchannel perfusion bioreactor</i>	376
7.10	<i>Oxygen transport in the Krogh tissue cylinder</i>	381
7.10.1	<i>Capillary oxygenated hemoglobin mass balance</i>	381
7.10.2	<i>Capillary unbound oxygen mass balance</i>	381
7.10.2.1	<i>The slope of the oxygen hemoglobin dissociation curve</i>	382
7.10.3	<i>Tissue oxygen mass balance</i>	383
7.11	<i>An approximate solution for oxygen transport in the Krogh tissue cylinder</i>	384
7.12	<i>Artificial blood</i>	387
	<i>Problems</i>	391

---

<b>8 Pharmacokinetic analysis . . . . .</b>	<b>399</b>
8.1 Terminology	399
8.2 Entry routes for drugs	399
8.3 PK modeling approaches	401
8.3.1 Compartmental pharmacokinetic models	401
8.3.2 Physiological pharmacokinetic models	402
8.3.3 Model independent pharmacokinetic models	402
8.4 Factors that affect drug distribution	403
8.4.1 Drug distribution volumes	403
8.4.2 Apparent distribution volume	404
8.4.3 The Oie-Tozer equation for the apparent distribution volume	404
8.4.4 Drug metabolism	407
8.4.5 Renal excretion of the drug	408
8.5 Drug clearance	410
8.5.1 Renal clearance	410
8.5.2 Plasma clearance	412
8.5.3 Biological half-life	413
8.5.4 The area under the curve, $AUC^{0 \rightarrow \infty}$	413
8.5.5 Accumulation of the drug in urine	413
8.6 A model for intravenous injection of drug	414
8.7 Continuous infusion of a drug	415
8.7.1 Application to controlled release of drugs by osmotic pumps	418
8.7.2 Controlled release of drugs from transdermal patches	420
8.7.2.1 Predicting the permeability of the skin	423
8.7.2.2 Experimental measurement of stratum corneum solute permeability	424
8.7.3 Controlled release of drugs from implantable devices	427
8.8 First-order drug absorption and elimination	429
8.9 Two-compartment models	433
8.9.1 Two-compartment model for an intravenous injection	434
8.9.2 Two-compartment model for first order absorption	437
8.9.3 Two-compartment model with drug absorption from a transdermal patch	440
8.9.4 Two-compartment model with drug absorption from an implantable device	440
8.10 Superposition principle	440
Problems	441
<b>9 Extracorporeal devices . . . . .</b>	<b>451</b>
9.1 Applications	451
9.2 Contacting schemes	451
9.3 Solute transport in extracorporeal devices	453
9.3.1 Estimating the mass transfer coefficients	453
9.3.2 Estimating the solute diffusivity in blood	454

---

9.4	<i>Hemodialysis</i>	456
9.4.1	<i>Background</i>	456
9.4.2	<i>Dialysate composition</i>	457
9.4.3	<i>Role of ultrafiltration</i>	458
9.4.4	<i>Clearance and dialysance</i>	459
9.4.5	<i>Solute transfer</i>	460
9.4.6	<i>A single-compartment model of urea hemodialysis</i>	464
9.4.6.1	<i>Daily home hemodialysis</i>	466
9.4.7	<i>Peritoneal dialysis</i>	466
9.4.7.1	<i>Constant volume model of CAPD</i>	468
9.4.7.2	<i>A simple CAPD model that includes ultrafiltration</i>	469
9.4.8	<i>Aquapheresis</i>	470
9.5	<i>Blood oxygenators</i>	470
9.5.1	<i>Background</i>	470
9.5.2	<i>Operating characteristics of blood oxygenators</i>	471
9.5.3	<i>Types of oxygenators</i>	472
9.5.4	<i>Analysis of a membrane oxygenator: Oxygen transfer</i>	475
9.5.4.1	<i>Constant oxygen partial pressure in the gas phase</i>	478
9.5.4.2	<i>Constant oxygen partial pressure in the gas phase and external cross flow of the blood over the hollow fibers</i>	478
9.5.4.3	<i>Calculation of the blood-side mass transfer coefficient</i>	479
9.5.5	<i>Analysis of a membrane oxygenator: Carbon dioxide transfer</i>	482
9.5.6	<i>Example calculations for membrane oxygenators</i>	484
9.6	<i>Immobilized enzyme reactors</i>	488
9.6.1	<i>Background</i>	488
9.6.2	<i>Examples of medical application of immobilized enzymes</i>	489
9.6.3	<i>Enzyme reaction kinetics</i>	490
9.6.4	<i>Reaction and diffusion in immobilized enzyme systems</i>	493
9.6.5	<i>Solving the immobilized enzyme reaction-diffusion model</i>	495
9.6.6	<i>Special case of a first order reaction</i>	497
9.6.6.1	<i>Spherical enzyme particle</i>	497
9.6.6.2	<i>Cylindrical enzyme particle</i>	497
9.6.6.3	<i>Flat plate enzyme particle</i>	498
9.6.7	<i>Observed reaction rate</i>	499
9.6.8	<i>External mass transfer resistance</i>	499
9.6.8.1	<i>External mass transfer resistance for a first order reaction</i>	500
9.6.9	<i>Reactor design equations</i>	500
9.6.9.1	<i>Packed bed reactor</i>	501
9.6.9.2	<i>Packed bed reactor with first-order kinetics and internal and external diffusion limitations</i>	502
9.6.9.3	<i>Well-mixed reactor</i>	502
9.6.9.4	<i>Well-mixed reactor with first-order kinetics and internal and external diffusion limitations</i>	503

---

9.7	<i>Affinity adsorption</i>	505
9.7.1	<i>Affinity adsorption of preformed antibodies</i>	506
9.7.2	<i>Analysis of an affinity adsorption system to remove preformed antibodies</i>	507
	<i>Problems</i>	509
<b>10</b>	<b>Tissue engineering and regenerative medicine . . . . .</b>	<b>515</b>
10.1	<i>Introduction</i>	515
10.2	<i>Background</i>	515
10.2.1	<i>Cells for TERM</i>	516
10.2.2	<i>The tissue engineering process</i>	517
10.2.2.1	<i>Immunoprotection of the transplanted cells</i>	518
10.3	<i>The extracellular matrix</i>	519
10.3.1	<i>Glycosaminoglycans</i>	521
10.3.2	<i>Collagens</i>	521
10.3.3	<i>Elastin</i>	521
10.3.4	<i>Fibronectin</i>	521
10.3.5	<i>Aggrecan</i>	522
10.3.6	<i>Basement membrane</i>	522
10.4	<i>Cellular interactions</i>	522
10.4.1	<i>Cadherins</i>	523
10.4.2	<i>Selectins</i>	523
10.4.3	<i>Cell adhesion molecules</i>	523
10.4.4	<i>Integrins</i>	524
10.4.5	<i>Cytokines and growth factors</i>	525
10.5	<i>Support structures for tissue engineering applications</i>	526
10.5.1	<i>Biomaterials</i>	527
10.5.2	<i>Techniques for making polymeric scaffolds</i>	530
10.5.2.1	<i>3D printing</i>	531
10.5.2.2	<i>Bioprinting</i>	533
10.6	<i>Biocompatibility and the initial response to an implant</i>	534
10.6.1	<i>The body's response to an implant</i>	535
10.7	<i>Cell transplantation into scaffolds</i>	535
10.8	<i>Bioreactor design for tissue engineering</i>	537
	<i>Problems</i>	541
<b>11</b>	<b>Bioartificial organs. . . . .</b>	<b>545</b>
11.1	<i>Background</i>	545
11.2	<i>Some immunology</i>	545
11.2.1	<i>B-Lymphocytes</i>	546
11.2.2	<i>Antibodies</i>	546
11.2.3	<i>T-Lymphocytes</i>	548
11.2.4	<i>Interaction between APCs, B cells, and T cells</i>	550
11.2.5	<i>The immune system and transplanted cells</i>	551

---

<b>Contents</b>	
11.3 <i>Immunoisolation</i>	552
11.4 <i>Permeability of immunoisolation membranes</i>	555
11.5 <i>Membrane Sherwood number</i>	558
11.6 <i>Examples of bioartificial organs</i>	558
11.6.1 <i>The bioartificial pancreas</i>	559
11.6.1.1 <i>Bioartificial pancreas approaches</i>	561
11.6.1.2 <i>Intravascular devices</i>	561
11.6.1.3 <i>Microencapsulation</i>	563
11.6.1.4 <i>Macroencapsulation</i>	565
11.6.2 <i>Number of islets needed</i>	568
11.6.3 <i>Islet insulin release model</i>	569
11.6.4 <i>Pharmacokinetic modeling of glucose and insulin interactions</i>	572
11.6.5 <i>Using the pharmacokinetic model to evaluate the performance of a bioartificial pancreas</i>	575
11.7 <i>The bioartificial liver</i>	578
11.7.1 <i>Artificial liver systems</i>	579
11.7.2 <i>Bioartificial livers</i>	580
11.7.3 <i>Examples of extracorporeal bioartificial livers</i>	582
11.8 <i>The bioartificial kidney</i>	587
11.9 <i>Design considerations for bioartificial organs</i>	589
Problems	590
<b>References</b>	593
<b>Index</b>	611

# Preface

The challenge in presenting a text on biomedical engineering is the fact that it is a very broad field that encompasses a variety of different engineering disciplines and life sciences. There are many recent edited works and advanced textbooks that provide specialized treatments and summaries of current research in various areas of biomedical engineering and transport phenomena. These works tend to be written more for the biomedical researcher and the advanced student than for the beginning student. There is therefore a need for an entry-level book that introduces some of the basic concepts. This book is designed to meet this goal. This work brings together fundamental engineering and life science principles to provide a focused coverage of key momentum and mass transport concepts in biomedical engineering with applications to the design of medical devices.

In accomplishing this task within a finite volume, the coverage was limited to those areas that emphasize chemical and physical transport processes with applications toward the development of artificial organs, bioartificial organs, controlled drug delivery systems, and tissue engineering. With this focus, the book first provides a basic review of units and dimensions, some tips for solving engineering problems, and a discussion on material balances. This is then followed by a review of thermodynamic concepts with an emphasis on the properties of solutions. Following this, the remaining chapters focus on such topics as body fluids, osmosis and membrane filtration, the physical and flow properties of blood, solute transport, oxygen transport, and pharmacokinetic analysis. This is followed by the application of these principles to extracorporeal devices and the relatively new areas of tissue engineering, regenerative medicine, and bioartificial organs. Throughout the book, considerable emphasis is placed on developing a quantitative understanding of the underlying physical, chemical, and biological phenomena. Therefore, mathematical models are developed using the conceptually simple “shell balance” or compartmental approaches.

Numerous examples are presented based on these mathematical models, and they are compared in many cases with actual experimental data from the research literature. The student is encouraged to rework these examples using the mathematical software package of their choice. Working through the examples and the end-of-chapter problems using mathematical software packages will develop skill and expertise in engineering problem solving while at the same time making the mathematics less formidable. These mathematical software packages also provide the student with the opportunity to explore various aspects of the solution on their own or apply these techniques as starting points for the solution to their own problems. In this way, the student should be able to gain confidence in the development of mathematical models for relatively simple systems and then be able to apply these concepts to a wide variety of problems of even greater complexity.

## Preface

---

It is hoped that this book is timely and useful to engineers and researchers in the biomedical community, as well as to students in chemical engineering, mechanical engineering, biotechnology, bioengineering, medicine, and the life sciences.

**Ronald L. Fournier**

MATLAB® is a registered trademark of The MathWorks, Inc. For product information, please contact:

The MathWorks, Inc.  
3 Apple Hill Drive  
Natick, MA 01760-2098 USA  
Tel: 508-647-7000  
Fax: 508-647-7001  
E-mail: [info@mathworks.com](mailto:info@mathworks.com)  
Web: [www.mathworks.com](http://www.mathworks.com)

# Notation

$a$	Molecular radius
$a_f$	Radius of a macromolecule
$A$	Helmholtz free energy defined as $U - TS$
$A$	Area
$A_{\text{drug}}$	Total amount of a drug in the body
$A_E$	Total amount of a drug in the extracellular fluid
$A_P$	Total amount of a drug in the plasma
$A_R$	Total amount of a drug everywhere else in the body
$A_p$	Total cross-sectional area of pores in a membrane
$A_s$	Surface area
$A_{xs}$	Cross-sectional area of a reactor
$\text{AUC}^{0 \rightarrow \infty}$	Area under the concentration time curve
$\bar{B}, \bar{C}, \bar{D}$ and $B, C, D$	Virial coefficients
$c$	Weight concentration
$C$	Concentration
$C_{50}$	Concentration where drug response is 50% of maximum response
$C_b, C_{\text{blood}}$	Concentration in the blood
$C'_b$	Concentration of oxygen bound to hemoglobin in the blood
$C_d$	Concentration in the exchange fluid
$C_g$	Concentration in the gas
$C_G$	Concentration of glucose
$C_{\text{CAPD}}$	Concentration of a solute in the CAPD exchange fluid
$C_E$	Total concentration of a drug in the extracellular fluid
$C_{EB}$	Concentration of bound drug in the extracellular fluid
$C_L$	Ligand concentration
$C_{L \cdot M}$	Ligand-macromolecule concentration
$C_{\max}$	Maximum concentration
$C_M$	Macromolecule concentration
$C_P, C_{\text{plasma}}$	Concentration in the plasma
$C_{\text{tissue}}$	Concentration in the tissue
$C_R$	Total concentration of a drug everywhere else in the body
$C_{\text{SS}}$	Steady-state concentration
$C_U$	Unbound concentration of a drug
$C'$	Concentration of oxygen bound to hemoglobin
$C'_{\text{SAT}}$	Concentration of oxygen-saturated hemoglobin

## Notation \_\_\_\_\_

$\bar{C}$	Concentration in the tissue
$CL$	Clearance
$CL_{CAPD}$	Clearance of continuous ambulatory peritoneal dialysis
$CL_D$	Clearance of dialysis
$CL_{\text{plasma}}$	Plasma clearance
$CL_{\text{renal}}$	Clearance due to the kidneys
$C_p$	Heat capacity at constant pressure
$C_{\text{total}}$	Total concentration of a drug, bound and unbound
$C_v$	Heat capacity at constant volume
$\Delta C_{LM}$	Log mean concentration difference
$d$	Diameter
$D_{AB}$	Diffusivity in a homogeneous fluid, usually used for water at 37 °C
$D_{\text{blood}}$	Diffusivity in the blood
$D_{\text{drug}}$	Dose of a drug
$D_0$	Diffusivity in interstitial fluid or a fluid other than water
$Da$	Damkohler number
$D_B$	Dialysance
$D_{\text{cell}}$	Diffusivity in the cell
$D_e$	Effective diffusivity
$D_{\text{effective}}$	Effective diffusivity in the blood
$d_H$	Hydraulic diameter
$D_m$	Membrane diffusivity
$D_{\text{plasma}}$	Diffusivity in the plasma
$D_T$	Diffusivity in the tissue
$E$	Enzyme concentration
$E$	Extraction factor
$E$	Extraction ratio
$E$	Solute extraction factor
$E_K$	Kinetic energy
$E_p$	Gravitational potential energy
$f$	Fraction of drug absorbable
$f$	Fraction of macromolecule bound to ligand
$f$	Friction factor
$f$	Fugacity
$f_i$	Fugacity of pure component i
$\hat{f}_i$	Fugacity of component i in a mixture
$f_R$	Cumulative fraction of the drug released
$f_U$	Fraction of unbound drug
$f_{UT}$	Fraction of unbound drug in the tissue
$F$	Faraday's constant
$F$	Volumetric flowrate to the device
$F$	Force
$g$	Acceleration of gravity
$g$	Membrane conductance
$G$	Gibbs free energy defined as $H - TS$

---

$\bar{G}_i$	Partial molar Gibbs free energy species i
$G_B$	Glucose concentration in the blood
$G^E$	Excess Gibbs free energy
$\bar{G}_i^E$	Partial molar excess Gibbs free energy
GFR	Glomerular filtration rate
$G_I$	Glucose concentration in the implant chamber
$h, H$	Height, thickness, or capillary rise height
$h_{\text{friction}}$	Frictional effects affecting the flow of a fluid
H	Enthalpy defined as $U + PV$
H	Hematocrit
$H_C$	Hematocrit of core
$H_F$	Hematocrit of feed
$H_T$	Tube hematocrit
H	Henry's constant
$\Delta H^m$	Enthalpy of fusion
$\Delta H^{\text{vap}}$	Heat of vaporization
i	Refers to the current flow of a particular component
$\tilde{i}, \tilde{j}, \tilde{k}$	Unit vectors in $x, y$ , and $z$ directions
I	Current
$I_B$	Plasma insulin concentration
$I_I$	Insulin concentration in the implant chamber
$I_{IF}$	Interstitial fluid insulin concentration
$I_0$	Drug infusion rate
$\dot{j}_i$	Mass flux of solute $i$ relative to $\tilde{v}$
$\dot{j}_i^+$	Mass flux of solute $i$ relative to $\tilde{v}^+$
$\dot{J}_i$	Molar flux of solute $i$ relative to $\tilde{v}$
$\dot{J}_i^+$	Molar flux of solute $i$ relative to $\tilde{v}^+$
k	First-order rate constant
$k_f, k_r$	Forward and reverse rate constants
$k_a$	Absorption rate constant
$k_b$	Mass transfer coefficient for blood
$k_{\text{cat}}$	Enzyme rate constant
$k_e$	Mass transfer coefficient for exchange fluid
$k_g$	Mass transfer coefficient for a gas
$k_i$	$i$ th elimination rate constant
$k_m$	Length averaged mass transfer coefficient
$k_m^{\text{local}}$	Local mass transfer coefficient
$k_{\text{metabolic}}$	First-order rate constant for metabolic drug consumption
$k_{pt}, k_{tp}$	Rate constants for transport of a drug between plasma and tissue
$k_{\text{renal}}$	Renal elimination rate constant
$k_{te}$	Total elimination rate constant
K	Partition coefficient
K	Distribution coefficient
$K, K_{\text{eq}}$	Equilibrium constant
K	Overall rate constant

---

$K_a$	Drug-protein affinity constant
$K_{fitting}$	Fitting friction factor
$K_i$	Distribution coefficient for component $i$
$K_m$	Constant in the Michaelis-Menten model
$K_{O/W}$	Octanol-water partition coefficient
$K_O$	Overall mass transfer coefficient
$L$	Latent heat of a phase change
$L$	Length
$L$	Liquid flow rate
$\bar{L}$	Membrane thickness
$L_p$	Hydraulic conductance of a membrane
$m$	Slope of the oxygen-hemoglobin dissociation curve
$m_i$	Mass of species $i$
$m_{solute}$	Mass concentration of a solute
$\dot{m}$	Mass flow rate
$M$	Molar property value
$M$	Mass
$M^E$	Excess property value
$M_i$	Molar property value of component $i$
$\dot{m}_A$	Mass transfer rate of solute A
$\bar{M}_i$	Partial molar property value of component $i$
$M_{urine}$	Mass of a drug in the urine
$\tilde{M}_t$	Mass flux of species $i$
$MW$	Molecular weight
$n$	Constant in the Hill equation
$n, N$	Number of moles
$n_i, N_i$	Number of moles of component $i$
$N$	Number of equilibrium stages
$N$	Number of pores
$N_A$	Avogadro's number
$N_{fiber}$	Number of fibers in a hollow fiber unit
$N_T$	Number of transfer units
$N_V$	Volumetric gas transport rate
$\tilde{N}_t$	Molar flux of species $i$
$P$	Absolute pressure
$P_B$	Pressure of bloodstream
$P_D$	Pressure of dialysate stream
$pCO_2$	Partial pressure of carbon dioxide
$pH$	$-\log_{10}$ (hydrogen ion concentration)
$pK$	$-\log_{10}$ (dissociation equilibrium constant)
$pO_2$	Partial pressure of oxygen
$\langle pO_2 \rangle$	Average partial pressure of oxygen
$P$	Power
$P_{50}$	Constant in the Hill equation
$P_C$	Hydrodynamic pressure in the capillary
$P_c$	Critical pressure

---

Pe	Peclet number
$P_i$	Partial pressure of component i
$P_{IF}$	Hydrodynamic pressure of interstitial fluid
$P_m$	Membrane permeability
$P_o$	Overall membrane permeability
$P^{SAT}, P^{vap}$	Saturation or vapor pressure
$P_{SC}$	Permeability of the stratum corneum
$\Delta P$	Effective pressure drop
q	Filtration flux
$q_b$	Tissue blood perfusion rate
Q	Blood flow rate
Q	Filtration rate
Q	Heat
Q	Volumetric flow rate of a fluid
$Q_b$	Volumetric flow rate of blood
$Q_d$	Volumetric flow rate of exchange fluid
$Q_f$	Filtration volumetric flow rate
$Q_g$	Volumetric flow rate of a gas
$Q_{capillary}$	Volumetric flow rate in a capillary
r	Ratio of ion concentration inside to that outside
r	Radius of a bubble or droplet
$r_{anoxic}$	Radius defining anoxic region in the Krogh tissue cylinder
$r_c$	Capillary radius
$r_{G\ in}$	Glucose input rate
$r_H$	Hydraulic radius
$r_{islet}$	Islet insulin release rate
$r_s$	Rate of substrate consumption in an enzyme reaction
$r_T$	Krogh tissue cylinder radius
$R''_{metabolic}$	Metabolic rate of drug consumption
$R''_A$	Chemical reaction rate at a surface
$R_A''$	Chemical reaction rate within a volume
R	Universal gas constant
R	Radius
$R_0$	Zero order volumetric reaction rate
Re	Reynolds number
$Re_x$	Local Reynolds number at x
$R_{E/I}$	Ratio of the amount of drug-binding protein in the extracellular fluid to that in the plasma
$R_{max}$	Saturation drug response at high drug concentration
s	Parameter in the Casson equation
s	Capillary surface area per volume of tissue
S	Entropy
S	Substrate concentration
S	Surface area of a membrane
$S_a$	Sieving coefficient in the absence of concentration polarization

---

$S_c$	Capillary surface area
$S_o$	Sieving coefficient at high filtration rates with concentration polarization
$Sc$	Schmidt number
$Sh$	Sherwood number
$SSE$	Sum of the square of the errors
$t$	Temperature in °C or °F
$t$	Time
$t_{1/2}$	Half-life
$T$	Absolute temperature in K or R
$T_C$	Critical temperature
$T_f$	Freezing temperature of a mixture
$T_m$	Normal melting temperature
$T_{tp}$	Triple point temperature
$U$	Internal energy
$\bar{U}$	Reduced average velocity
$U_B$	Bosanquet velocity
$v$	Capillary volume fraction in the tissue
$v_i$	Molar volume of a liquid
$v_x$	Velocity in the x direction
$v_y$	Velocity in the y direction
$v_z$	Velocity in the z direction
$\tilde{v}$	Mass average velocity
$\tilde{v}_i$	Mass average velocity of species $i$
$\tilde{v}^+$	Molar average velocity
$V$	Molar, specific volume, or total volume
$V$	Velocity, usually of a plate or bulk solution
$V$	Voltage
$V_{\text{apparent}}$	Apparent volume of distribution
$V_{\text{average}}$	Average velocity
$V_{Bg}$	Glucose distribution volume
$V_{Bi}$	Insulin distribution volume
$V_C$	Critical volume
$V_{\text{CAPD}}$	Volume of exchange fluid in continuous ambulatory peritoneal dialysis
$V_d$	Apparent dialysate fluid velocity
$V_{\text{device}}$	Device volume
$V_E$	Extracellular fluid volume
$V_{IF}$	Interstitial fluid distribution volume
$V_{\max}$	Constant in the Michaelis-Menten model
$V_0$	Superficial velocity
$V_p, V_{\text{plasma}}$	Plasma volume
$V_R$	Fluid volume of all other body fluids
$V_{\text{tissue}}$	Tissue volume
$V_T$	Total gas volume
$V_T$	Total volume of tissue
$W$	Width
$W$	Work

---

$W_b$	Membrane area per unit length on the blood side
$W_g$	Membrane area per unit length on the gas side
$\bar{W}_L$	Log mean membrane area
$W_s$	Shaft work as in a flow process
$x_i$	Mole fraction of component $i$ , usually the liquid phase
$X$	Conversion of a species
$y_i$	Mole fraction of component $i$ , usually the vapor or gas phase
$Y$	Fraction of hemoglobin that is saturated
$z$	Ion charge
$z$	Local position
$z$	Ratio of blood flow rate to exchange fluid flow rate
$Z$	Compressibility factor
$Z$	Elevation relative to a datum level
$\bar{Z}_i$	Partial molar compressibility factor for species $i$
$Z_M$	Charge on a macromolecule

## Superscripts

0	Initial value
AVG, avg	Average value
c	Core
E	Excess property value
G	Refers to the gas
I, II, ... $\pi$	Phase I, phase II, ... phase $\pi$
L	Refers to the liquid
p	Plasma
(P)	Refers to a planar surface
R	Denotes a residual thermodynamic property
S	Refers to the solid
Sat	Refers to the saturated state
SS	Steady-state value
STP	Refers to standard temperature and pressure (0 °C, 1 atm)
T	Refers to the tissue
V, Vap	Refers to the vapor
$\infty$	Denotes the value at infinite dilution
$\infty$	Denotes the value after a very long time

## Subscripts

0	Initial value
0	Interstitial fluid value
A	Species A
A	Arterial value
AVG, Avg, average	Average value

## Notation

---

b	Refers to the blood
bs	Refers to the value at the surface of a membrane or particle
B, bulk	Refers to the value in a bulk solution
BP	Refers to the boiling point
c	Core
C	Capillary
C	Value at the critical point
CAPD	Refers to continuous ambulatory peritoneal dialysis
d	Refers to dialysate fluid
e	Equilibrium value
f	Filtrate side of the membrane
g	Refers to the gas
i	A particular solute in a solution
IF	Interstitial fluid
local	At a specific location
L	Local value at $x = L$
L	Liquid
L	Ligand
m	Membrane value
m	Manometer value
M	Macromolecule
max, maximum	A maximum of the value
min, minimum	A minimum of the value
p	Plasma
plasma	Plasma
S	Shaft work
S	Value at the surface
SC	Stratum corneum
tube	A tube or other conduit
T	Tissue
urine	Refers to the urine
V	Venous value
W	The wall
W	Water
x	Local value at position x

## Greek letters

$\alpha$	Kinetic energy correction term
$\beta$	Dimensionless surface substrate concentration
$\gamma$	Heat capacity ratio defined as $C_p/C_v$
$\gamma$	Surface energy, surface tension
$\dot{\gamma}$	Shear rate
$\dot{\gamma}_w$	Shear rate at the wall
$\gamma_i$	Activity coefficient of component i

---

$\Gamma$	Gamma function
$\Gamma_{\text{oxygen}}$	Cellular oxygen consumption rate
$\Gamma'_{\text{oxygen}}$	Tissue oxygen consumption rate
$\delta$	Marginal or plasma layer thickness
$\delta$	Thickness of the velocity boundary layer
$\delta_C$	Concentration boundary layer thickness
$\delta_{\text{cell}}$	Thickness of a cellular layer
$\delta_{\text{device}}$	Device thickness
$\delta_i$	Solubility parameter for species i
$\delta_{\text{film}}$	Thickness of mass transfer film
$\delta_{\text{SC}}$	Thickness of the stratum corneum
$\Delta$	Ratio of concentration and velocity boundary thicknesses
$\varepsilon$	Tissue void volume fraction
$\varepsilon$	Void volume
$\varepsilon_R$	Reactor void volume
$\varepsilon_j$	Extent of reaction j
$\varepsilon_{\text{SC}}$	Void volume fraction of the stratum corneum
$\eta$	Effectiveness factor
$\eta$	Overall efficiency of an equilibrium stage
$\eta$	Efficiency of a pump or a turbine
$\lambda$	Ratio of the molecular radius to the pore radius
$\lambda$	Eigenvalue
$\mu$	Viscosity
$\mu_{\text{apparent}}$	Apparent viscosity
$\mu_i$	Chemical potential of component i
$\nu$	Kinematic viscosity, $\mu/\rho$
$\nu_{ij}$	Stoichiometric coefficient of species i in reaction j
$\Pi$	Osmotic pressure
$\rho$	Mass density
$\rho_i$	Mass concentration of species i
$\sigma$	Reflection coefficient
$\tau$	Residence time
$\tau$	Shear stress
$\tau$	Tortuosity of a membrane
$\tau_{\text{diffusion}}$	Characteristic time for diffusion
$\tau_{\text{max}}$	Time when concentration peaks
$\tau_z$	Shear stress, viscous transport flux of z momentum in the r direction
$\tau_w$	Wall shear stress
$\tau_y$	Yield stress
$\tau_{yx}$	Shear stress, viscous transport flux of x momentum in the y direction
$\phi$	Cell volume fraction
$\phi$	Thiele modulus
$\phi_i$	Fugacity coefficient of pure component i
$\hat{\phi}_i$	Fraction of site $i$ on a macromolecule bound to ligand
$\tilde{\phi}_i$	Fugacity coefficient of component i in a mixture

$\Phi_1$	Volume fraction of the solvent
$\omega_r$	Hindered diffusion parameter
$\omega$	Angular velocity
$\omega_i$	Mass fraction of species i

## Additional Notes

$\bar{\phantom{x}}$	Partial molar property
$\hat{\phantom{x}}$	Value of a property in a mixture
$\Delta$	Difference operator, final state minus initial state
$\sim$	Over a variable denotes a vector

## Greek Alphabet

A $\alpha$	alpha	N $\nu$	nu
B $\beta$	beta	$\Xi \xi$	xi
$\Gamma \gamma$	gamma	O o	omicron
$\Delta \delta$	delta	$\Pi \pi$	pi
E $\epsilon$	epsilon	P $\rho$	rho
Z $\zeta$	zeta	$\Sigma \sigma$	sigma
H $\eta$	eta	T $\tau$	tau
$\Theta \theta$	theta	$\Upsilon \upsilon$	upsilon
I $\iota$	iota	$\Phi \varphi$	phi
K $\kappa$	kappa	X $\chi$	chi
$\Lambda \lambda$	lambda	$\Psi \psi$	psi
$\mu \mu$	mu	$\Omega \omega$	omega

# Author

**Ronald L. Fournier** is a professor in the Department of Bioengineering at The University of Toledo in Ohio. He was also the founding chair of this department. During his 32 years at Toledo, he has taught a variety of chemical engineering and bioengineering subjects, including courses in biochemical engineering, chemical reactor engineering, biomedical engineering transport phenomena, design and entrepreneurship, biomechanics, and artificial organs. His research interests and scholarly publications are in the areas of bioartificial organs, tissue engineering, novel bioreactors, photodynamic therapy, and pharmacokinetics. In addition to his professional career, he also observes variable stars and is a member of the *American Association of Variable Star Observers*.



Taylor & Francis

Taylor & Francis Group

<http://taylorandfrancis.com>

# Chapter 1 Introduction

Before we can begin our study of biomedical engineering transport phenomena, let us first review some basic concepts that are essential for understanding the material in this book. You may have come across some of this material in other courses such as in chemistry, physics, and perhaps thermodynamics. Reviewing these concepts once again is still very important since these concepts form the basis of our approach to analyzing and solving biomedical engineering problems.

## 1.1 Review of units and dimensions

### 1.1.1 Units

Careful attention must be given to *units* and *dimensions* when solving engineering problems; otherwise, serious errors can occur in your calculations.

*Units* are how we describe the size or amount of a dimension. For example, a second is a common unit that is used for the dimension of time. In this book, we use primarily the *International System of Units*, which is also known by its abbreviation SI, for *Système international d'unités*. Other systems of units are also used, such as the English and American engineering systems and the centimeter-gram-second (cgs) system. We will come across some of these non-SI units as well in our study. The units of these other systems may be related to the SI units by appropriate conversion factors. [Table 1.1](#) provides a convenient summary of common conversion factors that relate these other units to the SI system.

It is important to remember that in engineering calculations you must always attach units to the numbers that arise in your calculations, unless they are already unitless. Furthermore, within a calculation, it is important to use a consistent system of units, and in this book we recommend that you work with the SI system. In the event that a number has a non-SI unit, you will first need to convert those units into SI units using the conversion factors found in [Table 1.1](#). Also, remember to treat the units associated with a number as algebraic symbols. Then, as long as the units are the same, you can perform operations such as addition, subtraction, multiplication, and division on the like units, thereby combining and, in some cases, even cancelling them out.

### 1.1.2 Fundamental dimensions

The measurement of the physical properties we are interested in are derived from the *fundamental dimensions* of length, mass, time, temperature, and mole. [Table 1.2](#) summarizes the basic SI units for these fundamental dimensions. The SI unit for *length* is the meter (m) and that for *time* is the second (sec).

Table 1.1 Conversion Factors

<b>Dimension</b>	<b>Conversion Factors</b>	
Length	1 m = 100 cm	
	1 m = 3.28084 ft	
	1 m = 39.37 in.	
Volume	1 m <sup>3</sup> = 10 <sup>6</sup> cm <sup>3</sup>	1 liter (L) = 1000 cm <sup>3</sup>
	1 m <sup>3</sup> = 35.3147 ft <sup>3</sup>	1 gallon (US) = 3.7853 L
	1 m <sup>3</sup> = 61,023.38 in. <sup>3</sup>	1 gallon (US) = 0.1337 ft <sup>3</sup>
Mass	1 kg = 1000 g	1 lb <sub>m</sub> = 454 g
	1 kg = 2.20462 lb <sub>m</sub>	
Force	1 N = 1 kg m sec <sup>-2</sup>	1 dyne = 1 g cm sec <sup>-2</sup>
	1 N = 100,000 dynes	
	1 N = 0.22481 lb <sub>f</sub>	
Pressure	1 bar = 100,000 kg m <sup>-1</sup> sec <sup>-2</sup>	1 Pa = 1 N m <sup>-2</sup>
	1 bar = 100,000 N m <sup>-2</sup>	100,000 Pa = 1 bar
	1 bar = 10 <sup>6</sup> dynes cm <sup>-2</sup>	1 atm = 760 mmHg
	1 bar = 0.986923 atm	1 atm = 14.7 psi
	1 bar = 14.5038 psi	1 atm = 101,325 Pa
	1 bar = 750.061 mmHg or torr	
Density	1 g cm <sup>-3</sup> = 1000 kg m <sup>-3</sup>	
	1 g cm <sup>-3</sup> = 62.4278 lb <sub>m</sub> ft <sup>-3</sup>	
Energy	1 J = 1 kg m <sup>2</sup> sec <sup>-2</sup>	
	1 J = 1 N m	
	1 J = 1 m <sup>3</sup> Pa	
	1 J = 10 <sup>-5</sup> m <sup>3</sup> bar	
	1 J = 10 cm <sup>3</sup> bar	
	1 J = 9.86923 cm <sup>3</sup> atm	
	1 J = 10 <sup>7</sup> dyne cm	
	1 J = 10 <sup>7</sup> erg	
	1 J = 0.239 cal	
	1 J = 5.12197 × 10 <sup>-3</sup> ft <sup>3</sup> psia	
	1 J = 0.7376 ft lb <sub>f</sub>	
	1 J = 9.47831 × 10 <sup>-4</sup> Btu	
Power	1 kW = 10 <sup>3</sup> W	1 HP = 550 ft lb <sub>f</sub> sec <sup>-1</sup>
	1 kW = 1000 kg m <sup>2</sup> sec <sup>-3</sup>	
	1 kW = 1000 J sec <sup>-1</sup>	
	1 kW = 239.01 cal sec <sup>-1</sup>	
	1 kW = 737.562 ft lb <sub>f</sub> sec <sup>-1</sup>	
	1 kW = 0.947831 Btu sec <sup>-1</sup>	
	1 kW = 1.34102 HP	
Viscosity	1 P = 1 g cm <sup>-1</sup> sec <sup>-1</sup>	1 P = 0.1 Pa sec
	1 P = 100 cP	1 cP = 0.001 Pa sec
	1 P = 1 dyne sec cm <sup>-2</sup>	1 cP = 0.01 g cm <sup>-1</sup> sec <sup>-1</sup>
	1 P = 0.1 N sec m <sup>-2</sup>	

Table 1.2 SI Units for the Fundamental Dimensions

Fundamental Dimension	Unit	Abbreviation
Length	Meter	m
Mass	Kilogram	kg
Time	Second	sec or s
Temperature	Kelvin	K
Mole	Mole	mol

**1.1.2.1 Mass and weight** The *mass* of an object refers to the total amount of material that is in the object. The mass is a property of matter and is the same no matter where the object is located. For example, the mass of an object is the same on Earth, on Neptune, or if it is just floating along somewhere in space. In SI units we measure the mass of an object in kilograms (kg). Remember that the mass of an object is different than the weight of an object. *Weight* is the force exerted by gravity on the object. Since weight is a force, we can use Newton's second law ( $F = ma$ ) to relate weight ( $F$ ) and mass ( $m$ ).

In the United States, with its American engineering system of units, a very confusing situation can occur when working with mass and force (weight). The following discussion should be sufficient for you to see the advantages of working in the SI system of units. However, the American engineering system of units is still widely used, and it is important that you understand the following in order to handle these units properly in the event they arise in your calculations.

What is commonly referred to as a pound is really a *pound force* (weight) in the American engineering system of units. The pound force is abbreviated as  $lb_f$ , where the subscript *f* must be present to indicate that this is a pound force. Mass is also expressed as pounds, but in reality what is meant is the *pound mass* ( $lb_m$ ) and, once again, the subscript *m* must be present to indicate that this is a pound mass. Using Newton's second law, we can develop the following relationship between the pound force and the pound mass:

$$(Force) lb_f = (Mass) lb_m \times (\text{Acceleration of gravity}) ft sec^{-2} \times 1/g_c \quad (1.1)$$

The  $g_c$  term in [Equation 1.1](#) is a conversion factor needed to make the units in [Equation 1.1](#) work out properly, i.e., to convert the  $lb_m$  to  $lb_f$ . Note that unlike the acceleration due to gravity, the value of  $g_c$  does not depend on location and is a constant. In the American engineering system of units, the value of force (pound force or  $lb_f$ ) and mass (pound mass or  $lb_m$ ) are defined in such a way so as to be the same at sea level at  $45^\circ$  latitude. The acceleration of gravity ( $g$ ) in the American system of units at sea level and  $45^\circ$  latitude is  $32.174 \text{ ft sec}^{-2}$ . The value of  $g_c$  in [Equation 1.1](#) is therefore  $32.174 \text{ ft lb}_m \text{ sec}^{-2} \text{ lb}_f^{-1}$ . It is important to recognize though that the acceleration of gravity depends on location. A pound force and a pound mass have the same value only at sea level, where the acceleration of gravity is  $32.174 \text{ ft sec}^{-2}$  or whenever the ratio of the local acceleration of gravity to  $g_c$  is equal to one. For calculations done on the surface of the Earth, it is usually just assumed that a pound mass ( $lb_m$ ) equals a pound force ( $lb_f$ ), since the acceleration of gravity really does not vary

that much. So, if an object with a mass of  $10 \text{ lb}_m$  is on Earth, then for practical purposes its weight is  $10 \text{ lb}_f$ . However, if this object is taken to the moon, where the acceleration of gravity is  $5.309 \text{ ft sec}^{-2}$ , the mass is still  $10 \text{ lb}_m$ ; however by [Equation 1.1](#), its weight is quite a bit lower, as shown in the following calculation:

$$10 \text{ lb}_m \times 5.309 \frac{\text{ft}}{\text{sec}^2} \times \frac{\text{sec}^2 \text{ lb}_f}{32.174 \text{ ft lb}_m} = 1.65 \text{ lb}_f$$

### Example 1.1

Calculate the weight in newtons and in  $\text{lb}_f$  of an average person on the Earth.

#### Solution

On Earth, the acceleration due to gravity ( $g$ ) is  $9.8 \text{ m sec}^{-2}$ . The average mass of a human is  $75 \text{ kg}$ , so on Earth, the weight of the average human is  $75 \text{ kg} \times 9.8 \text{ m sec}^{-2} = 735 \text{ kg m sec}^{-2}$ . Next, we will see that 1 newton (N) is a special SI unit defined as  $1 \text{ kg m sec}^{-2}$ , so our average human also has a weight of 735 N. From [Table 1.1](#) we find that  $1 \text{ newton} = 0.22481 \text{ lb}_f$  giving a weight of  $735 \text{ N} \times 0.22481 \text{ lb}_f \text{ N}^{-1} = 165.2 \text{ lb}_f$ .

**1.1.2.2 Temperature** Temperature is defined as an *absolute* temperature instead of a relative temperature like the commonly used Fahrenheit and Celsius scales. The Fahrenheit scale is based on water freezing at  $32^\circ\text{F}$  and boiling at  $212^\circ\text{F}$ , whereas the Celsius scale sets these at  $0^\circ\text{C}$  and  $100^\circ\text{C}$ , respectively. The following equations may be used to relate a Celsius temperature to a Fahrenheit temperature and vice versa:

$$t^\circ\text{F} = 1.8t^\circ\text{C} + 32 \quad \text{or} \quad t^\circ\text{C} = \frac{5}{9}(t^\circ\text{F} - 32) \quad (1.2)$$

Our SI unit for the measurement of absolute temperature is Kelvin (K). The absolute temperature scale sets the absolute zero point, or 0 Kelvin (0 K), as the lowest possible temperature at which matter can exist. The temperature unit of the absolute Kelvin temperature scale is the same as that of the Celsius scale, so  $1 \text{ K} = 1^\circ\text{C}$ . The following equation may be used to relate the Celsius temperature ( $t$ ) scale to the absolute Kelvin temperature ( $T$ ) scale. In Celsius units, the absolute zero point is therefore  $-273.15^\circ\text{C}$ :

$$t^\circ\text{C} = TK - 273.15 \quad (1.3)$$

The absolute temperature can also be defined by the same unit of temperature measurement as the Fahrenheit scale. This is referred to as the absolute Rankine (R) temperature scale and  $1 \text{ R} = 1^\circ\text{F}$ . Note that 0 K is the same as 0 R since the absolute Kelvin and the absolute Rankine temperature scales are based on the same reference point of absolute zero. [Equation 1.4](#) can be used to relate the Fahrenheit temperature scale ( $t$ ) to the absolute Rankine temperature ( $T$ ) scale. In Fahrenheit units, the absolute zero point is  $-459.67^\circ\text{F}$ :

$$t^\circ\text{F} = TR - 459.67 \quad (1.4)$$

Using Equations 1.2 through 1.4, one can also show that the relationship between the Rankine and Kelvin temperatures is given by

$$T_R = 1.8 T_K \quad (1.5)$$

**1.1.2.3 Mole** The *mole* is used to describe the amount of a substance that contains the same number of atoms or molecules as there are atoms in 0.012 kilograms (or 12 g) of carbon-12, i.e.,  $6.023 \times 10^{23}$  atoms, which is also called *Avogadro's number*. This is also called the gram mole, which can be written as *gmole*, *mole*, or just *mol*. In the American engineering system, the *pound mole* (lb mole or lb mol) is used and is defined as  $6.023 \times 10^{23} \times 454$  atoms. Therefore, 1 pound mole is equal to 454 gram moles.

The *molecular weight* is defined as the mass per mole of a given substance. For example, the molecular weight of glucose is  $0.180 \text{ kg mole}^{-1}$ , whereas the molecular weight of water is  $0.018 \text{ kg mole}^{-1}$ . A mole of glucose or a mole of water both contain the Avogadro's number of molecules. Even though one mole of glucose and water contains the same number of molecules, the masses of each are quite different because the molecules of glucose are much larger than those of water. That is, one mole of glucose has a mass of  $0.180 \text{ kg}$  and one mole of water has a mass of  $0.018 \text{ kg}$ .

### 1.1.3 Derived dimensional quantities

From these fundamental dimensions, we can derive the units for a variety of other dimensional quantities of interest. Some of these quantities will occur so often that it is useful to list them as shown in Table 1.3. In addition, some of these quantities, like force and energy, have their own special SI units, whereas others, like mass density, are based on the fundamental dimensions listed in Table 1.2. Many times, we will use special symbols to denote a quantity. For example, the Greek symbol  $\rho$  (rho) is used to denote the mass density and  $\mu$  (mu) is often used for the viscosity of a substance. The viscosity, discussed in Chapter 4, is a physical property of a fluid and is a measure of its resistance to flow. A listing of the symbols used in this book to denote a variety of quantities is given in the *Notation* section that follows the *Table of Contents*.

Table 1.3 SI Units for Other Common Dimensional Quantities

Quantity	Unit	Abbreviation	Fundamental Units	Derived Units
Force	Newton	N	$\text{kg m sec}^{-2}$	$\text{J m}^{-1}$
Energy, work, heat	Joule	J	$\text{kg m}^2 \text{ sec}^{-2}$	$\text{N m}$
Pressure and stress	Pascal	Pa	$\text{kg m}^{-1} \text{ sec}^{-2}$	$\text{N m}^{-2}$
Power	Watt	W	$\text{kg m}^2 \text{ sec}^{-3}$	$\text{J sec}^{-1}$
Volume	—	—	$\text{m}^3$	—
Mass density	—	—	$\text{kg m}^{-3}$	—
Molar concentration	—	—	$\text{mol m}^{-3}$	—
Specific volume	—	—	$\text{m}^3 \text{ kg}^{-1}$	—
Viscosity	—	—	$\text{kg m}^{-1} \text{ sec}^{-1}$	$\text{Pa sec}$
Diffusivity	—	—	$\text{m}^2 \text{ sec}^{-1}$	—
Permeability, mass transfer coefficient	—	—	$\text{m sec}^{-1}$	—

Table 1.4 Common Prefixes for SI Units

Prefix	Multiplication Factor	Symbol
Femto	$10^{-15}$	f
Pico	$10^{-12}$	p
Nano	$10^{-9}$	n
Micro	$10^{-6}$	$\mu$
Milli	$10^{-3}$	m
Centi	$10^{-2}$	c
Deci	$10^{-1}$	d
Deka	10	da
Hecto	$10^2$	h
Kilo	$10^3$	k
Mega	$10^6$	M
Giga	$10^9$	G
Tera	$10^{12}$	T

Oftentimes, a particular unit is expressed as a multiple or a decimal fraction. For example, 1/1000th of a meter is known as a millimeter, where the prefix “milli-” means to multiply the base unit of meter by the factor of  $10^{-3}$ . The prefix “kilo-” means to multiply the base unit by 1000. So, a kilogram is the same as 1000 grams. Table 1.4 summarizes a variety of prefixes that are commonly used to scale a base unit.

**1.1.3.1 Pressure** Pressure is defined as a force per unit area. Pressure is also expressed in either a relative or an absolute scale, and its unit of measure in the SI system is the Pascal (Pa), which is equal to a newton of force per square meter or  $N\ m^{-2}$ . How the pressure is measured will affect whether or not it is a relative or an absolute pressure. *Absolute pressure* is based on reference to a perfect vacuum. A *perfect vacuum* on the absolute pressure scale defines the zero point or 0 Pa. The zero point for a relative pressure scale is usually the pressure of the air or atmosphere where the measurement is taken. This local pressure is called either the *atmospheric pressure* or the *barometric pressure* and is measured by a *barometer*, which is a device for measuring atmospheric pressure. It is important to remember that the pressure of the surrounding air or atmosphere is not a constant but depends on location, elevation, and other factors related to the weather. That is why it is always important to log in your record book the atmospheric pressure in the laboratory when doing experiments that involve pressure measurements.

Most pressure measurement devices, or pressure gauges, measure the pressure relative to the surrounding atmospheric pressure or barometric pressure. These so-called *gauge pressures* are also relative pressures. A good example of a gauge pressure is the device used to measure the inflation pressure of your tires. If the tire pressure gauge has a reading of 250 kPa, then that means that the pressure in the tire is 250 kPa *higher* than the surrounding atmospheric pressure. A gauge pressure of 0 Pa means that the pressure is the same as the local atmospheric pressure, or you have a flat tire! A negative gauge pressure (i.e., suction or partial vacuum) means that the pressure is that amount *below* the atmospheric pressure. If the pressure measurement device measures the pressure relative to a perfect vacuum, then that pressure reading is referred to as

---

**Table 1.5 The Standard Atmosphere in a Variety of Units**

1.000 atmosphere (atm)
14.696 pounds force per square inch (psi)
760 millimeters of mercury (mmHg)
33.91 feet of water (ft H <sub>2</sub> O) = 10.34 meters of water (m H <sub>2</sub> O)
29.92 inches of mercury (in. Hg)
101,325 pascals (Pa)

---

an absolute pressure reading. The relationship between relative or gauge pressure and absolute pressure is given by the following equation:

$$(\text{Gauge pressure}) + (\text{Atmospheric pressure}) = (\text{Absolute pressure}) \quad (1.6)$$

The *standard atmosphere* is equivalent to the absolute pressure exerted at the bottom of a column of mercury that is 760 mm in height at a temperature of 0°C. This value is nearly the same as the atmospheric pressure that one may find on a typical day at sea level. The standard atmosphere in a variety of units is summarized in [Table 1.5](#). Using [Equation 1.6](#), and the pressure conversion factors shown in [Table 1.5](#), we can say that your tire pressure is 250 kPa gauge or 351.325 kPa absolute.

**1.1.3.2 Volume** *Volume* refers to the amount of space that an object occupies and depends on the mass of the object. The *mass density* is the mass of an object divided by the volume of space that it occupies. *Specific volume* is the volume of an object divided by its mass. Specific volume is, therefore, just the inverse of the mass density. For solids and liquids, the volume of an object of a given mass is not strongly dependent on the temperature or the pressure. For solids and liquids, the volume is then the mass multiplied by the specific volume or the mass divided by the density of the object. For gases, the volume of a gas is also strongly dependent on both the temperature and the pressure. For gases, we need to use an equation of state to properly relate the volume of the gas to the temperature, pressure, and moles (mass divided by molecular weight).

**1.1.3.3 Equations of state** An *equation of state* is a mathematical relationship that relates the pressure, volume, and temperature of a gas, liquid, or solid. For our purposes, the ideal gas law is an equation of state that will work just fine for the types of problems involving gases that we will consider here. Recall that an ideal gas has mass; however, the gas molecules themselves have no volume and these molecules do not interact with one another. The ideal gas law works well for gases like hydrogen and oxygen and air at pressures around atmospheric. Recall that the ideal gas law is given by the following relationship:

$$PV = nRT \quad (1.7)$$

In this equation

P denotes the absolute pressure

V is the volume

T is the absolute temperature

n is the number of moles

R is called the *universal gas constant*, and a suitable value must be used to make the units in [Equation 1.7](#) work out properly

[Table 1.6](#) summarizes commonly used values of the gas constant in a variety of different units.

Table 1.6 Gas Constant (R)

**Gas Constant**

8.314 m <sup>3</sup> Pa mol <sup>-1</sup> K <sup>-1</sup>
8.314 J mol <sup>-1</sup> K <sup>-1</sup>
82.06 cm <sup>3</sup> atm mol <sup>-1</sup> K <sup>-1</sup>
0.0821 L atm mol <sup>-1</sup> K <sup>-1</sup>
0.7302 ft <sup>3</sup> atm lb mol <sup>-1</sup> R <sup>-1</sup>
10.73 ft <sup>3</sup> psi absolute lb mol <sup>-1</sup> R <sup>-1</sup>

## 1.2 Dimensional equation

A *dimensional equation* is an equation that contains both numbers and their associated units. The dimensional equation usually arises from the use of a specific formula that is being used to solve a problem or when a particular number has nonstandard units associated with it. In the latter case, a series of conversion factors are used to put the number in some other system of units, e.g., the SI system of units. To arrive at the final answer, which is usually a number with its associated units, the dimensional equation is solved by performing the arithmetical operations on the numbers and, as discussed earlier, algebraic operations on the various units.

**Example 1.2** illustrates the use of the dimensional equation to convert a quantity in nonstandard units to SI units. **Example 1.3** illustrates the use of the dimensional equation to determine the volume of a gas at a given temperature and pressure. When solving engineering problems, make sure to use the dimensional equation approach illustrated in these examples. In this way, you can easily handle the conversion of the units associated with the quantities involved in your calculation and arrive at the correct answer. Remember to refer to **Tables 1.1 and 1.3 through 1.6**, where appropriate.

### Example 1.2

A particular quantity was reported to have a value of  $1.5 \text{ cm}^3 \text{ hr}^{-1} \text{ m}^{-2} \text{ mmHg}^{-1}$ . Recall that mmHg is a measurement of pressure, where 760 mm of mercury (Hg) is equal to a pressure of 1 atmosphere (1 atm). Convert this dimensional quantity to SI units of meter squared ( $\text{m}^2$ ) second (sec) per kilogram ( $\text{kg}^{-1}$ ), i.e.,  $\text{m}^2 \text{ sec kg}^{-1}$ .

#### Solution

The dimensional equation for the conversion of this quantity to SI units is

$$\begin{aligned}
 & 1.5 \frac{\text{cm}^3}{\text{hr m}^2 \text{ mmHg}} \times \frac{1 \text{ hr}}{3600 \text{ sec}} \times \frac{760 \text{ mmHg}}{1 \text{ atm}} \times \frac{1 \text{ atm}}{101,325 \text{ Pa}} \times \frac{1 \text{ Pa}}{1 \text{ N m}^{-2}} \\
 & \times \frac{1 \text{ N}}{\text{kg m sec}^{-2}} \times \frac{1 \text{ m}^3}{(100 \text{ cm})^3} = 3.125 \times 10^{-12} \frac{\text{m}^2 \text{ sec}}{\text{kg}}
 \end{aligned}$$

**Example 1.3**

Calculate the volume occupied by 100 lb<sub>m</sub> of oxygen (molecular weight equals 0.032 kg mole<sup>-1</sup>) at a pressure of 40 feet of water and a temperature of 20°C. Express the volume in cubic meters (m<sup>3</sup>).

**Solution**

The dimensional equation for the calculation of the volume of oxygen is based on [Equation 1.7](#) rearranged to solve for the volume, i.e., V = nRT/P:

$$V = \left( 100\text{lb}_m \times \frac{1\text{ kg}}{2.2046\text{ lb}_m} \times \frac{1\text{ mole}}{0.032\text{ kg}} \right) \times 8.314 \frac{\text{m}^3 \text{ Pa}}{\text{mole K}} \times (273.15 + 20) \text{ K}$$

$$\times \frac{1}{40 \text{ ft of water} \times \frac{1 \text{ atm}}{33.91 \text{ ft of water}} \times \frac{101,325 \text{ Pa}}{1 \text{ atm}}} = 28.90 \text{ m}^3$$

## 1.3 Conservation of mass

One of the most fundamental relationships that should always be considered when performing an engineering analysis on a system is the *conservation of mass*. This is also called a *material balance*. In its simplest terms, conservation of mass is the statement of the fact that the sum of the masses of all substances that enter the system must equal the sum of the masses of all the substances that leave the system. However, there can be changes in the individual masses or amounts of various chemical entities because of chemical reactions that may also be occurring within the system. Remember that mass is always conserved and moles are not necessarily conserved if chemical reactions occur in the system. The only exception to conservation of mass is for nuclear reactions where energy is converted to mass and vice versa. Nuclear reactions are not included in the systems that we will be considering.

### 1.3.1 Law of conservation

The following equation provides a generalized statement of the *law of conservation* for our system, which we will find extremely useful for the solution of a variety of problems:

$$\text{Accumulation} = \text{In} - \text{Out} + \text{Generation} - \text{Consumption} \quad (1.8)$$

This equation may be used to account for changes in quantities such as mass, moles, energy, momentum, and even money.

The *Accumulation* term accounts for the change with time of the quantity of interest within the system volume. The accumulation term in this equation is a time derivative of the quantity of interest and defines what is called an *unsteady problem*. The accumulation term can be either positive or negative. If the accumulation term is zero, then the quantity of interest within the volume of the system is not changing with time, and we refer to this situation as a *steady-state problem*.

The *In* term accounts for the entry of the quantity of interest into the system by all routes. For example, as carried in by the flow of fluid that is also called convection, or by the mechanism of diffusion.

The *Out* term is similar to the *In* term but accounts for the loss of the quantity of interest from the system. The *Generation* term accounts for the production of the quantity of interest within the system volume, whereas the *Consumption* term represents the loss of the quantity of interest within the system. The generation and consumption of the quantity of interest occurs through chemical reactions and the metabolic processes that occur within cells.

The following *nonengineering* example illustrates a practical application of [Equation 1.8](#), which is calculating the periodic payment on a loan. Remember this example since you can use the results to calculate payments for such items as automobiles, your house, and your credit card balance.

### Example 1.4

You just graduated from college as a bioengineer and have accepted your first job with a medical device company. You decide to buy yourself a nice sports car and in order to buy it you will need to borrow from the bank a total of \$65,000. The bank is offering you a 5 year loan at an annual interest rate of 6% compounded continuously.\* What is your monthly payment? What is the total amount that you will pay back to the bank? How much interest will you pay?

### Solution

We will let  $A$  represent the amount of money at any time that you owe the bank and  $R$  will represent the annual payment that you make to the bank on the loan. The interest rate is represented by  $i$ . The amount of interest that the bank charges you for the loan is equal to the interest rate multiplied by the amount at any time that you owe them. Using [Equation 1.8](#), we can then write the following equation that expresses how the amount you owe the bank changes with time:

$$\frac{dA}{dt} = iA - R$$

Note that the amount you owe the bank *Accumulates* or, in this case, since this is a loan, *Deaccumulates*, according to the term  $dA/dt$ . The amount you owe is also *Generated* or increased by the interest term represented by  $iA$ , and the amount you owe is decreased (*Out*) by the amount of your annual payment represented by  $R$ . Since  $R$  will be greater than  $iA$ , then  $dA/dt$  will be  $<0$ , and the amount that you owe the bank will decrease with time. This is a first order differential equation and represents what is also called an initial value problem. In order to solve this equation, we need to specify an initial condition (IC), which is the amount you owe the bank at time equal to zero, which is when you take out the loan. The initial condition can be written as

$$IC : t = 0 \quad A = A_0 = \$65,000$$

There are several methods that can be used to solve the above differential equation to include integrating factors and Laplace transforms. [Table 4.4](#) summarizes the Laplace transforms for a variety of functions, and one of the end-of-chapter problems asks you to resolve this example using Laplace transforms. However, an easy way to solve the differential equation (since  $R$  is

---

\* Note that most loans are compounded on some basis where interest is calculated, e.g., yearly, quarterly, monthly, or even daily, in the limit being continuous compounding. For practical purposes, the basis of the compounding is not a significant factor in estimating a loan payment.

a constant) is to let  $A$  be the sum of the homogeneous solution (i.e., when  $R = 0$ ) represented by  $A_h$  and a constant  $C_1$  yet to be determined. So, we let  $A = A_h + C_1$ . We then substitute this equation into the differential equation above, and we obtain

$$\frac{dA_h}{dt} = iA_h \quad \text{and} \quad -iC_1 = -R$$

We immediately see that  $C_1 = R/i$  and the homogeneous differential equation can be readily integrated to give  $A_h = C_2 e^{it}$ , where  $C_2$  is another constant that we evaluate from the initial condition. Our solution for the amount that we owe the bank at any time is then given by

$$A(t) = C_2 e^{it} + \frac{R}{i}$$

Now we use the initial condition that at  $t = 0$ ,  $A = A_0$  and we find that the constant  $C_2 = A_0 - (R/i)$ . Our result for the amount that you owe the bank at any time after the loan inception is then given by

$$A(t) = A_0 e^{it} + \left( \frac{R}{i} \right) (1 - e^{it})$$

Now, what we want to find is the annual payment needed to pay off the loan after  $T$  years. Then, since  $A(T) = 0$ , we can solve the above equation for  $R$  and obtain the following equation for the annual loan payment:

$$R = \frac{iA_0}{1 - e^{-iT}}$$

We can now insert the numbers to calculate the loan payment amount:

$$R = \frac{\frac{0.06}{\text{yr}} \times \$65,000}{1 - e^{\frac{-0.06 \times 5 \text{ yrs}}{\text{yr}}}} = \$15,047.35 \frac{1}{\text{yr}} = \$1,253.95 \frac{1}{\text{month}}$$

So, we see that the monthly payment for the sports car is about \$1254 per month. The total amount paid to the bank over the 5-year period of the loan is  $\$15,047.35 \text{ yr}^{-1} \times 5 \text{ yrs} = \$75,236.77$ , and the total amount of interest paid to the bank for the loan is  $\$75,236.77 - \$65,000 = \$10,236.77$ .

### 1.3.2 Chemical reactions

In the case of chemical reactions or cellular metabolism occurring within the system, you must also take into account, in your mass balances, the reaction stoichiometry as given by your balanced chemical equations for those substances that are involved in the chemical reactions. In addition, it is important to remember that for biological reactions, there can be an increase in the number of cells and your balanced chemical reaction must also consider the formation of biomass from the substances that take part in the reaction, as shown in the following example.

**Example 1.5**

Consider the anaerobic fermentation of glucose to ethanol by yeast. Glucose ( $C_6H_{12}O_6$ ) is converted into yeast, ethanol ( $C_2H_5OH$ ), the by-product glycerol ( $C_3H_8O_3$ ), carbon dioxide, and water. An empirical chemical formula for yeast can be taken as  $CH_{1.74}N_{0.2}O_{0.45}$  (Shuler and Kargi, 2002). Assuming ammonia ( $NH_3$ ) is the nitrogen source, we can write the following empirical chemical equation to describe the fermentation:



Suppose, we found that 0.12 moles of glycerol was formed for each mole of ethanol produced and 0.08 moles of water were formed for each mole of glycerol. Determine the *stoichiometric coefficients*, which are the letters a, b, c, d, e, and f in front of the chemical formulas in the above equation. Remember that the stoichiometric coefficients need to be determined so that the total number of carbon, hydrogen, oxygen, and nitrogen atoms are the same on each side of the equation.

**Solution**

Balancing the above equation by inspection is not an easy thing to do. Hence, we use the more formal approach as outlined below where we write a balance for each element, i.e., carbon, hydrogen, oxygen, and nitrogen:

$$\text{Carbon balance: } 6 = b + 2c + 3d + e$$

$$\text{Hydrogen balance: } 12 + 3a = 1.74b + 6c + 8d + 2f$$

$$\text{Oxygen balance: } 6 = 0.45b + c + 3d + 2e + f$$

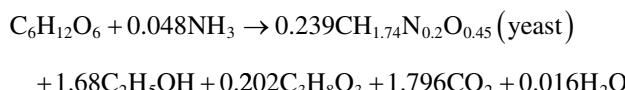
$$\text{Nitrogen balance: } a = 0.2b$$

$$\text{Other constraints: } d = 0.12c \text{ and } f = 0.08d$$

These relationships for each element can then be arranged into matrix form as follows. We see that the solution for a, b, c, d, e, and f involves the solution of six algebraic equations for these six unknowns:

$$\begin{bmatrix} 0 & 1 & 2 & 3 & 1 & 0 \\ -3 & 1.74 & 6 & 8 & 0 & 2 \\ 0 & 0.45 & 1 & 3 & 2 & 1 \\ 1 & -0.2 & 0 & 0 & 0 & 0 \\ 0 & 0 & -0.12 & 1 & 0 & 0 \\ 0 & 0 & 0 & 0.08 & 0 & -1 \end{bmatrix} \begin{bmatrix} a \\ b \\ c \\ d \\ e \\ f \end{bmatrix} = \begin{bmatrix} 6 \\ 12 \\ 6 \\ 0 \\ 0 \\ 0 \end{bmatrix}$$

Solution of this matrix gives  $a = 0.048$ ,  $b = 0.239$ ,  $c = 1.68$ ,  $d = 0.202$ ,  $e = 1.796$ , and  $f = 0.016$ . The balanced chemical equation for the anaerobic fermentation of glucose by yeast can then be written as shown here:



### 1.3.3 The extent of a chemical reaction

It is also convenient when analyzing chemical reactions to express the differential change in the moles of each species  $i$ , i.e.,  $dn_i$ , in terms of the differential *extent of reaction*  $j$ , i.e.,  $d\varepsilon_j$ . The extent of reaction  $j$  ( $\varepsilon_j$ ) will have units of moles and for a constant volume system ( $V$ ) can also be expressed in units of concentration. We also let  $v_{ij}$  represent the stoichiometric coefficient of species  $i$  in reaction  $j$ . If  $v_{ij} > 0$ , then the species is a product, and if  $v_{ij} < 0$ , then it is a reactant.

With these definitions, the following equation relates the differential change in the moles of species  $i$  as a result of its participation in each of the  $M$  reactions being considered. If species  $i$  does not participate in reaction  $j$ , then for that reaction  $v_{ij} = 0$ :

$$dn_i = \sum_{j=1}^M v_{ij} d\varepsilon_j \quad (1.9)$$

This equation can then be integrated from the initial state where  $\varepsilon_j = 0$  and the initial moles of species  $i$  is  $n_i = n_i^0$ , to the final state of  $n_i$  and  $\varepsilon_j$ :

$$n_i = n_i^0 + \sum_{j=1}^M v_{ij} \varepsilon_j \quad (1.10)$$

[Equation 1.10](#) then provides the moles of each species after the reaction has been completed ( $n_i$ ), in terms of the extent of each reaction ( $\varepsilon_j$ ). The total moles of all species ( $n$ ) can be found by summing [Equation 1.10](#) over  $i$  as shown by the next equation:

$$n = \sum_{i=1}^N n_i^0 + \sum_{i=1}^N \sum_{j=1}^M v_{ij} \varepsilon_j \quad (1.11)$$

In [Equations 1.9 through 1.11](#), the  $n_i$ 's represent the moles of species  $i$  in a given reaction volume of interest. If the reaction occurs in a flow-through system, then these  $n_i$ 's would be the molar flow rate of each species  $i$ .

Note that the concentrations of the respective species and the total concentration can be obtained by dividing [Equations 1.10](#) and [1.11](#) by the solution volume ( $V$ ), provided the solution volume remains constant throughout the course of the reaction. Also, the mole fraction of species  $i$  in the solution is given by  $x_i = n_i/n$ .

The conversion of a key component in a reaction is denoted by  $X$  and is defined as follows in terms of moles (the  $n_i$ 's) or the concentrations, if the volume is constant:

$$X = 1 - \frac{n_i}{n_i^0} = 1 - \frac{C_i}{C_i^0} \quad (1.12)$$

The actual conversion for a given reaction requires knowledge of the chemical kinetics or the rate law for a reaction and also depends on the reactor design equation. We will explore this in [Section 9.6](#)

for the special case of enzyme reactions. In some cases, we can make the assumption that the reaction is at equilibrium, and this is discussed in [Section 2.6.3.15](#) for the special case of equilibrium reactions in dilute aqueous solutions. An excellent resource for chemical reaction engineering is the book by Fogler (2005).

### Example 1.6

The continuous anaerobic fermentation of glucose was carried out at steady state in a well-mixed bioreactor. The feed stream to the bioreactor contained no yeast cells (sterile feed), ethanol, or glycerol. The feed flow rate to the bioreactor was  $100 \text{ L h}^{-1}$  and the concentration of glucose in this stream was equal to  $100 \text{ g L}^{-1}$ . Determine the amounts in  $\text{g h}^{-1}$  of the glucose, yeast cells, water produced, ethanol, glycerol, and carbon dioxide leaving the bioreactor for 97% conversion of glucose within the bioreactor. Also, determine the minimum amount of ammonia that is needed in  $\text{g h}^{-1}$ . Use the balanced chemical equation for anaerobic fermentation of glucose by yeast that was obtained in [Example 1.5](#). The volume of the liquid phase within the bioreactor is 2000 L.

### Solution

Since we only have one reaction, [Equations 1.10](#) and [1.11](#) simplify to

$$n_i = n_i^0 + v_i \epsilon \quad \text{and} \quad n = \sum_{i=1}^N n_i^0 + \epsilon \sum_{i=1}^N v_i$$

where  $\epsilon$  is the extent of the anaerobic fermentation reaction. In these equations the subscript  $i$  denotes the species, so let  $1 = \text{glucose}$ ,  $2 = \text{yeast}$ ,  $3 = \text{ethanol}$ ,  $4 = \text{glycerol}$ ,  $5 = \text{carbon dioxide}$ ,  $6 = \text{water}$ , and  $7 = \text{ammonia}$ . The molar rate at which glucose enters the reactor,  $n_1^0$ , is equal to the feed flow rate times the glucose concentration in this feed divided by the glucose molecular weight, i.e.

$$n_1^0 = 100 \frac{\text{L}}{\text{hr}} \times 100 \frac{\text{g}}{\text{L}} \times \frac{1 \text{ mole}}{180 \text{ g}} = 55.56 \frac{\text{moles}}{\text{hr}}$$

From the definition of conversion, we can show using [Equations 1.10](#) and [1.12](#) that the extent of this reaction is then related to the glucose conversion as follows:

$$\epsilon = n_1^0 X = 55.56 \frac{\text{moles}}{\text{hr}} \times 0.97 = 53.89 \frac{\text{moles}}{\text{hr}}$$

We can then use this extent of reaction, along with the stoichiometric coefficient for each component in the anaerobic fermentation reaction, to calculate the moles of each species leaving the reactor as follows:

*Glucose*

$$n_1 = 55.56 \frac{\text{moles}}{\text{hr}} - 53.89 \frac{\text{moles}}{\text{hr}} = 1.67 \frac{\text{moles}}{\text{hr}} \times 180 \frac{\text{g}}{\text{mole}} = 300.6 \frac{\text{g}}{\text{hr}}$$

*Yeast*

$$n_2 = 0 \frac{\text{moles}}{\text{hr}} + 0.239 \times 53.89 \frac{\text{moles}}{\text{hr}} = 12.88 \frac{\text{moles}}{\text{hr}} \times 23.74 \frac{\text{g}}{\text{mole}} = 305.8 \frac{\text{g}}{\text{hr}}$$

*Ethanol*

$$n_3 = 0 \frac{\text{moles}}{\text{hr}} + 1.68 \times 53.89 \frac{\text{moles}}{\text{hr}} = 90.54 \frac{\text{moles}}{\text{hr}} \times 46 \frac{\text{g}}{\text{mole}} = 4164.6 \frac{\text{g}}{\text{hr}}$$

*Glycerol*

$$n_4 = 0 \frac{\text{moles}}{\text{hr}} + 0.202 \times 53.89 \frac{\text{moles}}{\text{hr}} = 10.89 \frac{\text{moles}}{\text{hr}} \times 92 \frac{\text{g}}{\text{mole}} = 1001.5 \frac{\text{g}}{\text{hr}}$$

*Carbon dioxide*

$$n_5 = 0 \frac{\text{moles}}{\text{hr}} + 1.796 \times 53.89 \frac{\text{moles}}{\text{hr}} = 97.79 \frac{\text{moles}}{\text{hr}} \times 44 \frac{\text{g}}{\text{mole}} = 4258.6 \frac{\text{g}}{\text{hr}}$$

*Water (produced)*

$$n_6 = 0 \frac{\text{moles}}{\text{hr}} + 0.016 \times 53.89 \frac{\text{moles}}{\text{hr}} = 0.86 \frac{\text{moles}}{\text{hr}} \times 18 \frac{\text{g}}{\text{mole}} = 15.52 \frac{\text{g}}{\text{hr}}$$

The minimum amount of ammonia that is needed according to the fermentation reaction is

$$n_7^0 = 0 \frac{\text{moles}}{\text{hr}} + 0.048 \times 53.89 \frac{\text{moles}}{\text{hr}} = 2.59 \frac{\text{moles}}{\text{hr}} \times 17 \frac{\text{g}}{\text{mole}} = 43.97 \frac{\text{g}}{\text{hr}}$$

### 1.3.4 Material balances

In applying the law of mass conservation to your system, you can write a material balance using [Equation 1.8](#) for each component. If you have N components, then this will provide a total of N equations. You can also write a total material balance that gives an additional equation for a total of N + 1 equations. However, these N + 1 equations are not independent since we can also obtain the total material balance equation by just summing the N component material balances. Remember that you need as many equations as you have unknowns in order to completely describe your system. If you have more unknowns than equations relating these unknowns, then you have that many *degrees of freedom*, i.e.

$$\text{Degrees of freedom} = \text{Number of unknowns} - \text{Number of equations} \quad (1.13)$$

and you must specify the values of some of these unknowns. In solving engineering problems or designing equipment and devices, it is quite common to have more unknowns than equations that relate these unknowns. These degrees of freedom are also referred to as design variables and are quantities that you specify as part of the design of the system.

The following two examples illustrate the application of material balance principles.

**Example 1.7**

Drug B has a solubility of  $2.5 \text{ g B } 100^{-1} \text{ g}^{-1}$  water at  $80^\circ\text{C}$  and at  $4^\circ\text{C}$  the solubility of B is only  $0.36 \text{ g B } 100^{-1} \text{ g}^{-1}$  of water. If a saturated drug solution at  $80^\circ\text{C}$  has 1000 g of drug in it, determine how much water (W) is also present with the drug. The solution is then cooled to  $4^\circ\text{C}$  and the drug precipitate is separated from the saturated drug solution. How much of the drug will be precipitated (P) from the initial solution?

**Solution**

**Figure 1.1** illustrates the problem. As a basis for the calculation, we start with the fact that there is 1000 g of drug (D) in the initial solution. Since the drug has a solubility of  $2.5 \text{ g } 100^{-1} \text{ g}^{-1}$  of water at  $80^\circ\text{C}$ , we can calculate the amount of water (W) present in this saturated solution as follows:

$$W = \frac{100 \text{ g water}}{2.5 \text{ g B}} \times 1,000 \text{ g B} = 40,000 \text{ g water}$$

So, the initial saturated solution consists of 1,000 g of drug B and 40,000 g of water. This solution is then cooled to  $4^\circ\text{C}$  and the decrease in drug solubility results in the precipitation of B out of the solution. Here, we see that the 40,000 g of water is conserved within the cooled solution; however the mass of drug B in the supernatant solution (X) at  $4^\circ\text{C}$  and in the precipitate (P) are unknown. Let F denote the mass of the initial solution, i.e.,  $F = W + D = 40,000 \text{ g} + 1,000 \text{ g} = 41,000 \text{ g}$ . Also, let S represent the total mass of the saturated supernatant solution after cooling to  $4^\circ\text{C}$ , and P is the mass of drug B in the solid precipitate. A total mass balance on this process says that

$$F = S + P = 41,000 \text{ g}$$

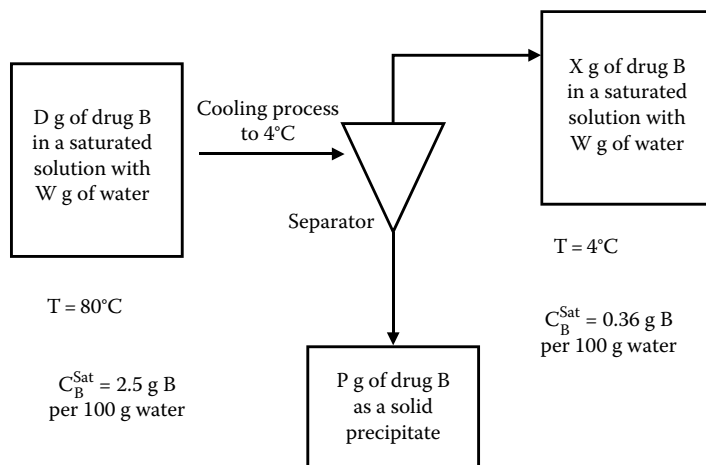


Figure 1.1 A drug precipitation process.

Therefore, the total mass balance says that  $F = 41,000 \text{ g} = S + P$ . Here, we still have two unknowns,  $S$  and  $P$ , so we need another equation in order to solve for  $S$  and  $P$ . A component material balance on drug B can also be written to find the mass of the drug precipitate, i.e.,  $P$ :

$$D = X + P = C_B^{\text{sat}} W + P$$

The term on the left side is the amount of drug B in the original solution ( $D$ ), the first term in the center portion provides the amount of drug B that can exist in the saturated supernatant solution at  $4^\circ\text{C}$ , and  $P$  is the mass of the drug precipitate.  $X$  can also be written as the product of the solubility of B at  $4^\circ\text{C}$  and the amount of water ( $W$ ) with the result that we can now solve for the amount of the precipitate:

$$1,000 \text{ g B} = \frac{0.36 \text{ g B}}{100 \text{ g water}} \times 40,000 \text{ g water} + P$$

$$P = 856 \text{ g of drug B in the precipitate}$$

With  $P$  now known, the overall material balance can be used to find the mass of the cooled supernatant solution:

$$S = F - P = 41,000 \text{ g} - 856 \text{ g} = 40,144 \text{ g}$$

The percentage recovery in the precipitate of drug B from the initial saturated solution at  $80^\circ\text{C}$  by cooling to a saturated solution at  $4^\circ\text{C}$  is given by

$$\% \text{ Drug B recovery} = \frac{\text{Mass in precipitate}}{\text{Mass in original solution}} = \frac{856 \text{ g drug B}}{1000 \text{ drug B}} \times 100 = 85.6\%$$

### Example 1.8

A continuous membrane separation process is being used to separate components A and B into a product stream that is mostly A and a waste stream that is primarily B. A and B enter the process together at a total flow rate ( $F$ ) of  $100 \text{ kg hr}^{-1}$ . The composition of this feed stream is 40% A and 60% B by mass. The product stream ( $P$ ) being removed from the process has a composition of 90% A and 10% B, whereas the waste stream ( $W$ ) leaving the process has a composition of 2% A and 98% B. Calculate the mass flow rates of the product ( $P$ ) and waste streams ( $W$ ).

### Solution

[Figure 1.2](#) illustrates the problem. First we can write an overall material balance that says,  $F = 100 \text{ kg hr}^{-1} = P + W$ . With two unknowns  $P$  and  $W$ , there is a need for another equation. So, we can write a component material balance on A that says,  $0.40 \times 100 \text{ kg hr}^{-1} = 0.90 \times P + 0.02 \times W$ . Since  $W = 100 \text{ kg hr}^{-1} - P$  from the overall material balance, the component material balance can be rewritten in terms of just  $P$ , or  $40 \text{ kg hr}^{-1} = 0.90 P + 2 \text{ kg hr}^{-1} - 0.02 P$ . Solving for the product flow rate, we obtain  $P = 43.18 \text{ kg hr}^{-1}$ . From the overall material balance, we then find that  $W = 100 \text{ kg hr}^{-1} - 43.182 \text{ kg hr}^{-1} = 56.82 \text{ kg hr}^{-1}$ .

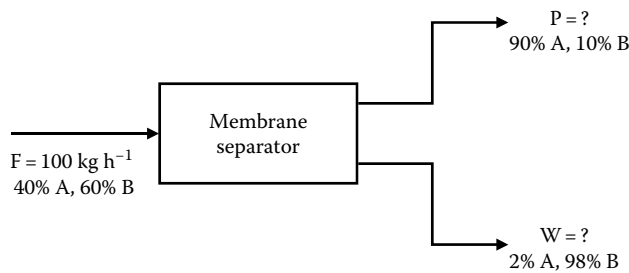


Figure 1.2 A continuous membrane separation process.

## 1.4 Tips for solving engineering problems

In this section, we outline a basic strategy that can be used to solve the type of engineering problems considered in this book and those you are likely to encounter as a biomedical engineer. This basic strategy is useful since it eliminates approaching the solution of each new problem or system as if it is a unique situation. The numerous examples throughout the book as well as the problems at the end of each chapter will provide you with the opportunity to apply the strategy outlined here and, at the same time, develop your skills in using the engineering analysis techniques discussed in this book. One of the unique and challenging aspects of engineering is that the number of problems that you may come across during the course of your career is limitless. However, it is important to understand that the underlying engineering principles and the solution strategy are always the same.

The engineering problems we will consider derive from some type of process. A *process* is defined as any combination of physical operations and chemical reactions that act on or change the substances involved in the process. A process also occurs within what is also more generally called the *system*. Everything else that is affected by the system or interacts with the system is known as the *surroundings*. The engineering analysis of all problems can therefore be considered within the context of the system and its surroundings.

There are several important steps that you should follow before attempting to make any engineering calculations on a system and its surroundings. For ease of reference, these steps are also summarized in [Table 1.7](#). One of the first things that you should do when solving a particular problem is to draw a sketch that defines your system. Drawing a sketch of the system for a given problem will allow you to identify and focus your attention on the key features of the problem. The sketch does not have to be elaborate; you can use boxes to represent the system and lines with arrows can be used to indicate the flow of streams that enter and leave the system. The solutions for [Examples 1.7](#) and [1.8](#) both have sketches, as shown in [Figures 1.1](#) and [1.2](#).

If you know them or can easily calculate them, make sure you also write down the flow rates of the flowing streams and the amount or concentration of each substance in each of the flowing streams. On your sketch, you will also write down the available data that you already have concerning the problem. Examples of additional data that may be important in solving your problem include temperatures, pressures, experimental data, physical properties, and even conversion factors. Next, you should obtain any additional information or data needed to solve the problem. You should also write down any chemical reactions that need to be considered and make sure that these are also balanced.

Table 1.7 Steps for Solving Engineering Problems

**Problem Solving Steps**

1. Draw a sketch that defines your system.
2. Indicate with lines and arrows the flow of streams that enter and leave the system.
3. Indicate the flow rates and the amounts or concentrations of each of the substances in each of the flowing streams.  
For those that are unknown see if you can easily calculate them using material balance equations.
4. Write down any chemical reactions that need to be considered and make sure that these are also balanced.
5. Write down the available data that you already have concerning the problem.
6. Obtain any additional information or data needed to solve the problem.
7. Identify the specific engineering principles and formulas that govern the physical and chemical operations that occur within your system.
8. Solve the problem using the above information.

Obtaining the answer to the problem illustrated by your sketch of the system will require the use of specific engineering principles and formulas that govern the physical and chemical operations that occur within your process. Formulating the solution and solving engineering problems is a skill that one needs to develop and refine in order to be successful in engineering. That is the goal of this book, to provide you with the mathematical techniques and skills for solving a variety of biomedical engineering problems that involve chemical reactions and such transport processes as fluid flow and mass transfer. Building on the skills learned in this book, you will then be able to design biomedical equipment and devices.

## 1.5 Useful numerical methods

The solution of many biomedical engineering problems will require the use of a numerical method. In other words, an analytical solution is very difficult to obtain or a simple hand calculation is not possible. In some cases, you may also want to illustrate your solution on a graph. In these situations you will need to write a computer program. In this section you will find eight examples that show how to solve many common problems that you may encounter. In each example, a numerical solution is shown using MATLAB®, a commercial engineering software package that is commonly used by engineers and scientists. You can use these example solutions as a template that can be easily modified to solve the particular problem you are working on. Additional details on how to program in MATLAB can be found in Hahn and Valentine (2013).

### Example 1.9: Comparing a model equation to a set of experimental data

**Table 1.8** summarizes the data obtained from a viscometer\* for the shear stress ( $\tau$ , Pa) of ketchup as a function of the shear rate ( $\dot{\gamma}$ , sec<sup>-1</sup>). These data were obtained from an online technical report presented by TA Instruments.<sup>†</sup> The Casson equation is a model that can be used to describe the shear stress and shear rate relationship for complex fluids like ketchup.

\* See Chapter 4 for more information on viscosity and the flow of fluids.

† [http://www.tainstruments.co.jp/application/pdf/Rheology\\_Library/Solutions/RS013.PDF](http://www.tainstruments.co.jp/application/pdf/Rheology_Library/Solutions/RS013.PDF).

Table 1.8 Shear Stress versus Shear Rate for Ketchup

Shear Rate ( $\text{sec}^{-1}$ )	Shear Stress (Pa)
0	58
25	80
50	87
100	105
150	115
200	120
300	138
400	155
500	170

The Casson equation is given by

$$\tau^{1/2} = \tau_y^{1/2} + s\gamma^{1/2} \quad (\text{A})$$

where  $\tau_y$  and  $s$  are constants. The Casson equation says that a plot of the square root of the shear stress versus the square root of the shear rate should give a straight line, i.e., compare the above equation with  $y = b + mx$ , where the  $y$  intercept ( $b$ ) of the graph is the square root of the yield stress, i.e.,  $\sqrt{\tau_y}$ , and the slope ( $m$ ) is  $s$ . From the data given in [Table 1.8](#), we can estimate the value of  $\tau_y$  as 58 Pa, and the value of  $s$  can be approximated from the rise over the run of the data starting at the  $y$  intercept of 58 Pa:

$$s = \frac{\tau^{1/2} - \tau_y^{1/2}}{\gamma^{1/2} - 0} = \frac{170^{1/2} - 58^{1/2}}{500^{1/2}} = 0.243 \left( \text{Pa sec} \right)^{1/2}$$

With these values of  $\tau_y$  and  $s$ , make a graph using MATLAB that compares the Casson equation, using these values of  $\tau_y$  and  $s$ , to the data given in [Table 1.8](#). Note that in the graph the data must be shown by symbols and the prediction by the Casson equation as a solid line.

### Solution

The MATLAB program for solving this problem is shown below. [Figure 1.3](#) shows a comparison between the data given in [Table 1.8](#) and the prediction of the Casson equation for the estimated values of  $\tau_y$  and  $s$ . We see that the Casson equation with these values of  $\tau_y$  and  $s$  provides an excellent representation of these data.

```
%Comparing an equation to a set of experimental data
clear
clc
clf
%enter the data as vectors gamma and tau, these data represent the
%shear rate and shear stress
gamma=[0,25,50,100,150,200,300,400,500];
tau=[58,80,87,105,115,120,138,155,170];
%now apply any transformation to these data, for example here we
```

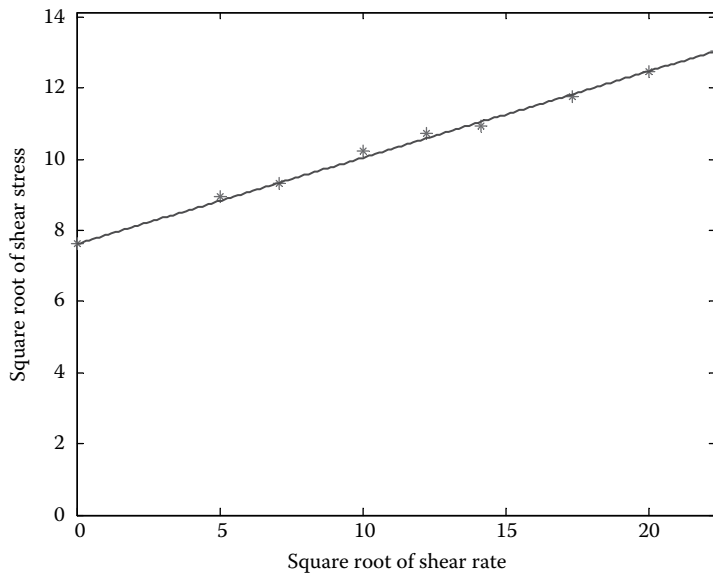


Figure 1.3 Comparison of the Casson equation to the shear stress and shear rate data for ketchup.

```
%take the square root of each quantity
x=sqrt(gamma);
y=sqrt(tau);
%now plot the transformed data set x and y with xlower and xupper
%defining the x range and ylower and yupper defining the y range
xlower=0;
xupper=sqrt(500);
ylower=0;
yupper=sqrt(200);
plot(x,y,'*b');
axis([xlower,xupper,ylower,yupper]);
xlabel('Square Root of Shear Rate'), ylabel('Square Root of Shear
Stress');
title('Comparing an Equation to a Set of Experimental Data');
hold on;
%now enter the equation and its parameters that you want to compare
%to the experimental data
s=0.243;
tauy=58;
%now define a vector of 200 points along the abscissa for the equation
%to calculate the predicted ordinate values from
xline=linspace(min(x),max(x),200);
%now calculate the predicted ordinate values for each value of xline
%using in this case the Casson equation
yline=sqrt(tau)+s*xline;
%now plot yline versus xline on the same graph with the data to obtain
%a comparison between the experimental data and the model equation
plot(xline,yline,'r-')
```

**Example 1.10: Linear regression of experimental data**

Using the data found in [Table 1.8](#), find the parameters  $\tau_y$  and  $s$  in the Casson equation that provides the best fit to these data.

**Solution**

The Casson equation says that if we replot the experimental data as the square root of the shear stress versus the square root of the shear rate, the result should be linear. According to the Casson equation, see [Equation A](#) in the previous example, these transformed data will have an intercept equal to the square root of the yield stress, i.e.,  $\sqrt{\tau_y}$ , and a slope equal to  $s$ . Our goal is then to find the values of  $\tau_y$  and  $s$  that minimize the error between these transformed experimental values and the values predicted by the Casson equation. The criterion that is often used to determine the best fit is the sum of the square of the error (SSE) between the experimental ordinate values and those predicted by the model equation. The SSE using the Casson equation is defined by

$$\text{SSE} = \sum_{n=1}^N \left( \tau_{\text{experimental},n}^{1/2} - \tau_{\text{Casson},n}^{1/2} \right)^2$$

where  $N$  is the total number of data points. The MATLAB program for performing the linear regression is shown below. [Figure 1.4](#) shows a comparison between the data given in [Table 1.8](#) and the prediction of the Casson equation. The values for  $\tau_y$  and  $s$  are found to be, respectively, 59.3 Pa and  $(\text{Pa sec})^{1/2}$ . The value of the correlation coefficient, i.e.,  $r^2 = 0.997$  and indicates that the Casson equation with these values of  $\tau_y$  and  $s$  provides an excellent representation of these data.

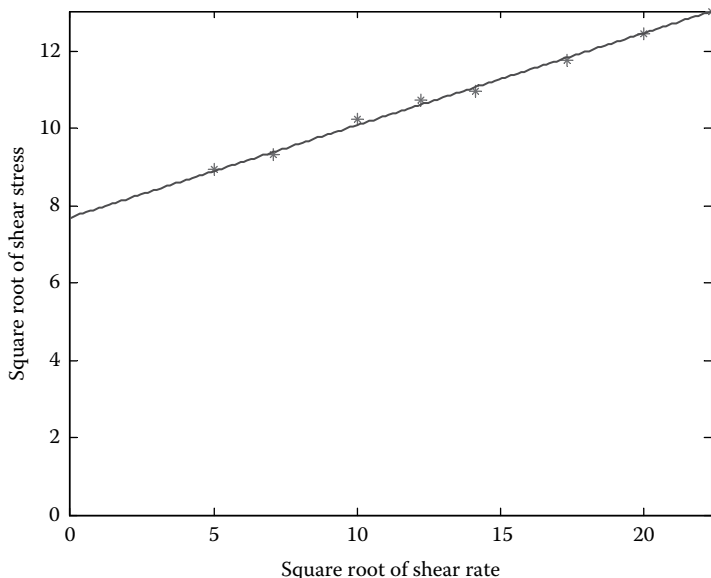


Figure 1.4 Linear regression of the Casson equation to the shear stress and shear rate data for ketchup.

```
%Linear regression
clear
clc
clf
%enter the data as vectors gamma and tau, these data represent the
%shear rate and shear stress
gamma=[0,25.,50.,100.,150.,200.,300.,400.,500.];
tau=[58.,80.,87.,105.,115.,120.,138.,155.,170.];
%now apply your transformation to these data, for example, here we
%take the square root of each quantity
x=sqrt(gamma);
y=sqrt(tau);
%now plot the transformed data set x and y with xlower and xupper
%defining the x range and ylower and yupper defining the y range
xlower=0;
xupper=sqrt(500);
ylower=0;
yupper=sqrt(170);
plot(x,y,'*b');
axis([xlower,xupper,ylower,yupper]);
xlabel('Square Root of Shear Rate'), ylabel('Square Root of Shear
    Stress');
title('Linear Regression');
hold on;
%now do the linear regression using polyfit with N=1 since the
%degree of a linear equation in x is 1
coeff=polyfit(x,y,1);
%now display the results of the regression, where m is the slope of the
%regression line, and b is the line's intercept
disp(['m= ',num2str(coeff(1))])
disp(['b= ',num2str(coeff(2))])
%now let's plot the best fit line to the data to see how well the
%regression line fits the data, to do this (1) define a vector of 200
%x-points in the range of the x data, (2) then calculate the
%corresponding vector of the predicted y values, (3) then display the
%predicted results as a line on the same figure as the data
xline=linspace(min(x),max(x),200);
%now calculate the predicted y values for each value of xline
yline=coeff(2)+xline*coeff(1);
%now plot yline versus xline on the same graph with the data
plot(xline,yline,'r-')
%now we calculate the correlation coefficient, or the r^2
%as a statistical measure of how good the fit for our regression is, if
%r^2 is 0 the fit is horrible, if +1 (positive slope) or -1 (negative
%slope) the fit is perfect, we usually want a abs(r^2)>0.90 for a good
%fit, so now we calculate the value of r^2
%first calculate the predicted value of y for each value of x
yest=coeff(1)*x+coeff(2);
%next calculate the average value of the y data
yavg=mean(y);
```

```
%now calculate the SSE and the SST
SSE=sum((y-yest).^2);
SST=sum((y-yavg).^2);
%then calculate the r^2 using this formula
rsqr=1-SSE/SST;
disp(['r-squared= ',num2str(rsqr)])
%now show both the regression equation and the
%r^2 on the graph as text
a1str=num2str(coeff(1));
a0str=num2str(coeff(2));
eqnstr=['y= (',a1str,')*x + (',a0str,')'];
rsqr = ['r^2 = ',num2str(rsqr)];
%then use the gtext command to position these strings on your graph
%where you want them to be
gtext({eqnstr,rsqr})
```

### Example 1.11: Linear regression of experimental data with a zero intercept

From the data given in [Table 1.8](#), we see that when the shear rate is zero, the shear stress is 58 Pa, and this would be equal to the yield stress,  $\tau_y$ . Using this as the value for  $\tau_y$ , we can rearrange the Casson equation as

$$\tau^{1/2} - \tau_y^{1/2} = s\dot{\gamma}^{1/2}$$

Now we see that a plot of  $\tau^{1/2} - \tau_y^{1/2}$  versus  $\dot{\gamma}^{1/2}$  would be linear with a slope equal to  $s$  and an intercept of zero. We can perform a linear regression of the data shown in [Table 1.8](#) using the above form of the Casson equation and obtain the slope,  $s$ , of the resulting regression line using  $\tau_y = 58$  Pa. However, in performing this linear regression, we need to use a linear regression method that constrains the  $y$  intercept to zero.

### Solution

The MATLAB program for performing the linear regression with the constraint of a zero intercept is shown below. [Figure 1.5](#) shows a comparison between the data given in [Table 1.8](#) and the prediction using the above equation. We find that the regression line has a slope, i.e.,  $s$ , equal to  $0.243$   $(\text{Pa sec})^{1/2}$ . The value of  $r^2 = 0.996$ , which shows that this approach also provides an excellent representation of these data.

```
%Linear regression with a zero intercept
clear
clc
clf
%enter the data as vectors gamma and tau, these data represent the
%shear rate and shear stress
gamma=[0,25.,50.,100.,150.,200.,300.,400.,500.];
tau=[58.,80.,87.,105.,115.,120.,138.,155.,170.];
%now subtract the square root of tau-y = 58 from the square
%root of these tau values and call the result y, also let x
```

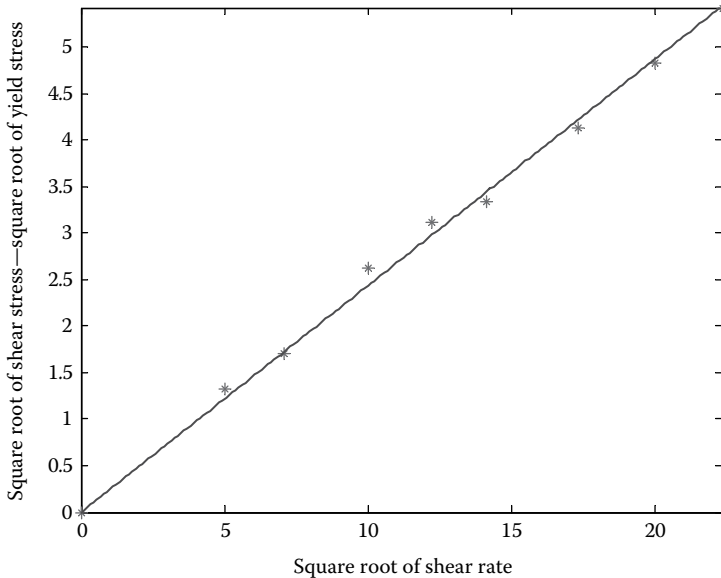


Figure 1.5 Zero intercept linear regression of the Casson equation to the shear stress and shear rate data for ketchup.

```
%equal the square root of the gamma's
y=sqrt(tau)-sqrt(58.)
x=sqrt(gamma)
%now plot these data with xlower and xupper defining the x range
%and ylower and yupper defining the y range
xlower=0.;
xupper=sqrt(500);
ylower=0.;
yupper=sqrt(170)-sqrt(58.);
plot(x,y,'*b');
axis([xlower,xupper,ylower,yupper]);
xlabel('Square Root of Shear rate')
ylabel('Square Root of Shear stress - Square Root of Yield Stress');
title('Linear Regression with a Zero Intercept');
hold on;
%now do the linear regression, note this is how it is done when the
%intercept must equal zero
m=x(:)\y(:);
%now display the results of the regression
disp(['m=',num2str(m)]);
%now let's plot the best fit line to the data to see how well the
%regression line fits the data, to do this (1) define a vector of 200
%x-points in the range of the x data, (2) then calculate the
%corresponding vector of y points, (3) display the calculated x and y
%points as a line on the same figure as the data
xline=linspace(min(x),max(x),200);
```

```
%now calculate the y values for each value of xline
yline=xline*m;
%now plot yline versus xline on the same graph with the data
plot(xline,yline,'r-')
%now use the correlation coefficient, or the
% $r^2$  as a statistical measure of how good the fit for the regression
%is, if  $r^2$  is 0 the fit is horrible, if +1 (positive slope) or -1
%(negative slope) the fit is perfect, usually  $\text{abs}(r^2) > 0.90$  for a
%good
%fit, first calculate the predicted value of y for each value of x
yest=m*x;
%next calculate the average value of the y data
yavg=mean(y);
%now calculate the SSE and the SST
SSE=sum((y-yest).^2);
SST=sum((y-yavg).^2);
%then calculate the  $r^2$  using this formula
rsqr=1-SSE/SST;
disp(['r-squared= ',num2str(rsqr)])
%now show both the regression equation and the
% $r^2$  on the graph as text
a1str=num2str(m);
eqnstr=['y= ',a1str,'*x'];
rsqr = ['r^2 = ',num2str(rsqr)];
%then use the gtext command to position these strings on your graph
%where you want them to be
gtext({eqnstr,rsqr})
```

### Example 1.12: Nonlinear regression of experimental data

Suppose we did not transform the data shown in [Table 1.8](#) but just plotted the data as shear stress versus shear rate. In this case we would find that the plot is not linear. Given a model like the Casson equation, we can rearrange it to express the shear stress in terms of the shear rate as given by

$$\tau = \left( \tau_y^{1/2} + s\dot{\gamma}^{1/2} \right)^2$$

Note that now the shear stress is related to the shear rate in a nonlinear way. The SSE in this case is defined by  $\text{SSE} = \sum_{n=1}^N (\tau_{\text{experimental},n} - \tau_{\text{Casson},n})^2$ . MATLAB has a built-in function (*nlinfit*) that can perform nonlinear regressions to find the parameters in the model equation above, i.e.,  $\tau_y$  and  $s$ , to minimize the error between the measured shear stress and the values predicted by the model equation.

### Solution

The MATLAB program for performing the nonlinear regression is shown below. [Figure 1.6](#) shows a comparison between the data given in [Table 1.8](#) and the prediction assuming the ketchup behaves like a Casson fluid. The nonlinear regression analysis gives a  $\tau_y = 59.55 \text{ Pa}$  and the value of  $s$  is  $0.237 \text{ (Pa sec)}^{1/2}$ .

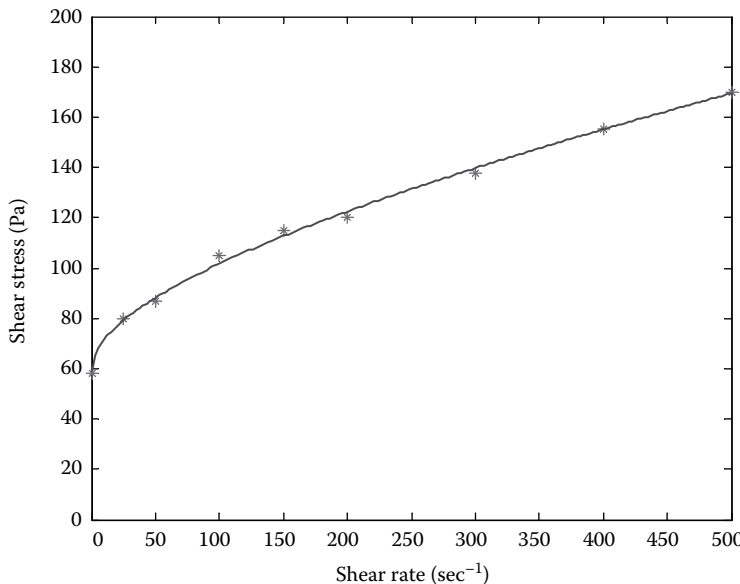


Figure 1.6 Nonlinear regression of the Casson equation to the shear stress and shear rate data for ketchup.

```
% Nonlinear Regression
clear
clc
clf
format compact
% enter the data as vectors gamma and tau, the shear rate and shear
stress
gamma=[0,25.,50.,100.,150.,200.,300.,400.,500.];
tau=[58.,80.,87.,105.,115.,120.,138.,155.,170.];
%now enter the function to fit these data tauh is the predicted ordinate
value, where b is the vector of the regression parameters, in
%this case b(1) is the yield stress and b(2) is s
tauh=@(b,gamma)(sqrt(b(1))+b(2)*sqrt(gamma)).^2;
% now enter guess values for the b parameters
b0=[60,0.25];
% plot the raw data
xlower=0;
xupper=500;
ylower=0;
yupper=200;
plot(gamma,tau,'*b');
axis([xlower,xupper,ylower,yupper]);
xlabel('Shear Rate, 1/sec'), ylabel('Shear Stress, Pa');
title('Nonlinear Regression')
hold on
```

```
% determine the best values of the b's to fit the function tauh to
% the data using the nlinfit routine
bhat=nlinfit(gamma,tau,tauh,b0);
%plot the results of the nonlinear regression
disp(['yield stress= ',num2str(bhat(1))])
disp(['s =',num2str(bhat(2))])
% plot the predicted values
xline=linspace(min(gamma),max(gamma),200);
plot(xline,tauh(bhat,xline),'r-');
legend('original data','fit to the data','location','Best')
```

### Example 1.13: Integration of a function

There are many times when we need to integrate a function, and sometimes it turns out that this cannot be done analytically. In addition, the solution to many first order differential equations can be obtained by performing an integration if the terms containing the dependent and independent variables are separable. So a method for numerically integrating a function can be very useful. Consider [Example 1.4](#) where the following differential equation described how the amount of money owed to the bank ( $A$ ) changes with time ( $t$ ) for a given annual payment ( $R$ ) and interest rate ( $i$ ):

$$\frac{dA}{dt} = iA - R$$

This equation can be rearranged and integrated to find the time it would take to pay off ( $t_{\text{payoff}}$ ) the loan ( $A_0$ ) for given values of  $i$  and  $R$ :

$$\int_0^{t_{\text{payoff}}} dt = t_{\text{payoff}} = - \int_0^{A_0} \frac{dA}{iA - R}$$

Using the values for  $A_0$ ,  $i$ , and  $R$  from [Example 1.4](#), calculate the time to pay off the loan by performing the above integration numerically.

### Solution

The MATLAB program for solving this problem is shown below. With  $A_0 = \$65,000$ ,  $i = .06/\text{yr}$ , and  $R = \$15,047.35$ , we find that  $t_{\text{payoff}} = 5$  years.

```
%Integration of a function
clear
clc
clf
%Use the matlab 'quad' command to perform the single variable
%integration where for a given f(x) with limits xlower and xupper we
%would write this as quad('f(x)',xlower,xupper)
Alower=0;
Aupper=65000;
i=.06;
R=15047.35;
f=@(A) -1./(i*A-R);
```

---

```
%for this example the quad command is written as follows
tpayoff=integral(f,Alower,Aupper);
%display the results
disp(['Payoff time, years= ',num2str(tpayoff)])
```

### Example 1.14: Solving a first order ordinary differential equation

In [Example 1.4](#), the following first order differential equation described how the amount of money owed to the bank ( $A$ ) changes with time ( $t$ ) for a given annual payment ( $R$ ) and interest rate ( $i$ ):

$$\frac{dA}{dt} = iA - R$$

This equation can also be solved numerically using a differential equation solver. Using the values for  $A_0$ ,  $i$ , and  $R$  from [Example 1.4](#), calculate the time to pay off the loan by solving this differential equation numerically.

#### Solution

The MATLAB program for solving this problem is shown below. The solution for how the amount owed,  $A(t)$ , changes with time is shown in [Figure 1.7](#), using  $A_0 = \$65,000$ ,  $i = .06/\text{yr}$ , and  $R = \$15,047.35$ . We find that  $t_{\text{payoff}} = 5$  years.

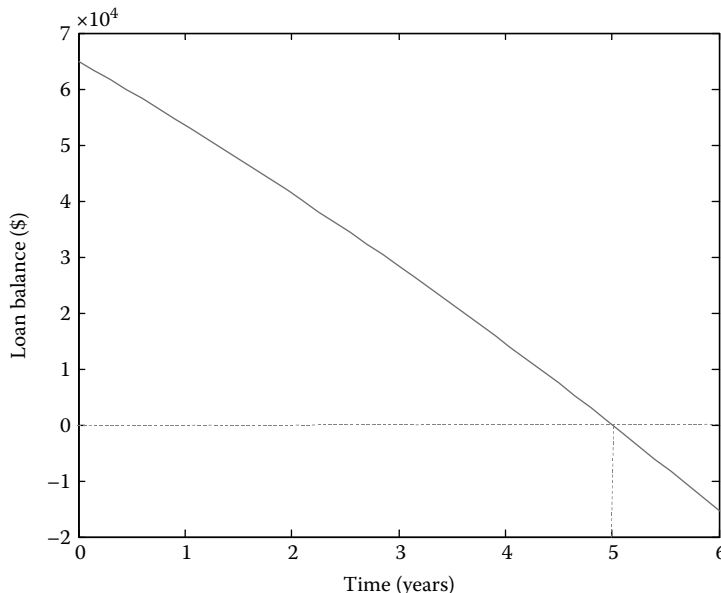


Figure 1.7 Loan balance as a function of time, payoff is 5 years.

```
%Solving a first order differential equation, dy/dx=f(x,y)
clear
clc
clf
%Enter the constants
A0=65000.;
i=.06;
R=15047.35;
%Enter the function f(x,y)
dAdt=@(t,A) (i*A-R);
%Enter the range of the independent variable
tstart=0.;
tend=6.;
Ainitial=A0;
%Now solve the differential equation using the ODE45 routine
[t,A]=ode45(dAdt,[tstart,tend],Ainitial);
%Now plot the solution as A vs t
plot(t,A);
xlabel('Time, years'), ylabel('Loan Balance, $');
title('Solution to Example 1.4');
hold on
```

### **Example 1.15: Solving a second order ordinary differential equation**

A second order ordinary differential equation can be solved by converting it into two first order ordinary differential equations. For example, consider the classic damped harmonic oscillation described by the following second order differential equation:

$$\frac{d^2x}{dt^2} + 2b\frac{dx}{dt} + a^2x = 0$$

The above equation can be rewritten as two first order differential equations by letting  $z = dx/dt$  and  $dz/dt = d^2x/dt^2$ . Substituting these into the above equation, we then obtain two first order differential equations:

$$\begin{aligned}\frac{dx}{dt} &= z \\ \frac{dz}{dt} &= -\left(2bz + a^2x\right)\end{aligned}$$

Now solve these two equations for  $x(t)$  from  $t = 0$  to  $t = 10$  with  $a = 1$  and  $b = .25$ . Two initial conditions are also needed, so let  $x|_{t=0} = 1$  and  $(dx/dt)|_{t=0} = z = 0$ .

#### **Solution**

The MATLAB program for solving this problem is shown below.\* In this MATLAB solution, you will need to write a *function file* to define the right-hand sides of the first order

---

\* Note that this solution can also be easily generalized to the solution of multiple first order ordinary differential equations.

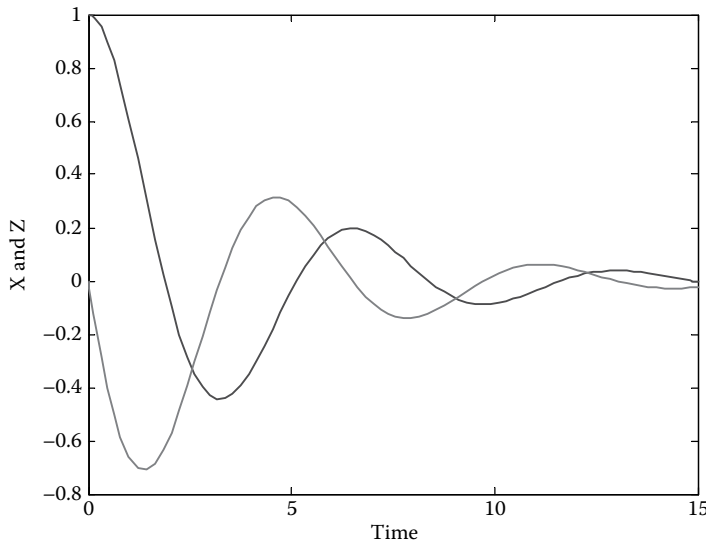


Figure 1.8 Solution to a second order ordinary differential equation.

differential equations. This *function file*, named here as *multipleode.m*, is then called by the *command file*, named here *call\_multipleode.m*. The solution for  $x(t)$  and  $z(t)$  is shown in Figure 1.8.

```
%This is the command file and solves multiple first order ordinary
% differential equations
function[t,x]=call_multipleode()
%enter the range of the independent variable
tspan=[0 15];
%enter the initial conditions for the dependent variables, note that in
%this example x1 is our x and x2 is our z
x1_0=1;
x2_0=0;
%enter any parameters in the ODE functions
a=1;
b=.25;
%now use the Matlab ODE solver to find how x changes with t
[t,x]=ode45(@multipleode,tspan,[x1_0 x2_0],[],a,b);
%now display the results on a graph
plot(t,x);
xlabel('Time'), ylabel('X and Z');
title('Multiple 1st Order Ordinary Differential Equations');
%This is the function file and defines the functions of the set of
% 1st order ODE's
%enter any constants to be used
function dxdt=multipleode(t,x,a,b)
dxdt=zeros(2,1);
dxdt(1)=x(2);
dxdt(2)=-(2*b*x(2)+a^2*x(1));
end
```

**Example 1.16: Finding the zero of a function of one variable, the root finder**

Many times an analysis results in a nonlinear equation where it is not possible to solve explicitly for the variable of interest. For example, given a function like  $\alpha(x) = \beta$ , we want to find the value of  $x$  that satisfies this equation. A root finder does this for us by finding the zero of a function, i.e.,  $f(x)$ , defined as  $f(x) = \alpha(x) - \beta$ . The root finder finds the value of  $x$  that makes  $f(x) = 0$ . In [Example 1.4](#), we showed that the following equation gives the annual payment for given interest rate,  $i$ , initial loan amount  $A_0$ , and loan period  $T$ :

$$R = \frac{iA_0}{1 - e^{-iT}}$$

Suppose we wanted to find, for a loan amount of  $A_0 = \$65,000$  and a loan period of 5 years, the annual interest rate that gives an annual payment of \$18,000. The above equation cannot be solved explicitly for  $i$ , so we would need to use a root finder method in order to solve this problem.

**Solution**

The following MATLAB program shows how to solve this type of problem. In this case the annual interest rate is found to be  $i = 0.1381$ . [Figure 1.9](#) shows a graph of  $f(i)$  versus  $i$ .

```
%this example shows you how to find the root of a nonlinear function
%i.e., find the value of x that makes f(x) = 0
clear
clc
clf
```

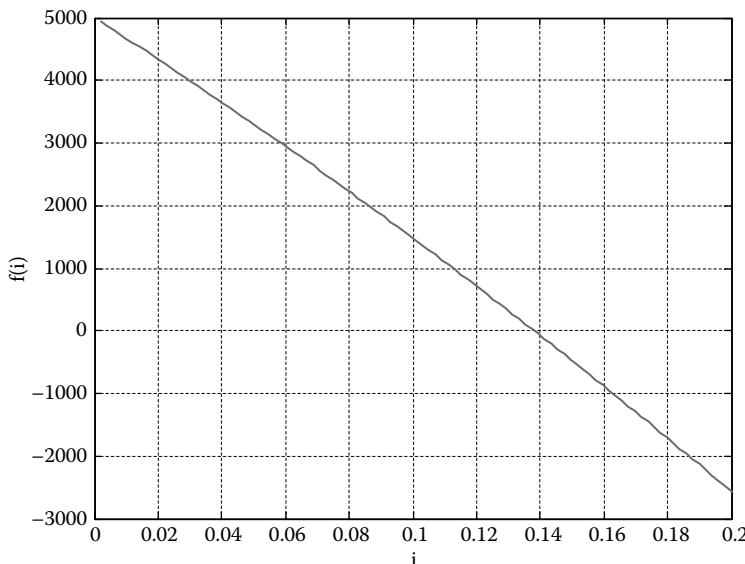


Figure 1.9 The root occurs when  $f(i) = 0$ , i.e.  $i \sim .139$ .

```
%enter the parameters in the function, f(x)
R=18000; A0=65000; t=5;
%define the function, f(x), here the unknown x is i
f=@(i) R-i*A0./(1-exp(-i*t));
%define the interval where the root is expected to occur
i=linspace(0,.2);
y=f(i);
%plot to show that the root is correct and to help with an initial
guess
plot(i,y);
axis([0,.20,-3000,5000]);
xlabel('i'); ylabel('f(i)');
title('root finder example-plot of f(i) vs i');
grid on
%now use the matlab function fzero to find the exact value of the
root
%using an initial guess from the graph found above
i=fzero(f,0.1);
disp(['i= ',num2str(i)]);
```

## Problems

- 1.1  $R = 8.314 \text{ J mol}^{-1} \text{ K}^{-1}$ , find the equivalent in  $\text{cal mol}^{-1} \text{ K}^{-1}$ .
- 1.2 Convert  $98.6^\circ\text{F}$  to  $^\circ\text{C}$  and then  $\text{K}$ .
- 1.3 During cell migration, fibroblasts can generate traction forces of approximately  $2 \times 10^4 \mu\text{dynes}$ . What is the equivalent force in  $\text{kN}$ ?
- 1.4 Endothelial cells in random motion were recorded to move at the *lightning speed* of  $27 \mu\text{m h}^{-1}$ , what would their speed be in miles per second?
- 1.5 A process requires 48 MW of power to convert A to B. What is the power needed in  $\text{cg cm}^2 \text{ hr}^{-3}$ ? What about in  $\text{kJ}$  per minute?
- 1.6 Which is moving faster, a plane moving at 400 miles per hour or a molecule moving at  $6.25 \times 10^{15} \text{ nm min}^{-1}$ ? Show the answer in units of mm per second.
- 1.7 Resolve [Example 1.4](#) using the Laplace transform technique.
- 1.8 Rework [Example 1.5](#) assuming there are 0.21 moles of glycerol formed for each mole of ethanol and 0.13 moles of water formed for each mole of glycerol.
- 1.9 A hollow fiber membrane separator with a nominal molecular weight cutoff of 100,000 is fed a solution of proteins at the rate of  $250 \text{ mL min}^{-1}$ . The composition of the protein solution is protein A ( $4 \text{ g L}^{-1}$ , MW = 20,000), protein B ( $7 \text{ g L}^{-1}$ , 150,000), and protein C ( $6 \text{ g L}^{-1}$ , MW = 300,000). The filtrate flow rate is found to be  $116.2 \text{ mL min}^{-1}$  and the flow rate of the retentate is  $133.8 \text{ mL min}^{-1}$ . The concentration of protein A in the retentate is found to be  $5.84 \text{ g L}^{-1}$ . What is the concentration of protein A in the filtrate? Also what are the concentrations of proteins B and C in the filtrate and in the retentate?
- 1.10 An artificial kidney is a device that removes water and wastes from the blood. In one such device, i.e., the hollow fiber hemodialyzer, blood flows from an artery through the insides of a bundle of cellulose acetate fibers. Dialyzing fluid, which consists of water and various dissolved salts, flows on the outside of the fibers. Water and wastes—principally urea, creatinine, uric acid, and phosphate ions—pass through the fiber walls into the dialyzing fluid, and

the purified blood is returned to a vein. At some time during the dialysis of a patient in kidney failure, the arterial and venous blood conditions are as follows:

	Arterial Blood—In	Venous Blood—Out
Flow rate ( $\text{mL min}^{-1}$ )	200	195
Urea concentration ( $\text{mg mL}^{-1}$ )	1.90	1.75

- a. Calculate the rates at which urea and water are being removed from the blood.
- b. If the dialyzing fluid enters at the rate of  $1500 \text{ mL min}^{-1}$  and the exiting dialyzing solution (dialysate) leaves at about the same rate, calculate the concentration of urea in the dialysate.
- c. Suppose we want to reduce the patient's urea level from an initial value of  $2.7 \text{ mg mL}^{-1}$  to a final value of  $1.1 \text{ mg mL}^{-1}$ . If the total blood volume is  $5.0 \text{ L}$  and the average rate of urea removal is that calculated in part (a), how long must the patient be dialyzed? (Neglect the loss in total blood volume due to the removal of water in the dialyzer.)

# Chapter 2 A review of thermodynamic concepts

Thermodynamics (power from heat) as a science began its development during the nineteenth century and was first used to understand the operation of work-producing devices such as steam engines. In broadest terms, thermodynamics is concerned with the relationships between different types of energy. Here, we are mainly interested in a specialized area of thermodynamics related to solutions. But before we can understand solution thermodynamics, we first must review some basic concepts of thermodynamics that will then lead us to the relationships we need for understanding the thermodynamics of solutions. Our goal here is to understand the mathematical basis of the field and apply the most useful results to our study of biomedical engineering transport phenomena.

## 2.1 The first law of thermodynamics

There are three general laws of thermodynamics, and these will be stated here in the forms that do not consider the effects of nuclear reactions. The *first law* is a statement of energy conservation and must be applied to both the system and the surroundings. In order to describe how the system and surroundings may exchange energy, we first need to define the type of system that is being considered. The most basic type of system is called an *isolated system*. In an isolated system, there is no exchange of mass or energy between the system and its surroundings. Therefore, for an isolated system, its energy and mass is constant. We define a *closed system* as a system that can exchange energy with its surroundings but not mass. Hence, the mass of a closed system does not change. The *open system* is defined as one that can exchange both mass and energy with its surroundings. We will discuss open systems in greater detail during our discussion of solution thermodynamics.

### 2.1.1 Closed systems

Energy exchange between a closed system and its surroundings is in the form of *heat* ( $Q$ ) and *work* ( $W$ ). Careful attention must be given to the signs of  $Q$  and  $W$ . The sign convention that is used is that  $Q$  and  $W$  are positive for transfer of energy from the surroundings to the system. Hence, if heat is added to the system, or work is done on the system, then  $Q$  and  $W$  are positive.

The total energy of a closed system consists of a summation of its *internal energy* ( $U$ ) and external energies known as the *potential energy* ( $E_p$ ) and *kinetic energy* ( $E_k$ ). The potential energy depends on the position of the system in a gravitational field, and the kinetic energy is a result of system motion. The internal energy of the system is energy possessed by the molecules that make up the chemical substances within the system. These molecular energies include the kinetic energy of translation, rotation, vibration, and intermolecular forces.

With respect to the system, we are usually not really interested in the absolute values of these energies but only in their changes. Hence, we can state that the change in the total energy of the system is equal to  $\Delta U + \Delta E_p + \Delta E_k$ , where the Greek symbol delta ( $\Delta$ ) signifies the final state minus the initial state.

For a closed system, the change in the total energy of the system ( $\Delta U + \Delta E_p + \Delta E_k$ ) must be equal to the energy transferred as heat and work with the surroundings. [Equation 2.1](#) is therefore a statement of the *first law of thermodynamics* for a closed system:

$$\Delta U + \Delta E_p + \Delta E_k = Q + W \quad (2.1)$$

If there are no changes in the kinetic and potential energies of the system, then we simply have that for a closed system

$$\Delta U = Q + W \quad (2.2)$$

Most of the time,  $\Delta E_p$  and  $\Delta E_k$  are much smaller than  $\Delta U$ ,  $Q$ , and  $W$ , and we can just use [Equation 2.2](#). The exceptions are those cases where large changes in system position or velocity are expected or desired. For an isolated system, we have  $\Delta U = 0$  since both  $Q$  and  $W$  are zero.

## 2.1.2 Steady flow processes

We can also apply the first law of thermodynamics to the steady flow process shown in [Figure 2.1](#). We now consider the energy changes that occur within a unit mass of material that enters at plane 1 and leaves the process at plane 2. We take our system to be this unit mass of material. The total energy of this unit mass of fluid can change as a result of changes in its internal energy, potential energy, and kinetic energy. [Equation 2.1](#) still applies to this situation as well; however, the kinetic energy term represents the change in kinetic energy of the unit mass of flowing fluid, and the potential energy term represents the change in potential energy of the unit mass of flowing fluid due to changes in its elevation within its gravitational field. Also, it is important to remember that the work term  $W$  also includes the work done on or by the unit mass of fluid as it flows through the process. This work that is done on or by the unit mass of fluid is called the *shaft work* ( $W_s$ ).

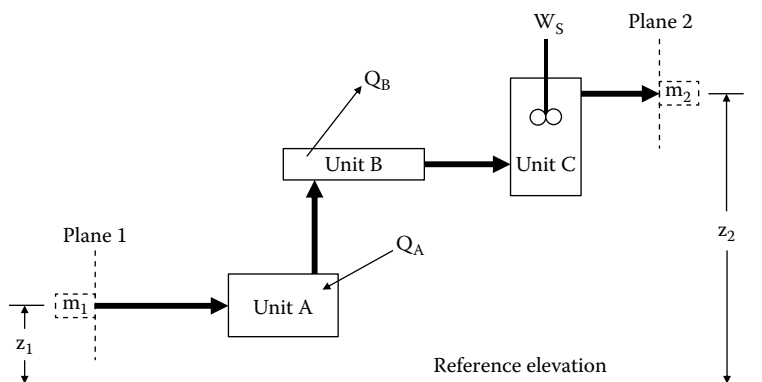


Figure 2.1 A steady state flow process.

Examples of shaft work include the work effect associated with reciprocating engines, pumps, turbines, and compressors. Therefore, in [Equation 2.1](#),  $W$  represents the shaft work as well as the work done on or by the unit mass of fluid as it enters and exits the process. Recall that work is defined as the displacement of an external force, i.e.,  $W = - \int_{x_1}^{x_2} F_{\text{external}} dx$ . Here, the force would be the pressure at the entrance of the process ( $P_1$ ) multiplied by the cross-sectional area ( $A_1$ ) normal to the flow of the unit mass of fluid. The displacement of our unit mass of fluid would equal the specific volume of our fluid ( $V_1$ ) divided by the cross-sectional area ( $A_1$ ). So, the work performed by the surroundings to push our unit mass of fluid into the process at the entrance is given by

$$W_1 = P_1 A_1 \times \frac{V_1}{A_1} = P_1 V_1 \quad (2.3)$$

Note that  $W_1$  is positive since work is done by the surroundings on the unit mass of fluid. At the exit of the process, the work is done by the system on the surroundings and  $W_2$  is given by the following expression:

$$W_2 = -P_2 V_2 \quad (2.4)$$

For our system taken as a unit mass of fluid, we can now rewrite [Equation 2.1](#) and obtain the following equation between planes 1 and 2 as shown in [Figure 2.1](#):

$$\Delta U + \Delta E_P + \Delta E_K = Q + W_S + P_1 V_1 - P_2 V_2 \quad (2.5)$$

This equation can also be rearranged and written as

$$\Delta(U + PV) + \Delta E_P + \Delta E_K = Q + W_S \quad (2.6)$$

The combination of the internal energy ( $U$ ) and the quantity  $PV$  is defined as the *enthalpy* ( $H$ ), and we can write [Equation 2.6](#) as

$$\Delta H + \Delta E_P + \Delta E_K = Q + W_S \quad (2.7)$$

In many cases, as mentioned earlier, the changes in the potential and kinetic energy of the fluid are negligible in comparison to the other terms, so [Equation 2.7](#) simplifies to

$$\Delta H = Q + W_S \quad (2.8)$$

[Equations 2.7](#) and [2.8](#) are expressions of the first law of thermodynamics for steady flow processes, as shown in [Figure 2.1](#). Recall that for a closed nonflow system, the first law is given by [Equations 2.1](#) and [2.2](#).

As written, [Equations 2.2](#) and [2.8](#) apply for finite changes in the energy quantities  $\Delta U$  and  $\Delta H$ . We will find it useful later to work with differential changes of these energy quantities, and [Equations 2.2](#) and [2.8](#) may then be written in their differential form as

$$dU = dQ + dW \quad \text{and} \quad dH = dQ + dW_S \quad (2.9)$$

## 2.2 The second law of thermodynamics

The *second law of thermodynamics* states that there is a property of matter called the *entropy* ( $S$ ) and that for any process, the sum of the entropy changes of the system and the surroundings (i.e.,  $\Delta S_{\text{Total}}$ ) is always greater than or equal to zero. Therefore, entropy is not conserved like energy. No process is feasible if the total change in entropy is less than zero. This statement of the second law of thermodynamics is given by the following equation:

$$\Delta S_{\text{Total}} = \Delta S_{\text{System}} + \Delta S_{\text{Surroundings}} \geq 0 \quad (2.10)$$

For an isolated system, there is no exchange of mass or energy between the system and the surroundings, so  $\Delta S_{\text{Surroundings}} = 0$  and  $\Delta S_{\text{System}} (\text{isolated}) \geq 0$ .

At the molecular level, entropy is a measure of disorder. The more disorder, the higher the entropy. It is important to recognize that a system can become more organized ( $\Delta S_{\text{System}} < 0$ ); however, there must be an even greater increase in the disorder of the surroundings such that in an overall sense, [Equation 2.10](#) is satisfied. The *third law of thermodynamics* sets a lower limit on the entropy. The third law states that at a temperature of absolute zero, the entropy for a perfectly ordered crystal of a given substance is zero.

### 2.2.1 Reversible processes

Processes for which  $\Delta S_{\text{Total}} > 0$  are known as *irreversible processes*, whereas processes for which  $\Delta S_{\text{Total}} = 0$  are known as *reversible processes*. A reversible process is one that can be reversed by an infinitesimal change in the variable that controls the process; in other words, the system is only infinitesimally removed from its equilibrium state.

In thermodynamics, an equilibrium state is defined as one in which there is no tendency for change on a macroscopic scale. For example, for a mechanically reversible process, imagine a frictionless piston that confines a gas within a cylinder closed at one end. At equilibrium, the pressure of the gas within the cylinder exactly balances the weight of the piston and the pressure of the surroundings. A reversible expansion of this gas requires that the pressure within the cylinder be increased an infinitesimal amount. Similarly, a reversible compression requires that the pressure of the surroundings be increased by an infinitesimal amount. The driving force for the reversible expansion or compression of the gas within the cylinder is the infinitesimal difference in pressure between the confined gas and the surroundings.

Similarly, thermal equilibrium requires that an object and its surroundings be at the same temperature. Reversible heat transfer occurs when the object and its surroundings differ in temperature by an infinitesimal amount, the driving force being the infinitesimal difference in temperature between the object and its surroundings.

A reversible process is an idealization since no real process is reversible. However, it is a useful concept since it does allow us to set limits on a real process and perform useful calculations. For example, for a mechanically reversible process like the piston and cylinder example discussed earlier, the work term in [Equations 2.1](#) and [2.2](#) can be evaluated as follows. Recall that work is defined as the displacement of an external force, i.e.,  $W = - \int_{x_1}^{x_2} F_{\text{external}} dx$ . Then, for the reversible work, we

can replace the external force by the product of the gas pressure,  $P$ , and the cross-sectional area of the cylinder,  $A$ , which gives the force generated by the gas pressure within the cylinder. Since the external and internal forces are only infinitesimally different, then  $F_{\text{external}} = PA$ . The differential displacement of the piston (i.e.,  $dx$ ) by the expanding or contracting gas within the cylinder would be equivalent to the differential change in volume of the gas divided by the cross-sectional area of cylinder, i.e.,  $dx = dV/A$ . Therefore, [Equation 2.11](#) results for the mechanically reversible work of the gas contained within our piston cylinder system:

$$W_{\text{Reversible}} = - \int_{V_1}^{V_2} P \, dV \quad (2.11)$$

or in differential form, we can say that  $dW_{\text{Reversible}} = -P \, dV$ . Provided we know how the pressure  $P$  varies with the change in the volume, we can evaluate the integral in [Equation 2.11](#) and obtain the reversible work,  $W_{\text{Reversible}}$ .

### Example 2.1

Consider the reversible expansion or compression of 1 mole of an ideal gas at constant temperature (isothermal) from an initial volume,  $V_1$ , to a final volume,  $V_2$ . Find an expression for the heat and work effects of this reversible isothermal process.

#### Solution

For an isothermal process involving an ideal gas, there is no change in the internal energy since the temperature is constant, so  $\Delta U = 0$ , and from [Equation 2.2](#) for a reversible process, we have that  $Q = -W_{\text{Reversible}}$ . For an ideal gas, we can also use the ideal gas law with  $P = RT/V$  and substitute this into [Equation 2.11](#). On integration, we obtain the following equations for the heat and reversible work per mole of gas:

$$Q = -W_{\text{Reversible}} = \int_{V_1}^{V_2} \frac{RT}{V} dV = RT \ln\left(\frac{V_2}{V_1}\right) = RT \ln\left(\frac{P_1}{P_2}\right)$$

## 2.3 Properties

Through the previous discussion of the three laws of thermodynamics, we have introduced three new properties of matter. These are the internal energy ( $U$ ), enthalpy ( $H$ ), and entropy ( $S$ ). Along with the pressure ( $P$ ), volume ( $V$ ), and temperature ( $T$ ), these are all known as properties or state variables. State variables only depend on the state of the system and not on how one arrived at that state.  $Q$  and  $W$  (or  $W_s$ ) are not properties since, according to [Equations 2.2](#) and [2.8](#), one can envision different processes or paths involving the transfer of  $Q$  and  $W$  (or  $W_s$ ), all giving the same change in the internal energy ( $\Delta U$ ), the enthalpy ( $\Delta H$ ), or the entropy ( $\Delta S$ ). Therefore,  $Q$  and  $W$  (or  $W_s$ ) are path-dependent quantities and depend on how the process is actually carried out. For example, for a mechanically reversible process, [Equation 2.11](#) allows calculation of the work, provided one knows how  $P$  changes with  $V$ .

For a pure substance, only two of these properties (i.e., T, P, V, U, and S) need to be specified in order to define completely the thermodynamic state of the substance. Our equation of state also provides an additional relationship between P, V, and T. Usually, we fix the state of a pure component by specifying the temperature and the pressure. So, from the equation of state, we can calculate the volume. Other properties, such as internal energy, enthalpy, and entropy, are also known since they too will depend only on the temperature and pressure, as shown in the following discussion.

### 2.3.1 Heat capacity

Calculating the changes in the internal energy, enthalpy, and entropy is facilitated by the definition of heat capacities. The *heat capacity* relates the change in temperature of an object to the amount of heat that was added to it. However, heat (Q) is not a property but is dependent on how the process of heat transfer was carried out. So, it is convenient to define heat capacity in such a manner that it too is a property. Therefore, we have two types of heat capacity, one defined at constant volume ( $C_V$ ) and the other defined at constant pressure ( $C_P$ ), as given by the following equations:

$$C_V \equiv \left( \frac{\partial U}{\partial T} \right)_V \quad \text{Heat capacity at constant volume} \quad (2.12)$$

$$C_P \equiv \left( \frac{\partial H}{\partial T} \right)_P \quad \text{Heat capacity at constant pressure} \quad (2.13)$$

Since  $C_V$  and  $C_P$  only depend on properties, they are also properties of a substance and their values for specific substances may be found or estimated as described in such reference books as Poling et al. (2001). For monoatomic gases,  $C_P$  is approximately  $(5/2)R$ , and for diatomic gases like nitrogen, oxygen, and air,  $C_P$  is approximately  $(7/2)R$ . We will also show in [Example 2.2](#) that for an ideal gas,  $C_P = C_V + R$ .

Now, for a constant volume process, or for any process where the final volume is the same as the initial volume, [Equation 2.12](#), when integrated, tells us that the change in internal energy is given by

$$\Delta U = \int_{T_1}^{T_2} C_V dT \quad (2.14)$$

If the process occurs reversibly and at constant volume, i.e., the volume never changes, then from [Equation 2.11](#),  $W_{\text{Reversible}} = 0$ , and  $Q = \Delta U$ . So, for a constant volume process, the heat transferred is equal to the change in the internal energy.

In a similar manner, for the constant pressure process, or a process in which the initial and final pressures are the same, [Equation 2.13](#) can be integrated to obtain the change in enthalpy:

$$\Delta H = \int_{T_1}^{T_2} C_P dT \quad (2.15)$$

If the process occurs reversibly and at constant pressure, i.e., the pressure never changes, then from Equations 2.2 and 2.11, we have that  $W_{\text{Reversible}} = -P \Delta V$  and that  $\Delta U = Q - P \Delta V$  or  $Q = \Delta H$ . Hence, for a constant pressure process, the heat transferred is equal to the change in the enthalpy.

### 2.3.2 Calculating the change in entropy

The entropy change of a closed system during a reversible process has been shown to be given by the following equation:

$$\Delta S = \int \frac{dQ_{\text{Reversible}}}{T} \quad (2.16)$$

In differential form, we can write this as  $dQ_{\text{Reversible}} = T dS$ .

**2.3.2.1 Entropy change of an ideal gas** We can use Equation 2.16 to calculate the entropy change for a substance. First, we consider an ideal gas and assume that we have 1 mole of gas and write the first law of thermodynamics for a reversible process as  $dU = dQ_{\text{Reversible}} - P dV = T dS - P dV$ . Next, we use the definition of enthalpy ( $H = U + PV$ ) and write this in differential form, i.e.,  $dH = dU + P dV + V dP$ . Next, we replace  $dU$  with  $T dS - P dV$  in this equation for  $dH$  to obtain the following expression for  $dS$ :

$$dS = \frac{dH}{T} - \frac{V}{T} dP \quad (2.17)$$

For 1 mole of an ideal gas, we know that  $dH = C_p dT$ , and from the ideal gas law,  $V/T = R/P$ , so Equation 2.17 becomes

$$dS = C_p \frac{dT}{T} - R \frac{dP}{P} \quad (2.18)$$

This equation can then be integrated from an initial state  $(T_1, P_1)$  to a final state  $(T_2, P_2)$  as given by

$$\Delta S = \int_{T_1}^{T_2} C_p \frac{dT}{T} - R \ln\left(\frac{P_2}{P_1}\right) \quad (2.19)$$

Note, all that is needed to calculate the entropy change of an ideal gas is the heat capacity  $C_p$ . Also, at constant  $P$ ,  $\Delta S = \int_{T_1}^{T_2} C_p (dT/T)$ .

For a constant volume process, we can use the fact that from the ideal gas law  $dP/P = R dT/PV = dT/T$  and from Example 2.2, we have that for an ideal gas,  $C_p = C_v + R$ , so when these two relationships are used in Equation 2.18 and the result is integrated, we obtain  $\Delta S = \int_{T_1}^{T_2} C_v (dT/T)$  for the constant volume process.

It is important to note that although we started the derivation of Equations 2.18 and 2.19 assuming a reversible process, the resulting equations only contain properties and are therefore independent

of how the process was actually carried out between the initial state of  $(T_1, P_1)$  and the final state of  $(T_2, P_2)$ . Therefore, Equations 2.18 and 2.19 can be used to calculate the entropy change of an ideal gas regardless of whether or not the process is reversible.

### Example 2.2

Calculate the final temperature and the work produced for the reversible adiabatic expansion of 10 mol of an ideal gas from 10 atm and 500 K to a final pressure of 1 atm. Assume that  $C_V = (5/2)R$  and that the heat capacity ratio  $\gamma = C_p/C_v$  is also a constant and equal to 1.4.

#### Solution

Since the process is reversible, we can state that  $\Delta S_{\text{Total}} = \Delta S_{\text{System}} + \Delta S_{\text{Surroundings}} = 0$ . An adiabatic process means that there is no heat transfer (i.e.,  $Q = 0$ ) between the system (i.e., the gas) and its surroundings. Therefore,  $\Delta S_{\text{Surroundings}} = 0$  and we then have that  $\Delta S_{\text{System}} = 0$ . A process for which  $\Delta S_{\text{System}} = 0$  is also called an *isentropic process*. Next, we can use Equation 2.19 and set that equal to zero and obtain

$$C_p \ln\left(\frac{T_2}{T_1}\right) = R \ln\left(\frac{P_2}{P_1}\right)$$

Next, we solve this equation for the final temperature  $T_2$ , which is given by

$$\frac{T_2}{T_1} = \left(\frac{P_2}{P_1}\right)^{R/C_p} = \left(\frac{P_2}{P_1}\right)^{(\gamma-1)/\gamma}$$

Note that we have used the fact that since  $H = U + PV$ , then for an ideal gas,  $H = U + RT$  and  $dH = dU + R dT$ . Since  $dH = C_p dT$  and  $dU = C_v dT$ , we have for an ideal gas that  $C_p = C_v + R$ . The heat capacity ratio is defined by  $\gamma = C_p/C_v$ . We can now use the previous equation to calculate the final temperature of the gas following the reversible expansion:

$$T_2 = 500 \text{ K} \left(\frac{1 \text{ atm}}{10 \text{ atm}}\right)^{(1.4-1)/1.4} = 258.98 \text{ K}$$

Next, we can calculate the amount of work that is done by the 10 mol of gas. For a closed system, we have from the first law of thermodynamics that  $n \Delta U = Q + W$ , where  $n$  is the number of moles of gas. Since the process is adiabatic, then  $Q = 0$  and  $W = n \Delta U = n C_v (T_2 - T_1)$ . Now  $C_v = (5/2)R$ , and using the value of  $R = 8.314 \text{ J mol}^{-1} \text{ K}^{-1}$  from Table 1.6 gives a value of  $C_v = 20.78 \text{ J mol}^{-1} \text{ K}^{-1}$ . So the work effect of this expansion can now be calculated as

$$\begin{aligned} W &= 10 \text{ mol} \times 20.78 \text{ J mol}^{-1} \text{ K}^{-1} \times (258.98 - 500 \text{ K}) \\ &= -50,084 \text{ J} = -50.084 \text{ kJ} \end{aligned}$$

In this example, the system is doing work on the surroundings, so the sign is negative. The change in the internal energy is also the same as the work in this case, so the energy used to perform work by the system is at the expense of the internal energy of the gas. That is why the final temperature of the gas is much lower than the initial temperature of the gas.

### 2.3.3 The Gibbs and Helmholtz free energy

In addition to the internal energy ( $U$ ), entropy ( $S$ ), and enthalpy ( $H = U + PV$ ), there are two additional properties that can be derived from the primary properties of  $P$ ,  $V$ ,  $T$ ,  $U$ , and  $S$ . These are the *Gibbs free energy* ( $G$ ) and the *Helmholtz free energy* ( $A$ ).

**2.3.3.1 Gibbs free energy** The Gibbs free energy ( $G$ ) is also a property and is defined in terms of the enthalpy, temperature, and entropy as  $G = H - TS$  or  $G = U + PV - TS$ . The Gibbs free energy change ( $\Delta G$ ) at constant temperature can be calculated from the change in the enthalpy and entropy as  $\Delta G = \Delta H - T \Delta S$ . The Gibbs free energy can be shown to equal the maximum amount of useful work that can be obtained from a reversible process at constant  $T$  and  $P$ . This can be shown as follows.

We have at constant temperature and pressure that  $\Delta G = \Delta H - T \Delta S = \Delta U + P \Delta V - T \Delta S$ . But for a reversible process at constant temperature, we also know that  $\Delta U = Q_{\text{Reversible}} + W_{\text{Reversible}} = T \Delta S + W_{\text{Reversible}}$ . Therefore,  $\Delta G = W_{\text{Reversible}} + P \Delta V$ . At constant pressure,  $-P \Delta V$  represents the work ( $W_{PV}$ ) as a result of any volume changes that occur in the system. So, we define the useful work over and above any  $PV$  work as  $W_{\text{Useful}} = W_{\text{Reversible}} - W_{PV} = \Delta G$ .

The Gibbs free energy is also useful for determining whether or not a given process will occur at constant temperature and pressure. For example, from the second law of thermodynamics, we know that for an isolated system,  $\Delta S = (Q_{\text{Reversible}}/T) \geq 0$ . From the first law of thermodynamics, we know that for a reversible process at constant pressure,  $Q_{\text{Reversible}} = \Delta U + P \Delta V = \Delta H$ . Therefore, we have that  $\Delta S \geq \Delta H/T$  or  $\Delta H - T \Delta S \leq 0$ . But  $\Delta H - T \Delta S$  is the same as  $\Delta G$  at constant temperature, so  $\Delta G \leq 0$ . We thus obtain the following criterion for determining the feasibility of a given process at constant temperature and pressure:

$$\begin{aligned} &\text{Spontaneous process } \Delta G < 0, \\ &\text{Equilibrium } \Delta G = 0, \\ &\text{No spontaneous process } \Delta G > 0. \end{aligned} \tag{2.20}$$

**2.3.3.2 Helmholtz free energy** The Helmholtz free energy ( $A$ ) is defined in terms of the internal energy, temperature, and entropy as  $A = U - TS$ . The Helmholtz free energy is useful for determining whether or not a given process will occur at constant temperature and volume. The criterion for feasibility of a process at constant temperature and volume is

$$\begin{aligned} &\text{Spontaneous process } \Delta A < 0 \\ &\text{Equilibrium } \Delta A = 0 \\ &\text{No spontaneous process } \Delta A > 0 \end{aligned} \tag{2.21}$$

## 2.4 The fundamental property relations

With this background on the first and second laws of thermodynamics, we can now develop what are known as the *fundamental property relations* for 1 mole of a single fluid phase of constant composition. From [Equation 2.9](#) in differential form, we have that  $dU = dQ + dW$ .

For a reversible process (cf. Equations 2.11 and 2.16), we also have that  $dQ_{\text{Reversible}} = T dS$  and  $dW_{\text{Reversible}} = -P dV$ . Hence

$$dU = T dS - P dV \quad (2.22)$$

As we discussed before, even though this equation was derived for the special case of a reversible process, since it only contains properties of the system, it is valid for all processes, reversible or not.

Now, since  $H = U + PV$ , we can differentiate this to obtain  $dH = dU + P dV + V dP$ . We can then substitute for  $dU$  from Equation 2.22 to obtain  $dH = T dS - P dV + P dV + V dP$ . So, we obtain that  $dH = T dS + V dP$ . Next, we have that  $G = H - TS$ , so then  $dG = dH - T dS - S dT$ . Using the relationship we just obtained for  $dH$ , we then get that  $dG = T dS + V dP - T dS - S dT$  and obtain the result that  $dG = -S dT + V dP$ . Finally, since  $A = U - TS$ , we then have  $dA = dU - T dS - S dT$ . Using Equation 2.22, we get  $dA = T dS - P dV - T dS - S dT$  and we obtain that  $dA = -P dV - S dT$ .

So, for 1 mole of a single fluid phase of constant composition, we can state our fundamental property relationships as follows:

$$dU = T dS - P dV \quad (2.23)$$

$$dH = T dS + V dP \quad (2.24)$$

$$dG = -S dT + V dP \quad (2.25)$$

$$dA = -P dV - S dT \quad (2.26)$$

These equations also provide functional relationships for  $U$ ,  $H$ ,  $G$ , and  $A$ . Therefore, we have that  $U = U(S, V)$ ,  $H = H(S, P)$ ,  $G = G(T, P)$ , and  $A = A(V, T)$ .

### 2.4.1 Exact differentials

The fundamental property relations shown earlier are also exact differentials. Recall from calculus that the total differential of a function  $F(x, y)$  is given by

$$dF = \left( \frac{\partial F}{\partial x} \right)_y dx + \left( \frac{\partial F}{\partial y} \right)_x dy = M dx + N dy \quad (2.27)$$

with  $M = (\partial F / \partial x)_y$  and  $N = (\partial F / \partial y)_x$ . We can also differentiate  $M$  and  $N$  with respect to  $y$  and  $x$  and obtain

$$\left( \frac{\partial M}{\partial y} \right)_x = \frac{\partial^2 F}{\partial y \partial x} \quad \text{and} \quad \left( \frac{\partial N}{\partial x} \right)_y = \frac{\partial^2 F}{\partial x \partial y} \quad (2.28)$$

Because the order of the differentiation with respect to  $x$  and  $y$  in the above equations is not important, we obtain

$$\left( \frac{\partial M}{\partial y} \right)_x = \left( \frac{\partial N}{\partial x} \right)_y, \quad (2.29)$$

which is the criterion for exactness of the total differential given by [Equation 2.27](#). We can now use [Equation 2.29](#) on our fundamental property relations given in [Equations 2.23 through 2.26](#) to obtain a set of relationships between our properties. These relationships are known as the *Maxwell equations* and several of these, derived from [Equations 2.23 through 2.26](#), are

$$\begin{aligned} \left(\frac{\partial T}{\partial V}\right)_S &= -\left(\frac{\partial P}{\partial S}\right)_V \\ \left(\frac{\partial T}{\partial P}\right)_S &= \left(\frac{\partial V}{\partial S}\right)_P \\ \left(\frac{\partial V}{\partial T}\right)_P &= -\left(\frac{\partial S}{\partial P}\right)_T \\ \left(\frac{\partial P}{\partial T}\right)_V &= \left(\frac{\partial S}{\partial V}\right)_T \end{aligned} \quad (2.30)$$

The Maxwell equations and the fundamental property relations are useful for deriving thermodynamic relationships between the various properties. The following example illustrates this.

### Example 2.3

Obtain expressions for the T and P dependence of the enthalpy and the entropy, i.e.,  $H(T, P)$  and  $S(T, P)$ .

#### Solution

The approach is to use the fundamental property relations and the Maxwell equations to obtain final expressions that only depend on P, V, T and the heat capacity,  $C_p$ , P, V, and T in these final expressions can then be related by an equation of state, the simplest being the ideal gas law for which  $PV = RT$ , or experimental PVT data. With this as our strategy, we first take the total differential of H and S and obtain

$$dH = \left(\frac{\partial H}{\partial T}\right)_P dT + \left(\frac{\partial H}{\partial P}\right)_T dP \quad \text{and} \quad dS = \left(\frac{\partial S}{\partial T}\right)_P dT + \left(\frac{\partial S}{\partial P}\right)_T dP$$

Now, since  $(\partial H / \partial T)_P = C_p$ , from [Equation 2.24](#) we can also get that

$$\left(\frac{\partial H}{\partial T}\right)_P = T \left(\frac{\partial S}{\partial T}\right)_P \quad \text{and} \quad \left(\frac{\partial S}{\partial T}\right)_P = \frac{1}{T} \left(\frac{\partial H}{\partial T}\right)_P = \frac{C_p}{T}$$

From [Equation 2.24](#), we can also write that  $(\partial H / \partial P)_T = T(\partial S / \partial P)_T + V$ . Using the third Maxwell equation in [Equation 2.30](#), replace  $(\partial S / \partial P)_T$  with  $-(\partial V / \partial T)_P$  and we then have that  $(\partial H / \partial P)_T = V - T(\partial V / \partial T)_P$ . Our expressions for  $dH$  and  $dS$  can then be written as follows:

$$dH = C_p dT + \left[ V - T \left(\frac{\partial V}{\partial T}\right)_P \right] dP \quad \text{and} \quad dS = C_p \frac{dT}{T} - \left(\frac{\partial V}{\partial T}\right)_P dP$$

These equations can be integrated to obtain the change in the enthalpy and entropy between two states,  $(T_1, P_1)$  and  $(T_2, P_2)$ :

$$\Delta H = \int_{T_1}^{T_2} C_P dT + \int_{P_1}^{P_2} \left[ V - T \left( \frac{\partial V}{\partial T} \right)_P \right] dP \quad \text{and} \quad \Delta S = \int_{T_1}^{T_2} C_P \frac{dT}{T} - \int_{P_1}^{P_2} \left( \frac{\partial V}{\partial T} \right)_P dP$$

These equations provide the temperature and pressure dependence for the enthalpy and entropy for 1 mole of a single phase fluid of constant composition. The heat capacity and experimental PVT data, or an equation of state, is needed to solve these equations. For the special case of an ideal gas, we can use the fact that  $PV = RT$  and that for an ideal gas  $(\partial V / \partial T)_P = R/P$ . On substituting this expression into the previous equations, we obtain the following results for an ideal gas:

$$\Delta H = \int_{T_1}^{T_2} C_P dT \quad \text{and} \quad \Delta S = \int_{T_1}^{T_2} C_P \frac{dT}{T} - R \ln \left( \frac{P_2}{P_1} \right)$$

Note that we obtain the result that, for an ideal gas, the enthalpy and, for that matter, the internal energy only depend on temperature. However, the entropy of an ideal gas depends on both the temperature and the pressure. Also, note that this result for  $\Delta S$  for the special case of the ideal gas is the same result we obtained earlier as [Equation 2.19](#).

## 2.5 Single phase open systems

Now, suppose that we have a single phase open system containing  $N$  chemical substances. For an open system, there can be an exchange of matter between the system and the surroundings. Therefore, the composition or the number of moles of each substance present in the system can change. Let  $n$  represent the total moles of these  $N$  chemical substances that are present. So, for a total of  $n$  moles and any property  $M$ , we can state that  $nM = nM(T, P, n_1, n_2, n_3, \dots, n_N)$  and  $n_i$  represent the moles of each substance that is present in the system. This tells us that the property  $M$  depends on the temperature, the pressure, and the number of moles of each species present in the solution. The total differential of  $nM$  is then given by

$$d(nM) = \left[ \frac{\partial(nM)}{\partial T} \right]_{P,n} dT + \left[ \frac{\partial(nM)}{\partial P} \right]_{T,n} dP + \sum_i \left[ \frac{\partial(nM)}{\partial n_i} \right]_{T,P,n_j} dn_i \quad (2.31)$$

In the last term of [Equation 2.31](#), the summation is over all substances that are present, and the partial derivative within the bracketed term in the summation is taken with respect to substance  $i$ , at temperature, pressure, and the number of moles of all other substances held constant.

## 2.5.1 Partial molar properties

In solution thermodynamics, the partial derivative of a property ( $M$ ) with respect to the number of moles of a given substance ( $n_i$ ) is called a *partial molar property* ( $\bar{M}_i$ ) and, in general, is defined by the following equation:

$$\bar{M}_i = \left[ \frac{\partial(nM)}{\partial n_i} \right]_{T,P,n_j} \quad (2.32)$$

Of particular interest in subsequent discussions is the partial molar Gibbs free energy ( $\bar{G}_i$ ), which is also known as the *chemical potential* ( $\mu_i$ ) of component  $i$  in the mixture. The chemical potential is therefore defined as

$$\mu_i = \bar{G}_i = \left[ \frac{\partial(nG)}{\partial n_i} \right]_{T,P,n_j} \quad (2.33)$$

We can use [Equation 2.32](#) and rewrite [Equation 2.31](#) as follows:

$$d(nM) = \left[ \frac{\partial(nM)}{\partial T} \right]_{P,n} dT + \left[ \frac{\partial(nM)}{\partial P} \right]_{T,n} dP + \sum_i \bar{M}_i dn_i \quad (2.34)$$

Next, we can define the mole fraction of substance  $i^*$  as  $x_i = n_i/n$ , so  $n_i = x_i n$  and  $\sum_i x_i = 1$ . We also have that  $dn_i = x_i dn + n dx_i$  and  $d(nM) = n dM + M dn$ . Using these relations, and recognizing that  $n$  in the first two bracketed terms of [Equation 2.34](#) is constant, [Equation 2.34](#) can be rearranged into the following form:

$$\left[ dM - \left( \frac{\partial M}{\partial T} \right)_{P,x} dT - \left( \frac{\partial M}{\partial P} \right)_{T,x} dP - \sum_i \bar{M}_i dx_i \right] n + \left[ M - \sum_i x_i \bar{M}_i \right] dn = 0 \quad (2.35)$$

Since  $n$  and  $dn$  are arbitrary, the only way that [Equation 2.35](#) can be satisfied is for both bracketed terms to equal zero. Hence, we obtain the following two equations:

$$dM = \left( \frac{\partial M}{\partial T} \right)_{P,x} dT + \left( \frac{\partial M}{\partial P} \right)_{T,x} dP + \sum_i \bar{M}_i dx_i, \quad (2.36)$$

$$M = \sum_i x_i \bar{M}_i \quad \text{or} \quad nM = \sum_i n_i \bar{M}_i \quad (2.37)$$

---

\* Note that most of the time  $x$  is used to denote liquid phase mole fractions and  $y$  is used for vapor or gas phase mole fractions.

Now [Equation 2.36](#) is nothing more than [Equation 2.34](#) written on a mole fraction basis. [Equation 2.37](#), however, shows how the mixture property  $M$  depends on the composition of the solution. Note that the mixture property is a mole fraction or mole-weighted average of the component partial molar property  $\bar{M}_i$ . The partial molar property for component  $i$  represents the property value for that component as it exists in the solution, which can be quite different from the pure component value of that property,  $M_i$ .

From [Equation 2.37](#), we can also write that  $dM = \sum_i x_i d\bar{M}_i + \sum_i \bar{M}_i dx_i$ . Using this relationship along with [Equation 2.36](#) results in

$$\left(\frac{\partial M}{\partial T}\right)_{P,x} dT + \left(\frac{\partial M}{\partial P}\right)_{T,x} dP - \sum_i x_i d\bar{M}_i = 0 \quad (2.38)$$

[Equation 2.38](#) places another restriction on the property changes for a single phase solution. This equation is known as the *Gibbs-Duhem equation* and can be used to test the thermodynamic consistency of experimental mixture property data, since this equation must be satisfied. For the special case of constant temperature and pressure, we have that

$$\sum_i x_i d\bar{M}_i = 0 \quad (2.39)$$

**2.5.1.1 Binary systems** To illustrate the application of the previous equations, let us apply them to a binary solution at constant temperature and pressure. For a binary solution, we can write from [Equation 2.37](#) that

$$M = x_1 \bar{M}_1 + x_2 \bar{M}_2 \quad \text{and} \quad dM = x_1 d\bar{M}_1 + \bar{M}_1 dx_1 + x_2 d\bar{M}_2 + \bar{M}_2 dx_2 \quad (2.40)$$

The Gibbs-Duhem equation for a binary system can be written as follows:

$$x_1 d\bar{M}_1 + x_2 d\bar{M}_2 = 0 \quad (2.41)$$

Since  $x_1 + x_2 = 1$  and  $dx_1 = -dx_2$ , we can combine [Equations 2.40](#) and [2.41](#) and obtain

$$dM = \bar{M}_1 dx_1 - \bar{M}_2 dx_1 \quad \text{or} \quad \frac{dM}{dx_1} = \bar{M}_1 - \bar{M}_2 \quad (2.42)$$

Now we can solve for  $\bar{M}_1$  and  $\bar{M}_2$  from [Equation 2.40](#) and substitute these results into [Equation 2.42](#) to obtain the following expressions for  $\bar{M}_1$  and  $\bar{M}_2$ :

$$\bar{M}_1 = M + (1-x_1) \frac{dM}{dx_1} \quad \text{and} \quad \bar{M}_2 = M - x_1 \frac{dM}{dx_1} \quad (2.43)$$

The above equations are very important since they allow for the calculation at constant temperature and pressure of the partial molar properties  $\bar{M}_1$  and  $\bar{M}_2$  from the composition dependence of the mixture property  $M$ . Note that as  $x_2 \rightarrow 0$ , then component 2 is becoming infinitely dilute and from [Equation 2.43](#),  $\bar{M}_2 \rightarrow \bar{M}_2^\infty \rightarrow M_1 - (dM/dx_1)|_{x_1 \rightarrow 1}$  where also  $\bar{M}_1 \rightarrow M_1$  or the pure component

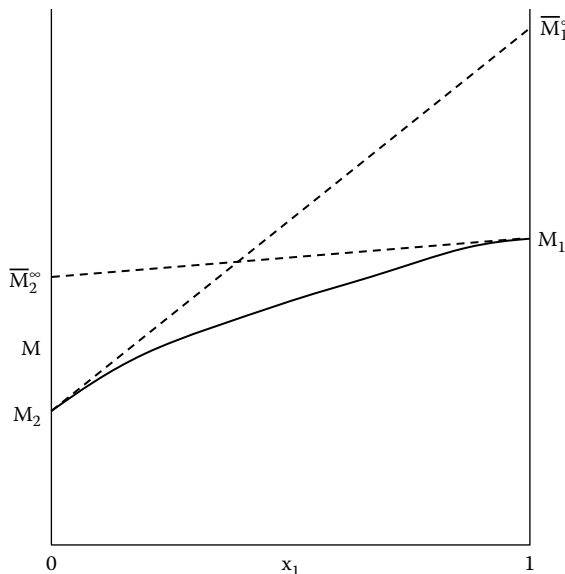


Figure 2.2 Partial molar properties in a binary system at constant T and P.

property value  $M_1$  and the superscript  $\infty$  on  $\bar{M}_2$  denotes that component 2 is infinitely dilute. Likewise, as  $x_1 \rightarrow 0$ , then component 1 is becoming infinitely dilute and  $\bar{M}_1 \rightarrow M_2$  or the pure component property value  $M_2$  and  $\bar{M}_1 \rightarrow \bar{M}_1^\infty \rightarrow M_2 + (dM/dx_1)|_{x_2 \rightarrow 1}$ . Figure 2.2 shows the composition dependence of these property values at constant T and P. Note that  $(dM/dx_1)|_{x_1 \rightarrow 1}$  and  $(dM/dx_1)|_{x_2 \rightarrow 1}$  are the respective tangents of the M curve as  $x_2 \rightarrow 0$  and  $x_1 \rightarrow 0$ .

**2.5.1.2 Property changes of mixing** The difference between the mixture property value ( $M$ ) and the mole fraction ( $y_i$ ) weighted sum of the pure component property values ( $\sum_i y_i M_i$ ) evaluated at the same T and P is known as the *property change of mixing* ( $\Delta M^{\text{mix}}$ ) and is given by the following equation:

$$\Delta M^{\text{mix}} = \sum_i y_i \bar{M}_i - \sum_i y_i M_i = M - \sum_i y_i M_i \quad (2.44)$$

**2.5.1.3 Ideal gas** The previous relationships are valid for describing the solution behavior of real solutions whether they are solids, liquids, or gases. Now let us see what these relationships tell us for the special case of an ideal gas. Recall that the ideal gas model assumes that the molecules have negligible volume and that the molecules do not interact with one another. In other words, each species in the ideal gas acts as if no other species are present and all of the gas molecules can move independently within the whole volume ( $V_T$ ) of the container.

Consider an ideal gas consisting of a total of  $n$  moles and  $N$  components at a given temperature  $T$  and in a total volume  $V_T$ . We know from the ideal gas law that  $P = nRT/V_T$ . For the same value of the temperature, each of the  $n_i$  moles of component  $i$  considered separately will also occupy the same total volume  $V_T$ . Therefore, each component  $i$  exerts a contribution to the total pressure  $P$  called the

*partial pressure* ( $P_i$ ), which is given by  $P_i = n_i RT/V_T$ . The ratio of  $P_i$  to  $P$  is given by  $P_i/P = n_i/n = y_i$ , which defines the gas phase mole fraction of component  $i$  in the mixture, i.e.,  $y_i$ . Hence, we obtain the fact that the *partial pressure* of component  $i$  in an ideal gas mixture is given by the following relationship:

$$P_i = y_i P \quad \text{with } y_i = \frac{n_i}{n} = \frac{P_i}{P} \quad (2.45)$$

Since the  $\sum_i y_i = 1$ , then  $\sum_i P_i = P$ , or the sum of the partial pressures of all components equals the total pressure. In addition, we can deduce that for an ideal gas, the partial molar volume for component  $i$  is  $\bar{V}_i^{\text{ideal gas}} = V_i^{\text{ideal gas}} = RT/P$ . Since  $V_T = \sum_i n_i V_i^{\text{ideal gas}}$ , then we have that  $V_T = \sum_i n_i V_i^{\text{ideal gas}} = \sum_i n_i (RT/P) = nRT/P$ , and we see that this definition of the ideal gas partial molar volume satisfies the ideal gas law for the mixture. Therefore, for an ideal gas, the partial molar volume is the same for all components and is equal to  $RT/P$ .

With the exception of the volume, for any other property, the partial molar value of the property for component  $i$  in an ideal gas mixture at  $T$  and  $P$  is the same as the corresponding pure component molar property at the mixture temperature and at a pressure that is equal to that component's partial pressure in the mixture, i.e.,

$$\bar{M}_i^{\text{ideal gas}}(T, P) = M_i^{\text{ideal gas}}(T, P_i) \quad (2.46)$$

In [Example 2.3](#), we showed that for an ideal gas the enthalpy and the internal energy do not depend on the pressure. Furthermore, since there are no molecular interactions in an ideal gas, the enthalpy or internal energy of component  $i$  in the mixture for a given  $T$  and  $P$  is the same as its pure component value at  $T$  and  $P_i$ . Therefore, for an ideal gas, we can state that  $\bar{H}_i(T, P) = H_i^{\text{ideal gas}}(T, P_i)$  and  $\bar{U}_i(T, P) = U_i^{\text{ideal gas}}(T, P_i)$ , where  $H_i^{\text{ideal gas}}$  and  $U_i^{\text{ideal gas}}$  represent the pure component ideal gas values of the enthalpy and internal energy at the mixture  $T$  and at component  $i$ 's partial pressure,  $P_i$ . Hence from [Equation 2.37](#), for an ideal gas mixture we have that

$$H^{\text{ideal gas}} = \sum_i y_i H_i^{\text{ideal gas}} \quad \text{and} \quad U^{\text{ideal gas}} = \sum_i y_i U_i^{\text{ideal gas}} \quad (2.47)$$

and this can be generalized using [Equation 2.46](#) for any ideal gas property  $M$  as

$$M^{\text{ideal gas}}(T, P) = \sum_i y_i M_i^{\text{ideal gas}}(T, P_i) \quad (2.48)$$

We also saw in [Example 2.3](#) that the entropy of an ideal gas depends on the pressure and the temperature. Consider pure component  $i$  at  $T$  and  $P_i$ . We can ask what is the entropy change for component  $i$  when it is placed in an ideal gas mixture at  $T$  and  $P$ ? Since the  $T$  is constant and the pressure changes from  $P_i$  to  $P$ , we can use the result for the entropy change of an ideal gas that was obtained in [Example 2.3](#), i.e.,

$$\Delta S_i^{\text{ideal gas}} = S_i^{\text{ideal gas}}(T, P) - S_i^{\text{ideal gas}}(T, P_i) = -R \ln\left(\frac{P}{P_i}\right) = -R \ln\left(\frac{P}{y_i P}\right) = R \ln y_i \quad (2.49)$$

and after rearranging we obtain the result that

$$S_i^{\text{ideal gas}}(T, P_i) = S_i^{\text{ideal gas}}(T, P) - R \ln y_i \quad (2.50)$$

Using [Equation 2.48](#), we then obtain the following expression for the entropy of an ideal gas mixture:

$$S^{\text{ideal gas}} = \sum_i y_i S_i^{\text{ideal gas}}(T, P) - R \sum_i y_i \ln y_i \quad (2.51)$$

### Example 2.4

Determine an expression for the enthalpy, internal energy, and entropy change that occurs when  $N$  pure components at  $T$  and  $P$  are mixed to form 1 mole of a solution at the same  $T$  and  $P$ . Assume that the pure components and the resulting mixture are ideal gases.

#### Solution

[Equation 2.44](#) defines the property change of mixing as

$$\Delta M^{\text{mix}} = M - \sum_i y_i M_i$$

Comparing the above equation with [Equation 2.47](#) shows that the enthalpy and internal energy change of mixing is zero for the formation of an ideal gas mixture from its pure components. However, using [Equation 2.51](#), the entropy change of mixing for this case is given by

$$\Delta S^{\text{mix}} = S^{\text{ideal gas}} - \sum_i y_i S_i^{\text{ideal gas}}(T, P) = -R \sum_i y_i \ln y_i$$

The  $-R \sum_i y_i \ln y_i$  term is always positive, indicating that the process of mixing results in an increase in the entropy of the system. Since the enthalpy of mixing is also zero, there is no change in the entropy of the surroundings, so the total entropy change is also positive. Therefore, mixing these pure ideal gas components is an irreversible process.

**2.5.1.4 Gibbs free energy of an ideal gas mixture** With the entropy of an ideal gas mixture given by [Equation 2.51](#), we can now calculate the Gibbs free energy of an ideal gas mixture, i.e.,  $G^{\text{ideal gas}} = H^{\text{ideal gas}} - T S^{\text{ideal gas}}$ . Using the above-mentioned relationships that were derived for  $H^{\text{ideal gas}}$  and  $S^{\text{ideal gas}}$ , we can obtain the following expression for the Gibbs free energy of an ideal gas mixture:

$$G^{\text{ideal gas}} = \sum_i y_i H_i^{\text{ideal gas}} - T \left( \sum_i y_i S_i^{\text{ideal gas}} - R \sum_i y_i \ln y_i \right) \quad (2.52)$$

which can also be written as follows, since  $G_i^{\text{ideal gas}} = H_i^{\text{ideal gas}} - TS_i^{\text{ideal gas}}$ :

$$G^{\text{ideal gas}} = \sum_i y_i G_i^{\text{ideal gas}} + RT \sum_i y_i \ln y_i \quad (2.53)$$

Comparing [Equation 2.53](#) with [Equations 2.46](#) and [2.48](#), we see that the partial molar Gibbs free energy, or the chemical potential, of component i in an ideal gas mixture is then given by

$$\mu_i^{\text{ideal gas}} = \bar{G}_i^{\text{ideal gas}} = G_i^{\text{ideal gas}} + RT \ln y_i \quad (2.54)$$

We also know from our fundamental property relations (see [Equation 2.25](#)) for pure component i at constant T that  $dG_i^{\text{ideal gas}} = V_i^{\text{ideal gas}} dP = (RT/P) dP = RT d \ln(P)$ . This result can be integrated from an arbitrary pressure  $P_0$  to the pressure P to give the following result for the pure component Gibbs free energy of an ideal gas:

$$G_i^{\text{ideal gas}} = (G_i^{0,\text{ideal gas}} - RT \ln P_0) + RT \ln P = G_i^{0,\text{ideal gas}} + RT \ln \frac{P}{P_0} = \mu_i^{0,\text{ideal gas}} + RT \ln \frac{P}{P_0} \quad (2.55)$$

where  $G_i^{0,\text{ideal gas}}$  or  $\mu_i^{0,\text{ideal gas}}$  depends only on the temperature and is the Gibbs free energy or chemical potential per mole of pure component i at a pressure equal to  $P_0$ . Combining the previous result with [Equation 2.54](#) provides the following alternative expression for the chemical potential of component i in an ideal gas mixture at T and P relative to a reference pressure  $P_0$ :

$$\mu_i^{\text{ideal gas}} = \mu_i^{0,\text{ideal gas}} + RT \ln \left( \frac{y_i P}{P_0} \right) \quad (2.56)$$

## 2.5.2 Pure component fugacity

For a pure component (i.e.,  $y_i = 1$ ) in the ideal gas state, [Equation 2.56](#) tells us that the pure component Gibbs free energy of an ideal gas is given by the following expression:  $G_i^{\text{ideal gas}} = (\mu_i^{0,\text{ideal gas}} - RT \ln P_0) + RT \ln P$ . This result can be generalized to the real gas by defining a new property called the *pure component fugacity* ( $f_i$ ) to replace the pressure P. The fugacity may be thought of as a “corrected” pressure that provides the value of the pure component Gibbs free energy of a real gas at pressure P. Therefore, the following expression defines the pure component fugacity for a real gas:

$$G_i = (\mu_i^{0,\text{ideal gas}} - RT \ln P_0) + RT \ln f_i \quad (2.57)$$

Now, if we subtract [Equation 2.55](#) from [Equation 2.57](#), we obtain the following result:

$$G_i - G_i^{\text{ideal gas}} = RT \ln \frac{f_i}{P} = RT \ln \phi_i \quad (2.58)$$

The pure component fugacity coefficient,  $\phi_i$ , is defined as the ratio of the pure component fugacity,  $f_i$ , to the pressure, P. Therefore,  $\phi_i = f_i/P$ . Clearly, we see that for an ideal gas, the pure component fugacity,  $f_i$ , is equal to the pressure, or  $f_i^{\text{ideal gas}} = P$  and  $\phi_i^{\text{ideal gas}} = 1$ .

The difference in the Gibbs free energy in [Equation 2.58](#), i.e.,  $G_i - G_i^{\text{ideal gas}}$ , defines what is also called a *residual property* or in this case the residual Gibbs free energy,  $G_i^R = G_i - G_i^{\text{ideal gas}}$ , where

both  $G_i$  and  $G_i^{\text{ideal gas}}$  are evaluated at the same T and P. This leads to the following general definition of a residual property as the difference between the actual value of a property and its value in the ideal gas state:

$$M^R = M - M^{\text{ideal gas}} \quad (2.59)$$

Equation 2.59 applies to any of our properties, i.e., U, H, S, G, A, V.

**2.5.2.1 Calculating the pure component fugacity** As shown in the following development, the pure component fugacity ( $f_i$ ) can be calculated from experimental PVT data or an appropriate equation of state. First, it is convenient to define the *compressibility factor* (Z), which describes the deviation of a real gas from the ideal gas state. The compressibility factor is a dimensionless quantity and is defined by

$$Z = \frac{PV}{RT} \quad (2.60)$$

Note that for an ideal gas,  $Z = 1$ . A variety of equation of states have been developed for calculating the compressibility factor for real gases and liquids at high pressures (Poling et al., 2001).

To determine the pure component fugacity ( $f_i$ ), we expand this differential, i.e.,  $d(G/RT)$ , and we obtain

$$d\left(\frac{G}{RT}\right) = \frac{RTdG - GRdT}{(RT)^2} = \frac{1}{RT}dG - \frac{G}{RT^2}dT, \quad (2.61)$$

and then substituting for  $dG$  from Equation 2.25 and recognizing that  $G = H - TS$ , we have that

$$d\left(\frac{G}{RT}\right) = \frac{V}{RT}dP - \frac{H}{RT^2}dT \quad (2.62)$$

From this equation, we can also write the following additional relationships at constant pressure and constant temperature:

$$\frac{H}{RT} = -T \left[ \frac{\partial(G/RT)}{\partial T} \right]_P \quad \text{and} \quad \frac{V}{RT} = \left[ \frac{\partial(G/RT)}{\partial P} \right]_T \quad (2.63)$$

The above relationships are also valid for the residual properties  $G^R$ ,  $H^R$ , and  $V^R$  as well by simply adding a superscript to the property.

Now the residual volume,  $V^R$ , is defined as  $V - V^{\text{ideal gas}}$ . So, we can write the residual volume as follows, using the definition from Equation 2.60 for the compressibility factor:

$$V^R = \frac{RT}{P}(Z-1) \quad (2.64)$$

Using the previous relationships, we can now obtain the following expressions for the residual properties. First, we can take the second expression in [Equation 2.63](#) at constant temperature and write it for the residual property. Then, we integrate at constant temperature from zero pressure ( $G^R$  is equal to zero since this is an ideal gas state) to any pressure  $P$ :

$$\frac{G^R}{RT} = \int_0^P \frac{V^R}{RT} dP = \int_0^P (Z-1) \frac{dP}{P} \quad (\text{constant } T) \quad (2.65)$$

To obtain the residual enthalpy, we can use the first expression in [Equation 2.63](#). Next, we evaluate  $[\partial(G^R/RT)/\partial T]_P$  using [Equation 2.65](#) and then we obtain

$$\frac{H^R}{RT} = -T \int_0^P \left( \frac{\partial Z}{\partial T} \right)_P \frac{dP}{P} \quad (\text{constant } T) \quad (2.66)$$

Since  $TS^R = H^R - G^R$ , we can also write that  $S^R/R = (H^R/RT) - (G^R/RT)$  and we can use these relationships for  $H^R$  and  $G^R$  to obtain

$$\frac{S^R}{R} = -T \int_0^P \left( \frac{\partial Z}{\partial T} \right)_P \frac{dP}{P} - \int_0^P (Z-1) \frac{dP}{P} \quad (\text{constant } T) \quad (2.67)$$

[Equations 2.65 through 2.67](#) are very important relationships since they allow us to calculate the real property value  $M$  from the residual property value  $M^R$  and the ideal gas property value  $M_{\text{ideal gas}}$ . Provided we have experimental PVT data, or an appropriate equation of state, we can use these equations to calculate the values of the Gibbs free energy, the enthalpy, and the entropy for real gases and even liquids at high pressures. In addition, we can also use [Equation 2.65](#) to now calculate the fugacity of a pure component at any  $T$  and  $P$ . Comparing [Equation 2.65](#) with [Equation 2.58](#), we see that [Equation 2.65](#) is also equal to the natural logarithm of the fugacity coefficient ( $\phi_i$ ) or  $f_i/P$ , i.e.,

$$\ln \phi_i = \ln \left( \frac{f_i}{P} \right) = \int_0^P (Z-1) \frac{dP}{P} \quad (2.68)$$

Therefore, [Equation 2.68](#) allows us to determine the fugacity of a pure component at any  $T$  and  $P$  from knowledge of its PVT behavior.

### Example 2.5

Obtain an expression for the fugacity coefficient using the pressure explicit form of the virial equation of state truncated after the second coefficient. If the second virial coefficient ( $\bar{B}$ ) of a particular gas is  $-0.01 \text{ atm}^{-1}$ , calculate the compressibility factor and the fugacity of this gas at a temperature of 500 K and a pressure of 10 atm.

### Solution

The simplest equation of state for a real gas is the virial equation of state given by the following volume and pressure explicit forms:

$$Z = 1 + \frac{B}{V} + \frac{C}{V^2} + \frac{D}{V^3} + \dots$$

$$Z = 1 + \bar{B}P + \bar{C}P^2 + \bar{D}P^3 + \dots$$

where  $B$ ,  $C$ ,  $D$  and  $\bar{B}$ ,  $\bar{C}$ ,  $\bar{D}$  are known as the second, third, and fourth virial coefficients, respectively, and are only a function of temperature. If we truncate the above series after the second coefficient, then we have for the pressure explicit form that  $Z = 1 + \bar{B}P$  or  $Z - 1 = \bar{B}P$ . Using [Equation 2.68](#), we then obtain

$$\ln \phi_i = \bar{B} \int_0^P dP = \bar{B}P$$

Hence, the value of  $Z = 1 - 0.01 \text{ atm}^{-1} \times 10 \text{ atm} = 0.90$ , and the fugacity coefficient and fugacity is calculated as

$$\ln \phi_i = -0.01 \text{ atm}^{-1} \times 10 \text{ atm} = -0.10$$

$$\phi_i = 0.905 \quad \text{and since } \frac{f_i}{P} = \phi_i, \quad \text{then } f_i = 0.905 \times 10 \text{ atm} = 9.05 \text{ atm}$$

and we see that the fugacity of this gas at these conditions is 9.05 atm compared to 10 atm if the gas were an ideal gas.

### 2.5.3 Fugacity of a component in a mixture

For a component in a mixture of real gases or a liquid solution, we can generalize [Equation 2.57](#) for an ideal gas mixture to provide the fugacity of component  $i$  as it exists in the real mixture:

$$\mu_i = (\mu_i^{0,\text{ideal gas}} - RT \ln P_0) + RT \ln \hat{f}_i \quad (2.69)$$

where  $\hat{f}_i$  is defined as the fugacity of component  $i$  as it exists in the mixture. We can also solve [Equation 2.57](#) for the value of  $(\mu_i^{0,\text{ideal gas}} - RT \ln P_0)$  in terms of the pure component values of  $G_i$  and  $f_i$  to obtain

$$\mu_i = \bar{G}_i = G_i + RT \ln \left( \frac{\hat{f}_i}{f_i} \right) \quad (2.70)$$

[Equation 2.70](#) shows the relationship between the chemical potential of component  $i$  as it exists in the mixture in terms of its pure component Gibbs free energy and fugacity ( $G_i$  and  $f_i$ ) and its mixture fugacity ( $\hat{f}_i$ ).

Now, if we subtract [Equation 2.56](#) from [Equation 2.69](#) for the same T and P, we obtain

$$\mu_i - \mu_i^{\text{ideal gas}} = \bar{G}_i^R = RT \ln \left( \frac{\hat{f}_i}{y_i P} \right) = RT \ln \hat{\phi}_i \quad (2.71)$$

where  $\hat{\phi}_i = \hat{f}_i / y_i P$  is defined as the component fugacity coefficient. For component i in an ideal gas,  $\hat{\phi}_i = 1$  since  $\mu_i = \mu_i^{\text{ideal gas}}$ , and we have

$$\hat{f}_i = \hat{f}_i^{\text{ideal gas}} = y_i P \quad (2.72)$$

We can calculate the values of  $\hat{\phi}_i$  provided we have mixture PVT data or an equation of state that describes the mixture (Poling et al., 2001). To see how this is done, we can rewrite [Equation 2.65](#) for n moles of our mixture as follows:

$$\frac{nG^R}{RT} = \int_0^P (nZ - n) \frac{dP}{P} \quad (\text{constant } T) \quad (2.73)$$

Then, from [Equation 2.71](#), we have that  $\ln \hat{\phi}_i = \bar{G}_i^R / RT = (1/RT) \left[ \partial(nG^R) / \partial n_i \right]_{T,P,n_j}$ , which allows us to perform this operation on [Equation 2.73](#), giving the following result:

$$\ln \hat{\phi}_i = \int_0^P \left[ \frac{\partial(nZ - n)}{\partial n_i} \right]_{T,P,n_j} \frac{dP}{P} = \int_0^P (\bar{Z}_i - 1) \frac{dP}{P}, \quad (2.74)$$

with the partial molar compressibility factor  $\bar{Z}_i = \left[ \partial(nZ) / \partial n_i \right]_{T,P,n_j}$  and  $\partial n / \partial n_i = 1$ . Provided we have mixture PVT data or a mixture equation of state, we can use [Equation 2.74](#) to calculate the component fugacity coefficient (Poling et al., 2001).

## 2.5.4 The ideal solution

The ideal solution model includes ideal gas mixtures as well as liquids and solids. The ideal solution model is useful for describing mixtures of substances whose molecules do not differ much in their size and chemical nature. For example, a liquid solution of ethanol and propanol would be expected to form an ideal solution, whereas a solution of ethanol and water would be expected to form a nonideal or real solution. The ideal solution model therefore serves as a useful basis of comparison to real solution behavior.

Recall that for an ideal gas, the chemical potential of component i was given by [Equation 2.54](#). For an ideal solution, we generalize this result by replacing the Gibbs free energy of component i in the ideal gas state,  $G_i^{\text{ideal gas}}$ , with  $G_i$ , the pure component Gibbs free energy at the same T, P, and physical state (i.e., solid, liquid, or gas) as the mixture. Therefore, an ideal solution is defined by [Equation 2.75](#) for the partial molar Gibbs free energy or chemical potential of component i:

$$\mu_i^{\text{ideal solution}} = \bar{G}_i^{\text{ideal solution}} = G_i + RT \ln x_i, \quad (2.75)$$

where  $x_i$  is defined as the mole fraction of component  $i$  in the mixture. We can also write [Equation 2.70](#) for an ideal solution as  $\mu_i^{\text{ideal solution}} = G_i + RT \ln(\hat{f}_i^{\text{ideal solution}}/f_i)$ , and combining this result with [Equation 2.75](#), we obtain the important result that

$$\hat{f}_i^{\text{ideal solution}} = x_i f_i. \quad (2.76)$$

[Equation 2.76](#) is also known as the *Lewis-Randall rule* and says that the fugacity of a component in an ideal solution is proportional to its mole fraction. Furthermore, the proportionality constant is the pure component fugacity evaluated at the same  $T$  and  $P$  as the solution being considered. Since  $\hat{\phi}_i = \hat{f}_i/x_i P$ , we then see, using [Equation 2.76](#), that for an ideal solution,  $\hat{\phi}_i^{\text{ideal solution}} = f_i/P = \phi_i$ .

### Example 2.6

Show using [Equation 2.75](#), which gives the partial molar Gibbs free energy of component  $i$  in an ideal solution, that the enthalpy of mixing, the internal energy of mixing, and the volume of mixing are equal to zero for an ideal solution.

#### Solution

Based on [Equation 2.31](#) we can write the mixture Gibbs free energy as

$$d(nG) = \left[ \frac{\partial(nG)}{\partial T} \right]_{P,n} dT + \left[ \frac{\partial(nG)}{\partial P} \right]_{T,n} dP + \sum_i \left[ \frac{\partial(nG)}{\partial n_i} \right]_{T,P,n_j} dn_i$$

For a closed system containing  $n$  moles, we can also write from [Equation 2.25](#) that  $d(nG) = -(nS)dT + (nV)dP$ . Comparing this result to the first two terms of the previous equation for constant  $n$ , we see that the first two partial derivatives can be replaced by  $-(nS)$  and  $(nV)$ , respectively. In addition, we know that  $\left[ \frac{\partial(nG)/\partial n_i}{\partial n_i} \right]_{T,P,n_j} = \bar{G}_i = \mu_i$ , the chemical potential of component  $i$ . Therefore, the previous equation may be written as

$$d(nG) = -(nS)dT + (nV)dP + \sum_i \mu_i dn_i$$

We can now use the criterion of exactness ([Equation 2.29](#)) on this equation and obtain the following relationships:

$$\left( \frac{\partial \mu_i}{\partial T} \right)_{P,n} = - \left( \frac{\partial(nS)}{\partial n_i} \right)_{P,T,n_j} = -\bar{S}_i \quad \text{and} \quad \left( \frac{\partial \mu_i}{\partial P} \right)_{T,n} = \left( \frac{\partial(nV)}{\partial n_i} \right)_{P,T,n_j} = \bar{V}_i$$

Using the above-mentioned relationships, along with [Equation 2.75](#), we then have for an ideal solution:

$$\left( \frac{\partial \mu_i^{\text{ideal solution}}}{\partial T} \right)_{P,n} = -\bar{S}_i^{\text{ideal solution}} = \left( \frac{\partial G_i}{\partial T} \right)_P + R \ln x_i$$

$$\left( \frac{\partial \mu_i^{\text{ideal solution}}}{\partial P} \right)_{T,n} = \bar{V}_i^{\text{ideal solution}} = \left( \frac{\partial G_i}{\partial P} \right)_T$$

Next, we can use our fundamental property relations for component  $i$  (Equation 2.25) to show that  $(\partial G_i / \partial T)_P = -S_i$  and  $(\partial G_i / \partial P)_T = V_i$ . Hence, we obtain the following equations for the partial molar entropy and partial molar volume for an ideal solution:

$$\bar{S}_i^{\text{ideal solution}} = S_i - R \ln x_i \quad \text{and} \quad \bar{V}_i^{\text{ideal solution}} = V_i$$

By Equation 2.44, we easily can see that the volume change of mixing for an ideal solution is zero and that  $V^{\text{ideal solution}} = \sum_i x_i V_i$ . For the enthalpy change of mixing, we can use the fact that  $\bar{H}_i^{\text{ideal solution}} = \bar{G}_i^{\text{ideal solution}} + T \bar{S}_i^{\text{ideal solution}}$  and using the above-mentioned relationships we obtain that  $\bar{H}_i^{\text{ideal solution}} = G_i + TS_i = H_i$ . Therefore, the enthalpy change of mixing for an ideal solution is also zero and  $H^{\text{ideal solution}} = \sum_i x_i H_i$ . In a similar fashion, we can use the fact that  $\bar{U}_i^{\text{ideal solution}} = \bar{H}_i^{\text{ideal solution}} - PV_i^{\text{ideal solution}} = H_i - PV_i = U_i$  with the result that the internal energy change of mixing is also zero.

## 2.6 Phase equilibrium

With this background on solution thermodynamics, we can now address the criterion for equilibrium between two phases (I and II) contained within a closed system. Equilibrium between the two phases also implies that the two phases are at the same temperature. Also, the two phases must have the same pressure, unless they are separated by a semipermeable rigid barrier or membrane. We will consider the situation where the pressures may be different later in this chapter when we discuss osmotic equilibrium.

Each phase is also an open system and is free to exchange mass with the other phase. Since we are considering the closed system containing the two phases to be at constant  $T$  and  $P$ , we can use the result from Example 2.6 that  $d(nG) = -(nS)dT + (nV)dP + \sum_i \mu_i dn_i$  and write this equation for phase I and phase II as

$$\begin{aligned} d(nG)^I &= -(nS)^I dT + (nV)^I dP + \sum_i \mu_i^I dn_i^I \\ d(nG)^{II} &= -(nS)^{II} dT + (nV)^{II} dP + \sum_i \mu_i^{II} dn_i^{II} \end{aligned} \quad (2.77)$$

For the closed system containing phases I and II, we can also write that

$$\begin{aligned} d(nG) &= -(nS)dT + (nV)dP = d(nG)^I + d(nG)^{II} \\ &= -[(nS)^I + (nS)^{II}]dT + [(nV)^I + (nV)^{II}]dP + \sum_i \mu_i^I dn_i^I + \sum_i \mu_i^{II} dn_i^{II} \end{aligned} \quad (2.78)$$

Since  $(nS)^I + (nS)^{II} = (nS)$  and  $(nV)^I + (nV)^{II} = (nV)$ , Equation 2.78, at constant  $T$  and  $P$ , simplifies to

$$\sum_i \mu_i^I dn_i^I + \sum_i \mu_i^{II} dn_i^{II} = 0 \quad (2.79)$$

where  $dn_i^I$  and  $dn_i^{II}$  represent the differential changes in the moles of component  $i$  as a result of mass transfer between phases I and II. Clearly, the law of mass conservation requires that  $dn_i^I = -dn_i^{II}$ . With this result, [Equation 2.79](#) may then be written as

$$\sum_i (\mu_i^I - \mu_i^{II}) dn_i^I = 0 \quad (2.80)$$

The values of  $dn_i^I$  and  $dn_i^{II}$  are arbitrary, so the only way [Equation 2.80](#) can be satisfied is for each term in parentheses (i.e.,  $\mu_i^I - \mu_i^{II}$ ) to be equal to zero. So, our criterion for phase equilibrium in a two-phase system can be expressed by

$$\mu_i^I = \mu_i^{II}, \quad (2.81)$$

which simply states that the chemical potential for each component  $i$  is the same in phase I and phase II at the given  $T$  and  $P$ .

This result can be easily generalized to provide the criterion for phase equilibrium in  $\pi$  phases at the same  $T$  and  $P$  as

$$\mu_i^I = \mu_i^{II} = \dots = \mu_i^\pi \quad (2.82)$$

If we only have a pure component in each phase, [Equations 2.81](#) or [2.82](#) still apply, and since in this case  $\mu_i = \bar{G}_i = G_i$ , then for a pure component, phase equilibrium requires that

$$G_i^I = G_i^{II} = \dots = G_i^\pi \quad (\text{pure component}) \quad (2.83)$$

Using [Equation 2.82](#), along with  $\mu_i = \bar{G}_i = G_i + RT \ln(\hat{f}_i/f_i)$  from [Equation 2.70](#), we can write an alternative expression for the criterion for phase equilibrium in multicomponent systems in terms of the component mixture fugacities as

$$\hat{f}_i^I = \hat{f}_i^{II} = \dots = \hat{f}_i^\pi \quad (2.84)$$

## 2.6.1 Pure component phase equilibrium

[Figure 2.3](#) shows a pressure-volume or PV curve for a pure component. Shown in the figure are several dashed lines of constant temperature or isotherms. The area within the dome-shaped region defines conditions, where two phases, e.g., vapor and liquid, are at equilibrium for a given  $T$  and  $P$ . At the top of the dome is the *critical point* (C), where the liquid and vapor phases become identical and thus have the same physical properties. The isotherm that passes through the critical point is known as the critical isotherm,  $T_C$ . The critical temperature, pressure, and volume ( $T_C$ ,  $P_C$ , and  $V_C$ ) are also pure component physical properties and play an important role in the estimation of a variety of physical properties (Poling et al., 2001).

Below this critical isotherm, we see that the other isotherms (i.e., subcritical isotherms) have three separate segments. Within the dome, we see that the isotherm is horizontal and represents the constant temperature and pressure phase change between the *saturated liquid* and *saturated vapor* states. The leftmost point on this horizontal segment denotes the saturated liquid and the rightmost point on the horizontal segment denotes the saturated vapor. Saturated means that for the pure component,

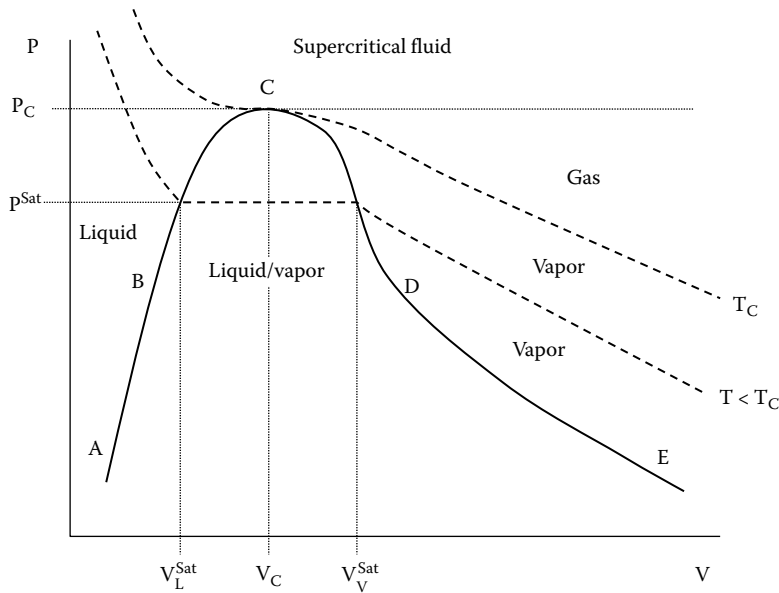


Figure 2.3 PV diagram for a pure component.

the vapor and liquid phases are at equilibrium at  $T = T^{Sat}$  and  $P = P^{Sat}$ , where  $P^{Sat}$  is called the *saturation pressure* or the *vapor pressure* of the pure component.  $P^{Sat}$  for a pure component only depends on the saturation temperature, i.e.,  $P^{Sat} = P^{Sat}(T^{Sat})$ . The normal boiling point ( $T_{BP}$ ) of a pure component occurs when the value of  $P^{Sat}$  is the same as the atmospheric pressure or  $P^{Sat} = 1 \text{ atmosphere} = P^{Sat}(T^{Sat}) = P^{Sat}(T_{BP})$ . Points along the curve ABC define saturated liquids, and the points along the curve CDE define saturated vapor. Points along the horizontal isotherm within the dome represent saturated mixtures of liquid and vapor. The actual molar volume of the vapor/liquid mixture will depend on the relative amounts of each phase present, i.e.,  $V = (1 - x)V^{Lsat} + xV^{Vsat}$ , where  $x$  is the vapor fraction of the vapor/liquid mixture.

The region to the left of the curve ABC denotes the liquid state, and the isotherms here rise very quickly because liquid volume changes are very small as the pressure is increased and, for the most part, liquids at modest pressures are therefore considered to be incompressible. The region to the right of curve CDE denotes the vapor state provided  $T < T_c$  and  $P < P_c$  and a gas for  $T > T_c$  and  $P > P_c$ . The conditions where  $T > T_c$  and  $P > P_c$  is known as the supercritical fluid region.

Now let us consider the vapor (V) and liquid (L) equilibrium of a pure component i at T and  $P = P^{Sat}(T)$ . From [Equation 2.83](#), we can write that  $G^V = G^L$ , and it follows that  $dG^V = dG^L$ . Next, we can use [Equation 2.25](#) and express the previous result as

$$dG^V = -S^V dT + V^V dP^{Sat} = -S^L dT + V^L dP^{Sat} = dG^L \quad (2.85)$$

This equation may be rearranged as follows:

$$\frac{dP^{Sat}}{dT} = \frac{S^V - S^L}{V^V - V^L} = \frac{\Delta S^{LV}}{\Delta V^{LV}} \quad (2.86)$$

Now  $\Delta S^{LV}$  and  $\Delta V^{LV}$  represent the changes in the entropy and volume of the pure component when it is transferred from the liquid phase to the vapor phase at the equilibrium temperature ( $T$ ) and pressure ( $P^{Sat}$ ). If we integrate [Equation 2.24](#) for the change in phase from liquid to vapor at constant  $T$  and  $P$ , we obtain  $\Delta H^{LV} = T\Delta S^{LV}$  or  $\Delta S^{LV} = \Delta H^{LV}/T$ .  $\Delta H^{LV}$  is also known as the *heat of vaporization* ( $\Delta H^{Vap}$ ) and represents the difference in enthalpy between the saturated vapor and the saturated liquid. These results can be substituted into [Equation 2.86](#) to give

$$\frac{dP^{Sat}}{dT} = \frac{\Delta H^{Vap}}{T\Delta V^{LV}} \quad (2.87)$$

This equation is also known as the *Clausius-Clapeyron* equation and is an equilibrium relationship between the saturated liquid and the saturated vapor. For a given change in the temperature ( $dT$ ), [Equation 2.87](#) provides the change in the pressure ( $dP^{Sat}$ ) required to maintain equilibrium between the saturated liquid and its saturated vapor. For solid-liquid or solid-vapor equilibrium, one may substitute the *enthalpy of melting* or the *enthalpy of sublimation* for the enthalpy of vaporization in [Equation 2.87](#).

For liquid-vapor and solid-vapor phase changes at saturation pressures near atmospheric, one can neglect the molar volume of the solid or liquid phase in comparison to the volume of the vapor and assume that the vapor phase behaves as an ideal gas, i.e.,  $\Delta V^{LV} = V^V = RT/P^{Sat}$ . [Equation 2.87](#) may then be written as

$$\frac{d \ln P^{Sat}}{d \frac{1}{T}} = -\frac{L}{R} \quad (2.88)$$

where  $L$  now represents either  $\Delta H^{LV}$  (heat of vaporization) or  $\Delta H^{SV}$  (heat of sublimation). [Equation 2.88](#) provides a relationship between the saturation pressure and the temperature in terms of the enthalpy change associated with the phase change. Over narrow ranges of temperature,  $L$  is pretty much constant, and [Equation 2.88](#) can be integrated from an arbitrary temperature ( $T_0$ ) to provide an approximate relationship between the saturation pressure and the temperature:

$$\ln P^{Sat} = \left( \ln P_0^{Sat} + \frac{L}{RT_0} \right) - \left( \frac{L}{R} \right) \frac{1}{T} = A - \frac{B}{T} \quad (2.89)$$

where  $A$  and  $B$  represent constants that can be fitted to pure component vapor pressure data. [Equation 2.89](#) shows that over a narrow range of temperatures, there is a linear relationship between the natural logarithm of the saturation pressure and the inverse of the temperature. Additional empirical equations for determining the saturation or vapor pressure of a given component as a function of temperature can be found in Poling et al. (2001).

Since we have a pure component  $i$ , [Equation 2.84](#) can be written in terms of the pure component fugacities as

$$f_i^L = f_i^V = f_i^{Sat} \quad (2.90)$$

where  $f_i^{Sat}$  denotes the fugacity of either the saturated liquid or the saturated vapor.

Since  $f_i^{\text{Sat}} = \phi_i^{\text{Sat}} P_i^{\text{Sat}}$ , we then have that

$$f_i^L = f_i^V = f_i^{\text{Sat}} = \phi_i^{\text{Sat}} P_i^{\text{Sat}} \quad (2.91)$$

where  $\phi_i^{\text{Sat}}$  would be given by [Equation 2.68](#) with  $P = P^{\text{Sat}}$  using an appropriate set of PVT data or an equation of state to perform the integration. Therefore

$$f_i^L = f_i^V = f_i^{\text{Sat}} = P_i^{\text{Sat}} \exp\left(\int_0^{P_i^{\text{Sat}}} (Z-1) \frac{dP}{P}\right) \quad (2.92)$$

**2.6.1.1 Fugacity of a pure component as a compressed liquid** For a given temperature  $T$ , if the pressure  $P$  is greater than the value of  $P^{\text{Sat}}(T)$  for a pure component, then the liquid is considered to be subcooled or a compressed liquid and is not in equilibrium with its vapor. Calculation of the fugacity of a pure component  $i$  as a compressed liquid starts with our fundamental property relation ([Equation 2.25](#)), i.e.,  $dG_i = -S_i dT + V_i dP$ . For constant temperature, we can write this as  $dG_i = V_i dP$  and integrate this equation from  $P_i^{\text{Sat}}$  to  $P$  as

$$G_i - G_i^{\text{Sat}} = \int_{P_i^{\text{Sat}}}^P V_i dP \quad (2.93)$$

Using [Equation 2.57](#), we can rewrite [Equation 2.93](#) as

$$G_i - G_i^{\text{Sat}} = RT \ln \frac{f_i}{f_i^{\text{Sat}}} = \int_{P_i^{\text{Sat}}}^P V_i dP \quad (2.94)$$

As mentioned earlier, liquid molar volumes do not depend that strongly on  $P$ , so [Equation 2.94](#) can be written as follows, after setting the subcooled molar liquid volume ( $V_i$ ) equal to the saturated liquid volume ( $V_i^{\text{Sat}}$ ) at the same  $T$ :

$$f_i = f_i^{\text{Sat}} \exp\left(\frac{V_i^{\text{Sat}} (P - P_i^{\text{Sat}})}{RT}\right) = \phi_i^{\text{Sat}} P_i^{\text{Sat}} \exp\left(\frac{V_i^{\text{Sat}} (P - P_i^{\text{Sat}})}{RT}\right) \quad (2.95)$$

Comparing [Equation 2.95](#) with [Equation 2.91](#), we see that the exponential term is a correction of the saturated fugacity to account for the fact that the pressure of the subcooled liquid is greater than its saturation pressure for a given  $T$ . The exponential term is also known as the *Poynting factor*.

## 2.6.2 Excess properties

Recall that we previously defined a residual property as the difference between the real property value and its corresponding value as an ideal gas ( $M^R = M - M^{\text{ideal gas}}$ ). We showed in [Section 2.5.2.1](#) that the residual properties can be determined from PVT data or an equation of state. We also

found that the definition of the residual properties provided a convenient method for calculating the pure component fugacity coefficient and the fugacity coefficient of a component in a mixture, i.e., [Equations 2.68](#) and [2.74](#). Accordingly, residual properties and fugacity coefficients are usually used for describing the behavior of real gases, since the residual properties and the fugacity coefficients express the deviation of the real gas from ideal gas behavior.

For liquids, it is usually easier to compare real liquid solution behavior to an ideal solution. An excess property ( $M^E$ ) is then defined as the difference between the property value in a real solution and the value it would have in an ideal solution at the same T, P, and composition. Therefore, we have that

$$M^E = M - M^{\text{ideal solution}} \quad (2.96)$$

In terms of partial molar properties, [Equation 2.96](#) becomes

$$\bar{M}_i^E = \bar{M}_i - \bar{M}_i^{\text{ideal solution}} \quad (2.97)$$

For phase equilibrium calculations, we are primarily interested in the Gibbs free energy, so the partial molar excess Gibbs free energy is given by the following equation:

$$\bar{G}_i^E = \bar{G}_i - \bar{G}_i^{\text{ideal solution}} \quad (2.98)$$

Using [Equations 2.70](#) and [2.75](#) for  $\bar{G}_i$  and  $\bar{G}_i^{\text{ideal solution}}$ , we obtain using [Equation 2.98](#)

$$\bar{G}_i^E = \bar{G}_i - \bar{G}_i^{\text{ideal solution}} = RT \ln \frac{\hat{f}_i}{x_i f_i} = RT \ln \gamma_i \quad (2.99)$$

The term  $\hat{f}_i/x_i f_i$  is dimensionless and is also known as the *activity coefficient*,  $\gamma_i$ . In terms of the activity coefficient, we can then express the fugacity of component  $i$  as it exists in the solution as  $\hat{f}_i = \gamma_i x_i f_i$ . Note that for an ideal solution, the  $\gamma_i$  equals unity and  $\hat{f}_i^{\text{ideal solution}} = x_i f_i$ . We can then write the partial molar excess Gibbs free energy in terms of the activity coefficient as

$$\bar{G}_i^E = \left[ \frac{\partial(nG^E)}{\partial n_i} \right]_{T,P,n_j} = RT \ln \gamma_i \quad (2.100)$$

Using [Equation 2.37](#) and the Gibbs-Duhem relationship ([Equation 2.39](#)) at constant T and P, we also have that

$$G^E = RT \sum_i x_i \ln \gamma_i \quad (2.101)$$

$$\sum_i x_i d \ln \gamma_i = 0 \quad (2.102)$$

Activity coefficients for a component in a mixture are obtained from experimental data, and the results are correlated with a model of how the excess Gibbs free energy depends on the composition of all the components within the mixture, i.e.,  $G^E/RT = f(x_1, x_2, \dots, x_N)$  at constant T, since for the most part, we can ignore the effect of pressure on the activity coefficients.

[Equation 2.102](#) serves as a thermodynamic consistency check of experimentally determined activity coefficients or empirical equations that are used to calculate activity coefficients. For a binary system at constant T and P, [Equation 2.102](#) can also be written as follows:

$$x_1 \left( \frac{\partial \ln \gamma_1}{\partial x_1} \right)_{T,P} + x_2 \left( \frac{\partial \ln \gamma_2}{\partial x_1} \right)_{T,P} = 0 \quad (2.103)$$

For a binary system, we can also write [Equation 2.101](#) as

$$\frac{G^E}{RT} = x_1 \ln \gamma_1 + x_2 \ln \gamma_2 \quad (2.104)$$

[Equation 2.104](#) can then be differentiated with respect to  $x_1$  at constant T and P to give

$$\frac{d(G^E/RT)}{dx_1} = x_1 \frac{\partial \ln \gamma_1}{\partial x_1} + \ln \gamma_1 + x_2 \frac{\partial \ln \gamma_2}{\partial x_1} + \ln \gamma_2 \frac{dx_2}{dx_1} \quad (2.105)$$

Since  $dx_2/dx_1 = -1$  and using the Gibbs-Duhem from [Equation 2.103](#), we then have that

$$\frac{d(G^E/RT)}{dx_1} = \ln \left( \frac{\gamma_1}{\gamma_2} \right) \quad (2.106)$$

This equation can then be integrated over  $x_1$ , as shown in the following equation:

$$\int_0^1 \frac{d(G^E/RT)}{dx_1} dx_1 = \left. \frac{G^E}{RT} \right|_{x_1=1} - \left. \frac{G^E}{RT} \right|_{x_1=0} = \int_0^1 \ln \left( \frac{\gamma_1}{\gamma_2} \right) dx_1 \quad (2.107)$$

Now the excess Gibbs free energy at  $x_1 = 0$  and  $x_1 = 1$  by definition is zero; hence we obtain the following as a condition on the activity coefficients:

$$\int_0^1 \ln \left( \frac{\gamma_1}{\gamma_2} \right) dx_1 = 0 \quad (2.108)$$

[Equation 2.108](#) is also called the *area test* of activity coefficients. It provides a convenient method for testing the thermodynamic consistency of activity coefficient data. One can simply plot the values of  $\ln(\gamma_1/\gamma_2)$  versus  $x_1$ , and if the area under the resulting curve is equal to zero, then the test for thermodynamic consistency is satisfied.

A variety of models of varying complexity for describing the excess Gibbs free energy of liquid solutions have been developed (Poling et al., 2001). Most of the modern activity coefficient models

easily handle multicomponent solutions. In addition, the so-called *UNIFAC model* allows the activity coefficients to be predicted from the molecular structure of the species that are in the solution. The following example illustrates the calculation of an expression for the activity coefficients for a binary system from a model of the excess Gibbs free energy.

### Example 2.7

The simplest model to describe the excess Gibbs free energy of a binary liquid solution is given by the following power series:

$$\frac{G^E}{x_1 x_2 RT} = A_0 + A_1(x_1 - x_2) + A_2(x_1 - x_2)^2 + \dots$$

Retaining only the lead constant  $A_0$ , find expressions for  $\gamma_1$  and  $\gamma_2$ .

#### Solution

We therefore have that  $G^E/RT = A_0 x_1 x_2 = A_0(n_1/n)(n_2/n)$  where  $n_1$  and  $n_2$  are the moles of components 1 and 2, respectively, and  $n = n_1 + n_2$ . Multiplying both sides of this expression by  $n$  and using [Equation 2.100](#), we have that

$$\begin{aligned}\ln \gamma_1 &= \left[ \frac{\partial(nG^E/RT)}{\partial n_1} \right]_{T,P,n_2} = \frac{(n_1 + n_2)A_0 n_2 - A_0 n_1 n_2}{(n_1 + n_2)^2} = A_0 \frac{n_2}{n} - A_0 \frac{n_1 n_2}{n^2} \\ &= A_0(x_2 - x_1 x_2) = A_0 x_2(1 - x_1) = A_0 x_2^2\end{aligned}$$

So, we find that the activity coefficient for component 1 based on this model for  $G^E$  is given by  $\ln \gamma_1 = A_0 x_2^2$ . In a similar manner, we can show that the activity coefficient for component 2 is given by  $\ln \gamma_2 = A_0 x_1^2$ . Expressions for the activity coefficients based on more complex models of  $G^E$  for both binary and multicomponent systems may be found in Poling et al. (2001).

### Example 2.8

From the previous example, determine the expressions for the activity coefficients of components 1 and 2 at infinite dilution.

#### Solution

At infinite dilution for component 1, we have that  $x_1 = 0$  and  $x_2 = 1$ . Therefore, from the results in [Example 2.7](#), we have that  $\ln \gamma_1^\infty = A_0$  and  $\ln \gamma_2 = 0$  or  $\gamma_2 = 1$ . At infinite dilution for component 2, we have that  $x_1 = 1$  and  $x_2 = 0$ . Hence,  $\ln \gamma_1 = 0$  or  $\gamma_1 = 1$  and  $\ln \gamma_2^\infty = A_0$ . In this example, for either component, the natural logarithm of the activity coefficient at infinite dilution is equal to  $A_0$ .

### Example 2.9

Show that the activity coefficient expressions found in [Example 2.7](#) satisfy the Gibbs-Duhem relationship, i.e., [Equation 2.103](#).

**Solution**

For a binary system, [Equation 2.103](#) states that

$$x_1 \left( \frac{\partial \ln \gamma_1}{\partial x_1} \right)_{T,P} + x_2 \left( \frac{\partial \ln \gamma_2}{\partial x_1} \right)_{T,P} = 0$$

Substituting in the fact that  $\ln \gamma_1 = A_0 x_2^2$  and  $\ln \gamma_2 = A_0 x_1^2$ , we then have that

$$\begin{aligned} 2A_0 x_1 (1-x_1)(-1) + 2A_0 x_1 (1-x_1) &= 0 \\ \text{or} \\ 0 &= 0 \end{aligned}$$

which shows that the expression used in [Example 2.7](#) for the excess Gibbs free energy satisfies the Gibbs-Duhem consistency test.

## 2.6.3 Applications of equilibrium thermodynamics

With the development of the above thermodynamic equilibrium relationships, we can now address specific topics in solution thermodynamics, such as the solubility of a solid in a liquid solvent, freezing point depression, solid-gas equilibrium, gas solubility, osmotic pressure, the distribution of a solute between two liquid phases, vapor-liquid equilibrium, flammability limits, the thermodynamics of surfaces, equilibrium dialysis, and chemical equilibrium in an ideal solution. The following discussion will form the foundation for our understanding in later chapters of solute transport in biological systems. Solute transport occurs across the interface between phases, and at the interface, we assume that the solute is in phase equilibrium.

**2.6.3.1 Solubility of a solid in a liquid solvent** We will consider a binary system where the solvent is denoted by subscript 1 and the solute by subscript 2. We assume that the solvent has negligible solubility in the solid; hence, the solid solute will exist as a pure phase. We can then use [Equation 2.84](#) and the definition of the activity coefficient given by [Equation 2.99](#) to express the solute phase equilibrium between the solid and liquid phases:

$$f_2^S = \gamma_2 x_2 f_2^L, \quad (2.109)$$

where

$f_2^S$  refers to the fugacity of the pure solid solute

$x_2$  represents the equilibrium solubility of the solid in the solvent phase expressed as a mole fraction

$f_2^L$  represents the fugacity of pure liquid solute at the equilibrium temperature and pressure of the solution

Since this temperature must be less than the melting temperature of the solid solute, it follows that the solute in the solution exists as a subcooled liquid. Since the solute does not ordinarily exist as a liquid at these conditions, we will have to estimate the value of  $f_2^L$  as shown in the discussion below.

With these assumptions, we can rearrange [Equation 2.109](#) to solve for the solubility ( $x_2$ ) as follows:

$$x_2 = \frac{f_2^S}{\gamma_2 f_2^L} \quad (2.110)$$

[Equation 2.110](#) shows that the solute solubility in the solvent is directly proportional to the ratio of the pure component fugacities of the solid and its subcooled liquid and inversely proportional to the value of the activity coefficient of the solid in the solvent solution.

To determine an expression for the solid solubility, we first must calculate the ratio of these fugacities for the pure solute. This can be accomplished by recognizing the fact that the *triple point* ( $T_{tp}$ ) for a pure substance (see [Figure 2.4](#)) defines that unique equilibrium temperature and pressure where all three phases (solid, liquid, and vapor) coexist in equilibrium. In addition, as shown in [Figure 2.4](#), the melting temperature ( $T_m$ ) of a pure substance does not depend strongly on the pressure and is therefore very close to the triple point temperature. Now, from [Equation 2.57](#), we can write that at constant temperature  $dG = RT d \ln f$ . Combining this result with [Equation 2.62](#), we have that

$$d\left(\frac{G}{RT}\right) = d \ln f = -\frac{H}{RT^2}dT + \frac{V}{RT}dP \quad (2.111)$$

This equation may then be written for the solid and subcooled liquid phases, with the difference between the solid and subcooled liquid fugacities then given by

$$d \ln \frac{f_2^S}{f_2^L} = \frac{H^L - H^S}{RT^2}dT - \frac{V^L - V^S}{RT}dP \quad (2.112)$$

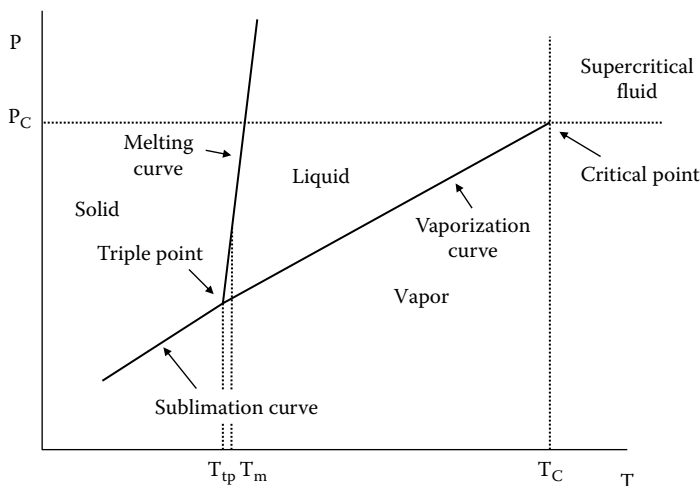


Figure 2.4 PT diagram for a pure component.

The term  $(H^L - H^S)$  is the *enthalpy of fusion* and is dependent on the temperature. Using the enthalpy of fusion at the triple point temperature ( $T_{tp}$ ) as a reference, we can write that  $H^L - H^S$  at some other temperature  $T$  is given by

$$H^L - H^S = \left( H^L \Big|_{T_{tp}} + \int_{T_{tp}}^T C_{PL} dT \right) - \left( H^S \Big|_{T_{tp}} + \int_{T_{tp}}^T C_{PS} dT \right) \quad (2.113)$$

which can also be written as follows assuming that the heat capacities do not vary much with the temperature between  $T_{tp}$  and  $T$ :

$$H^L - H^S = \Delta H_{tp} + \Delta C_P (T - T_{tp}) \quad (2.114)$$

where

$\Delta H_{tp}$  is the enthalpy of fusion of the solid at the triple point temperature

$\Delta C_P$  represents the difference in the heat capacities,  $\Delta C_P = C_{PL} - C_{PS}$

We can now substitute [Equation 2.114](#) into [Equation 2.112](#) and integrate between  $(T_{tp}, P_{tp})$  and the conditions of interest (i.e.,  $T, P$ ). In performing this integration, we also make use of the fact that, for the most part, the difference in the specific volumes ( $\Delta V = V^L - V^S$ ) is independent of the pressure. In addition, we recognize that at the triple point  $f_2^L = f_2^S$

$$\ln \frac{f_2^S}{f_2^L} = \frac{\Delta H_{tp}}{R} \left( \frac{1}{T_{tp}} - \frac{1}{T} \right) - \frac{\Delta C_P}{R} \left( \ln \frac{T_{tp}}{T} - \frac{T_{tp}}{T} + 1 \right) - \frac{\Delta V}{RT} (P - P_{tp}) \quad (2.115)$$

We can now substitute [Equation 2.115](#) into [Equation 2.110](#) and obtain the following general equation for the solubility of a solid in a liquid solvent at  $T$  and  $P$ :

$$x_2 = \frac{1}{\gamma_2} \exp \left[ \frac{\Delta H_{tp}}{R} \left( \frac{1}{T_{tp}} - \frac{1}{T} \right) - \frac{\Delta C_P}{R} \left( \ln \frac{T_{tp}}{T} - \frac{T_{tp}}{T} + 1 \right) - \frac{\Delta V}{RT} (P - P_{tp}) \right] \quad (2.116)$$

We can now make some reasonable approximations that simplify the use of [Equation 2.116](#). In most cases, the pressure correction in the last term of [Equation 2.116](#) is negligible. In addition, the heat capacity difference also provides only a minor contribution and can be ignored. In addition, as mentioned earlier, the triple point temperature ( $T_{tp}$ ) is close to the melting point temperature ( $T_m$ ) (cf. [Figure 2.4](#)) of the solid at atmospheric pressure, and we can then replace the enthalpy of fusion at  $T_{tp}$  with the enthalpy of fusion at the normal melting temperature, i.e.,  $\Delta H^m$ . For a variety of organic molecules, the ratio of the enthalpy of fusion ( $\Delta H^m$ , calories per gram mole) to the normal atmospheric melting point ( $T_m$ , K) is approximately in the range from 9 to 11. With these simplifications, [Equation 2.116](#) may be written as

$$x_2 = \frac{1}{\gamma_2} \exp \left[ \frac{\Delta H^m}{R} \left( \frac{1}{T_m} - \frac{1}{T} \right) \right] \quad (2.117)$$

If the solid solute and the solvent are chemically similar, then we would expect them to form an ideal solution. For an ideal solution, we can set  $\gamma_2$  in [Equation 2.117](#) equal to unity. For an ideal solution with  $\gamma_2 = 1$ , the solubility of the solid solute can be predicted from only the enthalpy of fusion and the melting temperature. Note that the ideal solubility (i.e.,  $\gamma_2 = 1$ ) is based only on the pure component properties of the solute and is the same regardless of the solvent. For nonideal solutions, we must use an appropriate solution model for the activity coefficient ( $\gamma_2$ ) (Poling et al., 2001) in order to calculate the solubility. In the limit of negligible solubility in the solvent, we may use the infinite dilution activity coefficient ( $\gamma_2^\infty$ ).

In the case of nonpolar solutes and solvents, it is worth mentioning at this point that the *Scatchard-Hildebrand equation* allows estimation of the solute activity coefficient from the pure component properties of the solute and the solvent. Using the Scatchard-Hildebrand equation, the solute activity coefficient is given by

$$\ln \gamma_2 = \frac{V_2^L (\delta_1 - \delta_2)^2 \Phi_1^2}{RT}, \quad (2.118)$$

where  $V_2^L$  represents the molar volume of the solute as a subcooled liquid that, in practice, is usually taken to be the same as the molar volume of the solute as a liquid at the melting temperature, the  $\delta$ 's are the *solubility parameters* for the solute and the solvent, and  $\Phi_1$  is the volume fraction of the solvent defined by the following equation:

$$\Phi_1 = \frac{x_1 V_1^L}{x_1 V_1^L + x_2 V_2^L} \quad (2.119)$$

The square of the solubility parameter ( $\delta_i^2$ ) is defined as the ratio of the change in the internal energy for complete vaporization to the molar liquid volume. The internal energy change of vaporization is the same as the enthalpy of vaporization minus RT assuming an ideal gas. The solubility parameter for component i is then given by the following equation:

$$\delta_i = \left( \frac{\Delta H_i^{\text{Vap}} - RT}{V_i^L} \right)^{1/2} \quad (2.120)$$

One usually ignores the temperature dependence of  $\Delta H_i^{\text{Vap}}$  and  $V_i^L$  and simply uses the values at the normal melting point for the solute and at 25°C for the solvent. For a solid solute, the heat of vaporization would also be equal to the difference between the heat of sublimation and the heat of fusion, i.e.,  $\Delta H^{\text{Vap}} = \Delta H^{\text{Sub}} - \Delta H^m$ . If an expression for the vapor pressure of the solid is known, e.g., from an equation like [Equation 2.89](#), then the heat of sublimation can be calculated using the Clausius-Clapeyron equation, i.e., [Equation 2.88](#). The more chemically similar the solute and solvent are, the closer the values of their respective solubility parameters, and from [Equation 2.118](#), we see that the resulting solution then approaches ideality. Hence, comparing the solubility parameters provides a quick method for determining chemical similarity and the degree of nonideality between the solute and the solvent.

**Example 2.10**

A drug has a molecular weight of 230 and a melting temperature of 155°C. Estimate the solubility of this drug in benzene and in n-hexane at 25°C, assuming they form an ideal solution. Also, determine the solubility based on the Scatchard-Hildebrand equation. The following data are also provided:

Heat of fusion of the drug	4300 cal mol <sup>-1</sup>
Density of the drug	1.04 g cm <sup>-3</sup>
Vapor pressure of the solid drug	$\ln P^{\text{Sat}} (\text{mmHg}) = 27.3 - \frac{8926}{T(\text{K})}$
Molar volume of benzene	89.4 cm <sup>3</sup> mol <sup>-1</sup>
Solubility parameter for benzene	9.2 (cal cm <sup>-3</sup> ) <sup>1/2</sup>
Molar volume of n-hexane	131.6 cm <sup>3</sup> mol <sup>-1</sup>
Solubility parameter for n-hexane	7.3 (cal cm <sup>-3</sup> ) <sup>1/2</sup>

**Solution**

To calculate the ideal solubility of the drug, we use [Equation 2.117](#) with  $\gamma_2 = 1$ :

$$x_2 = \exp\left[\frac{4300 \text{ cal g mol}^{-1}}{1.987 \text{ cal g mol}^{-1} \text{ K}^{-1}} \left( \frac{1}{273.15 + 155} - \frac{1}{298.15} \right) \text{ K}^{-1}\right] = 0.110$$

This is the same value whether the solvent is benzene or n-hexane. To calculate the solubility based on the Scatchard-Hildebrand equation, we need to estimate the solubility parameter for the drug. First, the heat of sublimation can be found as follows from the vapor pressure of the solid drug using [Equation 2.88](#):

$$\Delta H^{\text{Sub}} = -R \frac{d \ln P^{\text{Sat}}}{d(1/T)} = 1.987 \text{ cal g mol}^{-1} \text{ K}^{-1} \times 8926 \text{ K} = 17736.9 \text{ cal mol}^{-1}$$

Then the solubility parameter for the drug is found from [Equation 2.120](#) assuming that the molar volume of the drug as a liquid and as a solid is similar:

$$\delta_2 = \left( \frac{17736.9 \text{ cal mol}^{-1} - 4300 \text{ cal mol}^{-1} - 1.987 \text{ cal mol}^{-1} \text{ K}^{-1} \times 298.15 \text{ K}}{(1/1.04) \text{ cm}^3 \text{ g}^{-1} \times 230 \text{ g mol}^{-1}} \right)^{1/2} = 7.62 \left( \text{cal mol}^{-1} \right)^{1/2}$$

Next, we can combine [Equations 2.117 through 2.119](#) to give

$$x_2 = \frac{\exp\left[\frac{\Delta H^m}{R}\left(\frac{1}{T_m} - \frac{1}{T}\right)\right]}{\exp\left\{\frac{V_2^L (\delta_1 - \delta_2)^2}{RT} \left[ \frac{(1-x_2)V_1^L}{(1-x_2)V_1^L + x_2 V_2^L} \right]^2\right\}} \quad (\text{A})$$

The equation is an implicit algebraic equation in the solubility  $x_2$ . Numerical techniques need to be used to solve for the value of  $x_2$ . One approach that can be used is *direct iteration*.

In this technique one assumes a value for  $x_2$ , substitutes this value on the right-hand side of [Equation A](#), and calculates a new value of  $x_2$  called  $\hat{x}_2$ . One then lets  $x_2 = \hat{x}_2$ , and this new value of  $x_2$  is then substituted into the right-hand side of the previous equation, and the process is repeated until there is no longer any significant difference in the values of  $x_2$  and  $\hat{x}_2$  and convergence is then obtained. Although direct iteration is simple to implement, there is no guarantee for convergence to the solution. In addition, numerous iterations are sometimes required. The second approach is based on *Newton's method*. Newton's method has more reliable convergence and requires fewer iterations. To implement Newton's method, we first form the following difference equation from [Equation A](#):

$$f(x_2) = x_2 - \frac{\exp\left[\frac{\Delta H^m}{R}\left(\frac{1}{T_m} - \frac{1}{T}\right)\right]}{\exp\left\{\frac{V_2^L (\delta_1 - \delta_2)^2}{RT} \left[ \frac{(1-x_2)V_1^L}{(1-x_2)V_1^L + x_2 V_2^L} \right]^2\right\}}$$

The goal is to find the value of  $x_2$  that makes  $f(x_2) = 0$ . This is accomplished through the following iterative equation that provides an update for the value of  $x_2$  based on the evaluation of  $f(x_2)$  and  $df(x_2)/dx_2$  at the previous value of  $x_2$ :

$$\hat{x}_2 = x_2 - \frac{f(x_2)}{df(x_2)/dx_2}$$

One then assumes  $x_2 = \hat{x}_2$ , and the process is repeated until convergence. In terms of choosing an initial starting value of  $x_2$  for either approach, we could use the ideal solubility or simply assume that  $x_2 = 0$ . After substituting in the values of the known quantities into the earlier equation for  $f(x_2)$  and performing the iterative calculations, it is found that the solubility based on the Scatchard-Hildebrand model for the solute activity coefficient is  $x_2 = 0.054$  when the solvent is benzene and  $x_2 = 0.107$  when the solvent is n-hexane. The drug and n-hexane solubility parameters are nearly identical, and the solubility of the drug is nearly the same as that found assuming an ideal solution. On the other hand, for benzene as the solvent, the drug solubility is considerably lower than the value based on an ideal solution.

**2.6.3.2 Depression of the freezing point of a solvent by a solute** Consider a small amount of a solute dissolved in a solvent. As the temperature of this solution is decreased, a temperature ( $T_f$ ) is reached where the pure solvent just starts to separate out of the solution as a solid phase. The freezing temperature of this mixture is  $T_f$ . This temperature is lower than the freezing point of the pure solvent ( $T_m$ ). We are usually interested in determining the freezing point depression, which is then defined as  $\Delta T = T_m - T_f$ . This problem is very similar to the one we just addressed concerning the solubility of a solute in a solvent. However, now the focus is on the solvent, which is component 1.

To solve this problem, we assume that equilibrium exists between the first amount of solvent that freezes and the rest of the solution. We also assume that the solvent that freezes exists as pure solvent, and we assume that the minute amount of solid solvent formed has no effect on the composition of the solution. We can then write an equilibrium equation like [Equation 2.109](#), but now for the solvent

$$f_i^S = \gamma_i x_i f_i^L \quad (2.121)$$

which can be rearranged to give

$$\ln \gamma_1 x_1 = \ln \frac{f_i^S}{f_i^L} \quad (2.122)$$

Following a similar development we used for the solute (see [Equation 2.112](#)) in the previous section, we can write that

$$d \ln \frac{f_i^S}{f_i^L} = \frac{H^L - H^S}{RT^2} dT - \frac{V^L - V^S}{RT} dP \quad (2.123)$$

and we also have that

$$H^L - H^S = \Delta H^m + \Delta C_P (T_f - T_m) \quad (2.124)$$

where for the solvent, we use the normal melting temperature of the pure solvent as the reference temperature, and  $T_f$  is the mixture freezing temperature. We also assumed that the heat capacities do not vary much as the temperature changes from  $T_m$  to  $T_f$ . We can now substitute [Equation 2.124](#) into [Equation 2.123](#) and integrate between  $(T_m, P_m)$  and the conditions of interest, i.e.,  $(T_f, P_f)$ . In performing this integration, we also make use of the fact that, for the most part, the difference in the specific volumes ( $\Delta V = V^L - V^S$ ) is independent of the pressure. In addition, we recognize that at the melting point of the pure solvent,  $f_i^L = f_i^S$

$$\ln \frac{f_i^S}{f_i^L} = \frac{\Delta H^m}{R} \left( \frac{1}{T_m} - \frac{1}{T_f} \right) - \frac{\Delta C_P}{R} \left( \ln \frac{T_m}{T_f} - \frac{T_m}{T_f} + 1 \right) - \frac{\Delta V}{RT} (P_f - P_m) \quad (2.125)$$

Combining [Equation 2.125](#) with [Equation 2.122](#), we obtain

$$\ln \gamma_1 x_1 = \frac{\Delta H^m}{R} \left( \frac{1}{T_m} - \frac{1}{T_f} \right) - \frac{\Delta C_P}{R} \left( \ln \frac{T_m}{T_f} - \frac{T_m}{T_f} + 1 \right) - \frac{\Delta V}{RT} (P_f - P_m) \quad (2.126)$$

Once again, we can ignore the effect of the pressure term, and since  $T_f \approx T_m$ , we obtain

$$\ln \gamma_1 x_1 = \frac{\Delta H^m}{R} \left( \frac{1}{T_m} - \frac{1}{T_f} \right) = -\frac{\Delta H^m}{RT_m^2} (T_m - T_f) \quad (2.127)$$

The freezing point depression is then given by

$$\Delta T = T_m - T_f = -\frac{RT_m^2}{\Delta H^m} \ln \gamma_1 x_1 \quad (2.128)$$

Note that if the freezing depression is measured, then [Equation 2.128](#) provides a convenient means for determining the activity coefficient of the solvent for a solution of given composition.

For ideal solutions, we have that  $\gamma_1 = 1$ . For solutions that are very dilute in the solute,  $\gamma_1 \approx 1$  and  $\ln x_1 = \ln(1 - x_2) \approx -x_2$ . So, for dilute solutions we can write that

$$\Delta T = T_m - T_f = \frac{RT_m^2}{\Delta H^m} x_2 \quad (2.129)$$

where  $x_2$  is the mole fraction of the solute in the mixture.

**Example 2.11**

Estimate the freezing point depression of a benzene solution containing the drug considered in [Example 2.10](#). Assume that the drug concentration is  $0.04 \text{ g cm}^{-3}$ . The normal melting point for benzene is  $278.7 \text{ K}$ .

**Solution**

We expect the mole fraction of the drug at this concentration to be very small. We can therefore assume that the density of the liquid solution is the same as that of pure benzene, which is  $0.885 \text{ g cm}^{-3}$ . As a basis for the calculation of the mole fraction, assume that we have  $1 \text{ cm}^3$  of the liquid mixture. Then, for the drug mole fraction in benzene, we can write that

$$x_2 = \frac{\frac{0.04 \text{ g}}{\text{cm}^3} \times 1 \text{ cm}^3 \text{ solution} \times \frac{1 \text{ mol of drug}}{230 \text{ g}}}{\left( \frac{0.04 \text{ g}}{\text{cm}^3} \times \frac{1 \text{ mol of drug}}{230 \text{ g}} + \frac{0.885 - 0.04 \text{ g}}{\text{cm}^3} \times \frac{1 \text{ mol benzene}}{78 \text{ g}} \right) \times 1 \text{ cm}^3 \text{ solution}}$$

and we get that  $x_2 = 0.0158$ . Now using [Equation 2.129](#)

$$\Delta T = T_m - T_f = \frac{1.987 \text{ cal mol}^{-1} \text{ K}^{-1} 278.7^2 \text{ K}^2}{2350 \text{ cal mol}^{-1}} \times 0.0158 = 1.038 \text{ K}$$

**2.6.3.3 Equilibrium between a solid and a gas phase** Now, we consider a pure solid phase that is in equilibrium with a surrounding gas phase. Here, the question that can be addressed is, for a given  $T$  and  $P$ , what is the equilibrium composition of the gas phase? We let component 1 represent the gas and component 2 is the material that makes up the pure solid phase. We also assume that the gas has negligible solubility in the solid phase, so the solid phase is pure. Equilibrium requires that the solid phase fugacity of component 2 equals the fugacity of component 2 in the gas phase. We use [Equation 2.71](#) to describe the fugacity of component 2 in the gas phase and obtain the following statement for equilibrium between the pure solid phase and the gas:

$$f_2^S = \hat{\phi}_2 y_2 P \quad (2.130)$$

The mole fraction of component 2 in the gas phase is then given by

$$y_2 = \frac{f_2^S}{\hat{\phi}_2 P} \quad (2.131)$$

If the pressure is significantly above atmospheric, then a mixture equation of state is needed to calculate the fugacity coefficient of component 2 in the gas phase, as described by [Equation 2.74](#) (Poling et al., 2001). However, for most applications in biomedical engineering, the pressure will be near atmospheric and we can treat the gas phase as an ideal gas for which  $\hat{\phi}_2 = 1$ .

The fugacity of the pure solid is given by [Equation 2.95](#), recognizing that we are now considering a subcooled or compressed solid rather than that of a liquid for which we derived [Equation 2.95](#):

$$f_2^S = f_2^{\text{Sat}} \exp\left(\frac{V_2^{\text{S,Sat}} (P - P_2^{\text{Sat}})}{RT}\right) = \phi_2^{\text{Sat}} P_2^{\text{Sat}} \exp\left(\frac{V_2^{\text{S,Sat}} (P - P_2^{\text{Sat}})}{RT}\right) \quad (2.132)$$

$P_2^{\text{Sat}}$  is the sublimation pressure (or vapor pressure) wherein the solid will vaporize directly to a vapor without first forming a liquid. Since the sublimation pressure is generally very small at ambient temperatures, the saturated fugacity coefficient ( $\phi_2^{\text{Sat}}$ ) is equal to one. If the pressure is low and on the order of  $P_2^{\text{Sat}}$ , then the exponential term is also equal to unity. Therefore, for this case, we get that the pure component solid phase fugacity of component 2 is simply equal to its sublimation or vapor pressure. Hence, we can write that

$$y_2 = \frac{P_2^{\text{Sat}}}{P} \quad (2.133)$$

### Example 2.12

Estimate the gas phase equilibrium mole fraction of the drug considered in [Example 2.10](#) at a temperature of 35°C. The pressure of the gas is 1 atm.

#### Solution

Since the pressure is 1 atm, we assume that the gas phase is ideal and set  $\phi_2^{\text{Sat}} = 1$ . We then calculate the fugacity of the drug as a solid using [Equation 2.132](#):

$$f_2^S = P_2^{\text{Sat}} \exp\left(\frac{V^{S,\text{Sat}}(P - P_2^{\text{Sat}})}{RT}\right)$$

We also assume that the molar volume of the solid at the saturation T and P is the same as the molar volume of the solid at ambient conditions. For  $P_2^{\text{Sat}}$ , we were given an expression in [Example 2.10](#). For the given T, we calculate that  $P_2^{\text{Sat}} = 0.189 \text{ mmHg}$ . Using the previous equation, we then calculate the fugacity of the pure solid as

$$f_2^S = 0.189 \text{ mmHg} \times \exp\left(\frac{\frac{1 \text{ cm}^3}{1.04 \text{ g}} \times \frac{1 \text{ L}}{1000 \text{ cm}^3} \times 230 \frac{\text{g}}{\text{mol}} \times (760 - 0.189) \text{ mmHg} \times \frac{1 \text{ atm}}{760 \text{ mmHg}}}{0.082 \frac{\text{atm L}}{\text{K mol}} \times 308.15 \text{ K}}\right)$$

$$f_2^S = 0.189 \text{ mmHg} \times 1.0088 = 0.191 \text{ mmHg}$$

As expected, because of the low pressure, we see in the previous calculation that the exponential correction to the solid fugacity is negligible and that the fugacity of the solid is nearly the same as its vapor pressure. Using [Equation 2.133](#), we then find that the gas phase mole fraction of the drug is  $y_2 = 0.191 \text{ mmHg}/760 \text{ mmHg} = 0.00025$ .

**2.6.3.4 Solubility of a gas in a liquid** We now consider the calculation of the equilibrium solubility of a sparingly soluble gas (taken as component 2) in a liquid, i.e.,  $x_2 \rightarrow 0$ . Our phase equilibrium relationship, i.e., [Equation 2.84](#), requires for the solute gas that

$$\hat{f}_2^L = \hat{f}_2^G \quad (2.134)$$

The definition of the activity coefficient in [Equation 2.99](#), where  $\gamma_2 = \hat{f}_2^L / x_2 f_2^L$ , provides an approach for calculating the fugacity of component 2 within the liquid phase:

$$\hat{f}_2^L = \gamma_2 x_2 f_2^L, \quad (2.135)$$

where  $f_2^L$  is the pure component liquid fugacity at the mixture T and P and is given by [Equation 2.95](#). Recall from [Equation 2.71](#) that we also defined the component mixture fugacity coefficient as  $\hat{\phi}_2 = \hat{f}_2^G / y_2 P$ , which also says that the fugacity of component 2 within a vapor or gas mixture is given by

$$\hat{f}_2^G = y_2 \hat{\phi}_2 P \quad (2.136)$$

By [Equation 2.84](#), Equations [2.135](#) and [2.136](#) are equal, so

$$y_2 \hat{\phi}_2 P = \gamma_2 x_2 f_2^L \quad (2.137)$$

We then assume that the solvent has a negligible vapor pressure; hence,  $y_2 = 1$  and  $\hat{\phi}_2 = \phi_2$ . The gas solubility in the solvent expressed as a mole fraction is then given by

$$x_2 = \frac{\phi_2 P}{\gamma_2 f_2^L} = \frac{f_2^G}{\gamma_2 f_2^L} \quad (2.138)$$

Usually, the temperature of interest will be much higher than the critical temperature of the soluble gas being considered, so we have that  $T > T_{C2}$ . For example, the critical temperature and other physical properties for several common gases are summarized in [Table 2.1](#).

Although [Equation 2.138](#) provides a convenient means of calculating the gas solubility, it is encumbered by the fact that the soluble gas does not really exist as a liquid since  $T > T_{C2}$ . If by chance the soluble gas is below its critical temperature, then this problem of the gas existing as a hypothetical liquid is not an issue.

One approach to solving this problem involves using [Equation 2.138](#) with the Scatchard-Hildebrand equation for the activity coefficient of the solute. When [Equation 2.118](#) is substituted into [Equation 2.138](#) for  $\gamma_2$ , we obtain

$$x_2 = \frac{f_2^G}{f_2^L} \exp \left[ -\frac{V_2^L (\delta_1 - \delta_2)^2 \Phi_1^2}{RT} \right] \quad (2.139)$$

Table 2.1 Physical Properties of Some Common Gases

Gas	Critical Properties $T_C$ , K and $P_C$ , MPa	Liquid Volume $V^L$ , $\text{cm}^3 \text{ mol}^{-1}$	Solubility Parameter $\delta$ , $(\text{cal cm}^{-3})^{1/2}$
Oxygen	154.6, 5.046	33.0	4.0
Nitrogen	126.2, 3.394	32.4	2.58
Carbon dioxide	304.2, 7.376	55	6.0

Prausnitz and Shair (1961) used [Equation 2.139](#) to correlate known solubility data for a number of gases in a variety of solvents and obtained the three parameters in [Equation 2.139](#), which describe the soluble gas as a hypothetical liquid, i.e., the pure liquid fugacity ( $f_2^L$ ), the liquid volume ( $V_2^L$ ), and the gas solubility parameter ( $\delta_2$ ). [Table 2.1](#) summarizes for several gases the values of ( $V_2^L$ ) and ( $\delta_2$ ) that were found, and [Equation 2.140](#) provides the fugacity of the soluble gas as a hypothetical pure liquid at a pressure of 1.013 bar:

$$\ln\left(\frac{f_2^L}{P_{C2}}\right) = 7.81 - \frac{8.06}{T/T_{C2}} - 2.94 \ln\left(\frac{T}{T_{C2}}\right) \quad (2.140)$$

If the pressure is greater than 1.013 bar, then the liquid phase fugacity ( $f_2^L$ ) calculated from [Equation 2.140](#) needs to be corrected for the effect of the pressure, as shown in [Equation 2.95](#), after changing the reference pressure from  $P^{sat}$  to atmospheric pressure of 1.013 bar:

$$f_2^L(P) = f_2^L(1.013 \text{ bar}) \exp\left[\frac{V_2^L(P - 1.013 \text{ bar})}{RT}\right] \quad (2.141)$$

### Example 2.13

Estimate the solubility of oxygen and carbon dioxide in toluene at a gas partial pressure of 1 atm and 25°C. The solubility parameter for toluene is 8.91 (cal cm<sup>-3</sup>)<sup>1/2</sup>.

#### Solution

Since the pressure is atmospheric, we can neglect the pressure correction to the liquid fugacity. From [Equation 2.140](#), we then calculate the fugacity of oxygen and carbon dioxide in the liquid state at 25°C. For carbon dioxide, we then have that

$$\begin{aligned} \ln\left(\frac{f_2^L}{P_{C2}}\right) &= 7.81 - \frac{8.06}{\frac{298.15}{304.2}} - 2.94 \ln\left(\frac{298.15}{304.2}\right) = -0.3545 \\ f_2^L &= 7.376 \text{ MPa} \times \exp(-0.3545) \times \frac{10^6 \text{ Pa}}{1 \text{ MPa}} \times \frac{1 \text{ atm}}{101,325 \text{ Pa}} = 51.07 \text{ atm} \end{aligned}$$

and for oxygen we have that

$$\begin{aligned} \ln\left(\frac{f_2^L}{P_{C2}}\right) &= 7.81 - \frac{8.06}{\frac{298.15}{154.6}} - 2.94 \ln\left(\frac{298.15}{154.6}\right) = 1.70 \\ f_2^L &= 5.046 \text{ MPa} \times \exp(1.70) \times \frac{10^6 \text{ Pa}}{1 \text{ MPa}} \times \frac{1 \text{ atm}}{101,325 \text{ Pa}} = 272.6 \text{ atm} \end{aligned}$$

Since the gas partial pressure is only 1 atm, we can treat the gas phase as an ideal gas and set the gas phase fugacity equal to the partial pressure. From [Equation 2.139](#), we can then

calculate the mole fraction of carbon dioxide and oxygen in toluene. Note that we have set  $\Phi_1 = 1$  since we expect the solubility of these gases in toluene to be very small. For carbon dioxide, we then get that

$$x_2 = \frac{1\text{ atm}}{51.07\text{ atm}} \exp \left[ -\frac{55\text{ cm}^3\text{ g mol}^{-1}(6-8.91)^2\text{ cal cm}^{-3} \times 1}{1.987\text{ cal mol}^{-1}\text{ K}^{-1} \times 298.15\text{ K}} \right] = 0.0089$$

and for oxygen, we obtain

$$x_2 = \frac{1\text{ atm}}{272.6\text{ atm}} \exp \left[ -\frac{33\text{ cm}^3\text{ g mol}^{-1}(4-8.91)^2\text{ cal cm}^{-3} \times 1}{1.987\text{ cal mol}^{-1}\text{ K}^{-1} \times 298.15\text{ K}} \right] = 0.0010$$

The reported solubility of carbon dioxide in toluene at 25°C and at a partial pressure of 1 atm is 0.010 and that for oxygen in toluene is 0.0009. Calculating the % error, we see that the error for prediction of the carbon dioxide and oxygen solubility using the Scatchard-Hildebrand model is 11% for both gases.

The use of [Equation 2.139](#) for predicting the solubility of a gas in a liquid is limited by the assumptions made in the development of the Scatchard-Hildebrand model for estimating activity coefficients. Generally, the prediction will be better for nonpolar gases and liquids. Also, the accuracy will rapidly diminish as the absolute magnitude of the difference between the solubility parameter of the gas and the solvent increases. For example, consider the solubility of oxygen in ethanol ( $\delta_{\text{ethanol}} = 12.8\text{ (cal cm}^{-3})^{1/2}$ ). The difference in the solubility parameters of oxygen and ethanol is quite large, and we would therefore expect greater error in the prediction of the solubility. We can use the results from [Example 2.13](#) and calculate the predicted oxygen solubility in ethanol as  $4.91 \times 10^{-5}$ , whereas the reported value is about  $6 \times 10^{-4}$ . So, in this case, we have underestimated the solubility of oxygen by over a factor of 10.

Because of these limitations on predicting gas solubility, a more empirical approach is often used. At a given temperature and pressure, it has been found that, for the most part, the gas phase fugacity is directly proportional to the gas solubility expressed as a mole fraction ( $x_2$ ), i.e.,  $\hat{f}_2^G = y_2 \hat{\phi}_2 P = H x_2$ . The proportionality constant  $H$  is called *Henry's constant*. If the gas phase is ideal, then  $\hat{\phi}_2 = 1$ , and  $y_2 P$  is also just the partial pressure of the solute gas, i.e.,  $P_2$  or  $pX$ , where  $X$  is the name of the solute gas. For example, the partial pressure of oxygen can be written as either  $P_{\text{oxygen}}$  or as  $pO_2$ . So, we can write that  $P_2 = pX = Hx_2$ . It is important to remember though that Henry's constant for a specific gas will depend on the solvent, the temperature, and to some extent the pressure.

In some cases, Henry's constant is based on the solute concentration of the solute in the solvent. This is common, e.g., in describing the solubility of oxygen in blood where we write that the  $pO_2 = HC_{\text{oxygen}}$ . The partial pressure of oxygen in the gas phase is represented by  $pO_2$ , and  $C_{\text{oxygen}}$  is the molar concentration of dissolved oxygen in the blood. The value of Henry's constant ( $H$ ) for describing the solubility of oxygen in blood is  $0.74\text{ mmHg }\mu\text{M}^{-1}$ .

The thermodynamic basis for Henry's constant can be obtained from [Equation 2.135](#), where we have the following expression for the liquid phase fugacity:  $\hat{f}_2^L = \gamma_2 x_2 f_2^L$ . The product of  $\gamma_2$  and  $f_2^L$  as

$x_2 \rightarrow 0$  is Henry's constant. Substituting H for the product of  $\gamma_2$  and  $f_2^L$  results in Henry's law for describing gas solubility, i.e.,

$$\hat{f}_2^L = \gamma_2 x_2 f_2^L = H x_2 \quad (2.142)$$

For sparingly soluble gases, where  $x_2 \rightarrow 0$ , the activity coefficient approaches, in the limit of infinite dilution, a value that becomes independent of the solute mole fraction, i.e.,  $\gamma_2 \rightarrow \gamma_2^\infty$ . Hence, from [Equation 2.142](#), we would expect Henry's constant to be nearly independent of the solute mole fraction. Since H is also related to the pure component liquid fugacity, we would also expect H to be somewhat dependent on the temperature and only weakly dependent on the pressure.

### Example 2.14

Calculate the concentration of oxygen dissolved in blood for a gas phase partial pressure of oxygen equal to 95 mmHg.

#### Solution

Using Henry's law and the value of H given earlier for oxygen and blood, we can write that

$$C_{\text{oxygen}} = \frac{pO_2}{H} = \frac{95 \text{ mmHg}}{0.74 \text{ mmHg } \mu\text{M}^{-1}} = 128.4 \mu\text{M}$$

**2.6.3.5 Osmotic pressure** Consider the situation illustrated in [Figure 2.5](#) where a rigid semipermeable membrane separates region A from region B. Region B contains only pure solvent, whereas region A contains the solvent and a solute. The membrane that separates region A from region B is only permeable to the solvent; hence, the solute is completely retained in region A. Solvent will diffuse from region B into region A in an attempt to satisfy the requirement that at equilibrium (see [Equations 2.82](#) and [2.84](#)), the chemical potential or fugacity of the solvent on each side of the membrane must be equal. This movement of solvent from region B to region A is called *osmosis* and

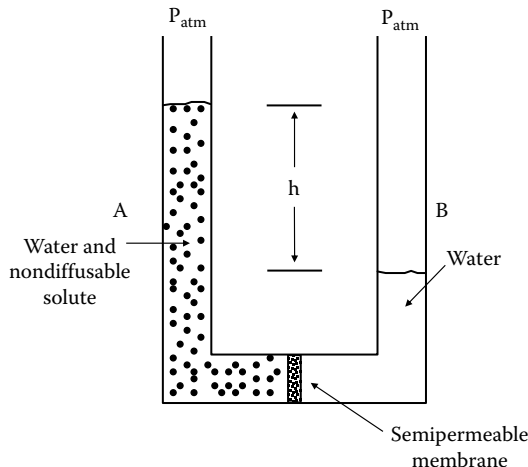


Figure 2.5 Concept of osmotic pressure.

will tend to increase the level of region A until the increase in hydrostatic pressure stops the flow of solvent from region B and equilibrium is attained.

The pressure difference across the membrane between regions A and B at this point of equilibrium is the osmotic pressure of region A relative to that of the pure solvent in region B. The osmotic pressure is represented by  $\Pi$  and is equal to  $(P_A - P_B)$ , which is also equal to  $\rho gh$  for the situation shown in [Figure 2.5](#).

A quantitative understanding of osmosis is needed for a variety of calculations and concepts involving solutions and mass transport across semipermeable membranes. We can easily derive an expression for the osmotic pressure of a solution by starting with the fundamental requirement that at equilibrium, the temperature and fugacity of the solvent in regions A and B must be equal:

$$\hat{f}_{\text{solvent}}^A(T, P_A) = f_{\text{solvent}}^B(T, P_B) \quad (2.143)$$

Note that at equilibrium, the temperatures of regions A and B will be the same; however, the pressures on either side of the membrane surface will not be the same. [Equation 2.143](#) can be rewritten as follows using an activity coefficient model (see [Equation 2.99](#)) to describe the fugacity of the solvent in region A:

$$\gamma_{\text{solvent}}^A x_{\text{solvent}}^A f_{\text{solvent}}^A(T, P_A) = f_{\text{solvent}}^B(T, P_B) \quad (2.144)$$

The pure component solvent fugacity in region A at T and  $P_A$  can be related to that in region B at T and  $P_B$  through the use of [Equation 2.95](#) after changing the reference pressure from  $P_{\text{sat}}$  to  $P_B$ . Hence, we can write that

$$f_{\text{solvent}}^A(T, P_A) = f_{\text{solvent}}^B(T, P_B) \exp\left(\frac{V_{\text{solvent}}^L(P_A - P_B)}{RT}\right) \quad (2.145)$$

Substituting [Equation 2.145](#) into [Equation 2.144](#) results in [Equation 2.146](#) for the osmotic pressure  $(P_A - P_B)$ . This osmotic pressure difference is given the symbol  $\Pi$  and represents the osmotic pressure of the solution in region A relative to that of the pure solvent in region B:

$$\Pi = (P_A - P_B) = \frac{-RT}{V_{\text{solvent}}^L} \ln(\gamma_{\text{solvent}}^A x_{\text{solvent}}^A) \quad (2.146)$$

Note that measurement of the osmotic pressure of a solution also provides a convenient method through the use of [Equation 2.146](#) to determine the activity coefficient of the solvent. For nonideal solutions, a variety of theoretical and empirical models exist for estimating the activity coefficient in [Equation 2.146](#) (Poling et al., 2001; also see [Problems 2.28](#) and [2.29](#) at the end of this chapter).

[Equation 2.146](#) can be simplified for the special case where the solvent and solute form an ideal solution. In this case,  $\gamma_{\text{solvent}}^A = 1$ , and since  $x_{\text{solvent}}^A$  is close to unity, we can rewrite [Equation 2.146](#) as

$$\Pi = \frac{RT}{V_{\text{solvent}}^L} x_{\text{solute}}^A = RTC_{\text{solute}} \quad (2.147)$$

where  $x_{\text{solute}}^A$  represents the mole fraction of the solute in region A. Since the solute mole fraction is generally quite small, we can approximate this as  $x_{\text{solute}}^A = V_{\text{solvent}}^L C_{\text{solute}}$ , where  $C_{\text{solute}}$  is the molar concentration of the solute and  $V_{\text{solvent}}^L$  is the molar volume of the solvent. This ideal dilute solution osmotic pressure, described by [Equation 2.147](#), is known as *van't Hoff's law*. If the solution contains N ideal solutes, then the total osmotic pressure of the solution is the summation of the osmotic pressure generated by each nondissociating solute according to [Equation 2.147](#):

$$\Pi = RT \sum_{i=1}^N C_{\text{solute}_i} \quad (2.148)$$

Osmotic pressure is not determined on the basis of the mass of the solute in the solution, but rather, on the number of particles that are formed by a given solute. Each nondiffusing or retained particle in the solution contributes the same amount to the osmotic pressure regardless of the size of the particle. Thus, if we take 1/1000th of an Avogadro's number of glucose molecules, or 1/1000th of an Avogadro's number of albumin molecules, and form a 1 L solution of each with water, we have a 1 mM (1 mmol L<sup>-1</sup>) solution of each solute. According to [Equation 2.147](#), the ideal osmotic pressure of these two solutions is the same. However, the mass of glucose added to the solution is 180 mg, whereas the mass of albumin added to the solution is nearly 70 g, demonstrating that it is not the mass of solute in the solution that is important in determining the osmotic pressure.

### Example 2.15

Consider the situation shown in [Figure 2.5](#) where on side A of the membrane, we have a solution that has a water mole fraction of 0.99. On side B of the membrane, we have pure water. If the temperature is 25°C, estimate the pressure drop needed across the membrane, i.e.,  $(P_A - P_B)$ , to stop the osmosis of water from region B. What will happen if this pressure difference was increased above this value?

### Solution

Assuming the solution in region A is an ideal solution, we can use [Equation 2.147](#) to calculate the osmotic pressure of region A relative to the pure water of region B, i.e.,

$$\Pi = (P_A - P_B) = \frac{8.314 \frac{\text{Pa m}^3}{\text{mol K}} \times \frac{1 \text{atm}}{101,325 \text{Pa}} \times 298 \text{K}}{18 \times 10^{-6} \frac{\text{m}^3}{\text{mol}}} \times 0.01 = 13.6 \text{ atm}$$

To stop the flow of water from region B to region A by osmosis, the pressure drop across the membrane, i.e.,  $(P_A - P_B)$ , must equal the osmotic pressure of the solution in region A. If the pressure drop across the membrane, i.e.,  $(P_A - P_B)$ , is greater than the osmotic pressure of region A, then water will move from region A into region B and this process is called *reverse osmosis*.

Since small pressures are easy to measure, the osmotic pressure is also useful for determining the molecular weight of macromolecules such as proteins. For example, letting  $m_{\text{solute}}$  represent the mass

concentration (e.g., in grams per liter) of the solute in the solution, then from [Equation 2.147](#) we can write the molecular weight of the solute ( $MW_{\text{solute}}$ ) in terms of the osmotic pressure of the solution as

$$MW_{\text{solute}} = \frac{RT m_{\text{solute}}}{\Pi} \quad (2.149)$$

### Example 2.16

The osmotic pressure of a solution containing a macromolecule is equivalent to the pressure exerted by 8 cm of water. The mass concentration of the protein in the solution is  $15 \text{ g L}^{-1}$ . Estimate the molecular weight of this macromolecule.

#### Solution

We can use [Equation 2.149](#) to estimate the molecular weight as follows:

$$MW_{\text{solute}} = \frac{8.314 \frac{\text{m}^3 \text{ Pa}}{\text{mol K}} \times 298 \text{ K} \times \frac{15 \text{ g}}{\text{L}} \times \frac{1 \text{ L}}{1000 \text{ cm}^3} \times \frac{(100 \text{ cm})^3}{\text{m}^3} \times \frac{1 \text{ atm}}{101,325 \text{ Pa}}}{8 \text{ cm H}_2\text{O} \times \frac{1 \text{ in.}}{2.54 \text{ cm}} \times \frac{1 \text{ ft}}{12 \text{ in.}} \times \frac{1 \text{ atm}}{33.91 \text{ ft H}_2\text{O}}} \\ MW_{\text{solute}} = 47,400 \text{ g mol}^{-1}$$

**2.6.3.6 Distribution of a solute between two liquid phases** Many purification processes are based on the unequal distribution of a solute between two partially miscible liquid phases. For example, through the process of liquid extraction, a drug produced by fermentation can be extracted from the aqueous fermentation broth into a suitable solvent and then be purified. Factors to consider in the selection of the solvent include its toxicity, cost, degree of miscibility with the fermentation broth, and selectivity for the solute.

Consider the resulting batch-type equilibrium where  $N_1$  moles of solute 1 are mixed with  $N_2$  moles of solvent 2, and  $N_3$  moles of solvent 3. The two solvents are partially miscible and form two liquid phases. The equilibrium distribution of these three components between the two resulting liquid phases (I and II) can be written for component i as follows using [Equations 2.84](#) and [2.99](#):

$$\gamma_i^I x_i^I f_i^I(T, P) = \gamma_i^{II} x_i^{II} f_i^{II}(T, P) \quad (2.150)$$

Now the pure component fugacities of component i are the same in phases I and II, since component i exists in the same state at the same temperature and pressure in each of the two phases. Therefore, [Equation 2.150](#) becomes

$$\gamma_i^I x_i^I = \gamma_i^{II} x_i^{II} \quad (2.151)$$

The ratio of the mole fractions of component i in the two phases is called the *distribution coefficient* ( $K_i$ ) and is defined as follows after rearranging [Equation 2.151](#):

$$K_i = \frac{x_i^I}{x_i^{II}} = \frac{\gamma_i^{II}}{\gamma_i^I} \quad (2.152)$$

It is important to remember that in liquid-liquid equilibrium problems, the solvents that form the two partially miscible liquid phases form highly nonideal solutions. Therefore, the activity coefficients of each component in each phase tend to be strong functions of the composition and need to be determined by multicomponent activity coefficient models that have the capability to describe liquid-liquid equilibrium problems as discussed in Poling et al. (2001).

In this type of problem, it is desired to determine the values of the mole fractions of the three components in the two liquid phases and the amounts of each phase, i.e.,  $N^I$  and  $N^{II}$ . For the three components and two phases, we therefore have eight unknowns, i.e., the six mole fractions and  $N^I$  and  $N^{II}$ . So, we need a total of eight relationships between these variables in order to obtain a solution. The equilibrium relationships ([Equation 2.152](#)) provide us with three equations and we can also write a mole balance for each component as

$$N_i = x_i^I N^I + x_i^{II} N^{II} \quad (2.153)$$

providing us with an additional three equations. In addition, we can use the fact that the mole fractions in each phase must sum to unity, i.e.,  $\sum_{i=1}^3 x_i^I = 1$  and  $\sum_{i=1}^3 x_i^{II} = 1$ . Solution of these eight equations provides the desired solution. However, it should be pointed out that this is a somewhat challenging problem to solve because of the strong nonlinear dependence of the activity coefficients on the composition of each phase.

The problem can be simplified by assuming that the two solvents are immiscible. Usually, solvents are selected to minimize their mutual solubility, so in a practical sense, this is a pretty good assumption. As given by [Equation 2.152](#), the distribution coefficient for the solute taken as component 1 will depend on the composition of each of the two phases. In many biological applications, the solute concentration is so low that the activity coefficients approach their infinite dilution values and the distribution coefficient is a constant. Also, since the solute is present in such a small amount, the values of  $N_2$  and  $N_3$  for solvents 2 and 3 are assumed to be constant and equal to  $N^I$  and  $N^{II}$ , respectively. With these assumptions, a mole balance on the solute can then be written as

$$N_1 = x_1^I N_2 + x_1^{II} N_3 \quad (2.154)$$

and with  $x_1^I = Kx_1^{II}$  from [Equation 2.152](#), we can solve for the mole fraction of the solute in phase II as follows:

$$x_1^{II} = \frac{N_1}{KN_2 + N_3} \quad (2.155)$$

### Example 2.17

The octanol-water partition coefficient ( $K_{OW}$ ) is frequently used to describe lipophilicity and to estimate the distribution of a drug between the aqueous and lipid regions of the body.  $K_{OW}$  is the same as the distribution coefficient described earlier with component 2 and phase I being the octanol phase and component 3 and phase II being the aqueous phase. Suppose we have 0.01 mol ( $N_1$ ) of drug dissolved in 100 mol of water ( $N_3$ ). The mole fraction of the drug in the aqueous phase is therefore equal to  $0.01 \times 100^{-1} = 10^{-4}$ . We then add to this phase 100 mol

(N<sub>2</sub>) of octanol. Estimate the mole fractions of the drug in the two phases once equilibrium has been attained. Also, determine the percent extraction of the drug from the aqueous phase. The octanol-water partition coefficient for the drug in this example is 89.

### Solution

Using [Equation 2.155](#), we can calculate the mole fraction of the drug in the aqueous phase once equilibrium has been reached:

$$x_1^{\text{II}} = \frac{0.01}{89 \times 100 + 100} = 1.11 \times 10^{-6}$$

The corresponding mole fraction of the drug in the octanol phase is given by [Equation 2.152](#):

$$x_1^{\text{I}} = Kx_1^{\text{II}} = 89 \times 1.11 \times 10^{-6} = 9.89 \times 10^{-5}$$

The percent extraction of the drug from the aqueous phase is calculated as

$$\% \text{Extraction} = \frac{N_1 - x_1^{\text{II}} N_3}{N_1} = \frac{0.01 - 1.11 \times 10^{-6} \times 100}{0.01} \times 100 = 98.89\%$$

**2.6.3.7 Single-stage solute extraction** Now, consider the situation shown in [Figure 2.6](#) where, e.g., a pure flowing solvent stream at molar flow rate L<sup>I</sup> is contacted in an extractor with an aqueous stream flowing at L<sup>II</sup> with a solute of mole fraction x<sub>in</sub><sup>II</sup>. Also, the solvent and water are immiscible, and we assume that the amount of solute is small, so there is no appreciable change in either L<sup>I</sup> or L<sup>II</sup>. Our mole balance on the solute can then be written as

$$L^{\text{II}} x_{\text{in}}^{\text{II}} = L^{\text{I}} x_{\text{out}}^{\text{I}} + L^{\text{II}} x_{\text{out}}^{\text{II}} \quad (2.156)$$

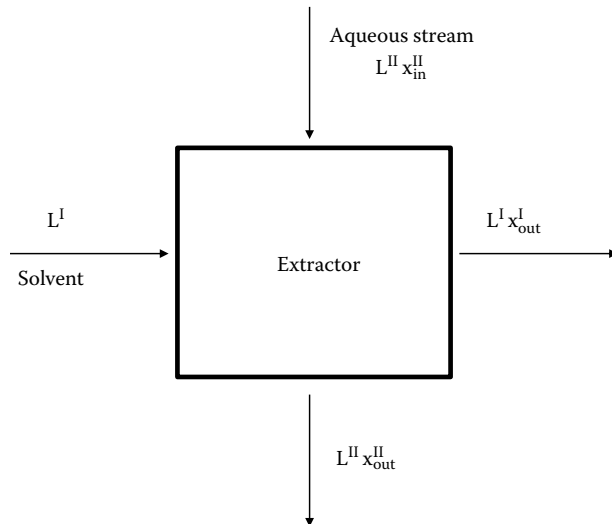


Figure 2.6 A single stage liquid-liquid extractor.

The streams exiting the extractor are at equilibrium, so from [Equation 2.152](#), we can write that  $x_{\text{out}}^{\text{I}} = Kx_{\text{out}}^{\text{II}}$ . Using this relationship in [Equation 2.156](#), we can solve for  $x_{\text{out}}^{\text{II}}$  as

$$\frac{x_{\text{out}}^{\text{II}}}{x_{\text{in}}^{\text{II}}} = \frac{1}{1+E} \quad (2.157)$$

where E is defined as the extraction factor, i.e.,  $E = L^{\text{I}}K/L^{\text{II}}$ . The percent extraction of the solute from the aqueous phase II is given by

$$\% \text{Extraction} = \left( 1 - \frac{x_{\text{out}}^{\text{II}}}{x_{\text{in}}^{\text{II}}} \right) \times 100 \quad (2.158)$$

### Example 2.18

Suppose a drug is in an aqueous stream flowing at  $100 \text{ mol min}^{-1}$  at a drug mole fraction of 0.01. The aqueous stream is then contacted within a single stage extractor with a solvent that is flowing at  $200 \text{ mol min}^{-1}$ . The solvent has a distribution coefficient of 6 for this particular drug. What is the equilibrium mole fraction of the drug in the streams exiting the extractor? What is the percent extraction of the drug from the aqueous stream entering the extractor?

### Solution

First, we find that the extraction factor is 12. Then, from [Equation 2.157](#), the mole fraction of the drug in the aqueous stream that leaves the extractor is

$$x_{\text{out}}^{\text{II}} = 0.01 \times \frac{1}{1+12} = 7.69 \times 10^{-4}$$

The mole fraction of the drug in the exiting solvent stream by [Equation 2.152](#) is

$$x_{\text{out}}^{\text{I}} = 6 \times 7.69 \times 10^{-4} = 4.62 \times 10^{-3}$$

and the percent extraction of the solute from [Equation 2.158](#) works out to be 92.3%.

**2.6.3.8 Multistage solute extraction** A percent extraction in [Example 2.18](#) of 92.3% results in the potential for loss of valuable product. Therefore, extraction is frequently carried out in a countercurrent multistage extractor. [Figure 2.7](#) illustrates this for N equilibrium stages of extraction. Since we again assume the phases are immiscible and the solute concentration is low, then  $L^{\text{I}}$  and  $L^{\text{II}}$  are constant within the extractor. In addition, the distribution coefficient K is also assumed to be constant. A solute mole balance around the dashed box enclosing stages 1–n of the extractor provides [Equation 2.159](#) for the mole fraction of the solute entering stage n in phase II:

$$x_{n+1}^{\text{II}} = \frac{L^{\text{I}}}{L^{\text{II}}} x_n^{\text{I}} + \frac{L^{\text{II}} x_n^{\text{II}} - L^{\text{I}} x_0^{\text{I}}}{L^{\text{II}}} \quad (2.159)$$

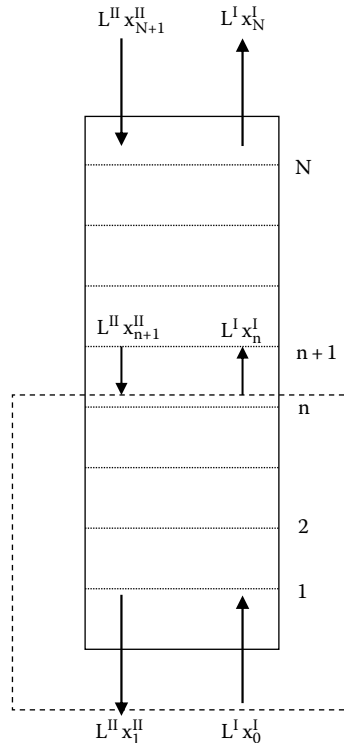


Figure 2.7 N stage liquid-liquid extractor.

The streams exiting stage  $n$  will be in equilibrium, so from [Equation 2.152](#), we can write that  $x_n^I = Kx_n^{II}$ , where  $K$  is the distribution coefficient. Substituting this result into [Equation 2.159](#) results in

$$x_{n+1}^{II} = Ex_n^{II} + x_1^{II} - \left( \frac{E}{K} \right) x_0^I \quad (2.160)$$

We can now use [Equation 2.160](#) in a stepwise manner to calculate successive values of  $x_{n+1}^{II}$  starting with stage 1. Note that in the following, we have also made use of the fact that we can replace  $x_0^I$  in [Equation 2.160](#) with  $Kx_e^{II}$ , where  $x_e^{II}$  is the solute concentration in phase II that would be in equilibrium with the solute concentration that enters in phase I. So for stage 1, we have that

$$n = 1 : \quad x_2^{II} = Ex_1^{II} + x_1^{II} - Ex_e^{II} = (E + 1)x_1^{II} - Ex_e^{II} \quad (2.161)$$

For stage 2, we can eliminate  $x_2^{II}$  by using [Equation 2.161](#), which then gives

$$n = 2 : \quad x_3^{II} = Ex_2^{II} + x_1^{II} - Ex_e^{II} = x_1^{II}(1 + E + E^2) - x_e^{II}(E + E^2)$$

and for stage 3, we obtain the following result after using the previous equation to eliminate  $x_3^{II}$ :

$$n = 3 : \quad x_4^{II} = x_1^{II}(1 + E + E^2 + E^3) - x_e^{II}(E + E^2 + E^3)$$

This equation can then be generalized for the  $n$ th stage with the following result:

$$x_{n+1}^{\text{II}} = x_1^{\text{II}} \left( 1 + E + E^2 + \dots + E^n \right) - x_e^{\text{II}} \left( E + E^2 + \dots + E^n \right) \quad (2.162)$$

Using [Equation 2.162](#), we can then write for stage N that

$$x_{N+1}^{\text{II}} = x_1^{\text{II}} \left( 1 + E + E^2 + \dots + E^N \right) - x_e^{\text{II}} \left( E + E^2 + \dots + E^N \right) \quad (2.163)$$

The summations in [Equation 2.163](#) are geometric progressions wherein the ratio of each successive term to the previous term is a constant, in this case E. The first series is then given by  $(1-E^{N+1})/(1-E)$ , and the second series is given by  $E(1-E^N)/(1-E)$ . Using these relationships for the series, [Equation 2.163](#) can then be written as

$$x_{N+1}^{\text{II}} = x_1^{\text{II}} \left( \frac{1-E^{N+1}}{1-E} \right) - x_e^{\text{II}} E \left( \frac{1-E^N}{1-E} \right) \quad (2.164)$$

In [Equation 2.164](#), e.g., phase II represents the aqueous phase, and we would know the incoming mole fraction of the solute, i.e.,  $x_{N+1}^{\text{II}}$ . Recall that  $x_e^{\text{II}} = x_0^{\text{I}}/K$  and we would also know the amount of solute in the solvent feed stream, i.e.,  $x_0^{\text{I}}$ . Therefore, for a given number of equilibrium stages (N), [Equation 2.164](#) can be solved to provide the amount of solute present in phase II as it exits the extractor, i.e.,  $x_1^{\text{II}}$ . If there is no solute in the entering solvent phase, then  $x_0^{\text{I}} = 0$  and we have that

$$\frac{x_1^{\text{II}}}{x_{N+1}^{\text{II}}} = \frac{E-1}{E^{N+1}-1} \quad (2.165)$$

The percent extraction of the solute from phase II is then given by

$$\% \text{Extraction} = \left( 1 - \frac{x_1^{\text{II}}}{x_{N+1}^{\text{II}}} \right) \times 100 \quad (2.166)$$

[Equation 2.164](#) can also be rearranged and solved to give the number of equilibrium stages (N) for specified solute mole fractions:

$$N = \frac{\ln \left( \frac{x_{N+1}^{\text{II}} - x_N^{\text{II}}}{x_1^{\text{II}} - x_e^{\text{II}}} \right)}{\ln E} \quad (2.167)$$

with  $x_N^{\text{II}} = x_N^{\text{I}}/K$  and  $x_e^{\text{II}} = x_0^{\text{I}}/K$ . The number of actual stages will be greater than that calculated from [Equation 2.167](#) since equilibrium is seldom achieved in each stage of the extractor. To find the actual number of stages, we can use the overall efficiency ( $\eta$ ) of an equilibrium stage defined as follows:

$$\eta = \frac{N}{N_{\text{actual}}} \quad (2.168)$$

Equilibrium stage efficiencies can be obtained from manufacturer's information on their extractor or from experimental data.

**Example 2.19**

Rework the previous example and determine the number of equilibrium and actual stages needed to achieve a 99.99% extraction of the drug from the aqueous phase. Assume that the efficiency of an equilibrium stage is 60%. Let phase II represent the aqueous phase and phase I the solvent. No solute is present in the solvent stream that enters the extractor.

**Solution**

From [Equation 2.166](#), we can calculate the mole fraction of the solute in the aqueous phase that exits the extractor:

$$x_1^{\text{II}} = \left(1 - \frac{\% \text{extraction}}{100}\right) x_{N+1}^{\text{II}} = (1 - 0.9999) 0.01 = 1 \times 10^{-6}$$

Next, we can write an overall solute mole balance around the extractor that can be used to solve for the mole fraction of the solute in the exiting solvent stream:

$$x_N^{\text{I}} = x_0^{\text{I}} + \left(\frac{L^{\text{II}}}{L^{\text{I}}}\right)(x_{N+1}^{\text{II}} - x_1^{\text{II}}) = 0 + \left(\frac{100}{200}\right)(0.01 - 1 \times 10^{-6}) = 4.9995 \times 10^{-3}$$

Next, we use [Equation 2.167](#) to find the number of equilibrium stages:

$$N = \frac{\ln\left(\frac{x_{N+1}^{\text{II}} - (x_N^{\text{I}}/K)}{x_1^{\text{II}} - (x_N^{\text{I}}/K)}\right)}{\ln E} = \frac{\ln\left(\frac{0.01 - (4.9995 \times 10^{-3})/6}{10^{-6}}\right)}{\ln 12} = 3.67 \approx 4$$

So we need 4 equilibrium stages or  $4/0.6 \approx 7$  actual stages.

**2.6.3.9 Vapor-liquid equilibrium** Vapor-liquid equilibrium plays an important role in understanding and designing separation processes that involve distillation, gas absorption, and the removal of solutes from liquids by contact with another gas stream, also known as stripping. These separation processes are widely used in the chemical process industry, and the design of these processes falls within the realm of chemical engineering. Here, we will illustrate vapor-liquid equilibrium calculations by determining the *bubble point* (boiling point) and *dew point* (condensation) temperatures of mixtures. We will also use these concepts to develop an understanding of the flammability or explosive limits of combustible materials.

Consider now the equilibrium distribution of N components at a given T and P between a vapor and a liquid. Our phase equilibrium relationship, i.e., [Equation 2.84](#), requires for component i that

$$\hat{f}_i^{\text{L}} = \hat{f}_i^{\text{V}} \quad (2.169)$$

For nonideal liquid solutions, an activity coefficient model is once again required to describe the behavior of the components of the liquid phase. For a nonideal liquid solution, we can then use the activity coefficient defined by [Equation 2.99](#), where  $\gamma_i = \hat{f}_i^{\text{L}} / x_i f_i^{\text{L}}$ , to calculate the fugacity of component i within the liquid phase:

$$\hat{f}_i^{\text{L}} = \gamma_i x_i f_i^{\text{L}}, \quad (2.170)$$

where  $f_i^L$  is the pure component liquid fugacity at the mixture T and P and is given by [Equation 2.95](#). In addition, at pressures considerably greater than atmospheric pressure, the vapor phase will deviate from that of an ideal gas, and a mixture equation of state is also needed to calculate the mixture fugacity coefficient of each species in the vapor phase as given by [Equation 2.74](#) (Poling et al., 2001). Recall from [Equation 2.71](#) that the component mixture fugacity coefficient is defined as  $\hat{\phi}_i = \hat{f}_i^V/y_i P$ , which also says that the fugacity of component i within a nonideal vapor mixture is given by

$$\hat{f}_i^V = y_i \hat{\phi}_i P \quad (2.171)$$

By [Equation 2.84](#), [Equations 2.170](#) and [2.171](#) are equal, so we can write [Equation 2.172](#), which expresses the equilibrium condition for each component i in the vapor-liquid mixture:

$$y_i \hat{\phi}_i P = \gamma_i x_i f_i^L \quad (2.172)$$

If the total pressure (P) and the component vapor pressures are on the order of atmospheric pressure, then we can usually treat the vapor phase as an ideal gas and set  $\hat{\phi}_i = 1$  and  $\phi_i^{\text{Sat}} = 1$ . Then, from [Equation 2.95](#), we also have for these conditions that the  $f_i^L \approx P_i^{\text{Sat}}$ . Therefore, we can write [Equation 2.172](#) as follows:

$$y_i P = \gamma_i x_i P_i^{\text{Sat}} = P_i \quad (2.173)$$

with  $P_i$  equal to the partial pressure of component i. Once again, we also have the constraint on the mole fractions that  $\sum_i x_i = \sum_i y_i = 1$ .

For an ideal liquid solution, we also have  $\gamma_i = 1$ , and then we have that

$$y_i P = x_i P_i^{\text{Sat}} = P_i \quad (2.174)$$

[Equation 2.174](#) is also known as *Raoult's law*, which shows that the partial pressure of a component ( $P_i = y_i P$ ) in an ideal liquid solution is equal to the product of its mole fraction and its vapor pressure.

Now, consider a liquid solution consisting of N components and mole fraction  $x_i$  for each component i. For a given pressure P, we can ask at what temperature would this liquid solution just start to boil, i.e., it first forms a vapor bubble? This temperature is known as the *bubble point temperature* and can be calculated as follows. When the liquid mixture is at its bubble point temperature, it is also referred to as a saturated liquid solution. Below the bubble point temperature, the liquid is a subcooled liquid.

First, we solve [Equation 2.172](#) for the equilibrium mole fraction of component i in the vapor bubble that is formed when the solution reaches the bubble point temperature:

$$y_i = \frac{\gamma_i x_i f_i^L}{\hat{\phi}_i P} \quad (2.175)$$

Since  $\sum_i y_i = 1$ , we then have [Equation 2.176](#), which can be solved to find the bubble point temperature:

$$\sum_i \frac{\gamma_i x_i f_i^L}{\hat{\phi}_i} = P \quad (2.176)$$

It is important to recognize that [Equation 2.176](#) depends on temperature through the terms that include the component liquid phase fugacities and the vapor phase fugacity coefficient. The activity coefficient may also have a temperature dependence. We then solve the nonlinear algebraic equation given by [Equation 2.176](#) for the temperature that makes the left-hand side of [Equation 2.176](#) equal to the pressure. This temperature is then known as the bubble point temperature or the boiling temperature of the liquid mixture. The composition of the first vapor bubble that is formed is then given by [Equation 2.175](#). If the liquid continues to boil, then the composition of the liquid and vapor phases will change as the more volatile components escape from the liquid to the vapor phase. This is the essence of distillation. The design of distillation processes falls within the study of staged processes and will not be considered here.

If the pressure is low, we can once again replace the liquid phase fugacity of each component with its vapor pressure and set the component mixture fugacity coefficient to one. If the liquid also forms an ideal solution, then the activity coefficients can also be set to unity. In this latter case, which is Raoult's law ([Equation 2.174](#)), we have for the bubble point temperature the requirement that

$$\sum_i x_i P_i^{\text{Sat}}(T) = P \quad (2.177)$$

The only temperature dependence remaining in [Equation 2.177](#) is in the component vapor pressures. [Equation 2.177](#) can then be solved for the bubble point temperature.

A similar analysis leads to the calculation of the dew point or condensation temperature of a vapor mixture of composition  $y_i$  for component  $i$ . When the vapor mixture is at its *dew point temperature*, it is also referred to as a saturated vapor. Above the dew point temperature, the vapor is referred to as superheated.

First, we solve [Equation 2.172](#) for the equilibrium mole fraction of component  $i$  in the first drop of liquid that is formed when the vapor is cooled to its dew point temperature:

$$x_i = \frac{\hat{\phi}_i y_i P}{\gamma_i f_i^L} \quad (2.178)$$

Since  $\sum_i x_i = 1$ , we then get [Equation 2.179](#), which can be solved to find the dew point temperature:

$$\sum_i \frac{\hat{\phi}_i y_i}{\gamma_i f_i^L} = \frac{1}{P} \quad (2.179)$$

where once again  $\hat{\phi}_i$ ,  $\gamma_i$ , and  $f_i^L$  will depend on the temperature. The temperature that satisfies [Equation 2.179](#) is then the dew point temperature of the vapor mixture. The composition of the liquid drop that is just formed is given by [Equation 2.178](#).

If the pressure is low, we can once again replace the liquid phase fugacity of each component with its vapor pressure and set the component mixture fugacity coefficient to one. If the liquid also forms an ideal solution, then the activity coefficients can also be set to unity. In this latter case, which is Raoult's law, we have that

$$\sum_i \frac{y_i}{P_i^{\text{Sat}}(T)} = \frac{1}{P} \quad (2.180)$$

The temperature dependence is only in the component vapor pressures, and [Equation 2.180](#) can then be solved for the dew point temperature.

### Example 2.20

Estimate the normal (i.e.,  $P = 1$  atmosphere) bubble point or boiling temperature of a liquid solvent solution consisting of 25 mol% benzene ( $C_6H_6$ , MW = 78.11,  $T_B = 353.3$  K), 45 mol% toluene ( $C_7H_8$ , MW = 92.14,  $T_B = 383.8$  K), and 30 mol% ethylbenzene ( $C_8H_{10}$ , MW = 106.17,  $T_B = 409.3$  K), where the chemical formula, molecular weight, and normal boiling point are given in parenthesis after each of the components. What is the composition of the vapor bubble that is formed at the bubble point temperature? The vapor pressures of these components are given by the Antoine vapor pressure equation (Reid et al., 1977) with the vapor pressure in mmHg and the temperature in Kelvin.

$$\ln P_{\text{benzene}}^{\text{Sat}} = 15.9008 - \frac{2788.51}{T - 52.36}$$

$$\ln P_{\text{toluene}}^{\text{Sat}} = 16.0137 - \frac{3096.52}{T - 53.67}$$

$$\ln P_{\text{ethylbenzene}}^{\text{Sat}} = 16.0195 - \frac{3279.47}{T - 59.95}$$

### Solution

Since these molecules are all chemically similar, we will assume that they form an ideal solution. [Equation 2.177](#) may therefore be used to calculate the bubble point temperature. The approach for solving this problem is as follows:

1. Assume a value of the bubble point temperature,  $T$ .
2. Calculate the vapor pressures for each component at  $T$ .
3. Calculate the  $\sum_i x_i P_i^{\text{Sat}} = \hat{P}$ .
4. If  $\hat{P} = P$ , which in this problem is 1 atm, then  $T$  is the bubble point temperature.
5. If  $\hat{P} > P$ , then the assumed  $T$  is too high; decrease  $T$  and go back to step 2.
6. If  $\hat{P} < P$ , then the assumed  $T$  is too low; increase  $T$  and go back to step 2.

After following the above-mentioned procedure, we obtain the following results:

$$\text{Bubble point temperature} = 377.81 \text{ K}$$

$$y_{\text{benzene}} = 0.503$$

$$y_{\text{toluene}} = 0.379$$

$$y_{\text{ethylbenzene}} = 0.118$$

Note the change in the distribution of the components between the liquid and the vapor bubble that is formed. Benzene, being the most volatile component, has a near twofold increase in its mole fraction, whereas ethylbenzene, being considerably less volatile than benzene, has its mole fraction in the vapor decreased by nearly a factor of three as compared to its composition in the liquid phase.

### Example 2.21

Repeat the above calculation, but this time, find the dew point temperature and the composition of the first drop of liquid that is formed.

#### Solution

Equation 2.180 may be used to calculate the dew point temperature. The approach for solving this problem is as follows:

1. Assume a value of the dew point temperature, T.
2. Calculate the vapor pressures for each component at T.
3. Calculate the  $\sum_i y_i / P_i^{\text{Sat}} = 1/\hat{P}$ .
4. If  $\hat{P} = P$ , which in this problem is 1 atm, then T is the dew point temperature.
5. If  $\hat{P} > P$ , then the assumed T is too high; decrease T and go back to step 2.
6. If  $\hat{P} < P$ , then the assumed T is too low; increase T and go back to step 2.

After following the above procedure, we obtain the following results:

$$\text{Dew point temperature} = 389.6 \text{ K}$$

$$y_{\text{benzene}} = 0.092$$

$$y_{\text{toluene}} = 0.382$$

$$y_{\text{ethylbenzene}} = 0.526$$

Note that the dew point temperature is greater than the bubble point temperature. This makes sense since if we first consider that we have a subcooled liquid of the given composition, then as we heat this liquid mixture, we will reach the bubble point temperature that we found in Example 2.20. Then, as we continue to add heat at constant pressure, we will vaporize more and more of the components in the liquid phase until, when we reach the dew point temperature, we have vaporized all of the components and we have a saturated vapor of the same composition as the original liquid mixture. As we continue heating, the temperature rises above the dew point temperature, and we have a superheated vapor.

**2.6.3.10 Flammability limits** Most manufacturing processes employ a variety of flammable substances. It is important that these materials be handled and processed in a safe manner in order to avoid fires and explosions that can have devastating consequences. The ignition, combustion, or explosion of flammable substances in air only occurs within a narrow range of composition called the *flammability limits*. Below a certain concentration of the flammable substance in air, the mixture is too “lean” to burn, while above a certain concentration, the mixture is too “rich” to burn. The flammable or explosive range lies within these limits. This is important in the design and operation of combustion engines, furnaces, and incinerators. It is also important from a safety viewpoint to prevent fires and explosions in manufacturing and other processes that involve the use or storage of flammable compounds.

A fire or explosion requires three elements: the fuel, a source of oxygen, and an ignition source. This is referred to as the *fire triangle*. The fuel can be the flammable substances in your manufacturing process. Oxygen is in the air and air certainly exists outside of your manufacturing equipment and may also be within your manufacturing process. Also, you can count on Mother Nature to provide the ignition source, although other likely ignition sources in a manufacturing facility can include hot surfaces and flames, sparks, unstable chemicals, and static electricity. Flammability limits for a large number of organic chemicals are available in the literature.

These flammability limits are provided as the lower and upper flammability (or explosion) limits. The upper (UFL) and lower flammability limit (LFL) is stated as the volume percent (which is the same as the mole percent) of the flammable chemical in air. If the flammable compound's volume percent or mole percent in air at a given T and P lies within the LFL to UFL range, then that mixture is ignitable or explosive. If the volume percent or mole percent of the flammable chemical in air is less than the LFL, or greater than the UFL, then that mixture is not ignitable or explosive.

[Table 2.2](#) summarizes from a variety of sources the LFL and UFL for some common chemicals in air. Note that different sources may give slightly different numbers than those reported in [Table 2.2](#).

For a flammable substance, it is important to remember that it is not the liquid that actually burns but the vapors that are produced from that liquid. In many cases involving the processing or storage of flammable chemicals, we can assume that the vapor and liquid phases are in equilibrium. We can then use our vapor liquid equilibrium calculations, as discussed earlier, to determine the equilibrium composition of the vapor phase. This vapor phase composition can then be compared to the flammability limits to determine whether or not there may be an issue regarding a fire or explosion. This type of calculation is illustrated in the next example.

Table 2.2 Flammability Limits of Some Common Substances  
in Air at Atmospheric Pressure

Chemical	Lower Flammability Limit, vol.% or mol%	Upper Flammability Limit, vol.% or mol%
Acetylene	2.5	100
Acetic acid	5.4	16.0
Acetone	2.6	13.0
Ammonia	15	28.0
Benzene	1.4	8.0
Ethanol	3.3	19.0
n-Butane	1.8	8.4
Methanol	6.7	36.0
Diethyl ether	1.9	36.0
Propane	2.1	9.5
Octane	1.0	6.5
Gasoline	1.3	7.6
Toluene	1.3	7.0
Hydrogen	4.0	75.0

**Example 2.22**

Consider the storage at ambient conditions (25°C and 1 atm) of a solvent such as benzene in a large storage tank in a manufacturing facility. Determine whether or not the vapor phase composition in this tank lies within the flammability limits for benzene.

**Solution**

In a closed and partially full storage tank, the vapor phase may be assumed to be in equilibrium with the liquid benzene, provided there have been no recent transfers of benzene into or out of the storage tank. At 25°C, the vapor pressure of benzene is 94.5 mmHg, using the vapor pressure equation previously used in [Example 2.20](#). From Raoult's law

$$P_{\text{benzene}} = P_{\text{benzene}} = P_{\text{benzene}}^{\text{Vap}} x_{\text{benzene}} = P_{\text{benzene}}^{\text{Vap}}$$

and the partial pressure of benzene in the vapor phase is 94.5 mmHg. Since the total pressure in the vapor space is 1 atm, this means that the partial pressure of air in the vapor space of the tank is  $760 - 94.5 \text{ mmHg} = 655.5 \text{ mmHg}$ . From Raoult's law, we can then calculate the mole fraction of benzene in the vapor space as

$$y_{\text{benzene}} = \frac{P_{\text{benzene}}^{\text{Vap}}}{P} = \frac{94.5 \text{ mmHg}}{760 \text{ mmHg}} = 0.1243$$

Therefore, the mole percent or volume percent of benzene in the vapor space is 12.4%. Comparing this value to the LFL and UFL values for benzene in [Table 2.2](#) indicates that the vapor space in the benzene storage tank at ambient conditions is not flammable or explosive assuming that the liquid and vapor phases are in equilibrium. However, nonequilibrium events, such as the removal of benzene from the tank will result in the addition of fresh air that will temporarily decrease the concentration of benzene in the vapor space from the above value until equilibrium is reestablished. It is possible during these transfer periods for the benzene concentration to fall within the flammability limits. In addition, for outside storage tanks, seasonal variations of temperature should also be considered. For example, at 40°F or 4.4°C, the vapor pressure of benzene decreases to 33.5 mmHg, giving at equilibrium a vapor phase benzene concentration of 4.4 mol% or 4.4 vol.%. Now, even at equilibrium, the vapor phase lies well within the flammability range. If an ignition source is present, then there is the possibility that this vapor mixture will be ignited and cause a fire or explosion.

[Example 2.22](#) illustrates that the storage of flammable substances can result in vapor mixtures that lie within the flammability range. In large storage tanks under these conditions, nitrogen gas is frequently supplied as a replacement rather than simply using ambient air. The use of nitrogen gas therefore eliminates the formation of flammable mixtures within a storage tank. For smaller tanks and portable containers for which this is not possible, it is important to make sure that these tanks and containers are properly grounded to eliminate static discharges that can serve as an ignition source. In addition, all vent openings into the tank or container can be fitted with flame arrestors to prevent the propagation of a fire from outside of the tank to inside the tank. Commercial flame arrestors are relatively simple and inexpensive devices made of screens or mesh-like materials with small openings on the order of a millimeter or so. The design and construction of flame arrestors is based

on the fact that flame propagation can be suppressed and eliminated if the flame has to pass through a large number of narrow openings. There exists a critical opening size below which the flame is quenched, and this is called the *quenching distance*. Quenching distances for a variety of flammable substances may be found in the combustion literature.

**2.6.3.11 Thermodynamics of surfaces** So far, we have discussed the thermodynamic properties of solutions containing solids, liquids, and gases. However, when two phases are in contact, a surface is formed at the interface. The surface that is formed may have properties that are quite different than the bulk phases. Understanding the thermodynamics of surfaces is important in many biomedical applications that involve the wetting of surfaces, as well as for understanding such processes as capillary flow and wicking.

Consider the differential increase in surface area ( $dA_S$ ) of a fluid of arbitrary shape. The Gibbs free energy change for this differential increase in the surface area may be written as follows:

$$dG = -SdT + VdP + \gamma dA_S \quad (2.181)$$

where the additional term  $\gamma dA_S$  represents the increase in the Gibbs free energy due to the change in the surface area  $dA_S$ . The *surface energy* is denoted by  $\gamma$  and is defined at constant T and P by

$$\gamma = \left( \frac{\partial G}{\partial A_S} \right)_{T,P} \quad (2.182)$$

For a pure component,  $\gamma$  is the same as the *surface tension*.

The surface energy acts as a restoring force that resists the addition of new surface area. At constant T and P, the work ( $dW$ ) required to change the surface area an amount  $dA_S$  is given by  $dW = \gamma dA_S$ . Typical units for the surface tension are dynes per centimeter and millinewton (mN) per meter. The surface tension of pure water in air at 25°C is about 72 mN m<sup>-1</sup>.

In order to develop some useful relationships, let us first consider a soap bubble. A soap bubble consists of a very thin spherical film of liquid. The film is relatively thick on a molecular level, so the innermost portion of the film acts like the bulk liquid. This film has two surfaces that are exposed to the outside atmosphere and the air trapped within the soap bubble. According to [Equation 2.181](#), at constant T and P, the soap bubble can decrease its free energy by decreasing its surface area. Hence, the bubble will decrease in size, placing more of the liquid film molecules in the innermost portion of the film. However, as the bubble shrinks in size, the internal pressure ( $P_B$ ) will increase until a point is reached where the soap bubble can shrink no further. At this point, the net force due to the pressure difference across the bubble film balances the forces in the surface of the bubble trying to shrink the bubble. An equilibrium state then occurs, and we can write that

$$\gamma dA_S = (P_B - P_A) A_S dr \quad (2.183)$$

The left-hand side of the [Equation 2.183](#) represents the work effect needed to expand or contract the bubble by an amount equal to  $dA_S$ . The right-hand side represents the net force acting on the surface  $A_S$ , and this force multiplied by the displacement of the interface,  $dr$ , is the work needed

to change the area of the bubble by an amount,  $dA_S$ . At equilibrium, [Equation 2.183](#) must be satisfied for any fluctuation in  $dA_S$ .

Recall that for a sphere of radius  $r$ , the surface area is  $4\pi r^2$ . For a soap bubble, there are two interfaces that have a change in area, the inside and outside surfaces of the liquid film, so  $dA_S$  in this case is equal to  $d(2 \times 4\pi r^2) = 16\pi r dr$ . For a droplet or a gas bubble, where we have either a drop of liquid suspended in a gas, or a gas bubble suspended in a liquid, there is only one interface and  $dA_S = d(4\pi r^2) = 8\pi r dr$ . Substituting in for  $dA_S$  and  $A_S$  in [Equation 2.183](#), we get [Equations 2.184](#) and [2.185](#) for the pressure difference  $P_B - P_A$ :

$$2 \text{ interfaces } P_B - P_A = \frac{4\gamma}{r} \quad (2.184)$$

$$1 \text{ interface } P_B - P_A = \frac{2\gamma}{r} \quad (2.185)$$

[Equations 2.184](#) and [2.185](#) are known as the *Laplace-Young* equation and shows that the excess pressure ( $P_B - P_A$ ) is inversely proportional to the radius of the bubble or the droplet. The radius  $r$  in the above equations is always considered to have its center of curvature in the phase in which  $P_B$  is measured. Hence, for a gas bubble in a liquid,  $P_B$  is the pressure within the bubble, which is then greater than the pressure ( $P_A$ ) in the liquid phase that surrounds the bubble.

### Example 2.23

Consider a droplet of water, 1  $\mu\text{m}$  in diameter, that is suspended in air at 1 atm and 25°C. What is the pressure of the water inside the droplet?

#### Solution

The center of curvature for the droplet of water lies within the droplet. Therefore,  $P_B$  represents the pressure within the droplet. Using [Equation 2.185](#) for the droplet, we have

$$P_B - 1 \text{ atm} = \frac{2 \times 72 \times 10^{-3} \text{ N m}^{-1}}{0.5 \times 10^{-6} \text{ m}} = 288,000 \text{ Pa} = 2.84 \text{ atm}$$

$$P_B = 3.84 \text{ atm}$$

Now, consider a liquid droplet suspended in its own vapor. The liquid and vapor phases are therefore in equilibrium. The Gibbs free energy for the droplet phase may be written as follows, assuming we have only a single component i:

$$dG = -SdT + VdP + \gamma dA_S + \mu_i^{(P)} dn_i \quad (2.186)$$

The chemical potential in this case is defined as  $\mu_i^{(P)} = (\partial G / \partial n_i)_{T, P, A_S, n_j}$ . Superscript P on the chemical potential denotes the fact that the transfer of  $dn_i$  moles does not change the surface area of the droplet, since in the above definition of the chemical potential,  $A_S$  is constant. The only way that this can occur is if  $\mu_i^{(P)}$  refers to the chemical potential of component i as a planar surface.

For a spherical droplet, the surface area of the droplet will depend on how much material is in the droplet. With  $v_i$  the molar volume of liquid  $i$ , we can then write that

$$dV = v_i dn_i = d\left(\frac{4}{3}\pi r^3\right) = 4\pi r^2 dr \quad (2.187)$$

Similarly, we can write for the surface area of the droplet that

$$dA_S = d(4\pi r^2) = 8\pi r dr = \frac{2dV}{r} = \frac{2v_i}{r} dn_i \quad (2.188)$$

Using [Equation 2.188](#), we can then rewrite [Equation 2.186](#) as

$$dG = -SdT + VdP + \left(\mu_i^{(P)} + \frac{2v_i\gamma}{r}\right)dn_i \quad (2.189)$$

The parenthetical term represents the chemical potential of component  $i$  as a droplet and takes into account the free energy change associated with changes in the droplet surface area.

Since the droplet is at equilibrium with its vapor at constant  $T$  and  $P$ , then we must have that

$$\mu_i^V = \mu_i^L = \mu_i^{(P)} + \frac{2v_i\gamma}{r} \quad (2.190)$$

From [Equation 2.56](#), we can write that

$$\mu_i^{L \text{ ideal gas}} = C_i(T) + RT \ln(P_i^{VAP}) \quad \text{and} \quad \mu_i^{(P) \text{ ideal gas}} = C_i(T) + RT \ln(P_i^{(P)VAP}) \quad (2.191)$$

where the  $y_i P$ , or the partial pressure for a pure component, would be the same as the vapor pressure by Raoult's law.  $C_i(T)$  is just a temperature-dependent constant that includes the reference state terms. Substituting the relationships in [Equation 2.191](#) into [Equation 2.190](#) provides the following result:

$$\ln\left(\frac{P_i^{VAP}}{P_i^{(P)VAP}}\right) = \frac{2v_i\gamma}{rRT} \quad (2.192)$$

This equation is also known as the *Kelvin equation* and shows that the vapor pressure of a small droplet of liquid of radius  $r$  is higher than the corresponding value as a planar layer of liquid. If the surface is concave toward the vapor side, e.g., a gas or vapor bubble in a liquid phase, then use a minus sign on the right-hand side of [Equation 2.192](#).

[Equation 2.192](#) shows that a swarm of liquid droplets of uniform radius at equilibrium with its vapor is unstable in terms of its radius. For example, if one droplet has a slight increase in its radius, then by [Equation 2.192](#), the vapor pressure of the droplet will decrease and there will be a corresponding transfer of mass from the vapor state to the liquid state, thereby increasing the size of the droplet and so on. On the other hand, if a droplet has a slight decrease in radius, then its vapor pressure will increase, and there will be transfer of mass from the liquid state to the vapor state, thereby decreasing the size of the droplet and so on. This means that in a mixture of droplets of different sizes, the larger droplets will grow at the expense of the smaller droplets, and this is the phenomenon that leads to the formation of clouds and rain.

**Example 2.24**

Consider a droplet of water, 1  $\mu\text{m}$  in diameter, that is suspended in air at 1 atm and 25°C. What is the vapor pressure of the water droplet? At 25°C, the vapor pressure of planar water is 3.166 kPa, and the molar volume of liquid water is 18.05  $\text{cm}^3 \text{ mol}^{-1}$ .

**Solution**

We can use [Equation 2.192](#) to calculate the vapor pressure of the droplet of water as

$$\ln\left(\frac{P_w^{\text{VAP}}}{P_w^{(P)\text{VAP}}}\right) = \frac{2 \times 18.05 \text{ cm}^3 \text{ mol}^{-1} \times 1 \text{ m}^3 (100 \text{ cm})^{-3} \times 72 \times 10^{-3} \text{ N m}^{-1}}{0.5 \times 10^{-6} \text{ m} \times 8.314 \text{ m}^3 \text{ N m}^{-2} \text{ mol}^{-1} \text{ K}^{-1} \times 298 \text{ K}} = 0.0021$$

$$P_w^{\text{VAP}} = e^{0.0021} \times 3.166 \text{ kPa} = 3.173 \text{ kPa}$$

**2.6.3.12 Equilibrium dialysis** In the laboratory, equilibrium dialysis is a useful method for studying the binding of a small molecule (called the *ligand*) to a much larger macromolecule such as a protein. An important example is determining by this method what fraction of a drug is bound to the proteins found in blood. Another important example of this, which we will study later in [Chapter 7](#), is the binding of oxygen with the protein hemoglobin that is found in the red blood cell. The equilibrium binding of oxygen with hemoglobin will depend on the partial pressure of oxygen ( $P_{\text{oxygen}} = y_{\text{oxygen}} P$ ) in the gas phase. In order to understand the oxygenation of tissue and to design blood oxygenators used in heart surgery, we need to know for a given partial pressure of oxygen how much oxygen is actually bound to the hemoglobin.

The simplest approach to performing equilibrium dialysis experiments is to form a membrane bag. The membrane bag can be formed by taking a membrane tube and tying off both ends. Usually, an aqueous solution containing the macromolecule of interest is placed within the membrane bag, and then the membrane bag is immersed into a well-stirred solution containing the ligand. Stirring the solution facilitates the transport of the ligand and shortens the time to reach equilibrium.

These experiments can also be performed within specially designed dialysis cells that consist of two well-stirred chambers separated by the dialysis membrane. Initially, one of these chambers holds a solution containing only the ligand, and the other chamber contains a solution of the macromolecule.

Equilibrium dialysis experiments employ semipermeable membranes. The membrane has small pores that are large enough to allow the free passage of the ligand and the solvent while retaining the macromolecules. The ligand then diffuses across the dialysis membrane into the solution containing the macromolecule. The ligand will then bind with the macromolecule, and this process continues until the system reaches a state of equilibrium. At equilibrium, we can use [Equation 2.84](#) to express the equilibrium of the ligand molecules (L) inside and outside the membrane bag:

$$\hat{f}_L^{\text{inside}} = \hat{f}_L^{\text{outside}} \quad (2.193)$$

Using [Equation 2.99](#), we can express the ligand fugacity in the solution inside and outside the membrane as

$$\gamma_L^{\text{inside}} x_L^{\text{inside}} f_L = \gamma_L^{\text{outside}} x_L^{\text{outside}} f_L \quad (2.194)$$

In this case, unlike for osmosis discussed earlier, the temperature and pressure inside and outside the membrane bag are the same, so the pure component ligand fugacity ( $f_L$ ) is the same in both regions. Also, the usual assumption is that the ligand forms an ideal solution; therefore, the ligand activity coefficients are equal to unity. Furthermore, assuming the ligand concentration is small, the ligand mole fractions may be approximated as  $x_L^{\text{inside}} = V_{\text{solvent}}^L C_L^{\text{inside}}$  and  $x_L^{\text{outside}} = V_{\text{solvent}}^L C_L^{\text{outside}}$ . With these substitutions into [Equation 2.194](#), the net result is that at equilibrium,  $C_L^{\text{inside}} = C_L^{\text{outside}}$ . The binding of the ligand to the macromolecule acts to concentrate the ligand inside the bag, even though at equilibrium, the concentrations of the ligand inside and outside the membrane bag are the same.

The goal of these equilibrium dialysis experiments is to develop an expression that describes, for a given concentration of ligand, the amount of ligand that is bound to the macromolecule. This requires in general that we know the equilibrium constant that describes the binding of the ligand to the macromolecule as well as the number of ligand binding sites per macromolecule. The simplest case is when the macromolecule has only a single site that can bind to the ligand. In this case, the binding of the ligand molecule (L) with the macromolecule (M) can be described by the following chemical equation:



where  $L \cdot M$  is the ligand-macromolecule complex.

Recall that the chemical equilibrium constant is defined in terms of the concentration of the ligand ( $C_L$ ), the free or unbound macromolecule concentration ( $C_M$ ), and the concentration of the ligand-macromolecule complex ( $C_{L \cdot M}$ ) and is given by

$$K = \frac{C_{L \cdot M}}{C_L C_M} \quad (2.196)$$

In order to calculate the value of K and the fraction of the macromolecules that are bound to the ligand, the above-mentioned concentrations need to be related to the measured ligand, macromolecule, and ligand-macromolecule complex concentrations. The total concentration of the macromolecule, i.e.,  $C_M^{\text{total}}$ , is known at the start of the experiment and this value is conserved over time within the membrane bag. At any time during the experiment,  $C_M^{\text{total}}$  is given by the sum of the free macromolecule concentration and that bound to the ligand by

$$C_M^{\text{total}} = C_M + C_{L \cdot M} \quad (2.197)$$

In a similar manner, the total amount of ligand inside the bag is the sum of the free ligand and that bound with the macromolecule as

$$C_L^{\text{total}} = C_L^{\text{inside}} + C_{L \cdot M} \quad (2.198)$$

where  $C_L^{\text{inside}}$  is the concentration of unbound ligand inside the membrane bag, which at equilibrium, is the same as that outside the membrane bag, i.e.,  $C_L = C_L^{\text{inside}} = C_L^{\text{outside}}$ . In terms of the previous definitions, it can be shown that the equilibrium constant (K) is then given by the following equation:

$$K = \frac{C_{L \cdot M}}{C_L (C_M^{\text{total}} - C_{L \cdot M})} \quad (2.199)$$

To facilitate the use of [Equation 2.199](#), it is convenient to define the fraction of the macromolecules ( $f$ ) that are bound to the ligand. This is given by

$$f \equiv \frac{C_{L \cdot M}}{C_{L \cdot M} + C_M} \quad (2.200)$$

Combining [Equations 2.199](#) and [2.200](#), the following equations are obtained for the relationship between  $f$  and  $K$ :

$$K = \frac{f}{(1-f)C_L} \quad \text{and} \quad f = \frac{KC_L}{1+KC_L} \quad (2.201)$$

These equations then provide the relationship between the ligand concentration, the equilibrium constant, and the fraction of the macromolecules that are bound to the ligand at equilibrium. The previous expressions can also be rearranged into a convenient form for data analysis as shown by the following equation:

$$\frac{f}{C_L} = K(1-f) = K - Kf \quad (2.202)$$

[Equation 2.202](#) is known as the *Scatchard equation* and shows that for a given ligand concentration ( $C_L$ ), if one determines the fraction of macromolecules that are bound to the ligand ( $f$ ), then a plot of  $f/C_L$  versus  $f$  should be linear with a slope equal to  $-K$  and an intercept equal to  $K$ .

The use of [Equation 2.202](#) is illustrated in the following example for the binding of oxygen to myoglobin. Myoglobin is an oxygen-binding protein found in muscles that store oxygen molecules and release the oxygen when the oxygen partial pressure becomes low, e.g., during strenuous exercise. Myoglobin has only one site available for the binding of oxygen. The absorption spectra of myoglobin bound to oxygen is different than that for free myoglobin and this can be used to determine, at a given partial pressure of oxygen, the fraction of myoglobin that is bound to oxygen.

### Example 2.25

The following data express the fractional binding of oxygen to myoglobin as a function of the partial pressure of oxygen. From these data, determine the value of the equilibrium constant for the binding of oxygen to myoglobin. Also, determine the  $P_{50}$ , which is the partial pressure of oxygen where the fractional binding of the myoglobin molecules is 50%.

Oxygen Partial Pressure, $pO_2$ , mmHg	Fraction of Myoglobin Bound to Oxygen, $f$
0.5	0.25
1.0	0.40
1.5	0.50
2.0	0.61
2.5	0.65
4.5	0.76
6.0	0.8

Source: Tinoco, I. et al., *Physical Chemistry: Principles and Applications in Biological Sciences*, 4th ed., Prentice-Hall, Inc., New York, 2001.

**Solution**

Since the  $pO_2$  of oxygen is related to the dissolved oxygen concentration ( $C_{\text{oxygen}}$ ) by Henry's law (see [Example 2.14](#), i.e.,  $pO_2 = HC_{\text{oxygen}}$ ), we can first rewrite [Equation 2.202](#) as follows, where  $H$  is Henry's constant:

$$\frac{f}{pO_2} = \frac{K}{H} - \frac{K}{H} f$$

$P_{50}$  is that value of the partial pressure of oxygen where one-half of the myoglobin molecules are bound to oxygen (i.e.,  $f = 0.5$ ). In terms of the  $P_{50}$ , it is easy to show using the previous equation that  $K/H = 1/P_{50}$ . Our regression equation in terms of  $P_{50}$  then becomes

$$\frac{f}{pO_2} = \frac{1}{P_{50}} - \frac{f}{P_{50}} \quad \text{and} \quad f = \frac{pO_2}{P_{50} + pO_2}$$

Performing a linear regression on the data given in the table, according to the previous equation on the left, we find that the  $P_{50}$  based on the average of the values obtained from the slope and the intercept is equal to 1.53 mmHg. We see in [Figure 2.8](#) that the previous equation on the right for  $f$  with the value of  $P_{50}$  found from the regression of the data provides an excellent fit to these data on oxygen binding to myoglobin.

In many cases, a macromolecule may have several binding sites for the ligand. In the general case, there are  $N$  sites available and it is also assumed that these sites are independent and have the same affinity for the ligand. This means that the binding of a ligand at a particular site has no effect on the binding of ligand at the other sites on the macromolecule. Each of these sites are therefore

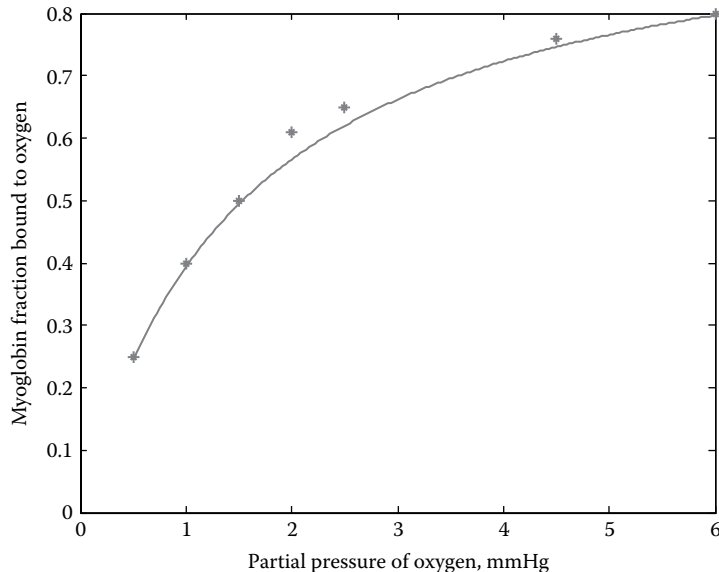


Figure 2.8 Binding of oxygen to myoglobin.

independent, and they will have the same ligand equilibrium constant  $K$ . The binding of ligand to the  $i$ th site on the macromolecule is given by the following equilibrium equation:



We can then let  $\phi_i$  be defined as the fraction of site  $i$  on the macromolecules that are bound to the ligand. This is given by

$$\phi_i = \frac{C_{L \cdot M_i}}{C_{M_i} + C_{L \cdot M_i}} \quad (2.204)$$

The equilibrium constant for the binding of the ligand to site  $i$  is given by

$$K = \frac{C_{L \cdot M_i}}{C_L C_{M_i}} \quad (2.205)$$

[Equations 2.204](#) and [2.205](#) can then be combined to give the following equation for the fraction of site  $i$  that is bound to the ligand:

$$\phi_i = \frac{KC_L}{1 + KC_L} \quad (2.206)$$

This equation can then be summed over all  $N$  sites on the macromolecule, recognizing that  $f = \sum_{i=1}^N \phi_i$ , where  $f$  is given by [Equation 2.200](#) and defines the moles of ligand bound per mole of macromolecule, which is also the same as the average number of ligand molecules that are bound to a macromolecule. The result is that  $f$  is given by [Equation 2.207](#) for the case of a macromolecule containing  $N$  identical and independent ligand binding sites:

$$f = \frac{NKC_L}{1 + KC_L} \quad (2.207)$$

For ease of data analysis, this equation can be rearranged as

$$\eta = \frac{f}{C_L} = K(N - f) = KN - Kf \quad (2.208)$$

This is the *Scatchard equation* for  $N$  binding sites on a macromolecule, which are all identical and independent. [Equation 2.208](#) shows that for a given ligand concentration ( $C_L$ ), if one determines the moles of ligand that are bound to a mole of macromolecule ( $f$ ), then a plot of  $\eta = f/C_L$  versus  $f$  should be linear with a slope equal to  $-K$  and a  $y$  intercept equal to  $NK$ , or an  $x$  intercept of  $N$ .

If the plot of the data based on [Equation 2.208](#) is not linear, then this is an indication that the binding sites for the ligand are not identical or not independent. For example, an important case where the Scatchard equation does not apply is the binding of oxygen to hemoglobin. Although hemoglobin has four oxygen binding sites, these sites are not independent and exhibit what is known as *cooperative binding*.\* As we will discuss in [Chapter 7](#), the binding of oxygen to hemoglobin enhances the

---

\* See [Section 7.2](#).

binding of additional oxygen molecules. In [Chapter 7](#), we will develop an equation that can be used to describe cooperative binding.

The use of [Equation 2.208](#) is illustrated in the following example for the binding of Mg-ATP (a complex of Mg and ATP) to the enzyme tetrahydrofolate synthetase.

### Example 2.26

The data shown in the following table express the binding of Mg-ATP complex to the enzyme tetrahydrofolate synthetase in terms of  $f$  and  $f/C_{\text{Mg-ATP}}$ . The enzyme consists of four identical subunits. From these data, determine the value of the equilibrium constant ( $K$ ) for the binding of Mg-ATP complex to this enzyme and show that the number of binding sites ( $N$ ) on the enzyme is consistent with there being one Mg-ATP binding site on each subunit of the enzyme.

$f$ , Fraction of Mg-ATP Bound to Enzyme	$f/C_{\text{Mg-ATP}}$
0.8	45,500
1.0	49,000
1.1	40,000
1.7	32,000
1.75	37,000
2.0	24,000
2.05	29,000
2.8	19,000
3.1	15,500
3.2	12,000
3.45	10,000
3.55	12,500
3.7	9,500
3.9	8,000

*Source:* Tinoco, I. et al., *Physical Chemistry: Principles and Applications in Biological Sciences*, 4th ed., Prentice-Hall, Inc., New York, 2001.

### Solution

Performing a linear regression on the data given in the table according to [Equation 2.208](#), we find that the value of  $K$  based on the slope is equal to  $1.29 \times 10^4 \text{ M}^{-1}$ . The number of binding sites  $N$  on the enzyme for the Mg-ATP complex is 4.33, which is consistent with the enzyme being comprised of four identical subunits. We also see in [Figure 2.9](#) that regression of the data according to [Equation 2.208](#) provides an excellent fit to these data on the binding of Mg-ATP to the enzyme.

**2.6.3.13 The Gibbs-Donnan effect** Now, consider a macromolecule in an aqueous solution with a concentration of  $C_M$ . The macromolecule is separated by a semipermeable membrane from

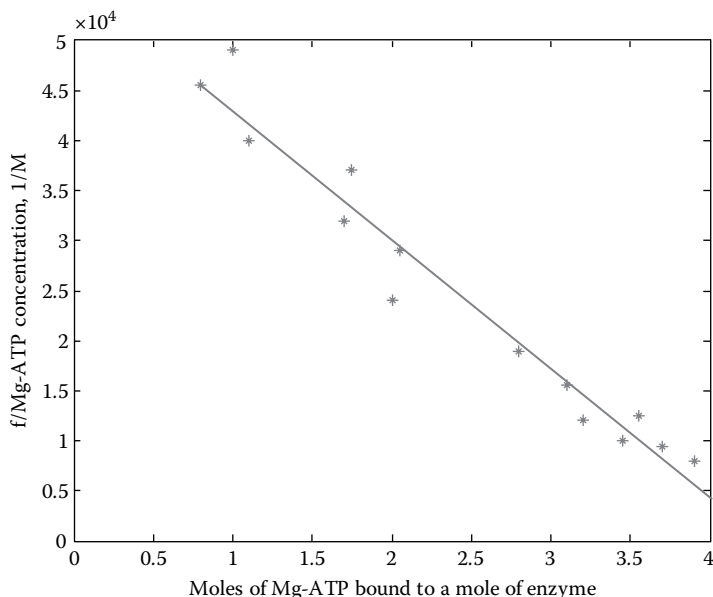


Figure 2.9 Binding of Mg-ATP to tetrahydrofolate synthetase.

another aqueous solution containing a strong electrolyte,\* such as NaCl. Only the ions formed from the strong electrolyte are free to cross the semipermeable membrane. These ions, in this case  $\text{Na}^+$  and  $\text{Cl}^-$ , will freely cross the semipermeable membrane and interact in a complex way with the macromolecule. The result will be that, depending on the solution pH, these ions along with the  $\text{H}^+$  will bind with the macromolecule with the result that the macromolecule will carry a net charge,  $Z_M$ .

The net charge of the macromolecule will create, at equilibrium, an uneven distribution of these small ions between the region that contains the macromolecule and the region on the other side of the semipermeable membrane that does not have the macromolecule. This difference in the concentrations of these ions will then create an osmotic pressure difference across the semipermeable membrane because the “solvent” on the macromolecule side of the semipermeable membrane is not the same as the “solvent” on the opposite side of the semipermeable membrane. This means that when finding the osmotic pressure of the macromolecule in an electrolyte solution, we will need to correct for what is known as the Gibbs-Donnan effect. Here, we will find an expression that allows for the calculation of this correction to the osmotic pressure of a macromolecule in a solution with a 1:1 electrolyte like NaCl.

The solution that is opposite or *outside* the solution containing the macromolecule must remain electrically neutral. If  $C_{\text{NaCl}}^{\text{outside}}$  is the total concentration of NaCl in the outside solution, then electrical neutrality of this solution requires that

$$C_{\text{NaCl}}^{\text{outside}} = C_{\text{Na}^+}^{\text{outside}} = C_{\text{Cl}^-}^{\text{outside}} \quad (2.209)$$

\* A strong electrolyte is a substance that completely dissociates into charged ions when placed in water.

The semipermeable membrane allows the transport of NaCl, so when equilibrium occurs between the *inside* macromolecule-containing solution and the *outside* solution that is free of macromolecule, we can use [Equation 2.82](#) and write this equilibrium for NaCl as

$$\mu_{\text{NaCl}}^{\text{inside}} = \mu_{\text{NaCl}}^{\text{outside}} \quad (2.210)$$

Since NaCl is a strong electrolyte, [Equation 2.210](#) can also be rewritten using [Equation 2.70](#) in terms of Na<sup>+</sup> and Cl<sup>-</sup>, where use is made of the fact that  $\mu_{\text{NaCl}} = \mu_{\text{Na}^+} + \mu_{\text{Cl}^-}$ ; therefore

$$\begin{aligned} & \left( G_{\text{Na}^+}^{\text{inside}} + G_{\text{Cl}^-}^{\text{inside}} \right) + RT \ln \left( \frac{\hat{f}_{\text{Na}^+}^{\text{inside}}}{f_{\text{Na}^+}} \right) + RT \ln \left( \frac{\hat{f}_{\text{Cl}^-}^{\text{inside}}}{f_{\text{Cl}^-}} \right) \\ &= \left( G_{\text{Na}^+}^{\text{outside}} + G_{\text{Cl}^-}^{\text{outside}} \right) + RT \ln \left( \frac{\hat{f}_{\text{Na}^+}^{\text{outside}}}{f_{\text{Na}^+}} \right) + RT \ln \left( \frac{\hat{f}_{\text{Cl}^-}^{\text{outside}}}{f_{\text{Cl}^-}} \right) \end{aligned} \quad (2.211)$$

In this equation, the pure component value of the Gibbs free energy and the fugacity for each pure species are the same on the inside and the outside solutions, since these are both at the same temperature and pressure. We can also make use of the fact from [Equation 2.99](#) that  $\hat{f}_i = \gamma_i x_i f_i$ . Hence, [Equation 2.211](#) becomes

$$\ln \left( x_{\text{Na}^+}^{\text{inside}} \gamma_{\text{Na}^+}^{\text{inside}} \right) + \ln \left( x_{\text{Cl}^-}^{\text{inside}} \gamma_{\text{Cl}^-}^{\text{inside}} \right) = \ln \left( x_{\text{Na}^+}^{\text{outside}} \gamma_{\text{Na}^+}^{\text{outside}} \right) + \ln \left( x_{\text{Cl}^-}^{\text{outside}} \gamma_{\text{Cl}^-}^{\text{outside}} \right) \quad (2.212)$$

If it is also assumed that  $\gamma_i^{\text{inside}} \approx \gamma_i^{\text{outside}}$  and  $x_i^{\text{inside}} = V_{\text{solvent}}^L C_i^{\text{inside}}$  and  $x_i^{\text{outside}} = V_{\text{solvent}}^L C_i^{\text{outside}}$ , then [Equation 2.212](#) can be shown to simplify to the following result:

$$C_{\text{Na}^+}^{\text{inside}} C_{\text{Cl}^-}^{\text{inside}} = C_{\text{Na}^+}^{\text{outside}} C_{\text{Cl}^-}^{\text{outside}} = (C_{\text{NaCl}}^{\text{outside}})^2 \quad (2.213)$$

This equation can then be solved for the Cl<sup>-</sup> concentration in the inside solution containing the macromolecule as

$$C_{\text{Cl}^-}^{\text{inside}} = \frac{(C_{\text{NaCl}}^{\text{outside}})^2}{C_{\text{Na}^+}^{\text{inside}}} \quad (2.214)$$

If the macromolecule is positively charged, then the electroneutrality of the inside solution will require that the following equation be satisfied:

$$C_{\text{Cl}^-}^{\text{inside}} = Z_M C_M + C_{\text{Na}^+}^{\text{inside}} \quad (2.215)$$

whereas if the macromolecule is negatively charged, then

$$C_{\text{Cl}^-}^{\text{inside}} = -Z_M C_M + C_{\text{Na}^+}^{\text{inside}} \quad (2.216)$$

When  $Z_M > 0$ , Equations 2.214 and 2.215 can then be combined to obtain the following expression for the equilibrium concentration of  $\text{Na}^+$  in the solution containing the macromolecule:

$$C_{\text{Na}^+}^{\text{inside}} = \frac{-Z_M C_M + \sqrt{(Z_M C_M)^2 + 4(C_{\text{NaCl}}^{\text{outside}})^2}}{2} \quad (2.217)$$

Of particular interest is the ratio of the ion concentrations for the inside and outside solutions. By letting  $r = C_{\text{Na}^+}^{\text{inside}} / C_{\text{Na}^+}^{\text{outside}} = C_{\text{Na}^+}^{\text{inside}} / C_{\text{NaCl}}^{\text{outside}}$ , Equation 2.217 may be rewritten in terms of  $r$ :

$$r = \frac{-Z_M C_M}{2C_{\text{NaCl}}^{\text{outside}}} + \sqrt{\left(\frac{Z_M C_M}{2C_{\text{NaCl}}^{\text{outside}}}\right)^2 + 1} \quad (2.218)$$

The ratio of the  $\text{Cl}^-$  concentrations inside and outside can also be shown to be related to  $r$  where  $C_{\text{Cl}^-}^{\text{inside}} / C_{\text{Cl}^-}^{\text{outside}} = 1/r$ .

Equation 2.218 shows that for a macromolecule with no charge, the value of  $r = 1$ , and the  $\text{Na}^+$  and  $\text{Cl}^-$  ion concentrations inside and outside at equilibrium are the same as expected. However, for a macromolecule with a very large positive charge, Equation 2.218 shows that for this case,  $r \rightarrow 0$ , which means that the  $\text{Na}^+$  are excluded from the inside solution due to the excessive positive charge carried by the macromolecule. This also means that the  $\text{Cl}^-$  concentration in the inside solution is much larger than that on the outside, and this occurs in order to offset the positive charge of the macromolecule and makes the inside solution electrically neutral. In general, for a positively charged macromolecule within the inside solution,  $r < 1$  and  $C_{\text{Na}^+}^{\text{inside}} < C_{\text{Na}^+}^{\text{outside}}$  and  $C_{\text{Cl}^-}^{\text{inside}} > C_{\text{Cl}^-}^{\text{outside}}$ .

This unequal distribution of the  $\text{Na}^+$  and  $\text{Cl}^-$  at equilibrium is due to the presence of the charged macromolecule, and this is called the *Gibbs-Donnan effect*. This unequal distribution of these ions also means that the osmotic pressure of the “solvent” on the inside and the outside solutions are not the same.

A similar analysis for a negatively charged macromolecule leads to the following expression for the value of  $r$ :

$$r = \frac{Z_M C_M}{2C_{\text{NaCl}}^{\text{outside}}} + \sqrt{\left(\frac{Z_M C_M}{2C_{\text{NaCl}}^{\text{outside}}}\right)^2 + 1} \quad (2.219)$$

where  $Z_M < 0$ . Also, the ratio of the  $\text{Cl}^-$  concentrations inside and outside is given by  $C_{\text{Cl}^-}^{\text{inside}} / C_{\text{Cl}^-}^{\text{outside}} = 1/r$ . Once again, if the macromolecule contains no charge, then from Equation 2.219,  $r = 1$ , and the  $\text{Na}^+$  and  $\text{Cl}^-$  ion concentrations inside and outside at equilibrium are the same as expected. However, for a macromolecule with a very large negative charge, Equation 2.219 shows for this case that  $r \gg 1$ , which means that the  $\text{Na}^+$  are concentrated in the inside solution due to the excessive negative charge carried by the macromolecule, and this occurs in order to offset the negative charge of the macromolecule and make the inside solution electrically neutral. This also means that the  $\text{Cl}^-$  concentration in the inside solution is much smaller than that on the outside. In general, for a negatively charged macromolecule within the inside solution,  $r > 1$  and  $C_{\text{Na}^+}^{\text{inside}} > C_{\text{Na}^+}^{\text{outside}}$  and  $C_{\text{Cl}^-}^{\text{inside}} < C_{\text{Cl}^-}^{\text{outside}}$ .

Using the previous relationships, we can now calculate the osmotic pressure of the macromolecule contained in the inside solution in the presence of a 1:1 electrolyte like NaCl. The following analysis assumes ideal solution behavior of both the inside and outside solutions at equilibrium. Assuming the macromolecule carries a positive charge,  $Z_M$ , we can write the osmotic pressure of the macromolecule solution as

$$\Pi = \left( RTC_M^{\text{inside}} + RTC_{\text{Na}^+}^{\text{inside}} + RTC_{\text{Cl}^-}^{\text{inside}} \right) - \left( RTC_{\text{Na}^+}^{\text{outside}} + RTC_{\text{Cl}^-}^{\text{outside}} \right) \quad (2.220)$$

The first parenthetical term on right-hand side of this equation is the ideal osmotic pressure (see [Equation 2.147](#)) due to the macromolecule and the  $\text{Na}^+$  and  $\text{Cl}^-$  ions that are present in the inside solution. The second parenthetical term in [Equation 2.220](#) is the osmotic pressure of the outside solution due to the  $\text{Na}^+$  and  $\text{Cl}^-$  ions. Note that if there is no electrolyte present, then the previous equation simplifies to  $\Pi = RTC_M^{\text{inside}}$ , as expected. From [Equation 2.220](#), we see then that this quantity,  $RT \left[ \left( C_{\text{Na}^+}^{\text{inside}} + C_{\text{Cl}^-}^{\text{inside}} \right) - \left( C_{\text{Na}^+}^{\text{outside}} + C_{\text{Cl}^-}^{\text{outside}} \right) \right]$ , is the correction to the osmotic pressure of the macromolecule as a result of the Gibbs-Donnan effect.

Using [Equation 2.215](#) to replace  $C_{\text{Cl}^-}^{\text{inside}}$  and replacing  $C_{\text{Na}^+}^{\text{inside}}$  with  $C_{\text{NaCl}}^{\text{outside}}$  using the definition of  $r$ , and then substituting for  $r$  using [Equation 2.118](#), the previous equation after some algebra becomes

$$\Pi = RTC_M^{\text{inside}} + RT \left\{ 2 \left[ \left( \frac{Z_M C_M}{2} \right)^2 + \left( C_{\text{NaCl}}^{\text{outside}} \right)^2 \right]^{1/2} - 2 C_{\text{NaCl}}^{\text{outside}} \right\} \quad (2.221)$$

The same result is obtained for a negatively charged macromolecule.

[Equation 2.221](#) gives the osmotic pressure of a macromolecule in a 1:1 electrolyte solution like NaCl. The first term on the right-hand side of this equation is the ideal osmotic pressure of the macromolecule based on van't Hoff's equation, i.e., [Equation 2.147](#). The second term on the right-hand side of [Equation 2.221](#) is the correction to this osmotic pressure as a result of the Gibbs-Donnan effect. At high concentrations of the salt, i.e.,  $C_{\text{NaCl}}^{\text{outside}}$ , or values of the macromolecule charge,  $Z_M$ , approaching zero, the term representing the Gibbs-Donnan effect in [Equation 2.221](#) becomes negligible. This means that the "solvent" on each side of the semipermeable membrane is the same.

### Example 2.27

Vilker et al. (1981) measured the osmotic pressure of solutions of the protein bovine serum albumin in solutions containing NaCl. Their experiments were conducted in an osmometer at a temperature of 25°C. In one experiment, the solution pH was 7.4 and the NaCl concentration, i.e.,  $C_{\text{NaCl}}^{\text{outside}}$ , was equal to 0.15 M. For an albumin concentration of 84 grams per liter, the osmotic pressure was found to be 48 mmHg. How does this measured value of the osmotic pressure compare to the value predicted by [Equation 2.221](#)? At a pH of 7.4, they also showed that the net charge on an albumin molecule is  $-20.5$ . The molecular weight of the bovine serum albumin is  $69,000 \text{ g mol}^{-1}$ .

**Solution**

With  $Z_M = -20.5$ ,  $C_M = 84 \text{ g L}^{-1} \times 1 \text{ mol} (69,000 \text{ g})^{-1} = 0.0012 \text{ M}$ , and  $C_{\text{NaCl}}^{\text{outside}} = 0.15 \text{ M}$ , then from [Equation 2.221](#), it is found that

$$\Pi = 0.0821 \text{ L atm mol}^{-1} \text{ K}^{-1} \times 298 \text{ K} \times 0.0012 \text{ mol L}^{-1} + \dots$$

$$0.0821 \text{ L atm mol}^{-1} \text{ K}^{-1} \times 298 \text{ K} \left\{ 2 \left[ \left( \frac{-20.5 \times 0.0012}{2} \right)^2 + 0.15^2 \right]^{1/2} - 2 \times 0.15 \right\} \text{ mol L}^{-1}$$

$$\Pi = 0.0294 \text{ atm} + 0.0246 \text{ atm} = 0.054 \text{ atm} \times 760 \text{ mmHg atm}^{-1} = 41.067 \text{ mmHg}$$

We see in this calculation that the correction to the ideal osmotic pressure of albumin due to the Gibbs-Donnan effect, i.e., 0.0246 atm, is comparable in magnitude to the ideal osmotic pressure of albumin, i.e., 0.0294 atm. However, this predicted value of the ideal osmotic pressure for albumin at these conditions is about 14% less than the measured value, and this is because at this albumin concentration, the albumin solution behavior is nonideal. [Problem 2.50](#) in the chapter problems shows how to handle the nonideal behavior of albumin at these concentrations.

**Example 2.28**

In [Example 2.27](#), the concentration of the macromolecule is 0.0012 M. The macromolecule also carries a net negative charge of  $-20.5$  at the given solution pH. The NaCl concentration in the solution is 0.15 M. Calculate the ratio of the concentration of the  $\text{Na}^+$  in the solution containing the macromolecule (inside) to that in the solution outside. Also find the ratio of the concentration of the  $\text{Cl}^-$  inside to that outside.

**Solution**

With  $Z_M = -20.5$ ,  $C_M = 0.0012 \text{ M}$ , and  $C_{\text{NaCl}}^{\text{outside}} = 0.15 \text{ M}$ , then from [Equation 2.219](#), it is found that

$$r = \frac{20.5 \times 0.0012 \text{ M}}{2 \times 0.15 \text{ M}} + \sqrt{\left( \frac{20.5 \times 0.0012 \text{ M}}{2 \times 0.15 \text{ M}} \right)^2 + 1} = 1.0854$$

Therefore, the ratio of the  $\text{Na}^+$  concentration inside with the macromolecule to that outside is 1.0854, and the ratio of  $\text{Cl}^-$  inside to that outside is  $1/r = 0.9214$ .

Although the solutions on the inside and the outside are electrically neutral, there is, as shown in [Example 2.28](#), an unequal distribution of the ions, which is caused by the charged macromolecules in the inside solution. For example, in [Example 2.28](#), the  $\text{Na}^+$  are concentrated inside to counter the negative charges on the macromolecules. The  $\text{Cl}^-$  are repulsed by the negative charges on the macromolecules and are concentrated in the solution that is outside. This means that there is a concentration gradient of  $\text{Na}^+$  that would tend to cause these ions to diffuse from the inside solution to the outside solution. Similarly, a concentration gradient of  $\text{Cl}^-$  is also formed, which would tend to cause

these ions to diffuse from outside the bag to the inside. To counter these concentration gradients, at equilibrium, there exists an attractive electrical force caused by the negative charges of the macromolecules that counters the loss of these  $\text{Na}^+$  from the inside solution due to the presence of their concentration gradient. These same negative charges on the macromolecule oppose the diffusion of the  $\text{Cl}^-$  from the solution outside to the inside solution containing the macromolecule. This transmembrane electrical potential is known as the *Donnan potential* and is described in the next section.

**2.6.3.14 Donnan potential** We can obtain an equation that relates the equilibrium membrane potential ( $V$ ), i.e., the difference in electrical potential between the inside ( $V_{\text{inside}}$ ) and the outside ( $V_{\text{outside}}$ ) solutions, to the equilibrium concentrations of the ions on either side of the semipermeable membrane. The presence of an electrical field across the membrane will produce a force on the ions as a result of their charge. Hence, the ions will move and their motion causes a current to flow. Recall that voltage ( $V$ ) times current ( $I$ ) is equal to the power and power is the rate of doing work. Electrical work is therefore done on the ion and is given by

$$W_{\text{electrical}} = -VI \quad (2.222)$$

If we are only infinitesimally removed from equilibrium, then  $W_{\text{electrical}}$  becomes  $W_{\text{reversible electrical}}$  and from our earlier discussion in [Section 2.3.3.1](#), the reversible electrical work (maximum work at constant  $T$  and  $P$ ) is equal to the change in the Gibbs free energy. Also, the product of the current and the time in [Equation 2.222](#) is equal to the total charge that is transferred. Faraday's constant ( $F$ ) is defined as the charge carried by a gram mole of ions of unit positive valency and is equal to  $9.649 \times 10^4$  coulombs mol $^{-1}$ , or  $2.306 \times 10^4$  cal V $^{-1}$  mol $^{-1}$ . We can now rewrite [Equation 2.222](#) for a gram mole of ions as

$$W_{\text{reversible electrical}} = \Delta G_{\text{electrical}} = -zFV \quad (2.223)$$

where  $z$  is the charge on the ion being considered. For example, for a sodium ion ( $\text{Na}^+$ )  $z = +1$ , for a calcium ion ( $\text{Ca}^{2+}$ )  $z = 2$ , and for a chloride ion ( $\text{Cl}^-$ )  $z = -1$ .

In addition to the movement of these ions by the electrical field, there is also movement of the ions as a result of the concentration gradient. The change in the Gibbs free energy due to the transport of a solute from the inside macromolecule-containing solution to the outside solution is given by

$$-\Delta G_{\text{transport}} = \bar{G}_{\text{inside}} - \bar{G}_{\text{outside}} = \mu_{\text{inside}} - \mu_{\text{outside}} \quad (2.224)$$

Recall from [Equation 2.75](#) that for an ideal solution, we can write that

$$\mu_{\text{inside}}^{\text{ideal solution}} = G'_{\text{inside}} + RT \ln C_{\text{inside}} \quad \text{and} \quad \mu_{\text{outside}}^{\text{ideal solution}} = G'_{\text{outside}} + RT \ln C_{\text{outside}} \quad (2.225)$$

where we have replaced the mole fraction with the concentration and the  $G'$ 's are pure component constants. Also, since the state of the ion is the same in the two regions, then  $G'_{\text{inside}} = G'_{\text{outside}}$ , and we can write that

$$\Delta G_{\text{transport}} = RT \ln \frac{C_{\text{outside}}}{C_{\text{inside}}} \quad (2.226)$$

The total change in the Gibbs free energy for the movement of the ion by transport and the electrical field is given by the sum of Equations 2.223 and 2.226. At equilibrium, this total change in the Gibbs free energy is zero:

$$\Delta G_{\text{total}} = RT \ln \frac{C_{\text{outside}}}{C_{\text{inside}}} - zFV = 0 \quad (2.227)$$

Solving for V, we obtain Equation 2.228, which is known as the *Nernst equation*. This equation can be used to calculate the equilibrium membrane potential for a particular ion in equilibrium with a charged macromolecule:

$$V = \frac{RT}{zF} \ln \frac{C_{\text{outside}}}{C_{\text{inside}}} = -\frac{RT}{zF} \ln \frac{C_{\text{inside}}}{C_{\text{outside}}} \quad (2.228)$$

In this equation

R represents the gas constant (e.g., 1.987 cal mol<sup>-1</sup> K<sup>-1</sup>)

T is the temperature in K

z is the charge on the ion

F is Faraday's constant (2.3 × 10<sup>4</sup> cal V<sup>-1</sup> mol<sup>-1</sup>)

At 25°C for a univalent ion, |RT/zF| is equal to 25.68 mV, whereas at 37°C, the value is 26.71 mV.

### Example 2.29

With the results from Example 2.28, calculate the transmembrane electrical potential based on the Na<sup>+</sup> concentration and the Cl<sup>-</sup> concentrations within the inside and outside solutions.

#### Solution

In Equation 2.228, we can replace C<sub>inside</sub>/C<sub>outside</sub> with r, where we have shown earlier that r = C<sub>Na<sup>+</sup></sub><sup>inside</sup>/C<sub>Na<sup>+</sup></sub><sup>outside</sup> = C<sub>Na<sup>+</sup></sub><sup>inside</sup>/C<sub>NaCl</sub><sup>outside</sup> = 1.0854 for Na<sup>+</sup> and C<sub>Cl<sup>-</sup></sub><sup>inside</sup>/C<sub>Cl<sup>-</sup></sub><sup>outside</sup> = 1/r = 1/1.0854 for Cl<sup>-</sup>. Hence, for Na<sup>+</sup> with z = +1, we have that

$$V = -\frac{RT}{zF} \ln \frac{C_{\text{inside}}}{C_{\text{outside}}} = -25.68 \text{ mV} \ln(1.0854) = -2.104 \text{ mV}$$

and for Cl<sup>-</sup> with z = -1, we obtain the same answer as above, i.e.,

$$V = -\frac{RT}{zF} \ln \frac{C_{\text{inside}}}{C_{\text{outside}}} = 25.68 \text{ mV} \ln\left(\frac{1}{1.0854}\right) = -2.104 \text{ mV}$$

**2.6.3.15 Chemical equilibrium in ideal aqueous solutions** In the previous discussion on the Gibbs-Donnan effect, the aqueous solution contained a strong electrolyte such as NaCl. Recall that a strong electrolyte in water completely dissociates into its constituent ions. Oftentimes, in biological systems, our aqueous solutions will also contain weak electrolytes such as weak acids or weak bases. Weak acids and bases only partially dissociate. An important example of a weak acid is acetic acid (CH<sub>3</sub>COOH or HOAc), and an example of a weak base is aqueous ammonia or ammonium hydroxide (NH<sub>4</sub>OH). Weak acids and weak bases, because of their partial dissociation, will affect the concentration of H<sup>+</sup> and, as a result, the pH of the solution.

In addition, water can also partially dissociate into  $H^+$  and  $OH^-$ . At  $25^\circ C$ , the dissociation equilibrium constant for water ( $K_W$ ) is given by

$$K_W = C_{H^+} C_{OH^-} = 10^{-14} M^2 \quad (2.229)$$

Since water must remain electrically neutral, this means that  $C_{H^+} = C_{OH^-}$ , and using [Equation 2.229](#), this means that  $(C_{H^+})^2 = 10^{-14} M^2$ , which says that for pure water at  $25^\circ C$ , the  $C_{H^+} = C_{OH^-} = 10^{-7} M$ .

The pH of an aqueous solution is defined in terms of the  $H^+$  concentration ( $M$ ) and is given by

$$pH \equiv -\log_{10} C_{H^+} \quad (2.230)$$

For pure water at  $25^\circ C$ , we showed that  $C_{H^+} = 10^{-7} M$ ; hence from [Equation 2.230](#) for pure water, the  $pH = 7$ , which is referred to as neutral since this value of the pH just expresses the normal concentration of  $H^+$  due to the equilibrium dissociation of water. As the pH decreases below 7, e.g., by adding an acid to water, the concentration of  $H^+$  increases from the neutral value where the  $pH = 7$  ( $C_{H^+} = 10^{-7} M$ ), and if the pH increases above 7, e.g., by adding a base to water, the concentration of  $H^+$  decreases.

If a weak electrolyte such as acetic acid is added to pure water, then additional hydrogen ions will be added to the solution due to the partial dissociation of the weak acid, i.e.,  $HOAc \leftrightarrow H^+ + OAc^-$ , where  $OAc^-$  denotes the acetate anion. The release of the  $H^+$  from the acetic acid in solution will lower the pH of the solution at equilibrium. In solving a chemical equilibrium problem such as this, involving the addition of acetic acid to water, the goal is usually to determine the concentrations of all the species that are present in the solution at equilibrium. For example, for the case of adding acetic acid ( $HOAc$ ) to water, this means finding the concentrations at equilibrium of  $HOAc$ ,  $OAc^-$ ,  $H^+$ ,  $OH^-$ , and  $HOH$ . This requires that we have the same number of independent equations as there are unknowns.

The equations used to find these unknowns are of three general types and include those of chemical equilibrium for each dissociation reaction, conservation of mass on the N species involved in the M reactions, and conservation of electrical charge. The equilibrium dissociation constants ( $K_j$ ) are specific for each reaction ( $j$ ) and depend on the temperature and can be affected by the presence of other species. For most reactions of interest, these values are tabulated in chemistry handbooks or may be found by Internet searches. Since the equilibrium dissociation constant for weak electrolytes can span many orders of magnitude, oftentimes the equilibrium constant for a particular reaction  $j$  is given as the base 10 logarithm of the equilibrium constant. Hence, the dissociation of a weak electrolyte by reaction  $j$  is given as  $pK_j$ , where  $pK_j$  is defined in terms of  $K_j$  by [Equation 2.231](#). Note that the  $pK_j$  is *not* the same as the dissociation equilibrium constant:

$$pK_j \equiv -\log_{10} K_j \quad (2.231)$$

Note that  $pK_W$  for water is  $-\log_{10}(10^{-14})$  and is equal to 14, whereas for a weak acid like acetic acid, the  $pK_{HOAc}$  is equal to 4.745.

Recall that in [Section 1.3.3](#) we defined for reaction  $j$  the differential change in the moles of each species  $i$ , i.e.,  $dn_i$ , in terms of the differential *extent of reaction*  $j$ , i.e.,  $d\epsilon_j$ . The extent of reaction  $j$  ( $d\epsilon_j$ ) has units of moles. We also let  $\nu_{ij}$  represent the stoichiometric coefficient of species  $i$  in reaction  $j$ .

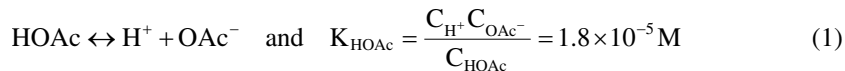
With these definitions and [Equations 1.9 through 1.11](#), we can calculate the concentrations of all the species at chemical equilibrium. The solution of these equations for the concentrations of the species will involve a lot of algebra as well as clever approximations that simplify the process of finding a solution. The following two examples illustrate the approach for solving chemical equilibrium problems.

### Example 2.30

Determine the equilibrium concentrations of all species in a 0.05 M solution of acetic acid. Also find the pH of the solution.

#### Solution

There are two dissociation reactions that must be considered: one is for acetic acid and the other is for water. These are shown below along with their corresponding equations for chemical equilibrium. The equilibrium constants are from Tinoco et al. (2001):



It is convenient to first take as a basis 1 L of solution and let  $n_{\text{HOAc}}^0$  represent the initial moles of HOAc added to make the 1 L solution. Hence, in this example, to make a 0.05 M solution,  $n_{\text{HOAc}}^0 = 0.05$  mol. In terms of the extent of each of the previous reactions, we can make use of [Equations 1.10](#) and [1.11](#) and write the following equations that express conservation of mass for each of the species that are present in the solution:

$$n_{\text{HOAc}} = n_{\text{HOAc}}^0 - \varepsilon_1 \quad (3)$$

$$n_{\text{OAc}^-} = \varepsilon_1 \quad (4)$$

$$n_{\text{H}^+} = \varepsilon_1 + \varepsilon_2 \quad (5)$$

$$n_{\text{OH}^-} = \varepsilon_2 \quad (6)$$

$$n_{\text{HOH}} = n_{\text{HOH}}^0 - \varepsilon_2 \quad (7)$$

Note that in writing these equations, there is no OAc<sup>-</sup>, OH<sup>-</sup>, and H<sup>+</sup> present initially in the solution since we start with undissociated water and acetic acid. If we now divide these equations by the 1 L volume of solution taken as our basis, we can then express  $n_i$  in terms of concentration  $C_i$ , where the extents now have units of moles per liter or molar concentration:

$$C_{\text{HOAc}} = C_{\text{HOAc}}^0 - \varepsilon_1 \quad (8)$$

$$C_{\text{OAc}^-} = \varepsilon_1 \quad (9)$$

$$C_{H^+} = \varepsilon_1 + \varepsilon_2 \quad (10)$$

$$C_{OH^-} = \varepsilon_2 \quad (11)$$

$$C_{HOH} = C_{HOH}^0 - \varepsilon_2 \quad (12)$$

Addition of Equations 8 and 9 expresses the fact that at equilibrium,  $C_{HOAc}^0 = C_{HOAc} + C_{OAc^-}$ . We can also insert the previous equations into the equilibrium relationships given by Equations 1 and 2 to give two equations in terms of the two unknown extents  $\varepsilon_1$  and  $\varepsilon_2$ :

$$\frac{(\varepsilon_1 + \varepsilon_2)\varepsilon_1}{0.05 - \varepsilon_1} = 1.8 \times 10^{-5} \quad (13)$$

$$(\varepsilon_1 + \varepsilon_2)(\varepsilon_2) = 10^{-14} \quad (14)$$

Since we are dealing with the dissociation of an acid in water, we expect that at equilibrium, the  $C_{H^+} \gg C_{OH^-}$ . This means from Equation 11 that  $C_{H^+} \gg \varepsilon_2$ , and from Equation 10, this is the same as saying that  $\varepsilon_1 \gg \varepsilon_2$ . As a result of these assumptions, Equation 13 can be simplified to give

$$\frac{\varepsilon_1^2}{0.05 - \varepsilon_1} = 1.8 \times 10^{-5} \quad \text{or} \quad \varepsilon_1^2 + 1.8 \times 10^{-5}\varepsilon_1 - 9.0 \times 10^{-7} = 0 \quad (15)$$

The quadratic form on the right-hand side of Equation 15 can then be solved for  $\varepsilon_1 = 9.4 \times 10^{-4}$  M. Note that the other root is invalid since it is negative. Equation 14 can then be solved for  $\varepsilon_2 = 1.064 \times 10^{-11}$  M. Note that  $\varepsilon_1 \gg \varepsilon_2$  as we assumed earlier. With the extents of the reactions known, we can now use Equations 8 through 12 to calculate the concentrations of the species at equilibrium, as shown below. Note that the concentration of pure water, i.e.,  $C_{HOH}^0$ , is equal to  $1000 \text{ g L}^{-1} \times 1 \text{ mol } 18^{-1} \text{ g}^{-1} = 55.56 \text{ M}$  and for practical purposes is constant:

$$C_{HOAc} = C_{HOAc}^0 - \varepsilon_1 = 0.05 - 9.4 \times 10^{-4} = 0.0491 \text{ M} \quad (16)$$

$$C_{OAc^-} = \varepsilon_1 = 9.4 \times 10^{-4} \text{ M} \quad (17)$$

$$C_{H^+} = \varepsilon_1 + \varepsilon_2 = 9.4 \times 10^{-4} \text{ M} \quad (18)$$

$$C_{OH^-} = \varepsilon_2 = 1.064 \times 10^{-11} \text{ M} \quad (19)$$

$$C_{HOH} = C_{HOH}^0 - \varepsilon_2 = 55.6 \text{ M} \quad (20)$$

The pH of the solution at equilibrium is  $-\log_{10}(9.4 \times 10^{-4}) = 3.03$ . Also, electroneutrality requires that  $C_{H^+} = C_{OAc^-} + C_{OH^-}$  and we see from the above solution that this requirement is also satisfied.

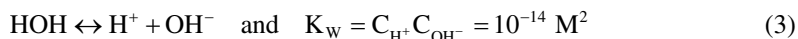
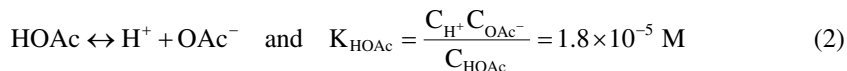
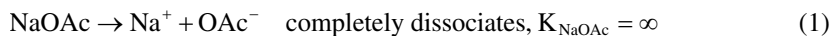
In biological systems, it is also very important to control the pH at some particular value, and buffers are substances that are employed to make the solution pH less sensitive to changes in the pH or the concentration of H<sup>+</sup> ions. These buffers usually consist of a weak acid or a weak base and their corresponding salt. For example, in a solution made from a particular acid, the addition of the salt of this acid will buffer the solution by consuming excess H<sup>+</sup>, thereby keeping the pH of the solution relatively constant. This is illustrated in the following example.

### Example 2.31

Determine the amount of sodium acetate (NaOAc) needed to form a buffer solution of pH = 4.5 in a 1 L solution containing 0.05 M acetic acid.

#### Solution

In [Example 2.30](#), it was shown that the pH of a 0.05 M solution of acetic acid is 3.03. NaOAc acts as a strong electrolyte dissociating into Na<sup>+</sup> and OAc<sup>-</sup>. The acetate anions will tend to consume the H<sup>+</sup>, and the problem is to find how much NaOAc is needed to raise the pH to 4.5. Now we have three dissociation reactions:



As in the previous example, we can express the concentrations of each species in terms of the extent of each of the above reactions as shown by the following equations:

$$C_{\text{NaOAc}} = C_{\text{NaOAc}}^0 - \varepsilon_1 \quad (4)$$

$$C_{\text{Na}^+} = \varepsilon_1 \quad (5)$$

$$C_{\text{HOAc}} = C_{\text{HOAc}}^0 - \varepsilon_2 \quad (6)$$

$$C_{\text{OAc}^-} = \varepsilon_1 + \varepsilon_2 \quad (7)$$

$$C_{\text{H}^+} = \varepsilon_2 + \varepsilon_3 \quad (8)$$

$$C_{\text{OH}^-} = \varepsilon_3 \quad (9)$$

$$C_{\text{HOH}} = C_{\text{HOH}}^0 - \varepsilon_3 \quad (10)$$

Since NaOAc is a strong electrolyte, and completely dissociates, then from [Equation 4](#),  $C_{\text{NaOAc}} = 0$  and  $\varepsilon_1 = C_{\text{NaOAc}}^0$ . Also by [Equations 5](#) and [7](#), we have that  $C_{\text{Na}^+} = \varepsilon_1 = C_{\text{NaOAc}}^0$  and  $C_{\text{OAc}^-} = \varepsilon_1 + \varepsilon_2 = C_{\text{NaOAc}}^0 + \varepsilon_2$ . Adding [Equations 6](#) and [7](#), we also get that  $C_{\text{HOAc}} + C_{\text{OAc}^-} = C_{\text{HOAc}}^0 + \varepsilon_1 = C_{\text{HOAc}}^0 + C_{\text{NaOAc}}^0 = C_A^0 + C_S^0$ . Here we generalize the result by denoting  $C_A^0$  and  $C_S^0$  as the initial concentrations of the acid and the salt in the solution that is formed.

A charge balance can also be written by summing Equations 5 and 8 for the cations and Equations 7 and 9 for the anions, and these must be equal, giving the following result:

$$C_{\text{Na}^+} + C_{\text{H}^+} = C_{\text{OAc}^-} + C_{\text{OH}^-} \quad (11)$$

To form a buffer solution, the amount of NaOAc or salt that must be added is usually significant. Therefore, we expect that  $C_{\text{Na}^+} \gg C_{\text{H}^+}$  and  $C_{\text{OAc}^-} \gg C_{\text{OH}^-}$ . This means that  $\varepsilon_1 \gg \varepsilon_2 + \varepsilon_3$  as well as  $\varepsilon_1 \gg \varepsilon_3$ . From the charge balance given by Equation 11

$$C_{\text{Na}^+} = C_{\text{OAc}^-} = C_{\text{NaOAc}}^0 = \varepsilon_1 \quad (12)$$

In addition, as shown in Example 2.30, the dissociation of the weak acid, in this case acetic acid by Equation 6, is very small; hence,  $C_{\text{HOAc}} \approx C_{\text{HOAc}}^0$ . Therefore, the equilibrium constant for the HOAc can be written as follows:

$$K_{\text{HOAc}} = \frac{C_{\text{H}^+} C_{\text{OAc}^-}}{C_{\text{HOAc}}} \approx \frac{C_{\text{H}^+} C_{\text{NaOAc}}^0}{C_{\text{HOAc}}^0} = \frac{C_{\text{H}^+} C_S^0}{C_A^0} \quad (13)$$

This equation can then be solved for  $C_{\text{H}^+}$  as follows:

$$C_{\text{H}^+} = K_{\text{HOAc}} \frac{C_A^0}{C_S^0} \quad (14)$$

$$\log_{10} C_{\text{H}^+} = \log_{10} K_{\text{HOAc}} + \log \frac{C_A^0}{C_S^0} \quad (15)$$

The previous equations can then be rewritten in terms of the pH and the pK of the acid (A) as shown below. This equation is known as the *Henderson-Hasselbalch equation*:

$$\text{pH} = \text{pK}_A + \log_{10} \frac{C_S^0}{C_A^0} \quad (16)$$

This equation is a general result that can be used to prepare buffer solutions. Since  $C_S^0 \approx C_A^0$ , we usually select a weak acid with a  $\text{pK}_A$  close to the desired pH. Recall that the subscript S refers to the salt of the weak acid A and  $\text{pK}_A$  is for the weak acid. For this example, we have that  $\text{pK}_A = 4.745$  and  $C_A^0 = 0.05 \text{ M}$ . Also, the final solution pH is to be 4.5. The Henderson-Hasselbalch equation can then be solved for the concentration of the salt, i.e., NaOAc in this example, as shown below:

$$4.5 = 4.745 + \log_{10} \frac{C_S^0}{0.05 \text{ M}} \quad \text{which gives } C_S^0 = 0.0284 \text{ M}$$

If the solution formed has a volume equal to 1 L, this means that 0.0284 mol of NaOAc is needed. The molecular weight of NaOAc is  $82 \text{ g mol}^{-1}$ , so the amount of NaOAc needed is  $0.0284 \text{ mol} \times 82 \text{ g mol}^{-1} = 2.33 \text{ g}$ . In obtaining this solution, we have assumed that the solutions are ideal. In actual practice, the pH of the solution may need some minor tweaking to account for nonideal solution behavior.

## Problems

- 2.1** Assuming that air is an ideal gas, calculate the change in entropy and enthalpy when 100 mol of air at 25°C and 1 atm is heated and compressed to 300°C and 10 atm. Use the following equation for  $C_p$ :

$$\frac{C_p}{R} = A + B \cdot T + C \cdot T^{-2}$$

where  $A = 3.355$ ,  $B = 0.575 \times 10^{-3}$ , and  $C = -0.016 \times 10^5$ , with  $T$  in K.

- 2.2** Calculate the reversible work required to compress adiabatically (i.e.,  $Q = 0$ ) 60 mol of carbon dioxide initially at 25°C and 1 atm to 350°C and 10 atm. Assume that  $C_p = 37.1 \text{ J K}^{-1} \text{ mol}^{-1}$ . Assume that carbon dioxide is an ideal gas.
- 2.3** A toy rocket consists of a Styrofoam rocket snuggly fitted into a long tube of volume equal to 0.5 L. The pressure in the tube is increased to a final pressure of 3 atm and a temperature of 30°C at which time the rocket takes off. If the rocket weighs 50 g, estimate the maximum initial velocity of the rocket and the maximum expected height of the rocket. Assume air is an ideal gas and has a  $C_v = (5/2)R$ . Explain why the rocket would not be expected to achieve this elevation.
- 2.4** Air at 400 kPa and 400 K passes through a turbine. The turbine is well insulated. The air leaves the turbine at 125 kPa. Find the maximum amount of work that can be obtained from the turbine and the exit temperature of the air leaving the turbine. Assume air is an ideal gas with a  $C_p = (7/2)R$ .
- 2.5** Consider the slow adiabatic expansion of a closed volume of gas for which  $C_p = (7/2)R$ . If the initial gas temperature is 825 K and the ratio of the final pressure to the initial pressure is 1/3, what is the change in enthalpy of the gas, the change in internal energy, the heat transferred  $Q$ , and the work  $W$ ? Assume a basis of 1 mol of gas.
- 2.6** Air at 125 kPa and 350 K passes through a compressor. The compressor is well insulated. The air leaves the compressor at 600 kPa and 650 K. Find the work required to do this compression. Is this change of state of the air possible? Assume air is an ideal gas with a  $C_p = (7/2)R$ .
- 2.7** Consider the slow adiabatic compression of a closed volume of gas for which  $C_p = 3.5 R$ . If the initial gas temperature is 320 K and the ratio of the final pressure to the initial pressure is 4, what is the change in enthalpy of the gas, the change in internal energy, the heat transferred  $Q$ , and the work  $W$ ? Assume a basis of 1 mol of gas.
- 2.8** One mole of an ideal gas, initially at 30°C and 1 atm, undergoes the following reversible changes. It is first compressed isothermally to a point such that when it is heated at constant volume to 150°C, its final pressure is 12 atm. Calculate  $Q$ ,  $W$ ,  $\Delta E$ , and  $\Delta H$  for the process. Take  $C_p = 3.5 R$  and  $C_v = 2.5 R$ .
- 2.9** A rigid vessel of 75 L volume contains an ideal gas at 400 K and 1 atm. If heat in the amount of 15,000 J is transferred to the gas, determine the entropy change of the gas. Assume  $C_v = 2.5 R$  and  $C_p = 3.5 R$ .
- 2.10** An osmotic pump (see Figure 8.7) is a device used to deliver a drug at a constant rate within the body. An excess of NaCl is used to form a continuously saturated solution that is contained within a compartment called the *osmotic engine*, which is located between a semipermeable membrane that is exposed to the interstitial fluid and a piston, which acts on a reservoir containing the drug. In operation, water from the surrounding tissue is brought into the osmotic

engine by osmosis. The resulting expansion of the osmotic engine drives the piston that forces drug from the drug reservoir out of the osmotic pump at a constant rate. The drug delivery rate ( $R$ ) can be shown to be proportional to the osmotic pressure of the fluid within the osmotic engine and the concentration ( $C$ ) of the drug in the reservoir. The delivery rate of the drug is therefore given by

$$R = k\pi C$$

At  $37^\circ\text{C}$ , the saturation concentration of NaCl in water is equal to 5.4 M. For a particular osmotic pump, it was found that the drug release rate ( $R$ ) was  $125 \mu\text{g day}^{-1}$ . The drug concentration ( $C$ ) was  $370 \text{ mg mL}^{-1}$ . What is the value of the proportionality constant ( $k$ , in  $\text{mL day}^{-1} \text{ atm}^{-1}$ ) for this osmotic pump?

- 2.11** The Navy is considering an osmotic device in their submarines in order to desalinate water when the submarine is submerged. When the submarine is below a critical depth, the osmotic device converts seawater into pure water that would be available for use on the submarine. The density of seawater is  $1024 \text{ kg m}^{-3}$  and the composition of the seawater is equivalent to a 0.5 M NaCl solution. What is the critical depth in meters below which this proposed desalination process will work?
- 2.12** One mole of an ideal gas initially at  $25^\circ\text{C}$  and 1 atm is heated and allowed to expand against an external pressure of 1 atm until the final temperature is  $400^\circ\text{C}$ . For this gas,  $C_V = 20.8 \text{ J mol}^{-1} \text{ K}^{-1}$ .
- Calculate the work done by the gas during the expansion.
  - Calculate the change in internal energy and the change in enthalpy of the gas during the expansion.
  - How much heat is absorbed by the gas during the expansion?
  - What is the change in entropy of the gas?
- 2.13** At  $50^\circ\text{C}$ , the vapor pressure of A and B as pure liquids are 268.0 and 236.2 mmHg, respectively. At this temperature, calculate the total pressure and the composition of the vapor, which is in equilibrium with the liquid containing a mole fraction of A of 0.25.
- 2.14** When 0.013 mol of urea is dissolved in 1000 g of water, the freezing point of water decreases by 0.024 K. How does this measured freezing point depression compare to that based on the ideal solution theory?
- 2.15** Gas in a cylinder expands slowly by pushing on a frictionless piston. The following data shows what happens to the gas in the cylinder. How much work ( $W$ ) is done by the gas? Assuming  $C_V = 2.5 \text{ R}$ , what is the change in the internal energy ( $\Delta E$ ) of the gas? How much heat was transferred during the process ( $Q$ )?

Gas Pressure, bar	Volume of Gas, L	Temperature of Gas, $^\circ\text{C}$
10	15	70
7	17	23
5	20	10
3	24	50
6	28	150
8	35	450

- 2.16** Cubic equations of state are commonly used for PVT calculations. Most of the modern cubic equations of state derive from that first developed by van der Waals in 1873. The van der Waals equation of state is given by

$$\left( P + \frac{a}{V^2} \right) (V - b) = RT$$

where

$a$  is called the attraction parameter

$b$  is referred to as the repulsion parameter or the effective molecular volume

Note that with  $a$  and  $b$  equal to zero, this equation simplifies to the ideal gas law. These constants are found by either fitting the above equation to actual PVT data, or as we shall see next, we can use the critical point to define them in terms of the component critical properties.

- a. Show that the previous equation can also be written in the following cubic forms in terms of volume or the compressibility factor:

$$V^3 - \left( b + \frac{RT}{P} \right) V^2 + \frac{a}{P} V - \frac{ab}{P} = 0$$

$$Z^3 - \left( \frac{bP}{RT} + 1 \right) Z^2 + \frac{aP}{(RT)^2} Z - \frac{abP^2}{(RT)^3} = 0$$

For isotherms ( $T$ ) below the critical isotherm and  $P = P^{\text{Sat}}(T)$  (also refer to [Figure 2.3](#)), the solution to either of the previous equations will produce three roots for either  $V$  or  $Z$ . The smallest of these roots will correspond to the saturated liquid value, i.e., point B in [Figure 2.3](#), and the largest of these roots will correspond to the saturated vapor value, i.e., point D in [Figure 2.3](#). The middle root has no physical meaning. At the critical point, point C in [Figure 2.3](#), these three roots become equal, i.e.,  $V_L^{\text{Sat}} = V_V^{\text{Sat}} = V_C = Z_C RT_C / P_C$ , where the subscript C denotes the critical values of PVT and Z. Hence, at the critical point, we have that  $(V - V_C)^3 = 0$  or when this is expanded, we have that  $V^3 - 3V_C V^2 + 3V_C^2 V - V_C^3 = 0$ .

- b. Comparing the like powers of the expanded volume equation at the critical point to those in the volume explicit form of the van der Waals equation, show that the van der Waals parameters are given by the following equations in terms of the critical properties:

$$a = \frac{27R^2 T_C^2}{64P_C} \quad b = \frac{RT_C}{8P_C} \quad R = \frac{8P_C V_C}{3T_C} \quad Z_C = 0.375$$

Although the value for the gas constant  $R$  is found to depend on the component-critical properties, the usual practice is to use the universal value of the gas constant (shown in [Table 1.5](#)) in PVT calculations. In this way, the van der Waals equation of state becomes the ideal gas law at low pressures.

- c. For water at 250°C, the vapor pressure is 3977.6 kPa and the specific volumes of the saturated vapor and liquid are 50.04 and 1.251 cm<sup>3</sup> g<sup>-1</sup>. Compare these specific volumes to those predicted by the van der Waals equation of state using the following critical properties for water:

$$T_C = 647.1 \text{ K} \quad P_C = 220.55 \text{ bar} \quad (1 \text{ bar} = 100 \text{ kPa})$$

- 2.17** A new drug has a molecular weight of 325 and a melting temperature of 310°C. Estimate the solubility of this drug in hexane at 25°C. Use the Scatchard-Hildebrand equation to estimate the activity coefficient of the drug. Additional information needed to solve this problem is shown subsequently and in [Example 2.10](#).

Heat of fusion of the drug	4825 cal mol <sup>-1</sup>
Density of the drug	1.028 g cm <sup>-3</sup> at 25°C
Vapor pressure of the solid drug	$\ln P^{\text{Sat}} \text{ (mmHg)} = 26.3 - \frac{8780}{T(K)}$

- 2.18** Estimate the gas phase equilibrium mole fraction of the drug considered in [Problem 2.17](#) at a temperature of 45°C. The pressure of the gas is 1 atm.
- 2.19** A protein solution containing 0.75 g of protein per 100 mL of solution has an osmotic pressure of 22 mmH<sub>2</sub>O at 25°C. What is the molecular weight of the protein?
- 2.20** Consider the situation where a semipermeable membrane separates a bulk fluid (region A) with an osmotic pressure of 1750 mmHg from another *enclosed* fluid (region B) with an osmotic pressure of 10,000 mmHg. The hydrodynamic gauge pressure of region A is 760 mmHg. The solvent in both regions A and B is water. Assuming the container and membrane enclosing region B is rigid, what is the equilibrium hydrodynamic gauge pressure in region B, i.e., the situation wherein there is no net flow of water across the membrane?
- 2.21** When 0.5 mol of sucrose is dissolved in 1000 g of water, the osmotic pressure at 20°C is found to be 12.75 atm. Calculate the activity coefficient of water.
- 2.22** It is desired to extract from water a drug with a mole fraction of 0.02. A single equilibrium stage extractor is to be used. The flow rate of the aqueous stream to the extractor is 50 mol min<sup>-1</sup>, and the flow rate of the solvent to the extractor is 150 mol min<sup>-1</sup>. If 90% of the drug is to be removed from the aqueous stream, what should the distribution coefficient of the solvent for this drug be?
- 2.23** Using the results for the distribution coefficient from [Problem 2.22](#), what would the percent extraction of the drug be if four equilibrium extraction stages were used?
- 2.24** The activity coefficients of ethanol (1) and water (2) can be described by the van Laar equation, where

$$\ln \gamma_1 = A_{12} \left( \frac{A_{21}x_2}{A_{12}x_1 + A_{21}x_2} \right)^2$$

$$\ln \gamma_2 = A_{21} \left( \frac{A_{12}x_1}{A_{12}x_1 + A_{21}x_2} \right)^2$$

The infinite dilution activity coefficient ( $\gamma_1^\infty$ ) of ethanol in water is 4.66 and that for water in ethanol ( $\gamma_2^\infty$ ) is 2.64. At 25°C, the vapor pressure of water is 3.166 kPa and the vapor pressure of ethanol is 7.82 kPa. Assuming a liquid phase contains 50 wt% ethanol, estimate the composition of the vapor phase that is in equilibrium with the liquid phase. Would this vapor phase composition be explosive? The density of pure water at 25°C is 0.9971 g cm<sup>-3</sup>, and the

density of pure ethanol is  $0.7851 \text{ g cm}^{-3}$ . The density of a 50 wt% solution of ethanol in water is  $0.9099 \text{ g cm}^{-3}$ .

- 2.25 Explain why a water bug can walk on water.
- 2.26 A droplet of water at  $25^\circ\text{C}$  has a diameter of  $0.1 \mu\text{m}$ . Calculate the pressure within the droplet of water.
- 2.27 What is the vapor pressure of the water within a droplet of water at  $25^\circ\text{C}$  that has a diameter of  $10 \text{ nm}$ ?
- 2.28 Consider the situation of a liquid mixture where the solute molecules are much larger than those of the solvent. An example of such a mixture would be a polymer in a solvent or a protein solution. In the solution model developed by Flory and Huggins (Sandler, 1989), the entropy change as a result of mixing a solvent (1) with a much larger solute (2) is given by the following expression:

$$\Delta S^{\text{mix}} = -R(x_1 \ln \phi_1 + x_2 \ln \phi_2)$$

where

$x_1$  and  $x_2$  are the mole fractions

$\phi_1$  and  $\phi_2$  are the volume fractions of the solvent and the solute, respectively

The volume fractions are given by

$$\phi_1 = \frac{x_1}{x_1 + rx_2} \quad \text{and} \quad \phi_2 = \frac{rx_2}{x_1 + rx_2}$$

with  $r = V_2/V_1$ , where  $V_1$  and  $V_2$  are the molar volumes of each species. Using Equations 2.44 and 2.96 that define the property change of mixing and the excess property, respectively, along with the result from Example 2.6 that  $S_i^{\text{ideal solution}} = S_i - R \ln x_i$ , show that the excess entropy of the solution is given by

$$S^E = -R \left( x_1 \ln \frac{\phi_1}{x_1} + x_2 \ln \frac{\phi_2}{x_2} \right)$$

Note that if the volumes of the solvent and solute are comparable in size, then from the above expression  $S^E = 0$ , and the solution is then an ideal solution. So, we see that it is the difference in the size of the solvent and the solute that leads to the nonideal solution behavior in the model proposed by Flory and Huggins. The excess enthalpy ( $H^E$ ) was then expressed by the following equation:

$$H^E = \chi RT(x_1 + rx_2) \phi_1 \phi_2$$

where  $\chi$  is an adjustable parameter known as the Flory-Huggins interaction parameter. The Flory-Huggins interaction parameter for nonpolar systems can be shown to be related to the solubility parameters of the solvent and the solute by the following equation (Prausnitz et al., 1986):

$$\chi = \frac{V_1}{RT} (\delta_1 - \delta_2)^2$$

A good solvent for the polymer or macromolecule is one for which  $\chi$  is very small or  $\delta_1 \sim \delta_2$ . In addition, to ensure that the solvent and polymer are completely miscible, the largest value of  $\chi$  is equal to 0.5. If  $\chi > 0.5$ , the solvent and solute are only partially miscible.

Since  $G^E = H^E - TS^E$ , show that the above two equations for  $S^E$  and  $H^E$  can be combined to give the Flory-Huggins model for the excess Gibbs free energy of the solution

$$\frac{G^E}{RT} = \left( x_1 \ln \frac{\phi_1}{x_1} + x_2 \ln \frac{\phi_2}{x_2} \right) + \chi(x_1 + rx_2)\phi_1\phi_2$$

Using [Equation 2.100](#), show (if you can) that the Flory-Huggins activity coefficients for the solvent (1) and the solute (2) are given by the following expressions:

$$\ln \gamma_1 = \ln \frac{\phi_1}{x_1} + \left( 1 - \frac{1}{r} \right) \phi_2 + \chi \phi_1^2$$

$$\ln \gamma_2 = \ln \frac{\phi_2}{x_2} + (r - 1) \phi_1 + \chi \phi_2^2$$

Recall from [Equation 2.146](#) that the osmotic pressure of the solution containing our solvent (1) and solute (2) is given by

$$\Pi = -\frac{RT}{V_1} \ln(\gamma_1 x_1)$$

Show that if the activity coefficient of solvent (1) is described by the Flory-Huggins activity coefficient model, then the osmotic pressure is given by the following expression. Note that for a dilute solute solution, we can expand the solvent and solute volume fraction in an infinite series where

$$\ln \phi_1 = \ln(1 - \phi_2) \approx -\phi_2 - \frac{\phi_2^2}{2} - \frac{\phi_2^3}{3} - \dots$$

$$\Pi = \frac{RT}{V_1} \left[ \frac{\phi_2}{r} + \left( \frac{1}{2} - \chi \right) \phi_2^2 + \frac{1}{3} \phi_2^3 + \dots \right]$$

From the definition of the solute volume fraction given above, we can then write for a dilute solution that  $\phi_2 = x_2 V_2 / V_1 = V_2 C_2$ , where  $C_2$  is the molar concentration of the solute. Substituting this result for  $\phi_2$  into the previous equation for  $\Pi$ , show that in a general sense the osmotic pressure for a nonideal solution can be described by a power series in the molar concentration of the solute (or a virial series) as shown below:

$$\Pi = RTC_2 \left( 1 + \bar{B}C_2 + \bar{C}C_2^2 + \dots \right)$$

where  $\bar{B}$  and  $\bar{C}$  are known as the second and third virial coefficients. Note that for an ideal solution,  $\bar{B}$  and  $\bar{C}$  are equal to zero and  $\Pi = RTC_2$ , which is also the result given by [Equation 2.147](#). Usually with polymers and macromolecules, the solute concentration is expressed in weight concentration, e.g., grams per liter. Letting  $c_2$  represent the weight concentration of the

solute,  $C_2 = c_2/MW_2$  and then  $\phi_2 = V_2(c_2/MW_2)$ . Substituting this result for  $\phi_2$  into the previous equation for  $\Pi$  and neglecting terms higher than the second order in  $\phi_2$ , show that the following result is obtained for the osmotic pressure:

$$\Pi = \frac{RTc_2}{MW_2} \left[ 1 + \frac{MW_2}{V_1\rho_2^2} \left( \frac{1}{2} - \chi \right) c_2 \right]$$

Also show that the second virial coefficient is equal to  $(MW_2/V_1\rho_2^2)((1/2) - \chi)$ .

- 2.29** The following data for the osmotic pressure of hemoglobin ( $MW = 68,000 \text{ g mol}^{-1}$ ) in an aqueous solution at  $0^\circ\text{C}$  are presented by Freeman (1995).

Hemoglobin Concentration, g $100^{-1} \text{ cm}^{-3}$ Solution	Osmotic Pressure, mmHg
2.5	8
5	15
8	25
10	37
12	42
15	65
19.5	100
23.4	150
24.5	167
27.5	229
28.6	254

Make a graph of the above-mentioned data and compare the data to regression fits of the following virial expression derived in [Problem 2.28](#) for the osmotic pressure, i.e.,  $\pi = (RTc_2/MW_2) [1 + \bar{B}c_2 + \bar{C}c_2^2]$ . Show that when  $\bar{B}$  and  $\bar{C}$  are equal to zero, the resulting expression, i.e., van't Hoff's law, fits the data quite well at low hemoglobin concentrations where the solution is expected to be ideal. Next, explore how the fit to these data improves by performing a nonlinear regression to find the value of  $\bar{B}$ , with  $\bar{C} = 0$ . Then, perform another nonlinear regression that includes  $\bar{B}$  and  $\bar{C}$ .

- 2.30** What is the predicted temperature of the seawater surrounding polar ice caps, assuming the seawater and the ice are in equilibrium? Assume the freezing point of pure water is  $0^\circ\text{C}$  and that the heat of fusion of pure water is  $6012 \text{ J mol}^{-1}$ .
- 2.31** A mountain climber has reached an elevation where the observed boiling point of water is  $97^\circ\text{C}$ . Estimate how high above sea level the climber is. Carefully state your assumptions and any references that you have consulted.
- 2.32** The concentration of a macromolecule in an aqueous solution contained inside a semipermeable membrane bag is  $0.002 \text{ M}$ . The macromolecule carries a net negative charge of minus 8. If the NaCl concentration in the solution outside the bag at equilibrium is  $0.05 \text{ M}$ , calculate the ratio of the concentration of the  $\text{Na}^+$  inside the bag to that outside the bag. Also, find the ratio of the concentration of the  $\text{Cl}^-$  inside the bag to that outside the bag. What is the transmembrane

voltage at equilibrium based on the  $\text{Na}^+$  concentration and the  $\text{Cl}^-$  concentration inside and outside the membrane bag?

- 2.33 Protein concentration in a membrane bag is 0.005 M with  $Z_M = +15$ .  $\text{NaCl}$  outside the bag is 0.15 M. Find  $\Pi$  of the protein in the bag.
- 2.34 Find the concentrations of the species at equilibrium for the case when a 0.10 M solution of sodium acetate ( $\text{NaOAc}$ ) is made.  $\text{NaOAc}$  is the salt of acetic acid ( $\text{HOAc}$ ). Also determine the pH of the resulting solution. Assume that sodium acetate as a salt is a strong electrolyte and that it completely dissociates in water to form  $\text{Na}^+$  and  $\text{OAc}^-$ . In this case, the high concentration of  $\text{OAc}^-$  will tend to consume  $\text{H}^+$  with the result that  $\text{HOAc}$  (acetic acid) will be formed and we expect the resulting solution to be basic. The water and  $\text{HOAc}$  dissociation equilibrium constants may be found in [Example 2.29](#).
- 2.35 *Tris*, i.e., tris-(hydroxymethyl) aminomethane (molecular weight = 121.14 g mol<sup>-1</sup>), is a weak base (i.e., removes  $\text{H}^+$ ) and a very important buffer used to make biological solutions. Although it is a weak base, it is still convenient in solving buffer problems to work instead with its acid dissociation reaction, which can be written as follows:  $\text{Tris}-\text{H}^+ \leftrightarrow \text{Tris} + \text{H}^+$ .  $\text{Tris}-\text{H}^+$  has a  $pK_A = 8.3$  at 20°C. If a 1 L solution contains 0.05 M of *Tris* and 0.03 M hydrochloric acid (HCl), what is the pH of this solution? Hydrochloric acid is a strong acid and will completely dissociate in an aqueous solution. Suppose after this solution is formed that an additional millimole of HCl is added. What is the pH now? Note that the addition of 1 mmol of HCl to 1 L of pure water gives a solution pH of 3.0.
- 2.36 A protein with a molecular weight of 67,396 g mol<sup>-1</sup> is added to water such that the concentration of the protein is 4.0 g 100<sup>-1</sup> cm<sup>-3</sup> of solution. Estimate the osmotic pressure (mmHg) of the resulting solution at a temperature of 0°C.
- 2.37 The osmotic pressure (mmHg) of a protein solution at a temperature of 30°C was found to be 10 mmHg. If the concentration of the protein is 4.0 g 100<sup>-1</sup> cm<sup>-3</sup> of solution, estimate the molecular weight of the protein molecule.
- 2.38 A peptide solution containing 0.35 g of protein per 100 mL of solution has an osmotic pressure of 36 mmH<sub>2</sub>O at 25°C. What is the molecular weight of the protein?
- 2.39 What is the osmotic pressure of a solution at 37°C containing a solute with a molecular weight of 75,000 at a concentration of 30 g L<sup>-1</sup> and a solute with a molecular weight of 20,000 at a concentration of 10 g L<sup>-1</sup>? The solute with a molecular weight of 75,000 is unstable in this solution and completely dissociates into four solutes of equal size.
- 2.40 A protein solution with an osmotic pressure of 45 mm of water needs to be prepared. If the molecular weight of the protein is 50,000 g mol<sup>-1</sup>, how many grams of the protein need to be in 100 mL of the solution at 25°C?
- 2.41 Estimate the osmotic pressure in mmHg of an aqueous solution containing a solute with a molecular weight of 120,000. The solute concentration is 15 g L<sup>-1</sup>, and the solute totally dissociates in water into three smaller solutes of equal size. You can assume the temperature is 37°C.
- 2.42 A protein with a molecular weight of 70,000 g mol<sup>-1</sup> is added to water at a temperature of 25°C. If the resulting osmotic pressure is found to be equal to 25 mmHg, estimate the required concentration of the protein in grams per 100 cm<sup>3</sup> of solution.
- 2.43 An aqueous solution (A) with an osmotic pressure of 5 atm is separated by a membrane from an aqueous solution (B) with an osmotic pressure of 2 atm. Both solutions are at a total pressure of 1 atm. The solutes in these two solutions cannot pass through the membrane.

Which way will the water flow, i.e., from (A) to (B) or from (B) to (A)? By how much must the hydrodynamic pressure be increased to stop the osmotic flow of water, and on which solution, (A) or (B), must this pressure increase be applied?

- 2.44** A protein is added to water such that the resulting protein concentration is equal to  $12 \text{ g } 100 \text{ cm}^{-3}$ . If the resulting osmotic pressure of this solution is found to be equal to  $35 \text{ mmHg}$  at a temperature of  $25^\circ\text{C}$ , estimate the molecular weight of this protein.
- 2.45** One hundred and twenty grams of a protein is added to water to make a  $1 \text{ L}$  solution. The molecular weight of this protein is  $72,000 \text{ g mol}^{-1}$ . However, when the protein is dissolved in water at  $20^\circ\text{C}$ , it dissociates into three equal-sized fragments. What is the osmotic pressure of this solution in mmHg?
- 2.46** A protein with a high molecular weight is added to water at a temperature of  $25^\circ\text{C}$ . If the resulting osmotic pressure of a  $94.2 \text{ g L}^{-1}$  solution of this protein is found to be equal to  $25 \text{ mmHg}$ , estimate the molecular weight of the protein in grams per mole.
- 2.47** A cell has a radius of  $5 \mu\text{m}$  and is in osmotic equilibrium with its surroundings at  $300 \text{ mOsM}$  for a temperature of  $25^\circ\text{C}$ . The cell is then placed in a  $155 \text{ mM}$  solution of NaCl at the same temperature. Will water now flow into the cell or out of the cell?
- 2.48** MoviPrep® is a low-volume colonoscopy preparation that is used to provide a clear view of the entire colon, thereby allowing your doctor to detect abnormal growths during the colonoscopy procedure. Each liter of a MoviPrep® solution contains in millimoles the following components:

PEG 3350 (polyethylene glycol, does not dissociate)	29.6
NaCl	45.6
Na <sub>2</sub> SO <sub>4</sub>	52.8
KCl	14.2
NaAscorbate (C <sub>6</sub> H <sub>7</sub> O <sub>6</sub> Na, strong electrolyte)	29.8

At  $37^\circ\text{C}$ , what is the osmotic pressure of this solution in mmHg?

- 2.49** A macromolecule is added at a concentration of  $18 \text{ g L}^{-1}$  to water at a temperature of  $10^\circ\text{C}$ . If the resulting osmotic pressure of this solution is found to be equal to  $12 \text{ mmHg}$ , estimate the molecular weight of the macromolecule in grams per mole.
- 2.50** Vilker et al. (1981) studied the osmotic pressure of bovine serum albumin in a  $0.15 \text{ M}$  sodium chloride solution at pHs of 4.5, 5.4, and 7.4. Their data at a pH of 7.4 is shown in the table below. Show that the following semiempirical equation represents these data. The first term on the right-hand side of this equation represents the contribution to the osmotic pressure due to the uneven distribution of the small ions between the solutions on each side of the membrane as a result of the Gibbs-Donnan effect, i.e., see the explanation regarding [Equation 2.221](#). The second term is a virial expansion that accounts for the nonideal behavior of albumin at these relatively high concentrations:

$$\pi = RT \left\{ 2 \left[ \left( \frac{ZC_p}{2M_p} \right)^2 + m_s^2 \right]^{1/2} - 2m_s \right\} + \frac{RT}{M_p} [C_p + A_2 C_p^2 + A_3 C_p^3]$$

What are the best values of the virial coefficients, i.e.,  $A_2$  and  $A_3$ ? In this equation,  $M_p$  is the albumin molecular weight ( $69,000 \text{ g mol}^{-1}$ ),  $m_s$  is the molar salt concentration, and  $C_p$  is the

albumin concentration in grams per liter of solution. Z is the charge carried by the albumin molecule in the solution and is equal to the difference between the number of bound protons ( $H^+$ ) and bound chloride ions ( $Cl^-$ ) on each albumin molecule. At a pH of 7.4, Z equals 20.5.

Osmotic Pressure of Albumin Solutions (Vilker et al., 1981)

Albumin Concentration, g L <sup>-1</sup>	Osmotic Pressure, $\pi$ , mmHg
84	48
91	59
211	332
211	334
289	844
325	996
325	996
354	1423
357	1638
413	2620
428	2806
448	3640

# Chapter 3 Physical properties of the body fluids and the cell membrane

## 3.1 Body fluids

To begin our study of transport phenomena in biomedical engineering, we first must examine the physical properties of the fluids that are within the human body. Many of our engineering calculations or the development and design of new procedures, devices, or treatments will either involve or affect the fluids that are within the human body. Therefore, we will focus our initial attention on the types and characteristics of the fluids that reside within the body.

The body fluids can be classified into three types: *extracellular*, *intracellular*, and *transcellular* fluids. As shown in [Table 3.1](#), nearly 60% of the body weight for an average 70 kg male is comprised of these body fluids, resulting in a total fluid volume of about 40 L.

The largest fraction of the fluid volume, about 36% of the body weight, consists of *intracellular fluid*, which is the fluid contained within the body's cells, e.g., the fluid found within red blood cells, muscle cells, and liver cells. *Extracellular fluid* consists of the *interstitial fluid* that comprises about 17% of the body weight and the *blood plasma* that comprises around 4% of the body weight. Interstitial fluid circulates within the spaces (*interstitium*) between cells. The interstitial fluid space represents about one-sixth of the body volume. The interstitial fluid is formed as a filtrate from the plasma portion of the blood that is within the *capillaries*. The capillaries are the smallest element of the cardiovascular system and represent the site where the exchange of vital substances occurs between the blood and the tissue surrounding the capillary. We shall see that the interstitial fluid composition is very similar to that of plasma.

The blood volume of a 70 kg male is 5 L, with 3 L consisting of plasma and the remaining 2 L representing the volume of the cells in the blood, primarily the red blood cells. The 2 L of cells found in the blood are filled with intracellular fluid. The fraction of the blood volume due to the red blood cells is called the *hematocrit*. The red blood cell volume fraction is found by centrifuging a given volume of blood in order to find the “packed” red cell volume. Since a small amount of plasma is trapped between the packed red blood cells, the true hematocrit (H) is about 96% of this measured hematocrit (Hct). The true hematocrit is about 40% for a male and about 36% for a female. The *transcellular fluids* are those fluids found only within specialized compartments and include the cerebrospinal, intraocular, pleural, pericardial, synovial, sweat, and digestive fluids. Some of these compartments have membrane surfaces that are in proximity to one another and have a thin layer of lubricating fluid between them.

Table 3.1 Body Fluids

Fluid	Fluid Volume (L)	Body Weight (wt%)
Intracellular	25	36
Extracellular	15	21
Interstitial	12	17
Plasma	3	4
Transcellular	—	—
Total	40	57

Source: Data from Guyton, A.C., *Textbook of Medical Physiology*, 8th ed., W.B. Saunders Co., Philadelphia, PA, 1991, p. 275.

Measurement of these fluid volumes can be achieved by using “tracer materials” that have the unique property of remaining in specific fluid compartments. The fluid volume of a specific compartment can then be found by adding a known mass of a tracer to a specific compartment and, after an appropriate period of time for dispersal, measuring the concentration (mass/volume) of the tracer in the fluid compartment. The compartment volume is then given by the ratio of the tracer mass that was added and the measured tracer concentration, i.e., mass/(mass/volume) = volume.

Examples of tracers used to measure fluid volumes include radioactive water for measuring *total body water* and radioactive sodium, radioactive chloride, or inulin for measuring *extracellular fluid volume*. Tracers that bind strongly with plasma proteins may be used for measuring the *plasma volume*. *Interstitial fluid volume* may then be found by subtracting the plasma volume from the extracellular fluid volume. Subtraction of the extracellular fluid volume from the total body water provides the *intracellular fluid volume*.

## 3.2 Fluid compositions

The compositions of the body fluids are presented in [Table 3.2](#) in terms of concentration in units of *milliosmolar* (mOsmole L<sup>-1</sup> of solution or mOsM). The term *osmole* has been introduced to account for the effect of a dissociating solute in an aqueous solution. One osmole is therefore defined as 1 mol of a nondissociating substance. Therefore, one mole of a dissociating substance such as NaCl is equivalent to 2 osmoles or a 1 molar (M) solution of NaCl is equivalent to a 2 osmolar (OsM) solution. However, one mole of glucose is the same as one osmole since glucose does not dissociate in solution. *Osmolarity* simply defines the number of osmoles per liter of solution.

Since the solutes listed in [Table 3.2](#) do not dissociate, these concentrations are the same as millimolar (mmol L<sup>-1</sup> or mM). Of particular interest is the fact that nearly 80% of the total osmolarity of the interstitial fluid and plasma is produced by sodium and chloride ions. As we discussed earlier, the interstitial fluid arises from filtration of plasma through the capillaries. We would therefore expect the composition of these two fluids to be very similar. This is shown in [Table 3.2](#). We find this to be true with the exception that the protein concentration in the interstitial fluid is significantly smaller in comparison to its value in the plasma.

Table 3.2 Osmolar Solutes Found in the Extracellular and Intracellular Fluids

Solute	Plasma (mOsM)	Interstitial (mOsM)	Intracellular (mOsM)
Na <sup>+</sup>	143	140	14
K <sup>+</sup>	4.2	4.0	140
Ca <sup>2+</sup>	1.3	1.2	0
Mg <sup>2+</sup>	0.8	0.7	20
Cl <sup>-</sup>	108	108	4
HCO <sub>3</sub> <sup>-</sup>	24	28.3	10
HPO <sub>4</sub> <sup>-</sup> , H <sub>2</sub> PO <sub>4</sub> <sup>-</sup>	2	2	11
SO <sub>4</sub> <sup>-</sup>	0.5	0.5	1
Phosphocreatine			45
Carnosine			14
Amino acids	2	2	8
Creatine	0.2	0.2	9
Lactate	1.2	1.2	1.5
Adenosine triphosphate			5
Hexose monophosphate			3.7
Glucose	5.6	5.6	
Protein	1.2	0.2	4
Urea	4	4	4
Others	4.8	3.9	11
Total (mOsM)	302.8	301.8	302.2
Corrected osmolar activity (mOsM)	282.5	281.3	281.3
Total osmotic pressure at 37°C (mmHg)	5450	5430	5430

Source: Data from Guyton, A.C., *Textbook of Medical Physiology*, 8th ed., W.B. Saunders Co., Philadelphia, PA, 1991, p. 277.

### 3.3 Capillary plasma protein retention

The retention of proteins by the walls of the capillary during filtration of the plasma is readily explained by comparing the molecular sizes of typical plasma protein molecules to the size of the pores within the capillary wall. Figure 3.1 illustrates the relative size of various solutes as a function of their molecular weight. The wall of a capillary, illustrated in Figure 3.2, consists of a single layer of *endothelial cells* that are surrounded on their outside by a *basement membrane*. The basement membrane is a mat-like cellular support structure, or extracellular matrix, that consists primarily of a protein called *type IV collagen*, and is joined to the cells by the glycoprotein called *laminin*. The basement membrane is about 50–100 nm thick. The total thickness of the capillary wall is about 0.5 µm.

As shown in Figure 3.2, there are several mechanisms that allow for the transport of solutes across the capillary wall. These include the *intercellular cleft* and *pinocytotic vesicles* and *channels*. The intercellular cleft is a thin slit or slit pore that is formed at the interface between adjacent endothelial cells. The size of the openings or pores in this slit is about 6–7 nm, just sufficient to retain plasma proteins such as albumin and other larger proteins.

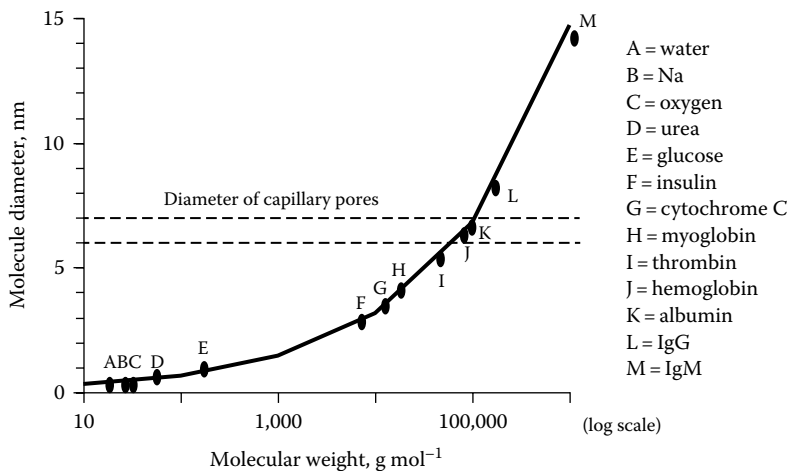


Figure 3.1 Approximate diameter of molecules as a function of their molecular weight.

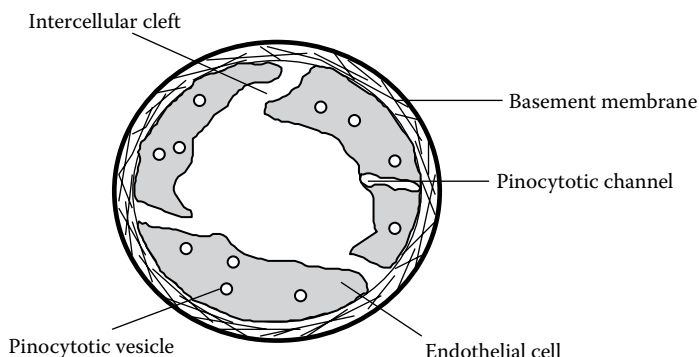


Figure 3.2 Cross section of a capillary.

The collective surface area of these openings represents less than 1/1000th of the total capillary surface area for a typical nonfenestrated capillary.

The plasma proteins are generally larger than the capillary slit pores. Although ellipsoidally shaped proteins, e.g., the clotting protein fibrinogen, may have a minor axis that is smaller than that of the capillary slit pore, the streaming effect caused by the fluid motion within the capillary orients the major axis of the proteins parallel to the flow axis and prevents their entry into the slit pore. This streaming effect is shown in [Figure 3.3](#). Therefore, the smaller substances found in the plasma, such as ions, glucose, and metabolic waste products, will readily pass through the slit pores of the capillary wall, whereas the plasma proteins will be retained in the lumen of the capillary. The composition of the plasma and interstitial fluid should therefore only differ in their protein content. This is shown in [Table 3.2](#).

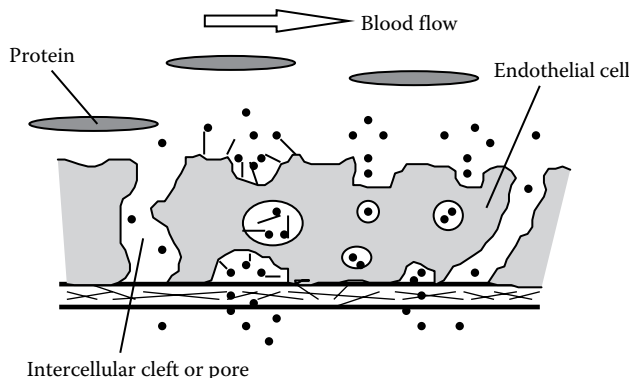


Figure 3.3 Orientation of ellipsoidal shaped proteins by streaming prevents their entry into the capillary pores.

### 3.4 Osmotic pressure

Retention of proteins in the plasma in comparison to the interstitial fluid creates an *osmotic pressure* between the plasma and the interstitial fluid. We discussed the thermodynamics of osmosis in [Section 2.6.3.5](#). Since the plasma proteins are the only constituent of the plasma that do not readily pass through the capillary wall, it is the plasma proteins that are responsible for the formation of the osmotic pressure between the interstitial and plasma fluids. The osmotic pressure created by these proteins is given the special name of *colloid osmotic pressure* or *oncotic pressure*. For human plasma, the colloid osmotic pressure is about 28 mmHg, with 19 mmHg caused by the plasma proteins and 9 mmHg caused by the cations within the plasma that are also retained through electrostatic interaction with the negative surface charges of these proteins (see Gibbs-Donnan Effect in [Section 2.6.3.13](#)).

The colloid osmotic pressure is actually quite small in comparison to the osmotic pressure that develops when a cell is placed in pure water. In this case, it is assumed that all of the species present within the intracellular fluid are retained by the cell membrane. As shown in [Table 3.2](#), the total osmotic pressure of the intracellular fluid in this case would be 5430 mmHg at 37°C.

#### 3.4.1 Osmolarity

Recognizing that it is the number of retained solute molecules that contributes to the osmotic pressure, we must be careful to make the distinction between a retained substance that dissociates and one that does not dissociate. The term “retained” means that the solute cannot move across the membrane that separates the solutions of interest. For example, compounds such as NaCl are strong electrolytes. In water, they completely dissociate to form two ions, i.e.,  $\text{Na}^+$  and  $\text{Cl}^-$ . For  $\text{CaCl}_2$ , we end up with three ions or entities, i.e.,  $\text{Ca}^{2+}$  and two  $\text{Cl}^-$ . Each ion or entity formed will exert its own osmotic pressure. It is important to note that the charge of the ion has no effect (assuming an ideal solution) on the osmotic pressure, so a sodium ion with a charge of +1 is equivalent to a calcium ion of charge +2. Substances such as glucose do not dissociate and their osmotic pressure is based on their nondissociated concentration only.

If a cell is placed within a solution that has a lower concentration of solutes or osmolarity, then the cell is in a *hypotonic solution*, and establishment of osmotic equilibrium requires the osmosis of water into the cell. This influx of water into the cell results in the swelling of the cell and a subsequent decrease in its osmolarity. On the other hand, if the cell is placed in a solution with a higher concentration of solutes or osmolarity, i.e., *hypertonic*, then osmotic equilibrium requires osmosis or diffusion of water out of the cell, concentrating the intracellular solution and resulting in shrinkage of the cell. An *isotonic* solution is a fluid that has the same osmolarity of the cell. When cells are placed in an isotonic solution, there is neither swelling nor shrinkage of the cell. A 0.9 wt% solution of sodium chloride or a 5 wt% solution of glucose is just about isotonic with respect to a cell.

### 3.4.2 Calculating the osmotic pressure

Recall from our discussion in [Chapter 2](#) on osmosis that for the special case where the solvent and solute form an ideal solution, the osmotic pressure given by [Equation 2.147](#) may be written as

$$\Pi = \frac{RT}{V_{\text{solute}}^L} x_{\text{solute}}^A = RTC_{\text{solute}} \quad (3.1)$$

Here,  $x_{\text{solute}}^A$  represents the mole fraction of the nondissociating solute in the solution, which is region A in [Figure 2.5](#). Recall that since the solute mole fraction is generally quite small, we may approximate this as  $x_{\text{solute}}^A = V_{\text{solvent}}^L C_{\text{solute}}$ , where  $C_{\text{solute}}$  is the concentration of the solute in gmoles per liter of solution and  $V_{\text{solvent}}^L$  is the molar volume of the solvent. This ideal dilute solution osmotic pressure, described by [Equation 3.1](#), is also known as *van't Hoff's law*.

If the solution contains N ideal nondissociating solutes, then the total osmotic pressure of the solution will be the summation of the osmotic pressure generated by each solute or entity according to [Equation 3.1](#):

$$\Pi = RT \sum_{i=1}^N C_{\text{solute}_i} \quad (3.2)$$

For physiological solutions, it is convenient to work in terms of milliosmoles (mOsm) or milliosmolar (mOsM). At a physiological temperature of 37°C, [Equation 3.2](#) may be written as follows to give the osmotic pressure in mmHg when the solute concentration of each nondissociating species is expressed in mOsM:

$$\Pi = 19.33 \sum_{i=1}^N C_{\text{solute}_i} \quad (3.3)$$

As we discussed in [Chapter 2](#), remember that osmotic pressure is not determined on the basis of the mass of the solute in the solution, but rather on the number of entities that are formed by a given solute. Each nondiffusing entity in the solution contributes the same amount to the osmotic pressure regardless its size. The following example shows how to apply [Equation 3.2](#) in a situation with many species that dissociate in water.

### Example 3.1

MoviPrep® is a low-volume colonoscopy prep that is used to provide a clear view of the entire colon, allowing your doctor to detect abnormal growths during the colonoscopy procedure. Each liter of a MoviPrep solution contains in millimoles the components shown in the following table.

PEG 3350 (polyethylene glycol, does not dissociate)	29.6
NaCl	45.6
Na <sub>2</sub> SO <sub>4</sub>	52.8
KCl	14.2
NaAscorbate (C <sub>6</sub> H <sub>7</sub> O <sub>6</sub> Na)	29.8

At 37°C, what is the osmotic pressure of this solution in mmHg?

#### Solution

The salt components will completely dissociate in the aqueous solution that is formed. We can do a dissociation balance on each entity to find its concentration in the final solution. The PEG 3350 does not dissociate so its concentration in the solution is 29.6 mM.

$$\text{Na}^+ = 45.6 + 2 \times 52.8 + 29.8 = 181 \text{ mOsM}$$

$$\text{Cl}^- = 45.6 + 14.2 = 59.8 \text{ mOsM}$$

$$\text{SO}_4^{2-} = 52.8 = 52.8 \text{ mOsM}$$

$$\text{K}^+ = 14.2 = 14.2 \text{ mOsM}$$

$$\text{Ascorbate}^- = 29.8 = 29.8 \text{ mOsM}$$

The osmotic pressure of the MoviPrep solution can then be calculated in mmHg using [Equation 3.3](#) provided the concentrations are expressed in mOsM.

$$\Pi = 19.33(29.6 + 181 + 59.8 + 52.8 + 14.2 + 29.8) = 7098 \text{ mmHg}$$

### 3.4.3 Other factors that may affect the osmotic pressure

The previous discussion assumed the mixture of solutes formed an ideal solution. However, the osmotic pressure should take into account the various secondary solute interactions that occur within the solution due to their charge, size, shape, and other effects. These effects will either increase or decrease the osmotic activity of a particular solute and results in the corrected osmolar activity shown in [Table 3.2](#). We see in [Table 3.2](#) that the ratio of the corrected osmolar concentration to the total osmolar concentration is about 0.93 for each of the body fluids. This value of 0.93 represents the overall average activity coefficient. In most cases, it is conventional practice to disregard the calculation of solute activity coefficients and calculate the osmotic pressure on the basis of solute

concentration only, as just discussed. Since we will primarily be concerned with differences in the osmotic pressure and the generation of fluid flow across a membrane due to a difference in osmotic pressure, this constant of 0.93 will become absorbed in other constants that generally need to be determined by experiment.

### 3.5 Filtration flow across a membrane

Recall that in general, a *flow* of something is proportional to a *driving force* and inversely proportional to the flow *resistance* or proportional to the flow *conductance*. The flow of fluid across the capillary wall, or, for that matter, any porous semipermeable membrane, is driven then by a difference in pressure across the membrane, which is the driving force. This pressure difference arises not only from hydrodynamic effects but also from the difference in osmotic pressure between the fluids separated by the membrane. The properties of the fluid as well as the physical nature of the membrane produce the resistance to this flow.

Figure 3.4 shows the hydrodynamic and osmotic pressures in the capillary and the surrounding interstitial fluid. In this case the capillary wall acts like a semipermeable membrane. The subscript C refers to the capillary space and the subscript IF refers to the interstitial fluid space that surrounds the capillary. The arrows indicate for each pressure the corresponding direction of fluid flow induced by that pressure. We can write that the volumetric fluid transfer rate ( $Q$ ) across the capillary membrane is directly proportional to the *effective pressure drop* ( $\overline{\Delta P}$ ) across the capillary membrane, as given by

$$Q = L_p S \left[ (P_C - P_{IF}) - (\Pi_C - \Pi_{IF}) \right] = L_p S \overline{\Delta P} \quad (3.4)$$

In Equation 3.4

$S$  is the total circumferential surface area of the capillary membrane, or the total membrane surface area

$L_p$  is the *hydraulic conductance* or *hydraulic permeability*, which is inversely related to the flow resistance of the capillary membrane

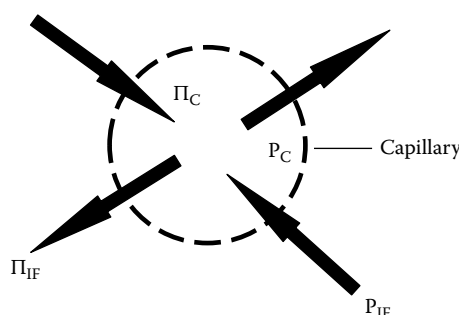


Figure 3.4 Forces acting to cause a flow of fluid across the capillary wall. Arrows indicate the direction of flow induced by each pressure.

The hydraulic conductance is usually best determined by experiment, although a model for its prediction is shown in [Section 3.5.1](#). Also remember that [Equation 3.4](#) applies not only to the capillary membrane but to any semipermeable membrane. However, the subscripts C and IF should be changed to reflect the situation being considered. For example, the high-pressure side of the membrane can be denoted as A and the low-pressure side of the membrane as B. In this case [Equation 3.4](#) becomes  $Q = L_p S[(P_A - P_B) - (\Pi_A - \Pi_B)]$ .

For the capillary membrane, Renkin (1977) reports values for  $L_p$  as low as  $3 \times 10^{-14} \text{ m}^2 \text{ s kg}^{-1}$  for the tight junctions between the endothelial cells found in the capillaries of the rabbit brain,  $5 \times 10^{-12} \text{ m}^2 \text{ s kg}^{-1}$  for nonfenestrated or continuous capillaries, and as high as  $1.5 \times 10^{-9} \text{ m}^2 \text{ s kg}^{-1}$  for the capillaries in the glomeruli of the kidney. In the synthetic membranes used, e.g., in a hemodialyzer,  $L_p$  is usually expressed in common engineering units and is on the order of  $3 \text{ mL h}^{-1} \text{ m}^{-2} \text{ mmHg}^{-1}$ . For silicon nanopore membranes,  $L_p$  can be as high as  $130 \text{ mL h}^{-1} \text{ m}^{-2} \text{ mmHg}^{-1}$  (Song et al., 2016).

It is important to note that [Equation 3.4](#) carries a sign sense with it in terms of the direction of the filtration flow, Q. For example, the first difference term in the brackets of [Equation 3.4](#) represents the difference between the hydrodynamic pressure of the capillary ( $P_C$ ) and the interstitial fluid ( $P_{IF}$ ). When this term is positive, fluid will leave the capillary. When this term is negative, fluid will flow from the interstitial fluid into the capillary. The second difference term within the brackets represents the difference in the osmotic pressure between the capillary ( $\Pi_C$ ) and the interstitial fluid ( $\Pi_{IF}$ ). When this parenthetical term is positive, there will be an osmotic flow of water from the interstitial fluid into the capillary, whereas if this difference is less than zero, there will be an osmotic flow of water out of the capillary. If the entire term in brackets in [Equation 3.4](#) is positive, then there is a net flow of fluid from the capillary into the interstitium. If the bracketed term is negative, then there will be a net flow of fluid from the interstitium into the capillary. If the bracketed term in [Equation 3.4](#) is zero, then there is no filtration flow and we have that  $(P_C - P_{IF}) = (\Pi_C - \Pi_{IF})$ .

[Equation 3.4](#) represents the filtration flow across the capillary membrane. It can also be used to describe the flow across any semipermeable membrane regardless of whether or not it is of biological or synthetic origin. We will find, e.g., that this equation applies to the dialysis membranes used in the artificial kidney as well in a variety of other membrane-based medical devices.

### 3.5.1 Predicting the hydraulic conductance

We can also develop a model for describing how the hydraulic conductance ( $L_p$ ), or the resistance to fluid flow across the membrane, depends on the membrane pore geometry and the physical properties of the filtrate fluid. First, we model the porous structure of the membrane as a series of parallel cylindrical pores. We will show in [Chapter 4](#) that Poiseuille's equation ([Equation 4.10](#)) provides a relationship between flow (Q) and the pressure drop ( $P_0 - P_L$ ) in a cylindrical tube or in this case a cylindrical pore:

$$Q = \frac{\pi R^4 (P_0 - P_L)}{8\mu L_{pore}} \quad (3.5)$$

where

$\mu$  is the viscosity (a measure of the flow resistance) of the fluid

R is the radius of the cylindrical tube or pore

$L_{pore}$  is the length of the tube or pore

[Equation 3.5](#) provides the flow rate across a single pore in the capillary wall or in a semipermeable membrane. If we have a total of  $N$  pores in a membrane of total surface area  $S$ , then we can equate [Equation 3.5](#) for  $N$  pores to [Equation 3.4](#) and obtain the result shown here:

$$Q = L_p S \overline{\Delta P} = N \left( \frac{\pi R^4}{8\mu\tau\bar{L}} \right) \overline{\Delta P} \quad (3.6)$$

where we have replaced  $(P_0 - P_L)$  in Poiseuille's equation with the effective pressure drop  $\overline{\Delta P}$ . The pore length, i.e.,  $L_{\text{pore}}$ , is usually longer than the thickness of the capillary wall or membrane ( $\bar{L}$ ) since the pores are not straight but tortuous. Hence, we replaced  $L_{\text{pore}}$  in [Equation 3.5](#) with the product of the tortuosity ( $\tau$ ) and the capillary wall or membrane thickness,  $\bar{L}$ . The tortuosity is a correction factor that accounts for pores that are longer than the thickness of the membrane.

The total cross-sectional area of the pores, i.e.,  $A_p$ , is equal to  $N\pi R^2$ . Substituting this into [Equation 3.6](#) allows us to solve for the hydraulic conductance as shown here:

$$L_p = \left( \frac{A_p}{S} \right) \frac{R^2}{8\mu\tau\bar{L}} = \varepsilon \frac{R^2}{8\mu\tau\bar{L}} \quad (3.7)$$

[Equation 3.7](#) provides a model that allows one to understand the factors that affect the hydraulic conductance. We see that the hydraulic conductance is directly proportional to the *porosity* ( $\varepsilon$ ) of the capillary wall, i.e.,  $(A_p/S)$ , and inversely proportional to the flow resistance of the fluid, i.e., its viscosity ( $\mu$ ), and the thickness of the capillary wall or membrane ( $\bar{L}$ ). In addition, the hydraulic conductance is directly proportional to the square of the pore radius.

### Example 3.2

Calculate the filtration flow rate ( $\text{cm}^3 \text{ s}^{-1}$ ) of a pure fluid across a  $100 \text{ cm}^2$  membrane. Assume the viscosity ( $\mu$ ) of the fluid is  $1.8 \text{ cP}$ . The porosity of the membrane is  $40\%$  and the thickness of the membrane is  $500 \mu\text{m}$ . The pores run straight through the membrane and these pores have a radius of  $0.225 \mu\text{m}$ . The pressure drop applied across the membrane is  $75 \text{ psi}$ . (From [Chapter 4](#) we have for the viscosity that  $1 \text{ cP} = 0.001 \text{ N s m}^{-2} = 0.001 \text{ Pa s}$ .)

### Solution

To find the filtration flow rate, we will use [Equations 3.4](#) and [3.7](#). Since there are no retained solutes, there are no osmotic effects and the effective pressure drop across the membrane is equal to the applied pressure drop of  $75 \text{ psi}$ . From the information about the membrane, we first calculate the value of the hydraulic conductance as shown here:

$$\frac{A_p}{S} = 0.4, \quad R = 0.225 \mu\text{m} = 2.25 \times 10^{-5} \text{ cm}, \quad \bar{L} = 500 \mu\text{m} = 0.05 \text{ cm},$$

$$\mu = 1.8 \text{ cP} = 0.0018 \text{ Pa s}, \quad \text{and} \quad \overline{\Delta P} = 75 \text{ psi} \times \frac{1 \text{ atm}}{14.7 \text{ psi}} \times \frac{10,1325 \text{ Pa}}{1 \text{ atm}} = 5.17 \times 10^5 \text{ Pa}$$

Now substituting these values in [Equation 3.7](#)

$$L_p = \frac{0.40 \times (2.25 \times 10^{-5} \text{ cm})^2}{8 \times 0.0018 \text{ Pa s} \times 0.05 \text{ cm}} = 2.813 \times 10^{-7} \frac{\text{cm}}{\text{Pa s}}$$

and from [Equation 3.4](#)

$$Q = 2.813 \times 10^{-7} \frac{\text{cm}}{\text{Pa s}} \times 100 \text{ cm}^2 \times 5.17 \times 10^5 \text{ Pa}$$

$$Q = 14.54 \frac{\text{cm}^3}{\text{s}}$$

**3.5.1.1 Rectangular pores** If the pores in the membrane are not circular, but rectangular slits, a similar approach as previously discussed can be used to calculate the hydraulic conductance. For flow in the rectangular space formed between two large parallel plates of length L (in the flow direction) and width W, it is shown in Problem 4.25 that the volumetric flow rate (Q) is given by

$$Q = \frac{2}{3} WH^3 \frac{(P_0 - P_L)}{\mu L} \quad (3.8)$$

where the plates are separated by a distance of 2H, and  $H \ll L$  and  $W$ . [Equation 3.8](#) gives the flow rate through a single rectangular pore. Assuming we have a total of N pores in the membrane of total surface area S, then we can equate [Equations 3.4](#) and [3.8](#) to obtain

$$Q = L_p S \overline{\Delta P} = N \left( \frac{2WH^3}{3\mu\tau\bar{L}} \right) \overline{\Delta P} \quad (3.9)$$

Once again we have replaced  $(P_0 - P_L)$  in [Equation 3.8](#) with the effective pressure drop  $\overline{\Delta P}$ . The actual pore length is also equal to  $\tau\bar{L}$  to account for pores that are not straight but tortuous. The total cross-sectional area of the slit pores, i.e.,  $A_p$ , is equal to  $N \times 2HW$ . Using this result to eliminate N in [Equation 3.9](#) gives the hydraulic conductance for slit pores

$$L_p = \left( \frac{A_p}{S} \right) \frac{H^2}{3\mu\tau\bar{L}} = \varepsilon \frac{H^2}{3\mu\tau\bar{L}} \quad (3.10)$$

Comparing the hydraulic conductance for a slit pore (i.e., [Equation 3.10](#)) to that for a cylindrical pore (i.e., [Equation 3.7](#)) with the slit pore half-thickness (H) equal to the cylindrical pore radius (R), we see that the slit pore, with everything else being the same, has a hydraulic conductance 2.67 times that of the cylindrical pore. This explains why we oftentimes see rectangular openings in many filtration situations. For example, in nature we see this in the capillary membrane with the slit pores or intercellular cleft formed between the endothelial cells that line the capillary or in the baleen plates of certain whales that trap their food by filtering the ocean water. We also see this in storm sewer drain covers and in the colander found in your kitchen. Rectangular openings maintain the desired size exclusion for filtration without impeding the flow of the fluid. Membranes based on rectangular slit pores are therefore receiving considerable attention for the next generation of a variety of membrane medical devices and artificial organs (Fissell et al., 2009, 2013; Kanani et al., 2010; Song et al., 2016).

### 3.6 Net capillary filtration rate

We can use [Equation 3.4](#) to estimate the *net capillary filtration rate* for the human body. To perform this calculation, we will first need to define nominal values for the properties of the capillaries that are in the body. These properties are summarized in [Table 3.3](#) (*Note*: these are gauge pressures or relative to atmospheric pressure of 760 mmHg). The capillary lumen lies within a circumferential ring of several endothelial cells, as shown earlier in [Figure 3.2](#). Note that capillaries are very small having diameters of about 8–10  $\mu\text{m}$  and lengths that are less than 1 mm. The residence time of blood in a capillary is also only on the order of 1 s. Each capillary can only supply nutrients and remove waste products from a very small volume of tissue that surrounds each capillary.

There are also three types of capillaries. They are referred to as continuous, fenestrated, and discontinuous. The *continuous capillaries* are found in the muscle, skin, lungs, fat, the nervous system, and in connective tissue. *Fenestrated capillaries* are much more permeable to water and small solutes in comparison to continuous capillaries. Hence, fenestrated capillaries have a very high hydraulic conductance in comparison to continuous capillaries. The fenestrated capillaries are found in tissues that are involved in the exchange of fluid or solutes such as hormones. For example, within the kidney they are found in the glomerulus and allow for a high filtration rate of the plasma. The endothelium of these capillaries is perforated by numerous small holes called *fenes-trae*. The fenes-trae are sometimes covered by a thin membrane that provides selectivity with regard to the size of solutes that are allowed to pass through. *Discontinuous capillaries* have large endothelial cell gaps that readily allow the passage of proteins and even red blood cells.

At the arterial end of the capillary, the capillary pressure is about 30 mmHg, and at the venous end of the capillary, the pressure is about 10 mmHg. The mean capillary pressure is considered to be about 17.3 mmHg and its bias to the lower end is based on the larger volume of the venous side of the capillaries in comparison to the arterial side of the capillaries. The interstitial fluid pressure has surprisingly been found to be subatmospheric and the accepted value is –3 mmHg. As mentioned before, the colloid osmotic pressure for human plasma is 28 mmHg and the value for the interstitial fluid is about 8 mmHg.

Table 3.3 Capillary Characteristics

Property	Value
Inside diameter ( $D_c$ )	10 $\mu\text{m}$
Length (L)	0.1 cm
Wall thickness ( $t_m$ )	0.5 $\mu\text{m}$
Average blood velocity (V)	0.05 cm $\text{s}^{-1}$
Pore fraction	0.001
Wall pore diameter ( $d_p$ )	6–7 nm
Inlet pressure	30 mmHg
Outlet pressure	10 mmHg
Mean pressure ( $P_c$ )	17.3 mmHg
Colloid osmotic pressure ( $\Pi_p$ )	28 mmHg
Interstitial fluid pressure ( $P_{IF}$ )	–3 mmHg
Interstitial fluid colloid osmotic pressure ( $\Pi_{IF}$ )	8 mmHg

At the arterial end of the capillary, we can calculate the flow rate of fluid across the capillary wall by using [Equation 3.4](#). Therefore,  $Q/L_pS = [(30 - (-3)) - (28 - 8)] = 13 \text{ mmHg}$ , which is positive, indicating that there is a net flow of fluid from the capillary into the interstitium. At the venous end of the capillary,  $Q/L_pS = [(10 - (-3)) - (28 - 8)] = -7 \text{ mmHg}$ , which is less than zero, indicating a net reabsorption of fluid from the interstitium back into the capillary.

This flow of fluid out of the capillary at the arterial end, and its reabsorption at the venous end, is called *Starling flow*, after E.H. Starling who first described it over a hundred years ago. [Equation 3.4](#) is also known as the *Starling equation*. If we base the filtration rate on the mean capillary pressure, then  $Q/L_pS = [(17.3 - (-3)) - (28 - 8)] = 0.3 \text{ mmHg}$ . Hence, on average, there is a slight imbalance in pressure resulting in more filtration of fluid out of the capillary than is reabsorbed.

Approximately 90% of the fluid that leaves at the arterial end of the capillary is reabsorbed at the venous end. However, the 10% that is not reabsorbed by the capillary collects within the interstitium and enters the lymphatic system where it is then returned to the cardiovascular system. The amount of this net filtration of fluid from the circulation for the human body can be estimated as illustrated in the following example.

### Example 3.3

Calculate the normal rate of net filtration for the human body. Assume the capillaries have a total surface area of  $500 \text{ m}^2$ , that the tortuosity of the slit pores ( $\tau$ ) is equal to 2, and that the slit pore surface area is 1/1000th of the total capillary surface area.

### Solution

We model the porous structure of the capillary wall as a series of parallel rectangular slit pores with a thickness of 7 nm. Plasma filtrate may be considered to be a Newtonian fluid with a viscosity of 1.2 centipoise (cP). The mean net filtration pressure, or the effective pressure drop for the capillary, was just calculated previously to be 0.3 mmHg. Using [Equation 3.10](#), we can calculate the hydraulic conductance and then the net filtration rate:

$$L_p = \left( \frac{0.5 \text{ m}^2}{500 \text{ m}^2} \right) \frac{\left( 0.5 \times 7 \times 10^{-9} \text{ m} \right)^2}{3 \times 1.2 \text{ cP} \times \frac{0.01 \text{ P}}{\text{cP}} \times \frac{1 \text{ g}}{\text{cm} \cdot \text{s}} \times \frac{100 \text{ cm}}{\text{m}} \times \frac{1 \text{ kg}}{1000 \text{ g}} \times 2 \times 0.5 \times 10^{-6} \text{ m}} \\ = 3.40 \times 10^{-12} \frac{\text{m}^2 \cdot \text{s}}{\text{kg}}$$

Note that this prediction of  $L_p$  is consistent with the values reported by Renkin (1977) for the hydraulic conductance of continuous capillaries:

$$Q = 3.40 \times 10^{-12} \frac{\text{m}^2 \cdot \text{s}}{\text{kg}} \times 500 \text{ m}^2 \times 0.3 \text{ mmHg} \times \frac{1 \text{ atm}}{760 \text{ mmHg}} \times 101.33 \frac{\text{kPa}}{\text{atm}} \times \frac{1 \text{ Nm}^{-2}}{\text{Pa}} \\ \times \frac{1000 \text{ Pa}}{\text{kPa}} \times \frac{\text{kg ms}^{-2}}{\text{N}} \times \frac{60 \text{ s}}{\text{min}} \times \frac{(100 \text{ cm})^3}{\text{m}^3} \\ Q = 4.1 \frac{\text{cm}^3}{\text{min}}$$

We find that the *total net filtration rate* due to the pressure imbalance at the capillaries for the human body is on the order of several  $\text{mL min}^{-1}$ .

### 3.6.1 A comparison of the blood flow into the capillary with the capillary filtration flow rate

We see in the previous example that some of the blood plasma that enters the capillary will be filtered across the capillary wall by the combined effect of the hydrodynamic and oncotic pressure differences that exist between the capillary and the surrounding interstitial fluid. This perfusion of plasma across the capillary wall is also known as *plasmapheresis*. In the following example, we will compare the capillary filtration rate to the flow rate of the blood entering the capillary.

#### **Example 3.4**

Calculate the filtration flow rate of plasma across the capillary wall and compare this to the flow rate of blood entering the capillary.

#### **Solution**

Using the capillary properties provided in [Table 3.3](#) and the value of the hydraulic conductance, i.e.,  $L_p$ , from [Example 3.3](#), we can then calculate the filtration rate for a capillary using [Equation 3.4](#). Note that the hydraulic conductance of  $3.40 \times 10^{-12} \text{ m}^2 \text{ s kg}^{-1}$  found in [Example 3.3](#) is equal to  $1.63 \text{ cm}^3 \text{ h}^{-1} \text{ m}^{-2} \text{ mmHg}^{-1}$ :

$$\begin{aligned} Q_{\text{filtration}} &= \frac{1.63 \text{ cm}^3}{\text{h m}^2 \text{ mmHg}} \times \pi \times 10 \times 10^{-6} \text{ m} \times 0.001 \text{ m} \times [(17.3 - 3) - (28 - 8)] \text{ mmHg} \\ &= 1.54 \times 10^{-8} \text{ cm}^3 \text{ h}^{-1} = 1.54 \times 10^{-5} \mu\text{L h}^{-1} \end{aligned}$$

We can compare this value of the plasma filtration flow rate across the capillary wall to the total flow rate of blood entering the capillary, i.e.,  $Q_{\text{capillary}} = (\pi/4)d_{\text{capillary}}^2 V$ :

$$\begin{aligned} Q_{\text{capillary}} &= \frac{\pi}{4} (10 \times 10^{-6} \text{ m})^2 \times \frac{0.05 \text{ cm}}{\text{s}} \times \left( \frac{100 \text{ cm}}{\text{m}} \right)^2 \times \frac{3600 \text{ s}}{\text{h}} \\ &= 1.41 \times 10^{-4} \text{ cm}^3 \text{ h}^{-1} = 0.14 \mu\text{L h}^{-1} \end{aligned}$$

We find for the special case of a capillary that the volumetric flow rate of blood entering the capillary ( $Q_{\text{capillary}}$ ) is significantly higher than the filtration flow of plasma ( $Q_{\text{filtration}}$ ) across the capillary wall. We may therefore assume that the blood flow, i.e.,  $Q_{\text{capillary}}$ , is constant along the length of the capillary.

## 3.7 Lymphatic system

We must now address where this total net filtration of fluid from the capillaries ultimately goes. It clearly cannot continue to collect within the interstitium since this would lead to *edema* or excess fluid (swelling) within the tissues of the body.

Edema is an excess extracellular fluid and is caused either by too much filtration of fluid from the capillaries as just discussed, a failure to drain this excess fluid from the interstitium, or retention of salt and water as a result of impaired kidney function. Edema can also be caused by

intracellular accumulation of fluid as a result of cellular metabolic problems or inflammation. In these cases either the sodium ion pumps are impaired (see [Section 3.10](#)) or the cell membrane permeability to sodium is increased. In either case, the excess sodium in the cell causes osmosis of water into the cell.

The *lymphatic system* is an accessory flow or circulatory system in the body that drains excess fluid from the interstitial spaces and returns it to the blood. The lymphatics consist of a system of lymphatic capillaries and ducts that empty into the venous system at the junctures of the left and right internal jugular and subclavian veins. The lymphatic system is also responsible for the removal of large proteins and other substances that cannot be reabsorbed into the capillary from the interstitial space. Like the capillaries of the vascular system, the lymphatic capillaries are also formed by endothelial cells. However, the lymphatic endothelial cells have much larger intercellular junctions and the cells overlap in such a manner to form a valve-like structure. Interstitial fluid can force the valve open to flow into the lymphatic capillary; however, backflow of lymphatic fluid from the lymphatic capillary is prevented.

### 3.8 Solute transport across the capillary endothelium

Lipid-soluble substances such as oxygen and carbon dioxide can diffuse directly through the endothelial cells that line the capillary wall without the use of the intercellular cleft slit pores. Accordingly, their rate of transfer across the capillary wall is significantly higher than water-soluble, but lipid-insoluble substances, such as sodium ions, chloride ions, and glucose, for which the cell membrane of the endothelial cell is essentially impermeable. The transport of these latter substances across the capillary wall is through the use of the capillary intercellular cleft slit pores.

In addition to the slit pores, there are two other pathways that can provide an additional route for the transport of large lipid-insoluble solutes, such as proteins, across the endothelium of the capillary wall. These pathways are called *pinocytosis* and *receptor-mediated transcytosis* (Lauffenburger and Linderman, 1993).

Pinocytosis is not solute specific and, as shown in [Figure 3.5](#), involves the ingestion by the cell of the surrounding extracellular fluid and its associated solutes. A small portion of the cell's plasma membrane forms a pocket containing the extracellular fluid. This pocket grows in size and finally

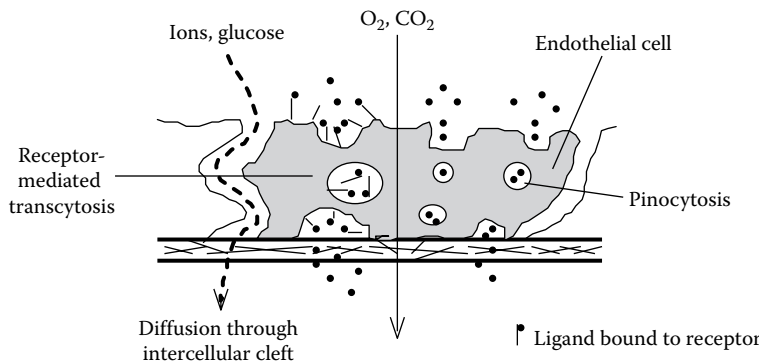


Figure 3.5 Mechanisms for solute transport across the capillary endothelium.

pinches off to form the intracellular pinocytotic vesicles. This ingestion of extracellular material by the cell is also known as *endocytosis*. The pinocytotic vesicles are either processed, and their contents used internally, or they migrate through the cell and reattach to the cell membrane on the opposite side, where they release their contents to the surrounding milieu. This release of material from the pinocytotic vesicle is known as *exocytosis*. Because of its nonspecific nature, pinocytosis is usually not a significant solute transport mechanism.

However, *receptor-mediated transcytosis* can provide for significant transport of specific solutes across the capillary endothelium. This process is also shown in [Figure 3.5](#). The solute, referred to as a *ligand*, first binds with complementary receptors that are located on the surface of the cell membrane. Unlike the nonspecific process of pinocytosis, receptor-mediated transcytosis can concentrate a particular ligand by many orders of magnitude. This solute-concentrating mechanism by the cell-surface receptors is responsible for the significant transport rates that can be achieved by this process. The ligand-receptor complexes are then endocytosed forming transcytotic vesicles. These vesicles are either processed internally or they can move through the cell and reattach themselves to the opposite side of the cell. The transcytotic vesicle then releases its contents by exocytosis.

The importance of receptor-mediated transcytosis of large lipid-insoluble solutes is provided by the following example. In vitro studies of insulin transport across vascular endothelial cells have shown that 80% of the insulin was transported by receptor-mediated processes. The remaining 20% was transported either through the slit pores between the endothelial cells or by nonspecific pinocytosis (Hachiya et al., 1988).

### 3.9 The cell membrane

The cell membrane, illustrated in [Figure 3.6](#), is composed mainly of a *lipid bilayer*. Lipid molecules are insoluble in water but readily dissolve in organic solvents such as benzene. Three classes of lipids are found in cellular membranes. These are *phospholipids*, *cholesterol*, and *glycolipids*. The lipid bilayer results because the lipid molecule has a head and tail configuration, as shown in [Figure 3.6](#). The head of the lipid molecule is polar and thus hydrophilic, whereas the tail of the lipid molecule is nonpolar and hydrophobic (typically derived from a fatty acid). Such molecules are also called *amphipathic* because the molecule has both hydrophilic and hydrophobic properties. The term *lipid bilayer* indicates their

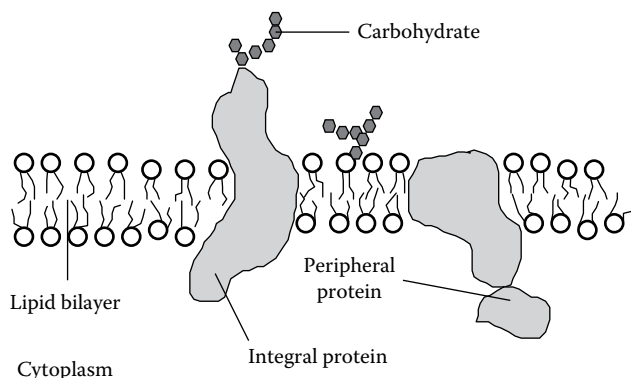


Figure 3.6 Cell membrane structure.

## Physical properties of the body fluids and the cell membrane

tendency to form bimolecular sheets when surrounded on all sides by an aqueous environment, as is the case for a cell membrane. Thus, the hydrophilic heads of the lipid molecules face into the aqueous environment, and the hydrophobic tails are sandwiched between the heads of the lipid molecules.

The lipid bilayer forms the basic structure of the cell membrane. However, other molecules such as proteins are scattered throughout the lipid bilayer of the cell membrane and serve many important functions. For example, special proteins allow for the transport of specific molecules across the cell membrane. Other proteins have catalytic activity and mediate chemical reactions that occur within the cell membrane. These proteins are known as *enzymes*. Still other proteins provide structural support to the cell or provide connections to surrounding cells or other extracellular materials. Some proteins found in the cell membrane act as receptors to extracellular substances or chemical signals and, through transduction of these signals, control intracellular events. Other proteins present foreign materials to the immune system or identify the cell as self.

Protein molecules associated with the cell membrane can be classified into two broad categories. The *transmembrane proteins* are also amphipathic and extend through the lipid bilayer. They typically have hydrophobic regions that may travel across the membrane several times and hydrophilic ends that are exposed to water on either side of the membrane. Integral membrane proteins are transmembrane proteins that are held tightly within the cell membrane through chemical linkages with other components of the cell membrane. Integral proteins have major functions related to the transport of water-soluble but lipid-insoluble substances across the cell membrane. The *peripheral membrane proteins* are not located within the plasma membrane but associate on either side of the membrane with transmembrane or integral proteins. Peripheral proteins mostly function as enzymes.

For the most part, the cell membrane is impermeable to polar or other water-soluble molecules. Hence, large neutral polar molecules, like glucose, have very low cell membrane permeabilities. Charged molecules and ions, such as  $H^+$ ,  $Na^+$ ,  $K^+$ , and  $Cl^-$ , also have very low permeabilities. Hydrophobic molecules, such as oxygen and nitrogen, readily dissolve in the lipid bilayer and show very high permeabilities. Smaller neutral polar molecules, such as  $CO_2$ , urea, and water, are able to permeate the lipid bilayer because of their much smaller size and neutral charge.

The transport of essential water-soluble molecules across the cell membrane is achieved through the use of special transmembrane proteins that have a high specificity for a certain type or class of molecules. These membrane transport proteins come in two basic types: *carrier proteins* and *channel proteins*. The carrier proteins bind to the solute and then undergo a change in shape or conformation (*ding* to *dong*; see Figure 3.7), which allows the solute to traverse the cell membrane. The carrier protein, therefore,

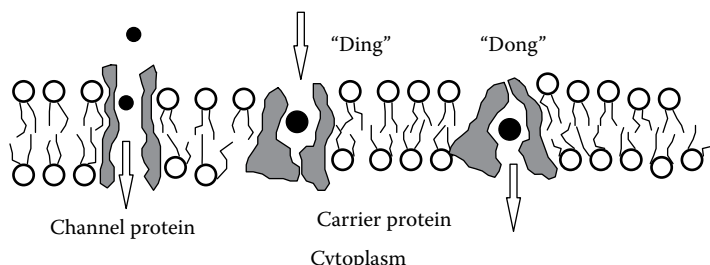


Figure 3.7 Membrane transport proteins. Carrier protein exists in two conformational states, “Ding” and “Dong”.

changes between two shapes, alternately presenting the solute-binding site to either side of the membrane. Channel proteins actually form water-filled pores that penetrate across the cell membrane. Solutes that cross the cell membrane by either carrier or channel proteins are said to be passively transported.

**Figure 3.7** illustrates the passive transport of solutes through the cell membrane by either carrier proteins or channel proteins. Carrier proteins can transport only a single solute across the membrane, a process called *uniport*, or there can be transport of two different solutes, called *coupled transport*. The passive transport of glucose into a cell by glucose transporters is an example of a uniport. In coupled transport, the transfer of one solute occurs in combination with the transport of another solute. This coupled transport of the two solutes can occur with both solutes transported in the same direction, *symport*, or in opposite directions, *antiport*. An example of coupled transport is the sodium ion gradient–driven symport of glucose and sodium ions.

In general, the driving force for the passive transport of these solutes is due to the combined effect of their concentration gradient and the electric potential difference that exists across the membrane. Neutral molecules diffuse from regions of high concentration to regions of low concentration. However, if the molecule carries an electrical charge, then both the concentration gradient and the electric potential difference, or voltage gradient, across the cell membrane will affect the transport of the molecule. The *electrochemical gradient* is the term used to describe the combined effect of charge and solute concentration on the transport of a molecule. The voltage gradient for a cell membrane is such that the inside of the cell membrane is negative in comparison to the outside. This membrane potential ( $V_M$ ) for cells at rest is about  $-90$  mV, which means that the potential inside the cell is  $90$  mV lower than the potential outside the cell.

The flow of charged molecules through channels in the cell membrane is responsible for the creation of the membrane potential. For example, the higher concentration of potassium ions within the cell relative to the surroundings will tend to cause a leakage of these ions out of the cell through the potassium ion leak channels. The loss of these positive ions will make the interior of the cell negative in charge. This creates an electric field that is called the membrane potential. The growth of this membrane potential with continued loss of potassium ions will reach a point where the negative charge created within the cell begins to retard the loss of the positively charged potassium ions due to the difference in potassium concentration. When these two forces balance each other, there is no net flow of the ion, and the ion is at equilibrium. This balance or equilibrium of the concentration and voltage gradients for an ion is known as the *Nernst equilibrium membrane potential* for that ion. Recall from [Chapter 2](#) that the following equation ([Equation 2.228](#)), known as the *Nernst equation*, can be used to calculate the Nernst equilibrium membrane potential for a particular ion:

$$V = \frac{RT}{zF} \ln \frac{C_{\text{outside}}}{C_{\text{inside}}} = - \frac{RT}{zF} \ln \frac{C_{\text{inside}}}{C_{\text{outside}}} \quad (3.11)$$

In this equation

R represents the gas constant ( $1.987 \text{ cal g mol}^{-1} \text{ K}^{-1}$ )

T is the temperature in kelvin

z is the charge on the ion

F is Faraday's constant ( $2.3 \times 10^4 \text{ cal V}^{-1} \text{ g mol}^{-1}$ )

At 25°C, for a univalent ion,  $|RT/zF|$  is equal to 25.68 mV, whereas at 37°C the value is 26.71 mV.

Considering potassium ions, the intracellular concentration from [Table 3.2](#) is 140 mOsM and the interstitial concentration is 4 mOsM. Therefore, the Nernst equilibrium membrane potential calculated from [Equation 3.11](#) for this ion is equal to about -95 mV. Since this value is less than zero, this indicates that there are more negative charges within the cell than outside the cell. When this calculation is done for Cl<sup>-</sup> ions, the equilibrium membrane potential is about -90 mV. Since these Nernst equilibrium membrane potentials for K<sup>+</sup> and Cl<sup>-</sup> ions are pretty close to the resting membrane potential of -90 mV, these ions are at equilibrium and their net transport across the cell membrane is zero.

However, when we calculate the Nernst equilibrium membrane potential for Na<sup>+</sup> and Ca<sup>++</sup> using the values given in [Table 3.2](#),\* we find values of about 60 and 250 mV, respectively, for these ions. These Nernst equilibrium membrane potentials for Na<sup>+</sup> and Ca<sup>++</sup> are far different from the actual resting membrane potential ( $V_M$ ) of about -90 mV, and we conclude that these ions are not at equilibrium. So we see that for a resting cell, the large concentration gradients for K<sup>+</sup> and Cl<sup>-</sup> ions between the inside and outside of the cell are balanced by the electric potential difference across the cell membrane. However, for Na<sup>+</sup> and Ca<sup>++</sup>, their large concentration gradients are not balanced by the resting cell membrane potential, and these ions exist in a nonequilibrium state and will cross the cell membrane into the cell.

The net driving force for the transport of an ion due to the combined effect of the concentration gradient and the resting membrane potential, i.e., the electrochemical gradient, is proportional to the difference between the actual membrane potential,  $V_M$ , and the ion's Nernst equilibrium potential,  $V$ . If the quantity ( $V_M - V$ ) is greater than zero, then the ion will be transported out of the cell through either the channel protein pores or by membrane carrier proteins. However, if this quantity is less than zero, then the ion will be transported into the cell.

We shall soon see in [Section 3.10](#) that the cell must expend cellular energy in order to maintain these large nonequilibrium sodium and calcium ion gradients, thereby maintaining its resting membrane potential.

### 3.9.1 Action potentials

In nerve and muscle cells, the resting membrane potential can change very rapidly. This rapid change in the membrane potential is called an *action potential* and provides for the conduction of a nerve signal from neuron to neuron or the contraction of a muscle fiber. Any stimulus to the cell that raises the membrane potential above a threshold value will lead to the generation of a self-propagating action potential. It is also important to note that the action potential is an all-or-nothing response. The development of an action potential is dependent on the presence of voltage-gated sodium and potassium channels. The voltage-gated sodium channels only open or become active when the membrane potential is less negative than during the resting state. They typically begin to open when the membrane potential is about -65 mV. These sodium gates remain open for only a few tenths of a millisecond after which time they close or become inactive. The voltage-gated sodium channels remain in this inactive or closed state until the

---

\* Here we have set the interior Ca ion concentration at 0.0001 mOsM since the table value is 0.

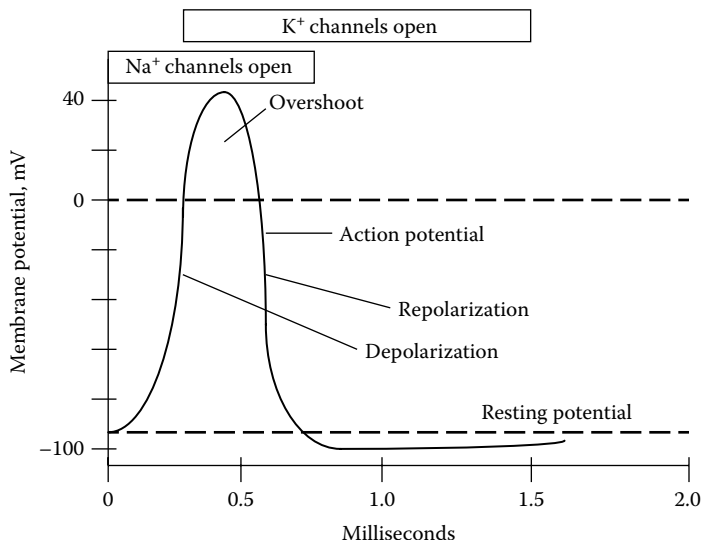


Figure 3.8 Action potential.

membrane potential has returned to near its resting value. The voltage-gated potassium channels also open when the membrane potential becomes less negative than during the resting state; however, unlike the sodium channels, they open more slowly and become fully opened only after the sodium channels have closed. The potassium channels then remain open until the membrane potential has returned to near its resting potential. [Figure 3.8](#) illustrates the events during the generation of an action potential.

The first stage of an action potential is a rapid *depolarization* of the cell membrane. The cell membrane becomes very permeable to sodium ions because of the opening of the voltage-gated sodium channels. This rapid influx of sodium ions, carrying a positive charge, increases the membrane potential in the positive direction and, in some cases, can result in a positive membrane potential (overshoot) for a brief period of time. This depolarization phase may last only a few tenths of a millisecond. Following the depolarization of the membrane, the sodium channels close and the potassium channels, which are now fully opened, allow for the rapid loss of positively charged potassium ions from the cell, thus reestablishing within milliseconds the normal negative resting potential of the cell membrane (repolarization). However, for a brief period of time following an action potential, the sodium channels remain inactive and they cannot open again, regardless of external stimulation, for several milliseconds. This is known as the *refractory period*.

The transport of ions across the cell membrane generates a current ( $i$ ) that is given by the product,  $g(V_M - V)$ . The proportionality constant for the transport of an ion ( $g$ ) due to its electrochemical gradient is referred to as the *membrane conductance* ( $g$ ), which is the inverse of the membrane resistance. This current, or flow of charge, can be related to the flow of the ions themselves using the definitions summarized in [Table 3.4](#). The following example illustrates the calculation of the flow of ions through a membrane channel.

## Physical properties of the body fluids and the cell membrane

Table 3.4 Physical Constants Used to Describe the Electrical Properties of the Cell Membrane

<b>Basic Electrical Properties</b>	<b>Units</b>
Charge	Coulomb (C), charge carried by $6.2 \times 10^{18}$ univalent ions
Electric potential	Volt (V), potential caused by separation of charges
Current	Ampere (A), flow of charge, $C\ s^{-1}$
Capacitance	Farad (F), amount of charge needed on either side of a membrane to produce a given potential, $C/V$
Conductance	Siemens (S), ability of a membrane to conduct a flow of charge, $A/V$
<b>Electrical Properties of Cells</b>	<b>Typical Values</b>
Membrane potential	-20 to -200 mV
Membrane capacitance	$\sim 0.01\ pF\ \mu m^{-2}$ of cell membrane surface area
Conductance of a single ion channel	1–150 pS
Number of specific ion channels	$\sim 75\ \mu m^{-2}$ of cell membrane surface area
<b>Other Relationships</b>	
milli (m) = $10^{-3}$ , micro ( $\mu$ ) = $10^{-6}$	nano (n) = $10^{-9}$ , pico (p) = $10^{-12}$

Source: Data from Alberts, B. et al., *Molecular Biology of the Cell*, 2nd ed., Garland Publishing, Inc., New York, 1989, p. 1067.

### Example 3.5

Calculate the flow of sodium ions through the voltage-gated sodium channels in a cell membrane during depolarization. Assuming the cell membrane has a surface area of  $1\ \mu m^2$ , how long would it take to change the membrane potential by 100 mV? Assume the equilibrium membrane potential for sodium ions is 62 mV (see Table 3.2 and Equation 3.11), that the threshold membrane potential for the sodium channels is -65 mV, and that at the peak of the action potential the membrane potential is 35 mV. In addition, the membrane conductance for the Na ions is  $4 \times 10^{-12}\ S\ channel^{-1}$ .

### Solution

Since the membrane potential rapidly changes during depolarization from the threshold value of -65 mV to the peak value of 35 mV, assume for calculation of the sodium ion flow that the “average” membrane potential during this phase is -15 mV. The flow or current of sodium ions may then be calculated from the following equation:

$$i_{Na} = g_{Na} (V_M - V_{Na})$$

$$i_{Na} = \frac{4 \times 10^{-12}\ S}{channel} \times \frac{1\ A\ V^{-1}}{S} \times \frac{1\ C\ s^{-1}\ V^{-1}}{A} \times \frac{6.2 \times 10^{18}\ \oplus}{C} \times \frac{1\ V}{1000\ mV} \times \frac{1\ Na}{\oplus} \times \frac{75\ channels}{\mu m^2}$$

$$\times (-15 - 62)\ mV = -1.43 \times 10^8\ Na\ s^{-1}\ \mu m^{-2}$$

This flow of sodium ions into the cell is also equivalent to a current of  $-23\ pA\ \mu m^{-2}$ . The flow of sodium ions transfers charge across the membrane, thereby changing the membrane potential. We can relate this change in charge and membrane potential to the membrane capacitance by the following relationship,  $C_{membrane} = i_{Na} t / \Delta V_M$ . Recall from Table 3.4 that the membrane capacitance is

about  $.01 \text{ pF } \mu\text{m}^{-2}$ . For the calculated sodium ion current and the 100 mV change in the membrane potential, we can then solve for the time required to achieve this change in membrane potential:

$$t = \frac{\frac{.01 \text{ pF}}{\mu\text{m}^2} \times \frac{1 \text{ C}}{\text{VF}} \times \frac{1 \text{ V}}{1000 \text{ mV}} \times 100 \text{ mV}}{23 \frac{\text{pA}}{\mu\text{m}^2} \times \frac{1 \text{ C}}{\text{s A}} \times \frac{1 \text{ s}}{1000 \text{ ms}}} = 0.043 \text{ ms}$$

This example shows that the membrane potential is rapidly depolarized during the initial phase of the action potential.

### 3.10 Ion pumps maintain nonequilibrium state of the cell

Cells also have the ability to “pump” certain solutes against their electrochemical gradient. This process is known as *active transport* and involves the use of special carrier proteins. Since this is an “uphill” process, active transport requires the expenditure of cellular energy.

As discussed earlier, the large concentration gradient and the favorable electrical field of the cell’s resting membrane potential will tend to drive the transport of sodium and calcium ions across the cell membrane and into the cell. There will also be some leakage of potassium and chloride ions out of the cell. However, as we have discussed, proper functioning of the cell requires that these concentration differences be maintained in order to preserve the cell’s resting membrane potential. Substances cannot diffuse against their own electrochemical gradient without the expenditure of energy. Therefore, to compensate for the loss of potassium ions by leakage through the cell membrane, the cell must have a “pump” mechanism to shuttle potassium ions from the external environment back into the cell. Similarly, sodium ions leak into the cell and the cell needs a “pump” to remove these ions. This process of shuttling substances across the cell membrane against their electrochemical gradient and at the expense of cellular energy is called *active transport*.

The energy for active transport is provided by the cellular energy storage molecule called *adenosine triphosphate* (ATP). ATP is a nucleotide consisting of three components: a base called adenine, a ribose sugar, and a triphosphate group. Through the action of the enzyme *ATPase*, a molecule of ATP can be converted into a molecule of ADP (adenosine diphosphate) and a free high-energy phosphate bond that can cause conformational changes in special cell membrane carrier proteins.

The best example of active transport is the *sodium-potassium pump* present in all cells. The Na-K pump transports sodium ions out of the cell and at the same time transfers potassium ions into the cell. [Figure 3.9](#) illustrates the essential features of the Na-K pump. The carrier protein protrudes through both sides of the cell membrane. Within the cell, the carrier protein has three receptor sites for binding sodium ions and also has ATPase activity. On the outside of the cell membrane, the carrier protein has two receptor sites for binding potassium ions. When these ions are bound to their respective receptor sites, the ATPase then becomes activated liberating the high-energy phosphate bond ( $P_i$ ) from ATP. The energy in the phosphate bond causes a shape or conformational change in the carrier protein that allows for passage of the sodium and potassium ions. The Na-K ATPase pump is electrogenic, i.e., removing a net positive charge from the cell equivalent to about  $-4 \text{ mV}$ . Similar active transport carrier proteins are also available to transfer other ions such as  $\text{Cl}^-$ ,  $\text{Ca}^{2+}$ ,  $\text{Mg}^{2+}$ , and  $\text{HCO}_3^-$ . The only difference in the carrier proteins would be their preference for a specific ion.

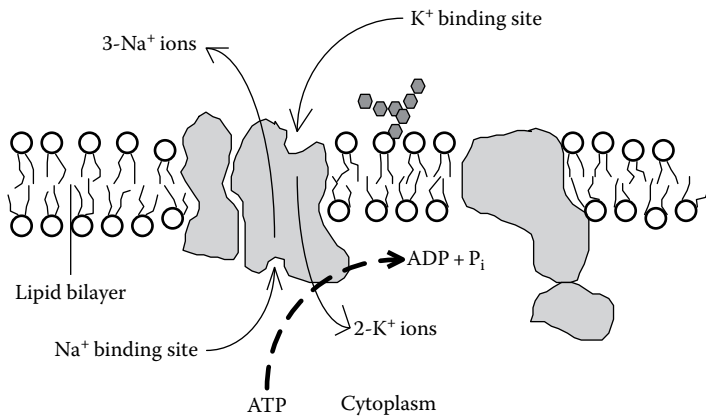


Figure 3.9 The sodium-potassium pump.

Active transport of a solute can also be driven by ion gradients, a process referred to as secondary active transport. For example, the higher concentration of sodium ions outside of the cell can lead to a conformational change in a carrier protein that favors the symport of another solute. The other solute is therefore pumped into the cell against its own electrochemical gradient. The sodium ion gradient that drives this pump is maintained by the Na-K ATPase pump discussed earlier. Sodium ion antiports are also used to control intracellular pH. In this case, the removal of excess hydrogen ions generated by acid-forming reactions within the cell is coupled with the influx of sodium ions.

## Problems

- 3.1** Derive [Equation 3.3](#).
- 3.2** A membrane has pure water on one side and a protein solution on the other side. The membrane has pores equivalent in size to a spherical molecule with a molecular weight of 100,000. The protein solution consists of albumin ( $40 \text{ g L}^{-1}$ ; MW = 69,000), globulins ( $70 \text{ g L}^{-1}$ ; MW = 150,000), and fibrinogen ( $60 \text{ g L}^{-1}$ ; MW = 340,000). Assuming that the proteins form an ideal solution, what is the osmotic pressure of the protein solution? What would be the osmotic pressure of the protein solution if the membrane was completely impermeable to the proteins?
- 3.3** Explain why osmotic pressure is based on the molar concentration of the solute and not the solute mass concentration.
- 3.4** Explain the difference between a mole and an osmole. Cite some examples.
- 3.5** You are concentrating a solution containing a polypeptide of modest molecular weight by pressure filtration through a membrane. The solute concentration on the feed side of the membrane is 0.10 M and the temperature is 25°C. The applied pressure on the feed side of the membrane is 6 atm (gauge), and the pressure on the opposite side of the membrane is 0 atm (gauge). If the polypeptide solute is completely rejected by the membrane, what is the “effective” pressure drop across the membrane? If the hydraulic conductance of the membrane is  $3 \text{ mL h}^{-1} \text{ m}^{-2} \text{ mmHg}^{-1}$ , what is the filtration rate? Assume the membrane has a total surface area of 1 m<sup>2</sup>.

- 3.6** The following clean water flow rates were reported for a particular series of ultrafiltration membranes.

Nominal Molecular Weight Cutoff (NMWCO)	Clean Water Flow Flux (mL min <sup>-1</sup> cm <sup>-2</sup> at 50 psi)
10,000	0.90
30,000	3.00
100,000	8.00

From these data, calculate the hydraulic conductance for each case ( $L_p$ ). Assuming the membranes have similar porosity and thickness, what is the relationship between the value of  $L_p$  and the NMWCO? Hint: Base your analysis on [Equation 3.7](#) and assume that the NMWCO is for a spherical molecule having the same size as the pores in the membrane. Show that the radius of a spherical molecule is proportional to the molecular weight to the 1/3 power as given by [Equation 5.41](#).

- 3.7** Perform a literature search and write a short paper on the biomedical applications of liposomes.  
**3.8** Look up in a biochemistry text the chemical structures of collagen, laminin, cholesterol, and the various lipids found in the cell membrane.  
**3.9** Search the literature and write a short paper on the biomedical applications of osmotic pumps.  
**3.10** How many potassium ions must a cell lose in order to produce a membrane potential of -95 mV for potassium? How does this compare to the number of potassium ions within the cell?  
**3.11** Consider a membrane that is permeable to Ca<sup>2+</sup> ions. On one side of the membrane the Ca<sup>2+</sup> concentration is 100 mM, and on the other side of the membrane the Ca<sup>2+</sup> concentration is 1 mM. The electric potential of the high-concentration side of the membrane relative to the low-concentration side of the membrane is +10 mV. How much reversible work is required to move each mole of Ca<sup>2+</sup> from the low-concentration side of the membrane to the high-concentration side of the membrane? What is the equilibrium membrane potential?  
**3.12** The cell membrane is permeable to many different ions. Therefore, the equilibrium membrane potential for the case of multiple ions will depend not only on the concentrations of the ions within and outside the cell but also on the permeability (P) of the cell membrane to each ion. The Goldman equation may be used to calculate the equilibrium membrane potential for the case of multiple ions. For example, considering Na<sup>+</sup> and K<sup>+</sup> ions, the Goldman equation may be written as

$$V = 26.71 \times \ln \left( \frac{P_{Na}C_{Na,0} + P_KC_{K,0}}{P_{Na}C_{Na,i} + P_KC_{K,i}} \right), \text{ mV}$$

For a cell at rest,  $P_{Na}$  is much smaller than  $P_K$ ; typically,  $P_{Na}$  is about 0.01P<sub>K</sub>. Calculate the equilibrium membrane potential for a cell under these conditions. During the depolarization phase of an action potential, the sodium ion permeability increases dramatically due to the opening of the voltage-gated sodium ion channels. Under these conditions,  $P_K$  is about 0.5P<sub>Na</sub>. Under these conditions, recalculate the value of the equilibrium membrane potential.

- 3.13** Composite membranes are often used in membrane filtration and in hemodialysis (Clark and Gao, 2002). One of these membranes is used to provide structural support and can be tens or even hundreds of microns in thickness. This structural membrane is usually microporous to minimize its flow resistance and will therefore have pore diameters on the order of a micron. Attached to this structural membrane is a much thinner permselective membrane skin on the order of a micron in thickness that will have pores whose diameter is defined in terms of their nominal molecular weight cutoff (NMWCO; see [Equation 5.41](#), which can be used to relate the molecular radius of a solute to its molecular weight). Hence, solutes whose molecular weight is less than the NMWCO of the selective membrane will travel across the membrane through the pores, whereas those solutes whose molecular weights are larger than the NMWCO will not cross the permselective membrane. Since the filtration flow rate,  $Q_i$  (see [Equation 3.4](#), where  $L_p$  and  $\Delta P$  are, respectively, the hydraulic conductance and the effective pressure drop across the  $i$ th membrane), through each membrane layer  $i$  has to be the same, show that the overall hydraulic conductance for three membranes that are stacked together is given by the following equation. Note that in this equation,  $L_{P_i}$  is the hydraulic conductance for the  $i$ th membrane, as calculated by [Equation 3.7](#) or [3.10](#), or as found by independent filtration flow measurements for that particular membrane:

$$L_{P_{\text{composite}}} = \frac{1}{\sum_{i=1}^3 \frac{1}{L_{P_i}}}$$

- 3.14** Consider a composite membrane that is being used to filter plasma from blood. Plasma has a viscosity of 1.2 cP. The composite membrane consists of a microporous sponge-like material that provides structural support. This membrane is 25  $\mu\text{m}$  thick and has pores that are 2  $\mu\text{m}$  in diameter. These pores are also tortuous and have a tortuosity (i.e.,  $\tau$ ) of 1.67. The porosity of this membrane (i.e.,  $A_p/S$ ) is also equal to 0.60. Attached to this microporous membrane is a thin permselective skin 3.23  $\mu\text{m}$  thick that has a NMWCO of 1000. The pores in this membrane skin are therefore about 0.0015  $\mu\text{m}$  in diameter. The tortuosity of the pores in the membrane skin is also equal to 1.67, and the porosity of the membrane skin is equal to 0.60. Use the formula found in [Problem 3.13](#) to predict the overall hydraulic conductance for this composite membrane. Find the total filtration flow rate ( $\text{mL h}^{-1}$ ) across this composite membrane assuming the total surface area of the membrane is 1  $\text{m}^2$  and that the overall effective pressure drop across the composite membrane is 160 mmHg.
- 3.15** Consider a solution of glucose on one side of a membrane that is impermeable to the transport of glucose. The temperature of the glucose solution is 20°C. What pressure must be applied on the glucose side of the membrane to stop the flow of water into the glucose solution? Assume the glucose concentration is 1 mg  $\text{mL}^{-1}$  and that the molecular weight of glucose is 180 g  $\text{mol}^{-1}$ .
- 3.16** A hollow fiber membrane cartridge is being evaluated for use in an aquapheresis system. In one experiment using blood, a cartridge with a surface area of 1.5  $\text{m}^2$  had a filtration flow across the hollow fiber membranes of 1000  $\text{mL h}^{-1}$ . The average pressure of the blood flowing inside the tubes of the hollow fiber membranes was 120 mmHg, and the suction pressure on the filtrate side of the hollow fibers averaged -150 mmHg. Assuming that the plasma proteins were totally retained on the blood side of the hollow fiber membrane, estimate the hydraulic conductance of these membranes in  $\text{mL h}^{-1} \text{ m}^{-2} \text{ mmHg}^{-1}$ .

- 3.17** An aqueous solution (A) with an osmotic pressure of 5 atm is separated by a membrane from an aqueous solution (B) with an osmotic pressure of 2 atm. Both solutions are at a total pressure of 1 atm. The solutes in these two solutions cannot pass through the membrane. Which way will the water flow, from (A) to (B) or from (B) to (A)? By how much must the hydrodynamic pressure be increased to stop the osmotic flow of water and on which solution, (A) or (B), must this pressure increase be applied?
- 3.18** The nephron is the functional unit of the kidney. Fluid enters the space within Bowman's capsule through filtration across the glomerular capillaries. The walls of these capillaries will allow small ions and other solutes to pass from the plasma phase of the blood to the filtrate in Bowman's capsule. However, proteins are too big to cross the capillary, and these are retained within the capillaries. Estimate the total glomerular filtration rate (GFR) if the average glomerular pressure is 60 mmHg and the pressure within the Bowman's capsule that collects the filtrate is 20 mmHg. The osmotic pressure of the retained plasma proteins is 25.6 mmHg. The value of  $L_p S$  for the glomerular capillaries is about  $8.7 \text{ mL min}^{-1} \text{ mmHg}^{-1}$ .
- 3.19** The hydraulic conductance for pure water of a porous membrane ( $L_p$ ) was found to be  $0.1350 \text{ cm mmHg}^{-1} \text{ h}^{-1}$ . The porosity ( $\epsilon$ ) of the membrane was found to be 0.52 and the thickness ( $\bar{L}$ ) of the membrane was  $32 \mu\text{m}$ . Assuming the pores in this membrane are rectangular slits and that they run straight through the membrane (i.e.,  $\tau = 1$ ), estimate the size of the slit opening (i.e.,  $2H$ ) in microns. Water under these conditions has a viscosity ( $\mu$ ) of  $0.0008 \text{ Pa s}$ .
- 3.20** A membrane has a porosity ( $\epsilon$ ) of 0.60 and a thickness ( $\bar{L}$ ) of  $45 \mu\text{m}$ , and the pores in this membrane are tortuous with a radius of  $0.05 \mu\text{m}$  and tortuosity ( $\tau$ ) of 1.3. Estimate the hydraulic conductance ( $L_p$ ) of this membrane for plasma. Your answer for  $L_p$  should be in units of  $\text{cm mmHg}^{-1} \text{ h}^{-1}$ . You can assume that plasma has a viscosity ( $\mu$ ) of  $0.0012 \text{ Pa s}$ .
- 3.21** Estimate the filtrate flux ( $\text{mL cm}^{-2} \text{ min}^{-1}$ ) at  $20^\circ\text{C}$  for the filtration of a protein solution across a membrane that is impermeable to the protein. The hydraulic conductance of this membrane is equal to  $0.01 \text{ mL cm}^{-2} \text{ psi}^{-1} \text{ min}^{-1}$ . The hydrodynamic pressure drop applied across the membrane is equal to 15 psi, and the protein concentration in the solution being filtered is equal to 22 g per 100 mL. The molecular weight of the protein is  $69,000 \text{ g mol}^{-1}$ .
- 3.22** A drug delivery catheter consists of a cylindrical needle whose wall contains very small pores allowing the drug solution to leave the needle into the surrounding tissue. The hydraulic conductance of the needle wall is  $10^{-5} \text{ cm}^2 \text{ s g}^{-1}$ . The needle has a length of 2 cm and the diameter of the needle is  $200 \mu\text{m}$ . The sharp end of the needle is closed off so that any flow of drug solution into the needle must flow out through the porous wall of the needle. The drug solution has a viscosity of 1 cP. If the pressure driving the drug solution into the needle is 5 mmHg, how long will it take in seconds for this catheter to deliver  $100 \mu\text{L}$  of the drug solution into the surrounding tissue? Assume that the pressure is constant at 5 mmHg (gauge) within the 2 cm length of the needle and that the pressure in the surrounding tissue is 0 mmHg (gauge). Also assume that the pores in the needle wall are of such a size that no solutes are retained.
- 3.23** Estimate the hydraulic conductance ( $\text{cm}^3 \text{ dyne}^{-1} \text{ s}^{-1}$ ) of a dialysis membrane for water. The radius of the pores in the membrane through which water is filtered is  $2.3 \text{ nm}$ , the porosity of the dialysis membrane is 0.4, and the total length of a pore is  $150 \mu\text{m}$ . Assume the viscosity of water is 1 cP.

- 3.24** Estimate the hydraulic conductance, in  $\text{mL} (\text{h m}^2 \text{ mmHg})^{-1}$ , of a silicon nanopore membrane. Assume the pores are rectangular slits and run straight through the membrane. The slit height ( $2H$ ) is 7 nm and the slit width is 2  $\mu\text{m}$ . The thickness of the nanopore membrane is 300 nm and the porosity of the membrane is 0.0002. The fluid being filtered is human plasma with a viscosity of 1.2 cP and a density of 1.02 g  $\text{cm}^{-3}$ .
- 3.25** The hydraulic conductance of a 2  $\mu\text{m}$  thick silicon nanopore membrane was found to be  $1200 \text{ mL h}^{-1} \text{ m}^{-2} \text{ mmHg}^{-1}$  for human plasma having a viscosity of 1.2 cP and a density of 1.02 g  $\text{cm}^{-3}$ . If the pores in this membrane run straight through the membrane, estimate the diameter of the membrane pores in nanometers (nm). The porosity of the membrane is 40%.



Taylor & Francis

Taylor & Francis Group

<http://taylorandfrancis.com>

# Chapter 4 The physical and flow properties of blood and other fluids

## 4.1 Physical properties of blood

Blood is a viscous fluid mixture consisting of plasma and cells. [Table 4.1](#) summarizes the most important physical properties of blood. Recall that the chemical composition of the plasma was previously shown in [Table 3.2](#). Proteins represent about 7–8 wt% of the plasma. The major proteins found in plasma are albumin ( $MW = 69,000$ ;  $4.5 \text{ g } 100 \text{ mL}^{-1}$ ), the globulins ( $MW = 35,000\text{--}1,000,000$ ;  $2.5 \text{ g } 100 \text{ mL}^{-1}$ ), and fibrinogen ( $MW = 400,000$ ;  $0.3 \text{ g } 100 \text{ mL}^{-1}$ ). *Albumin* has a major role in regulating the pH and the colloid osmotic pressure of blood. The so-called *alpha* and *beta globulins* are involved in solute transport, whereas the *gamma globulins* are the antibodies that fight infection and form the basis of the humoral component of the immune system. *Fibrinogen*, through its conversion to long strands of *fibrin*, has a major role in the process of blood clotting. *Serum* is simply the fluid remaining after blood is allowed to clot. For the most part, the composition of serum is the same as that of plasma, with the exception that the clotting proteins, primarily fibrinogen, and the cells have been removed.

## 4.2 Cellular components

The cellular component of blood consists of three main cell types. The most abundant cells are the red blood cells (RBCs) or *erythrocytes* comprising about 95% of the cellular component of blood. Their major role is the transport of oxygen by the hemoglobin contained within the RBC. Note from [Table 4.1](#) that the density of an RBC is higher than that of plasma. Therefore, in a quiescent fluid, the RBCs will tend to settle. The RBC volume fraction is called the *hematocrit* and typically varies between 40% and 50%. The true hematocrit (H) is about 96% of the measured hematocrit (Hct).

The RBC has a unique shape described as a *biconcave discoid*. [Figure 4.1](#) illustrates the size of the RBC and [Table 4.2](#) summarizes its typical dimensions. RBCs can form stacked coin-like structures called *rouleaux*. Rouleaux can also clump together to form larger RBC structures called *aggregates*. Both rouleaux and aggregates break apart under conditions of increased blood flow or higher shear rates.

*Platelets* are the next most abundant cell type, comprising about 4.9% of the blood cell volume. The platelets are major players in blood coagulation and *hemostasis*, which is the prevention of blood loss. The remaining 0.1% of the cellular component of blood consists of the white blood cells (WBCs) or *leukocytes*, which form the basis of the cellular component of the immune system. Since the WBCs and platelets only comprise about 5% of the cellular component of blood, their effect on the macroscopic flow characteristics of blood is negligible.

Table 4.1 Physical Properties of Adult Human Blood

Property	Value
Whole blood	
pH	7.35–7.40
Viscosity (37°C)	3.0 cP (at high shear rates)
Specific gravity (25/4°C)	1.056
Venous hematocrit	
Male	0.47
Female	0.42
Whole blood volume	~78 mL kg <sup>-1</sup> body weight
Plasma or serum	
Colloid osmotic pressure	~330 mm H <sub>2</sub> O
pH	7.3–7.5
Viscosity (37°C)	1.2 cP
Specific gravity (25/4°C)	1.0239
Formed elements	
Erythrocytes (RBCs)	
Specific gravity (25/4°C)	1.098
Count	
Male	5.4 × 10 <sup>9</sup> mL <sup>-1</sup> whole blood
Female	4.8 × 10 <sup>9</sup> mL <sup>-1</sup> whole blood
Average life span	120 days
Production rate	4.5 × 10 <sup>7</sup> mL <sup>-1</sup> whole blood/day
Hemoglobin concentration	0.335 g mL <sup>-1</sup> of erythrocyte
Leukocytes	
Count	~7.4 × 10 <sup>6</sup> mL <sup>-1</sup> whole blood
Diameter	7–20 μm
Platelets	
Count	~2.8 × 10 <sup>8</sup> mL <sup>-1</sup> whole blood
Diameter	~2–5 μm

Source: Data from Cooney, D.O., *Biomedical Engineering Principles*, Marcel Dekker, New York, 1976, p. 39.

### 4.3 Rheology

The field of rheology concerns the deformation and flow behavior of fluids. The prefix *rheo-* is from the Greek and refers to something that flows. Due to the particulate nature of blood, we expect the rheological behavior of blood to be somewhat more complex than a simple fluid such as water.

Our understanding of the flow behavior of fluids begins by exploring the relationship between *shear stress* ( $\tau$ ) and the *shear rate* ( $\dot{\gamma}$ ). To develop this relationship, consider the situation shown in Figure 4.2. A fluid is contained between two large parallel plates both of area A. The plates are separated by a small distance equal to h. Initially the system is at rest. At time t = 0, the lower plate is set into

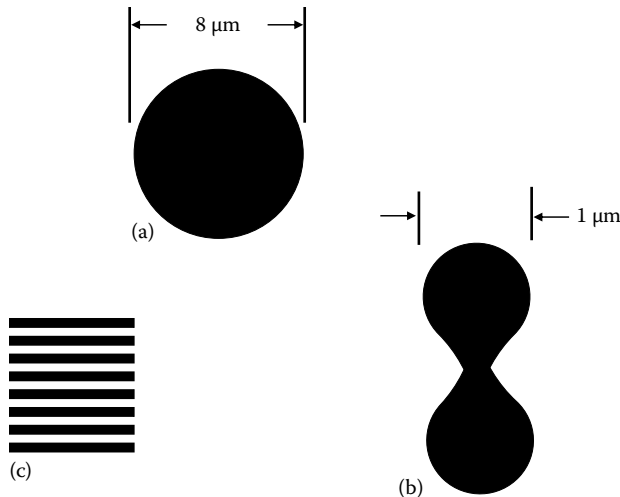


Figure 4.1 The dimensions of the red blood cell. (a) Top view, (b) side view, and (c) rouleaux.

Table 4.2 Dimensions of the Normal Red Blood Cell

Property	Value
Diameter	$8.1 \pm 0.43 \mu\text{m}$
Greatest thickness	$2.7 \pm 0.15 \mu\text{m}$
Least thickness	$1.0 \pm 0.3 \mu\text{m}$
Surface area	$138 \pm 17 \mu\text{m}^2$
Volume	$95 \pm 17 \mu\text{m}^3$

Source: Data from Burton, A.C., *Physiology and Biophysics of the Circulation*, 2nd ed., Year Book Medical Publishers, Inc., Chicago, IL, 1972.

motion in the x direction at a constant velocity V. The velocity of the lower plate is sufficiently low such that the fluid motion is not turbulent, i.e., macroscopic or convective mixing of the fluid in the y direction does not occur. Rather, the fluid motion is *laminar*. In laminar flow, the fluid flows without any mixing in the y direction. This means that adjacent layers of fluid will slide past one another in a manner analogous to what is seen when a deck of playing cards is deformed.

The fluid velocity is a vector and will have three components, which in these Cartesian coordinates are  $v_x$ ,  $v_y$ , and  $v_z$ . For the situation shown in Figure 4.2,  $v_y$  and  $v_z$  are both zero;  $v_x$  is zero because the plates extend to a great distance in the z direction and the lower plate only moves in the x direction, so we conclude that there is no flow of fluid in the z direction;  $v_y$  is zero since there is no motion of the lower or upper plate in the y direction and there are no holes in either of the plates that would cause the fluid to flow in the y direction. So we see that for the situation shown in Figure 4.2, the only velocity component is that in the x direction, i.e.,  $v_x$ , and this will depend, in general, on  $(x,y,z,t)$ .

Since the lower plate is set into motion at  $t = 0$ , and the fluid initially is not moving, there will be a transient period during which successive layers of the fluid will be set into motion. This means that

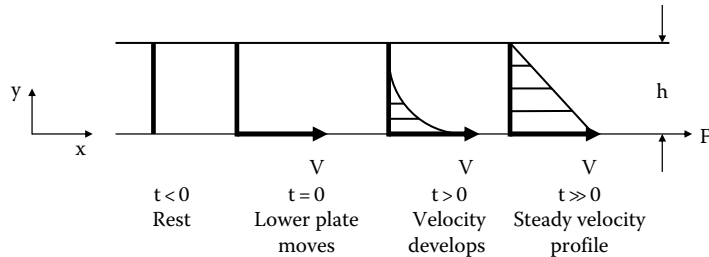


Figure 4.2 Velocity profile development for flow of a fluid between two parallel plates.

the flow is inherently unsteady and dependent on time, i.e.,  $t$ . The plate separation, i.e.,  $h$ , is constant in the  $x$  direction so this means that  $v_x$  will not depend on  $x$ . Since the lower plate is moving at  $V$  and the upper plate is stationary,  $v_x$  will depend only on  $y$ . However, since the plates are very large in the  $z$  direction compared to their separation, i.e.,  $h$ ,  $v_x$  at a given  $y$  and  $t$  will be the same for any value of  $z$ . So we conclude that  $v_x$  can only be a function of  $y$  and  $t$ , i.e.,  $v_x(y,t)$ .

As time proceeds, momentum is transferred in the  $y$  direction to successive layers of fluid from the lower plate that is in motion in the  $x$  direction. In laminar flow, momentum transport occurs by diffusion and we say that momentum “flows or diffuses” from a region of high velocity to a region of low velocity. After a sufficient length of time, a steady-state velocity profile is obtained, i.e., a linear function of  $y$ , i.e.,  $v_x(y) = \frac{V}{h}(h - y)$ .

At steady state, a constant force ( $F$ ) must be applied to overcome the resistance of the fluid and maintain the motion of the lower plate at velocity  $V$ . For the situation shown in Figure 4.2, the shear stress on the lower plate is defined as  $F/A$  and is given the symbol  $\tau_{yx}$ , where the subscript  $yx$  denotes the viscous flux\* of  $x$  momentum in the  $y$  direction (Bird et al., 2002). The shear stress, i.e.,  $\tau_{yx}$ , can also be interpreted as a force acting in the  $x$  direction on a surface that is perpendicular to the  $y$  direction. The shear rate at any position  $y$  in the fluid is defined as  $-\frac{dv_x(y)}{dy} = \frac{V}{h} = \dot{\gamma}$ . The shear rate is given the symbol  $\dot{\gamma}$ . Notice that shear rate has units of reciprocal time. The shear rate is also the same as the strain rate or the rate of deformation.

*Newton's law of viscosity* states that for *laminar flow* (nonturbulent) the shear stress is proportional to the shear rate. The proportionality constant is called the *viscosity*,  $\mu$ , which is a physical property of the fluid and is a measure of the flow resistance of the fluid. Viscosity is usually expressed in the following units where  $1 \text{ P}$  (poise) =  $100 \text{ cP}$  (centipoise) =  $1 \text{ g cm}^{-1} \text{ s}^{-1}$  =  $1 \text{ dyne s cm}^{-2}$  =  $0.1 \text{ N s m}^{-2}$  =  $0.1 \text{ Pa s}$ . Also  $1 \text{ cP} = 0.001 \text{ Pa s}$ . For the situation shown in Figure 4.2, Newton's law of viscosity can be stated as follows:

$$\frac{F}{A} = \tau_{yx} = \mu \frac{V}{h} = \mu \dot{\gamma} \quad (4.1)$$

Most simple homogeneous liquids and gases obey this law and are called *Newtonian fluids*.

\* A flux is a flow that has been normalized with respect to the area that is perpendicular to the direction of the flow.

For more complicated geometries, the steady-state velocity profile is not linear. However, Newton's law of viscosity can be stated at any point in the laminar flow field. In Cartesian coordinates ( $x, y, z$ ), and in cylindrical coordinates ( $r, \theta, z$ ), we can write Newton's law of viscosity as

$$\tau_{yx} = -\mu \frac{dv_x}{dy} = \mu \dot{\gamma} \quad (4.2a)$$

$$\tau_{rz} = -\mu \frac{dv_z}{dr} = \mu \dot{\gamma} \quad (4.2b)$$

where

$v_x$  is the velocity in the  $x$  direction at position  $y$

$v_z$  is the velocity in the  $z$  direction at position  $r$

These equations tell us that the momentum flows in the direction of decreasing velocity. The velocity gradient is therefore the driving force for momentum transport much like the temperature gradient is the driving force for heat transfer, and the concentration gradient is the driving force for mass transport.

A fluid whose *shear stress-shear rate relationship* does not follow [Equation 4.1](#) is known as a *non-Newtonian fluid*. [Figure 4.3](#) illustrates the type of shear stress-shear rate relationships that are typically observed for non-Newtonian fluids. The Newtonian fluid is shown for comparison. Note from [Equation 4.2a](#) and [b](#) that the shear stress-shear rate relationship for a Newtonian fluid is linear with the slope equal to the viscosity. For non-Newtonian fluids, we can also define the observed or *apparent viscosity* for given values of  $\tau_{yx}$  and  $\dot{\gamma}$ . Hence, from [Equation 4.2a](#) and [b](#), and for given values of  $\tau_{yx}$  and  $\dot{\gamma}$ , the apparent viscosity ( $\mu_{\text{apparent}}$ ) for a non-Newtonian fluid is given by  $\tau_{yx}/\dot{\gamma}$  or  $\tau_{rz}/\dot{\gamma}$ . Note that the apparent viscosity is not constant and will depend on the shear rate,  $\dot{\gamma}$ .

A *dilatant* fluid thickens or has an increase in apparent viscosity as the shear rate increases. An example of a dilatant fluid is a solution of cornstarch and water, which allows one to “walk on water.” As a person quickly walks or runs across this fluid, each step induces a high shear rate in the fluid surrounding the foot increasing the fluid viscosity and the resulting shear stress that is generated

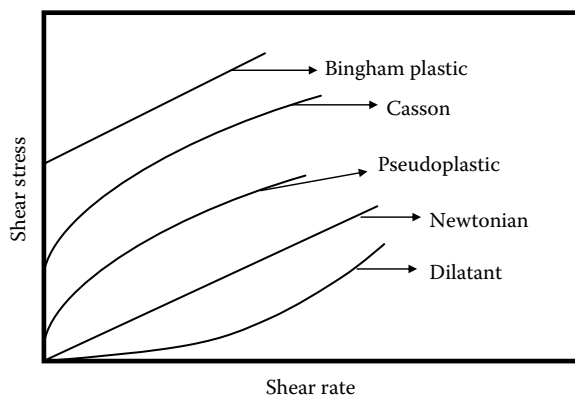


Figure 4.3 Types of shear stress–shear rate relationship.

supports the person and they do not sink into the fluid. A *pseudoplastic* fluid, on the other hand, tends to thin out, or its apparent viscosity decreases, with an increase in shear rate. Paint is an example of a pseudoplastic fluid, since it thins out as it is brushed or quickly shears as it is applied to a surface.

Heterogeneous fluids that contain a particulate phase that forms aggregates at low rates of shear exhibit a yield stress,  $\tau_y$ . The yield stress must be exceeded in order to get the material to flow. Two types of fluids that exhibit this behavior are the *Bingham plastic* and the *Casson fluid*. The Casson fluid has been used to describe liquids that contain particulates that also aggregate, forming large complex structures. An example of this type of fluid is the ink used in ball point pens. When the pen is not being used, the ink thickens and cannot flow out of the pen. As one writes, the rotating ball at the point of the pen shears the fluid, thinning it out so it can be applied to the paper. In the case of the Bingham plastic, once the yield stress is exceeded, the fluid behaves as if it were Newtonian. For the Casson fluid, we see that as the shear rate increases, the apparent viscosity decreases, indicating that the particulate aggregates are getting smaller and smaller and, at some point, the fluid behaves as a Newtonian fluid. Blood is a heterogeneous fluid, with the particulates consisting primarily of RBCs. As mentioned earlier and shown in [Figure 4.1](#), the RBCs form rouleaux and aggregates at low shear rates. We will see in the ensuing discussion that the rheology of blood behaves like that of the Casson fluid.

#### 4.4 The capillary viscometer and laminar flow in tubes

The simplest approach for examining the shear stress-shear rate behavior of blood or other fluids is through the use of the capillary viscometer shown in [Figure 4.4](#). The diameter of the capillary tube is typically on the order of 500  $\mu\text{m}$ . To eliminate entrance and exit effects, the ratio of the capillary length ( $L$ ) to its radius ( $R$ ) should be greater than 100 (Rosen, 1993). For a given flow rate of fluid,  $Q$ , the pressure drop across the viscometer,  $-\Delta P = P_0 - P_L$ , is measured. From this information, it is possible to deduce an analytical expression for the shear stress-shear rate relationship, i.e.,  $\dot{\gamma} = \dot{\gamma}(\tau_{rz})$ .

Analysis of the flow of a fluid in the horizontal cylindrical capillary tube illustrated in [Figure 4.4](#) requires the use of cylindrical coordinates ( $r, \theta, z$ ). In cylindrical coordinates, the components of the velocity vector are  $v_r$ ,  $v_\theta$ , and  $v_z$ . With steady-state flow, i.e., no dependence on time, we can make the following simplifying assumptions: the length of the tube ( $L$ ) is much greater than the tube radius ( $R$ ) (i.e.,  $L/R \sim 100$ ) to eliminate entrance effects; the flow is incompressible (i.e., constant density) and isothermal (i.e., constant temperature); no external forces are acting on the fluid; no holes are in the tube so that there is no radial velocity component  $v_r$ ; there is no axisymmetric flow or no swirls so that the tangential velocity  $v_\theta$  is also zero; and the *no-slip condition* at the wall requires that  $v_z = 0$

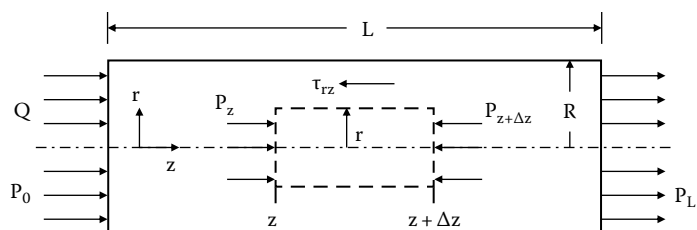


Figure 4.4 Forces acting on a cylindrical fluid element within a capillary viscometer.

at  $r = R$ . Continuity or conservation of mass for an incompressible fluid with these assumptions therefore requires that only an axial velocity component exists, and it will be a function of the tube radius only; therefore  $v_z = v_z(r)$ .

Now consider in [Figure 4.4](#) a cylindrical volume of fluid of radius  $r$  and length  $\Delta z$ . For steady flow, the viscous force acting to retard the fluid motion, i.e.,  $\tau_{rz} 2\pi r \Delta z$ , must be balanced by the force developed by the pressure drop acting on the volume of fluid of length  $\Delta z$ , i.e.,  $\pi r^2 (P_l - P_{z+\Delta z})$ . Equating these forces, dividing by  $\Delta z$ , and taking the limit as  $\Delta z \rightarrow 0$ , the following equation is obtained for the shear stress distribution for the fluid flowing within the capillary tube:

$$\frac{\tau_{rz}(r)}{r} = -\frac{1}{2} \frac{dP}{dz} = \frac{(P_0 - P_L)}{2L} \quad (4.3)$$

In [Equation 4.3](#), the first term on the left-hand side of the equation is only a function of  $r$ , and the middle term of the equation is only a function of  $z$ . Hence, both of these terms must equal the same constant, and this means that  $-dP/dz$  is equal to the pressure drop per unit length of the tube, i.e.,  $(P_0 - P_L)/L$ .

We note that the shear stress vanishes at the centerline of the capillary and achieves its maximum value,  $\tau_w$ , at the wall where  $r = R$ . The *wall shear stress* is easily calculated by the following equation in terms of the measured pressure drop ( $P_0 - P_L$ ) and the tube dimensions ( $R$  and  $L$ ):

$$\tau_w = \tau_{rz}(R) = -\frac{R}{2} \frac{dP}{dz} = \frac{(P_0 - P_L)R}{2L} \quad (4.4)$$

It should also be pointed out that [Equations 4.3](#) and [4.4](#) hold whether the fluid is Newtonian or non-Newtonian. Nothing has been said so far about the relationship between a particular fluid's shear stress and shear rate. Using [Equation 4.4](#), one can rewrite [Equation 4.3](#) to give the shear stress in terms of the wall shear stress and the fractional distance from the centerline of the capillary tube, i.e.,  $r/R$ :

$$\tau_{rz}(r) = \tau_w \frac{r}{R} \quad (4.5)$$

#### [4.4.1 Hagen-Poiseuille equation for laminar flow of a Newtonian liquid in a cylindrical tube](#)

Let's first consider the flow of a Newtonian liquid in a cylindrical tube. Liquids are considered to be incompressible and their density is constant. For a Newtonian liquid flowing in a cylindrical horizontal tube, we know from [Equation 4.2b](#) that  $\tau_{rz} = -\mu(dv_z/dr)$ . Substituting this relation for  $\tau_{rz}$  into [Equation 4.3](#), we obtain

$$\tau_{rz} = -\mu \frac{dv_z}{dr} = \frac{(P_0 - P_L)r}{2L} \quad (4.6)$$

This equation can be easily integrated using the no-slip boundary condition (BC) that says that, at  $r = R$ ,  $v_z = 0$ . The result of this integration provides an equation that describes the velocity profile

for laminar flow of a Newtonian liquid in a cylindrical tube. The following equation shows that the velocity profile will have a parabolic shape:

$$v_z(r) = \frac{(P_0 - P_L)R^2}{4\mu L} \left[ 1 - \left( \frac{r}{R} \right)^2 \right] \quad (4.7)$$

Note that the maximum velocity ( $V_{\text{maximum}}$ ) occurs at the centerline of the cylindrical tube, where  $r = 0$ ; hence the maximum velocity is given by

$$V_{\text{maximum}} = \frac{R^2(P_0 - P_L)}{4\mu L} \quad (4.8)$$

The total volumetric flow rate of the liquid in a cylindrical tube is given by

$$Q = 2\pi \int_0^R v_z(r) r dr \quad (4.9)$$

Substituting [Equation 4.7](#) for  $v_z(r)$  into [Equation 4.9](#) and performing the integration gives

$$Q = \frac{\pi R^4 (P_0 - P_L)}{8\mu L} = \frac{\pi d^4 (P_0 - P_L)}{128\mu L} \quad (4.10)$$

where  $d$  is the tube diameter.

[Equation 4.10](#) is the *Hagen-Poiseuille law* for laminar flow of a Newtonian liquid in a cylindrical tube. It provides a simple relationship between the volumetric flow rate in the tube given by  $Q$  and the pressure drop between the entrance and the exit of the tube, i.e.,  $P_0 - P_L$ , for the given dimensions of the tube  $R$  and  $L$ , and the fluid viscosity  $\mu$ .

Using the analogy that flow is proportional to a driving force divided by a resistance, we see that the driving force is the pressure drop,  $P_0 - P_L$ , and the resistance is given by  $8\mu L/\pi R^4$ . This resistance term is very important since it shows that for laminar flow within blood vessels, small changes in the radius of the vessel can have a significant effect on the blood flow rate for a given pressure drop. To achieve this control of the blood flow rate, the arterioles, the smallest elements of the arterial system with diameters less than 100  $\mu\text{m}$ , consist of an inner endothelial cell lining that is surrounded by a layer of vascular smooth muscle cells. Contraction or relaxation of the smooth muscle layer provides a reactive method for controlling arteriole diameter and hence the blood flow rate within organs and tissues.

For laminar flow in a network of tubes or small capillaries, the overall pressure drop across the network is  $P_0 - P_L$ , and the resistance for the  $i$ th element of the network is  $8\mu L_i/\pi R_i^4$ , where  $L_i$  and  $R_i$  are, respectively, the length and radius of the  $i$ th element. We can then draw on the analogy to an electrical circuit with resistors in series and in parallel to solve for the overall flow ( $Q$ ) in the network and for the flow ( $Q_i$ ) in each element of the network.

If the entrance of the tube is at a height  $Z_0$  above a reference elevation, and the exit of the tube is at a height  $Z_L$  relative to the same reference elevation, then the pressure difference term in [Equation 4.10](#) must account for the change in the hydrostatic pressure between the entrance and exit of the tube. Hence, in this case, we can write the pressure difference term in [Equation 4.10](#) as  $[(P_0 - P_L) + \rho g(Z_0 - Z_L)]$ .

The average velocity ( $V_{\text{average}}$ ) of the fluid flowing within a cylindrical tube is defined as the ratio of the volumetric flow rate ( $Q$ ) to the cross-sectional area (i.e.,  $A = \pi R^2$ ) of the tube normal to the flow direction, i.e.,  $V_{\text{average}} = Q/A$ . Using [Equation 4.10](#) for  $Q$ , the average velocity is then given by

$$V_{\text{average}} = \frac{R^2(P_0 - P_L)}{8 \mu L} = \frac{1}{2} V_{\text{maximum}} \quad (4.11)$$

### Example 4.1

[Equation 4.10](#) was derived under the assumption of the laminar flow of a Newtonian liquid. What happens if the fluid is a Newtonian gas? Develop an expression for the pressure change over the length of the tube, i.e.,  $(P_0 - P_L)$ , for a gas in laminar flow.

### Solution

Unlike a liquid whose density is constant, the density of a gas will change along the flow path because of the decrease in pressure. However, conservation of mass will require that the mass flow rate of the gas in the tube is constant, which means that at any axial location within the tube, we must have that  $\dot{m} = \rho Q$ . Now assuming we have an ideal gas, the gas density is then given by  $\rho = P/RT$ . If we also assume that the gas flow in the tube is isothermal, then between the tube entrance, i.e.,  $z = 0$ , and any location in the tube,  $z$ , we have that  $P(z)/P(0) = \rho(z)/\rho_0$ . Now at some location  $z$  within the tube, the local volumetric flow rate for a Newtonian gas is given by [Equation 4.10](#), where we have replaced  $(P_0 - P_L)/L$  with  $-dP/dz$ , to account for the change in the gas density as the pressure changes:

$$Q(z) = \frac{\dot{m}}{\rho(z)} = \frac{\dot{m} P_0}{\rho_0 P(z)} = -\frac{\pi R^4}{8 \mu} \frac{dP}{dz}$$

This is a differential equation that can then be solved for the isothermal pressure change of a gas flowing in a cylindrical tube. Hence,

$$Q_0 = \frac{\dot{m}}{\rho_0} = \left( \frac{\pi R^4}{8 \mu L} \right) \left( \frac{P_0 + P_L}{2} \right) \left( \frac{P_L - P_0}{P_0} \right) \quad (\text{A})$$

where  $Q_0$  is the volumetric flow rate of the gas at the tube entrance.

Gas viscosities at normal pressures are considerably less than liquids. For example, the viscosity of water is 1 cP at room temperature, whereas the viscosity of air is only 0.018 cP. Comparing [Equation A](#) in [Example 4.1](#) for a gas, with [Equation 4.10](#) for a liquid, with everything but the viscosity the same, we see that the flow rate of the gas in a tube would be about 50 times larger than that of the liquid. Conversely, for the same flow rate of the gas and liquid, the pressure drop for the gas would be about 50 times less than that for the liquid. Hence, in most biomedical engineering applications, the pressure drop for gas flow is usually negligible.

**Example 4.2**

A hollow fiber module is being designed for a bioreactor application. Mammalian liver cells will be grown in the shell space surrounding the hollow fibers, and nutrient media will flow through the inside of the hollow fibers. The module will contain a total of 7000 hollow fibers with inside diameter of 500 µm and length 35 cm. If the pressure drop over the length of these fibers is 25 mmHg, estimate the total flow rate in mL min<sup>-1</sup> of the nutrient media through the hollow fiber module. The nutrient media has a viscosity of 0.85 cP and a density of 1 g cm<sup>-3</sup>, and the flow is laminar.

**Solution**

Since the pressure drop over the length of each hollow fiber has to be the same, this means that we can calculate the flow rate for one hollow fiber and then multiply that value by the number of fibers to obtain the total flow rate. Using [Equation 4.10](#), we have

$$Q_{\text{fiber}} = \frac{\pi(0.05 \text{ cm})^4 \times 25 \text{ mmHg} \times 1 \text{ atm} / 760 \text{ mmHg} \times 101,325 \text{ Pa/atm}}{128 \times 0.00085 \text{ Pas} \times 35 \text{ cm}} = 0.0172 \frac{\text{cm}^3}{\text{s}}$$

$$Q_{\text{total}} = Q_{\text{fiber}} \times \# \text{ of fibers} = 0.0172 \frac{\text{cm}^3}{\text{s}} \times 7000 \times \frac{60 \text{ s}}{\text{min}} = 7224 \frac{\text{mL}}{\text{min}}$$

**4.4.1.1 Laminar flow of a Newtonian fluid through a tube of very short length** If the length of the tube is comparable to the radius of the tube, then the Hagen-Poiseuille equation needs to take into account entrance effects. This can happen, e.g., in nanoengineered ultrathin membranes. This means that the velocity profile has to develop in the tube from its flat entrance profile to the parabolic velocity profile given by [Equation 4.7](#). Dagan et al. (1982) obtained a solution to this problem, and in this case the volumetric flow rate is given by

$$Q = \frac{R^3(P_0 - P_L)}{\mu \left[ 3 + \frac{8}{\pi} \left( \frac{L}{R} \right) \right]} \quad (4.12)$$

If  $\frac{8}{\pi} \left( \frac{L}{R} \right) \gg 3$ , then [Equation 4.12](#) reduces to [Equation 4.10](#).

## 4.4.2 Hagen-Poiseuille equation for laminar flow of a Newtonian liquid in tubes of noncircular cross section

Solutions for laminar flow of a Newtonian fluid through tubes of noncircular cross sections have also been described in the literature (Lamb, 1932; Bird et al., 2002; Lekner, 2007). For laminar flow in the annular space formed by two concentric cylindrical tubes

$$Q = \frac{\pi R^4 (P_0 - P_L)}{8 \mu L} \left[ \left( 1 - \kappa^4 \right) - \frac{(1 - \kappa^2)^2}{\ln(1/\kappa)} \right] \quad (4.13)$$

where

R is the radius of the outer tube

$\kappa R$  is the radius of the inner tube

For an ellipsoidal tube cross section of major axis  $a$  and minor axis  $b$ , we have that

$$Q = \frac{\pi(P_0 - P_L)}{4\mu L} \frac{(ab)^3}{a^2 + b^2} \quad (4.14)$$

For laminar flow through the rectangular slit of height  $2H$  formed between two large parallel and horizontal plates of width  $W$  and length  $L$  in the flow direction

$$Q = \frac{2}{3}WH^3 \frac{P_0 - P_L}{\mu L} \quad (4.15)$$

## 4.5 The Rabinowitsch equation for the flow of a non-Newtonian fluid in a cylindrical tube

Through the use of the data obtained from the capillary viscometer of given length,  $L$ , and radius,  $R$ , a general relationship between the shear rate and some function of the shear stress can be determined in terms of the measurable quantities  $Q$  and  $(P_0 - P_L)$ .

Recall that for the capillary viscometer shown in [Figure 4.4](#), we can write the total flow rate  $Q$  in terms of the axial velocity profile as follows:

$$Q = 2\pi \int_0^R v_z(r) r dr \quad (4.16)$$

Next, we integrate [Equation 4.16](#) by parts to obtain the following equation:

$$Q = -\pi \int_0^R r^2 \left( \frac{dv_z(r)}{dr} \right) dr \quad (4.17)$$

Since  $\dot{\gamma} = -dv_z/dr$  and from [Equation 4.5](#) we have that  $r = R(\tau_{rz}/\tau_w)$ , we can show that the following equation is obtained. This is called the *Rabinowitsch equation*:

$$Q = \frac{\pi R^3}{\tau_w^3} \int_0^{\tau_w} \dot{\gamma}(\tau_{rz}) \tau_{rz}^2 d\tau_{rz} \quad (4.18)$$

For data obtained from a given capillary viscometer, the experiments will provide  $Q$  as a function of the observed pressure drop, i.e.,  $P_0 - P_L$ . The wall shear stress,  $\tau_w$ , is related to  $P_0 - P_L$  by [Equation 4.4](#). The appropriate shear rate and shear stress relationship, i.e.,  $\dot{\gamma} = \dot{\gamma}(\tau_{rz})$ , is the one that best fits the data according to [Equation 4.18](#).

For example, consider the simplest case of a Newtonian fluid. [Equation 4.19](#) provides the relationship for  $\dot{\gamma}(\tau_{rz})$ :

$$\dot{\gamma}(\tau_{rz}) = \frac{\tau_{rz}}{\mu} \quad (4.19)$$

Substituting this equation into [Equation 4.18](#) and integrating, we can readily obtain the result obtained earlier, i.e., [Equation 4.10](#), for the laminar volumetric flow rate of a Newtonian liquid flowing in a cylindrical tube.

## 4.6 Other useful flow relationships

Some other useful relationships for Newtonian flow in a cylindrical tube may be obtained by combining Equations 4.4 and 4.10. First, we obtain the following expression that relates the wall shear stress to the volumetric flow rate:

$$\tau_w = \left( \frac{4\mu}{\pi} \right) \frac{Q}{R^3} \quad (4.20)$$

Also, by writing Equation 4.19 at the tube wall and using Equation 4.20, it is found that the shear rate at the wall is given by

$$\dot{\gamma}_w = \frac{4Q}{\pi R^3} = \frac{4V_{\text{average}}}{R} = \frac{8V_{\text{average}}}{d} \quad (4.21)$$

The reduced average velocity  $\bar{U}$  is related to the wall shear rate and is defined as the ratio of the average velocity and the tube diameter. It is given by the following equation:

$$\bar{U} = \frac{V_{\text{average}}}{d} = \frac{4Q}{\pi d^3} = \frac{1}{8} \dot{\gamma}_w \quad (4.22)$$

The Rabinowitsch equation (4.18) can also be rewritten in terms of  $\bar{U}$ , i.e.,

$$\bar{U} = \frac{4Q}{\pi d^3} = \frac{1}{2\tau_w^2} \int_0^{\tau_w} \dot{\gamma}_w (\tau_{rz}) \tau_{rz}^2 d\tau_{rz} \quad (4.23)$$

This equation predicts that the reduced average velocity is only a function of the wall shear stress.

Table 4.3 provides a summary of these key flow equations.

### Example 4.3

A large artery can have a diameter of about 0.5 cm, whereas a large vein may have a diameter of about 0.8 cm. The average blood velocity in these arteries and veins is, respectively, on the order of 40 and 20 cm s<sup>-1</sup>. Calculate for these blood flows the wall shear rate,  $\dot{\gamma}_w$ .

#### Solution

We can use Equation 4.21 to calculate the wall shear rates.

For the large artery

$$\dot{\gamma}_w = \frac{4 \times 40 \text{ cm s}^{-1}}{0.25 \text{ cm}} = 640 \text{ s}^{-1}$$

and for the large vein

$$\dot{\gamma}_w = \frac{4 \times 20 \text{ cm s}^{-1}}{0.40 \text{ cm}} = 200 \text{ s}^{-1}$$

Table 4.3 Summary of Key Flow Equations

Relationship	Non-Newtonian	Newtonian
Shear stress, $\tau_{rz} =$	$\frac{(P_0 - P_L)r}{2L} = \tau_w \frac{r}{R}$	$\frac{(P_0 - P_L)r}{2L} = \tau_w \frac{r}{R}$
Wall shear stress, $\tau_w =$	$\frac{(P_0 - P_L)R}{2L}$	$\frac{(P_0 - P_L)R}{2L}$
Shear rate, $\dot{\gamma} =$	$-\frac{dv_z}{dr} = \dot{\gamma}(\tau_{rz})$	$-\frac{dv_z}{dr} = \frac{\tau_{rz}}{\mu}$
Volumetric flow rate, $Q =$	$\frac{\pi R^3}{\tau_w^3} \int_0^{\tau_w} \dot{\gamma}(\tau_{rz}) \tau_{rz}^2 d\tau_{rz}$	$\frac{\pi R^4 \Delta P}{8 \mu L}$
Wall shear stress, $\tau_w =$	—	$\frac{4\mu Q}{\pi R^3}$
Wall shear rate, $ \dot{\gamma}_w  =$	—	$\frac{4Q}{\pi R^3}$
Reduced average velocity, $\bar{U} =$	$\frac{4Q}{\pi d^3}$	$\frac{4Q}{\pi d^3}$

#### Example 4.4

Nutrient media is flowing at the rate of  $1.5 \text{ L min}^{-1}$  in a tube that is  $5 \text{ mm}$  in diameter. The walls of the tube are covered with antibody-producing cells, and these cells are anchored to the tube wall by their interaction with a special coating material that was applied to the surface of the tube. If one of these cells has a surface area of  $500 \mu\text{m}^2$ , what is the amount of the force that each cell must resist as a result of the flow of this fluid in the tube? Assume the viscosity of the nutrient media is  $1.2 \text{ cP} = 0.0012 \text{ Pa s}$ .

#### Solution

We can use [Equation 4.20](#) to find the shear stress acting on the cells that cover the surface of the tube:

$$\tau_w = \left( \frac{4 \times 0.0012 \text{ Pa s}}{\pi} \right) \frac{1500 \text{ cm}^3}{\min(0.25 \text{ cm})^3} \times \frac{1 \text{ min}}{60 \text{ s}} = 2.44 \text{ Pa} = 2.44 \text{ N m}^{-2}$$

Multiplying  $\tau_w$  by the surface area of a cell gives the force acting on that cell as a result of the fluid flow. Therefore

$$F_{\text{cell}} = 500 \mu\text{m}^2 \times \frac{(10^{-6} \text{ m})^2}{\mu\text{m}^2} \times 2.44 \frac{\text{N}}{\text{m}^2} \times \frac{10^{12} \text{ pN}}{\text{N}} = 1220 \text{ pN}$$

## 4.7 The rheology of blood and the Casson equation

The apparent viscosity of blood as a function of shear rate is illustrated in Figure 4.5 at a temperature of 37°C. At low shear rates, the apparent viscosity of blood is quite high due to the presence of rouleaux and aggregates. However, at shear rates above about 100–200 s<sup>-1</sup>, blood behaves as if it were a Newtonian fluid. We then approach the asymptotic high shear rate limit for the apparent viscosity of blood, which is about 3–4 cP.

At high shear rates, where blood is basically a Newtonian fluid, the following equations can be used to express the dependence of the blood viscosity on temperature and hematocrit (Charm and Kurland, 1974):

$$\mu = \mu_{\text{plasma}} \frac{1}{1 - \alpha H}, \quad \text{for } H \leq 0.6$$

$$\text{where } \alpha = 0.070 \exp \left[ 2.49H + \frac{1107}{T} \exp(-1.69H) \right] \quad (4.24)$$

In the previous equations, temperature (T) is in K. These equations may be used to a hematocrit of 0.60 and the stated accuracy is within 10%.

### 4.7.1 The Casson equation

The shear stress-shear rate relationship for blood can be described by the following empirical equation known as the *Casson equation*:

$$\tau^{1/2} = \tau_y^{1/2} + s \dot{\gamma}^{1/2} \quad (4.25)$$

In this equation,  $\tau_y$  is the yield stress and s is a constant, both of which can be determined from viscometer data. The yield stress represents the fact that a minimum force must be applied to stagnant

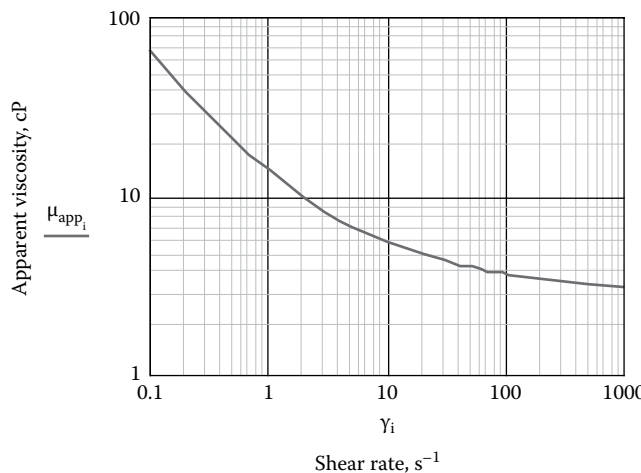


Figure 4.5 Apparent viscosity of blood at 37°C.

blood before it will flow. This was illustrated in [Figure 4.3](#). The yield stress for blood at 37°C is about 0.04 dynes cm<sup>-2</sup>. It is important to point out, however, that the effect of the yield stress on the flow of blood is small, as the following example will show.

### Example 4.5

Estimate the pressure drop in a small blood vessel that is needed to just overcome the yield stress.

#### Solution

We can use [Equation 4.4](#) to solve for the pressure drop needed to overcome the yield stress ( $\tau_y = \tau_w$ ):

$$(P_0 - P_L)_{\min} = \frac{2L\tau_y}{R}$$

Using the yield stress of 0.04 dynes cm<sup>-2</sup> and an L/R of 200 for a blood vessel, the pressure drop required to just initiate the flow is

$$(P_0 - P_L)_{\min} = 2 \times 200 \times 0.04 \text{ dynes cm}^{-2} \times \frac{1 \text{ bar}}{10^6 \text{ dynes cm}^{-2}} \times \frac{750.061 \text{ mmHg}}{1 \text{ bar}} = 0.012 \text{ mmHg}$$

This result is considerably less than the mean blood pressure, which is on the order of 100 mmHg.

At large values of the shear rate, the apparent viscosity of blood approaches its asymptotic value as shown in [Figure 4.5](#). From [Equation 4.25](#) at large shear rates, we see that the parameter s can be interpreted as the square root of the asymptotic Newtonian viscosity. The asymptotic viscosity of blood is about 3 cP; therefore, the parameter s is  $\sqrt{3cP} = 1.732(\text{cP})^{1/2}$  or 0.173 (dynes s cm<sup>-2</sup>)<sup>1/2</sup>. It should be stressed that the values of the yield stress and the parameter s will also depend on plasma protein concentrations, hematocrit, and temperature. Therefore, one must be careful to properly calibrate the Casson equation to the actual blood and the conditions used in the viscometer or the situation under study.

## 4.7.2 Using the Casson equation

For a Casson fluid like blood, we can rearrange [Equation 4.25](#) and solve for the shear rate, i.e.,  $\dot{\gamma}(\tau_{rz})$ , in terms of the shear stress,  $\tau_{rz}$ :

$$\dot{\gamma}(\tau_{rz}) = \frac{[\tau_{rz}^{1/2} - \tau_y^{1/2}]^2}{s^2} \quad (4.26)$$

This equation can be substituted into [Equation 4.23](#) and the resulting equation integrated to obtain the following fundamental equation that describes the flow of the Casson fluid in a cylindrical tube. This equation depends on only two parameters,  $\tau_y$  and s, which can be determined from experimental data:

$$\bar{U} = \frac{1}{2s^2} \left[ \frac{\tau_w}{4} - \frac{4}{7} \sqrt{\tau_y} \sqrt{\tau_w} - \frac{1}{84} \frac{\tau_y^4}{\tau_w^3} + \frac{\tau_y}{3} \right] \quad (4.27)$$

Using [Equation 4.22](#), we can replace the reduced average velocity in [Equation 4.27](#) with the volumetric flow rate, i.e.,  $Q$ , and obtain

$$Q = \frac{\pi R^4 (P_0 - P_L)}{8\mu_\infty L} \left[ 1 - \frac{16}{7} \sqrt{\frac{\tau_y}{\tau_w}} + \frac{4}{3} \frac{\tau_y}{\tau_w} - \frac{1}{21} \left( \frac{\tau_y}{\tau_w} \right)^4 \right] \quad (4.28)$$

where

$\mu_\infty$  is equal to  $s^2$  and is the viscosity of the fluid at high shear rates

$\tau_w$  is given by [Equation 4.4](#)

[Equation 4.28](#) is the Casson fluid equivalent to the Hagen-Poiseuille equation, i.e., [Equation 4.10](#).

### Example 4.6

Merrill et al. (1965) in a series of classic experiments studied the flow of blood in capillary tubes of various diameters. The blood had a hematocrit of 39.3 and the temperature was 20°C. They measured the pressure drop as a function of the flow rate for five tube diameters ranging from 288 to 850  $\mu\text{m}$ . When they expressed the measured pressure drops in terms of the wall shear stress ([Equation 4.4](#)), and the volumetric flow rates in terms of the reduced average velocity ([Equation 4.22](#)), all of the data for the various tube sizes formed, within the experimental accuracy, a single line as predicted by [Equation 4.23](#). From their results they provide the following values of the Casson parameters at 20°C:  $\tau_y = 0.0289 \text{ dynes cm}^{-2}$  and  $s = 0.229 (\text{dynes s cm}^{-2})^{1/2}$ . Using these values for  $\tau_y$  and  $s$ , show that [Equation 4.27](#) provides an excellent fit to their data summarized in the following table.

$\tau_w, \text{dynes cm}^{-2}$	$\bar{U}, \text{s}^{-1}$
0.06	0.01
0.10	0.05
0.15	0.10
0.40	0.50
0.70	1.0
2.7	5.0
4.4	10.0
17.0	50.0
30.0	100.0

### Solution

[Figure 4.6](#) shows a good comparison between the data given in the previous table and the predicted reduced average velocity from [Equation 4.27](#) using the parameter values from Merrill et al. (1965).

### 4.7.3 The velocity profile for tube flow of a Casson fluid

We can also use the Casson equation to obtain an expression for the axial velocity profile for the flow of blood in a cylindrical tube or vessel. The maximum shear stress,  $\tau_w$ , is at the wall. If the yield stress,  $\tau_y$ , is greater than  $\tau_w$ , then there will be no flow of the fluid. On the other hand, if  $\tau_w$  is

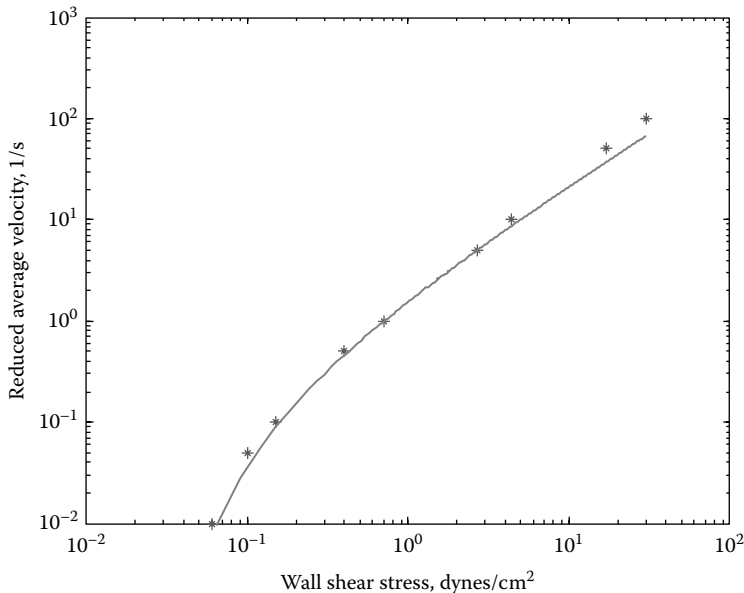


Figure 4.6 Reduced average velocity versus wall shear stress.

greater than  $\tau_y$ , there will be flow; however, there will be a critical radius ( $r_{critical}$ ) at which the local shear stress will equal  $\tau_y$ . From the tube centerline to this critical radius, this core fluid will have a flat velocity profile, i.e.,  $v_z(r) = v_{core}$ , and will move as if it were a solid body or in what is known as “plug flow.” For the region from the critical radius to the tube wall ( $r_{critical} \leq r \leq R$ ), [Equation 4.3](#) describes the shear stress distribution as a function of radial position. We can set this equation equal to the shear stress relation provided by the Casson equation [\(4.25\)](#) and rearrange to obtain the following equation for the shear rate:

$$\dot{\gamma} = -\frac{dv_z(r)}{dr} = \left\{ \frac{P_0 - P_L}{2L} r - 2\tau_y^{1/2} \left[ \frac{P_0 - P_L}{2L} r \right]^{1/2} + \tau_y \right\} \frac{1}{s^2} \quad (4.29)$$

This equation can be integrated to find  $v_z(r)$  using the boundary condition that at  $r = R$ ,  $v_z(R) = 0$ , thereby obtaining the following result:

$$v_z(r) = \frac{R\tau_w}{2s^2} \left\{ \left[ 1 - \left( \frac{r}{R} \right)^2 \right] - \frac{8}{3} \sqrt{\frac{\tau_y}{\tau_w}} \left[ 1 - \left( \frac{r}{R} \right)^{3/2} \right] + 2 \left( \frac{\tau_y}{\tau_w} \right) \left( 1 - \frac{r}{R} \right) \right\} \quad (4.30)$$

[Equation 4.30](#) applies for the region defined by  $r_{critical} \leq r \leq R$ . At this point, however, we need to determine the value of  $r_{critical}$ . Since the shear stress at  $r_{critical}$  must equal the yield stress, i.e.,  $\tau_{rz} = \tau_y$ , it is easy to then show from [Equation 4.5](#) that  $r_{critical} = R(\tau_y/\tau_w)$ . For locations from the centerline to the critical radius, the velocity of the core is given by [Equation 4.30](#) after setting  $r/R = r_{critical}/R = \tau_y/\tau_w$ .

#### 4.7.4 Tube flow of blood at low shear rates

At low shear rates RBC aggregates start to form due to the effect of plasma proteins like fibrinogen that make the RBCs stick together. This causes the apparent viscosity of blood to increase rapidly at low shear rates as we see in [Figure 4.5](#). As these aggregates grow, their characteristic size can also become comparable to that of the tube diameter. The assumption of blood being a homogeneous fluid is then no longer correct. However, for practical purposes, blood flow in the body and through medical devices will be at significantly higher shear rates.

Therefore, we really need not concern ourselves with the limiting case of blood flow at these very low shear rates.

### 4.8 The effect of tube diameter at high shear rates

Tube flow of blood at high shear rates (i.e.,  $>100 \text{ s}^{-1}$ ) in tubes less than about  $500 \mu\text{m}$  shows two anomalous effects that involve the tube diameter. These are the *Fahraeus effect* and the *Fahraeus-Lindqvist effect* (Barbee and Cokelet, 1971a,b; Gaehtgens, 1980; Pries et al., 1996).

#### 4.8.1 The Fahraeus effect

To understand the effect of tube diameter on blood flow, consider the conceptual model illustrated in [Figure 4.7](#). In this figure, blood flows from a larger vessel, such as an artery, into a smaller vessel, after which the blood flows into a larger vessel as in a vein. We make the distinction between the hematocrit found in the feed to the smaller vessel, represented by  $H_F$ , the hematocrit in the vessel of interest  $H_T$ , and the discharge hematocrit  $H_D$ . All of these hematocrits are averaged over the entire cross-sectional area of the tube.

In tubes with diameters from about 10 to  $500 \mu\text{m}$ , it is found that the tube hematocrit ( $H_T$ ) is actually less than that of the discharge hematocrit (at steady state,  $H_D = H_F$ , to satisfy the mass balance on the RBCs). This is called the *Fahraeus effect* and  $H_T/H_D$  reaches its minimal value of about 0.6–0.7 in tubes with a diameter of about 10–20  $\mu\text{m}$ .

Pries et al. (1996) have shown that the experimental data for  $H_T/H_D$  can be described by the following equation that depends on the tube diameter ( $d$ , microns) and the discharge hematocrit ( $H_D$ ):

$$\frac{H_T}{H_D} = H_D + (1 - H_D) \left( 1 + 1.7e^{-0.415d} - 0.6e^{-0.011d} \right) \quad (4.31)$$

To explain the Fahraeus effect, it has been shown both by *in vivo* and *in vitro* experiments that the RBCs do not distribute themselves evenly across the tube cross section. Instead, the RBCs tend to

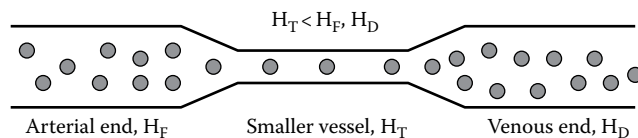


Figure 4.7 The Fahraeus effect.

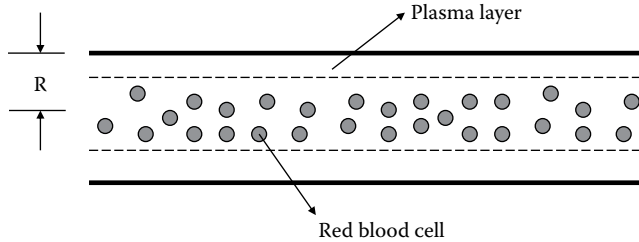


Figure 4.8 Axial accumulation of red blood cells.

accumulate along the tube axis forming, in a statistical sense, a thin cell-free layer along the tube wall. This is illustrated in Figure 4.8. Recall from Equation 4.7 that the fluid velocity is maximal along the tube axis. The axial accumulation of RBCs, in combination with the higher fluid velocity near the tube axis, maintains the RBC balance ( $H_F = H_D$ ) even though the hematocrit in the tube is reduced. The thin cell-free layer along the tube wall is called the *plasma layer* ( $\delta$ ). The thickness of the plasma layer depends on the tube diameter and the hematocrit and is typically on the order of several microns.

#### 4.8.2 The Fahraeus-Lindqvist effect

Because of the Fahraeus effect, it is found that as the tube diameter decreases below about 500  $\mu\text{m}$ , the *apparent viscosity* of blood also decreases, reaching a minimum value at a tube diameter of about 7  $\mu\text{m}$ . Even though the shear rate is high enough for the blood to behave like a Newtonian fluid, the blood viscosity is no longer constant and just a material property of the blood, but also depends on the tube diameter. The decreased viscosity is a direct result of the decrease in the tube hematocrit and the presence of the cell-free plasma layer near the wall of the tube, which has the effect of reducing the flow resistance of the blood. This reduction in the viscosity of the blood as the tube diameter gets smaller is known as the *Fahraeus-Lindqvist effect*.

For the laminar flow of blood in tubes less than 500  $\mu\text{m}$ , we can still use Equation 4.10 to express how the flow rate, i.e.,  $Q$ , depends on the pressure drop and the tube dimensions  $R$  and  $L$ . However, we will need to replace the viscosity, i.e.,  $\mu$ , by its apparent value, i.e.,  $\mu_{\text{apparent}}$ , to account for the effect of the tube diameter. Hence, we can write Equation 4.10 as follows:

$$Q = \frac{\pi R^4 \Delta P}{8 \mu_{\text{apparent}} L} \quad (4.32)$$

Pries et al. (1996) have shown that the *in vitro* experimental data for the apparent viscosity of blood as a function of tube diameter ( $d$ ,  $\mu\text{m}$ ) and the discharge hematocrit ( $H_D$ ) can be described by the following set of equations:

$$\frac{\mu_{\text{apparent}}}{\mu_{\text{plasma}}} = 1 + (\eta_{0.45} - 1) \frac{(1 - H_D)^C - 1}{(1 - 0.45)^C - 1} \quad (4.33)$$

where  $\eta_{0.45}$  is the ratio of the apparent viscosity of blood to plasma at a hematocrit of 0.45 and is given by

$$\eta_{0.45} = 220e^{-1.3d} + 3.2 - 2.44e^{-0.06d^{0.645}} \quad (4.34)$$

and the curve fitting parameter C is given by

$$C = \left(0.8 + e^{-0.075d}\right) \left(-1 + \frac{1}{1 + 10^{-11}d^{12}}\right) + \frac{1}{1 + 10^{-11}d^{12}} \quad (4.35)$$

For the in vivo case, Pries et al. (1996) provided the following expression for the apparent viscosity of blood as a function of the vessel diameter ( $d$ ,  $\mu\text{m}$ ) and the discharge hematocrit ( $H_D$ ):

$$\frac{\mu_{\text{apparent}}}{\mu_{\text{plasma}}} = \left[ 1 + \left( \eta_{0.45}^* - 1 \right) \frac{(1-H_D)^C - 1}{(1-0.45)^C - 1} \left( \frac{d}{d-1.1} \right)^2 \right] \left( \frac{d}{d-1.1} \right)^2 \quad (4.36)$$

with C given by [Equation 4.35](#) and  $\eta_{0.45}^*$  given by

$$\eta_{0.45}^* = 6e^{-0.085d} + 3.2 - 2.44e^{-0.06d^{0.645}} \quad (4.37)$$

The in vivo apparent viscosity of blood in vessels with diameters in the range of 4–30  $\mu\text{m}$  is significantly higher than the in vitro apparent viscosity in tubes of the same diameter. This is likely due to the presence of macromolecules on the endothelial surface of blood vessels retarding the flow of plasma.

### Example 4.7

Blood is flowing within a small hollow fiber module containing a total of 10,000 fibers. Each fiber has an internal diameter of 60  $\mu\text{m}$  and a length of 20 cm. If the total flow rate of the blood is 10  $\text{mL min}^{-1}$ , estimate the pressure drop in mmHg across the hollow fibers. Also calculate the tube hematocrit,  $H_T$ . Assume the discharge hematocrit of the blood is 0.40 and that the Newtonian viscosity of blood in large tubes is 3 cP. The plasma viscosity is 1.2 cP.

### Solution

Since the hollow fiber diameter is less than 500  $\mu\text{m}$ , we will need to take into account the Fahraeus and the Fahraeus-Lindqvist effects. First, we can calculate the tube hematocrit using [Equation 4.31](#):

$$\frac{H_T}{0.40} = 0.40 + (1 - 0.40) \left( 1 + 1.7e^{-0.415 \times 60} - 0.6e^{-0.011 \times 60} \right)$$

$$H_T = 0.326$$

Next, we calculate the apparent viscosity of blood using Equations 4.33 through 4.35:

$$C = \left(0.8 + e^{-0.075 \times 60}\right) \left(-1 + \frac{1}{1 + 10^{-11} 60^{12}}\right) + \frac{1}{1 + 10^{-11} 60^{12}} = -0.811$$

$$\eta_{0.45} = 220e^{-1.3 \times 60} + 3.2 - 2.44e^{-0.06 \times 60^{0.645}} = 2.148$$

$$\frac{\mu_{\text{apparent}}}{1.2 \text{ cP}} = 1 + (2.148 - 1) \frac{(1 - 0.40)^{-0.811} - 1}{(1 - 0.45)^{-0.811} - 1} = 1.944$$

$$\mu_{\text{apparent}} = 1.944 \times 1.2 \text{ cP} = 2.333 \text{ cP} = 0.00233 \text{ Pas}$$

The flow rate for a given fiber is

$$Q_{\text{fiber}} = 10 \frac{\text{cm}^3}{\text{min}} \times \frac{1 \text{ min}}{60 \text{ s}} \times \frac{1}{10,000 \text{ fibers}} = 1.667 \times 10^{-5} \text{ cm}^3 \text{ s}^{-1}$$

We can now rearrange Equation 4.32 and solve for the pressure drop across the hollow fiber as shown next:

$$\Delta P = \frac{8 \mu_{\text{apparent}} L Q}{\pi R^4} = \frac{8 \times 0.00233 \text{ Pa s} \times 20 \text{ cm} \times 1.667 \times 10^{-5} \text{ cm}^3 \text{ s}^{-1}}{\pi \times (0.003 \text{ cm})^4}$$

$$\Delta P = 24,422 \text{ Pa} \times \frac{1 \text{ atm}}{101,325 \text{ Pa}} \times \frac{760 \text{ mmHg}}{1 \text{ atm}} = 183.2 \text{ mmHg}$$

### 4.8.3 Marginal zone theory

The marginal zone theory proposed by Haynes (1960) may be used to characterize the Fahraeus-Lindqvist effect in the range from about 4–7 to 500  $\mu\text{m}$ . Using this theory, it is possible to obtain an expression for the apparent viscosity in terms of the plasma layer thickness, tube diameter, and the core and plasma viscosities. Development of the marginal zone theory makes use of the relationships for a Newtonian fluid that we developed earlier. These are summarized in Table 4.3.

As shown in Figure 4.8, the blood flow within a tube or vessel is divided into two regions: a central core that contains the RBCs with a viscosity  $\mu_{\text{core}}$  and the cell-free marginal or plasma layer that consists only of plasma with a thickness of  $\delta$  and a viscosity equal to that of the plasma given by the symbol  $\mu_{\text{plasma}}$ . Note that the tube hematocrit (i.e., averaged over the entire tube cross section) is related to the core hematocrit by the expression  $H_T = \left(1 - \frac{\delta}{R}\right)^2 H_C$ .

In each of these regions, the flow is considered to be Newtonian and Equation 4.6 applies to each. For the core region, we can then write

$$\tau_{rz} = \frac{(P_0 - P_L)r}{2L} = -\mu_{\text{core}} \frac{dv_z^{\text{core}}}{dr}$$

$$\text{BC1: } r = 0, \quad \frac{dv_z^{\text{core}}}{dr} = 0 \quad (4.38)$$

$$\text{BC2: } r = R - \delta, \quad \tau_{rz}|_{\text{core}} = \tau_{rz}|_{\text{plasma}}$$

The first boundary condition (BC1) expresses the fact that the axial velocity profile is symmetric about the axis of the tube and the velocity is also a maximum at the centerline of the tube. The second boundary condition (BC2) derives from the fact that the transport of momentum must be continuous across the interface between the core and the plasma layer.

For the plasma layer, the following equations apply:

$$\begin{aligned} \tau_{rz} &= \frac{(P_0 - P_L)r}{2L} = -\mu_{\text{plasma}} \frac{dv_z^{\text{plasma}}}{dr} \\ \text{BC3: } r &= R - \delta, \quad v_z^{\text{core}} = v_z^{\text{plasma}} \\ \text{BC4: } r &= R, \quad v_z^{\text{plasma}} = 0 \end{aligned} \quad (4.39)$$

The third boundary condition (BC3) states the requirement that the velocity in each region must be the same at their interface. The last boundary condition (BC4) simply requires that the axial velocity is zero at the tube wall.

[Equations 4.38](#) and [4.39](#) can be readily integrated to give the following expressions for the axial velocity profiles in the core and plasma regions:

$$v_z^{\text{plasma}}(r) = \frac{(P_0 - P_L)R^2}{4\mu_{\text{plasma}}L} \left[ 1 - \left( \frac{r}{R} \right)^2 \right] \quad \text{for } R - \delta \leq r \leq R \quad (4.40)$$

$$v_z^{\text{core}}(r) = \frac{(P_0 - P_L)R^2}{4\mu_{\text{plasma}}L} \left\{ 1 - \left( \frac{R - \delta}{R} \right)^2 - \frac{\mu_{\text{plasma}}}{\mu_{\text{core}}} \left( \frac{r}{R} \right)^2 + \frac{\mu_{\text{plasma}}}{\mu_{\text{core}}} \left( \frac{R - \delta}{R} \right)^2 \right\} \quad \text{for } 0 \leq r \leq R - \delta \quad (4.41)$$

The plasma and core volumetric flow rates are given by the following equations:

$$\begin{aligned} Q_{\text{plasma}} &= 2\pi \int_{R-\delta}^R v_z^{\text{plasma}}(r) r dr \\ Q_{\text{core}} &= 2\pi \int_0^{R-\delta} v_z^{\text{core}}(r) r dr \end{aligned} \quad (4.42)$$

Integration of [Equation 4.42](#) with the values of  $v_z^{\text{plasma}}$  and  $v_z^{\text{core}}$  from [Equations 4.40](#) and [4.41](#) provides the following result for the volumetric flow rates of the plasma layer and the core:

$$Q_{\text{plasma}} = \frac{\pi(P_0 - P_L)}{8\mu_{\text{plasma}}L} \left[ R^2 - (R - \delta)^2 \right]^2 \quad (4.43)$$

$$Q_{\text{core}} = \frac{\pi(P_0 - P_L)R^2}{4\mu_{\text{plasma}}L} \left[ (R - \delta)^2 - \left( 1 - \frac{\mu_{\text{plasma}}}{\mu_{\text{core}}} \right) \frac{(R - \delta)^4}{R^2} - \frac{\mu_{\text{plasma}}}{\mu_{\text{core}}} \frac{(R - \delta)^4}{2R^2} \right] \quad (4.44)$$

The total flow rate of blood within the tube is equal to the sum of the flow rates in the core and plasma regions. After adding Equations 4.43 and 4.44, we obtain the following expression for the total flow rate:

$$Q = \frac{\pi R^4 (P_0 - P_L)}{8 \mu_{\text{plasma}} L} \left[ 1 - \left( 1 - \frac{\delta}{R} \right)^4 \left( 1 - \frac{\mu_{\text{plasma}}}{\mu_{\text{core}}} \right) \right] \quad (4.45)$$

Comparing Equation 4.45 with Equation 4.32 allows one to develop a relationship for the apparent viscosity based on the marginal zone theory. We then arrive at the following expression for the apparent viscosity in terms of  $\delta$ ,  $R$ ,  $\mu_{\text{core}}$ , and  $\mu_{\text{plasma}}$ :

$$\mu_{\text{apparent}} = \frac{\mu_{\text{plasma}}}{1 - \left( 1 - \frac{\delta}{R} \right)^4 \left( 1 - \frac{\mu_{\text{plasma}}}{\mu_{\text{core}}} \right)} \quad (4.46)$$

As  $\delta/R \rightarrow 0$ , then  $\mu_{\text{apparent}} \rightarrow \mu_{\text{core}} \rightarrow \mu$ , which is the viscosity of blood in a large tube at high shear rates, i.e., a Newtonian fluid, as one would expect. We can use Equations 4.45 and 4.46 for blood flow calculations in tubes less than 500  $\mu\text{m}$  in diameter provided that we know the thickness of the plasma layer,  $\delta$ , and the viscosity of the core,  $\mu_{\text{core}}$ . The next section shows how to determine the thickness of the plasma layer,  $\delta$ , and the viscosity of the core,  $\mu_{\text{core}}$ , using apparent viscosity data.

**4.8.3.1 Using the marginal zone theory** If we have apparent viscosity data for blood at high shear rates in tubes of various diameters, we can use Equation 4.46 to fit these data. First, we can use the binomial series to approximate the term  $(1 - r/R)^4$  as follows:

$$\left( 1 - \frac{\delta}{R} \right)^4 \approx 1 - \frac{4\delta}{R} \quad (4.47)$$

Substituting Equation 4.47 into Equation 4.46 and rearranging, we obtain

$$\frac{1}{\mu_{\text{apparent}}} = \frac{1}{\mu_{\text{core}}} + \left[ \frac{4\delta}{\mu_{\text{core}}} \left( \frac{\mu_{\text{core}}}{\mu_{\text{plasma}}} - 1 \right) \right] \frac{1}{R} \quad (4.48)$$

Equation 4.48 shows us that a plot of  $1/\mu_{\text{apparent}}$  versus  $1/R$  should be linear with a y intercept equal to  $1/\mu_{\text{core}}$  and a slope equal to the bracketed term. For a given plasma viscosity, the core viscosity can then be obtained from the y intercept, and we can solve for the thickness of the plasma layer ( $\delta$ ) from the slope. Example 4.8 shows how this is done.

### Example 4.8

Find the values of  $\delta$  and  $\mu_{\text{core}}$  that represent the data for the apparent viscosity of blood as a function of tube diameter given in the paper by Gaehtgens (1980) and summarized in the following table. Assume a plasma viscosity of 1.2 cP.

Tube Diameter, $\mu\text{m}$	$\mu_{\text{apparent}}, \text{cP}$
25	1.89
30	2.07
40	2.31
60	2.46
80	2.70
100	2.79
130	3.0

### Solution

Figure 4.9 shows a plot of  $1/\mu_{\text{apparent}}$  versus  $1/R$ . The line shown in Figure 4.9 is the result of a linear regression that provided an intercept of  $b = 0.2986 \text{ cP}^{-1}$  and a slope of  $m = 2.8367 \mu\text{m cP}^{-1}$  and a  $r^2 = 0.988$ . From Equation 4.48, we see that the core viscosity is equal to  $1/b = \mu_{\text{core}} = 3.349 \text{ cP}$ . From the slope  $m$ , we can solve for the value of the plasma layer thickness, i.e.,  $\delta$ :

$$\delta = \frac{m\mu_{\text{core}}}{4\left(\frac{\mu_{\text{core}}}{\mu_{\text{plasma}}} - 1\right)} = \frac{2.8367 \mu\text{m cP}^{-1} \times 3.349 \text{ cP}}{4\left(\frac{3.349 \text{ cP}}{1.2 \text{ cP}} - 1\right)} = 1.326 \mu\text{m}$$

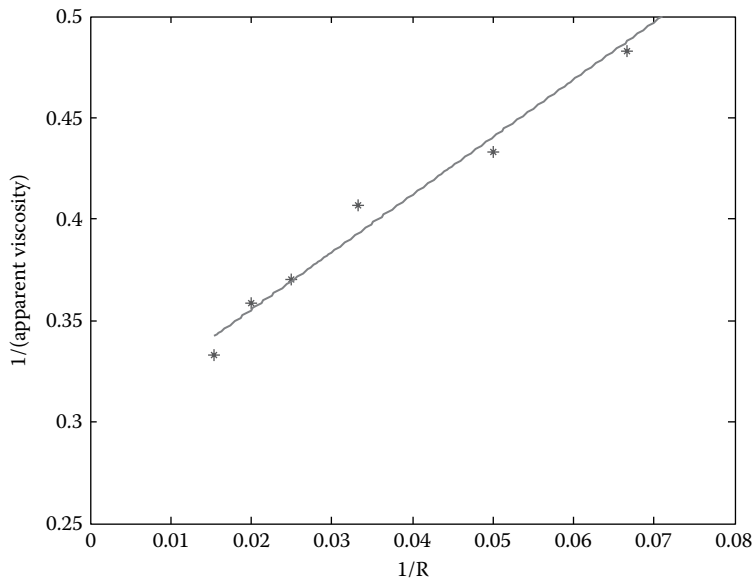


Figure 4.9 Regression using Equation 4.48.

## 4.9 Boundary layer theory

Describing the flow of a fluid near a surface is extremely important in a wide variety of engineering problems. Generally, the effect of the fluid viscosity is such that the fluid velocity changes from zero at the surface to the free stream value over a narrow region near the surface that is referred to as the *boundary layer*. It is the presence of this boundary layer that affects the rates of mass transfer and heat transfer between the surface and the fluid. Recall that the transport of something like momentum, mass, or energy is proportional to a driving force divided by a resistance. We will see that the boundary layer creates the resistance to the transport of momentum, mass, and energy. Interestingly, we will find that the thickness of the boundary layer is inversely proportional to the square root of the free stream velocity.

Analysis of these types of problems using boundary layer theory for relatively simple cases can provide a great deal of insight on how the flow of the fluid affects the transport of momentum, mass, and energy and lead to the rational development of correlations to describe their transport in more complex geometries and flow systems. We will use these correlations in later chapters in problems that involve the transport of mass across a bounding surface into a flowing fluid.

### 4.9.1 The flow near a wall that is set in motion

Consider the situation shown in [Figure 4.10](#). A semi-infinite quantity of a viscous fluid is contacted from below by a flat and horizontal plate. For  $t < 0$ , the plate and the fluid are not moving. At  $t = 0$ , the

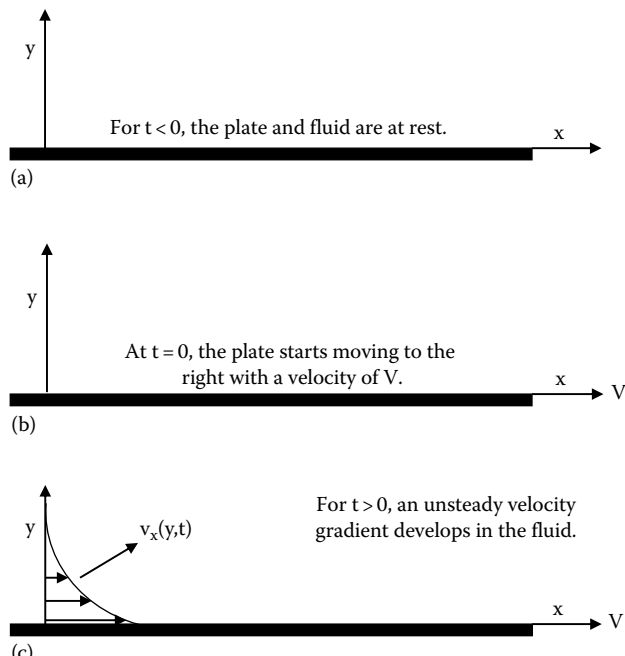


Figure 4.10 Flow of a fluid near a flat plate that is set in motion. (a) Plate and fluid at rest, (b) plate begins to move, and (c) plate moves at constant velocity  $V$ .

plate is set in motion with a constant velocity ( $V$ ) to the right, as shown in [Figure 4.10](#). There are no pressure gradients or gravitational forces acting on the fluid, so the motion of the fluid is solely due to the momentum transferred from the plate to the fluid. The flow is also laminar, meaning there is no mixing of fluid elements in the  $y$  direction. The velocity in Cartesian coordinates will have components  $v_x$ ,  $v_y$ , and  $v_z$ , and these will depend, in general, on  $x$ ,  $y$ ,  $z$ , and  $t$ . Since the plate does not move in the  $y$  direction, and we have no holes in the plate,  $v_y$  is zero. Also, the fluid and plate are assumed to be infinite in the  $z$  direction, so  $v_z$  is zero. The only component of the fluid velocity is therefore  $v_x$ . Since the plate and the fluid are infinite in the  $x$  and  $z$  directions,  $v_x$  can only depend on  $y$ , which makes sense since momentum is transported from the plate into the fluid in the  $y$  direction only. As time progresses, the  $x$  momentum of the plate is transported into the fluid in the  $y$  direction. In other words, for this laminar flow, the momentum diffuses in the  $y$  direction from a region of high velocity to a region of low velocity. This creates a velocity profile in the  $y$  direction that will depend on time.

We can arbitrarily define the boundary layer thickness ( $\delta$ ) for this problem as the distance perpendicular to the plate surface where the fluid has just been set into motion, and this distance is defined as that point where the local velocity is equal to 1% of  $V$ . Our goal here is now to determine the velocity profile  $v_x(y,t)$  and the boundary layer thickness,  $\delta(t)$ .

The concept of a shell balance can be used to analyze this problem. The shell balance is an important technique for developing mathematical models to describe the transport of such quantities as momentum, mass, and energy. The shell balance approach is conceptually easy to use and is based on the application of the generalized balance equation ([Equation 1.8](#)) to a given finite volume of interest.

In [Figure 4.10](#), consider a small volume element of the fluid  $\Delta x \Delta y W$ , where  $W$  is the width of the plate in the  $z$  direction (normal to the page) and is assumed to be very large. Recall that momentum is (mass)  $\times$  (velocity) and we can write the momentum per unit volume of the fluid as  $\rho v_x$ . The rate of accumulation of momentum within this volume element of the fluid is equal to  $\rho \frac{\partial v_x}{\partial t} \Delta x \Delta y W$ . This term has units of force and is also equal to the sum of the forces acting on this volume element of the fluid. The only forces acting on this volume element of fluid are the shear forces acting on the surfaces at  $y$  and  $y + \Delta y$ , i.e.,  $\tau_{yx}|_y$  and  $\tau_{yx}|_{y+\Delta y}$ . These terms also, respectively, represent the flux of  $x$  momentum in the  $y$  direction at  $y$  and  $y + \Delta y$ , respectively. Hence, our momentum shell balance on the volume element can be written as

$$\rho \frac{\partial v_x}{\partial t} \Delta x \Delta y W = \left( \tau_{yx}|_y - \tau_{yx}|_{y+\Delta y} \right) \Delta x W \quad (4.49)$$

Eliminating  $\Delta x$  and  $W$ , and then dividing by  $\Delta y$  and taking the limit as  $\Delta y \rightarrow 0$ , we obtain the following partial differential equation:

$$\rho \frac{\partial v_x}{\partial t} = - \frac{\partial \tau_{yx}}{\partial y} \quad (4.50)$$

This equation is valid for any fluid, Newtonian or non-Newtonian. For the special case of the Newtonian fluid, we can use Newton's law of viscosity, i.e., [Equation 4.2a](#), for  $\tau_{yx}$ , and obtain

$$\frac{\partial v_x}{\partial t} = \nu \frac{\partial^2 v_x}{\partial y^2} \quad (4.51)$$

where  $\nu$  is the *kinematic viscosity* and is defined as  $\mu/\rho$ . The initial condition (IC) and boundary conditions are

$$\begin{aligned} \text{IC: } t = 0, v_x = 0 & \quad \text{for all values of } y \\ \text{BC1: } y = 0, v_x = V & \quad \text{for all values of } t > 0 \\ \text{BC2: } y = \infty, v_x = 0 & \quad \text{for all values of } t > 0 \end{aligned} \quad (4.52)$$

[Equation 4.51](#) can easily be solved using the Laplace transform technique. Recall that the Laplace transform of a function  $f(t)$  is defined by the following equation:

$$L[f(t)] = \bar{f}(s) = \int_0^{\infty} e^{-st} f(t) dt \quad (4.53)$$

Tables of Laplace transforms may be found in a variety of calculus textbooks and mathematical handbooks. [Table 4.4](#) summarizes some of the more commonly used Laplace transforms.

Taking the Laplace transform of [Equation 4.51](#) results in the following equation:

$$s\bar{v}_x - v_x(t=0) = \nu \frac{d^2\bar{v}_x}{dy^2} \quad (4.54)$$

where  $\bar{v}_x$  denotes the Laplace transform of the velocity. From the initial condition ([Equation 4.52](#)), we have that  $v_x(t=0) = 0$ , and the other boundary conditions, when transformed, become

$$\begin{aligned} \text{BC1: } y = 0, \quad \bar{v}_x &= \frac{V}{s} \\ \text{BC2: } y = \infty, \quad \bar{v}_x &= 0 \end{aligned} \quad (4.55)$$

[Equation 4.54](#) can then be written as

$$\frac{d^2\bar{v}_x}{dy^2} - a^2 \bar{v}_x = 0 \quad (4.56)$$

with  $a^2 = s/\nu$ . [Equation 4.56](#) is a homogeneous second order differential equation having the general solution

$$\bar{v}_x = C_1 e^{ay} + C_2 e^{-ay} \quad (4.57)$$

The constants  $C_1$  and  $C_2$  can then be found from the transformed boundary conditions given by [Equation 4.55](#). Using these boundary conditions, we find that  $C_1 = 0$  and  $C_2 = V/s$ . Hence, our solution in the Laplace transform space is

$$\frac{\bar{v}_x}{V} = \frac{1}{s} e^{-ay} = \frac{1}{s} e^{-\frac{y}{\sqrt{\nu}} \sqrt{s}} \quad (4.58)$$

Table 4.4 Some Commonly Used Laplace Transforms

ID	Function	Transform
1	$C_1 f(t) + C_2 g(t)$	$C_1 \bar{f}(s) + C_2 \bar{g}(s)$
2	$\frac{df(t)}{dt}$	$s \bar{f}(s) - f(0+)$
3	$\frac{\partial^n f(x_i, t)}{\partial x_i^n}$	$\frac{\partial^n \bar{f}(x_i, s)}{\partial x_i^n}$
4	$\int_0^t f(\tau) d\tau$	$\frac{1}{s} \bar{f}(s)$
5	$f(\alpha t)$	$\frac{1}{\alpha} \bar{f}\left(\frac{s}{\alpha}\right)$
6	$e^{-\beta t} f(t)$	$\bar{f}(s + \beta)$
7	$\int_0^t f(t - \tau) g(\tau) d\tau$	$\bar{f}(s) \bar{g}(s)$
8	1	$\frac{1}{s}$
9	$t$	$\frac{1}{s^2}$
10	$\frac{1}{(\pi t)^{1/2}}$	$\frac{1}{s^{1/2}}$
11	$-\frac{1}{2\pi^{1/2} t^{3/2}}$	$s^{1/2}$
12	$e^{-\alpha t}$	$\frac{1}{s + \alpha}$
13	$\frac{e^{-\beta t} - e^{-\alpha t}}{\alpha - \beta}$	$\frac{1}{(s + \alpha)(s + \beta)}$
14	$t e^{-\alpha t}$	$\frac{1}{(s + \alpha)^2}$
15	$\frac{(\gamma - \beta)e^{-\alpha t} + (\alpha - \gamma)e^{-\beta t} + (\beta - \alpha)e^{-\gamma t}}{(\alpha - \beta)(\beta - \gamma)(\gamma - \alpha)}$	$\frac{1}{(s + \alpha)(s + \beta)(s + \gamma)}$
16	$\frac{1}{2} t^2 e^{-\alpha t}$	$\frac{1}{(s + \alpha)^3}$
17	$\frac{\alpha e^{-\alpha t} - \beta e^{-\beta t}}{\alpha - \beta}$	$\frac{s}{(s + \alpha)(s + \beta)}$

(Continued)

Table 4.4 (Continued) Some Commonly Used Laplace Transforms

ID	Function	Transform
18	$\frac{(\beta-\gamma)\alpha e^{-at} + (\gamma-\alpha)\beta e^{-bt} + (\alpha-\beta)\gamma e^{-ct}}{(\alpha-\beta)(\beta-\gamma)(\gamma-\alpha)}$	$\frac{s}{(s+\alpha)(s+\beta)(s+\gamma)}$
19	$\sin \alpha t$	$\frac{\alpha}{s^2 + \alpha^2}$
20	$\cos \alpha t$	$\frac{s}{s^2 + \alpha^2}$
21	$\sinh \alpha t$	$\frac{\alpha}{s^2 - \alpha^2}$
22	$\cosh \alpha t$	$\frac{s}{s^2 - \alpha^2}$
23	$\frac{x}{2(\pi at^3)^{1/2}} e^{-x^2/4at}$	$e^{-qx}, \quad q = \left(\frac{s}{a}\right)^{1/2}$
24	$\left(\frac{a}{\pi t}\right)^{1/2} e^{-x^2/4at}$	$\frac{e^{-qx}}{q}, \quad q = \left(\frac{s}{a}\right)^{1/2}$
25	$\operatorname{erfc}\left(\frac{x}{2(at)^{1/2}}\right)$	$\frac{e^{-qx}}{s}, \quad q = \left(\frac{s}{a}\right)^{1/2}$
26	$2\left(\frac{at}{\pi}\right)^{1/2} e^{-x^2/4at} - x \operatorname{erfc}\left(\frac{x}{2(at)^{1/2}}\right)$	$\frac{e^{-qx}}{qs}, \quad q = \left(\frac{s}{a}\right)^{1/2}$
27	$\left(t + \frac{x^2}{2a}\right) \operatorname{erfc}\left(\frac{x}{2(at)^{1/2}}\right) - x \left(\frac{t}{\pi a}\right)^{1/2} e^{-x^2/4at}$	$\frac{e^{-qx}}{s^2}$

Source: Arpaci, V.S., *Conduction Heat Transfer*, Addison-Wesley, Reading, MA, 1966.

Now inverting [Equation 4.58](#), we find the function  $v_x(t)$  whose Laplace transform is the above equation. From [Table 4.4](#), we use transform pair 25 and then find that the inverse of [Equation 4.58](#) provides the following solution for  $v_x(t)$ :

$$\frac{v_x(y,t)}{V} = \operatorname{erfc}\left(\frac{y}{\sqrt{4vt}}\right) = 1 - \operatorname{erf}\left(\frac{y}{\sqrt{4vt}}\right) \quad (4.59)$$

This solution is in terms of a new function called the *error function* and the *complementary error function*, which are abbreviated as “*erf*” and “*erfc*,” respectively. The error function is defined by the following equation:

$$\operatorname{erf}(x) = \frac{2}{\sqrt{\pi}} \int_0^x e^{-t^2} dt \quad \text{and} \quad \operatorname{erfc}(x) = 1 - \operatorname{erf}(x) \quad (4.60)$$

Note in [Equation 4.60](#) that the integral of  $e^{-x^2}$  cannot be obtained analytically. Since this integral is quite common in the solution of many engineering problems, this function has been tabulated in mathematical handbooks and mathematical software and can be treated as a known function, much like logarithmic and trigonometric functions.

Recall that we defined the boundary layer thickness as that distance  $y$  from the surface of the plate where the velocity has decreased to a value of 1% of  $V$ . The complementary error function of  $y/\sqrt{4vt} = 1.821$  provides a value of  $v_x/V$  that is equal to 0.01. Hence, we can define the boundary layer thickness,  $\delta(t)$ , as follows:

$$\delta(t) = 3.642\sqrt{vt} \approx 4\sqrt{vt} \quad (4.61)$$

The value of  $\delta$  can also be interpreted as the distance to which momentum from the moving plate has penetrated into the fluid at time  $t$ .

### Example 4.9

Calculate the boundary layer thickness 1 s after the plate has started to move. Assume the fluid is water for which  $\nu = 1 \times 10^{-6} \text{ m}^2 \text{ s}^{-1}$ .

#### Solution

Using [Equation 4.61](#), we can calculate the thickness of the boundary layer as

$$\delta = 4\sqrt{10^{-6} \text{ m}^2 \text{ s}^{-1} \times 1 \text{ s}} = 0.004 \text{ m} = 4 \text{ mm}$$

### 4.9.2 Laminar flow of a fluid along a flat plate

Now consider the situation shown in [Figure 4.11](#) for the steady laminar flow of a fluid along a flat plate. The plate is assumed to be semi-infinite and the fluid approaches the plate at a uniform

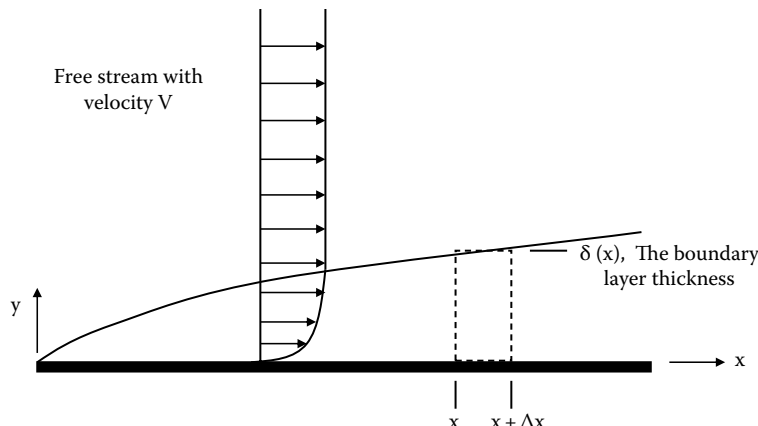


Figure 4.11 Laminar boundary layer flow of a fluid over a flat plate.

velocity of  $V$  in the direction of the plate length, which is  $L$ . The velocity in Cartesian coordinates will have components  $v_x$ ,  $v_y$ , and  $v_z$ , and these will depend, in general, on  $x$ ,  $y$ ,  $z$ . However, since the plate is large in the  $z$  direction, there will be no  $v_z$  component of the velocity. Since the fluid velocity at the surface of the plate is zero, a boundary layer is formed near the surface of the plate, and within this boundary layer,  $v_x$  increases from zero at the plate surface to its free stream value of  $V$ .

We can estimate the boundary layer thickness as follows (Schlichting, 1979). Recall for the plate suddenly set into motion that from [Equation 4.61](#), the boundary layer thickness,  $\delta$ , is proportional to  $\sqrt{vt}$ , where  $t$  is the time, since the plate was set into motion. For the situation shown in [Figure 4.11](#), we can think of  $t$  as the time it takes to travel from the leading edge of the flat plate to a downstream location  $x$ . Hence, we can replace  $t$  in [Equation 4.61](#) with  $x/V$ , and we obtain the following approximate relationship for how the boundary layer thickness,  $\delta(x)$ , changes along the surface of the flat plate:

$$\delta(x) = 4\sqrt{\frac{vx}{V}} \quad (4.62)$$

The growth of the boundary layer along the surface of the plate will also cause the fluid flow to be displaced in the  $y$  direction, and this means that, in addition to the  $v_x$  component of the velocity, there will also be a  $v_y$  component. Both of these velocity components will depend on  $x$  and  $y$ .

**4.9.2.1 Approximate solution for laminar boundary flow over a flat plate** In the following discussion, we will obtain an approximate solution for the boundary layer flow over a flat plate. The approximate solution is very close to the exact solution. Details on exact solutions to the boundary layer equations may be found in Schlichting (1979).

Consider the shell volume shown in [Figure 4.11](#) and located from  $x$  to  $x + \Delta x$  and from  $y = 0$  to  $y = \delta(x)$ . We first perform a steady-state mass balance on this shell volume that is given by

$$\int_0^{\delta(x)} \left[ W\rho v_x|_x - W\rho v_x|_{x+\Delta x} \right] dy - \rho v_y|_{y=\delta(x)} W\Delta x = 0 \quad (4.63)$$

The integral term in [Equation 4.63](#) is the net rate (i.e., In – Out) at which mass is being added to the shell volume. The second term accounts for the loss of mass from the shell volume at the top of the boundary layer due to flow in the  $y$  direction. Eliminating  $\rho$  and  $W$ , and dividing by  $\Delta x$ , followed by taking the limit as  $\Delta x \rightarrow 0$ , provides the following equation\* for  $v_y|_{y=\delta(x)}$ :

$$v_y|_{y=\delta(x)} = - \int_0^{\delta(x)} \frac{\partial v_x}{\partial x} dy = - \frac{d}{dx} \int_0^{\delta(x)} v_x dy + V \frac{d\delta(x)}{dx} \quad (4.64)$$

---

\* Here we have used Leibnitz's rule, i.e.,  $\frac{d}{dt} \left( \int_{a(t)}^{b(t)} f(x,t) dx \right) = \int_{a(t)}^{b(t)} \frac{\partial f}{\partial t} dx + f[b(t),t] \frac{db(t)}{dt} - f[a(t),t] \frac{da(t)}{dt}$

In a similar manner, we can write an x momentum balance on the shell volume as

$$\int_0^{\delta(x)} \left[ W\rho v_x v_x \Big|_x - W\rho v_x v_x \Big|_{x+\Delta x} \right] dy - \rho v_y \Big|_{y=\delta(x)} V W \Delta x + W \Delta x \tau_{yx} \Big|_{y=0} = 0 \quad (4.65)$$

The first term from the left in [Equation 4.65](#) represents the net rate at which x momentum is being added to the shell volume. The second term represents the rate at which x momentum per volume of fluid ( $\rho V$ ) at the top of the boundary layer is being lost due to the flow of fluid out of the boundary layer in the y direction. The last term in this equation represents the loss of momentum as a result of the shear stress generated by the fluid at the surface of the plate.

After eliminating W and dividing by  $\Delta x$ , taking the limit as  $\Delta x \rightarrow 0$ , using Leibnitz's rule\* and [Equation 4.64](#) to eliminate  $v_y$ , we can write [Equation 4.65](#) as

$$-\tau_{yx} \Big|_{y=0} = \frac{d}{dx} \left( \int_0^{\delta(x)} \rho(V - v_x) v_x dy \right) \quad (4.66)$$

For a Newtonian fluid, we can use [Equation 4.2a](#) and obtain

$$\mu \frac{\partial v_x}{\partial y} \Big|_{y=0} = \frac{d}{dx} \left( \int_0^{\delta(x)} \rho(V - v_x) v_x dy \right) \quad (4.67)$$

[Equation 4.67](#) is also known as the *von Karman* momentum balance equation and forms the basis for obtaining an approximate solution to the boundary layer flow over a flat plate. To obtain an approximate solution, we first need to approximate the shape of the velocity profile within the boundary layer, i.e.,  $v_x(x,y)$ . The simplest function that reasonably approximates the shape of the velocity profile is a simple cubic equation:

$$v_x(y) = a + by + cy^2 + dy^3 \quad (4.68)$$

This velocity profile also has to satisfy the following boundary conditions:

$$\begin{aligned} BC1: \quad & y = 0, \quad v_x = 0 \\ BC2: \quad & y = \delta(x), \quad v_x = V \\ BC3: \quad & y = \delta(x), \quad \frac{\partial v_x}{\partial y} = 0 \\ BC4: \quad & y = 0, \quad \frac{\partial^2 v_x}{\partial y^2} = 0 \end{aligned} \quad (4.69)$$

---

\* Here we have used Leibnitz's rule, i.e.,  $\frac{d}{dt} \left( \int_{a(t)}^{b(t)} f(x,t) dx \right) = \int_{a(t)}^{b(t)} \frac{\partial f}{\partial t} dx + f[b(t),t] \frac{db(t)}{dt} - f[a(t),t] \frac{da(t)}{dt}$

The first boundary condition (BC1) is referred to as the “no-slip” boundary condition, which requires that the velocity of the fluid at the surface of the plate be the same as the velocity of the plate, which, in this case, is zero. The last boundary condition (BC4) expresses the fact that the stress at the surface of the plate only depends on  $x$  and not on  $y$ . The second and third boundary conditions (BC2 and BC3) state that beyond the boundary layer, the velocity is constant and equal to the free stream value,  $V$ .

When the above boundary conditions are imposed on [Equation 4.68](#), the following expression is obtained for the velocity profile within the boundary layer:

$$\frac{v_x(x,y)}{V} = \frac{3}{2} \left( \frac{y}{\delta(x)} \right) - \frac{1}{2} \left( \frac{y}{\delta(x)} \right)^3 \quad (4.70)$$

[Equation 4.70](#) shows that  $v_x$  depends on  $\delta(x)$ , which is still not known. However, we can insert this equation into the von Karman momentum balance equation ([Equation 4.67](#)), and after some simplification we obtain

$$\delta \frac{d\delta}{dx} = \frac{140}{13} \left( \frac{\mu}{\rho V} \right) \quad (4.71)$$

with the condition that at  $x = 0$ ,  $\delta = 0$ . Integration of this equation results in the following expression for the boundary layer thickness,  $\delta(x)$ :

$$\delta(x) = 4.64 \sqrt{\frac{vx}{V}} \quad (4.72)$$

This equation is very similar to the approximate relationship we got earlier, i.e., [Equation 4.62](#). We can also rearrange [Equation 4.72](#) and express the boundary layer thickness relative to the downstream location  $x$  as

$$\frac{\delta(x)}{x} = \frac{4.64}{\sqrt{\frac{\rho V x}{\mu}}} = 4.64 Re_x^{-1/2} \quad (4.73)$$

In this equation,  $Re_x = \rho V x / \mu$  is defined as the local value (i.e., at location  $x$ ) of the *Reynolds number*. The Reynolds number is a very important dimensionless number in the field of fluid mechanics. We see that the Reynolds number represents the ratio of the inertial forces ( $\rho V \times V L^2 = \rho V^2 L^2$ ) acting on the fluid to the viscous forces ( $\mu(V/L) \times L^2 = \mu VL$ ) acting on the fluid, where  $L$  is a characteristic dimension. A high Reynolds number indicates that the inertial forces dominate the viscous forces. On the other hand, a low Reynolds number means viscous forces are much larger than the inertial forces. The Reynolds number also provides insight into when the fluid transitions from uniform laminar flow to turbulent flow. This critical Reynolds number for transition from laminar to turbulent flow depends on the geometry of the flow being considered. For example, for boundary layer flow over the flat plate, experiments show that the flow is laminar provided  $Re_x < 300,000$ , whereas for flow in a cylindrical tube of diameter  $d$ , the flow is laminar if the  $Re_d < \sim 2300$  and can transition to turbulent

flow at a  $Re_d > \sim 4000$ . In this case of flow in a cylindrical tube, note that the characteristic dimension is the diameter of the cylindrical tube ( $d$ ). For flow over the flat plate of length  $L$ , the Reynolds number is  $Re_L = \rho VL/\mu$ .

The approximate velocity profile within the boundary layer for laminar flow on a flat plate is then given by the combination of Equations 4.70 and 4.72 as shown here:

$$\frac{v_x(x,y)}{V} = 0.3233 \left( y \sqrt{\frac{V}{vx}} \right) - 0.005 \left( y \sqrt{\frac{V}{vx}} \right)^3 \quad (4.74)$$

Note that  $v_x(x,y)/V$  depends on the single dimensionless parameter  $\eta$ , where  $\eta = y\sqrt{V/vx}$ .

Equation 4.74 provides an excellent representation of the actual measured velocity profile for laminar boundary flow over a flat plate (see Problem 4.27 at the end of this chapter).

We can also use Equation 4.64 to calculate the  $y$  component of the velocity at the outer edge of the boundary layer, i.e.,  $v_y|_{y=\delta(x)}$ , using Equation 4.74 for  $v_x(x,y)$  and Equation 4.72 for  $\delta(x)$ :

$$v_y|_{y=\delta(x)} = 0.87V \sqrt{\frac{v}{Vx}} = 0.87V \sqrt{\frac{\mu}{\rho Vx}} = 0.87V \sqrt{\frac{1}{Re_x}} \quad (4.75)$$

The exact value of  $v_y|_{y=\delta(x)}$  given by Schlichting (1979) has the constant in Equation 4.75 as 0.8604 instead of the value given by our approximate solution of 0.87. Equation 4.75 shows that at the outer edge of the boundary layer, there is an outward flow of fluid in the  $y$  direction that is caused by the growth of the boundary layer thickness in the direction of flow, i.e.,  $\delta(x)$ , as given by Equation 4.72.

With the velocity profile given by Equation 4.74, we can also calculate the drag force exerted by the fluid on the plate. For a plate of length  $L$  and width  $W$ , the force that acts on the surface of both sides of the plate in the positive  $x$  direction is given by

$$F_x = 2 \int_0^W \int_0^L \left( \mu \frac{\partial v_x}{\partial y} \Big|_{y=0} \right) dx dz = 1.293 \sqrt{\rho \mu L W^2 V^3} \quad (4.76)$$

The exact solution, as well as experimental data for the drag force on the flat plate, is about 3% greater than that predicted by the approximate solution to the flat plate boundary layer problem given by Equation 4.76. The constant in Equation 4.76 being 1.328 for the exact solution. Hence, we see that this approximate solution to the flat plate boundary layer problem is quite good not only predicting the  $x$  and  $y$  velocity profiles but also the drag as well.

We can also calculate the power needed to overcome the drag force. Recall that power is defined as (force  $\times$  velocity), so after multiplying Equation 4.76 by  $V$ , the power is given by

$$P = VF_x = 1.293 \sqrt{\rho \mu L W^2 V^5} \quad (4.77)$$

The *friction factor* ( $f$ ) is defined as the ratio of the shear stress at the wall and the kinetic energy per volume of the fluid based on the free stream velocity. The local value of the friction factor is then given by

$$f_x = \frac{\tau_{yx}|_{y=0}}{\frac{1}{2}\rho V^2} = \frac{\mu \left| \frac{\partial v_x}{\partial y} \right|_{y=0}}{\frac{1}{2}\rho V^2} = \frac{3\mu}{\rho V \delta(x)} = \frac{0.646}{\sqrt{Re_x}} \quad (4.78)$$

For a plate of length  $L$  and width  $W$ , the average value of the friction factor ( $f$ ) is given by integrating Equation 4.78 as shown here:

$$f = \frac{\int_0^W \int_0^L \frac{0.646}{\sqrt{Re_x}} dx dz}{WL} = 1.293 \frac{1}{\sqrt{Re_L}} \quad (4.79)$$

where  $Re_L = \rho VL/\mu$ . The definition of the friction factor given by Equation 4.78 means that the force acting on both sides of the plate (i.e.,  $F_x$ ) is given by the product of the kinetic energy per volume of the fluid ( $(1/2)\rho V^2$ ), the area of the flat plate ( $2LW$ ), and the friction factor ( $f$ ) and is given by the next equation:

$$F_x = \frac{1}{2} \rho V^2 \times (\text{Area}) \times f = \frac{1}{2} \rho V^2 \times (2LW) \times 1.293 \frac{1}{\sqrt{Re_L}} = 1.293 \sqrt{\rho \mu L W^2 V^3} \quad (4.80)$$

This result for  $F_x$  is, as expected, the same as that given by Equation 4.76. As shown by Equations 4.79 and 4.80, the friction factor is a convenient method for finding the force acting on a surface as a result of fluid motion. When the flow is across or over an object, the friction factor is also known as the *drag coefficient* ( $f = C_D$ ) since it allows for the calculation of the drag force exerted on the object by the flowing fluid.

### Example 4.10

Water ( $\mu = 0.001 \text{ Pa s}$ ,  $\rho = 1000 \text{ kg m}^{-3}$ ) is flowing over a flat plate at a speed of  $0.1 \text{ m s}^{-1}$ . Over what length of the plate (cm) is the boundary layer flow laminar? What is the boundary layer thickness (cm) at the location where the flow becomes turbulent? If the plate has a width of 25 cm, what is the drag force (N) acting on the flat plate over this length?

### Solution

The flow will transition to turbulent flow once the Reynolds number reaches 300,000. Letting this distance be where  $x = L$ , the Reynolds number can be solved for the value of  $L$  as

$$L = \frac{Re_L \mu}{\rho V} = \frac{300,000 \times 0.001 \frac{\text{Ns}}{\text{m}^2} \times \frac{\text{kgm}}{\text{s}^2 \text{N}}}{1000 \frac{\text{kg}}{\text{m}^3} \times 0.1 \frac{\text{m}}{\text{s}}} = 3.0 \text{ m} = 300 \text{ cm}$$

From [Equation 4.72](#), the thickness of the boundary layer at this location (i.e., L) can be found:

$$\delta(L) = 4.64 \sqrt{\frac{\mu L}{\rho V}} = 4.64 \sqrt{\frac{0.001 \frac{\text{Ns}}{\text{m}^2} \times 3.0 \text{ m} \times \frac{\text{kgm}}{\text{s}^2 \text{N}}}{1000 \frac{\text{kg}}{\text{m}^3} \times 0.1 \frac{\text{m}}{\text{s}}}} = 0.0254 \text{ m} = 2.54 \text{ cm}$$

The drag force acting on the plate can be found from [Equation 4.76](#):

$$F_{\text{drag}} = 1.293 \sqrt{1000 \frac{\text{kg}}{\text{m}^3} \times 0.001 \frac{\text{Ns}}{\text{m}^2} \times 3.0 \text{ m} \times 0.25^2 \text{ m}^2 \times 0.1^3 \frac{\text{m}^3}{\text{s}^3} \times \frac{1 \text{ Ns}^2}{\text{kgm}}} = 0.018 \text{ N}$$

### Example 4.11

Consider a manta ray swimming along in the ocean at  $0.75 \text{ m s}^{-1}$ . Assuming the ray approximates a rectangular shape with a length of  $0.30 \text{ m}$  and a width of  $0.75 \text{ m}$ , estimate how much power the ray is expending to move through the water as a result of the drag force of the water on its surface? Assume the density of the water is  $1000 \text{ kg m}^{-3}$  and the viscosity of the water is  $1 \text{ cP} = 0.001 \text{ Pa s} = 0.001$ .

#### Solution

Assume the geometry of the manta ray approximates that of a flat plate, and we can assume that we have laminar flow of the seawater over a flat plate. Using [Equation 4.77](#) we can calculate the power requirement as follows:

$$P = 1.293 \sqrt{1000 \text{ kgm}^{-3} \times 0.001 \text{ kgm}^{-1} \text{s}^{-1} \times 0.3 \text{ m} \times 0.75^2 \text{ m}^2 \times 0.75^5 \text{ m}^5 \text{s}^{-5}} \\ = 0.26 \text{ kgms}^{-2} \text{ ms}^{-1} = 0.26 \text{ Js}^{-1} = 0.26 \text{ W}$$

As shown here, the Reynolds number calculation shows that the flow is laminar over the surface of the manta ray since it is less than 300,000 at  $x = L = 0.30 \text{ m}$ :

$$Re_L = \frac{1000 \text{ kgm}^{-3} \times 0.75 \text{ ms}^{-1} \times 0.30 \text{ m}}{0.001 \text{ kgm}^{-1} \text{s}^{-1}} = 225,000$$

## 4.10 Generalized mechanical energy balance equation

[Equation 4.10](#) provides a useful relationship for describing the laminar flow of a liquid in a cylindrical tube of constant cross section. Oftentimes, we will need a more generalized relationship that can handle turbulent flow and account for not only the effect of the pressure drop on fluid flow but also the effect of changes in elevation, tube cross section, changes in fluid velocity, sudden contractions or expansions, pumps, as well as the effect of fittings such as valves. This general relationship for the flow of a fluid is called the *Bernoulli equation* and is valid for laminar or turbulent flow.

The Bernoulli equation accounts for the effect of changes in fluid pressure, potential energy, and kinetic energy on the flow of the fluid. It also accounts for the energy added to the fluid by pumps, the energy removed by turbines, and accounts for energy losses due to a variety of frictional effects.

For steady-state flow of an incompressible fluid (density  $\rho = \text{constant}$ ) from inlet station “1” to exit station “2” (see [Figure 2.1](#)), the Bernoulli equation can be written as follows (McCabe et al., 1985; Bird et al., 2002):

$$\frac{P_1}{\rho} + gZ_1 + \frac{\alpha_1 V_1^2}{2} + W_{\text{device}} = \frac{P_2}{\rho} + gZ_2 + \frac{\alpha_2 V_2^2}{2} + h_{\text{friction}} \quad (4.81)$$

In this equation

$P$  represents the pressure

$Z$  is the elevation relative to a reference plane

$V$  is the average fluid velocity

Gravitational acceleration is represented by  $g$  and in SI units is equal to  $9.8 \text{ m s}^{-2}$ . The  $\alpha$ 's are kinetic energy correction terms that account for the shape of the velocity profile. For laminar flow in a cylindrical tube, i.e., for a  $Re = \rho d_{\text{tube}} V / \mu < 2300$ ,  $\alpha = 2.0$ , and for turbulent flow  $\alpha = 1.0$ . The work effect per unit mass of fluid is  $W_{\text{device}}$ . If  $W_{\text{device}} > 0$ , then work is done on the fluid, e.g., by a pump. The actual work required to achieve these changes in the fluid properties will be greater than  $W_{\text{device}}$  due to frictional losses and mechanical inefficiencies within the pump. If  $W_{\text{device}} < 0$ , then the fluid produces work, e.g., by a turbine. The actual amount of work that is generated will be less than this value because of frictional losses and mechanical inefficiencies within the turbine. Other frictional effects between positions 1 and 2 due to the tube itself, contractions, expansions, and fittings are accounted for by the term  $h_{\text{friction}}$ .

The units of each term in [Equation 4.81](#) must be consistent with one another and are expressed in terms of energy per unit mass of fluid. In SI units, each term in [Equation 4.81](#) will have units of  $\text{m}^2 \text{ s}^{-2}$ . If these units of  $\text{m}^2 \text{ s}^{-2}$  are multiplied by  $\text{kg kg}^{-1}$ , then as we see in the following equation, the units are the same as a  $\text{J kg}^{-1}$ :

$$\frac{\text{m}^2}{\text{s}^2} = \frac{\text{m}^2}{\text{s}^2} \times \frac{\text{kg}}{\text{kg}} = \frac{\text{kg m}}{\text{s}^2} \times \frac{\text{m}}{\text{kg}} = \frac{\text{Nm}}{\text{kg}} = \frac{\text{J}}{\text{kg}} \quad (4.82)$$

In addition to the Bernoulli equation, we also need to write a mass balance on the fluid. At steady state, this simply says that the rate of mass leaving the system, or a region of interest at position 2, must equal the rate at which mass enters the system at position 1. For steady-state flow, this can be expressed by the mass conservation or continuity equation given here:

$$\dot{m} = (\rho VS)_1 = (\rho VS)_2 = \text{constant} \quad (4.83)$$

In this equation

$\dot{m}$  is the mass flow rate

$S$  represents the cross-sectional area of the tube

The frictional effects in [Equation 4.81](#) are described by

$$h_{\text{friction}} = \left( 4 \sum_i f_i \frac{L_i V_i^2}{2d_i} + \sum_j \frac{V_j^2}{2} K_{\text{fitting}_j} \right) \quad (4.84)$$

In this equation,  $f_i$  is the friction factor and accounts for the loss in fluid energy per unit mass of fluid in tube segment  $i$  of length  $L_i$  and diameter  $d_i$ .  $V_i$  represents the average velocity,

$$V_i = \frac{\text{Volumetric flow rate}}{\pi d_i^2 / 4}, \quad \text{within tube section } i.$$

The friction factor  $f$ , also known as the *Fanning friction factor*, is defined as the ratio of the wall shear stress ( $\tau_w$ ) and the average kinetic energy per unit mass of fluid, also called the *velocity head*, i.e.,  $\rho V^2 / 2$ . For laminar flow, it is easy to show from [Equation 4.10](#) that  $f = 16/\text{Re}$ . For turbulent flow ( $\text{Re} > \sim 2300$ ) in smooth tubes, the friction factor may be evaluated from either of the following equations (McCabe et al., 1985; Bird et al., 2002):

$$\begin{aligned} \frac{1}{\sqrt{f}} &= 4.07 \log(\text{Re} \sqrt{f}) - 0.60 \\ f &= \frac{0.0791}{\text{Re}^{1/4}} \end{aligned} \quad (4.85)$$

The second equation is valid up to a  $\text{Re} = 100,000$  and is more convenient to use since  $f$  is explicit in  $\text{Re}$ . If the flow is turbulent, and the walls are not smooth, then the friction factor charts in McCabe et al. or Bird et al. should be consulted (i.e., graphs of  $f$  versus  $\text{Re}$  with surface roughness as a parameter).

The term in the second summation of [Equation 4.84](#), represented by  $K_{\text{fitting}}$ , accounts for energy loss in the fluid due to tube contractions, expansions, or fittings such as valves. It is important to note that for the most part, these fitting losses tend to be negligible for laminar flow of a fluid.

The average velocity in this second summation of [Equation 4.84](#) is for the fluid just downstream of the contraction, expansion, or fitting. A  $K_{\text{fitting}}$  for such items as valves is highly dependent on the valve's degree of openness and on the type of valve used. It is generally best to consult the manufacturer's literature for the particular valve being considered. As examples, a gate valve that is wide open has a  $K_{\text{fitting}}$  of about 0.2 and a value of about 6 when half open. A globe valve that is wide open may have a value as high as 10. Simple fittings, such as a tee, has a  $K_{\text{fitting}}$  value of 2.0, and a  $90^\circ$  elbow has a value of about 1.0.

For sudden contractions and expansions of the fluid, the following equations can be used to estimate  $K_{\text{fitting}}$ . Once again,  $S$  refers to the cross-sectional area of the tube:

$$\begin{aligned} K_{\text{contraction}} &= 0.45 \left( 1 - \frac{S_{\text{downstream}}}{S_{\text{upstream}}} \right), \quad \text{sudden contraction, turbulent flow} \\ K_{\text{expansion}} &= \left( \frac{S_{\text{downstream}}}{S_{\text{upstream}}} - 1 \right)^2, \quad \text{sudden expansion, turbulent flow} \end{aligned} \quad (4.86)$$

If for an expansion  $S_{\text{downstream}} \gg S_{\text{upstream}}$ , then  $K_{\text{expansion}} = 1$ , and the velocity upstream of the expansion is used in [Equation 4.84](#). In this case, the expansion means that we essentially lose all of the kinetic energy per mass of fluid (i.e.,  $V_{\text{upstream}}^2/2$ ) as it goes through the expansion.

#### 4.10.1 The hydraulic diameter

If the tube through which a fluid flows is not circular, then the *hydraulic diameter* can be used in the above calculations. The hydraulic diameter for flow in tubes of noncircular cross section is defined as four times the *hydraulic radius* (i.e.,  $4 \times r_H$ ). The hydraulic radius is defined as the ratio of the cross-sectional area of the flow channel to the wetted perimeter of the tube. The factor of four is needed so that  $d_H = d$  for a circular tube:

$$d_H = 4 \times r_H = \frac{4 \times (\text{Cross sectional area})}{(\text{Wetted perimeter})} \quad (4.87)$$

The hydraulic diameter is then used in the calculation of the Reynolds number, i.e.,  $Re = \rho V d_H / \mu$ , and in [Equation 4.84](#). However, the average velocity ( $V$ ) is still defined as the volumetric flow rate ( $Q$ ) divided by the cross-sectional area normal to the flow. It is also important to note that the hydraulic diameter should only be used for turbulent flow.

For flow in a cylindrical annulus with an inner tube of outer diameter  $d_i$  and an outer tube with inner diameter  $d_o$ , the hydraulic diameter is found from [Equation 4.87](#) to be  $(d_o - d_i)$ . For flow between two parallel plates of width,  $W$ , separated by a distance,  $H$ , and completely filled with fluid, the hydraulic diameter is equal to  $2WH/(W+H)$ . Note that for a very wide rectangular duct where  $W \gg H$ , the hydraulic diameter for this slit flow is  $2H$ , or twice the separation of the plates.

The following examples illustrate the use of the Bernoulli equation and the above relationships.

#### Example 4.12

Consider the flow of a fluid through an orifice located at the bottom of a tank. The cross-sectional area of the tank is  $S_1$ , and the area of the orifice located at the bottom surface of the tank is  $S_2$ . The fluid stream leaving through the orifice will tend to contract (called the *vena contracta*) such that at a short distance downstream of the orifice, its cross-sectional area will be about 0.64 times that of the area of the orifice or  $S_{\text{vena contracta}} = 0.64 S_2$ . If the pressure in the tank is maintained at  $P_1$ , and if the fluid leaving through the orifice is at atmospheric pressure, develop an expression for the average fluid velocity at the vena contracta, assuming the height of the fluid in the tank is given by  $h$ .

#### Solution

First, we write the Bernoulli equation (4.81) for this situation, where the index 1 denotes the surface of the fluid within the tank. Note that there are no work devices and we ignore any frictional effects and assume the flow leaving the tank through the orifice is turbulent. We also set  $g(Z_1 - Z_2) = g h$ . Hence, for this situation we can write the Bernoulli equation as

$$\frac{P_1}{\rho} + gh + \frac{V_1^2}{2} = \frac{P_{\text{vena contracta}}}{\rho} + \frac{V_{\text{vena contracta}}^2}{2}$$

Since  $P_{\text{vena contracta}}$  is the same as the atmospheric pressure ( $P_{\text{atm}}$ ), this equation can be rewritten as

$$V_{\text{vena contracta}}^2 = V_1^2 + 2 \frac{(P_1 - P_{\text{atm}})}{\rho} + 2 gh$$

Mass conservation given by [Equation 4.83](#) allows for the calculation of the velocity of the fluid surface within the tank in terms of the velocity at the vena contracta, i.e.,

$$V_1 = V_{\text{vena contracta}} \frac{S_{\text{vena contracta}}}{S_1}$$

Using the previous equation to eliminate  $V_1$  in the previous equation for  $V_{\text{vena contracta}}$  allows for the calculation of the average velocity of the fluid in the vena contracta as

$$V_{\text{vena contracta}} = \sqrt{\frac{2 \left( \frac{P_1 - P_{\text{atm}}}{\rho} \right) + 2 gh}{1 - \left( \frac{S_{\text{vena contracta}}}{S_1} \right)^2}}$$

For the flow of a fluid from a tank through an orifice, we usually have that  $S_1 \gg S_{\text{vena contracta}}$ . Hence, in this case

$$V_{\text{vena contracta}} = \sqrt{2 \left( \frac{P_1 - P_{\text{atm}}}{\rho} \right) + 2 gh}$$

And if the tank is open to the atmosphere, then  $P_1 = P_{\text{atm}}$  and we obtain what is known as the *Torricelli equation*:

$$V_{\text{vena contracta}} = \sqrt{2 gh}$$

Based on this result, the volumetric flow rate of the fluid, i.e.,  $Q = S_{\text{vena contracta}} \times V_{\text{vena contracta}}$ , is given by the next result:

$$Q = S_{\text{vena contracta}} \sqrt{2 gh} \approx 0.64 S_{\text{orifice}} \sqrt{2 gh}$$

If the flow through the orifice is driven by the pressure difference and not by the potential energy of the fluid, i.e., if  $\left( \frac{P_1 - P_{\text{atm}}}{\rho} \right) \gg 2 gh$ , then we have

$$V_{\text{vena contracta}} = \sqrt{\frac{2(P_1 - P_{\text{atm}})}{\rho}}$$

And in this case,  $Q$  is given by

$$Q = S_{\text{vena contracta}} \sqrt{\frac{2(P_1 - P_{\text{atm}})}{\rho}} \approx 0.64 S_{\text{orifice}} \sqrt{\frac{2(P_1 - P_{\text{atm}})}{\rho}} \quad (\text{A})$$

### Example 4.13

Consider a patient being evaluated for stenosis (narrowing) of their aortic valve. Catheterization of the heart gave a cardiac output of  $5000 \text{ mL min}^{-1}$ , a mean systolic pressure drop across the aortic valve of  $50 \text{ mmHg}$ , a heart rate of  $80 \text{ beats min}^{-1}$ , and a systolic ejection period of  $0.33 \text{ s}$ . From these data, estimate the cross-sectional area of the aortic valve.

#### Solution

We can use [Equation A](#) developed in the previous example to determine the cross-sectional area of the aortic valve ( $S_{\text{orifice}} = S_{\text{aortic valve}}$ ) from these data. From [Table 4.1](#), the density of blood is  $1.056 \text{ g cm}^{-3} = 1056 \text{ kg m}^{-3}$ . From the cardiac output and the number of heartbeats per minute, we find that each beat of the heart moves a volume of blood given by  $\frac{5000 \text{ cm}^3}{\text{min}} \times \frac{1 \text{ min}}{80 \text{ beats}} = 62.5 \frac{\text{cm}^3}{\text{beat}}$ . If the aortic valve remains open for  $0.33$  seconds for each beat, then each beat of the heart gives a flow rate of blood through the valve of  $\frac{62.5 \text{ cm}^3}{\text{beat}} \times \frac{1 \text{ beat}}{0.33 \text{ s}} = 189.4 \frac{\text{cm}^3}{\text{s}}$ . Solving [Equation A](#) for the area of the aortic valve

$$S_{\text{aortic valve}} = \frac{Q}{0.64 \sqrt{\frac{2\Delta P_{\text{systolic}}}{\rho}}} = \frac{189.4 \frac{\text{cm}^3}{\text{s}}}{0.64 \sqrt{\frac{2 \times 50 \text{ mmHg}}{1056 \text{ kg/m}^3} \times \frac{101,325 \text{ Pa}}{760 \text{ mmHg}} \times \frac{\text{N}}{\text{m}^2 \text{Pa}} \times \frac{\text{kgm}}{\text{s}^2 \text{N}} \times \frac{10^4 \text{ cm}^2}{\text{m}^2}}}$$

$$S_{\text{aortic valve}} = 0.83 \text{ cm}^2$$

We can also calculate the Reynolds number at the vena contracta of the blood flowing out of the aortic valve. At the vena contracta, the cross-sectional area is  $0.64 \times 0.83 \text{ cm}^2 = 0.53 \text{ cm}^2$ , which gives a diameter for the vena contracta of  $0.82 \text{ cm}$ . The average velocity of the blood at the vena contracta is given by

$$V = \frac{189.4 \text{ cm}^3}{\text{s}} \times \frac{1}{0.64 \times 0.83 \text{ cm}^2} = 356.6 \frac{\text{cm}}{\text{s}}$$

From [Table 4.1](#), we have that the viscosity of blood is  $3 \text{ cP}$ . Therefore, we can calculate the Reynolds number as

$$Re = \frac{\rho V d_{\text{vena contracta}}}{\mu_{\text{blood}}} = \frac{1.056 \frac{\text{g}}{\text{cm}^3} \times 356.6 \frac{\text{cm}}{\text{s}} \times 0.82 \text{ cm}}{3 \text{ cP} \times 0.01 \frac{\text{g}}{\text{cP cms}}} = 10,293$$

Hence, we conclude that the flow of the blood through the aortic valve under these conditions is turbulent and that the assumptions used to calculate the aortic valve cross-sectional area that were based on the results of the previous example are valid.

**Example 4.14**

A *Pitot tube* (see [Figure 4.12](#)) is a simple device for measuring the velocity of a fluid that is passing nearby. This device is used to measure the airspeed on airplanes and can be inserted into pipes to measure the velocity of the flowing fluid. As shown in [Figure 4.12](#), the Pitot tube is aligned with the axis of the flow. At the tip of this tube (1), there is a small opening into an inner tube that leads to a pressure measuring system. In this case, the pressure measuring system is a simple manometer that contains a denser fluid such as mercury with density  $\rho_m$ . The fluid that impinges at the tip of the Pitot tube (1) stagnates or has a zero velocity (i.e.,  $V_1 = 0$ ), and its kinetic energy is converted according to the Bernoulli equation into what is called the *stagnation pressure*,  $P_1$ . Surrounding or coaxial to this tube is another tube, and along the sides of this tube are small holes that are also connected to the pressure measuring system. These small holes along the side of this outer tube sense the static pressure ( $P_2$ ) of the surrounding fluid that passes by at a velocity of  $V_2$ . From this information, develop an expression for the velocity of the fluid flowing near a Pitot tube in terms of the pressure difference ( $P_1 - P_2$ ).

Also, write this expression for the velocity in terms of the manometer reading ( $h$ ) for a manometer fluid of density  $\rho_m$ .

**Solution**

For the fluid flowing past the Pitot tube, there is no change in elevation. Also, since in this case we are measuring the local velocity of the fluid and not the average velocity, there is no kinetic energy correction term; hence  $\alpha$  is equal to one. If we also neglect any work and frictional effects, the Bernoulli equation (4.81) can be written between the stagnation point (1) (note  $V_1 = 0$ ) and the static holes (2) as

$$\frac{P_1}{\rho} = \frac{P_2}{\rho} + \frac{V_2^2}{2}$$

Note that this equation says that the stagnation pressure ( $P_1$ ) is equal to the static pressure ( $P_2$ ) plus the dynamic pressure, or the velocity head of the fluid, i.e.,  $\frac{1}{2}\rho V_2^2$ ; hence  $P_1 = P_2 + \frac{1}{2}\rho V_2^2$ .

This equation can then be rearranged and solved to give the velocity of the fluid passing near the static holes along the sides of the Pitot tube:

$$V_2 = \sqrt{\frac{2(P_1 - P_2)}{\rho}}$$

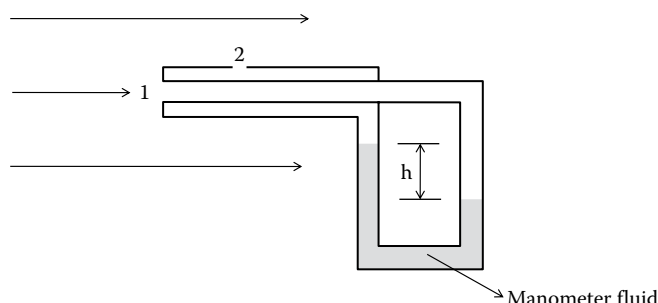


Figure 4.12 The Pitot tube.

If a manometer is used as shown in [Figure 4.12](#) to measure the pressure difference ( $P_1 - P_2$ ), then the Bernoulli equation can be used to express this pressure difference in terms of the difference in height ( $h$ ) between the legs of the manometer fluid. At the surface of the upper leg of the manometer fluid, the pressure is  $P_2$  and the velocity of this surface is equal to zero. Similarly, at the surface of the lower leg of the manometer fluid, the pressure is  $P_1$  and the velocity of this surface is also zero. Neglecting work and frictional effects, the Bernoulli equation for this situation becomes

$$\frac{P_1}{\rho_m} + gZ_1 = \frac{P_2}{\rho_m} + gZ_2$$

Letting  $Z_2 - Z_1 = h$ , this equation can be solved for  $(P_1 - P_2)$  in terms of  $h$  for a manometer fluid of density  $\rho_m$ . This result is also known as the *manometer equation*:

$$(P_1 - P_2) = \rho_m gh$$

Using this result, we can express the velocity for the Pitot tube of [Figure 4.12](#) as

$$V_2 = \sqrt{\frac{2\rho_m gh}{\rho}}$$

### Example 4.15

Farmer Jones needs to pump water from the Maumee River to irrigate his soybean fields. He figures that he will need 250 ft of 2 in. inside diameter steel pipe and four 90° elbows to bring the water from the river to his water tower where the water is then stored. The total change in elevation from the river surface to where the water flows into the top of the water tower is 100 ft. Farmer Jones wants the water flow rate in this system to be 100 gal min<sup>-1</sup>. Assuming the pump down by the river has an efficiency of 80%, estimate the required horsepower of the pump that is needed.

#### Solution

We assume that the storage tank is vented to the atmosphere and that the pipe enters at the top of the storage tank where the water flows into the storage tank. We also let location (1) be the surface of the river and location (2) is the plane at the exit of the pipe. With these assumptions, the pressure at the surface of the river is the same as that inside the storage tank; hence we have  $P_1 = P_2$ . We also assume that the surface of the river adds no kinetic energy to the flow in the pipe, which means that  $V_1 = 0$ . With these assumptions, we can then write the Bernoulli equation ([4.81](#)) from the surface of the lake (1) to where the water leaves the pipe (2):

$$gZ_1 + W_{device} = gZ_2 + \frac{\alpha_2 V_2^2}{2} + h_{friction}$$

We now use [Equation 4.84](#) for  $h_{friction}$  to account for the resistance of the pipe of length  $L$  and diameter  $d$  and the fittings. The above equation then becomes

$$W_{device} = g(Z_2 - Z_1) + \frac{\alpha_2 V_2^2}{2} + \frac{4fLV_2^2}{2d} + \sum_j \frac{V_j^2}{2} K_{fitting_j}$$

The second to the last term in the previous equation accounts for the loss of energy per unit mass as the water flows at velocity  $V_2$  through the 2 in. pipe ( $d$ ) that is 250 ft in length ( $L$ ). The friction factor ( $f$ ) in this term can be calculated after we find the Reynolds number and determine whether the flow in the pipe is laminar or turbulent. To find the Reynolds number, we first need to determine the velocity,  $V_2$ , in the pipe as

$$V_2 = \frac{4Q}{\pi d^2} = \frac{4 \times 100 \frac{\text{gal}}{\text{min}} \times \frac{1 \text{ min}}{60 \text{ s}} \times \frac{0.13368 \text{ ft}^3}{\text{gal}} \times \frac{(12 \text{ in.})^3}{\text{ft}^3} \times \frac{(2.54 \text{ cm})^3}{\text{in.}^3}}{\pi \times (2 \text{ in.})^2 \times \frac{(2.54 \text{ cm})^2}{\text{in.}^2}} = 311.3 \frac{\text{cm}}{\text{s}}$$

Assuming that water has a density of  $1 \text{ g cm}^{-3}$  and a viscosity of  $1 \text{ cP}$ , we can now calculate the value of the Reynolds number:

$$Re = \frac{\rho dV}{\mu} = \frac{1 \frac{\text{g}}{\text{cm}^3} \times 2 \text{ in.} \times \frac{2.54 \text{ cm}}{\text{in.}} \times 311.3 \frac{\text{cm}}{\text{s}}}{1 \text{ cP} \times \frac{1 \text{ g}}{\text{cm s } 100 \text{ cP}}} = 158,140$$

The flow in the pipe is therefore turbulent and  $\alpha_2 = 1.0$ . We can also use [Equation 4.85](#) to find the friction factor, which is found to be equal to 0.0041.

Next, the contraction of the fluid as it enters the pipe from the river and the effect of the four elbows is calculated as

$$\sum_j \frac{V_j^2}{2} K_{fitting_j} = \frac{1}{2} V_2^2 \times (4 \times K_{elbow}) + 0.45 \left(1 - \frac{S_{\text{pipe}}}{S_{\text{river}}}\right) \times \frac{1}{2} V_2^2 = 2.225 V_2^2$$

This result is obtained when the value of  $K_{elbow}$  is set equal to 1. We also assume for the contraction from the river into the pipe that  $S_{\text{river}} \gg S_{\text{pipe}}$ . The Bernoulli equation then becomes

$$W_{\text{device}} = g(Z_2 - Z_1) + \left(\frac{1}{2} + \frac{4fL}{2d} + 2.225\right) V_2^2$$

Now inserting the numerical values where the elevation change was given as 100 ft (30.48 m), the pipe length is 250 ft (76.2 m), the diameter of the pipe is 2 in. (0.051 m), along with  $f$  equal to 0.0041, and  $V_2 = 311.3 \text{ cm s}^{-1} = 3.11 \text{ m s}^{-1}$ , we then obtain

$$W_{\text{device}} = 9.8 \frac{\text{m}}{\text{s}^2} \times 30.48 \text{ m} + \left(2.725 + \frac{4 \times 0.0041 \times 76.2 \text{ m}}{2 \times 0.051 \text{ m}}\right) \frac{3.11^2 \text{ m}^2}{\text{s}^2} = 443.6 \frac{\text{m}^2}{\text{s}^2}$$

If this result is then multiplied by  $\text{kg kg}^{-1}$  (see [Equation 4.82](#)), then  $W_{\text{device}} = 443.6 \text{ J kg}^{-1}$ . Next, we multiply this result by the mass flow rate of the water, which is calculated next:

$$\dot{m} = \frac{\pi d^2}{4} \rho V_2 = \frac{\pi \times 0.051^2 \text{ m}^2}{4} \times 1000 \frac{\text{kg}}{\text{m}^3} \times 3.11 \frac{\text{m}}{\text{s}} = 6.35 \frac{\text{kg}}{\text{s}}$$

So, the total amount of work required to pump the water is given by

$$W_{\text{total}} = \dot{m} W_{\text{device}} = 6.35 \frac{\text{kg}}{\text{s}} \times 443.6 \frac{\text{J}}{\text{kg}} = 2816.6 \frac{\text{J}}{\text{s}} \times \frac{1 \text{ W}}{\text{Js}^{-1}} = 2816.6 \text{ W}$$

Because of the inefficiencies of the pump, this value needs to be divided by the efficiency of the pump (here 0.80) to find the actual work required. This would be the rating of the pump. So, dividing this result by the efficiency gives a value of  $W_{\text{actual}} = 3.52 \text{ kW}$ , since  $1 \text{ kW} = 1000 \text{ W}$ . In terms of horsepower (HP), which is a common unit of power still used in the United States, we multiply this result by the conversion factor of  $1.341 \text{ HP kW}^{-1}$  and obtain  $W_{\text{actual}} = 4.72 \text{ HP}$ .

### Example 4.16

Consider the design of a power injector that rapidly injects a bolus of imaging contrast agent into a blood vessel. The diameter of the injector barrel is 2.5 cm, and this is connected to a catheter with an inside diameter of 0.98 mm and a total length of 50 cm. Calculate the pressure (PSI) inside the power injector barrel and the force (N and  $\text{lb}_f$ ) required to deliver a flow rate of the contrast agent of  $8 \text{ cm}^3 \text{ s}^{-1}$  through the catheter. The contrast agent has a viscosity of  $2.5 \text{ cP}$  and a density of  $1 \text{ g cm}^{-3}$ . The gauge pressure in the blood vessel is equal to  $8 \text{ mmHg}$  (gauge pressure\*). Assume the power injector is horizontal and at the same level as the injection site on the patient's arm. Also, you can neglect any frictional force developed between the power injector's plunger and the barrel wall that encloses the contrast agent within the power injector. In addition, the pressure losses due to fluid motion within the barrel itself are negligible in comparison to the pressure loss within the catheter and the pressure loss due to the contraction of the fluid as it enters the catheter. This means the pressure of the contrast agent fluid within the power injector barrel is constant.

### Solution

We let location (1) be the contrast agent within the barrel of the power injector, and location (2) is the plane at the catheter exit where the contrast agent leaves and enters the blood vessel. We also assume that the velocity of the contrast agent within the catheter, i.e.,  $V_2$ , is much greater than the velocity of the contrast agent in the barrel of the power injector during the injection process, i.e.,  $V_1$ . With these assumptions, the Bernoulli equation, as given by [Equation 4.81](#), simplifies to give

$$\frac{P_1}{\rho} = \frac{P_2}{\rho} + \frac{\alpha_2 V_2^2}{2} + h_{\text{friction}}$$

From [Equation 4.84](#), we can write  $h_{\text{friction}}$  as

$$h_{\text{friction}} = 4f \frac{LV_2^2}{2d} + \frac{V_2^2}{2} K_{\text{contraction}}$$

---

\* Recall that gauge pressure is that pressure relative to the local atmospheric pressure. Absolute pressure is gauge pressure plus local atmospheric pressure.

Using [Equation 4.86](#), we can calculate the value of  $K_{\text{contraction}}$ . Since the diameter of the power injector barrel is much larger than the diameter of the catheter, we have that  $K_{\text{contraction}} = 0.45$ . The velocity of the contrast agent in the catheter tube ( $V_2$ ) is

$$V_2 = 8 \frac{\text{cm}^3}{\text{s}} \times \frac{4}{\pi(0.098 \text{ cm})^2} = 1060.6 \frac{\text{cm}}{\text{s}}$$

With this value of  $V_2$ , we can calculate the Reynolds number as

$$Re = \frac{\rho d V_2}{\mu} = \frac{1 \frac{\text{g}}{\text{cm}^3} \times 0.098 \text{ cm} \times 1060.6 \frac{\text{cm}}{\text{s}}}{2.5 \text{ cP} \times \frac{0.01 \text{ g}}{\text{cm s cP}}} = 4157.5$$

The flow in the catheter is therefore turbulent since  $Re > 2300$ . Using [Equation 4.85](#), we calculate the friction factor and obtain  $f = 0.0099$ . Next, we can calculate the value of  $h_{\text{friction}}$ :

$$\begin{aligned} h_{\text{friction}} &= 4f \frac{LV_2^2}{2d} + \frac{V_2^2}{2} K_{\text{contraction}} \\ &= \left[ 2 \times 0.0099 \times \frac{50 \text{ cm}}{0.098 \text{ cm}} + 0.5(0.45) \right] \left[ 1060.6 \frac{\text{cm}}{\text{s}} \right]^2 = 1.162 \times 10^7 \frac{\text{cm}^2}{\text{s}^2} \end{aligned}$$

The pressure in the vein ( $P_2$ ) is given as 8 mmHg and this is equal to 1066.6 Pa. We can then use the Bernoulli equation to calculate the pressure within the power injector, i.e.,  $P_1$  as

$$\begin{aligned} P_1 &= P_2 + \frac{\rho V_2^2}{2} + \rho h_{\text{friction}} = 1066.6 \text{ Pa} + \frac{1 \frac{\text{g}}{\text{cm}^3} \times \left( 1060.6 \frac{\text{cm}}{\text{s}} \right)^2}{2} + 1 \frac{\text{g}}{\text{cm}^3} \times 1.162 \times 10^7 \frac{\text{cm}^2}{\text{s}^2} \\ &= 1066.6 \text{ Pa} + (5.624 \times 10^5 + 1.162 \times 10^7) \frac{\text{g}}{\text{cm s}^2} \times \frac{100 \text{ cm}}{\text{m}} \times \frac{1 \text{ kg}}{1000 \text{ g}} \times \frac{1 \text{ Pa}}{\frac{\text{kg}}{\text{m s}^2}} \end{aligned}$$

$$P_1 = 1.22 \times 10^6 \text{ Pa} = 12.03 \text{ atm} = 176.9 \text{ PSI}$$

Now we can calculate the force needed to push the plunger

$$F = P_1 \times A_{\text{plunger}} = 1.22 \times 10^6 \text{ Pa} \times \frac{\text{m}^2}{\text{Pa}} \times \pi \frac{(2.5 \text{ cm})^2}{4} \times \frac{1 \text{ m}^2}{(100 \text{ cm})^2} = 598.9 \text{ N} = 134.6 \text{ lb}_f$$

The next example illustrates a pseudo-steady-state application\* of the Bernoulli equation to estimate the draining time of an IV bag.

\* [Problem 4.7](#) at the end of this chapter discusses an unsteady-state solution.

### Example 4.17

The simplest patient infusion system is that of gravity flow from an intravenous (IV) bag. A 500 mL IV bag containing an aqueous solution is connected to a vein in the forearm of a patient. Venous pressure in the forearm is about 8 mmHg. The IV bag is placed on a stand such that the entrance to the tube leaving the IV bag is exactly 1 m above the vein into which the IV fluid enters. The length of the IV bag is 30 cm. The IV fluid is fed through a tube with an internal diameter of 0.953 mm and the total length of the tube is 2 m. Calculate the flow rate of the IV fluid. Also estimate the time needed to empty the bag.

#### Solution

We apply the Bernoulli equation from the surface of the fluid in the IV bag (“1”) to the entrance to the vein (“2”). We expect the flow of the fluid through the bag and the tube to be laminar and therefore neglect the contraction at the entry to the feed tube and the expansion at the vein. The pressure at the surface of the fluid in the bag will be atmospheric ( $P_1 = 760$  mmHg absolute), since the bag collapses as the fluid leaves the bag. The venous pressure, or  $P_2$ , is 8 mmHg gauge or 768 mmHg absolute. Because the fluid takes some length of time to leave the bag, we neglect the velocity of the surface of the fluid in the bag in comparison to the fluid velocity at the exit of the tube. Therefore, we assume  $V_1 = 0$  and  $V_2 \gg V_1$ . We also set the reference elevation as the entrance to the patient’s arm; hence  $Z_2 = 0$ . Therefore,  $Z_1$  is equal to the elevation of the bag relative to the position where the fluid enters the patient’s arm. This would equal 1 m plus the 30 cm length of the bag. Since there are no work devices in the system,  $W_{\text{device}} = 0$ . We can now write the Bernoulli equation for this particular problem as

$$\frac{P_1}{\rho} + gZ_1 = \frac{P_2}{\rho} + V_2^2 + \left(4f \frac{L}{D}\right) \frac{V_2^2}{2}$$

Recall that the friction factor for laminar flow in a cylindrical tube is equal to  $16/Re$ . We can substitute this relationship into the above equation to obtain the following quadratic equation that can be solved for the exiting velocity,  $V_2$ :

$$V_2^2 + \left( \frac{32 \mu L}{\rho D^2} \right) V_2 - \left[ gZ_1 + \frac{1}{\rho} (P_1 - P_2) \right] = 0$$

This equation may now be solved for the exit velocity recognizing that this quantity must be positive:

$$V_2 = \frac{-\left( \frac{32 \mu L}{\rho D^2} \right) + \sqrt{\left( \frac{32 \mu L}{\rho D^2} \right)^2 + 4 \left[ gZ_1 + \frac{1}{\rho} (P_1 - P_2) \right]}}{2}$$

Assuming the IV fluid has the same properties as water, and substituting the appropriate values for the parameters in this equation, the exit velocity is calculated as shown here. Note that  $P_1 - P_2$  equals  $-8 \text{ mmHg}$ , which is equal to  $-0.0105 \text{ atm}$  or  $-1066.58 \text{ kg m}^{-1} \text{ s}^{-2}$ :

$$V_2 =$$

$$\frac{-\left( \frac{32 \times 0.001 \frac{\text{kg ms}}{\text{s}^2 \text{m}^2} \times 2.0 \text{ m}}{1000 \frac{\text{kg}}{\text{m}^3} \times 0.000953^2 \text{ m}^2} \right) + \left[ \left( \frac{32 \times 0.001 \frac{\text{kg ms}}{\text{s}^2 \text{m}^2} \times 2.0 \text{ m}}{1000 \frac{\text{kg}}{\text{m}^3} \times 0.000953^2 \text{ m}^2} \right)^2 + 4 \left( 9.8 \frac{\text{m}}{\text{s}^2} \times 1.3 \text{ m} - \frac{1066.58 \frac{\text{kg}}{\text{ms}^2}}{1000 \frac{\text{kg}}{\text{m}^3}} \right) \right]^{1/2}}{2}$$

$$V_2 = 0.1652 \frac{\text{m}}{\text{s}} \times \frac{100 \text{ cm}}{\text{m}} \times \frac{60 \text{ s}}{\text{min}} = 991.49 \frac{\text{cm}}{\text{min}}$$

$$Q = 991.49 \frac{\text{cm}}{\text{min}} \times \frac{\pi}{4} (0.0953 \text{ cm})^2 \times \frac{\text{mL}}{\text{cm}^3} = 7.072 \frac{\text{mL}}{\text{min}}$$

The time to empty the 500 mL bag based on this fluid flow rate of  $7.072 \text{ mL min}^{-1}$  is then given by

$$t_{\text{empty}} \approx \frac{V_{\text{bag}}}{Q} = \frac{500 \text{ mL}}{7.072 \frac{\text{mL}}{\text{min}}} = 70.7 \text{ min}$$

With the exit velocity of the fluid now estimated, we need to check the Reynolds number to see if our assumption of laminar flow is valid:

$$Re = \frac{\rho d V_2}{\mu} = \frac{1000 \frac{\text{kg}}{\text{m}^3} \times 0.000953 \text{ m} \times 0.1652 \frac{\text{m}}{\text{s}}}{0.001 \frac{\text{kg}}{\text{ms}}} = 157$$

Since the  $Re < 2300$ , our assumption of laminar flow is correct.

## 4.11 Capillary rise and capillary action

Numerous processes depend on capillary action, i.e., the ability of liquids to penetrate freely into small pores, cracks, and openings. Capillary action is responsible for transporting water to the uppermost parts of tall trees and has a variety of applications in the fields of printing, textiles, agriculture, cleaning and sanitation products, and medical devices.

### 4.11.1 Equilibrium capillary rise

Consider the situation shown in [Figure 4.13](#). A small capillary tube is placed within a liquid. The liquid is drawn into the capillary as a result of the surface forces acting on the liquid wetting the inside surfaces of the capillary tube. These surface forces cause a curvature, called a *meniscus*, in the liquid surface as shown at position 3 in [Figure 4.13](#), which, according to the *Laplace-Young equation*

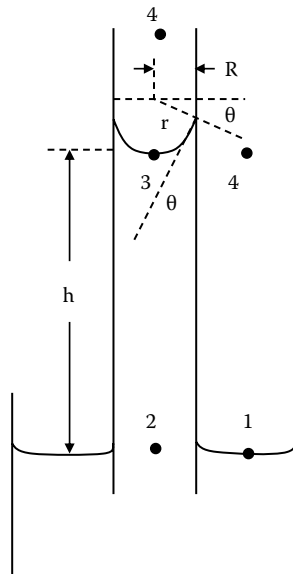


Figure 4.13 Capillary rise of a liquid in a small diameter tube of radius  $R$ .

(i.e., [Equation 2.185](#)), lowers the pressure there relative to that outside of the capillary tube. This creates a suction that draws the fluid into the capillary tube. The liquid continues to rise up in the capillary until the forces tending to draw up the liquid are balanced by the downward force of gravity acting on the fluid.

The angle ( $\theta$ ) at the meniscus between the liquid surface and the wall of the capillary is called the *contact angle*. The radius of curvature of the meniscus ( $r$ ) is related to the radius of the capillary tube ( $R$ ) and the contact angle by the following equation:

$$r = \frac{R}{\cos \theta} \quad (4.88)$$

The equilibrium capillary rise ( $h$ ) can be found from an analysis of the pressures at points 1, 2, 3, and 4, shown in [Figure 4.13](#). From the Laplace-Young equation that we developed in [Chapter 2](#) (i.e., [Equation 2.185](#)), we can write at the meniscus interface that

$$P_4 - P_3 = \frac{2\gamma}{r} \quad (4.89)$$

The pressure at point 2 is greater than the pressure at point 3 by an amount equal to  $\rho_L gh$  and the pressure at point 1 is greater than the pressure at point 4 by  $\rho_V gh$ ; hence we can write that  $P_1 = P_4 + \rho_V gh$ ,  $P_2 = P_3 + \rho_L gh$ . We also have the requirement that at equilibrium,  $P_1 = P_2$ . Therefore,  $P_4 - P_3 = (\rho_L - \rho_V)gh$ . Using this result, [Equation 4.89](#) can be solved for the capillary rise as shown in the following equation, recognizing that  $\rho_L \gg \rho_V$ :

$$h = \frac{2\gamma \cos \theta}{\rho_L R g} \quad (4.90)$$

Note that this equation also provides a simple means to determine the surface tension ( $\gamma$ ) of a liquid by measuring its capillary rise.

**Example 4.18**

Calculate the capillary rise for water in a tube with a diameter of 1 mm. Assume that  $\cos \theta \approx 1$  and that the surface tension of water is  $72 \text{ mN m}^{-1}$ .

**Solution**

Using [Equation 4.90](#), we can calculate the capillary rise:

$$h = \frac{2 \times 72 \times 10^{-3} \text{ Nm}^{-1} \times 1}{0.0005 \text{ m} \times 1000 \text{ kgm}^{-3} \times 9.8 \text{ ms}^{-2}} = 0.0294 \text{ m} = 29.4 \text{ mm} = 1.16 \text{ in.}$$

#### 4.11.2 Dynamics of capillary action

Suppose it is desired to estimate the rate at which the fluid enters the capillary, i.e., find how the capillary flow rate,  $Q$ , and the rise height,  $h$ , depend on time. For the situation shown in [Figure 4.13](#), the liquid is drawn into the capillary by forces arising from the surface tension, and this *capillary force* is retarded by the *inertial force* due to the mass of the rising fluid, the *viscous force*, and the *gravitational force* acting on the fluid. In a general sense, this is a very difficult problem; however, an approximate solution can be obtained if we assume that the flow in the capillary tube is laminar ( $Re < 2300$ ) and that the velocity profile maintains the same parabolic shape (i.e., [Equation 4.7](#)) as the liquid is drawn into the capillary tube.

The capillary force draws fluid into the tube as a result of the suction pressure developed between positions 4 and 3 of [Figure 4.13](#). This is given by the following expression, where we have also made use of [Equations 4.88](#) and [4.89](#):

$$F_{\text{capillary force}} = \pi R^2 (P_4 - P_3) = \pi R^2 \frac{2\gamma}{r} = 2\pi\gamma R \cos\theta \quad (4.91)$$

The gravitational force acts on the mass of fluid ( $\rho_L \pi R^2 h(t)$ ) within the tube at time  $t$ . This is given by the following equation where  $\rho_L$  is the density of the fluid:

$$F_{\text{gravitational force}} = \rho_L g \pi R^2 h(t) \quad (4.92)$$

The viscous force arises as a result of the flow of the fluid as it is drawn into the capillary tube by the capillary force. It is assumed that the flow is laminar and that the Hagen-Poiseuille law ([Equation 4.10](#)) can be used to describe this unsteady flow. The driving force for this flow of fluid into the capillary tube is the pressure drop between points 2 and 3 as shown in [Figure 4.13](#). Since the fluid is incompressible, the average velocity of the fluid (i.e.,  $V$ ) is the same as the observed meniscus velocity, which is  $dh(t)/dt$ . With these assumptions, the volumetric flow rate of the fluid at time  $t$  is given by

$$Q(t) = \pi R^2 V(t) = \pi R^2 \frac{dh(t)}{dt} = \frac{\pi R^4 (P_2 - P_3)}{8\mu h(t)} \quad (4.93)$$

The wall shear stress (i.e.,  $\tau_w$ ) is also related to  $(P_2 - P_3)$  through [Equation 4.4](#), so we can solve this equation for  $(P_2 - P_3)$  in terms of the wall shear stress as shown here:

$$(P_2 - P_3) = \frac{2h(t)\tau_w}{R} \quad (4.94)$$

Substituting [Equation 4.94](#) into [Equation 4.93](#) and solving for  $dh(t)/dt$  gives the next result:

$$\frac{dh(t)}{dt} = \frac{2\pi Rh(t)\tau_w}{8\pi\mu h(t)} \quad (4.95)$$

The viscous force is the wall shear stress times the circumferential area, which is the numerator of the right-hand side of [Equation 4.95](#). Therefore, we obtain

$$F_{\text{viscous force}} = 8\pi\mu h(t) \frac{dh(t)}{dt} \quad (4.96)$$

The inertial force is the mass of the fluid in the capillary tube multiplied by its acceleration. This is given by Newton's second law:

$$F_{\text{inertial force}} = \lim_{t \rightarrow 0} \frac{mV|_{t+\Delta t} - mV|_t}{\Delta t} = \frac{d(mV)}{dt} = \frac{d}{dt} \left( m \frac{dh(t)}{dt} \right) = \rho_L \pi R^2 \frac{d}{dt} \left( h(t) \frac{dh(t)}{dt} \right) \quad (4.97)$$

The inertial force is then equal to the sum of all the forces acting on the fluid as it rises in the tube through capillary action. The capillary force draws the fluid into the capillary tube and the viscous and gravitational forces work in opposition. Using the expressions developed earlier, we can then write that

$$\rho_L \pi R^2 \frac{d}{dt} \left( h(t) \frac{dh(t)}{dt} \right) = 2\gamma R \cos \theta - 8\pi\mu h(t) \frac{dh(t)}{dt} - \rho_L g \pi R^2 h(t) \quad (4.98)$$

Next, we rearrange [Equation 4.98](#) and obtain what is known as the *Bosanquet equation* (Zhmud et al., 2000; Kornev and Neimark, 2001):

$$\frac{d}{dt} \left( h(t) \frac{dh(t)}{dt} \right) + \left( \frac{8\mu}{\rho_L R^2} \right) h(t) \frac{dh(t)}{dt} = \frac{2\gamma \cos \theta}{\rho_L R} - gh(t) \quad (4.99)$$

[Equation 4.99](#) can then be solved for the rise of the fluid in the capillary tube as a function of time, provided suitable initial conditions can be defined. The initial conditions can be found by considering a solution to [Equation 4.99](#) that is valid for short contact times when penetration of the fluid just begins. In this case, only the inertial and capillary forces are dominant and [Equation 4.99](#) becomes

$$\frac{d}{dt} \left( h(t) \frac{dh(t)}{dt} \right) = \frac{2\gamma \cos \theta}{\rho_L R} \quad (4.100)$$

Integration of [Equation 4.100](#) with the initial condition that  $h(0) = 0$  gives

$$h(t) \frac{dh(t)}{dt} = \left( \frac{2 \gamma \cos \theta}{\rho_L R} \right) t \quad (4.101)$$

The left-hand side of [Equation 4.101](#) is proportional to the fluid momentum,  $\rho_L \pi R^2 h(t) \frac{dh(t)}{dt}$ , and shows that as  $t \rightarrow 0$ , the momentum of the fluid approaches zero. Since  $h(0) = 0$ , this implies for  $t \rightarrow 0$  that there is a finite velocity during the initial fluid entry phase, which is known as the *Bosanquet velocity* ( $U_B$ ), that is defined by the following relationships:

$$\text{For } t \rightarrow 0, \quad \frac{dh(t)}{dt} \approx U_B \quad \text{or} \quad h(t) \approx U_B t \quad (4.102)$$

[Equation 4.102](#) predicts that during the initial time of fluid penetration, the capillary rise increases linearly with time. Upon substitution of the results from the previous equation into [Equation 4.101](#), we can solve for the initial fluid velocity as it enters the capillary tube due to the capillary force:

$$U_B = \left( \frac{2 \gamma \cos \theta}{\rho_L R} \right)^{1/2} \quad (4.103)$$

Hence, from [Equations 4.102](#) and [4.103](#), the initial conditions for [Equation 4.99](#) are  $h(0) = 0$  and  $dh(0)/dt = U_B$ .

At long times, the fluid in the capillary reaches a stationary level, which represents a balance between the capillary forces and the gravitational forces. At this equilibrium,  $dh(t)/dt = 0$ , and [Equation 4.99](#) simplifies to the following equation for the capillary rise, which is the same as [Equation 4.90](#) that was found earlier:

$$h_{\text{equilibrium}} = \frac{2 \gamma \cos \theta}{\rho_L R g} \quad (4.104)$$

For intermediate times, the first term representing the fluid inertia in [Equation 4.99](#) can be neglected and we then obtain the *Lucas-Washburn equation*. This equation describes the rise of the fluid after the initial entry of the fluid into the tube, since the fluid acceleration is decreasing and the inertial force is much smaller for these times than the viscous and gravitational forces:

$$\left( \frac{8\mu}{\rho_L R^2} \right) h(t) \frac{dh(t)}{dt} = \frac{2 \gamma \cos \theta}{\rho_L R} - gh(t) \quad (4.105)$$

If the capillary rise is not large, then the gravitational force can also be neglected, and [Equation 4.105](#) can be integrated to give the following result for the capillary rise as a function of time:

$$h(t) = \sqrt{\frac{R \gamma \cos \theta t}{2 \mu}} \quad (4.106)$$

This equation predicts that the capillary rise is directly proportional to  $\sqrt{t}$ . Also, since  $V(t) = \frac{dh(t)}{dt}$  and  $Q(t) = \pi R^2 V(t)$ , we obtain the following equations for the average velocity and the volumetric flow rate after differentiating [Equation 4.106](#) with respect to  $t$ :

$$V(t) = \sqrt{\frac{\gamma R \cos \theta}{8 \mu t}} \quad \text{and} \quad Q(t) = \pi R^2 \sqrt{\frac{\gamma R \cos \theta}{8 \mu t}} \quad (4.107)$$

[Equation 4.107](#) predicts that for long times,  $V$  and  $Q$  decrease in proportion to  $1/\sqrt{t}$ . Notice also that [Equation 4.107](#) at  $t = 0$  gives the result that  $V$  and  $Q$  are infinite. This is a result of the neglect of the inertial forces when the fluid is first being drawn into the capillary tube.

### Example 4.19

Estimate the time for water at 25°C to reach a height of 15 mm in a capillary tube that has a diameter of 1 mm. Assume that  $\cos \theta \approx 1$  and that the surface tension of water is 72 mN m<sup>-1</sup>.

#### Solution

Using [Equation 4.106](#), we can solve for the time for the fluid to reach a particular height:

$$t = \frac{2\mu h^2}{R\gamma \cos \theta} = \frac{2 \times 0.001 \text{ Nsm}^{-2} \times 0.015^2 \text{ m}^2}{0.0005 \text{ m} \times 72 \times 10^{-3} \text{ Nm}^{-1} \times 1} = 0.0125 \text{ s} = 12.5 \text{ ms}$$

## Problems

- 4.1 Derive [Equations 4.18](#) and [4.27](#).
- 4.2 Derive [Equation 4.30](#).
- 4.3 Derive [Equations 4.40](#) and [4.41](#).
- 4.4 Derive [Equation 4.64](#) and then [Equation 4.75](#).
- 4.5 Derive [Equation 4.66](#).
- 4.6 Starting with [Equations 4.51](#) and [4.52](#), work the steps to obtain [Equation 4.59](#).
- 4.7 In [Example 4.17](#), we obtained an estimate of the time needed to drain the IV bag. However, the IV bag has a length of 30 cm, and as the fluid drains from the bag, the potential energy ( $Z_1$ ) of the remaining fluid that drives the flow will change with time. Therefore, to obtain a better estimate of the time to drain the bag, we also need to include how  $Z_1$  changes with time. This can be obtained by combining the expression for the exit velocity ( $V_2$ ) derived in [Example 4.17](#) with an unsteady mass balance on the fluid in the bag itself. Letting  $M(t)$  denote the mass of IV fluid remaining in the bag at any time  $t$ , we can write the IV bag mass balance as follows:

$$\frac{dM(t)}{dt} = \rho_L S_{\text{bag}} \frac{d(Z_1(t) - H)}{dt} = -\rho_L \pi \frac{d_{\text{tube}}^2}{4} V_2$$

In this equation,  $H$  represents the height of the catheter tube leaving the bottom of the bag relative to where this tube then enters the patient's arm. For this problem,  $H$  is equal to 1 m and  $Z_1 - H$  is then the depth of the remaining fluid in the bag.  $S_{\text{bag}}$  is the cross-sectional area

of the IV bag, and  $d_{\text{tube}}$  is the diameter of the tube. Use this equation, and the expression from [Example 4.17](#) for  $V_2$  to obtain the time to just drain the bag. How does this time compare to the pseudo-steady-state estimate of drain time obtained in [Example 4.17](#)?

- 4.8** Derive [Equation 4.10](#). Start with [Equation 4.18](#) and the assumption of a Newtonian fluid. Also show that [Equation 4.10](#) can be obtained by integrating  $v_z(r)$  in [Equation 4.7](#) using [Equation 4.16](#).
- 4.9** The cardiac output in a human is about  $6 \text{ L min}^{-1}$ . Blood enters the right side of the heart at a pressure of about  $0 \text{ mmHg}$  gauge and flows via the pulmonary arteries to the lungs at a mean pressure of  $11 \text{ mmHg}$  gauge. Blood returns to the left side of the heart through the pulmonary veins at a mean pressure of  $8 \text{ mmHg}$  gauge. The blood is then ejected from the heart through the aorta at a mean pressure of  $90 \text{ mmHg}$  gauge. Use the Bernoulli equation to obtain an estimate of the total work performed by the heart. Carefully state any assumptions and express your answer in watts.
- 4.10** Use the Bernoulli equation to describe the expected velocity and pressure changes upstream, within, and downstream of an arterial stenosis. A stenosis is a partial blockage or narrowing of an artery by formation of plaque (atherosclerosis).
- 4.11** Blood is flowing through a bundle of hollow fiber tubes that are each  $50 \mu\text{m}$  in diameter. There are 10,000 tubes in the bundle. The hollow fiber tube length is  $12 \text{ cm}$  and the pressure drop across each tube is found to be  $250 \text{ mmHg}$ . The hematocrit of the blood is  $0.40$ . Estimate the blood flow rate for these conditions in each tube.
- 4.12** Blood enters a hollow fiber unit that is used as an artificial kidney, i.e., for hemodialysis. The unit consists of 10,000 hollow fibers arranged in a shell and tube configuration. Blood flows from an artery in the patient's arm through a catheter tube and is uniformly distributed to the fibers via an arterial head space region at the entrance of the unit. The blood then leaves each fiber through the venous head space region of the unit and is returned to a vein in the patient's arm. Each hollow fiber has an inside diameter of  $220 \mu\text{m}$  and a length of  $25 \text{ cm}$ . Assuming the maximum available pressure drop across the hollow fiber unit is  $90 \text{ mmHg}$ , estimate the total flow rate of blood through the hollow fiber unit.
- 4.13** You are designing a hollow fiber unit. The fiber diameter is  $800 \mu\text{m}$  and their length is  $30 \text{ cm}$ . You want a blood flow rate of  $8 \text{ mL min}^{-1}$  for each fiber. What should be the pressure drop in  $\text{mmHg}$  across each fiber length to achieve this flow rate?
- 4.14** Using the data shown in [Figure 4.5](#), find the best values of  $s$  and  $\tau_y$  in the Casson equation that fit these data. Recall that the shear stress can be found from the data shown in [Figure 4.5](#) from the following relationship,  $\tau = \mu_{\text{apparent}} \dot{\gamma}$ . Also, from the Casson equation, note that a plot of  $\tau^{1/2}$  versus  $\dot{\gamma}^{1/2}$  should be linear with a slope equal to  $s$  and an intercept of  $\tau_y^{1/2}$ . Express the units of  $s$  as  $(\text{dynes s cm}^{-2})^{1/2}$  and  $\tau_y$  in  $(\text{dynes cm}^{-2})$ .
- 4.15** The following values were obtained for the apparent viscosity of blood ( $H = 40\%$ ) in tubes of various diameters. Estimate the thickness of the plasma layer ( $\delta$ ) in microns and the core viscosity in  $\text{cP}$  from these data. The viscosity of the plasma is  $1.09 \text{ cP}$ .

Tube Radius, $R, \mu\text{m}$	Apparent Viscosity, $\text{cP}$
20	1.68
40	2.25
60	2.49
100	2.88
300	3.00

- 4.16** A bioartificial liver has a plasma flow of  $1000 \text{ mL min}^{-1}$  through a hollow fiber unit that contains hepatocytes on the shell side. The hollow fiber unit contains 10,000 fibers. The fiber length is 75 cm and the inside diameter of the fibers is 300  $\mu\text{m}$ . What is the pressure drop across each fiber in mmHg?
- 4.17** A design for a novel aortic cannula for use on a blood pump oxygenator consists of a smooth thin-walled polyethylene tube 7 mm in diameter and 40 cm in length. For a flow rate of blood of  $5 \text{ L min}^{-1}$  through the cannula, estimate the pressure drop (mmHg) over the length of the cannula.
- 4.18** For a cell-free plasma layer of 3  $\mu\text{m}$  and a blood hematocrit of 40%, calculate the apparent viscosity for blood flowing in a 100  $\mu\text{m}$  diameter tube. Assume the plasma viscosity is 1.093 cP and the core viscosity is 3.7 cP.
- 4.19** You are designing a small implantable microfluidic pump for the continuous delivery of a drug. The pump is a two-compartment cylindrical chamber: one compartment contains the drug dissolved within a solvent, and the other compartment is the pump engine. These two compartments are separated by a movable piston that pushes on the drug compartment as the pump engine operates. At the other end of the drug compartment, there is an exit tube through which the drug solution flows. The exit tube of the pump through which the drug leaves the pump has an internal diameter of 10  $\mu\text{m}$  and a total length of 15 cm. What gauge pressure is needed in mmHg within the drug compartment to maintain a flow rate of the drug solution of  $350 \text{ }\mu\text{g day}^{-1}$ ? You may assume that the drug solution has a density of  $1 \text{ g cm}^{-3}$  and a viscosity of 3 cP.
- 4.20** You are part of a team developing an osmotic pump for the delivery of a drug. An osmotic pump has two compartments; one compartment, the osmotic engine, contains an osmotic agent that is retained by a membrane and imbibes water when placed within the body. This compartment also has a piston that expands against another compartment containing the drug solution as water is imbibed from the surroundings. The movement of the piston then forces the drug solution out into the body. A question has been raised as to what would be the maximum pressure within the device if after implantation the exit tube that delivers the drug becomes blocked? Assume the interstitial fluid pressure is -3 mmHg and its osmotic pressure is 8 mmHg. If the concentration of the osmotic agent is 0.05 OsM, what would be the maximum hydrodynamic pressure within the device assuming the delivery tube becomes blocked?
- 4.21** A viscometer has been used to measure the viscosity of a fluid at  $20^\circ\text{C}$ . The data of the shear stress versus the shear rate when plotted on a log-log graph is linear. Is this fluid Newtonian? Explain your answer.
- 4.22** Blood flows through a bundle of hollow fibers at a total flow rate of  $250 \text{ mL min}^{-1}$ . There are a total of 7500 fibers. The diameter of each fiber is 75  $\mu\text{m}$  and the length of a fiber is 15 cm. What is the pressure drop across a fiber in mmHg?
- 4.23** Commercially available spermicidal or contraceptive gels have been developed for the purpose of preventing sperm transport and thus blocking fertilization (Owen et al., 2000). Current interest has also led to the possible use of contraceptive gels as a means to reduce the spread of sexually transmitted diseases such as AIDS, and has led to interest in developing formulations of these gels for both prophylaxis and contraception. The physical properties of these gels must be such that, when applied, they spread to coat the vaginal epithelia, and then stay in place long enough to provide contraception, as well as adequate protection from disease causing agents such as bacteria and viruses. This is accomplished by gel formulations that

deliver topically bioactive compounds, such as microbiocides, and also by the physical barrier to infection provided by the coating layer. The spreading and retention of intravaginal contraceptive formulations are fundamental to their efficacy and these performance characteristics are governed in part by their rheological properties.

In vivo, these contraceptive gels will experience a wide range of shear rates as a result of movements of the vaginal epithelial surfaces, gravity, capillary flow, and sex. It is estimated that these shear rates may range from as low as 0.1/s to as high as 100/s during sex. The polymeric nature of these gels suggests that they will exhibit non-Newtonian rheological behavior.

A popular model for describing the rheological behavior of non-Newtonian gels is that of the two-parameter power law model. This model is shown by the following equations for flow in a cylindrical tube:

$$\tau_{rz} = m\dot{\gamma}^n = -m\dot{\gamma}^{n-1} \frac{dv_z}{dr} = -\mu_{\text{apparent}} \frac{dv_z}{dr} = \mu_{\text{apparent}} \dot{\gamma}$$

$$\mu_{\text{apparent}} = m\dot{\gamma}^{n-1}$$

In this equation,  $m$  and  $n$  are constants characterizing the fluid, and  $\dot{\gamma}$  is the shear rate equal to  $-\frac{dv_z}{dr}$ . Using this equation, derive an expression for the axial velocity profile,  $v_z(r)$ , and the mass flow rate ( $\dot{m} = \rho_L Q$ ) of a fluid described by the power law model.

The following table shows data obtained from a rheometer for the commercially available gel called *Conceptrol*.

Apparent Viscosity of Conceptrol versus Shear Rate

Shear Rate, s <sup>-1</sup>	Viscosity, Pa s
0.01	6000
0.05	2000
0.1	800
0.5	400
1	100
5	80
10	40
50	15
100	5
500	0.80
1000	0.2

Source: Owen, D.H. et al., *Contraception*, 62, 321, 2000.

Perform a regression analysis of the data in this table and find the power law parameters  $m$  and  $n$ . Compare your model predictions to the data shown in this table. Carefully state the units these parameters have.

- 4.24** Bush et al. (1997) studied the flow of urine in an anatomical model of the human female urethra as shown in [Figure 4.14](#).

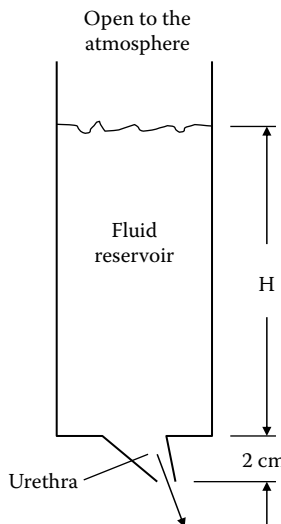


Figure 4.14 An in vitro fluid flow model of the human urethra. (From Bush, M.B. et al., *J. Biomech.*, 30, 967, 1997.)

They obtained the following data shown in the table from their experimental model.

Flow Rate, $\text{cm}^3 \text{s}^{-1}$	Pressure Difference, $\Delta P$ , $\text{cm of H}_2\text{O}$
5	2.0
8	4.5
10	8.0
13	14.0
15	21.0
17	28.0
20	38.0
23	52.0
25	60.0

The pressure difference represents the reservoir head ( $H$ ) shown in Figure 4.14 plus the additional 2 cm from the bottom of the reservoir to the exit of the urethra. Use the Bernoulli equation (Equation 4.81) to predict the pressure difference for each of the flow rates given in this table. Show your results as a graphical comparison between the data and the model. Assume that the diameter of the urethra is 3.25 mm and that its length is 4 cm. Determine whether the flow is laminar or turbulent. If the model does not fit the data, what parameters in the model can you change to improve the fit, e.g., what is the effect of the average urethral diameter?

- 4.25** Consider the steady laminar flow of a Newtonian fluid in the thin channel formed between two large parallel and horizontal plates of length  $L$  in the flow direction and width  $W$ . The plates

are separated by a distance of  $2H$  and  $H \ll L$  and  $W$ . Show that the velocity profile,  $v_z(y)$ , and the volumetric flow rate,  $Q$ , are given by the following expressions:

$$v_z(y) = \frac{(P_0 - P_L)H^2}{2\mu L} \left[ 1 - \left( \frac{y}{H} \right)^2 \right]$$

$$Q = \frac{2}{3} WH^3 \frac{(P_0 - P_L)}{\mu L}$$

with  $P_0$  and  $P_L$  as the inlet and exit pressures, respectively.

- 4.26** Using the results from [Problem 4.25](#), show that the following expression approximates the penetration of liquid,  $L(t)$ , by capillary action into a slit channel used in a diagnostic device:

$$L(t) = 2 \left[ \frac{H\gamma \cos \theta}{3\mu} \right]^{1/2} t^{1/2}$$

A diagnostic device makes use of a thin rectangular channel to draw in a sample of blood. Assuming the blood sample has a viscosity of 3 cP and that the plates forming the channel are separated by a distance of 1 mm, estimate the time for the sample of blood to travel a distance of 15 mm in the channel. Assume the blood has a surface tension of 0.06 N m<sup>-1</sup> and that the contact angle is 70°.

- 4.27** The following table shows data for the measured velocity profile for the laminar boundary layer flow of a fluid across a flat plate (from Schlichting, 1979). Make a plot of these data and compare to the approximate velocity profile given by [Equation 4.74](#).

$y \sqrt{\frac{V}{vx}}$	$\frac{v_x(x,y)}{V}$
0.25	0.1
0.50	0.175
1.0	0.34
1.5	0.495
2.0	0.63
2.5	0.745
3.0	0.85
3.5	0.92
4.0	0.955
5.0	0.98

- 4.28** Zhmud et al. (2000) obtained the following data for the capillary rise of dodecane in a 200 μm diameter capillary tube. Compare these results to those predicted by the Lucas-Washburn

equation, i.e., [Equation 4.106](#). The physical properties for dodecane are as follows: viscosity =  $1.7 \times 10^{-3}$  Pa s, surface tension =  $2.5 \times 10^{-2}$  N m<sup>-1</sup>, and density = 750 kg m<sup>-3</sup>. What is the value of the contact angle that gives the best fit to these data using the Lucas-Washburn equation?

Time, s	$h(t)$ , mm
0.03	2
0.06	4.3
0.1	6.1
0.13	7.9
0.16	9
0.20	10
0.23	11
0.26	12
0.30	12.8
0.33	13.5
0.36	14.2
0.40	14.8
0.42	15.5
0.46	16.1
0.50	16.3

- 4.29** In the paper by Zhmud et al. (2000), the capillary rise for diethyl ether in a 1 mm diameter capillary tube was found to be 8.6 mm at equilibrium. How does this value compare with the value predicted by [Equation 4.90](#)? The physical properties for diethyl ether are as follows: surface tension =  $1.67 \times 10^{-2}$  N m<sup>-1</sup>, density = 710 kg m<sup>-3</sup>, contact angle = 26°.
- 4.30** Prove that for laminar flow in a cylindrical tube, the kinetic energy correction factor,  $\alpha$ , in the Bernoulli equation is equal to 2.
- 4.31** Show that  $f=16/Re$  for laminar flow in a cylindrical tube.
- 4.32** A small airplane is flying at 3000 m above sea level. The density of air at this altitude is 0.83 kg m<sup>-3</sup>. A Pitot tube gives a difference between the stagnation pressure and the static pressure of 50 mmHg. Based on this information, how fast is the airplane traveling in miles per hour?
- 4.33** The viscosity of a fluid ( $\mu_{\text{test}}$ ) may be found in terms of the viscosity of another reference fluid whose viscosity is known ( $\mu_{\text{reference}}$ ) by measuring the time it takes for the fluid ( $t_{\text{test}}$ ) to drain by gravity a certain distance within a vertical tube of constant cross section, and then comparing that time to the time ( $t_{\text{reference}}$ ) for the reference fluid whose viscosity is known. Show that for either fluid the velocity of the fluid exiting the tube is related to the change in height ( $z$ ) of the fluid by the following equation:

$$\frac{dz}{dt} = -V_2$$

where  $V_2$  is the velocity of the fluid exiting the bottom of the tube. Next, apply the Bernoulli equation to the fluid in the tube from the top of the fluid surface (1) to the bottom of the tube (2).

Assuming laminar flow of the fluid with  $f = 16/Re$  and using the above equation for  $V_2$ , show that  $dz/dt$  is also given by the following equation:

$$\frac{dz}{dt} = -\frac{\rho d^2 g}{32\mu}$$

where

$d$  is the inside diameter of the tube

$g$  is the acceleration of gravity

Next, integrate this equation and show that the time for the fluid to drain a distance equal to  $\Delta z$  is given by

$$\Delta z = \frac{\rho d^2 g t}{32\mu}$$

Now, if both fluids drain the same distance, i.e.,  $\Delta z_{\text{test}} = \Delta z_{\text{reference}}$ , show that the following equation may be used to relate their viscosities in terms of their drain times and densities:

$$\frac{\mu_{\text{test}}}{\mu_{\text{reference}}} = \frac{\rho_{\text{test}} t_{\text{test}}}{\rho_{\text{reference}} t_{\text{reference}}}$$

Shown below are some data for the drain time of different concentrations of chitosan in water that were obtained by one of my former PhD students, Prasanjit Das. Pure water was used as the reference fluid with a viscosity of 0.001 Pa s or 1 cP and a density of 997 kg m<sup>-3</sup>. The time ( $t_{\text{reference}}$ ) for the water to flow by gravity for a defined distance ( $\Delta z_{\text{test}} = \Delta z_{\text{reference}}$ ) in a capillary tube was found to be 0.120 s. Calculate the viscosity (cP) of the chitosan solution for each of the concentration values given in the following table.

Chitosan Concentration, ppm	Chitosan Solution Density, kg m <sup>-3</sup>	Drain Time ( $t_{\text{test}}$ ), s
10	997	0.120
100	997	0.120
200	997	0.230
500	997	0.290
1000	998	0.480

- 4.34** The formation of a small droplet at the tip of a capillary tube can be used to determine the surface tension of a fluid. This is known as the hanging droplet method. The droplet can grow in size until the gravitational force exceeds the surface tension force that holds the droplet to the periphery of the tube, i.e.,

$$\gamma\pi D_{\text{tube}} = \frac{4}{3}\pi R^3 \rho_L g$$

where

$\gamma$  is the surface tension of the fluid

$R$  is the radius of the spherical droplet formed

Show that the surface tension is then given by the following equation:

$$\gamma = \frac{0.1667 d^3 \rho_L g}{D_{\text{tube}}}$$

where  $d$  is the diameter of the droplet that just releases itself from the tube. Shown below are some data that were obtained by my former PhD student, Prasanjit Das, on droplets formed at the tip of a 1 mm outside diameter capillary tube for different concentrations of chitosan in water. From these data, calculate the surface tension ( $\text{mN m}^{-1}$ ) of the chitosan solution for each of the concentration values given in the following table.

Chitosan Concentration, ppm	Chitosan Solution Density, $\text{kg m}^{-3}$	Droplet Diameter, mm
10	997	3.48
100	997	3.46
200	997	3.43
500	997	3.40
1000	998	3.38

- 4.35** Bazilevsky et al. (2003) measured the entry capillary flow rate of water into a 0.65 mm diameter capillary tube. The average entry flow rate of the water was found to be  $220 \text{ mm}^3 \text{ s}^{-1}$ . What is the entrance velocity of the water and how does this compare to that predicted by the Bosanquet equation? Assume the surface tension of water is  $0.071 \text{ N m}^{-1}$  and its viscosity is  $0.001 \text{ Pa s}$ . Also  $\theta = 0^\circ$ .
- 4.36** A concentrated solution of sugar dissolved in water is flowing through a capillary tube with an inside diameter of 2 mm. The capillary tube will be used to find the viscosity of this solution. The length of the capillary tube is 10 cm. The density of the solution is  $1200 \text{ kg m}^{-3}$ . For a flow rate of  $60 \text{ cm}^3 \text{ min}^{-1}$ , the pressure drop per length of the tube was found to be  $1.0 \text{ mmHg cm}^{-1}$ . What is the viscosity (Pa s) of the fluid?
- 4.37** A polymeric fluid having a viscosity of  $0.40 \text{ Pa s}$ , a density of  $800 \text{ kg m}^{-3}$ , and a surface tension of  $0.02 \text{ N m}^{-1}$  is drawn by capillary action into a glass tube of radius 0.025 cm. If the contact angle is such that the  $\cos \theta \sim 1$ , estimate the time required for the fluid to reach a height equal to 90% of its equilibrium rise. Also, find the initial flow rate of this fluid into the tube in  $\text{cm}^3 \text{ s}^{-1}$ .
- 4.38** The capillary rise,  $h(t)$ , as a function of time,  $t$ , for a biofluid was measured in a capillary tube of radius 0.3 mm. When the data was plotted as  $h(t)$  versus  $t^{1/2}$  the data was found to be linear with a slope equal to  $0.06 \text{ m s}^{-1/2}$ . If the fluid has a viscosity of  $1.2 \times 10^{-3} \text{ Pa s}$ , and the contact angle  $\sim 0^\circ$ , estimate the surface tension of the fluid in  $\text{N m}^{-1}$ .
- 4.39** A particular fluid has a shear stress of  $0.005 \text{ N m}^{-2}$  at a shear rate of  $1 \text{ s}^{-1}$  and a shear stress of  $2 \text{ N m}^{-2}$  at a shear rate of  $50 \text{ s}^{-1}$ . Present an argument as to whether this fluid is Newtonian or non-Newtonian.
- 4.40** Blood is flowing at a flow rate of  $7 \text{ L min}^{-1}$  through a tube that is 6 mm in diameter and 50 cm in length. Estimate the pressure drop of the blood over this length of tubing in mmHg.
- 4.41** The apparent viscosity of blood flowing in a  $100 \mu\text{m}$  diameter tube was found to be 2.6 cP. Assuming that the core viscosity of blood is about 3.7 cP, estimate the thickness of the marginal zone layer. Assume the plasma viscosity is 1.1 cP.

- 4.42** Blood flows through a 100  $\mu\text{m}$  diameter glass tube that is 0.1 cm in length. Estimate the volumetric flow rate of the blood in  $\text{cm}^3 \text{ h}^{-1}$  if the pressure difference over the length of the tube is 6000 Pa.
- 4.43** You are designing a hollow fiber unit with 10,000 fibers. The fiber diameter is 1000  $\mu\text{m}$  and their length is 50 cm. You want a flow rate of 100  $\text{L min}^{-1}$  for the entire unit. What should the pressure drop (mmHg) be across the unit to achieve this flow rate?
- 4.44** The broth from a continuous fermentor has a density of  $1.02 \text{ g cm}^{-3}$  and a viscosity of 1.8 cP. The broth is being pumped from the fermentor into the bottom of a filtration feed tank that leads into a filtration system. The surface of the liquid contained in the filtration feed tank is 20 feet above the surface of the liquid in the fermentor. The pressure in the fermentor is maintained at 1 atm and the pressure in the feed tank is maintained at 6 atm in order to facilitate the downstream filtration process. The pipe connecting the fermentor and the feed tank is equivalent to 75 ft of pipe with an inside diameter of 3 in., where, this equivalent length includes the additional resistance of any valves and pipe fittings. The desired flow rate of the fermentation broth as it is pumped to the feed tank is  $100 \text{ gal min}^{-1}$ . What power (kilowatts) must be delivered by the pump to the fluid in order to effect this transfer of broth from the fermentor to the feed tank?
- 4.45** Water at  $20^\circ\text{C}$  is pumped through 3000 cm of pipe with an internal diameter of 7.8 cm into an overhead storage tank that vents to the surroundings. The total elevation change is 1000 cm. The valves and other pipe fittings are equivalent to an additional pipe length equal to 15 pipe diameters. What outlet pressure in atmospheres of the pump is needed to move the water at a flow rate of  $70 \text{ L min}^{-1}$ ? At  $20^\circ\text{C}$  the viscosity of water is 1.002 cP and the density is  $0.9982 \text{ g cm}^{-3}$ .
- 4.46** The pressure drop of a nutrient fluid flowing through the hollow fibers of a bioreactor cannot exceed 50 mmHg. There are 10,000 fibers in the bioreactor, and the total flow rate of the nutrient media to the bioreactor is  $50 \text{ L min}^{-1}$ . Estimate the allowable length of these fibers assuming the hollow fiber radius is 0.1 cm and the viscosity of the nutrient fluid is 0.05 Pa s.
- 4.47** You are studying in the laboratory the laminar boundary layer flow of a fluid across a very thin flat plate. The flat plate is suspended vertically from a spring in the range where Hooke's law applies, i.e.,  $F = k \Delta\lambda$ , where  $\Delta\lambda$  is the amount of spring extension from the unloaded position of the spring and  $k$  is the spring constant. Under conditions of no air flow, the extension of the spring due to the weight of the flat plate is  $\Delta\lambda_{\text{plate}} = 5 \text{ cm}$ . When there is an upward flow of air, the resulting drag opposes the weight of the flat plate. Find the air flow in  $\text{m s}^{-1}$  for which the spring extension is zero, i.e.,  $\Delta\lambda = 0$ . Use the following data to find your answer:
- Mass of the plate,  $M = 0.001 \text{ kg}$
- Plate length,  $L = 0.2 \text{ m}$
- Plate width,  $W = 0.1 \text{ m}$
- Air speed,  $V = \text{find this}$
- Air density,  $\rho = 1.2 \text{ kg m}^{-3}$
- Air kinematic viscosity,  $\nu = 1.51 \times 10^{-5} \text{ m}^2 \text{ s}^{-1}$
- 4.48** Estimate the maximum power that is generated in megawatts from a wind turbine whose blades are 300 ft in diameter. Assume the wind speed averages 20 miles  $\text{h}^{-1}$  and that the density of air is  $1.2 \text{ kg m}^{-3}$ . Carefully state your assumptions.
- 4.49** Estimate the pressure drop in mmHg of blood flowing in the annulus formed by two concentric cylindrical tubes. The inner tube has an outer diameter of 8 mm and the outer tube has an

inner diameter of 15 mm. The blood flow rate is  $15,000 \text{ mL min}^{-1}$ , and the overall length of the tube section being considered is 40 cm.

- 4.50 For the flow of a fluid through a small tube that is 0.9 mm in diameter, the flow rate was  $0.3 \text{ cm}^3 \text{ s}^{-1}$  and the pressure drop over the length of the 50 cm tube was found to be 50 kPa. Estimate the viscosity of this fluid in Pa s.
- 4.51 The rheological properties of a new personal lubricant were studied in a viscometer. A linear regression of these data was performed after first taking the natural log of the apparent viscosity (cP) and the natural log of the shear rate (1/sec). The equation for the regression line is:  $\ln \mu_{\text{apparent}} = 11.02 - 0.75 \ln \dot{\gamma}$ . What are the parameters in an appropriate viscosity model? Be sure to state what the viscosity model is and any units on your parameters. Is this lubricant's behavior Newtonian or Non-Newtonian?
- 4.52 The equilibrium rise height of a rather viscous fluid in a small capillary tube of diameter equal to 0.1 mm was found to be 65 mm. The contact angle was also measured to be  $75^\circ$ . Estimate the surface tension of this fluid if its viscosity is  $\mu = 0.75 \text{ Pa s}$  and  $\rho_L = 800 \text{ kg m}^{-3}$ .
- 4.53 Water at  $70^\circ\text{F}$  enters a pump through a 3 in. schedule 40 pipe at atmospheric pressure and is being pumped at a rate of  $100 \text{ gal min}^{-1}$  (1 gal =  $3.7853 \text{ L}$ ) through a pipe system made up of 500 ft of 3 in. schedule 40 steel pipe (internal diameter = 3.068 in.). The pipe circuit includes  $4^\circ$ – $90^\circ$  elbows. The total change in elevation from the pump entrance to the discharge of the water into the atmosphere is equal to 400 ft. Find the horsepower (HP) required for the pump assuming the pump efficiency is 70%. The viscosity of water under these conditions is 0.96 cP and the density of water is  $1 \text{ g cm}^{-3}$ .
- 4.54 A Newtonian fluid with a density of  $1.06 \text{ g cm}^{-3}$  is flowing through a horizontal tube with a length of 50 cm and a diameter of 6 mm at a flow rate of  $7.5 \text{ L min}^{-1}$ . The pressure drop across this length of tube was found to be 200 mmHg. Estimate the viscosity of this fluid in cP.
- 4.55 A fluid with a density of  $1.03 \text{ g cm}^{-3}$  is flowing at the rate of  $1.8 \text{ L h}^{-1}$  through a small tube that is 1.5 mm in diameter and 50 cm in length. If the viscosity of this fluid is 2.8 cP, estimate the pressure drop over the tube length in mmHg.
- 4.56 A Newtonian fluid with a density of  $1.03 \text{ g cm}^{-3}$  is flowing through a horizontal tube with a diameter of 4 mm at a flow rate of  $15 \text{ L min}^{-1}$ . The viscosity of this fluid is 1.1 cP. What pressure drop in mmHg would you expect over a 50 cm length of this tube?
- 4.57 Consider the rise of water in a capillary tube of radius equal to  $50 \mu\text{m}$ . What is the equilibrium rise height in cm of the water after one end of the tube is immersed in water? Assume the viscosity of water is  $0.001 \text{ Pa s}$ , the surface tension of the water is  $7.3 \times 10^{-2} \text{ N m}^{-1}$ , and the density of the water is  $1000 \text{ kg m}^{-3}$ . Assume  $\cos \theta = 1$ .
- 4.58 A woman decides to build a log cabin at the base of a tall mountain and is looking at the feasibility of tapping into a snow melt fed lake that is about 500 ft above her cabin for her water supply. The plan is to install a small pipeline that runs from the lake into a water storage tank that will then provide water as needed to her cabin, which is located nearby. The change in elevation from the surface of the lake to where the water would empty into the storage tank is 475 ft. The plan is to use a 1.25 in. inside diameter pipe that would have an overall length of 600 ft. Included in the piping circuit is a priming pump (which only runs to get the water flowing, sort of like a siphon) with a  $K_{\text{pump}} = 1.5$  and there are also  $8$ – $90^\circ$  elbows ( $K_{\text{elbow}} = 1.0$ ). When the water is flowing, what is the flow rate of the water in gallons per minute as it exits the pipe into the top of the storage tank? Assume that the water exiting the pipe is not submerged in the water. Also assume that the tank is vented to the atmosphere. You can also neglect the difference in barometric pressure

between the lake and the cabin. The water is at 41°F and its viscosity and density at this temperature are, respectively, 1.519 cP and 1000 kg m<sup>-3</sup>.

- 4.59** A Newtonian fluid with a density of 1.10 g cm<sup>-3</sup> and a viscosity of 1.5 cP is flowing through a horizontal tube with a diameter of 5 mm. If the pressure drop across the length of the tube cannot exceed 2000 mmHg, estimate the maximum length of the tube in cm. The flow rate of the fluid is 7 L min<sup>-1</sup>.
- 4.60** A fluid with a density of 1.03 g cm<sup>-3</sup> is flowing through a small horizontal tube that is 1.25 mm in diameter and 75 cm in length. If the viscosity of this fluid is 1.8 cP, and the pressure drop over this length of tube is 60 mmHg, estimate the flow rate of the fluid in mL h<sup>-1</sup>.
- 4.61** A droplet of a nerve agent lands on the surface of a soldier's clothing and covers an area of 2.8 cm<sup>2</sup>. The surface tension of the nerve agent is 0.028 N m<sup>-1</sup>. The material in the person's clothing is such that the weave makes tiny cylindrical openings that have a diameter of 0.5 mm. The cylindrical openings cover 45% of the clothing area. The contact angle ( $\theta$ ) of the agent and clothing material is such that the  $\cos \theta = 0.9063$ . From this information, estimate the *initial* mass flow rate of the nerve agent into the clothing material in grams per second. The density of the nerve agent is 1.04 g cm<sup>-3</sup>.
- 4.62** Blood flows through a vein that is 0.71 cm in diameter and 20 cm in length. If the blood has a viscosity of 4 cP and a density of 1.04 g cm<sup>-3</sup>, what is the flow rate of the blood in cm<sup>3</sup> s<sup>-1</sup> if the pressure drop over the length of the vein is equal to 1 mmHg?
- 4.63** The rheology of an infant gruel formula is being evaluated in a capillary viscometer. The viscometer is a glass tube that has an internal diameter of 1.25 mm and is 5 cm in length. When the flow rate of the gruel was 1 cm<sup>3</sup> min<sup>-1</sup>, the pressure drop over the length of the viscometer was found to be 137 mmHg. What is the apparent viscosity of the gruel in units of Pa s?
- 4.64** A Newtonian fluid with a density of 1.06 g cm<sup>-3</sup> is flowing through a horizontal tube with a length of 50 cm and a diameter of 6 mm at a flow rate of 7.5 L min<sup>-1</sup>. The viscosity of the fluid is equal to 2.55 cP. What is the pressure drop across this length of tube?
- 4.65** A fluid with a density of 1.03 g cm<sup>-3</sup> is flowing through a small tube that is 1.5 mm in diameter and 50 cm in length. If the viscosity of this fluid is 2.8 cP, and the pressure drop over the tube length is 42.3 mmHg, what is the flow rate of the fluid in L h<sup>-1</sup>?
- 4.66** Calculate the pressure drop in mmHg for the flow of a liquid material in a horizontal, smooth, and circular tube 1000 cm in length that has an inside diameter of 3 cm. The liquid material flows through the tube at a mass rate of 1028 g s<sup>-1</sup> and has a density of 0.935 g cm<sup>-3</sup> and a viscosity of 1.95 cP.
- 4.67** A container of a viscous liquid makes contact with an open capillary tube that is vertical. The capillary tube has a diameter of 0.1 mm. The equilibrium rise height of this fluid in the capillary was found to be 0.0765 m. How long will it take for the viscous liquid to rise within the capillary tube to a height of 0.069 m? The contact angle of the liquid with the capillary tube is 60°, the viscosity of the liquid is 1 Pa s, and its density is 0.8 g cm<sup>-3</sup>.
- 4.68** The equilibrium rise height of a rather viscous fluid in a small capillary tube of diameter equal to 0.1 mm was found to be 65 mm. The contact angle was also measured to be 75°. Estimate the surface tension of this fluid if its viscosity is  $\mu = 0.75$  Pa s and  $\rho_L = 800$  kg m<sup>-3</sup>.
- 4.69** A rapid blood bag infusion system is being designed that involves effectively squeezing the bag of blood through a tube (4.0 mm internal diameter with a total length of 2 m) into a vein in the patient's arm. The blood bag is placed within another pressurizing bag that is pressurized with air that squeezes the blood bag at constant pressure. It is desired to empty the bag of blood using this method in 10 seconds. The bag contains 500 mL of blood. What pressure

(mmHg) is needed in the pressurizing bag to make this possible? Assume the pressure in the patient's vein is 8 mmHg and that the bag of blood is 0.5 m above the point of entry of the blood into the patient's arm. The density of blood is  $1.06 \text{ g cm}^{-3}$  and its viscosity is 3 cP. Also neglect any frictional losses due to the flow of blood within the blood bag.

- 4.70** A Newtonian fluid with a viscosity of 1300 cP needs to be pumped through a tube that has an internal diameter of 1.25 mm and a length of 10 cm. If the flow rate of this fluid is  $1 \text{ cm}^3 \text{ min}^{-1}$ , what is the pressure drop (in mmHg) over the length of the tube that is needed to produce this flow?
- 4.71** Estimate the radius of a capillary tube (mm) from these measurements taken for the flow of a viscous fluid through the tube: capillary tube length = 50.02 cm, kinematic viscosity =  $4.03 \times 10^{-5} \text{ m}^2 \text{ s}^{-1}$ , fluid density ( $\rho$ ) =  $0.9552 \times 10^3 \text{ kg m}^{-3}$ , pressure drop across the tube in a horizontal position = 4.766 atm, mass flow rate through the tube of the viscous fluid =  $0.1798 \text{ kg min}^{-1}$ .
- 4.72** Calculate the pressure drop in mmHg for a fluid flowing within a smooth tube that is 0.8 cm in diameter and 20 cm in length. The fluid velocity in the tube is  $200 \text{ cm s}^{-1}$ , and the fluid has a density of  $1.04 \text{ g cm}^{-3}$  and a kinematic viscosity of  $0.04 \text{ cm}^2 \text{ s}^{-1}$ .
- 4.73** A small bubble of air in water ( $\gamma = 0.073 \text{ N m}^{-1}$ ) has a radius of 0.10 mm. Find the difference in pressure in mmHg between the inside and outside of the bubble.
- 4.74** A rectangular conduit 200 cm in length is needed to convey water at a flow rate of  $18 \text{ mL s}^{-1}$ . The conduit cross section has a height of 0.23 cm and a width of 0.45 cm. Calculate the pressure drop (mmHg) over the length of the conduit to obtain this flow rate. Assume the kinematic viscosity ( $\nu$ ) of water is  $0.01 \text{ cm}^2 \text{ s}^{-1}$  and its density is  $1 \text{ g cm}^{-3}$ .
- 4.75** Water at  $16^\circ\text{C}$  (viscosity 1.13 cP and density  $1 \text{ g cm}^{-3}$ ) is pumped from a large lake to the top of a mountain through a 6 in. steel pipe at an average velocity of  $10 \text{ ft s}^{-1}$ . The inside diameter of this schedule of pipe is 5.501 in. The pipe discharges into the atmosphere at a level 4000 ft above the level in the lake. The pipeline is 5000 ft in total length. You can neglect the pressure loss due to any valves and fittings. The overall efficiency of the pump and its motor is 70%. If electricity costs \$.11 per kWh, what will it cost to pump this water for 1 h?
- 4.76** A commercial size hollow fiber bioreactor contains 1000 tubes, and each fiber has a length of 100 cm and an inside diameter of 6 mm. A Newtonian culture fluid with a density of  $1.06 \text{ g cm}^{-3}$  is flowing into the bioreactor at a flow rate of  $125 \text{ L s}^{-1}$ , and this flow is evenly distributed into each of these fiber tubes. The viscosity of the fluid is 15 cP. Is the flow in each tube laminar or turbulent? Estimate the pressure drop in mmHg across the bioreactor.
- 4.77** The following data were obtained for the flow of a viscous fluid in a capillary tube:  $L = 50 \text{ cm}$ ,  $\mu = 5 \text{ cP}$ ,  $Q = 0.3 \text{ cm}^3 \text{ s}^{-1}$ , and  $\Delta P = 0.375 \text{ mmHg}$ . Estimate the diameter (cm) of this capillary tube from these data.
- 4.78** A capillary viscometer was used to measure the viscosity of a fluid at room temperature. At a pressure drop per unit length of  $0.28 \text{ mmHg cm}^{-1}$ , i.e.,  $\Delta P/L$ , the measured flow rate of the fluid through the capillary viscometer was found to be  $0.0125 \text{ cm}^3 \text{ s}^{-1}$ . When the value of  $\Delta P/L$  was increased to  $0.79 \text{ mmHg cm}^{-1}$ , the flow rate of the fluid was found to be  $.047 \text{ cm}^3 \text{ s}^{-1}$ . Under these conditions, is the fluid Newtonian or non-Newtonian? Be sure to justify your answer.
- 4.79** A fire suppression system (FSS) for a tall building pumps water from a river and delivers the water through a long pipe to where the water flows on top of the water already in a storage tank at the top of the building. When the pump is running, the water flows into the storage tank at  $30 \text{ L s}^{-1}$ . The water exits the pipe 30 m above the surface of the river. The pipe has an internal diameter of 10 cm. What pumping power (HP) is needed to deliver the water? The viscosity of water is 1 cP and the density of the water is  $1 \text{ g cm}^{-3}$ . Assume  $h_{\text{friction}} = 100.32 \text{ m}^2 \text{ s}^{-2}$ .

- 4.80** An absorbent material is being designed to clean up a toxic liquid material. The surface tension of the toxic material is  $0.028 \text{ N m}^{-1}$ . The absorbent material has within its structure tiny cylindrical openings that have a diameter of 0.5 mm. The cylindrical openings cover 45% of the absorbent material's surface. The contact angle ( $\theta$ ) of the toxic substance and the absorbent material is such that the  $\cos \theta = 0.9105$ . From this information estimate the initial mass flux (grams per second per  $\text{cm}^2$  of absorbent material) of the toxic material into the absorbent material. The density of the toxic substance is  $1.04 \text{ g cm}^{-3}$ .
- 4.81** A polymeric material is being extruded as a very thin ribbon of thickness 3 mm and width 25 mm. As part of the extrusion process, the material is to be treated with an antistatic agent as it leaves the extruder. This antistatic agent wicks into the porous space of the polymeric material. The radius of the pores in the polymeric material is  $5 \mu\text{m}$ . It is desired that the antistatic agent penetrate  $150 \mu\text{m}$  into the material. Estimate how long will it take for the antistatic agent to enter into the pores of the polymeric material. The antistatic agent has a viscosity of 38 cP and a surface tension of 30 milliN  $\text{m}^{-1}$ . The cosine of the contact angle, i.e.,  $\cos \theta$ , is equal to 0.84.
- 4.82** An adhesive material was studied in a viscometer. A linear regression equation based on the Casson equation was found to describe the data as  $\tau^{1/2} = 0.238\dot{\gamma}^{1/2} + 7.7$ , where  $\tau$  is the shear stress in Pa and  $\dot{\gamma}$  is the shear rate in  $\text{s}^{-1}$ . An adhesive applicator system is being designed that will dispense this adhesive material through a polymeric tube with an inside diameter of 2.3 mm and a total length of 100 cm. If the pressure drop over the length of this tube is 2000 mmHg, estimate the flow rate of the adhesive material through the tube in  $\text{cm}^3 \text{ min}^{-1}$ .
- 4.83** A drug injection system consists of a large chamber (length to diameter ratio = 10) that contains the drug solution and a small catheter tube that goes to the patient. This chamber contains a moving piston that separates the drug containing region from the region of the chamber where air is introduced to pneumatically drive the piston to induce flow of the drug solution. The air is maintained at a constant pressure during the drug injection process. The drug solution is injected into the patient at a flow rate of  $10 \text{ cm}^3 \text{ s}^{-1}$  through a catheter tube that has an inner diameter of 1 mm and a length of 15 cm. Also, the drug solution has a viscosity of 0.85 cP and a density of  $1.02 \text{ g cm}^{-3}$ . The drug is injected into the abdominal cavity of the patient where the local pressure is 0 mmHg gauge. Assume the drug chamber is horizontal and that you can neglect any frictional force developed between the piston and the walls of the chamber containing the drug solution. Also, any pressure losses due to fluid motion within the drug solution chamber are negligible in comparison to the frictional losses within the tubing that leads from the drug solution chamber and into the patient. What air pressure (mmHg) is required to achieve this flow rate of the drug solution?
- 4.84** Nutrient media is being transferred through a horizontal 2 in. diameter pipe from the feed-stock building to the fermentation building at a flow rate of  $60 \text{ gal min}^{-1}$ . Pressure gauges are installed in the pipe in each building to monitor the transfer operation. If the length of the transfer pipe between these two pressure gauges is 75 ft, what would be the expected pressure drop in mmHg? At the planned operating conditions the nutrient media has a viscosity of 0.85 cP and a density of  $1 \text{ g cm}^{-3}$ .
- 4.85** Experiments on a viscous biological fluid were done in a capillary viscometer having an internal diameter of 1.75 mm. The data for eight experiments when plotted as the volumetric flow rate,  $Q$ , versus the pressure drop over the length of the capillary tube, i.e.,  $\Delta P/L$ , showed a

linear relationship between  $Q$  and  $\Delta P/L$ . A regression line through these data with a zero intercept gave a slope of  $83.5 \text{ mL cm min}^{-1} \text{ mmHg}^{-1}$ , and the maximum flow rate for these experiments was  $Q = 50 \text{ mL min}^{-1}$ . Based on this information, estimate the viscosity ( $\mu$ ) of the solution in cP. Assume the density of this solution is about  $1 \text{ g cm}^{-3}$ .

- 4.86** The Carreau viscosity model has been shown to describe the apparent viscosity of blood (Lee et al., 2014).

$$\mu_{\text{apparent}} = \mu_{\infty} + (\mu_0 - \mu_{\infty}) \left[ 1 + (\lambda \dot{\gamma})^2 \right]^{\frac{n-1}{2}}$$

In this equation,  $\mu_{\text{apparent}}$  is the non-Newtonian apparent viscosity of the fluid,  $n$  is the power law index, and  $\lambda$  is the relaxation time.  $\mu_0$  and  $\mu_{\infty}$  are, respectively, the fluid viscosity at zero shear rate and at infinite shear rate. Using the data shown in [Figure 4.5](#), find the best values of the parameters in the Carreau viscosity model.

- 4.87** Blood flows through a  $75 \mu\text{m}$  diameter glass tube that is  $10 \text{ cm}$  in length. This particular blood has a core viscosity of  $3.3 \text{ cP}$  and a marginal zone layer thickness (or plasma layer) of  $2.4 \mu\text{m}$ , i.e.,  $\delta$ . Estimate the volumetric flow rate of the blood in  $\text{cm}^3 \text{ h}^{-1}$  if the pressure difference over the length of the tube is  $8000 \text{ Pa}$ . The plasma viscosity of this blood is  $1.2 \text{ cP}$ .
- 4.88** Using the Carreau viscosity model described in Problem 4.86, if the shear rate on a Carreau fluid is  $3 \text{ s}^{-1}$ , what is the shear stress on the fluid (Pa)? Use the following values for these parameters given by Lee et al. (2014):

$$\mu_0 = 0.056 \text{ Pa s}$$

$$\mu_{\infty} = 0.0035 \text{ Pa s}$$

$$\lambda = 3.313 \text{ s}$$

$$n = 0.3568$$

- 4.89** A fire suppression system (FSS) at a remote resort in Jasper, Alberta, is being designed to take water from a river and send it through a hose where it exits through a nozzle at a turbulent velocity of  $30 \text{ m s}^{-1}$ . The pump must be able to deliver  $2000 \text{ L min}^{-1}$  of water. The inside diameter of the hose is  $0.10 \text{ m}$  and the equivalent length of the hose, which includes the losses due to entrance and exit effects, valves, and fittings, is  $90 \text{ m}$ . Also, the FSS must be able to lift the water  $30 \text{ m}$  from the river surface to where it exits the nozzle. How much power must the pump in the FSS have to meet these conditions? The viscosity of water is  $1 \text{ cP}$  and its density is  $1 \text{ g cm}^{-3}$ .

- 4.90** Derive [Equation A](#) in [Example 4.1](#).

- 4.91** A capillary viscometer is being used to measure the viscosity of a liquid at  $20 \text{ C}$ . The capillary tube is  $0.01 \text{ cm}$  in diameter and has a length of  $100 \text{ cm}$ . When the pressure drop over the length of this capillary tube was  $2 \text{ atm}$ , the flow rate of the liquid was found to be  $1.0 \text{ cm}^3 \text{ h}^{-1}$ . What is the viscosity of the liquid in cP? The density of the liquid is  $1.025 \text{ g cm}^{-3}$ .

- 4.92** Two tanks are connected by  $300 \text{ m}$  of  $7.5 \text{ cm}$  diameter steel pipe. One of the tanks is open to the atmosphere (tank 2) and the other tank (tank 1) is maintained at an internal pressure of  $P_1$ . The diameter of each tank is quite large so that the velocities of the liquid surface in each tank is negligible. The fluid in the tanks is a polymeric fluid with a viscosity of  $100 \text{ cP}$  and a density of  $0.80 \text{ g cm}^{-3}$ . What should the pressure be in the closed tank, i.e.,  $P_1$ , relative to atmospheric pressure, i.e.,  $P_2$ , so that the flow rate of the oil from tank 1 to tank 2 is  $7 \text{ kg s}^{-1}$ . Express the pressure in units of mmHg. The surface of the liquid contained in tank 1 lies  $9 \text{ m}$  below the surface of the liquid in tank 2.



Taylor & Francis

Taylor & Francis Group

<http://taylorandfrancis.com>

# Chapter 5 Mass transfer fundamentals

## 5.1 Description of solute mass transfer

In this chapter, we will focus our discussion on the mass transfer of solutes. Our focus is on a homogeneous solution where a solvent contains the solute of interest. Solute mass transfer occurs both through bulk fluid motion, also known as *convection*, and by solute *diffusion* due to the presence of solute concentration gradients.

## 5.2 Important definitions used in solute mass transfer

In order to understand solute transport, we first need to define what we mean by the *concentration* of the solute in our solution of interest. The concentration of a solute in a solution is the amount of the solute per volume of solution. We can define the amount of the solute in terms of either its mass or by the number of moles. Hence, we have for a given solute, the *mass concentration* ( $\rho_i$ ) or the *molar concentration* ( $C_i$ ). The mass concentration for solute  $i$  is defined as the mass of solute  $i$  ( $m_i$ ) per unit volume ( $V$ ) of solution, i.e.,  $\rho_i = m_i/V$ . The molar concentration for solute  $i$  is defined as the moles of solute  $i$  ( $n_i$ ) per unit volume ( $V$ ) of solution, or  $C_i = n_i V^{-1} = \rho_i MW_i^{-1}$ , where  $MW_i$  is the solute molecular weight.

We can also define the mole fraction of species  $i$ , i.e.,  $x_i$ , as the molar concentration of  $i$ , i.e.,  $C_i$ , divided by the total molar concentration of the solution, i.e.,  $C = \sum_{i=1}^N C_i$ , where  $N$  is the number of components in the solution. Hence,  $x_i = C_i/C$ . In a similar manner, we can define the mass fraction of species  $i$  as  $\omega_i = \rho_i/\rho$ , where  $\rho$  is the mass density of the solution.

In order to solve mass transfer problems, we will need to determine the amount of solute transported by convection, i.e., as carried along by the bulk motion of the fluid, and the amount of solute transported by diffusion. We assume that the total transport rate of the solute is the sum of that due to convection and that due to diffusion. We can think of the solute transport by diffusion as being superimposed on the transport of the solute due to the bulk motion of the solution.

Now, to understand the role of convection and diffusion on the transport of the solute, it is first convenient to define the *mass average velocity* and the *molar average velocity* of the solution, both of which are defined relative to a stationary coordinate system. Also, recall that velocity is a vector and we will denote vectors with the additional decoration of a  $\sim$  on top of the symbol used for the vector variable name.

The *mass average velocity vector* for the  $i$ th species relative to stationary coordinates is given by  $\tilde{v}_i$ . It is important to note that this species velocity is not the velocity of an individual molecule but is the

average velocity of a very large number of species  $i$  molecules within a very small volume of the solution. The mass average velocity vector  $\tilde{v}$  is then defined by

$$\tilde{v} = \frac{\sum_{i=1}^N m_i \tilde{v}_i}{\sum_{i=1}^N m_i} = \frac{1/V \sum_{i=1}^N m_i \tilde{v}_i}{1/V \sum_{i=1}^N m_i} = \frac{\sum_{i=1}^N \rho_i \tilde{v}_i}{\sum_{i=1}^N \rho_i} = \frac{\sum_{i=1}^N \rho_i \tilde{v}_i}{\rho} = \sum_{i=1}^N \omega_i \tilde{v}_i \quad (5.1)$$

In [Equation 5.1](#)

$\rho_i$  is the mass concentration of species  $i$

$N$  is the total number of species in the solution

In a similar manner, we can define the *molar average velocity vector*,  $\tilde{v}^+$ , as follows:

$$\tilde{v}^+ = \frac{\sum_{i=1}^N n_i \tilde{v}_i}{\sum_{i=1}^N n_i} = \frac{1/V \sum_{i=1}^N n_i \tilde{v}_i}{1/V \sum_{i=1}^N n_i} = \frac{\sum_{i=1}^N C_i \tilde{v}_i}{\sum_{i=1}^N C_i} = \frac{\sum_{i=1}^N C_i \tilde{v}_i}{C} = \sum_{i=1}^N x_i \tilde{v}_i \quad (5.2)$$

In mass transfer, we frequently work in terms of the mass and molar fluxes of species  $i$ . The mass and molar flux is defined as the mass or moles of species  $i$  that cross a given area per unit time. We can write these mass and molar fluxes, which are also vectors and relative to stationary coordinates, as

$$\text{Mass flux } \tilde{M}_i = \rho_i \tilde{v}_i \quad (5.3)$$

$$\text{Molar flux } \tilde{N}_i = C_i \tilde{v}_i \quad (5.4)$$

The species mass and molar fluxes can also be written relative to the mass average velocity, i.e.,  $\tilde{v}$ , and the molar average velocity, i.e.,  $\tilde{v}^+$ , as

$$\text{Mass flux } \tilde{j}_i = \rho_i (\tilde{v}_i - \tilde{v}) \quad \text{and} \quad \tilde{j}^+ = \rho_i (\tilde{v}_i - \tilde{v}^+) \quad (5.5)$$

$$\text{Molar flux } \tilde{J}_i = C_i (\tilde{v}_i - \tilde{v}) \quad \text{and} \quad \tilde{J}_i^+ = C_i (\tilde{v}_i - \tilde{v}^+) \quad (5.6)$$

The velocity differences in [Equations 5.5](#) and [5.6](#), i.e.,  $(\tilde{v}_i - \tilde{v})$  and  $(\tilde{v}_i - \tilde{v}^+)$ , are the velocity of species  $i$  relative to the mass and molar average velocity of all the species in the solution, respectively. This relative velocity of species  $i$  is the result of the diffusion of that particular species relative to the bulk motion of the solution.

The molar flux of species  $i$  relative to the molar average velocity, i.e.,  $\tilde{J}_i^+$ , can be written in terms of the molar flux of species  $i$  relative to stationary coordinates, i.e.,  $\tilde{N}_i$ , as follows. First, we use [Equation 5.2](#) to eliminate  $\tilde{v}^+$  in [Equation 5.6](#), and then we use [Equation 5.4](#) to replace  $C_i \tilde{v}_i$  with  $\tilde{N}_i$ . We then obtain

$$\tilde{J}_i^+ = C_i (\tilde{v}_i - \tilde{v}^+) = C_i \tilde{v}_i - C_i \tilde{v}^+ = C_i \tilde{v}_i - \frac{C_i}{C} \sum_{j=1}^N C_j \tilde{v}_j = \tilde{N}_i - x_i \sum_{j=1}^N \tilde{N}_j \quad (5.7)$$

### 5.2.1 Binary diffusion

For most diffusion problems that we will be discussing, we can treat the problem as a two component or binary system, i.e., the solute, which we will denote by the symbol A, and the solvent, which we will denote by B. In biological systems, the solvent is usually a mixture comprised of a complex collection of other species dissolved in water. This means that, in a strict sense, the diffusivity of A in this complex mixture is really an apparent diffusivity of this solute in the mixture B.

Using [Equation 5.7](#), we can then write the molar flux of solute A relative to stationary coordinates as

$$\tilde{N}_A = \tilde{J}_A^+ + x_A (\tilde{N}_A + \tilde{N}_B) \quad (5.8)$$

In [Equation 5.8](#), the term given by  $x_A (\tilde{N}_A + \tilde{N}_B)$  represents the molar flux of solute A due to the convective or bulk flow of the solution.

### 5.2.2 Fick's first law

Diffusion is the result of the random motion of molecules superimposed on the bulk motion of the fluid itself. In a statistical sense, it is observed that molecules will tend to spread from a region of high concentration to a region of lower concentration. The  $\tilde{J}_A^+$  term in [Equation 5.8](#) represents the molar flux of A relative to the molar average velocity of the solution, and this is a result of solute diffusion. Recall from [Chapter 4](#) that for laminar flow of a fluid between two parallel plates, we obtained Newton's law of viscosity to express the momentum transport flux, i.e.,  $\tau_{yx}$ , in terms of the velocity gradient,  $dv_x/dy$ . Hence, we found that  $\tau_{yx} = -\mu \frac{dv_x}{dy}$ , where  $\mu$  was the viscosity of the fluid.

The diffusion flux of solute A is analogous to this diffusive transport of momentum, and this is given by *Fick's first law*, where  $\tilde{J}_A^+$  is proportional to the mole fraction gradient, which we can express in three dimensions as  $\tilde{\nabla}x_A$ , where the mole fraction gradient in Cartesian coordinates is given by

$$\tilde{\nabla}x_A = \tilde{i} \frac{\partial x_A}{\partial x} + \tilde{j} \frac{\partial x_A}{\partial y} + \tilde{k} \frac{\partial x_A}{\partial z} \quad (5.9)$$

The proportionality constant in Fick's first law is called the diffusivity of solute A in solution B, or  $D_{AB}$ . The units of diffusivity are typically  $\text{cm}^2 \text{s}^{-1}$ . Hence, we can write Fick's first law as

$$\tilde{J}_A^+ = -CD_{AB}\tilde{\nabla}x_A \quad (5.10)$$

We can combine Fick's first law given by [Equation 5.10](#) with [Equation 5.8](#) to obtain the expression for the molar flux of solute A relative to stationary coordinates:

$$\tilde{N}_A = x_A (\tilde{N}_A + \tilde{N}_B) - CD_{AB}\tilde{\nabla}x_A \quad (5.11)$$

[Equation 5.11](#) is our usual starting point for mass transfer problems. In a similar manner, we can also obtain an expression for the mass flux of A relative to stationary coordinates, which is given by

$$\tilde{M}_A = \omega_A (\tilde{M}_A + \tilde{M}_B) - \rho D_{AB} \tilde{\nabla} \omega_A \quad (5.12)$$

### 5.2.3 Simplifications of Fick's first law

Many of our problems will also be one dimensional, so we will only need to consider one component of the molar flux of A, e.g.,  $N_{Az}$ , where, e.g., z is in the direction of the bulk flow. Hence, [Equation 5.11](#) becomes for one-dimensional mass transfer:

$$N_{Az} = x_A (N_{Az} + N_{Bz}) - CD_{AB} \frac{dx_A}{dz} \quad (5.13)$$

There are also four common physical situations that will allow for some simplification of [Equation 5.11](#). These are *forced convection*, a *stagnant or quiescent fluid*, a *dilute solution*, and *equimolar countercdiffusion*.

**5.2.3.1 The case of forced convection** In some cases, the transport of solute A is dominated by the bulk flow of the solution. This means that the diffusion of A in the direction of the flow, e.g., in the z direction, is much smaller than the amount of A carried along by the flow in the z direction. In this case, [Equation 5.13](#) simplifies to

$$N_{Az} = x_A (N_{Az} + N_{Bz}) = x_A (C_A v_{Az} + C_B v_{Bz}) = x_A C_A v_z^+ = C_A v_z^+ \quad (5.14)$$

Now, in [Equation 5.14](#),  $C_A v_z^+$  is the rate at which the moles of A are passing through a given unit cross section of area that is perpendicular to the molar average velocity,  $v_z^+$ . In the design of a medical device, e.g., this forced convective flow is often occurring within a tube of cross-sectional area,  $A_{tube}$ . Hence, we can also say that the molar flux of A in the direction of the flow, i.e.,  $N_{Az}$ , is the same as the volumetric flow rate of the fluid, i.e., Q, times the molar concentration of A, i.e.,  $C_A$ , divided by the cross-sectional area of the tube, i.e.,  $A_{tube}$ . Hence,  $N_{Az} = QC_A/A_{tube}$ . If the x direction is perpendicular to the direction of the flow, then in the case of forced convection in the z or axial direction, with negligible axial diffusion, the molar flux of A at some value of x becomes

$$N_{Az}(x) = C_A v_z^+ = C_A v_z(x) \quad (5.15)$$

It is important to remember though that the molar diffusion flux of A ( $\tilde{J}_A^+$ ) relative to the molar average velocity ( $\tilde{v}^+$ ) is a vector, and although the z component of this vector can be negligible, the other two components of  $\tilde{J}_A^+$  may not be negligible. For example, if there were a chemical reaction occurring at the surface of a cylindrical tube that was consuming A, then there will be a significant concentration gradient of A in the radial direction.

**5.2.3.2 The case of a stagnant or quiescent fluid** If the fluid phase B is not moving, or stagnant, then relative to a stationary coordinate system,  $\tilde{N}_B = 0$ . [Equation 5.11](#) then simplifies to

$$\tilde{N}_A = x_A \tilde{N}_A - CD_{AB} \tilde{\nabla} x_A = -\frac{1}{1-x_A} CD_{AB} \tilde{\nabla} x_A \quad (5.16)$$

If  $x_A$  is also much smaller than unity, then [Equation 5.16](#) simplifies to

$$\tilde{N}_A = -CD_{AB} \tilde{\nabla} x_A \quad (5.17)$$

**5.2.3.3 The case of dilute solutions** Oftentimes we have a dilute solution, which means that  $x_A \ll 1$ . For example, in biological solutions, the molar concentration of water is 55.6 M. Most solutes of interest will have concentrations that are significantly less than 55.6 M, as we see, e.g., in Table 3.2. So if we had a particular solute with a concentration of 0.1 M, then its mole fraction in this solution would be equal to  $\frac{C_A}{C_A + C_{\text{water}}} = \frac{0.1 \text{ M}}{0.1 \text{ M} + 55.6 \text{ M}} = 0.0018$ . This means we can neglect the term,  $x_A (\tilde{N}_A + \tilde{N}_B)$ , in Equation 5.11. Also, because the solution is dilute, the total concentration, i.e.,  $C$ , is also constant. With these assumptions, Equation 5.11 becomes

$$\tilde{N}_A = -CD_{AB}\tilde{\nabla}x_A = -D_{AB}\tilde{\nabla}C_A \quad (5.18)$$

Most mass transfer calculations begin with Equation 5.18 and are based therefore on the assumption of a dilute solution. Although this seems like a serious limitation, this assumption of a dilute solution works surprisingly well in most cases.

**5.2.3.4 Equimolar counterdiffusion** Equimolar counterdiffusion means that for each mole of A that diffuses in a particular direction, a mole of B diffuses in the opposite direction. We see this many times in a chemical reaction occurring at the surface of an object. For example, suppose an enzyme is immobilized on the surface of a solid support. This enzyme catalyzes a simple isomerization of A to form B. The reaction stoichiometry, i.e.,  $A \rightarrow B$ , says that for every mole of A that diffuses to the surface, one mole of the reaction product, i.e., B, diffuses away from the surface. This means that  $\tilde{N}_A = -\tilde{N}_B$  and Equation 5.11 in this case becomes

$$\tilde{N}_A = -CD_{AB}\tilde{\nabla}x_A \quad (5.19)$$

## 5.2.4 Boundary conditions for diffusion problems

When we solve a diffusion problem, we will have conditions on the solute concentration that must be satisfied at the boundaries of the region of interest. These are called the *boundary conditions* and come about because of the physical nature of the situation we are considering. If the concentration of the solute is also changing with time, we also need to know what the concentration distribution in the region of interest is at time equal to zero. This is known as the *initial condition* (IC). In most cases, the initial concentration of the solute in the region of interest is uniform, and if the solute is not present initially, then its concentration is equal to zero.

The boundary conditions specify what we know about the behavior of the solute concentration at the boundaries. There are several types of common boundary conditions that come up in mass transfer problems.

**5.2.4.1 Concentration is known at the boundary** The first type of boundary condition (BC) is when we know the value of the concentration at the boundary surface. So, e.g., in the following discussion, if we let the  $y$  direction extend outward and normal to the boundary, then we can write at the boundary surface

$$C_A|_{y=0} = C_{AS} \quad (5.20)$$

Many times the concentration of solute A at the surface, i.e.,  $C_{AS}$ , is just the equilibrium solubility of the solute A in B. This means that the solute dissolves very quickly in comparison to the mass

transfer of the solute into the bulk fluid. Hence, the solute concentration at the boundary surface is constant and equal to its equilibrium solubility in the solvent. If there is a very fast or instantaneous reaction occurring at the surface of a boundary, then the concentration of the reactant is zero at the surface, and we can set  $C_{AS} = 0$ .

**5.2.4.2 Zero solute flux at the boundary** The second situation involves specifying the flux of the solute at a boundary. If a boundary is impermeable to the solute, or if the boundary is a symmetry plane, then the solute flux across this boundary is zero, and from [Equation 5.18](#) for a dilute solution, where we let the  $y$  direction extend outward and is normal to the boundary, we have for the  $y$  component of the solute flux

$$N_{Ay}\Big|_{y=0} = -D_{AB} \frac{dC_A}{dy}\Big|_{y=0} = 0. \quad (5.21)$$

**5.2.4.3 Convective transport at the boundary** In other cases, as we will discuss later, there can be a fluid that is flowing over the surface. In this case, the mass transfer flux will depend on the nature of this flow over the surface. For this situation, the mass transfer flux of solute A across the surface is proportional to the difference in concentration between the surface, i.e.,  $C_{AS} = C_A|_{y=0}$ , and the concentration of A in the bulk solution, i.e.,  $C_{A\text{ bulk}}$ . The proportionality constant is called the *mass transfer coefficient*,  $k_m$ , and will depend on the geometry and the nature of the flow over the surface. The boundary condition at the surface for this case is

$$N_{Ay}\Big|_{y=0} = -D_{AB} \frac{dC_A}{dy}\Big|_{y=0} = k_m (C_A|_{y=0} - C_{A\text{ bulk}}) = k_m (C_{AS} - C_{A\text{ bulk}}) \quad (5.22)$$

**5.2.4.4 Chemical reaction at the boundary** If there is a chemical reaction occurring at the boundary, then at steady state, the molar flux of solute A at the surface has to be equal to the rate of the reaction on the surface. This means

$$N_{Ay}\Big|_{y=0} = -D_{AB} \frac{dC_A}{dy}\Big|_{y=0} = k_m (C_{AS} - C_{A\text{ bulk}}) = -R''_A \quad (5.23)$$

where  $R''_A$  is the rate of the surface chemical reaction and has typical units like  $\text{mol cm}^{-2} \text{ s}^{-1}$ .  $R''_A$  is positive for the consumption of solute A, and the  $y$  direction extends outward and normal to the boundary. [Equation 5.23](#) also says that at steady state, the rate of mass transfer of the solute to the surface has to equal the solute reaction rate at the surface.

Now let us consider the common situation where the surface reaction can be described by a first order reversible reaction, i.e.,  $A \leftrightarrow C$ . By the law of mass action, the reaction rates are proportional to the concentrations of  $C_A$  and  $C_C$  at the surface. The proportionality constants are the first order rate constants for the forward and reverse reactions, i.e.,  $k_f$  and  $k_r$ . Hence, we can write the surface reaction rate for solute A as

$$R''_A = k_f C_{AS} - k_r C_{CS} \quad (5.24)$$

We can also define the equilibrium constant for the reaction as

$$K_{eq} = \left( \frac{C_{CS}}{C_{AS}} \right)_{eq} = \frac{k_f}{k_r} \quad (5.25)$$

and then we can rewrite [Equation 5.24](#) in terms of the equilibrium constant:

$$R_A'' = k_f \left( C_{AS} - \frac{1}{K_{eq}} C_{CS} \right) \quad (5.26)$$

Next, we recognize that in this situation where we have diffusion and a surface chemical reaction, the overall observed rate consists of three steps in series. First, the solute A must diffuse from the bulk solution to the surface, then it reacts at the surface reversibly to produce solute C, and then solute C diffuses back into the bulk solution. The surface reaction rate of solute A is given by [Equation 5.26](#). The diffusion steps can be written in terms of the mass transfer coefficient using [Equation 5.22](#) as

$$\begin{aligned} N_{Ay} \Big|_{y=0} &= k_{mA} (C_{A\ bulk} - C_{AS}) \\ N_{Cy} \Big|_{y=0} &= k_{mC} (C_{CS} - C_{C\ bulk}) \end{aligned} \quad (5.27)$$

[Equations 5.26](#) and [5.27](#) have been written to have a positive sense for the reaction of solute A. We also recognize that at steady state,  $N_{Ay}$ ,  $N_{Cy}$ , and  $R_A''$  are all the same. If we divide the  $N_{Cy}$  molar flux in [Equation 5.27](#) by  $K_{eq}$ , and then do some algebraic manipulation, we can combine [Equations 5.26](#) and [5.27](#) and obtain a single equation for  $N_{Ay}$ ,  $N_{Cy}$ , and  $R_A''$  in terms of the bulk concentrations of solutes A and C,

$$N_{Ay} \Big|_{y=0} = N_{Cy} \Big|_{y=0} = R_A'' = K \left( C_{A\ bulk} - \frac{C_{C\ bulk}}{K_{eq}} \right) \quad (5.28)$$

where K is the overall rate constant and includes the effects of both solute diffusion and the surface reaction rate on the observed transport rate of solutes A and C. The overall rate constant is given by

$$\frac{1}{K} = \frac{1}{k_{mA}} + \frac{1}{k_f} + \frac{1}{K_{eq} k_{mC}} \quad (5.29)$$

Each term on the right-hand side of [Equation 5.29](#) represents a resistance, and in analogy to an electric circuit, we see that the overall resistance, represented by  $1/K$ , is equal to the sum of the individual resistances due to the mass transfer of solutes A and C and the surface chemical reaction.

There are also some special cases that need to be considered. First, suppose the mass transfer rates are very high, e.g., the bulk fluid is moving very fast, or being mixed very well. In this case, which is called *reaction controlling*, the mass transfer coefficients, i.e.,  $k_{mA}$  and  $k_{mC}$ , are much larger than the reaction rate constant,  $k_f$ . In this case, [Equation 5.28](#) becomes

$$N_{Ay} \Big|_{y=0} = N_{Cy} \Big|_{y=0} = R_A'' = k_f \left( C_{A\ bulk} - \frac{C_{C\ bulk}}{K_{eq}} \right) \quad (5.30)$$

If the reaction rate is very fast, then we have the situation of *mass transfer controlling*, and we can write [Equation 5.28](#) as

$$N_{Ay} \Big|_{y=0} = N_{Cy} \Big|_{y=0} = R''_A = \left( \frac{1}{\frac{1}{k_{mA}} + \frac{1}{K_{eq} k_{mC}}} \right) \left( C_{A \text{ bulk}} - \frac{C_{C \text{ bulk}}}{K_{eq}} \right) \quad (5.31)$$

If the reaction is also irreversible and very fast, i.e.,  $K_{eq}$  is really big, then [Equation 5.31](#) becomes

$$N_{Ay} \Big|_{y=0} = N_{Cy} \Big|_{y=0} = R''_A = k_{mA} (C_{A \text{ bulk}} - 0) = k_{mA} C_{A \text{ bulk}} \quad (5.32)$$

Here, we see that the observed reaction rate is just the mass transfer rate of solute A to the surface. Also, since the surface reaction rate is also very fast, the surface concentration of solute A is equal to zero.

Finally, for the special case of a finite irreversible reaction, [Equation 5.28](#) becomes

$$N_{Ay} \Big|_{y=0} = N_{Cy} \Big|_{y=0} = R''_A = \left( \frac{1}{\frac{1}{k_{mA}} + \frac{1}{k_f}} \right) C_{A \text{ bulk}} \quad (5.33)$$

### 5.3 Estimating the diffusivity

To solve diffusion problems, we will also need to know the diffusivity of the solute, i.e.,  $D_{AB}$ . The diffusivity typically has units of  $\text{cm}^2 \text{ s}^{-1}$  or  $\text{m}^2 \text{ s}^{-1}$ . The solute diffusivity generally depends on the size of the solute, its concentration, the temperature and pressure, and the physical properties of the fluid or material in which the solute is diffusing.

The value of the diffusivity for a given solute is best found from experimental data. Literature searches can be used to see if the diffusivity has been determined for a particular solute. Cussler (1984) and Tyn and Gusek (1990) also provide data on the diffusivity for a variety of solutes. However, many times, experimental data do not exist for the solute and medium of interest, and performing experiments to measure the solute diffusivity can be time consuming and expensive. Hence, we must resort to methods that allow us to estimate the diffusivity. Cussler (1984) and Bird et al. (2002) summarize methods for estimating diffusivities in gases, liquids, and solids. Young et al. (1980) have also developed a correlation for estimating the diffusivity of proteins.

For gases, the diffusivity is on the order of 0.1 to 1.0  $\text{cm}^2 \text{ s}^{-1}$ . According to the Chapman-Enskog theory of solute diffusion in a gas (Cussler, 1984), the diffusivity of the solute is inversely proportional to the pressure and directly proportional to the temperature in K to the nth power, i.e.,  $D_{AB} \propto \frac{T^n}{P}$ , where n ranges from 1.5 to 1.8. If a gas diffusivity is known at conditions  $(T_1, P_1)$ , then its value at conditions  $(T_2, P_2)$  can be estimated by

$$D_{AB} \Big|_2 = D_{AB} \Big|_1 \left( \frac{P_1}{P_2} \right) \left( \frac{T_2}{T_1} \right)^n \quad (5.34)$$

where the temperature is absolute.

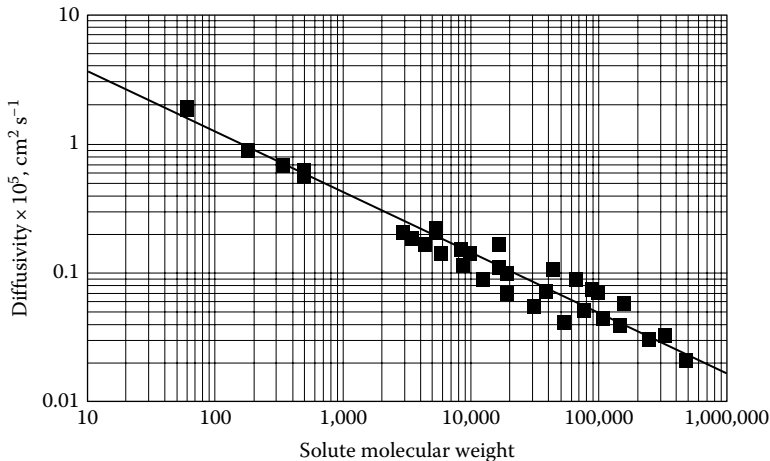


Figure 5.1 Solute diffusivity in water at 37°C. (Based on data from Renkin, E.M. and Curry, F.E., Transport of water and solutes across capillary endothelium, in: *Membrane Transport in Biology*, vol. 4, Giebisch, G. and Tosteson, D.C. (eds.), Springer-Verlag, New York, 1979, [Chapter 1](#).)

In liquids such as water, the diffusivity is around  $10^{-5} \text{ cm}^2 \text{ s}^{-1}$  for molecules with a MW on the order of 100. For example, the diffusivity of oxygen in water at 37°C was found to be  $2.76 \times 10^{-5} \text{ cm}^2 \text{ s}^{-1}$  (Yoshida and Ohshima, 1966), and at 25°C the value is  $2.1 \times 10^{-5} \text{ cm}^2 \text{ s}^{-1}$  (Cussler, 1984). For large macromolecules like a polypeptide, the diffusivity in water is on the order of  $10^{-6} \text{ cm}^2 \text{ s}^{-1}$ , and protein molecules can have a diffusivity in water on the order of  $10^{-7} \text{ cm}^2 \text{ s}^{-1}$ . In polymers, the diffusivity is on the order of  $10^{-8} \text{ cm}^2 \text{ s}^{-1}$ , and in solids the diffusivity can be as low as  $10^{-10} \text{ cm}^2 \text{ s}^{-1}$ .

Figure 5.1 presents a plot of diffusivity data (Renkin and Curry, 1979) for a variety of solutes in dilute aqueous solutions at 37°C as a function of solute MW. Note that the diffusivity for the data shown in this figure has been multiplied by  $10^5$ . The solid line through the data is the result of a linear least squares regression. The following empirical equation based on the data in Figure 5.1 provides a useful relationship for estimating the diffusivity of a solute in water at 37°C knowing only the MW of the solute.

$$D_{AB} = 1.013 \times 10^{-4} (\text{MW})^{-0.46}, \text{ cm}^2 \text{ s}^{-1} \quad (5.35)$$

### 5.3.1 Stokes-Einstein equation

The diffusivity of a solute in a dilute liquid solution can also be estimated from the *Stokes-Einstein equation* (Einstein, 1956; Cussler, 1984; Bird et al., 2002). We assume that the solute can be represented as a solid sphere of radius  $a$  moving through a continuous solvent phase where we assume that the solvent molecules are much smaller than the solute molecules. The steady motion of the solute molecule represents a balance between the drag force exerted on the solute molecule as the solvent flows across its surface and the force exerted on the solute molecule due to its concentration gradient (Einstein, 1956).

For a spherical object of radius  $a$  moving slowly through a quiescent fluid, Stokes law (Bird et al., 2002) says that the drag force on the object, i.e.,  $F_{\text{drag}}$ , is given by  $6\pi\mu av_\infty$ , where  $\mu$  is the fluid

viscosity and  $v_\infty$  is the velocity of the spherical object relative to that of the solvent. In terms of the velocity of the solute molecule, we then have

$$v_\infty = \frac{F_{\text{drag}}}{6\pi\mu a} \quad (5.36)$$

Now if we focus on the steady motion of solute A in the x direction only, then to balance the drag force on the solute molecule, Einstein (1956) showed that the gradient of the osmotic pressure of the solute, i.e.,  $-\frac{d\Pi}{dx}$ , is equal to the force per unit volume of solution exerted on the solute molecules that causes their motion in the x direction. We can express this force on each solute molecule as

$$F = -\frac{1}{N_A C_A} \frac{d\Pi}{dx} = -\frac{RT}{N_A C_A} \frac{dC_A}{dx} = -\frac{1}{N_A} \frac{d\mu_A^{\text{ideal solution}}}{dx} \quad (5.37)$$

where  $N_A$  is Avogadro's number and we have used van't Hoff's law, i.e., [Equation 2.147](#), to replace  $\Pi$  with  $RT C_A$ . Then, using [Equation 2.75](#), we see that this force is also equal to the chemical potential gradient, assuming we have an ideal dilute solution. Substituting [Equation 5.37](#) for  $F_{\text{drag}}$  in [Equation 5.36](#), we obtain

$$v_\infty = -\frac{RT}{6\pi\mu a N_A} \frac{1}{C_A} \frac{dC_A}{dx} \quad (5.38)$$

If the solute concentration at some position  $x$  is  $C_A$ , then by [Equation 5.4](#), the molar flux of solute A relative to stationary coordinates, i.e.,  $N_{Ax}$ , is given by  $v_\infty C_A$ ; hence, we have using [Equation 5.38](#) that

$$N_{Ax} = -\frac{RT}{6\pi\mu a N_A} \frac{dC_A}{dx} \quad (5.39)$$

For a dilute solution, [Equation 5.18](#) says that  $N_{Ax} = -D_{AB} \frac{dC_A}{dx}$ , and comparing this with the result given by [Equation 5.39](#), we obtain the Stokes-Einstein equation for the diffusivity:

$$D_{AB} = \frac{RT}{6\pi\mu a N_A} \quad (5.40)$$

In [Equation 5.40](#)

$R$  is the ideal gas constant

$T$  is the absolute temperature

$a$  is the solute radius

$N_A$  is Avogadro's number ( $6.023 \times 10^{23} \text{ mol}^{-1}$ )

$\mu$  is the solution viscosity

For solute diffusion in water, the viscosity is 0.691 cP at 37°C, 0.89 cP at 25°C, and 1.002 cP at 20°C. For solute diffusion in plasma, the viscosity at 37°C is 1.2 cP. Recall that 1cP = 1 centipoise = 0.01 g cm<sup>-1</sup> s<sup>-1</sup> = 0.001 Pa s.

If the diffusivity for a solute in a given solvent is known, then [Equation 5.40](#) can also be used to obtain an estimate of the molecular radius ( $a$ ) of the solute. This value is known as the *Stokes-Einstein radius*.

If the radius of the solute, i.e.,  $a$ , is not known, it can be estimated from its MW by the following equation. This equation assumes that a molecule of the solute is a sphere with a density ( $\rho \approx 1 \text{ g cm}^{-3}$ ) equal to that of the solute in the solid phase.

$$a = \left( \frac{3\text{MW}}{4\pi\rho N_A} \right)^{1/3} \quad (5.41)$$

If we use [Equation 5.41](#) to find the solute radius and use this in the Stokes-Einstein equation, i.e., [Equation 5.40](#), we find that the diffusivity, i.e.,  $D_{AB}$ , is directly proportional to the following quantity, i.e.,  $\frac{T}{\mu\text{MW}^{1/3}}$ . In the paper by Young et al. (1980), the proportionality constant was found by analyzing the measured diffusivity of 143 proteins. For  $D_{AB}$  in  $\text{cm}^2 \text{ s}^{-1}$ , the proportionality constant was found to be  $8.34 \times 10^{-8}$ , with the solution viscosity in cP, the temperature in absolute K, and the MW in  $\text{g mol}^{-1}$ .

If the solute diffusivity in a liquid is known at conditions  $(T_1, \mu_1)$ , then its value at conditions  $(T_2, \mu_2)$  can be estimated from [Equation 5.40](#) as shown next:

$$D_{AB}|_2 = D_{AB}|_1 \left( \frac{\mu_1}{\mu_2} \right) \left( \frac{T_2}{T_1} \right) \quad (5.42)$$

### Example 5.1

Using the Stokes-Einstein equation, estimate the diffusivity of ovalbumin ( $\text{MW} = 45,000$ ) in water at  $25^\circ\text{C}$ . Cussler (1984) reports a value for the diffusivity of ovalbumin of  $7.8 \times 10^{-7} \text{ cm}^2 \text{ s}^{-1}$ . Also estimate the ovalbumin diffusivity using the correlation developed by Young et al. (1980), i.e.,  $D_{AB} = 8.34 \times 10^{-8} \left( \frac{T}{\mu\text{MW}^{1/3}} \right)$ . The viscosity of water at  $25^\circ\text{C}$  is 0.89 cP.

### Solution

We assume ovalbumin is spherical and we estimate the radius of this molecule using [Equation 5.41](#):

$$a = \left( \frac{3 \times 45,000 \text{ g mol}^{-1}}{4\pi \times 1 \text{ g cm}^{-3} \times 6.023 \times 10^{23} \frac{1}{\text{mol}}} \right)^{1/3} = 2.61 \times 10^{-7} \text{ cm} \times \frac{1 \text{ m}}{100 \text{ cm}} \times \frac{10^9 \text{ nm}}{\text{m}} = 2.61 \text{ nm}$$

Next, using the Stokes-Einstein equation, we have

$$D_{AB} = \frac{8.314 \text{ J mol}^{-1} \text{ K}^{-1} \times 298 \text{ K} \times \frac{\text{kg m m}}{\text{s}^2 \text{ J}} \times \frac{(100 \text{ cm})^2}{\text{m}^2}}{6\pi \times 0.89 \text{ cP} \times \frac{0.01 \text{ g cm}^{-1} \text{ s}^{-1}}{\text{cP}} \times 2.61 \times 10^{-7} \text{ cm} \times 6.023 \times 10^{23} \frac{1}{\text{mol}} \times \frac{1 \text{ kg}}{1000 \text{ g}}}$$

$$D_{AB} = 9.39 \times 10^{-7} \text{ cm}^2 \text{ s}^{-1}$$

Using the correlation developed by Young et al. (1980):

$$D_{AB} = 8.34 \times 10^{-8} \left( \frac{T}{\mu MW^{1/3}} \right) = 8.34 \times 10^{-8} \left( \frac{298}{0.89 \times 45,000^{1/3}} \right) = 7.85 \times 10^{-7} \text{ cm}^2 \text{ s}^{-1}$$

Very large molecules like the protein considered in this example can be solvated or hydrated making the radius of the actual solvated solute larger than the radius estimated from the solute MW using [Equation 5.41](#). This would make the diffusivity of the solvated solute smaller than the value calculated from the Stokes-Einstein equation. The Young et al. (1980) correlation gives a diffusivity for ovalbumin that compares very well with the value reported by Cussler (1984).

### Example 5.2

Estimate the diffusivity of oxygen in water at 25°C. The oxygen diffusivity in water at 37°C was found to be  $2.76 \times 10^{-5} \text{ cm}^2 \text{ s}^{-1}$  by Yoshida and Ohshima (1966).

#### Solution

We can use [Equation 5.42](#), which is based on the Stokes-Einstein equation ([Equation 5.40](#)), to estimate the diffusivity of oxygen in water at 25°C. The viscosity of water is 0.691 cP at 37°C and 0.89 cP at 25°C. Hence, we calculate the oxygen diffusivity as follows:

$$D_{AB}|_{25^\circ\text{C}} = 2.76 \times 10^{-5} \text{ cm}^2 \text{ s}^{-1} \left( \frac{0.691}{0.89} \right) \left( \frac{298}{310} \right) = 2.06 \times 10^{-5} \text{ cm}^2 \text{ s}^{-1}$$

The value for the oxygen diffusivity in water at 25°C is reported to be  $2.1 \times 10^{-5} \text{ cm}^2 \text{ s}^{-1}$  (Cussler, 1984).

## 5.4 Fick's second law

Consider the situation shown in [Figure 5.2](#). The surface of a semi-infinite plate of length L in the x direction contains a solute that maintains a constant concentration,  $C_{AS}$ , along the surface of the plate at  $y = 0$ . At  $t = 0$ , this surface is contacted with a stagnant medium that has a uniform initial

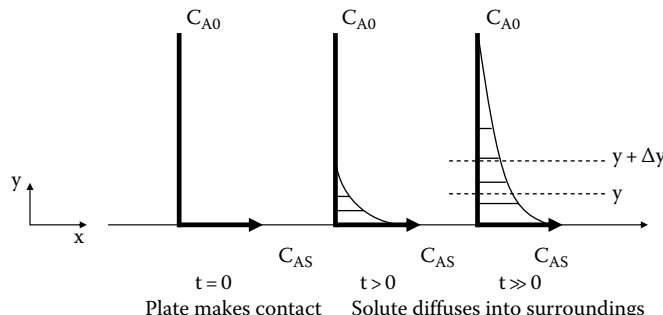


Figure 5.2 Solute concentration in the vicinity of a flat plate of constant surface concentration.

concentration of the solute equal to  $C_{A0}$ , and we assume, e.g., that  $C_{AS} > C_{A0}$ . The solute therefore diffuses from the surface of the plate into the stagnant medium. As time progresses, the solute will penetrate more and more into the stagnant medium.

[Figure 5.2](#) shows a thin slice of fluid of thickness  $\Delta y$ , with a surface area normal to the  $y$  direction of  $S$ , giving a shell volume of  $S \Delta y$ . The rate at which the solute enters and leaves this thin shell volume by diffusion at  $y$  and  $y + \Delta y$  is given by our one-dimensional diffusion equation, i.e., [Equation 5.13](#), written here in terms of the  $y$  component of the diffusion flux, i.e.,  $N_{Ay}$ .

$$N_{Ay} = x_A (N_{Ay} + N_{By}) - CD_{AB} \frac{dx_A}{dy} \quad (5.43)$$

Assuming a dilute medium, [Equation 5.43](#) simplifies to

$$N_{Ay} = -CD_{AB} \frac{dx_A}{dy} \quad (5.44)$$

Now, we perform an unsteady solute mass balance on our shell volume equal to  $S\Delta y$ . We can then write, using [Equation 1.8](#) as our guide, that

$$S\Delta y \frac{\partial C_A}{\partial t} = N_{Ay} S|_y - N_{Ay} S|_{y+\Delta y} = S \left( -CD_{AB} \frac{\partial x_A}{\partial y} \Big|_y - -CD_{AB} \frac{\partial x_A}{\partial y} \Big|_{y+\Delta y} \right) \quad (5.45)$$

The term on the left of the first equal sign in [Equation 5.45](#) represents the accumulation of the solute within the control volume  $S \Delta y$ . The terms on the right of this equal sign express the net rate at which the solute enters the control volume by diffusion according to Fick's first law. We can eliminate  $S$  in [Equation 5.45](#), and after dividing by  $\Delta y$ , taking the limit as  $\Delta y \rightarrow 0$ , and assuming that  $D_{AB}$  and  $C$  are constant, we obtain the following result that is known as *Fick's second law*:

$$\frac{\partial C_A}{\partial t} = D_{AB} \frac{\partial^2 C_A}{\partial y^2} \quad (5.46)$$

[Equation 5.46](#) is the one-dimensional form of *Fick's second law*, which describes solute diffusion in a stagnant or quiescent medium.

[Equation 5.46](#) can be extended to give Fick's second law in three dimensions, and other coordinate systems such as Cartesian, cylindrical, and spherical, by recognizing that the second derivative of  $C_A$  with respect to  $y$  can be generalized as the *Laplacian* of the scalar  $C_A$ . Hence, [Equation 5.46](#) can be written in terms of the *Laplacian operator* as

$$\frac{\partial C_A}{\partial t} = D_{AB} \nabla^2 C_A \quad (5.47)$$

The *Laplacian operator* for scalar variable  $s$  in Cartesian, cylindrical, and spherical coordinates is shown next:

$$\text{Cartesian coordinates } (x, y, z) \quad \nabla^2 s = \frac{\partial^2 s}{\partial x^2} + \frac{\partial^2 s}{\partial y^2} + \frac{\partial^2 s}{\partial z^2} \quad (5.48)$$

$$\text{Cylindrical coordinates } (r, \theta, z) \quad \nabla^2 s = \frac{1}{r} \frac{\partial}{\partial r} \left( r \frac{\partial s}{\partial r} \right) + \frac{1}{r^2} \frac{\partial^2 s}{\partial \theta^2} + \frac{\partial^2 s}{\partial z^2} \quad (5.49)$$

$$\text{Spherical coordinates } (r, \theta, \phi) \quad \nabla^2 s = \frac{1}{r^2} \frac{\partial}{\partial r} \left( r^2 \frac{\partial s}{\partial r} \right) + \frac{1}{r^2 \sin \theta} \frac{\partial}{\partial \theta} \left( \sin \theta \frac{\partial s}{\partial \theta} \right) + \frac{1}{r^2 \sin^2 \theta} \frac{\partial^2 s}{\partial \phi^2} \quad (5.50)$$

## 5.5 Some solutions to Fick's second law

Next, we will consider several cases where we can obtain an analytical solution to Fick's second law as given by [Equation 5.47](#).

### 5.5.1 Solution for the concentration profile for diffusion from a flat plate into a semi-infinite stagnant medium

[Equation 5.46](#) describes the situation in [Figure 5.2](#), and we can obtain a solution in terms of the concentration relative to  $C_{A0}$ . We can also write the following initial condition and boundary conditions for solute A within the stagnant medium:

$$\begin{aligned} \text{IC: } t = 0, \quad C_A &= C_{A0} \\ \text{BC1: } y = 0, \quad C_A &= C_{AS} \\ \text{BC2: } y = \infty, \quad C_A &= C_{A0} \end{aligned} \quad (5.51)$$

Next, we let  $\theta = C_A - C_{A0}$ , and [Equations 5.46](#) and [5.51](#) then become in terms of  $\theta$

$$\frac{\partial \theta}{\partial t} = D_{AB} \frac{\partial^2 \theta}{\partial y^2} \quad (5.52)$$

and

$$\begin{aligned} \text{IC: } t = 0, \quad \theta &= 0 \\ \text{BC1: } y = 0, \quad \theta_s &= C_{AS} - C_{A0} \\ \text{BC2: } y = \infty, \quad \theta &= 0 \end{aligned} \quad (5.53)$$

[Equations 5.52](#) and [5.53](#) are analogous to the problem we examined in [Chapter 4](#) for the flat plate that is set in motion within a semi-infinite fluid, which is described by [Equations 4.51](#) and [4.52](#). In that case, we used Laplace transforms to obtain a solution for the unsteady velocity profile within the fluid, i.e.,  $v_x(y, t)$ . We can therefore use that result here, i.e., [Equation 4.59](#), by simply recognizing that we can replace  $v_x$  with  $\theta$ ,  $V$  with  $\theta_s$ , and the kinematic viscosity,  $\nu$ , by the diffusivity,  $D_{AB}$ . Hence, we obtain the following result for the concentration profile within a stagnant semi-infinite medium, at any location  $y$ , and time  $t$ :

$$\frac{\theta(y, t)}{\theta_s} = \frac{C_A(y, t) - C_{A0}}{C_{AS} - C_{A0}} = \operatorname{erfc} \left( \frac{y}{\sqrt{4D_{AB}t}} \right) = 1 - \operatorname{erf} \left( \frac{y}{\sqrt{4D_{AB}t}} \right) \quad (5.54)$$

We can also define a concentration boundary layer thickness,  $\delta_C$ , as that distance where the relative concentration, i.e.,  $\frac{\theta(\delta_C, t)}{\theta_s}$ , has decreased to 1% of the value at the surface of the plate. Recall from [Chapter 4](#) that the complementary error function (erfc) of  $\frac{y}{\sqrt{4D_{AB}t}} = 1.821$  provides a value of  $\theta/\theta_s$  that is equal to 0.01. Hence, we can define the concentration boundary layer thickness,  $\delta_C$ , as follows:

$$\delta_C(t) = 3.642 \sqrt{D_{AB}t} \approx 4\sqrt{D_{AB}t} \quad (5.55)$$

The value of  $\delta_C$  can also be interpreted as the distance to which the solute from the plate has penetrated into the fluid at time  $t$ . Note that this penetration distance is proportional to the square root of time. This result also tells us that the characteristic time for the diffusion of a solute, i.e.,  $\tau_{\text{diffusion}}$ , is proportional to the square of a characteristic dimension, i.e.,  $L$ , divided by the solute diffusivity, i.e.,  $\tau_{\text{diffusion}} \propto \frac{L^2}{D_{AB}}$ .

### Example 5.3

Calculate the concentration boundary layer thickness 1 second after the plate has made contact with the medium. Assume that the medium is water and that the solute diffusivity is  $D_{AB} = 1 \times 10^{-5} \text{ cm}^2 \text{ s}^{-1}$ .

#### Solution

Using [Equation 5.55](#), we can calculate the thickness of the concentration boundary layer as shown below:

$$\delta_C = 4\sqrt{10^{-5} \text{ cm}^2 \text{ s}^{-1} \times 1 \text{ s}} = 0.0126 \text{ cm} = 126 \mu\text{m}$$

### Example 5.4

A polymeric material is being used as a barrier for a protective garment. The polymeric material has a thickness of 0.075 in. For a particular toxic agent, the diffusivity in this material was found to be equal to  $1 \times 10^{-6} \text{ cm}^2 \text{ s}^{-1}$ . If the protective garment comes into contact with the toxic agent, estimate the time it will take for the toxic agent to just penetrate the garment.

#### Solution

Assume that there is no toxic agent within the material before contact is made. Hence,  $C_{A0} = 0$ . We can then use [Equation 5.54](#) to estimate the breakthrough time, assuming that  $C_A/C_{AS} = 0.001$  is a reasonable criterion for breakthrough of the toxic agent. Hence, we have that

$$\text{erf}\left(\frac{y}{\sqrt{4D_{AB}t}}\right) = 1 - 0.001 = 0.999$$

From this equation, we have for this case that  $\text{erf}(2.327) = 0.999$ . Therefore,

$$\frac{y}{\sqrt{4D_{AB}t}} = 2.327 = \frac{0.075 \text{ in.} \times 2.54 \text{ cm in.}^{-1}}{\sqrt{4 \times 1 \times 10^{-6} \text{ cm}^2 \text{ s}^{-1} \times t}}$$

Solving for the time, we get that  $t = 1675 \text{ s}$  or  $28 \text{ min}$ .

**5.5.1.1 Calculation of the solute flux at the surface of the plate** The flux of solute diffusing at any location  $y$  for the situation shown in Figure 5.2 is given by Equation 5.43 for this one-dimensional problem. Assuming we also have a dilute solution, then Equation 5.43 at the plate surface becomes

$$N_{Ay} \Big|_{y=0} = -D_{AB} \frac{dC_A}{dy} \Big|_{y=0} \quad (5.56)$$

We can find  $\frac{\partial C_A}{\partial y} \Big|_{y=0}$  by differentiating Equation 5.54 with respect to  $y$  and evaluating this result at  $y = 0$ . We find for this case that

$$N_{Ay} \Big|_{y=0} = \frac{(C_{AS} - C_{A0}) D_{AB}}{\sqrt{\pi D_{AB} t}} \quad (5.57)$$

If  $C_{AS} > C_{A0}$ , then the diffusion flux is from the surface of the plate into the medium. Letting  $S$  be the area normal to the  $y$  direction, the total amount of solute taken up by the medium at any time  $t$ , i.e.,  $M(t)$ , can be found by integrating Equation 5.57 with respect to time. The result is given by

$$M(t) = S \int_0^t N_A \Big|_{y=0} dt = 2(C_{AS} - C_{A0}) S \left( \frac{D_{AB} t}{\pi} \right)^{1/2} \quad (5.58)$$

If  $C_{AS} < C_{A0}$ , then the diffusion flux is from the medium to the surface of the plate. In this case, Equation 5.57 still applies; however, the flux will carry a negative sign because the direction of this flux is opposite to the  $y$  direction. The total amount of solute removed from the medium in this case is still given by Equation 5.58, with the understanding that the negative sign in this case represents loss of the solute from the medium to the surface.

## 5.5.2 Solution for the concentration profile for diffusion from a planar source into an infinite stagnant medium

Now consider in Figure 5.3 that the surface at  $y = 0$  initially contains a finite amount of solute A contained within an infinitesimally thin planar volume at  $y = 0$ . As time progresses, solute A spreads

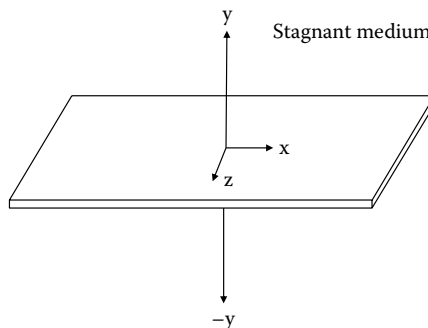


Figure 5.3 A very thin planar surface of area  $S$  containing a finite amount of solute A surrounded by a stagnant medium.

by diffusion into the stagnant medium, and in this case, we let the medium be symmetrical about the plane  $y = 0$ , so this means the medium now extends in both the  $+y$  and the  $-y$  directions.

Once again we can use Fick's second law to describe this one-dimensional diffusion of solute A into the medium.

$$\frac{\partial C_A}{\partial t} = D_{AB} \frac{\partial^2 C_A}{\partial y^2} \quad (5.59)$$

The initial condition and the boundary conditions are given next. Here, we assume that solute A is not present initially in the surrounding medium.

$$\begin{aligned} IC: \quad & t = 0, \quad C_A = 0 \\ BC1: \quad & y = \infty, \quad C_A = 0 \\ BC2: \quad & y = -\infty, \quad C_A = 0 \end{aligned} \quad (5.60)$$

The following equation can be shown to be a general solution to [Equation 5.59](#):

$$C_A(y,t) = \frac{N}{\sqrt{t}} \exp\left(-\frac{y^2}{4D_{AB}t}\right) \quad (5.61)$$

In [Equation 5.61](#), N is an arbitrary constant, and we also note that this solution is symmetrical about the plane  $y = 0$  and tends to zero as  $y$  goes to infinity in either the  $+y$  or  $-y$  directions.

Letting S denote the surface area normal to the  $y$  direction, the total amount of solute A in the medium at time  $t$ , i.e.,  $M(t)$ , is given by

$$M(t) = S \int_{-\infty}^{\infty} C_A(y,t) dy \quad (5.62)$$

Substituting [Equation 5.61](#) into [Equation 5.62](#) for  $C_A(y,t)$ , we obtain

$$M(t) = \frac{SN}{\sqrt{t}} \int_{-\infty}^{\infty} \exp\left(-\frac{y^2}{4D_{AB}t}\right) dy \quad (5.63)$$

Now in [Equation 5.63](#), we let  $z^2 = \frac{y^2}{4D_{AB}t}$ , which also gives  $dy = 2\sqrt{D_{AB}t}dz$ , and substituting these relationships into [Equation 5.63](#), we have

$$M(t) = 2SN\sqrt{D_{AB}} \int_{-\infty}^{\infty} \exp(-z^2) dz \quad (5.64)$$

The integral term in [Equation 5.64](#) is a form of the Gaussian integral and is equal to  $\sqrt{\pi}$ . Therefore, [Equation 5.64](#) becomes

$$M(t) = 2SN\sqrt{\pi D_{AB}} \quad (5.65)$$

[Equation 5.65](#) gives the interesting result that the amount of solute A within the medium at any time  $t$  is a constant and must therefore be equal to the original amount deposited on the area  $S$  on the plane at  $y = 0$ , i.e.,  $M_0$ . This means that we can use [Equation 5.65](#) to solve for the value of the arbitrary constant we denoted earlier by  $N$  in [Equation 5.61](#), which gives  $N = \frac{M_0}{2S\sqrt{\pi D_{AB}t}}$ , and with this result, [Equation 5.61](#) becomes

$$C_A(y, t) = \frac{M_0}{2S\sqrt{\pi D_{AB}t}} \exp\left(-\frac{y^2}{4D_{AB}t}\right) \quad (5.66)$$

[Equation 5.66](#) is also known as a Gaussian distribution and gives the concentration of solute A in the medium for any value of  $y$  and  $t$ . The total width of the distribution will broaden with time, and we let  $\delta_C$  represent the distance into the medium to which the solute has just penetrated; hence,

$$\delta_C = 4\sqrt{D_{AB}t} \quad (5.67)$$

### 5.5.3 Solution for the concentration profile for diffusion from a point source into an infinite planar stagnant medium

Now let us consider the solution for the diffusion of a solute from a point source on the planar surface of an infinite stagnant medium, which is shown in [Figure 5.4](#). In a Cartesian coordinate system, this planar surface exists at  $z = 0$  and extends in both the  $-x$ ,  $x$  and  $-y$ ,  $y$  directions. The point source, defined at  $x = 0$  and  $y = 0$ , initially contains a finite amount of solute A deposited upon an infinitesimally small area. We define  $C_A$  as the amount of solute A per unit surface area. As time progresses, solute A spreads by diffusion into the plane of the stagnant medium in both the  $-x$ ,  $x$  and  $-y$ ,  $y$  directions.

We can write Fick's second law in two dimensions for a dilute solution to describe the diffusion of solute A into the surrounding planar medium.

$$\frac{\partial C_A}{\partial t} = D_{AB} \left( \frac{\partial^2 C_A}{\partial x^2} + \frac{\partial^2 C_A}{\partial y^2} \right) \quad (5.68)$$

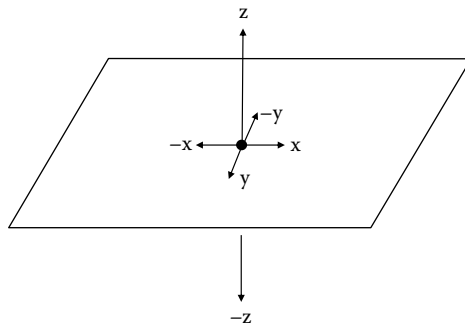


Figure 5.4 Diffusion from a point source located at  $(0,0,0)$  on an infinite planar surface at  $z = 0$ .

The initial condition and the boundary conditions are given next. Here, we assume that solute A is not present initially in the surrounding medium.

$$\begin{aligned} \text{IC: } & t = 0, \quad C_A = 0 \\ \text{BC1: } & x = \infty, \quad C_A = 0 \\ \text{BC2: } & x = -\infty, \quad C_A = 0 \\ \text{BC3: } & y = \infty, \quad C_A = 0 \\ \text{BC4: } & y = -\infty, \quad C_A = 0 \end{aligned} \quad (5.69)$$

The following equation is a general solution to [Equation 5.68](#), i.e.,

$$C_A(x, y, t) = \frac{N}{t} \exp\left(-\frac{x^2 + y^2}{4D_{AB}t}\right) \quad (5.70)$$

where we let N be an arbitrary constant.

The total amount of solute A in the medium at time t, i.e., M(t), is given by

$$M(t) = \int_{-\infty}^{\infty} \int_{-\infty}^{\infty} C_A(x, y, t) dx dy \quad (5.71)$$

Substituting [Equation 5.70](#) into [Equation 5.71](#) for C<sub>A</sub>(x, y, t), and integrating, we obtain

$$M(t) = 4\pi ND_{AB} \quad (5.72)$$

[Equation 5.72](#) shows that the amount of solute A within the medium at any time t is a constant and must therefore be equal to the original amount deposited at the point source located at x = 0 and y = 0, i.e., M<sub>0</sub>. Hence, we have that N =  $\frac{M_0}{4\pi D_{AB}}$ , and using this result, [Equation 5.70](#) becomes

$$C_A(r, t) = \frac{M_0}{4\pi D_{AB}t} \exp\left(-\frac{r^2}{4D_{AB}t}\right) \quad (5.73)$$

where r is the radial distance from the point source, i.e.,  $r = \sqrt{x^2 + y^2}$ .

### Example 5.5

An interesting application of [Equation 5.73](#) is its use to describe the dispersal of an insect population (Kareiva, 1983). As we have been discussing, diffusion is the result of the random motion of molecules, and molecules will tend to spread from a region of high concentration to a region of lower concentration. The same can be said about the movement of an insect population. Insects will move in a random walk from where they are at a high concentration to a location where their numbers are lower. This random walk of an insect population can be shown to be described by Fick's second law of diffusion (Phillips et al., 2013). In this case,

we let  $C_A$  represent the population density, i.e., the number of insects per unit area, and  $D_{AB}$  is the insect diffusivity.  $M_0$  represents the initial number of insects at the point source. Suppose 1000 *Trirhabda virgata*, a leaf beetle, are placed on a goldenrod. Kareiva (1983) gives a diffusivity for this beetle of  $0.41 \text{ m}^2 \text{ day}^{-1}$ . After 14 days, what radial distance from the point source on the goldenrod will contain 95% of these beetles? Assume that all of the beetles are still alive.

### Solution

The number of beetles confined within a circle of radius  $R$  at some time  $t$  is given by

$$M(R,t) = 2\pi \int_0^R C_A(r,t) r dr$$

When [Equation 5.73](#) is substituted into the previous equation, we obtain after integration

$$M(R,t) = M_0 \left( 1 - e^{-\frac{R^2}{4D_{AB}t}} \right) \quad (\text{A})$$

[Equation A](#) can then be solved for  $R$ :

$$R = \sqrt{4D_{AB}t} \left\{ -\ln \left[ 1 - \frac{M(R,t)}{M_0} \right] \right\}^{1/2}$$

With  $\frac{M(R,t)}{M_0} = 0.95$  and  $D_{AB} = 0.41 \text{ m}^2 \text{ day}^{-1}$ , we can solve the above equation for the value of  $R$  at 14 days:

$$R = \sqrt{4 \times 0.41 \text{ m}^2 \text{ day}^{-1} \times 14 \text{ days}} \times \left\{ -\ln(1 - 0.95) \right\}^{1/2} = 8.29 \text{ m}$$

## 5.6 The mass transfer coefficient

The solution of many diffusion problems is facilitated through the use of the *mass transfer coefficient*,  $k_m$ . This is especially true for problems where there is both convection and diffusion, which means the solute is diffusing through a fluid that is also flowing.

The mass transfer coefficient is used to calculate the solute flux at the surface of a boundary and was defined earlier by [Equation 5.22](#):

$$N_{Ay} \Big|_{y=0} = -D_{AB} \frac{dC_A}{dy} \Big|_{y=0} = k_m (C_A \Big|_{y=0} - C_{A \text{ bulk}}) = k_m (C_{AS} - C_{A \text{ bulk}}) \quad (5.74)$$

The mass transfer coefficient, i.e.,  $k_m$ , can be thought of as the proportionality constant that relates the flux of the solute at a boundary surface, i.e.,  $N_{Ay}|_{y=0}$ , to the overall concentration driving force,

i.e.,  $(C_A|_{y=0} - C_{A\text{ bulk}}) = (C_{AS} - C_{A\text{ bulk}})$ , where  $C_{AS}$  is the solute concentration at the surface and  $C_{A\text{ bulk}}$  is the solute concentration in the flowing medium.

The total mass transfer rate of the solute from a surface, i.e.,  $\dot{m}_A$ , is given by the product of the solute flux, i.e.,  $k_m (C_{AS} - C_{A\text{ bulk}})$ , and the surface area normal to that solute flux, i.e.,  $S$ :

$$\dot{m}_A = k_m S (C_{AS} - C_{A\text{ bulk}}) \quad (5.75)$$

The solution of most mass transfer problems will begin with [Equation 5.75](#) and involves solving for one of the variables in this equation.

### 5.6.1 The Sherwood number

The mass transfer coefficient is usually expressed in terms of the dimensionless group known as the *Sherwood number* ( $Sh$ ). The Sherwood number is the ratio of the transport rate of the solute by convection to that by diffusion and is defined as  $Sh = \frac{k_m L}{D_{AB}}$ , where  $L$  is a characteristic length. For example, for convective mass transfer within a cylindrical tube, the characteristic length is the tube diameter,  $d_{\text{tube}}$ .

The mass transfer coefficient, and hence the Sherwood number, is usually found from engineering correlations that are based on mass transfer experiments. However, there are special situations where an analytical solution for the mass transfer coefficient and the Sherwood number can be obtained. These situations usually have well-defined geometries and laminar flow of the fluid. We will now take a closer look at several situations where an analytical solution can be found for the mass transfer coefficient and the Sherwood number.

## 5.7 Diffusion from a flat plate into a semi-infinite stagnant medium

Recall the problem considered in [Section 5.5.1](#), i.e., solute diffusion from a flat plate into a semi-infinite stagnant medium shown in [Figure 5.2](#). [Equation 5.57](#) gave the flux of solute A at the surface of the flat plate as

$$N_{Ay}|_{y=0} = \frac{(C_{AS} - C_{A0}) D_{AB}}{\sqrt{\pi D_{AB} t}} \quad (5.76)$$

Comparing [Equation 5.76](#) with [Equation 5.74](#), and recognizing that  $(C_A|_{y=0} - C_{A\text{ bulk}}) = (C_{AS} - C_{A0})$ , we see that the mass transfer coefficient is then given by

$$k_m = \frac{D_{AB}}{\sqrt{\pi D_{AB} t}} = \frac{4 D_{AB}}{\sqrt{\pi \delta_C(t)}} \quad (5.77)$$

where we recall from [Equation 5.55](#) that  $\delta_C(t) = 4\sqrt{D_{AB}t}$ . For this unsteady diffusion problem shown in [Figure 5.2](#), we see that the mass transfer coefficient is not constant but decreases as the concentration boundary layer thickness, i.e.,  $\delta_C(t)$ , increases over time.

### 5.7.1 Film theory

From [Equation 5.77](#), we also see that the mass transfer coefficient is directly proportional to the solute diffusivity and inversely proportional to the concentration boundary layer thickness.

This shows us that the mass transfer coefficient can be thought of as the solute diffusivity divided by the thickness of a thin film of the medium over which the concentration change occurs, i.e.,  $(C_A|_{y=0} - C_{A \text{ bulk}}) = (C_{AS} - C_{A0})$ . Hence, this so-called *film theory* of diffusion says that the mass transfer coefficient is given by

$$k_m = \frac{D_{AB}}{\delta_{\text{film}}} \quad (5.78)$$

where in this case for the diffusion of the solute from a flat plate into a stagnant medium, the film thickness, i.e.,  $\delta_{\text{film}}$ , from [Equation 5.77](#) is equal to  $\frac{1}{4}\sqrt{\pi}\delta_C(t)$ .

The film thickness will depend on the geometry and the physical properties of the medium through which the solute is diffusing and will be affected by the bulk flow of the medium. Recall from laminar boundary layer flow over a flat plate that the boundary layer thickness, i.e.,  $\delta(x)$ , is inversely proportional to the square root of the local Reynolds number (see [Equation 4.73](#)). Hence, we would expect that as the bulk flow rate, or the free stream velocity, increases, which gives a higher Reynolds number, the film thickness ( $\delta_{\text{film}}$ ) should decrease in a manner similar to that of the momentum boundary layer thickness. This will increase the mass transfer coefficient and, by [Equation 5.75](#), the solute mass transfer rate. This will be shown to be the case when we look at mass transfer in laminar boundary flow over a flat plate in [Section 5.9.3](#).

Although film theory gives us some insight into the nature of the mass transfer coefficient, it really just lumps everything into a new unknown quantity, the film thickness.

#### Example 5.6

Calculate the value of the mass transfer coefficient for the situation described in [Example 5.3](#).

#### Solution

Using [Equation 5.77](#), and the concentration boundary layer thickness of 0.0126 cm after 1 s of contact, we can calculate the mass transfer coefficient as shown below:

$$k_m = \frac{D_{AB}}{\sqrt{\pi D_{AB} t}} = \frac{4D_{AB}}{\sqrt{\pi \delta_C(t)}} = \frac{4 \times 10^{-5} \text{ cm}^2 \text{ s}^{-1}}{\sqrt{\pi \times 0.0126 \text{ cm}}} = 0.0018 \text{ cm s}^{-1}$$

#### Example 5.7

A flat plate is coated with a layer of a volatile material. Air flows along the surface of the plate. After 12 days, it is found that the thickness of the layer of volatile material has decreased by 1 mm. Estimate the mass transfer coefficient and the mass transfer film thickness. The saturation concentration of the volatile material in air for these conditions is  $1.85 \times 10^{-9} \text{ mol cm}^{-3}$ , and its diffusivity in air is  $0.068 \text{ cm}^2 \text{ s}^{-1}$ . The density of the volatile material as coated on the flat plate is  $1.21 \text{ g cm}^{-3}$ , and its MW is 140.2.

**Solution**

We assume that the evaporation of the volatile material from the plate surface does not affect the mass transfer process. Also, the concentration of the volatile material in the bulk air is negligible in comparison to the saturation concentration. The mass transfer rate of the volatile material is then given by [Equation 5.75](#), i.e.,

$$\dot{m}_A = k_m S(C_{AS} - 0) \quad (\text{A})$$

In this case, we can choose as a basis for our calculation that  $S = 1 \text{ cm}^2$  of the plate surface. Over the 12-day period of time, we lose 1 mm of volatile material from the plate surface; hence, the mass of volatile material that is lost from the surface of the plate is given by the product of the volume of this lost material and its density, i.e.,

$$M_{\text{lost}} = 1 \text{ mm} \times S \times \rho = 1 \text{ mm} \times \frac{1 \text{ cm}}{10 \text{ mm}} \times 1 \text{ cm}^2 \times 1.21 \text{ g cm}^{-3} = 0.121 \text{ g}$$

The mass transfer rate is then given by the mass lost divided by the length of time:

$$\dot{m}_A = \frac{M_{\text{lost}}}{12 \text{ days}} = \frac{0.121 \text{ g}}{12 \text{ days} \times 24 \text{ h day}^{-1} \times 3600 \text{ s h}^{-1}} = 1.167 \times 10^{-7} \text{ g s}^{-1}$$

We can then calculate the value of  $k_m$  from [Equation A](#):

$$k_m = \frac{\dot{m}_A}{S(C_{AS} - 0)} = \frac{1.167 \times 10^{-7} \text{ g s}^{-1}}{1 \text{ cm}^2 \times 1.85 \times 10^{-9} \text{ mol cm}^{-3} \times 140.2 \text{ g mol}^{-1}} = 0.45 \text{ cm s}^{-1}$$

The film thickness is then given by

$$\delta_{\text{film}} = \frac{D_{AB}}{k_m} = \frac{0.068 \text{ cm}^2 \text{ s}^{-1}}{0.45 \text{ cm s}^{-1}} = 0.15 \text{ cm} = 1.5 \text{ mm}$$

## 5.8 Mass transfer from the surface of a sphere into an infinite quiescent medium

Next, we will determine the mass transfer coefficient and the Sherwood number for the steady-state transport of a solute from the surface of a sphere into a quiescent medium. The concentration of the solute at the surface of the sphere is given by  $C_{AS}$ , and its concentration far from the surface of the sphere is  $C_{A\infty}$ . We can use Fick's second law given by [Equation 5.47](#) for a dilute solution, which says for this steady-state situation that  $\nabla^2 C_A = 0$ . Using [Equation 5.50](#) to express the Laplacian of  $C_A$  in spherical coordinates, and recognizing that diffusion is only in the radial direction, we get the following differential equation for the solute concentration ( $C_A$ ) in the fluid surrounding the sphere:

$$\frac{d}{dr} \left( r^2 \frac{dC_A}{dr} \right) = 0 \quad (5.79)$$

The boundary conditions for the previous equation are

$$\begin{aligned} BC1: \quad r = R, \quad C_A = C_{AS} \\ BC2: \quad r = \infty, \quad C_A = C_{A\infty} \end{aligned} \quad (5.80)$$

If the differential equation given by [Equation 5.79](#) is integrated twice, we then obtain

$$C_A(r) = -\frac{C_1}{r} + C_2 \quad (5.81)$$

Applying the boundary conditions to this equation allows us to find the integration constants  $C_1$  and  $C_2$ . Hence, it is easily shown that  $C_2 = C_{A\infty}$  and  $C_1 = R(C_{A\infty} - C_{AS})$ . With these constants, the concentration profile and its first derivative in the fluid surrounding the sphere are given by

$$\begin{aligned} C_A(r) &= C_{A\infty} - (C_{A\infty} - C_{AS}) \frac{R}{r} \\ \frac{dC_A}{dr} &= (C_{A\infty} - C_{AS}) \frac{R}{r^2} \end{aligned} \quad (5.82)$$

From [Equation 5.74](#), we can next write the solute flux at the surface of the sphere as

$$N_{Ar}\Big|_{r=R} = -D_{AB} \frac{dC_A}{dr} \Big|_{r=R} = k_m (C_{AS} - C_{A\infty}) \quad (5.83)$$

However, from [Equation 5.82](#),  $-\frac{dC_A}{dr} \Big|_{r=R} = \frac{C_{AS} - C_{A\infty}}{R}$ , and when this is substituted into [Equation 5.83](#) for  $\frac{dC_A}{dr} \Big|_{r=R}$ , we obtain the result that  $k_m = \frac{D_{AB}}{R}$ . When this result is rearranged with the characteristic length based on the sphere diameter ( $d_{sphere} = 2R$ ), we find that the Sherwood number is equal to 2 for the case of steady diffusion of a solute from the surface of a sphere into a quiescent fluid, i.e.,

$$Sh = \frac{k_m d_{sphere}}{D_{AB}} = 2 \quad (5.84)$$

### Example 5.8

A drug has an equilibrium solubility in water of  $1.5 \text{ g L}^{-1}$ . The diffusivity of the drug in water is  $0.6 \times 10^{-5} \text{ cm}^2 \text{ s}^{-1}$ . One gram of the drug is made into particles that are  $0.1 \text{ cm}$  in diameter, and these particles have a density of  $1.15 \text{ g cm}^{-3}$ . These particles are then vigorously mixed in a stirred vessel containing  $1 \text{ L}$  of water. After mixing for  $10 \text{ min}$ , the drug concentration in the solution was  $0.03 \text{ g L}^{-1}$ . Estimate the value of the mass transfer coefficient ( $\text{cm s}^{-1}$ ) for the drug under these conditions. Also find the Sherwood number ( $Sh$ ). Assume that the particle size does not change significantly during the  $10 \text{ min}$ .

### Solution

The concentration of the drug at the surface of the particles is equal to the equilibrium solubility of the drug in water, which is equal to  $1.5 \text{ g L}^{-1}$ . This is  $C_{AS}$  in [Equation 5.75](#). The concentration of the drug dissolved in the solution, i.e.,  $C_{A\text{bulk}}$ , starts at  $0 \text{ g L}^{-1}$  and increases after

10 min to 0.03 g L<sup>-1</sup>. Although C<sub>A bulk</sub> is changing with time, which means the mass transfer driving force, i.e., (C<sub>AS</sub> - C<sub>A bulk</sub>), is also changing with time, we can approximate C<sub>A bulk</sub> in [Equation 5.75](#) by the average of these values, or 0.015 g L<sup>-1</sup>, since C<sub>A bulk</sub> ≪ C<sub>AS</sub>. The total amount of drug that was dissolved over the 10 min period is equal to 0.03 g L<sup>-1</sup> × 1 L = 0.03 g. The average dissolution rate is therefore 0.03 g of drug in 10 min or 5.0 × 10<sup>-5</sup> g s<sup>-1</sup>. The dissolution rate of the drug (m<sub>A</sub>) is then given by [Equation 5.75](#), where the total area available for mass transfer is equal to the number of particles in the solution (N<sub>particles</sub>) times the surface area of a single particle (S<sub>particle</sub>).

$$\dot{m}_A = k_m N_{\text{particles}} S_{\text{particle}} (C_{\text{AS}} - C_{\text{A bulk}}) = k_m N_{\text{particles}} S_{\text{particle}} \times (1.5 - 0.015) \text{ g L}^{-1} = 5.0 \times 10^{-5} \text{ g s}^{-1}$$

The area of a single drug particle is given by 4πR<sup>2</sup>, where R is the particle radius. Hence, we find that S<sub>particle</sub> = 0.0314 cm<sup>2</sup>. The number of particles can be found by dividing the mass of drug placed into the solution by the drug density, which gives the total volume of particles, and then dividing this result by the volume of a given particle. When this is done, it is found that 1 g of the drug is equivalent to 1661 particles. With these parameters found, the previous equation can now be solved for the mass transfer coefficient as follows:

$$k_m = \frac{5.0 \times 10^{-5} \text{ g s}^{-1}}{1.485 \text{ g L}^{-1} \times \frac{1 \text{ L}}{1000 \text{ cm}^3}} \times \frac{1}{1661 \text{ particles} \times \frac{0.0314 \text{ cm}^2}{\text{particle}}} = 6.46 \times 10^{-4} \text{ cm s}^{-1}$$

The Sherwood number is calculated as

$$Sh = \frac{k_m d_{\text{particle}}}{D_{AB}} = \frac{6.46 \times 10^{-4} \text{ cm s}^{-1} \times 0.1 \text{ cm}}{0.6 \times 10^{-5} \text{ cm}^2 \text{ s}} = 10.76$$

In this case, the Sh is greater than 2 indicating that solute transport from the drug particles is a result of convection and diffusion.

### Example 5.9

In [Example 5.8](#), the concentration of drug dissolved in the solution, i.e., C<sub>A bulk</sub>, starts at 0 g L<sup>-1</sup> and increases after 10 min to 0.03 g L<sup>-1</sup>. Thus, C<sub>A bulk</sub> is changing with time, which means the mass transfer driving force, i.e., (C<sub>AS</sub> - C<sub>A bulk</sub>), is also changing with time. However, in [Example 5.8](#), we approximated C<sub>A bulk</sub> in [Equation 5.75](#) by the average of the initial bulk concentration and the value at 10 min, or 0.015 g L<sup>-1</sup>, since C<sub>A bulk</sub> was much smaller than C<sub>AS</sub>. Compare the results obtained in [Example 5.8](#) to a rigorous solution that accounts for the changing bulk concentration of the solute.

### Solution

We assume that the particle size does not change significantly over the course of the 10 min. We can then write the following unsteady mass balance on the solute dissolved in the bulk fluid phase using [Equation 1.8](#) as a guide. In this case, the accumulation of solute mass in the bulk solution is equal to the solute mass transfer rate.

$$V_{\text{bulk}} \frac{dC_{\text{A bulk}}}{dt} = N_{\text{particles}} S_{\text{particle}} k_m (C_{\text{AS}} - C_{\text{A bulk}})$$

The previous equation can be rearranged and integrated to obtain an expression for the mass transfer coefficient as shown next:

$$k_m = -\frac{1}{t} \left( \frac{V_{bulk}}{N_{particles} S_{particle}} \right) \ln \left( \frac{C_{AS} - C_{A bulk}(t)}{C_{AS}} \right) \quad (A)$$

Substituting in the values of the parameters in [Equation A](#):

$$k_m = -\frac{1}{10 \text{ min} \times 60 \text{ s min}^{-1}} \left( \frac{1000 \text{ cm}^3}{1661 \times 0.0314 \text{ cm}^2} \right) \ln \left( \frac{1.5 - 0.03}{1.5} \right)$$

$$k_m = 6.46 \times 10^{-4} \text{ cm s}^{-1}$$

We see that the rigorous solution that accounts for the changing bulk solute concentration gives the same result for the mass transfer coefficient that was found in [Example 5.8](#). This is because when  $C_{A bulk} \ll C_{AS}$ , the two solutions can be shown to be the same. In [Example 5.8](#), we expressed the mass transfer rate of the solute as

$$\dot{m}_A = \frac{V_{bulk} C_{A bulk}(t)}{t} = k_m N_{particles} S_{particle} (C_{AS} - C_{A bulk}(t)) \approx k_m N_{particles} S_{particle} C_{AS}$$

which can be solved for the mass transfer coefficient:

$$k_m = \frac{1}{t} \left( \frac{V_{bulk}}{N_{particles} S_{particle}} \right) \frac{C_{A bulk}(t)}{C_{AS}} \quad (B)$$

In [Equation A](#), when  $C_{A bulk} \ll C_{AS}$ , then  $\ln \left( \frac{C_{AS} - C_{A bulk}(t)}{C_{AS}} \right) \approx -\frac{C_{A bulk}(t)}{C_{AS}}$ , and when this result is substituted into [Equation A](#) for the natural log term, we then get [Equation B](#), showing that the two solutions are equivalent when  $C_{A bulk} \ll C_{AS}$ .

### Example 5.10

If the drug particles in [Example 5.8](#) are placed in a very large volume of water and gently mixed, how long will it take for them to totally dissolve into the bulk solution?

#### Solution

In this case, the gentle mixing of the particles means that the Sherwood number is equal to 2. Also, since the particles are placed in a large volume of water, we can assume that  $C_{A bulk} \sim 0$ . Using [Equation 1.8](#) as a guide, and [Equation 5.75](#) as the rate of mass transfer from the particle surface, we can write an unsteady mass balance on a drug particle:

$$\frac{dM_{particle}}{dt} = \rho_{particle} \frac{dV_{particle}}{dt} = -k_m S_{particle} (C_{AS} - C_{A bulk}) = -k_m S_{particle} C_{AS} \quad (A)$$

Next, assuming a spherical particle, we let  $S_{\text{particle}} = 4\pi R^2$  and  $V_{\text{particle}} = \frac{4}{3}\pi R^3$ . Also, since  $\text{Sh} = 2$ , we also have that  $k_m = \frac{D_{AB}}{R}$ . We also recognize in this problem that  $R$  depends on time. Substituting these previous relationships into [Equation A](#), we get

$$\frac{dR}{dt} = -\frac{D_{AB}}{\rho_{\text{particle}} R} C_{AS} \quad (\text{B})$$

With the initial condition that at  $t = 0$ ,  $R = R_0$ , we can integrate [Equation B](#) for the dissolution time, which is when  $R$  becomes equal to zero.

$$t_{\text{dissolution}} = \frac{\rho_{\text{particle}} R_0^2}{2C_{AS} D_{AB}}$$

Using the data given in [Example 5.8](#), we then calculate the dissolution time for the drug particles as

$$t_{\text{dissolution}} = \frac{1.15 \text{ g cm}^{-3} \times 0.05^2 \text{ cm}^2}{2 \times 0.0015 \text{ g cm}^{-3} \times 0.6 \times 10^{-5} \text{ cm}^2 \text{ s}^{-1}} = 1.6 \times 10^5 \text{ s} = 44.4 \text{ h}$$

### 5.8.1 Mass transfer between the surface of a sphere and a flowing fluid

If the relative velocity between the sphere and fluid is  $v_\infty$ , then the Sherwood number will be greater than 2. In this case, it has been found that the Sherwood number is given by

$$\text{Sh} = \frac{k_m d_{\text{sphere}}}{D_{AB}} = 2.0 + 0.6 \left( \frac{\rho d_{\text{sphere}} v_\infty}{\mu} \right)^{1/2} \left( \frac{\mu}{\rho D_{AB}} \right)^{1/3} = 2.0 + 0.6 \text{Re}^{1/2} \text{Sc}^{1/3} \quad (5.85)$$

where  $\text{Sc} = \frac{v}{D_{AB}} = \frac{\mu}{\rho D_{AB}}$  is a dimensionless number known as the *Schmidt number*. The Schmidt number is the ratio of momentum diffusivity ( $v = \frac{\mu}{\rho}$ ) to the mass diffusivity, i.e.,  $D_{AB}$ . For solutes diffusing through liquids, the Schmidt number is much greater than unity, and for solutes diffusing through gases, the Schmidt number is on the order of unity.

## 5.9 Solute transport by convection and diffusion

Now we will consider several examples where we can obtain an analytical solution for mass transfer problems where there is both convection and diffusion of the solute. In all of these problems, the fluid is in laminar flow. The mass transfer coefficient for situations involving the much more complex nature of turbulent flow needs to be found from experimental data.

### 5.9.1 Solute mass transfer from a gas into a falling liquid film: short contact time solution

Consider the situation shown in [Figure 5.5](#) for the diffusion of a gas into a falling liquid film. Here, we have a thin liquid film that flows in laminar flow down a flat vertical surface of width  $W$  in the  $y$  direction. One side of this liquid film wets the surface of the plate and the other side of the film is exposed to a gas containing solute A, which is only sparingly soluble in the liquid.

To analyze the mass transfer of solute A into the liquid film, we perform a steady-state mass balance on the small shell volume given by  $\Delta x \Delta z W$ . We also neglect any entrance and exit effects and assume the film thickness, i.e.,  $\delta$ , at any value of  $z$ , is constant. In this case, we also recognize that the solute flux relative to stationary coordinates has the following two components, i.e.,  $N_{Ax}$  and  $N_{Az}$ .

With these conditions, we can write our solute A mass balance as

$$W\Delta x N_{Az}|_z - W\Delta x N_{Az}|_{z+\Delta z} + W\Delta z N_{Ax}|_x - W\Delta z N_{Ax}|_{x+\Delta x} = 0 \quad (5.86)$$

Now, if we divide through by  $\Delta x \Delta z W$  and take the limits as  $\Delta x$  and  $\Delta z$  become infinitesimally small, we then obtain

$$\frac{\partial N_{Az}}{\partial z} + \frac{\partial N_{Ax}}{\partial x} = 0 \quad (5.87)$$

Next, we make some reasonable assumptions that will lead us to an analytical solution to this problem. First, we seek a solution in which solute A has only penetrated a short distance into the liquid film, i.e., the penetration distance is much less than the thickness of the film. This will also be the region of the film where the velocity is pretty much equal to the maximum film velocity, which is at the film surface, so we can let  $v_z(x) = v_{max}$ . This is also known as a *short contact time solution* since the exposure time of the liquid film to the gas over a given length  $L$ , i.e.,  $L/v_{max}$ , is small.

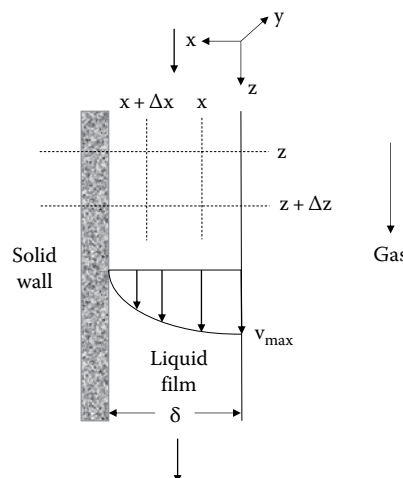


Figure 5.5 Diffusion from a gas into a falling liquid film.

Since the penetration depth of the solute for any value of  $z$  is much less than the film thickness, the short contact time solution means that the diffusion of the solute is unaffected by the presence of the wall at  $x = \delta$ . In other words, the solute does not “know” how thick the liquid film really is. So, this means that we can replace the boundary condition at  $x = \delta$  with the condition that at  $x = \infty, C_A = 0$ .

Because the film is flowing in the  $z$  direction, we also expect that the transport of solute A will be greater in that direction by convection than by diffusion. For example, the amount of solute A being carried along by the bulk flow of the fluid is on the order of  $v_{\max} C_A$ , and the amount of diffusion in the  $z$  direction over the length  $L$  is on the order of  $\frac{D_{AB}C_A}{L}$ . The ratio of these two quantities is known as the *Peclet number* ( $Pe$ ), which is a dimensionless number. If  $Pe = \frac{v_{\max}L}{D_{AB}} \gg 1$ , then we can ignore axial diffusion in comparison to axial convection. This means that we can use [Equation 5.15](#) and write that  $N_{Az} = C_A v_z(x) = C_A v_{\max}$ . Since solute A is also sparingly soluble in the liquid film, we have by [Equation 5.18](#) that  $N_{Ax} = -D_{AB} \frac{\partial C_A}{\partial x}$ . Substituting these for  $N_{Az}$  and  $N_{Ax}$  in [Equation 5.87](#), we obtain

$$v_{\max} \frac{\partial C_A}{\partial z} = D_{AB} \frac{\partial^2 C_A}{\partial x^2} \quad (5.88)$$

The solution to [Equation 5.88](#) is subject to the following boundary conditions:

$$\begin{aligned} BC1: \quad & z = 0, \quad C_A = 0 \\ BC2: \quad & x = 0, \quad C_A = C_{AS} \\ BC3: \quad & x = \infty, \quad C_A = 0 \end{aligned} \quad (5.89)$$

where we have assumed that there is no solute A in the entering liquid film and we let  $C_{AS}$  equal the equilibrium solubility of solute A in the liquid film.

Now, to obtain a solution to [Equations 5.88](#) and [5.89](#), let us first transform the  $z$  direction into time. We can do this by defining  $t$  as the time it takes for an element of fluid in the film to reach a position  $z$ ; hence,  $t = z/v_{\max}$ . Hence, we have that  $z = v_{\max} t$  and  $dz = v_{\max} dt$ , and we can transform [Equations 5.88](#) and [5.89](#) as follows:

$$\frac{\partial C_A}{\partial t} = D_{AB} \frac{\partial^2 C_A}{\partial x^2} \quad (5.90)$$

with

$$\begin{aligned} BC1: \quad & t = 0, \quad C_A = 0 \\ BC2: \quad & x = 0, \quad C_A = C_{AS} \\ BC3: \quad & x = \infty, \quad C_A = 0 \end{aligned} \quad (5.91)$$

[Equations 5.90](#) and [5.91](#) are identical to the problem we solved earlier in [Section 5.5.1](#) for the diffusion of a solute from a planar surface into a semi-infinite stagnant medium. We can therefore use

the solution there, as given by [Equation 5.54](#), with  $C_{A0} = 0$  and replacing  $y$  with  $x$ , to obtain the following expression for the solute A concentration within the liquid film.

$$\frac{C_A(x,t)}{C_{AS}} = \operatorname{erfc}\left(\frac{x}{\sqrt{4D_{AB}t}}\right) = 1 - \operatorname{erf}\left(\frac{x}{\sqrt{4D_{AB}t}}\right) \quad (5.92)$$

In terms of  $x$  and  $z = v_{max} t$ , we can write [Equation 5.92](#) as

$$\frac{C_A(x,z)}{C_{AS}} = \operatorname{erfc}\left(\frac{x}{\sqrt{\frac{4D_{AB}z}{v_{max}}}}\right) \quad (5.93)$$

The maximum distance to which the solute has penetrated into the liquid film at the distance  $L$  is given by [Equation 5.55](#) where we now let  $t = L/v_{max}$ . Therefore, the maximum concentration boundary layer thickness is given by

$$\delta_C(L) = 3.642 \sqrt{\frac{D_{AB}L}{v_{max}}} \approx 4 \sqrt{\frac{D_{AB}L}{v_{max}}} \quad (5.94)$$

In [Example 5.9](#), we will show that the liquid film thickness  $\delta$  is given by the following equation:

$$\delta = \left( \frac{3 \mu Q}{\rho g W} \right)^{1/3} \quad (5.95)$$

where  $Q$  is the volumetric flow rate. If  $\delta_C(L) \ll \delta$ , then the short contact time solution is valid.

In a mass transfer problem such as this, we are also interested in knowing the solute mass transfer flux at the surface of the film, i.e., at  $x = 0$ , since by [Equation 5.74](#), this allows us to find the mass transfer coefficient. Hence, at the surface of the film, we have by [Equation 5.74](#)

$$N_{Ax}(z) \Big|_{x=0} = -D_{AB} \frac{\partial C_A}{\partial x} \Big|_{x=0} = k_m (C_{AS} - C_{A \text{ bulk}}) = k_m C_{AS} \quad (5.96)$$

since  $C_{A \text{ bulk}} = 0$ . Using [Equation 5.93](#) to find  $\frac{\partial C_A}{\partial x} \Big|_{x=0}$ , and substituting that result into [Equation 5.96](#), we obtain

$$N_{Ax}(z) \Big|_{x=0} = C_{AS} \sqrt{\frac{D_{AB}V_{max}}{\pi z}} = k_m C_{AS} \quad (5.97)$$

From [Equation 5.97](#), we then see that the mass transfer coefficient is given by

$$k_{m \text{ local}} = \sqrt{\frac{D_{AB}V_{max}}{\pi z}} \quad (5.98)$$

It is important to recognize that the value of the mass transfer coefficient given by [Equation 5.98](#) is a *local* value of the mass transfer coefficient since it depends on the value of  $z$ , which is the axial position in the direction of the film flow.

From [Equation 5.95](#), the volumetric flow rate of the liquid film is given by  $Q = \frac{\rho g W \delta^3}{3 \mu}$ . The average and maximum velocity of the liquid film are also given by

$$v_{\text{avg}} = \frac{Q}{\delta W} = \frac{\rho g \delta^2}{3 \mu} = \frac{2}{3} v_{\text{max}} \quad (5.99)$$

Using [Equation 5.99](#) to replace  $v_{\text{max}}$  with  $v_{\text{avg}}$  in [Equation 5.98](#) gives the following expression for the local value of the Sherwood number:

$$Sh_{\text{local}} = \frac{k_m \text{local} Z}{D_{AB}} = 0.69 \sqrt{\frac{v_{\text{avg}} Z}{D_{AB}}} \quad (5.100)$$

Over the entire liquid film surface of width  $W$  and length  $L$ , the total mass transfer rate of solute A that is transported from the gas into the liquid film is given by integrating the surface flux of solute A given by [Equation 5.97](#) over the entire surface:

$$\dot{m}_A = \iint_{0,0}^{W,L} N_{Ax} \Big|_{x=0} dz dy = WC_{AS} \sqrt{\frac{D_{AB} v_{\text{max}}}{\pi}} \int_0^L z^{-1/2} dz = 2LWC_{AS} \sqrt{\frac{D_{AB} v_{\text{max}}}{\pi L}} \quad (5.101)$$

Comparing this result to [Equation 5.75](#) with  $S = LW$ , we see that the average mass transfer coefficient and Sherwood number, i.e.,  $Sh = \frac{k_m L}{D_{AB}}$ , based on the total surface area, where  $S = LW$ , is given by

$$k_m = 2 \sqrt{\frac{D_{AB} v_{\text{max}}}{\pi L}} = 1.38 \sqrt{\frac{D_{AB} v_{\text{avg}}}{L}} \\ Sh = 1.38 \sqrt{\frac{v_{\text{avg}} L}{D_{AB}}} \quad (5.102)$$

### Example 5.11

Yoshida and Ohshima (1966) used a falling liquid film on the outside vertical surface of a cylindrical tube of outside diameter  $d$  to determine the diffusivity of oxygen in serum. Serum is the fluid portion of the blood that remains after the blood has clotted. They used [Equation 5.101](#) to find  $D_{AB}$  from the measured oxygen absorption rate, i.e.,  $\dot{m}_A$ . Analyze some of their data and find the value of  $D_{AB}$  for serum at 37°C.

### Solution

In order to understand how Yoshida and Ohshima (1966) analyzed their data, we first need to find the velocity profile for the laminar flow of a liquid film on a vertical surface. For the

situation shown in [Figure 5.5](#), we can write the following  $z$  momentum balance over a fluid shell volume of length  $L$  defined as  $\Delta x LW$ :

$$WL \tau_{xz}|_x - WL \tau_{xz}|_{x+\Delta x} + W\Delta x \rho v_z v_z|_{z=0} - W\Delta x \rho v_z v_z|_{z=L} + W\Delta x L \rho g = 0 \quad (\text{A})$$

The first and second terms in this equation represent the transport of  $z$  momentum in the  $x$  direction, recognizing that momentum is transported from a region of high velocity to that of lower velocity. The third and fourth terms represent the momentum of the fluid entering and leaving the shell volume by bulk flow. Since the velocity in the  $z$  direction for any value of  $x$  is the same at  $z = 0$  and at  $z = L$ , these terms cancel out. The last term is the force of gravity acting on the mass of fluid within the shell volume.

Now we divide [Equation A](#) by  $LW\Delta x$  and take the limit as  $\Delta x \rightarrow 0$  and obtain

$$\frac{d\tau_{xz}}{dx} = \rho g \quad (\text{B})$$

For a Newtonian fluid, we have that  $\tau_{xz} = -\mu \frac{dv_z}{dx}$ , and when this is substituted into [Equation B](#), we get

$$\frac{d^2v_z}{dx^2} = -\frac{\rho g}{\mu} \quad (\text{C})$$

[Equation C](#) is then integrated twice, and the following boundary conditions are used to find the integration constants:

$$\begin{aligned} \text{BC1: } x = 0, \quad & \frac{dv_z}{dx} = 0 \\ \text{BC2: } x = \delta, \quad & v_z = 0 \end{aligned} \quad (\text{D})$$

Using these boundary conditions, the velocity profile is

$$v_z(x) = \frac{\rho g \delta^2}{2 \mu} \left[ 1 - \left( \frac{x}{\delta} \right)^2 \right] \quad (\text{E})$$

Because we assume that the oxygen does not penetrate very far into the liquid film, i.e., the short contact time solution, the velocity in the region near  $x = 0$  is  $v_{\max}$ , which is then given by

$$v_{\max} = \frac{\rho g \delta^2}{2 \mu} \quad (\text{F})$$

The total volumetric flow, i.e.,  $Q$ , is given by integrating  $v_z(x)$ , i.e., [Equation E](#), over the area normal to the bulk flow:

$$Q = \iint_{0 \ 0}^{W \ L} v_z(x) dx dy = \frac{\rho g W \delta^3}{3 \mu} \quad (\text{G})$$

which is [Equation 5.95](#) given earlier.

The average film velocity is then given by

$$v_{\text{avg}} = \frac{Q}{W\delta} = \frac{\rho g \delta^2}{3\mu} = \frac{2}{3} v_{\text{max}} \quad (\text{H})$$

We then use [Equation G](#) to replace  $\delta$  in terms of  $Q$ , i.e.,  $\delta = \left( \frac{3\mu Q}{\rho g W} \right)^{1/3}$ , and for flow down the outside of a vertical tube of outside diameter  $d$ , where  $\delta$  is much smaller than  $d$ , we can let  $W = \pi d$ . Substituting these into [Equation F](#), we obtain

$$v_{\text{max}} = \frac{3}{2} \left( \frac{\rho g}{3\mu} \right)^{1/3} \left( \frac{Q}{\pi d} \right)^{2/3} \quad (\text{I})$$

Yoshida and Ohshima (1966) then defined the liquid film exposure time as  $t = L/v_{\text{max}} = LFQ^{-2/3}$ , where  $F$  is a constant defined as

$$F = \frac{2}{3} \left( \frac{3\mu}{\rho g} \right)^{1/3} (\pi d)^{2/3} \quad (\text{J})$$

Letting  $L/v_{\text{max}} = LFQ^{-2/3}$  in [Equation 5.101](#), we then obtain

$$\dot{m}_A = 2C_{AS}dL^{1/2}Q^{1/3} \sqrt{\frac{\pi D_{AB}}{F}} \quad (\text{K})$$

In a given experiment, if the data are plotted as  $\frac{\dot{m}_A^2}{Q^{2/3}}$  versus the length of the liquid film, i.e.,  $L$ , then [Equation K](#) says that the value of the oxygen diffusivity, i.e.,  $D_{AB}$ , can be obtained from the slope of this plot, i.e.,  $m = 4C_{AS}^2 d^2 \left( \frac{\pi D_{AB}}{F} \right)$ . Although their data showed the presence of entrance and exit effects, the slope is not affected by these entrance and exit effects, and there was a region where the data showed a constant slope, and from the slope of these data, the diffusivity can be found. For example, the table below presents some of their data for the transport of oxygen into a liquid film of ox serum. The solubility of oxygen in the serum at the gas-liquid interface, i.e.,  $C_{SA}$ , was equal to  $2.87 \times 10^{-5} \text{ g cm}^{-3}$ . The outside diameter of the vertical glass tube, i.e.,  $d$ , was 1.03 cm.

Length of Wetted Wall, $L, \text{ cm}$	Film Flow Rate, $Q,$ $\text{cm}^3 \text{ s}^{-1}$	Oxygen Absorption Rate, $\dot{m}_A, \text{ g s}^{-1}$	$\dot{m}_A^2/Q^{2/3},$ $\text{g}^2 \text{ cm}^{-2} \text{ s}^{-4/3}$
6.72	0.933	$2.73 \times 10^{-6}$	$7.81 \times 10^{-12}$
6.76	0.902	$2.87 \times 10^{-6}$	$8.82 \times 10^{-12}$
8.89	0.881	$4.19 \times 10^{-6}$	$1.91 \times 10^{-11}$
9.51	0.949	$4.65 \times 10^{-6}$	$2.24 \times 10^{-11}$
13.54	0.876	$5.84 \times 10^{-6}$	$3.73 \times 10^{-11}$
16.22	0.887	$6.92 \times 10^{-6}$	$5.19 \times 10^{-11}$
16.3	0.924	$7.22 \times 10^{-6}$	$5.49 \times 10^{-11}$

A linear regression of the data, i.e.,  $\dot{m}_A^2/Q^{2/3}$  versus  $L$ , in the previous table gave a slope ( $m$ ) of  $4.635 \times 10^{-12} \text{ g}^2 \text{ cm}^{-3} \text{ s}^{-4/3}$  and a correlation constant ( $r^2$ ) of 0.994 indicating an excellent fit to the data. Next, we calculate the value of  $F$  from [Equation J](#) using a value of the serum viscosity at  $37^\circ\text{C}$  of 1.01 cP. This gives  $F = 0.0458 \text{ cm sec}^{1/3}$ . Then, since the slope, i.e.,  $m = 4C_{AS}^2 d^2 \left( \frac{\pi D_{AB}}{F} \right)$ , we can calculate the value of  $D_{AB}$  as shown next:

$$D_{AB} = \frac{mF}{4\pi C_{AS}^2 d^2} = \frac{4.635 \times 10^{-12} \text{ g}^2 \text{ cm}^{-3} \text{ s}^{-4/3} \times 0.0458 \text{ cm sec}^{1/3}}{4\pi (2.87 \times 10^{-5} \text{ g cm}^{-3})^2 \times (1.03 \text{ cm})^2}$$

$$D_{AB} = 1.93 \times 10^{-5} \text{ cm}^2 \text{ s}^{-1}$$

The diffusivity of oxygen at  $37^\circ\text{C}$  in the fluid portion of blood is therefore on the order of  $1.9 \times 10^{-5} \text{ cm}^2 \text{ s}^{-1}$ . The value measured for the diffusivity of oxygen in water at  $37^\circ\text{C}$  by Yoshida and Ohshima (1966) using the same method was found to be  $2.76 \times 10^{-5} \text{ cm}^2 \text{ s}^{-1}$ .

**5.9.1.1 A general solution for gas absorption into a laminar falling liquid film** If the short contact time solution obtained previously is not valid, i.e.,  $\delta_C \sim \delta$ , then we have to assume that the solute concentration profile extends across the film thickness. In this case, we can use the following exact analytical solution obtained by Al-Malah (2013) to calculate the average mass transfer coefficient

$$Sh = \frac{k_m L}{D_{AB}} = \frac{8 \delta v_{avg}}{D_{AB}} \sum_{n=1}^{\infty} \frac{1}{\pi^2 (2n-1)^2} \left( 1 - e^{-\frac{(2n-1)^2 \pi^2 D_{AB} L}{4 v_{avg} \delta^2}} \right) \quad (5.103)$$

where in this case the mass transfer rate is defined as  $\dot{m}_A = k_m L W (C_{AS} - C_{A0})$ .

### Example 5.12

A device for the oxygenation of plasma consists of 10 vertical plates with air flowing between the plates. The plates are 10 cm in width ( $W$ ) and 25 cm in length ( $L$ ). The air flow is sufficiently high so that we can assume the concentration of oxygen in the gas is constant. Plasma at  $37^\circ\text{C}$  containing no dissolved oxygen enters the oxygenator at a flow rate of  $1000 \text{ mL min}^{-1}$  and is evenly distributed to each side of each plate. The plasma flows down the surface of each side of the plate in laminar flow. The saturation concentration of oxygen in plasma is  $216 \mu\text{M}$ , the viscosity of the plasma is 1.2 cP, and the diffusivity of oxygen in the plasma is  $1.9 \times 10^{-5} \text{ cm}^2 \text{ s}^{-1}$ . Calculate the total oxygen transfer rate and estimate the maximum dissolved oxygen concentration ( $\mu\text{M}$ ) in the plasma as it leaves the oxygenator.

### Solution

We assume that the oxygen transport for each side of the vertical plates is the same and we neglect entrance and exit effects. We can calculate the oxygen transported into the plasma on one side of a plate and then multiply that value by 20 (2 sides per plate  $\times$  10 plates) to find how much oxygen was transported into the plasma. We then use an overall oxygen mass balance across the oxygenator to find the exiting dissolved oxygen concentration in the plasma.

First, we calculate the film thickness from [Equation 5.95](#) with the flow rate on one side of the plate equal to  $0.83 \text{ cm}^3 \text{ s}^{-1}$ .

$$\delta = \left( \frac{3 \mu Q}{\rho g W} \right)^{1/3} = \left( \frac{3 \times 1.2 \text{ cP} \times 0.01 \text{ g cm}^{-1} \text{ s}^{-1} \text{ cP}^{-1} \times 0.83 \text{ cm}^3 \text{ s}^{-1}}{1.024 \text{ g cm}^{-3} \times 980 \text{ cm s}^{-2} \times 10 \text{ cm}} \right)^{1/3} = 0.0144 \text{ cm}$$

Then, we calculate the average velocity of the liquid film from [Equation 5.99](#), which gives

$$v_{\text{avg}} = \frac{Q}{\delta W} = \frac{0.83 \text{ cm}^3 \text{ s}^{-1}}{0.0144 \text{ cm} \times 10 \text{ cm}} = 5.77 \text{ cm s}^{-1}$$

From [Equation 5.94](#), we can calculate the maximum solute boundary layer thickness for a  $v_{\text{max}} = 1.5v_{\text{avg}} = 8.66 \text{ cm sec}^{-1}$ .

$$\delta_C = 4 \sqrt{\frac{1.9 \times 10^{-5} \text{ cm}^2 \text{ s}^{-1} \times 25 \text{ cm}}{8.66 \text{ cm s}^{-1}}} = 0.03 \text{ cm}$$

Since  $\delta_C$  is greater than the actual film thickness, we need to calculate the mass transfer coefficient from [Equation 5.103](#). Here, we only need the first two terms since the series converges quickly:

$$\begin{aligned} Sh &= \frac{8 \times 0.0144 \text{ cm} \times 5.77 \text{ cm s}^{-1}}{1.9 \times 10^{-5} \text{ cm}^2 \text{ s}^{-1}} \\ &\times \left[ \frac{1}{\pi^2} \left( 1 - e^{-\frac{\pi^2 \times 1.9 \times 10^{-5} \text{ cm}^2 \text{ s}^{-1} \times 25 \text{ cm}}{4 \times (0.0144 \text{ cm})^2}} \right) + \frac{1}{9\pi^2} \left( 1 - e^{-\frac{9\pi^2 \times 1.9 \times 10^{-5} \text{ cm}^2 \text{ s}^{-1} \times 25 \text{ cm}}{4 \times (0.0144 \text{ cm})^2}} \right) \right] = 3927.3 \end{aligned}$$

The average mass transfer coefficient over one side of the plate of area  $LW$  is then given by

$$k_m = \frac{Sh D_{AB}}{L} = \frac{3927.3 \times 1.9 \times 10^{-5} \text{ cm}^2 \text{ s}^{-1}}{25 \text{ cm}} = 0.003 \text{ cm s}^{-1}$$

And the mass transfer rate of oxygen into the liquid film of plasma on one side of the vertical plate is given by

$$\dot{m}_A = k_m L W C_{AS} = 0.003 \text{ cm s}^{-1} \times 25 \text{ cm} \times 10 \text{ cm} \times 0.216 \mu\text{mol cm}^{-3} = 0.161 \mu\text{mol s}^{-1}$$

Next, we multiply the previous result by 20 to get the total oxygen transport rate for the oxygenator:

$$\dot{m}_A^{\text{total}} = 0.161 \mu\text{mol s}^{-1} \times 20 = 3.22 \mu\text{mol s}^{-1}$$

Then, we perform a steady-state overall oxygen balance over the oxygenator to find the exiting oxygen concentration in the plasma.

$$Q^{\text{total}} C_A^{\text{in}} + \dot{m}_A^{\text{total}} = Q^{\text{total}} C_A^{\text{out}}$$

Since there is no oxygen in the entering plasma, we can then write that

$$C_A^{\text{out}} = \frac{\dot{m}_A^{\text{total}}}{Q^{\text{total}}} = \frac{3.22 \mu\text{mol s}^{-1} \times 60 \text{ s min}^{-1}}{1000 \text{ cm}^3 \text{ min}^{-1}} = 0.193 \mu\text{mol cm}^{-3} = 193 \mu\text{M}$$

Recall that the saturation concentration of oxygen in the plasma is 216  $\mu\text{M}$ , which means that this oxygenator design has reached 89% of the saturation value.

### 5.9.2 Mass transfer from a rotating disk

Now, as shown in Figure 5.6, we consider the mass transfer of a solute from the surface of a flat circular disk of radius  $R$  that is rotating about the  $z$  axis that is perpendicular to the disk surface. The disk rotates within a large volume of fluid, which itself is at rest. The rotation of the disk causes a thin layer of fluid at its surface to flow outward in the radial direction as a result of the centrifugal forces caused by the rotation of the disk. This flow of the fluid will create a boundary layer near the surface of the plate where the velocity and solute concentration changes will be confined. There will also be a flow of the fluid toward the surface of the disk to maintain this outward radial flow of fluid along the disk surface.

Clearly, this is a very complex 3D flow. However, with some reasonable assumptions, a solution can be obtained that describes the mass transfer rate of the solute very well when compared to experimental data. We can use cylindrical coordinates to describe the solution to this problem, so we have velocity and solute molar flux components in the  $r$ ,  $\theta$ , and  $z$  directions. However, because of axial symmetry about the  $z$  axis, these velocity and molar flux components do not vary in the  $\theta$  direction.

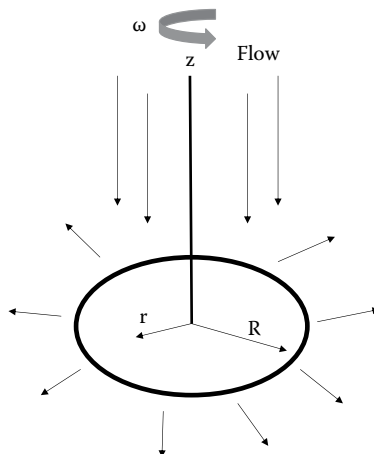


Figure 5.6 Mass transfer from a rotating disk.

Schlichting (1979) has also shown that the momentum boundary layer thickness along the surface of the rotating disk is given by

$$\delta \approx \sqrt{\frac{v}{\omega}} \quad (5.104)$$

where

- $\omega$  is defined as the disk rotation rate in radians per second
- $v$  is the kinematic viscosity

This result is also consistent with the momentum boundary layer thickness given by [Equation 4.72](#) for flow over a flat plate if we let  $x = R$  and replace  $V$  with the angular velocity,  $\omega R$ . If we assume that this momentum boundary layer thickness is much smaller than the disk radius, i.e.,  $\delta \ll R$ , then we can assume to a good approximation that the solute concentration will only depend on the axial position  $z$ .

This means that near the surface of the rotating disk, we can write a steady-state solute balance in the  $z$  direction over a thin annular shell volume, i.e.,  $2\pi r \Delta r \Delta z$ , of radial thickness  $\Delta r$  and axial thickness  $\Delta z$ :

$$v_z(z)(2\pi r \Delta r)C_A|_z - v_z(z)(2\pi r \Delta r)C_A|_{z+\Delta z} + D_{AB}(2\pi r \Delta r) \frac{dC_A}{dz}|_{z+\Delta z} - D_{AB}(2\pi r \Delta r) \frac{dC_A}{dz}|_z = 0 \quad (5.105)$$

Next, we divide [Equation 5.105](#) by  $2\pi r \Delta r \Delta z$  and take the limit as  $\Delta z \rightarrow 0$  and obtain

$$v_z(z) \frac{dC_A}{dz} = D_{AB} \frac{d^2C_A}{dz^2} \quad (5.106)$$

The boundary conditions for [Equation 5.106](#) are

$$\begin{aligned} BC1 : \quad z = 0, \quad C_A &= C_{AS} \\ BC2 : \quad z = \infty, \quad C_A &= 0 \end{aligned} \quad (5.107)$$

Next, we introduce a dimensionless distance from the surface of the rotating disk, i.e.,  $\zeta = \frac{z}{\delta} = z\sqrt{\frac{\omega}{v}}$ , and a dimensionless velocity, i.e.,  $H(\zeta) = \frac{v_z(z)}{\delta\omega} = \frac{v_z(z)}{\sqrt{v\omega}}$ . Substituting these quantities into [Equation 5.106](#), we get

$$H(\zeta) \frac{dC_A}{d\zeta} = \frac{D_{AB}}{v} \frac{d^2C_A}{d\zeta^2} = \frac{1}{Sc} \frac{d^2C_A}{d\zeta^2} \quad (5.108)$$

where  $Sc = \frac{v}{D_{AB}} = \frac{\mu}{\rho D_{AB}}$ . The boundary conditions can also be written in terms of  $\zeta$ :

$$\begin{aligned} BC1 : \quad \zeta = 0, \quad C_A &= C_{AS} \\ BC2 : \quad \zeta = \infty, \quad C_A &= 0 \end{aligned} \quad (5.109)$$

To facilitate the integration of [Equation 5.108](#), we let  $Y = \frac{dC_A}{d\zeta}$  and substitute this into that equation to give

$$\frac{dY}{d\zeta} = ScH(\zeta)Y \quad (5.110)$$

Integration of [Equation 5.110](#) then gives

$$\ln Y = Sc \int_0^{\zeta} H(\bar{\zeta}) d\bar{\zeta} + \ln C_1 \quad (5.111)$$

and then

$$\frac{dC_A}{d\zeta} = C_1 \exp \left[ Sc \int_0^{\zeta} H(\bar{\zeta}) d\bar{\zeta} \right] \quad (5.112)$$

[Equation 5.112](#) can then be integrated to give

$$C_A(\zeta) = C_1 \int_0^{\zeta} \exp \left[ Sc \int_0^{\bar{\zeta}} H(s) ds \right] d\bar{\zeta} + C_2 \quad (5.113)$$

Next, we use the boundary conditions given by [Equation 5.109](#) to eliminate  $C_1$  and  $C_2$ , which then gives the following equation for the solute concentration in the fluid:

$$\frac{C_A(\zeta)}{C_{AS}} = 1 - \frac{\int_0^{\zeta} \exp \left[ Sc \int_0^{\bar{\zeta}} H(s) ds \right] d\bar{\zeta}}{\int_0^{\infty} \exp \left[ Sc \int_0^{\bar{\zeta}} H(s) ds \right] d\bar{\zeta}} \quad (5.114)$$

Provided that we know  $H(\zeta)$ , we can solve the previous equation for the solute concentration in the fluid above the surface of the disk.

Recall that the axial velocity is given by  $v_z(\zeta) = H(\zeta)\delta\omega = H(\zeta)\sqrt{v\omega}$ . We will skip the details here on the solution for the velocity profiles since it is a rather involved calculation. However, Schlichting (1979) outlines the solution procedure for obtaining the velocity profiles and provides a graph and table for the values of  $H(\zeta)$  as a function of  $\zeta = \frac{z}{\delta} = z\sqrt{\frac{\omega}{v}} = z\sqrt{\frac{\omega}{D_{AB}Sc}}$ .

Now for a large value of  $Sc$ , and in the region near the surface of the disk, we expect  $\zeta < 1$ . In this region, which is of the most interest to us since the solute flux at the surface is given by  $-D_{AB} \frac{dC_A}{d\zeta} \Big|_{\zeta=0}$ ,

we find from Schlichting's results that  $H(\zeta) \approx -0.510\zeta^2$ . When this expression for  $H(\zeta)$  is substituted into [Equation 5.114](#), and the integral term within the exponential is evaluated, we obtain

$$\frac{C_A(\zeta)}{C_{AS}} = 1 - \frac{\int_0^\zeta \exp[-0.17Sc\bar{\zeta}^3] d\bar{\zeta}}{\int_0^\infty \exp[-0.17Sc\bar{\zeta}^3] d\bar{\zeta}} \quad (5.115)$$

The integral in the denominator of [Equation 5.115](#) can be evaluated analytically in terms of the *gamma function*, which is defined as  $\Gamma(j) \equiv \int_0^\infty e^{-x} x^{j-1} dx$ , along with the gamma function property that  $j \Gamma(j) = \Gamma(j + 1)$ . Hence, [Equation 5.115](#) becomes

$$\frac{C_A(\zeta)}{C_{AS}} = 1 - \frac{(0.17Sc)^{1/3} \int_0^\zeta \exp[-0.17Sc\bar{\zeta}^3] d\bar{\zeta}}{\Gamma\left(\frac{4}{3}\right)} \quad (5.116)$$

The solute molar flux in the  $z$  direction is then given by

$$N_{Az} = -D_{AB} \frac{dC_A}{dz} = C_{AS} D_{AB} \frac{(0.17Sc)^{1/3}}{\Gamma\left(\frac{4}{3}\right)} \exp(-0.17Sc\zeta^3) \frac{d\zeta}{dz} \quad (5.117)$$

$$N_{Az} = C_{AS} D_{AB} \frac{(0.17Sc)^{1/3}}{\Gamma\left(\frac{4}{3}\right)} \exp(-0.17Sc\zeta^3) \sqrt{\frac{\omega}{v}}$$

in which  $\frac{d\zeta}{dz} = \sqrt{\frac{\omega}{v}}$ .

Now, we can use [Equation 5.74](#) with [Equation 5.117](#) to find the solute flux at the surface of the rotating disk and then the mass transfer coefficient:

$$N_{Az}|_{z=0} = -D_{AB} \frac{dC_A}{dz} \Big|_{z=0} = k_m (C_{AS} - 0) = C_{AS} D_{AB} \frac{(0.17Sc)^{1/3}}{\Gamma\left(\frac{4}{3}\right)} \sqrt{\frac{\omega}{v}} \quad (5.118)$$

$$N_{Az}|_{z=0} = k_m C_{AS} = 0.62 C_{AS} D_{AB} Sc^{1/3} \sqrt{\frac{\omega}{v}}$$

[Equation 5.118](#) has the interesting property that the solute flux at the surface of the rotating disk is independent of the disk diameter,  $d_{disk}$ . This also means that the mass transfer coefficient is also independent of the disk diameter. Because of this property, the rotating disk is a very useful device for mass transfer studies.

The mass transfer coefficient expressed by the Sherwood number can then be shown to be given by

$$Sh = \frac{k_m d_{disk}}{D_{AB}} = 0.62 \left( \frac{\rho d_{disk}^2 \omega}{\mu} \right)^{1/2} \left( \frac{\mu}{\rho D_{AB}} \right)^{1/3} = 0.62 Re^{1/2} Sc^{1/3} \quad (5.119)$$

### Example 5.13

Tao et al. (1974) provides the following data for the dimensionless mass transfer rate of benzoic acid from the surface of a rotating disk into water. According to Equations 5.118 and 5.119, the dimensionless mass transfer rate is equal to the Sh as shown in Equation A below:

$$\text{Mass transfer rate} = \frac{N_{Az}|_{z=0} d_{disk}}{D_{AB} C_{AS}} = Sh = 0.62 \left( \frac{\rho d_{disk}^2 \omega}{\mu} \right)^{1/2} \left( \frac{\mu}{\rho D_{AB}} \right)^{1/3} \quad (A)$$

According to Equation A, when the dimensionless mass transfer rate, i.e., Sh, is plotted versus the  $Re^{1/2}$ , the slope of the line is equal to  $m = 0.62 Sc^{1/3}$ . The diffusivity of benzoic acid in water, i.e.,  $D_{AB}$ , at  $25^\circ\text{C}$  is  $0.9 \times 10^{-5} \text{ cm}^2 \text{ s}^{-1}$  (Noult and Lealst, 1987). Using this value of the diffusivity gives  $Sc = 989$ . For benzoic acid in water, the value of the slope  $m$  should then equal 6.18. Compare this theoretical value of the slope, i.e.,  $m = 6.18$ , to the slope of the line for the benzoic acid mass transfer data shown below.

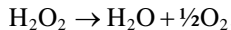
$(\text{Reynolds Number})^{1/2} = \left( \frac{\rho d_{disk}^2 \omega}{\mu} \right)^{1/2}$	$\frac{N_{Az} _{z=0} d_{disk}}{D_{AB} C_{AS}} = \frac{k_m d_{disk}}{D_{AB}}$ Dimensionless Mass Transfer Rate
20.82	137.52
27.48	175.02
34.98	225.02
58.32	366.70
59.98	375.04
78.30	495.88
81.64	516.70
82.46	525.04
135.78	858.40
139.12	875.08

### Solution

We perform a linear regression with a zero intercept on the data in the table and obtain a value of the slope equal to 6.318, which compares very well with the theoretical value of 6.18. The error in the slope from Equation 5.119 and these data is equal to 2.23%. The correlation constant is also equal to 0.9998, which indicates an excellent fit to the data.

**Example 5.14**

A design for a contact lens cleaning system uses a 3% hydrogen peroxide ( $H_2O_2$ ) solution to kill any microorganisms on the lenses. The killing of the microorganisms occurs very quickly when the lens is in this solution. However, the remaining hydrogen peroxide needs to be neutralized before the lenses can be worn again. It is proposed to neutralize the hydrogen peroxide by having within the lens cleaning container a thin rotating disk that has a catalyst on its surface. The disk is rotated at 60 RPM. As the catalyst disk rotates, the residual hydrogen peroxide moves to the surface of the disk where it is decomposed into water and oxygen according to the following irreversible equation:



At  $25^\circ C$ , the density of the hydrogen peroxide solution is  $1 \text{ g cm}^{-3}$  and its viscosity is  $0.90 \text{ cP}$ . The diffusivity of hydrogen peroxide in water is  $1.43 \times 10^{-5} \text{ cm}^2 \text{ s}^{-1}$ , and the MW of hydrogen peroxide is 34. The hydrogen peroxide volume in the cleaning container is  $15 \text{ cm}^3$ . If the catalyst disk ( $d_{\text{disk}}$ ) is  $5/8$  inch in diameter, and both sides of the disk are catalytically active, estimate how long it will take for 99.99% of the hydrogen peroxide to be removed from the cleaning solution. The decomposition of the hydrogen peroxide at the surface of the disk is a first order reaction, i.e.,  $R_A'' = k_f C_{A\text{S}}$ , where  $k_f$  is the first order rate constant for the decomposition reaction and is equal to  $0.008 \text{ cm s}^{-1}$ . How long will it take if the surface reaction was instantaneous?

**Solution**

Since the hydrogen peroxide reaction at the surface of the rotating disk is a first order irreversible reaction, we can use the result given by [Equation 5.33](#) to calculate the mass transfer flux of the solute at the disk surface.

$$N_{Az}\Big|_{z=0} = R_A'' = \left( \frac{1}{\frac{1}{k_{mA}} + \frac{1}{k_f}} \right) C_{A\text{ bulk}} \quad (\text{A})$$

We can also write the following unsteady mass balance equation for hydrogen peroxide in the solution using [Equation 1.8](#) as a guide:

$$V \frac{dC_{A\text{ bulk}}}{dt} = -2 \frac{\pi d_{\text{disk}}^2}{4} N_{Az}\Big|_{z=0} = -2 \frac{\pi d_{\text{disk}}^2}{4} \left( \frac{1}{\frac{1}{k_{mA}} + \frac{1}{k_f}} \right) C_{A\text{ bulk}}$$

The previous equation can then be integrated to give

$$C_{A\text{ bulk}}(t) = C_{A\text{ bulk}}^0 \exp\left(-\frac{\pi d_{\text{disk}}^2}{2V} Kt\right) \quad (\text{B})$$

where we let  $\frac{1}{K} = \frac{1}{k_{mA}} + \frac{1}{k_f}$ . If 99.99% of the hydrogen peroxide is to be removed, then  $\frac{C_{A\text{ bulk}}(t)}{C_{A\text{ bulk}}^0} = 0.0001$ . Now we calculate the value of the overall rate constant, i.e.,  $K$ , which

includes the solute mass transfer coefficient and the surface reaction rate constant. We can estimate  $k_{mA}$  from [Equation 5.119](#). First, we calculate the Re:

$$Re = \frac{\rho d_{disk}^2 \omega}{\mu} = \frac{\frac{1 \text{ g}}{\text{cm}^3} \times (1.59 \text{ cm})^2 \times \frac{60 \text{ rev}}{\text{min}} \times \frac{1 \text{ min}}{60 \text{ s}} \times \frac{2 \pi}{1 \text{ rev}}}{0.9 \text{ cP} \times \frac{0.01 \text{ g cm}^{-1} \text{ s}^{-1}}{1 \text{ cP}}} = 1765$$

The Sc is then

$$Sc = \frac{\mu}{\rho D_{AB}} = \frac{0.9 \text{ cP} \times \frac{0.01 \text{ g cm}^{-1} \text{ s}^{-1}}{\text{cP}}}{1 \text{ g cm}^{-3} \times 1.43 \times 10^{-5} \text{ cm}^2 \text{ s}^{-1}} = 629$$

The mass transfer coefficient is then calculated as

$$k_{mA} = 0.62 \frac{D_{AB}}{d_{disk}} Re^{1/2} Sc^{1/3} = 0.62 \times \frac{1.43 \times 10^{-5} \text{ cm}^2 \text{ s}^{-1}}{1.59 \text{ cm}} \times 1765^{1/2} \times 629^{1/3} = 0.002 \text{ cm s}^{-1}$$

Using this value of  $k_{mA}$  and the given value of  $k_f = 0.008 \text{ cm s}^{-1}$ , we calculate that  $K = 0.0016 \text{ cm s}^{-1}$ . We can then solve [Equation B](#) for the time to remove 99.99% of the hydrogen peroxide:

$$t = -\frac{2V}{\pi d_{disk}^2 K} \ln\left(\frac{C_A(t)}{C_A^0}\right) = -\frac{2 \times 15 \text{ cm}^3}{\pi (1.59 \text{ cm})^2 \times 0.0016 \text{ cm s}^{-1}} \ln(0.0001) = 21,744 \text{ s} = 6.04 \text{ h}$$

If the surface reaction is instantaneous, then  $K = k_{mA}$  and we obtain

$$t = -\frac{2V}{\pi d_{disk}^2 k_{mA}} \ln\left(\frac{C_A(t)}{C_A^0}\right) = -\frac{2 \times 15 \text{ cm}^3}{\pi (1.59 \text{ cm})^2 \times 0.002 \text{ cm s}^{-1}} \ln(0.0001) = 17,395 \text{ s} = 4.83 \text{ h}$$

### 5.9.3 Mass transfer in laminar boundary layer flow over a flat plate

[Figure 5.7](#) shows the laminar flow of a fluid across a semi-infinite flat plate of length L. The surface of the plate maintains a constant concentration of a solute ( $C_{AS}$ ), and the concentration of the solute in the fluid is given by  $C_A$ . Unlike the situation shown in [Figure 5.1](#), here the solute diffuses from the surface of the plate and is then swept away by the flowing fluid. Hence, in this problem, the solute is transported away from the flat plate surface by a combination of diffusion and convection. We also assume that the bulk of the fluid is free of the solute except in the region adjacent to the flat plate, which is defined as the concentration boundary layer. If the fluid approaching the plate has a solute concentration of  $C_{A \text{ bulk}}$ , then the following analysis still applies; however, the concentration will need to be defined as  $\bar{C}_A = C_A - C_{A \text{ bulk}}$ .

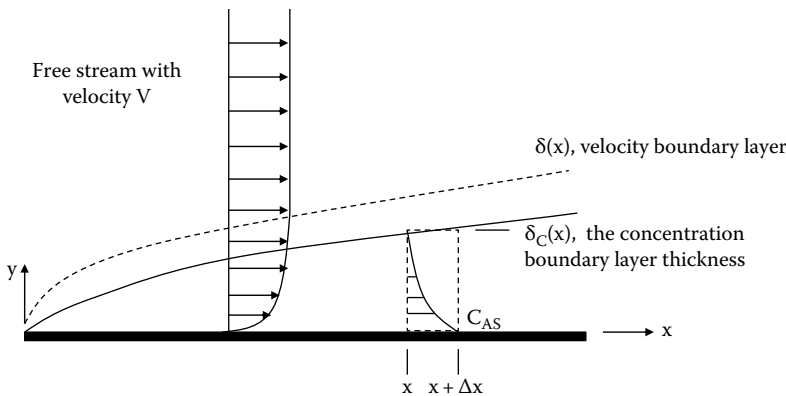


Figure 5.7 Laminar boundary layer flow in the vicinity of a flat plate of constant surface concentration.

In [Section 4.9.2](#), we developed an approximate solution for the steady laminar flow of a fluid along a flat plate and determined the velocity profile within the boundary layer that is formed along the length of the plate. Here, we will extend this solution to determine the concentration profile of the solute in the concentration boundary layer that is also formed along the surface of the flat plate.

Consider the shell volume shown in [Figure 5.7](#) of width  $W$  and located from  $x$  to  $x + \Delta x$  and from  $y = 0$  to  $y = \delta_C(x)$ , where  $\delta_C$  is the concentration boundary layer thickness. We first perform a steady-state solute balance on this shell volume, which is given by

$$\int_0^{\delta_C(x)} \left[ WC_A v_x|_x - WC_A v_x|_{x+\Delta x} \right] dy - C_A v_y|_{y=\delta_C(x)} W \Delta x + N_{Ay}|_{y=0} W \Delta x = 0 \quad (5.120)$$

The integral term in [Equation 5.120](#) represents the net rate at which the solute is being added to the shell volume by flow of the fluid in the  $x$  direction. The second term represents the loss of the solute from the top of the shell volume as a result of flow in the  $y$  direction. The last term represents the rate at which the solute is diffusing away from the surface of the flat plate. After eliminating the plate width,  $W$ , and dividing by  $\Delta x$ , and taking the limit as  $\Delta x \rightarrow 0$ , we can write [Equation 5.120](#) as

$$N_{Ay}|_{y=0} = \frac{d}{dx} \int_0^{\delta_C(x)} C_A v_x dy + C_A v_y|_{y=\delta_C(x)} \quad (5.121)$$

Assuming a dilute solution, we can use the form of Fick's first law given by [Equation 5.18](#) for  $N_{Ay}|_{y=0}$  and obtain

$$-D_{AB} \frac{dC_A}{dy} \Big|_{y=0} = \frac{d}{dx} \int_0^{\delta_C(x)} C_A v_x dy + C_A v_y|_{y=\delta_C(x)} \quad (5.122)$$

The solution of [Equation 5.122](#) requires that we know how  $v_x$  and  $C_A$  depend on  $x$  and  $y$  in their respective boundary layers. Since we only want to obtain an approximate solution, we can use our previous result for  $v_x(x, y)$ , i.e., [Equation 4.70](#):

$$\frac{v_x(x, y)}{V} = \frac{3}{2} \left( \frac{y}{\delta(x)} \right) - \frac{1}{2} \left( \frac{y}{\delta(x)} \right)^3 \quad (4.70)$$

and in a similar fashion propose that the concentration profile in the concentration boundary layer is approximately described by the following cubic equation:

$$C_A(y) = a_C + b_C y + c_C y^2 + d_C y^3 \quad (5.123)$$

The concentration profile described by [Equation 5.123](#) also has to satisfy the following boundary conditions:

$$\begin{aligned} BC1: \quad & y = 0, \quad C_A = C_{AS} \\ BC2: \quad & y = \delta_C(x), \quad C_A = 0 \\ BC3: \quad & y = \delta_C(x), \quad \frac{\partial C_A}{\partial y} = 0 \\ BC4: \quad & y = 0, \quad \frac{\partial^2 C_A}{\partial y^2} = 0 \end{aligned} \quad (5.124)$$

The first boundary condition (BC1) expresses the fact that the concentration of the solute is constant along the surface of the flat plate. The second and third boundary conditions (BC2 and BC3) state that beyond the concentration boundary layer, the solute is not present. This allows us to eliminate the last term in [Equation 5.122](#), which then becomes

$$-D_{AB} \frac{dC_A}{dy} \Big|_{y=0} = \frac{d}{dx} \int_0^{\delta_C(x)} C_A v_x dy \quad (5.125)$$

The fourth boundary condition (BC4) expresses the fact that the flux of solute along the surface of the plate is only a function of  $x$ .

After imposing the boundary conditions given by [Equation 5.124](#) on [Equation 5.123](#), the following expression is obtained for the concentration profile within the concentration boundary layer in terms of the concentration boundary thickness,  $\delta_C(x)$ , which at this time still needs to be determined.

$$\frac{C_A(x, y)}{C_{AS}} = 1 - \frac{3}{2} \left( \frac{y}{\delta_C(x)} \right) + \frac{1}{2} \left( \frac{y}{\delta_C(x)} \right)^3 \quad (5.126)$$

We now can substitute Equations 4.70 and 5.126 into Equation 5.125. We also assume that the ratio of the boundary layer thicknesses, i.e.,  $\Delta = \frac{\delta_C(x)}{\delta(x)}$ , is a constant. The algebra is a bit overwhelming, but one can obtain the following differential equation for the thickness of the concentration boundary layer:

$$(0.15 \Delta - 0.0107 \Delta^3) \frac{d\delta_C}{dx} = \frac{3}{2} \frac{D_{AB}}{V \delta_C} \quad (5.127)$$

with the boundary condition that at  $x = 0$ ,  $\delta_C = 0$ . The solution of Equation 5.127 is then given by

$$\delta_C(x) = \sqrt{\frac{3}{(0.15 \Delta - 0.0107 \Delta^3)}} \frac{D_{AB}x}{V} \quad (5.128)$$

Recall from Equation 4.72 that the momentum boundary layer thickness  $\delta$  is given by

$$\delta(x) = 4.64 \sqrt{\frac{vx}{V}} = 4.64 \sqrt{\frac{\mu x}{\rho V}} \quad (4.72)$$

Dividing Equation 5.128 by Equation 4.72, and simplifying, results in the following equation for  $\Delta = \frac{\delta_C(x)}{\delta(x)}$ :

$$1.0765 \Delta^3 - 0.0768 \Delta^5 = \frac{\rho D_{AB}}{\mu} = \frac{1}{Sc} \quad (5.129)$$

where  $Sc = \frac{\mu}{\rho D_{AB}}$  is once again the dimensionless number known as the *Schmidt number*. For solutes diffusing through liquids, the Schmidt number is generally much greater than unity; hence, from Equation 5.129, we have that  $\Delta < 1$  and  $\delta > \delta_C$ . This shows that for liquids, the concentration boundary layer lies within the velocity or momentum boundary layer. For solutes diffusing through gases, the Schmidt number is on the order of unity and  $\Delta$  is approximately equal to unity and  $\delta \approx \delta_C$ . For solutes diffusing through materials like liquid metals, the Schmidt number is much less than unity and then  $\Delta > 1$  and  $\delta_C > \delta$ .

In general, if one knows the value of the Schmidt number for the mass transfer problem being considered, then Equation 5.129 can be solved for the value of  $\Delta$ . The velocity boundary layer thickness is then given by Equation 4.72, and the concentration boundary layer thickness is equal to  $\Delta \delta(x)$ .

For many mass transfer problems of interest to biomedical engineers, the solute is diffusing within a liquid, and this means the Schmidt number is much larger than unity. This makes the right-hand side of Equation 5.129 much smaller than unity. The only way this can happen is if  $\Delta$  is also much smaller than unity. This means that the concentration boundary layer lies well within the boundary layer for the velocity. Hence, for  $\Delta \ll 1$ , Equation 5.129 simplifies to the following result:

$$\Delta = \frac{\delta_C(x)}{\delta(x)} \approx Sc^{-1/3} \quad (5.130)$$

Combining this with [Equation 4.72](#) results in [Equation 5.131](#) for the thickness of the concentration boundary layer:

$$\frac{\delta_C(x)}{x} = 4.64 \left( \frac{\mu}{\rho V x} \right)^{1/2} \left( \frac{\rho D_{AB}}{\mu} \right)^{1/3} = 4.64 \left( \frac{V}{Vx} \right)^{1/2} \left( \frac{D_{AB}}{V} \right)^{1/3} = 4.64 \left( \frac{1}{Re_x} \right)^{1/2} \left( \frac{1}{Sc} \right)^{1/3} \quad (5.131)$$

Note that the concentration boundary layer thickness depends on two dimensionless parameters that describe the nature of the flow, as given by the Reynolds number ( $Re_x$ ), and the physical properties of the solute and the fluid, as given by the Schmidt number ( $Sc$ ).

Recall that the mass transfer coefficient is proportional to the solute diffusivity and inversely proportional to the concentration boundary layer thickness (see [Equation 5.78](#)). This means that since  $\delta_C$  depends on  $x$ , the mass transfer coefficient will depend on the location along the surface of the flat plate. We can calculate this local value of the mass transfer coefficient using [Equation 5.74](#), which says the local mass transfer coefficient is given by

$$k_{m \text{ local}} = - \frac{D_{AB}}{(C_{AS} - C_{A \text{ bulk}})} \frac{dC_A}{dy} \Big|_{y=0} = - \frac{D_{AB}}{C_{AS}} \frac{dC_A}{dy} \Big|_{y=0} \quad (5.132)$$

After substituting [Equation 5.126](#) into the above expression, and replacing  $\delta_C(x)$  with [Equation 5.131](#), we obtain the following expression for the local mass transfer coefficient for laminar flow over a flat plate:

$$Sh_{\text{local}} = \frac{k_{m \text{ local}} x}{D_{AB}} = 0.323 \left( \frac{\rho V x}{\mu} \right)^{1/2} \left( \frac{\mu}{\rho D_{AB}} \right)^{1/3} = 0.323 Re_x^{1/2} Sc^{1/3} \quad (5.133)$$

where  $Sh_{\text{local}}$  is the local Sherwood number at location  $x$ . Recall that the Sherwood number is the ratio of the transport rate of the solute by convection to that by diffusion. In [Equation 5.133](#),  $k_{m \text{ local}}$  is the local value of the mass transfer coefficient. As the fluid progresses down the length of the plate, the concentration boundary layer thickness increases, and by [Equation 5.133](#), we see that  $k_{m \text{ local}}$  decreases in inverse proportion to  $x^{1/2}$ .

For a plate of length  $L$ , the average mass transfer coefficient is given by

$$k_m = \frac{1}{L} \int_0^L k_{m \text{ local}}(x) dx \quad (5.134)$$

Substituting [Equation 5.133](#) into [Equation 5.134](#) results in [Equation 5.135](#), which is also known as the *length averaged mass transfer coefficient*.

$$\frac{k_m L}{D_{AB}} = Sh = 0.646 \left( \frac{\rho V L}{\mu} \right)^{1/2} \left( \frac{\mu}{\rho D_{AB}} \right)^{1/3} = 0.646 Re^{1/2} Sc^{1/3} \quad (5.135)$$

[Equations 5.133](#) and [5.135](#) describe the mass transfer of a solute from a flat plate for laminar boundary layer flow provided that the local value of the Reynolds number is less than 300,000.

For flow over one side of a flat plate of length  $L$  and width  $W$ , the solute transport rate can then be written as follows according to [Equation 5.75](#). In [Equation 5.136](#), recall that  $C_{AS}$  is the concentration of the solute at the surface of the plate and  $C_{A\text{bulk}}$  is the concentration of the solute in the fluid outside the boundary layer. Note that  $k_m$  is calculated from [Equation 5.135](#), which is the average value of the mass transfer coefficient for the surface area, i.e.,  $S = LW$ .

$$\dot{m}_A = k_m LW (C_{AS} - C_{A\text{bulk}}) \quad (5.136)$$

### Example 5.15

Blood is flowing across the flat surface of a polymeric material coated with an anticoagulant drug. Equilibrium studies of the drug coated on the polymer show that the drug has a solubility of  $100 \text{ mg L}^{-1}$  of blood. The fluid adjacent to the plate equilibrates quickly; hence, the concentration of the drug at the surface of the plate, i.e.,  $C_{AS}$ , is for practical purposes the same as this equilibrium value. Find the following:

- The distance at which the laminar boundary layer for flow over the surface of the polymeric material ends
- The thickness of the velocity and concentration boundary layers at the end of the polymeric material
- The local mass transfer coefficient at the end of the polymeric material and the average mass transfer coefficient for the drug
- The average mass transfer flux of the drug from the polymeric material assuming the concentration of the drug in the blood is much smaller than at the surface, i.e.,  $C_{A\text{bulk}} = 0$

Assume that the blood traveling across the polymeric material has a free stream velocity, i.e.,  $V$ , of  $40 \text{ cm s}^{-1}$ . The polymeric material has a length in the direction of the flow of  $30 \text{ cm}$ . The diffusivity of the drug in blood is  $4.3 \times 10^{-6} \text{ cm}^2 \text{ s}^{-1}$ .

### Solution

For part (a), we use the fact that the transition to turbulence begins at a  $\text{Re}_x = \rho V x / \mu = 300,000$ . Hence, we can solve this equation for the value of  $x$  at this transition as follows:

$$x = \frac{300,000 \times 3 \text{ cP} \times \frac{1 \text{ g cm}^{-1} \text{ s}^{-1}}{100 \text{ cP}}}{1.056 \text{ g cm}^3 \times 40 \text{ cm s}^{-1}} = 213 \text{ cm}$$

Note that this distance for the transition to turbulence is much greater than the actual length of the flat polymeric material; hence, the flow is laminar over the region of interest. For part (b), we use [Equations 4.72](#) and [5.130](#) to calculate the boundary layer thicknesses at the end of the polymeric material as shown below. The thickness of the velocity boundary layer is therefore

$$\delta = 4.64 \sqrt{\frac{3 \text{ cP} \times \frac{1 \text{ g cm}^{-1} \text{ s}^{-1}}{100 \text{ cP}} \times 30 \text{ cm}}{1.056 \text{ g cm}^{-3} \times 40 \text{ cm s}^{-1}}} = 0.68 \text{ cm}$$

Next, we calculate the Schmidt number:

$$Sc = \frac{\mu}{\rho D} = \frac{3 \text{ cP} \times \frac{1 \text{ g cm}^{-1} \text{ s}^{-1}}{100 \text{ cP}}}{1.056 \text{ g cm}^{-1} \times 4.3 \times 10^{-6} \text{ cm}^2 \text{ s}^{-1}} = 6607$$

We see that  $Sc \gg 1$  in this case and the concentration boundary layer will therefore lie well within the velocity boundary layer calculated above as shown below:

$$\delta_C = \delta Sc^{-1/3} = 0.68 \text{ cm} \times 6607^{-1/3} = 0.036 \text{ cm}$$

Note that both  $\delta$  and  $\delta_C$  are much larger than the plasma layer thickness (see [Section 4.8](#)); hence, we are justified in using the properties of whole blood in these calculations.

For part (c), we use [Equations 5.133](#) and [5.135](#) to calculate the local and average mass transfer coefficients, respectively. The Reynolds number at the end of the polymeric surface is given by

$$\left( \frac{\rho Vx}{\mu} \right) = \frac{1.056 \text{ g cm}^{-3} \times 40 \text{ cm s}^{-1} \times 30 \text{ cm}}{3 \text{ cP} \times \frac{1 \text{ g cm}^{-1} \text{ s}^{-1}}{100 \text{ cP}}} = 42,240$$

and from [Equation 5.133](#)

$$k_{m \text{ local}} = 0.323 \times \frac{4.3 \times 10^{-6} \text{ cm}^2 \text{ s}^{-1}}{30 \text{ cm}} \times 42,240^{1/2} \times 6,607^{1/3} = 1.78 \times 10^{-4} \text{ cm s}^{-1}$$

Since the average mass transfer coefficient up to a given location is twice the local value, we then have that  $k_m = 3.56 \times 10^{-4} \text{ cm s}^{-1}$ . The average mass transfer flux of the drug from the polymeric surface is found from [Equation 5.136](#) where the solute flux at the surface is given by  $N_{Ay}|_{y=0} = \frac{\dot{m}_A}{LW}$ ; hence,

$$N_{Ay}|_{y=0} = k_m \times C_{AS} = 3.56 \times 10^{-4} \text{ cm s}^{-1} \times 100 \text{ mg L}^{-1} \times \frac{1 \text{ L}}{1000 \text{ cm}^3}$$

$$N_{Ay}|_{y=0} = 3.56 \times 10^{-5} \text{ mg cm}^{-2} \text{ s}^{-1}$$

## 5.9.4 Mass transfer between the wall of a cylindrical tube and a fluid in laminar flow

Next, we consider the situation shown in [Figure 5.8](#). A fluid in laminar flow is flowing through a cylindrical tube and comes into contact with a section of the tube that maintains a constant concentration of a solute that diffuses into the fluid. We want to determine the mass transfer rate of the solute from the surface. Hence, we will need to find an expression for the mass transfer coefficient in terms of dimensionless quantities such as the Reynolds number and the Schmidt number. In order

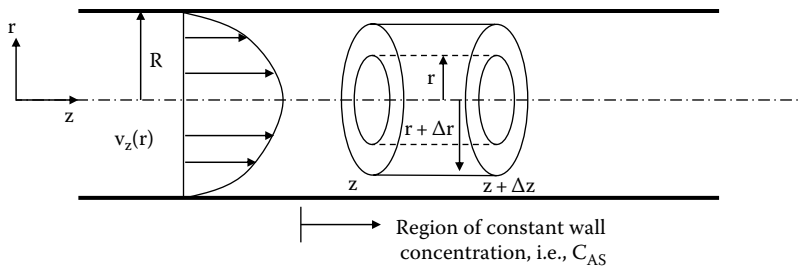


Figure 5.8 Laminar flow of a fluid in a tube with constant concentration of the solute along the surface.

to obtain an analytical solution to this rather complex problem, we will make a simplifying assumption, i.e., we will only be interested in obtaining what is known as a *short contact time solution*. This means that the solute does not penetrate very far from the surface of the tube. Hence, the change in concentration of the solute occurs only near the surface of the tube wall.

From [Chapter 4](#), we know that the velocity profile for laminar flow in a tube is given by the following expression, i.e., [Equation 4.7](#):

$$v_z(r) = \frac{(P_0 - P_L)R^2}{4\mu L} \left[ 1 - \left( \frac{r}{R} \right)^2 \right] \quad (4.7)$$

Next, we perform a steady-state solute balance on the cylindrical shell volume shown in [Figure 5.8](#).

$$\begin{aligned} & 2\pi r \Delta r \left( v_z C_A|_z - v_z C_A|_{z+\Delta z} \right) + 2\pi r \Delta r \left( D_{AB} \frac{\partial C_A}{\partial z} \Big|_{z+\Delta z} - D_{AB} \frac{\partial C_A}{\partial z} \Big|_z \right) \\ & + 2\pi r \Delta z \left( D_{AB} \frac{\partial C_A}{\partial r} \Big|_{r+\Delta r} - D_{AB} \frac{\partial C_A}{\partial r} \Big|_r \right) = 0 \end{aligned} \quad (5.137)$$

The first parenthetical term in [Equation 5.137](#) represents the net rate at which solute is added to the shell volume by bulk flow of the fluid. The second term in parentheses represents the net rate at which solute is added to the shell volume by diffusion of solute in the  $z$  direction. The final parenthetical term in [Equation 5.137](#) represents the net rate at which solute enters the shell volume by diffusion in the  $r$  direction. Now, if we divide through by  $2\pi r \Delta r \Delta z$  and then take the limit as  $\Delta r$  and  $\Delta z \rightarrow 0$ , we then obtain the following partial differential equation that describes the transport of solute at any value of  $r$  and  $z$  within the tube:

$$v_z \frac{\partial C_A}{\partial z} = D_{AB} \left( \frac{1}{r} \frac{\partial}{\partial r} \left( r \frac{\partial C_A}{\partial r} \right) + \frac{\partial^2 C_A}{\partial z^2} \right) \quad (5.138)$$

The term on the left-hand side of [Equation 5.138](#) represents the solute transport in the flowing fluid by axial ( $z$ ) convection or bulk flow of the fluid. The right-hand side represents the transport of the solute by diffusion in the radial ( $r$ ) and axial ( $z$ ) directions.

Generally, more solute is transported in the  $z$  direction by convection than is transported by axial diffusion. For example, the amount of solute A carried along by the bulk flow of the fluid is on the order of  $V_{\text{average}} C_A$ , and the amount of diffusion in the  $z$  direction over the tube length  $L$  is on the order of  $\frac{D_{AB} C_A}{L}$ . The ratio of these two quantities is the dimensionless Peclet number ( $Pe$ ). If  $Pe = \frac{V_{\text{average}} L}{D_{AB}} \gg 1$ , then we can ignore axial diffusion in comparison to axial convection. This means

in [Equation 5.138](#) that  $v_z \frac{\partial C_A}{\partial z} \gg D_{AB} \frac{\partial^2 C_A}{\partial z^2}$ , and in this case [Equation 5.138](#) becomes

$$v_z \frac{\partial C_A}{\partial z} = D_{AB} \frac{1}{r} \frac{\partial}{\partial r} \left( r \frac{\partial C_A}{\partial r} \right) \quad (5.139)$$

Next, we let  $s = R - r$  represent the distance from the wall of the tube. Since we are only interested in a solution near the wall,  $s$  will be small relative to  $R$  and we can neglect the effect of the curvature of the tube. With these assumptions, [Equation 5.139](#) becomes

$$v_z \frac{\partial C_A}{\partial z} = D_{AB} \frac{\partial^2 C_A}{\partial s^2} \quad (5.140)$$

We also recognize that near the tube wall the velocity profile is nearly linear in  $s$ , and from [Equations 4.7](#) and [4.11](#), we see that  $v_z \approx \frac{(P_0 - P_L)R}{2 \mu L} s \approx \frac{4V_{\text{average}}s}{R}$ . Using this result for  $v_z$ , [Equation 5.140](#) can then be written as

$$\frac{(P_0 - P_L)R}{2 \mu L} s \frac{\partial C_A}{\partial z} = \frac{4V_{\text{average}}s}{R} \frac{\partial C_A}{\partial s} = D_{AB} \frac{\partial^2 C_A}{\partial s^2} \quad (5.141)$$

The boundary conditions for [Equation 5.141](#) are as follows:

$$\begin{aligned} BC1: \quad & z = 0, \quad \text{and all } s, \quad C_A = 0 \\ BC2: \quad & s = 0, \quad \text{and } z > 0, \quad C_A = C_{AS} \\ BC3: \quad & s = \infty, \quad \text{and } z > 0, \quad C_A = 0 \end{aligned} \quad (5.142)$$

The last boundary condition (BC3) results from the short contact time assumption, which means that the solute does not penetrate very far into the fluid. We have also assumed that the bulk of the fluid is free of the solute except in the region adjacent to the tube wall. If the fluid has a solute concentration of  $C_{A \text{ bulk}}$ , then the following analysis still applies; however, the concentration will need to be defined as  $C_A = C_A - C_{A \text{ bulk}}$ .

The solution of [Equations 5.141](#) and [5.142](#) is facilitated by rewriting these equations in terms of dimensionless variables defined as follows. We let  $\theta \equiv \frac{C_A}{C_{AS}}$ ,  $\varepsilon \equiv \frac{z}{R}$ , and  $\sigma \equiv \frac{s}{R}$ , where  $\theta$  is defined

as a dimensionless concentration,  $\varepsilon$  is a dimensionless axial position, and  $\sigma$  is a dimensionless distance from the tube wall. If these dimensionless variables replace  $C_A$ ,  $z$ , and  $s$  in Equations 5.141 and 5.142, the following result is obtained:

$$N\sigma \frac{\partial \theta}{\partial \varepsilon} = \frac{\partial^2 \theta}{\partial \sigma^2} \quad (5.143)$$

where  $N \equiv \frac{R^3(P_0 - P_L)}{2 \mu D_{AB} L} = \frac{4RV_{\text{average}}}{D_{AB}}$ . The boundary conditions become

$$\begin{aligned} \text{BC1: } \varepsilon &= 0, \text{ and all } \sigma, \theta = 0 \\ \text{BC2: } \sigma &= 0, \text{ and } \varepsilon > 0, \theta = 1 \\ \text{BC3: } \sigma &= \infty, \text{ and } \varepsilon > 0, \theta = 0 \end{aligned} \quad (5.144)$$

Now to solve Equations 5.143 and 5.144, the *similarity transform technique* or *combination of variables* approach can be used. In this approach, we define a new independent variable  $\eta$  that is a suitable combination of  $\varepsilon$  and  $\sigma$  that converts Equation 5.143 from a partial differential equation into an ordinary differential equation that only depends on  $\eta$ . If we let  $\eta \equiv \left( \frac{N\sigma^3}{9\varepsilon} \right)^{1/3} = s \left( \frac{4V_{\text{average}}}{9D_{AB}Rz} \right)^{1/3}$ , then

it can be shown with a little bit of effort that Equations 5.143 and 5.144 become

$$\frac{d^2\theta}{d\eta^2} + 3\eta^2 \frac{d\theta}{d\eta} = 0 \quad (5.145)$$

and the boundary conditions become

$$\begin{aligned} \text{BC1: } \eta &= \infty, \theta = 0 \\ \text{BC2: } \eta &= 0, \theta = 1 \end{aligned} \quad (5.146)$$

The integration of Equations 5.145 and 5.146 then gives the following result for the solute concentration profile as a function of  $\eta \equiv \left( \frac{N\sigma^3}{9\varepsilon} \right)^{1/3} = s \left( \frac{4V_{\text{average}}}{9D_{AB}Rz} \right)^{1/3}$ :

$$C_A(\eta) = C_{AS} \frac{\int_{\eta}^{\infty} e^{-\eta^3} d\eta}{\Gamma\left(\frac{4}{3}\right)} \quad (5.147)$$

Obtaining the solution given by Equation 5.147 involves the use of the *gamma function*, which is defined as  $\Gamma(j) \equiv \int_0^{\infty} e^{-x} x^{j-1} dx$ , along with the gamma function property that  $j\Gamma(j) = \Gamma(j+1)$ . The  $\Gamma(4/3) = 0.893$ .

We can also use Equation 5.147 to define the concentration boundary layer thickness at any position  $z$  as that distance away from the tube wall where  $C_A(\eta) = 0.01C_{AS}$ . Hence, letting  $\frac{C_A(\eta)}{C_{AS}} = 0.01$ ,

we can solve [Equation 5.147](#), and we find that the value of  $\eta$  is equal to 1.404. From the definition of  $\eta$ , we can then find the value of  $\delta_C$  with  $s$  now equal to  $\delta_C$ , i.e.,  $\eta = 1.404 = \left( \frac{N\sigma^3}{9\varepsilon} \right)^{1/3} = \left( \frac{4V_{\text{average}}}{9D_{AB}Rz} \right)^{1/3} \delta_C$ . We can then solve this previous result for  $\delta_C$  and obtain

$$\delta_C = 1.84 \left( \frac{zRD_{AB}}{V_{\text{average}}} \right)^{1/3} \quad (5.148)$$

The above result gives the thickness of the concentration boundary layer as a function of the axial tube position  $z$ . Since we are considering a short contact time solution, this means that the solute has not penetrated very far into the fluid from the surface of the tube; hence, this type of solution is valid as long as  $\delta_C \ll R$ .

The solute flux from the tube surface at any value of  $z$  is given by [Equation 5.18](#) for a dilute solution, which in cylindrical coordinates is

$$N_{Ar} \Big|_{r=R} = -D_{AB} \frac{\partial C_A}{\partial r} \Big|_{r=R} = \frac{D_{AB}C_{AS}}{R} \frac{\partial \theta}{\partial \sigma} \Big|_{\sigma=0} = 0.855 D_{AB} C_{AS} \left( \frac{V_{\text{average}}}{D_{AB}Rz} \right)^{1/3} \quad (5.149)$$

From [Equation 5.149](#), the local value of the mass transfer coefficient, defined by [Equation 5.22](#), can then be written as

$$k_{m \text{ local}} = \frac{N_{Ar} \Big|_{r=R}}{(C_{AS} - 0)} = 1.077 D_{AB} \left( \frac{V_{\text{average}}}{D_{AB}d_{\text{tube}}z} \right)^{1/3} \quad (5.150)$$

where the average velocity of the fluid in the tube is equal to the volumetric flow rate ( $Q$ ) of the fluid divided by the tube cross-sectional area, i.e.,  $V_{\text{average}} = \frac{Q}{\pi R^2}$ .

In terms of the local Sherwood number, [Equation 5.150](#) becomes

$$Sh_{\text{local}} = \frac{k_{m \text{ local}} d_{\text{tube}}}{D_{AB}} = 1.077 \left( \frac{\rho V_{\text{average}} d_{\text{tube}}}{\mu} \right)^{1/3} \left( \frac{\mu}{\rho D_{AB}} \right)^{1/3} \left( \frac{d_{\text{tube}}}{z} \right)^{1/3} \quad (5.151)$$

where  $Sh_{\text{local}}$  is the local Sherwood number at location  $z$ .

The average mass transfer coefficient over the length of the tube is given by

$$k_m = \frac{1}{L} \int_0^L k_{m \text{ local}} dz = 1.077 D_{AB} \left( \frac{V_{\text{average}}}{D_{AB}d_{\text{tube}}} \right)^{1/3} \times \frac{1}{L} \int_0^L z^{-1/3} dz \quad (5.152)$$

Integration of [Equation 5.152](#) provides the following result for the average Sherwood number:

$$Sh = \frac{k_m d_{\text{tube}}}{D_{AB}} = 1.615 Re^{1/3} Sc^{1/3} \left( \frac{d_{\text{tube}}}{L} \right)^{1/3} \quad (5.153)$$

where the Reynolds number in [Equation 5.153](#) is defined as  $\text{Re} \equiv \frac{\rho d_{\text{tube}} V_{\text{average}}}{\mu}$  and the Schmidt number is given by  $\text{Sc} = \frac{\mu}{\rho D_{AB}}$ .

The total mass transfer rate of the solute from the surface of the tube is given by

$$\dot{m}_A = k_m 2 \pi R L \left( C_{AS} - C_A|_{z=0} \right) \quad (5.154)$$

Since this is a short contact time solution, the bulk concentration of the solute is constant and equal to the concentration of the solute as it enters the tube. Any change in the solute concentration in the fluid flowing through the tube is confined to a very thin region near the tube wall. Thus, the mass transfer driving force over the length of the tube is constant and equal to  $(C_{AS} - C_A|_{z=0})$ .

**5.9.4.1 Overall solute mass balance for the short contact time solution** If the fluid exiting the cylindrical tube considered in [Section 5.9.4](#) is then completely mixed, we can find the mixed solute concentration by performing an overall steady-state solute mass balance between the entrance to the tube at  $z = 0$  and the tube exit at  $z = L$ :

$$\pi R^2 V_{\text{average}} C_A|_{z=L} = \pi R^2 V_{\text{average}} C_A|_{z=0} + k_m 2 \pi R L \left( C_{AS} - C_A|_{z=0} \right) \quad (5.155)$$

[Equation 5.155](#) says that the rate at which solute is leaving the tube at  $z = L$  is equal to the rate at which the solute enters the tube at  $z = 0$  plus the rate at which the solute is being transported from the tube surface as given by [Equation 5.154](#).

[Equation 5.155](#) can then be solved to give the mixed concentration of the solute exiting the tube as

$$C_A|_{z=L} = C_A|_{z=0} + \left( \frac{2 k_m L}{R V_{\text{average}}} \right) \left( C_{AS} - C_A|_{z=0} \right) \quad (5.156)$$

### Example 5.16

Plasma is flowing at an average velocity of  $15 \text{ cm s}^{-1}$  through a tube that is  $1 \text{ cm}$  in diameter. The walls of the tube are coated over a length of  $10 \text{ cm}$  with a drug that diffuses from the surface of the tube into the flowing fluid. The equilibrium concentration of the drug in plasma is  $100 \text{ mg L}^{-1}$ . Find the average mass transfer coefficient over the  $10 \text{ cm}$  length of the tube that is coated with the drug. Also, find the total transport rate of the solute and the mixed concentration of the drug in the plasma after the coated section of the tube. Show that the short contact time solution is a valid approach for solving this problem. The diffusivity of the drug in plasma is estimated to be  $4 \times 10^{-6} \text{ cm}^2 \text{ s}^{-1}$ .

### Solution

First, we calculate the  $\text{Re}$  as shown below:

$$\text{Re} = \frac{\rho d_{\text{tube}} V_{\text{average}}}{\mu} = \frac{1.024 \text{ g cm}^{-3} \times 1 \text{ cm} \times 15 \text{ cm s}^{-1}}{1.2 \text{ cP} \times \frac{1 \text{ g cm}^{-1} \text{ s}^{-1}}{100 \text{ cP}}} = 1280$$

Therefore, based on this  $Re$ , the flow is laminar. The  $Sc$  is then calculated as

$$Sc = \frac{\mu}{\rho D_{AB}} = \frac{1.2 \text{ cP} \times \frac{1 \text{ g cm}^{-1} \text{ s}^{-1}}{100 \text{ cP}}}{1.024 \text{ g cm}^{-1} \times 4 \times 10^{-6} \text{ cm}^2 \text{ s}^{-1}} = 2929.7$$

Using [Equation 5.153](#), we can calculate the average  $Sh$  as shown in the following calculation:

$$Sh = 1.615 Re^{1/3} Sc^{1/3} \left( \frac{d_{tube}}{L} \right)^{1/3} = 1.615 \times 1280^{1/3} \times 2929.7^{1/3} \times \left( \frac{1 \text{ cm}}{10 \text{ cm}} \right)^{1/3} = 116.46$$

From this value of the  $Sh$ , we can then calculate the average mass transfer coefficient over the 10 cm section of the tube as

$$k_m = \frac{Sh D_{AB}}{d_{tube}} = \frac{116.4 \times 4 \times 10^{-6} \text{ cm s}^{-1}}{1 \text{ cm}} = 4.66 \times 10^{-4} \text{ cm s}^{-1}$$

From [Equation 5.154](#), we can calculate the mass transfer rate of the solute from the coated surface of the tube.

$$\begin{aligned} \dot{m}_A &= k_m 2 \pi R L \left( C_{AS} - C_A \Big|_{z=0} \right) \\ &= 4.66 \times 10^{-4} \text{ cm s}^{-1} \times 2 \times \pi \times 0.5 \text{ cm} \times 10 \text{ cm} \times 100 \text{ mg L}^{-1} \times \frac{1 \text{ L}}{1000 \text{ cm}^3} \\ &= 0.0015 \text{ mg s}^{-1} \end{aligned}$$

The mixed concentration of the drug in the plasma after the coated section of the tube can then be found from [Equation 5.156](#).

$$C_A \Big|_{z=L} = \left( \frac{2 k_m L}{R V_{average}} \right) C_{AS} = \left( \frac{2 \times 4.66 \times 10^{-4} \text{ cm s}^{-1} \times 10 \text{ cm}}{0.5 \text{ cm} \times 15 \text{ cm s}^{-1}} \right) \times 100 \text{ mg L}^{-1} = 0.124 \text{ mg L}^{-1}$$

The thickness of the concentration boundary layer at the end of the coated section of the tube can be found from [Equation 5.148](#):

$$\delta_C = 1.84 \left( \frac{z R D_{AB}}{V_{average}} \right)^{1/3} = 1.84 \left( \frac{10 \text{ cm} \times 0.5 \text{ cm} \times 4 \times 10^{-6} \text{ cm s}^{-1}}{15 \text{ cm s}^{-1}} \right)^{1/3} = 0.020 \text{ cm}$$

This value of  $\delta_C$  is significantly less than the tube radius of 0.5 cm; hence, the short contact time solution is valid for the mass transfer conditions in this example. Another way to look at whether the short contact solution is valid is to compare the characteristic time for solute convection and the time for radial diffusion within the tube. In terms of convection, the solute

residence time within the tube for this example is on the order of  $\frac{L}{V_{\text{average}}} = \frac{10 \text{ cm}}{15 \text{ cm s}^{-1}} = 0.67 \text{ s}$ .

The radial diffusion time for the solute is on the order of  $\frac{R^2}{D_{AB}} = \frac{(0.5 \text{ cm})^2}{4 \times 10^{-6} \text{ cm}^2 \text{ s}^{-1}} = 62,500 \text{ s}$ .

Hence, we see that the time for the solute to diffuse far from the tube surface to the center of the tube is many orders of magnitude longer than the time the solute actually spends in the tube once it is released from the surface of the tube. In this example, we see that the solute will not be able to penetrate very far from the surface of the tube wall. Therefore, the short contact time solution is valid for these conditions.

## 5.10 The general case of mass transfer between the wall of a cylindrical tube and a flowing fluid

In [Section 5.9.4](#), we obtained a short contact time solution for the mass transfer of a solute between the tube wall and a fluid in laminar flow. In this case, we assume that the solute does not penetrate very far from the surface of the tube and this means as well that the bulk concentration of the solute in the flowing fluid remains constant along the length of the flow path.

However, in many situations, the assumption of a short contact time solution is not valid. This means we need to take into account the fact that the bulk concentration of the solute will be changing along the length of the flow path. This also means that the concentration driving force is no longer constant as we assumed in [Equation 5.154](#) but now changes with the axial position in the tube. This is shown in [Figure 5.9](#) for the case of mass transfer of the solute from the surface of the tube into a flowing fluid. Clearly, the concentration driving force at the entrance of the tube is much larger in this case than at the exit of the tube.

We can still write our solute mass transfer rate in terms of the length averaged mass transfer coefficient, i.e.,  $k_m$ , and the circumferential area of the tube, but the question becomes how do we express the solute concentration difference? The analysis in [Section 5.10.1](#) will show that the proper concentration driving force in this case is the *log mean concentration difference* given by  $\Delta C_{LM}$ .

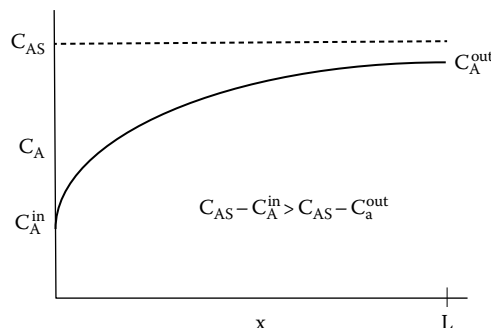


Figure 5.9 Concentration profile for mass transfer from the wall of a cylindrical tube to a flowing fluid.

### 5.10.1 Derivation of the log mean concentration difference

Consider the flow of a fluid in a cylindrical tube of radius  $R$  and length  $L$ . The fluid flow can be either laminar or turbulent. The average velocity of the fluid is  $V_{\text{average}}$ , and the solute concentration at the tube surface is  $C_{\text{AS}}$ . The bulk concentration of the solute in the fluid is  $C_A$  and is defined as the mixing cup average concentration, which is given by

$$C_A = \frac{\int_A v_z(r) C_A(r) dA}{\int_A v_z(r) dA} \quad (5.157)$$

In the above equation,  $v_z(r)$  is the axial velocity in the tube, and the integrations are over the cross-sectional area normal to this flow. The numerator of this equation reflects the fact that, in general, the flow is higher near the axis of the tube, so this flow will bring more solute into the mixing cup than the slower flow near the wall of the tube. The denominator is just the volumetric flow rate.

We can then perform a steady-state shell balance on the solute in the direction of the flow from  $z$  to  $z + \Delta z$  as shown below:

$$V_{\text{average}} \pi R^2 C_A|_{z+\Delta z} = V_{\text{average}} \pi R^2 C_A|_z + 2 \pi R \Delta z k_{\text{m local}} (C_{\text{AS}} - C_A) \quad (5.158)$$

Note that in [Equation 5.158](#), we use the local value of the mass transfer coefficient to describe the mass transfer rate in the region from  $z$  to  $z + \Delta z$ .

When the solute mass balance given by [Equation 5.158](#) is divided by  $\Delta z$  and the limit taken as  $\Delta z \rightarrow 0$ , we get

$$\frac{dC_A}{dz} = \frac{2 k_{\text{m local}}}{V_{\text{average}} R} (C_{\text{AS}} - C_A) \quad (5.159)$$

with the boundary condition that at  $z = 0$ ,  $C_A = C_A^{\text{in}}$  and at  $z = L$ ,  $C_A = C_A^{\text{out}}$ .

The integration of [Equation 5.159](#) over the tube length ( $L$ ) gives the following result:

$$\frac{C_{\text{AS}} - C_A^{\text{out}}}{C_{\text{AS}} - C_A^{\text{in}}} = \exp\left(-\frac{2 k_m L}{V_{\text{average}} R}\right) = \exp\left(-\frac{4 k_m L}{V_{\text{average}} d_{\text{tube}}}\right) \quad (5.160)$$

Note that when we integrate [Equation 5.159](#), the average mass transfer coefficient is introduced and is defined in terms of the local mass transfer coefficient by  $k_m \equiv \frac{1}{L} \int_0^L k_{\text{m local}} dz$ .

Note that if  $V_{\text{average}} R \gg 2 k_m L$ , then  $C_A^{\text{out}} \rightarrow C_A^{\text{in}}$ , and this situation is called *diffusion limited*, and in the limit there is no transfer of the solute into the fluid. If  $2 k_m L \gg V_{\text{average}} R$ , then  $C_A^{\text{out}} \rightarrow C_{\text{AS}}$ , and the solute transport is *flow limited*, and in the limit the solute concentration leaving the tube approaches that at the tube surface.

We can also write a total mass balance on the solute over the tube length ( $L$ ) and obtain the following result that expresses the total solute transport rate ( $\dot{m}_A$ ):

$$\dot{m}_A = V_{\text{average}} \pi R^2 (C_A^{\text{out}} - C_A^{\text{in}}) = 2 \pi RL k_m \Delta C_{\text{LM}} \quad (5.161)$$

Here, we let  $\Delta C_{\text{LM}}$  represent the concentration driving force that when multiplied by the average mass transfer coefficient ( $k_m$ ) and the total surface area available for mass transfer ( $2\pi RL$ ) gives the solute transport rate. We can solve for  $\Delta C_{\text{LM}}$  from the previous equation:

$$\Delta C_{\text{LM}} = \frac{V_{\text{average}} R (C_A^{\text{out}} - C_A^{\text{in}})}{2 k_m L} \quad (5.162)$$

From [Equation 5.160](#), we have that

$$\frac{2 k_m L}{V_{\text{average}} R} = \ln \left( \frac{C_{\text{AS}} - C_A^{\text{in}}}{C_{\text{AS}} - C_A^{\text{out}}} \right) \quad (5.163)$$

Using this result in [Equation 5.162](#), we obtain the following equation for  $\Delta C_{\text{LM}}$ :

$$\Delta C_{\text{LM}} = \frac{V_{\text{average}} R (C_A^{\text{out}} - C_A^{\text{in}})}{2 k_m L} = \frac{(C_A^{\text{out}} - C_A^{\text{in}})}{\ln \left( \frac{C_{\text{AS}} - C_A^{\text{in}}}{C_{\text{AS}} - C_A^{\text{out}}} \right)} = \frac{(C_{\text{AS}} - C_A^{\text{in}}) - (C_{\text{AS}} - C_A^{\text{out}})}{\ln \left( \frac{C_{\text{AS}} - C_A^{\text{in}}}{C_{\text{AS}} - C_A^{\text{out}}} \right)} \quad (5.164)$$

[Equation 5.164](#) defines the *log mean concentration difference* ( $\Delta C_{\text{LM}}$ ), and this is the proper driving force to be used when calculating the total solute mass transfer rate from [Equation 5.161](#). [Equation 5.161](#) can also be used to determine the average mass transfer coefficient, i.e.,  $k_m$ , from measurements of the entering and exiting solute concentrations as shown below:

$$k_m = \frac{\dot{m}_{\text{solute}}}{2 \pi RL \Delta C_{\text{LM}}} = \frac{V_{\text{average}} \pi R^2 (C_A^{\text{out}} - C_A^{\text{in}})}{2 \pi RL \Delta C_{\text{LM}}} = \frac{V_{\text{average}} \pi R^2}{2 \pi RL} \ln \left( \frac{C_{\text{AS}} - C_A^{\text{in}}}{C_{\text{AS}} - C_A^{\text{out}}} \right) \quad (5.165)$$

## 5.10.2 Mass transfer in a tube of arbitrary cross section

We can generalize the results obtained in [Section 5.10.1](#) to a tube of constant arbitrary cross section. In this case, we let  $Q$  represent the volumetric flow rate of the fluid and  $S$  represents the total mass transfer area over the tube of length  $L$ . Hence,

$$\frac{C_{\text{AS}} - C_A^{\text{out}}}{C_{\text{AS}} - C_A^{\text{in}}} = \exp \left( - \frac{k_m S}{Q} \right) \quad (5.166)$$

[Equation 5.161](#) can also be written for this case as

$$\dot{m}_{\text{solute}} = Q (C_A^{\text{out}} - C_A^{\text{in}}) = k_m S \Delta C_{\text{LM}} \quad (5.167)$$

where  $\Delta C_{LM}$  is given by [Equation 5.164](#):

$$\Delta C_{LM} = \frac{\left(C_A^{out} - C_A^{in}\right)}{\ln\left(\frac{C_{AS} - C_A^{in}}{C_{AS} - C_A^{out}}\right)} = \frac{\left(C_{AS} - C_A^{in}\right) - \left(C_{AS} - C_A^{out}\right)}{\ln\left(\frac{C_{AS} - C_A^{in}}{C_{AS} - C_A^{out}}\right)} \quad (5.168)$$

## 5.11 A summary of useful mass transfer coefficient correlations

The earlier mass transfer coefficient and Sherwood number equations that we developed for specific situations also provide valuable insight as to how to develop correlations for mass transfer coefficients in more complicated flows and geometries. In many cases, we find that mass transfer coefficient data can be correlated with general functions that are very similar in form to these equations. For example, for problems involving forced convection where the fluid is flowing over the surface, we can propose a functional dependence for the Sh on the Re and Sc that is very similar to [Equations 5.135](#) and [5.153](#), i.e., the  $Sh = A Re^m Sc^n$ . The values of A, m, and n can then be found by fitting this equation to experimental mass transfer data. [Table 5.1](#) provides a summary (Cussler, 1984) of some useful mass transfer coefficient correlations for a variety of geometries and flow situations, i.e., both laminar and turbulent flows.

### 5.11.1 Mass transfer for undeveloped laminar flow in a cylindrical tube

A particularly important mass transfer coefficient correlation is for the general case of laminar flow of a fluid within a cylindrical tube. When a fluid containing a solute enters a tube, we assume that the velocity profile and the concentration profile are flat and everywhere the same in the radial direction at the tube entrance. This means that the velocity and concentration profiles in the radial direction will change with axial position as the fluid experiences drag and momentum is lost at the tube wall, and solute mass transfer occurs between the bulk fluid and the surface of the tube. The length averaged mass transfer coefficient ( $k_m$ ) for this particular case can be estimated from the following equation (Thomas, 1992):

$$Sh = \frac{k_m d_{tube}}{D_{AB}} = 3.66 + \frac{0.104 Re Sc \left( \frac{d_{tube}}{L} \right)}{1 + 0.016 \left[ Re Sc \left( \frac{d_{tube}}{L} \right) \right]^{0.8}} \quad (5.169)$$

where  $Re = \frac{\rho d_{tube} V_{average}}{\mu}$  and  $Sc = \frac{\mu}{\rho D_{AB}}$ .

[Equation 5.169](#) is generally applicable to this case of undeveloped laminar flow in a cylindrical tube. Recall that a fully developed laminar flow velocity profile is parabolic and is given by [Equation 4.7](#). For the velocity profile to be fully developed at any axial position  $z$ , experiments show that  $z > 0.05 Re d_{tube}$ . For the concentration profile to be fully developed, we have that  $z > 0.05 Re Sc d_{tube}$ . If both of these conditions are satisfied, i.e., the flow is fully developed in terms of the velocity and

Table 5.1 A Selection of Useful Mass Transfer Coefficient Correlations

Physical Situation	Correlation
Sphere in a stagnant fluid	$\frac{k_m d_{sphere}}{D_{AB}} = 2$
Forced convection around a sphere	$\frac{k_m d_{sphere}}{D_{AB}} = 2.0 + 0.6 \left( \frac{\rho d_{sphere} V}{\mu} \right)^{1/2} \left( \frac{\mu}{\rho D_{AB}} \right)^{1/3}$
Laminar flow over a flat plate at location z	$\frac{k_m d_{local}}{D_{AB}} = 0.323 \left( \frac{\rho V z}{\mu} \right)^{1/2} \left( \frac{\mu}{\rho D_{AB}} \right)^{1/3}$
Laminar flow over a flat plate	$\frac{k_m L}{D_{AB}} = 0.646 \left( \frac{\rho V L}{\mu} \right)^{1/2} \left( \frac{\mu}{\rho D_{AB}} \right)^{1/3}$
Laminar flow in a circular tube, short contact time solution	$\frac{k_m d_{tube}}{D_{AB}} = 1.615 \left( \frac{\rho V d_{tube}}{\mu} \right)^{1/3} \left( \frac{\mu}{\rho D_{AB}} \right)^{1/3} \left( \frac{d_{tube}}{L} \right)^{1/3}$
Laminar flow in a circular tube, short contact time solution, at location z	$\frac{k_m d_{local,tube}}{D_{AB}} = 1.077 \left( \frac{\rho V d_{tube}}{\mu} \right)^{1/3} \left( \frac{\mu}{\rho D_{AB}} \right)^{1/3} \left( \frac{d_{tube}}{z} \right)^{1/3}$
Laminar flow in a circular tube, undeveloped flow	$\frac{k_m d_{tube}}{D_{AB}} = 3.66 + \frac{0.104 \left( \frac{\rho V d_{tube}}{\mu} \right) \left( \frac{\mu}{\rho D_{AB}} \right) \frac{d_{tube}}{L}}{1 + 0.016 \left( \left( \frac{\rho V d_{tube}}{\mu} \right) \left( \frac{\mu}{\rho D_{AB}} \right) \frac{d_{tube}}{L} \right)^{0.8}}$
Laminar flow in a circular tube, fully developed flow and concentration profiles	$\frac{k_m d_{tube}}{D_{AB}} = 3.66$
Turbulent flow within a horizontal slit	$\frac{k_m d_{slit}}{D_{AB}} = 0.026 \left( \frac{\rho d_{slit} V}{\mu} \right)^{0.8} \left( \frac{\mu}{\rho D_{AB}} \right)^{1/3},$ with $d_{slit} = \frac{2}{\pi} (\text{slit width})$
Turbulent flow through a circular tube	$\frac{k_m d_{tube}}{D_{AB}} = 0.026 \left( \frac{\rho d_{tube} V}{\mu} \right)^{0.8} \left( \frac{\mu}{\rho D_{AB}} \right)^{1/3}$
Laminar flow in a circular tube	$\frac{k_m d_{tube}}{D_{AB}} = 1.86 \left( \frac{\rho d_{tube} V}{\mu} \frac{\mu}{\rho D_{AB}} \frac{d_{tube}}{L} \right)^{1/3}$ for $\frac{L}{d_{tube}} < 0.01 \text{Re Sc}$
Spinning disk	$\frac{k_m d_{disk}}{D_{AB}} = 0.62 \left( \frac{\rho d_{disk}^2 \omega}{\mu} \right)^{1/2} \left( \frac{\mu}{\rho D_{AB}} \right)^{1/3}$

where  $\omega$  is the disk rotation rate in radians  $s^{-1}$

(Continued)

Table 5.1 (Continued) A Selection of Useful Mass Transfer Coefficient Correlations

Physical Situation	Correlation
Packed beds	$\frac{k_m}{V_0} = 1.17 \left( \frac{\rho d_{\text{particle}} V_0}{\mu} \right)^{-0.42} \left( \frac{\mu}{\rho D_{AB}} \right)^{-0.67}$ <p>where <math>V_0</math> is the superficial velocity defined as the volumetric flow rate divided by the unpacked tube cross-sectional area</p>
Falling film at location z	$\frac{k_m \text{local} z}{D_{AB}} = 0.69 \left( \frac{z V_{\text{film}}}{D_{AB}} \right)^{1/2}$
Falling film, average	$\frac{k_m L}{D_{AB}} = 1.38 \left( \frac{L V_{\text{film}}}{D_{AB}} \right)^{1/2}$

Source: Cussler, E.L., *Diffusion: Mass Transfer in Fluid Systems*, Cambridge University Press, Cambridge, U.K., 1984.

Notes:  $\rho$  is the fluid density,  $\mu$  is the fluid viscosity,  $D_{AB}$  is the solute diffusivity,  $d_{\text{disk}}$  is the disk diameter,  $d_{\text{particle}}$  is the particle diameter,  $d_{\text{sphere}}$  is the sphere diameter,  $d_{\text{tube}}$  is the tube diameter,  $k_m \text{local}$  is the local mass transfer coefficient,  $k_m$  is the length averaged mass transfer coefficient,  $L$  is the tube length,  $R$  is the tube radius,  $V$  is the average fluid velocity,  $V_{\text{film}}$  is the average film velocity,  $z$  is the axial position.

concentration profiles, the Sherwood number for laminar flow in a cylindrical tube then attains its asymptotic value of 3.66. Otherwise, [Equation 5.169](#) must be used to find the Sherwood number.

The length averaged mass transfer coefficient for undeveloped laminar flow in cylindrical tubes and channels can also be estimated from the following equation (Thomas, 1992):

$$Sh = \frac{k_m d_{\text{tube}}}{D_{AB}} = 1.86 Re^{1/3} Sc^{1/3} \left( \frac{d_{\text{tube}}}{L} \right)^{1/3} \quad \text{for } \frac{d_{\text{tube}}}{Re Sc} < 0.01 \quad (5.170)$$

where  $Re = \frac{\rho d_{\text{tube}} V_{\text{average}}}{\mu}$  and  $Sc = \frac{\mu}{\rho D_{AB}}$ .

For noncylindrical flow channels, the diameter of the tube ( $d_{\text{tube}}$ ) in the mass transfer coefficient correlations can be replaced with the *hydraulic diameter*,  $d_H$ , which is defined by the following equation:

$$d_H = \frac{4 \times (\text{cross-sectional area})}{(\text{wetted perimeter})} \quad (5.171)$$

### Example 5.17

A bioreactor is being designed to remove a toxic substance from plasma. The plasma will flow through the bioreactor at a total flow rate of  $250 \text{ mL min}^{-1}$ . The bioreactor consists of a bundle of hollow fibers. The plasma flows on the inside of the hollow fibers and is evenly distributed among them. The total circumferential surface area of these hollow fibers is  $5000 \text{ cm}^2$ , the length of each fiber is  $25 \text{ cm}$ , and the inside diameter of each fiber is  $300 \mu\text{m}$ . The inside surface of these hollow fibers is covered with an enzyme that rapidly converts the toxic material into a harmless product. Determine from this information the performance of this proposed

bioreactor in terms of the % removal of the toxic substance =  $100 \left( 1 - \frac{C_A^{\text{out}}}{C_A^{\text{in}}} \right)$ . The diffusivity for the toxic material in plasma is  $6 \times 10^{-6} \text{ cm}^2 \text{ s}^{-1}$ .

### Solution

Since the enzyme reaction at the surface of the hollow fiber is very fast, this means that  $C_{AS} = 0$ . The % removal of each hollow fiber will be the same since the plasma flow rate and the enzyme loading for each hollow fiber are assumed to be the same. Hence, we only need to focus on what happens in a given hollow fiber. From the given circumferential surface area ( $S$ ) of the hollow fibers, we can find the number of hollow fibers in the bioreactor since  $S = N_{\text{fibers}} \pi d_{\text{fiber}} L$ ; hence,

$$N_{\text{fibers}} = \frac{S}{\pi d_{\text{fiber}} L} = \frac{5000 \text{ cm}^2}{\pi \times 0.03 \text{ cm} \times 25 \text{ cm}} = 2122$$

The flow rate of the plasma in a given hollow fiber is then given by

$$Q = \frac{250 \text{ cm}^3 \text{ min}^{-1} \times \frac{1 \text{ min}}{60 \text{ s}}}{2122} = 0.002 \text{ cm}^3 \text{ s}^{-1}$$

and the average plasma velocity in a hollow fiber is given by

$$V_{\text{average}} = \frac{4Q}{\pi d_{\text{fiber}}^2} = \frac{4 \times 0.002 \text{ cm}^3 \text{ s}^{-1}}{\pi \times (0.03 \text{ cm})^2} = 2.83 \text{ cm s}^{-1}$$

Next, we calculate the Sc and the Re:

$$\begin{aligned} Sc &= \frac{\mu}{\rho D_{AB}} = \frac{1.2 \text{ cP} \times \frac{0.01 \text{ g}}{\text{cm s cP}}}{1.024 \text{ g cm}^{-3} \times 6 \times 10^{-6} \text{ cm s}^{-1}} = 1953 \\ Re &= \frac{\rho d_{\text{fiber}} V_{\text{average}}}{\mu} = \frac{1.024 \text{ g cm}^{-3} \times 0.03 \text{ cm} \times 2.83 \text{ cm s}^{-1}}{1.2 \text{ cP} \times \frac{0.01 \text{ g}}{\text{cm s cP}}} = 7.24 \end{aligned}$$

The Re indicates that the flow of the plasma within the hollow fiber is laminar. This means we can use [Equation 5.169](#) to calculate the mass transfer coefficient:

$$\begin{aligned} Sh &= \frac{k_m d_{\text{fiber}}}{D_{AB}} = 3.66 + \frac{0.104 Re Sc \left( \frac{d_{\text{fiber}}}{L} \right)}{1 + 0.016 \left[ Re Sc \left( \frac{d_{\text{fiber}}}{L} \right) \right]^{0.8}} \\ &= 3.66 + \frac{0.104 \times 7.24 \times 1953 \times \frac{0.03 \text{ cm}}{25 \text{ cm}}}{1 + 0.016 \left[ 7.24 \times 1953 \times \frac{0.03 \text{ cm}}{25 \text{ cm}} \right]^{0.8}} = 5.19 \end{aligned}$$

From this value of the Sh, we can calculate  $k_m$  as

$$k_m = \frac{Sh D_{AB}}{d_{fiber}} = \frac{5.19 \times 6 \times 10^{-6} \text{ cm}^2 \text{ s}^{-1}}{0.03 \text{ cm}} = 0.001 \text{ cm s}^{-1}$$

Now we can calculate the % removal of the toxic substance using [Equation 5.160](#) with  $C_{AS} = 0$ .

$$\frac{0 - C_A^{out}}{0 - C_A^{in}} = \frac{C_A^{out}}{C_A^{in}} = \exp\left(-\frac{4k_m L}{V_{average} d_{fiber}}\right) = \exp\left(-\frac{4 \times 0.001 \text{ cm s}^{-1} \times 25 \text{ cm}}{2.83 \text{ cm s}^{-1} \times 0.03 \text{ cm}}\right) = 0.295$$

$$\% \text{ removal} = 100 \left(1 - \frac{C_A^{out}}{C_A^{in}}\right) = 70.6\%$$

## Problems

- 5.1** Hemoglobin has a MW of 64,460. Estimate its molecular radius and diffusivity in water at 37°C using [Equations 5.35](#) (or [Figure 5.1](#)) and [5.40](#). Explain why these results differ.
- 5.2** Show graphically that the Stokes-Einstein equation ([Equation 5.40](#)) provides a reasonable estimation of the data shown in [Figure 5.1](#).
- 5.3** The following data for the mass transfer coefficient of water flowing within hollow fiber tubes was reported by Yang and Cussler (1986). Compare their results to the correlation given by [Equation 5.170](#). The Peclet number in this case is given by  $Pe = Re Sc \frac{d_{tube}}{L}$ .

Pe	$Sh = \frac{k_m d_{tube}}{D_{AB}}$
30	4.8
50	6.0
100	7.6
300	9.8
500	13.0
1000	18.0
3000	30.0

- 5.4** A new photosensitizer drug has a MW of 1400. Estimate the diffusivity of this drug in water at 37°C using [Equations 5.35](#) and [5.40](#). Express your answer in  $\text{cm}^2 \text{ s}^{-1}$ .
- 5.5** Blood is flowing through a hollow fiber that is 800 μm in diameter and 30 cm in length. The average velocity of the blood within the hollow fiber is  $25 \text{ cm s}^{-1}$ . The concentration of a drug is maintained at  $10 \text{ mg L}^{-1}$  along the inside surface of the hollow fiber. The diffusivity of the drug in blood is  $4 \times 10^{-6} \text{ cm}^2 \text{ s}^{-1}$ . Estimate the mass transfer coefficient  $k_m$  for the drug. Assuming no drug enters the hollow fiber with the blood, estimate the exiting concentration of the drug in the blood.
- 5.6** Derive [Equation 5.126](#).

- 5.7** Derive Equations 5.127 and 5.129.
- 5.8** Starting with Equation 5.143, derive Equation 5.145.
- 5.9** Derive Equation 5.147.
- 5.10** A stainless steel disk is coated on one side with a drug called *Rocketinfusiola* having a MW of 341. The radius of the disk is 0.9 cm. The coated disk is placed in a solution of ethanol, and the disk is then rotated at an angular speed of 80 RPM (RPM = revolutions per minute). The density of ethanol is  $0.80 \text{ g cm}^{-3}$  and its viscosity is 1.198 cP. Estimate the dissolution rate of the *Rocketinfusiola*. The drug's equilibrium solubility in ethanol is equal to  $5.86 \text{ mg cm}^{-3}$ . Assume the concentration of the *Rocketinfusiola* in the bulk solution surrounding the spinning disk is zero and the temperature is  $20^\circ\text{C}$ .
- 5.11** The antibody IgG has a MW of 150,000. Estimate its diffusivity in water at a temperature of  $20^\circ\text{C}$ .
- 5.12** Consider the flow of an aqueous solution within a  $400 \mu\text{m}$  diameter hollow fiber that is 20 cm in length. A drug is impregnated into the wall of the fiber, and the equilibrium solubility of the drug in water is  $3 \text{ mg L}^{-1}$ . The Reynolds number for the flow conditions is 16,000 and the Schmidt number is 10,000. If the diffusivity of the solute of interest in the water is  $0.6 \times 10^{-6} \text{ cm}^2 \text{ s}^{-1}$ , what is the maximum total mass transfer rate ( $\text{mg h}^{-1}$ ) of the drug from the fiber surface?
- 5.13** A particular drug is a solid at  $300 \text{ K}$  and is soluble in water. The equilibrium solubility of the drug in water is  $0.005 \text{ g cm}^{-3}$ . The MW of the drug is 600. 100 g of the drug is made into particles that are 0.2 cm in diameter. The density of the drug particles is  $1.05 \text{ g cm}^{-3}$ . These particles are then very gently mixed in a stirred vessel containing 100 L of water. After 10 min of mixing, estimate how many grams of the drug have dissolved into the water.
- 5.14** Estimate the diffusivity of a drug in a solvent at  $315 \text{ K}$ . The MW of the drug is 526. The viscosity of the solvent at this temperature is 0.295 cP.
- 5.15** A flat plate coated with a layer of a volatile organic material is exposed to a parallel flow of air at  $20^\circ\text{C}$  with a free stream air velocity of  $5 \text{ m s}^{-1}$ . The length of the flat plate in the direction of the flow is 0.5 m. Estimate how long it will take for the average thickness of the volatile organic layer to decrease by 1 mm. The saturation concentration of the organic material in air at these conditions is  $1.85 \times 10^{-9} \text{ mol cm}^{-3}$ , and its diffusivity in air is  $0.068 \text{ cm}^2 \text{ s}^{-1}$ . The density of the volatile organic material as a solid is  $1.21 \text{ g cm}^{-3}$  and its MW is 140.2. Also the kinematic viscosity of air at these conditions is  $0.155 \text{ cm}^2 \text{ s}^{-1}$ .
- 5.16** A cylindrical tube 1 cm in diameter and 10 cm in length has a drug immobilized on its surface. The equilibrium solubility of the drug in the fluid flowing through the tube is  $100 \text{ mg L}^{-1}$ . The fluid flows through the tube at an average velocity of  $10 \text{ cm s}^{-1}$ . If the exiting concentration ( $C_A^{\text{out}}$ ) of the drug in the fluid is  $0.163 \text{ mg L}^{-1}$ , estimate the average value of the mass transfer coefficient ( $k_m$ ) assuming that there is no drug in the fluid that enters the tube.
- 5.17** A liquid extraction process is proposed for removing a drug from the solution leaving a fermentation system. As part of the design process, you need to provide an estimate of the diffusivity of this drug at  $17^\circ\text{C}$  in the extraction solvent cyclohexane. The MW of the drug is  $765 \text{ g mol}^{-1}$ . The viscosity of cyclohexane at this temperature is 1.02 cP.
- 5.18** A spinning disk is being proposed as a room deodorizer. The deodorizer is basically a small cylindrical disk 5 cm in diameter. One side of the disk is coated with a layer of a volatile substance that smells really good. The disk will rotate at 300 RPM, and the average room temperature is  $20^\circ\text{C}$ . Estimate how long it will take (in hours) for the average thickness of the volatile

substance layer to decrease by 1 mm. The saturation concentration of the volatile substance in air at these conditions is  $3 \times 10^{-8}$  mol cm $^{-3}$ , and the diffusivity of the volatile substance in air is given by  $D_{AB} = 0.06$  cm $^2$  s $^{-1}$ . Also, the kinematic viscosity of air at these conditions is 0.151 cm $^2$  s $^{-1}$ . The density of the volatile substance layer is 1.1 g cm $^{-3}$  and its MW is 175 g mol $^{-1}$ .

- 5.19** A rotating disk 1 cm in diameter is coated on one side with a drug that bears a fluorescent tag that allows for determining its concentration in solution. The spinning disk is placed in 100 cm $^3$  of pure water at 37°C and the disk is spun at 25 RPM. After 60 min, the concentration of the drug in the water was found to equal 0.075 g L $^{-1}$ . The equilibrium solubility of the drug in water at these conditions is 3.0 g L $^{-1}$ . From this information, estimate the diffusivity of the drug in water in cm $^2$  s $^{-1}$ .
- 5.20** Water containing a solute is flowing through a 0.2 cm diameter tube, which is 50 cm in length, at an average velocity of 1 cm s $^{-1}$ . The temperature of the water is 37°C. The walls of the tube are coated with an enzyme that makes the solute disappear instantly. The solute enters the tube at a concentration of 0.1 M and the solute has a MW of 300 g mol $^{-1}$ . Estimate the fraction of the solute that leaves the tube.
- 5.21** Yoshida and Ohshima (1966) used a falling liquid film on the outside vertical surface of a cylindrical tube of outside diameter  $d_{\text{tube}}$  to determine the diffusivity of oxygen in water. The table below presents some of their data for the oxygen and water experiments at 37°C. The solubility of oxygen in water at the gas-liquid interface, i.e.,  $C_{SA}$ , was found to be  $3.12 \times 10^{-5}$  g cm $^{-3}$ . The outside diameter of the vertical glass tube, i.e.,  $d_{\text{tube}}$ , was 1.03 cm. Analyze their data and find the value of  $D_{AB}$  for oxygen diffusion in water at 37°C.

Length of Wetted Wall, L, cm	Film Flow Rate, Q, cm $^3$ s $^{-1}$	Oxygen Absorption Rate, M $_{\text{Total}}$ , g s $^{-1}$	M $_{\text{Total}}^{2/3}/Q^{2/3}$ , g $^2$ cm $^{-2}$ s $^{-4/3}$
3.66	0.871	$2.67 \times 10^{-6}$	$7.82 \times 10^{-12}$
8.00	1.01	$5.56 \times 10^{-6}$	$3.07 \times 10^{-11}$
8.41	1.072	$6.63 \times 10^{-6}$	$4.20 \times 10^{-11}$
10.13	1.012	$7.37 \times 10^{-6}$	$5.39 \times 10^{-11}$
10.98	1.112	$8.29 \times 10^{-6}$	$6.40 \times 10^{-11}$
12.94	1.049	$8.77 \times 10^{-6}$	$7.45 \times 10^{-11}$
13.97	1.088	$9.34 \times 10^{-6}$	$8.25 \times 10^{-11}$
15.20	1.041	$10.0 \times 10^{-6}$	$9.74 \times 10^{-11}$
15.26	1.054	$10.0 \times 10^{-6}$	$9.66 \times 10^{-11}$

- 5.22** A system for sterilizing a contact lens before they are packaged for shipment consists of spinning the contact lens in a solution comprised of a disinfectant dissolved in water. The volume of this disinfectant solution surrounding the contact lens is 50 ml. The disinfectant material has a diffusivity in water of  $7.5 \times 10^{-6}$  cm $^2$  s $^{-1}$ , the viscosity of the solution is 1 cP, and its density is 1 g cm $^{-3}$ . The initial concentration of the disinfectant in this solution is 7.5 mg L $^{-1}$ . The lens is spun at 100 RPM. How long will it take in hours for the disinfectant concentration to decrease to 1 mg L $^{-1}$  assuming that the disinfectant agent reacts instantaneously at the surface of the contact lens? You can treat the contact lens as a flat disk that is 14.5 mm in diameter.
- 5.23** A drug with a MW of 700 g mol $^{-1}$  is added to a solvent at a temperature of 25°C. The solvent viscosity at 25°C is 1.5 cP. Estimate the solute diffusivity in this solvent at this temperature.

- 5.24** The diffusivity of a drug in a solvent is  $2.8 \times 10^{-6} \text{ cm}^2 \text{ s}^{-1}$  at a temperature of  $25^\circ\text{C}$ . The solvent viscosity at  $25^\circ\text{C}$  is 1.25 cP. Estimate the MW of the drug.
- 5.25** A system for sterilizing a thin cylindrical bone scaffold disk before they are packaged for shipment consists of spinning the disk in a sterilization solution. The disinfectant material in this solution has a diffusivity in the solution of  $3.0 \times 10^{-6} \text{ cm}^2 \text{ s}^{-1}$ , and the viscosity of the solution is 1.2 cP and its density is  $1.05 \text{ g cm}^{-3}$ . The initial concentration of the disinfecting agent in this solution is  $10 \text{ mg L}^{-1}$ . The scaffold material is a flat disk that is 15 mm in diameter. The disk is spun at 200 RPM. What volume of disinfecting solution is needed if the requirement is to decrease the disinfectant concentration to  $1 \text{ mg L}^{-1}$  in 3.5 h? You can assume that the disinfectant agent reacts instantaneously at the surface of the disk.
- 5.26** A hollow fiber enzyme reactor (HFER) consists of 5000 fibers. Each fiber has an internal diameter of 0.04 cm, and on the inside surface of the fibers, an enzyme has been immobilized that removes a toxin from plasma that is flowing through the inside of the fibers. The enzyme reaction is very fast so a good assumption is that the concentration of the toxin at the surface of the hollow fiber is equal to zero. The HFER operates at  $37^\circ\text{C}$  and the plasma enters at a total flow rate of  $200 \text{ mL min}^{-1}$ . The concentration of the toxin in the plasma that enters the HFER is  $1 \text{ mg L}^{-1}$  and its MW is  $636 \text{ g mol}^{-1}$ . If the fibers in the HFER are 50 cm in length, what is the concentration of the toxin in the plasma as it leaves the HFER?
- 5.27** A spheroid of hepatocytes is suspended within a large amount of stagnant nutrient media containing a drug. The experiment is being done to measure the rate of metabolism of this drug by the cells in the spheroid. The spheroid has a diameter of 0.08 cm. At a particular time during the experiment, it was found that the drug concentration in the bulk media solution was equal to  $0.190 \mu\text{mol cm}^{-3}$  and the drug concentration at the surface of the spheroid of cells was found to be  $0.07 \mu\text{mol cm}^{-3}$ . From these data, determine the reaction rate per volume of spheroid (i.e.,  $\mu\text{mol L}^{-1} \text{ s}^{-1}$ ) at which the hepatocyte cells in the spheroid are metabolizing the drug. The diffusivity of this drug in the nutrient media is  $7.35 \times 10^{-6} \text{ cm}^2 \text{ s}^{-1}$ .
- 5.28** The diffusivity of a drug in water at  $37^\circ\text{C}$  was found to be  $6.5 \times 10^{-6} \text{ cm}^2 \text{ s}^{-1}$ . What would its diffusivity be in a solvent A at  $20^\circ\text{C}$ ? The viscosity of solvent A at this temperature is 0.86 cP.
- 5.29** A solid sphere with a diameter of 2 mm has a thin film of a drug ( $\text{MW} = 475 \text{ g mol}^{-1}$ ) coated on its surface. Water at  $37^\circ\text{C}$  flows past the sphere with an average velocity of  $2 \text{ cm s}^{-1}$ . The equilibrium solubility of the drug in water at these conditions is  $20 \mu\text{M}$ . If the drug concentration far from the surface of the sphere is zero, calculate the mass transfer rate of the drug from the surface of the sphere in  $\text{ng s}^{-1}$ .
- 5.30** It is desired to remove a toxic substance from plasma by passing the plasma through the inside of the hollow fibers of a bioreactor. The flow rate of the plasma is  $2000 \text{ cm}^3 \text{ min}^{-1}$ , and the bioreactor contains 1000 hollow fibers each with a diameter of  $800 \mu\text{m}$  and a length of 50 cm. The walls of these hollow fibers contain an enzyme coated on their surface that rapidly converts the toxic material into a harmless substance. The toxic substance has a diffusivity in plasma of  $6 \times 10^{-6} \text{ cm}^2 \text{ s}^{-1}$ , and the viscosity of the plasma is 1.2 cP and its density is  $1.02 \text{ g cm}^{-3}$ . Estimate the % removal of the toxic substance from the plasma by this device.
- 5.31** A drug has a measured diffusivity of  $5 \times 10^{-6} \text{ cm}^2 \text{ s}^{-1}$  at  $37^\circ\text{C}$ . What is this drug's Stokes-Einstein radius in nm?
- 5.32** As part of the design of a bioartificial liver, there is a hollow fiber membrane cartridge that treats plasma with activated carbon to remove toxic components that are in the plasma. The plasma to this device comes from a plasmapheresis unit that separates a portion of the plasma from the patient's blood. The activated carbon particles are in the shell space that surrounds

the hollow fibers. The plasma therefore flows within the hollow fibers. The plasma flow rate to the device is  $250 \text{ mL min}^{-1}$ , and there are 6500 hollow fibers in the device. The inside diameter of the hollow fibers is  $400 \mu\text{m}$ . These fibers are microporous and have a very high solute permeability. During the early period of time after the device has been in contact with the plasma, the activated carbon has a very large capacity for the adsorption of toxic materials that are present in the plasma. Hence, it is reasonable to assume that the concentration of any toxic material in the plasma is zero at the inside surface of the hollow fibers. For a target toxin having a MW of  $300 \text{ g mol}^{-1}$ , the diffusivity of this solute in the plasma would be about  $4.5 \times 10^{-6} \text{ cm}^2 \text{ s}^{-1}$ . If the hollow fibers are 40 cm in length, estimate the fractional removal of this toxin during the early phase of the device's operation. Assume the density of the plasma is  $1.024 \text{ g cm}^{-3}$  and the viscosity is 1.2 cP.

- 5.33** Air at  $100^\circ\text{F}$  and 2 atm is being passed over a shallow bed of naphthalene spheres that are 0.5 inch in diameter at a superficial velocity ( $V_0$ ) of  $5 \text{ ft s}^{-1}$ . The MW of naphthalene is  $128.2 \text{ g mol}^{-1}$ , and its diffusivity in air at these operating conditions is  $0.033 \text{ cm}^2 \text{ s}^{-1}$ . The porosity of the bed is 0.40, and the total surface area of the naphthalene particles is  $86.3 \text{ ft}^2$  for each  $1 \text{ ft}^3$  of packed bed. The viscosity of air under these conditions is 0.0184 cP and the density of air is  $0.0023 \text{ g cm}^{-3}$ . The equilibrium concentration of naphthalene in the air under these conditions is  $0.006 \text{ mol L}^{-1}$ . Assuming the concentration of the naphthalene in the air stream is negligible, estimate the initial evaporation rate of the naphthalene in pounds per second from  $1 \text{ ft}^3$  of bed.
- 5.34** Genetically modified endothelial cells are grown on the inside surface of a cylindrical hollow fiber with an internal diameter of  $200 \mu\text{m}$  and a length of 15 cm. This bioreactor is being used to remove toxin A from plasma at  $37^\circ\text{C}$ . These cells carry on their surface an enzyme that instantly converts toxin A into a harmless substance. The plasma flows through the hollow fiber at the rate of  $0.75 \text{ cm}^3 \text{ min}^{-1}$ . If toxin A enters the bioreactor at a concentration of  $0.01 \text{ mol L}^{-1}$ , find the toxin concentration at the outlet of the hollow fiber bioreactor. The toxin has a MW of  $785 \text{ g mol}^{-1}$ .
- 5.35** A drug has a Stokes-Einstein radius of 0.6 nm. What is its diffusivity ( $\text{cm}^2 \text{ s}^{-1}$ ) in a solvent at  $20^\circ\text{C}$  having a viscosity of 0.8 cP?
- 5.36** The diffusivity of a molecule in a solvent at  $25^\circ\text{C}$  was experimentally found to be equal to  $4 \times 10^{-6} \text{ cm}^2 \text{ s}^{-1}$ . The viscosity of the solvent at these conditions is 0.86 cP. Estimate the molecular radius of this molecule in nanometers (nm).
- 5.37** A new design for a contact lens cleaning system uses a 3% hydrogen peroxide ( $\text{H}_2\text{O}_2$ ) solution to kill any bacteria on the lenses. The killing of the bacteria occurs quickly when the lens is in this solution. However, the remaining hydrogen peroxide needs to be neutralized before the lenses can be worn again. It is proposed to neutralize the hydrogen peroxide by having within the lens cleaning container a thin rotating disk that has a catalyst on its surface. The disk is rotated at 200 RPM. As the catalyst disk rotates, the residual hydrogen peroxide diffuses to the surface of the disk where it is instantly converted into water and oxygen according to the following equation:  $\text{H}_2\text{O}_2 \rightarrow \text{H}_2\text{O} + \frac{1}{2}\text{O}_2$ . At  $25^\circ\text{C}$ , the density of the hydrogen peroxide solution may be assumed to be  $1 \text{ g cm}^{-3}$ , and the viscosity is 0.90 cP. The diffusivity of hydrogen peroxide in water is  $1.43 \times 10^{-5} \text{ cm}^2 \text{ s}^{-1}$ . The initial concentration of hydrogen peroxide is pretty close to  $0.03 \text{ g cm}^{-3}$ . The MW of hydrogen peroxide is  $34 \text{ g mol}^{-1}$ . If the catalyst disk is  $5/8$  inch in diameter, and both sides of the disk are catalytically active, estimate initially how many milliliters of oxygen per minute will be evolved at a temperature of  $25^\circ\text{C}$  and a pressure of 1 atm. The molar density of oxygen as a gas at these conditions is  $0.041 \text{ mol L}^{-1}$ .

- 5.38** Chloropicrin, also known as PS and nitrochloroform, is a chemical compound currently used as a broad-spectrum antimicrobial, fungicide, herbicide, insecticide, and nematicide. In World War I, the Germans used it as tear gas since it is also an airway irritant. This substance is a liquid at room temperatures. Suppose there was a small spill of this material on a paved surface at a chemical plant. The spill has a width of 0.8 ft and a length of 2.5 ft. The prevailing wind is 10 miles per hour in a direction parallel to the length of the spilled material. Estimate the rate of evaporation in grams per hour of this material. Chloropicrin has a diffusivity in air of  $0.088 \text{ cm}^2 \text{ s}^{-1}$ . At  $25^\circ\text{C}$ , its vapor pressure is such that its equilibrium concentration in air would be equal to  $0.211 \text{ g L}^{-1}$ . The kinematic viscosity of air under these conditions is  $0.157 \text{ cm}^2 \text{ s}^{-1}$ . Carefully state your assumptions.
- 5.39** Design a hollow fiber plasma oxygenator. The operating conditions are as in [Example 5.12](#). Assume there is no oxygen in the entering plasma and that the saturation oxygen level in plasma is  $216 \mu\text{M}$ .
- 5.40** Air at  $100^\circ\text{C}$  and 1 atm flows over a flat plate of a volatile substance at a free stream velocity of  $3 \text{ m s}^{-1}$ . The plate is 2 m in length and 0.5 m in width. The viscosity of air at these conditions is 0.0215 cP and the density of the air is  $948 \text{ g m}^{-3}$ . The equilibrium concentration of the volatile substance in the air at the surface of the plate is  $64.5 \text{ g m}^{-3}$ . What is the total mass transfer rate of the volatile substance from the plate to the air in  $\text{g min}^{-1}$ ? The concentration of the substance in the air far from the surface is zero, and the diffusivity of the volatile substance in the air is  $0.094 \text{ cm}^2 \text{ s}^{-1}$ .
- 5.41** Estimate the liquid diffusivity of acetic acid at  $25^\circ\text{C}$  in a dilute solution of ethyl acetate. Molecular models of the acetic acid molecule give a molecular radius of about 0.22 nm. The viscosity of the ethyl acetate is 0.462 cP.
- 5.42** As part of the design of a bioartificial liver, there is a hollow fiber membrane cartridge that first treats the plasma with a mix of immobilized enzymes to remove any toxic components that are in the plasma. The plasma to this device comes from a plasmapheresis unit that separates a portion of the plasma from the patient's blood. The immobilized enzyme particles are in the shell space that surrounds the hollow fibers. The plasma therefore flows within the hollow fibers. The plasma flow rate to the device is  $250 \text{ mL min}^{-1}$  and there are 6500 hollow fibers in the device. The inside diameter of the hollow fibers is  $400 \mu\text{m}$ . The enzyme loading in the shell space is quite large, and the enzyme reactions may be considered to be very fast in comparison to the mass transfer processes. Hence, it is reasonable to assume that the concentration of any toxic material in the plasma is zero at the inside surface of the hollow fibers. For a target toxin having a MW of  $300 \text{ g mol}^{-1}$ , and if the hollow fibers are 25 cm in length, estimate the fractional removal of this toxin from this device. Assume the density of the plasma is  $1.024 \text{ g cm}^{-3}$ , the viscosity is 1.2 cP, and that the device operates at  $37^\circ\text{C}$ .
- 5.43** A hazardous chemical was spilled into a quiescent pond. The chemical is immiscible with water and has a density of  $0.9 \text{ g cm}^{-3}$ . A hazmat team estimated that there is a layer of the chemical on the pond surface that is 2 cm in thickness. Measurements made with a portable gas chromatograph show that the vapor film layer above the surface of this chemical layer is about 0.5 cm in thickness. The diffusivity of this chemical in air is known to be  $0.03 \text{ cm}^2 \text{ s}^{-1}$ . Since the pond is in a remote location, it has been decided to just let the chemical evaporate into the air. Assuming the concentration of the chemical in the bulk air is so low that it can be neglected, estimate how many days this will take. The saturation concentration of the chemical in the air is  $6.73 \times 10^{-5} \text{ g cm}^{-3}$ .



Taylor & Francis

Taylor & Francis Group

<http://taylorandfrancis.com>

# Chapter 6 Mass transfer in heterogeneous materials

The heterogeneous nature of biological tissues and medical devices complicates the description of solute mass transfer in these systems. There will be regions where the solute molecule will encounter obstacles that either will hinder the movement of the solute or cannot be penetrated. For example, solutes will need to diffuse through porous structures such as the capillary wall or a polymeric membrane, around or through cells, and through fluids containing a variety of macromolecules. The mass transfer of the solute will therefore be affected by the presence of these heterogeneous structures and the components found in complex macromolecular solutions. Hence, we will have to make suitable adjustments to the solute diffusivity and be careful with how we apply Fick's first and second laws in these situations.

## 6.1 Solute diffusion within heterogeneous media

To understand mass transfer in heterogeneous materials, we will need to expand our understanding of solute diffusion to see how these heterogeneous structures affect solute diffusion.

We will begin by considering as an example the transport of a solute from the blood across the capillary wall into the surrounding tissue space. The concepts introduced by this example are general and can be applied to other heterogeneous structures, such as mass transfer across a variety of membranes.

Figure 6.1 illustrates the situation for the diffusion of a solute from the blood, through the cell-free plasma layer, across the capillary wall, and into the surrounding tissue space. The figure shows many of the types of solute diffusivity that we will need to consider. These are the solute diffusivity in blood or tissue ( $D_T$ ), the diffusivity in plasma ( $D_{\text{plasma}}$ ), the diffusivity within a pore of the capillary wall ( $D_{\text{pore}}$ ), the diffusivity in the interstitial fluid ( $D_0$ ), and the diffusivity through cells ( $D_{\text{cell}}$ ). The following discussion will show how to relate these various solute diffusivities to the diffusivity of the solute in a homogeneous medium, like water, where we defined the solute diffusivity as  $D_{AB}$ .

### 6.1.1 Solute transport across thin porous membranes

For solute transport by diffusion through the pores of the capillary wall, or a porous membrane in general, the available surface area for mass transfer of the solute is not the total surface area of the membrane, i.e.,  $S$ , but the pore area,  $A_p$ . The porosity, i.e.,  $\epsilon$ , of the membrane is the volume fraction of the porous void volume within the membrane divided by the total membrane volume. The porosity, i.e.,  $\epsilon$ , of the membrane is then given by  $A_p/S$ .

The solute itself is only soluble in the fluid contained within the pores and is not soluble in the continuous nonporous phase. Furthermore, in many cases, the pores are not perfectly straight and will have a length greater than the membrane thickness,  $\bar{L}$ . This means the solute must follow a path through the pores that is tortuous, making the diffusion distance greater than the thickness

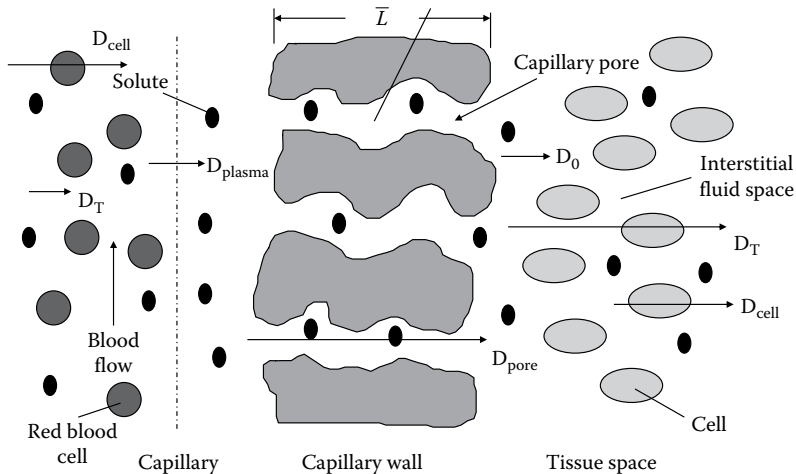


Figure 6.1 Solute transport from blood.

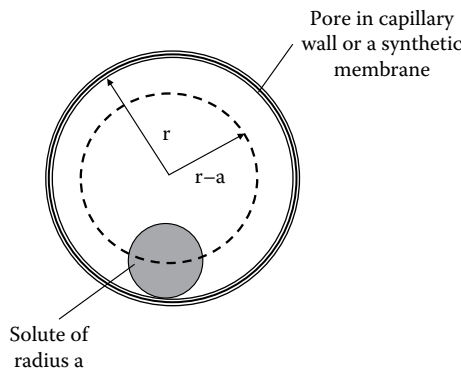


Figure 6.2 Steric exclusion.

of the membrane. We account for this tortuous diffusion distance by the *tortuosity* ( $\tau$ ), which when multiplied by the thickness of the membrane, i.e.,  $\tau \times \bar{L}$ , gives the total pore diffusion distance.

**6.1.1.1 Steric exclusion and hindered diffusion** In many cases in pore diffusion, the solute radius, i.e.,  $a$ , is also comparable to that of the pore radius,  $r$ . This leads to two additional effects, both reducing the diffusivity of the solute within the pore. The first effect, called *steric exclusion*, is illustrated in Figure 6.2. Steric exclusion restricts the ability of the solute from entering the pore from the bulk solution. In Figure 6.2, we see that to a first approximation, a solute can get no closer to the pore wall than its radius ( $a$ ). Therefore, only a fraction of the pore cross-sectional area is available to the molecule. The fraction of the pore cross-sectional area available to the solute is given by the following ratio:

$$K = \frac{\pi(r-a)^2}{\pi r^2} = \left(1 - \frac{a}{r}\right)^2 = \frac{C_{A_{\text{pore}}}}{C_{A_{\text{bulk}}}} \Big|_{\text{pore mouth}} \quad (6.1)$$

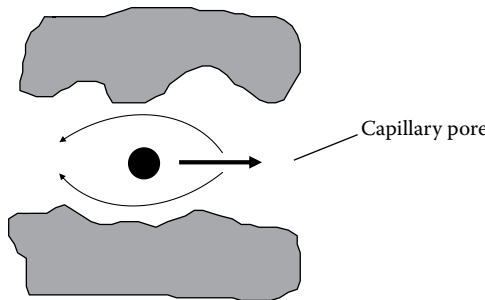


Figure 6.3 Solvent flow across solute in small pores increases drag.

where  $K$  is also known as the solute *partition coefficient*. Because of steric exclusion, the equilibrium concentration of the solute is lower at the pore mouth than in the bulk solution adjacent to the pore entrance, i.e.,  $C_{A\text{pore}}|_{\text{pore mouth}} < C_{A\text{bulk}}|_{\text{pore mouth}}$ . This simple expression for  $K$  ignores any secondary attractive or repulsive interactions between the solute and the pore and basically treats the molecule as a hard sphere. Attractive forces between the solute and the pore will tend to increase the value of  $K$ , and repulsive forces will decrease the value of  $K$ , relative to that based on steric exclusion alone. In these cases, it is best to measure  $K$  experimentally.

As the solute molecule diffuses through the pore, it experiences hydrodynamic drag caused by the flow of the solvent over the surface of the solute. This is shown in Figure 6.3. As the solute radius increases relative to that of the pore radius, this hydrodynamic drag increases, reducing or restricting the diffusion of the solute through the pore compared to its motion in the bulk fluid. This drag effect on the solute in the pore results in a decrease in the solute diffusivity within the pore relative to its value in the bulk solution and is called *restricted or hindered diffusion*.

**6.1.1.2 Solute diffusion in a single pore of a thin planar membrane** Now we can apply Fick's first law to the situation of solute diffusion through a single straight cylindrical pore. Letting  $x$  denote the direction along the length of the pore, we can write the following steady-state solute balance over a control volume from  $x$  to  $x + \Delta x$  as shown below:

$$0 = -\pi r^2 D_{\text{pore}} \frac{dC_{A\text{pore}}}{dx} \Big|_x - \pi r^2 D_{\text{pore}} \frac{dC_{A\text{pore}}}{dx} \Big|_{x+\Delta x} \quad (6.2)$$

In Equation 6.2

$D_{\text{pore}}$  is the diffusivity of the solute in the fluid contained within the pore

$C_{A\text{pore}}$  is the solute concentration within the pore

Dividing by  $\Delta x$ , and taking the limit as  $\Delta x \rightarrow 0$ , Equation 6.2 becomes

$$\frac{d^2C_{A\text{pore}}}{dx^2} = 0 \quad (6.3)$$

If we integrate Equation 6.3 once, we find that  $dC_{A\text{pore}}/dx = C_1$ , which says that the solute flux within the pore of a thin planar membrane is equal to a constant. If we integrate this result, we then get that  $C_{A\text{pore}}(x) = C_1 x + C_2$ , where  $C_1$  and  $C_2$  are the integration constants. This shows that the solute concentration profile within the pore of a thin planar membrane is linear.

The integration constants, i.e.,  $C_1$  and  $C_2$ , can be found from the boundary conditions (BCs) at the entrance and exit of the pore. At the pore entrance, where  $x = 0$ , we have that  $C_{A\text{pore}} = C_{A\text{pore}}^{x=0}$ , and at the pore exit, where  $x = \bar{L}$ , we have  $C_{A\text{pore}} = C_{A\text{pore}}^{x=\bar{L}}$ . Using these boundary conditions, we find for a thin planar membrane that  $C_2 = C_{A\text{pore}}^{x=0}$  and  $C_1 = (C_{A\text{pore}}^{x=\bar{L}} - C_{A\text{pore}}^{x=0})/\bar{L} = dC_{A\text{pore}}/dx$ . The concentration profile along the length of the pore is then given by

$$C_{A\text{pore}}(x) = C_{A\text{pore}}^{x=0} - (C_{A\text{pore}}^{x=0} - C_{A\text{pore}}^{x=\bar{L}}) \frac{x}{\bar{L}} \quad (6.4)$$

From Fick's first law for a dilute solution, we have for the solute flux within the pore that

$$N_{Ax}^{\text{pore}} = -D_{\text{pore}} \frac{dC_{A\text{pore}}}{dx} = -D_{\text{pore}} \frac{C_{A\text{pore}}^{x=\bar{L}} - C_{A\text{pore}}^{x=0}}{\bar{L}} \quad (6.5)$$

The solute concentration within the pore is difficult to measure. However, the bulk concentrations of the solute outside the membrane are known. We can relate the solute concentrations within the pore at the entrance and exit of the pore to the bulk solute concentration just outside the pore by the partition coefficient given by [Equation 6.1](#). Hence, [Equation 6.5](#) can be written as

$$N_{Ax}^{\text{pore}} = -D_{\text{pore}} \frac{C_{A\text{pore}}^{x=\bar{L}} - C_{A\text{pore}}^{x=0}}{\bar{L}} = -D_{\text{pore}} K \frac{C_{A\text{bulk}}^{x=\bar{L}} - C_{A\text{bulk}}^{x=0}}{\bar{L}} \quad (6.6)$$

Next, we can account for the tortuous nature of the pore by increasing the membrane thickness, i.e.,  $\bar{L}$ , by the tortuosity,  $\tau$ . Also, because of the hindered or restricted diffusion effect within the pore, the value of  $D_{\text{pore}}$  will be smaller than the value of  $D_{AB}$  by a factor we will call  $\omega_r$ , which we expect to depend on the ratio of the solute radius to the pore radius, i.e.,  $a/r$ . With these adjustments, [Equation 6.6](#) becomes

$$N_{Ax}^{\text{pore}} = -D_{\text{pore}} K \frac{C_{A\text{bulk}}^{x=\bar{L}} - C_{A\text{bulk}}^{x=0}}{\bar{L}} = -D_{AB} \left( \frac{K\omega_r}{\tau} \right) \frac{C_{A\text{bulk}}^{x=\bar{L}} - C_{A\text{bulk}}^{x=0}}{\bar{L}} \quad (6.7)$$

[Equation 6.7](#) gives the solute flux in a given pore of a thin planar membrane written in terms of the measurable bulk solute concentrations at the surface on either side of the membrane. From [Equation 6.7](#), we see that the diffusivity of the solute in the pore, i.e.,  $D_{\text{pore}}$ , and the solute diffusivity across a single membrane pore relative to the bulk solute concentrations, i.e.,  $D_m$ , are defined as

$$\begin{aligned} D_{\text{pore}} &= D_{AB} \frac{\omega_r}{\tau} \\ D_m &= K D_{\text{pore}} = D_{AB} \left( \frac{K\omega_r}{\tau} \right) \end{aligned} \quad (6.8)$$

**6.1.1.3 Solute diffusion across a thin planar membrane** To find the solute flux for a membrane of total surface area  $S$ , and a total cross-sectional pore area of  $A_p$ , we multiply  $N_{Ax}^{\text{pore}}$  by the total area of all the pores, i.e.,  $A_p$ , which gives the total mass transfer rate, and then we divide that result by the total membrane area, i.e.,  $S$ , to get the solute flux based on the total membrane area, i.e.,  $N_{Ax}$ :

$$N_{Ax} = \frac{A_p}{S} \times N_{Ax}^{\text{pore}} = -D_{AB} \frac{A_p}{S} \left( \frac{K\omega_r}{\tau} \right) \frac{C_{A\text{bulk}}^{x=\bar{L}} - C_{A\text{bulk}}^{x=0}}{\bar{L}} = -D_e \frac{C_{A\text{bulk}}^{x=\bar{L}} - C_{A\text{bulk}}^{x=0}}{\bar{L}} \quad (6.9)$$

where  $D_e$  is called the *effective diffusivity* of the solute for a heterogeneous membrane material.  $D_e$  is then given by the following equation:

$$D_e = D_{AB} \frac{A_p}{S} \left( \frac{K\omega_r}{\tau} \right) = \frac{\varepsilon D_{AB}}{\tau} K\omega_r = \varepsilon K D_{pore} = \varepsilon D_m \quad (6.10)$$

where  $\varepsilon = A_p/S$  is the porosity of the membrane.

For mass transfer across a thin planar membrane placed between two well-stirred solutions, the solute mass transfer rate across the membrane of total surface area  $S$  is then given by

$$\dot{m}_A = SD_e \frac{C_{A\text{bulk}}^{x=0} - C_{A\text{bulk}}^{x=\bar{L}}}{\bar{L}} \quad (6.11)$$

**6.1.1.4 The Renkin equation** Beck and Schultz (1970) studied the diffusion of a variety of solutes across track-etched mica membranes. The mica membranes were bombarded with  $U^{235}$  fission fragments. The etched particle tracks that were formed resulted in relatively straight pores (i.e.,  $\tau = 1$ ) with a narrow pore size distribution. Their data for a number of solutes is shown in Figure 6.4, where the ratio of the solute diffusivity in a membrane pore ( $D_m$ ) based on the bulk solute concentrations and the bulk diffusivity ( $D_{AB}$ ) is plotted as function of the ratio of the solute radius to pore radius, i.e.,  $\lambda = a/r$ . We see that this hindered diffusion effect significantly affects the solute diffusivity. Note from Figure 6.4 that when the solute radius is only one-tenth of the pore radius, the solute diffusivity is reduced by about 40%. When  $\lambda$  is equal to 0.40, the solute diffusivity has been reduced by nearly 90%.

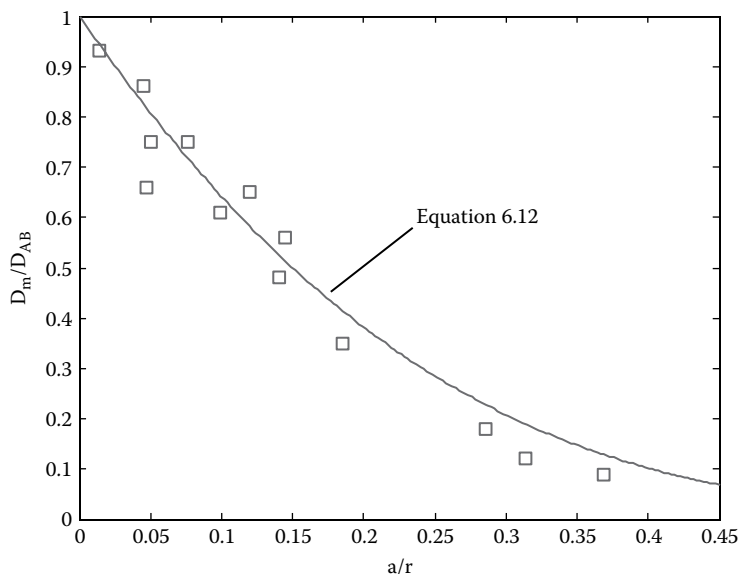


Figure 6.4 Solute diffusivity in the pores of a membrane. (Data from Beck, R.E. and Schultz, J.S., *Science*, 170, 1302, 1970.)

According to [Equation 6.8](#), we have  $\tau = 1$  in their experiments,  $D_m/D_{AB} = K\omega_r$ , and the data in [Figure 6.4](#) shows that  $K\omega_r$  is only a function of  $\lambda = a/r$ . The solid line in [Figure 6.4](#) represents the fit of the Renkin equation (1954) to their data, which is given by the following expression:

$$\left(\frac{D_m}{D_{AB}}\right)_{\tau=1} = K\omega_r = \left(1 - \frac{a}{r}\right)^2 \left[ 1 - 2.1\left(\frac{a}{r}\right) + 2.09\left(\frac{a}{r}\right)^3 - 0.95\left(\frac{a}{r}\right)^5 \right] \quad (6.12)$$

We see that the Renkin equation describes their data rather well. The first term in parentheses on the right-hand side of [Equation 6.12](#) is the partition coefficient, i.e.,  $K$ , given by [Equation 6.1](#), and represents the effect of steric exclusion, or the reduction in the solute concentration at the pore mouth compared to its value in the well-stirred bulk solution. The bracketed term on the right-hand side of [Equation 6.12](#) is the hindered diffusion term, i.e.,

$$\omega_r = \left( 1 - 2.1\left(\frac{a}{r}\right) + 2.09\left(\frac{a}{r}\right)^3 - 0.95\left(\frac{a}{r}\right)^5 \right) \quad (6.13)$$

and accounts for the increased hydrodynamic drag in a pore comparable in size to that of the solute. Additional expressions for describing the hindered diffusion of large molecules in liquid-filled pores can be found in the review paper by Deen (1987).

### Example 6.1

Estimate the diffusivity ( $D_m$ ) of ovalbumin at 25°C through the cylindrical pores of a membrane that are 28 nm in diameter. The pores have a tortuosity of 1.2. Assume that the molecule enters the pores of the membrane from a well-stirred bulk solution.

#### Solution

Cussler (1984) gives the ovalbumin diffusivity as  $7.8 \times 10^{-7}$  cm<sup>2</sup> s<sup>-1</sup>. In [Example 5.1](#), we estimated that this solute has a radius of 2.61 nm. The pore radius is given as 14 nm, so  $\lambda = 2.61 \text{ nm}/14 \text{ nm} = 0.186$ . With these values, we can then use [Equation 6.12](#) to find  $K\omega_r$ , which is equal to 0.413. Next, we calculate  $D_m$  from [Equation 6.8](#):

$$D_m = D_{AB} \left( \frac{K\omega_r}{\tau} \right) = 7.8 \times 10^{-7} \text{ cm}^2 \text{ s}^{-1} \left( \frac{0.413}{1.2} \right) = 2.685 \times 10^{-7} \text{ cm}^2 \text{ s}^{-1}$$

### Example 6.2

Suppose the concentration of ovalbumin in the previous example is 5 g L<sup>-1</sup> in the bulk solution at the entrance to the pore and 0 g L<sup>-1</sup> at the pore exit. Calculate the ovalbumin solute flux in g cm<sup>-2</sup> s<sup>-1</sup> through a 28 nm diameter pore assuming its length is 0.02 cm and the tortuosity of the pore is 1.2. Consider next a membrane with a total surface area of 100 cm<sup>2</sup> that consists of a multitude of these pores such that the porosity of the membrane ( $\epsilon$ ) is 0.40. Calculate the total ovalbumin transport rate in g h<sup>-1</sup> for the membrane.

### Solution

To calculate the solute flux across a single pore, we use [Equation 6.7](#) and the value of  $D_m$  from [Example 6.1](#):

$$N_{Ax}^{pore} = -D_{AB} \left( \frac{K\omega_r}{\tau} \right) \frac{C_{A\text{bulk}}^{x=\bar{L}} - C_{A\text{bulk}}^{x=0}}{\bar{L}} = -D_m \frac{C_{A\text{bulk}}^{x=\bar{L}} - C_{A\text{bulk}}^{x=0}}{\bar{L}}$$

$$N_{Ax}^{pore} = -2.685 \times 10^{-7} \text{ cm}^2 \text{ s}^{-1} \times \frac{(0-5) \text{ g L}^{-1} \times \frac{1 \text{ L}}{1000 \text{ cm}^3}}{0.02 \text{ cm}} = 6.713 \times 10^{-8} \text{ g cm}^{-2} \text{ s}^{-1}$$

To calculate the total solute mass transfer rate across a  $100 \text{ cm}^2$  membrane, we use [Equation 6.11](#). From [Equation 6.10](#), we have that  $D_e = \varepsilon D_m$

$$\dot{m}_A = SD_e \frac{C_{A\text{bulk}}^{x=0} - C_{A\text{bulk}}^{x=\bar{L}}}{\bar{L}} = \varepsilon SD_m \frac{C_{A\text{bulk}}^{x=0} - C_{A\text{bulk}}^{x=\bar{L}}}{\bar{L}} = \varepsilon SN_{Ax}^{pore}$$

$$\dot{m}_A = 0.4 \times 100 \text{ cm}^2 \times 6.713 \times 10^{-8} \text{ g cm}^{-2} \text{ s}^{-1} \times 3600 \text{ s h}^{-1} = 0.0097 \text{ g h}^{-1}$$

**6.1.1.5 Solute membrane permeability** [Equation 6.11](#) shows that the solute mass transfer rate across a membrane of total surface area  $S$  is proportional to the solute concentration difference in the bulk fluid adjacent to either side of the membrane and the ratio of the solute effective diffusivity, i.e.,  $D_e$ , and the membrane thickness,  $\bar{L}$ . This ratio, i.e.,  $D_e/\bar{L}$ , is called the *membrane permeability* ( $P_m$ ) and is often used to describe solute transport across a membrane. The membrane permeability lumps together all of the membrane properties that affect the transport of the solute across the membrane. In terms of the membrane permeability, we can rewrite [Equation 6.11](#) for the solute mass transfer rate across the membrane as

$$\dot{m}_A = P_m S \left( C_{A\text{bulk}}^{x=0} - C_{A\text{bulk}}^{x=\bar{L}} \right) \quad (6.14)$$

From [Equations 6.9](#) and [6.10](#), we see that for microporous membranes, the membrane permeability can be expressed in terms of the membrane properties as

$$P_m = \frac{D_e}{\bar{L}} = \frac{D_{AB}}{\bar{L}} \left( \frac{A_p}{S} \right) \left( \frac{K\omega_r}{\tau} \right) \quad (6.15)$$

For a membrane with cylindrically shaped pores, the quantity  $K\omega_r$  can be estimated from the Renkin equation given by [Equation 6.12](#). The porosity of the membrane, i.e.,  $\varepsilon = A_p/S$ , is usually known or easily measured for a given membrane. The tortuosity, i.e.,  $\tau$ , is best measured from experiments of solute mass transfer rates across the membrane. Tortuosity usually falls in the range from 2 to 6 (Cussler, 1984) and, in the absence of any other information, is on the order of  $1/\varepsilon$ .

**6.1.1.6 Capillary wall solute permeability** We can also use [Equation 6.14](#) to describe solute transport across the capillary wall. The intercellular cleft, as shown in [Figures 3.2](#) and [3.3](#), forms pores through which the solute diffuses. The capillary wall for many solutes that are lipid insoluble is therefore like a microporous membrane.

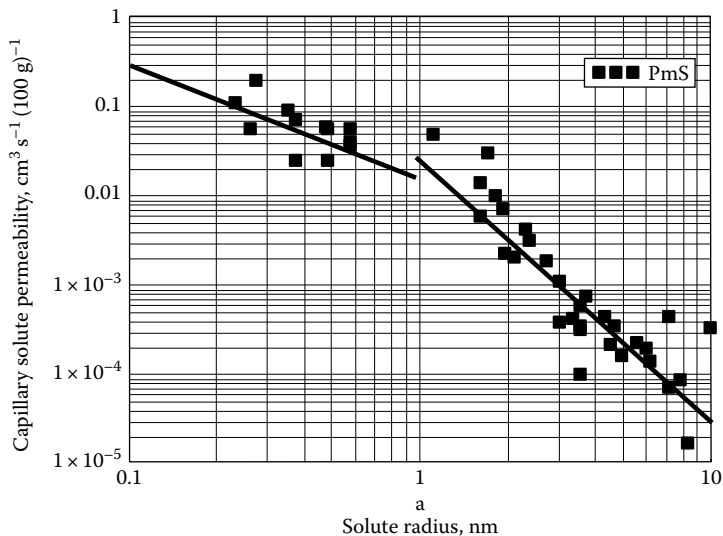


Figure 6.5 Solute permeability of capillaries. (Based on data from Renkin, E.M. and Curry, F.E., Transport of water and solutes across capillary endothelium, in: *Membrane Transport in Biology*, vol. 4, Giebisch, G. and Tosteson, D.C. (eds.), Springer-Verlag, New York, 1979, [Chapter 1](#).)

For solute transport by diffusion through capillary pores, it is more convenient to work with the product of  $P_m$  and  $S$ , rather than specific values of  $P_m$  or  $S$ . Hence, Renkin and Curry (1979) summarized their results for solutes of various sizes in continuous capillaries in terms of  $P_mS$ . These data are shown in [Figure 6.5](#). Note that in some cases for a given solute size, the value of  $P_mS$  can vary by almost an order of magnitude. This arises from molecular shape effects, hydration of the solute that increases the effective diffusion size of the solute, and other interactions between the solute and the capillary wall. In addition, fenestrated and discontinuous capillaries can have  $P_mS$  values that are several orders of magnitudes higher than those given in [Figure 6.5](#).

The solid lines in [Figure 6.5](#) represent a linear least square regression of the data. The following empirical equations can be used to estimate capillary  $P_mS$  values for a given solute of radius ( $a$ ). Note that the units on  $P_mS$  are  $\text{cm}^3 \text{s}^{-1} (100 \text{ g})^{-1}$  of tissue.

$$\begin{aligned} P_mS &= 0.0184a^{-1.223}, & a < 1 \text{ nm} \\ P_mS &= 0.0287a^{-2.92}, & a > 1 \text{ nm} \end{aligned} \quad (6.16)$$

**6.1.1.7 Membrane permeability and the overall mass transfer coefficient** In many medical devices, a membrane separates two fluid regions. The solute is transported from one fluid region, across the membrane, and then into the other fluid region. These transport processes are illustrated in [Figure 6.6](#) where the solute is transported from region 1 to region 2, since we will assume that  $C_A^{\text{bulk}1} > C_A^{\text{bulk}2}$ . The concentrations of the solute at the fluid-membrane interfaces are assumed to be at equilibrium, and the partition coefficient ( $K$ ) is used to describe the solute equilibrium at the membrane surfaces.

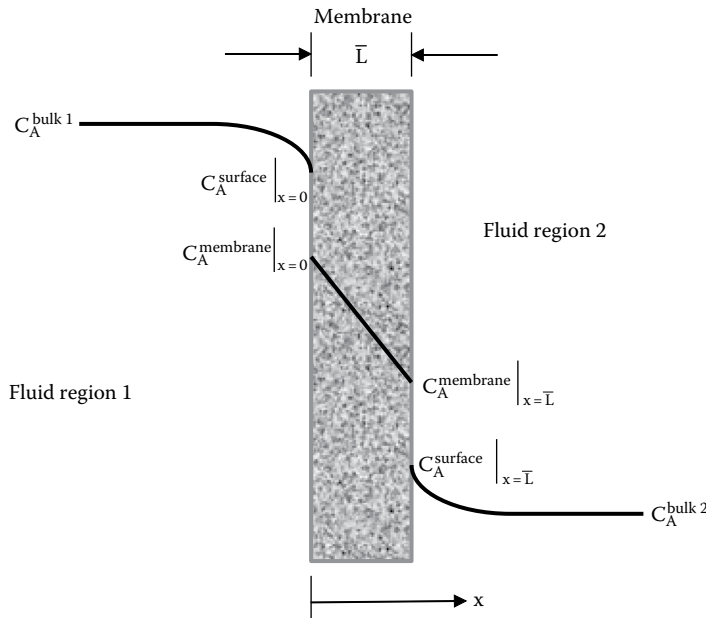


Figure 6.6 Solute mass transfer across a membrane.

As shown in Figure 6.6, the solute concentration just inside the membrane is related to the bulk concentration adjacent to the outside of the membrane surface by the following relationships,  $C_A^{\text{membrane}}|_{x=0} = K C_A^{\text{surface}}|_{x=0}$  and  $C_A^{\text{membrane}}|_{x=L} = K C_A^{\text{surface}}|_{x=L}$ . If a fluid region is well mixed, then the solute concentration at the surface of the membrane is the same as its concentration in the bulk fluid, i.e.,  $C_A^{\text{bulk}1}$  or  $C_A^{\text{bulk}2}$ .

Each of these fluid regions, as well as the membrane itself, acts as a resistance to the transport of the solute. These individual mass transfer resistances can be combined into an overall mass transfer coefficient ( $K_O$ ) defined in terms of the overall mass transfer driving force based on the bulk fluid concentrations, i.e.,  $(C_A^{\text{bulk}1} - C_A^{\text{bulk}2})$ . The solute mass transfer rate is then given as

$$\dot{m}_A = K_O S (C_A^{\text{bulk}1} - C_A^{\text{bulk}2}) \quad (6.17)$$

The overall mass transfer coefficient can be written in terms of the mass transfer coefficients of the respective fluid regions, i.e.,  $k_m^{(1)}$  and  $k_m^{(2)}$ , and the membrane permeability,  $P_m$ . The mass transfer coefficients and  $P_m$  are conductances, and their reciprocal represents the solute mass transfer resistance. These mass transfer resistances occur in a series, and by analogy to an electrical circuit, we can then write that the overall resistance is the sum of the individual resistances. The overall mass transfer coefficient is then given by

$$\frac{1}{K_O} = \frac{1}{k_m^{(1)}} + \frac{1}{P_m} + \frac{1}{k_m^{(2)}} \quad (6.18)$$

The smallest value of  $k_m^{(1)}$ ,  $P_m$ , or  $k_m^{(2)}$  for a given solute is said to be the *controlling resistance*.

The mass transfer coefficients in [Equation 6.18](#) can be estimated using the correlations we discussed in [Chapter 5](#). The mass transfer coefficients depend on the physical properties of the fluid regions and the nature of the flow in each of the fluid regions. They also can depend on the position due to boundary layer growth, so we usually use length-averaged values of the mass transfer coefficients in [Equation 6.18](#). The membrane permeability, although best measured experimentally (Dionne et al., 1996; Baker et al., 1997), is defined by [Equation 6.15](#).

### 6.1.2 Diffusion of a solute from within a porous polymeric material

Biocompatible polymers are widely used in a variety of medical devices and for the controlled release of a variety of drugs (Ritger and Peppas, 1987; Serra et al., 2006). Many of these polymeric materials also have a microporous structure.

Consider the situation shown in [Figure 6.7](#). A drug is uniformly distributed within a microporous polymeric disk of radius  $R$  and thickness  $L$ . The disk is very thin so  $R \gg L$  making the diffusion process one dimensional in the  $x$  direction. All of the surfaces of the disk are coated with an impermeable material except for the surface located at  $x = L$ . Since the drug release is assumed to occur over a long period of time, which can be many days or weeks, the rate-limiting process for the release of the drug from the polymeric support at  $x = L$  is diffusion of the drug through the polymeric material.

The concentration of the solute is expressed in terms of the void volume of the polymeric structure, where  $\varepsilon$  is the void volume fraction or the porosity. An unsteady solute mass balance in the volume from  $x$  to  $x + \Delta x$  says  $S\Delta x\varepsilon \frac{\partial C_A}{\partial t} = -S\varepsilon \frac{D_{AB}\omega_r}{\tau} \frac{\partial C_A}{\partial x} \Big|_x + S\varepsilon \frac{D_{AB}\omega_r}{\tau} \frac{\partial C_A}{\partial x} \Big|_{x+\Delta x}$ . Dividing by  $S\varepsilon\Delta x$ , and taking the limit as  $\Delta x \rightarrow 0$ , gives Fick's second law for the one-dimensional diffusion of the solute within the polymeric material:

$$\frac{\partial C_A}{\partial t} = D_e \frac{\partial^2 C_A}{\partial x^2} \quad (6.19)$$

Since the solute is diffusing through a heterogeneous polymeric structure, we use the effective diffusivity, i.e.,  $D_e$ , to describe the diffusion of the solute through the void space within the polymeric material. In this case,  $D_e = D_{AB}(\omega_r/\tau)$ , where we adjust the solute diffusivity in the solvent-filled pores to account for hindered diffusion and the tortuosity of the void space.

The initial concentration of the drug in the material is  $C_A^0$ , and the drug concentration at  $x = L$  is zero since we assume the drug is immediately taken up by the surroundings, a process that is much faster

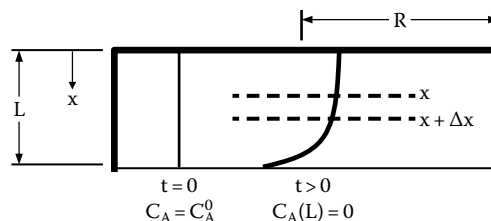


Figure 6.7 Diffusion of a solute within a polymeric disk.

than the diffusion of the drug through the polymeric material. The initial and boundary conditions can then be written as

$$\begin{aligned} \text{IC: } t = 0, \quad C_A(x, t) &= C_A^0 \\ \text{BC1: } x = 0, \quad \frac{\partial C_A}{\partial x} &= 0 \\ \text{BC2: } x = L, \quad C_A &= 0 \end{aligned} \quad (6.20)$$

Boundary condition 1 expresses the additional fact that the solute cannot diffuse out through the top surface of the polymeric disk since this surface is coated with an impermeable material.

A solution to Equations 6.19 and 6.20 can be obtained using the *separation of variables* technique, which will be briefly described in the following discussion (check out any advanced calculus book for more information on this technique). We let  $C_A(x, t)$  be given by the product of a function that depends only on  $x$ , i.e.,  $F(x)$ , and we define another function that depends only on  $t$ , i.e.,  $T(t)$ . Therefore,  $C_A(x, t) = F(x) T(t)$ . We substitute this equation into Equation 6.19 and obtain

$$\frac{1}{TD_e} \frac{dT}{dt} = \frac{1}{F} \frac{d^2F}{dx^2} = -\lambda^2 \quad (6.21)$$

Note that the term on the left side of the previous equation depends only on  $t$  and the term in the middle only depends on  $x$ . The only way they can then be equal to each other is if they equal the same constant, i.e.,  $\lambda^2$ . The minus sign is in front of  $\lambda^2$  in order to obtain a solution that remains finite as time increases. Equation 6.21 can then be rearranged to give the following two ordinary differential equations:

$$\frac{dT}{dt} = -\lambda^2 D_e T \quad \text{and} \quad \frac{d^2F}{dx^2} + F\lambda^2 = 0 \quad (6.22)$$

These equations can then be integrated to give

$$T = C_1 e^{-\lambda^2 D_e t} \quad \text{and} \quad F = C_2 \sin \lambda x + C_3 \cos \lambda x \quad (6.23)$$

Applying boundary conditions 1 and 2 on the expression for  $F$ , we obtain that  $C_2 = 0$  and that  $C_3 \cos \lambda L = 0$ .  $C_3$  cannot be equal to zero since that provides a trivial solution. Because of the periodic nature of the cosine function, there are an infinite number of  $\lambda$ 's that can satisfy the condition that the  $\cos \lambda L = 0$ . It is easy to show that these  $\lambda$ 's are given by

$$\lambda_n = \left( \frac{2n+1}{2} \right) \frac{\pi}{L} \quad \text{for } n = 0, 1, 2, \dots \infty \quad (6.24)$$

The  $\lambda_n$  are also known as *eigenvalues*, and the  $\cos \lambda_n x$  are known as the *eigenfunctions*.

The  $n$ th value of our solution is then given by  $C_{An}(x, t) = C_n e^{-\lambda_n^2 D_e t} \cos \lambda_n x$ , for  $n=0, 1, 2, \dots \infty$ . Each value of  $n$  gives us a solution to the original partial differential equation, i.e., Equation 6.19, that

satisfies boundary conditions 1 and 2. We can also sum all of these  $n$  solutions and obtain the following general solution:

$$C_A(x,t) = \sum_{n=0}^{\infty} C_n e^{-\lambda_n^2 D_e t} \cos \lambda_n x \quad (6.25)$$

The  $C_n$ 's can then be obtained by requiring that this equation satisfies the initial condition in [Equation 6.20](#); hence, at  $t = 0$ , [Equation 6.25](#) becomes

$$C_A^0 = \sum_{n=0}^{\infty} C_n \cos \lambda_n x \quad (6.26)$$

Next, we multiply both sides of [Equation 6.26](#) by  $\cos \lambda_m x$  and integrate from  $x = 0$  to  $x = L$ .

$$\int_0^L C_A^0 \cos \lambda_m x dx = \int_0^L \cos \lambda_m x \left( \sum_{n=0}^{\infty} C_n \cos \lambda_n x \right) dx \quad (6.27)$$

[Equation 6.27](#) can also be written as

$$\frac{C_A^0}{\lambda_n} \sin \lambda_n L = \sum_{n=0}^{\infty} C_n \int_0^L \cos \lambda_m x \cos \lambda_n x dx = C_n \int_0^L \cos^2 \lambda_n x dx \quad (6.28)$$

where  $\int_0^L \cos \lambda_m x \cos \lambda_n x dx = 0$  except when  $m = n$ . Hence, we then can solve [Equation 6.28](#) for  $C_n$ , which is given by

$$C_n = \frac{4C_A^0 (-1)^n}{(2n+1)\pi} \quad (6.29)$$

Combining [Equations 6.25](#) and [6.29](#) then provides the solution for the concentration distribution of the drug or solute within the polymeric material.

$$C_A(x,t) = \frac{4C_A^0}{\pi} \sum_{n=0}^{\infty} \frac{(-1)^n}{2n+1} e^{-\frac{(2n+1)^2 \pi^2 D_e t}{4L^2}} \cos \frac{(2n+1)\pi x}{2L} \quad (6.30)$$

Of particular interest is the flux of drug leaving the polymeric disk, which from Fick's first law is given by  $N_{Ax}|_{x=L} = -D_e \frac{\partial C_A}{\partial x}|_{x=L}$ . Using [Equation 6.30](#) to find  $\frac{\partial C_A}{\partial x}|_{x=L}$ , we can solve for the flux of the drug crossing the surface at  $x = L$  as

$$N_{Ax}|_{x=L} = \frac{2D_e C_A^0}{L} \sum_{n=0}^{\infty} (-1)^n e^{-\frac{(2n+1)^2 \pi^2 D_e t}{4L^2}} \quad (6.31)$$

For thin drug patches that are applied to the skin, [Equation 6.31](#) can also be combined with a pharmacokinetic model for drug distribution in the body to predict how the drug concentration in the body changes with time. This is discussed later in [Chapter 8](#).

The amount of drug or solute remaining in the polymeric material at any time  $t$  is also of interest. Since  $S$  is the total surface area of the polymeric material normal to the diffusion direction, then the total amount of drug ( $A_0$ ) initially present in the polymeric material is equal to  $A_0 = C_A^0 \varepsilon S L$ , where  $C_A^0$  was defined in terms of the void volume of the polymeric material that contains the drug or solute. The amount of drug remaining in the polymeric material at time  $t$ , i.e.,  $A(t)$ , is then given by integrating the concentration distribution at any time  $t$ , i.e., [Equation 6.30](#), from  $x = 0$  to  $x = L$ :

$$A(t) = \varepsilon S \int_0^L C_A(x, t) dx = \frac{8}{\pi^2} A_0 \sum_{n=0}^{\infty} \frac{1}{(2n+1)^2} e^{-\frac{(2n+1)^2 \pi^2 D_e t}{4L^2}} \quad (6.32)$$

We can also define the cumulative fraction of the drug ( $f_R$ ) that has been released as the amount of drug released, i.e.,  $A_0 - A(t)$ , divided by the amount of drug originally present, i.e.,  $A_0$ . Hence,

$$f_R = \frac{A_0 - A(t)}{A_0} = 1 - \frac{8}{\pi^2} \sum_{n=0}^{\infty} \frac{1}{(2n+1)^2} e^{-\frac{(2n+1)^2 \pi^2 D_e t}{4L^2}} \quad (6.33)$$

**6.1.2.1 A solution valid for short contact times** For short contact times, the drug concentration change occurs only over a thin region near where  $x = L$ . In this case, [Equation 6.19](#) still describes the diffusion of the drug within the polymeric material; however, we replace  $x$  with  $y$ , which represents the distance into the material from the exposed surface. The boundary conditions are given by

$$\begin{aligned} \text{IC: } & t = 0, \quad C_A(y, t) = C_A^0 \\ \text{BC1: } & y = 0, \quad C_A = 0 \\ \text{BC2: } & y = \infty, \quad C_A = C_A^0 \end{aligned} \quad (6.34)$$

Boundary condition 2 expresses the fact that at distances far from the exposed surface, the drug concentration within the polymeric material is still equal to its initial value.

[Equations 6.19](#) and [6.34](#) can be solved using the Laplace transform technique. If we let  $C'_A \equiv C_A^0 - C_A$ , then [Equation 6.19](#) remains the same with the exception that  $C_A$  is replaced by  $C'_A$  and the initial and boundary conditions given in [Equation 3.4](#) become

$$\begin{aligned} \text{IC: } & t = 0, \quad C'_A(y, t) = 0 \\ \text{BC1: } & y = 0, \quad C'_A = C_A^0 \\ \text{BC2: } & y = \infty, \quad C'_A = 0 \end{aligned} \quad (6.35)$$

The solution to this problem for  $C'_A$  using Laplace transforms is identical to the solution we obtained earlier for Equations 5.46 and 5.51, which is given by Equation 5.54. Using that solution, it is easy to show that

$$C_A(y,t) = C_A^0 \operatorname{erf} \left( \frac{y}{\sqrt{4D_e t}} \right) \quad (6.36)$$

The flux of a drug from the surface at  $x = L$  is given by  $N_{Ay} \Big|_{y=0} = -D_e \frac{\partial C_A}{\partial y} \Big|_{y=0}$ . Using Equation 6.36 to find  $\frac{\partial C_A}{\partial y} \Big|_{y=0}$ , we can solve for the flux of the drug crossing the surface at  $x = L$  as

$$N_{Ay} \Big|_{y=0} = \frac{C_A^0 D_e}{\sqrt{\pi D_e t}} \quad (6.37)$$

The amount of drug still in the polymeric material at time  $t$ , i.e.,  $A(t)$ , is given by the difference between the initial amount of drug, i.e.,  $A_0 = C_A^0 \varepsilon S L$ , and the amount of the drug that has left the polymeric structure, i.e.,  $\varepsilon S \int_0^t N_{Ay} \Big|_{y=0} dt$ ; hence,

$$A(t) = A_0 - \varepsilon S \int_0^t N_{Ay} \Big|_{y=0} dt = A_0 - \frac{\varepsilon S C_A^0 D_e^{1/2}}{\sqrt{\pi}} \int_0^t t^{-1/2} dt = A_0 - \varepsilon S C_A^0 \sqrt{\frac{4D_e t}{\pi}} \quad (6.38)$$

We can also define the cumulative fraction of the drug ( $f_R$ ) that has been released as the amount of drug released (i.e.,  $A_0 - A(t)$ ) divided by the amount of drug originally present, i.e.,  $A_0 = \varepsilon S L C_A^0$ . Hence,

$$f_R = \frac{A_0 - A(t)}{A_0} = \frac{1}{L} \sqrt{\frac{4D_e t}{\pi}} = 4 \sqrt{\frac{D_e}{4\pi L^2} t^{1/2}} \quad (6.39)$$

Equation 6.39 shows that for short contact times, a plot of the fraction of the drug released, i.e.,  $f_R$ , versus  $t^{1/2}$  is linear with a zero intercept and a slope,  $m$ , equal to  $4 \sqrt{\frac{D_e}{4\pi L^2}}$ . This provides a convenient method for finding the effective diffusivity of a solute within a polymeric structure as illustrated in Example 6.3. This short contact time solution is valid for  $0 \leq f_R \leq 0.4$ .

### Example 6.3

Bawa et al. (1985) investigated the release of macromolecules from small slabs of a polymeric material made of ethylene-vinyl acetate copolymer. The polymeric material was formed into slabs that were  $1 \text{ cm} \times 1 \text{ cm}$  and  $1 \text{ mm}$  in thickness. All surfaces of the slab were coated with paraffin except one  $1 \text{ cm} \times 1 \text{ cm}$  face, which was exposed to the surroundings. During the

formation of the polymeric slabs, bovine serum albumin (BSA) particles were incorporated within the polymer, forming a system of interconnected pores after the BSA became solubilized when the polymeric slabs were immersed in an aqueous solution. In one case, the BSA particles ranged in size from 106 to 150  $\mu\text{m}$ , and the cumulative fraction of BSA released (i.e.,  $f_R$ ) as a function of the square root of the time was measured as shown in the table. From these data, estimate the effective diffusivity of BSA within the polymeric material.

Time $^{1/2}$ , h $^{1/2}$	Cumulative Fraction of BSA Released ( $f_R$ )
2.5	0.05
5.0	0.1
7.0	0.12
11.0	0.20
13.0	0.22
15.5	0.28
17.5	0.30
20.0	0.32
22.0	0.35

### Solution

Figure 6.8 shows a plot of the  $f_R$  versus  $t^{1/2}$  data from the previous table. The solid line is a linear regression of these data with a zero intercept. As shown in the figure, we obtain an excellent fit of Equation 6.39 to the experimental data. The slope of this line is  $0.01678 \text{ h}^{-1/2}$ .

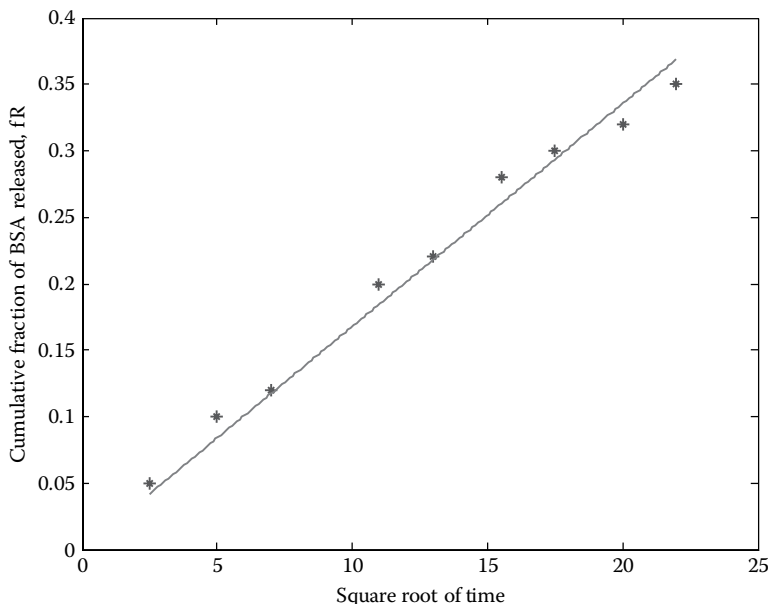


Figure 6.8 Cumulative fraction of BSA released as a function of  $(\text{time})^{1/2}$ .

From [Equation 6.39](#), this value of the slope, i.e.,  $m$ , is equal to  $4\sqrt{\frac{D_e}{4\pi L^2}}$ . Hence, we can solve for the value of  $D_e$  as shown next:

$$D_e = \frac{1}{4} m^2 \pi L^2 = \frac{1}{4} \times (0.01678)^2 \text{ h}^{-1} \times \pi \times (0.1 \text{ cm})^2 = 2.21 \times 10^{-6} \text{ cm}^2 \text{ h}^{-1}$$

The same value of  $D_e$  was also found when a nonlinear regression of these data was done using the exact solution for  $f_R$  versus  $t$  given by [Equation 6.33](#).

**6.1.2.2 A solution valid for long contact times** For long contact times, the summation term in [Equation 6.33](#) for the fractional release converges rapidly. In this case, we can use just the  $n = 0$  term of the summation for which [Equation 6.33](#) becomes

$$f_R = 1 - \frac{8}{\pi^2} e^{-\frac{\pi^2 D_e t}{4L^2}} \quad (6.40)$$

This equation has been found to be valid for  $0.4 \leq f_R \leq 1$ . [Equation 6.40](#) can be rearranged to give a form that is convenient for analyzing fractional release data.

$$\ln(1 - f_R) = \ln\left(\frac{8}{\pi^2}\right) - \left(\frac{\pi^2 D_e}{4L^2}\right)t \quad (6.41)$$

[Equation 6.41](#) shows that a plot of  $\ln(1 - f_R)$  versus  $t$  will be linear and from the slope,  $m$ , we can find the value of  $D_e$ , i.e.,

$$D_e = -\frac{4L^2 m}{\pi^2} \quad (6.42)$$

### 6.1.3 Diffusion in blood and tissue

In heterogeneous regions like the blood or tissue, the solute can diffuse through both the continuous fluid space and through the cells themselves. For solute diffusion in the blood or the tissue, we let  $D_T$  represent the *effective diffusivity* of the solute through this heterogeneous region.

One approach for estimating  $D_T$  is based on a model developed by Maxwell (1873).

$$\frac{D_T}{D_0} = \frac{2D_0 + D_{cell} - 2\phi(D_0 - D_{cell})}{2D_0 + D_{cell} + \phi(D_0 - D_{cell})} \quad (6.43)$$

Interestingly, we see that [Equation 6.43](#) does not depend on the size of the cells, but only on their volume fraction,  $\phi$ . In [Equation 6.43](#),  $D_{cell}$  is the diffusivity of the solute in the cells. For a

lipid-insoluble solute,  $D_{\text{cell}}$ , in the absence of any data, can be taken to be equal to zero. If  $D_{\text{cell}} = 0$ , then [Equation 6.43](#) simplifies to

$$\frac{D_T}{D_0} = \frac{2(1-\phi)}{2+\phi} = \frac{2\varepsilon}{3-\varepsilon} \quad (6.44)$$

where  $\varepsilon$  is the void fraction within the tissue space, which is equal to  $1 - \phi$ . If the cell volume fraction is 0.85 and  $D_{\text{cell}} = 0$ , then the solute diffusivity is about 10% of its value in the fluid phase.

Riley et al. (1994, 1995a–c, 1996) have developed an empirical relation based on Monte Carlo simulations for  $D_T/D_0$  that shows good agreement with available data throughout a wide range of cell volume fractions, i.e.,  $0.04 < \phi < 0.95$ .

$$\frac{D_T}{D_0} = 1 - \left(1 - \frac{D_{\text{cell}}}{D_0}\right) \left(1.727\phi - 0.8177\phi^2 + 0.09075\phi^3\right) \quad (6.45)$$

In [Equations 6.43 through 6.45](#),  $D_0$  is the diffusivity of the solute through the interstitial fluid space or, in the case of blood, through plasma, for which  $D_0 = D_{\text{plasma}}$ . For plasma, we can use the Stokes-Einstein relation, i.e., [Equations 5.40](#) and [5.42](#), to estimate the solute diffusivity in plasma, i.e.,  $D_0 = D_{\text{plasma}}$ . In order to do this, we adjust the diffusivity of the solute in water, i.e.,  $D_{\text{AB}}$ , for the increased viscosity of plasma relative to that of water. Using this approach, the diffusivity of a solute in plasma at 37°C is given by the following equation:

$$D_{\text{plasma}} = D_{\text{AB}} \times \left( \frac{0.691 \text{ cP}}{1.2 \text{ cP}} \right) = 0.576 D_{\text{AB}} \quad (6.46)$$

**6.1.3.1 Diffusion in the interstitial fluid and other gel-like materials** The interstitial fluid that lies between the cells has a hydrogel-like consistency due to the presence of a variety of macromolecules like collagen and glycosaminoglycans. Therefore, the solute must diffuse through and around this random network of macromolecular obstacles. The reduction in the solute diffusivity relative to its value in pure water ( $D_{\text{AB}}$ ) due to this network of macromolecules within the interstitial fluid or a gel-like material can be described by the following equation developed by Brinkman (1947).

$$\frac{D_0}{D_{\text{AB}}} = \omega_r = \frac{1}{1 + \kappa a + \frac{1}{3}(\kappa a)^2} \quad (6.47)$$

where the ratio of  $D_0$  to  $D_{\text{AB}}$  is equal to the solute diffusional hindrance caused by the macromolecules in the interstitial fluid and depends on the solute radius, i.e.,  $a$ , and one adjustable parameter,  $\kappa$ .  $\kappa$  is a function of the gel's microstructure and can be found by fitting the above equation to experimental data for solute diffusion in the gel.

The steric exclusion, or equilibrium partitioning, of a solute upon entrance from a bulk solution into a gel-like material such as the interstitial fluid can be described by the following equation developed by Ogston (1958):

$$K = \exp \left[ -\phi \left( 1 + \frac{a}{a_f} \right)^2 \right] \quad (6.48)$$

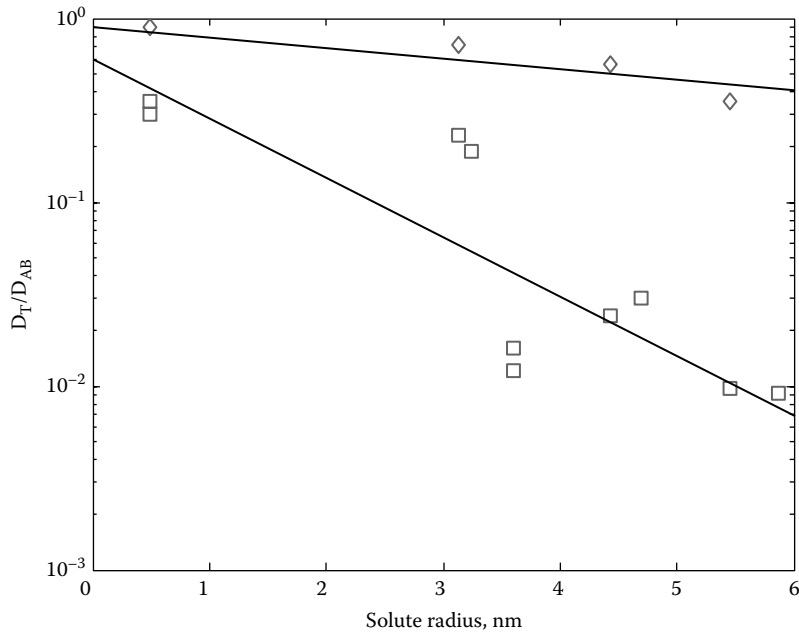


Figure 6.9 Effective diffusivity ( $D_T$ ) in tissue as a function of the solute radius. Diamond and square symbols represent solute diffusion data for tumor and normal tissue, respectively. Solid lines are an aid for estimating solute tissue diffusivity. (From Nugent, L.J. and Jain, R.K., *Cancer Res.*, 44, 238, 1984a.)

In this equation,  $a_f$  represents the radius of the macromolecules, which are assumed to form very long cylindrical fibers. If the length of these fibers per volume of gel is given in terms of  $l$ , then the volume fraction of these macromolecular fibers is given by  $\phi = \pi a_f^2 l$  (Tong and Anderson, 1996).

Nugent and Jain (1984a,b) examined the diffusion of various-sized solutes through normal and tumor tissue. Their results are shown in [Figure 6.9](#), where we see the ratio of the solute diffusivity in tissue, i.e.,  $D_T$ , to its aqueous diffusivity, i.e.,  $D_{AB}$ , plotted as a function of the solute radius. This figure can also be used to estimate solute diffusivities in tissue.

#### 6.1.4 Solute transport across gel membranes

The effective diffusivity, i.e.,  $D_e$ , of a solute diffusing from one fluid region across a gel-like membrane into a second fluid region, as in [Figure 6.6](#), is given by  $D_e = K D_0 = K \omega_i D_{AB}$ . In terms of [Equations 6.47](#) and [6.48](#), this becomes

$$D_e = D_{AB} \frac{\exp\left[-\phi\left(1 + \frac{a}{a_f}\right)^2\right]}{1 + \kappa a + \frac{1}{3}\left(\kappa a\right)^2} \quad (6.49)$$

The solute mass transfer rate across a gel-like membrane of thickness  $\bar{L}$  is then

$$\dot{m}_A = \frac{D_e S}{\bar{L}} (C_{A\text{bulk}}^{x=0} - C_{A\text{bulk}}^{x=\bar{L}}) = P_m S (C_{A\text{bulk}}^{x=0} - C_{A\text{bulk}}^{x=\bar{L}}) \quad (6.50)$$

where  $P_m = D_e / \bar{L}$ .

Tong and Anderson (1996) showed that [Equation 6.49](#) provided excellent representation of the partitioning and diffusion of two representative globular proteins (albumin and ribonuclease-A) in a polyacrylamide gel (see [Problems 6.2, 6.3, and 6.5](#) at the end of this chapter).

#### Example 6.4

The antibody IgG is diffusing from a bulk solution across a 5% agarose hydrogel membrane into another bulk solution. The membrane is 1 mm in thickness and the temperature of this system is at 37°C. The radius ( $a$ ) of the IgG molecule based on [Equation 5.41](#) and its molecular weight of 150,000 is estimated to be 3.90 nm. The polymer fibers in the hydrogel have a radius ( $a_f$ ) of 2.79 nm. The volume fraction of the polymer fibers in the hydrogel is  $\phi = 0.05$  and the value of  $\kappa$  is 0.57. Estimate the effective diffusivity and the membrane permeability of IgG in this hydrogel membrane.

#### Solution

Since the IgG is diffusing across a gel membrane in contact with bulk solutions on either side of the membrane, we can use [Equation 6.49](#) to find the effective diffusivity of this solute. The diffusivity of IgG in water at 37°C can be estimated from [Figure 5.1](#) or by [Equation 5.35](#) from which we find that  $D_{AB} = 4.21 \times 10^{-7} \text{ cm}^2 \text{ s}^{-1}$ . Hence, we have

$$D_e = D_{AB} \frac{\exp \left[ -\phi \left( 1 + \frac{a}{a_f} \right)^2 \right]}{1 + \kappa a + \frac{1}{3} (\kappa a)^2}$$

$$D_e = 4.21 \times 10^{-7} \text{ cm}^2 \text{ s}^{-1} \frac{\exp \left[ -0.05 \left( 1 + \frac{3.9 \text{ nm}}{2.79 \text{ nm}} \right)^2 \right]}{1 + 0.57 \frac{1}{\text{nm}} \times 3.9 \text{ nm} + \frac{1}{3} \left( 0.57 \frac{1}{\text{nm}} \times 3.9 \text{ nm} \right)^2} = 6.48 \times 10^{-8} \text{ cm}^2 \text{ s}^{-1}$$

From this value of  $D_e$ , we can calculate the membrane permeability for IgG as

$$P_m = \frac{6.48 \times 10^{-8} \text{ cm}^2 \text{ s}^{-1}}{0.1 \text{ cm}} = 6.48 \times 10^{-7} \text{ cm s}^{-1}$$

## 6.2 The irreversible thermodynamics of membrane transport

The transport of solvent and solute across membranes can occur as a result of several driving forces. These driving forces include differences in pressure, concentration, and even the electrical potential across the membrane. In this discussion, we will ignore electrical potential gradients and just focus

on the pressure and concentration driving forces. Electrical potential effects are discussed in Cussler (1984) and Grodzinsky (2011).

The presence of pressure and concentration differences across a membrane means that solute mass transfer can occur by a combination of bulk flow or convection, and by diffusion. The convective flow across a membrane is also called a filtration flow.

In some cases, the relative magnitudes of the diffusive and convective transport rates for a given solute are comparable, and we must consider the fact that these processes are therefore interdependent. This interaction makes the description of the solute transport rate much more complicated and to arrive at the proper result requires an understanding of the thermodynamics of irreversible processes.

The application of irreversible thermodynamics to membrane transport was developed by Staverman (1948) and Kedem and Katchalsky (1958). For dilute solutions, the theory of irreversible thermodynamics states that the filtration rate of the solvent ( $Q$ ) across the membrane and the filtration rate due to the solute relative to that of the solvent ( $Q_V$ ) both depend in a linear manner on the driving forces  $\Delta P$  and  $RT\Delta C_A$ . This linear combination of the driving forces is then given by the following equations for a membrane of surface area  $S$ :

$$Q = SL_P\Delta P + SL_{PS}RT\Delta C_A \quad (6.51)$$

$$Q_V = SL_{SP}\Delta P + SL_SRT\Delta C_A \quad (6.52)$$

$Q$  and  $Q_V$  must have the correct sign sense for proper interpretation. This is easily accomplished if we simply assume in our analyses a vertical orientation for the membrane. The solute concentration is higher in the solution to the left of the membrane than in the solution to the right of the membrane. The flow of solvent and solute from left to right is considered positive. The  $\Delta$  sign in this case also represents the value of the property ( $P$  or  $C_A$ ) on the left side of the membrane minus the corresponding value on the right side of the membrane.

The cross coefficients ( $L_{PS}$  and  $L_{SP}$ ) in Equations 6.51 and 6.52 represent secondary effects that are caused by the primary driving forces. For example, the primary  $\Delta P$  driving force generates the filtration flow ( $Q$ ) and also induces a relative flow ( $Q_V$ ) between solute and solvent represented by  $L_{SP}\Delta P$ . This relative flow between the solute and solvent is capable of producing a separation of solute and solvent and is referred to as *ultrafiltration*.

Along the same line of reasoning, the  $RT\Delta C_A$  primary driving force is responsible for solute diffusion. This diffusive transport produces an additional contribution to the filtration flow that is given by  $L_{PS}RT\Delta C_A$ , and from Equation 3.1, Van't Hoff's equation, we recognize this as an osmotic flow. The coefficient  $L_P$  in Equation 6.51 is the hydraulic conductance of the membrane defined earlier by Equations 3.4 and 3.7. We will soon show that  $L_S$  in Equation 6.52 is related to the permeability of the membrane, i.e.,  $P_m$ .

Another basic theorem from the work of Onsager is that the cross coefficients  $L_{SP}$  and  $L_{PS}$  are equal. We can then simplify Equations 6.51 and 6.52 as follows:

$$Q = L_P S (\Delta P - \sigma RT \Delta C_A) \quad (6.53)$$

$$Q_V = L_p S \left( -\sigma \Delta P + \frac{L_s}{L_p} RT \Delta C_A \right) \quad (6.54)$$

The parameter  $\sigma$ , defined as  $-(L_{sp}/L_p)$  or  $-(L_{ps}/L_p)$ , is called the Staverman *reflection coefficient*.

Note the similarity between the filtration flow rate ( $Q$ ) in [Equation 6.53](#) and that given by [Equation 3.4](#), recognizing that  $RT\Delta C$  is equivalent to  $(\Pi_C - \Pi_{IF})$ . These equations are identical when  $\sigma = 1$ , which implies that the pores of the membrane are impermeable to the solute as required by the derivation of [Equation 3.4](#). The solute is therefore completely “reflected” by the membrane, and the  $RT\Delta C_A$  term in [Equation 6.53](#) is the osmotic pressure difference across the membrane.

When  $\sigma = 0$  in [Equation 6.53](#), we have that  $Q = L_p S \Delta P$ . This result is also known as *Darcy's law*, which says that the filtration flow of the solution is proportional to the pressure drop across the membrane. Also, in this case, there is no secondary effect of osmotic flow caused by the primary concentration difference driving force. This means that the solute flows through the pores completely unimpeded, just as easily as the solvent; hence, the solute is not “reflected” and  $\sigma = 0$ . The concept of the reflection coefficient is illustrated in [Figure 6.10](#).

The total mass transfer rate of the solute, i.e.,  $\dot{m}_A$ , across the membrane is given by the product of the average solute concentration ( $\tilde{C}_A$ ) within the membrane and the combined flow rate of the solution due to the applied pressure and concentration differences, i.e.,  $\dot{m}_A = \tilde{C}_A (Q + Q_V)$ . Combining [Equations 6.53](#) and [6.54](#) in this fashion results in [Equation 6.55](#) for the mass transfer rate of the solute across the membrane.

$$\dot{m}_A = \tilde{C}_A L_p S \left[ (1 - \sigma) \Delta P + \left( \frac{L_s}{L_p} - \sigma \right) RT \Delta C_A \right] \quad (6.55)$$

This equation can be rewritten by using [Equation 6.53](#) to express  $\Delta P$  as a function of  $Q$  and  $\Delta C_A$ . Hence, we then obtain

$$\dot{m}_A = \tilde{C}_A (1 - \sigma) Q + \tilde{C}_A S L_p \left( \frac{L_s}{L_p} - \sigma^2 \right) RT \Delta C_A \quad (6.56)$$

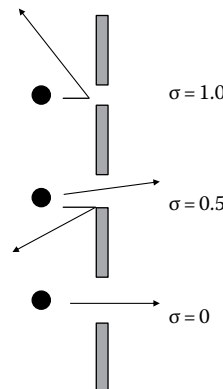


Figure 6.10 The reflection coefficient.

The second term in [Equation 6.56](#) has the following factor, i.e.,  $((L_S/L_P) - \sigma^2)$ , that must be determined. Recognizing for the case of no filtration flow that  $Q = 0$  and diffusion is the only solute transport mechanism, then by [Equation 6.53](#) we have

$$\Delta P|_{Q=0} = \sigma RT \Delta C_A|_{Q=0} \quad (6.57)$$

Substituting this expression into [Equation 6.54](#) for the case where  $Q = 0$  and with  $\dot{m}_A = \tilde{C}_A Q_V$  gives [Equation 6.58](#), where we must recognize that in the absence of  $Q$ , the transport rate of the solute across the membrane must be equal to our previous result given by [Equation 6.14](#) or [6.50](#).

$$\dot{m}_A|_{Q=0} = \tilde{C}_A L_P S (RT \Delta C_A)|_{Q=0} \left( \frac{L_S}{L_P} - \sigma^2 \right) = P_m S \Delta C_A|_{Q=0} \quad (6.58)$$

We can then solve [Equation 6.58](#) for  $((L_S/L_P) - \sigma^2)$ , which is given by

$$\left( \frac{L_S}{L_P} - \sigma^2 \right) = \frac{P_m}{L_P R T \tilde{C}_A} \quad (6.59)$$

where  $P_m$  is the membrane permeability. [Equation 6.56](#) can now be simplified using [Equation 6.59](#) to give our final result for the solute transport across a membrane, recognizing that  $Q$  is the filtration flow rate given earlier by [Equation 6.53](#).

$$\dot{m}_A = \tilde{C}_A (1 - \sigma) Q + P_m S \Delta C_A \quad (6.60)$$

where

$\tilde{C}_A$  represents the average solute concentration in the membrane

$\Delta C_A$  is the solute concentration difference across the membrane

This is an interesting result. We went through a lot of mathematics to get a result that confirms our engineering intuition. [Equation 6.60](#) says that the solute mass transfer rate across the membrane is the sum of the amount carried by the filtration flow plus the amount that diffuses. That is, the first term on the right-hand side of [Equation 6.60](#) represents the amount of solute transported by the convective or filtration flow of the solvent across the membrane corrected for solute reflection and the second term represents the contribution of diffusion to the solute transport rate.

### 6.2.1 Finding $L_P$ , $P_m$ , and $\sigma$

In a general sense, we must know the three parameters,  $L_P$ ,  $P_m$ , and  $\sigma$ , in [Equations 6.53](#) and [6.60](#) to calculate the mass transfer of a solute across a membrane. Recall that  $L_P$  is the hydraulic conductance and it can be estimated using [Equation 3.7](#) for cylindrical pores or [Equation 3.10](#) for slit pores. The hydraulic conductance can also be measured for a given membrane by using a pure solvent whose value of  $\sigma = 0$ , and measuring the flow rate  $Q$  across the membrane for a given  $\Delta P$ . Then from [Equation 6.53](#), which simplifies to Darcy's law, we have

$$L_P = \frac{Q}{S \Delta P} \Big|_{\sigma=0} \quad (6.61)$$

Recall that  $P_m$  is the permeability of the solute in the membrane and can be estimated from the solute's effective diffusivity, i.e.,  $D_e$ , by Equations 6.15 and 6.49. Alternatively, in the absence of any bulk flow across the membrane (i.e.,  $Q = 0$ ), the permeability can be obtained by measuring the solute mass transfer rate ( $\dot{m}_A$ ) for a given concentration difference. Then from Equation 6.60, the permeability is given by

$$P_m = \frac{\dot{m}_A}{S\Delta C_A} \Big|_{Q=0} \quad (6.62)$$

The reflection coefficient,  $\sigma$ , can be measured by one of two ways. In the first method, one employs a pressure drop across the membrane and measures the filtration flow rate,  $Q$ , as well as the transport rate of the solute,  $\dot{m}_A$ , across the membrane in the absence of a solute concentration difference across the membrane. Then, from Equation 6.60, we obtain that

$$(1 - \sigma) = \frac{\dot{m}_A}{C_A Q} \Big|_{\Delta C_A = 0} \quad (6.63)$$

where  $C_A$  is the solute concentration in the feed solution.

Alternatively, we can measure the filtration flow rate,  $Q$ , in the absence of a pressure drop across the membrane, but under the control of a concentration difference across the membrane (osmotic flow). Then from Equation 6.53, the reflection coefficient is given by

$$\sigma = -\frac{Q}{SL_p RT \Delta C_A} \Big|_{\Delta P = 0} \quad (6.64)$$

**6.2.1.1 Estimating the reflection coefficient** The reflection coefficient can also be estimated using theories developed to describe the motion of particles in small pores. Anderson and Quinn (1974) reexamined the basic hydrodynamic equations that describe hindered particle motion in small pores in which a fluid is flowing. Under the assumptions of a rigid and spherical solute, and no electrostatic interactions with the pore wall, which is assumed to be inert, they showed that the *sieving coefficient*,  $S_a \equiv \dot{m}_A / C_A Q$ , is the same as  $(1 - \sigma)$ , where  $C_A$  is the concentration of the solute on the feed side of the membrane pore. The sieving coefficient is defined as the ratio of the solute concentration in the filtrate to that at the surface of the membrane on the feed side. This definition of  $S_a$  also implies that solute transport by diffusion through the pore is negligible in comparison to the solute transported through the pore by convection or filtration.

Theoretical expressions based on the motion of a spherical solute moving through a cylindrical pore have been developed to estimate the value of the sieving coefficient (Anderson and Quinn, 1974; Deen, 1987). The development of these expressions neglects the secondary effects between the solute and the membrane pore, e.g., electrostatic, hydrophobic, and van der Waals interactions. The following expression can be used to estimate the sieving coefficient.

$$S_a = (1 - \lambda)^2 \left[ 2 - (1 - \lambda)^2 \right] \left[ 1 - \frac{2}{3} \lambda^2 - 0.163 \lambda^3 \right] \quad (6.65)$$

In this equation,  $\lambda$  is defined as the ratio of the solute radius ( $a$ ) to the capillary pore radius ( $r$ ). If no other information is available, the solute radius can be estimated from the solute molecular weight using [Equation 5.41](#).

Since  $S_a = (1 - \sigma)$ , [Equation 6.65](#) can be rearranged to give the following predictive equation for the reflection coefficient.

$$\sigma = 1 - (1 - \lambda)^2 \left[ 2 - (1 - \lambda)^2 \right] \left[ 1 - \frac{2}{3} \lambda^2 - 0.163 \lambda^3 \right] \quad (6.66)$$

### 6.2.2 Multicomponent membrane transport

[Equations 6.53](#) and [6.60](#) describe the filtration flow rate and the solute transport rate in a system comprised of only a single solute and a solvent. However, similar equations can be derived for a multicomponent solute and solvent system by recognizing that now [Equations 6.51](#) and [6.52](#) become

$$Q = SL_p \Delta P + SRT \sum_{i=1}^N L_{PS_i} \Delta C_i \quad (6.67)$$

$$Q_V = S \Delta P \sum_{i=1}^N L_{SP_i} + SRT \sum_{i=1}^N L_{S_i} \Delta C_i \quad (6.68)$$

The summations are over each solute in the system. Using the approach outlined earlier for the derivation of [Equations 6.53](#) and [6.60](#), the following equations are obtained for the filtration rate ( $Q$ ) and the transport rate of solute  $i$ , i.e.,  $\dot{m}_i$ , across the membrane in multicomponent systems:

$$Q = SL_p \left[ \Delta P - RT \sum_{i=1}^N \sigma_i \Delta C_i \right] \quad (6.69)$$

$$\dot{m}_i = \tilde{C}_i (1 - \sigma_i) Q + P_{m_i} S \Delta C_i \quad (6.70)$$

### 6.2.3 Membrane Peclet number

We can use the Peclet number ( $Pe$ ) as a means to determine in membrane solute transport the relative importance of solute convection (filtration) and solute diffusion. The membrane Peclet number is defined as the amount of solute transported across the membrane by convection or filtration to that transported by diffusion. From [Equation 6.60](#), we can write this as

$$Pe_{\text{membrane}} = \frac{(1 - \sigma) Q}{P_m S} \quad (6.71)$$

assuming that  $\tilde{C}_A \approx \text{order}(\Delta C_A)$ .

If the  $Pe_{\text{membrane}} \ll 1$ , then we can conclude that the amount of solute carried across the membrane by filtration flow is much smaller than that transported by diffusion. On the other hand, if  $Pe_{\text{membrane}} \gg 1$ , then transport of solute by filtration dominates and transport by diffusion is negligible.

### 6.3 Solute transport by filtration and diffusion across the capillary wall

In this section, we will use the capillary wall as a representative membrane to illustrate in the following examples the calculation of solute transport rates using the relationships developed in the previous sections. [Table 3.3](#) summarizes the characteristics of a typical capillary. In our discussion, we will find it convenient to classify solutes into three categories: The first category concerns the transport of small water-soluble but lipid-insoluble substances such as  $\text{Na}^+$  and  $\text{K}^+$  ions, glucose, amino acids, many drugs, and other metabolites. The second category of solutes is lipid-soluble substances such as oxygen and carbon dioxide, and the third category we will discuss is the transport of large lipid-insoluble substances such as proteins (macromolecules).

#### Example 6.5

Calculate the rate of transport by filtration and diffusion of a small water-soluble but lipid-insoluble solute, such as glucose, with a molecular weight of  $180 \text{ g mol}^{-1}$ , across the capillary wall at  $37^\circ\text{C}$ . Using [Equations 5.35](#) and [5.41](#), the *diffusivity of glucose* ( $D_{AB}$ ) in water is estimated to be  $0.93 \times 10^{-5} \text{ cm}^2 \text{ s}^{-1}$  and its molecular radius is 0.41 nm. The average concentration of glucose in plasma is about  $5 \mu\text{mol cm}^{-3}$ , and it is assumed that all the glucose transported to the extracapillary space is consumed instantly by the cells. We will also assume that all of the plasma proteins are retained by the capillary wall and that they generate an oncotic or colloid osmotic pressure of 28 mmHg. We will also assume that the tortuosity of the capillary wall is equal to 2.

#### Solution

The filtration flow rate of plasma ( $Q$ ) across the capillary wall is given by [Equation 6.53](#) with  $\sigma = 1.0$  and was shown earlier in [Example 3.4](#) to be equal to  $1.54 \times 10^{-8} \text{ cm}^3 \text{ h}^{-1}$ . [Equation 6.60](#) can be used to calculate the solute transport rate of glucose across the capillary wall. We first need to estimate the reflection coefficient ( $\sigma$ ) for glucose. [Equation 6.66](#) can be used to obtain an estimate. The slit pores of the capillary wall have a thickness of 7 nm, and from [Equation 5.171](#), the hydraulic diameter for this slit is 14 nm.

$$\sigma = 1 - \left(1 - \frac{0.41}{7}\right)^2 \left[ 2 - \left(1 - \frac{0.41}{7}\right)^2 \right] \left[ 1 - \frac{2}{3} \left(\frac{0.41}{7}\right)^2 - 0.163 \left(\frac{0.41}{7}\right)^3 \right]$$

$$\sigma = 0.015$$

From [Equation 6.46](#), the diffusivity of glucose in plasma is estimated to be  $0.54 \times 10^{-5} \text{ cm}^2 \text{ s}^{-1}$ . The permeability of glucose in the capillary wall can be estimated using [Equation 6.15](#), and the quantity  $K_o$  can be obtained from [Equation 6.12](#).

$$P_m = \frac{0.54 \times 10^{-5} \text{ cm}^2 \text{ s}^{-1}}{2 \times 0.5 \times 10^{-6} \text{ m}} \times \frac{1 \text{ m}}{100 \text{ cm}} \times 0.001 \times \left(1 - \frac{0.41 \text{ nm}}{7 \text{ nm}}\right)^2 \\ \times \left[1 - 2.1 \left(\frac{0.41 \text{ nm}}{7 \text{ nm}}\right) + 2.09 \left(\frac{0.41 \text{ nm}}{7 \text{ nm}}\right)^3 - 0.95 \left(\frac{0.41 \text{ nm}}{7 \text{ nm}}\right)^5\right] = 4.2 \times 10^{-5} \text{ cm s}^{-1}$$

We can now calculate, by [Equation 6.60](#), the transport rate of glucose across the capillary wall.

$$\dot{m}_A = \frac{1}{2} (5+0) \mu\text{mol cm}^{-3} (1-0.015) \times 1.54 \times 10^{-8} \text{ cm}^3 \text{ h}^{-1} + 4.2 \times 10^{-5} \text{ cm s}^{-1} \times \pi \times 10 \times 10^{-6} \text{ m} \\ \times 0.001 \text{ m} \times (5-0) \mu\text{mol cm}^{-3} \times \frac{(100 \text{ cm})^2}{\text{m}^2} \times \frac{3600 \text{ s}}{\text{h}} \\ \dot{m}_A = 3.792 \times 10^{-8} \mu\text{mol h}^{-1} + 2.375 \times 10^{-4} \mu\text{mol h}^{-1} = 2.375 \times 10^{-4} \mu\text{mol h}^{-1}$$

The first term in the calculation of  $\dot{m}_A$  by [Equation 6.60](#) represents the transport rate of glucose by the convective filtration flow. The second term represents the transport rate by diffusion. Comparing these values, we find that the transport rate of small water-soluble but lipid-insoluble solutes such as glucose across the capillary wall is several thousand times higher by diffusion than by convection or filtration! The membrane Peclet number also confirms this conclusion. From [Equation 6.71](#), we obtain

$$Pe_{\text{membrane}} = \frac{(1-\sigma)Q}{P_m S} = \frac{(1-0.015) \times 1.54 \times 10^{-8} \text{ cm}^3 \text{ h}^{-1}}{4.2 \times 10^{-5} \text{ cm s}^{-1} \times 3600 \text{ s h}^{-1} \times \pi \times 10^{-4} \text{ cm} \times 0.1 \text{ cm}} \\ Pe_{\text{membrane}} = 0.0032$$

Since the  $Pe_{\text{membrane}} \ll 1$ , this shows as well that we can neglect the amount of solute carried across the membrane by filtration flow in comparison to the amount of solute that is transported by diffusion. We can therefore neglect the convective or filtration transport of a small molecule like glucose across the capillary wall and base our calculations on the diffusive transport of the solute alone.

### Example 6.6

Now consider the transport rate of lipid-soluble solutes such as oxygen across the capillary wall. In this case, the entire surface area of the capillary wall is available for transport. Oxygen has a considerable solubility in the cell membrane and will readily diffuse through the endothelial cells of the capillary wall. Oxygen can also diffuse through the pores in the capillary wall. The *diffusivity of oxygen* ( $D_{AB}$ ) in water at  $37^\circ\text{C}$  is  $2.76 \times 10^{-5} \text{ cm}^2 \text{ s}^{-1}$  (Yoshida and Ohshima, 1966), and its molecular radius from [Equation 5.41](#) is estimated to be 0.23 nm.

The average concentration of oxygen in the capillary is  $0.09 \text{ } \mu\text{mol cm}^{-3}$ . Once again we will assume that the tortuosity of the capillary wall is 2.

### Solution

The filtration flow rate of plasma ( $Q$ ) across the capillary wall was shown earlier in [Example 3.4](#) to be equal to  $1.54 \times 10^{-8} \text{ cm}^3 \text{ h}^{-1}$ . [Equation 6.60](#) can be used to calculate the solute transport rate of oxygen through the pores in the capillary wall. We first need to estimate the reflection coefficient for oxygen. [Equation 6.66](#) can be used to obtain an estimate assuming the hydraulic diameter of the capillary pores is 14 nm.

$$\sigma = 1 - \left(1 - \frac{0.23}{7}\right)^2 \left[2 - \left(1 - \frac{0.23}{7}\right)^2\right] \left[1 - \frac{2}{3} \left(\frac{0.23}{7}\right)^2 - 0.163 \left(\frac{0.23}{7}\right)^3\right]$$

$$\sigma = 0.0049$$

From [Equation 6.46](#), the diffusivity of oxygen in plasma is estimated to be  $1.59 \times 10^{-5} \text{ cm}^2 \text{ s}^{-1}$ . The permeability of oxygen in the capillary wall due to the pores can be estimated using [Equation 6.15](#), and the quantity  $K_{\omega_f}$  can be obtained from [Equation 6.12](#).

$$P_m = \frac{1.59 \times 10^{-5} \text{ cm}^2 \text{ s}^{-1}}{2 \times 0.5 \times 10^{-6} \text{ m}} \times \frac{1 \text{ m}}{100 \text{ cm}} \times 0.001 \times \left(1 - \frac{0.23 \text{ nm}}{7 \text{ nm}}\right)^2$$

$$\times \left[1 - 2.1 \left(\frac{0.23 \text{ nm}}{7 \text{ nm}}\right) + 2.09 \left(\frac{0.23 \text{ nm}}{7 \text{ nm}}\right)^3 - 0.95 \left(\frac{0.23 \text{ nm}}{7 \text{ nm}}\right)^5\right] = 1.385 \times 10^{-4} \text{ cm s}^{-1}$$

We can now calculate by [Equation 6.60](#) the transport rate of oxygen through the pores of the capillary wall.

$$\dot{m}_A = \frac{1}{2} (0.09 + 0) \mu\text{mol cm}^{-3} (1 - 0.0049) \times 1.54 \times 10^{-8} \text{ cm}^3 \text{ h}^{-1} + 1.385 \times 10^{-4} \text{ cm s}^{-1} \times \pi \times 10 \times 10^{-6} \text{ m}$$

$$\times 0.001 \text{ m} \times (0.09 - 0) \mu\text{mol cm}^{-3} \times \frac{(100 \text{ cm})^2}{\text{m}^2} \times \frac{3600 \text{ s}}{\text{h}}$$

$$\dot{m}_A = 0.689 \times 10^{-9} \mu\text{mol h}^{-1} + 1.410 \times 10^{-5} \mu\text{mol h}^{-1} = 1.410 \times 10^{-4} \mu\text{mol h}^{-1}$$

Comparing the contributions of filtration and diffusion in this result, we again find that the transport rate of small molecules like oxygen through the capillary pores is several thousand times higher by diffusion than by convection. An upper limit for the permeability of oxygen through the capillary wall itself is given by assuming the capillary wall diffusional resistance is that of plasma. Then,  $P_m$  is given by the ratio of the oxygen diffusivity in plasma divided by the thickness of the capillary wall

$$P_m \approx \frac{D_{\text{plasma}}}{\bar{L}} = \frac{1.59 \times 10^{-5} \text{ cm}^2 \text{ s}^{-1}}{0.5 \times 10^{-6} \text{ m}} \times \frac{1 \text{ m}}{100 \text{ cm}} = 0.32 \text{ cm s}^{-1}$$

The accepted value for the oxygen permeability is about  $0.1 \text{ cm s}^{-1}$ . The oxygen transport rate from the capillary is given by [Equation 6.50](#) and is equal to

$$\dot{m}_A = 0.10 \text{ cm s}^{-1} \times \pi \times 10 \times 10^{-6} \text{ m} \times 0.001 \text{ m} \times (0.09 - 0) \mu\text{mol cm}^{-3} \times \frac{(100 \text{ cm})^2}{\text{m}^2} \times \frac{3600 \text{ s}}{\text{h}}$$

$$\dot{m}_A = 0.01 \mu\text{mol h}^{-1}$$

This is the total oxygen transport rate from the capillary since the contribution due to the capillary pores found earlier is negligible in comparison. The smaller value of the oxygen transport rate through the pores ( $1.41 \times 10^{-4} \mu\text{mol h}^{-1}$ ) in comparison to the value given previously for the entire capillary wall ( $0.01 \mu\text{mol h}^{-1}$ ) represents the fact that the pore surface area is 1/1000th that of the capillary wall. Since the permeability of oxygen through the pores of the capillary and the capillary wall itself need to be multiplied by the same values of  $S$  and  $\Delta C_A$  to calculate the transport rate of oxygen, it is seen that regardless of these values, the diffusive transport of oxygen is 1000-fold higher through the endothelial cells lining the capillary walls than what is transported by diffusion through the capillary pores. Thus, we can conclude that the dominant mode for transport of oxygen is simple diffusion across the entire surface area of the capillary walls.

### Example 6.7

Our final category of solute to consider is a lipid-insoluble macromolecule such as a protein. Here, the molecular radius is comparable to the size of the pores in the capillary wall. Calculate the rate of transport by filtration and diffusion through the capillary wall of a protein with a molecular weight of 50,000. Assume the concentration of the protein in the plasma is  $0.05 \mu\text{mol cm}^{-3}$ .

### Solution

The filtration flow rate of plasma ( $Q$ ) across the capillary wall is given by [Equation 6.53](#) and was shown earlier in [Example 3.4](#) to be equal to  $1.54 \times 10^{-8} \text{ cm}^3 \text{ h}^{-1}$ . Since we only know the molecular weight of the protein, we need to first estimate its radius and its diffusivity. From [Equation 5.41](#), we find that the radius of the solute is equal to 2.71 nm. We can also use [Equation 5.35](#) to estimate the diffusivity. Therefore, we find that  $D_{AB} = 7 \times 10^{-7} \text{ cm}^2 \text{ s}^{-1}$ . From [Equation 6.46](#), the diffusivity of the protein in plasma is estimated to be  $4.03 \times 10^{-7} \text{ cm}^2 \text{ s}^{-1}$ . [Equation 6.60](#) can be used to calculate the solute transport rate of the protein across the capillary wall. We first need to estimate the reflection coefficient ( $\sigma$ ) from [Equation 6.66](#). The slit pores of the capillary wall have a thickness of 7 nm, and from [Equation 5.171](#), the hydraulic diameter for this slit is 14 nm.

$$\sigma = 1 - \left(1 - \frac{2.71}{7}\right)^2 \left[2 - \left(1 - \frac{2.71}{7}\right)^2\right] \left[1 - \frac{2}{3} \left(\frac{2.71}{7}\right)^2 - 0.163 \left(\frac{2.71}{7}\right)^3\right]$$

$$\sigma = 0.457$$

The permeability of the protein for the capillary wall can be estimated using [Equation 6.15](#), and the quantity  $K_{\omega_r}$  can be obtained from [Equation 6.12](#).

$$P_m = \frac{4.03 \times 10^{-7} \text{ cm}^2 \text{ s}^{-1}}{2 \times 0.5 \times 10^{-6} \text{ m}} \times \frac{1 \text{ m}}{100 \text{ cm}} \times 0.001 \times \left(1 - \frac{2.71 \text{ nm}}{7 \text{ nm}}\right)^2 \\ \times \left[1 - 2.1 \left(\frac{2.71 \text{ nm}}{7 \text{ nm}}\right) + 2.09 \left(\frac{2.71 \text{ nm}}{7 \text{ nm}}\right)^3 - 0.95 \left(\frac{2.71 \text{ nm}}{7 \text{ nm}}\right)^5\right] = 4.541 \times 10^{-7} \text{ cm s}^{-1}$$

We can now calculate, by [Equation 6.60](#), the transport rate of the protein across the capillary wall by filtration and diffusion.

$$\dot{m}_A = \frac{1}{2}(0.05 + 0) \mu\text{mol cm}^{-3} (1 - 0.457) \times 1.54 \times 10^{-8} \text{ cm}^3 \text{ h}^{-1} + 4.541 \times 10^{-7} \text{ cm}^3 \text{ s}^{-1} \times \pi \times 10 \times 10^{-6} \text{ m} \\ \times 0.001 \text{ m} \times (0.05 - 0) \mu\text{mol cm}^{-3} \times \frac{(100 \text{ cm})^2}{\text{m}^2} \times \frac{3600 \text{ s}}{\text{h}} \\ \dot{m}_A = 2.091 \times 10^{-10} \mu\text{mol h}^{-1} + 2.568 \times 10^{-8} \mu\text{mol h}^{-1} = 2.589 \times 10^{-8} \mu\text{mol h}^{-1}$$

Once again, we observe that even for a macromolecular solute with a molecular weight of 50,000, the diffusive solute transport across the capillary wall is still significantly higher than the amount of solute transported by convection. Convection accounts for only about 1% of the total solute transport. The membrane Peclet number also confirms this conclusion. From [Equation 6.71](#), we obtain

$$Pe_{\text{membrane}} = \frac{(1-\sigma)Q}{P_m S} = \frac{(1-0.457) \times 1.54 \times 10^{-8} \text{ cm}^3 \text{ h}^{-1}}{4.541 \times 10^{-7} \text{ cm s}^{-1} \times 3600 \text{ s h}^{-1} \times \pi \times 10^{-4} \text{ cm} \times 0.1 \text{ cm}} \\ Pe_{\text{membrane}} = 0.163$$

Since the  $Pe_{\text{membrane}}$  is still quite smaller than unity, this shows that even for a rather large macromolecule, we can still neglect the amount of solute carried across the membrane by filtration flow in comparison to the amount of solute that is transported by diffusion.

## 6.4 Transport of a solute between a capillary and the surrounding tissue space

Now that we have developed an understanding of solute transport across a semipermeable membrane like the capillary wall, it is possible to develop a model for the spatial distribution and consumption or production of a particular species within the tissue space surrounding a given capillary. The following equations also describe the transport of a solute between a fluid flowing within a hollow fiber and the cylindrical space surrounding the hollow fiber under conditions where diffusion dominates the solute transport. From [Equation 6.71](#), this means that the  $Pe_{\text{membrane}} \ll 1$ . In the

case of oxygen transport where the flowing fluid is blood, the situation is somewhat more complex since the red blood cell provides an additional source or sink of oxygen through interactions with hemoglobin. We will discuss oxygen transport from blood later in [Chapter 7](#).

### 6.4.1 The Krogh tissue cylinder

Microscopic studies support, somewhat, the notion that a bed of capillaries in tissue can be represented as a repetitive arrangement of capillaries surrounded by a cylindrical layer of tissue. [Figure 6.11](#) shows an idealized sketch of the capillary bed and the corresponding cylindrical layer of tissue of thickness equal to  $r_T$ . Krogh (1919) used this cylindrical capillary-tissue model to study the supply of oxygen to muscle. This approach is now known as the *Krogh tissue cylinder model*.

A steady-state mathematical model for the transport of a solute can be developed using the Krogh tissue cylinder model. Although this model is developed for a single capillary surrounded by tissue, it can also be extended to a single hollow fiber membrane found in a bioartificial organ or in a bioreactor. In the case of the hollow fiber, the radius and length of the fiber is much larger than the dimensions of a single capillary.

We will treat the tissue space surrounding the capillary as a continuous phase and ignore the fact that it is comprised of discrete cells. Therefore, the diffusion of the solute in the tissue space may be described by an effective diffusivity ( $D_T$ ) as defined earlier by [Equations 6.43](#) and [6.45](#). The driving force for diffusion of the solute is created by the consumption (or production) of the solute by the cells within the tissue space.

We also need to have an expression that relates the consumption or production of the solute to the concentration of the solute in the tissue space, i.e.,  $\bar{C}_A$ . The *Michaelis-Menten equation* can be used to describe the metabolic consumption (or production) of the solute in the tissue space. The Michaelis-Menten equation can be written as follows:

$$R''_A = \frac{V_{\max} \bar{C}_A}{K_m + \bar{C}_A} \quad (6.72)$$

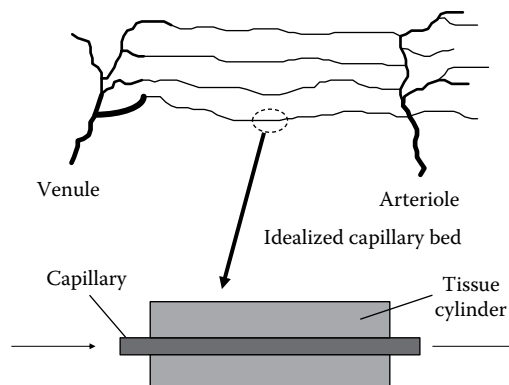


Figure 6.11 The Krogh tissue cylinder.

For consumption of the solute, the solute reaction rate, i.e.,  $R''_A$ , will be assumed to have a positive value, whereas if the solute is produced, then  $R''_A$  will have a negative value. The units on  $R''_A$  are in moles A per volume of tissue per time, e.g., mol L<sup>-1</sup> s<sup>-1</sup>.

In [Equation 6.72](#),  $V_{\max}$  represents the maximum reaction rate. The maximum reaction rate occurs when  $\bar{C}_A \gg K_m$ , and the reaction rate is then said to be zero order in the solute concentration, i.e.,  $\bar{C}_A^0$ .  $K_m$  is called the Michaelis constant and represents the value of  $\bar{C}_A$  for which the reaction rate is one-half the maximal value. When  $\bar{C}_A \ll K_m$ , then  $R''_A = V_{\max} \bar{C}_A / K_m$ , and the reaction is first order in the solute concentration, i.e.,  $\bar{C}_A^1$ . In many cases for biological reactions,  $\bar{C}_A \gg K_m$ , and we can reasonably assume that the reaction is zero order and that  $R''_A = V_{\max} = R_A^{\max}$ . In [Chapter 7](#), we will see this is the case for oxygen consumption by cells. This will considerably simplify the following mathematical analysis and allow us to find an analytical solution for solute diffusion in the tissue space that surrounds a given capillary.

## 6.4.2 A model of the Krogh tissue cylinder

[Figure 6.12](#) illustrates the Krogh tissue cylinder that surrounds a capillary. Within the capillary, the solute is transported primarily by convection in the axial direction and by diffusion in the radial direction. Diffusion of the solute from the blood and through the capillary wall is proportional to the concentration difference of the solute between that in the bulk fluid and that at the interface between the outer capillary wall and the surrounding tissue, i.e., at  $r = r_c + \bar{L}$ . This concentration difference is multiplied by the overall mass transfer coefficient, i.e.,  $K_o$ , defined earlier by [Equation 6.18](#). This gives the local solute flux across the capillary wall and into the tissue space. The overall mass transfer coefficient represents the combined resistance of the fluid flowing through the capillary, i.e.,  $k_m$ , on the blood or capillary side, and the permeability of the solute in the capillary wall, i.e.,  $P_m$ . The local solute flux across the capillary wall is given by dividing both sides of [Equation 6.60](#) by  $S$ . Unless there is known to be a significant filtration flow across the capillary wall or membrane, the convective solute flux in [Equation 6.60](#), i.e.,  $C_A(1-\sigma)Q/S$ , is negligible in comparison to the amount of solute transported by diffusion, i.e.,  $P_m \Delta C_A$ . From [Equation 6.71](#), this also means that the  $Pe_{\text{membrane}} \ll 1$ .

When calculating the value of  $k_m$ , one needs to determine whether the transport properties, as represented by the viscosity and the solute diffusivity, should be based on their respective plasma values or on those of blood. Recall from [Chapter 4](#) that the red blood cells have a tendency to accumulate along their axis of flow. This creates a cell-free plasma layer ( $\delta_{\text{plasma}}$ ) adjacent to the capillary wall that is on the order of a few microns in thickness. Also, the thickness of the concentration boundary layer can be approximated from the fact that  $k_m \approx D_0/\delta_C$ . Hence, we can first determine the value of  $k_m$  using the properties of blood. Then the concentration boundary layer thickness is approximately given by

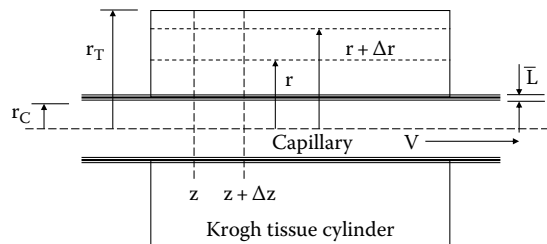


Figure 6.12 Geometry of the Krogh tissue cylinder.

$\delta_C \approx D_0/k_m$ . If  $\delta_C > \delta_{\text{plasma}}$ , then the value of  $k_m$  should be based on the properties of blood since the concentration boundary layer is expected to be comprised of blood. Otherwise, if  $\delta_C < \delta_{\text{plasma}}$ , then the concentration boundary layer lies within the plasma layer and the physical properties should be those of plasma.

In developing the Krogh tissue cylinder model, we will also treat the blood as a continuous phase and ignore the finite size of the red blood cells. We will assume that the blood flows through the capillary with an average velocity of  $V$ . With these assumptions, a steady-state shell balance on the solute in the blood from  $z$  to  $z + \Delta z$  (see [Figure 6.12](#)) provides the following equation:

$$V\pi r_c^2 C_A|_z - V\pi r_c^2 C_A|_{z+\Delta z} = 2\pi r_c \Delta z K_O \left( C_A - \bar{C}_A|_{r_c + \bar{L}} \right) \quad (6.73)$$

Dividing by  $\Delta z$ , and taking the limit as  $\Delta z \rightarrow 0$ , results in the following differential equation for the solute concentration in the blood.

$$-V \frac{dC_A}{dz} = \frac{2}{r_c} K_O \left( C_A - \bar{C}_A|_{r_c + \bar{L}} \right) \quad (6.74)$$

A steady-state shell balance at a given value of  $z$  from  $r$  to  $r + \Delta r$  can also be written for the solute concentration in the tissue space.

$$-D_T \frac{d\bar{C}_A}{dr} 2\pi r \Delta z|_r + -D_T \frac{d\bar{C}_A}{dr} 2\pi r \Delta z|_{r+\Delta r} = R''_A 2\pi r \Delta z \quad (6.75)$$

This equation neglects axial diffusion in comparison to radial diffusion within the tissue space. After dividing by  $2\pi r \Delta r$ , and taking the limit as  $\Delta r \rightarrow 0$ , the following differential equation results for the solute concentration in the tissue space:

$$\frac{D_T}{r} \frac{d}{dr} \left( r \frac{d\bar{C}_A}{dr} \right) = R''_A \quad (6.76)$$

The boundary conditions for [Equations 6.74](#) and [6.76](#) are

$$\begin{aligned} BC1: \quad z = 0, \quad C_A = C_A^0 \\ BC2: \quad r = r_c + \bar{L}, \quad \bar{C}_A = \bar{C}_A|_{r_c + \bar{L}} \\ BC3: \quad r = r_T, \quad \frac{d\bar{C}_A}{dr} = 0 \end{aligned} \quad (6.77)$$

It should be noted that even though we neglect axial diffusion in the tissue space in comparison to radial diffusion, the solute concentration in the tissue space will still have an axial dependence. This axial dependence of the tissue space solute concentration results from the boundary condition at  $r = r_c + \bar{L}$  and the solute flux term,  $K_O \left( C_A - \bar{C}_A|_{r_c + \bar{L}} \right)$ , which couples the solutions for the solute concentration within the capillary and the tissue space. In this way, the axial variation of the solute concentration in the capillary is impressed on that of the tissue space.

The solute concentration in the tissue space is then easily found by solving [Equation 6.76](#) subject to boundary conditions 2 and 3 in [Equation 6.77](#). Here, we assume the consumption of solute is

zero order as discussed earlier; hence  $R''_A = V_{\max} = R_A^{\max}$  is a constant. The following equation is then obtained:

$$\bar{C}_A(r,z) = \bar{C}_A(z) \Big|_{r_c + \bar{L}} + \frac{R_A^{\max}}{4D_T} \left[ \left( r^2 - (r_c + \bar{L})^2 \right) \right] - \frac{R_A^{\max} r_T^2}{4D_T} \ln \left( \frac{r}{r_c + \bar{L}} \right) \quad (6.78)$$

This equation provides no information on the value of the solute concentration at the interface between the capillary wall and the tissue space, i.e.,  $\bar{C}_A(z) \Big|_{r_c + \bar{L}}$ . However, at any axial position  $z$  from the capillary entrance, we must have at steady state that the change in solute concentration within the blood must equal the consumption of solute in the tissue space. Therefore, we can express this requirement by writing the following equation:

$$V\pi r_c^2 C_A^0 - V\pi r_c^2 C_A \Big|_z = \pi \left[ r_T^2 - (r_c + \bar{L})^2 \right] z R_A^{\max} \quad (6.79)$$

This equation can be rearranged to give [Equation 6.80](#), which provides for the axial variation of the solute concentration in the capillary.

$$C_A(z) = C_A^0 - \frac{R_A^{\max}}{Vr_c^2} \left[ r_T^2 - (r_c + \bar{L})^2 \right] z \quad (6.80)$$

[Equation 6.80](#) can now be used to find  $dC_A/dz$  in [Equation 6.74](#) with the result that we can solve for  $\bar{C}_A(z) \Big|_{r_c + \bar{L}}$ , which is given by

$$\bar{C}_A(z) \Big|_{r_c + \bar{L}} = C_A(z) - \frac{R_A^{\max}}{2r_c K_O} \left( r_T^2 - (r_c + \bar{L})^2 \right) \quad (6.81)$$

Note that  $C_A(z)$  in [Equation 6.81](#) makes  $\bar{C}_A(z) \Big|_{r_c + \bar{L}}$  depend on  $z$ , and by [Equation 6.78](#), the tissue space solute concentration then depends on both  $r$  and  $z$  as discussed earlier. [Equations 6.78, 6.80, and 6.81](#) can now be combined to give [Equation 6.82](#) for the solute concentration in the tissue space.

$$\begin{aligned} \bar{C}_A(r,z) &= C_A^0 - \frac{R_A^{\max}}{Vr_c^2} \left[ r_T^2 - (r_c + \bar{L})^2 \right] z - \frac{R_A^{\max}}{2r_c K_O} \left[ r_T^2 - (r_c + \bar{L})^2 \right] \\ &\quad + \frac{R_A^{\max}}{4D_T} \left[ r^2 - (r_c + \bar{L})^2 \right] - \frac{R_A^{\max} r_T^2}{2D_T} \ln \left( \frac{r}{r_c + \bar{L}} \right) \end{aligned} \quad (6.82)$$

**6.4.2.1 The critical radius** Under some conditions, the delivery of the solute to the capillary is limited by the capillary flow rate, or limited by the transport rate of the solute across the capillary wall, or the consumption of the solute by the tissue is very rapid. Any one of these conditions can lead to regions of the tissue that have no solute. We can then define a *critical radius* in the tissue,  $r_{\text{critical}}(z)$ , defined as the distance beyond which no solute is present in the tissue. For this situation, we need to modify boundary condition 3 in [Equation 6.77](#) to the following:

$$\text{BC3'}: \quad r = r_{\text{critical}}(z), \quad \frac{d\bar{C}_A}{dr} = 0 \quad \text{and} \quad \bar{C}_A = 0 \quad (6.83)$$

Under these conditions, the solute concentrations in the capillary, i.e.,  $C_A(z)$ , at the interface between the capillary and the tissue space, i.e.,  $\bar{C}_A(z)|_{r_c+L}$ , and in the tissue space itself, i.e.,  $\bar{C}_A(r,z)$ , are still given respectively by Equations 6.80, 6.81, and 6.82. However, the Krogh tissue cylinder radius in these equations, i.e.,  $r_T$ , is replaced with  $r_{\text{critical}}(z)$  once the solute concentration in the tissue at a particular location has reached zero.

The critical radius is found by recognizing that at  $r_{\text{critical}}(z) = 0$ ,  $\bar{C}_A(r,z) = 0$ . Thus, we can use Equation 6.82, with  $r_T = r_{\text{critical}}(z)$  and  $\bar{C}_A(r,z) = 0$ , to obtain the following expression for the critical radius.

$$\left(\frac{r_{\text{critical}}(z)}{r_c + L}\right)^2 \ln\left(\frac{r_{\text{critical}}(z)}{r_c + L}\right)^2 - \left(\frac{r_{\text{critical}}(z)}{r_c + L}\right)^2 + 1 = \left(\frac{4D_T C_A^0}{R_A^{\max} (r_c + L)^2}\right) - \frac{4D_T}{Vr_c^2} \left[ \left(\frac{r_{\text{critical}}(z)}{r_c + L}\right)^2 - 1 \right] z - \frac{2D_T}{r_c K_o} \left[ \left(\frac{r_{\text{critical}}(z)}{r_c + L}\right)^2 - 1 \right] \quad (6.84)$$

This is a nonlinear algebraic equation that can be solved for the critical radius at a given axial position,  $z$ , along the length of the capillary. Of particular interest are the conditions under which the solute just begins to be depleted within the tissue space. The depletion of the solute will start at the downstream corner of the Krogh tissue cylinder represented by the coordinates  $z = L$  and  $r = r_T$ . Equation 6.82 can be used to explore the conditions when the solute depletion just begins by recognizing that  $\bar{C}(r_T, L) = 0$ .

### Example 6.8

Calculate the glucose concentration at the exit of an exercising muscle capillary. Also calculate the glucose concentration in the tissue space at  $r = r_T$  and  $z = L$ . Assume the capillary properties summarized in Table 3.3 apply and that the glucose consumption rate,  $R_A^{\max}$ , is equal to  $0.007 \mu\text{mol cm}^{-3} \text{s}^{-1}$  and the glucose concentration in the blood entering the capillary is  $5 \mu\text{mol cm}^{-3}$ . Also assume that the Krogh tissue cylinder radius,  $r_T$ , is  $40 \mu\text{m}$ .

#### Solution

From Equation 6.80, we can calculate the glucose concentration in the blood as it exits the capillary:

$$C_A(L) = 5 \mu\text{mol cm}^{-3} - \frac{0.007 \mu\text{mol cm}^{-3} \text{s}^{-1}}{0.05 \text{ cm s}^{-1} \times (0.0005 \text{ cm})^2} \times \left[ (0.004 \text{ cm})^2 - (0.0005 \text{ cm} + 0.00005 \text{ cm})^2 \right] \times 0.1 \text{ cm}$$

$$C_A(L) = 4.12 \mu\text{mol cm}^{-3}$$

We will assume that within the capillary, the red blood cells are spaced by intervals of plasma. Hence, the properties of plasma will be used to describe the blood in the capillary. In Example 6.5, the diffusivity of glucose in plasma was estimated to be  $0.54 \times 10^{-5} \text{ cm}^2 \text{s}^{-1}$ . For plasma flowing in a capillary, we find that Reynolds number ( $Re$ ) = 0.0043 and Schmidt number ( $Sc$ ) = 2188.

For the velocity profile to be fully developed in a capillary, the distance downstream must be greater than  $0.05Re d_{\text{capillary}}$ . This distance is equal to  $2 \times 10^{-7} \text{ cm}$ , which is much smaller than the capillary length of  $0.1 \text{ cm}$ , so we conclude that the velocity profile is fully developed in the capillary. For the concentration profile to be fully developed, the distance downstream must be greater than  $0.05Re Sc d_{\text{capillary}}$ , which is equal to  $0.00047 \text{ cm}$ , and we conclude that the concentration profile is also fully developed. From [Equation 5.169](#), we have that  $Sh = 3.66$ . From this asymptotic value of the  $Sh$ , we can calculate the blood-side mass transfer coefficient:

$$k_m = 3.66 \times \frac{D_{\text{plasma}}}{d_{\text{capillary}}} = 3.66 \times \frac{0.54 \times 10^{-5} \text{ cm}^2 \text{ s}^{-1}}{0.001 \text{ cm}} = 0.02 \text{ cm s}^{-1}$$

From [Example 6.5](#), the capillary wall glucose permeability, i.e.,  $P_m$ , was estimated to be  $4.2 \times 10^{-5} \text{ cm s}^{-1}$ . We see that  $P_m \ll k_m$  and we conclude that the bulk of the mass transfer resistance is in the capillary wall, and we can ignore the blood-side mass transfer resistance since it is much smaller in comparison to that of the capillary wall. Therefore, from [Equation 6.18](#), we have that  $K_O \approx P_m = 4.2 \times 10^{-5} \text{ cm s}^{-1}$ . We can estimate the diffusivity of glucose in the tissue using the results shown in [Figure 6.9](#). For a glucose radius of  $0.41 \text{ nm}$ , we have  $D_T/D_{AB} \approx 0.5$ . With  $D_{AB} = 0.93 \times 10^{-5} \text{ cm}^2 \text{ s}^{-1}$ , this gives a  $D_T = 0.47 \times 10^{-5} \text{ cm}^2 \text{ s}^{-1}$ . Next, we use [Equation 6.82](#) to calculate the glucose concentration in the tissue at  $r = r_T$  and  $z = L$ .

$$\begin{aligned} \bar{C}_A(r_T, L) &= 4.12 \mu\text{mol cm}^{-3} - \frac{0.007 \mu\text{mol cm}^{-3} \text{ s}^{-1}}{2 \times 0.0005 \text{ cm} \times 4.2 \times 10^{-5} \text{ cm s}^{-1}} \\ &\quad \times \left[ (0.004 \text{ cm})^2 - (0.0005 \text{ cm} + 0.00005 \text{ cm})^2 \right] \\ &\quad + \frac{0.007 \mu\text{mol cm}^{-3} \text{ s}^{-1}}{4 \times 4.7 \times 10^{-6} \text{ cm}^2 \text{ s}^{-1}} \left[ (0.004 \text{ cm})^2 - (0.0005 \text{ cm} + 0.00005 \text{ cm})^2 \right] \\ &\quad - \frac{0.007 \mu\text{mol cm}^{-3} \text{ s}^{-1} (0.004 \text{ cm})^2}{2 \times 4.7 \times 10^{-6} \text{ cm}^2 \text{ s}^{-1}} \\ &\quad \times \ln \left( \frac{0.004 \text{ cm}}{(0.0005 + 0.00005) \text{ cm}} \right) \\ \bar{C}_A(r_T, L) &= 1.48 \mu\text{mol cm}^{-3} \end{aligned}$$

**6.4.2.2 A comparison of convection and diffusion effects** Recall that in developing our model for solute transport between a capillary and the Krogh tissue cylinder, i.e., [Equations 6.80](#) and [6.82](#), we ignored axial diffusion of the solute within the capillary in comparison to axial convection of solute, i.e., the solute carried along by the flowing blood. We can easily check the validity of this assumption through the following arguments. The amount of solute carried by convection in a capillary of diameter,  $d_c$ , is on the order of

$$\text{Solute transport by axial convection} = \frac{\pi d_c^2}{4} V C_A^0 \quad (6.85)$$

and the amount of solute carried by axial diffusion is on the order of

$$\text{Solute transport by axial diffusion} = \frac{\pi d_c^2}{4} \left( \frac{D_{AB}(C_A^0 - 0)}{L} \right) \quad (6.86)$$

where

$D_{AB}$  is the solute diffusivity

$L$  is the length of the capillary

By taking the ratio of Equations 6.85 and 6.86, we obtain the *Peclet number*, whose magnitude in this case represents the importance of axial solute convection in comparison to axial solute diffusion. The criterion for ignoring axial diffusion is then given by the fact that  $Pe = VL/D_{AB} \gg 1$ . For the example problems presented previously,  $Pe = VL/D_{AB} = (0.05 \text{ cm s}^{-1} \times 0.1 \text{ cm})/(0.93 \times 10^{-5} \text{ cm}^2 \text{ s}^{-1}) = 538 \gg 1$  and we conclude that we can ignore axial diffusion in comparison to axial convection.

A similar line of reasoning can be applied to the tissue space to support the neglect of axial diffusion in comparison to radial diffusion. The solute transport by radial diffusion is on the order of

$$\text{Solute transport by radial diffusion} = 2\pi r_c L \left( \frac{D_T(C_A^0 - 0)}{r_T - r_c} \right) \quad (6.87)$$

and the amount of solute transport by axial diffusion is on the order of

$$\text{Solute transport by axial diffusion} = \pi(r_T^2 - r_c^2) \left( \frac{D_T(C_A^0 - 0)}{L} \right) \quad (6.88)$$

The ratio of Equations 6.87 and 6.88 is a measure of the relative importance of radial diffusion in comparison to axial diffusion. If this ratio, i.e.,  $\frac{2r_c L^2}{(r_T - r_c)(r_T^2 - r_c^2)} \gg 1$ , then axial diffusion can be neglected. For a typical capillary, we then have

$$\frac{2r_c L^2}{(r_T - r_c)(r_T^2 - r_c^2)} = \frac{2 \times 0.5 \times 10^{-3} \text{ cm} \times (0.1 \text{ cm})^2}{(4 \times 10^{-3} - 0.5 \times 10^{-3}) \left[ (4 \times 10^{-3})^2 - (0.5 \times 10^{-3})^2 \right] \text{cm}^3} = 181 \gg 1$$

and we conclude that we can ignore axial diffusion in the tissue space.

### 6.4.3 The Renkin-Crone equation

The previous analysis can also be simplified considerably for the special case where the solute concentration in the tissue space is zero or much smaller than the concentration in the blood. We can also assume that the blood offers little resistance to the solute transport rate in comparison to that of

the capillary wall; hence  $K_O \approx P_m$ . For these conditions, [Equation 6.74](#) simplifies to

$$\frac{dC_A}{dz} = -\frac{2P_m}{Vr_c} C_A = -\frac{2\pi r_c P_m}{Q} C_A \quad (6.89)$$

Here, we have replaced the capillary blood velocity ( $V$ ) with the volumetric flow rate of blood in the capillary ( $Q$ ). [Equation 6.89](#) is easily integrated to obtain the solute concentration in the capillary at any axial position  $z$ .

$$E = \frac{C_A^0 - C_A(z)}{C_A^0} = 1 - \exp\left(-\frac{2\pi r_c P_m z}{Q}\right) \quad (6.90)$$

where  $C_A^0$  is the solute concentration in the blood that enters the capillary.

[Equation 6.90](#) is known as the *Renkin-Crone equation* and describes how the solute concentration varies along the length of the capillary for the special case where the solute concentration in the tissue space is very small in comparison to its value in the blood.

The solute extraction is represented by  $E$ , which is the ratio of the actual amount of solute transported across the capillary, i.e.,  $Q(C_A^0 - C_A)$ , to the maximum amount of solute that can be transported across the capillary,  $QC_A^0$ . Hence,  $E \times QC_A^0$  represents the actual solute transport rate for the given conditions. The solute extraction is therefore a measure of the removal efficiency of the solute from the capillary. [Equation 6.90](#) shows that solute transport from the capillary is strongly dependent on the ratio of the permeability of the capillary wall ( $2\pi r_c P_m z$ ) to the blood flow rate ( $Q$ ). This ratio can be used to define conditions under which the solute transport is either flow limited or diffusion limited as follows:

$$\begin{aligned} &\text{if } \frac{2\pi r_c P_m z}{Q} \gg 1, \text{ then flow limited and } E \rightarrow 1 \\ &\text{if } \frac{2\pi r_c P_m z}{Q} \ll 1, \text{ then diffusion limited and } E \rightarrow 0 \end{aligned} \quad (6.91)$$

*Flow limited* means that the mass transport rate of the solute by diffusion out of the capillary and into the tissue space is much faster than the rate at which the solute is entering the capillary by the flowing blood. In this situation, solute transport to the tissue surrounding a given capillary can only be increased by increasing the blood flow rate. In the *diffusion-limited* case, blood supply is more than adequate and the limitation is the difficulty of transporting the solute across the capillary wall.

[Equation 6.90](#) is for a single capillary. For regions of tissue containing many capillaries, we can replace the quantity  $2\pi r_c P_m z$  with the group  $P_m S$ , where  $S$  represents the total surface area of the capillaries within the tissue region of interest. Hence, [Equation 6.90](#) for a tissue becomes

$$E = \frac{C_A^0 - C_A(z)}{C_A^0} = 1 - \exp\left(-\frac{P_m S}{Q}\right) \quad (6.92)$$

**6.4.3.1 Determining the value of  $P_mS$**  The multiple tracer indicator diffusion technique can be used to obtain a test solute's permeability ( $P_mS$ ) across the capillary wall in organs and large tissue regions. This technique can also be used to evaluate the solute permeability in medical devices that employ membranes, e.g., in hemodialyzers, bioreactors, and bioartificial organs.

In this technique, a solution containing equal concentrations of a permeable test solute and a non-permeable reference solute, typically labeled albumin, is rapidly injected into a main artery leading to the region of interest (Levick, 1991). Venous blood samples are then collected over the next few seconds and analyzed for the concentrations of the test and reference solutes. Because the test solute is permeable to the capillary wall, its concentration in the venous blood will initially fall below that of the reference solute due to its diffusion into the tissue space that surrounds the capillaries. This is shown in Figure 6.13. Because of the transient nature of this technique and the mass transfer resistance of the capillary wall, the concentration of the test solute in the tissue space surrounding the capillaries can be assumed to be close to zero or much smaller than the value within the blood. The concentration of the reference solute in the venous blood provides an estimate of what the test solute concentration would have been at a particular time if no transport of the test solute out of the capillaries had occurred. After several seconds, the reference solute concentration in the blood will fall below that of the test solute since the reference solute has been nearly washed out of the capillary and the test solute concentration in the tissue space is now larger than that in the blood. Hence, the test solute starts to diffuse back into the blood.

The concentrations of the test and reference solutes,  $C_{\text{test}}$  and  $C_{\text{reference}}$ , in the venous blood at a particular time can then be used to calculate, using Equation 6.92, the test solute extraction (E) and the value of  $P_mS$  for a given blood flow rate (Q). From Equation 6.92, we then have at a particular time,  $t$ ,

$$E = \frac{C_{\text{reference}}(t) - C_{\text{test}}(t)}{C_{\text{reference}}(t)} = 1 - \exp\left(-\frac{P_mS}{Q}\right) \quad (6.93)$$

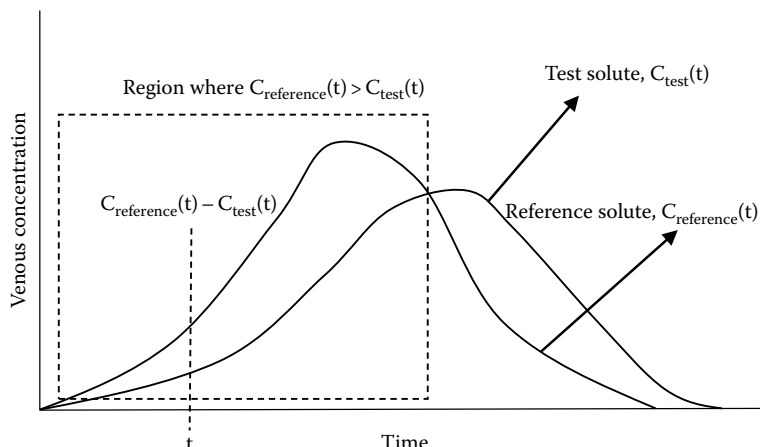


Figure 6.13 Multiple tracer indicator diffusion technique.

It is important to note that accurate results require that the test be repeated at increasing blood flow rates ( $Q$ ) to ensure that the solute transport is not flow limited. To show that the solute transport is not flow limited, it is convenient to express [Equation 6.92](#) in terms of the *clearance*. The term clearance is often used to describe the removal of a solute from a flowing fluid such as in a capillary. Clearance, given the symbol  $CL$ , is the volumetric flow rate of the fluid that has been totally cleared of the solute. Clearance is then defined by the following expression where we see that  $CL = QE$ .

$$CL(z) \equiv \frac{Q(C_A^0 - C_A(z))}{C_A^0} = QE = Q \left( 1 - e^{-\frac{P_m S}{Q}} \right) \quad (6.94)$$

This expression shows that capillary solute clearance is linearly dependent on the flow rate, i.e.,  $CL = Q$ , under flow-limited conditions where  $P_m S \gg Q$  and  $E \approx 1$ . However, under diffusion-limited conditions, where  $P_m S \ll Q$ , the parenthetical term in the above equation becomes equal to  $P_m S/Q$  and we obtain the result that the clearance becomes independent of the flow rate  $Q$  and is equal to the capillary wall permeability, i.e.,  $CL = P_m S$ . Hence, in experiments to determine the value of  $P_m S$  using the multiple tracer indicator diffusion technique, the value of  $P_m S$  should not be dependent on the flow rate,  $Q$ .

### Example 6.9

Blood is flowing through a hollow fiber-based bioartificial organ at a flow rate ( $Q$ ) of  $8 \text{ cm}^3 \text{ min}^{-1}$  for each fiber. Surrounding the fibers in the shell space are living cells obtained from a pig's liver. Each fiber has a diameter of  $800 \mu\text{m}$  and a length of  $30 \text{ cm}$ . At time equal to zero, equal concentrations of a permeable (relative to the fiber wall) test solute and labeled albumin (impermeable) are injected into the blood entering the device. Exiting blood samples are collected over the next few seconds and analyzed for the concentrations of the test solute ( $C_{\text{test}}$ ) and the reference solute, albumin ( $C_{\text{reference}}$ ). At a particular time, the value of  $C_{\text{test}}/C_{\text{reference}}$  was found to equal 0.60. Estimate the solute permeability ( $P_m$ ) of the hollow fiber membrane ( $\text{cm s}^{-1}$ ).

### Solution

We can use [Equation 6.94](#) to first calculate the clearance of a given hollow fiber for the test solute as shown below.

$$CL = Q \left( 1 - \frac{C_{\text{test}}}{C_{\text{reference}}} \right) = 8 \text{ cm}^3 \text{ min}^{-1} \times (1 - 0.6) = 3.2 \text{ cm}^3 \text{ min}^{-1}$$

Next, we calculate from [Equation 6.94](#) the value of  $P_m$ .

$$P_m = -\frac{Q}{S} \ln \left( 1 - \frac{CL}{Q} \right) = -\frac{8 \text{ cm}^3 \text{ min}^{-1} \times \frac{1 \text{ min}}{60 \text{ s}}}{2\pi \times 0.04 \text{ cm} \times 30 \text{ cm}} \ln \left( 1 - \frac{3.2 \text{ cm}^3 \text{ min}^{-1}}{8 \text{ cm}^3 \text{ min}^{-1}} \right) = 0.009 \text{ cm s}^{-1}$$

#### 6.4.4 Solute transport in vascular beds: The well-mixed assumption

The Krogh tissue cylinder model provides a description of solute transport within the tissue region surrounding a single capillary. In many cases, a model is needed to describe the solute transport in a much larger region containing numerous capillaries, as illustrated for the capillary bed shown in [Figure 6.11](#). One simple approach to describe solute transport in this situation is to treat the blood in the capillary bed and the tissue space as separate well-mixed regions.

To facilitate the analysis, we introduce two parameters that characterize the degree of vascularization in the region of interest. The first parameter is the *surface area capillary density* ( $s$ ), which is the capillary surface area per unit volume of tissue. Assuming the geometry of the Krogh tissue cylinder shown in [Figure 6.11](#), the following equation provides an estimate of ( $s$ ) based on the given values of the capillary radius,  $r_c$ , and the Krogh tissue cylinder radius,  $r_T$ .

$$s = \frac{2r_c}{r_T^2} \quad (6.95)$$

The second parameter is the *volume of capillaries per unit volume of tissue* ( $v$ ). In terms of the Krogh tissue cylinder model, this may also be expressed in terms of  $r_c$  and  $r_T$ .

$$v = \left( \frac{r_c}{r_T} \right)^2 \quad (6.96)$$

A steady-state solute balance, assuming only diffusion is relevant for solute transport across the capillary wall, can then be written for the capillary bed illustrated in [Figure 6.11](#). We can write that the solute carried into the capillary bed by blood flow must equal the amount removed by diffusion across the capillary walls and that which leaves with the blood flow.

$$Q C_A^0|_{in} = P_m S (C_A - \bar{C}) + Q C_A|_{out} \quad (6.97)$$

In this equation,  $Q$  is the volumetric flow rate of blood to the region of interest. If  $V_T$  is the volume of the tissue region considered, then  $q_b = Q/V_T$ , defined as the *tissue blood perfusion rate*. Assuming a capillary of length  $L$ , and blood velocity within the capillary of  $V$ , it is easily shown that

$$q_b = \left( \frac{r_c}{r_T} \right)^2 \left( \frac{V}{L} \right) = \frac{V}{\tau} \quad (6.98)$$

where  $\tau$  is the blood residence time in the capillary, i.e.,  $\tau = L/V = 0.1 \text{ cm}/0.05 \text{ cm s}^{-1} = 2 \text{ s}$ .

At steady state, the amount of solute diffusing out of the capillaries must equal the consumption rate of the solute in the tissue space. Hence, the diffusion term,  $P_m S (C_A - \bar{C}_A)$ , must equal  $V_T R_A^{\max}$ , for a zero order reaction occurring within the tissue space. After equating these two expressions, we can write the solute concentration in the tissue space as

$$\bar{C}_A = C_A - \frac{V_T R_A^{\max}}{P_m S} \quad (6.99)$$

Replacing the diffusion term in [Equation 6.97](#) with  $V_T R_A^{\max}$  allows for the calculation of the solute concentration in the blood exiting the tissue region of interest.

$$C_A = C_A^0 - \frac{V_T R_A^{\max}}{Q} = C_A^0 - \frac{R_A^{\max}}{q_b} \quad (6.100)$$

When this equation is substituted into [Equation 6.99](#) for  $C_A$ , the solute concentration within the tissue space is then given by the following equation:

$$\bar{C}_A = C_A^0 - R_0 \left[ \frac{1}{q_b} + \frac{V_T}{P_m S} \right] \quad (6.101)$$

The following example illustrates the use of these equations.

### Example 6.10

Consider the transport of glucose from the capillary blood to an exercising muscle tissue. As a basis, consider 1 g of tissue. The glucose consumption of the tissue is  $60 \mu\text{mol min}^{-1} (100 \text{ g})^{-1}$  or  $0.01 \mu\text{mol s}^{-1} \text{ g}^{-1}$ . Blood flow to the region is  $60 \text{ cm}^3 \text{ min}^{-1} (100 \text{ g})^{-1}$  or  $0.01 \text{ cm}^3 \text{ s}^{-1} \text{ g}^{-1}$ . The arterial glucose concentration is  $5 \text{ mM}$  ( $5 \mu\text{mol cm}^{-3}$ ). The value of  $P_m S$  based on capillary recruitment during exercise is  $0.33 \text{ cm}^3 \text{ s}^{-1} (100 \text{ g})^{-1}$  or, for the 1 g of tissue considered here,  $0.0033 \text{ cm}^3 \text{ s}^{-1}$ . Calculate the glucose concentration in the tissue space and in the exiting blood (based on data provided in Levick, 1991).

### Solution

From [Equation 6.100](#), we have

$$C_A = 5 \mu\text{mol cm}^{-3} - \frac{0.01 \mu\text{mol g}^{-1} \text{ s}^{-1}}{0.01 \text{ cm g s}^{-1}} = 4.0 \mu\text{mol cm}^{-3} = 4 \text{ mM}$$

and by [Equation 6.101](#)

$$\begin{aligned} \bar{C}_A &= 5 \mu\text{mol cm}^{-3} - 0.01 \mu\text{mol g}^{-1} \text{ s}^{-1} \left( \frac{1}{0.01 \text{ cm g s}^{-1}} + \frac{1}{0.0033 \text{ cm g s}^{-1}} \right) \\ &= 0.97 \mu\text{mol cm}^{-3} = 0.97 \text{ mM} \end{aligned}$$

## 6.5 Solute transport by filtration flow across a membrane

The filtration of blood across the capillary wall, or a microporous membrane, to form a filtrate of plasma, is known as *plasmapheresis*. Because of the size of the pores in the capillary wall or the membrane, this filtration flow can also be used to separate the solutes on the basis of their size. For example, for the capillary wall, the pores in the membrane will stop the transport of the cellular components of the blood, and the smaller solutes like ions, glucose, and amino acids will readily pass through the capillary pores. However, larger proteins will be hindered to varying degrees in their passage across the capillary wall based on the relative size of these components in comparison to the size

of the pores. This selective filtration is used in a variety of membrane systems that are used in bioreactors, in processes for bioseparations, and in medical devices like artificial organs. In these membrane filtration applications, the solute transport by filtration is usually much greater than that by diffusion. From [Equation 6.71](#), this means that the membrane Peclet number is much greater than unity.

The solute selectivity during this membrane filtration process is described by the *actual* sieving coefficient ( $S_a$ ), which was given earlier by [Equation 6.65](#). The actual sieving coefficient was defined as the ratio of the solute concentration in the filtrate ( $C_A^{\text{filtrate}}$ ) to the solute concentration at the surface of the membrane on the feed side ( $C_A^{\text{surface}}$ ). Hence,

$$S_a = \frac{C_A^{\text{filtrate}}}{C_A^{\text{surface}}} = (1-\lambda)^2 \left[ 2 - (1-\lambda)^2 \right] \left[ 1 - \frac{2}{3} \lambda^2 - 0.163\lambda^3 \right] \quad (6.102)$$

where  $\lambda$  is defined as the ratio of the solute radius ( $a$ ) to the membrane pore radius ( $r$ ).

However, under most membrane filtration conditions, the filtration rates are much higher than those for which [Equation 6.102](#) applies. These higher filtration rates will lead to the formation of a layer of retained or hindered solutes that will concentrate along the surface on the feed side of the membrane. These retained solutes will have a higher concentration near the surface of the membrane than in the bulk solution. This effect, which is shown in [Figure 6.14](#), is called *concentration polarization*, and the layer of retained solutes will affect the transport of the solutes. Concentration polarization is particularly important at the higher filtration rates used in commercial membrane-based plasmapheresis systems used for separating plasma from the cellular components of blood, as well as in membrane systems used to purify protein solutions.

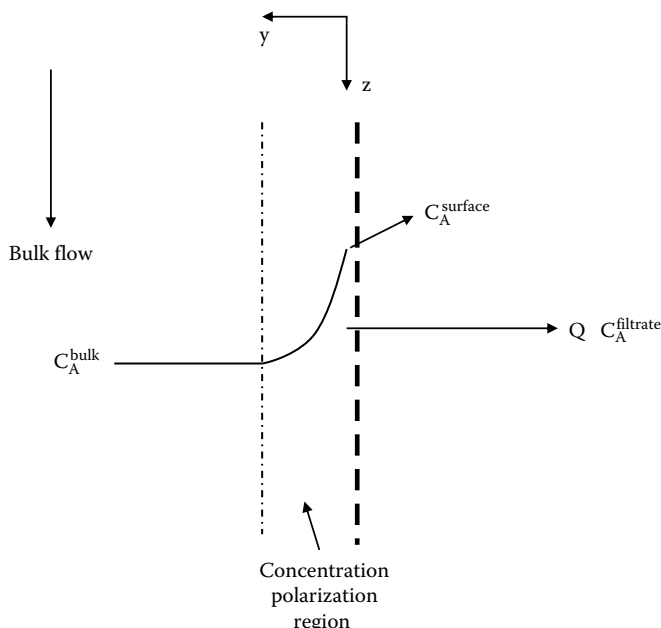


Figure 6.14 Sieving and concentration polarization.

The *observed* sieving coefficient for the case of concentration polarization ( $S_O$ ) is defined as the ratio of the solute concentration in the filtrate ( $C_A^{\text{filtrate}}$ ) to that in the bulk solution on the feed side of the membrane ( $C_A^{\text{bulk}}$ ).

An expression for the observed sieving coefficient can be developed as follows using film theory to describe the solute mass transfer. The convective transport rate of solute at any position  $y$  in the concentration polarization region shown in [Figure 6.14](#) has to equal the rate at which the solute is diffusing back toward the bulk solution plus the rate the solute is carried away by the filtration flow. This can be expressed by the following equation:

$$QC_A \Big|_y = -D_0 S \frac{dC_A}{dy} \Big|_y + QC_A^{\text{filtrate}} \quad (6.103)$$

where

$S$  is the surface area of the membrane normal to the direction of the filtration flow

$D_0$  is the solute diffusivity within the concentration polarization region

$Q$ , the filtration flow rate across the membrane, is given by [Equation 6.53](#)

[Equation 6.103](#) can then be rearranged and integrated across the concentration polarization region having a film thickness  $\delta_C$  as follows:

$$q \int_0^{\delta_C} dy = -D_0 \int_{C_A^{\text{surface}}}^{C_A^{\text{bulk}}} \frac{dC_A}{C_A - C_A^{\text{filtrate}}} \quad (6.104)$$

where the filtration flux  $q$  is equal to  $Q/S$ . After performing the integration, we obtain

$$q = -\frac{D_0}{\delta_C} \ln \left( \frac{C_A^{\text{bulk}} - C_A^{\text{filtrate}}}{C_A^{\text{surface}} - C_A^{\text{filtrate}}} \right) = -k_m \ln \left( \frac{C_A^{\text{bulk}} - C_A^{\text{filtrate}}}{C_A^{\text{surface}} - C_A^{\text{filtrate}}} \right) \quad (6.105)$$

In [Equations 6.104](#) and [6.105](#),  $\delta_C$  is defined as the film thickness of the concentration polarization region, and from our discussion of mass transfer and film theory in [Section 5.7.1](#), we can replace  $D_0/\delta_C$  with the mass transfer coefficient,  $k_m$ .

[Equation 6.105](#) can then be rearranged, and after some algebra, we obtain the following expression for the observed sieving coefficient:

$$S_O = \frac{C_A^{\text{filtrate}}}{C_A^{\text{bulk}}} = \frac{S_a}{(1 - S_a) e^{-\frac{q}{k_m}} + S_a} \quad (6.106)$$

where

$S_a$  is given by [Equation 6.102](#)

$k_m$  is the mass transfer coefficient, which, as discussed in [Section 5.11](#), is dependent on the fluid properties and the nature of the flow field

Note that in [Equation 6.106](#), if the ratio of the filtration flux to the mass transfer coefficient, i.e.,  $q/k_m$ , approaches zero, meaning that the filtration flow is small in comparison to solute mass transfer, then  $S_o \rightarrow S_a$ . On the other hand, if  $q/k_m$  is much greater than unity, meaning that the solute transport by the filtration flow is much larger than that by diffusion, then  $S_o \rightarrow 1$  and the solute concentration in the filtrate is the same as that in the bulk solution on the feed side of the membrane.

### Example 6.11

A protein with a MW of 15,000 in an aqueous solution is being filtered at 20°C through a microporous membrane within a 25 mm diameter stirred ultrafiltration cell. The membrane has a nominal molecular weight cutoff (NMWCO) of 30,000. The stirring speed is 1000 RPM. Estimate the observed sieving coefficient,  $S_o$ . The filtration flux, i.e.,  $q = Q/S$ , is equal to  $1.5 \times 10^{-3} \text{ cm s}^{-1}$ .

#### Solution

First, we calculate the radius of the protein and the radius of the membrane pores using [Equation 5.41](#):

$$r = \left( \frac{3 \times 30,000 \text{ g mol}^{-1}}{4 \times \pi \times 1 \text{ g cm}^{-3} \times 6.023 \times 10^{23} \text{ mol}^{-1}} \right)^{1/3} = 2.283 \times 10^{-7} \text{ cm} = 2.283 \text{ nm}$$

$$a = \left( \frac{3 \times 15,000 \text{ g mol}^{-1}}{4 \times \pi \times 1 \text{ g cm}^{-3} \times 6.023 \times 10^{23} \text{ mol}^{-1}} \right)^{1/3} = 1.812 \times 10^{-7} \text{ cm} = 1.812 \text{ nm}$$

Next, we calculate  $\lambda = a/r = 0.794$ . From [Equation 6.102](#), we find the actual sieving coefficient:

$$S_a = (1 - 0.794)^2 \left[ 2 - (1 - 0.794)^2 \right] \left[ 1 - \frac{2}{3} \times 0.794^2 - 0.163 \times 0.794^3 \right] = 0.0414$$

The protein diffusivity can be estimated from [Equation 5.35](#), which is also corrected to 20°C using [Equation 5.42](#).

$$D_{AB} = 1.013 \times 10^{-4} (15,000)^{-4.6} \left( \frac{0.691}{1.002} \right) \left( \frac{293}{310} \right) = 7.92 \times 10^{-7} \text{ cm}^2 \text{ s}^{-1}$$

For a stirred ultrafiltration cell, Mochizuki and Zydny (1992) provide the following correlation for finding the mass transfer coefficient:

$$\frac{k_m r_{cell}}{D_{AB}} = 0.23 Re^{0.567} Sc^{0.33} = 0.23 \left( \frac{\rho \omega r_{cell}^2}{\mu} \right)^{0.567} \left( \frac{\mu}{\rho D_{AB}} \right)^{0.33}$$

where

$r_{cell}$  is the radius of the stirred cell ultrafiltration chamber

$\omega$  is the stirring speed

Hence,

$$\begin{aligned}
 \frac{k_m r_{cell}}{D_{AB}} &= 0.23 \left( \frac{1 \text{ g cm}^{-3} \times 1000 \text{ RPM} \times 2\pi \text{ rev}^{-1} \times \frac{1 \text{ min}}{60 \text{ s}} \times (1.25 \text{ cm})^2}{1.002 \text{ cP} \times 0.01 \text{ g cm}^{-1} \text{ s}^{-1}} \right)^{0.567} \\
 &\quad \times \left( \frac{1.002 \text{ cP} \times 0.01 \text{ g cm}^{-1} \text{ s}^{-1}}{1 \text{ g cm}^{-3} \times 7.92 \times 10^{-7} \text{ cm}^2 \text{ s}^{-1}} \right)^{0.33} \\
 &= 0.23 (16,329.8)^{0.567} (12,651.52)^{0.33} = 1,311.80 \\
 k_m &= 1,311.80 \times \frac{7.92 \times 10^{-7} \text{ cm}^2 \text{ s}^{-1}}{1.25 \text{ cm}} = 8.312 \times 10^{-4} \text{ cm s}^{-1}
 \end{aligned}$$

We can now solve for  $S_0$  using [Equation 6.106](#):

$$S_0 = \frac{S_a}{(1 - S_a) e^{-\frac{q}{k_m}} + S_a} = \frac{0.0414}{(1 - 0.0414) \exp \left( -\frac{1.5 \times 10^{-3} \text{ cm s}^{-1}}{8.312 \times 10^{-4} \text{ cm s}^{-1}} \right) + 0.0414}$$

$$S_0 = 0.208$$

### 6.5.1 The change in the bulk flow of a fluid flowing within a hollow fiber with filtration

Consider the filtration of a fluid flowing within a hollow fiber. Assume the length of the hollow fiber is given by  $L$  and the radius of the hollow fiber is  $R$ . We need to develop the differential equation that describes the steady-state change with axial position ( $z$ ) of the volumetric flow rate of the fluid ( $F$ ) as a result of filtration across the walls of the hollow fiber.

We can write a shell balance across a finite axial shell volume of the hollow fiber equal to  $\pi R^2 \Delta z$ . The amount of the fluid filtered across the wall of the hollow fiber within the shell volume is equal to  $2\pi R \Delta z q$ , where  $2\pi R \Delta z$  is the circumferential surface area of the shell volume and  $q(z)$  is the local filtration flux, which is given by [Equation 6.53](#) with  $q = Q/S$ :

$$q(z) = L_p (\Delta P - \sigma RT \Delta C_A) \quad (6.107)$$

In [Equation 6.107](#),  $\Delta P$  is the local hydrodynamic pressure difference that is driving the filtration flow across the membrane, i.e.,  $\Delta P = P_{fiber} - P_{filtrate}$ , where  $P_{fiber}$  is the pressure of the fluid flowing inside the hollow fiber and  $P_{filtrate}$  is the pressure of the filtrate fluid. The osmotic pressure effect on the filtration flow is given by  $\sigma RT \Delta C_A$ , where  $\Delta C_A$  is the local solute concentration difference across the membrane, i.e.,  $\Delta C_A = C_A^{surface} - C_A^{filtrate}$ . Because the local values of the pressures and solute concentrations can be changing along the length of the hollow fiber, this means that in general the filtration flux is dependent on the axial fiber position, i.e.,  $z$ .

Our steady-state shell balance assuming constant fluid density can then be written as

$$0 = F|_z - F|_{z+\Delta z} - 2\pi R \Delta z q(z) \quad (6.108)$$

Dividing [Equation 6.108](#) by  $\Delta z$ , and taking the limit as  $\Delta z \rightarrow 0$ , results in the following differential equation that describes the axial variation of the volumetric flow rate within the hollow fiber:

$$\frac{dF}{dz} = -2\pi R q(z) = -2\pi R L_p (\Delta P - \sigma RT \Delta C_A) \quad (6.109)$$

If  $q(z)$  is constant, then [Equation 6.109](#) can be integrated to give

$$F(z) = F_0 - 2\pi R q z \quad (6.110)$$

where  $F_0$  is the volumetric feed rate to the hollow fiber.

### 6.5.2 Describing the change in the bulk concentration of a solute in a fluid flowing in a hollow fiber with filtration

We can perform a solute mass balance on solute A over the length of a fiber from  $z$  to  $z + \Delta z$ . We assume that the filtration rate is high enough so that the transport of solute A across the membrane is by convection (filtration) and not by diffusion. Therefore,  $P_e_{\text{membrane}} \gg 1$ . We also use the observed sieving coefficient, i.e.,  $S_o$ , defined by [Equation 6.106](#), to relate the solute concentration in the filtrate to that in the bulk fluid flowing within the hollow fiber.

$$FC_A^{\text{bulk}} \Big|_z - FC_A^{\text{bulk}} \Big|_{z+\Delta z} = 2\pi R \Delta z q C_A^{\text{filtrate}} = 2\pi R \Delta z S_o C_A^{\text{bulk}} \quad (6.111)$$

After dividing by  $\Delta z$ , and taking the limit as  $\Delta z \rightarrow 0$ , we obtain

$$\frac{dFC_A^{\text{bulk}}}{dz} = F \frac{dC_A^{\text{bulk}}}{dz} + C_A^{\text{bulk}} \frac{dF}{dz} = -2\pi R q S_o C_A^{\text{bulk}} \quad (6.112)$$

From [Equation 6.109](#), we also have that  $dF/dz = -2\pi R q(z)$ , and using this result, we can write [Equation 6.112](#) as

$$\frac{dC_A^{\text{bulk}}}{dz} = \frac{2\pi R (1 - S_o) q(z)}{F(z)} C_A^{\text{bulk}} \quad (6.113)$$

[Equation 6.113](#) can then be solved, along with [Equation 6.109](#), to find how the flow rate and bulk solute concentration vary along the length of the hollow fiber.

If the filtration flux  $q(z)$  is constant along the length of the fibers, then we can use [Equation 6.110](#) to describe  $F(z)$ , and [Equation 6.113](#) becomes

$$\frac{dC_A^{\text{bulk}}}{dz} = \frac{2\pi R (1 - S_o) q(z)}{F(z)} C_A^{\text{bulk}} = \frac{2\pi R (1 - S_o) q}{F_0 - 2\pi R q z} C_A^{\text{bulk}} \quad (6.114)$$

[Equation 6.114](#) can then be readily integrated to obtain an expression for how the bulk solute concentration changes with position in the hollow fiber for the case when the filtration flux is constant. First, we rearrange and separate the variables in [Equation 6.114](#) as shown next:

$$\int_{C_A^{\text{bulk}}(0)}^{C_A^{\text{bulk}}(z)} \frac{dC_A^{\text{bulk}}}{C_A^{\text{bulk}}} = 2\pi R (1 - S_o) q \int_0^z \frac{dz}{F_0 - 2\pi R q z} \quad (6.115)$$

[Equation 6.115](#) is then integrated to give

$$C_A^{\text{bulk}}(z) = C_A^{\text{bulk}}(0) \left[ 1 - \left( \frac{2\pi R q}{F_0} \right) z \right]^{-(1-S_o)} \quad (6.116)$$

Note that if the solute is totally retained by the hollow fiber membrane, then  $S_o = 0$ , and [Equation 6.116](#) simplifies to give

$$C_A^{\text{bulk}}(0) F_0 = C_A^{\text{bulk}}(z) (F_0 - 2\pi R q z) = C_A^{\text{bulk}}(z) F(z) \quad (6.117)$$

[Equation 6.117](#) says that for a retained solute, the mass rate at which that solute enters the hollow fiber equals the mass rate at which that solute crosses any axial position  $z$  in the hollow fiber.

### Example 6.12

Consider a hollow fiber module that is being used to concentrate a protein solution at 37°C. The module contains 10,000 fibers, and each fiber has a diameter of 400 μm and a length of 20 cm. The pore length in the wall of the hollow fibers is 75 μm. The NMWCO for the hollow fibers is 100,000, and the porosity of the hollow fibers ( $\epsilon = A_p/S$ ) is equal to 0.40. The protein solution has a viscosity of 0.001 Pa s. The protein solution enters the hollow fiber module at a flow rate of 250 mL min<sup>-1</sup>. The composition of the protein solution is protein A (4 g L<sup>-1</sup>, MW = 20,000), protein B (7 g L<sup>-1</sup>, MW = 150,000), and protein C (6 g L<sup>-1</sup>, MW = 300,000). The diffusivity of protein A in the solution is  $6.42 \times 10^{-7}$  cm<sup>2</sup> s<sup>-1</sup>. Determine the total filtration flow rate across the hollow fibers assuming the average pressure drop across the hollow fiber membrane wall is 750 mmHg. What is the composition of the fluid leaving on the filtrate side? What is the fractional removal of protein A from the feed solution to the hollow fiber module? What is the composition of the fluid leaving the hollow fibers?

### Solution

To obtain a solution, we will need to make some reasonable assumptions. Proteins B and C are retained by the hollow fiber membranes. We can estimate their osmotic pressure from [Equation 3.3](#).

$$\begin{aligned} \Pi_{BC} &= 19.33 \text{ mmHg mM}^{-1} \left( 7 \text{ g L}^{-1} \times \frac{1 \text{ mol}}{150,000} + 6 \text{ g L}^{-1} \times \frac{1 \text{ mol}}{300,000} \right) \\ &\times \frac{1,000 \text{ mmol}}{\text{mol}} \times \frac{1 \text{ mM L}}{\text{mmol}} = 1.29 \text{ mmHg} \end{aligned}$$

In comparison to the average pressure drop across the hollow fiber membrane wall of 750 mmHg, this osmotic pressure of the retained solutes is rather small; hence, from [Equation 6.107](#), we can assume that the filtration flux is constant along the length of the hollow fibers. Next, we calculate the hydraulic conductance of the hollow fiber membrane from [Equation 3.7](#), assuming that the radius of the membrane pores can be found from the NMWCO using [Equation 5.41](#).

$$r = \left( \frac{3 \times 100,000 \text{ g mol}^{-1}}{4\pi \times 1 \text{ g cm}^{-3} \times 6.023 \times 10^{23} \frac{1}{\text{mol}}} \right)^{1/3} = 3.41 \times 10^{-7} \text{ cm}$$

and

$$L_P = \frac{0.40 \times (3.41 \times 10^{-7} \text{ cm})^2}{8 \times 0.001 \text{ Pa s} \times 0.0075 \text{ cm}} = 7.75 \times 10^{-10} \text{ cm Pa}^{-1} \text{ s}^{-1}$$

Next, we can calculate the total filtration flow for the hollow fiber module using [Equation 3.4](#).

$$Q = 7.75 \times 10^{-10} \text{ cm Pa}^{-1} \text{ s}^{-1} \times 10,000 \times 2\pi \times 0.02 \text{ cm} \times 20 \text{ cm} \times (750 - 1.29) \text{ mmHg} \\ \times \frac{1 \text{ atm}}{760 \text{ mmHg}} \times \frac{101,325 \text{ Pa}}{1 \text{ atm}} = 1.94 \text{ cm}^3 \text{ s}^{-1}$$

The filtration flow rate is almost 50% of the total flow rate entering the hollow fiber module, which is  $250 \text{ cm}^3 \text{ min}^{-1}$  or  $4.17 \text{ cm}^3 \text{ s}^{-1}$ . Thus, the flow rate of fluid leaving the fibers of the hollow fiber module is therefore

$$F(L) = (4.17 - 1.94) \text{ cm}^3 \text{ s}^{-1} = 2.23 \text{ cm}^3 \text{ s}^{-1}$$

The filtration flux ( $q$ ) equals  $Q$  divided by the total circumferential surface area of the fibers. Therefore,

$$q = \frac{1.94 \text{ cm}^3 \text{ s}^{-1}}{2\pi \times 0.02 \text{ cm} \times 20 \text{ cm} \times 10,000} = 7.72 \times 10^{-5} \text{ cm s}^{-1}$$

We now need to calculate the sieving coefficient, or  $S_O$ , which is also dependent on  $k_m$  according to [Equation 6.106](#). To find  $k_m$ , we will need to know the fluid velocity within the hollow fiber. Because of filtration, the fluid velocity will change along the length of the hollow fiber. We will base the calculation of  $k_m$  on the average velocity of the fluid in the hollow fiber. The average of the entrance and exit flow rates is

$$F_{\text{average}} = \frac{1}{2} (4.17 + 2.23) \text{ cm s}^{-1} = 3.2 \text{ cm}^3 \text{ s}^{-1}$$

We can calculate the average velocity of the fluid in a hollow fiber by dividing  $F_{\text{average}}$  by the hollow fiber cross-sectional area, which is given by

$$V = 3.2 \text{ cm}^3 \text{ s}^{-1} \times \frac{1}{10,000} \times \frac{4}{\pi (0.04 \text{ cm})^2} = 0.25 \text{ cm s}^{-1}$$

The average Reynolds number of the fluid flowing in a hollow fiber is

$$Re = \frac{\rho V d_{\text{tube}}}{\mu} = \frac{1 \text{ g cm}^{-1} \times 0.04 \text{ cm} \times 0.25 \text{ cm s}^{-1}}{0.01 \text{ g cm}^{-1} \text{ s}^{-1}} = 1.0$$

Therefore, the flow of the fluid within the fibers is laminar. The diffusivity of protein A is given as  $6.42 \times 10^{-7} \text{ cm}^2 \text{ s}^{-1}$ , and the Schmidt number is then calculated as follows:

$$Sc = \frac{\mu}{\rho D_{AB}} = \frac{0.01 \text{ g cm}^{-1} \text{ s}^{-1}}{1 \text{ g cm}^{-3} \times 6.42 \times 10^{-7} \text{ cm}^2 \text{ s}^{-1}} = 15,576$$

Previously, we discussed that the velocity profile is fully developed if  $z > d_{\text{tube}} \times 0.05 Re$ . In this case, the velocity profile is fully developed if  $z > 0.002 \text{ cm}$ . Since this is much smaller than the fiber length of 20 cm, we conclude that the velocity profile within the hollow fiber is fully developed. For the concentration profile to be fully developed, we have that  $z > d_{\text{tube}} \times 0.05 Re Sc$ , which in this case gives that  $z > 31 \text{ cm}$ , which is longer than the given length of the hollow fibers. Hence, the concentration profile is not fully developed and we should use [Equation 5.169](#) to calculate the value of  $k_m$  as shown below.

$$Sh = 3.66 + \frac{0.104 \times 1.0 \times 15,576 \times \frac{0.04 \text{ cm}}{20 \text{ cm}}}{1 + 0.016 \left( 1.0 \times 15,576 \times \frac{0.04 \text{ cm}}{20 \text{ cm}} \right)^{0.8}} = 6.25$$

The mass transfer coefficient is then calculated as shown next.

$$k_m = \frac{D_{AB} Sh}{d_{\text{tube}}} = \frac{6.42 \times 10^{-7} \text{ cm}^2 \text{ s}^{-1} \times 6.25}{0.04 \text{ cm}} = 1.0 \times 10^{-4} \text{ cm s}^{-1}$$

Next, we can use [Equation 6.102](#) to find the value of  $S_a$ . The radius of protein A ( $a$ ) can be estimated from the molecular weight using [Equation 5.41](#).

$$a = \left( \frac{3 \times 20,000 \text{ g mol}^{-1}}{4\pi \times 1 \text{ g cm}^{-3} \times 6.023 \times 10^{23} \frac{1}{\text{mol}}} \right)^{1/3} = 1.99 \times 10^{-7} \text{ cm} = 1.994 \text{ nm}$$

and the value of  $\lambda = a/r = 1.994 \text{ nm}/3.41 \text{ nm} = 0.585$ . Hence, the actual sieving coefficient, in the absence of concentration polarization, is given by

$$S_a = (1 - 0.585)^2 \left[ 2 - (1 - 0.585)^2 \right] \left[ 1 - \frac{2}{3} \times 0.585^2 - 0.163 \times 0.585^3 \right] = 0.233$$

From [Equation 6.106](#), we can then include the effect of concentration polarization on the sieving coefficient as shown below in the calculation of  $S_O$ .

$$S_O = \frac{0.233}{(1 - 0.233) e^{-\frac{7.72 \times 10^{-5} \text{ cm s}^{-1}}{1.0 \times 10^{-4} \text{ cm s}^{-1}}} + 0.233} = 0.398$$

Next, we can calculate from [Equation 6.116](#) the concentration of protein A exiting ( $z = L$ ) the hollow fiber module.

$$C_A^{\text{bulk}} \Big|_{z=L} = 4 \text{ g L}^{-1} \left( 1 - \left( \frac{2\pi \times 0.02 \text{ cm} \times 7.72 \times 10^{-5} \text{ cm s}^{-1}}{4.17 \text{ cm}^3 \text{ s}^{-1} \times \frac{1}{10,000}} \right) \times 20 \text{ cm} \right)^{-(1-0.398)} = 5.83 \text{ g L}^{-1}$$

An overall solute balance can then be used to find the concentration of protein A in the filtrate leaving the hollow fiber module.

$$(QC_A^{\text{filtrate}}) \Big|_{\text{out}} = (FC_A^{\text{bulk}}) \Big|_{z=0} - (FC_A^{\text{bulk}}) \Big|_{z=L}$$

$$C_A^{\text{filtrate}} \Big|_{\text{out}} = \frac{(FC_A^{\text{bulk}}) \Big|_{z=0} - (FC_A^{\text{bulk}}) \Big|_{z=L}}{Q} = \frac{4.17 \text{ cm}^3 \text{ s}^{-1} \times 4 \text{ g L}^{-1} - 2.23 \text{ cm}^3 \text{ s}^{-1} \times 5.83 \text{ g L}^{-1}}{1.94 \text{ cm}^3 \text{ s}^{-1}}$$

$$C_A^{\text{filtrate}} \Big|_{\text{out}} = 1.90 \text{ g L}^{-1}$$

The % removal of protein A from the stream entering the hollow fiber module is then given by the following calculation.

$$\% \text{ Removal of A} = \frac{(FC_A^{\text{bulk}}) \Big|_{z=0} - (FC_A^{\text{bulk}}) \Big|_{z=L}}{(FC_A^{\text{bulk}}) \Big|_{z=0}}$$

$$= \frac{4.17 \text{ cm}^3 \text{ s}^{-1} \times 4 \text{ g L}^{-1} - 2.23 \text{ cm}^3 \text{ s}^{-1} \times 5.83 \text{ g L}^{-1}}{4.17 \text{ cm}^3 \text{ s}^{-1} \times 4 \text{ g L}^{-1}} \times 100 = 22\%$$

The concentrations of the retained proteins, i.e., B and C, in the fluid exiting the hollow fibers can also be calculated by [Equation 6.117](#):

$$C_B^{\text{bulk}} \Big|_{z=L} = \frac{(FC_B^{\text{bulk}}) \Big|_{z=0}}{F \Big|_{z=L}} = \frac{4.17 \text{ cm}^3 \text{ s}^{-1} \times 7 \text{ g L}^{-1}}{2.23 \text{ cm}^3 \text{ s}^{-1}} = 13.1 \text{ g L}^{-1}$$

$$C_C^{\text{bulk}} \Big|_{z=L} = \frac{(FC_C^{\text{bulk}}) \Big|_{z=0}}{F \Big|_{z=L}} = \frac{4.17 \text{ cm}^3 \text{ s}^{-1} \times 6 \text{ g L}^{-1}}{2.23 \text{ cm}^3 \text{ s}^{-1}} = 11.2 \text{ g L}^{-1}$$

Recall that the average pressure drop across the hollow fiber membrane that drives the filtration flow was given as 750 mmHg. How does this value compare with the pressure drop in the direction of the fluid flowing within the hollow fibers? Recall that the total flow rate of the protein solution to the hollow fiber unit is  $4.17 \text{ cm}^3 \text{ s}^{-1}$  and the flow rate leaving the hollow fibers is  $2.23 \text{ cm}^3 \text{ s}^{-1}$ . This gives an average flow rate within the hollow fiber unit of  $3.2 \text{ cm}^3 \text{ s}^{-1}$  or  $Q_{\text{fiber}} = 3.2 \times 10^{-4} \text{ cm}^3 \text{ s}^{-1}$  in each of the hollow fibers. Since the flow in the fibers is laminar,

we can calculate the pressure drop using this average value of the flow rate according to [Equation 4.10](#) as follows:

$$\Delta P = \frac{8Q_{fiber}\mu L}{\pi R^4} = \frac{8 \times 3.2 \times 10^{-4} \text{ cm}^3 \text{ s}^{-1} \times 0.001 \text{ Pa s} \times 20 \text{ cm}}{\pi \times (0.02 \text{ cm})^4} \times \frac{760 \text{ mmHg}}{101,325 \text{ Pa}} = 0.76 \text{ mmHg}$$

This pressure drop over the length of the hollow fiber is negligible in comparison to the pressure that is driving the filtration flow. Therefore, our assumption in this case of a constant average filtration pressure of 750 mmHg is reasonable. In this example, we also assumed that solute transport by filtration was much greater than that by diffusion across the hollow fiber membrane. We can calculate the membrane Peclet number from [Equation 6.71](#) to see if this assumption is reasonable. First, we calculate  $P_m$  from [Equation 6.15](#) with  $K_{\omega_r}$  calculated by the Renkin equation, i.e., [Equation 6.12](#), with  $\lambda = 1.994/3.41 = 0.585$ :

$$P_m = \frac{6.42 \times 10^{-7} \text{ cm}^2 \text{ s}^{-1}}{0.0075 \text{ cm}} \times 0.40 \left[ (1 - 0.585)^2 (1 - 2.1 \times 0.585 + 2.09 \times 0.585^3 - 0.95 \times 0.585^5) \right]$$

$$P_m = 7.36 \times 10^{-7} \text{ cm s}^{-1}$$

We then calculate the membrane Peclet number as shown next:

$$Pe_{membrane} = \frac{(1-\sigma)Q}{P_m S} = \frac{S_o q}{P_m} = \frac{0.398 \times 7.72 \times 10^{-5} \text{ cm s}^{-1}}{7.36 \times 10^{-7} \text{ cm s}^{-1}} = 41.74 > 1$$

Since the membrane Peclet number is much greater than unity, we conclude that filtration is the dominant mode of solute transport across the hollow fiber membranes.

## Problems

- 6.1** Consider a polymeric membrane within a 6 cm diameter stirred ultrafiltration cell. The membrane is 30  $\mu\text{m}$  thick. The membrane has pores equivalent in size to a spherical molecule with a molecular weight of 100,000, a porosity of 80%, and a tortuosity of 2.5. On the feed side of the membrane, we have a solution containing a protein at a concentration of 8 g  $\text{L}^{-1}$  with these properties:  $a = 3 \text{ nm}$  and  $D_{AB} = 6.0 \times 10^{-7} \text{ cm}^2 \text{ s}^{-1}$ . The solution viscosity is 1 cP. The hydrodynamic pressure on the protein side of the membrane is 20 pounds per square inch (psi) higher than on the filtrate side of the membrane. Determine the convective flow rate of the solution across the membrane and the rate at which the protein crosses the membrane. The solution on the feed side of the membrane is being stirred at 900 RPM.
- 6.2** Tong and Anderson (1996) obtained for BSA the following data in a polyacrylamide gel for the partition coefficient ( $K$ ) as a function of the gel volume fraction ( $\phi$ ). The BSA they used had a molecular weight of 67,000, a molecular radius of 3.6 nm, and a diffusivity of

$6 \times 10^{-7} \text{ cm}^2 \text{ s}^{-1}$ . Compare the Ogston equation ([Equation 6.48](#)) to their data and obtain an estimate for the radius of the cylindrical fibers ( $a_f$ ) that comprise the gel.

Gel Volume Fraction ( $\phi$ )	$K_{\text{BSA}}$
0.00	1.0
0.025	0.35
0.05	0.09
0.06	0.05
0.075	0.017
0.085	0.02
0.105	0.03

- 6.3 Tong and Anderson (1996) also obtained the following data for the diffusive permeability of BSA ( $D_e = KD_0$ ) in polyacrylamide gels as a function of the gel volume fraction ( $\phi$ ). Show that the product of the Brinkman and Ogston equations, i.e., [Equation 6.49](#), can be used to represent their data.

Gel Volume Fraction ( $\phi$ )	Diffusive Permeability ( $D_e = KD_0$ ), $\text{cm}^2 \text{ s}^{-1}$
0.00	$5.5 \times 10^{-7}$
0.02	$1.0 \times 10^{-7}$
0.025	$6.5 \times 10^{-8}$
0.05	$8.0 \times 10^{-9}$
0.065	$4.5 \times 10^{-9}$
0.075	$1.0 \times 10^{-9}$

- 6.4 Show for a protein with a molecular weight of 50,000 that  $S_O = S_a$  for blood flowing through a capillary.
- 6.5 The following data was obtained by Iwata et al. (1996) for the effective diffusivity of several solutes through a 5% agarose hydrogel. Show how well the product of the Brinkman (1947) and Ogston (1958) equations, i.e., [Equation 6.49](#), represents these data.

Solute	Molecular Weight	Gel Diffusivity ( $D_e = KD_0$ ), $\text{cm}^2 \text{ s}^{-1}$
Glucose	180	$4.5 \times 10^{-6}$
Vitamin B <sub>12</sub>	1,200	$1.7 \times 10^{-6}$
Myoglobin	17,000	$4.0 \times 10^{-7}$
BSA	69,000	$1.0 \times 10^{-7}$
IgG	150,000	$1.3 \times 10^{-7}$

- 6.6 Iwata et al. (1996) also measured the sieving coefficient for a variety of solutes using an XM-50 ultrafilter reported to have a nominal molecular weight cutoff of 50,000. Compare their measured sieving coefficients to predictions for the actual sieving coefficient calculated by [Equation 6.65](#). What pore diameter is needed to get a reasonable representation of the data?

Solute Molecular Weight	Sieving Coefficient
180	0.98
1,200	0.94
14,300	0.55
17,000	0.12
69,000	0.01

- 6.7 Starting with Equations 6.74 and 6.76, derive Equations 6.80 and 6.82. The boundary conditions are given by Equation 6.77.
- 6.8 Membrane plasmapheresis (Zydney and Colton, 1986; Zydney, 1995) is a technique used to separate plasma from the cellular components of the blood. The plasma that is collected can be processed further to yield a variety of substances that are useful for the treatment of a variety of blood disorders. Membrane-based systems employ blood flow that is parallel to the membrane. The filtrate of plasma is therefore perpendicular to the membrane. A cell-free filtrate with minimal retention of plasma proteins is obtained since the membrane pores are typically 0.2–1.0  $\mu\text{m}$  in diameter. The filtrate flux is limited, however, by the accumulation (concentration polarization) of blood cells along the surface of the membrane that provides an additional hydraulic resistance.

Figure 6.14 illustrates the situation. In this case, the solute is the cells, and the filtrate concentration of the cells, i.e.,  $C_{\text{cells}}^{\text{filtrate}}$ , is equal to zero since they are totally retained by the membrane wall of the hollow fibers. At any axial position ( $z$ ) from the device inlet, this layer of cells at steady state represents a balance between the flux of cells carried to the membrane surface by the filtration flux, i.e.,  $q(z) C_{\text{cells}}(z)$ , and the diffusive flux of cells carried away from the membrane, i.e.,  $-D_{\text{cells}} \frac{dC_{\text{cells}}(z)}{dy}$ . Hence, we can write

$$q(z) C_{\text{cells}}(z) = -D_{\text{cells}} \frac{dC_{\text{cells}}(z)}{dy}$$

Here

$q(z)$  is the filtration flux ( $Q(z)/S$ )

$C_{\text{cells}}(z)$  is the concentration of the cells in the blood

$D_{\text{cells}}$  is the diffusivity of the red blood cells

$y$  is the distance from the membrane surface on the blood side

Show that after equating these flux expressions as above and integrating over the thickness of the cell boundary layer ( $\delta_{\text{cells}}$ ), the following expression is obtained for the filtrate flux:

$$q(z) = \frac{D_{\text{cells}}}{\delta_{\text{cells}}} \ln \left( \frac{C_{\text{cells}}^{\text{surface}}}{C_{\text{cells}}^{\text{bulk}}} \right) = k_m \ln \left( \frac{C_{\text{cells}}^{\text{surface}}}{C_{\text{cells}}^{\text{bulk}}} \right)$$

where

$k_m$  represents the film mass transfer coefficient (i.e.,  $D_{\text{cells}}/\delta_{\text{cells}}$ )

$C_{\text{cells}}^{\text{surface}}$  and  $C_{\text{cells}}^{\text{bulk}}$  represent the cell concentration at the membrane surface and in the bulk blood, on the blood side of the membrane, respectively

Also, the thickness of the cell boundary layer is much thinner than that of the flow channel. Hence, under these conditions, the axial velocity profile will vary linearly across the cell boundary layer and the mass transfer coefficient for this situation is given by what is known as the Leveque approximation, which gives a result similar to [Equation 5.151](#) with the lead constant of 1.077 replaced with the value of 1.03. The shear-induced diffusivity of the red blood cells was found through experimental measurements to be described by the following equation (Zydney and Colton, 1986).

$$D_{\text{cells}} = 0.03a^2 \dot{\gamma}_w$$

Here

$a$  represents the radius of the red blood cells, about  $4.2 \mu\text{m}$

$\dot{\gamma}_w$  is the wall shear rate given by the following equation for flow of blood in a single cylindrical hollow fiber of radius equal to  $R$  (see [Equation 4.21](#))

$$\dot{\gamma}_w = \frac{4F(z)}{\pi R^3}$$

Show that [Equation 5.151](#) (with 1.077 replaced with 1.03) can be rewritten as follows for the flow of blood in the hollow fiber membrane.

$$k_m = 0.05 \left( \frac{a^4}{z} \right)^{1/3} \dot{\gamma}_w$$

The previous expressions can then be substituted into [Equation 6.109](#) to obtain an expression for the axial change of the volumetric flow rate of the blood, i.e.,  $F(z)$ , as a result of plasma filtration.

$$\frac{dF(z)}{dz} = -2\pi R k_m (z) = -2\pi R \times 0.05 \left( \frac{a^4}{z} \right)^{1/3} \times \frac{4F(z)}{\pi R^3} \times \ln \left( \frac{C_{\text{cells}}^{\text{surface}}}{C_{\text{cells}}^{\text{bulk}}} \right)$$

The plasma filtration rate ( $Q_f$ ) is defined as the difference between the flow rate of the entering blood, i.e.,  $F(0)$ , and that leaving the device, i.e.,  $F(L)$ . With  $Q_f = F(0) - F(L)$ , the previous differential equation can be integrated over the length of the hollow fibers ( $L$ ) to find the fractional filtrate yield, defined as the ratio of the total plasma filtrate formed ( $Q_f$ ) and the inlet blood flow rate  $F(0)$ . However, to obtain an analytical expression that is useful for design calculations, several assumptions are needed. Zydney and Colton (1986) assumed that

$$\ln \left( \frac{C_{\text{cells}}^{\text{surface}}}{C_{\text{cells}}^{\text{bulk}}} \right) \approx \ln \left( \frac{C_{\text{cells}}^{\text{surface}}}{C_{\text{cells}}^{\text{bulk}}(0)} \right); \text{ hence, the bulk cell concentration remained constant at its inlet}$$

value, i.e.,  $C_{\text{cells}}^{\text{bulk}}(0)$ . Using these assumptions, show that the following equation is obtained for the fractional filtration yield,  $\frac{Q_f}{F(0)}$ .

$$\frac{Q_f}{F(0)} = 1 - \exp \left[ -0.90\beta \ln \left( \frac{C_{\text{cells}}^{\text{surface}}}{C_{\text{cells}}^{\text{bulk}}(0)} \right) \right] \quad \text{where } \beta = \frac{2}{3} \left( \frac{a^2 L}{R^3} \right)^{2/3}$$

In this equation,  $\beta$  is a dimensionless length. Zydny and Colton (1986) provided the following performance data for a variety of membrane plasmapheresis units. Show that the previous equation provides a good prediction of the fractional filtration yield for these units. Use 0.35 and 0.95 for the concentration of the red blood cells entering in the blood and at the wall, respectively.

$\beta$	Fractional Filtrate Yield
0.20	0.12
0.27	0.20
0.27	0.23
0.32	0.22
0.32	0.25
0.35	0.25
0.40	0.30
0.42	0.32
0.43	0.30
0.44	0.39
0.45	0.38
0.49	0.36
0.51	0.35
0.58	0.40
0.60	0.35
0.62	0.37
0.70	0.41

- 6.9** In a discussion of glucose transport through exercising muscle capillaries, Renkin (1977) reports the capillary glucose permeability ( $P_m$ ) to be on the order of  $12 \times 10^{-6} \text{ cm s}^{-1}$  with a capillary surface area ( $S$ ) of  $7000 \text{ cm}^2$  per  $100 \text{ g}$  of tissue. How does the value of  $P_m S$  compare to the data shown in [Figure 6.5](#)?
- 6.10** Using the Renkin-Crone equation, make a graph of capillary solute extraction ( $E$ ) as a function of capillary position ( $z$ ) for various values of the ratio  $\frac{2\pi r_c P_m z}{Q}$ . Identify conditions on your plot for which the solute transport is flow limited and diffusion limited.
- 6.11** Levick (1991) presented the following data obtained by Renkin (1977) for the capillary clearance of antipyrine and urea as a function of blood flow in skeletal muscle. Based on this data, which of these solutes' transport rate is flow limited and which is diffusion limited? Calculate the value of  $P_m S$  for urea. How does this value of  $P_m S$  for urea compare to the results presented in [Figure 6.5](#)? Explain why the  $P_m S$  value for antipyrine cannot be found from these data.

Solute	Blood Flow $Q, \text{ mL min}^{-1} (100 \text{ g})^{-1}$	Clearance $CL, \text{ cm}^3 \text{ min}^{-1} (100 \text{ g})^{-1}$
Antipyrine	4.5	4
	4.5	4.5
	6.5	6.5

(Continued)

Solute	Blood Flow		Clearance
	Q, mL min <sup>-1</sup> (100 g) <sup>-1</sup>	CL, cm <sup>3</sup> min <sup>-1</sup> (100 g) <sup>-1</sup>	CL, cm <sup>3</sup> min <sup>-1</sup> (100 g) <sup>-1</sup>
Urea	10		10
	5		3.5
	5.5		3
	7		4
	8		2.5
	8.5		2.6
	8.5		4
	10		2.6
	10.5		2.5
	12		4.5
	13.5		2.6

- 6.12** Mann et al. (1979) obtained the following concentration versus time data for several solutes in cat fenestrated salivary glands using the multiple tracer indicator diffusion technique. The test solutes were cyanocobalamin (vitamin B<sub>12</sub>, MW = 1,353) and insulin (MW = 5,807). Albumin (MW = 69,000) served as the nonpermeable reference solute. The perfusion rate for the gland was 8 mL min<sup>-1</sup> g<sup>-1</sup>. The following table summarizes the concentration of these solutes (% dose per 0.2 mL of perfusate sample) for various periods of time following their injection into the gland. From this data, calculate the value of P<sub>m</sub>S for B<sub>12</sub> and insulin. How do these P<sub>m</sub>S values for B<sub>12</sub> and insulin compare to the results shown in [Figure 6.5](#)?

Time, s	C, B <sub>12</sub>	C, Insulin	C, Albumin
0.3	1.5	2.2	2.3
0.66	4.4	6.3	7.3
1.0	7.3	10.0	11.9
1.5	8.6	11.0	12.9
1.9	7.6	10.2	10.7
2.1	6.0	7.3	7.8
2.5	5.0	5.9	5.7
2.8	4.1	4.2	3.9
3.1	3.8	3.7	3.0
3.5	3.0	2.6	2.2
3.8	2.7	2.2	2.0

- 6.13** Estimate the pore diffusivity, the membrane diffusivity, and the effective diffusivity of a spherically shaped molecule with a molecular weight equal to 35,000 through a membrane containing straight cylindrical pores that are 8 nm in diameter. Assume that the molecule enters the pores of the membrane from a well-stirred bulk solution and that the porosity of the membrane is 0.40.

- 6.14** Some folks have suggested that the cell walls of living cells have pores that are 30 Å in diameter ( $1 \text{ \AA} = 10^{-8} \text{ cm}$ ). Estimate  $D_m (\text{cm}^2 \text{ s}^{-1})$  at 37°C for a solute 5 Å in diameter. Assume the pores are filled with a fluid that is similar to plasma.
- 6.15** A molecule with a radius of 2.5 nm enters, from a bulk solution, a membrane having pores with a radius of 7.5 nm. For a temperature of 37°C, and assuming the fluid phase is water, what is the effective diffusivity of the molecule in the pores of the membrane? Express your answer in  $\text{cm}^2 \text{ s}^{-1}$ . The porosity of the membrane is 40% and the tortuosity is 1.5.
- 6.16** Your group has developed a new drug for the treatment of hilariosis. This drug is lipid insoluble and has a molecular weight of 1200. As part of the design of a controlled release system for this drug, you have been asked to estimate the permeability in  $\text{cm}^3 \text{ s}^{-1} (100 \text{ g})^{-1}$  of this drug through the capillary wall.
- 6.17** Estimate the reflection coefficient for a molecule that has a radius of 0.75 nm assuming the pores in the membrane have a radius of 2.5 nm.
- 6.18** A single hollow fiber is placed within a larger diameter glass tube forming a shell space that surrounds the hollow fiber. The hollow fiber is 20 cm in length and has a diameter of 400  $\mu\text{m}$ . The flow rate of a liquid through the hollow fiber is  $1 \text{ cm}^3 \text{ min}^{-1}$ , and in the shell space, another liquid also flows through at a flow rate of  $100 \text{ cm}^3 \text{ min}^{-1}$ . The liquid entering the hollow fiber also contains a permeable solute. It is found that the concentration of the permeable solute exiting the hollow fiber is 10% of the concentration of this solute when entering the hollow fiber in the liquid. Estimate the permeability for this solute in  $\text{cm s}^{-1}$ .
- 6.19** Bawa et al. (1985) measured the drug distribution inside a polymer matrix material. These polymeric slabs of thickness 1 mm were loaded with albumin at an initial concentration of  $484 \text{ mg cm}^{-3}$  of slab. The table below shows two distributions of the drug concentration as a function of  $x/L$  after 6.5 and 172 h. Find the value of  $D_e$  that best fits these data using [Equation 6.30](#). How well does [Equation 6.36](#) fit the 6.5 h concentrations?

$x/L$	C at 6.5 h	C at 172 h
0.039	$484 \text{ mg cm}^{-3}$	$175 \text{ mg cm}^{-3}$
0.115	484	200
0.20	484	213
0.32	484	188
0.38	484	175
0.46	484	150
0.58	475	113
0.66	450	100
0.73	275	75
0.82	200	38
0.89	112	25
0.93	80	12.5

- 6.20** Bawa et al. (1985) obtained the following data for the cumulative fraction released ( $f_R$ ) for lysozyme from 1 mm thick polymeric slabs. Estimate the value of the  $D_e$  that best fits

these data. The initial concentration of lysozyme is about  $400 \text{ mg cm}^{-3}$ , and the diffusivity of lysozyme in water is  $3.74 \times 10^{-3} \text{ cm}^2 \text{ h}^{-1}$ .

Time <sup>1/2</sup> , h <sup>1/2</sup>	f <sub>R</sub>
3	0.03
5	0.12
7	0.18
8	0.21
9.5	0.24
13	0.32
15	0.40
16.5	0.45
18.5	0.50
21	0.52

- 6.21** The filtration flux across a membrane is  $5 \times 10^{-5} \text{ cm s}^{-1}$ . The mass transfer coefficient for a particular solute for this situation is  $10^{-4} \text{ cm s}^{-1}$ . The ratio of the solute radius to the radius of the membrane pores is  $\lambda = 0.4$ . If the concentration of this solute is  $0.5 \text{ g L}^{-1}$  in the bulk solution, estimate the concentration of the solute in the filtrate.
- 6.22** A well-mixed protein solution is being filtered across a semipermeable membrane. The nominal molecular weight cutoff of the membrane is 100,000, and the protein has a molecular weight of 20,000. The protein concentration on the feed side of the membrane in the filtration unit is  $1 \text{ g L}^{-1}$ . The protein's mass transfer coefficient is  $3 \times 10^{-4} \text{ cm s}^{-1}$ , and the filtration flux of the protein solution across the membrane is  $10^{-4} \text{ cm s}^{-1}$ . Assuming the protein has a molecular radius of 2.0 nm, what is the concentration of the protein in the filtrate solution?
- 6.23** A well-mixed protein solution is being filtered across a semipermeable membrane. The pores in the membrane have an average radius of 3.6 nm, and the radius of the protein molecule is 2.2 nm. The protein concentration in the filtration unit is  $1.5 \text{ g L}^{-1}$ . The protein's mass transfer coefficient is  $3.5 \times 10^{-4} \text{ cm s}^{-1}$ , and the filtration flux of the protein solution across the membrane is  $1.5 \times 10^{-4} \text{ cm s}^{-1}$ . What is the concentration of the protein in the filtrate solution?
- 6.24** Estimate the permeability of a spherically shaped molecule that has a molecular weight of  $42,000 \text{ g mol}^{-1}$  through a microporous polycarbonate membrane. Assume that the molecule enters the pores of the membrane from a well-stirred bulk solution that is at  $37^\circ\text{C}$ . The membrane pores are cylindrical and have a diameter of 32 nm with an overall length of 325  $\mu\text{m}$ . The membrane itself is 250  $\mu\text{m}$  in thickness. The pores comprise 42% of the membrane volume.
- 6.25** Calculate the critical radius at  $z = L$  for the capillary conditions used in [Example 6.8](#). Assume that the flow rate in the capillary has been reduced by a factor of ten to  $V = 0.005 \text{ cm s}^{-1}$ .
- 6.26** Shi et al. (2013) measured the diffusivity of fluorescein ( $\text{MW} = 332$ ), a fluorescent tracer, in the porcine temporomandibular joint (TMJ) disk using a technique known as fluorescence recovery after photobleaching (FRAP). The TMJ disk consists mostly of water and a large amount of type I collagen. The overall average diffusivity of fluorescein in the TMJ disk was found to be  $57.0 \text{ } \mu\text{m}^2 \text{ s}^{-1}$ . Using the Brinkman model, estimate the value of  $\kappa$  for fluorescein diffusion in the porcine TMJ disk.
- 6.27** Write a paper that describes how the solute diffusivity in tissue is determined using the technique known as FRAP.

- 6.28** A design for a hollow fiber membrane plasmapheresis module is based on a feed rate of blood of  $300 \text{ mL min}^{-1}$  giving a plasma filtration rate of  $120 \text{ mL min}^{-1}$ . If the length of the hollow fibers is 30 cm, what should be the inside diameter of the hollow fibers?
- 6.29** A hollow fiber plasmapheresis unit separates plasma from blood. If the plasma filtration flow rate is  $250 \text{ mL min}^{-1}$ , estimate the allowable blood flow rate to the device. Assume the hollow fibers have an inner diameter of  $400 \mu\text{m}$  and a length of 30 cm.
- 6.30** A protein with a MW of 15,000 in an aqueous solution ( $\mu = 1 \text{ cP}$ ,  $\rho = 1 \text{ cm}^3 \text{ s}^{-1}$ ) is being filtered at  $20^\circ\text{C}$  through a microporous membrane within a 25 mm diameter stirred ultrafiltration cell. The membrane has a NMWCO of 30,000. The stirring speed is 1000 RPM. Estimate the observed sieving coefficient, i.e.,  $S_o$ . The filtration flux, i.e.,  $q = Q/S$ , is equal to  $1.5 \times 10^{-3} \text{ cm s}^{-1}$ . For a stirred ultrafiltration cell, the following correlation can be used for the mass transfer coefficient:

$$\frac{k_m r_{cell}}{D} = 0.23 Re^{0.567} Sc^{0.33} = 0.23 \left( \frac{\rho \omega r_{cell}^2}{\mu} \right)^{0.567} \left( \frac{\mu}{\rho D} \right)^{0.33}$$

where

$r_{cell}$  is the radius of the stirred cell ultrafiltration chamber

$\omega$  is the stirring speed in radians per second



Taylor & Francis

Taylor & Francis Group

<http://taylorandfrancis.com>

# Chapter 7 Oxygen transport in biological systems

## 7.1 The diffusion of oxygen in multicellular systems

The growth of simple multicellular systems beyond a diameter of a hundred microns or so is limited by the availability of oxygen. The metabolic needs of the cells near the center of the cell aggregate exceed the supply of oxygen available by simple diffusion. This is illustrated in [Figure 7.1](#) for isolated insulin-producing islet organs (Brockmann bodies) of the fish, *Osphronemus goramy*. The islet organs, typically 800  $\mu\text{m}$  in diameter, were placed in culture media, and the oxygen partial pressure in the surrounding media and within the cells was measured radially using an oxygen microelectrode.

For the case with no convection in the media (diamond symbols), we see that the oxygen partial pressure drops sharply and has been reduced to nearly zero within a few hundred microns of the Brockmann bodies' surface (electrode position of 0  $\mu\text{m}$ ). Those cells that experience reduced oxygen levels suffer from *hypoxia*. If the oxygen level is reduced beyond some critical value, the cells may die, which is called *necrosis*. Note that with increased convection (fluid mixing) in the surrounding media (square symbols), the partial pressure of oxygen at the surface and core regions of the Brockmann bodies is increased significantly in comparison to the case without convection. This is a result of the decrease in the resistance to oxygen transport of the fluid surrounding the islets. However, we still observe a large decrease in the oxygen partial pressure within the islet bodies.

Clearly, the development of such complex cellular systems as vertebrates required the development of oxygen delivery systems that are more efficient than diffusion alone. This has been accomplished by the development of two specialized systems that enhance the delivery of oxygen to cells. The first is the circulatory system, which carries oxygen in the blood by convection to tiny blood vessels called *capillaries* in the neighborhood of the cells. Here, oxygen is released and then diffuses over much shorter distances to the cells. Second, a specialized oxygen carrier protein, called *hemoglobin*, is contained within the red blood cells (RBCs) that are suspended within the blood plasma. The presence of hemoglobin overcomes the very low solubility of oxygen in water. In this chapter, we will investigate the factors that affect oxygen delivery to cells.

### 7.1.1 $p\text{O}_2$ and Henry's constant

[Figure 7.1](#) provides measured values of the oxygen concentration within a spherical volume of cells. We see that the oxygen concentration is expressed in terms of the partial pressure of oxygen. It is quite common to express oxygen concentration in terms of its partial pressure in units of mmHg. Recall that the gas-phase equilibrium partial pressure of oxygen, or  $p\text{O}_2$ , above a liquid solution is related to the oxygen concentration in the solution by *Henry's law*, which is expressed by the following equation:

$$p\text{O}_2 \equiv P_{\text{y}_{\text{oxygen}}} = H_{\text{oxygen}} C_{\text{oxygen}} \quad (7.1)$$

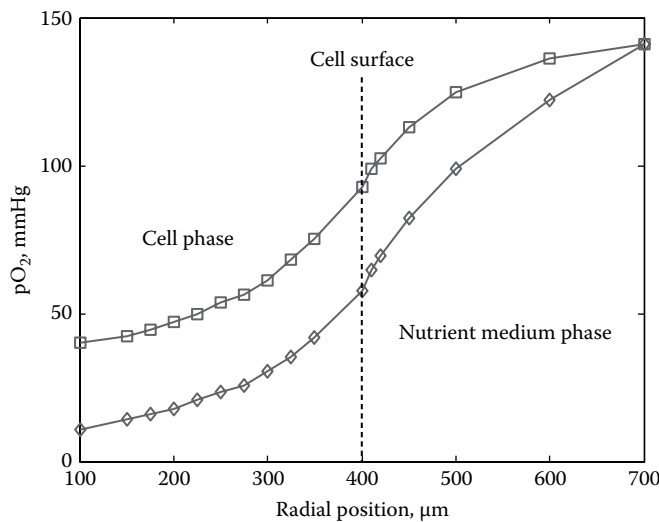


Figure 7.1  $pO_2$  profiles of Brockmann bodies with convection (square symbols) and without convection (diamond symbols) in the nutrient medium. (Data obtained from Schrezenmeir, J. et al., *Transplantation*, 57, 1308, 1994.)

Table 7.1 Henry's Constant for Oxygen in Water

Temperature, °C	$H_{\text{oxygen}}$ , mmHg $\mu\text{M}^{-1}$
0	0.349
10	0.447
15	0.494
20	0.551
25	0.603
30	0.655
35	0.697
40	0.738

Source: Bailey, J.E. and Ollis, D.F., *Biochemical Engineering Fundamentals*, 2nd ed., McGraw-Hill, New York, 1986.

In [Equation 7.1](#),  $H_{\text{oxygen}}$  is Henry's constant. Henry's constant for oxygen in water at temperatures from 0°C to 40°C is shown in [Table 7.1](#). Here, we will usually express the dissolved oxygen concentration ( $C_{\text{oxygen}}$ ) in  $\mu\text{M}$ , i.e., micromoles of oxygen per liter of solution. With the  $pO_2$  in mmHg, this means Henry's constant will have units of  $\text{mmHg } \mu\text{M}^{-1}$ . For blood at 37°C, Henry's constant is 0.74  $\text{mmHg } \mu\text{M}^{-1}$ .

## 7.1.2 Oxygen transport to a spherical volume of cells

We can develop a reaction-diffusion model that can be used to describe the  $pO_2$  profiles shown in [Figure 7.1](#). From this description we can also determine from data like that shown in [Figure 7.1](#) the oxygen consumption rate of the cells.

At steady state we can write an oxygen mass balance over a thin shell of a spherical volume of cells from  $r$  to  $r + \Delta r$ :

$$4\pi r^2 D_T \frac{dC_{\text{oxygen}}}{dr} \Big|_{r+\Delta r} - 4\pi r^2 D_T \frac{dC_{\text{oxygen}}}{dr} \Big|_r = 4\pi r^2 \Delta r \phi \Gamma_{\text{oxygen}} \quad (7.2)$$

The first two terms on the left-hand side of [Equation 7.2](#) represent the rate at which oxygen enters the shell volume by diffusion at  $r + \Delta r$  and leaves at  $r$ .  $C_{\text{oxygen}}$  is the oxygen concentration within a given volume of tissue, which includes the cells and surrounding interstitial fluid. The product of  $C_{\text{oxygen}}$  and this tissue volume gives the mass of oxygen in the volume of tissue.  $D_T$  is the effective oxygen diffusivity within the tissue and is described by [Equations 6.43](#) or [6.45](#). At 37°C, Bentley et al. (1993) found that  $D_T = 2.41 \times 10^{-5} \text{ cm}^2 \text{ s}^{-1}$ .

This difference in the diffusional oxygen transport rate at steady state must equal the amount of oxygen consumed by the cells, which is given by the expression on the right-hand side of [Equation 7.2](#).  $\Gamma_{\text{oxygen}}$  represents the rate of oxygen consumption by the cells contained within the volume of cells given by  $4\pi r^2 \Delta r \phi$ , where  $\phi$  is the volume fraction of the cells. The units on  $\Gamma_{\text{oxygen}}$  are moles of oxygen per volume of cells per unit time, which we will express in  $\mu\text{M s}^{-1}$ .

Now, if we divide [Equation 7.2](#) by  $\Delta r$  and take the limit as  $\Delta r \rightarrow 0$  and replace  $C_{\text{oxygen}}$  with the  $pO_2$  using [Equation 7.1](#), we obtain

$$\frac{D_T}{r^2} \frac{d}{dr} \left( r^2 \frac{dpO_2}{dr} \right) = \phi H_{\text{oxygen}} \Gamma_{\text{oxygen}} \quad (7.3)$$

The boundary conditions (BC) for [Equation 7.3](#) are

$$\begin{aligned} BC1 : \quad r = 0, \quad \frac{dpO_2}{dr} &= 0 \\ BC2 : \quad r = R, \quad pO_2 &= pO_2 \Big|_{r=R} \end{aligned} \quad (7.4)$$

The oxygen consumption rate for the tissue, i.e.,  $\Gamma_{\text{oxygen}}$ , can be described by Michaelis-Menten type kinetics,\* where the oxygen consumption rate of the tissue is dependent on the  $pO_2$  in the tissue:

$$\Gamma_{\text{oxygen}} = \frac{V_{\text{max}} pO_2}{K_m + pO_2} \quad (7.5)$$

It turns out that in most cases for oxygen consumption by cells,  $K_m \ll pO_2$ . For example, for the islets of Langerhans, the value of  $K_m$  is 0.44 mmHg (Dionne et al., 1989, 1991). Since the  $pO_2$  in tissue usually falls in the range of 10 to 100 mmHg, this means from [Equation 7.5](#) that  $\Gamma_{\text{oxygen}} \approx V_{\text{max}}$ , or  $\Gamma_{\text{oxygen}}$  is a constant.

$V_{\text{max}}$  is often expressed as the oxygen consumption rate on a per cell basis, and  $\rho_{\text{cell}}$  is the cell density, i.e., the number of cells per total volume, then  $\phi \Gamma_{\text{oxygen}} = \rho_{\text{cell}} V_{\text{max}}$ , where  $\phi$  is the

\* A derivation of the Michaelis-Menten equation can be found in [Section 9.6.3](#).

volume fraction of the cells within the total volume. In terms of the volume of a single cell, i.e.,  $V_{\text{cell}}$ , we also have that  $\phi = \rho_{\text{cell}} V_{\text{cell}}$ .

With  $\Gamma_{\text{oxygen}}$  a constant, we can then integrate Equations 7.3 and 7.4 to get

$$pO_2(r) = pO_2|_{r=R} - \frac{H_{\text{oxygen}} \phi \Gamma_{\text{oxygen}} R^2}{6D_T} \left[ 1 - \left( \frac{r}{R} \right)^2 \right] \quad (7.6)$$

If we have an external concentration boundary layer in the fluid phase surrounding the cells as shown in Figure 7.1, then we can add the external mass transfer resistance by incorporating the mass transfer coefficient into Equation 7.6. At steady state, the rate of mass transfer of oxygen from the bulk solution must equal the rate at which oxygen is being consumed by the cells. Hence, for constant  $\Gamma_{\text{oxygen}}$ , we can write

$$4\pi R^2 k_m \left( C_{\text{oxygen}}^{\text{bulk}} - C_{\text{oxygen}}|_{r=R} \right) = \frac{4}{3} \pi R^3 \phi \Gamma_{\text{oxygen}} \quad (7.7)$$

We can then solve Equation 7.7 for  $pO_2|_{r=R}$  after using Henry's law to replace  $C_{\text{oxygen}}$  with  $pO_2$  as the dependent variable; hence

$$pO_2|_{r=R} = pO_2^{\text{bulk}} - \frac{R \phi \Gamma_{\text{oxygen}} H_{\text{oxygen}}}{3k_m} \quad (7.8)$$

We can then substitute Equation 7.8 into Equation 7.6 for  $pO_2|_{r=R}$  to give

$$pO_2(r) = pO_2^{\text{bulk}} - \frac{R \phi \Gamma_{\text{oxygen}} H_{\text{oxygen}}}{3k_m} - \frac{H_{\text{oxygen}} \phi \Gamma_{\text{oxygen}} R^2}{6D_T} \left[ 1 - \left( \frac{r}{R} \right)^2 \right] \quad (7.9)$$

Equation 7.9 can then be used to describe data like that shown in Figure 7.1 for a spherical volume of cells.

### Example 7.1

Using the diamond symbol data shown in Figure 7.1, estimate the oxygen consumption rate of the Brockmann bodies, i.e., the value of  $\Gamma_{\text{oxygen}}$ . Assume the volume fraction of the cells in the Brockmann body is about 0.85. Also, compare the predicted value of the  $pO_2|_{r=R}$  from Equation 7.8 to the value given in Figure 7.1. Assume the Brockmann bodies have a diameter of 800  $\mu\text{m}$  and that Henry's constant for oxygen is 0.70 mmHg  $\mu\text{M}^{-1}$ .

### Solution

The data in the following table summarize the  $pO_2$  values as a function of radial position measured from the center of the Brockmann bodies.

Radial Position in the Brockmann Body, $\mu\text{m}$	$p\text{O}_2, \text{mmHg}$
100	10.58
150	14.10
175	16.22
200	17.63
225	20.68
250	23.5
275	25.85
300	30.55
325	35.25
350	41.83
400	57.58

We can perform a linear regression of the data in the table using [Equation 7.6](#). A plot of  $p\text{O}_2(r)$  versus  $1 - \left(\frac{r}{R}\right)^2$  should be linear with a slope,  $m$ , equal to  $-\frac{H_{\text{oxygen}}\phi\Gamma_{\text{oxygen}}R^2}{6D_T}$  and a y intercept equal to  $p\text{O}_{2,r=R}$ . [Figure 7.2](#) shows the results of the linear regression. The slope is found to be equal to  $-47.6456 \text{ mmHg}$ . In order to determine the value of  $\Gamma_{\text{oxygen}}$ , we need to estimate the value of  $D_T$  for oxygen. Bentley et al. (1993) provide a value of  $D_T = 2.41 \times 10^{-5} \text{ cm}^2 \text{ s}^{-1}$ . We can then calculate  $\Gamma_{\text{oxygen}}$ :

$$\Gamma_{\text{oxygen}} = -\frac{6D_T m}{H_{\text{oxygen}}\phi R^2} = \frac{6 \times 2.41 \times 10^{-5} \text{ cm}^2 \text{ s}^{-1} \times 47.65 \text{ mmHg}}{0.70 \text{ mmHg } \mu\text{M}^{-1} \times 0.85 \times (0.04 \text{ cm})^2}$$

$$\Gamma_{\text{oxygen}} = 7.24 \mu\text{M s}^{-1}$$

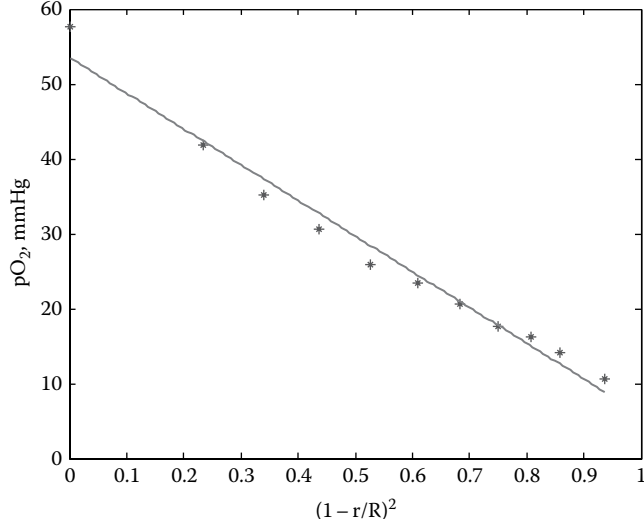


Figure 7.2 Linear regression of Brockmann body  $p\text{O}_2$  data.

From [Figure 7.1](#), the  $pO_2$  at the surface of the Brockmann bodies is 57.6 mmHg. From the linear regression of the data in the table, the  $y$  intercept was found to be 53.51 mmHg, which is the same as the surface value of the  $pO_2$ , and this value compares reasonably well with the measured value of 57.6 mmHg. We can also use [Equation 7.8](#) to find the value of  $pO_2|_{r=R}$ . From [Figure 7.1](#) we see that  $pO_2^{\text{bulk}} = 140$  mmHg. Also, for a sphere of cells like the Brockmann bodies in a stagnant fluid, the Sherwood number ( $Sh$ ) = 2. Assuming the nutrient media is mostly water, then  $D_{AB} \approx 2.76 \times 10^{-5} \text{ cm}^2 \text{ s}^{-1}$  (Yoshida and Ohshima, 1966). Therefore, the mass transfer coefficient for oxygen is

$$k_m = \frac{2 \times 2.76 \times 10^{-5} \text{ cm}^2 \text{ s}^{-1}}{2 \times 0.04 \text{ cm}} = 6.9 \times 10^{-4} \text{ cm s}^{-1}$$

and from [Equation 7.8](#)

$$\begin{aligned} pO_2|_{r=R} &= pO_2^{\text{bulk}} - \frac{R\phi\Gamma_{\text{oxygen}}H_{\text{oxygen}}}{3k_m} \\ &= 140 \text{ mmHg} - \frac{0.04 \text{ cm} \times 0.85 \times 7.24 \mu\text{M s}^{-1} \times 0.70 \text{ mmHg } \mu\text{M}^{-1}}{3 \times 0.00069 \text{ cm s}^{-1}} \\ pO_2|_{r=R} &= 56.76 \text{ mmHg} \end{aligned}$$

This value of the  $pO_2$  at the surface of the Brockmann bodies compares really well with the measured value and shows the reasonableness of the parameter values that were used.

## 7.2 Hemoglobin

[Figure 7.3](#) shows the basic structural features of the hemoglobin molecule. The hemoglobin found in adult humans is called *hemoglobin A*. Hemoglobin consists of four polypeptide chains (a polymer of amino acids), two of one kind called the  $\alpha$  chain and two of another kind called the  $\beta$  chain. These polypeptide chains of hemoglobin A are held together by noncovalent attractions. The hemoglobin molecule is nearly spherical with a diameter of about 5.5 nm and a molecular weight of 68,000.

The oxygen binding capacity of hemoglobin\* depends on the presence of a nonpolypeptide unit called the *heme group*. The iron atom within heme gives blood its distinctive red color. The heme group is also called a *prosthetic group* because it gives the hemoglobin protein its overall functional activity. The heme group consists of an organic part that binds through four nitrogen atoms with

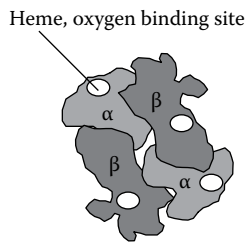


Figure 7.3 Structure of hemoglobin.

\* Abbreviated as Hb.

the iron atom within the center. The organic part is called the *protoporphyrin* and consists of four pyrrole rings linked by methene bridges. The iron atom can form up to six bonds, four of which are committed to the pyrrole rings. So we have two additional bonds available, one on each side of the heme plane. A heme group can therefore bind one molecule of oxygen.

The four heme groups in a hemoglobin molecule are located near the surface of the molecule, and the oxygen binding sites are about 2.5 nm apart. Each of the four chains contains a single heme group and therefore a single oxygen binding site. A molecule of hemoglobin therefore has the potential to bind four molecules of oxygen. Hemoglobin is an *allosteric protein*, and its oxygen binding properties are affected by interactions between these separate and nonadjacent oxygen binding sites. The binding of oxygen to hemoglobin enhances the binding of additional oxygen molecules. The binding of oxygen to hemoglobin is therefore said to be *cooperative*.\*

### 7.3 The oxygen-hemoglobin dissociation curve

The binding of oxygen with hemoglobin is described by the oxygen hemoglobin dissociation curve shown in [Figure 7.4](#). This is an equilibrium curve that expresses, for a given oxygen partial pressure (or  $p_{O_2}$ ), the fractional occupancy of the hemoglobin-oxygen binding sites ( $Y$ ) on a large number of hemoglobin molecules. The equilibrium partial pressure of oxygen, or  $p_{O_2}$ , above a solution of blood is related to the dissolved oxygen concentration by *Henry's law*, which is given by [Equation 7.1](#). In [Equation 7.1](#),  $H_{\text{oxygen}}$  is Henry's constant with a value for blood at 37°C of 0.74 mmHg  $\mu\text{M}^{-1}$ .  $C_{\text{oxygen}}$  is the dissolved oxygen concentration ( $\mu\text{M}$ ) in the blood. It is important to realize that the  $p_{O_2}$  is exerted only by the dissolved oxygen. Oxygen bound to hemoglobin does not directly affect the  $p_{O_2}$  but serves only as a source or sink for oxygen.

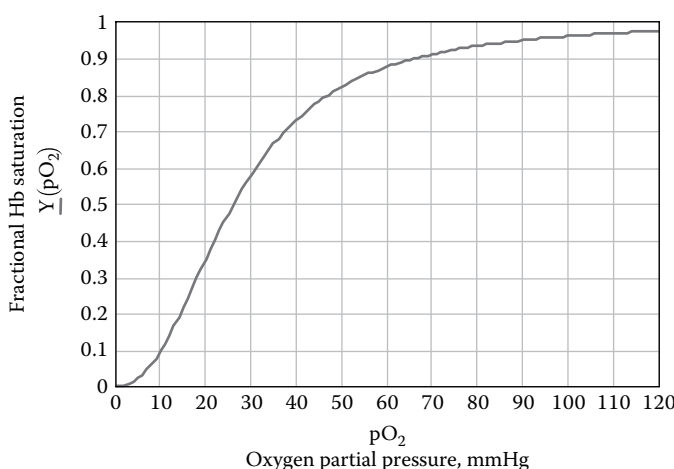


Figure 7.4 Oxygen-hemoglobin dissociation curve.

\* An analogy for cooperative binding would be several people entering a life raft from the water. Because of the high sides of the life raft it is very difficult for the first person to get aboard. Once one person is aboard she can help the next person. Two people on board make it even easier to load the next person and so on.

## 7.4 Oxygen levels in blood

Table 7.2 summarizes some typical properties of arterial and venous blood. The concentration of hemoglobin in blood (see Table 4.1) is about  $150 \text{ g L}^{-1} = 15 \text{ g dL}^{-1} = 2200 \mu\text{M}$ . Since each molecule of hemoglobin can bind at most four molecules of oxygen, the saturated ( $Y = 1$ ) concentration of oxygen bound to hemoglobin, i.e.,  $C'_{\text{SAT}}$ , is equal to  $8800 \mu\text{M}$ . Comparing this saturated value, or even the arterial or venous values shown in Table 7.2 (i.e., as oxyhemoglobin), to the arterial dissolved oxygen value of  $130 \mu\text{M}$  clearly shows that the bulk of the oxygen that is available in the blood is carried by hemoglobin. The  $P_{50}$  value represents the value of the oxygen partial pressure ( $pO_2$ ) at which 50% of the oxygen binding sites are filled, i.e.,  $Y = 0.5$ . From Figure 7.4, we see this occurs when the  $pO_2 \approx 26 \text{ mmHg}$ .

## 7.5 The Hill equation

In 1913, Archibald Hill proposed that the sigmoidal shape of the oxygen hemoglobin dissociation curve shown in Figure 7.4 can be described by the following equilibrium reaction:



In this equation,  $n$  represents the number of molecules of oxygen that bind with hemoglobin (Hb) to form oxyhemoglobin, i.e.,  $[\text{Hb(O}_2\text{)}_n]$ . Writing an elementary rate expression for the appearance of hemoglobin, with  $k_1$  and  $k_{-1}$  representing the reaction rate constants, we obtain

$$\frac{d[\text{Hb}]}{dt} = k_1 [\text{Hb(O}_2\text{)}_n] - k_{-1} [\text{Hb}] [\text{O}_2]^n = 0 \quad (7.11)$$

where the brackets imply the concentration of the respective chemical species. Assuming the reaction given by Equation 7.10 is at equilibrium, we can set Equation 7.11 equal to zero and solve for the concentration of oxygenated hemoglobin in terms of the free hemoglobin and dissolved oxygen concentrations:

$$[\text{Hb(O}_2\text{)}_n] = \kappa [\text{Hb}] [\text{O}_2]^n \quad (7.12)$$

Table 7.2 Oxygen Levels in Blood

Oxygen Property	Arterial	Venous
Partial pressure (tension), $pO_2$ , mmHg	95	40
Dissolved $O_2$ , $\mu\text{M}$	130	54
As oxyhemoglobin, $\mu\text{M}$	8500	6424
Total effective (dissolved + oxy - Hb), $\mu\text{M}$	8630	6478

Other useful data:  $H_{\text{oxygen}} = 0.74 \text{ mmHg } \mu\text{M}^{-1}$ ; saturated oxyhemoglobin =  $8800 \mu\text{M}$ ;  $P_{50} \sim 26 \text{ mmHg}$ ;  $n = 2.34$ .

In [Equation 7.12](#),  $\kappa$  is defined as  $k_{-1}/k_1$ . The fraction of hemoglobin that is saturated ( $Y$ ) is defined by the following relationship:

$$Y \equiv \frac{[\text{Hb(O}_2\text{)}_n]}{[\text{Hb(O}_2\text{)}_n] + [\text{Hb}]} = \frac{\frac{[\text{Hb(O}_2\text{)}_n]}{[\text{Hb}]}}{1 + \frac{[\text{Hb(O}_2\text{)}_n]}{[\text{Hb}]}} \quad (7.13)$$

This equation can be simplified using [Equations 7.1](#) and [7.12](#) to obtain the following result:

$$Y = \frac{\kappa[\text{O}_2]^n}{1 + \kappa[\text{O}_2]^n} = \frac{(p\text{O}_2)^n}{P_{50}^n + (p\text{O}_2)^n} \quad (7.14)$$

The  $P_{50}^n$  value was substituted for  $\frac{H_{\text{oxygen}}^n}{K}$ . [Equation 7.14](#) is called the *Hill equation* and can be used to provide a mathematical relationship between  $Y$  and  $p\text{O}_2$  that describes the behavior shown in [Figure 7.4](#) and is convenient to use in design calculations.

The regression analysis of  $Y$  and  $p\text{O}_2$  data is facilitated by the following rearrangement of the Hill equation:

$$\ln \frac{Y}{1-Y} = n \ln(p\text{O}_2) - n \ln P_{50} \quad (7.15)$$

A plot of  $\ln\left(\frac{Y}{1-Y}\right)$  versus  $\ln(p\text{O}_2)$  is linear with a slope equal to  $n$  and a y intercept equal to  $-n \ln P_{50}$ . This is called the *Hill plot*. The following example illustrates the use of the Hill equation to represent the oxygen hemoglobin dissociation curve.

### Example 7.2

The following table presents data that represents the oxygen hemoglobin dissociation. Show that the Hill equation provides excellent representation of this data.

Oxygen Partial Pressure, $p\text{O}_2$ , mmHg	Fractional Hemoglobin Saturation
10	0.12
20	0.28
30	0.56
40	0.72
50	0.82
60	0.88
70	0.91
80	0.93
90	0.95
100	0.96

Source: Guyton, A.C., *Textbook of Medical Physiology*, 8th ed., W.B. Saunders Co., Philadelphia, PA, 1991.

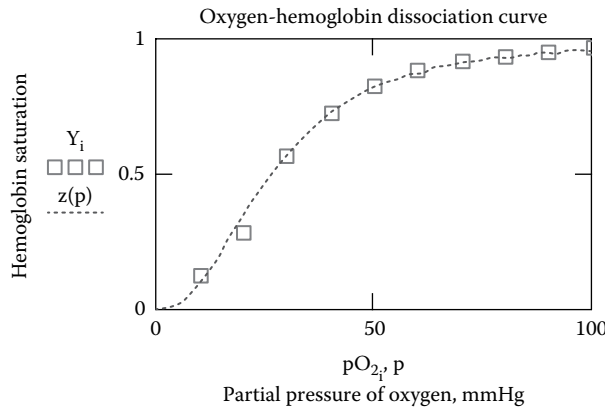


Figure 7.5 The Hill equation.

### Solution

Performing a linear regression analysis on the above data using [Equation 7.15](#), we find that the  $P_{50}$  value is 26 mmHg and the value of  $n$  is 2.34. We also see in [Figure 7.5](#) (dashed line) that the Hill equation provides for an excellent representation of the oxygen hemoglobin dissociation curve.

## 7.6 Other factors that can affect the oxygen-hemoglobin dissociation curve

Other molecules, such as  $H^+$ ,  $CO_2$ , and organic phosphates (such as 2,3-diphosphoglycerate [DPG]) also bind on specific sites on the hemoglobin molecule and greatly affect its oxygen binding ability through *allosteric interactions*. A lowering of the pH shifts the oxygen dissociation curve to the right as shown in [Figure 7.6](#). This decreases, for a given  $pO_2$ , the oxygen affinity of the hemoglobin

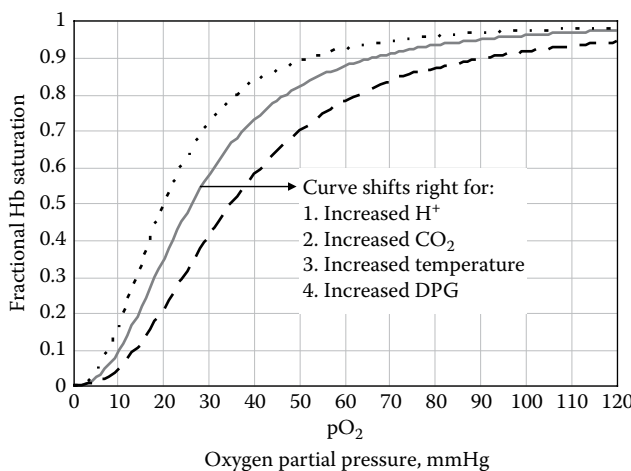


Figure 7.6 Shifts in the oxygen-hemoglobin dissociation curve.

molecule.  $\text{CO}_2$  at increased levels and constant pH also lowers the oxygen affinity of hemoglobin. In metabolically active tissues such as the muscle, the higher levels of  $\text{CO}_2$  and  $\text{H}^+$  in the capillaries have a beneficial effect by promoting the release of oxygen. This is called the *Bohr effect*.

As shown in [Figure 7.6](#), we see that the oxygen hemoglobin dissociation curve shifts to the right when the partial pressure of carbon dioxide ( $\text{pCO}_2$ ) is increased. Under these conditions,  $\text{CO}_2$  can reversibly bind to hemoglobin displacing oxygen to form a compound known as *carbaminohemoglobin*. The reverse process also occurs, i.e., oxygen binding to hemoglobin has the ability to displace  $\text{CO}_2$  that is bound to hemoglobin. This is important in both tissues and in the lungs. In the tissue capillaries, the higher  $\text{pCO}_2$  in the tissue space results in the formation of carbaminohemoglobin, which increases the release of oxygen from hemoglobin. Within the lungs, where the  $\text{pO}_2$  is much higher within the gas space of the alveoli, there is a displacement of  $\text{CO}_2$  from the hemoglobin by oxygen. This is called the *Haldane effect*.

The affinity of hemoglobin for oxygen within the RBC is significantly lower than that of hemoglobin in free solution. Within the RBC, there exists an organic phosphate called 2,3-diphosphoglycerate (DPG) at about the same concentration as hemoglobin. DPG binds to hemoglobin and reduces the oxygen binding capacity as shown in [Figure 7.6](#). Without DPG, the value of  $P_{50}$  is reduced to about 1 mmHg. This makes it very difficult for hemoglobin to release the bound oxygen at low values of the  $\text{pO}_2$ . Note that without DPG, there would be essentially no release of oxygen in the physiological range of  $\text{pO}_2$  values from 40 to 95 mmHg. Therefore, the presence of DPG within the RBC is vital for hemoglobin to perform its oxygen carrying role.

## 7.7 Tissue oxygenation

With this understanding of the oxygen binding ability of hemoglobin, we can now focus on tissue oxygenation. Hemoglobin rich with oxygen within the RBCs is transported by the circulatory system to the capillaries where the oxygen is able to diffuse out of the capillary to the tissue that surrounds each capillary. The consumption of oxygen by the tissues creates the driving force for oxygen diffusion and also causes the  $\text{pO}_2$  level to decrease along the length of the capillary, which causes a release of oxygen from the hemoglobin in the blood.

Consider the capillary bed shown earlier in [Figure 6.11](#). We can develop the following simple mathematical model to describe oxygen consumption by the tissue. We assume that the capillary bed and the surrounding tissue space are each well mixed with respect to oxygen. This assumption allows us to write the following mass balance equations for oxygen between the arterial and venous flows of the capillary blood and the tissue. We will let  $V_T$  represent the volume of the tissue space (including the capillaries), let  $q$  be the tissue blood perfusion rate, i.e.,  $Q/V_T$ , in units of  $\text{cm}^3$  of blood  $(\text{cm}^3 \text{ tissue})^{-1} \text{ min}^{-1}$ , and let  $\Gamma'_{\text{oxygen}}$  represent the tissue oxygen consumption rate ( $\mu\text{M s}^{-1}$ ) on a total tissue volume basis; hence,  $\Gamma'_{\text{oxygen}} = \phi \Gamma_{\text{oxygen}}$ .  $C_{\text{oxygen}}$  represents the dissolved oxygen concentration in the blood ( $\mu\text{M}$ ) and  $C'_{\text{HbO}}$  represents the concentration of oxygen in the blood that is bound to hemoglobin ( $\mu\text{M}$ ).  $\bar{C}_{\text{oxygen}}$  represents the concentration of oxygen in the tissue ( $\mu\text{M}$ ).  $P_C$  ( $\text{cm s}^{-1}$ ) is the permeability of oxygen through the capillary wall, and  $S_C$  represents the total surface area of the capillaries ( $\text{cm}^2$ ). With these definitions, we can then write the following steady-state oxygen mass balances for the blood and tissue regions:

$$0 = qV_T \left( C_{\text{oxygen}} + C'_{\text{HbO}} \right) \Big|_{\text{arterial}} - qV_T \left( C_{\text{oxygen}} + C'_{\text{HbO}} \right) \Big|_{\text{venous}} - P_C S_C \left( C_{\text{oxygen}} \Big|_{\text{venous}} - \bar{C}_{\text{oxygen}} \right) \quad (7.16)$$

$$0 = P_C S_C \left( C_{\text{oxygen}} \Big|_{\text{venous}} - \bar{C}_{\text{oxygen}} \right) - V_T \Gamma'_{\text{oxygen}} \quad (7.17)$$

Note that the convective terms (containing  $q$ ) in [Equation 7.16](#) include oxygen transported in the dissolved states as well as that bound to hemoglobin. However, the mass transfer of oxygen across the capillary wall is only based on the difference between the dissolved oxygen concentration in the blood and that within the tissue. [Equations 7.16](#) and [7.17](#) can then be added together and solved to give [Equation 7.18](#) for the value of the tissue oxygen consumption rate.

$$\Gamma'_{\text{oxygen}} = q \left[ \left( C_{\text{oxygen}} + C'_{\text{HbO}} \right)_{\text{arterial}} - \left( C_{\text{oxygen}} + C'_{\text{HbO}} \right)_{\text{venous}} \right] \quad (7.18)$$

### 7.7.1 Nominal tissue oxygen consumption rate

To solve [Equation 7.18](#) for the oxygen consumption rate of tissue requires a value of the tissue blood perfusion rate,  $q$ . [Table 7.3](#) provides representative values for the blood flow to various organs and tissues in the human body. The blood perfusion in this table is expressed on the basis of blood flow in milliliters per min per 100 g of tissue or organ. A nominal tissue perfusion rate is on the order of  $0.5 \text{ mL cm}^{-3} \text{ min}^{-1}$  (assuming the density of tissue,  $\rho_{\text{tissue}} \approx 1 \text{ g cm}^{-3}$ ). The nominal arterial and venous  $pO_2$  levels from [Table 7.2](#) are 95 and 40 mmHg, respectively. We can then use [Equation 7.18](#) to obtain an estimate of the nominal oxygen consumption rate,  $\Gamma'_{\text{oxygen}}$ , as shown in the following example.

#### Example 7.3

Calculate the oxygen consumption rate in  $\mu\text{M s}^{-1}$  using the previous nominal values for the blood perfusion rate and the arterial and venous  $pO_2$  levels.

Table 7.3 Blood Flow to Different Organs and Tissues under Basal Conditions

Organ	Percent	$\text{mL min}^{-1}$	$\text{mL min}^{-1} (\text{100 gm of tissue})^{-1}$
Brain	14	700	50
Heart	4	200	70
Bronchial	2	100	25
Kidneys	22	1100	360
Liver	27	1350	95
Portal	(21)	(1050)	
Arterial	(6)	(300)	
Muscle (inactive state)	15	750	4
Bone	5	250	3
Skin (cool weather)	6	300	3
Thyroid gland	1	50	160
Adrenal glands	0.5	25	300
Other tissues	35.5	175	1.3
Total	100.0	5000	—

Source: Guyton, A.C., *Textbook of Medical Physiology*, 8th ed., W.B. Saunders Co., Philadelphia, PA, 1991.

**Solution**

Using [Equation 7.18](#)

$$\begin{aligned}\Gamma'_{\text{oxygen}} &= \frac{0.5 \text{ mL}_{\text{blood}}}{\text{cm}^3_{\text{tissue}} \text{ min}} \times (8630 - 6478) \mu\text{M}_{\text{blood}} \times \frac{1 \text{ min}}{60 \text{ s}} \\ &\quad \times \frac{1000 \text{ cm}^3_{\text{tissue}}}{\text{Liter}_{\text{tissue}}} \times \frac{\mu\text{mol}_{\text{oxygen}}}{\text{Liter}_{\text{blood}} \mu\text{M}_{\text{blood}}} \times \frac{1 \text{ L}_{\text{blood}}}{1000 \text{ mL}_{\text{blood}}} \times \frac{\mu\text{M}_{\text{tissue}} \text{ L}_{\text{tissue}}}{\mu\text{mol}_{\text{oxygen}}} \\ &= 17.93 \mu\text{M}_{\text{tissue}} \text{ s}^{-1}\end{aligned}$$

This calculation shows that the tissue oxygen consumption rate is on the order of  $20 \mu\text{M s}^{-1}$ . The actual value for any given tissue will depend on the cells' specific requirement for oxygen. McMurtrey (2016) summarized the oxygen and glucose consumption rates for a variety of cell types.

### 7.7.2 Calculating the venous $\text{pO}_2$ for a given oxygen demand

If the value of  $\Gamma'_{\text{oxygen}}$  is known for a given tissue, then [Equation 7.18](#) can be rearranged to solve for the change in blood oxygenation in order to provide the oxygen demands of the tissue:

$$(C_{\text{oxygen}} + C'_{\text{HbO}})_{\text{venous}} = (C_{\text{oxygen}} + C'_{\text{HbO}})_{\text{arterial}} - \frac{\Gamma'_{\text{oxygen}}}{q} \quad (7.19)$$

To illustrate this type of calculation, where  $\Gamma'_{\text{oxygen}}$  is known, consider the *islet of Langerhans*. The islets of Langerhans are a specialized cluster of cells located within the pancreas. The islets amount to about 1%–2% of the pancreatic tissue mass. The cells that lie within the islet are responsible for the control of glucose metabolism through the secretion of the hormones insulin ( $\beta$  cells) and glucagon ( $\alpha$  cells). The loss of the  $\beta$  cells as a result of an autoimmune response of the immune system results in type I or insulin-dependent diabetes.

An islet of Langerhans is only about  $150 \mu\text{m}$  in diameter. The *single islet blood flow* has been determined to be about  $7 \text{ nL min}^{-1}$ , which gives an islet tissue perfusion rate of about  $4 \text{ mL cm}^{-3} \text{ min}^{-1}$  (Lifson et al., 1980). This value is about four times the blood perfusion rate of the pancreas itself and is probably related to the hormonal function of the islet.

The oxygen consumption rate for tissues like islets can be described by Michaelis-Menten type kinetics as given by [Equation 7.5](#). For islets, the value of  $K_m$  is  $0.44 \text{ mmHg}$  and the value of  $V_{\text{max}}$  is  $26 \mu\text{M s}^{-1}$  when the islets are exposed to basal levels of glucose ( $100 \text{ mg dL}^{-1}$ ) and  $46 \mu\text{M s}^{-1}$  under stimulated glucose levels ( $300 \text{ mg dL}^{-1}$ ) (Dionne et al., 1989, 1991).

Because of the small value of  $K_m$ , the tissue oxygen consumption rate is generally independent of the tissue  $\text{pO}_2$  until the  $\text{pO}_2$  in the tissue reaches a value of just a few mmHg. Cellular metabolic processes are therefore relatively insensitive to the local  $\text{pO}_2$  level until it reaches a value of about 5 mmHg. Therefore, we can approximate the value of  $\Gamma_{\text{oxygen}}$  as simply the value of  $V_{\text{max}}$ . Only at very low  $\text{pO}_2$  levels would this approximation be no longer valid.

From [Equation 7.19](#), we know the value of  $\Gamma'_{\text{oxygen}}$ , and the value of  $(C_{\text{oxygen}} + C'_{\text{HbO}})_{\text{arterial}}$  is the nominal arterial value of  $8630 \mu\text{M}$  (from [Table 7.2](#)). We can now solve for the value of  $(C_{\text{oxygen}} + C'_{\text{HbO}})_{\text{venous}}$  recognizing that  $C'_{\text{HbO}}$  (the amount of oxygen bound to hemoglobin) depends on  $C_{\text{oxygen}}$  (the dissolved oxygen concentration) through the Hill equation ([Equation 7.14](#)), where we make use of the fact that  $pO_2 = H_{\text{oxygen}} C_{\text{oxygen}}$  (i.e., Henry's law). Hence,  $C'_{\text{HbO}}$  is given by

$$C'_{\text{HbO}} = \frac{C'_{\text{SAT}} (H_{\text{oxygen}} C_{\text{oxygen}})^n}{P_{50}^n + (H_{\text{oxygen}} C_{\text{oxygen}})^n} \quad (7.20)$$

where  $C'_{\text{SAT}}$  is the saturated amount of oxygen bound to hemoglobin, which is  $8800 \mu\text{M}$ . Substituting this equation into [Equation 7.19](#) for the venous value of  $C'_{\text{HbO}}$ , we obtain [Equation 7.21](#) for the dissolved oxygen concentration in the venous blood:

$$\left[ C_{\text{oxygen}} + \frac{C'_{\text{SAT}} (H_{\text{oxygen}} C_{\text{oxygen}})^n}{P_{50}^n + (H_{\text{oxygen}} C_{\text{oxygen}})^n} \right]_{\text{venous}} = (C_{\text{oxygen}} + C'_{\text{HbO}})_{\text{arterial}} - \frac{\Gamma'_{\text{oxygen}}}{q} \quad (7.21)$$

For the given values of  $q$ ,  $\Gamma'_{\text{oxygen}}$ , and  $(C_{\text{oxygen}} + C'_{\text{HbO}})_{\text{arterial}}$ , [Equation 7.21](#) can be solved for the dissolved oxygen concentration ( $C_{\text{oxygen}}$ ) in the blood leaving the tissue, which in this case is an islet of Langerhans. Once we have obtained the value of  $C_{\text{oxygen}}$ , then the concentration of oxygen bound to hemoglobin,  $C'_{\text{HbO}}$ , can be found from [Equation 7.20](#). The  $pO_2$  of the exiting blood is then given by Henry's law, i.e., [Equation 7.1](#). The following example illustrates these calculations.

#### Example 7.4

Calculate the change in blood oxygenation within an islet of Langerhans. Perform the calculations under conditions of normal blood perfusion for basal and stimulated levels of glucose. Also find the critical blood perfusion rate to maintain the exiting  $pO_2$  at  $20 \text{ mmHg}$  under conditions of basal and stimulated levels of glucose.

#### Solution

[Equation 7.21](#) allows us to make these calculations. Since this equation is nonlinear in  $C_{\text{oxygen}}$ , an implicit root-finding method is needed to solve for  $C_{\text{oxygen}}$  in the venous blood. For the case of basal glucose stimulation, the venous dissolved oxygen concentration is found to be  $102.7 \mu\text{M}$ . The corresponding value of the exiting  $pO_2$  from [Equation 7.1](#) is  $76 \text{ mmHg}$ , and the fractional saturation of the hemoglobin from [Equation 7.14](#), or [Figure 7.4](#), is  $0.925$ . The exiting oxygen levels under stimulated glucose conditions are found to be  $86.7 \mu\text{M}$  with a  $pO_2$  of  $64 \text{ mmHg}$  and a fractional saturation of  $0.89$ . In both of these cases, we observe a modest decrease in oxygen levels in the blood exiting the islet. This is because the islets are highly perfused with blood. The critical perfusion rate is defined as the blood flow rate to the tissue that just maintains a critical  $pO_2$  level, e.g.,  $20 \text{ mmHg}$ . Hence, we solve [Equation 7.21](#) for the value of the blood perfusion rate, i.e.,  $q$ . We then find that the critical blood perfusion rate for an islet is  $0.28 \text{ mL cm}^{-3} \text{ min}^{-1}$  under basal glucose conditions. A similar calculation shows that the critical blood perfusion rate is  $0.50 \text{ mL cm}^{-3} \text{ min}^{-1}$  under stimulated glucose conditions.

## 7.8 Oxygen transport in blood oxygenators, bioartificial organs, and tissue engineered constructs

This discussion on oxygen transport is also of critical importance in the design of blood oxygenators (see [Section 9.5](#)), bioartificial organs (Colton, 1995, 2014), and engineered constructs used for tissue engineering (Radisic et al., 2006; McMurtrey, 2016).

In one type of bioartificial organ proposed for the treatment of diabetes, therapeutic cells such as the islets of Langerhans, or other insulin-secreting cells, are sandwiched between two permselective membranes that are surrounded by vascularized tissue or adjacent to a polymer matrix material that has been vascularized by the host. The permselective membrane has a porous structure at the molecular level such that small molecules like oxygen, key nutrients, and the therapeutic agent are readily permeable; however, the components of the host immune system cannot cross the membrane. The cells are therefore said to be *immunoprotected*.\*

In tissue engineering applications,<sup>†</sup> cells are placed within porous polymeric constructs that in many cases can be represented as thin disks. In these applications, key nutrients are brought to the cells primarily by diffusion, and in most cases, the critical species that affects the design is the transport of oxygen.

The following discussion will first look at an oxygen mass balance for a blood oxygenator. We will then focus on calculating the oxygen gradient in thin planar or one-dimensional disks that contain cells with the goal of providing sufficient oxygen to the cells. In general, the oxygen gradient will depend on the cell density in the region of interest, the viability of the cells, and the metabolic activity of the cells.

### 7.8.1 Oxygen mass balance for a blood oxygenator

These concepts can also be used to determine the amount of oxygen transported to blood in medical devices such as blood oxygenators. In this case, a steady-state oxygen mass balance says that the amount of oxygen transported into the blood is equal to the difference between the amount of oxygen in the blood leaving and entering the oxygenator. Hence,

$$\dot{m}_{\text{oxygen}} = Q_{\text{blood}} \left[ \left( C_{\text{oxygen}} + C'_{\text{HbO}} \right)_{\text{out}} - \left( C_{\text{oxygen}} + C'_{\text{HbO}} \right)_{\text{in}} \right] \quad (7.22)$$

In this equation

$\dot{m}_{\text{oxygen}}$  is the amount of oxygen transported to the blood

$Q_{\text{blood}}$  is the blood flow rate through the oxygenator

[Example 7.5](#) illustrates the application of [Equation 7.22](#).

#### Example 7.5

Blood travels through a membrane oxygenator at a flow rate of  $5000 \text{ mL min}^{-1}$ . The entering  $p\text{O}_2$  of the blood is  $30 \text{ mmHg}$  and the exiting blood  $p\text{O}_2$  is  $100 \text{ mmHg}$ . Calculate the amount of oxygen transported into the blood in  $\mu\text{mol s}^{-1}$ .

\* We will discuss immunoprotection in greater detail in [Chapter 11](#).

<sup>†</sup> Tissue engineering is discussed in [Chapter 10](#).

### Solution

First, we need to find the amount of oxygen that is dissolved in the blood at 30 mmHg and at 100 mmHg. This can be found from Henry's law given by [Equation 7.1](#).

$$C_{\text{oxygen}}^{\text{in}} = \left( \frac{pO_2}{H} \right)_{\text{in}} = \frac{30 \text{ mmHg}}{0.74 \text{ mmHg } \mu\text{M}^{-1}} = 40.54 \mu\text{M}$$

$$C_{\text{oxygen}}^{\text{out}} = \left( \frac{pO_2}{H} \right)_{\text{out}} = \frac{100 \text{ mmHg}}{0.74 \text{ mmHg } \mu\text{M}^{-1}} = 135.14 \mu\text{M}$$

The amount of oxygen bound to hemoglobin can be found from [Figure 7.4](#). At 30 mmHg, the hemoglobin saturation is  $Y = 0.58$ , and at 100 mmHg, it is  $Y = 0.97$ . Therefore, we have

$$C'_{\text{HbO}}^{\text{in}} = 0.58 \times 8800 \mu\text{M} = 5104 \mu\text{M}$$

$$C'_{\text{HbO}}^{\text{out}} = 0.97 \times 8800 \mu\text{M} = 8536 \mu\text{M}$$

Using these values, we can calculate the amount of oxygen transported to the blood.

$$\dot{m}_{\text{oxygen}} = Q_{\text{blood}} \left[ (C_{\text{oxygen}} + C'_{\text{HbO}})_{\text{out}} - (C_{\text{oxygen}} + C'_{\text{HbO}})_{\text{in}} \right]$$

$$= 5000 \text{ mL min}^{-1} \times [(135.14 + 8536) - (40.54 + 5104)] \mu\text{M}$$

$$\times 1 \mu\text{mol L}^{-1} \mu\text{M}^{-1} \times \frac{1 \text{ min}}{60 \text{ s}} \times \frac{1 \text{ L}}{1000 \text{ mL}}$$

$$Q_{\text{oxygen}} = 293.9 \mu\text{mol s}^{-1}$$

### 7.8.2 Oxygen transport in planar bioartificial organs

Consider the bioartificial organ shown in [Figure 7.7](#). The planar immunoisolation membranes enclose the layer of cells. We will prescribe the  $pO_2$  level at the outer surface of the immunoisolation membrane to be some average of the blood  $pO_2$  found in the capillaries adjacent to this membrane. A steady-state shell balance for oxygen over a thickness  $\Delta x$  of the cell layer of cross-sectional area  $S$  can be written as follows:

$$0 = -SD_T \frac{dC_{\text{oxygen}}}{dx} \Big|_x + SD_T \frac{dC_{\text{oxygen}}}{dx} \Big|_{x+\Delta x} - \Gamma_{\text{oxygen}} S \Delta x \phi \quad (7.23)$$

$C_{\text{oxygen}}$  is the oxygen concentration within a given volume of tissue, i.e., the cells and surrounding interstitial fluid. The product of  $C_{\text{oxygen}}$  and this tissue volume gives the mass of oxygen in the volume of tissue. Note that the volumetric oxygen consumption rate of the tissue,  $\Gamma_{\text{oxygen}}$  (assumed constant), is multiplied by the cell volume, i.e.,  $S\Delta x \phi$ , to get the amount of oxygen consumed by the tissue in the shell of thickness  $\Delta x$ . The volume fraction of the cells or tissue is given by  $\phi$ .

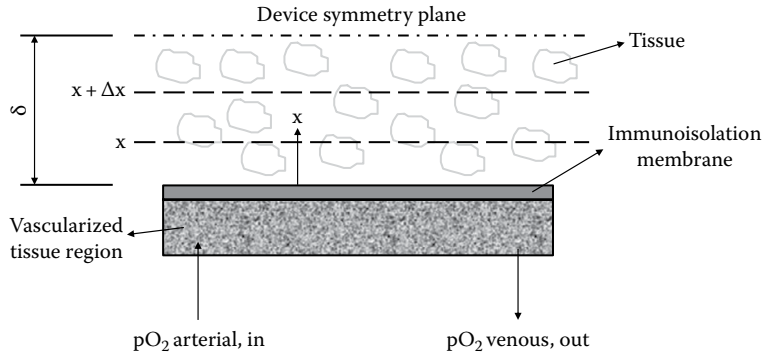


Figure 7.7 Conceptual model for a bioartificial organ.

$D_T$  is the effective diffusivity of oxygen within the tissue and was defined earlier in [Chapter 6](#), e.g., by [Equations 6.43](#) and [6.45](#). Since oxygen is lipid soluble, we would expect  $D_T$  for oxygen in tissue at 37°C to be on the order of its diffusivity in water, i.e.,  $2.76 \times 10^{-5} \text{ cm}^2 \text{ s}^{-1}$  (Yoshida and Ohshima, 1966). For example, Bentley et al. (1993) give a value of  $D_T$  for oxygen diffusion in tissue of  $2.41 \times 10^{-5} \text{ cm}^2 \text{ s}^{-1}$ . For plasma and interstitial fluid, Goldstick et al. (1976) give a value of the oxygen diffusivity of  $2.18 \times 10^{-5} \text{ cm}^2 \text{ s}^{-1}$ , and for blood with a normal hematocrit of 42%, the oxygen diffusivity is  $1.62 \times 10^{-5} \text{ cm}^2 \text{ s}^{-1}$ .

After dividing [Equation 7.23](#) by  $\Delta x$ , and taking the limit as  $\Delta x \rightarrow 0$ , [Equation 7.24](#) is obtained, where Henry's law was used to express the oxygen concentration in terms of the oxygen partial pressure, i.e.,  $pO_2 = H_{\text{oxygen}} C_{\text{oxygen}}$ :

$$D_T \frac{d^2 pO_2}{dx^2} = \Gamma_{\text{oxygen}} H_{\text{oxygen}} \phi \quad (7.24)$$

Since this equation is a second order differential equation, we require the following two boundary conditions in order to obtain the solution for the  $pO_2$  profile within the tissue layer:

$$\begin{aligned} BC1 : \quad & x = 0, \quad pO_2 = pO_2^{x=0} \\ BC2 : \quad & x = \delta, \quad \frac{dpO_2}{dx} = 0 \end{aligned} \quad (7.25)$$

The first boundary condition (BC1) expresses the  $pO_2$  level at the interface between the immunoisolation membrane and the layer of cells. The second boundary condition (BC2) results from the device symmetry and expresses the fact that there is no net flow of oxygen across the symmetry plane.

[Equation 7.24](#) can now be integrated twice and [Equation 7.25](#) can be used to find the integration constants. [Equation 7.26](#) is then obtained for the oxygen profile within the tissue layer:

$$pO_2(x) = pO_2^{x=0} + \left[ \frac{\Gamma_{\text{oxygen}} H_{\text{oxygen}} \phi \delta^2}{2 D_T} \right] \left[ \left( \frac{x}{\delta} \right)^2 - 2 \left( \frac{x}{\delta} \right) \right] \quad (7.26)$$

At this point, the value of  $pO_2^{x=0}$  in [Equation 7.26](#) is unknown. In order to determine  $pO_2^{x=0}$ , we need to develop an additional equation that relates the transport rate of oxygen across the immunoisolation membrane to the total consumption of oxygen by the cells. This is given by

$$\frac{SP_m}{H_{\text{oxygen}}} (pO_2^{\text{AVG}} - pO_2^{x=0}) = S\delta\phi\Gamma_{\text{oxygen}} \quad (7.27)$$

where

$P_m$  is the oxygen permeability of the immunoisolation membrane  
 $pO_2^{\text{AVG}}$  is the average partial pressure of oxygen in the blood in the vascularized region adjacent to the immunoisolation membrane, which is assumed to be known

Rearranging [Equation 7.27](#) provides the value of  $pO_2^{x=0}$ :

$$pO_2^{x=0} = pO_2^{\text{AVG}} - \left[ \frac{\Gamma_{\text{oxygen}} H_{\text{oxygen}} \phi \delta}{P_m} \right] \quad (7.28)$$

Combining this result for  $pO_2^{x=0}$  with [Equation 7.26](#), we can now write the  $pO_2$  gradient within the cell layer as

$$pO_2(x) = pO_2^{\text{AVG}} - \left[ \frac{\Gamma_{\text{oxygen}} H_{\text{oxygen}} \phi \delta}{P_m} \right] + \left[ \frac{\Gamma_{\text{oxygen}} H_{\text{oxygen}} \phi \delta^2}{2D_T} \right] \left[ \left( \frac{x}{\delta} \right)^2 - 2 \left( \frac{x}{\delta} \right) \right] \quad (7.29)$$

The previous equations can now be used for basic calculations on the effect of oxygen transport on the design of a bioartificial organ. These calculations are illustrated in the following examples.

### Example 7.6

Consider a bioartificial organ such as that shown in [Figure 7.7](#). Assume the value of  $pO_2^{\text{AVG}}$  is the mean of the arterial and venous oxygen values, i.e., 68 mmHg. Let the cells be the islets of Langerhans, assumed to be spheres with a diameter of 150  $\mu\text{m}$ , with the basal oxygen consumption rate of  $25.9 \mu\text{M s}^{-1}$ . The half-thickness ( $\delta$ ) of the islet layer is 200 microns and the cell volume fraction ( $\phi$ ) is equal to 0.15. The islets are suspended within a hydrogel for which the effective oxygen diffusivity, i.e.,  $D_T$ , is estimated to be  $1.67 \times 10^{-5} \text{ cm}^2 \text{ s}^{-1}$ . The oxygen permeability of the membrane ( $P_m$ ) is equal to  $4 \times 10^{-3} \text{ cm s}^{-1}$ . Calculate the  $pO_2$  profile in the islet layer of the bioartificial organ. Also find the  $pO_2$  at the center of the device, i.e., at  $x = \delta$ .

### Solution

[Equation 7.29](#) can be used to obtain the solution for the given values of the parameters. [Figure 7.8](#) shows a plot of the  $pO_2$  profile within the islet layer of the bioartificial organ.

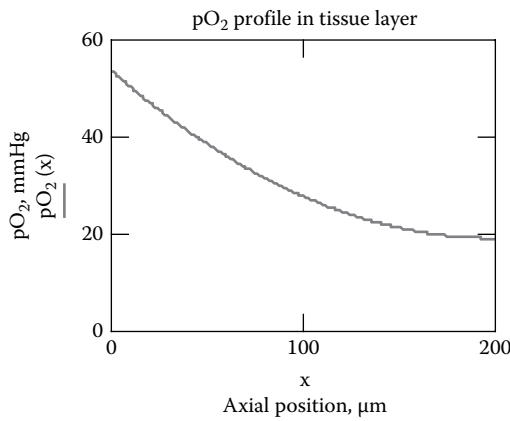


Figure 7.8 Oxygen profile in a bioartificial organ.

The graph shows that for these conditions, the tissue layer is fully oxygenated. The  $pO_2$  at the centerline can be found using [Equation 7.29](#) by setting  $x = \delta$ :

$$\begin{aligned}
 pO_2(x = \delta) &= pO_2^{\text{AVG}} - \left[ \frac{\Gamma_{\text{oxygen}} H_{\text{oxygen}} \phi \delta}{P_m} \right] + \left[ \frac{\Gamma_{\text{oxygen}} H_{\text{oxygen}} \phi \delta^2}{2D_T} \right] (-1) \\
 pO_2(x = \delta) &= 68 \text{ mmHg} - \left( \frac{25.9 \mu\text{M s}^{-1} \times 0.74 \text{ mmHg } \mu\text{M}^{-1} \times 0.15 \times 0.02 \text{ cm}}{0.004 \text{ cm s}^{-1}} \right) \\
 &\quad - \left( \frac{25.9 \mu\text{M s}^{-1} \times 0.74 \text{ mmHg } \mu\text{M}^{-1} \times 0.15 \times 0.02 \text{ cm} \times 0.02 \text{ cm}}{2 \times 1.67 \times 10^{-5} \text{ cm}^2 \text{ s}^{-1}} \right) \\
 pO_2(x = \delta) &= 68 \text{ mmHg} - 14.37 \text{ mmHg} - 34.43 \text{ mmHg} = 19.2 \text{ mmHg}
 \end{aligned}$$

### 7.8.3 Oxygen transport in planar tissue engineered constructs

Consider a planar tissue engineered construct where the cells are incorporated into the voids formed within a polymeric construct. On the surface of the construct, there can also be a thin membrane to provide mechanical stability to the entire tissue engineered structure. When implanted in the body, this tissue engineered construct will have vascularized tissue adjacent to this membrane. For this polymeric scaffold, we let  $\epsilon_{\text{scaffold}}$  represent the fraction of the total construct volume that is available for the tissue.

When performing an oxygen mass balance over a thin shell of the construct of total cross-sectional area  $S$  from  $x$  to  $x + \Delta x$ , we see that [Equation 7.23](#) still applies; however, each term in that expression needs to be multiplied by  $\epsilon_{\text{scaffold}}$ , and in the end we still get [Equation 7.29](#). Although [Equation 7.29](#) was derived for the case of the bioartificial organ shown in [Figure 7.7](#), we see that it can be generalized to other situations involving tissue engineered constructs.

If the tissue construct does not have the membrane on its surface, then the  $pO_2$  at the surface of the construct is equal to  $pO_2^{\text{AVG}}$ , which is the average partial pressure of oxygen in the blood in the

vascularized region adjacent to the construct which is assumed to be known. In this case, we then have that  $pO_2^{x=0} = pO_2^{\text{AVG}}$ , and [Equation 7.26](#) gives the  $pO_2$  profile within the tissue construct as

$$pO_2(x) = pO_2^{\text{AVG}} + \left[ \frac{\Gamma_{\text{oxygen}} H_{\text{oxygen}} \phi \delta^2}{2D_T} \right] \left[ \left( \frac{x}{\delta} \right)^2 - 2 \left( \frac{x}{\delta} \right) \right] \quad (7.30)$$

**7.8.3.1 *In vitro culture of planar tissue engineered constructs*** The cells in tissue engineered constructs are often first grown in culture in a bioreactor before implantation. In this case, the tissue engineered construct is immersed within a well-stirred nutrient medium. If this nutrient medium is not sufficiently agitated, then there will also exist a concentration boundary layer in the fluid surrounding the cell layer construct. This external mass transfer resistance to oxygen transport can be accounted for by a mass transfer coefficient,  $k_m$ .

In this case, we can add an additional resistance to [Equation 7.29](#) like the term for the membrane resistance. Hence, [Equation 7.29](#) becomes

$$pO_2(x) = pO_2^{\text{bulk}} - \Gamma_{\text{oxygen}} H_{\text{oxygen}} \phi \delta \left[ \frac{1}{P_m} + \frac{1}{k_m} \right] + \left[ \frac{\Gamma_{\text{oxygen}} H_{\text{oxygen}} \phi \delta^2}{2D_T} \right] \left[ \left( \frac{x}{\delta} \right)^2 - 2 \left( \frac{x}{\delta} \right) \right] \quad (7.31)$$

where  $pO_2^{\text{bulk}}$  is the partial pressure of oxygen in the bulk nutrient media solution. Note that if the external mass transfer resistance is small and there is no membrane, then [Equation 7.31](#) simplifies to

$$pO_2(x) = pO_2^{\text{bulk}} + \left[ \frac{\Gamma_{\text{oxygen}} H_{\text{oxygen}} \phi \delta^2}{2D_T} \right] \left[ \left( \frac{x}{\delta} \right)^2 - 2 \left( \frac{x}{\delta} \right) \right] \quad (7.32)$$

### Example 7.7

Malda et al. (2004) measured oxygen gradients in tissue engineered cartilaginous constructs. Using a microelectrode, oxygen concentrations were measured as a function of distance into the tissue engineered constructs containing the chondrocytes. In addition, they also determined the chondrocyte distribution as a function of position with the construct. The average number of chondrocytes per  $\text{cm}^3$  of total construct, i.e., the cell density, 28 days after seeding, is about  $1.5 \times 10^8 \text{ cells cm}^{-3}$ . The table below summarizes the  $pO_2$  levels that were measured within the construct as a function of the distance from the exposed surface of the construct.

Depth, $\mu\text{m}$	$pO_2$ , mmHg
0	160
250	114
500	95
750	76
1000	61
1250	53
1500	42
1750	38
2000	30
2500	19

They also estimated the diffusivity of oxygen in the construct to be  $3.8 \times 10^{-6} \text{ cm}^2 \text{ s}^{-1}$ . From these data, estimate the oxygen consumption rate of the chondrocytes in  $\mu\text{M s}^{-1}$  assuming the diameter of a chondrocyte is  $20 \mu\text{m}$ .

### Solution

We can use [Equation 7.32](#) to describe the oxygen partial pressure within the construct since the oxygen concentration is given at the surface of the construct. The volume of one cell, i.e.,  $V_{\text{cell}}$ , is equal to  $4.19 \times 10^{-9} \text{ cm}^3 \text{ cell}^{-1}$ . Multiplying the cell volume by the cell density, i.e.,  $\rho_{\text{cell}}$ , provides the value of the cell volume fraction  $\phi$ . Hence, we have that  $\phi = V_{\text{cell}} \rho_{\text{cell}}$  and in this case  $\phi = 0.63$ . A regression analysis can then be performed to find the best value of  $\Gamma_{\text{oxygen}}$  in [Equation 7.32](#) that fits the data in the table. [Figure 7.9](#) shows the results of these calculations.  $\Gamma_{\text{oxygen}}$  is found to equal  $0.037 \mu\text{M s}^{-1}$  and we see that [Equation 7.32](#) provides a good representation of the data. It is also important to note that chondrocytes have a very low oxygen consumption rate, which helps them survive in the relatively avascular regions of cartilage tissue. Heywood et al. (2006) in a study involving bovine articular chondrocytes reported oxygen consumption rates ranging from  $9.6 \times 10^{-16} \text{ mol cell}^{-1} \text{ h}^{-1}$  at basal levels of glucose to  $18.4 \times 10^{-16} \text{ mol cell}^{-1} \text{ h}^{-1}$  at reduced levels of glucose. On the basis of a cell diameter of  $20 \mu\text{m}$ , this equates to a metabolic oxygen consumption rate for chondrocytes of  $0.06\text{--}0.12 \mu\text{M s}^{-1}$ , which is of the same order as found here for the data obtained by Malda et al. (2004).

### Example 7.8

A thin tissue engineered construct of genetically transformed cells is a cylindrical disk  $5 \text{ cm}$  in diameter. The construct is suspended in a nutrient solution at  $37^\circ\text{C}$ , and the disk is rotated at  $50 \text{ rpm}$  as shown in [Figure 5.6](#). The nutrient solution has a density of  $1 \text{ g cm}^{-3}$  and a viscosity of  $0.8 \text{ cP}$ . The oxygen diffusivity in the nutrient solution was found to be  $2.65 \times 10^{-5} \text{ cm}^2 \text{ s}^{-1}$ ,

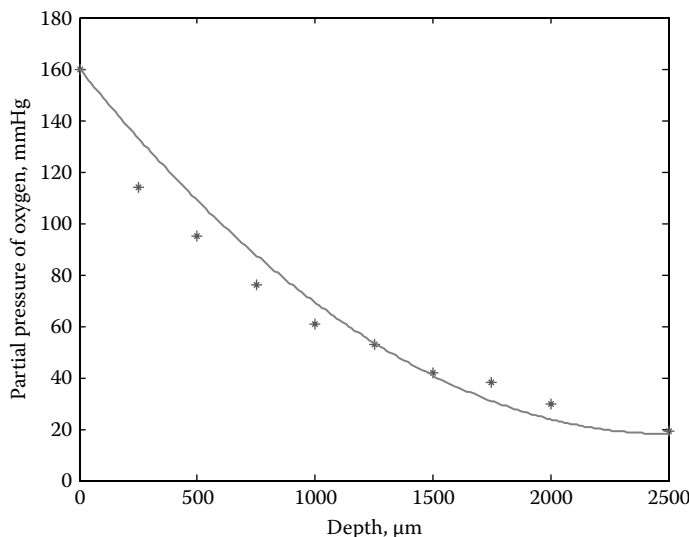


Figure 7.9 Measured and predicted oxygen gradients in engineered cartilaginous constructs.

and the effective diffusivity of oxygen through the construct containing the immobilized cells is  $2.3 \times 10^{-5} \text{ cm}^2 \text{ s}^{-1}$ . The half-thickness of the disk ( $\delta$ ) that contains the cells is  $150 \mu\text{m}$  and the cell volume fraction in the disk is 0.35. The consumption rate of oxygen on a per cell volume basis is  $18.5 \mu\text{M s}^{-1}$ . If the  $pO_2$  of oxygen in the bulk nutrient solution is  $150 \text{ mmHg}$ , estimate the oxygen level at the centerline of the disk (i.e.,  $x = \delta$ ). Assume that Henry's constant for the oxygen in this nutrient solution is equal to  $0.71 \text{ mmHg } \mu\text{M}^{-1}$ .

### Solution

We can use [Equation 7.31](#) to solve this problem. Since there is no membrane on the surface of the construct, this equation can be written with  $x = \delta$  as

$$pO_2(x = \delta) = pO_2^{\text{bulk}} - \frac{\Gamma_{\text{oxygen}} H_{\text{oxygen}} \phi \delta}{k_m} - \left[ \frac{\Gamma_{\text{oxygen}} H_{\text{oxygen}} \phi \delta^2}{2D_T} \right] \quad (\text{A})$$

We can then calculate the value of  $k_m$  using [Equation 5.119](#) for a rotating disk. The rotation speed is given as 50 rpm, which is equal to  $5.24 \text{ s}^{-1}$ .

$$\begin{aligned} \frac{k_m d_{\text{disk}}}{D_{\text{AB}}} &= 0.62 \left( \frac{\rho d_{\text{disk}}^2 \omega}{\mu} \right)^{1/2} \left( \frac{\mu}{\rho D_{\text{AB}}} \right)^{1/3} = 0.62 \left( \frac{1 \text{ g cm}^{-3} (5 \text{ cm})^2 5.24 \text{ s}^{-1}}{0.8 \text{ cP} \times 0.01 \text{ g cm}^{-1} \text{ s}^{-1} \text{ cP}^{-1}} \right)^{1/2} \\ &\times \left( \frac{0.8 \text{ cP} \times 0.01 \text{ g cm}^{-1} \text{ s}^{-1} \text{ cP}^{-1}}{1 \text{ g cm}^{-3} \times 2.65 \times 10^{-5} \text{ cm s}^{-1}} \right)^{1/3} = 0.62 \times 127.96 \times 6.71 = 532.21 \\ k_m &= 532.21 \times \frac{2.65 \times 10^{-5} \text{ cm}^2 \text{ s}^{-1}}{5 \text{ cm}} = 2.821 \times 10^{-3} \text{ cm s}^{-1} \end{aligned}$$

Next, we substitute the parameter values into [Equation A](#) and calculate the  $pO_2$  at  $x = \delta$ :

$$\begin{aligned} pO_2(x = \delta) &= 150 \text{ mmHg} - \frac{18.5 \mu\text{M s}^{-1} \times 0.71 \text{ mmHg } \mu\text{M}^{-1} \times 0.35 \times 0.015 \text{ cm}}{2.821 \times 10^{-3} \text{ cm s}^{-1}} \\ &- \left[ \frac{18.5 \mu\text{M s}^{-1} \times 0.71 \text{ mmHg } \mu\text{M}^{-1} \times 0.35 \times (0.015 \text{ cm})^2}{2 \times 2.3 \times 10^{-5} \text{ cm s}^{-1}} \right] \\ &= 150 \text{ mmHg} - 24.44 \text{ mmHg} - 22.49 \text{ mmHg} \\ pO_2(x = \delta) &= 103.07 \text{ mmHg} \end{aligned}$$

**7.8.3.2 Maximum thickness of planar tissue engineered constructs** We can use [Equations 7.29](#) and [7.31](#), and the various simplifications of those equations discussed previously, to determine for a given set of conditions the maximum half-thickness of the tissue engineered construct or a bioartificial organ. The maximum half-thickness is that value of  $\delta$ , which makes the  $pO_2(x = \delta)$  a certain limiting value. For example, the  $pO_2(x = \delta)$  cannot be less than zero. This is illustrated in [Example 7.9](#).

**Example 7.9**

A design for a bioartificial liver consists of a thin layer of hepatocytes that are immobilized within a gel-like material that coats the inside surface of hollow fiber membranes. The hepatocyte cell fraction in the gel-like layer is 0.40, and these cells consume oxygen at a rate of  $29.5 \text{ } \mu\text{M s}^{-1}$ . The perfusing fluid is plasma at an average  $\text{pO}_2$  of 70 mmHg and a temperature of  $37^\circ\text{C}$ . The plasma velocity within the hollow fiber is  $5 \text{ cm s}^{-1}$ , and the plasma has a viscosity of 1.2 cP and a density of  $1.07 \text{ g cm}^{-3}$ . Separate experiments have shown that the oxygen diffusivity within the layer of immobilized hepatocytes is  $2.1 \times 10^{-5} \text{ cm}^2 \text{ s}^{-1}$ , the diffusivity of oxygen in the plasma is  $2.2 \times 10^{-5} \text{ cm}^2 \text{ s}^{-1}$ , and Henry's constant is  $0.72 \text{ mmHg } \mu\text{M}^{-1}$ . The hollow fibers have an inside diameter of 4 mm and a length of 40 cm. What is the maximum thickness of the layer of hepatocytes that can line the inside surface of the hollow fiber membranes assuming that the lowest allowable  $\text{pO}_2$  within the layer of hepatocytes is 15 mmHg? Since the radius of the hollow fibers is much larger than the expected thickness of the cell layer, you can neglect the effect of curvature.

**Solution**

We can solve [Equation 7.31](#) for  $\delta$  for the given  $\text{pO}_2^{\text{bulk}} = 70 \text{ mmHg}$  and the minimal  $\text{pO}_2$  in the cell layer of 15 mmHg. Rearranging [Equation 7.31](#), we obtain

$$\left[ \frac{\Gamma_{\text{oxygen}} H_{\text{oxygen}} \phi}{2D_T} \right] \delta^2 + \Gamma_{\text{oxygen}} H_{\text{oxygen}} \phi \left[ \frac{1}{P_m} + \frac{1}{k_m} \right] \delta + (\text{pO}_2^{x=\delta} - \text{pO}_2^{\text{bulk}}) = 0$$

This is a quadratic equation, which can be solved for  $\delta$ . We let

$$\begin{aligned} a &= \left[ \frac{\Gamma_{\text{oxygen}} H_{\text{oxygen}} \phi}{2D_T} \right] \\ b &= \Gamma_{\text{oxygen}} H_{\text{oxygen}} \phi \left[ \frac{1}{P_m} + \frac{1}{k_m} \right] \\ c &= (\text{pO}_2^{x=\delta} - \text{pO}_2^{\text{bulk}}) \\ a\delta^2 + b\delta + c &= 0 \end{aligned} \tag{A}$$

Since there is no membrane, we can eliminate  $1/P_m$  in the  $b$  term. The only parameter left to find is the mass transfer coefficient, i.e.,  $k_m$ . This can be found based on the laminar flow of the plasma in a cylindrical tube using [Equation 5.169](#). First, we calculate the Reynolds number to confirm that the flow is in fact laminar:

$$Re = \frac{\rho d_{\text{fiber}} V}{\mu} = \frac{1.07 \text{ g cm}^{-3} \times 0.4 \text{ cm} \times 5 \text{ cm s}^{-1}}{1.2 \text{ cP} \times 0.01 \text{ g cm}^{-3} \text{ s}^{-1} \text{ cP}^{-1}} = 178.33$$

So the plasma flow in the hollow fiber is laminar. Next, we calculate the Schmidt number for oxygen in plasma:

$$Sc = \frac{\mu}{\rho D_{AB}} = \frac{1.2 \text{ cP} \times 0.01 \text{ g cm}^{-3} \text{ s}^{-1} \text{ cP}^{-1}}{1.07 \text{ g cm}^{-3} \times 2.2 \times 10^{-5} \text{ cm}^2 \text{ s}^{-1}} = 509.77$$

Now we can use [Equation 5.169](#) to calculate the mass transfer coefficient:

$$Sh = 3.66 + \frac{0.104 \times 178.33 \times 509.77 \left( \frac{0.4}{40} \right)}{1 + 0.016 \left[ 178.33 \times 509.77 \left( \frac{0.4}{40} \right) \right]^8} = 3.66 + 20.01 = 23.67$$

$$k_m = Sh \times \frac{D_{AB}}{d_{fiber}} = 23.67 \times \frac{2.2 \times 10^{-5} \text{ cm}^2 \text{ s}^{-1}}{0.4 \text{ cm}} = 0.0013 \text{ cm s}^{-1}$$

And we can calculate the value of a, b, and c given in [Equation A](#):

$$a = \left[ \frac{\Gamma_{\text{oxygen}} H_{\text{oxygen}} \phi}{2D_T} \right] = \frac{29.5 \mu\text{M s}^{-1} \times 0.72 \text{ mmHg } \mu\text{M}^{-1} \times 0.4}{2 \times 2.1 \times 10^{-5} \text{ cm}^2 \text{ s}^{-1}} = 202,285.71 \text{ mmHg cm}^{-2}$$

$$b = \Gamma_{\text{oxygen}} H_{\text{oxygen}} \phi \left[ \frac{1}{P_m} + \frac{1}{k_m} \right] = 29.5 \mu\text{M s}^{-1} \times 0.72 \text{ mmHg } \mu\text{M}^{-1} \times 0.4 \times \frac{1}{0.0013 \text{ cm s}^{-1}}$$

$$= 6,535.38 \text{ mmHg cm}^{-1}$$

$$c = (pO_2^{x=\delta} - pO_2^{\text{bulk}}) = (15 - 70) \text{ mmHg} = -55 \text{ mmHg}$$

Using these values of a, b, and c, we see that the units of  $\delta$  will be in cm. So, from the quadratic formula we have

$$\delta = \frac{-b \pm \sqrt{b^2 - 4ac}}{2a}$$

$$= \frac{-6,535.38 \pm \sqrt{(6,535.38)^2 - 4 \times 202,285.71 \times -55}}{2 \times 202,285.71} = \frac{-6,535.38 \pm 9,338.85}{404,571.42}$$

$$\delta = 0.0069 \text{ cm} = 69.3 \mu\text{m}$$

So we see that the maximum thickness of the layer of cells that line the inside surface of the hollow fibers is 69  $\mu\text{m}$ .

## 7.9 Oxygen transport in perfusion bioreactors

As shown in [Figures 7.8](#) and [7.9](#), there can be rather sharp decreases in the oxygen levels within the layer of cells contained in a bioartificial organ or a tissue engineered construct. This places severe limitations on the thickness of the cell layer in devices that rely solely on diffusion to provide the oxygen needed by the cells (Ehsan and George, 2013). Some research groups are working to either generate oxygen *in situ* within the bioartificial organ or tissue engineered construct or periodically inject exogenous oxygen to the device as discussed in [Example 11.2](#) (Ludwig et al., 2013; Neufeld et al., 2013).

Another approach for enhancing the delivery of oxygen within these devices is to perfuse a fluid through the layer of cells. This is shown conceptually in [Figure 7.10](#). For an implantable device, a

perfusion flow of plasma through the device can be obtained by connecting the device between an artery and a vein and filtering the blood through a microporous membrane. The pressure difference between the artery and the vein will produce a flow of plasma through the device, which will carry with it dissolved oxygen and other nutrients needed by the cells.

### 7.9.1 A model of convective and diffusive transport of oxygen through a planar layer of cells

We can develop a mathematical model for the convective and diffusive transport of oxygen to the cells contained within the structure shown in Figure 7.10. The thickness of the layer of cells is given by  $\delta$  and the cell fraction is  $\phi$ . The filtration rate of the fluid through the layer of cells, i.e.,  $Q_{\text{filtrate}}$ , is given by Equation 3.4 for the given effective pressure drop over the layer of cells.

A steady-state oxygen balance over a thin shell volume of cross-sectional area  $S$  extending from  $x$  to  $x + \Delta x$  is

$$0 = -SD_T \frac{dC_{\text{oxygen}}}{dx} \Big|_x + SD_T \frac{dC_{\text{oxygen}}}{dx} \Big|_{x+\Delta x} + Q_{\text{filtrate}} C_{\text{oxygen}} \Big|_x - Q_{\text{filtrate}} C_{\text{oxygen}} \Big|_{x+\Delta x} - \Gamma_{\text{oxygen}} S \Delta x \phi \quad (7.33)$$

We then divide by  $\Delta x$  and take the limit as  $\Delta x \rightarrow 0$ . We also define the fluid *superficial velocity* as  $v_{\text{filtrate}} = \frac{Q_{\text{filtrate}}}{S}$ . Hence, we get

$$D_T \frac{d^2 C_{\text{oxygen}}}{dx^2} - v_{\text{filtrate}} \frac{dC_{\text{oxygen}}}{dx} = \phi \Gamma_{\text{oxygen}} \quad (7.34)$$

This second order differential equation requires two boundary conditions, which are

$$\begin{aligned} \text{BC1 : } & x = 0, \quad v_{\text{filtrate}} C_{\text{oxygen}}^{\text{in}} = -D_T \frac{dC_{\text{oxygen}}}{dx} \Big|_{x=0} + v_{\text{filtrate}} C_{\text{oxygen}} \Big|_{x=0} \\ \text{BC2 : } & x = \delta, \quad \frac{dC_{\text{oxygen}}}{dx} \Big|_{x=\delta} = 0 \end{aligned} \quad (7.35)$$

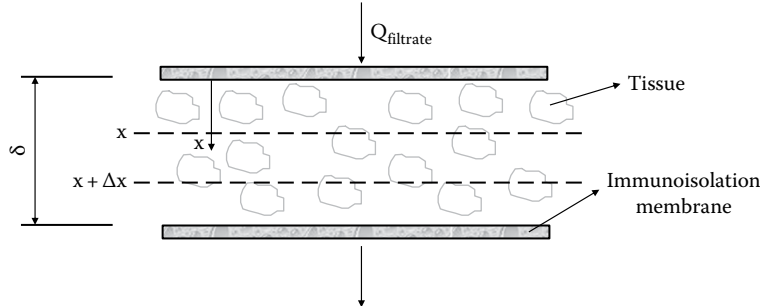


Figure 7.10 Perfusion of a planar cellular construct.

These are known as the *Danckwerts' boundary conditions*. BC1 expresses the fact that the convective rate at which oxygen enters the cellular layer on the feed side of  $x = 0$  has to equal the rate at which oxygen is transported by diffusion and convection within the layer of cells at  $x = 0$ . The concentration of oxygen in the fluid exiting the cellular layer is not known and must be found from the solution to [Equation 7.34](#). BC2 is a requirement on the oxygen profile at  $x = \delta$  so that the following mass balance condition is satisfied, i.e.,  $v_{\text{filtrate}} C_{\text{oxygen}}^{\text{out}} = v_{\text{filtrate}} C_{\text{oxygen}}|_{x=\delta}$ .

The solution of [Equations 7.34](#) and [7.35](#) is facilitated by defining a dimensionless oxygen concentration and a dimensionless distance in the cellular layer, where  $\theta \equiv \frac{C_{\text{oxygen}}}{C_{\text{oxygen}}^{\text{in}}} = \frac{pO_2}{pO_2^{\text{in}}}$  and  $\eta \equiv \frac{x}{\delta}$ . Upon substituting these dimensionless variables for  $C_{\text{oxygen}}$  and  $x$  into [Equations 7.34](#) and [7.35](#), we get

$$\begin{aligned} \frac{d^2\theta}{d\eta^2} - \left( \frac{v_{\text{filtrate}}\delta}{D_T} \right) \frac{d\theta}{d\eta} &= \left[ \frac{\phi\Gamma_{\text{oxygen}}\delta^2}{D_T C_{\text{oxygen}}^{\text{in}}} \right] \\ \frac{d^2\theta}{d\eta^2} - Pe \frac{d\theta}{d\eta} &= Da \end{aligned} \quad (7.36)$$

In [Equation 7.36](#) we also have formed two dimensionless groups. The first is the *Peclet number* ( $Pe$ ) that is given by  $Pe = \frac{v_{\text{filtrate}}\delta}{D_T}$  and the *Damkohler number* ( $Da$ ) that is given by  $Da = \left[ \frac{\phi\Gamma_{\text{oxygen}}\delta^2}{D_T C_{\text{oxygen}}^{\text{in}}} \right]$ .

The Peclet number represents the ratio of the rate of the convective transport of oxygen to the diffusive transport rate of oxygen. If the  $Pe \gg 1$ , then convection will dominate the transport of oxygen within the cellular layer. If the  $Pe \ll 1$ , then the diffusive transport of oxygen dominates.

The Damkohler number represents the ratio of the rate of oxygen consumption by the cells to the diffusive transport rate of oxygen. If  $Da \gg 1$ , then the cells' oxygen consumption rate is much higher than the rate at which diffusion can provide the oxygen needed by the cells. In this case, we would expect to see large decreases in the oxygen concentration or  $pO_2$  within the layer of cells. On the other hand, if  $Da \ll 1$ , then in comparison, the oxygen consumption rate by the cells is much smaller than the rate at which oxygen can be supplied by diffusion, and we would expect very little change in the oxygen concentration or the  $pO_2$  through the layer of cells.

Using these dimensionless variables, the boundary conditions in [Equation 7.35](#) become

$$\begin{aligned} BC1: \quad \eta = 0, \quad 1 &= - \frac{1}{Pe} \frac{d\theta}{d\eta} \Big|_{\eta=0} + \theta \Big|_{\eta=0} \\ BC2: \quad \eta = 1, \quad \frac{d\theta}{d\eta} \Big|_{\eta=1} &= 0 \end{aligned} \quad (7.37)$$

Since the  $Pe$  and  $Da$  are constant in the situation we are considering, we can obtain an analytical solution to [Equations 7.36](#) and [7.37](#). After solving [Equation 7.36](#) and finding the two integration constants using [Equation 7.37](#), we obtain

$$\theta(\eta) = 1 - \left( \frac{Da}{Pe^2} \right) \left( 1 - e^{-Pe(1-\eta)} \right) - \left( \frac{Da}{Pe} \right) \eta \quad (7.38)$$

If  $\text{Pe} \gg \text{Da}$  and  $\text{Pe} \gg 1$ , then Equation 7.38 says that  $\theta(\eta)=1$  or that the concentration of oxygen, or the  $p\text{O}_2$  throughout the cellular layer, is the same as the oxygen concentration or  $p\text{O}_2$  in the fluid entering the construct, i.e.,  $C_{\text{oxygen}}(\eta) = C_{\text{oxygen}}^{\text{in}}$  and  $p\text{O}_2(\eta) = p\text{O}_2^{\text{in}}$ . The same result occurs for  $\text{Da} = 0$ , meaning that there is no consumption of oxygen by the cells.

The exiting oxygen concentration or  $p\text{O}_2$  can be found from Equation 7.38 by setting  $\eta = 1$ . Hence,

$$\theta^{\text{out}} = 1 - \frac{\text{Da}}{\text{Pe}} \quad (7.39)$$

Since  $\theta^{\text{out}}$  has to be greater than a minimum critical value, i.e.,  $\theta_{\text{critical}}$ , this means that Equation 7.39 imposes a condition on  $\text{Da}$  and  $\text{Pe}$ , i.e.,

$$\frac{\text{Da}}{\text{Pe}} \leq 1 - \theta_{\text{critical}} \quad \text{or} \quad 0 \leq \theta_{\text{critical}} \leq 1 - \frac{\text{Da}}{\text{Pe}} \quad (7.40)$$

If  $\theta_{\text{critical}} = 0$ , then we see from Equation 7.40 that  $\frac{\text{Da}}{\text{Pe}} \leq 1$  or  $\text{Pe} \geq \text{Da}$ .

### Example 7.10

Consider a thin planar tissue engineered construct (see Figure 7.10) with a thickness ( $\delta$ ) of 400  $\mu\text{m}$ . The device is connected between an artery and a vein that generates a plasma filtrate flow with a superficial residence time within the device of 2 s. If the plasma entering the device has a  $p\text{O}_2 = 70 \text{ mmHg}$ , calculate the  $p\text{O}_2$  of the plasma leaving the device. The cellular oxygen consumption rate is  $25 \mu\text{M s}^{-1}$ , and the effective diffusivity of oxygen through the layer of cells is  $2.4 \times 10^{-5} \text{ cm}^2 \text{ s}^{-1}$ . Henry's constant for oxygen is  $0.74 \text{ mmHg } \mu\text{M}^{-1}$ . The volume fraction of cells in the device is 0.6. If the device could only rely on the diffusion of oxygen, at what distance into the device would the  $p\text{O}_2 = 10 \text{ mmHg}$ ?

### Solution

We can use Equation 7.39 to find the  $p\text{O}_2$  of oxygen in the plasma leaving the device. First, we calculate the Damkohler number:

$$\text{Da} = \left[ \frac{\phi \Gamma_{\text{oxygen}} \delta^2}{D_T C_{\text{oxygen}}^{\text{in}}} \right] = \frac{0.6 \times 25 \mu\text{M s}^{-1} \times (0.04 \text{ cm})^2}{2.4 \times 10^{-5} \text{ cm}^2 \text{ s}^{-1} \times \frac{70 \text{ mmHg}}{0.74 \text{ mmHg } \mu\text{M}^{-1}}} = 10.57$$

From the superficial residence time ( $\tau$ ) within the device of 2 s, we can calculate the superficial velocity of the plasma flow in the device:

$$v_{\text{filtrate}} = \frac{\delta}{\tau} = \frac{0.04 \text{ cm}}{2 \text{ s}} = 0.02 \text{ cm s}^{-1}$$

Hence, the Peclet number is

$$\text{Pe} = \frac{v_{\text{filtrate}} \delta}{D_T} = \frac{0.02 \text{ cm s}^{-1} \times 0.04 \text{ cm}}{2.4 \times 10^{-5} \text{ cm}^2 \text{ s}^{-1}} = 33.33$$

From [Equation 7.39](#) we can calculate the value of  $\theta^{\text{out}}$ :

$$\theta^{\text{out}} = 1 - \frac{Da}{Pe} = 1 - \frac{10.57}{33.33} = 0.683$$

$$pO_2^{\text{out}} = \theta^{\text{out}} \times pO_2^{\text{in}} = 0.683 \times 70 \text{ mmHg} = 47.80 \text{ mmHg}$$

If we let a  $pO_2 = 10 \text{ mmHg}$  be the limiting value, then we see that the filtration flow of plasma through the layer of cells provides sufficient oxygen to the cells in the construct since  $pO_2^{\text{out}}$  is greater than 10 mmHg. If diffusion is the only mechanism for oxygen transport to these cells, then we can use [Equation 7.26](#) to find the value of  $\delta$ , which makes the  $pO_2(x = \delta) = 10 \text{ mmHg}$ . Hence,

$$pO_2(x = \delta) = pO_2^{x=0} - \left[ \frac{\Gamma_{\text{oxygen}} H_{\text{oxygen}} \phi \delta^2}{2 D_T} \right]$$

and

$$\delta_{\text{diffusion}} = \sqrt{\frac{2 D_T (pO_2^{x=0} - pO_2(x = \delta))}{\phi \Gamma_{\text{oxygen}} H_{\text{oxygen}}}} = \sqrt{\frac{2 \times 2.4 \times 10^{-5} \text{ cm}^2 \text{ s}^{-1} (70 - 10) \text{ mmHg}}{0.6 \times 25 \mu\text{M s}^{-1} \times 0.74 \text{ mmHg } \mu\text{M}^{-1}}}$$

$$\delta_{\text{diffusion}} = 0.0161 \text{ cm} = 161 \mu\text{m}$$

### 7.9.2 A microchannel perfusion bioreactor

Tilles et al. (2001), Allen and Bhatia (2003), and Mehta and Linderman (2006) describe oxygen transport in microchannel perfusion bioreactor systems. The microchannel bioreactor also serves as a model system for the flow channels that are formed in perfusion bioreactors that are used for the production of tissue engineered constructs. The oxygen concentration within the bioreactor can be controlled by adjusting the flow rate of media thru the device.

[Figure 7.11](#) illustrates the parallel-plate microchannel bioreactor used by Allen and Bhatia (2003). Nutrient media flows through the bioreactor with an average velocity equal to  $V$ . On the lower surface, there is a monolayer of attached cells that consume the oxygen that is in the flowing stream. The entering oxygen concentration is  $C_{\text{oxygen}}^{\text{in}}$ . A steady-state shell balance for oxygen on a shell volume of the fluid of width  $W$  from  $x$  to  $x + \Delta x$  and from  $y$  to  $y + \Delta y$  can be written as

$$V \Delta y W C_{\text{oxygen}} \Big|_x - V \Delta y W C_{\text{oxygen}} \Big|_{x+\Delta x} + D_{AB} \Delta x W \frac{\partial C_{\text{oxygen}}}{\partial y} \Big|_{y+\Delta y} - D_{AB} \Delta x W \frac{\partial C_{\text{oxygen}}}{\partial y} \Big|_y = 0 \quad (7.41)$$

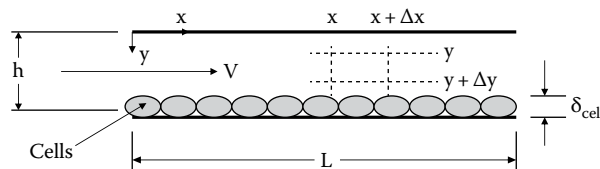


Figure 7.11 Parallel-plate microchannel bioreactor.

The amount of oxygen carried in the  $x$  direction by the fluid flow is assumed to be much greater than any solute diffusion in the  $x$  direction. However, solute diffusion in the  $y$  direction is important in this case. After dividing by  $\Delta x \Delta y$  and taking the limit as  $\Delta x$  and  $\Delta y \rightarrow 0$ , the following differential equation is obtained:

$$V \frac{\partial C_{\text{oxygen}}}{\partial x} = D_{AB} \frac{\partial^2 C_{\text{oxygen}}}{\partial y^2} \quad (7.42)$$

This is a convective-diffusion equation and describes the transport of oxygen within the parallel-plate microchannel bioreactor. The term on the left-hand side of [Equation 7.42](#) represents the transport of oxygen by convection, or the bulk flow of the fluid flowing through the bioreactor, and the term on the right-hand side represents oxygen transport by diffusion in the  $y$  direction. Recall that we have assumed that the transport of oxygen in the axial direction ( $x$ ) by convection is much larger than that transported by axial diffusion. This means that the Peclet number is much larger than unity, or  $Pe_L = \frac{VL}{D_{AB}} \gg 1$ .

The boundary conditions for [Equation 7.42](#) are

$$\begin{aligned} BC1: \quad & x = 0, \quad C_{\text{oxygen}}(0, y) = C_{\text{oxygen}}^{\text{in}} \\ BC2: \quad & y = h, \quad -D_{AB} \left. \frac{\partial C_{\text{oxygen}}}{\partial y} \right|_{y=h} = \phi \Gamma_{\text{oxygen}} \delta_{\text{cell}} \\ BC3: \quad & y = 0, \quad \left. \frac{\partial C_{\text{oxygen}}}{\partial y} \right|_{y=0} = 0 \end{aligned} \quad (7.43)$$

BC1 expresses the fact that fluid flowing through the bioreactor enters at a uniform oxygen concentration, i.e.,  $C_{\text{oxygen}}^{\text{in}}$ . BC2 expresses the fact that the flux of oxygen at the cellular surface is equal to the rate of oxygen consumption by the cells. The thickness of the cellular layer along the lower surface is  $\delta_{\text{cell}}$ , and  $\phi$  represents the volume fraction of the cells along the lower surface. BC3 says that oxygen is not consumed or lost from the upper surface of the bioreactor.

Next, we introduce the following dimensionless variables:

$$\xi \equiv \frac{x}{L}, \quad \eta \equiv \frac{y}{h}, \quad \theta \equiv \frac{C_{\text{oxygen}}}{C_{\text{oxygen}}^{\text{in}}} \quad (7.44)$$

After substituting these dimensionless variables into [Equations 7.42](#) and [7.43](#), the following dimensionless equations are obtained:

$$\frac{\partial \theta}{\partial \xi} = \frac{\alpha}{Pe_h} \frac{\partial^2 \theta}{\partial \eta^2} \quad (7.45)$$

$$\text{BC1: } \xi = 0, \quad \theta = 1$$

$$\text{BC2: } \eta = 1, \quad \left. \frac{\partial \theta}{\partial \eta} \right|_{\eta=1} = -Da \quad (7.46)$$

$$\text{BC3: } \eta = 0, \quad \left. \frac{\partial \theta}{\partial \eta} \right|_{\eta=0} = 0$$

The Peclet number ( $Pe_h$ ) in [Equation 7.45](#) is based on the flow channel thickness ( $h$ ) and is defined as  $Pe_h = \frac{Vh}{D_{AB}}$ . Also, in [Equation 7.45](#), we have the geometrical factor,  $\alpha = \frac{L}{h}$ . The Peclet number, i.e.,  $Pe_h$ , in [Equation 7.45](#) represents the ratio of oxygen transport by convection in the  $x$  direction to that transported by diffusion in the  $y$  direction. The Peclet number based on the length in the direction of flow, i.e.,  $Pe_L = \frac{VL}{D_{AB}}$ , is equal to  $Pe_h \times \alpha$ . In [Equation 7.46](#), the dimensionless oxygen flux is also known as the *Damkohler number*, defined as  $Da = \frac{\phi \Gamma_{\text{oxygen}} h \delta_{\text{cell}}}{D_{AB} C_{\text{oxygen}}^{\text{in}}}$ .

[Equations 7.45](#) and [7.46](#) can be solved analytically using separation of variables. The resulting dimensionless oxygen concentration profile can be shown to be given by [Equation 7.47](#) (Allen and Bhatia, 2003):

$$\theta(\xi, \eta) = 1 + Da \left[ \frac{1-3\eta^2}{6} - \frac{\alpha}{Pe_h} \xi + \frac{2}{\pi^2} \sum_{n=1}^{\infty} \frac{(-1)^n}{n^2} \exp\left(-\frac{\alpha n^2 \pi^2 \xi}{Pe_h}\right) \cos(n\pi\eta) \right] \quad (7.47)$$

[Equation 7.47](#) provides the oxygen concentration within the bioreactor at any position given by the dimensionless variables  $(\xi, \eta)$ . For large Peclet numbers, the summation term in [Equation 7.47](#) becomes insignificant a short distance into the bioreactor, and this solution can then be approximated by the following result:

$$\theta(\xi, \eta) \approx 1 + Da \left( \frac{1-3\eta^2}{6} - \frac{\alpha}{Pe_h} \xi \right) \quad (7.48)$$

Of particular interest is the location along the cell surface where the oxygen concentration becomes equal to zero, i.e.,  $\theta(\xi_{\text{critical}}, \eta=1)=0$ . We can then solve [Equation 7.48](#) for this critical value, which is given by

$$\xi_{\text{critical}} = \frac{x_{\text{critical}}}{L} \approx \frac{Pe_h}{\alpha} \left( \frac{1}{Da} - \frac{1}{3} \right) \quad (7.49)$$

We can also calculate the average oxygen concentration at any value of  $\xi$  by integrating [Equation 7.47](#) from  $\eta=0$  to  $\eta=1$ . The following result is then obtained for the average oxygen concentration in the bioreactor as a function of  $\xi = \frac{x}{L}$ :

$$\theta_{\text{average}}(\xi) = \frac{C_{\text{oxygen}}^{\text{average}}}{C_{\text{oxygen}}^{\text{in}}} = 1 - \left( \frac{\alpha Da}{Pe_h} \right) \xi = 1 - \left( \frac{\alpha Da}{Pe_h} \right) \frac{x}{L} \quad (7.50)$$

**Example 7.11**

Calculate the distance into the bioreactor where the cell surface  $pO_2$  reaches 0 mmHg. The flow rate through the bioreactor is  $0.5 \text{ cm}^3 \text{ min}^{-1}$ , and the inlet  $pO_2$  is 76 mmHg. Use the bioreactor parameters in the table below from Allen and Bhatia (2003). The measured Henry's constant was  $\approx 0.83 \text{ mmHg } \mu\text{M}^{-1}$ .

Parameter	Value	Units
$D_{AB}$ , oxygen diffusivity	$2 \times 10^{-5}$	$\text{cm}^2 \text{ s}^{-1}$
$V_{max}$ , max. $O_2$ uptake	0.38	$\text{nmol s}^{-1} (10^6 \text{ cells})^{-1}$
$\rho$ , surface cell density	$1.7 \times 10^5$	$\text{cells cm}^{-2}$
$pO_2^{in}$ , inlet $pO_2$	75	mmHg
$Q$ , flow rate	0.5	$\text{cm}^3 \text{ min}^{-1}$
$h$ , height of flow channel	100	microns
$W$ , width of flow channel	2.8	cm
$L$ , length of flow channel	5.5	cm

**Solution**

First we need to calculate  $\alpha$ , Da, and  $Pe_h$ .  $\alpha = L/h = 550$ . For the Da we also recognize that  $\rho V_{max} = \Gamma_{oxygen} \phi \delta_{cell}$ . Therefore, we can calculate the Da as shown in the next calculation. Note that we have divided the inlet  $pO_2$  by Henry's constant for oxygen in media to estimate the inlet oxygen concentration as  $91.6 \text{ nmol cm}^{-3}$ .

$$Da = \frac{\rho V_{max} h}{D_{AB} C_{oxygen}^{in}} = \frac{1.7 \times 10^5 \text{ cells cm}^{-2} \times 0.38 \text{ nmol s}^{-1} 10^{-6} \text{ cell}^{-1} \times 0.01 \text{ cm}}{2 \times 10^{-5} \text{ cm}^2 \text{ s}^{-1} \times 91.6 \text{ nmol cm}^{-3}} = 0.353$$

The Peclet number is then calculated as follows:

$$Pe_h = \frac{Vh}{D_{AB}} = \frac{\left( \frac{Q}{h \times W} \right) h}{D_{AB}} = \frac{0.5 \text{ cm}^3 \text{ min}^{-1} \times \frac{1 \text{ min}}{60 \text{ s}} \times \frac{1}{(0.01 \text{ cm} \times 2.8 \text{ cm})} \times 0.01 \text{ cm}}{2 \times 10^{-5} \text{ cm}^2 \text{ s}^{-1}} = 148.8$$

Using the above values of  $\alpha$ , Da, and  $Pe_h$ , we find that both Equations 7.47 and 7.49 give an  $\xi = 0.676$  or an  $x_{critical}$  of  $0.676 \times 5.5 \text{ cm} = 3.72 \text{ cm}$ .

**Example 7.12**

Allen and Bhatia (2003) obtained the following outlet  $pO_2$ 's (equivalent to the average  $pO_2$  at  $x = L$ ) for their bioreactor discussed in the previous example at various flow rates for an inlet  $pO_2 = 158 \text{ mmHg}$ . Compare these results to that predicted by Equation 7.50. Find the value of  $\rho V_{max} = \Gamma_{oxygen} \phi \delta_{cell}$  that best fits the data.

Flow Rate, $\text{cm}^3 \text{ min}^{-1}$	$pO_2$ out, mmHg
0.5	42
0.75	73
1.0	92
1.5	112
2.0	122
3.0	133

**Solution**

First, we need to calculate  $\alpha$ ,  $Da$ , and  $Pe_h$ . From before  $\alpha = L/h = 550$ . We then calculate the  $Da$  as shown below. The value of  $\rho V_{max}$  was adjusted from the value based on the data in the table from the previous example, which gives  $0.0646 \text{ nmol cm}^{-2} \text{ s}^{-1}$  to  $0.08 \text{ nmol cm}^{-2} \text{ s}^{-1}$  in order to improve the fit to the data. Note that we have divided the inlet  $pO_2$  by Henry's constant for oxygen to estimate the inlet oxygen concentration as  $190.4 \text{ nmol cm}^{-3}$ :

$$Da = \frac{\rho V_{max} h}{D_{AB} C_{oxygen}^{in}} = \frac{0.08 \text{ nmol cm}^{-2} \text{ s}^{-1} \times 0.01 \text{ cm}}{2.0 \times 10^{-5} \text{ cm}^2 \text{ s}^{-1} \times 190.4 \text{ nmol cm}^{-3}} = 0.21$$

For the Peclet number, we have to calculate a value for each of the flow rates:

$$Pe_h = \frac{Vh}{D_{AB}} = \frac{\left( \frac{Q}{h \times W} \right) h}{D_{AB}} = \frac{Q \text{ cm}^3 \text{ min}^{-1} \times \frac{1 \text{ min}}{60 \text{ s}} \times \frac{1}{(0.01 \text{ cm} \times 2.8 \text{ cm})} \times 0.01 \text{ cm}}{2.0 \times 10^{-5} \text{ cm}^2 \text{ s}^{-1}} = 298Q$$

We can then rewrite [Equation 7.50](#) at  $x = L$  as shown below replacing the concentrations with the  $pO_2$ 's and recognizing that the units on  $Q$  are  $\text{cm}^3 \text{ min}^{-1}$ :

$$pO_{2out} = pO_{2in} \left( 1 - \frac{\alpha Da}{Pe_h} \right) = 158 \text{ mmHg} \left( 1 - \frac{550 \times 0.21}{298Q} \right) = 158 \text{ mmHg} \left( 1 - \frac{0.388}{Q} \right)$$

[Figure 7.12](#) shows the comparison between the measured outlet  $pO_2$  values and those predicted by [Equation 7.50](#) as given by the previous equation derived for this example. The agreement between the data and the model is quite good when we make this modest adjustment to the value of  $\rho V_{max}$ .

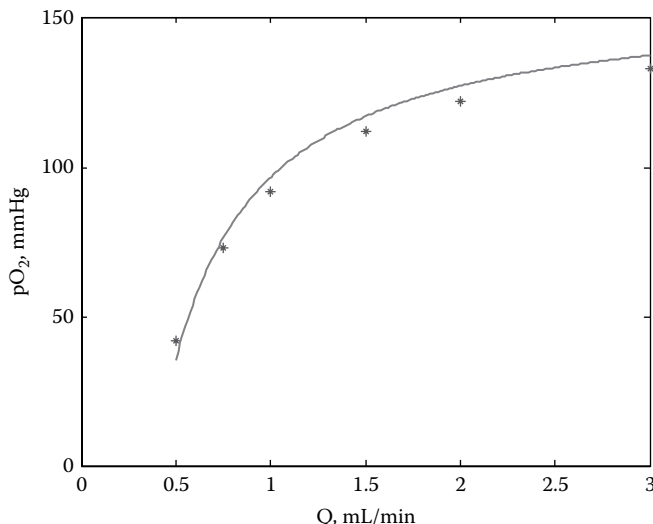


Figure 7.12 Comparison of actual and predicted exiting  $pO_2$  levels from the parallel-plate microchannel bioreactor.

## 7.10 Oxygen transport in the Krogh tissue cylinder

We can use the Krogh tissue cylinder approach (Krogh, 1919) developed earlier in [Chapter 6](#) to analyze oxygen transport to the tissue surrounding a given capillary. The Krogh tissue model is a good place to start before considering more advanced models that are described in the literature (Mirhashemi et al., 1987; Tsai et al., 1990; Lagerlund and Low, 1993; Secomb et al., 1993; Intaglietta, 1997; Li et al., 1997; Vadapalli et al., 2002; Lee et al., 2014).

### 7.10.1 Capillary oxygenated hemoglobin mass balance

[Figure 6.12](#) illustrates a concentric shell of the Krogh tissue cylinder. Considering blood first, the shell balance equation for oxygenated hemoglobin can be written as follows\*:

$$(2\pi r \Delta r \Delta z) \frac{\partial C'_{\text{HbO}}}{\partial t} = 2\pi r \Delta r V C'_{\text{HbO}} \Big|_z - 2\pi r \Delta r V C'_{\text{HbO}} \Big|_{z+\Delta z} + (2\pi r \Delta r \Delta z) R''_{\text{HbO}} \quad (7.51)$$

In [Equation 7.51](#), we ignore the particulate nature of blood as well as the mass transfer resistance of the RBC membrane. The blood is assumed to be in plug flow with an average velocity represented by  $V$ . Also, note that the hemoglobin is carried along by the RBC at the average blood velocity ( $V$ ) and accordingly there is no diffusive transport of hemoglobin.  $R''_{\text{HbO}}$  represents the production rate of oxygenated hemoglobin per unit volume of blood. After dividing by  $2\pi r \Delta r \Delta z$  and taking the limit as  $\Delta z \rightarrow 0$ , we obtain the following differential equation that describes the mass balance for oxygenated hemoglobin within the blood flowing through the capillary:

$$\frac{\partial C'_{\text{HbO}}}{\partial t} + V \frac{\partial C'_{\text{HbO}}}{\partial z} = R''_{\text{HbO}} \quad (7.52)$$

### 7.10.2 Capillary unbound oxygen mass balance

A shell balance for the free or unbound oxygen in the blood is given by the next equation:

$$\begin{aligned} (2\pi r \Delta r \Delta z) \frac{\partial C_{\text{oxygen}}}{\partial t} &= 2\pi r \Delta r V C_{\text{oxygen}} \Big|_z - 2\pi r \Delta r V C_{\text{oxygen}} \Big|_{z+\Delta z} \\ &\quad - 2\pi r \Delta z D_{\text{oxygen}} \frac{\partial C_{\text{oxygen}}}{\partial r} \Big|_r + 2\pi r \Delta z D_{\text{oxygen}} \frac{\partial C_{\text{oxygen}}}{\partial r} \Big|_{r+\Delta z} \\ &\quad - 2\pi r \Delta r D_{\text{oxygen}} \frac{\partial C_{\text{oxygen}}}{\partial z} \Big|_z + 2\pi r \Delta r D_{\text{oxygen}} \frac{\partial C_{\text{oxygen}}}{\partial z} \Big|_{z+\Delta z} \\ &\quad + 2\pi r \Delta r \Delta z R''_{\text{oxygen}} \end{aligned} \quad (7.53)$$

In addition to the convective flow of oxygen in blood, i.e., the  $VC_{\text{oxygen}}$  terms in [Equation 7.53](#), we have also included both the axial and radial diffusion of the oxygen, i.e., the

\* Unlike the shell balances developed in [Chapter 6](#), we will now leave in the accumulation term so that we can consider, if necessary, unsteady-state problems.

$D_{\text{oxygen}} \frac{\partial C_{\text{oxygen}}}{\partial z}$  and  $D_{\text{oxygen}} \frac{\partial C_{\text{oxygen}}}{\partial r}$  terms, where  $D_{\text{oxygen}}$  is the diffusivity of oxygen in blood. In [Equation 7.53](#),  $R''_{\text{oxygen}}$  represents the production rate of oxygen per unit volume of blood. Once again, we divide by  $2\pi r \Delta r \Delta z$  and take the limit as  $\Delta r$  and  $\Delta z \rightarrow 0$ . We then obtain the following differential equation that describes the mass balance on dissolved oxygen within the capillary blood:

$$\frac{\partial C_{\text{oxygen}}}{\partial t} + V \frac{\partial C_{\text{oxygen}}}{\partial z} = D_{\text{oxygen}} \left[ \frac{1}{r} \frac{\partial}{\partial r} \left( r \frac{\partial C_{\text{oxygen}}}{\partial r} \right) + \frac{\partial^2 C_{\text{oxygen}}}{\partial z^2} \right] + R'''_{\text{oxygen}} \quad (7.54)$$

The two reaction rate terms in [Equations 7.53](#) and [7.54](#) are simply the negative of each other; therefore,  $R''_{\text{HbO}} = -R''_{\text{oxygen}}$ . This is true since the rate of disappearance of dissolved oxygen in the blood must equal the rate of appearance of oxygenated hemoglobin within the RBCs.

We can also make use of the oxygen hemoglobin dissociation curve to relate  $C'_{\text{HbO}}$  to  $C_{\text{oxygen}}$  as follows:

$$\begin{aligned} \frac{\partial C'_{\text{HbO}}}{\partial t} &= \frac{\partial C_{\text{oxygen}}}{\partial t} \left( \frac{\partial C'_{\text{HbO}}}{\partial C_{\text{oxygen}}} \right) = m \frac{\partial C_{\text{oxygen}}}{\partial t} \\ \frac{\partial C'_{\text{HbO}}}{\partial z} &= \frac{\partial C_{\text{oxygen}}}{\partial z} \left( \frac{\partial C'_{\text{HbO}}}{\partial C_{\text{oxygen}}} \right) = m \frac{\partial C_{\text{oxygen}}}{\partial z} \end{aligned} \quad (7.55)$$

where  $m = \frac{dC'_{\text{HbO}}}{dC_{\text{oxygen}}}$  is the slope of the oxygen hemoglobin dissociation curve.

[Equations 7.52](#) and [7.54](#) can now be added together, using [Equation 7.55](#) and Henry's law ([Equation 7.1](#)), to express the dissolved oxygen concentration in terms of the  $pO_2$ . We then obtain [Equation 7.56](#), which expresses the mass balance for the unbound dissolved oxygen within the capillary in terms of the oxygen partial pressure.

$$(1+m) \frac{\partial pO_2}{\partial t} + V(1+m) \frac{\partial pO_2}{\partial z} = D_{\text{oxygen}} \left[ \frac{1}{r} \frac{\partial}{\partial r} \left( r \frac{\partial pO_2}{\partial r} \right) + \frac{\partial^2 pO_2}{\partial z^2} \right] \quad (7.56)$$

**7.10.2.1 The slope of the oxygen hemoglobin dissociation curve** Before we go any further, let us take a closer look at how to evaluate the parameter  $m$ . Recall that  $m \equiv \frac{dC'_{\text{HbO}}}{dC_{\text{oxygen}}}$ , which is the slope of the oxygen hemoglobin dissociation curve. Recognizing that  $Y \equiv \frac{C'_{\text{HbO}}}{C'_{\text{SAT}}}$ , we then have that  $m = C'_{\text{SAT}} \frac{dY}{dC_{\text{oxygen}}}$ . From Henry's law, i.e.,  $pO_2 = H_{\text{oxygen}} C_{\text{oxygen}}$ , we then get

$$m = H_{\text{oxygen}} C'_{\text{SAT}} \frac{dY}{dpO_2} \quad (7.57)$$

Note that  $m$  is also dimensionless. Using Hill's equation (Equation 7.14), we can then evaluate  $\frac{dY}{dpO_2}$  in Equation 7.57 and obtain the following expression for the dependence of  $m$  on the local  $pO_2$ :

$$m = nP_{50}^n H_{\text{oxygen}} C'_{\text{SAT}} \frac{pO_2^{n-1}}{(P_{50}^n + pO_2^n)^2} \quad (7.58)$$

### 7.10.3 Tissue oxygen mass balance

A shell balance on the oxygen within the tissue surrounding the capillary can be written as follows:

$$(2\pi r \Delta r \Delta z) \frac{\partial \bar{C}_{\text{oxygen}}}{\partial t} = (-2\pi r \Delta z) D_T \left. \frac{\partial \bar{C}_{\text{oxygen}}}{\partial r} \right|_r + (2\pi r \Delta z) D_T \left. \frac{\partial \bar{C}_{\text{oxygen}}}{\partial r} \right|_{r+\Delta r} + (-2\pi r \Delta r) D_T \left. \frac{\partial \bar{C}_{\text{oxygen}}}{\partial z} \right|_z \\ + (2\pi r \Delta r) D_T \left. \frac{\partial \bar{C}_{\text{oxygen}}}{\partial z} \right|_{z+\Delta z} - 2\pi r \Delta r \Delta z \phi \Gamma_{\text{oxygen}} \quad (7.59)$$

where  $\bar{C}_{\text{oxygen}}$  is the oxygen concentration within a given volume of tissue, which consists of the cells and surrounding interstitial fluid. The product of  $\bar{C}_{\text{oxygen}}$  and this tissue volume gives the mass of oxygen in the volume of tissue.

After dividing by  $2\pi r \Delta r \Delta z$  and taking the limit as  $\Delta r$  and  $\Delta z \rightarrow 0$ , the following differential equation is obtained for the oxygen mass balance within the tissue region. Henry's law was used to express the oxygen concentration in the tissue in terms of the tissue region oxygen partial pressure,  $p\bar{O}_2$ :

$$\frac{\partial p\bar{O}_2}{\partial t} = D_T \left[ \frac{1}{r} \frac{\partial}{\partial r} \left( r \frac{\partial p\bar{O}_2}{\partial r} \right) + \frac{\partial^2 p\bar{O}_2}{\partial z^2} \right] - \phi \Gamma_{\text{oxygen}} H_{\text{oxygen}} \quad (7.60)$$

The boundary conditions needed to solve Equations 7.56 and 7.60 are

$$\begin{aligned} BC1: \quad & z = 0, \quad pO_2 = pO_2^{\text{in}}(t) \quad \text{and} \quad \frac{\partial p\bar{O}_2}{\partial z} = 0 \\ BC2: \quad & z = L, \quad \frac{\partial p\bar{O}_2}{\partial z} = 0 \quad \text{and} \quad \frac{\partial p\bar{O}_2}{\partial z} = 0 \\ BC3: \quad & r = 0, \quad \frac{\partial p\bar{O}_2}{\partial r} = 0 \\ BC4: \quad & r = r_C, \quad pO_2 = p\bar{O}_2 \quad \text{and} \quad D_{\text{oxygen}} \frac{\partial pO_2}{\partial r} = D_T \frac{\partial p\bar{O}_2}{\partial r} \\ BC5: \quad & r = r_T, \quad \frac{\partial p\bar{O}_2}{\partial r} = 0 \end{aligned} \quad (7.61)$$

BC1 expresses the fact that the  $pO_2$  of the blood entering the capillary is assumed to be known and can be a function of time. BC2 simply states that oxygen cannot leave the capillary in the

axial direction in either the blood or the tissue by axial diffusion. BC3 says that the oxygen profile is symmetric with respect to the capillary centerline. BC4 assumes the capillary wall has negligible mass transfer resistance\* and also expresses the requirement that the oxygen concentrations and the oxygen flux are continuous at the interface between the capillary and tissue regions. BC1 also says that oxygen cannot cross the boundary of the Krogh tissue cylinder by axial diffusion at the entrance of the capillary. BC5 states that the oxygen profile in the tissue region between capillaries spaced a distance  $2r_T$  (the Krogh tissue cylinder diameter) apart is symmetric.

Under certain conditions, anoxic regions can develop within the tissue region. These regions will be defined by a *critical radius*,  $r_{\text{anoxic}}(z)$ , a distance beyond which there is no oxygen in the tissue. If an anoxic region exists, then BC5 becomes

$$\text{BC6 : } r = r_{\text{anoxic}}(z), \quad \frac{\partial p\bar{O}_2}{\partial r} = 0 \quad \text{and} \quad p\bar{O}_2 = 0 \quad (7.62)$$

## 7.11 An approximate solution for oxygen transport in the Krogh tissue cylinder

The solution of the previous equations for the oxygen concentrations within the blood and tissue regions is a formidable problem and requires a numerical solution (Lagerlund and Low, 1993). However, with some simplifications, a reasonable analytical solution can be obtained, which is a good starting point for exploring the key factors that govern the oxygenation of the tissue surrounding a given capillary. We can also limit ourselves to a steady-state solution, thereby eliminating the time derivatives in these equations. Another useful approximation is to treat  $m$  as a constant. Recall that  $m$  is related to the slope of the oxygen hemoglobin dissociation curve and is given by [Equation 7.58](#). An average value of  $m$  can then be used in the range of  $pO_2$  levels of interest. Since the capillary is much longer in length than the Krogh tissue cylinder radius, we can also ignore axial diffusion within the tissue region. This greatly simplifies the equation for the tissue region, and [Equation 7.60](#) becomes

$$\frac{1}{r} \frac{\partial}{\partial r} \left( r \frac{\partial p\bar{O}_2}{\partial r} \right) = \frac{\phi \Gamma_{\text{oxygen}} H_{\text{oxygen}}}{D_T} \quad (7.63)$$

Within the capillary, we can ignore axial diffusion in comparison to axial convection, and from [Equation 7.56](#), we obtain

$$V(1+m) \frac{\partial pO_2}{\partial z} = D_{\text{oxygen}} \left[ \frac{1}{r} \frac{\partial}{\partial r} \left( r \frac{\partial pO_2}{\partial r} \right) \right] \quad (7.64)$$

[Equation 7.64](#) is a partial differential equation and is still tough to solve. One approximate approach is to eliminate the radial diffusion term by lumping (i.e., integrating the equation) over the  $r$  direction.

---

\* Recall that oxygen is lipid soluble and readily permeates the entire surface of the capillary wall.

The radial averaging of the capillary oxygen levels is appropriate here since the bulk of the oxygen mass transfer resistance is not within the capillary. Hence, we do not expect steep gradients in the oxygen concentration in the radial direction within the blood. So, lumping [Equation 7.64](#) in the  $r$  direction, we obtain

$$2\pi \int_0^{r_c} V(1+m) \frac{\partial pO_2}{\partial z} r dr = 2\pi D_{\text{oxygen}} \int_0^{r_c} \left[ \frac{1}{r} \frac{\partial}{\partial r} \left( r \frac{\partial pO_2}{\partial r} \right) \right] r dr \quad (7.65)$$

This equation can then be integrated and written as

$$2\pi(1+m)V \frac{d}{dz} \int_0^{r_c} pO_2 r dr = 2\pi D_{\text{oxygen}} r_c \frac{\partial pO_2}{\partial r} \Big|_{r_c} \quad (7.66)$$

We next recognize that the radially averaged  $pO_2$  level in the blood, i.e.,  $\langle pO_2 \rangle$ , at a given axial location  $z$  is defined by

$$\langle pO_2 \rangle = \frac{2\pi \int_0^{r_c} pO_2 r dr}{\pi r_c^2} \quad (7.67)$$

This allows [Equation 7.66](#) to be rewritten in terms of the average  $pO_2$  level in the blood as given by

$$(1+m) \frac{d\langle pO_2 \rangle}{dz} = \frac{2D_{\text{oxygen}}}{r_c V} \frac{\partial pO_2}{\partial r} \Big|_{r_c} = \frac{2D_T}{r_c V} \frac{\partial \bar{pO}_2}{\partial r} \Big|_{r_c} \quad (7.68)$$

Note that the solutions for the average oxygen level in the blood, i.e.,  $\langle pO_2 \rangle$ , and the oxygen level in the tissue region, i.e.,  $\bar{pO}_2$ , are connected through the oxygen flux terms on the right-hand side of [Equation 7.68](#), which arises from the use of BC4 in [Equation 7.61](#).

We can now proceed to obtain an analytical solution for the oxygen levels within the capillary and the tissue region. First, we integrate [Equation 7.63](#) two times and use BC4 and BC5 in [Equation 7.61](#) to obtain

$$\bar{pO}_2(r, z) = \langle pO_2(z) \rangle - \frac{r_c^2 \phi \Gamma_{\text{oxygen}} H_{\text{oxygen}}}{4D_T} \left[ 1 - \left( \frac{r}{r_c} \right)^2 \right] - \frac{r_c^2 \phi \Gamma_{\text{oxygen}} H_{\text{oxygen}}}{2D_T} \ln \left( \frac{r}{r_c} \right) \quad (7.69)$$

Although we ignored axial diffusion within the tissue region, note that the axial average capillary  $pO_2$  level, i.e.,  $\langle pO_2(z) \rangle$ , impresses an axial dependence on the tissue region  $pO_2$  level. Thus, [Equation 7.69](#) depends on the local capillary oxygen  $pO_2$  and is valid so long as  $pO_2^T > 0$  throughout the tissue region.

In some cases, part of the tissue region can become anoxic and [Equation 7.63](#) must be solved using the anoxic boundary condition given by [Equation 7.62](#). In this case, the tissue pO<sub>2</sub> is given by

$$p\bar{O}_2(r, z) = \langle pO_2(z) \rangle - \frac{r_c^2 \phi \Gamma_{oxygen} H_{oxygen}}{4D_T} \left[ 1 - \left( \frac{r}{r_c} \right)^2 \right] - \frac{r_{anoxic}^2(z) \phi \Gamma_{oxygen} H_{oxygen}}{2D_T} \ln \left( \frac{r}{r_c} \right) \quad (7.70)$$

We can find r<sub>anoxic</sub>(z) from the additional condition in [Equation 7.62](#) that requires p̄O<sub>2</sub> = 0 at r<sub>anoxic</sub>(z). By setting the left-hand side of [Equation 7.70](#) equal to zero and letting r = r<sub>anoxic</sub>(z), we then obtain the following nonlinear equation that can be solved for r<sub>anoxic</sub>(z):

$$\left( \frac{r_{anoxic}(z)}{r_c} \right)^2 \ln \left( \frac{r_{anoxic}(z)}{r_c} \right)^2 - \left( \frac{r_{anoxic}(z)}{r_c} \right)^2 + 1 = \frac{4D_T \langle pO_2(z) \rangle}{r_c^2 H_{oxygen} \phi \Gamma_{oxygen}} \quad (7.71)$$

[Equations 7.69 through 7.70](#) provide the pO<sub>2</sub> level within the tissue region under both nonanoxic and anoxic conditions for a given average capillary pO<sub>2</sub> level at axial position z.

The capillary pO<sub>2</sub> level changes with axial position and can now be found by solving [Equation 7.68](#). The solution of this equation requires that we know the value of D<sub>T</sub>  $\frac{dp\bar{O}_2}{dr} \Big|_{r_c}$ . We can get this by differentiating either [Equation 7.69](#) or [7.70](#) and evaluating the derivative at r<sub>C</sub>. On substitution of this result for the nonanoxic case, we obtain

$$\frac{d \langle pO_2(z) \rangle}{dz} = - \frac{\phi \Gamma_{oxygen} H_{oxygen}}{(1+m)V} \left[ \left( \frac{r_T}{r_c} \right)^2 - 1 \right] \quad (7.72)$$

This equation can be integrated to give the following result for the axial change in the capillary oxygen partial pressure. Note that this equation predicts that the capillary pO<sub>2</sub> level decreases linearly with axial position in the capillary:

$$\langle pO_2(z) \rangle = pO_2^{in} - \frac{\phi \Gamma_{oxygen} H_{oxygen}}{(1+m)V} \left[ \left( \frac{r_T}{r_c} \right)^2 - 1 \right] z \quad (7.73)$$

For anoxic conditions, we can simply replace r<sub>T</sub> by r<sub>anoxic</sub>(z) in [Equation 7.73](#).

At a given value of z, we can substitute the anoxic version of [Equation 7.73](#) into [Equation 7.71](#) to obtain the axial dependence of r<sub>anoxic</sub>(z). This would be the radial position for a given z at which the tissue pO<sub>2</sub> is equal to zero:

$$\left( \frac{r_{anoxic}(z)}{r_c} \right)^2 \ln \left( \frac{r_{anoxic}(z)}{r_c} \right)^2 - \left( \frac{r_{anoxic}(z)}{r_c} \right)^2 + 1 = \left[ \frac{4D_T pO_2^{in}}{r_c^2 \phi \Gamma_{oxygen} H_{oxygen}} \right] - \frac{4D_T}{(1+m)r_c^2 V} \left[ \left( \frac{r_{anoxic}(z)}{r_c} \right)^2 - 1 \right] z \quad (7.74)$$

Of particular interest are the conditions under which anoxia first begins. Anoxia will first start at the corner of the Krogh tissue cylinder represented by the coordinates  $z = L$  and  $r = r_T$ . This critical tissue  $pO_2$  level, equal to zero at the *anoxic corner*, can be found by first solving [Equation 7.73](#) for the  $pO_2$  level in the blood exiting the capillary. [Equation 7.69](#) can then be solved with  $r = r_T$  to find the value of  $p\bar{O}_2$  at the anoxic corner. One can then adjust various parameters such as  $V$  and  $\phi\Gamma_{\text{oxygen}} = \Gamma'_{\text{oxygen}}$  until  $p\bar{O}_2 = 0$  at the anoxic corner.

The Krogh tissue cylinder approach assumes that we know the Krogh tissue cylinder radius ( $r_T$ ). In [Chapter 6](#), we showed that the blood perfusion rate can be related to the Krogh tissue cylinder radius, the capillary radius and length, and the average blood velocity. This relationship is given by [Equation 6.98](#), which when solved for  $r_T$  gives the following equation:

$$r_T = r_c \sqrt{\frac{V}{q_b}} \quad (7.75)$$

## 7.12 Artificial blood

Blood is crucial for our survival and is frequently needed for the treatment of life-threatening injuries, to replace blood loss during surgery, and to treat a variety of blood disorders. The world demand for blood amounts to over 100 million units\* of blood per year. Within the United States, a blood transfusion occurs about every 4 s (Lewis, 1997). Blood banking provides in most cases an immediate source of blood to meet these needs. However, blood banking requires an extensive infrastructure for collection, testing for disease, cross-matching, and storage. In addition to potential contamination of the blood supply with infectious agents such as Zika virus, HIV, and hepatitis virus, blood itself can cause hemolytic transfusion reactions. The risks associated with blood transfusions include 0.0004%† for HIV infection, 0.001% for a fatal hemolytic reaction, 0.002%–0.03% for contracting the hepatitis virus, and 1% for a minor reaction (Intaglietta and Winslow, 1995).

Concern in recent years about the safety of the blood supply has resulted in major efforts to develop a substitute for blood. A blood substitute can replace human donor blood and potentially be used for trauma and surgery, as well as for the treatment of chronic blood disorders that require frequent transfusions. Blood substitutes are also of interest to the military because of the potential for a significant decrease in the special handling and logistical requirements of human blood on the modern battlefield.

An artificial blood must meet the two most important functions of blood given by transfusion. These are the replacement of lost plasma and the ability to transport sufficient amounts of oxygen. Hence, blood substitutes can be categorized as *volume expanders*, *oxygen carriers*, or *oxygen therapeutics*.

Blood substitutes, known as volume expanders, are inert aqueous materials that carry no more than dissolved oxygen, and these are used to increase blood volume to replace lost plasma. Examples of volume expanders include donated plasma, Ringer's solution, and a 5% dextrose solution.

\* A unit of blood is 1 pint equal to about 500 mL.

† 1% is equal to 1 transfusion incident per 100 units transfused.

Blood substitutes, known as oxygen therapeutics, also serve as volume expanders and have the capability to transport significant amounts of oxygen. These materials are designed to mimic the oxygen transport properties of human blood. The most promising oxygen therapeutics tend to be based on the use of compounds with enhanced oxygen solubility, like perfluorocarbons (PFCs) (Castro and Briceno, 2010), or solutions that contain hemoglobin or hemoglobin-like compounds.

The solubility of oxygen in solutions of PFCs can be a hundred times higher than that in plasma. Oxygen therapeutics that use hemoglobin are either using solutions containing stroma-free\* hemoglobin or camouflaged RBCs. Many products based on these approaches are in clinical trials and utilize some form of hemoglobin, PFCs, or camouflaged RBCs (Scott et al., 1997; Winslow, 1997; Goorha et al., 2003).

Both of these general approaches have their advantages and disadvantages and, regardless, a successful oxygen therapeutic must be as readily available as donated blood. Furthermore, these materials need to be universal or compatible across all blood types. They also must have minimal side effects, not cause allergic reactions, and be free of infectious agents. In order to be competitive in the marketplace, an oxygen therapeutic should also be relatively inexpensive and have a long storage life.

Several products are based on the use of stroma-free hemoglobin and are also known as *hemoglobin-based oxygen carriers*. The hemoglobin can be derived from a variety of sources. For example, hemoglobin can be of human or bovine origin; it can be derived from bacteria via genetic engineering techniques or by transgenic methods in animals and plants.

Hemoglobin, as discussed earlier, consists of four polypeptide chains, two  $\alpha$  chains and two  $\beta$  chains. The hemoglobin molecule outside of the RBC is not stable. For example, if hemoglobin is diluted in comparison to its concentration in RBCs, it will spontaneously dissociate into these smaller chains. These lower molecular weight chains are then rapidly removed from the circulation and excreted by the kidneys. Also, recall that hemoglobin by itself has a very high affinity for oxygen. Therefore, to be effective as a blood substitute, artificial blood based on hemoglobin must chemically modify the hemoglobin in order to improve its stability and to decrease its affinity for oxygen. Therefore, the  $P_{50}$  value obtained for artificial blood based on hemoglobin therefore needs to be comparable to that of normal human blood.

PFCs are hydrocarbons in which the bonds between C and H are replaced by the much stronger C and F bonds. These strong C-F bonds give PFCs their chemical inertness (Shah and Mehra, 1996). PFCs also exhibit high oxygen solubility and they are for the most part biocompatible and have a low cost. However, a disadvantage of PFCs is that they are immiscible with water. In order to be used as a blood substitute, they must first be emulsified into tiny droplets typically in the range of 0.1–0.2  $\mu\text{m}$  in diameter. The droplets are also frequently coated with phospholipids derived from egg yolk to stabilize the emulsion.

Oxygenated blood carries about 20 mL of oxygen (at 37°C and 760 mmHg) per 100 mL of blood. A pure PFC solution in equilibrium with oxygen at 760 mmHg has an average oxygen solubility of about 50 mL of oxygen per 100 mL of PFC (Gabriel et al., 1996). PFCs also exhibit a linear equilibrium relationship between the oxygen solubility and the  $\text{pO}_2$ . Unlike blood containing hemoglobin, PFCs do not saturate and they can therefore transport more oxygen by simply increasing the  $\text{pO}_2$  level in the gas breathed by the patient. Because of their relatively high vapor pressure, a portion of the PFCs is removed from the circulation by evaporation via respiration.

---

\* Stroma-free in this case means without the red blood cell and its cellular framework.

Artificial blood based on modified hemoglobin or PFCs still face some significant development problems. Key among these problems are gastrointestinal complaints and vasoconstriction (reduction in blood vessel diameter) when using hemoglobin products and flu-like symptoms and thrombocytopenia (very low quantity of platelets) when using PFCs. This artificial blood also exhibits short lifetimes in the circulation. Modified hemoglobin lasts on the order of 12 h to 2 days, whereas PFCs are removed in about 12 h. In comparison, normal RBCs have lifetimes of about 120 days. Until the lifetimes of these products can be significantly improved, they will only be able to be used for acute situations such as trauma and surgery (Winslow, 1997).

Another promising approach that can overcome some of the problems of artificial blood based on modified hemoglobin or PFCs (Scott et al., 1997) is to covalently bind substances like polyethylene glycol (PEG) to the surfaces of intact RBCs. The RBCs appear to be not affected by the presence of the PEG coat. The PEG molecules have the effect of masking or camouflaging the surface antigens on the RBC that lead to the various blood types in the case of human blood or that trigger rejection in the case of animal RBCs. The result is a universal blood type that could allow the use of unmatched human or animal RBCs. The camouflaged RBCs should have a lifetime that is comparable to that of a normal RBC.

### Example 7.13

Show that oxygenated blood carries about 20 mL of oxygen (based on 37°C and 760 mmHg) per 100 mL of blood.

#### Solution

First, we need to calculate the gas density of oxygen at these conditions as shown by the following calculation:

$$\rho_{\text{oxygen}} = \frac{P}{RT} = \frac{760 \text{ mmHg} \times \frac{1 \text{ atm}}{760 \text{ mmHg}}}{0.08206 \text{ atm L mol}^{-1} \text{ K}^{-1} \times 310 \text{ K}} = 0.0393 \text{ mol L}^{-1}$$

From [Table 7.2](#), oxygenated blood has a total oxygen (dissolved and bound to hemoglobin) concentration of 8620 μM. We can then recast this result in terms of the volume of oxygen as a gas that is dissolved in 100 mL of blood as

$$\begin{aligned} V_{\text{oxygen}} &= 8630 \text{ } \mu\text{M} \times \frac{\mu\text{mol oxygen}}{\mu\text{M} \times \text{L blood}} \times \frac{1 \text{ L blood}}{1000 \text{ mL blood}} \times \frac{100 \text{ mL blood}}{100 \text{ mL blood}} \times \frac{1 \text{ mol oxygen}}{10^6 \text{ } \mu\text{mol}} \\ &\quad \times \frac{1 \text{ L oxygen}}{0.0393 \text{ mol oxygen}} \times \frac{1000 \text{ mL oxygen}}{\text{L oxygen}} \\ &= 21.96 \frac{\text{mL oxygen}}{100 \text{ mL blood}} \end{aligned}$$

### Example 7.14

Based on the solubility of oxygen in a pure solution of PFC, show that Henry's constant is equal to about 0.04 mmHg μM<sup>-1</sup>. Also, show that a 40 vol.% PFC emulsion when saturated with pure oxygen at 760 mmHg has the same oxygen carrying capacity as oxygen saturated blood.

**Solution**

As previously discussed, the oxygen solubility in 100 mL of a pure solution of PFC is 50 mL at 37°C and 760 mmHg. Using the density of oxygen at these conditions found in [Example 7.13](#), we can calculate Henry's constant as

$$\begin{aligned} H_{\text{oxygen}}^{\text{PFC}} &= \frac{760 \text{ mmHg}}{\frac{50 \text{ mL oxygen}}{100 \text{ mL PFC}} \times \frac{1000 \text{ mL PFC}}{1 \text{ L PFC}} \times \frac{1 \text{ L oxygen}}{1000 \text{ mL oxygen}} \times \frac{0.0393 \text{ mol oxygen}}{\text{L oxygen}} \times \frac{10^6 \mu\text{M oxygen}}{1 \text{ mol oxygen L}^{-1}}} \\ H_{\text{oxygen}}^{\text{PFC}} &= 0.039 \text{ mmHg } \mu\text{M}^{-1} \end{aligned}$$

Since we are given that there is 50 mL of oxygen in 100 mL of a pure PFC solution, then if we have a solution that is 40% by volume PFC, the oxygen carrying capacity is reduced to 20 mL of oxygen in 100 mL of this solution, which is comparable to the oxygen carrying capacity of blood.

**Example 7.15**

An artificial blood-like fluid is flowing at the rate of 250 mL min<sup>-1</sup> through the lumens of a hollow fiber bioreactor that contains hepatoma cells on the shell side. Henry's constant for dissolved oxygen in the aqueous portion of the artificial blood is 0.71 mmHg μM<sup>-1</sup>. The artificial blood also contains an insoluble PFC material at a volume fraction of 0.60 that forms an emulsion of the PFC in the aqueous phase that has an enhanced solubility for oxygen. Henry's constant for the PFC material is equal to 0.04 mmHg μM<sup>-1</sup>, where the μM refers to the volume of the PFC oxygen-carrying material only. The pO<sub>2</sub> of the entering artificial blood is 160 mmHg. The exiting pO<sub>2</sub> of the artificial blood is 35 mmHg. Estimate the oxygen transport rate to the hepatoma cells in μmol s<sup>-1</sup> and in mL of oxygen (37°C and 760 mmHg) per minute.

**Solution**

The artificial blood can be considered to be a fluid where oxygen is dissolved in both the water phase and in the PFC emulsion phase that has enhanced oxygen solubility. The difference between the amount of oxygen in the artificial blood entering the bioreactor and leaving is equal to the amount of oxygen transported to the hepatoma cells. So we can use [Equation 7.22](#):

$$\dot{m}_{\text{oxygen}} = Q_{\text{artificial blood}} \left[ (0.4C_{\text{aqueous}} + 0.6C_{\text{PFC}})_{\text{in}} - (0.4C_{\text{aqueous}} + 0.6C_{\text{PFC}})_{\text{out}} \right]$$

Note that in the parenthetical terms, the flow rate of the artificial blood is multiplied by the respective volume fraction of the artificial blood that is the aqueous phase or the PFC emulsion phase. The dissolved oxygen concentration in each phase is represented by C<sub>aqueous</sub> and C<sub>PFC</sub>.

We can then express the dissolved oxygen concentrations in each of these phases using Henry's law as given by [Equation 7.1](#):

$$Q_{\text{oxygen}} = 250 \text{ mL min}^{-1} \times \frac{1 \text{ min}}{60 \text{ s}} \times \frac{1 \text{ L}}{1000 \text{ mL}}$$

$$\times \left[ \left( 0.40 \times \frac{160 \text{ mmHg}}{0.71 \text{ mmHg } \mu\text{M}^{-1}} + 0.60 \times \frac{160 \text{ mmHg}}{0.04 \text{ mmHg } \mu\text{M}^{-1}} \right)_{\text{in}} - \left( 0.40 \times \frac{35 \text{ mmHg}}{0.71 \text{ mmHg } \mu\text{M}^{-1}} + 0.60 \times \frac{35 \text{ mmHg}}{0.04 \text{ mmHg } \mu\text{M}^{-1}} \right)_{\text{out}} \right]$$

$$\times 1 \text{ } \mu\text{mol L}^{-1} \text{ } \mu\text{M}^{-1}$$

$$Q_{\text{oxygen}} = 8.1 \text{ } \mu\text{mol s}^{-1}$$

Using the density of oxygen at 37°C and 1 atm that was found in [Example 7.13](#), we can find the volumetric flow rate of oxygen that was transported to the hepatoma cells, as shown by the following calculation:

$$\dot{V}_{\text{oxygen}} = 8.1 \text{ } \mu\text{mol s}^{-1} \times 60 \text{ s min}^{-1} \times \frac{1 \text{ L}}{0.0393 \text{ mol}} \times \frac{1 \text{ mol}}{10^6 \text{ } \mu\text{mol}} \times 1000 \text{ ml L}^{-1}$$

$$\dot{V}_{\text{oxygen}} = 12.37 \text{ mL min}^{-1}$$

## Problems

- 7.1** The only life form that is present on the planet *Biophilus* is a small, slimy flat worm that is about 200 mm in length and about 20 mm in width. The worm survives through metabolic processes that are limited by the transport of methane present in the planet's atmosphere. The metabolic rate of methane consumption is estimated to be 15  $\mu\text{M s}^{-1}$  based on the total flesh volume, i.e.,  $\phi\Gamma_{\text{methane}}$ . The effective diffusivity ( $D_T$ ) of methane in the flesh of the worm is estimated to be about  $2.15 \times 10^{-5} \text{ cm}^2 \text{ s}^{-1}$ . The concentration of methane in the planet's atmosphere was found to be 0.20 moles  $\text{L}^{-1}$ , and the molar equilibrium solubility ratio of methane in the flesh of this worm relative to atmospheric methane is 0.10. Estimate the maximum thickness of this flat worm in millimeters.
- 7.2** Rework [Example 7.1](#) for the case of convection in the medium surrounding the Brockmann bodies and determine the volumetric tissue oxygen consumption rate ( $\Gamma_{\text{oxygen}}$ ,  $\mu\text{M s}^{-1}$ ) from the data shown in [Figure 7.1](#) for Brockmann bodies.
- 7.3** Calculate the external mass transfer coefficient ( $k_m$ ,  $\text{cm s}^{-1}$ ) for oxygen from the data shown in [Figure 7.1](#). Recall that the flux of oxygen into the spherical Brockmann body by diffusion must equal the oxygen transport rate from the bulk fluid as described by the following equation:

$$D_T \frac{d\bar{C}_{\text{oxygen}}}{dr} \Big|_{r=R} = k_m (C_{\text{oxygen}}^{\text{bulk}} - \bar{C}_{\text{oxygen}} \Big|_{r=R}) \approx \frac{1}{3} R_{\text{Brockmann body}} \Gamma'_{\text{oxygen}}$$

Show that for the case without convection, the Sherwood number (Sh) is equal to 2.

- 7.4** Derive [Equation 7.26](#).
- 7.5** For the situation described in [Example 7.6](#), determine the critical loading of islets, i.e., the void volume of the tissue space for which the  $pO_2$  becomes equal to zero at the centerline of the symmetric islet layer.
- 7.6** For the results obtained in [Example 7.6](#), determine an estimate of the blood flow rate needed to sustain a total of 750,000 islets. Each islet can be assumed to be 150 microns in diameter. What would be the diameter of such a device?
- 7.7** For the situation described in [Example 7.6](#), determine the critical oxygen permeability of the membrane, i.e., the value for which the  $pO_2$  becomes equal to zero at the centerline of the symmetric islet layer.
- 7.8** Write a short paper that discusses blood types.
- 7.9** Derive [Equation 7.69](#).
- 7.10** Derive [Equation 7.73](#).
- 7.11** Calculate the oxygen profiles within a capillary and its surrounding tissue for an islet of Langerhans. Assume blood enters the capillary at a  $pO_2 = 95$  mmHg. Also calculate the critical blood perfusion rate. Determine the anoxic boundary for a blood perfusion rate of  $0.25 \text{ mL cm}^{-3} \text{ min}^{-1}$ .
- 7.12** Consider a long and wide planar aggregate or slab of hepatocytes (liver cells) used in a bio-artificial liver. The slab is suspended in a growth medium at  $37^\circ\text{C}$  with no mass transfer limitations between the slab and the medium. The medium is saturated with air giving a  $pO_2$  of 160 mmHg, and Henry's constant for the oxygen in the medium is  $0.74 \text{ mmHg } \mu\text{M}^{-1}$ . The cell density in the slab is  $1.25 \times 10^8 \text{ cells cm}^{-3}$ . Each cell is spherical in shape and  $20 \mu\text{m}$  in diameter. The oxygen consumption rate of the cells may be described by the Michaelis-Menten relationship ([Equation 7.5](#)) with  $V_{\max} = 0.4 \text{ nmol (10}^6 \text{ cells)}^{-1} \text{ s}^{-1}$  and a  $K_m = 0.5 \text{ mmHg}$ . Estimate the maximum half-thickness of the slab of hepatocytes.
- 7.13** Photodynamic therapy (PDT) involves the localized photoirradiation of dye-sensitized tissue toward the end goal of causing cell death in tumors (Henderson and Dougherty, 1992). The tumor containing the photosensitizer is irradiated by a laser with light of the proper wavelength (around 630 nm) to generate excited singlet molecules of the sensitizer. In the presence of molecular oxygen, the singlet sensitizer forms a very reactive form of oxygen called singlet oxygen, which destroys the tumor. Therefore, sufficient levels of molecular oxygen are needed in the tissue to kill the tumor by PDT. The action of PDT on tissue oxygen levels is like having an additional sink for oxygen that is dependent on the laser fluence rate  $\phi_0$ . Foster (1993) states that this PDT-induced oxygen consumption rate can be estimated by the following equation:

$$\Gamma_{\text{PDT}} = 0.14 \left( \mu\text{M cm}^2 \text{ s}^{-1} \text{ mW}^{-1} \right) \times \phi_0 \left( \text{mW cm}^{-2} \right),$$

where  $\phi_0$  is the fluence rate.

Consider a typical capillary within the tumor undergoing PDT treatment. Assume a capillary diameter of  $8 \mu\text{m}$  and a capillary length of  $300 \mu\text{m}$ . The Krogh tissue cylinder radius is assumed to be  $40 \mu\text{m}$ . The cellular oxygen consumption rate is  $11.5 \mu\text{M s}^{-1}$ . The average velocity of blood in the capillary is  $0.04 \text{ cm s}^{-1}$ . The entering blood  $pO_2$  is 95 mmHg. Answer the following questions:

- What is the exiting  $pO_2$  of the blood from the capillary with the laser off?
- What is the  $pO_2$  in the lethal corner ( $z = L$  and  $r = r_T$ ) with the laser off?

- c. At what fluence rate is the  $pO_2$  in the lethal corner equal zero? Note this is the point at which PDT starts to be ineffective for those cancer cells at the outer periphery of the Krogh tissue cylinder.
- 7.14** Consider the design of a hollow fiber unit for an extracorporeal bioartificial liver. Blood flows through the lumens of the hollow fibers contained within the device at a flow rate of  $400 \text{ mL min}^{-1}$ . The unit consists of 10,000 fibers and the lumen diameter of a fiber is  $400 \mu\text{m}$ . The blood enters the fiber with a  $pO_2$  of  $95 \text{ mmHg}$  and must exit the device with a  $pO_2$  no lower than  $40 \text{ mmHg}$ . Surrounding each fiber is a multicellular layer of cloned human liver cells. These cells in the shell space have a volume fraction of 20%, and they consume oxygen at a rate of  $17.5 \mu\text{M s}^{-1}$  (based on cellular volume). The hollow fibers are  $25 \text{ cm}$  in length and the fiber wall provides negligible resistance to the transport of oxygen. Determine the maximum thickness of the layer of cells that can surround each fiber. Carefully state your assumptions.
- 7.15** A nonwoven mesh of polyglycolic acid (PGA) is proposed to serve as the support for growing cells *in vitro* for the regeneration of tissue. The PGA mesh is a square pad  $1 \text{ cm} \times 1 \text{ cm}$  and  $0.5 \text{ mm}$  thick. The PGA mesh has a porosity of 97% and the edges of the mesh are clamped within a support. The cells were found to consume oxygen at a rate of  $2.14 \times 10^{-13} \text{ mol cell}^{-1} \text{ h}^{-1}$ . Assuming the cells are cultured in a well-perfused growth media that is saturated with air, estimate the maximum number of cells that can be grown within each PGA mesh. Assume the diameter of a cell is about 20 microns. Carefully state your assumptions.
- 7.16** Blood perfuses a region of tissue at a flow rate of  $0.35 \text{ mL min}^{-1} \text{ cm}^{-3}$  of tissue. The  $pO_2$  of the entering blood is  $95 \text{ mmHg}$  and the exiting  $pO_2$  of the blood is  $20 \text{ mmHg}$ . Calculate the oxygen consumption rate of the tissue in  $\mu\text{M s}^{-1}$ .
- 7.17** Consider a slab layer of cells being grown within an artificial support structure. The layer of cells is immersed in a well-mixed nutrient medium maintained at a  $pO_2 = 150 \text{ mmHg}$ . The cells are known to consume oxygen at the rate of  $40 \mu\text{M s}^{-1}$ . Estimate the maximum half-thickness of the cell layer (cm) assuming the cell volume fraction in the tissue layer is 0.80.
- 7.18** A tumor spheroid, 400 microns in diameter, is suspended in a very large and quiescent media at  $37^\circ\text{C}$  with a  $pO_2$  of  $120 \text{ mmHg}$ . The  $pO_2$  at the surface of the spheroid was measured to be  $100 \text{ mmHg}$ . Estimate the oxygen consumption rate of the cells in the spheroid in  $\mu\text{M s}^{-1}$ . Assume  $H_{\text{oxygen}} = 0.74 \text{ mmHg } \mu\text{M}^{-1}$  and  $\phi = 0.15$ .
- 7.19** Blood flows through a membrane oxygenator at a flow rate of  $5000 \text{ mL min}^{-1}$ . The entering  $pO_2$  of the blood is  $40 \text{ mmHg}$  and the exiting blood  $pO_2$  is  $95 \text{ mmHg}$ . Calculate the amount of oxygen transported into the blood in  $\mu\text{mol s}^{-1}$  and in  $\text{mL}$  of oxygen per minute at  $37^\circ\text{C}$  and  $1 \text{ atm}$ .
- 7.20** Consider a slab layer of cells being grown between two microporous support membranes. The half-thickness of the cell layer is  $125 \mu\text{m}$  and the cell volume fraction is 0.10. The permeability of oxygen through the support membrane is estimated to be equal to  $1.5 \times 10^{-3} \text{ cm s}^{-1}$ . The layer of cells is immersed in a well-mixed nutrient medium maintained at a  $pO_2 = 150 \text{ mmHg}$ . An oxygen microelectrode placed at the centerline of the layer of cells gives a  $pO_2$  reading of  $15 \text{ mmHg}$ . Estimate the rate at which these cells are consuming oxygen in  $\mu\text{M s}^{-1}$ .
- 7.21** Blood is flowing at the rate of  $200 \text{ mL min}^{-1}$  through the lumens of a hollow fiber unit containing hepatocytes on the shell side. The  $pO_2$  of the entering blood is  $95 \text{ mmHg}$  and the exiting  $pO_2$  of the blood is  $20 \text{ mmHg}$ . The volume of hepatocytes on the shell side of the device is estimated to be about  $600 \text{ mL}$ . Estimate the metabolic oxygen consumption rate of the hepatocytes in  $\mu\text{M s}^{-1}$ .

- 7.22** Consider a slab layer of cells being grown within an artificial support structure. The layer of cells is immersed in a well-mixed nutrient medium maintained at a  $pO_2 = 130$  mmHg. The cells are known to consume oxygen at a rate of  $10 \mu M s^{-1}$ , and the half-thickness of the slab of cells is  $35 \mu m$ . Estimate the cell volume fraction in the tissue.
- 7.23** Blood perfuses a region of tissue at a flow rate of  $0.50 \text{ mL min}^{-1}\text{cm}^{-3}$  of tissue. The  $pO_2$  of the entering blood is 95 mmHg, and the exiting  $pO_2$  of the blood is 30 mmHg. Calculate the oxygen consumption rate of the tissue in  $\mu M s^{-1}$ .
- 7.24** Consider a slab layer of cells being grown within an artificial support structure. The layer of cells is immersed in a well-mixed nutrient medium maintained at a  $pO_2 = 140$  mmHg. The cells are known to consume oxygen at a rate of  $30 \mu M s^{-1}$ . Estimate the maximum half-thickness of the cell layer (microns) assuming the cell volume fraction in the tissue layer is 0.80.
- 7.25** In a tissue engineered vascularized tissue construct,  $pO_2$  measurements were taken *in vivo* in the region equidistant from the capillaries using luminescent oxygen-sensitive dyes. This  $pO_2$  value, which is basically at the Krogh tissue cylinder radius, was found to be 10 mmHg, and the average concentration of oxygen in the blood in the capillaries was  $100 \mu M$ . Histological analysis of the tissue samples indicated that the capillaries were pretty much parallel to each other. The average distance between the capillaries, measured center to center, was found to be  $130 \mu m$ . The capillaries themselves are  $7 \mu m$  in diameter, and the rate of oxygen uptake for the cells surrounding the capillaries is estimated to be  $30 \mu M s^{-1}$ . From these data, estimate the diffusivity of oxygen through the tissue surrounding the capillaries.
- 7.26** Islets of Langerhans are sequestered from the immune system in a device like that shown in [Figure 7.7](#). The  $pO_2$  of the blood in the capillaries adjacent to the immunoisolation membrane is 40 mmHg. The membrane oxygen permeability is  $9.51 \times 10^{-4} \text{ cm s}^{-1}$ . If the islets consume oxygen at the rate of  $25.9 \mu M s^{-1}$ , estimate the maximum half-thickness of the islet tissue in centimeters assuming a cell volume fraction in the islet layer of  $\phi = 0.05$ .
- 7.27** A laboratory-scale bioartificial liver consists of a single hollow fiber that is  $500 \mu m$  in diameter and 25 cm in length. The flow rate of blood through the fiber is  $0.2 \text{ mL min}^{-1}$ . The blood enters the fiber with a  $pO_2$  of 95 mmHg and exits the fiber at a  $pO_2$  of 35 mmHg. Surrounding the hollow fiber is a confluent layer of cloned human liver cells that consume oxygen at a rate of  $25 \mu M s^{-1}$  (based on cell volume). Assume the hollow fiber wall provides negligible resistance to the transport of oxygen. Determine the maximum thickness of the layer of cells that can surround the hollow fiber.
- 7.28** A laboratory-scale bioartificial liver consists of 10,000 hollow fibers that are  $500 \mu m$  in diameter and 25 cm in length. The blood enters the fibers with a  $pO_2$  of 95 mmHg and exits the fibers at a  $pO_2$  of 35 mmHg. Surrounding each of the hollow fibers is a single confluent layer of cloned human liver cells that consume oxygen at a rate of  $25 \mu M s^{-1}$ . The thickness of the layer of cells is  $25 \mu m$ . Assume the hollow fiber wall provides negligible resistance to the transport of oxygen. Determine the total flow rate of the blood in  $\text{mL min}^{-1}$  needed to provide these conditions.
- 7.29** Design a planar-disk bioartificial pancreas for the treatment of diabetes, i.e., find the dimensions of the device, the thickness, and the radius. Assume that the device will contain a total of 50 million genetically modified human  $\beta$  cells. Each of these cells has a diameter of  $15 \mu m$  and when packed into the device the cell volume fraction must be 0.85. The immunoisolation membrane has a thickness of  $50 \mu m$  and a porosity of 0.80. Assume the cells consume oxygen at a rate of  $25 \mu M s^{-1}$  and that the  $pO_2$  in the blood adjacent to the immunoisolation membrane is 40 mmHg.

- 7.30 Rework [Problem 7.29](#) assuming there are 500 million cells.
- 7.31 Generate the cell-surface oxygen concentration profiles in the bioreactor studied by Allen and Bhatia (2003) for an inlet flow rate of  $0.5 \text{ cm}^3 \text{ min}^{-1}$  and inlet oxygen concentrations from 90 to  $190 \text{ nmol cm}^{-3}$ . Other data can be found in [Example 7.11](#).
- 7.32 Starting with [Equation 7.11](#), derive [Equation 7.14](#), where Y is given in terms of the  $P_{50}$ , n, and  $pO_2$ . Also show how [Equation 7.14](#) can be rearranged to give [Equation 7.15](#).
- 7.33 Write a short paper that reviews the current state of artificial blood development.
- 7.34 Blood is flowing at a rate of  $250 \text{ mL min}^{-1}$  through the lumens of a hollow fiber unit that contains hepatoma cells on the shell side. The  $pO_2$  of the entering blood is 95 mmHg. The volume of the hepatoma cells is 500 mL. The hepatoma cells consume oxygen at a rate of  $20 \mu\text{M s}^{-1}$  (based on the cell volume). Show that the exiting  $pO_2$  of the blood is about 37.5 mmHg.
- 7.35 Consider the oxygen transport within a flat disk-shaped tumor of total thickness  $250 \mu\text{m}$ . The surfaces of the tumor are covered with capillaries such that the oxygen concentration at the surface of the tumor is equal to  $120 \mu\text{M}$ . A microelectrode placed at the center of the tumor showed that the  $pO_2$  was equal to 15 mmHg, and a tissue sample indicated that the volume fraction of the tumor cells was equal to 0.45. From these data, estimate the oxygen consumption rate of the tumor cells in  $\mu\text{M s}^{-1}$ .
- 7.36 A blood oxygenator for a small child needs to deliver  $0.5 \text{ mol h}^{-1}$  of oxygen to the blood. Assuming the blood enters the oxygenator at a  $pO_2$  of 40 mmHg and leaves at 95 mmHg, estimate the required flow rate of blood ( $\text{L min}^{-1}$ ) through this oxygenator.
- 7.37 A thin cylindrical disk of genetically transformed hepatocytes  $2.5 \text{ cm}$  in diameter is suspended in a nutrient solution at  $37^\circ\text{C}$ . The nutrient solution has a density of  $1 \text{ g cm}^{-3}$  and a viscosity of  $0.0012 \text{ Pa s}$ . The oxygen diffusivity in the nutrient solution was found to be  $2.5 \times 10^{-5} \text{ cm}^2 \text{ s}^{-1}$ . The half-thickness of the disk ( $\delta$ ) that contains the cells is  $150 \mu\text{m}$ , and the cell fraction is 0.35. The consumption rate of oxygen on a per cell volume basis by these cells is  $18.5 \mu\text{M s}^{-1}$ . If the  $pO_2$  of oxygen in the bulk nutrient solution is 150 mmHg, estimate the RPM that the disk needs to be rotated at so that the oxygen level at the centerline of the disk (i.e., at  $x = \delta$ ) is at least 25 mmHg. Assume Henry's constant for the oxygen in this nutrient solution is equal to  $0.73 \text{ mmHg } \mu\text{M}^{-1}$ .
- 7.38 A laboratory-scale bioartificial liver consists of a small cylindrical tube  $8 \text{ cm}$  in length. A single layer of hepatocytes lines the interior surface of the tube giving an internal diameter of the tube lumen of  $0.02 \text{ cm}$ . Nutrient media enters this tube at a flow rate of  $0.10 \text{ cm}^3 \text{ min}^{-1}$  at  $37^\circ\text{C}$  with an oxygen concentration of  $0.225 \mu\text{mol cm}^{-3}$ . Assuming the hepatocytes consume oxygen at a very fast rate, estimate the oxygen concentration in the nutrient media that leaves the tube. Assume the physical properties of the nutrient media are essentially the same as water, i.e., the density of the nutrient media is  $1 \text{ g cm}^{-3}$  and the viscosity is  $0.69 \text{ cP}$ .
- 7.39 Blood flows through an organ at a rate of  $500 \text{ mL min}^{-1}$ . The arterial  $pO_2$  of the blood is 70 mmHg and the venous  $pO_2$  is 20 mmHg. What is the oxygen consumption rate of the organ in  $\mu\text{mol s}^{-1}$ ?
- 7.40 An oxygen-impermeable contact lens is being considered for use as a drug delivery system to the eye. One concern is an inadequate supply of oxygen to the cells of the cornea. Without the contact lens in place, the oxygen comes from two sources, the aqueous humor ( $pO_2 = 55 \text{ mmHg}$ ) in contact with the inner surface of the cornea and from the tear layer ( $pO_2 = 155 \text{ mmHg}$ ) that covers the outer surface of the cornea. Since the cornea is thin with a thickness of  $0.6 \text{ mm}$ , we can neglect any curvature and consider the cornea to be flat. The diffusivity of oxygen in the cornea is  $10^{-5} \text{ cm}^2 \text{ s}^{-1}$ , and the oxygen consumption rate of the

corneal tissue expressed as  $\phi\Gamma_{\text{oxygen}}$  is equal to  $0.37 \mu\text{M s}^{-1}$ . Henry's constant for the oxygen in the aqueous humor and cornea is  $0.71 \text{ mmHg } \mu\text{M}^{-1}$ . From this information, estimate the  $p\text{O}_2$  at the interface between the contact lens and the cornea.

- 7.41** A thin circular disk of genetically transformed gecko hepatocytes 4 cm in diameter is suspended and exposed to nutrient media on both of its sides at  $37^\circ\text{C}$ . The media has a density of  $1.01 \text{ g cm}^{-3}$  and a viscosity of  $0.8 \text{ cP}$ . The oxygen diffusivity in the media was found to be  $2.4 \times 10^{-5} \text{ cm}^2 \text{ s}^{-1}$ . The half-thickness of the disk ( $\delta$ ) that contains the cells is  $150 \mu\text{m}$ , and the cell volume fraction in the disk is 0.35. The consumption rate of oxygen on a per cell volume basis by these cells is  $5 \mu\text{M s}^{-1}$ . If the  $p\text{O}_2$  in the nutrient media is maintained at  $158 \text{ mmHg}$ , estimate the oxygen level at the centerline of the disk of cells (i.e., at  $x = \delta$ ) if the disk is rotated at 10 rpm in the nutrient media. Assume Henry's constant for the oxygen in this media is equal to  $0.74 \text{ mmHg } \mu\text{M}^{-1}$ .
- 7.42** A water oxygenator consists of a cylindrical gas-permeable tube that is 1 mm in diameter and 200 cm in length. The water properties are such that its viscosity is close to 1 cP and its density is  $1 \text{ g cm}^{-3}$ . The tube wall is highly permeable to oxygen and the concentration of oxygen at the inside surface of the tube where the water is flowing is constant along the length of the tube at  $5.6 \mu\text{g cm}^{-3}$ . The diffusivity in the water flowing through the tube is equal to  $2.1 \times 10^{-5} \text{ cm}^2 \text{ s}^{-1}$ . The water is flowing through the oxygenator tube at a flow rate of  $2 \text{ cm}^3 \text{ min}^{-1}$ . If there is no oxygen in the water entering the oxygenator and the exiting oxygen concentration in the water leaving the oxygenator tube is equal to  $4.0 \mu\text{g cm}^{-3}$ , use these data to find the average mass transfer coefficient in  $\text{cm s}^{-1}$ .
- 7.43** For the conditions given in [Problem 7.42](#), make a prediction using a suitable mass transfer coefficient correlation of what the average mass transfer coefficient should be in  $\text{cm s}^{-1}$ .
- 7.44** Blood is being used to provide oxygen to one liter of cells growing in a bioreactor. If the blood enters the bioreactor with a  $p\text{O}_2 = 85 \text{ mmHg}$  and leaves the device at a  $p\text{O}_2$  of  $25 \text{ mmHg}$ , estimate what the flow rate of the blood ( $\text{mL min}^{-1}$ ) needs to be if the cells in the bioreactor consume oxygen at a rate  $20 \mu\text{M s}^{-1}$ .
- 7.45** A thin circular disk of genetically transformed cells 3 cm in diameter is suspended in a nutrient solution at  $37^\circ\text{C}$ . The nutrient solution has a density of  $1 \text{ g cm}^{-3}$  and a viscosity of  $1.2 \text{ cP}$ . The oxygen diffusivity in the nutrient solution was found to be  $2.2 \times 10^{-5} \text{ cm}^2 \text{ s}^{-1}$ , and the effective diffusivity of oxygen through the layer of immobilized cells is  $1.9 \times 10^{-5} \text{ cm}^2 \text{ s}^{-1}$ . The half-thickness of the disk ( $\delta$ ) that contains the cells is  $150 \mu\text{m}$ , and the cell fraction in the disk is 0.35. The metabolic consumption rate of oxygen on a per cell volume basis by these cells is  $18.5 \mu\text{M s}^{-1}$ . If the  $p\text{O}_2$  in the bulk nutrient solution is  $150 \text{ mmHg}$ , estimate the oxygen level at the centerline of the disk (i.e.,  $x = \delta$ ) if the disk is rotated at 25 rpm. Assume Henry's constant for the oxygen in this nutrient solution is equal to  $0.68 \text{ mmHg } \mu\text{M}^{-1}$ .
- 7.46** A tube that is 1 mm in diameter and 200 cm in length has a solution flowing within it. The viscosity of this solution is  $0.01 \text{ g cm}^{-1} \text{ s}^{-1}$  and has a density of  $1 \text{ g cm}^{-3}$ . The tube wall is porous to the transport of oxygen, and the oxygen concentration at the surface of the wall in contact with the solution is  $175 \mu\text{M}$ . The diffusivity of oxygen in the solution flowing through the tube is equal to  $2.3 \times 10^{-5} \text{ cm}^2 \text{ s}^{-1}$ . The pressure drop per unit length of the tube is  $0.1 \text{ mmHg cm}^{-1}$ . The solution entering the tube is free of oxygen. What is the concentration of oxygen ( $\mu\text{M}$ ) in the solution as it exits the tube?
- 7.47** Blood is being used as a source of oxygen for cells that are growing in a tissue engineered construct. The design assumes that blood enters the device with a  $p\text{O}_2 = 95 \text{ mmHg}$  and leaves the device with a  $p\text{O}_2 = 25 \text{ mmHg}$ . If the cells in the device consume oxygen at a rate

of  $20 \mu\text{M s}^{-1}$  and there are  $100 \text{ mL}$  of cells, what is the required flow rate of the blood in  $\text{mL min}^{-1}$  to meet this oxygen demand?

- 7.48** A perfusion bioreactor consists of a layer of cells  $1.5 \text{ mm}$  thick that is supported between two very thin macroporous titanium meshes. A nutrient medium flows through the bioreactor in the direction of the cell layer thickness. The cell volume fraction is  $0.35$  and the cells consume oxygen at a rate of  $21 \mu\text{M s}^{-1}$ . The effective diffusivity of oxygen within the layer of cells has been estimated to be  $2.05 \times 10^{-5} \text{ cm}^2 \text{ s}^{-1}$ . The oxygen concentration in the fluid that enters this bioreactor is equal to  $200 \mu\text{M}$ . The exiting oxygen concentration of the fluid leaving this bioreactor cannot be less than  $25 \mu\text{M}$ . Estimate the flow rate of the nutrient medium in  $\text{cm}^3 \text{ min}^{-1}$ . The cross-sectional area of the cell layer normal to the flow of the nutrient medium is  $64 \text{ cm}^2$ .
- 7.49** A laboratory-scale bioreactor consists of a small cylindrical tube  $10 \text{ cm}$  in length. A single layer of genetically modified cells lines the interior surface of the tube giving an internal diameter of the tube lumen of  $0.025 \text{ cm}$ . Nutrient media enters this tube at a flow rate of  $10 \text{ cm}^3 \text{ h}^{-1}$  at  $37^\circ\text{C}$  with an oxygen concentration of  $0.25 \mu\text{mol cm}^{-3}$ . Assuming the cells consume oxygen at a very fast rate, estimate the oxygen concentration ( $\mu\text{mol cm}^{-3}$ ) in the nutrient media that leaves the tube. The nutrient media has a viscosity of  $0.85 \text{ cP}$ , and its density is  $1 \text{ g cm}^{-3}$ . The oxygen diffusivity in the media is  $2 \times 10^{-5} \text{ cm}^2 \text{ s}^{-1}$ .
- 7.50** A monolayer of *Andromedian qwak* cells is being grown on one side of a  $4 \text{ cm}$  circular disk. The disk containing the cells is in nutrient media maintained at a temperature of  $37^\circ\text{C}$  and is spun at a rotation speed of  $15 \text{ rpm}$ . Oxygen is sparged into the media and the bulk  $\text{pO}_2$  is estimated to be  $160 \text{ mmHg}$ . Henry's constant for the oxygen in this media is  $0.7 \text{ mmHg } \mu\text{M}^{-1}$ . If the monolayer of qwak cells on the disk surface consumes oxygen at a rate of  $0.10 \text{ nmol cm}^{-2} \text{ s}^{-1}$ , estimate the  $\text{pO}_2$  in  $\text{mmHg}$  at the surface of the monolayer of cells. The media density is  $1 \text{ g cm}^{-3}$ , and its viscosity is  $0.70 \text{ cP}$ .
- 7.51** A design for a bioreactor consists of a thin layer of cultured cells that are immobilized within a gel-like material that coats the inside surfaces of a rectangular flow channel. Assume that the cell fraction in the gel-like layer is  $0.65$  and that these cells consume oxygen at a rate of  $19.5 \mu\text{M s}^{-1}$ . The nutrient media is fed to the bioreactor at a temperature of  $37^\circ\text{C}$  and at a sufficiently high flow rate that the average  $\text{pO}_2$  in the media flowing in the bioreactor can be taken as  $85 \text{ mmHg}$ . The flow channel cross section has a width of  $10 \text{ cm}$  and a slit thickness of  $0.2 \text{ cm}$  giving a hydraulic diameter of  $0.392 \text{ cm}$ . The length of the flow channel is  $20 \text{ cm}$ . The media average velocity within the flow channel is  $25 \text{ cm s}^{-1}$ , and the media has a viscosity of  $0.8 \text{ cP}$  and a density of  $1.03 \text{ g cm}^{-3}$ . Separate experiments have shown that the oxygen diffusivity within the layer of immobilized cells is  $1.95 \times 10^{-5} \text{ cm}^2 \text{ s}^{-1}$ , and Henry's constant is  $0.72 \text{ mmHg } \mu\text{M}^{-1}$ . The oxygen diffusivity in the bulk media is  $2.25 \times 10^{-5} \text{ cm}^2 \text{ s}^{-1}$ . Estimate the maximum thickness of the layer of cells that can coat the inside surface of the flow channel assuming that the lowest allowable  $\text{pO}_2$  within the layer of hepatocytes is  $18 \text{ mmHg}$ .
- 7.52** An artificial blood is being used as a source of oxygen for cells that are growing on the shell side in a hollow fiber bioreactor. This artificial blood has a linear oxygen dissociation relationship that is given by  $Y = (0.01 \text{ mmHg}^{-1}) \text{ pO}_2$ , where the  $\text{pO}_2$  is in  $\text{mmHg}$  and  $Y$ , i.e.,  $C'_{\text{oxygen}} / C'_{\text{SAT}}$ , is the fraction of the oxygen carrier molecules that are saturated. When the carrier molecules are saturated, i.e.,  $Y = 1$ , the associated oxygen concentration, i.e.,  $C'_{\text{SAT}}$ , is equal to  $9000 \mu\text{M}$ . Henry's constant for the artificial blood is  $0.78 \text{ mmHg } \mu\text{M}^{-1}$ . The design assumes that blood enters the device at a flow rate of  $30 \text{ mL min}^{-1}$  with a  $\text{pO}_2 = 90 \text{ mmHg}$  and

flows within the hollow fibers. If the cells in the device consume oxygen at the rate of  $20 \mu\text{M s}^{-1}$  and there are 100 mL of cells, what is the  $\text{pO}_2$  of the artificial blood leaving the bioreactor?

- 7.53** A plasma oxygenator consists of a multitude of hollow fibers. The plasma flows within these fibers at a rate of  $1 \text{ cm}^3 \text{ h}^{-1}$  per fiber. The hollow fibers have an internal diameter of 0.02 cm. Air flows through the shell space that surrounds the hollow fibers, and the concentration of oxygen at the inside surface of the hollow fibers is  $220 \mu\text{M}$ . The diffusivity of oxygen in the plasma is  $2 \times 10^{-5} \text{ cm}^2 \text{ s}^{-1}$ . Estimate how long the hollow fibers must be in order for the exiting oxygen concentration to equal 95% of the oxygen hollow fiber wall concentration. You can assume that the viscosity of the plasma is 1.2 cP and its density is  $1.024 \text{ g cm}^{-3}$ , and the entering plasma contains no oxygen.
- 7.54** In a packed bed bioreactor, mammalian cells are being grown within a hydrogel that coats the surface of solid spherical particles that are 4 mm in diameter. The volume fraction ( $\phi$ ) of the cells in the hydrogel layer that coats the spherical particles is 0.45. These cells consume oxygen at a rate of  $25 \mu\text{M s}^{-1}$ . Nutrient media flows through the packed bed bioreactor at a superficial velocity ( $V_0$ ) of  $1 \text{ cm s}^{-1}$ , with an average oxygen partial pressure ( $\text{pO}_2$ ) of 120 mmHg. If the thickness of the hydrogel layer containing the cells that coats the spherical particles is  $100 \mu\text{m}$ , estimate what the  $\text{pO}_2$  (mmHg) is at the interface between the hydrogel layer containing the cells and the surface of the spherical particle. The diffusivity of oxygen in the nutrient media is  $2.7 \times 10^{-5} \text{ cm}^2 \text{ s}^{-1}$ , and the diffusivity of oxygen in the hydrogel containing the cells is  $2.1 \times 10^{-5} \text{ cm}^2 \text{ s}^{-1}$ . The density of the nutrient media is  $1.01 \text{ g cm}^{-3}$ , and its viscosity is 0.7 cP. The nutrient media has Henry's constant of  $0.72 \text{ mmHg } \mu\text{M}^{-1}$ . Since the thickness of the hydrogel layer is much less than the radius of the spherical particle, you can neglect the curvature and assume that the oxygen diffusion in the hydrogel layer is one dimensional and planar.

# Chapter 8 Pharmacokinetic analysis

## 8.1 Terminology

In this chapter, we will focus our attention on some useful techniques in the field of pharmacokinetics. *Pharmacokinetics* (PK) is the study of the processes that affect drug distribution and the rate of change of drug concentrations within various regions of the body. These processes are also collectively referred to as ADMET for drug *adsorption*, *distribution*, *metabolism*, *excretion*, and *toxicity*. Although pharmacokinetics is of utmost importance in the treatment of diseases using drugs, our major focus will be on using this technique as a tool for understanding the transport processes in drug delivery systems and between an artificial device and the body.

We also need to distinguish pharmacokinetics from similar terms. Therefore, *pharmaceutics* concerns the formulation and preparation of the drug to achieve a desired drug availability within the body, and *pharmacodynamics* is concerned with the time course of the treatment response that results from a given drug. For example, how is the cholesterol concentration in the plasma affected by the daily doses of a particular drug? The actual physiological reason for the response that results from a drug is the subject of *pharmacology*.

## 8.2 Entry routes for drugs

There are two routes through which a drug can enter the body. The *enteral* route refers to drugs that are given via the gastrointestinal tract (GI tract). All other routes are called *parenteral*.

The enteral route includes drugs that are absorbed via one or more of the following components of the GI tract: the buccal cavity (mouth) and sublingual (beneath the tongue), gastric (stomach), intestinal (small and large intestines), and rectal. Once the drug is absorbed from the GI tract, the drug enters the blood and is distributed throughout the body. It is important, however, to point out that only drugs absorbed from the buccal cavity and the lower rectum enter the *systemic circulation* directly. Drugs absorbed from the stomach, intestines, colon, and upper rectum enter the *splanchnic circulation* (abdominal organs or viscera). The splanchnic circulation then takes the drug to the liver via the portal vein, and after leaving the liver, the drug enters the systemic circulation. Since the liver contains many enzymes capable of degrading the drug (metabolism), a significant portion of the drug can be removed during this first pass through the liver before the drug is available to the general circulation.

**Table 8.1** summarizes all of the other routes for drug administration that are called parenteral. For the most part, drugs given parenterally enter the systemic circulation directly.

As the drug is being absorbed into the body, its presence will be noticed within the circulation as its concentration in the plasma portion of the blood changes. Recall that plasma refers to the clear supernatant fluid that results from blood after the cellular components have been removed. If the blood sample is allowed to clot, then the resulting clear fluid is referred to as serum, since the

Table 8.1 Parenteral Routes for Drug Administration

Route	Result
Intravenous (IV)	Introduced directly into the venous circulation
Intramuscular	Within the muscle
Subcutaneous	Beneath the epidermal and dermal skin layers
Intradermal	Within the dermis, usually a local effect
Percutaneous	Topical treatment applied to the skin
Inhalation	Mouth/nose, pharynx, trachea, bronchi, bronchioles, alveolar sacs, alveoli
Intra-arterial	Introduced directly into an artery, regional drug delivery
Intrathecal	Cerebrospinal fluid, subarachnoid space
Intraperitoneal	Within the peritoneal cavity
Vaginal	Within the vagina

clotting proteins have been removed by the clotting process. For the most part, the concentration of a drug in plasma or serum is identical, and no distinction is needed. It is usually only the plasma drug concentration in the body that is known, and this is what is meant when we speak of the concentration of the drug in the body. For the most part, it has been found that the physiological activity of most drugs can be related to the plasma concentration of the drug. Pharmacokinetic modeling is then used to predict and/or adjust the dosing strategy for a particular drug.

Plasma drug concentration as measured is usually the total plasma concentration ( $C_{\text{total}}$ ) that includes the concentration of the drug that is bound to plasma proteins ( $C_P$ ) and that which is unbound ( $C_U$ ). Hence,  $C_{\text{total}} = C_P + C_U$ . However, the effect of a particular drug and its transport out of the circulatory system is due to the unbound drug concentration. The fraction of unbound drug or  $f_U$  is defined as

$$f_U = \frac{C_U}{C_P + C_U} = \frac{C_U}{C_{\text{total}}} \quad (8.1)$$

Now,  $f_U$  for a particular drug is usually constant, so either  $C_U$  or  $C_{\text{total}}$  can be used in a pharmacokinetic model; however, it is important to make sure you know and understand which concentration you are using.

[Figure 8.1](#) illustrates typical plasma drug concentrations as a function of time after their introduction to the body. Curve I illustrates the case where the drug is first slowly absorbed, resulting in increasing plasma concentrations, followed by a plateau, and then the plasma concentration decreases as the drug is eliminated by a variety of body processes. Curve II represents a very rapid injection (bolus) of the drug, usually intravenously (IV injection), where we see that the drug quickly reaches its peak plasma concentration near the time of injection, and then is slowly eliminated. Curve III results from a continuous infusion, usually intravenous (IV) or through a controlled release formulation. In this case, we see that after a short period of time, the drug reaches a steady-state plasma concentration, since the infusion rate is equal to the elimination rate of the drug. If the infusion is stopped, then the plasma drug concentration falls due to its elimination as shown by the dashed portion of the curve.

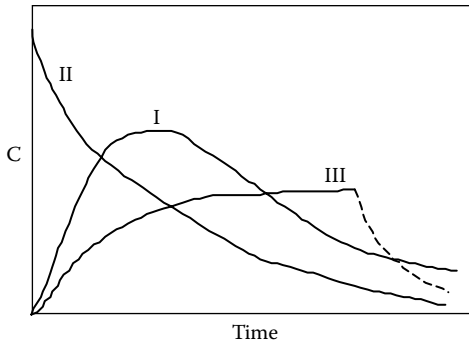


Figure 8.1 Plasma drug concentration following I: absorption, II: rapid intravenous, and III: continuous infusion.

### 8.3 PK modeling approaches

Our goal is then to develop mathematical models that can be used to describe profiles of plasma drug concentration such as those shown in Figure 8.1. This will allow for the description of the drug concentration in the body as a function of time. Through pharmacology and pharmacodynamics, the effects of the drug on the body can then be related to the plasma drug concentration. For example, the physiological response to a particular drug often saturates at high drug concentrations ( $C_{\text{total}}$ ) and can be described by the following equation:

$$R_{\text{drug}} = \frac{R_{\max} C_{\text{total}}^n}{C_{50}^n + C_{\text{total}}^n} \quad (8.2)$$

where

$R_{\text{drug}}$  represents the physiological response to the drug, often expressed in terms of a percent or fractional change in some key parameter. Common examples include body temperature, heart rate, glucose levels, cholesterol levels, and blood pressure

$R_{\max}$  is the saturation response at high drug concentrations where  $C_{\text{total}} \gg C_{50}$

$C_{50}$  is the drug concentration where  $R_{\text{drug}} = 0.50 R_{\max}$

The values of  $C_{\text{total}}$  in Equation 8.2 result from measurements of the drug concentration or from the solution to a pharmacokinetic model.

Pharmacokinetic models will incorporate several unknown parameters that we find by fitting our models to experimental drug concentration data. The development of pharmacokinetic models has generally followed three approaches—the *compartmental approach*, the *physiological approach*, and the *model independent approach*.

#### 8.3.1 Compartmental pharmacokinetic models

The compartmental approach assumes the drug distributes into one or more “compartments” in the body, which usually represent a particular region of the body, an organ, a group of tissues, or body fluids. The compartments are assumed to be well mixed, so that the concentration of the drug within the compartment is spatially uniform. Spatial distribution of the drug within the body is accounted for

by the use of multiple compartments. The assumption of well-mixed compartments is usually pretty good since the cardiac output in humans is nominally  $5 \text{ L min}^{-1}$  and the blood volume is about 5 L giving an effective residence time for one passage of the drug through the circulatory system of about 1 min. Also, recall that there is a net filtration of several milliliters per minute of the blood plasma forming the interstitial fluid that bathes and circulates around all of the cells in the body. Hence, the mixing time of the body fluids occurs much faster than the observed temporal changes of the drug concentration, which can occur over periods of hours or even days. Since drug distribution occurs over periods of hours, and the body's fluids are moving over periods of minutes, and mass transfer occurs on the order of seconds, the well-mixed assumption is appropriate. The movement of the drug between the compartments is usually described by simple irreversible or reversible first order rate processes, i.e., the rate of transport is proportional to the difference in the drug concentration between compartments.

### 8.3.2 Physiological pharmacokinetic models

In physiological models, the movement of drug is based on the blood flow rate through a particular organ or tissue and includes consideration of the rates of the mass transport processes within the region of interest. Experimental blood and tissue drug concentrations are needed to define the model parameters. Our Krogh tissue cylinder model developed in [Chapter 7](#) to describe the changes in oxygen levels within the capillary and the surrounding tissue region is an example of a physiological model. In this case, however, the “drug” is oxygen.

Since the liver plays a major role in the metabolism and excretion of drugs from the body, much attention has been focused on the development of physiological models to describe liver function (Bass and Keiding, 1988; Niro et al., 2003; van de Pas et al., 2012). Physiologically based pharmacokinetic models can become very complex. For example, van de Pas et al. (2012) describe a physiologically based model for predicting plasma cholesterol concentrations. Their model consists of eight compartments, each of which is described by a time-dependent differential equation, along with twenty-one chemical reactions for the various biochemical reactions controlling the disposition of cholesterol.

### 8.3.3 Model independent pharmacokinetic models

The model independent approach does not try to make any physiological connection like the compartmental approach or the physiological approach. Instead, one simply finds the best set of mathematical equations that describes the situation of interest (Notari, 1987). These models are considered to be linear if the plasma drug concentration can be represented by a simple weighted summation of exponential decays. For example, [Equation 8.3](#) can be used to describe the time course of the plasma drug concentration.

$$C_{\text{total}} = \sum_{i=1}^n a_i e^{-\lambda_i t} \quad (8.3)$$

where the constants  $\lambda_i$  and  $a_i$  are adjusted to provide the best fit to the drug concentration data as a function of time.

Our focus in this chapter will be on the use of compartmental models to describe pharmacokinetic data like that shown in [Figure 8.1](#). Compartmental models are commonly used and provide a convenient framework for building a pharmacokinetic model and are conceptually simple to use (Cooney, 1976; Gibaldi and Perrier, 1982; Welling, 1986; Notari, 1987, Rowland and Tozer, 1995; Tozer and Rowland, 2006; Hacker et al., 2009).

## 8.4 Factors that affect drug distribution

Before we can investigate some simple compartmental models, we must first discuss the following factors that influence how a particular drug is distributed throughout the body. [Table 8.2](#) summarizes these factors, and they are discussed in greater detail in the following discussion.

### 8.4.1 Drug distribution volumes

Recall that [Table 3.1](#) summarized the types of fluids found within the body. Since a drug can only distribute within these fluid volumes, we call these the *true distribution volumes*. If a drug only distributes within the plasma volume of the circulatory system, then the true distribution volume for this drug is about 3 L. If the drug readily penetrates the capillary walls, then it can also distribute throughout the extracellular fluid volume for a total true distribution volume of about 15 L. If the drug can also permeate the cell wall, then it will also be found within the intracellular fluid spaces, giving a total true distribution volume of about 40 L.

The rate at which the drug is distributed throughout these fluid volumes is controlled by the rate at which the drug is delivered to a region of interest by the blood, i.e., the tissue blood perfusion rate, and by the rate at which the drug diffuses from within the vascular system into the extravascular spaces. If the drug is lipid soluble, then its mass transfer across the capillary wall is usually not rate limiting and equilibrium is quickly reached between the amount of drug in the tissue region and that found in the blood. In this case, the distribution of the drug in a particular tissue region is limited by the blood flow and is *perfusion rate limited*. For lipid-insoluble drugs, the capillary membrane permeability controls the rate at which the drug distributes between the blood and tissue regions. The distribution of the drug is then said to be *diffusion rate limited*.

Drugs are also capable of binding to proteins found in the plasma and extravascular spaces. Albumin is perhaps the most common of the blood proteins that will bind with drugs. Recall that the major difference between plasma and interstitial fluids is the amount of protein that is present. For the most part, plasma proteins have a difficult time diffusing through the capillary wall to enter the extravascular space. Therefore, a drug that binds strongly with plasma proteins will for the most part be limited to just the volume of the plasma, i.e., about 3 L. On the other hand, extravascular proteins or cell-surface receptors that bind strongly to the drug will tend to accumulate the drug in the extravascular space at the expense of the plasma. In this case, the distribution volume of the drug can appear to be larger than the physical fluid volumes. Thus, protein binding of the drug can have a significant effect on the calculated or *apparent distribution volumes* as the following discussion will show.

Table 8.2 Factors Influencing Drug Distribution

- |                          |
|--------------------------|
| Blood perfusion rate     |
| Capillary permeability   |
| Drug biological affinity |
| Metabolism of drug       |
| Renal excretion          |

### 8.4.2 Apparent distribution volume

Most analytical methods measure the total drug concentration (bound and unbound) that is in the plasma. Since this total plasma concentration ( $C_{\text{total}}$ ) is readily measured, the *apparent distribution volume* ( $V_{\text{apparent}}$ ) of the drug is simply given by the following equation:

$$V_{\text{apparent}} = \frac{A_{\text{drug}}}{C_{\text{total}}} \quad (8.4)$$

where  $A_{\text{drug}}$  is the total amount of drug within the body. The amount of drug in the body is typically expressed in units of milligrams (mg), and the concentration of drug in micrograms per milliliter of plasma ( $\mu\text{g mL}^{-1}$ ), which is the same as milligrams per liter of plasma ( $\text{mg L}^{-1}$ ), resulting in the apparent distribution volume having units of liters (L).

It is also important to note that the concentration of drug within any particular tissue region can vary significantly from the concentration of the drug in the plasma. Therefore, although the apparent distribution volume seems to have some physical significance, it really is just a factor having units of volume that when multiplied by the plasma drug concentration provides the total amount of drug in the body at a particular time.

### 8.4.3 The Oie-Tozer equation for the apparent distribution volume

Because of the effect of protein binding, the apparent distribution volume calculated by [Equation 8.4](#) can be vastly different from the true distribution volume, i.e.,  $V$ , which is related to the volume of the various body fluids. To examine the effect of protein binding on the apparent distribution volume, consider the conceptual model shown in [Figure 8.2](#) (Oie and Tozer, 1979). In their model, unbound drug is free to distribute between three compartments: the plasma (P), the extracellular fluid outside of the plasma (E), and the remainder of the body (R), where the drug is bound to the surface of the

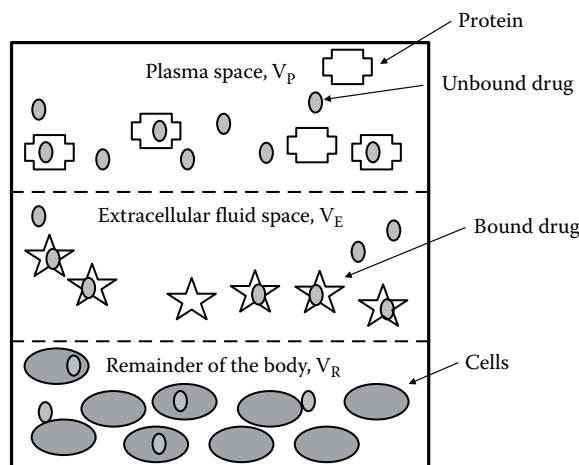


Figure 8.2 Drug distribution in the body with protein binding.

cell by cell-surface receptors, or internalized by the cell by a variety of cellular transport processes. A mass balance on the total amount of drug in the body ( $A_{\text{drug}}$ ) at any time can then be written as

$$A_{\text{drug}} = A_P + A_E + A_R \quad (8.5)$$

where  $A_P$ ,  $A_E$ , and  $A_R$  represent the total amount of drug in the plasma, the extracellular fluid, and the remainder of the body, respectively.

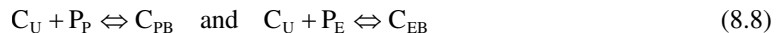
The amount of drug in any of these three compartments is also related to the corresponding concentration of total drug (bound and unbound) in a given compartment, i.e.,  $A_P = C_{\text{total}}V_P$ ,  $A_E = C_E V_E$ , and  $A_R = C_R V_R$ , where  $C_{\text{total}}$ ,  $C_E$ , and  $C_R$  are the respective total drug concentration in each compartment and  $V_P$ ,  $V_E$ , and  $V_R$  are the corresponding compartment volumes. Using these relationships and [Equation 8.4](#), we can rewrite [Equation 8.5](#) as

$$V_{\text{apparent}} = V_P + V_E \left( \frac{C_E}{C_{\text{total}}} \right) + V_R \left( \frac{C_R}{C_{\text{total}}} \right) \quad (8.6)$$

Ignoring active transport type processes, it is assumed that at distribution equilibrium, the unbound concentration of the drug, i.e.,  $C_U$ , is the same in all of the compartments. In addition, in the extracellular fluid compartment, we have that  $C_E = C_U + C_{EB}$ , where  $C_{EB}$  is the bound drug concentration in the extracellular fluid. We now define  $f_U$  as  $C_U/C_{\text{total}}$ , which is the fraction of unbound drug in the plasma, and we also define  $f_{UT}$  as  $C_U/C_R$ , which is the fraction of unbound drug in the extracellular space. Both  $f_U$  and  $f_{UT}$  are usually determined experimentally by equilibrating a known amount of a drug with plasma or extracellular fluid and determining from a drug mass balance the fraction of unbound drug. With these relationships, [Equation 8.6](#) becomes

$$V_{\text{apparent}} = V_P + V_E f_U \left( \frac{C_U + C_{EB}}{C_U} \right) + V_R \frac{f_U}{f_{UT}} \quad (8.7)$$

Unbound drug in the plasma and extracellular spaces can bind with proteins in the plasma ( $P_P$ ) and extracellular spaces ( $P_E$ ) as described by the following chemical reactions:



where  $C_{PB}$  and  $C_{EB}$  represent the concentrations of drug-bound protein in the plasma and extracellular spaces. Assuming that the binding sites on these proteins have the same affinity for the unbound drug, then at equilibrium we can write:

$$K_a = \frac{C_{PB}}{C_U P_P} = \frac{C_{EB}}{C_U P_E} \quad (8.9)$$

where  $K_a$  is the equilibrium or affinity constant for the drug binding to these proteins. The total protein concentration in the plasma ( $P_{PT}$ ) and extracellular spaces ( $P_{ET}$ ) must be equal to the concentration of the respective proteins that are bound to the drug ( $C_{PB}$  and  $C_{EB}$ ) plus the concentration of these proteins that are not bound to the drug ( $P_P$  and  $P_E$ ). Hence, we can write

$$P_P + C_{PB} = P_{PT} \quad \text{and} \quad P_E + C_{EB} = P_{ET} \quad (8.10)$$

Solving these equations for  $P_P$  and  $P_E$  and substituting this result into [Equation 8.9](#), taking the inverse of this equation, and solving for  $C_{EB}$ , we have

$$C_{EB} = C_{PB} \frac{P_{ET}}{P_{PT}} \quad (8.11)$$

Recall that  $P_{ET}$  and  $P_{PT}$  represent the total protein concentrations in the extracellular and plasma spaces, respectively. The total amount of drug-binding protein in the plasma and extracellular spaces equals  $P_{PT}V_P$  and  $P_{ET}V_E$ .  $R_{E/I}$  is then defined as the ratio of the total amount of drug-binding protein in the extracellular space to that in the plasma space, so we have that  $R_{E/I} = \frac{P_{PT}V_P}{P_{ET}V_E}$ . Therefore, [Equation 8.11](#) can be written as

$$C_{EB} = C_{PB}R_{E/I} \frac{V_P}{V_E} \quad (8.12)$$

Now, we can substitute [Equation 8.12](#) into [Equation 8.7](#) for  $C_{EB}$  and obtain

$$V_{apparent} = V_P + f_U \left( \frac{V_E C_U + C_{PB} V_P R_{E/I}}{C_U} \right) + V_R \frac{f_U}{f_{UT}} \quad (8.13)$$

Recognizing that  $\frac{C_{PB}}{C_U} = \frac{1 - f_U}{f_U}$ , we then obtain what is known as the *Oie-Tozer equation*:

$$V_{apparent} = V_P (1 + R_{E/I}) + f_U V_P \left( \frac{V_E}{V_P} - R_{E/I} \right) + \frac{V_R f_U}{f_{UT}} \quad (8.14)$$

From [Table 3.1](#), we have for a 70 kg man that the plasma volume,  $V_P$ , is  $\sim 3$  L and that the extracellular fluid volume outside of the plasma, i.e.,  $V_E$ , is  $\sim 12$  L. The intracellular fluid volume represented by  $V_R$  is in the range of 25–27 L. Also, the amount of drug-binding protein in the extracellular fluid space to that in the plasma, i.e.,  $R_{E/I}$ , is  $\sim 1.4$ . Using these values, [Equation 8.14](#) simplifies approximately to

$$V_{apparent} = 7 + 8f_U + V_R \frac{f_U}{f_{UT}} \quad (8.15)$$

The above equation shows that if a drug is only distributed within the extracellular fluid space and cannot enter the cells, i.e.,  $V_R = 0$ , the apparent distribution volume of the drug then attains its smallest value and is equal to  $V_{apparent}^{\min} = 7 + 8f_U$ . If, in addition, the drug is not bound to plasma proteins, i.e.,  $f_U = 1$ , then the apparent distribution volume of the drug is limited to 15 L, which is the extracellular fluid volume. On the other hand, if the drug is completely bound ( $f_U = 0$ ), then the distribution volume cannot be less than 7 L, and this corresponds to the distribution volume of albumin, which is found in both the plasma and the extracellular compartments.

If the drug enters the cells but is not significantly bound ( $f_U = 1$  and  $f_{UT} = 1$ ), then from [Equation 8.15](#), the apparent volume of distribution is that of the total body water, i.e., 40–42 L. An example of a

drug that distributes throughout the total body water is ethanol. Also note that as  $f_{UT} \rightarrow 0$ , [Equation 8.15](#) predicts that the apparent distribution volume will get very large and exceed that of the total body water volume of about 40 L. It is also important to note that for a large molecular weight drug ( $>60,000 \text{ g mol}^{-1}$ ), it is very difficult for the drug to diffuse across the capillary walls and leave the vascular system; hence, the distribution volume becomes that of the plasma volume, i.e., 3 L.

[Equations 8.14](#) and [8.15](#) are therefore useful for investigating a variety of factors that affect the apparent distribution volume of a drug. Many of these changes can occur as a result of age, disease, injury, and interactions with other drugs. Also, distribution volumes for drugs generally scale according to body weight, so these volumes can be increased or decreased in a proportional sense by dividing them by 70 kg and multiplying by the actual body weight.

### Example 8.1

A drug has an apparent distribution volume of 35 L and is found to be 95% bound to plasma proteins. Unbound drug is also found to freely distribute throughout the total volume of water found in the body. Estimate the fraction of unbound drug with the extracellular fluids, i.e.,  $f_{UT}$ .

#### Solution

The value of  $f_U$  is  $1 - 0.95 = 0.05$ . From [Equation 8.15](#), we can solve for the value of  $f_{UT}$  as shown by the following calculation:

$$f_{UT} = \frac{f_U V_R}{V_{\text{apparent}} - 7 - 8f_U} = \frac{0.05 \times 27 \text{ L}}{35 \text{ L} - 7 - 8 \times 0.05} = 0.0489$$

### 8.4.4 Drug metabolism

Once the drug is absorbed and distributed throughout the body, a variety of biochemical reactions will begin to degrade the drug. This breakdown of the drug is part of the body's natural defense against foreign materials. Metabolism of the drug is beneficial in the sense that it limits the time of drug action and, in some cases, it produces the active form of the drug. These biochemical reactions, driven by existing enzymes, occur in a variety of organs and tissues. However, the major site of drug metabolism is within the liver, and other important sites include the kidneys, lungs, blood, and the GI wall. The enzymatic destruction of the drug reduces its pharmacological activity because the active site related to the drug's molecular structure is destroyed. Also, the *metabolites* that result tend to have increased water solubility that decreases their capillary permeability and enhances their removal from the body via the kidneys.

Drug degradation typically follows the Michaelis-Menten rate model.\* This rate model lumps together all of the enzymatic and transport mechanisms that are responsible for the degradation of the drug into a single reaction rate model. The reaction rate for drug metabolism is given by the following expression:

$$R''_{\text{metabolic}} = \frac{V_{\max} C_{\text{total}}}{K_m + C_{\text{total}}} \quad (8.16)$$

\* A derivation of the Michaelis-Menten model can be found in [Section 9.6.3](#).

We usually assume that the drug degradation reactions occur either in the linear portion of [Equation 8.16](#), where the drug concentration is much smaller than the value of  $K_m$ , or in the saturated reaction rate region, where the drug concentration is much larger than  $K_m$  and the reaction rate is constant at  $V_{max}$ . Therefore, the rate at which the drug is degraded by metabolic reactions can be represented by

$$\begin{aligned} R''_{\text{metabolic}} &= k_{\text{metabolic}} C_{\text{total}} \quad \text{for } C_{\text{total}} \ll K_m \\ R''_{\text{metabolic}} &= V_{\text{max}} \quad \text{for } C_{\text{total}} \gg K_m \end{aligned} \quad (8.17)$$

where

$C_{\text{total}}$  represents the total plasma concentration of the drug

$k_{\text{metabolic}} = V_{\text{max}}/K_m$

$R''_{\text{metabolic}}$  represents the rate at which the drug is degraded on a per unit volume basis

At low concentrations, we see that the Michaelis-Menten equation, given by [Equation 8.16](#), simplifies to first order kinetics, i.e., first order in the total drug concentration. At high concentrations, the Michaelis-Menten equation (cf. [Equation 8.16](#)) simplifies to zero order kinetics, i.e., zero order in the total drug concentration. We will use [Equation 8.17](#) later when we write mass balances for the drug using compartmental models.

#### 8.4.5 Renal excretion of the drug

The kidneys also have a major role in the elimination of the drug from the body. A part of this elimination process is enhanced by the enzymatic degradation of the drug by the liver and the formation of more water-soluble products. The kidneys receive about  $1100 \text{ mL min}^{-1}$  of blood or about 22% of the cardiac output. On a per mass basis, they are the highest perfused organ in the body. Their primary purpose is to remove unwanted metabolic end products such as urea, creatinine, uric acid, and urates from the blood and to control the concentrations of such ions as sodium, potassium, chloride, and hydrogen. The concentrated urine that is formed from the kidneys amounts to about 1.5 L of urine per day.

[Figure 8.3](#) illustrates the basic functional unit of the kidney called the *nephron*. Each kidney contains about one million nephrons, and each nephron contributes to the formation of urine. The operation of the kidney can be explained by considering how an individual nephron functions. The nephron consists of the following major components: the *glomerulus* contained within *Bowman's capsule*, the *convoluted proximal tubule*, *Henle's loop*, the *convoluted distal tubule*, and finally the *collecting tubule* that branches into the *collecting duct*. The glomerulus, proximal tubule, and distal tubule have a major role in drug elimination from the kidney.

Blood enters the glomerulus via the *afferent arteriole* and leaves by the *efferent arteriole*. The glomerulus consists of a tuft of highly permeable fenestrated capillaries, several hundred times more permeable to solutes than the typical capillary. *Glomerular filtrate* is formed across these capillaries within the Bowman's capsule due to hydraulic and osmotic pressure differences that exist between the fluids within the glomerular capillaries and the Bowman space (cf. [Equation 3.4](#)). The glomerular capillary membrane for the most part is impermeable to the plasma proteins retaining those molecules with a molecular weight larger than about 69,000. The drugs that are bound to plasma proteins therefore cannot be removed from the bloodstream by filtration through

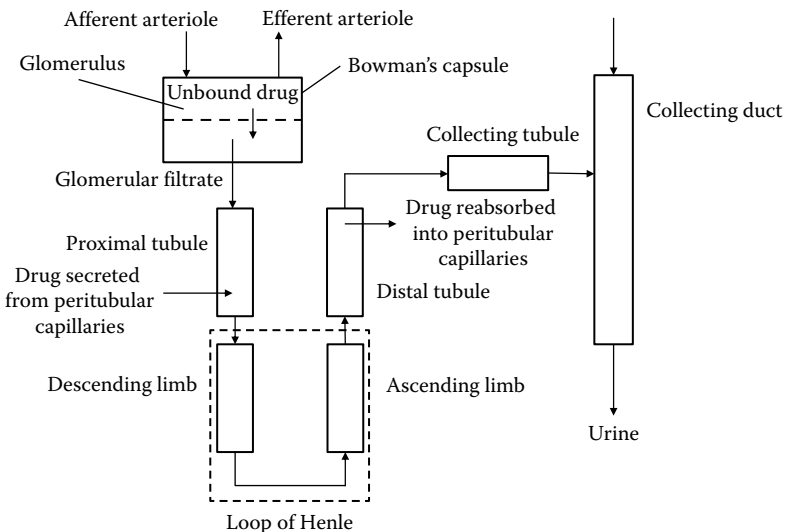


Figure 8.3 Basic structure of the nephron.

the glomerulus. However, unbound drugs with a molecular weight less than 69,000 are readily filtered out of the bloodstream with the glomerular filtrate.

The *glomerular filtration rate* (GFR) is the sum total of all the glomerular filtrate formed per unit time by the nephrons in the two kidneys. This is about  $125 \text{ mL min}^{-1}$  or about 180 L each day, which is more than twice the weight of the body. Clearly, this volume of fluid must be recovered, and we find that over 99% of the glomerular filtrate is reabsorbed in the tubules. The filtration rate of unbound drug in the glomerulus is given by the following equation:

$$\text{Unbound drug removal rate}_{\text{glomerulus}} = \text{GFR} \times C_U = f_U \times \text{GFR} \times C_{\text{total}} \quad (8.18)$$

After the glomerular filtrate leaves the Bowman's capsule, it enters the proximal tubule that is primarily concerned with the active reabsorption of sodium ions and water. Other substances such as glucose and amino acids are also reabsorbed. The proximal tubule is important in drug elimination in that it can also actively secrete drugs from the peritubular capillaries surrounding the proximal tubule. This active transport of the drug is sufficiently fast that even drugs that are bound to plasma proteins will dissociate freeing up the drug for active secretion across the tubule wall.

Within the descending portion of Henle's loop, continued reabsorption of water and other ions occurs primarily by passive diffusion. The ascending loop of Henle is considerably less permeable to water and urea resulting in a very dilute tubular fluid that is rich in urea. Henle's loop does not play a significant role in regard to drug elimination. The first portion of the distal tubule is similar to that of the ascending loop of Henle in that it continues to absorb ions but is impermeable to water and urea. Within the latter portions of the distal tubule and the collecting tubule, ions and water continue to be absorbed along with acidification of the urine thus controlling the acid-base balance of the body fluids.

The reabsorption rate of sodium ions is controlled by the hormone *aldosterone*. The water permeability of these distal segments is controlled by *antidiuretic hormone* providing a means for controlling the final volume of urine that is formed. Drugs can also be reabsorbed within the distal tubule thus affecting the rate of drug elimination from the body. The collecting duct continues to reabsorb water under the control of antidiuretic hormone and does not, for the most part, affect drug elimination.

We thus find that the kidney affects drug elimination through the following mechanisms: filtration through the glomerulus, secretion from the peritubular capillaries into the proximal tubule, and reabsorption within the distal tubule.

## 8.5 Drug clearance

### 8.5.1 Renal clearance

The elimination of drug by the kidney is described by the term *renal clearance*. The renal clearance is simply the volume of plasma that is totally “cleared” of the drug per unit time as a result of the drug’s elimination by the kidneys. Figure 8.4 illustrates the concept of renal clearance and allows for a mathematical definition for the case where the only elimination pathway for the drug is through the kidneys.

In this figure, a drug is uniformly distributed within a single compartment having an apparent distribution volume  $V_{\text{apparent}}$ , and a total plasma concentration represented by  $C_{\text{total}}$ .  $CL_{\text{renal}}$  represents the renal plasma flow rate (typically  $\text{mL min}^{-1}$ ) that is totally cleared of the drug, i.e.,  $C_{\text{total}} = 0$  in the blood leaving the kidneys. Therefore, by definition, the rate at which the drug is removed from the body by the kidneys is given by  $CL_{\text{renal}} \times C_{\text{total}}$ .

We can then write an unsteady mass balance on the drug in the body’s apparent distribution volume assuming that the only elimination pathway for the drug is through the kidneys:

$$V_{\text{apparent}} \frac{dC_{\text{total}}}{dt} = -CL_{\text{renal}} C_{\text{total}} \quad (8.19)$$

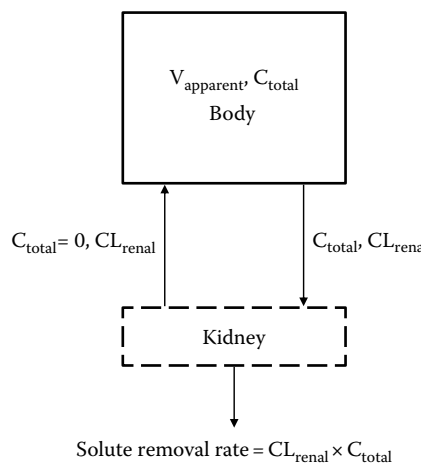


Figure 8.4 Concept of renal clearance.

This equation can be integrated to provide an equation for how the drug concentration within the body changes with time starting from an initial total plasma drug concentration  $C_{\text{total}}^0$ .

$$C_{\text{total}}(t) = C_{\text{total}}^0 e^{-(CL_{\text{renal}}/V_{\text{apparent}})t} = C_{\text{total}}^0 e^{-k_{\text{renal}}t} \quad (8.20)$$

We see that drug elimination by the kidneys can be described as a first order process exhibiting an exponential decay in plasma drug concentration with time. The renal elimination rate constant  $k_{\text{renal}}$  is related to the renal clearance and the apparent distribution volume by the following equation:

$$k_{\text{renal}} = \frac{CL_{\text{renal}}}{V_{\text{apparent}}} \quad (8.21)$$

At any particular time, if  $Q_{\text{urine}}$  represents the urine volumetric flow rate and  $C_{\text{urine}}$  is the concentration of drug in the urine, then the drug removal rate from the apparent distribution volume must equal the rate of its appearance in the urine, i.e.,

$$CL_{\text{renal}} C_{\text{total}} = Q_{\text{urine}} C_{\text{urine}} \quad \text{or} \quad CL_{\text{renal}} = \frac{Q_{\text{urine}} C_{\text{urine}}}{C_{\text{total}}} \quad (8.22)$$

This equation then provides a connection between the renal clearance and the flow rate of the urine that contains the excreted drug. [Equation 8.22](#) can be used to calculate the renal clearance if the urine flow rate and the plasma and urine drug concentrations are known.

The plant polysaccharide *inulin*, with a molecular weight of about 6000, is particularly important to mention at this point because its renal clearance can be used to measure kidney function. Inulin does not bind with plasma proteins, is not metabolized by the body, readily passes through the glomerular capillaries, and is neither reabsorbed nor secreted within the tubules. From [Equation 8.18](#) and [Figure 8.4](#), we have that the mass removal rate of unbound inulin across the glomerular capillaries is given by  $C_U \times CL_{\text{renal}} = GFR \times C_U = f_U \times GFR \times C_{\text{total}}$ . Since  $f_U$  is equal to unity for inulin and  $C_U = C_{\text{total}}$ , this result shows that the rate at which plasma is being cleared of inulin in the kidneys (i.e., renal clearance,  $CL_{\text{renal}}$ ) is the same as the GFR. Hence, for inulin,  $CL_{\text{renal}} = GFR$ .

Creatinine, another substance that is naturally found in the body, can also be used to determine the GFR. Creatinine is found in the plasma and is a product of endogenous protein degradation, specifically the breakdown of creatine phosphate in muscles. Creatinine, for the most part, is produced at a fairly constant rate by the body, although its production rate can depend on the muscle mass. So, for example, there will be a difference between males and females in the creatinine production rate, and a body builder is expected to have a higher production rate of creatinine than a normal person.

The production rate of creatinine ( $\dot{m}_{\text{creatinine}}$ ) in the body is about  $1.2 \text{ mg min}^{-1}$  in healthy young men and about  $1 \text{ mg min}^{-1}$  in healthy young women. Creatinine does not bind with the plasma proteins and, unlike inulin, is secreted by the tubules, which will affect the accuracy of GFR estimation from creatinine concentrations in the plasma. At steady state, the production rate of creatinine in the body has to be equal to the rate of creatinine appearance in the urine. This is expressed by the following equation where  $C_{\text{total}}$  is the plasma concentration of creatinine and  $C_{\text{urine}}$  is the urine concentration of creatinine:

$$\dot{m}_{\text{creatinine}} = GFR \times C_{\text{total}} = Q_{\text{urine}} \times C_{\text{urine}} \quad (8.23)$$

Knowing the urine flow rate and the plasma and urine creatinine concentrations, [Equation 8.23](#) can be used to calculate the GFR. Since the production rate of creatinine is relatively constant, [Equation 8.23](#) also provides a means for calculating the GFR based on a measured concentration of creatinine in the plasma, i.e.,

$$\text{GFR}_{\text{creatinine}} = \frac{\dot{m}_{\text{creatinine}}}{C_{\text{total}}} \quad (8.24)$$

### Example 8.2

The normal concentration of creatinine in the blood is about 1 mg 100 mL<sup>-1</sup> or 1 mg dL<sup>-1</sup>. Estimate the GFR for this value of the creatinine concentration. The normal GFR is about 125 mL min<sup>-1</sup>. Suppose the creatinine concentration in the blood was found to be 8 mg dL<sup>-1</sup>. What is the GFR now?

#### Solution

We can use [Equation 8.24](#) with  $\dot{m}_{\text{creatinine}}$  equal to 1.2 mg min<sup>-1</sup>. For a creatinine concentration of 1 mg dL<sup>-1</sup>, the GFR is 120 mL min<sup>-1</sup>, which compares favorably with the normal GFR of 125 mL min<sup>-1</sup>. If the creatinine concentration in the body rises to 8 mg dL<sup>-1</sup>, then the GFR decreases to a value of 15 mL min<sup>-1</sup>, which indicates a significant impairment of kidney function and the possible need for hemodialysis.

Most drugs, unlike inulin and creatinine, are secreted and reabsorbed in the tubules of the nephron making the calculation of renal clearance for these drugs more complicated. The secretion of the drug may be inferred when the rate of excretion ( $CL_{\text{renal}} \times C_{\text{total}}$ ) exceeds the rate of drug filtration by the glomeruli ( $f_U \times GFR \times C_{\text{total}}$ ) or when  $CL_{\text{renal}} > f_U \times GFR$ . Tubular reabsorption of the drug is important whenever the rate of drug excretion is less than the rate of drug filtration or when  $CL_{\text{renal}} < f_U \times GFR$ .

## 8.5.2 Plasma clearance

*Plasma clearance* ( $CL_{\text{plasma}}$ ) is the term used to represent the sum of all the drug elimination processes of the body. This includes the two primary ones already discussed, metabolism and renal clearance, and other secondary processes such as sweating, bile production, respiration, and bowel movement. We can write a drug mass balance for the amount of drug in the apparent distribution volume in terms of the plasma clearance as

$$V_{\text{apparent}} \frac{dC_{\text{total}}}{dt} = -CL_{\text{plasma}} C_{\text{total}} \quad (8.25)$$

where  $CL_{\text{plasma}} = CL_{\text{metabolism}} + CL_{\text{renal}} + CL_{\text{sweat}} + CL_{\text{bile}} + CL_{\text{respiration}} + CL_{\text{feces}}$ . We can also define a first order elimination rate constant\* for each elimination process as follows:

$$k_i = \frac{CL_i}{V_{\text{apparent}}} \quad (8.26)$$

where  $i = \text{metabolic, renal, sweat, bile, respiration, feces}$ .

---

\* First order means that the rate of elimination depends on the concentration to the first power.

The total first order elimination rate constant is given by  $k_{te}$  and is equal to the sum of the elimination rate constants for all of the elimination processes and is given by

$$k_{te} = \sum_i k_i = \frac{1}{V_{apparent}} \sum_i CL_i = \frac{CL_{plasma}}{V_{apparent}} \quad (8.27)$$

### 8.5.3 Biological half-life

The *biological half-life* ( $t_{1/2}$ ) of a drug is also a measure of the drug clearance and is the time needed for the drug concentration in the plasma to be reduced by one-half. To obtain the half-life for a drug distributed within a single compartment, we can write [Equation 8.25](#) in terms of the total elimination rate constant, i.e.,  $k_{te}$ :

$$\frac{dC_{total}}{dt} = -k_{te} C_{total} \quad (8.28)$$

We then integrate [Equation 8.28](#) with the initial condition that at  $t = 0$ ,  $C_{total} = C_{total}^0$ .

The change in drug concentration with time, taking into account all elimination processes, is then given by

$$C_{total}(t) = C_{total}^0 e^{-k_{te}t} \quad (8.29)$$

The half-life time, i.e.,  $t_{1/2}$ , can be found by simply letting  $\frac{C_{total}(t)}{C_{total}^0}$  equal 0.5 in the previous equation. When solved for  $t_{1/2}$ , the following result is obtained, which also shows how the drug half-life is related to the apparent distribution volume and the plasma clearance:

$$t_{1/2} = \frac{0.693}{k_{te}} = \frac{0.693V_{apparent}}{CL_{plasma}} \quad (8.30)$$

### 8.5.4 The area under the curve, $AUC^{0 \rightarrow \infty}$

The total area under a  $C_{total}$  versus  $t$  curve, such as those shown in [Figure 8.1](#), is given the special symbol  $AUC^{0 \rightarrow \infty}$  and is a measure of the body's exposure to the drug. Drug exposure depends on the drug dose and the drug clearance.  $AUC^{0 \rightarrow \infty}$  is defined mathematically as follows:

$$AUC^{0 \rightarrow \infty} \equiv \int_0^t C_{total}(t) dt \quad (8.31)$$

### 8.5.5 Accumulation of the drug in urine

As we discussed earlier, some of the drug will be eliminated by the kidneys and show up in the urine. In some cases, it may be convenient to use additional data on the amount of drug (not its metabolites) found in the urine to supplement a pharmacokinetic analysis. The rate at which the drug

accumulates in the urine is given by [Equation 8.32](#), where  $M_{\text{urine}}$  is the mass of drug (unchanged) in the urine at any given time.

$$\frac{dM_{\text{urine}}}{dt} = k_{\text{renal}} V_{\text{apparent}} C_{\text{total}} = CL_{\text{renal}} C_{\text{total}} \quad (8.32)$$

## 8.6 A model for intravenous injection of drug

[Equations 8.28](#) and [8.29](#) can also be used to describe how the drug concentration in the body changes with time after a rapid bolus IV injection of a drug. This model is based on a single drug distribution compartment with all the elimination processes lumped into a single first order elimination rate constant, i.e.,  $k_{\text{te}}$ . [Equation 8.29](#) predicts that the drug concentration decreases at an exponential rate with a general shape like that of curve II in [Figure 8.1](#).

The initial drug concentration is related to the drug dose ( $D_{\text{drug}}$ ) and the apparent distribution volume, as given by [Equation 8.33](#), where we assume that no drug is eliminated during the rapid injection phase of the drug.

$$C_{\text{total}}^0 = \frac{D_{\text{drug}}}{V_{\text{apparent}}} \quad (8.33)$$

If the dose and the initial concentration of the drug are known, then [Equation 8.33](#) can be used to solve for the apparent distribution volume of the drug.

An expression for  $AUC^{0 \rightarrow \infty}$  can be obtained by substituting [Equation 8.29](#) into [Equation 8.31](#), which gives

$$AUC^{0 \rightarrow \infty} = \frac{C_{\text{total}}^0}{k_{\text{te}}} = \frac{D_{\text{drug}}}{V_{\text{apparent}} k_{\text{te}}} = \frac{D_{\text{drug}}}{CL_{\text{plasma}}} \quad (8.34)$$

This equation then provides a simple relationship between the total area under the curve, the drug dose, and the plasma clearance. Note that the  $AUC^{0 \rightarrow \infty}$ , which is a measure of the drug exposure in the body, is directly proportional to the drug dose and inversely proportional to the plasma clearance.

We can also substitute [Equation 8.29](#) for the value of the drug concentration in the plasma at any time into [Equation 8.32](#) and integrate that result to obtain the following expression for the mass of unchanged drug in the urine at any time.

$$M_{\text{urine}}(t) = \left( \frac{k_{\text{renal}} C_{\text{total}}^0 V_{\text{apparent}}}{k_{\text{te}}} \right) \left( 1 - e^{-k_{\text{te}} t} \right) \quad (8.35)$$

After a sufficiently long period of time, i.e., as  $t \rightarrow \infty$ , [Equation 8.35](#) simplifies to provide the total amount of unchanged drug collected in the urine:

$$M_{\text{urine}}^{\text{total}} = \frac{k_{\text{renal}} C_{\text{total}}^0 V_{\text{apparent}}}{k_{\text{te}}} = D_{\text{drug}} \frac{k_{\text{renal}}}{k_{\text{te}}} = AUC^{0 \rightarrow \infty} CL_{\text{renal}} \quad (8.36)$$

Thus, we find a relationship exists between the total amount of drug collected in the urine, the renal clearance, and the total area under the curve. Note that if the only drug elimination pathway is through the kidneys, i.e.,  $k_{\text{renal}} = k_{\text{te}}$ , then the total amount of drug collected in the urine is equal to the total drug dose, as it should be.

## 8.7 Continuous infusion of a drug

So far, we have discussed the case of first order drug elimination following a rapid bolus injection of a drug. The drug was assumed to be uniformly distributed throughout a single compartment. In this case, the drug concentration versus time is expected to follow curve II of [Figure 8.1](#).

In many cases, a continuous infusion of the drug is given. Here, the concentration of the drug increases and reaches a steady-state level once a balance is reached between the drug infusion rate and the drug elimination rate. The concentration versus time curve for constant infusion follows something like curve III of [Figure 8.1](#). This result is similar to the so-called *controlled release* drug delivery systems that are commonly used, e.g., to treat motion sickness, for birth control, for extended chemotherapy, for pain management, and to help people quit smoking by delivering nicotine. The constant infusion of a drug can also be used to provide a steady starting concentration of the drug for pharmacokinetic studies.

[Figure 8.5](#) illustrates a single-compartment model for the continuous infusion of a drug.  $\dot{m}_{\text{drug}}$  represents the drug infusion rate ( $\text{mg min}^{-1}$ ) assumed here to be constant. However, one could generalize this infusion rate to be any arbitrary time varying function. For example, in [Section 6.1.2](#), we developed an analytical solution describing the diffusion of a solute from a polymeric material. In this case, the solute is the drug and the polymeric material is a controlled release device. The mass transport flux of the drug ( $N_{Ax}|_{x=L}$ ) out of the device was given by [Equation 6.31](#). Hence,  $\dot{m}_{\text{drug}}$  in [Equation 8.37](#) is given by  $\dot{m}_{\text{drug}}(t) = N_{Ax}|_{x=L} S$ , where  $S$  is the surface area of the device in contact with the skin.

Referring to [Figure 8.5](#), we can write an unsteady mass balance for the drug in the single compartment representing the body as

$$V_{\text{apparent}} \frac{dC_{\text{total}}}{dt} = \dot{m}_{\text{drug}} - CL_{\text{plasma}} C_{\text{total}} = \dot{m}_{\text{drug}} - V_{\text{apparent}} k_{\text{te}} C_{\text{total}} \quad (8.37)$$

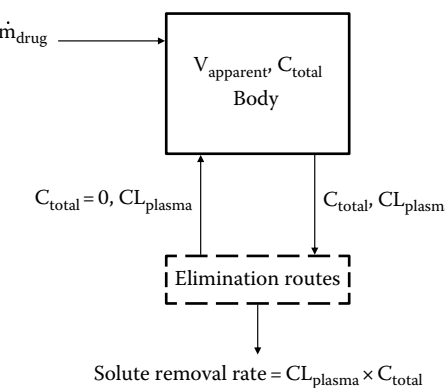


Figure 8.5 Single-compartment model for continuous infusion with first order elimination.

[Equation 8.37](#) can be integrated under the assumption of a constant infusion rate and that the initial drug concentration in the body is  $C_{\text{total}}^0$ , which gives

$$C_{\text{total}}(t) = C_{\text{total}}^0 e^{-k_{te}t} + \left( \frac{\dot{m}_{\text{drug}}}{k_{te}V_{\text{apparent}}} \right) \left( 1 - e^{-k_{te}t} \right) \quad (8.38)$$

The general shape of the curve described by this equation is that of curve III in [Figure 8.1](#). For long periods of time, this equation predicts a steady-state plasma drug concentration given by

$$C_{\text{drug}}^{\text{ss}} = \frac{\dot{m}_{\text{drug}}}{k_{te}V_{\text{apparent}}} = \frac{\dot{m}_{\text{drug}}}{CL_{\text{plasma}}} \quad (8.39)$$

When the infusion is stopped, then the drug is eliminated according to [Equation 8.29](#), where the initial drug concentration  $C_{\text{drug}}^0$  is equal to the steady-state drug concentration, i.e.,  $C_{\text{drug}}^{\text{ss}}$ , arising from the constant infusion. Now the drug concentration decreases as shown by the dotted line of curve III in [Figure 8.1](#).

### Example 8.3

The following table provides some data for the elimination of radioactive inulin from a 392 g laboratory rat. The animal was given a bolus injection at  $t = 0$  equivalent to  $1.01 \times 10^5$  cpm (counts per minute, where the radioactivity is directly proportional to the inulin concentration). This was done to hasten the development of a steady-state plasma inulin level. Next, a continuous infusion of inulin was started at the rate of  $2.76 \times 10^3$  cpm min $^{-1}$ . The inulin infusion was then stopped after a total of 80 min. From these data, determine the GFR, the renal elimination rate constant, and the apparent distribution volume for inulin.

Inulin Elimination from a Laboratory Rat (Sarver, 1994)

Time, min	Inulin Concentration, cpm mL $^{-1}$
0	0
30	849
40	845
60	903
70	888
75	873
80	882 infusion stopped
90	565
100	412
110	271

### Solution

We see that after about 30 min, a steady-state plasma inulin concentration of about 873 cpm mL $^{-1}$  is reached. Once the infusion is stopped, the plasma inulin concentration decreases rapidly. As discussed earlier, inulin is only removed by the kidneys, and its renal clearance is the same

as the GFR. Therefore, for the case of this experiment with inulin, [Equation 8.39](#) can be rearranged to solve for the GFR in terms of the known values of the infusion rate and the steady-state plasma concentration.

$$\text{GFR} = \frac{\dot{m}_{\text{drug}}}{C_{\text{total}}^{\text{ss}}} = \frac{2.76 \times 10^3 \text{ cpm min}^{-1}}{873 \text{ cpm mL}^{-1}} = 3.16 \text{ mL min}^{-1}$$

For the experimental conditions leading to the data shown in the previous table, the GFR is then calculated to be  $3.16 \text{ mL min}^{-1}$ . Since the GFR is proportional to body weight, this can be expressed as  $0.48 \text{ mL h}^{-1} \text{ gBW}^{-1}$ . The renal elimination rate constant, i.e.,  $k_{\text{renal}}$ , can be found by performing a regression analysis of the data obtained after the infusion is stopped using [Equation 8.29](#). Note that the time in this equation represents the time since the infusion was stopped. The initial concentration is equal to  $873 \text{ cpm mL}^{-1}$  and  $k_{\text{te}}$  is equal to  $k_{\text{renal}}$  since the only elimination process is that of the kidneys. Note that [Equation 8.29](#) can be linearized by taking the natural logarithm of each side. The regression equation is then given by

$$\ln C_{\text{total}}(t) = \ln C_{\text{total}}^0 - k_{\text{renal}} t$$

The intercept is the natural logarithm of the initial concentration, and the slope is the negative of the elimination rate constant. After performing the linear regression, we find that  $C_{\text{total}}^0 = 860.1 \text{ cpm mL}^{-1}$  and that  $k_{\text{renal}} = 0.038 \text{ min}^{-1}$ . [Figure 8.6](#) shows a comparison between

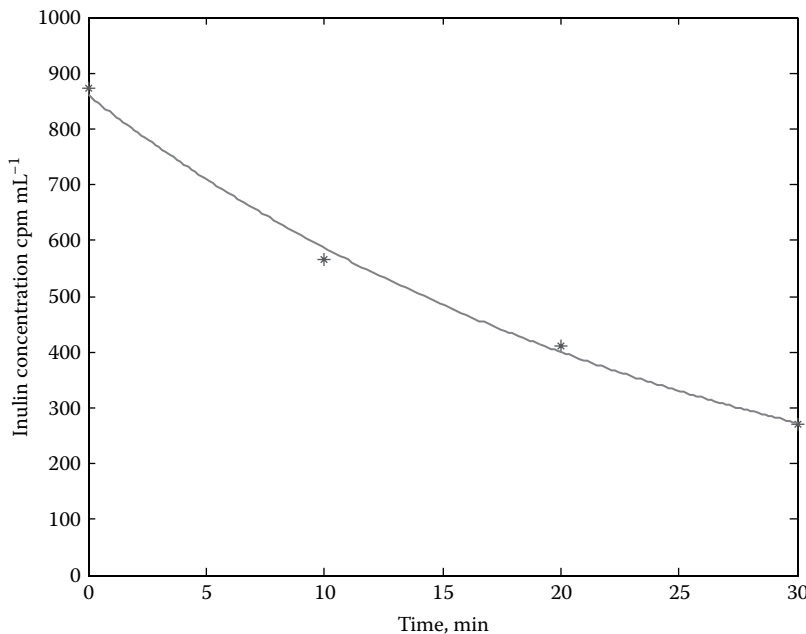


Figure 8.6 Measured and predicted inulin concentrations.

the data and the inulin concentrations predicted by [Equation 8.29](#). The apparent distribution volume for inulin can be found from the definition of the renal clearance, i.e.,  $GFR = CL_{\text{renal}} = k_{\text{renal}} V_{\text{apparent}}$ :

$$V_{\text{apparent}} = \frac{GFR}{k_{\text{renal}}} = \frac{3.16 \text{ mL min}^{-1}}{0.038 \text{ min}^{-1}} = 83.2 \text{ mL}$$

For these data, the apparent distribution volume is about 83 mL. Since the distribution volume is also proportional to the body weight, the apparent inulin distribution volume for a rat can be expressed as  $0.21 \text{ mL gBW}^{-1}$ .

### 8.7.1 Application to controlled release of drugs by osmotic pumps

There is considerable interest focused on the development of novel drug delivery systems (Verma et al., 2002). Novel drug delivery systems have several advantages including elimination of first-pass metabolism by the liver, minimal discomfort, lower risk of infections, sustained release of the drug, potential for reduced side effects, and better patient compliance, especially for chronic conditions.

Osmotic pumps are small implantable devices that can be used to deliver a drug at a constant infusion rate to a specific site in the body for very long periods of time. An example is the DUROS® osmotic pump (Wright et al., 2001) that was developed to deliver the gonadotropin-releasing hormone agonist leuprolide for the palliative treatment of advanced prostate cancer. The DUROS osmotic pump is made from a cylindrically shaped piece of titanium alloy and measures 4 mm in diameter and 45 mm in length. Serum leuprolide levels of about  $1 \text{ ng mL}^{-1}$  for long periods of time will reduce serum testosterone levels in humans to below castration levels, which is important in controlling the growth of prostate cancer cells. The device is inserted subcutaneously and is designed to deliver leuprolide at a constant rate for up to 1 year.

As shown in [Figure 8.7](#), an osmotic pump like the DUROS is basically a cylindrical device that is capped at one end by a permselective membrane and at the other end by a flow modulator through which the drug is released into the body. Within the device are two chambers separated by a piston. In the chamber between the permselective membrane and the piston, there is an osmotic agent that increases the osmotic pressure of the fluid within the chamber relative to the osmotic pressure of the body fluid that surrounds the device. The osmotic agent in the DUROS osmotic pump is NaCl at amounts much higher than the NaCl solubility. As water from the surroundings flows across the

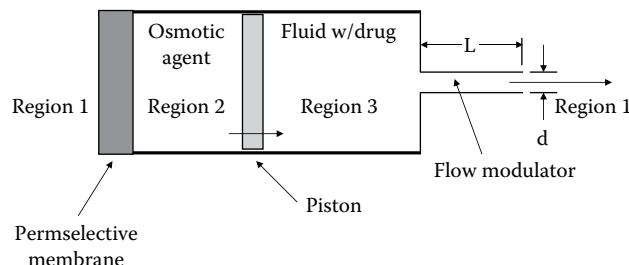


Figure 8.7 Osmotic pump drug delivery system.

permselective membrane by osmosis, the NaCl dissolves and, because of being in excess, maintains saturation levels and hence a constant osmotic pressure throughout the lifetime of the implant. As water enters the device by osmosis, the fluid volume containing the osmotic agent increases and exerts pressure on the piston, causing the piston to move to the right in [Figure 8.7](#). The movement of the piston then acts on the second chamber that contains a fluid with the drug. The piston movement then forces the fluid containing the drug out of the device through the flow modulator at a rate equal to the rate at which water enters the device by osmosis.

The rate at which water enters the device shown in [Figure 8.7](#) from the surroundings is given by [Equation 3.4](#), i.e.,

$$Q_{in} = L_p S \left[ (\Pi_2 - \Pi_1) - (P_2 - P_1) \right] \quad (8.40)$$

where

the numerical subscripts refer to the regions shown in [Figure 8.7](#)

$S$  refers to the surface area of the permselective membrane

Since the piston moves very slowly, we can also assume that the pressures in the osmotic agent chamber and the drug chamber are the same, i.e.,  $P_2 = P_3$ .

If the flow modulator is closed or plugged, then water continues to enter the device by osmosis until the hydrodynamic pressure difference, i.e.,  $(P_2 - P_1)$ , balances the osmotic pressure difference  $(\Pi_2 - \Pi_1)$  stopping the influx of water by osmosis, or

$$P_2 = P_1 + (\Pi_2 - \Pi_1) \quad \text{equilibrium pressure} \quad (8.41)$$

With the flow modulator open, there must be at steady state some value of the internal pressure, i.e.,  $P_2$  or  $P_3$ , which gives a flow rate out of the device that is equal to the rate at which water enters the device by osmosis. This value of  $P_2$  can be found by applying Bernoulli's equation, i.e., [Equation 4.81](#), across the flow modulator as shown by the next equation.

$$\frac{P_2}{\rho} = \frac{P_1}{\rho} + \frac{\alpha V_1^2}{2} + h_{friction} \quad (8.42)$$

In this equation,  $h_{friction}$  represents the frictional losses due to the contraction and expansion of the fluid as it enters and leaves the flow modulator as well as the friction loss as the drug solution flows through the flow modulator of length  $L$  and diameter  $d$ . Recall that  $h_{friction}$  is given by [Equation 4.84](#).  $V_1$  is the velocity of the drug-containing fluid as it exits the flow modulator. The volumetric flow rate of the drug-containing fluid leaving the osmotic pump is given by

$$Q_{out} = \frac{\pi d^2}{4} V_1 \quad (8.43)$$

At steady state, one needs to find the value of  $P_2$  in [Equation 8.42](#) that makes the  $Q_{out}$  calculated by [Equation 8.43](#) equal to the osmotic flow into the device as calculated by [Equation 8.40](#). The drug

delivery rate, or the drug infusion rate  $\dot{m}_{\text{drug}}$  in Equations 8.38 and 8.39, is then given by the product of  $Q_{\text{out}}$  and the drug concentration within the osmotic pump, i.e.,  $C_{\text{drug}}$ .

$$\dot{m}_{\text{drug}} = Q_{\text{out}} C_{\text{drug}} \quad (8.44)$$

Because the flow rate of the drug from the device is usually so small and occurs over such a long period of time, the pressures within the chambers of the osmotic pump, i.e.,  $P_2$  and  $P_3$ , are very close to the pressure of the surroundings, i.e.,  $P_1$ . In addition, the osmotic pressure of the osmotic agent, i.e.,  $\Pi_2$ , is much larger than the osmotic pressure of the body fluids surrounding the device, i.e.,  $\Pi_1$ . Hence, for these practical reasons, the values of  $Q_{\text{in}}$  and  $Q_{\text{out}}$  are given by the following equation, which results from a simplification of Equation 8.40:

$$Q_{\text{in}} = Q_{\text{out}} = L_p S \Pi_2 \quad (8.45)$$

Combining Equations 8.44 and 8.45 results in the following equation for the infusion rate of drug by an osmotic pump:

$$\dot{m}_{\text{drug}} = L_p S C_{\text{drug}} \Pi_2 \quad (8.46)$$

This equation shows that the infusion rate of the osmotic pump is directly proportional to the drug concentration within the device and the osmotic pressure of the osmotic agent that is used. The proportionality constant is the product of the surface area of the permselective membrane and its hydraulic conductance.

### 8.7.2 Controlled release of drugs from transdermal patches

The controlled release of a drug can also be accomplished using a transdermal patch to provide percutaneous drug absorption.

In the transdermal delivery of a drug, i.e., a skin drug patch (Panchagnula, 1997), the drug molecules diffuse across the skin and enter the systemic circulation. However, the passive transport of the drug across the skin can be a major problem. Skin acts as a major defense barrier for the body, and most drugs have very low skin permeability, which can limit the ability to achieve therapeutic drug levels in the body. Therefore, transdermal delivery of a drug is best suited for drugs that have high pharmacological activity (potency) and good skin permeability (lipophilic). Examples where transdermal delivery of drugs is being used include birth control, estrogen replacement and testosterone replacement therapies, and the treatment of hypertension, pain, overactive bladder, and motion sickness, and for cessation of smoking.

In other cases, as in cosmetics and for various skin lotions, the goal is for the active agent not to penetrate the skin and enter the systemic circulation. In these situations, the approach is to find an effective formulation that minimizes the permeation of the active ingredient across the skin (Wang et al., 2014).

The bulk of the resistance for the transport of a drug across the skin as shown in Figure 8.8 results from the *stratum corneum* (SC) (Mitragotri, 2003). The stratum corneum is the outermost layer of

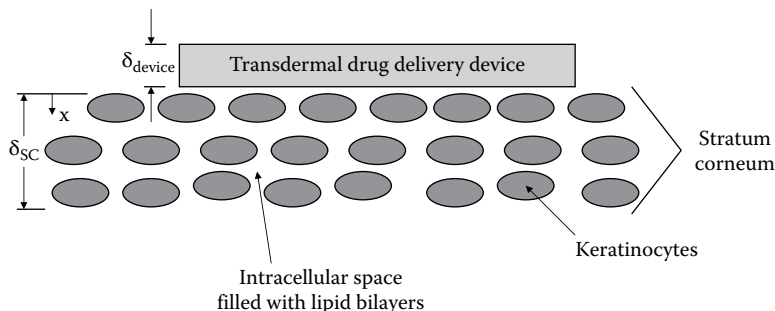


Figure 8.8 Transdermal delivery of drugs.

the skin consisting of about fifteen layers of keratin-filled cells (keratinocytes). The spaces between these cells are filled with lipid bilayers.

The rate of transdermal transport of a drug across the stratum corneum, i.e., the drug infusion rate, can be described by an equation similar to [Equation 6.14](#), where we treat the stratum corneum as a permeable membrane, i.e.,

$$\dot{m}_{drug} = P_{SC}S(C_{drug} - 0) = P_{SC}SC_{drug} \quad (8.47)$$

In [Equation 8.47](#)

we let  $P_{SC}$  describe the permeability of the drug in the stratum corneum

$S$  is the total surface area of the transdermal device

$C_{drug}$  is the average concentration of the drug within the transdermal device

The permeability of a drug across the stratum corneum can be measured experimentally using samples of skin (Wang et al., 2014), or it can be estimated as discussed in the next section. It is also assumed that the concentration of the drug at  $x = \delta_{SC}$  is zero since the drug is immediately taken up by the blood supply.

The stratum corneum permeability, i.e.,  $P_{SC}$ , can be described by an equation similar to [Equation 6.15](#):

$$P_{SC} = \frac{\epsilon_{SC}D_{SC}K}{\delta_{SC}} \quad (8.48)$$

where

$\epsilon_{SC}$  represents the volume fraction of the lipid bilayers through which the drug diffuses

$D_{SC}$  is the diffusivity of the drug in the lipid bilayer material

$K = \left. \frac{C_{SC}}{C_{drug}} \right|_{x=0}$  represents the equilibrium solubility of the drug in the stratum corneum, where  $C_{SC}$  is the drug concentration within the stratum corneum

In [Equation 8.47](#), the value of  $C_{drug}$  will change with time as the drug is depleted from the device. In the most rigorous case, we could use [Equation 6.30](#) to calculate the average concentration of the drug within the device at a given time where we also assume that the drug concentration within the device is many times larger than the concentration of the drug within the stratum corneum, thus satisfying the second boundary condition (BC2) in [Equation 6.20](#).

However, within the transdermal device, we can also make the reasonable assumption that the concentration profile of the drug at any time is flat since the device is very thin, and diffusion of the drug out of the device is a very slow process because the bulk of the mass transfer resistance for the drug lies within the stratum corneum. Therefore, an unsteady mass balance on the amount of drug within the device at any time can be written as

$$V_{\text{device}} \frac{dC_{\text{drug}}}{dt} = -P_{\text{SC}} S C_{\text{drug}} \quad (8.49)$$

With the initial condition that  $C_{\text{drug}} = C_{\text{drug}}^0$ , [Equation 8.49](#) can be integrated to provide the amount of drug within the transdermal delivery device at any time.

$$C_{\text{drug}}(t) = C_{\text{drug}}^0 e^{-\frac{P_{\text{SC}}}{\delta_{\text{device}}} t} \quad (8.50)$$

where  $\delta_{\text{device}} = \frac{V_{\text{device}}}{S}$  is the thickness of the transdermal patch.

[Equations 8.47](#) and [8.50](#) can then be combined with [Equation 8.37](#) to obtain the following differential equation that describes the concentration of the drug within the apparent distribution volume during continuous infusion of a drug by a transdermal delivery system:

$$V_{\text{apparent}} \frac{dC_{\text{total}}}{dt} + V_{\text{apparent}} k_{\text{te}} C_{\text{total}} = P_{\text{SC}} S C_{\text{drug}}^0 e^{-\frac{P_{\text{SC}}}{\delta_{\text{device}}} t} \quad (8.51)$$

with the initial condition that at  $t = 0$ ,  $C_{\text{total}} = C_{\text{total}}^0$ , where  $C_{\text{total}}^0$  is the initial concentration of the drug in the body.

[Equation 8.51](#) can be easily solved using Laplace transforms ([Table 4.4](#)) to give [Equation 8.52](#) for the plasma drug concentration as a function of time:

$$C_{\text{total}}(t) = C_{\text{total}}^0 e^{-k_{\text{te}} t} + \frac{P_{\text{SC}} S C_{\text{drug}}^0}{V_{\text{apparent}}} \left( \frac{e^{-\frac{P_{\text{SC}}}{\delta_{\text{device}}} t} - e^{-k_{\text{te}} t}}{k_{\text{te}} - \frac{P_{\text{SC}}}{\delta_{\text{device}}}} \right) \quad (8.52)$$

Note that if the device is very large, i.e.,  $\delta_{\text{device}} \gg 0$ , or the stratum corneum permeability is very small, then [Equation 8.52](#) simplifies to the previous result given by [Equation 8.38](#) with  $\dot{m}_{\text{drug}} = P_{\text{SC}} S C_{\text{drug}}^0$ .

[Equation 8.52](#) can also be used to follow the drug concentration in the body for successive applications of a transdermal patch. In this case, we assume the old patch is removed and then a new patch is applied, and  $C_{\text{total}}^0$  is the concentration of the drug in the body when the new patch is applied, with the understanding that  $t$  in [Equation 8.52](#) is the time since the new patch was applied.

In some cases, a transdermal device is designed with a rate-limiting membrane that is adjacent to the skin (Nachum et al., 2006). This is done in cases where the stratum corneum permeability for the drug is very high, or where there is wide variation in the stratum corneum permeability between different skin sites. In this way, the drug transport rate from the device is controlled by the transdermal device and not by any variations in the permeability of the skin. In this case, [Equation 8.52](#) can still

be used to describe the concentration of the drug in the apparent distribution volume; however,  $P_{SC}$  is now understood to represent the membrane permeability of the drug.

If the rate-limiting membrane permeability and the stratum corneum permeability are of the same order of magnitude, then the overall permeability, i.e.,  $P_O$ , is used in [Equation 8.52](#) in the place of  $P_{SC}$ , where the overall permeability for the case of a stratum corneum and a device membrane is given by  $\frac{1}{P_O} = \frac{1}{P_{SC}} + \frac{1}{P_{membrane}}$ .

**8.7.2.1 Predicting the permeability of the skin** Oftentimes for preliminary design calculations using [Equation 8.52](#), it may be necessary in the absence of experimental values to have an estimate of the permeability of a drug in the stratum corneum (Mitragotri et al., 2011; Moss et al., 2012). Potts and Guy (1992) developed a relatively simple model for the stratum corneum permeability based on the size of the drug molecule, i.e., its molecular weight, MW, and its octanol/water partition coefficient ( $K_{O/W}$ ). The octanol/water partition coefficient is a commonly used measure of the lipid solubility of a drug. They assumed that the diffusivity of a drug in the stratum corneum depends on the molecular weight of the drug as given by

$$\varepsilon_{SC} D_{SC} = (\varepsilon D)_{SC}^0 e^{-\beta MW} \quad (8.53)$$

Substituting [Equation 8.53](#) into [Equation 8.48](#) and replacing the equilibrium solubility of the drug in the lipid bilayers ( $K$ ) with the octanol/water partition coefficient ( $K_{O/W}$ ), we obtain

$$P_{SC} = K_{O/W} \frac{(\varepsilon D)_{SC}^0}{\delta_{SC}} e^{-\beta MW} \quad (8.54)$$

After taking the base ten log (log) of each side, [Equation 8.54](#) becomes

$$\log P_{SC} = \log \left[ \frac{(\varepsilon D)_{SC}^0}{\delta_{SC}} \right] + \alpha \log K_{O/W} - \beta MW \quad (8.55)$$

where  $\alpha$  is an adjustable constant added to improve the regression analysis and is expected to be on the order of unity.

Potts and Guy (1992) then performed a regression analysis using [Equation 8.55](#) on a data set of more than 90 drugs for which the stratum corneum permeability is known.

The drugs considered in their data set ranged in molecular weight from 18 to 750 and had octanol/water partition coefficients, i.e.,  $\log K_{O/W}$ , from -3 to +6. The regression analysis found the values of  $\left[ \frac{(\varepsilon D)_{SC}^0}{\delta_{SC}} \right]$ ,  $\alpha$ , and  $\beta$  that best represented the data set. Their regression analysis resulted in

$$\log P_{SC} \left( \text{cm s}^{-1} \right) = -6.3 + 0.71 (\log K_{O/W}) - 0.0061 \text{ MW} \quad (8.56)$$

This equation can be expected to yield the predicted values of  $P_{SC}$  that are within several fold of the actual values of the stratum corneum permeability for a given drug.

**Example 8.4**

Estimate the stratum corneum permeability for caffeine. The molecular weight of caffeine is 194, and its octanol/water partition coefficient,  $K_{O/W}$ , is equal to 1 (Joshi and Raje, 2002).

**Solution**

We use the Potts and Guy equation to estimate the stratum corneum permeability for caffeine as shown below:

$$\log P_{SC} = -6.3 + 0.71 \log 1 - 0.0061 \times 194 = -7.483$$

$$P_{SC} = 3.29 \times 10^{-8} \text{ cm s}^{-1} = 1.18 \times 10^{-4} \text{ cm h}^{-1}$$

The value reported by Joshi and Raje for the stratum corneum permeability of caffeine is  $1 \times 10^{-4} \text{ cm h}^{-1}$ , which compares quite well to the value predicted by the Potts and Guy equation.

**8.7.2.2 Experimental measurement of stratum corneum solute permeability** The measurement of the skin permeability for a particular drug or other substance can be done in a transdermal diffusion cell apparatus (Todo et al., 2013; Wang et al., 2014). A transdermal diffusion cell in a conceptual sense is similar to mass transfer across a membrane as shown in [Figure 6.6](#). The skin sample is placed horizontally between two compartments with the stratum corneum facing upward. The top donor compartment is where the sample containing the drug is placed. The receptor compartment contains a well-mixed fluid to receive the drug as it diffuses across the skin sample. Samples are taken over time from the receptor compartment to measure the drug concentrations.

We can then use Fick's second law as given by [Equation 6.19](#) to describe the diffusion of the drug through the skin sample:

$$\frac{\partial C_A}{\partial t} = D_e \frac{\partial^2 C_A}{\partial x^2} \quad (8.57)$$

where

$C_A$  is the drug concentration

$D_e$  is the effective diffusivity of the drug within the skin sample

[Equation 8.57](#) can be solved analytically if we assume that initially there is no drug in the skin sample, that the concentration of the drug in the donor compartment remains constant with time, and that the concentration of the drug in the receptor compartment is very low and can be taken as zero.

We can then write the initial condition (IC) and the boundary conditions for [Equation 8.57](#) as

$$\begin{aligned} \text{IC: } & t = 0, \quad C_A(x, 0) = 0 \\ \text{BC1: } & x = 0, \quad C_A(0, t) = KC_A^{\text{donor}} \\ \text{BC2: } & x = \bar{L}, \quad C_A(\bar{L}, t) = 0 \end{aligned} \quad (8.58)$$

where  $K$  is the drug partition coefficient between the drug in the donor compartment and the skin sample. Hence,  $C_A|_{x=0} = KC_A^{\text{donor}}$ . The thickness of the skin sample is given by  $\bar{L}$ .

Crank (1975) obtained a solution to Equations 8.57 and 8.58 using the method of separation of variables. The solution for the total mass of drug that has diffused through a skin sample of area S at time t is given by

$$\frac{M_A}{S\bar{L}Kc_A^{\text{donor}}} = \frac{D_e t}{\bar{L}^2} - \frac{1}{6} - \frac{2}{\pi^2} \sum_{n=1}^{\infty} \frac{(-1)^n}{n^2} \exp\left(-\frac{D_e n^2 \pi^2 t}{\bar{L}^2}\right) \quad (8.59)$$

For a skin of a given thickness, Equation 8.59 can be used to fit data of  $M_A/S$  versus time to find the values of K and  $D_e$ . The drug permeability of the skin, i.e.,  $P_{SC}$ , is then given by  $\frac{KD_e}{\bar{L}}$ .

As  $t \rightarrow \infty$ , Equation 8.59 simplifies to

$$\frac{M_A}{S} = \bar{L}Kc_A^{\text{donor}} \left( \frac{D_e t}{\bar{L}^2} - \frac{1}{6} \right) = \left( \frac{KD_e C_A^{\text{donor}}}{\bar{L}} \right) t - \frac{1}{6} \bar{L}Kc_A^{\text{donor}} \quad (8.60)$$

Equation 8.60 describes the drug permeation through the skin sample at steady state. We see that the cumulative amount of drug that crosses the skin sample increases in a linear fashion with time. Therefore, if we plot data for the cumulative amount of drug versus time, the slope of these data for large times can be used to find the stratum corneum permeability for the drug, i.e.,  $P_{SC}$ . Hence,

$$P_{SC} \equiv \frac{KD_e}{\bar{L}} = \frac{\text{slope}}{C_A^{\text{donor}}} \quad (8.61)$$

We can also write Equation 8.60 as

$$\frac{M_A}{S} = \frac{KD_e C_A^{\text{donor}}}{\bar{L}} \left( t - \frac{\bar{L}^2}{6D_e} \right) = P_{SC} C_A^{\text{donor}} (t - t_{\text{lag}}) \quad (8.62)$$

where  $t_{\text{lag}} \equiv \frac{\bar{L}^2}{6D_e}$  and is the lag time. The lag time is the time it takes for the drug to just penetrate the skin sample and begin to show itself in the receptor compartment. From Equation 8.62, we see that  $t_{\text{lag}}$  is the x intercept on a cumulative amount of drug versus time plot and can be used to find the value of  $D_e$ .

### Example 8.5

Todo et al. (2013) obtained the data shown in the table for the diffusion of methylparaben (MP) across hairless rat skin. MP is a preservative that is found in a variety of cosmetics and other personal care products. The molecular weight of MP is 152.2 and the log ( $K_{OW}$ ) is 1.96. The concentration of MP in the donor compartment was 10 mM, or  $1522 \mu\text{g cm}^{-3}$ . From these data, estimate the stratum corneum permeability of MP, the MP effective diffusivity, and the MP partition coefficient. Also, compare the value of  $P_{SC}$  obtained to that predicted by Equation 8.56. Assume the resistance to transport of MP across the skin is due to the stratum corneum with a thickness of  $15 \mu\text{m} = 0.0015 \text{ cm}$ .

Time, h	MP Permeated, $\mu\text{g cm}^{-2}$
1	4.1
2	13.4
3	23.2
4	35.5
5	46.4
6	57.3
7	69.6
8	81.9

### Solution

Figure 8.9 shows a plot of the data given in the table. We see that the data from 3 to 8 h lie along a straight line. The equation for this line is

$$\left( \frac{M_A}{A} \right)_{\text{predicted}} = (11.74 \mu\text{g cm}^{-2} \text{ h}^{-1})t - 12.02 \mu\text{g cm}^{-2} \quad (\text{A})$$

From the slope and Equation 8.61, we can calculate the value of  $P_{sc}$ :

$$P_{sc} = \frac{11.74 \mu\text{g cm}^{-2} \text{ h}^{-1}}{1522 \mu\text{g cm}^{-3}} \times \frac{1 \text{ h}}{3600 \text{ s}} = 2.14 \times 10^{-6} \text{ cm s}^{-1}$$

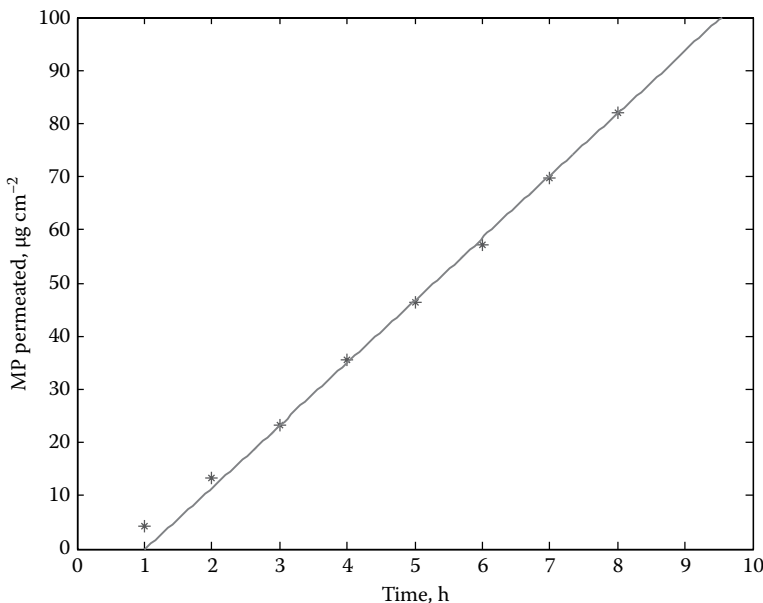


Figure 8.9 Skin permeation of MP.

The value of  $P_{SC}$  predicted by [Equation 8.56](#) is

$$P_{SC}^{\text{predicted}} = 10^{(-6.3+0.71 \times 1.96 - 0.0061 \times 152.2)} = 1.46 \times 10^{-6} \text{ cm s}^{-1}$$

The lag time from [Figure 8.9](#) is the x intercept, which is about 1 h. From [Equation A](#), we also have

$$t_{\text{lag}} = \frac{12.02 \mu\text{g cm}^{-2}}{11.74 \mu\text{g cm}^{-2} \text{ h}^{-1}} = 1.02 \text{ h} = 3672 \text{ s}$$

and since  $t_{\text{lag}} \equiv \frac{\bar{L}^2}{6D_e}$ , we can calculate the value of  $D_e$ :

$$D_e = \frac{\bar{L}^2}{6t_{\text{lag}}} = \frac{(0.0015 \text{ cm})^2}{6 \times 3672 \text{ s}} = 1.02 \times 10^{-10} \text{ cm}^2 \text{ s}^{-1}$$

The partition coefficient, i.e.,  $K$ , can be found from [Equation 8.61](#) as

$$K = \frac{P_{SC}\bar{L}}{D_e} = \frac{2.14 \times 10^{-6} \text{ cm s}^{-1} \times 0.0015 \text{ cm}}{1.02 \times 10^{-10} \text{ cm}^2 \text{ s}^{-1}} = 31.47$$

### 8.7.3 Controlled release of drugs from implantable devices

Drugs can also be contained within a polymeric structure and implanted to provide for a sustained release of the drug into the body. For example, Implanon® (Wenzl et al., 1998) is a nonbiodegradable rod made from ethylene vinyl acetate that contains a core of synthetic progestin etonogestrel (ENG). ENG is a nonestrogen that has a contraceptive effect by suppressing ovulation. This implant is 2 mm in diameter and 4 cm in length. When implanted, this device can provide effective contraception for up to 3 years.

Assuming the wall of a drug-releasing implant is the controlling resistance for the transport of the drug out of the implant, [Equation 6.14](#) can be used to describe the transport rate of the drug, i.e.,

$$\dot{m}_{\text{drug}} = P_m S_{\text{implant}} (C_{\text{drug}} - 0) = P_m S_{\text{implant}} C_{\text{drug}} \quad (8.63)$$

where

$P_m$  is the permeability of the material that contains the drug

$S_{\text{implant}}$  is the surface area for drug transport

$C_{\text{drug}}$  is the concentration of the drug within the implant

An unsteady mass balance on the amount of a drug within the implant is given by

$$V_{\text{implant}} \frac{dC_{\text{drug}}}{dt} = -P_m S_{\text{implant}} C_{\text{drug}} \quad (8.64)$$

With the initial condition that  $C_{\text{drug}} = C_{\text{drug}}^0$ , [Equation 8.64](#) can be integrated to provide the amount of a drug within the drug implant at any time:

$$C_{\text{drug}}(t) = C_{\text{drug}}^0 e^{-\frac{4P_m}{d_{\text{implant}}} t} \quad (8.65)$$

where  $d_{\text{implant}}$  is the diameter of the cylindrical implant.

[Equations 8.63](#) and [8.65](#) can then be combined with [Equation 8.37](#) to obtain the following differential equation that describes the concentration of the drug within the apparent distribution volume during continuous infusion of the drug from the implant:

$$V_{\text{apparent}} \frac{dC_{\text{total}}}{dt} + V_{\text{apparent}} k_{\text{te}} C_{\text{total}} = P_m S_{\text{implant}} C_{\text{drug}}^0 e^{-\frac{4P_m}{d_{\text{implant}}} t} \quad (8.66)$$

with the initial condition that at  $t = 0$ ,  $C_{\text{total}} = C_{\text{total}}^0$ , where  $C_{\text{total}}^0$  is the initial concentration of the drug in the body.

[Equation 8.66](#) can then be solved using Laplace transforms ([Table 4.4](#)) to give [Equation 8.67](#) for the plasma drug concentration as a function of time.

$$C_{\text{total}}(t) = C_{\text{total}}^0 e^{-k_{\text{te}} t} + \frac{P_m S_{\text{implant}} C_{\text{drug}}^0}{V_{\text{apparent}}} \left( \frac{\frac{e^{-\frac{4P_m}{d_{\text{implant}}} t} - e^{-k_{\text{te}} t}}{k_{\text{te}} - \frac{4P_m}{d_{\text{implant}}}}}{\frac{4P_m}{d_{\text{implant}}}} \right) \quad (8.67)$$

[Equation 8.67](#) can also be used to follow the drug concentration in the body for the successive applications of a drug implant. In this case, we assume the old implant is removed and then a new one is implanted, with  $C_{\text{total}}^0$  as the concentration of the drug in the body when the new device is implanted, with the understanding that  $t$  in [Equation 8.67](#) is the time since the new device was implanted.

### Example 8.6

The in vitro release rate kinetics for a batch of ENG implants gave  $75 \mu\text{g day}^{-1}$  after 3 months,  $55 \mu\text{g day}^{-1}$  at 1 year, and  $40 \mu\text{g day}^{-1}$  after 2 years (Wenzl et al., 1998). From these data, estimate the ENG permeability from the implant assuming the controlling mass transfer resistance is the wall of the implant. The device is 2 mm in diameter and 4 cm in length.

### Solution

The mass transfer rate of the drug out of the implant is given by a combination of [Equations 8.63](#) and [8.65](#), i.e.,

$$\dot{m}_{\text{drug}} = P_m S_{\text{implant}} C_{\text{drug}} = P_m S_{\text{implant}} C_{\text{drug}}^0 e^{-\frac{4P_m}{d_{\text{implant}}} t}$$

Taking the natural logarithm of both sides of this equation, we obtain

$$\ln(\dot{m}_{\text{drug}}) = \ln(P_m S_{\text{implant}} C_{\text{drug}}^0) - \left( \frac{4P_m}{d_{\text{implant}}} \right) t \quad (\text{A})$$

This equation says that if we plot the natural log of the drug release rate versus time, the resulting graph of the data should be linear with a slope, i.e.,  $m$ , equal to  $-4P_m/d_{\text{implant}}$ . After performing a linear regression of the release rate data using [Equation A](#), we find that  $m = -9.764 \times 10^{-4} \text{ day}^{-1}$ . We can then find  $P_m$ :

$$P_m = -\frac{md_{\text{implant}}}{4} = \frac{9.764 \times 10^{-4} \text{ day}^{-1} \times 0.2 \text{ cm}}{4} = 4.88 \times 10^{-5} \text{ cm day}^{-1}$$

## 8.8 First-order drug absorption and elimination

Many drugs are given orally or by injection. Other routes can include the nasal cavity or by inhalation. In all of these cases, the drug is first absorbed and makes its way into the plasma by diffusion where it becomes distributed throughout the body. The plasma concentration of the drug gradually increases and then finally decreases as the elimination processes begin to overcome the rate of drug absorption. Curve I of [Figure 8.1](#) illustrates the general trend of the plasma drug concentration with time during the absorption and elimination phases. Although the drug absorption rate is strongly affected by the dosage form, i.e., solution, capsule, tablet, suspension, it has been found that for the most part, the drug absorption process in many cases can be adequately described by simple first order kinetics.

[Figure 8.10](#) illustrates a single-compartment model for the case of first order drug absorption and elimination. Note a separate mass balance equation is needed for the drug whose amount decreases with time due to its absorption into the body. The factor ( $f$ ) accounts for the fraction of the dose ( $D_{\text{drug}}$ ) that is actually absorbable. An amount of the dose equal to  $(1 - f) D_{\text{drug}}$  is assumed to be removed from the body without ever entering the apparent distribution volume.

A mass balance on the amount of drug within the apparent distribution volume can be written as

$$V_{\text{apparent}} \frac{dC_{\text{total}}}{dt} = k_a A_{\text{drug}} - CL_{\text{plasma}} C_{\text{total}} = k_a A_{\text{drug}} - V_{\text{apparent}} k_{\text{te}} C_{\text{total}} \quad (8.68)$$

where

$A_{\text{drug}}$  represents the mass of the drug remaining to be absorbed

$k_a$  represents the drug's first order absorption rate constant

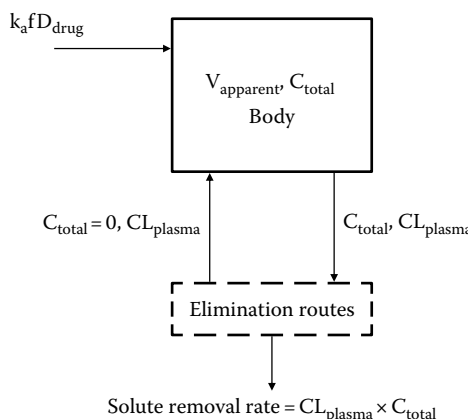


Figure 8.10 Single-compartment model with first order absorption and elimination.

A mass balance on the drug yet to be absorbed, i.e.,  $A_{\text{drug}}$ , is given by the following equation:

$$\frac{dA_{\text{drug}}}{dt} = -k_a A_{\text{drug}} \quad (8.69)$$

When this equation is integrated, recognizing that initially  $A_{\text{drug}}(t = 0) = fD_{\text{drug}}$ , then the amount of a drug at any time waiting to be absorbed is given by

$$A_{\text{drug}}(t) = fD_{\text{drug}} e^{-k_a t} \quad (8.70)$$

This equation can then be substituted into [Equation 8.68](#) to obtain an expression for the total amount of a drug in the plasma as a function of time, assuming the initial concentration of the drug is zero:

$$C_{\text{total}}(t) = \frac{fD_{\text{drug}}}{V_{\text{apparent}}} \left( \frac{k_a}{k_a - k_{\text{te}}} \right) \left( e^{-k_{\text{te}}t} - e^{-k_a t} \right) \quad (8.71)$$

We see that the concentration of a drug in the plasma is dependent on the first order rate constants for absorption and elimination, i.e.,  $k_a$  and  $k_{\text{te}}$ . The concentration is directly proportional to the fraction of the drug dose that is absorbable and inversely proportional to the apparent distribution volume.

An expression for the time at which the concentration peaks can be obtained by taking the derivative of [Equation 8.71](#) with respect to time, setting this result equal to zero, and solving for the time. This time, called  $\tau_{\text{max}}$ , is given by the following expression:

$$\tau_{\text{max}} = \frac{1}{k_a - k_{\text{te}}} \ln \left( \frac{k_a}{k_{\text{te}}} \right) \quad (8.72)$$

Note that the time the maximum concentration is reached is independent of the dose. The corresponding concentration at the time of the peak can be found by substituting  $\tau_{\text{max}}$  into [Equation 8.71](#) for the time and simplifying to obtain

$$C_{\text{max}} = \left( \frac{fD_{\text{drug}}}{V_{\text{apparent}}} \right) \left( \frac{k_a}{k_{\text{te}}} \right)^{\frac{k_{\text{te}}}{k_{\text{te}} - k_a}} \quad (8.73)$$

We can also find the value of  $AUC^{0 \rightarrow \infty}$  by substituting [Equation 8.71](#) into [Equation 8.31](#). Upon integration, the following result is obtained for the value of  $AUC^{0 \rightarrow \infty}$ :

$$AUC^{0 \rightarrow \infty} = \frac{fD_{\text{drug}}}{k_{\text{te}} V_{\text{apparent}}} = \frac{fD_{\text{drug}}}{CL_{\text{plasma}}} \quad (8.74)$$

It is interesting to note that the value of  $AUC^{0 \rightarrow \infty}$  does not depend on the absorption rate constant. However,  $AUC^{0 \rightarrow \infty}$  is directly proportional to the absorbed dose,  $fD_{\text{drug}}$ , and inversely proportional to the plasma clearance.  $AUC^{0 \rightarrow \infty}$  is a measure of the body's exposure to the drug.

To complete our mathematical description of the process shown in [Figure 8.10](#), the rate at which the drug enters the urine can be found from [Equation 8.32](#). Substituting [Equation 8.71](#) for the total

plasma drug concentration into this equation gives the following result for the amount of a drug in the urine at any given time:

$$M_{\text{urine}}(t) = \left( \frac{fD_{\text{drug}} k_{\text{renal}}}{k_{\text{te}}} \right) \left[ 1 - \frac{1}{k_a - k_{\text{te}}} (k_a e^{-k_{\text{te}}t} - k_{\text{te}} e^{-k_a t}) \right] \quad (8.75)$$

After all of the drug has cleared the body, i.e.,  $t \rightarrow \infty$ , the amount of drug in the urine is given by

$$M_{\text{urine}}^{\infty} = fD_{\text{drug}} \frac{k_{\text{renal}}}{k_{\text{te}}} \quad (8.76)$$

Note that if the only elimination pathway for the drug is through the kidneys, i.e.,  $k_{\text{renal}} = k_{\text{te}}$ , then  $M_{\text{urine}}^{\infty} = fD_{\text{drug}}$ .

If [Equation 8.76](#) is subtracted from [Equation 8.75](#), then an equation is obtained for the quantity of the drug remaining to be excreted by the kidneys. This equation is of a convenient form for determining the absorption and elimination rate constants from urinary excretion data:

$$M_{\text{urine}}^{\infty} - M_{\text{urine}}(t) = \frac{M_{\text{urine}}^{\infty}}{(k_a - k_{\text{te}})} (k_a e^{-k_{\text{te}}t} - k_{\text{te}} e^{-k_a t}) \quad (8.77)$$

The parameters, i.e.,  $k_a$  and  $k_{\text{te}}$ , can be determined by performing a nonlinear regression on urinary excretion data in a manner similar to that shown in [Example 8.7](#). Since  $M_{\text{urine}}^{\infty}$  is known from the urinary excretion data, one can then determine the renal elimination rate constant ( $k_{\text{renal}}$ ) from [Equation 8.76](#) given the dose actually absorbed ( $fD_{\text{drug}}$ ) and the value of  $k_{\text{te}}$ .

[Example 8.7](#) illustrates the use of the single-compartment model with first order absorption and elimination to describe the plasma concentration of an experimental drug after an oral dose of 500 mg. This example requires that a nonlinear regression be performed to find the three unknown parameters in [Equation 8.71](#), i.e.,  $\frac{fD_{\text{drug}}}{V_{\text{apparent}}}$ ,  $k_a$ , and  $k_{\text{te}}$ . There are a variety of mathematical software programs that have routines for solving multiple parameter nonlinear regression problems. It is important to note that many times when performing a nonlinear regression analysis, a unique solution may not be found. In other words, there can be different values of the regression parameters that can fit the data to the same level of accuracy.

To extract the values of  $f$  and  $V_{\text{apparent}}$  from the value of  $\frac{fD_{\text{drug}}}{V_{\text{apparent}}}$  requires additional data, such as that obtained from urinary excretion or IV injection studies. Other techniques based on graphical methods may also be used to determine pharmacokinetic parameters as discussed in the following references (Cooney, 1976; Gibaldi and Perrier, 1982; Welling, 1986; Notari, 1987) and in [Problem 8.5](#) at the end of this chapter.

### Example 8.7

The table below summarizes plasma concentration levels of an experimental drug following a 500 mg oral dose. From the data provided in this table, determine the pharmacokinetic parameters that describe the absorption and elimination of this drug. The drug was also found to have an absorption factor ( $f$ ) of 0.8.

Time, min	Plasma Drug Concentration, mg L <sup>-1</sup>
0	0
1	1.5
4	4.5
8	8.2
12	10.5
16	11.5
20	12.5
24	13.2
28	13.1
32	13.0
40	12.5
70	8.5
100	5.9
150	2.5
200	1.4
300	0.3

### Solution

One of the issues with the nonlinear regression analysis of pharmacokinetic data is obtaining suitable initial guesses of the parameters. In this example, we need to find the values of  $\frac{fD_{\text{drug}}}{V_{\text{apparent}}}$ ,  $k_a$ , and  $k_{te}$ . One approach for guessing  $\frac{fD_{\text{drug}}}{V_{\text{apparent}}}$  is to extrapolate the data after the concentration peak back to the value at  $t = 0$  since this represents in a sense what the initial drug concentration would be if the absorption process was very fast. This is usually facilitated by plotting the log of the concentration data versus time. For the above data, it is then found that

$\frac{fD_{\text{drug}}}{V_{\text{apparent}}} \sim 25 \text{ mg L}^{-1}$ . Since, in most cases, the absorption process is many times faster than the elimination process then for times after the peak concentration, the elimination processes dominate. Hence, [Equation 8.71](#) becomes

$$\ln C_{\text{total}} \Big|_{t \gg 0} \approx \ln \left[ \frac{fD_{\text{drug}}}{V_{\text{apparent}}} \left( \frac{k_a}{k_a - k_{te}} \right) \right] - k_{te} t$$

Therefore, if the  $\ln(C_{\text{total}})$  is plotted as a function of time for the data after the peak, the slope of these data is approximately equal to  $-k_{te}$ . In this case, an estimate of  $k_{te} = 0.014 \text{ min}^{-1}$  is found. Since the absorption process is much faster than the elimination process, a value of  $k_a \approx 10 \times k_{te}$  can be assumed as a starting point. [Figure 8.11](#) shows the results of the nonlinear regression. The open symbols are the data points from the previous table, and the solid line is the resulting best fit of [Equation 8.71](#) to these data. The value of

$$\frac{fD_{\text{drug}}}{V_{\text{apparent}}} = 19.9 \text{ mg L}^{-1},$$

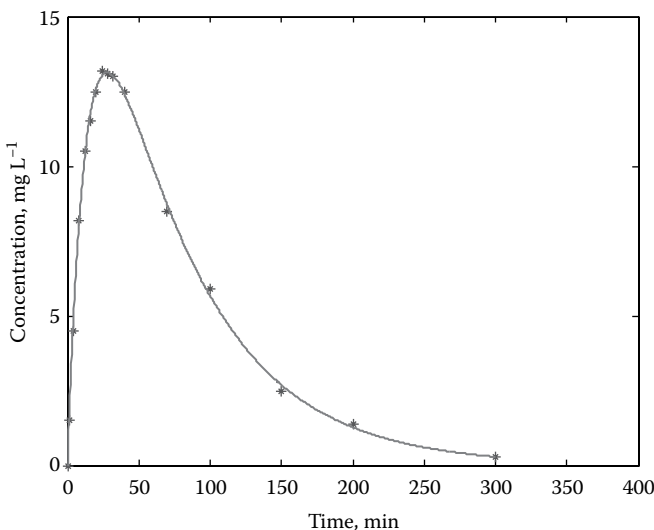


Figure 8.11 A comparison of actual and predicted plasma drug concentrations.

$k_a = 0.07 \text{ min}^{-1}$ , and  $k_{te} = 0.015 \text{ min}^{-1}$ . From [Equation 8.72](#), the predicted maximum in the plasma drug concentration occurs after 27.9 min, and the peak plasma concentration from [Equation 8.73](#) is  $13.1 \text{ mg L}^{-1}$ . The fit during the initial absorption phase and the elimination phase is excellent. Since the dose is given as 500 mg and the fraction of the dose absorbed is 0.8, we find that the apparent distribution volume for this drug is

$$V_{\text{apparent}} = \frac{0.8 \times 500 \text{ mg}}{19.9 \text{ mg L}^{-1}} = 20.1 \text{ L}$$

## 8.9 Two-compartment models

In many cases, the single-compartment model is not sufficient to represent the time course of the plasma drug concentration. The single-compartment model assumes that the drug rapidly distributes throughout a single homogeneous apparent distribution volume. In fact, the drug may distribute at different rates in different tissues of the body, and it may require an extended period of time before the drug concentration equilibrates between the different tissue and fluid regions of the body. Clearly, this a complex process, and one could envision building a model in which a central compartment representing the plasma is in direct communication with a multitude of other compartments representing other tissue and fluid regions of the body.

A reasonable simplification of this type of model is the two-compartment model shown in [Figure 8.12](#). A drug is introduced into the central compartment that generally represents the plasma and other fluids in which the drug rapidly equilibrates. The drug then slowly distributes into the

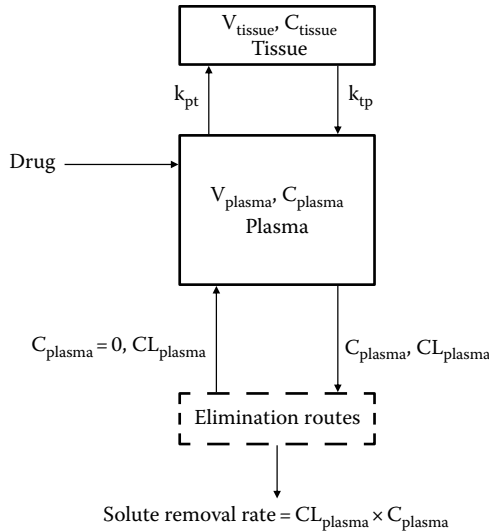


Figure 8.12 A two-compartment model.

remaining tissue and fluid spaces represented by a single tissue compartment. The total apparent distribution volume is then equal to the sum of the distribution volume for the plasma and that of the tissue.

The constants  $k_{pt}$  and  $k_{tp}$  represent the rate constants describing the first order transport between the plasma and tissue compartments. Also,  $k_{te}$  is the first order rate constant that is used to describe the total of all the drug elimination processes, and these elimination processes are assumed to be associated with the plasma compartment. Also, [Equation 8.32](#) can be used to describe the accumulation of the drug in the urine; however,  $V_{\text{apparent}}$  is now the plasma volume, i.e.,  $V_{\text{plasma}}$ , and  $C_{\text{total}}$  is the plasma drug concentration, i.e.,  $C_{\text{plasma}}$ .

The two-compartment model has a characteristic biphasic temporal plasma concentration profile that distinguishes it from the single-compartment model. During the early period after the drug absorption, the drug is eliminated at a more rapid pace from the plasma volume due to the combined effects of the usual elimination processes as well as drug absorption by the tissues and fluids of the secondary compartment. After a period of time, the two compartments equilibrate and the drug elimination rate falls off.

### 8.9.1 Two-compartment model for an intravenous injection

First, let us develop a pharmacokinetic model for the case of a bolus IV injection. A separate unsteady mass balance equation for the drug is then written for the plasma and the tissue compartments:

$$\text{Plasma compartment: } V_{\text{plasma}} \frac{dC_{\text{plasma}}}{dt} = k_{tp} V_{\text{tissue}} C_{\text{tissue}} - (k_{te} + k_{pt}) V_{\text{plasma}} C_{\text{plasma}} \quad (8.78)$$

$$\text{Tissue compartment: } V_t \frac{dC_t}{dt} = k_{pt} V_p C_p - k_{tp} V_t C_t \quad (8.79)$$

where

$V_{\text{plasma}}$  and  $V_{\text{tissue}}$  represent the apparent distribution volumes of the plasma and tissue compartments  
 $C_{\text{plasma}}$  and  $C_{\text{tissue}}$  represent the total concentrations of the drug within these respective compartments

These equations can be solved analytically using Laplace transforms with the following initial condition:  $t = 0$ ,  $C_{\text{plasma}} = D_{\text{drug}}/V_{\text{plasma}}$ , and  $C_{\text{tissue}} = 0$ . The equation for the concentration of the drug within the plasma compartment is given by

$$C_{\text{plasma}}(t) = \frac{D_{\text{drug}}}{V_{\text{plasma}}(A - B)} \left[ (k_{tp} - B)e^{-Bt} - (k_{tp} - A)e^{-At} \right] \quad (8.80)$$

and that for the concentration of the drug in the tissue compartment is then given by

$$C_{\text{tissue}}(t) = \frac{D_{\text{drug}} k_{pt}}{V_{\text{tissue}}(A - B)} \left[ e^{-Bt} - e^{-At} \right] \quad (8.81)$$

The constants A and B are given by the following equations in terms of the first order rate constants:

$$A = \frac{1}{2} \left\{ (k_{pt} + k_{tp} + k_{te}) + \left[ (k_{pt} + k_{tp} + k_{te})^2 - 4k_{tp}k_{te} \right]^{1/2} \right\} \quad (8.82)$$

$$B = \frac{1}{2} \left\{ (k_{pt} + k_{tp} + k_{te}) - \left[ (k_{pt} + k_{tp} + k_{te})^2 - 4k_{tp}k_{te} \right]^{1/2} \right\}$$

A nonlinear regression of plasma drug concentration data using [Equation 8.80](#) can be performed to obtain the constants in that equation, i.e.,  $V_{\text{plasma}}$ , A, B, and  $k_{tp}$ . The other first order rate constants,  $k_{pt}$  and  $k_{te}$ , can then be found through the following process. We first multiply A and B in [Equation 8.82](#) to obtain the following result:

$$k_{te} = \frac{AB}{k_{tp}} \quad (8.83)$$

Then, A and B in [Equation 8.82](#) are added together to give

$$k_{pt} = (A + B) - (k_{tp} + k_{te}) \quad (8.84)$$

[Equations 8.83](#) and [8.84](#) can then be solved to obtain the values of  $k_{te}$  and  $k_{pt}$  from the known values of A, B, and  $k_{tp}$ .

The apparent distribution volume of the tissue compartment can be found by assuming that once the two compartments are at equilibrium, then the derivative in [Equation 8.79](#) is equal to zero

and the concentrations in the two compartments are the same. [Equation 8.79](#) then simplifies to give the following result for the volume of the tissue space:

$$V_{\text{tissue}} = V_{\text{plasma}} \left[ \frac{k_{\text{pt}}}{k_{\text{tp}}} \right] \quad (8.85)$$

The overall apparent distribution volume is then equal to  $V_{\text{plasma}} + V_{\text{tissue}}$  and is given by

$$V_{\text{apparent}} = V_{\text{plasma}} \left[ 1 + \frac{k_{\text{pt}}}{k_{\text{tp}}} \right] \quad (8.86)$$

The data in [Example 8.8](#) illustrate how the pharmacokinetic parameters of the two-compartment model for an IV dose can be determined. Other techniques based on graphical methods can also be used to determine pharmacokinetic parameters (Welling, 1986; Notari 1987; Hacker et al., 2009). Oftentimes the graphical approaches can provide reasonable starting values for the parameters in a nonlinear regression.

### Example 8.8

The data shown in the table below from Putcha et al. (1989) provide the mean plasma concentration ( $N = 6$ ) following an IV injection of 0.4 mg of scopolamine. Scopolamine is a drug that is used to alleviate motion sickness. Determine the pharmacokinetic parameters of the two-compartment model given by [Equations 8.80](#) and [8.81](#).

Time, min	Plasma Scopolamine Concentration, pg mL <sup>-1</sup>
20	3495.8
30	2405.8
45	2260.5
60	1762.0
90	1139.3
120	784.1
180	447.6
300	199.2
360	180.3
480	106.8
600	83.3
720	69.1

### Solution

[Figure 8.13](#) shows the results of the nonlinear regression using the two-compartment IV model. The symbols are the data points from the previous table, and the solid line is the resulting best fit of [Equation 8.80](#) to these data. We see that the two-compartment model fits these

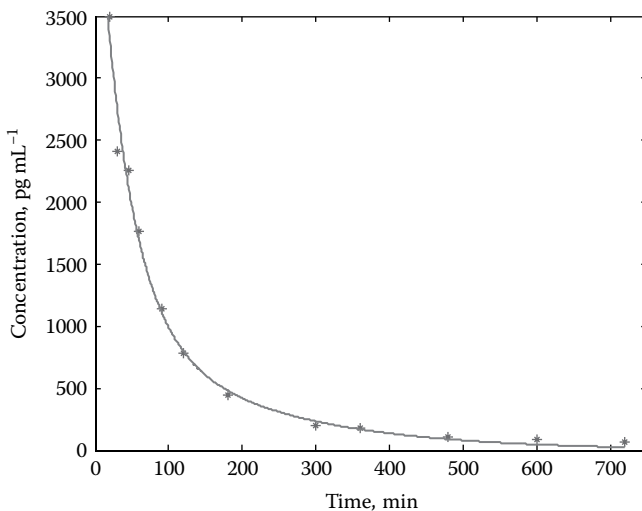


Figure 8.13 A comparison of actual and predicted plasma scopolamine levels.

data extremely well. The following table summarizes the results of the regression analysis. Note that the plasma clearance is given by  $CL_{\text{plasma}} = k_{\text{te}} V_{\text{plasma}}$ .

Parameter	Value
A	0.024 min⁻¹
B	0.0053 min⁻¹
$k_{\text{tp}}$	0.0098 min⁻¹
$k_{\text{pt}}$	0.0068 min⁻¹
$k_{\text{te}}$	0.0133 min⁻¹
$V_{\text{tissue}}$	56.8 L
$V_{\text{plasma}}$	82.1 L
$V_{\text{apparent}}$	138.9 L
$CL_{\text{plasma}}$	65.3 L min⁻¹

### 8.9.2 Two-compartment model for first order absorption

Continuing our discussion of the two-compartment model, consider the case now of the first order absorption of the drug. Unsteady mass balance equations can once again be written for each of the compartments. The equation for the tissue compartment is still given by [Equation 8.79](#), and the equation that describes the amount of drug yet to be absorbed ( $A_{\text{drug}}$ ) is still given by [Equations 8.69](#) and [8.70](#). The plasma compartment equation is then given by

$$V_{\text{plasma}} \frac{dC_{\text{plasma}}}{dt} = k_a A_{\text{drug}} + k_{\text{tp}} V_{\text{tissue}} C_{\text{tissue}} - (k_{\text{te}} + k_{\text{pt}}) V_{\text{plasma}} C_{\text{plasma}} \quad (8.87)$$

The initial conditions are that at time equal to zero, no drug is present in either compartment. These equations can then be solved using Laplace transforms to obtain the following expressions for the concentration of a drug within the plasma and tissue compartments. For the plasma concentration we have

$$C_{\text{plasma}}(t) = \frac{fD_{\text{drug}} k_a}{V_{\text{plasma}}} \left[ \frac{(k_{tp} - A)}{(k_a - A)(B - A)} e^{-At} + \frac{(k_{tp} - B)}{(k_a - B)(A - B)} e^{-Bt} + \frac{(k_{tp} - k_a)}{(A - k_a)(B - k_a)} e^{-k_a t} \right] \quad (8.88)$$

and for the tissue concentration

$$C_{\text{tissue}}(t) = \frac{fD_{\text{drug}} k_a k_{tp}}{V_{\text{tissue}}} \left[ \frac{e^{-At}}{(k_a - A)(B - A)} + \frac{e^{-Bt}}{(k_a - B)(A - B)} + \frac{e^{-k_a t}}{(A - k_a)(B - k_a)} \right] \quad (8.89)$$

The constants A and B have the same dependence on  $k_{pt}$ ,  $k_{tp}$ , and  $k_{te}$  as the two-compartment IV case and are also given by Equations 8.82. Depending on the type of data one has, Equation 8.88 can be fitted to plasma concentration data to obtain the unknown parameters:  $fD_{\text{drug}}/V_{\text{plasma}}$ ,  $k_a$ ,  $k_{tp}$ , A, and B. In some cases, it may not be possible to resolve the group  $fD_{\text{drug}}/V_{\text{plasma}}$  without additional data, perhaps from an IV bolus injection and/or urinary excretion data. Once these parameters have been determined, Equations 8.83 through 8.86 can be used to find the remaining parameters. Other techniques based on graphical methods may also be used to determine pharmacokinetic parameters as discussed in the references (Cooney, 1976; Gibaldi and Perrier, 1982; Welling, 1986; Notari, 1987).

**Example 8.9** illustrates the use of the two-compartment model with first order absorption to describe the mean plasma scopolamine levels following a 0.4 mg oral dose.

### Example 8.9

The data shown in the table below from Putcha et al. (1989) provide the mean plasma concentration ( $N = 6$ ) following an oral dose of 0.4 mg of scopolamine. Determine the pharmacokinetic parameters of the two-compartment model given by Equations 8.88 and 8.89.

Time, min	Plasma Scopolamine Concentration, pg mL <sup>-1</sup>
0	0
9.6	289.4
20	507
30	420.6
45	447.6
90	272
120	187.2
240	106.8
360	57.3
480	42
720	25.5

### Solution

Figure 8.14 illustrates the solution. We see that the two-compartment model fits these data rather well. Note that for the same dose of 0.4 mg, the IV administration of scopolamine resulted in a much higher peak plasma concentration (see Figure 8.13) than obtained when the dose is given orally (see Figure 8.14). Putcha et al. (1989) state that this may be a result of first-pass metabolism in the liver or poor absorption of the drug from the GI tract. Because of this lowered availability of the drug when given orally, we have adjusted the fraction of the drug actually absorbed, i.e.,  $f$ , to match the apparent distribution volume for scopolamine as found in Example 8.8. The value  $f$  was then found to be 0.129. The table below summarizes the results of the regression analysis.

Parameter	Value
$\frac{fD}{V_{\text{apparent}}}$	781.2 $\mu\text{g mL}^{-1}$
A	0.024 $\text{min}^{-1}$
B	0.0033 $\text{min}^{-1}$
$k_{\text{tp}}$	0.0085 $\text{min}^{-1}$
$k_{\text{pt}}$	0.0093 $\text{min}^{-1}$
$k_{\text{te}}$	0.0092 $\text{min}^{-1}$
$V_{\text{plasma}}$	66.05 L
$V_{\text{tissue}}$	73 L
$V_{\text{apparent}}$	139 L
$CL_{\text{plasma}}$	36.3 L $\text{min}^{-1}$

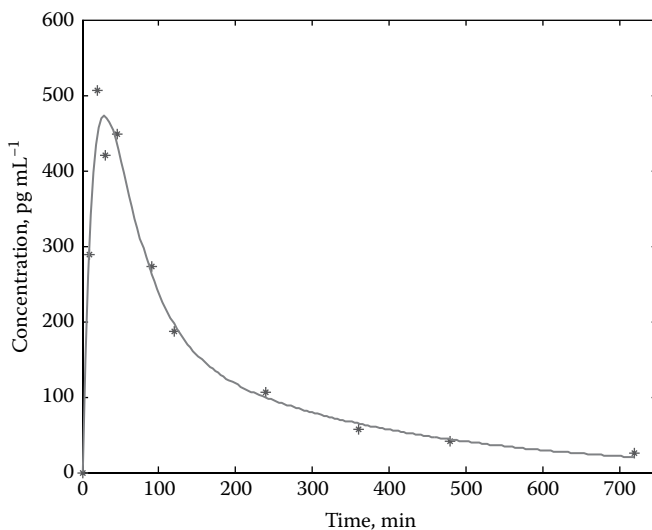


Figure 8.14 Comparison of actual and predicted plasma scopolamine levels.

### 8.9.3 Two-compartment model with drug absorption from a transdermal patch

If the drug is delivered transdermally from a thin skin patch of thickness  $\delta_{\text{device}}$  and cross-sectional area  $S$ , then we can replace the absorption rate term in [Equation 8.87](#), i.e.,  $k_a A_{\text{drug}} = k_a f D_{\text{drug}} e^{-k_a t}$ , with  $P_{\text{SC}} S C_{\text{drug}}^0 e^{-\left(\frac{P_{\text{SC}}}{\delta_{\text{device}}}\right)t}$ . Hence, [Equation 8.88](#) still describes the plasma drug concentration, however, with the understanding that  $k_a = \frac{P_{\text{SC}}}{\delta_{\text{device}}}$  and  $f D_{\text{drug}} k_a = P_{\text{SC}} S C_{\text{drug}}^0$ .

### 8.9.4 Two-compartment model with drug absorption from an implantable device

If the drug is delivered within the body from a cylindrical controlled release device with a diameter of  $d_{\text{implant}}$  and circumferential area  $S_{\text{implant}}$ , then we can replace in [Equation 8.87](#) the term,  $k_a A_{\text{drug}} = k_a f D_{\text{drug}} e^{-k_a t}$  with  $P_m S_{\text{implant}} C_{\text{drug}}^0 e^{-\left(\frac{4P_m}{d_{\text{implant}}}\right)t}$ . Hence, [Equation 8.88](#) still describes the plasma drug concentration, however, with the understanding that  $k_a = \frac{4P_m}{d_{\text{implant}}}$  and  $f D_{\text{drug}} k_a = P_m S_{\text{implant}} C_{\text{drug}}^0$ .

## 8.10 Superposition principle

The pharmacokinetic models we have developed so far are based on a single dose of the drug. In many cases, multiple sequential doses of a drug are given. The *superposition principle* argues that each drug dose behaves independently of any other dose that is given. The total concentration of a drug at a particular time  $t$  is the summation of the concentration at that particular time resulting from each dose that has been administered. Hence,

$$C_{\text{total}}(t) = C_{\text{total}}^{(1)}(t) + C_{\text{total}}^{(2)}(t) + C_{\text{total}}^{(3)}(t) + C_{\text{total}}^{(4)}(t) + \dots \quad (8.90)$$

where  $C_{\text{total}}^{(i)}(t)$  is the concentration of the drug from the  $i$ th dose at time  $t$ . The  $C_{\text{total}}^{(i)}(t)$  can be described by the previously developed single-dose pharmacokinetic models. Be careful though in your calculations since the single-dose model equations for a given dose are in terms of the time since that particular dose was given, i.e.,  $t'$ . Therefore, for the  $i$ th dose,  $t' = t - t_i$ , where  $t_i$  is when the  $i$ th dose was taken relative to  $t$ .

### Example 8.10

Write the mathematical expression that describes the plasma concentration for a drug given orally in two separate doses. Assume the pharmacokinetics of the drug can be described by a single-compartment model with first order absorption and elimination.

### Solution

The appropriate model is given by [Equation 8.71](#). We let  $D_1$  be the first drug dose taken at  $t_1$  and  $D_2$  is the second drug dose taken at  $t_2$ . At  $t = 0$ , the plasma concentration of the drug is zero. Using the superposition principle, the pharmacokinetic model is given by

$$C_{\text{total}}(t) = \theta(t - t_1) \left( \frac{fD_{\text{drug}}^{(1)}}{V_{\text{apparent}}} \right) \left( \frac{k_a}{k_a - k_{te}} \right) \left( e^{-k_{te}(t-t_1)} - e^{-k_a(t-t_1)} \right) \\ + \theta(t - t_2) \left( \frac{fD_{\text{drug}}^{(2)}}{V_{\text{apparent}}} \right) \left( \frac{k_a}{k_a - k_{te}} \right) \left( e^{-k_{te}(t-t_2)} - e^{-k_a(t-t_2)} \right)$$

where  $\theta(t - t_i)$  is the unit step function, which is equal to 0 when  $t - t_i < 0$  and equal to 1 when  $t - t_i > 0$ .

## Problems

- 8.1 Derive [Equation 8.38](#).
- 8.2 Derive [Equation 8.71](#).
- 8.3 Derive [Equations 8.72](#) and [8.73](#).
- 8.4 Derive [Equation 8.75](#).
- 8.5 The rate constants in [Equation 8.71](#) ( $k_a$  and  $k_{te}$ ) can also be found using a graphical technique called “feathering” (Notari, 1987). Note that the plasma concentration in [Equation 8.71](#) is related to the sum of two exponential terms. In most cases,  $k_a$  is larger than  $k_{te}$ ; hence, the second exponential term in [Equation 8.71](#) vanishes for long periods of time. Therefore, for long time periods, [Equation 8.71](#) can be approximated as

$$C(t)_{\text{TL}} \approx \frac{fD_{\text{drug}}}{V_{\text{apparent}}} \left( \frac{k_a}{k_a - k_{te}} \right) e^{-k_{te}t}$$

where  $C(t)_{\text{TL}}$  is the drug concentration along the terminal line (TL) during the drug elimination phase. From this equation, we see that a plot of  $\ln[C(t)_{\text{TL}}]$  versus time predicts that the concentration data for these times should form a straight line. This region is referred to as the terminal elimination phase. The slope of the terminal line that fits the data during this period of time is then equal to  $-k_{te}$  and the intercept is equal to  $\ln \left[ \frac{fD_{\text{drug}}}{V_{\text{apparent}}} \left( \frac{k_a}{k_a - k_{te}} \right) \right]$ . We can also use the equation for  $C(t)_{\text{TL}}$  to form the difference or residual, i.e., residual =  $C(t)_{\text{TL}} - C_{\text{total}}(t)$ , with the following result:

$$\text{Residual} = C(t)_{\text{TL}} - C_{\text{total}}(t) = \frac{fD_{\text{drug}}}{V_{\text{apparent}}} \left( \frac{k_a}{k_a - k_{te}} \right) e^{-k_a t}$$

This equation is valid for all values of time starting from time equal to zero. Note for short periods of time,  $C(t)_{\text{TL}}$  is obtained either by extrapolation of the terminal line or by estimating  $C(t)_{\text{TL}}$  by the first equation above. For long periods of time, this difference is equal to zero. Now, if a plot is made of the  $\ln [C(t)_{\text{TL}} - C_{\text{total}}(t)]$  versus time, the slope is equal to  $-k_a$  and the intercept is once again equal to  $\ln \left[ \frac{fD_{\text{drug}}}{V_{\text{apparent}}} \left( \frac{k_a}{k_a - k_{te}} \right) \right]$ . With  $k_a$  and  $k_{te}$  now known,  $fD_{\text{drug}}/V_{\text{apparent}}$  can be obtained from the value of the intercept.

Use this feathering technique to obtain the parameters for the data given in [Example 8.7](#). How do these parameters obtained using the feathering technique compare with those obtained from a nonlinear regression? Under what conditions do you expect the feathering technique to be difficult to use?

- 8.6** Putcha et al. (1989) gave the data in the table for the scopolamine urinary excretion rate following an IV dose to a subject of 0.4 mg. Develop a suitable pharmacokinetic model to evaluate these data. What is the renal clearance for scopolamine?

Time, min	Urinary Excretion Rate, $\mu\text{g h}^{-1}$
24.6	8.45
73.7	4.97
106.5	3.05
147.4	1.64
212.9	0.96
270.3	0.52
327.6	0.45
425.9	0.27
540.5	0.084
786.2	0.02

- 8.7** You are taking a final exam, it is unlike any exam you have taken before, plus you had a short night of sleep, you had car problems yesterday, you had too much to drink last night, and your cell phone kept ringing early this morning. The result is that you have a terrible headache, unlike any headache you have ever had before. You reach for your bottle of a new headache medicine that claims maximum relief within 30 min and contains a well-known pain reliever. An amazing coincidence is that the exam you are taking includes a problem related to the pharmacokinetics of this pain reliever. You are given the following information:

$$\text{Elimination rate constant} = 0.277 \text{ h}^{-1}$$

$$\text{Apparent distribution volume} = 35 \text{ L}$$

$$\text{Fraction absorbed} = 80\%$$

$$\text{Therapeutic range} = 10\text{--}20 \mu\text{g mL}^{-1}$$

You plan to take this pain reliever. What dose in milligrams should you take? At what time should you take another dose? How much should you take for the second dose?

- 8.8** The pharmacokinetics of nicotinamide was reported in humans (Petley et al., 1995). Nicotinamide, a derivative of the B vitamin niacin, is under investigation as a prevention for insulin-dependent diabetes mellitus. The drug was given orally to eight male subjects with a mean body weight of 75 kg. Two formulations were used, a standard powdered form and a sustained release form. The data below summarize the data obtained for the low-dose studies (standard =  $2.5 \text{ mg kg}^{-1} \text{ BW}^{-1}$  and sustained =  $6.7 \text{ mg kg}^{-1} \text{ BW}^{-1}$ ). Analyze these data using an appropriate pharmacokinetic model. Explain any differences in the pharmacokinetics of the two formulations used.

Time, h	Nicotinamide Plasma	Concentration, $\mu\text{g mL}^{-1}$
	Standard Dose	Sustained Release Dose
0	0	0
0.3	3.3	
0.5	2.45	1.75
0.75	1.90	
1.0	1.45	1.5
1.25	1.00	
1.5	0.80	1.1
1.75	0.55	
2.0	0.50	1.05
2.5	0.30	1.1
3.0	0.20	0.67
3.5		0.50
4.0		0.45
4.5		0.50
5.0		0.55
5.5		0.15

- 8.9** The following serum insulin levels were obtained following the intranasal administration of 150 U of insulin to 12 healthy men (Jacobs et al., 1993). Analyze these data using an appropriate pharmacokinetic model.

Time, min	Serum Insulin Concentration, $\mu\text{U mL}^{-1}$
0	10
15	150
20	220
25	230
30	260
35	250
40	210
45	170
60	140
75	105
90	80
105	50
120	45
150	35
180	35
240	35
300	35

- 8.10** The following plasma concentrations for the antibiotic imipenem were obtained from six patients suffering multiorgan failure (Hashimoto et al., 1997). All patients were also anuric

because of complete renal failure and were placed on continuous venovenous hemodialysis. The antibiotic was delivered by an IV infusion pump for 30 min resulting in an initial plasma concentration of  $32.47 \text{ } \mu\text{g mL}^{-1}$ . Following the infusion, blood samples were taken over the next 12 h. The initial dose was 500 mg, and 107.7 mg of imipenem was recovered in the dialysate fluid (“urine”). The table below summarizes the plasma concentrations.

Time, min	Plasma Concentration, $\mu\text{g mL}^{-1}$
0	32.47
30	24
60	18.5
120	13
180	10
360	4.6
540	2
720	1.12

Use an appropriate pharmacokinetic model to analyze these data.

- 8.11 Starting with [Equation 8.51](#), derive [Equation 8.52](#) using Laplace transforms.
- 8.12 Estimate the stratum corneum permeability for testosterone and estradiol. The molecular weight of testosterone and estradiol are 288 and 272, respectively. The respective values of their octanol/water partition coefficients ( $K_{O/W}$ ) are 2070 and 7000. The reported value of the stratum corneum permeability for testosterone is  $2.2 \times 10^{-3} \text{ cm h}^{-1}$ , and for estradiol, the value is  $3.2 \times 10^{-3} \text{ cm h}^{-1}$  (Joshi and Raje, 2002).
- 8.13 Consider the delivery of a drug from a patch applied to the skin. Assume that the patch has a surface area for drug transport of  $30 \text{ cm}^2$  and a thickness of  $0.6 \text{ mm}$ , that the concentration of the drug in the patch at any time after it has been applied is given by  $C_{\text{drug}}(t)$ , and that the stratum corneum permeability of the drug is given by  $P_{SC}$ , which for this particular drug has a value of  $3.66 \times 10^{-7} \text{ cm s}^{-1}$ . If the initial concentration of the drug in the patch is  $C_{\text{drug}}(0) = 25 \text{ mg mL}^{-1}$ , how long will it take to reduce the concentration of the drug in the patch to  $\frac{1}{2}C_{\text{drug}}(0)$ , i.e.,  $12.5 \text{ mg mL}^{-1}$ ?
- 8.14 Alora is a transdermal system designed to deliver estradiol continuously and consistently over a 3- to 4-day period when placed on the skin. Alora provides systemic estrogen replacement therapy in postmenopausal women. For a  $36 \text{ cm}^2$  patch, the release rate of the drug is  $0.1 \text{ mg}$  of estradiol per day. Clinical trials have provided the following pharmacokinetic data. In one study, following application of the patch, the peak concentration of estradiol was found to be  $144 \text{ pg mL}^{-1}$  ( $10^{12} \text{ pg} = 1 \text{ g}$ ) and the half-life of the estradiol was found to be  $1 \text{ h}$ . Over an  $84 \text{ h}$  dosing interval, the plasma clearance for the estradiol from the Alora patch was found to be  $61 \text{ L h}^{-1}$ . What is the steady-state plasma concentration for estradiol in  $\text{pg mL}^{-1}$ ? What is the apparent volume of distribution in  $\text{L}$ ?
- 8.15 Deponit is a nitroglycerin transdermal delivery system for the prevention of angina pectoris. The *in vivo* release rate of the  $16 \text{ cm}^2$  patch is  $0.2 \text{ mg h}^{-1}$ . The reported volume of distribution is  $3 \text{ L kg}^{-1} \text{ BW}^{-1}$  and the observed clearance rate is  $1 \text{ L kg}^{-1} \text{ BW}^{-1} \text{ min}^{-1}$ . What is the steady-state nitroglycerin concentration ( $\text{ng mL}^{-1}$ ) in a  $70 \text{ kg}$  human? What is the elimination rate constant? What is the half-life of nitroglycerin in minutes?

- 8.16** A pharmacokinetic study of a particular drug taken orally as a single dose provided an  $AUC^{0 \rightarrow \infty}$  of  $1085.5 \text{ ng h mL}^{-1}$ , a  $C_{\max}$  equal to  $98.5 \text{ ng mL}^{-1}$ , and a  $\tau_{\max}$  of  $2.1 \text{ h}$ . From these data, determine the values of  $V_{\text{apparent}}$  ( $\text{L}$ ),  $k_{\text{te}}$  ( $\text{min}^{-1}$ ), and  $k_a$  ( $\text{min}^{-1}$ ). The dose was  $80 \text{ mg}$  and the entire drug is available, i.e.,  $f = 1$ .
- 8.17** Design a skin patch to deliver nicotine. The goal is to have a patch that delivers nicotine for  $24 \text{ h}$ , then a new patch is added, and so on. Nicotine is somewhat water soluble and has a molecular weight of  $162.23$  and an octanol-water partition coefficient ( $\log K_{\text{O/W}}$ ) of  $1.2$ . The dose of nicotine to be absorbed into the body is  $21 \text{ mg}$  per  $24 \text{ h}$ , and the initial concentration of nicotine within the patch is  $25 \text{ mg mL}^{-1}$ . Assume that the total nicotine content of the patch is  $52.5 \text{ mg}$ . The volume of distribution for nicotine is  $2\text{--}3 \text{ L kg}^{-1}$  of body weight, and the average plasma clearance is  $1.2 \text{ L min}^{-1}$ . Estimate the surface area and the thickness of the patch. Also plot the predicted plasma concentration of nicotine in  $\text{ng mL}^{-1}$  over a period of  $7 \text{ days}$  assuming a new patch is applied every  $24 \text{ h}$ .
- 8.18** Krewson et al. (1995) presented the steady-state data in the table for the distribution of the nerve growth factor (NGF) in the vicinity of a thin cylindrical controlled drug release device implanted into the brain of a rat. The polymeric disks containing radiolabeled  $I^{125}\text{-NGF}$  were  $2 \text{ mm}$  in diameter and  $0.8 \text{ mm}$  in thickness. The NGF has a molecular weight of  $28,000 \text{ g mol}^{-1}$ . Assume that the NGF is eliminated from the brain tissue by a first order process, i.e., the rate of elimination is proportional to the concentration of NGF, i.e.,  $k_{\text{apparent}}C_{\text{NGF}}$  where  $k_{\text{apparent}}$  is the apparent first order elimination rate constant for the NGF and accounts for such processes as metabolism, cellular internalization, or uptake by the brain's systemic circulation. Then develop a steady-state reaction-diffusion model to analyze these data. The boundary conditions, assuming the origin of the Cartesian coordinate system to be the midline of the polymeric disk, are as follows:

$$C_{\text{NGF}} = C_0 \quad \text{at} \quad x = a \quad \text{and} \quad C_{\text{NGF}} = 0 \quad x = \infty$$

where  $a$  is the half-thickness of the polymeric disk. Estimate the value of the Thiele modulus  $\left( a \sqrt{\frac{k_{\text{apparent}}}{D_T}} \right)$  that provides the best estimate of the data.  $D_T$  represents the diffusivity of the NGF in the brain tissue which is estimated to be  $4 \times 10^{-7} \text{ cm}^2 \text{ s}^{-1}$ . Using this value of  $D_T$  for the NGF, what is the value of  $k_{\text{apparent}}$ ? Using [Equation 8.30](#), calculate the half-life of the NGF in the brain tissue. How does this value of the NGF half-life compare to the reported half-life of the NGF in brain tissue of about  $1 \text{ h}$ ?

Distance from Polymer/Tissue Interface, mm	NGF Concentration, $\mu\text{g mL}^{-1}$
0	37.0
0.1	31.5
0.2	20.0
0.3	15.0
0.4	10.5
0.5	8.5
0.6	6.5
0.8	3.5
1.0	2.2

- 8.19** The following table summarizes plasma nicotine levels in a 27-year-old man chewing one piece of gum containing 4 mg of nicotine (McNabb et al., 1982). Nicotine gum was developed to help people quit smoking by providing the same amount of plasma nicotine as obtained from cigarettes. Nicotine is absorbed from the gum over a 30 min period after an initial short period of chewing the gum to release the nicotine. Nicotine is then readily absorbed within the buccal cavity. From the data provided in this table, explore how well a single-compartment model with first order absorption and elimination fit these data. Can a better fit to these data be obtained by assuming that the nicotine is released at a constant rate during the initial 30 min period? In your analyses, determine the pharmacokinetic parameters that describe the absorption and elimination of nicotine.

Time, min	Plasma Nicotine Concentration, ng mL <sup>-1</sup>
0	0
2	2.5
3	4
6	4
8	5
10	6
12	7
13	8.5
16	10
18	11
20	12
24	13
28	12.5
32	12
35	11
41	10
48	9
52	9
65	7.5

- 8.20** A transdermal delivery system for a drug gives an in vivo release rate of  $40 \text{ mg h}^{-1}$ . If the apparent distribution volume for this drug is  $60 \text{ L}$  and the drug half-life is  $2.5 \text{ h}$ , estimate the steady-state drug concentration in  $\text{mg L}^{-1}$ .
- 8.21** Following the IV injection of  $500 \text{ mg}$  of a drug, the following data were obtained for the plasma concentrations of the drug as a function of time. Estimate the apparent distribution volume, the plasma clearance, the half-life, and the value of the total elimination rate constant  $k_{te}$ .

Time, min	Plasma Concentration, $\mu\text{g mL}^{-1}$
0	100
30	85

(Continued)

Time, min	Plasma Concentration, $\mu\text{g mL}^{-1}$
60	73
120	58
180	52
360	26
480	16
600	8
720	5
1000	1.6

- 8.22** Design an osmotic pump to deliver 150  $\mu\text{L}$  per 90 days of a drug solution. Assume this solution has a density of  $1 \text{ g cm}^{-3}$  and a viscosity of 1 cP. The flow moderator from which the solution exits the pump consists of a tube that is 50 mm in length with a diameter of 0.05 cm. An excess of sodium chloride is placed on the side opposite the drug compartment, and these compartments are separated by a frictionless piston of thickness 5 mm (see [Figure 8.7](#)). At  $37^\circ\text{C}$ , a saturated solution of NaCl is formed and the concentration of this solution is 36.6 g NaCl per 100 g of water. The density of the NaCl solution that is formed is  $1.186 \text{ g cm}^{-3}$ , and there is always enough solid NaCl in this compartment to maintain the saturated state. Assume that the pump has a cylindrical shape made of an alloy of steel and that an osmotic membrane is placed as an end cap on the compartment containing the NaCl. This membrane has a hydraulic conductance, i.e.,  $L_p$ , equal to  $6.29 \times 10^{-5} \mu\text{L day}^{-1} \text{ cm}^{-2} \text{ mmHg}^{-1}$ , and this membrane completely retains the NaCl solution. From this information, specify the diameter of the osmotic pump and provide a reasonable estimate of its length.
- 8.23** Todo et al. (2013) obtained the data shown in the table for the diffusion of methylparaben (MP) across a silicone membrane proposed as an alternative to the use of an animal skin for the prediction of skin permeation. MP is a preservative that is found in a variety of cosmetics and other personal care products. The molecular weight of MP is 152.2. The concentration of MP in the donor compartment was 10 mM, or  $1522 \mu\text{g cm}^{-3}$ . From these data, estimate the permeability of MP in the silicone membrane.

Time, min	MP Permeated, $\mu\text{g cm}^{-2}$
0.5	0.39
1	0.87
1.5	1.55
2	2.33
3	3.69
4	5.24

- 8.24** The serum concentrations of ENG after an IV bolus of 150  $\mu\text{g}$  for an individual with a body mass index (BMI) of  $20 \text{ kg m}^{-2}$  (Wenzl et al., 1998) are given in the table below. ENG is the

active ingredient released from the contraceptive implant known as Implanon. Find the values of the pharmacokinetic parameters that best describe these data.

Time, h	Concentration, pg mL <sup>-1</sup>
0.167	6300
0.5	5500
0.75	3800
1	2800
1.5	1900
2	1400
4	480
6	410
8	340
12	300
16	200
24	190
36	105
48	80
72	40

- 8.25** Using the pharmacokinetic parameters found in [Problem 8.24](#), compare the measured serum ENG concentrations as a function of time shown in the table after the implant of Implanon (Wenzl et al., 1998) to the predicted ENG concentrations based on a pharmacokinetic model for the implant. The implant contains 68 mg of ENG when it is implanted. The in vitro release rate kinetics for this batch of implants gave  $75 \mu\text{g day}^{-1}$  after 3 months,  $55 \mu\text{g day}^{-1}$  at 1 year, and  $40 \mu\text{g day}^{-1}$  after 2 years. The in vivo release rate was found to be 80% of these in vitro values.

Time, Days	Concentration, pg mL <sup>-1</sup>
0	0
80	282
156	235
240	200
429	170
720	165

- 8.26** The data shown in the table were given in Koushanpour (1976) and represents plasma inulin concentrations following a rapid IV injection of 4.5 g of inulin in an 80 kg human.

Determine the pharmacokinetic parameters of the two-compartment model given by Equations 8.80 and 8.81. Also calculate the GFR and compare to the normal value of about  $125 \text{ mL min}^{-1}$ .

Time, min	Plasma Inulin Concentration, $\mu\text{g mL}^{-1}$
10	440
20	320
40	200
60	150
90	110
120	80
150	60
175	48
210	35
240	25

- 8.27** The following table (McNabb et al., 1982) presents plasma nicotine levels in a 49-year-old man while smoking one cigarette yielding 0.8 mg of nicotine. Using the two-compartment model given by Equations 8.88 and 8.89, determine the pharmacokinetic parameters.

Time, min	Plasma Nicotine Concentration, $\text{ng mL}^{-1}$
0	0
2	5
3	7
4	11
5	10
6	14
8	12
9	13
11	13
12	12
15	12
21	9
25	9
35	8
41	7.5
49	7
59	7
71	6

- 8.28** The following table (Nachum et al., 2006) presents plasma scopolamine concentrations obtained from 15 individuals following the application of a transdermal delivery device. Using the model given by [Equation 8.52](#), determine the values of  $\frac{P_{SC}SC_{drug}^0}{V_{apparent}}$ ,  $\frac{P_{SC}}{\delta_{device}}$ , and  $k_{te}$ .

Time, h	Plasma Scopolamine Concentration, pg mL <sup>-1</sup>
0	0
2	8.82
3	20.59
4	29.41
6	55.88
10	83.82
24	105.88
48	101.46
72	92.64

# Chapter 9 Extracorporeal devices

In this chapter, we will discuss and analyze several examples of extracorporeal devices. These devices lie outside (*extra*) the body (*corporeal*) and are usually connected to the patient by an *arteriovenous shunt*.<sup>\*</sup> In some respects, they may be thought of as artificial organs. Their function is based on the use of physical and chemical processes to replace the function of a failed organ or to remove an unwanted substance from the blood. The patient's blood before entering these devices is infused with anticoagulating drugs such as *heparin*, to prevent clotting. A variety of ancillary equipment may also be present to complete the system. This may include items such as pumps, flow monitors, bubble and blood detectors, and pressure, temperature, and concentration control systems. It is important to note that these devices do not generally contain any living cells. Devices containing living cells are called bioartificial organs and these will be discussed in [Chapter 11](#).

## 9.1 Applications

A variety of extracorporeal devices have been developed. The best known of these are *blood oxygenators*, which are used in such procedures as open heart surgery, and *hemodialysis*, which replaces the function of failed kidneys. Other examples include *aquapheresis* for removing excess water from the body; *hemoperfusion*, wherein a bed of activated carbon particles are used for cleansing blood of toxic materials; *plasmapheresis*<sup>†</sup> to separate plasma from blood as a first step in the subsequent processing of the plasma; *immobilized enzyme reactors* to rid the body of a particular substance or to replace lost liver function; and *affinity columns* to remove agents of the immune system that attack the body's own cells, as in *autoimmune diseases* and in *sepsis*.

The primary functional unit of extracorporeal devices is typically provided as a sterile disposable cartridge. However, in some cases, considering mounting healthcare costs, the functional unit can be reused many times provided it is cleaned and sterilized between applications. Reused functional units are not shared between patients.

Certainly, there is no end to the possibilities for extracorporeal devices. However, whatever the functions of the device are, there will be some commonality among them in terms of their construction, use of membranes, and fluid contacting schemes.

## 9.2 Contacting schemes

Most devices, such as blood oxygenators and dialyzers, are typically based on the use of polymeric membranes to create the surface area needed to provide mass transfer between the blood stream and another exchange fluid stream. The membrane is physically retained within the device by a support structure that also creates the flow channels. As illustrated in [Figure 9.1](#) for hemodialyzers,

\* A shunt is a means of diverting flow, in this case blood from an artery through a device and then back into the body via a vein.

† See Problem 6.8 for a discussion and analysis of a membrane plasmapheresis system.

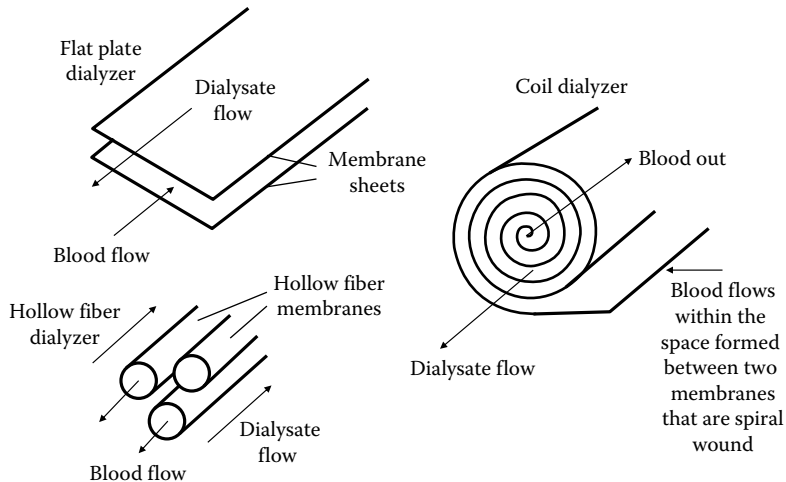


Figure 9.1 Membrane configurations.

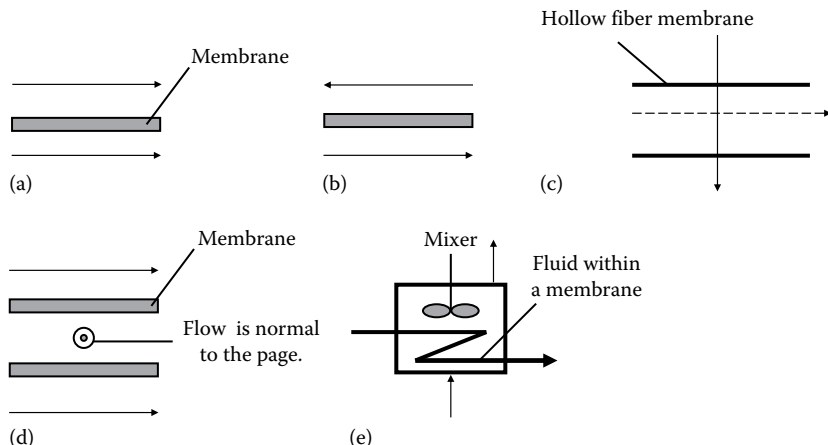


Figure 9.2 Fluid contacting patterns. (a) Cocurrent flow, (b) countercurrent flow, (c) cross flow over a hollow fiber membrane, (d) cross flow in a coiled membrane, and (e) bulk fluid is well mixed.

the membranes are typically arranged as stacks of flat sheets, coils of membrane sheets, or bundles of hollow fiber membranes. Hollow fiber membranes are finding increased use because of their low cost, ease of manufacture, and consistent quality.

A variety of contacting patterns between the blood and the exchange fluid are also possible as shown in [Figure 9.2](#). In *cocurrent flow*, the fluid streams flow in the same direction, whereas, in *countercurrent flow*, the fluid streams flow in opposite directions. In the *cross flow* pattern, the fluid streams flow in a perpendicular sense to each other.

Immobilized enzyme reactors and affinity columns have the active material, i.e., an *enzyme* or other *ligand*, firmly attached to a support particle. Support materials for immobilized enzyme reactors and

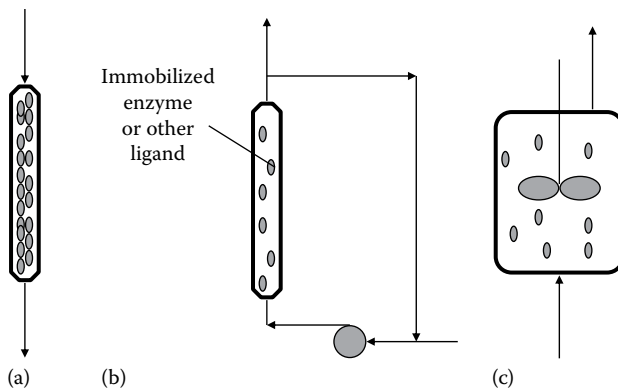


Figure 9.3 Immobilized enzyme and affinity reactor systems. (a) Packed bed, (b) completely mixed by fluid recycle, and (c) completely mixed by impeller.

affinity columns are typically made from a wide variety of polymeric materials such as alginates, agar, carrageenin, and polyacrylamide, or inorganic materials such as glass, silicas, aluminas, and activated carbon. As shown in Figure 9.3, the particles containing the immobilized material can be arranged as a packed bed or the particles can be suspended in a well-mixed device. The complete mixing of the fluid phase and suspended particles can be achieved either by a mechanical impeller or by fluid recirculation.

### 9.3 Solute transport in extracorporeal devices

In many extracorporeal devices, a solute is transported through the blood, perhaps across a membrane, and then into an exchange fluid. These transport processes were discussed in Section 6.1.1.7 and illustrated in Figure 6.6 for the case of simple diffusion.

Recall that we also defined an overall mass transfer coefficient, i.e.,  $K_O$ , (see Equation 6.17) in terms of the overall mass transfer driving force based on the bulk fluid concentrations of the solute as shown in Figure 6.6. The overall mass transfer coefficient is given by Equation 6.18 in terms of the individual film mass transfer coefficients on the blood and exchange fluid sides and the membrane permeability.

Recall that we discussed membrane permeability in much detail in Chapter 6. Membrane permeability, although best measured experimentally (Dionne et al., 1996; Baker et al., 1997), is defined by Equation 6.15. Also as discussed in Chapter 5, the individual film mass transfer coefficients depend on the physical properties of the fluid and the nature of the flow. They also depend on position due to boundary layer growth, so we usually use length-averaged values of these coefficients in Equation 6.18.

#### 9.3.1 Estimating the mass transfer coefficients

Techniques for estimating the individual film mass transfer coefficients for a variety of flow conditions were summarized in Section 5.11. For the laminar flow of fluids in a tube, we can use Equation 5.169 or 5.170 to estimate the film mass transfer coefficient. For other flow situations, Table 5.1 provides a summary of useful mass transfer coefficient correlations.

Blood flow through extracorporeal devices is typically laminar and, in some cases, the velocity and concentration profiles can be fully developed. Recall from Chapter 5 that the laminar flow velocity

profile is fully developed when  $z/d > 0.05Re$  and the concentration profile is fully developed when  $z/d > 0.05ReSc$ . Here,  $z$  is defined as the axial position in the direction of the flow path,  $d$  is the diameter of the tube,  $Re$  is the Reynolds number, and  $Sc$  is the Schmidt number. For solutes in liquids, the  $Sc \gg 1$ , so the velocity profile will develop much faster than the concentration profile. If the value of  $z$  is much less than the length of the flow path in the device, then we can assume that the particular profile, i.e., velocity or concentration, is fully developed within the device. However, if  $z$  is larger than the length of the flow path in the device, then the velocity or concentration profile is undeveloped within the device.

The exchange fluid will either be in laminar or turbulent flow. Generally, one operates on the exchange fluid side in such a manner that its contribution to the overall mass transfer resistance is negligible. If an estimate of the mass transfer coefficient for the solute in the exchange fluid is needed, then one can use [Equation 5.169](#) or [5.170](#) if the exchange fluid flow is laminar. For turbulent flow of the exchange fluid, one can consult [Table 5.1](#) or these additional references: Cussler (1984), Bird et al. (2002), and Thomas (1992).

### 9.3.2 Estimating the solute diffusivity in blood

The diffusivity of the solute in blood is given by  $D_T$  and can be quite different from the solute's diffusivity in the plasma ( $D_{\text{plasma}}$ ) alone because of the presence of the red blood cells. The factors influencing mass transfer within blood are summarized in [Table 9.1](#) (Colton and Lowrie, 1981).

The rheological behavior of blood is not a very important factor in describing solute transport since at the relatively high shear rates encountered in extracorporeal devices, blood behaves as a Newtonian fluid. Mass transport theories for Newtonian fluids are well developed, and we can make use of these for the special case of blood. The rotation and translation of red blood cells can influence mass transport to some degree; however, these effects can usually be neglected unless sufficient data is available to warrant their inclusion.

A complete description of solute transport in blood requires that one knows the solute diffusivity and its red blood cell permeability, its equilibrium distribution between the plasma and the fluid within the red blood cell, and the kinetics of any chemical reaction it may undergo with other solutes,

Table 9.1 Factors That Affect Mass Transport in Blood

<i>Suspension properties</i>
Volume fraction of red blood cells
Volume fraction of proteins
Red blood cell solute permeability
<i>Solute behavior</i>
Protein binding kinetics and equilibrium
Reactions with other solutes
<i>Flow-dependent behavior</i>
Rheological properties
Red blood cell dynamics
Rouleaux formation
Migration from the wall
Rotation and translation

typically proteins, that may be present. Clearly, this is a complex problem. The diffusion and reaction of oxygen with hemoglobin is a special case that is important in the design of blood oxygenators and is discussed in [Section 9.5](#). However, for most other solutes, we can treat the blood as a nonreactive fluid and assume either of the following two cases applies.

First, if the red blood cell permeability for the solute of interest is extremely large, then the solute will diffuse through the blood as if it were a pseudohomogeneous fluid and the solute diffusivity will not be affected by the presence of the red blood cells. For this case, one only needs to know the solute diffusivity in plasma, which can be obtained by estimating the aqueous diffusivity by use of [Figure 5.2](#), followed by a correction for the difference in viscosity between an aqueous solution and plasma using [Equation 6.46](#). Solute diffusion in plasma amounts to an estimated 40% reduction in comparison to the aqueous solute diffusivity.

For the second case, the red blood cell may be somewhat permeable to the solute. The solute must therefore diffuse around or through the red blood cells increasing the solute diffusion path and decreasing the solute effective diffusivity. We can use relationships such as those presented in [Chapter 6](#), i.e., [Equations 6.43](#) and [6.45](#), to describe this situation.

Another approach for estimating  $D_T$  has been described by Colton and Lowrie (1981). They investigated the diffusion of urea in both stagnant and flowing blood. They presented data for the ratio of the solute permeability in blood to that in plasma alone as a function of the hematocrit. These results were then used to develop an expression for the solute diffusivity in nonreactive blood.

The diffusion coefficient through blood, i.e.,  $D_T$ , was defined by the following equation for the x-component of the solute flux, which is similar to Fick's first law:

$$N_{\text{blood}} = -D_T \frac{dC_{\text{effective}}}{dx} \quad (9.1)$$

The effective concentration ( $C_{\text{effective}}$ ) represents the volume fraction-weighted sum of the solute concentration in the red blood cell phase ( $C_{\text{RBC}}$ ) and the continuous plasma phase ( $C_{\text{plasma}}$ ) and is given by

$$C_{\text{effective}} = HC_{\text{RBC}} + (1-H)C_{\text{plasma}} \quad (9.2)$$

where  $H$  represents the blood hematocrit. [Equation 9.2](#) treats the blood as a continuous pseudohomogeneous phase, which is a reasonable approximation for an extracorporeal device as long as the region being considered is much larger than the size of an individual red blood cell.

Diffusion of solute through just the continuous or plasma phase ( $H = 0$ ) is given by

$$N_{\text{plasma}} = -D_{\text{plasma}} \frac{dC_{\text{plasma}}}{dx} \quad (9.3)$$

Substituting [Equation 9.2](#) into [Equation 9.1](#) for  $C_{\text{effective}}$  and dividing the result by [Equation 9.3](#) provides a relationship for the solute diffusivity in blood in comparison to its value in plasma alone:

$$\frac{N_{\text{blood}}}{N_{\text{plasma}}} = \frac{D_T}{D_{\text{plasma}}} \left[ HK_{\text{RBC}} + (1-H) \right] \quad (9.4)$$

In this equation,  $K_{\text{RBC}} = C_{\text{RBC}}/C_{\text{plasma}}$  represents the equilibrium partition coefficient for the solute between the red blood cells and the plasma. Average values of  $K_{\text{RBC}}$  for some typical solutes are summarized in [Table 9.2](#).

Table 9.2 Values of  $K_{RBC}$  for Some Typical Solutes

Solute	$K_{RBC}$
Urea	0.86
Creatinine	0.73
Uric acid	0.54
Glucose	0.95

*Source:* Data from Colton, C.K. and Lowrie, E.G., Hemodialysis: Physical principles and technical considerations, in: *The Kidney*, 2nd ed., vol. II, Brenner, B.M. and Rector, F.C., Jr. (eds.), WB Saunders Co., Philadelphia, PA, 1981.

Colton and Lowrie (1981) have shown that [Equation 9.4](#) is also equal to the following expression (actually [Equation 6.43](#) with  $\phi = H$ ) assuming the red blood cell is impermeable to the solute ( $D_{cell} = 0$ ):

$$\frac{D_T}{D_{\text{plasma}}} \left[ HK_{RBC} + (1-H) \right] = \frac{2(1-H)}{2+H} \quad (9.5)$$

[Equation 9.5](#) can be used to estimate the diffusivity of a solute in blood, i.e.,  $D_T$ .

With this background on extracorporeal devices, the following discussion will focus on a description and analysis of five representative devices: hemodialyzers, aquapheresis, blood oxygenators, enzyme reactors, and affinity columns.

## 9.4 Hemodialysis

### 9.4.1 Background

The basic functional unit of the kidney is the nephron (shown earlier in [Figure 8.3](#)). Each kidney contains about 1 million nephrons. Only about one-third of these nephrons are needed to maintain normal levels of waste products in the blood. If about 90% of the nephrons lose their function, then the symptoms of *uremia* will develop in the patient. Uremia results when waste products normally removed from the blood by the kidneys start to accumulate in the blood and other fluid spaces. For example, water generated by normal metabolic processes is no longer removed and accumulates in the body, leading to *edema*, and in the absence of additional electrolytes, almost half of this water enters the cells rather than the extracellular fluid spaces due to osmotic effects.

The normal metabolic processes also produce more acid than base, and this acid is removed by the kidneys. Therefore, in kidney failure, there is a decrease in the pH of the body's fluids, called *acidosis*, which can result in a *uremic coma*. The end products of protein metabolism include such nitrogenous substances as urea, uric acid, and creatinine. These materials must be removed to ensure continued protein metabolism in the body. The accumulation of urea and creatinine in the blood, although not life threatening by themselves, is an important marker of the degree of renal failure. They are also used to measure the effectiveness of hemodialysis for the treatment of kidney failure. The kidneys also produce the hormone *erythropoietin* that is responsible for regulating the production of red blood cells in the bone marrow. In kidney failure, this hormone is diminished leading to a condition called *anemia* and a lowered hematocrit. If kidney failure is left untreated, death can occur within a few days to several weeks.

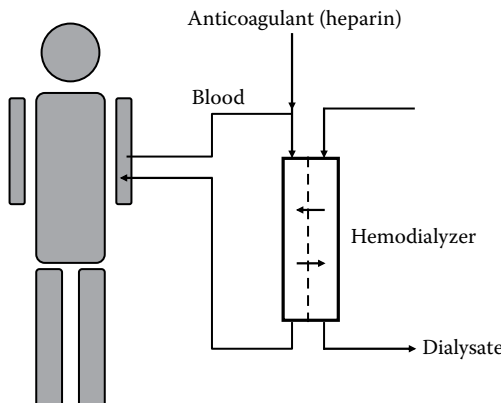


Figure 9.4 Hemodialysis.

Hemodialysis was developed in the 1940s (Kolff, 1947) to treat patients with degenerative kidney failure or end-stage renal disease. Hemodialysis has the ability to replace many functions of the failed kidneys. For example, hemodialysis removes the toxic waste products from the body, maintains the correct balance of electrolytes, and removes excess fluid from the body. Hemodialysis can keep patients alive for several years, and for many patients, allows them to survive long enough to receive a kidney transplant. Nearly 500,000 patients in the United States are currently being kept alive by hemodialysis, and another 200,000 patients have a functioning kidney obtained by transplantation.

Figure 9.4 illustrates the basic operation of hemodialysis. Heparinized blood flows through a membrane device known as the hemodialyzer. The dialysate or exchange fluid flows on the membrane side opposite the blood. Solutes are exchanged by diffusion between the blood and the dialysate fluid. A variety of membrane configurations are possible, and some of the typical ones were shown earlier in Figure 9.1. A variety of flow patterns for the blood and dialysate have been used, and these are also summarized in Figure 9.2. The membranes were originally made from cellulose and cellulose derivatives such as cellulose acetate; however, these have been replaced for the most part by synthetic polymers such as polyacrylonitrile, polycarbonate, polyvinylpyrrolidone, polyarylether-sulfone, and polyamide (Zelman, 1987; Galletti et al., 1995; Clark and Gao, 2002). The membrane surface area of the dialysis cartridge is on the order of 1–2 m<sup>2</sup>. Blood flow rates are in the range of several hundred mL min<sup>-1</sup> and the dialysate flow rate is about twice that of the blood.

#### 9.4.2 Dialysate composition

Table 9.3 compares the species present in normal and uremic plasma with those of a typical dialysate fluid. The composition of the dialysate is based on the need to restore the uremic plasma to the normal state. Note in particular the high levels of urea and creatinine in the uremic plasma. For the most part, the movement of the species in the above table between the uremic plasma and the dialysate is by diffusion. The higher level of HCO<sub>3</sub><sup>-</sup> in the dialysate fluid is used to decrease the acidity of the plasma through its buffering action. Because of the reduced concentrations, the osmolarity of the dialysate is about 265 milliosmolar in comparison to about 300 milliosmolar or so for the plasma. Hence, water will tend to leave the dialysate and enter the plasma by osmosis. Since the patient needs to have excess water removed during dialysis, it is then necessary to maintain the dialysate

Table 9.3 Composition of Normal and Uremic Plasma and Dialysate

Species Electrolytes, mEq L <sup>-1</sup>	Normal Plasma	Uremic Plasma	Dialysate
Na <sup>+</sup>	142	142	133
K <sup>+</sup>	5	7	1
Ca <sup>++</sup>	3	2	3
Mg <sup>++</sup>	1.5	1.5	1.5
Cl <sup>-</sup>	107	107	105
HCO <sub>3</sub> <sup>-</sup>	27	14	35.7
Lactate <sup>-</sup>	1.2	1.2	1.2
HPO <sub>4</sub> <sup>-</sup>	3	9	0
Urate <sup>-</sup>	0.3	2	0
SO <sub>4</sub> <sup>-</sup>	0.5	3	0
Nonelectrolytes, mg dL <sup>-1</sup>			
Glucose	100	100	125
Urea	26	200	0
Creatinine	1	6	0

Source: Data from Guyton, A.C., *Textbook of Medical Physiology*, 8th ed., W.B. Saunders Co., Philadelphia, PA, 1991.

Note: Equivalents (Eq) are the amounts of substances that have the same combining capacity in chemical reactions.

pressure below atmospheric pressure in order to develop a transmembrane pressure gradient that is sufficient to overcome osmosis and remove water from the patient.

The removal of waste products from the plasma must also be carefully controlled in order to avoid *disequilibrium syndrome*. If waste products are removed from the blood too fast by dialysis, then the osmolarity of the plasma becomes less than that of the cerebrospinal fluid, resulting in a flow of water from the plasma and into the spaces occupied by the brain and spinal cord. This increases the local pressure in these areas and can lead to serious side effects.

### 9.4.3 Role of ultrafiltration

The rate at which water is removed (ultrafiltration) from the plasma by the pressure gradient across the dialysis membrane can be estimated using [Equation 3.4](#). This equation can be simplified by assuming only the plasma proteins are impermeable. Hence, the following equation is obtained:

$$Q = L_p S (\Delta P_{\text{mean}} - \Pi_{\text{plasma}}) \quad (9.6)$$

where

$\Pi_{\text{plasma}}$  represents the oncotic pressure of the retained plasma proteins, about 28 mmHg

$\Delta P_{\text{mean}}$  is the average transmembrane pressure difference, which is given by

$$\Delta P_{\text{mean}} = \left[ \frac{P_{B,\text{in}} + P_{B,\text{out}}}{2} - \frac{P_{D,\text{in}} + P_{D,\text{out}}}{2} \right] \quad (9.7)$$

Note that to avoid problems with the calculations, it is best to simply use absolute pressures in [Equation 9.7](#), recognizing that since the dialysate is subatmospheric, its reported gauge pressure will be negative. The pressure drop on the blood side of the hemodialyzer is typically on the order

of 20 mmHg and that on the dialysate side is about 50 mmHg. The mean transmembrane pressure drop is on the order of a few hundred mmHg. The hydraulic conductance,  $L_p$ , is typically about  $3 \text{ mL h}^{-1} \text{ m}^{-2} \text{ mmHg}^{-1}$ . High-flux membranes can have values of the hydraulic conductance as high as  $20 \text{ mL h}^{-1} \text{ m}^{-2} \text{ mmHg}^{-1}$ ; however, protein deposition on the plasma side of the membrane can reduce this in a linear manner by about 6% per hour (Zelman, 1987). [Example 9.1](#) illustrates the calculation of the ultrafiltration rate in a typical membrane dialyzer.

### Example 9.1

Using the membrane properties listed in the discussion in [Section 9.4.3](#), calculate the ultrafiltration rate of water in a hemodialyzer with a membrane surface area of  $1 \text{ m}^2$ . How much water is removed after 6 h of dialysis? Assume blood enters the device at 120 mmHg (gauge) and leaves at 100 mmHg (gauge). The dialysate fluid enters at  $-150 \text{ mmHg}$  (gauge) and leaves at  $-200 \text{ mmHg}$  (gauge).

### Solution

Using [Equation 9.6](#),

$$\begin{aligned} Q &= 1 \text{ m}^2 \times 3 \text{ mL h}^{-1} \text{ m}^{-2} \text{ mmHg}^{-1} \\ &\times \left[ \frac{(120 + 760) + (100 + 760)}{2} - \frac{(760 - 150) + (760 - 200)}{2} - 28 \right] \text{ mmHg} \\ &= 771 \text{ mL h}^{-1} = 13 \text{ mL min}^{-1} \end{aligned}$$

After 6 h of dialysis, about 10 lb of water will have been removed.

### 9.4.4 Clearance and dialysance

Solute transfer in the dialyzer can be analyzed with the help of the model shown in [Figure 9.5](#), which shows a cocurrent flow of the blood and dialysate. The  $Q$ 's represent the volumetric flow rates of the blood (b) and the dialysate (d), and the  $C$ 's represent the concentration of a particular solute. The mass transfer rate of solute A across the dialysis membrane is given by the following equation:

$$\dot{m}_A = Q_b^{in} C_b^{in} - Q_b^{out} C_b^{out} = Q_d^{out} C_d^{out} - Q_d^{in} C_d^{in} \quad (9.8)$$

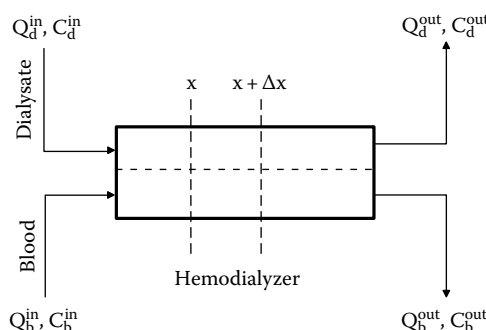


[Figure 9.5](#) Solute mass balance model for a cocurrent hemodialyzer.

The *clearance of the dialyzer* for a particular solute is defined as the volumetric flow rate of blood (typically  $\text{mL min}^{-1}$ ) entering the dialyzer that is completely cleared of the solute. The dialyzer clearance ( $CL_D$ ) for solute A is then given by the next equation:

$$CL_D = \frac{\dot{m}_A}{C_b^{in}} \quad (9.9)$$

The clearances for such solutes as urea, creatinine, and uric acid are on the order of  $100 \text{ mL min}^{-1}$ . Higher molecular weight solutes show a reduced clearance.

The term *dialysance* is also used to describe the solute removal characteristics of a dialyzer. Dialysance ( $D_B$ ) is defined by [Equation 9.10](#). We see that the solute mass transfer rate is now divided by the maximum solute concentration difference between the blood and the dialysate:

$$D_B = \frac{\dot{m}_A}{C_b^{in} - C_d^{in}} \quad (9.10)$$

For a single-pass dialyzer,  $C_d^{in} = 0$ , and the dialysance is then the same as the clearance.

Because of water removal, the inlet and outlet flow rates of the blood and dialysate streams are not equal. This water removal is by ultrafiltration across the hemodialysis membrane and is given by [Equation 9.11](#) in terms of the flow rates of the blood and dialysate streams:

$$Q = Q_b^{in} - Q_b^{out} = Q_d^{out} - Q_d^{in} \quad (9.11)$$

If ultrafiltration is important, then we can use this relationship in combination with [Equations 9.8](#) and [9.9](#) to derive an expression for the clearance that allows for the examination of the importance of ultrafiltration on the clearance of a given solute. Explicitly including the ultrafiltration flow given by  $Q$ , the solute clearance for a particular solute is expressed by the following equation:

$$CL_D = Q_b^{in} \left( \frac{C_b^{in} - C_b^{out}}{C_b^{in}} \right) + Q \left( \frac{C_b^{out}}{C_b^{in}} \right) \quad (9.12)$$

Since, in general, the value of  $C_b^{out} \ll C_b^{in}$ , the contribution of the ultrafiltration flow to the solute clearance is therefore less than the value of  $Q$ . As shown in [Example 9.1](#),  $Q$  is on the order of  $10 \text{ mL min}^{-1}$ , and earlier it was stated that the clearance of such solutes as urea is on the order of a  $100 \text{ mL min}^{-1}$ . Therefore, we can conclude that the effect of ultrafiltration on the clearance of low-molecular-weight solutes is quite small. However, for higher molecular weight solutes, the effect of ultrafiltration may be significant.

#### 9.4.5 Solute transfer

We can now develop relationships between solute clearance and the mass transfer characteristics of the membrane dialyzer. In order to perform this analysis, we first must choose one of the contacting patterns shown in [Figure 9.2](#) to describe the flow of blood and dialysate in the dialyzer. Here, we will use the cocurrent pattern as shown in [Figure 9.5](#). We will also assume that the overall mass transfer coefficient is constant within the hemodialyzer. The flow rates of the blood and dialysate are also assumed to be constant, i.e., ultrafiltration is ignored.

A shell mass balance for the blood and dialysate can then be written for a given solute as

$$\begin{aligned} Q_d C_d|_x - Q_d C_d|_{x+\Delta x} &= K_O W \Delta x (C_b - C_d) \\ Q_d C_d|_x - Q_d C_d|_{x+\Delta x} &= -K_O W \Delta x (C_b - C_d) \end{aligned} \quad (9.13)$$

The quantity,  $W\Delta x$ , represents the available mass transfer area within the shell volume  $\Delta V$  of the hemodialyzer. Hence,  $W$  is the membrane surface area per unit length of the dialyzer. If  $L$  is the length of the dialyzer, then the quantity  $A=L\times W$  is the total membrane area within the dialyzer. After dividing the previous equations by  $\Delta x$  and taking the limit as  $\Delta x$  approaches zero, the following two differential equations are obtained that provide the position dependence of the solute concentration in the dialyzer blood and dialysate:

$$\begin{aligned} Q_b \frac{dC_b}{dx} &= -K_O W (C_b - C_d) \\ Q_d \frac{dC_d}{dx} &= K_O W (C_b - C_d) \end{aligned} \quad (9.14)$$

[Equation 9.14](#) can be integrated analytically, provided we first can relate  $C_d$  and  $C_b$ . This can be obtained by adding the previous two equations, multiplying through by  $dx$ , and then integrating between the entrance and any arbitrary value of  $x$ . The following result is then obtained for the value of  $C_d$  in terms of  $C_b$ . Note that  $z \equiv Q_b/Q_d$ :

$$C_d(x) = C_d^{in} - z(C_b(x) - C_b^{in}) \quad (9.15)$$

Substituting this equation for  $C_d$  in [Equation 9.14](#), we obtain the following differential equation that describes the solute concentration on the blood side. We see that the only dependent variable is the blood concentration:

$$Q_b \frac{dC_b}{dx} = -K_O W \left[ (1+z) C_b - (C_d^{in} + z C_b^{in}) \right] \quad (9.16)$$

[Equation 9.16](#) can now be integrated analytically and rearranged to give the following result. This equation is known as the *performance equation* for a cocurrent hemodialyzer:

$$E = \frac{D_B}{Q_b} = \frac{C_b^{in} - C_b^{out}}{C_b^{in} - C_d^{in}} = \frac{1 - \exp[-N_T(1+z)]}{(1+z)} \quad (9.17)$$

Two additional dimensionless parameters have been defined in the derivation of this equation, the *extraction ratio* ( $E$ ), where  $0 \leq E \leq 1$ , and the *number of transfer units*,  $N_T = K_O A / Q_b$ . The number of transfer units provides a measure of the mass transfer effectiveness, i.e., the amount of solute transported across the membrane versus the amount of solute that enters the device in the blood. The concentration of a given solute in the blood exiting the dialyzer is then given by

$$C_b^{out} = C_b^{in} (1 - E) + E C_d^{in} \quad (9.18)$$

If the membrane area is infinite for a given value of  $z$ , i.e., for given values of the dialysate and blood flow rates, then we achieve the maximum possible extraction ratio, i.e.,  $E_{maximum} = 1/(1+z)$ . This corresponds to the best possible performance in a dialyzer for a given set of blood and dialysate flow

Table 9.4 Performance Equations for Hemodialyzers

Contacting Pattern	Performance Equation
Cocurrent	$E = \frac{1 - \exp[-N_T(1+z)]}{1+z}$
Countercurrent	$E = \frac{\exp[N_T(1-z)] - 1}{\exp[N_T(1-z)] - z}$
Well-mixed dialysate	$E = \frac{1 - \exp(-N_T)}{1 + z[1 - \exp(-N_T)]}$
Cross flow	$E = \frac{1}{N_T} \sum_{n=0}^{\infty} [S_n(N_T) S_n(N_T z)]$ where $S_n(x) = 1 - \exp(-x) \sum_{m=0}^n \left[ \frac{x^m}{m!} \right]$

Source: Colton, C.K. and Lowrie, E.G., Hemodialysis: Physical principles and technical considerations, in: *The Kidney*, 2nd ed., vol. II, Brenner, B.M. and Rector, F.C., Jr. (eds.), WB Saunders Co., Philadelphia, PA, 1981.

rates and is independent of the solute concentrations. This also implies that the solute concentrations in the exiting blood and dialysate are equal or in equilibrium, i.e.,  $C_b^{out} = C_d^{out} = C_{equilibrium}$ . For these conditions, the maximum achievable dialysance for any combination of the blood and dialysate flows is also given by  $D_{B,maximum} = Q_b/(z+1) = Q_b Q_d / (Q_b + Q_d)$ .

If  $z = 0$ , i.e., the dialysate flow rate is significantly higher than that of the blood, and if the membrane area is also infinite, then we obtain from [Equation 9.17](#) that  $E = 1$ . For these conditions, the solute concentration in the blood exiting the dialyzer achieves its lowest possible value, i.e., the value of the solute concentration in the entering dialysate fluid,  $C_d^{in}$ .

Performance equations for other fluid contacting patterns such as countercurrent, a well-mixed dialysate, and cross flow are summarized in [Table 9.4](#). More advanced multidimensional models for describing the hemodialyzer can be found in Ding et al. (2004, 2005) and Labecki et al. (1996).

### Example 9.2

Estimate the clearance of urea in a  $1 \text{ m}^2$  cocurrent and countercurrent hollow fiber hemodialyzer. The dialyzer hollow fibers are 25 cm in length, and they have an inside diameter of 250  $\mu\text{m}$ . The wall thickness of the fibers is 40  $\mu\text{m}$ . The void volume ( $\epsilon$ ) in the hemodialyzer is 50%. Blood flows within the hollow fibers and the dialysate flows in a single pass on the shell side of the device parallel to the fibers. The blood flow rate is  $200 \text{ mL min}^{-1}$ , and the dialysate flow rate is  $500 \text{ mL min}^{-1}$ . The membrane permeability,  $P_m$ , for urea is  $10^{-3} \text{ cm s}^{-1}$ .

### Solution

For the blood flowing through the fibers, the characteristic dimension in the Sherwood number (Sh) is the internal diameter of the fiber. For flow outside and parallel to the fibers, the

characteristic dimension in the dialysate Sherwood number is the hydraulic diameter,  $d_H$ , defined by [Equation 5.171](#) as (Yang and Cussler, 1986)

$$d_H = \frac{4(\text{Cross sectional area})}{\text{Wetted perimeter}}$$

Assuming the fibers are arranged on a square pitch, the following relationship can be developed to express the relationship between the diameter of the hollow fiber ( $d$ ), the dialyzer void fraction ( $\varepsilon$ ), and the hydraulic diameter ( $d_H$ ):

$$d_H = d \left( \frac{\varepsilon}{1-\varepsilon} \right) \text{ square pitch}$$

The apparent velocity of the dialysate through the void space between the fibers is equal to the dialysate volumetric flow rate ( $Q_d$ ) divided by the cross-sectional area of the void space. The cross-sectional area of the void space is equal to the void fraction ( $\varepsilon$ ) times the cross-sectional area of the dialyzer itself. A little algebra provides the following result for the apparent dialysate velocity where  $N_{fiber}$  is the number of hollow fibers in the dialyzer:

$$V_d = \frac{4(1-\varepsilon)Q_d}{N_{fiber}\varepsilon\pi d^2}$$

The number of fibers in the dialyzer can be found from the given membrane area and the dimensions of a single hollow fiber; hence  $N_{fiber} = A_{membrane}/\pi d L$ . After performing the calculations using the performance equations given in [Table 9.4](#) for the cocurrent and countercurrent cases, the predicted urea dialyzer clearance is about  $120 \text{ mL min}^{-1}$  for the cocurrent dialyzer and about  $133 \text{ mL min}^{-1}$  for the countercurrent case. These urea clearance values are typical of what is observed in actual practice. In comparison, the urea clearance of the two normal kidneys is about  $70 \text{ mL min}^{-1}$ . In general, the countercurrent dialyzer will provide the higher clearance, everything else being equal.

This is because the countercurrent flow pattern maintains a relatively constant mass transfer driving force along the length of the dialyzer. The cocurrent pattern provides a larger driving force at the entrance of the dialyzer, but this difference rapidly decreases along the length of the dialyzer, resulting in less overall mass transfer of the solute.

### Example 9.3

Ding et al. (2004) developed a double porous media model to describe the mass transfer in hollow fiber membrane hemodialyzers. They also provided experimental data using several hemodialyzers to validate their model. For the CT190G hemodialyzer module, the properties are as follows:

Effective length	24 cm
Membrane area	1.90 m <sup>2</sup>
Fiber inner diameter	200 μm
Fiber outer diameter	230 μm
Module diameter	3.5 cm

In their countercurrent flow experiments on this hemodialyzer module, they used a saline solution for blood and water for the dialysate fluid. The solution properties used were those of water at 37°C. The diffusivity of urea under these conditions is  $1.82 \times 10^{-5} \text{ cm}^2 \text{ s}^{-1}$ . The overall mass transfer coefficient was found by fitting their model to the experimental data obtained for blood ( $Q_b$ ) and dialysate ( $Q_d$ ) flow rates equal to  $400 \text{ mL min}^{-1}$ , which gave a  $K_O$  equal to  $0.001082 \text{ cm s}^{-1}$ . Ding et al. (2004) assumed this value of the overall mass transfer coefficient is a constant in the flow rate ranges studied in their experiments. Using this information, calculate the predicted urea clearance for each of the flow rate conditions shown in the table.

### Solution

For a blood flow of  $300 \text{ mL min}^{-1}$  and a dialysate flow of  $200 \text{ mL min}^{-1}$ , we can calculate the extraction ratio using the countercurrent flow performance equation given in [Table 9.4](#). The value of  $z$  is equal to 1.5, and the number of transfer units is given by

$$N_T = \frac{K_O A}{Q_b} = \frac{0.001082 \text{ cm s}^{-1} \times 19,000 \text{ cm}^2}{5 \text{ cm}^3 \text{ s}^{-1}} = 4.11$$

Using these values of  $z$  and  $N_T$ , we can calculate  $E$  as

$$E = \frac{\exp[N_T(1-z)] - 1}{\exp[N_T(1-z)] - z} = \frac{-0.872}{-1.372} = 0.636$$

The urea clearance is then given by  $EQ_b$ , which is  $190.7 \text{ mL min}^{-1}$ . Repeating this calculation for all of the combinations of the blood and dialysate flows given by Ding et al. (2004), we obtain the predicted clearance ( $CL_{pred}$ ) results shown in the table. Also shown in the table are the experimental clearances ( $CL_{exp}$ ) and the predicted clearances from their double porous media model ( $CL_{DPMM}$ ).

$Q_b, \text{ mL min}^{-1}$	$Q_d, \text{ mL min}^{-1}$	$CL_{exp}, \text{ mL min}^{-1}$	$CL_{DPMM}, \text{ mL min}^{-1}$	$CL_{pred}, \text{ mL min}^{-1}$
300	200	195.56	188.18	190.7
300	300	234.83	235.21	241.6
300	400	266.56	256.82	263.3
400	200	212.34	196.45	195.3
400	400	294.49	294.57	302.3
400	500	305.62	315.5	324.0

The average error between  $CL_{exp}$  and the  $CL_{DPMM}$  is 3.05%. The average error between the  $CL_{exp}$  and the predicted clearance ( $CL_{pred}$ ) using the much simpler countercurrent performance equation given in [Table 9.4](#) is 3.96%.

### 9.4.6 A single-compartment model of urea hemodialysis

Urea distributes throughout the total body water for an apparent distribution volume of about  $40 \text{ L}$  in a  $70 \text{ kg}$  human. The distribution volume (in liters) can also be estimated to be 58% of body weight (in kg) (Galletti et al., 1995). We can treat the body as a single well-mixed compartment and use the

hemodialyzer performance equations to predict how the amount of urea within the body changes with time during hemodialysis.

For some solutes, the solute removal from the hemodialyzer is so fast that the rate of solute transfer from the extravascular spaces into the plasma will be the rate-limiting step. For these cases, a two-compartment model may be needed to describe the kinetics of solute removal. The following references provide additional information on hemodialysis: Ramachandran and Mashelkar (1980); Colton and Lowrie (1981); Armer and Hanley (1986); Abbas and Tyagi (1987); Zelman (1987); Lee and Chang (1988); Lee et al. (1989); Shaoting et al. (1990); Capello et al. (1994); Galletti et al. (1995).

An unsteady mass balance for urea within the apparent distribution is given by

$$V_{\text{apparent}} \frac{dC_{\text{urea}}}{dt} = \dot{m}_{\text{urea}} - V_{\text{apparent}} k_{\text{te}} C_{\text{urea}} \quad (9.19)$$

In [Equation 9.19](#),  $\dot{m}_{\text{urea}}$  is the body's urea generation rate, which is assumed to be a constant value and is on the order of  $10 \text{ g day}^{-1}$ . It is also assumed that the only elimination pathway for urea is the hemodialyzer. Therefore,  $V_{\text{apparent}} k_{\text{te}}$  equals the urea hemodialyzer clearance. The solution to [Equation 9.19](#) is given by

$$C_{\text{urea}}(t) = C_{\text{urea}}^0 e^{-k_{\text{te}} t} + \left( \frac{\dot{m}_{\text{urea}}}{k_{\text{te}} V_{\text{apparent}}} \right) \left( 1 - e^{-k_{\text{te}} t} \right) \quad (9.20)$$

where  $C_{\text{urea}}^0$  is the concentration of urea in the distribution volume at the start of dialysis.

Once hemodialysis is completed, we then assume the kidney has no residual clearance for urea; hence,  $k_{\text{te}}$  is equal to zero. [Equation 9.19](#) still applies, and we find that during this time, the urea concentration will increase linearly with time after dialysis according to the following equation:

$$C_{\text{urea}}(t) = C_{\text{urea}}^{\text{end of dialysis}} + \left( \frac{\dot{m}_{\text{urea}}}{V_{\text{apparent}}} \right) t \quad (9.21)$$

#### Example 9.4

Using the urea hemodialyzer clearance value for a countercurrent unit obtained from [Example 9.2](#), calculate the time needed to reduce the urea concentration in the body by 60%. How long can one go before the next hemodialysis? Assume the maximum urea concentration is  $75 \text{ mg dL}^{-1}$  and the urea generation rate is  $10 \text{ g day}^{-1}$ .

#### Solution

A 60% reduction in the urea concentration means that  $C_{\text{urea}}/C_{\text{urea}}^0 = 0.40$ . Other parameters needed to solve the problem are

$$\dot{m}_{\text{urea}} = 10 \text{ g day}^{-1} = 1.16 \times 10^{-4} \text{ g s}^{-1}$$

$$V_{\text{apparent}} = 40,000 \text{ cm}^3$$

$$CL_{\text{hemodialyzer}} = 133 \text{ cm}^3 \text{ min}^{-1} = 2.22 \text{ cm}^3 \text{ s}^{-1}$$

$$k_{te} = \frac{CL_{\text{hemodialyzer}}}{V_{\text{apparent}}} = 5.54 \times 10^{-5} \text{ s}^{-1}$$

During the time of hemodialysis, the urea production rate is very low in comparison to the amount of urea removed by dialysis. Therefore, [Equation 9.20](#) simplifies in this case to

$$\frac{C_{\text{urea}}}{C_{\text{urea}}^0} = 0.40 = e^{-k_{te}t}$$

Solving for t:

$$t = -\frac{\ln 0.40}{k_{te}} = -\frac{\ln 0.40}{5.54 \times 10^{-5} \text{ s}^{-1}} = 4.6 \text{ h}$$

The urea concentration at the end of dialysis is  $0.4 \times 75 \text{ mg dL}^{-1}$ , which is equal to  $30 \text{ mg dL}^{-1}$ . After hemodialysis, the length of time before hemodialysis is needed again can be found from this rearrangement of [Equation 9.21](#):

$$t = \frac{(C_{\text{urea}}^{\max} - C_{\text{urea}}^{\text{end of dialysis}}) V_{\text{apparent}}}{m_{\text{urea}}} = \frac{(7.5 - 3) \times 10^{-4} \text{ g cm}^{-3} \times 40,000 \text{ cm}^3}{10 \text{ g day}^{-1}} = 1.8 \text{ days}$$

This result shows that hemodialysis will be required about 3–4 times per week.

**9.4.6.1 Daily home hemodialysis** Recently, daily home hemodialysis has become available for some patients. In this case, the treatment time is much shorter than at a hemodialysis center, on the order of two hours, but more frequent, e.g., 5–7 times per week.

## 9.4.7 Peritoneal dialysis

An alternative approach for treating kidney failure is called continuous ambulatory peritoneal dialysis (CAPD) (Lysaght and Farrell, 1989; Lysaght and Moran, 1995). Unlike the hemodialysis technique that was just described, CAPD has the advantage of the patient not being severely restricted by the regimen of multiple treatments per week at a hemodialysis center. Rather, the patient is responsible for performing a relatively simple maintenance process that can take place at home or even at work. The use of CAPD is growing rapidly. CAPD was used in about 4% of the total dialysis population in 1979 and now is used in about 15% of the dialysis population.

CAPD is based on the addition to the peritoneal cavity of a sterile hypertonic solution of glucose and electrolytes. The peritoneal cavity is a closed space formed by the peritoneum, a membrane-like tissue that lines the abdominal cavity and covers the internal organs such as the liver and the intestines. The peritoneum has excellent mass transfer characteristics for a process like CAPD. The peritoneum has the appearance of a fairly transparent sheath that is smooth and quite strong. The surface area (S)

of the peritoneum is about  $1.75 \text{ m}^2$ . Its thickness ranges from 200 to over 1000  $\mu\text{m}$ . The surface of the peritoneum presented to the CAPD dialysate solution consists of a single layer of mesothelial cells that is densely covered with microvilli or tiny hair-like projections. Beneath this layer of cells is the interstitium that has the characteristics of a gel-like material. Within the interstitium, there is a rich capillary network providing a total blood flow on the order of  $50 \text{ mL min}^{-1}$ .

The CAPD solution is added and later removed from the peritoneal cavity through an in-dwelling catheter. This process can also be automated such that all fluid exchanges are carried out by a pumping unit, even while the patient is asleep. This automated process is called automated peritoneal dialysis (APD).

The intraperitoneal CAPD fluid partially equilibrates across the peritoneal membrane with waste products in the plasma. Excess water from the patient's body is also removed by ultrafiltration across the peritoneal membrane as a result of osmotic gradients. Typically, four 2 L exchanges are made each day with an additional 2 L of water removed as a result of ultrafiltration. The average mass removal rate of a particular solute is given by the following equation:

$$\dot{m}_{\text{CAPD}} = \frac{V_{\text{CAPD}} C_{\text{CAPD}}}{t_{\text{CAPD}}} \quad (9.22)$$

In this equation

$V_{\text{CAPD}}$  represents the volume of the CAPD solution

$C_{\text{CAPD}}$  is the final concentration of the solute in this solution

The time the solution was in the peritoneal cavity is given by  $t_{\text{CAPD}}$ . Recall that the clearance of a solute is equal to its mass removal rate divided by the solute concentration in the blood. Therefore, solute clearance during CAPD is given by

$$CL_{\text{CAPD}} = \frac{\dot{m}_{\text{CAPD}}}{C_{\text{blood}}} = \frac{V_{\text{CAPD}} C_{\text{CAPD}}}{t_{\text{CAPD}} C_{\text{blood}}} \quad (9.23)$$

Since the CAPD solution is usually completely equilibrated with urea in the plasma, the urea clearance is then simply  $V_{\text{CAPD}}/t_{\text{CAPD}}$ . About 10 L of solution is used each day, which equates to a continuous urea clearance of about  $7 \text{ mL min}^{-1}$ .

The mass transfer characteristics of CAPD can be described using relationships we have already developed. For example, the ultrafiltration rate is given by [Equation 6.69](#):

$$Q = S L_P \left[ \Delta P - RT \sum_{i=1}^N \sigma_i (C_{\text{blood}} - C_{\text{CAPD}})_i \right] \quad (9.24)$$

CAPD usually begins with a solution containing about 4% glucose. The initial ultrafiltration rate for this solution is on the order of  $20 \text{ mL min}^{-1}$  and decreases rapidly with time as the glucose, initially in the peritoneal cavity dialysate fluid, is removed by the blood. Since  $\Delta P$  across the peritoneal membrane is small during CAPD and the osmotic pressure of the initial glucose solution is about 4300 mmHg, then the hydraulic conductance is on the order of  $0.15 \text{ mL h}^{-1} \text{ m}^{-2} \text{ mmHg}^{-1}$ .

Table 9.5 Transport Properties of the Peritoneal Membrane

Solute	Molecular Weight	Reflection Coefficient	$P_m S, \text{cm}^3 \text{ min}^{-1}$
Urea	60	0.26	21
Creatinine	113	0.35	10
Uric acid	158	0.37	10
Vitamin B12	1,355		5
Inulin	5,200	0.5	4
$\beta_2$ microglobulin	12,000		0.8
Albumin	69,000	0.99	

Source: Lysaght, M.J. and Moran, J., Peritoneal dialysis equipment, in: *The Biomedical Engineering Handbook*, Bronzino, J.D. (ed.), CRC Press, Inc., Boca Raton, FL, 1995, pp. 1923–1935.

The solute transport rate for species  $i$  is given by Equations 6.69 and 6.70, recognizing that initially significant quantities of solute may be transported by ultrafiltration represented by the first term in Equation 9.25:

$$\dot{m}_{\text{CAPD}} = \tilde{C}_i (1 - \sigma_i) Q + P_{m_i} S (C_{\text{blood}} - C_{\text{CAPD}})_i \quad (9.25)$$

Typical values of the reflection coefficient and the permeability-surface area product for several solutes are summarized in Table 9.5.

Mathematical models describing CAPD can also be developed to describe the time course of the treatment process. The patient is considered to be represented by a single well-mixed compartment of apparent distribution volume ( $V_{\text{apparent}}$ ) and a solute concentration in the body ( $C_{\text{body}}$ ), which is assumed to be the same as the solute concentration in the blood ( $C_{\text{blood}}$ ). The CAPD solution in the peritoneal cavity is in a much smaller variable volume (about 2 L at the start) represented by  $V_{\text{CAPD}}$  and solute concentration  $C_{\text{CAPD}}$ . The peritoneal membrane separates these two compartments. The peritoneal lymphatic system also removes fluid from the peritoneal cavity ( $Q_{\text{lymph}}$ ) at a rate of about 0.1 to as high as 10 mL min<sup>-1</sup>. During the initial phases of CAPD, the volume of fluid in the peritoneal cavity will increase due to the osmotic flow of water into the cavity; however, as time progresses and glucose is diluted and removed from the peritoneal cavity, the volume of fluid in the peritoneal cavity will decrease as a result of the lymphatic flow.

Models for describing CAPD are reviewed by Lysaght and Farrell (1989). These models range from relatively simple analytical solutions to much more complex models that include the selective transport of solutes, ultrafiltration, and the effects of lymphatic flow. These models all require numerical solutions. We will discuss two relatively simple analytical models for CAPD in the following discussion.

**9.4.7.1 Constant volume model of CAPD** The simplest analytical model neglects ultrafiltration and lymphatic flow and assumes that only the peritoneal dialysate concentration changes with time. This diffusion-only model, with the assumption that  $V_{\text{CAPD}}$  is constant, limits the use of this approach to the constant volume phase (isovolemic) that occurs about an hour or so after the CAPD

process begins. For this diffusion-only CAPD model, the solute mass balance equation only needs to be written for the fluid in the peritoneal cavity:

$$\frac{d(V_{\text{CAPD}}C_{\text{CAPD}})}{dt} = V_{\text{CAPD}} \frac{dC_{\text{CAPD}}}{dt} = P_m S(C_{\text{body}} - C_{\text{CAPD}}) \quad (9.26)$$

This equation is easily integrated to obtain the following equations. In these equations, the initial concentration of the solute in the CAPD solution is given by  $C_{\text{CAPD}}^0$ :

$$P_m S = \frac{V_{\text{CAPD}}}{t} \ln \left( \frac{C_{\text{body}} - C_{\text{CAPD}}^0}{C_{\text{body}} - C_{\text{CAPD}}(t)} \right) \quad (9.27)$$

$$C_{\text{CAPD}}(t) = C_{\text{body}} - (C_{\text{body}} - C_{\text{CAPD}}^0) \exp \left( -\frac{P_m S t}{V_{\text{CAPD}}} \right) \quad (9.28)$$

[Equation 9.27](#) allows for the determination of the value of  $P_m S$ , given information on the solute concentrations at a particular time. [Equation 9.28](#) allows for the prediction of the solute concentration in the CAPD dialysate solution as a function of time, assuming the transport properties of the peritoneal membrane are known.

**9.4.7.2 A simple CAPD model that includes ultrafiltration** A slightly more complex model than the one shown earlier can be developed that includes the effect of ultrafiltration (Garred et al., 1983). However, the solute concentration in the body is still assumed to be constant; the peritoneal membrane is not selective, i.e., the reflection coefficients are zero; and lymphatic flow is ignored. The solute balance for the CAPD solution for these conditions can be written as follows:

$$\frac{d(V_{\text{CAPD}}C_{\text{CAPD}})}{dt} = P_m S(C_{\text{body}} - C_{\text{CAPD}}) + C_{\text{body}} \frac{dV_{\text{CAPD}}}{dt} \quad (9.29)$$

The second term on the right-hand side, i.e.,  $(C_{\text{body}}(dV_{\text{CAPD}}/dt))$ , represents the ultrafiltration flow that carries with it the solute from the body. An integration of this equation still requires knowledge of how  $V_{\text{CAPD}}$  changes with time. This could be obtained from [Equation 9.24](#); however, an analytical solution would then be difficult to obtain. If one assumes that the initial and final CAPD volumes are known, then this equation can be integrated using an average value of  $V_{\text{CAPD}}$  to give the next two equations, where  $\bar{V}_{\text{CAPD}}$  is the average volume defined as the mean of the initial and final CAPD volumes:

$$P_m S = \frac{\bar{V}_{\text{CAPD}}}{t} \ln \left[ \frac{V_{\text{CAPD}}^0 (C_{\text{body}} - C_{\text{CAPD}}^0)}{V_{\text{CAPD}}(t) (C_{\text{body}} - C_{\text{CAPD}}(t))} \right] \quad (9.30)$$

$$C_{\text{CAPD}}(t) = C_{\text{body}} - \frac{V_{\text{CAPD}}^0}{\bar{V}_{\text{CAPD}}(t)} (C_{\text{body}} - C_{\text{CAPD}}^0) \exp \left( -\frac{P_m S t}{\bar{V}_{\text{CAPD}}} \right) \quad (9.31)$$

Once again, [Equation 9.30](#) can be used to estimate the mass transport properties of the peritoneal membrane from given values of the solute concentrations and volumes at a particular time. [Equation 9.31](#) allows determination of the time course of the solute concentration in the CAPD dialysate solution.

### 9.4.8 Aquapheresis

Congestive heart failure (CHF) is a very complex chronic disease in which the heart loses its ability to provide a sufficient flow of blood to meet the demands of the body. CHF is usually a result of myocardial infarctions (i.e., heart attack), heart disease such as cardiomyopathy, high blood pressure, and problems with the valves in the heart. Symptoms of CHF include shortness of breath (*dyspnea*), venous swelling or congestion, coughing, swelling of the lower extremities, and difficulty during exercise. CHF severely affects the quality of life since there are frequent life-threatening episodes where plasma fluid volume increases significantly and fluid accumulates (congestion) in the lungs, peripheral tissues, and abdominal organs such as the liver.

Because of the excess fluid in the body (fluid overload), treatment of CHF involves removing the excess sodium and water to achieve a proper fluid balance in the body. This can be achieved by treating the patient with a low-salt diet, restricting fluid intake, and using diuretic drugs, which increase urine production. However, in many cases these treatment methods periodically stop working and the patient requires hospitalization in order to make adjustments to their drug regimen so that the excess water can be removed and other health issues can be addressed. However, some of these patients with frequent hospitalization have also developed a resistance to diuretics, and other means are used to remove the excess water. One approach for these cases is to use *aquapheresis*.

Aquapheresis involves the use of hollow fiber membrane cartridges similar in some respects to those that are used in hemodialysis. However, in aquapheresis the goal is to only remove the excess salt and water. In this case, heparinized blood from the patient is pumped through the hollow fiber membrane cartridge and then returned to the patient. Water and salt are filtered across the membrane by ultrafiltration, and this fluid is collected in a bag and disposed. The flow rate of the water is controlled by the transmembrane pressure differences and by the properties of the hollow fiber membrane. Equations 9.6 and 9.7 can be used to predict the filtration flow of the water as shown in Example 9.1. In aquapheresis, up to 500 mL of water can be removed per hour, and the average rate is about  $250 \text{ mL h}^{-1}$ . The total treatment time for aquapheresis is about 24 h.

## 9.5 Blood oxygenators

### 9.5.1 Background

Heart surgery oftentimes requires that the heart be stopped or arrested (*cardioplegia*). Cardioplegia can be achieved by infusing a cold ( $4^\circ\text{C}$ ) cardioplegic solution into the coronary circulation. Once the heart is arrested, blood is no longer pumped throughout the body and the blood is no longer oxygenated by the lungs. Blood flow to the chambers of the heart is also stopped, providing a dry and bloodless field for surgery. Over 700,000 open heart surgeries are performed in the United States every year (Federspiel and Henchir, 2004). Special devices called heart-lung machines or extracorporeal blood pump-oxygenators (Richardson, 1987; Makarewicz et al., 1993; Galletti and Colton, 1995; Federspiel and Henchir, 2004) have been developed and used for over 50 years (Gibbon, 1954; Iwahashi et al., 2004) to replace the gas exchange function of the lungs and the pumping action of the heart during these open heart surgical procedures.

Blood flow to the blood pump-oxygenator is usually collected into a reservoir by a roller or peristaltic pump from the large systemic veins such as the vena cava or from the right atrium of the heart. This blood is then pumped through the oxygenator and returned to the body via the ascending portion of the aorta. Blood flow rates for a particular oxygenator are typically in the range of  $0.5\text{--}7 \text{ L min}^{-1}$ . A mixture of oxygen and carbon dioxide also passes through the blood oxygenator at flow rates between  $5$  and  $10 \text{ L min}^{-1}$ .

In order to meet the metabolic requirements of the body, the oxygenator will need to be able to deliver around  $250 \text{ mL min}^{-1}$  of oxygen and remove about  $200 \text{ mL min}^{-1}$  of carbon dioxide from the blood. These rates are based on body temperature and atmospheric pressure (BTP,  $37^\circ\text{C}$  and  $1 \text{ atm}$ ). In addition, there are also blood suction devices to minimize the loss of blood and to keep the surgical field free of blood. The suctioned blood is collected and filtered before being pumped into the venous reservoir where it is then sent to the oxygenator. Patients are also given heparin to prevent the clotting of blood in the pump-oxygenator flow circuit. In addition, all of the blood-contacting surfaces of the flow circuit are coated with proprietary heparin or anticoagulant formulations to minimize the risk of blood clot formation and to minimize the amount of systemic heparin that is given to the patient.

In addition to blood pump-oxygenators for heart surgery, much interest has also focused on the development of intravascular lung assist devices, or ILADs (Vaslef et al., 1989; Jurmann et al., 1992; Makarewicz et al., 1993; Fukui et al., 1994; Hewitt et al., 1998; Guzman et al., 2005), and microfluidic oxygenators to serve as an artificial placenta for newborns with respiratory problems (Rochow et al., 2014).

ILADs are being used for the treatment of patients that suffer from adult respiratory distress syndrome. ILADs consist of a bundle of hollow fiber membranes that are mounted on a catheter and then inserted into the vena cava. Pure oxygen is supplied within the hollow fibers by an external flow control system. Blood flows externally along the outer surfaces of the hollow fibers, and oxygen and carbon dioxide are exchanged.

### 9.5.2 Operating characteristics of blood oxygenators

There are several important differences between the operational characteristics of the lungs and blood oxygenators. These are summarized in [Table 9.6](#). The blood flow through the blood oxygenator is usually the same as that to the lungs since the blood oxygenator must provide the same level of blood oxygenation; that is increasing the oxygen partial pressure ( $\text{pO}_2$ ) of the venous blood from about  $40 \text{ mmHg}$  to the arterial  $\text{pO}_2$  of  $95 \text{ mmHg}$ . The capillaries in the lungs present the blood to the alveolar gas as a very thin film of blood with diffusional distances on the order of a few microns. This provides rapid gas transport in a very short time, typically a few tenths of a second. The total surface area available for oxygen transport in the lungs is about  $140 \text{ m}^2$ . In a blood oxygenator, the blood mass transfer film thickness is governed by the number and thickness of the blood flow channels, typically providing oxygen diffusional distances between the blood and the oxygen that are an order of magnitude larger than that found in the lungs. Also the blood contact time in an oxygenator is on the order of tens of seconds.

In the lungs, the  $\text{pO}_2$  of the alveolar air is about  $104 \text{ mmHg}$ . The average oxygen partial pressure driving force in the lungs is therefore on the order of  $40\text{--}50 \text{ mmHg}$ . Carbon dioxide has a partial pressure ( $\text{pCO}_2$ ) of about  $40 \text{ mmHg}$  in the alveolar space, and its level in the blood varies from

Table 9.6 Operational Characteristics of the Lungs and Blood Pump-Oxygenators

Characteristic	Lungs	Blood Oxygenator
Blood flow rate	5 L min <sup>-1</sup>	0.5–7 L min <sup>-1</sup>
Pressure head	12 mmHg	0–200 mmHg
Blood volume	1 L	1–4 L
Blood film thickness	5–10 µm	100–300 µm
Length of blood flow channel	100 µm	2–30 cm
Blood contact time	0.7 s	3–30 s
Surface area for mass transfer	140 m <sup>2</sup>	1–10 m <sup>2</sup>
Gas flow rates	7 L min <sup>-1</sup>	2–10 L min <sup>-1</sup>
pO <sub>2</sub> and pCO <sub>2</sub> blood in	40 and 45 mmHg	40 and 45 mmHg
pO <sub>2</sub> and pCO <sub>2</sub> blood out	95 and 40 mmHg	100–300 and 30–40 mmHg
Gas pO <sub>2</sub> and pCO <sub>2</sub> in	149 and 0.3 mmHg	250–713 and 0–20 mmHg
Gas pO <sub>2</sub> and pCO <sub>2</sub> out	120 and 27 mmHg	150–675 and 10–30 mmHg
pO <sub>2</sub> gradient	40–50 mmHg	650 mmHg
pCO <sub>2</sub> gradient	3–5 mmHg	30–50 mmHg

Sources: Cooney, D.O., *Biomedical Engineering Principles*, Marcel Dekker, Inc., New York, 1976; Galletti, P.M. and Colton, C.K., Artificial lungs and blood-gas exchange devices, in: *The Biomedical Engineering Handbook*, Bronzino, J.D. (ed.), CRC Press, Inc., Boca Raton, FL, 1995, pp. 1879–1997.

40 mmHg in arterial blood to 45 mmHg in venous blood. Therefore, the driving force for carbon dioxide transport is only a few mmHg and considerably smaller than that for oxygen. However, this smaller driving force is offset by the much higher permeability of carbon dioxide through the respiratory membranes, which is about 20 times that for oxygen.

One significant advantage of the blood oxygenator as compared to the lungs is the driving force for oxygen and carbon dioxide transport. In a blood oxygenator, humidified oxygen at atmospheric pressure can be used, resulting in a pO<sub>2</sub> of about 713 mmHg [760 mmHg – 47 mmHg (water saturation pressure at 37°C) = 713 mmHg]. Also, little or no carbon dioxide is present in this gas, so the driving force for carbon dioxide transport is considerably higher. This results in a considerable reduction in the mass transfer surface area of the blood oxygenator. Therefore, although the transport of oxygen is not as efficient within a blood oxygenator, these high mass transfer driving forces allow the resting metabolic needs of the patient to be met using blood oxygenators with mass transfer surface areas in the range from 1 to 10 m<sup>2</sup>.

### 9.5.3 Types of oxygenators

The design goal of a blood oxygenator is to present as large a surface area as possible between the blood and the oxygen-carrying gas stream. Several approaches have been developed to accomplish this, and they are summarized in [Figure 9.6](#) (Iwahashi et al., 2004).

*Bubble oxygenators* were the earliest systems developed for open heart surgery. Bubble oxygenators achieve the required surface area for gas exchange by the production within the blood of numerous small bubbles of gas. These gas bubbles are in direct contact with the blood and are typically several

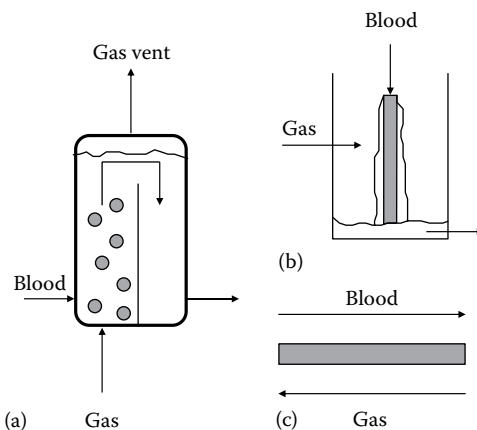


Figure 9.6 Types of blood oxygenators. (a) Bubble oxygenator, (b) film oxygenator, and (c) membrane oxygenator.

millimeters in diameter. Because these bubbles contact the blood, they induce mechanical stresses on the RBCs, which can damage them. Of particular concern in the operation of bubble oxygenators is the removal of foam and gas bubbles prior to the return of the blood to the patient. This is achieved through the use of filters and defoaming sponges as the blood leaves the oxygenator. The design of bubble oxygenators is complicated by the complex nature of bubble motion. For example, bubbles exist in many different sizes, and they tend to break up and coalesce during their passage through the oxygenator.

To avoid the problem with antifoaming and bubble removal, *film oxygenators* have also been developed. In these systems, a film of blood is created on a surface that may be stationary or rotating. The blood film is then exposed directly to the gas. To increase the mass transfer rates, stationary films often employ irregular surfaces to enhance internal mixing of the blood film.

Rotating disks whose bottom surface is in contact with a pool of blood create very thin films that are continuously renewed, resulting in the efficient exposure of the blood to the gas stream.

*Membrane oxygenators* have for the most part now replaced the earlier bubble and film oxygenators. In these systems, the membrane physically separates the blood and gas streams. Membrane systems offer the advantage of minimizing the trauma to the blood that is created in direct contact systems such as bubble and film oxygenators. The membrane and the associated fluid boundary layers, however, do present an additional mass transfer resistance. However, recent advances in membrane technology have resulted in membranes with significant oxygen and carbon dioxide permeabilities. The gas permeabilities for various membrane materials are shown in [Table 9.7](#).

Typical units of the thickness normalized membrane gas permeability ( $\hat{P}_m$ ) are mL (standard temperature and pressure [STP])  $\mu\text{m min}^{-1} \text{m}^{-2} \text{ atm}^{-1}$ , where the STP conditions are for the pure gas at  $0^\circ\text{C}$  and 1 atm. The volumetric transport rate of gas (mL(STP)  $\text{min}^{-1}$ ) is then given by the following equation:

$$N_V = \frac{\hat{P}_m \times (\text{Membrane surface area}) \times \Delta(\text{Gas partial pressure})}{\text{Membrane thickness}} \quad (9.32)$$

Table 9.7 Oxygen and Carbon Dioxide Permeability of Selected Membrane Materials

Material	O <sub>2</sub> Permeability, mL (STP) $\mu\text{m}$ $\text{min}^{-1} \text{m}^{-2} \text{atm}^{-1}$	CO <sub>2</sub> Permeability, mL (STP) $\mu\text{m}$ $\text{min}^{-1} \text{m}^{-2} \text{atm}^{-1}$
Air	$1.27 \times 10^9$	$1.02 \times 10^9$
Polydimethylsiloxane (silicone)	27,900	140,000
Water	3,810	68,600
Polystyrene	1,397	6,985
Polyisoprene (natural rubber)	1,270	7,620
Polybutadiene	1,016	7,112
Cellulose (cellophane)	635	11,430
Polyethylene	305	1,524
Polytetrafluoroethylene (Teflon)	203	610
Polyamide (nylon)	2.54	10.2
Polyvinylidene chloride (saran)	0.25	1.52

Source: Galletti, P.M. and Colton, C.K., Artificial lungs and blood-gas exchange devices, in: *The Biomedical Engineering Handbook*, Bronzino, J.D. (ed.), CRC Press, Inc., Boca Raton, FL, 1995, pp. 1879–1997.

The most common membrane material used in early versions of membrane devices used silicone with wall thicknesses on the order of 50–200  $\mu\text{m}$ . The oxygen permeability for a 130  $\mu\text{m}$  thick silicone membrane is about 215 mL (STP)  $\text{min}^{-1} \text{m}^{-2} \text{atm}^{-1}$  and that for carbon dioxide is about 1100 mL (STP)  $\text{min}^{-1} \text{m}^{-2} \text{atm}^{-1}$  (Cooney, 1976; Gray, 1981, 1984).

Recent hollow fiber systems employ hydrophobic microporous polypropylene membranes. Because these membranes are hydrophobic and have very small pores, there is sufficient surface tension to prevent plasma infiltration. Hence, these pores are gas filled, resulting in significantly higher transport rates of oxygen and carbon dioxide than if the pores were filled with liquid. This can be seen by comparing in [Table 9.7](#) the oxygen permeability through a column of air with that through a column of water of the same thickness. Therefore, these microporous hydrophobic membranes have very high gas permeabilities, and in most cases the resistance to the transport of oxygen and carbon dioxide across these membranes is negligible in comparison to the resistance offered by the flowing blood.

The hollow fiber membranes used in blood oxygenators typically have external diameters in the range of 250–400  $\mu\text{m}$  with wall thicknesses in the range of 20–50  $\mu\text{m}$ . The porosity of these membranes is in the range of 40%–60%, and the pores are typically on the order of 0.1  $\mu\text{m}$  in diameter. These membrane-based systems come in a variety of configurations, e.g., flat plate, coil, and hollow fiber arrangements as shown earlier in [Figure 9.1](#). Blood and gas stream contacting schemes can include cocurrent, countercurrent, and cross flow. Cross flow systems typically have the gas flowing through the lumen of the hollow fiber with blood flowing at right angles across the outer surface of the fibers. The cross flow of the blood results in a significant improvement in the performance as measured by gas exchange rates (Catapano et al., 1992; Vaslef et al., 1994; Wickramasinghe et al., 2002a,b, 2005; Federspiel and Henchir, 2004; Nagase et al., 2005; Wickramasinghe and Han, 2005).

### 9.5.4 Analysis of a membrane oxygenator: Oxygen transfer

The following mathematical model for a blood oxygenator is useful for illustrating the key concepts involved in the design of a blood oxygenator and serves as the foundation for the evaluation of other contacting schemes between the blood and the gas phases. Mathematical models such as the one shown in this section are also important for the evaluation of preliminary design calculations and for exploring the effects of operating conditions on device performance (Vaslef et al., 1994; Matsuda and Sakai, 2000; Nagase et al., 2005; Wickramasinghe and Han, 2005). The model is developed in a manner similar to that used earlier for hemodialysis; however, now we must make use of techniques developed in [Chapter 7](#) to account for the binding of oxygen with hemoglobin.

[Figure 9.7](#) shows the mass balance model where now we assume countercurrent flow of the blood and gas streams. We also assume the total flow rates of these streams are unchanged; hence,  $Q_g$  and  $Q_b$  are constant.  $C_b$  and  $C_g$  are the bulk concentrations of oxygen on the blood (b) and gas (g) sides of the membrane, and  $C'_b$  represents the concentration of oxygenated hemoglobin.  $C_{bm}$  and  $C_{gm}$  are the corresponding oxygen concentration values at the membrane surface on the blood and gas sides, respectively.

A shell balance on oxygen can be written as follows for the blood and gas sides of the membrane of length  $\Delta x$ :

$$\begin{aligned} Q_b \left( C_b + C'_b \right) \Big|_x - Q_b \left( C_b + C'_b \right) \Big|_{x+\Delta x} &= k_b W_b \Delta x (C_b - C_{bm}) \\ Q_g C_g \Big|_{x+\Delta x} - Q_g C_g \Big|_x &= k_g W_g \Delta x (C_g - C_{gm}) \end{aligned} \quad (9.33)$$

In these equations  $k_b$  and  $k_g$  are the blood- and gas-side mass transfer coefficients.  $W$  is the membrane area per unit length of membrane with the subscript denoting either the blood (b) or gas (g) side. This allows the application of this discussion to cylindrical fibers where the area normal to the direction of radial transport changes with radial position. For planar membranes we simply have that  $W_b = W_g = W$ .

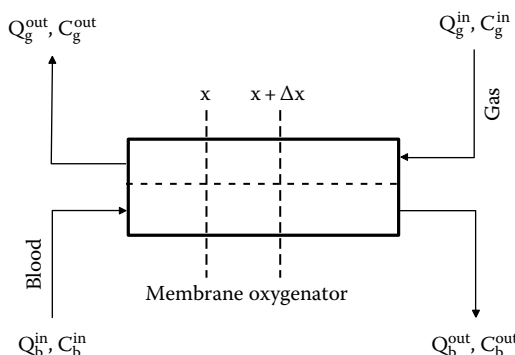


Figure 9.7 Solute mass balance model for a countercurrent membrane blood oxygenator.

After dividing by  $\Delta x$  and taking the limit as  $\Delta x \rightarrow 0$ , we obtain the following differential equations:

$$\begin{aligned} Q_b \frac{d(C_b + C'_b)}{dx} &= -k_b W_b (C_b - C_{bm}) \\ Q_g \frac{dC_g}{dx} &= k_g W_g (C_g - C_{gm}) \end{aligned} \quad (9.34)$$

Once again, we can make use of the fact that the slope of the oxygen-hemoglobin dissociation curve is given by  $m = dC'_b/dC_b$ . A value for  $m$  can be estimated from [Equation 7.57](#) or [7.58](#), and in general,  $m$  will depend on the local dissolved oxygen concentration or the  $pO_2$ . Assuming that  $m$  is constant and evaluated at the average of the venous and arterial  $pO_2$  values, the blood-side equation simplifies to the following result:

$$Q_b (1+m) \frac{dC_b}{dx} = -k_b W_b (C_b - C_{bm}) \quad (9.35)$$

It is now convenient to convert from the oxygen concentration to the oxygen partial pressure in our description of the mass transfer process. Recall for blood that the partial pressure of oxygen is related to the dissolved oxygen concentration by Henry's law, i.e.,  $pO_{2b} = H_{O2}C_b$ . The value of  $H_{O2}$  for blood is  $0.74 \text{ mmHg } \mu\text{M}^{-1}$ . On the gas side,  $pO_{2g} = RT C_g$ , using the ideal gas law. Our equations for the blood and gas sides may now be written as

$$\begin{aligned} Q_b (1+m) \frac{dpO_{2b}}{dx} &= -k_b W_b (pO_{2b} - pO_{2bm}) \\ Q_g \frac{dpO_{2g}}{dx} &= k_g W_g (pO_{2g} - pO_{2gm}) \end{aligned} \quad (9.36)$$

These equations can be rewritten in terms of the overall oxygen partial pressure driving force, i.e.,  $pO_{2g} - pO_{2b}$ , through the definition of the overall mass transfer coefficient,  $K_O$ , defined by

$$\frac{1}{K_O} = \frac{H_{O2}}{k_b} + \frac{W_b}{\rho^{\text{STP}} P_m \bar{W}_L} + \frac{RT W_b}{k_g W_g} \quad (9.37)$$

where  $\rho^{\text{STP}}$  represents the density of the gas at STP conditions ( $0^\circ\text{C}$  and 1 atm). The units on  $K_O$  are typically  $\text{mol cm}^{-2} \text{ mmHg}^{-1} \text{ s}^{-1}$ .  $K_O$  is also now based on the membrane area on the blood side, i.e.,  $W_b$ , where the log mean area of the membrane is given by  $\bar{W}_L \equiv \frac{W_g - W_b}{\ln(W_g/W_b)}$ .

As discussed earlier for blood oxygenators using microporous hydrophobic hollow fiber membranes, the membrane pores are gas filled and therefore have a permeability that is much larger than the blood-side mass transfer coefficient. Also, the solubility of the gases in blood is very low, which means that the gas-side mass transfer coefficient is also much larger than the liquid-side mass transfer coefficient. This means that the blood-side mass transfer resistance is usually controlling, and [Equation 9.37](#) simplifies to

$$K_O \approx \frac{k_b}{H_{O2}} \quad (9.38)$$

In terms of  $K_O$ , the blood- and gas-side equations become

$$\frac{Q_b(1+m)}{H_{O_2}} \frac{dpO_{2b}}{dx} = K_O W_b (pO_{2g} - pO_{2b}) \quad (9.39)$$

$$\frac{Q_g}{RT} \frac{dpO_{2g}}{dx} = K_O W_b (pO_{2g} - pO_{2b})$$

We can now solve these equations to provide an analytical solution to describe the performance of the oxygenator. First, we subtract the gas-side equation from the blood-side equation. This allows us to obtain a relationship between  $pO_{2g}$  and  $pO_{2b}$ :

$$\frac{Q_b(1+m)}{H_{O_2}} \frac{dpO_{2b}}{dx} - \frac{Q_g}{RT} \frac{dpO_{2g}}{dx} = 0 \quad (9.40)$$

This equation is then integrated from the entrance of the blood stream at  $x = 0$  to any arbitrary value of  $x$  to give

$$pO_{2g}(x) = \frac{Q_b}{Q_g} \frac{RT}{H_{O_2}} (1+m) [pO_{2b}(x) - pO_{2b}^{in}] + pO_{2g}^{out} \quad (9.41)$$

Now we can substitute this equation for  $pO_{2g}$  in the blood-side equation (9.39) to give

$$\frac{dpO_{2b}}{dx} = \left[ \frac{K_O W_b H_{O_2}}{Q_b (1+m)} \right] \left\{ \left[ \frac{Q_b}{Q_g} \frac{RT}{H_{O_2}} (1+m) - 1 \right] pO_{2b} + \left[ pO_{2g}^{out} - \frac{Q_b}{Q_g} \frac{RT}{H_{O_2}} (1+m) pO_{2b}^{in} \right] \right\} \quad (9.42)$$

This equation can then be integrated to give the following result for the blood-side membrane area ( $A_{oxygen}$ ) required for a given change in blood oxygenation:

$$A_{oxygen} = \frac{\alpha}{\beta} \ln \left( \frac{\beta pO_{2b}^{out} + \gamma}{\beta pO_{2b}^{in} + \gamma} \right) \quad (9.43)$$

where  $\alpha$ ,  $\beta$ , and  $\gamma$  are given by

$$\alpha = \frac{Q_b(1+m)}{K_O H_{O_2}}$$

$$\beta = \frac{Q_b}{Q_g} \frac{RT}{H_{O_2}} (1+m) - 1 \quad (9.44)$$

$$\gamma = pO_{2g}^{out} - \frac{Q_b}{Q_g} \frac{RT}{H_{O_2}} (1+m) pO_{2b}^{in}$$

The value of  $\alpha$  will typically have units of  $cm^2$ ,  $\beta$  is dimensionless, and  $\gamma$  will be in  $mmHg$ .

**9.5.4.1 Constant oxygen partial pressure in the gas phase** The change in the gas-side  $pO_2$  is usually not that great. Also, in an experimental study, the gas flow rate can be set at a high level to keep the  $pO_2$  change in the gas phase small. This means that we can treat the  $pO_2$  in the gas phase as a constant, i.e.,  $pO_{2g} = pO_{2g}^{\text{avg}} = \frac{1}{2}(pO_{2g}^{\text{in}} + pO_{2g}^{\text{out}})$ . In this case, from [Equation 9.39](#), we can then write the blood-side oxygen balance as

$$\frac{Q_b(1+m)}{H_{O_2}} \frac{dpO_{2b}}{dx} = K_O W_b (pO_{2g}^{\text{avg}} - pO_{2b}) \quad (9.45)$$

Integrating [Equation 9.45](#) over the length of the oxygenator gives the following equation for the blood-side membrane area:

$$A_{\text{oxygen}} = \alpha \ln \left( \frac{pO_{2g}^{\text{avg}} - pO_{2b}^{\text{in}}}{pO_{2g}^{\text{avg}} - pO_{2b}^{\text{out}}} \right) \quad (9.46)$$

where  $\alpha$  is given by the expression given in [Equation 9.44](#).

**9.5.4.2 Constant oxygen partial pressure in the gas phase and external cross flow of the blood over the hollow fibers** Next, we consider an oxygenator where the gas flows within the hollow fibers and the blood flows outside and across in a direction perpendicular to the hollow fibers. We will also assume that the gas flow is sufficiently high that the gas concentrations are constant along the length of the hollow fiber and the controlling mass transfer resistance is in the blood.

[Figure 9.8](#) shows the mass balance model. A shell balance on oxygen can be written as follows for the blood for a membrane of length  $\Delta x$  in the blood flow direction:

$$Q_b (C_b + C'_b) \Big|_x - Q_b (C_b + C'_b) \Big|_{x+\Delta x} = k_b W_b \Delta x (C_b - \bar{C}_g) \quad (9.47)$$

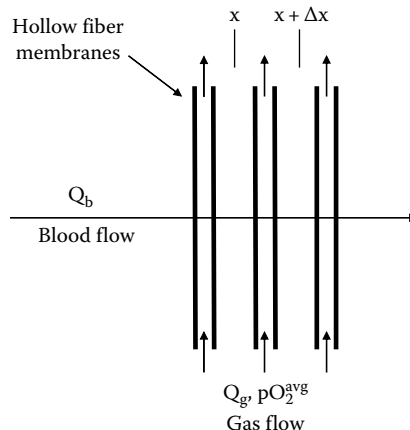


Figure 9.8 External cross flow of blood over hollow fiber membranes.

where, at the gas-blood interface,  $\bar{C}_g$  is the oxygen concentration in the blood assumed to be in equilibrium with the gas phase oxygen concentration, i.e.,  $\bar{C}_g = pO_{2g}^{avg}/H_{O_2}$ .

Next, we assume that  $m=dC_b/dC_b$  is a constant, divide through by  $\Delta x$ , and take the limit as  $\Delta x \rightarrow 0$ ; we then get

$$Q_b(1+m) \frac{dC_b}{dx} = -k_b W_b (C_b - \bar{C}_g) \quad (9.48)$$

Replacing the concentrations with the partial pressure of oxygen, we obtain

$$Q_b(1+m) \frac{dpO_{2b}}{dx} = -k_b W_b (pO_{2b} - pO_{2g}^{avg}) \quad (9.49)$$

Integrating [Equation 9.49](#) over the length of the oxygenator gives the following equation for the blood-side membrane area:

$$A_{oxygen} = \frac{Q_b(1+m)}{k_b} \ln \left( \frac{pO_{2g}^{avg} - pO_{2b}^{in}}{pO_{2g}^{avg} - pO_{2b}^{out}} \right) \quad (9.50)$$

**9.5.4.3 Calculation of the blood-side mass transfer coefficient** Since the oxygen solubility in blood is low, the mass transfer coefficient in the gas phase is much larger than that on the blood side, and for practical purposes the gas-side mass transfer resistance can be ignored. In addition, for hollow fiber membranes where the pores are filled with the gas, the membrane permeability is also very large. This means that in most cases, the controlling mass transfer resistance resides in the blood and we only need to find  $k_b$ .

The calculation of the blood-side mass transfer coefficient ( $k_b$ ) can be found from correlations that typically have the following general form, i.e.,  $Sh = aRe^bSc^{1/3}$ . The Sherwood number in the mass transfer coefficient correlation for  $k_b$  is defined as  $k_b d_H/D_{blood}$ , where  $D_{blood}$  is the diffusivity of oxygen in the whole blood and  $d_H$  is the hydraulic diameter.

The constants  $a$  and  $b$ , i.e., in  $Sh = aRe^bSc^{1/3}$ , depend on the geometry and the flow pattern that is used in a particular hollow fiber blood oxygenator. For blood flowing inside the hollow fibers, the mass transfer coefficients for tube flow found in [Table 5.1](#) can be used. For blood in external cross flow over a bed of hollow fibers, Vaslef et al. (1994) found that  $a$  ranged from 0.136 to 0.256 and  $b$  ranged from 0.751 to 0.832 in the three oxygenators they studied. Federspiel and Henchir (2004) averaged the values for  $a$  and  $b$  from a variety of correlations for external cross flow of blood in the literature and recommend a value of  $a$  equal to 0.524 and a value for  $b$  of 0.523. Wickramasinghe and Han (2005) for the cross flow of blood over mats of woven hollow fibers gave values of  $a$  and  $b$  as 0.8 and 0.59, respectively.

Yang and Cussler (1986) in their study found for external cross flow over hollow fibers that  $a$  is equal to 0.90 and  $b$  is equal to 0.40 when the void fraction in the hollow fiber cartridge was 0.93. When the void fraction in the hollow fiber bundle was 0.30, the values of  $a$  and  $b$  were found to equal 1.38 and 0.34, respectively.

The Reynolds and Sherwood numbers in the mass transfer correlations for  $k_b$  are defined as follows, i.e.,  $Re = \rho V d_H / \mu$  and  $Sh = k_b d_H / D_{blood}$ , where  $d_H$  is the hydraulic diameter, given by [Equation 5.171](#), and  $D_{blood}$  is the oxygen diffusivity in whole blood. The average velocity ( $V$ ) in the  $Re$  is the volumetric flow rate of the blood divided by the open cross-sectional area normal to the flow. For the flow of blood within a cylindrical hollow fiber of inside fiber diameter ( $d$ ), the average velocity of the blood is just  $4Q_b/\pi d^2$ . However, for the external flow of the blood across and perpendicular to a bank of hollow fibers,  $V$  is the blood velocity in the space between the hollow fibers. Hence,  $v$  is defined as the blood volumetric flow rate ( $Q_b$ ) divided by the open area between the hollow fibers. This open area is equal to the device frontal area ( $A_f$ ) normal to the blood flow multiplied by the hollow fiber module void fraction,  $\epsilon_{module}$ . Hence, we have that  $V = Q_b / \epsilon_{module} A_f$ .

For the flow of blood within a cylindrical hollow fiber, the hydraulic diameter is the same as the inside fiber diameter ( $d$ ). However, if the blood is flowing on the outside of the hollow fibers, this will require an understanding of the hollow fiber arrangement in order to calculate the wetted perimeter of the flow path and the cross-sectional area normal to the flow path. In the case of blood flow across a bank of hollow fibers, the hydraulic diameter can be calculated by the following equation (Wickramasinghe and Han, 2005):

$$d_H = \frac{\epsilon_{module}}{1 - \epsilon_{module}} d_O \quad (9.51)$$

where

- $\epsilon_{module}$  is the void fraction of the hollow fiber module
- $d_O$  is the outer diameter of the hollow fibers

The diffusivity of oxygen in whole blood with a % hematocrit of  $H$  can be estimated from [Equation 9.52](#) (Katoh and Yoshida, 1972). This equation neglects the binding reactions between the oxygen and the hemoglobin:

$$D_{blood} \left( \text{cm}^2 \text{s}^{-1} \right) = (2.13 - 0.0092 H) \times 10^{-5} \quad (9.52)$$

For blood with a 40% hematocrit, the value of  $D_{blood}$  is  $1.76 \times 10^{-5} \text{ cm}^2 \text{ s}^{-1}$ .

The diffusivity in the Schmidt number needs to account for the effect of oxygen binding with hemoglobin (Vaslef et al., 1994; Federspiel and Henchir, 2004; Wickramasinghe and Han, 2005). This means that we use an effective diffusivity in the Schmidt number, defined as follows, i.e.,  $Sc = \mu / \rho D_e = \nu / D_e$ .

To understand this phenomenon of how oxygen binding with hemoglobin affects the oxygen diffusivity in blood, consider the unsteady diffusion of oxygen across a stagnant layer of blood. We assume that only the oxygen dissolved in the plasma can diffuse since the hemoglobin resides within the red blood cells that are not moving since the blood is stagnant. Performing a shell balance on oxygen over a thin slice of blood from  $x$  to  $x + \Delta x$ , we can then write

$$S\Delta x \left( \frac{\partial C}{\partial t} + \frac{\partial C'}{\partial t} \right) = -SD_{blood} \frac{\partial C}{\partial x} \Big|_x - SD_{blood} \frac{\partial C}{\partial x} \Big|_{x+\Delta x} \quad (9.53)$$

In this equation,  $D_{blood}$  is the diffusivity of oxygen in whole blood, which is given by [Equation 9.52](#). The dissolved oxygen concentration is given by  $C$ , and  $C'$  represents the concentration of oxygen

bound to hemoglobin. Now, assuming the dissolved and bound oxygen are in equilibrium and after dividing by  $\Delta x$  and taking the limit as  $\Delta x \rightarrow 0$ , [Equation 9.53](#) becomes

$$\left( \frac{\partial C}{\partial t} + \frac{\partial C'}{\partial t} \right) = \left( \frac{\partial C}{\partial t} + \frac{\partial C'}{\partial C} \frac{\partial C}{\partial t} \right) = \left( 1 + \frac{\partial C'}{\partial C} \right) \frac{\partial C}{\partial t} = D_{\text{blood}} \frac{\partial^2 C}{\partial x^2} \quad (9.54)$$

Note that in [Equation 9.54](#),  $\partial C'/\partial C$  is the slope of the oxygen-hemoglobin dissociation curve, which was previously given by [Equations 7.57](#) and [7.58](#). Letting  $m = \partial C'/\partial C$ , [Equation 9.54](#) can then be written as follows:

$$\frac{\partial C}{\partial t} = \frac{D_{\text{blood}}}{1+m} \frac{\partial^2 C}{\partial x^2} = D_e \frac{\partial^2 C}{\partial x^2} \quad (9.55)$$

Hence, we find from this analysis that the effective diffusivity of oxygen ( $D_e$ ) in blood that we use in the Schmidt number is given by

$$D_e = \frac{D_{\text{blood}}}{1+m} \quad (9.56)$$

or in terms of [Equations 7.57](#) and [7.58](#), we can write the effective diffusivity as

$$D_e = \frac{D_{\text{blood}}}{1 + H_{O_2} C'_{\text{SAT}} \frac{dY}{dpO_2}} = \frac{D_{\text{blood}}}{1 + n P_{50}^n H_{O_2} C'_{\text{SAT}} \frac{pO_2^{n-1}}{(P_{50}^n + pO_2^n)^2}} \quad (9.57)$$

This approach has been found to work well in describing the oxygen mass transfer in blood oxygenators (Vaslef et al., 1994). As shown in [Example 9.7](#), we can use the average  $pO_2$  of the blood in the oxygenator to determine the value of  $D_e$  from [Equation 9.57](#).

In the absence of oxygen binding to hemoglobin, the mass transfer coefficient in the blood ( $k_b^{\text{without}}$ ) would be proportional to  $(Sc = \mu/\rho D_{\text{blood}})^{1/3}$ , whereas when we take the oxygen and hemoglobin binding into account as discussed previously, the blood-side mass transfer coefficient ( $k_b$ ) is proportional to  $(Sc = \mu/\rho D_e)^{1/3}$ . The ratio of  $(k_b)$  to  $(k_b^{\text{without}})$  is then equal to  $(D_{\text{blood}}/D_e)^{1/3} = (1+m)^{1/3}$ . This means that the binding of oxygen to hemoglobin in the blood enhances the blood-side mass transfer coefficient by a factor of  $E = (1+m)^{1/3}$ . Using [Equation 7.58](#) to evaluate  $m$ , we have that

$$k_b = k_b^{\text{without}} E = k_b^{\text{without}} (1+m)^{1/3} = k_b^{\text{without}} \left( 1 + n P_{50}^n H_{O_2} C'_{\text{SAT}} \frac{pO_2^{n-1}}{(P_{50}^n + pO_2^n)^2} \right)^{1/3} \quad (9.58)$$

At an average blood  $pO_2$  of 59.5 mmHg in the oxygenator, the value of  $m$  is equal to 28.2, which gives, according to [Equation 9.58](#), a blood-side oxygen mass transfer coefficient enhancement factor, i.e.,  $E$ , of 3, which means that the binding of oxygen to hemoglobin increases the mass transfer coefficient by a factor of 3.

### 9.5.5 Analysis of a membrane oxygenator: Carbon dioxide transfer

We also need to develop a similar set of equations for the transport of carbon dioxide in the oxygenator. Carbon dioxide can exist in blood in a variety of forms, such as a dissolved gas and in combinations with water, hemoglobin, and other proteins. Like oxygen, the total amount of carbon dioxide in the blood depends on its partial pressure, i.e.,  $p\text{CO}_2$ . The carbon dioxide dissociation curve shown in Figure 9.9 provides a relationship between the total amount of carbon dioxide in the blood and its  $p\text{CO}_2$ . The ordinate expresses the volume of carbon dioxide gas as a percentage of the blood volume. The volume percents are based on body conditions (BTP) of 37°C and 1 atm of pure gas. For example, there is about 50 mL of carbon dioxide at BTP in each 100 mL of blood, i.e., 50 vol.%, at a  $p\text{CO}_2$  of about 42 mmHg.

The change in the carbon dioxide concentration for normal blood is very narrow. For example, venous blood has a  $p\text{CO}_2$  of about 45 mmHg and a corresponding concentration of 52 vol.%. Arterial blood has a  $p\text{CO}_2$  of about 40 mmHg and a corresponding concentration of 48 vol.%.

Figure 9.7 can also be used to write shell balances on the blood and gas sides for carbon dioxide. A set of equations similar to those given by Equation 9.39 are obtained, where  $m$  is now equal to zero. Henry's law is also assumed to describe the relationship between the carbon dioxide concentration in the blood and its  $p\text{CO}_2$ . The overall mass transfer coefficient,  $K_O$ , is still given by Equation 9.37, recognizing that the physical properties of carbon dioxide are to be used. Hence, for carbon dioxide transport in the blood oxygenator we have

$$\begin{aligned} \frac{Q_b}{H_{\text{CO}_2}} \frac{dp\text{CO}_{2b}}{dx} &= K_O W_b (p\text{CO}_{2g} - p\text{CO}_{2b}) \\ \frac{Q_g}{RT} \frac{dp\text{CO}_{2g}}{dx} &= K_O W_g (p\text{CO}_{2g} - p\text{CO}_{2b}) \end{aligned} \quad (9.59)$$

As was done for oxygen, the gas-side equation can be subtracted from the blood-side equation and the result integrated to provide the following expression relating  $p\text{CO}_{2g}$  to  $p\text{CO}_{2b}$ :

$$p\text{CO}_{2g}(x) = \left( \frac{Q_b}{Q_g} \right) \left( \frac{RT}{H_{\text{CO}_2}} \right) [p\text{CO}_{2b}(x) - p\text{CO}_{2b}^{\text{in}}] + p\text{CO}_{2g}^{\text{out}} \quad (9.60)$$

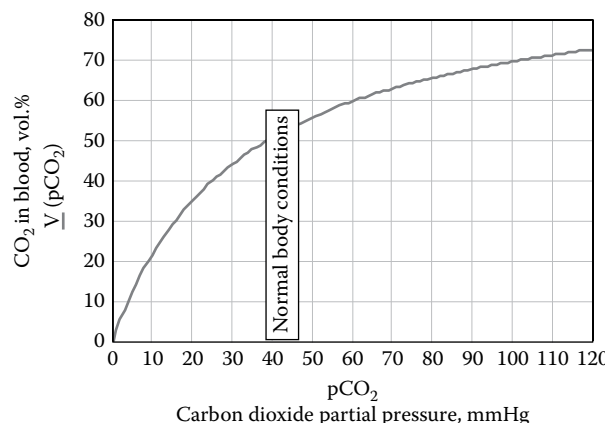


Figure 9.9 Carbon dioxide blood solubility curve.

This equation may be used in the blood equation (9.59) to obtain the following differential equation for  $pCO_{2b}$ :

$$\frac{dpCO_{2b}}{dx} = \left( \frac{K_O W_b H_{CO_2}}{Q_b} \right) \left\{ \left[ \left( \frac{Q_b}{Q_g} \left( \frac{RT}{H_{CO_2}} \right) - 1 \right) pCO_{2b} \right. \right. \\ \left. \left. + \left[ pCO_{2g}^{out} - \left( \frac{Q_b}{Q_g} \right) \left( \frac{RT}{H_{CO_2}} \right) pCO_{2b}^{in} \right] \right] \right\} \quad (9.61)$$

When this equation is integrated over the length of the oxygenator, the following result is obtained for the blood-side membrane surface area needed for the required carbon dioxide removal:

$$A_{carbon\ dioxide} = \frac{\alpha'}{\beta'} \ln \left[ \frac{\beta' pCO_{2b}^{out} + \gamma'}{\beta' pCO_{2b}^{in} + \gamma'} \right] \quad (9.62)$$

The constants  $\alpha'$ ,  $\beta'$ , and  $\gamma'$  are given by the next set of equations and have the same typical units as described earlier for oxygen:

$$\alpha' = \frac{Q_b}{K_O H_{CO_2}} \\ \beta' = \frac{Q_b}{Q_g} \left( \frac{RT}{H_{CO_2}} \right) - 1 \\ \gamma' = pCO_{2g}^{out} - \left( \frac{Q_b}{Q_g} \right) \left( \frac{RT}{H_{CO_2}} \right) pCO_{2b}^{in} \quad (9.63)$$

**Example 9.5** shows how to estimate the carbon dioxide Henry's constant ( $H_{CO_2}$ ).

### Example 9.5

Show that the observed Henry's constant for carbon dioxide in blood for the physiological range of  $pCO_2$  is about  $0.0022 \text{ mmHg } \mu\text{M}^{-1}$ .

#### Solution

First we define Henry's constant ( $H_{CO_2}$ ) by the following relationship:  $pCO_2 = H_{CO_2} C_{CO_2}$ , where  $C_{CO_2}$  is the total concentration of carbon dioxide in the blood.

Using the values obtained from Figure 9.9 at  $pCO_2$ 's of 40 and 45 mmHg, we can calculate the corresponding values of  $H_{CO_2}$ , i.e.,

$$H_{CO_2}(40 \text{ mmHg}) = \frac{40 \text{ mmHg}}{48 \text{ vol.\%}} = 0.833 \frac{\text{mmHg}}{\text{vol.\%}}$$

$$H_{CO_2}(45 \text{ mmHg}) = \frac{45 \text{ mmHg}}{52 \text{ vol.\%}} = 0.865 \frac{\text{mmHg}}{\text{vol.\%}}$$

The average value of  $H_{CO_2}$  in the physiological range of 40–45 mmHg is therefore 0.85 mmHg (vol.%)<sup>-1</sup>. We can then do some unit conversions on this value of  $H_{CO_2}$  to get this result into mmHg  $\mu M^{-1}$  as shown below:

$$H_{CO_2} = 0.85 \frac{\text{mmHg}}{\text{vol.}\%} \times \frac{1 \text{ vol.}\%}{\frac{1 \text{ mL CO}_2(\text{BTP})}{100 \text{ mL(blood)}} \times \frac{1000 \text{ mL(blood)}}{1 \text{ L(blood)}}}$$

$$H_{CO_2} = 0.085 \frac{\text{mmHg L(blood)}}{1 \text{ mL CO}_2(\text{BTP})}$$

Next, we need to find how many moles of carbon dioxide there are in 1 mL of gas at BTP. From the ideal gas law, i.e.,  $PV = nRT$ , we can then write that

$$1 \text{ mL CO}_2(\text{BTP}) = 0.001 \text{ L} = n_{CO_2} \times 0.082 \text{ atm L mol}^{-1} \text{ K}^{-1} \times \frac{310 \text{ K}}{1 \text{ atm}}$$

Solving this equation, we find  $n_{CO_2} = 3.93 \times 10^{-5}$  mol  $CO_2$ .

Therefore, we can now find the value of  $H_{CO_2}$  in units of mmHg and  $\mu M$  as shown next:

$$H_{CO_2} = 0.085 \frac{\text{mmHg L(blood)}}{1 \text{ mL CO}_2(\text{BTP})} \times \frac{1 \text{ mL CO}_2(\text{BTP})}{3.93 \times 10^{-5} \text{ mol CO}_2} \times \frac{1 \text{ mol}}{\frac{\text{L}}{\text{M}}} \times \frac{1 \text{ M}}{10^6 \mu M}$$

$$H_{CO_2} = 0.0022 \text{ mmHg } \mu M^{-1}$$

### 9.5.6 Example calculations for membrane oxygenators

Generally, it is recommended that experiments be performed to measure the oxygen transport rates for a given oxygenator design. Mathematical models, such as the ones developed here or in the papers by Vaslef et al. (1994) and Wickramasinghe et al. (2005), can then be used to correlate the results and provide accurate measurements of the blood-side mass transfer coefficient. A calibrated model can then be used to explore operations under a wide range of operating conditions and assist in the optimal development of the device. For example, Vaslef et al. (1994) and Wickramasinghe et al. (2005) were able to assess the performance of cross flow hollow fiber oxygenators using water and other blood analogues. Subsequent tests using bovine blood provided excellent comparisons between their measurements and model predictions of the oxygen transport rates.

The following examples will illustrate the calculation of the membrane area for a countercurrent hollow fiber membrane blood oxygenator and compare measured oxygen transport rates to the predicted values for a cross flow hollow fiber membrane blood oxygenator.

#### Example 9.6

Determine the hollow fiber membrane surface area for a blood oxygenator operating under the following conditions. Assume the fibers are made from microporous polypropylene. The gas membrane permeabilities are then based on diffusion through a stagnant layer of gas trapped

within the pores of the membrane. The length of each fiber is 50 cm with a wall thickness of 50  $\mu\text{m}$ . The inside diameter of a fiber is 400  $\mu\text{m}$ . The blood flow rate through the lumen of the fibers in the device is 5,000  $\text{mL min}^{-1}$ , and the gas flow rate on the outside of the fibers is 10,000  $\text{mL min}^{-1}$ , both at 37°C and 1 atm. The  $\text{pO}_2$  of the entering blood is 40 mmHg, and the amount of oxygen transported into the blood as it passes through the oxygenator must equal 250  $\text{mL min}^{-1}$  (BTP). The  $\text{pCO}_2$  of the entering blood is 45 mmHg, and the amount of carbon dioxide removed from the blood must equal 200  $\text{mL min}^{-1}$  (BTP). The entering gas is saturated with water ( $\text{pH}_2\text{O} = 47 \text{ mmHg}$  at BTP) and contains a small amount of carbon dioxide in order to decrease the driving force for carbon dioxide transport so that a proper *respiratory exchange ratio* (R) can be achieved and for the calculated surface areas for oxygen and carbon dioxide to be the same. The respiratory exchange ratio is defined as the ratio of carbon dioxide output to oxygen uptake and should be equal to 0.8. Estimate the surface area required to deliver 250  $\text{mL min}^{-1}$  of oxygen to the blood and remove 200  $\text{mL min}^{-1}$  of carbon dioxide under these conditions. The gas-side mass transfer resistance can be considered negligible because of the low solubility of oxygen and carbon dioxide in blood. As discussed earlier, the permeability of these polypropylene hollow fiber membranes is also very high, resulting in negligible mass transfer resistance. Hence, the bulk of the mass transfer resistance is a result of the boundary layer formed within the blood.

### Solution

The solution algorithm is based on first identifying all of the relevant dimensions and physical properties. There are also three unknowns that serve as iteration variables. The *first iteration variable* is the membrane area required for oxygen and carbon dioxide transport. The *second iteration variable* is the average value of the blood  $\text{pO}_2$  as it flows through the hollow fiber. This value is used to calculate, by [Equation 7.58](#), the value of m, which is the slope of the oxygen-hemoglobin dissociation curve. The average  $\text{pO}_2$  is chosen to make the oxygen mass transfer on the gas and blood sides balance. Hence, the amount of oxygen transferred to the blood must equal the amount of oxygen lost from the flowing gas. The *third iteration variable* is the  $\text{pCO}_2$  in the incoming gas. This value is adjusted to make the oxygen and carbon dioxide membrane surface areas, calculated by [Equations 9.43](#) and [9.62](#), result in the same value. In addition, an overall mass balance on oxygen and carbon dioxide is performed such that their respective transport rates are 250 and 200  $\text{mL min}^{-1}$  at BTP. To achieve these gas transport rates, the calculation gives a  $\text{pO}_2$  of the blood exiting the hollow fibers of 90 mmHg and a  $\text{pCO}_2$  of 41.55 mmHg. Once the three iteration variables are assumed, i.e.,  $A_{\text{membrane}}$ ,  $\text{pO}_{2b}^{\text{avg}}$ , and  $\text{pCO}_{2g}^{\text{in}}$ , the calculation approach is then to calculate the value of m by [Equation 7.58](#). From this value of m, the effective diffusivity of oxygen in blood is found from [Equation 9.57](#) using the assumed  $\text{pO}_{2b}^{\text{avg}}$ . Next, the number of hollow fibers based on the assumed membrane area is determined, i.e.,  $N_{\text{fibers}} = A_{\text{membrane}} / \pi d_{\text{outside}} L$ , where  $A_{\text{membrane}}$  is the assumed membrane area,  $d_{\text{outside}}$  is the external fiber diameter, and L is the fiber length. Knowing the number of hollow fibers, the average velocity of blood in a given hollow fiber can be found, i.e.,  $V_{\text{blood}} = 4Q_{\text{blood}} / N_{\text{fibers}} \pi d^2$ , where  $Q_{\text{blood}}$  is the total volumetric flow rate of the blood and d is the internal diameter of a hollow fiber. In this case, the velocity was found in the converged solution to be 23.2  $\text{cm s}^{-1}$ . Next, the value of Re and Sc are found, and from these, the blood-side mass transfer coefficient can be found from [Equation 5.169](#). The  $\text{pO}_2$  in the exiting gas can then be found from [Equation 9.41](#), which in this case is found to be 664.8 mmHg. Next, the surface area of the membrane for oxygen transport is found from [Equation 9.43](#).

This process is then repeated for carbon dioxide and ends with the calculation of the membrane area required for carbon dioxide transport using [Equation 9.62](#). For carbon dioxide, it is found that the exiting  $pCO_2$  in the gas is equal to 44.26 mmHg. Following this, the amount of oxygen and carbon dioxide transport is calculated from an overall mass balance for the gas and for the blood. The surface areas for oxygen and carbon dioxide transport must also come out to be the same for each respective gas, i.e.,  $A_{\text{membrane}} = A_{\text{oxygen}} = A_{\text{carbon dioxide}}$ . In addition, the oxygen and carbon dioxide mass balances must be equal between the gas and blood phases. If the solution has not converged in this manner, then adjustments need to be made to the three iteration variables until convergence is achieved. In this case, the membrane area required for oxygen and carbon dioxide transport was found to equal  $2.25 \text{ m}^2$ . The partial pressure of carbon dioxide in the feed gas was found to be 29.1 mmHg, and the average  $pO_2$  used for calculating the value of  $m$  was found to be 59.5 mmHg. The respiratory exchange ratio also equals 0.80.

### Example 9.7

Vaslef et al. (1994) measured the oxygen transport rate in a Sarns SMO1 oxygenator as a function of the blood flow rate. The oxygenator contained hollow fibers with an outer diameter of  $290 \mu\text{m}$ . The blood flowed external and perpendicular to the hollow fibers. The blood was obtained from cows and the properties of the blood were  $C'_{\text{sat}} = 7800 \mu\text{M}$ ,  $n = 2.85$ ,  $P_{50} = 29.1 \text{ mmHg}$ ,  $H = 37\%$ . The blood entering the oxygenator had an oxygen saturation of about 59%. Pure oxygen at a  $pO_2$  of 760 mmHg flowed within the hollow fibers. The total surface area of the hollow fibers available for oxygen transport was  $1.87 \text{ m}^2$ , and the void space, i.e.,  $\epsilon_{\text{module}}$ , within the oxygenator module was 0.576. The frontal area ( $A_f$ ) normal to the blood flow was  $36.88 \text{ cm}^2$ , and the blood flow path was 9.5 cm in length. Calculate the oxygen transport rate for blood flow rates of 1.41, 3.19, and  $4.86 \text{ L min}^{-1}$ . The measured values of the oxygen transport rates for these blood flows are 113.1, 234.9, and  $313.2 \text{ mL min}^{-1}$  (BTP), respectively. Use the mass transfer correlation they developed using water, which says that  $Sh = 0.136Re^{0.832}Sc^{1/3}$ .

### Solution

Since the blood is in external cross flow over a bank of hollow fibers, we can use [Equation 9.50](#) to find the change in the oxygenation of blood flowing through the oxygenator. Hence,

$$pO_{2b}^{\text{out}} = pO_{2g}^{\text{avg}} - \left( pO_{2g}^{\text{avg}} - pO_{2b}^{\text{in}} \right) e^{-\frac{A_{\text{oxygen}} k_b}{Q_b (1+m)}} \quad (\text{A})$$

Using this equation to guide our calculations, we have from the problem statement that  $pO_{2g}^{\text{avg}} = 760 \text{ mmHg}$ , and we can use the % saturation of the incoming blood to calculate from the Hill equation, for the given values of  $n$  and  $P_{50}$ , the value of  $pO_{2b}^{\text{in}} = 33 \text{ mmHg}$ . Next, we need to calculate the value of  $k_b$ , and the calculation will be shown for the highest flow rate, which is  $4.86 \text{ L min}^{-1}$ . The hydraulic diameter for the flow of the blood across the hollow fibers is given by

$$d_H = \frac{d\epsilon_{\text{module}}}{1 - \epsilon_{\text{module}}} = \frac{0.029 \text{ cm} \times 0.576}{1 - 0.576} = 0.0394 \text{ cm}$$

The Reynolds number is given by the next equation, where  $V$  is the velocity of the blood between the hollow fibers, and we assume the blood behaves as a Newtonian fluid with a viscosity of 3 cP:

$$\text{Re} = \frac{\rho V d_H}{\mu} = \frac{\rho Q_b d}{(1 - \varepsilon_{\text{module}}) A_f \mu} = \frac{1.056 \text{ g cm}^{-3} \times 81 \text{ cm}^3 \text{ s}^{-1} \times 0.029 \text{ cm}}{(1 - 0.576) \times 36.88 \text{ cm}^2 \times 0.03 \text{ g cm}^{-1} \text{ s}^{-1}} = 5.29$$

The hematocrit of the blood is given as 37%, and from [Equation 9.52](#) we calculate the oxygen diffusivity in the blood as  $D_{\text{blood}} = 1.79 \times 10^{-5} \text{ cm}^2 \text{ s}^{-1}$ . Next, we calculate the Schmidt number, taking into account the oxygen transport enhancement due to oxygen binding with hemoglobin. The effective diffusivity of oxygen in the blood is given by [Equation 9.57](#) where the  $pO_2$  is based on the average  $pO_2$  of the blood in the oxygenator. Since  $pO_{2b}^{\text{out}}$  is not known, we have to first assume a value of  $pO_{2b}^{\text{avg}}$ , calculate  $D_e$  from [Equation 9.57](#), find  $pO_{2b}^{\text{out}}$  from [Equation A](#), and then update  $pO_{2b}^{\text{avg}}$ , which is equal to  $\frac{1}{2}(pO_{2b}^{\text{in}} + pO_{2b}^{\text{out}})$ . This process is repeated until convergence is attained. For  $pO_{2b}^{\text{avg}} = 52 \text{ mmHg}$ , we calculate  $D_e$  from [Equation 9.57](#), which gives

$$D_e = \frac{D_{\text{blood}}}{1 + m} = \frac{D_{\text{blood}}}{1 + n P_{50}^n H_{\text{oxygen}} C'_{\text{SAT}} \frac{pO_2^{n-1}}{(P_{50}^n + pO_2^n)^2}} = 4.1 \times 10^{-7} \text{ cm}^2 \text{ s}^{-1}$$

From this value of  $D_e$ , we obtain a  $Sc = \mu / \rho D_e = 69,240$ . Also, in the above calculation we obtain an  $m = 42.6$ . From the given mass transfer coefficient correlation, i.e.,  $Sh = 0.136 Re^{0.832} Sc^{1/3}$ , we then obtain a  $Sh = 22.31$ . Since  $Sh = k_b d_H / D_{\text{blood}}$ , we calculate a  $k_b$  of

$$k_b = Sh \times \frac{D_{\text{blood}}}{d_H} = 22.31 \times \frac{1.79 \times 10^{-5} \text{ cm}^2 \text{ s}^{-1}}{0.0394 \text{ cm}} = 0.0101 \text{ cm s}^{-1}$$

We can now calculate the  $pO_2$  of the blood leaving the oxygenator from [Equation A](#):

$$pO_{2b}^{\text{out}} = pO_{2g}^{\text{avg}} - (pO_{2g}^{\text{avg}} - pO_{2b}^{\text{in}}) e^{-\frac{A_{\text{oxygen}} k_b}{Q_b (1+m)}} \\ pO_{2b}^{\text{out}} = 760 \text{ mmHg} - (760 - 33) \text{ mmHg} \times e^{-\frac{18,700 \text{ cm}^2 \times 0.0101 \text{ cm s}^{-1}}{81 \text{ cm}^3 \text{ s}^{-1} (1+42.6)}} = 70.83 \text{ mmHg}$$

Using this value of  $pO_{2b}^{\text{out}}$ , we now update the value of  $pO_{2b}^{\text{avg}}$ , which is equal to  $\frac{1}{2}(pO_{2b}^{\text{in}} + pO_{2b}^{\text{out}}) = \frac{1}{2}(33 + 70.83) \text{ mmHg} = 51.92 \text{ mmHg}$ , which is close enough to the assumed value of 52 mmHg. Once we have converged, we then can calculate the oxygen transport rate from

$$\dot{m}_{\text{oxygen}} = \frac{Q_b}{H_{\text{oxygen}}} (pO_{2b}^{\text{out}} - pO_{2b}^{\text{in}}) + Q_b C'_{\text{SAT}} (Y^{\text{out}} - Y^{\text{in}})$$

where  $Y$  is the hemoglobin saturation fraction given by Hill's equation. For the given values of  $n$  and  $P_{50}$ , we find that  $Y^{\text{out}}$  and  $Y^{\text{in}}$  are 0.927 and 0.589, respectively. Hence,

$$\begin{aligned}\dot{m}_{\text{oxygen}} &= \frac{4.86 \text{ L min}^{-1}}{0.74 \text{ mmHg } \mu\text{mol}^{-1} \text{ L}} (70.83 - 33) \text{ mmHg} \\ &\quad + 4.86 \text{ L min}^{-1} \times 7,800 \mu\text{mol L}^{-1} (0.927 - 0.589) = 13,061.4 \mu\text{mol min}^{-1}\end{aligned}$$

Next, we calculate the density of oxygen at BTP as

$$\begin{aligned}\rho_{\text{oxygen}} &= \frac{P}{RT} \\ &= \frac{1 \text{ atm}}{0.0821 \text{ L atm mol}^{-1} \text{ K}^{-1} \times 310 \text{ K}} \times 10^6 \mu\text{mol mol}^{-1} \times 0.001 \text{ L mL}^{-1} = 39.291 \mu\text{mol mL}^{-1}\end{aligned}$$

And then we calculate the oxygen transport rate of the blood oxygenator as

$$\dot{V}_{\text{oxygen}} = \frac{\dot{m}_{\text{oxygen}}}{\rho_{\text{oxygen}}} = \frac{13,061.4 \mu\text{mol min}^{-1}}{39.291 \mu\text{mol mL}^{-1}} = 332.4 \text{ mL min}^{-1}$$

The table summarizes the results of these calculations for the given flow rates and compares the calculated oxygen transport rates to the experimental oxygen transport rates given by Vaslef et al. (1994). The comparison between the cross flow oxygenator model given by Equation 9.50 and these data is quite good.

Blood Flow Rate ( $Q_b$ ), $\text{L min}^{-1}$	Experimental Oxygen Transport Rate, $\text{mL min}^{-1}$	Predicted Oxygen Transport Rate, $\text{mL min}^{-1}$	% Error
1.41	113.1	110.1	2.7
3.19	234.9	248.9	6
4.86	313.2	332.4	6.2

## 9.6 Immobilized enzyme reactors

### 9.6.1 Background

Another example of extracorporeal devices is the use of immobilized enzyme reactors to chemically change a species found in the blood. An enzyme is a protein that acts as a biochemical catalyst and offers great specificity in terms of the types of chemical species or substrates it acts on. For example, Qiao et al. (2011) describe an enzymatic bioreactor to assist in the treatment of leukemia by removing a key cancer cell nutrient, L-asparagine, from the patient's blood.

Enzymes are usually named after the substrate whose reaction is catalyzed. For example, the enzyme that hydrolyzes the substrate urea is called *urease*. Note that the suffix *-ase* is usually added to a portion of the name for the substrate the enzyme acts on.

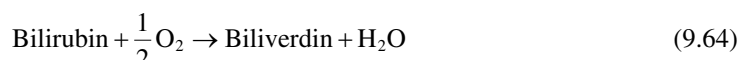
[Figure 9.3](#) shows several reactor arrangements that are possible when an enzyme is attached to or immobilized within a solid support. Enzyme immobilization offers several advantages. First, immobilization keeps the enzyme out of the bulk solution, which in the case of blood returning to the body, could be harmful or result in an allergic reaction to the foreign protein of the enzyme (Qiao et al., 2011). Second, immobilization offers the potential to reuse an enzyme, which may in fact be quite expensive. Finally, in many cases, the enzyme is stabilized (less labile) when immobilized, retaining its activity for longer periods of time.

## 9.6.2 Examples of medical application of immobilized enzymes

One example where immobilized enzyme reactors have been proposed is in the treatment of neonatal jaundice (Lavin et al., 1985; Sung et al., 1986). Newborns tend to have higher levels of the greenish-yellow pigment *bilirubin* than those found in adults. Bilirubin is a natural product derived from red blood cells after they have lived out their lifespan of about 120 days. Bilirubin is formed from the heme portion (the four pyrrole rings) of the hemoglobin molecule after the removal of the iron. The bilirubin binds to plasma albumin for transport to the liver where it is finally excreted from the body in the bile fluids.

The fetus's bilirubin readily crosses the placenta and is removed by the mother's liver. However, in the period after birth, the infant's liver is not fully functional for the first week, resulting in increased levels of plasma bilirubin. In some cases, the infant's bilirubin levels are sufficiently high, resulting in a *jaundiced* (yellow) appearance to the skin. High levels of plasma bilirubin can be toxic to a variety of tissues, and in these cases jaundiced infants are commonly treated by *phototherapy* or blood transfusions. In phototherapy, the infant is placed under a blue light that converts the bilirubin to a less toxic by-product. Phototherapy through the skin is not capable of controlling cases of severe jaundice. However, blood transfusions can replace the infant's blood with adult blood, effectively diluting the infant's plasma bilirubin levels. However, blood transfusions pose their own risk, particularly infectious diseases such as hepatitis and HIV.

An alternative approach to the treatment of neonatal jaundice is the use of a bilirubin-specific enzyme for the removal of bilirubin from the infant's blood (Lavin et al., 1985; Sung et al., 1986). The enzyme bilirubin oxidase catalyzes the oxidation of bilirubin according to the following reaction stoichiometry:



Calculations indicate that the amount of oxygen needed to convert all of the bilirubin found in the blood is about 100 times less than the actual oxygen content of blood. Therefore, no external supply of oxygen is needed within the enzyme reactor to carry out this reaction. Biliverdin itself is much less toxic than bilirubin and in fact is further oxidized by bilirubin oxidase to other less toxic substances. Experiments using a water-jacketed reactor (much like that in [Figure 9.3a](#)) containing bilirubin oxidase covalently attached to agarose beads showed that plasma bilirubin levels in rats decreased by 50% after 30 min of treatment. The rat's blood was recirculated through the 6 mL reactor volume at a flow rate of 1 mL min<sup>-1</sup>. Clearly, these results indicate that an immobilized bilirubin oxidase reactor could be an approach for the treatment of neonatal jaundice. It also shows the feasibility of using immobilized enzyme reactors for the specific removal of a harmful substance present in the blood.

Cells found in the liver and other organs carry out a wide variety of life-sustaining enzymatic reactions. There is considerable interest in using these cells or their enzymes to treat liver failure and other enzyme deficiency diseases. The discussion here focuses on the use of just the key enzymes. The use of immobilized cells as bioartificial organs, perhaps using liver cells (hepatocytes), is discussed in [Chapter 11](#). However, it is important to recognize that some of the techniques used in this chapter to design immobilized enzyme reactors are directly applicable to systems that employ immobilized cells.

Another example of an immobilized enzyme reactor that we will look at in considerably more detail is that for the removal of *heparin* (Bernstein et al., 1987a,b; Ameer et al., 1999a,b). Recall that heparin is used as an anticoagulant in extracorporeal treatments such as hemodialysis and blood oxygenators. Heparin is a large negatively charged conjugated polysaccharide molecule that is produced by many types of cells in the body. By itself, heparin has little anticoagulant activity at the typical concentrations found in blood. However, in some regions of the body such as the liver and lungs, it is produced in greater amounts. Therefore, heparin has an important role in preventing blood clots in the slow-moving venous blood flow entering the capillaries of the lungs and liver. By combining with *antithrombin III*, it increases by several orders of magnitude the ability of antithrombin to remove *thrombin*. Thrombin is an enzyme that converts the plasma protein fibrinogen into fibrin, leading to the fibrous mesh-like structure characteristic of a blood clot. Therefore, this synergistic combination of heparin with antithrombin III results in a powerful anticoagulant.

Over 20 million extracorporeal procedures using heparin are performed each year, and in about 15% of these, complications due to heparin arise. Certainly, the removal of heparin from the blood before it is returned to the body could significantly improve the safety of these procedures. The enzyme heparinase has the ability to degrade heparin into less harmful by-products, and one could envision an immobilized heparinase reactor for the removal of heparin from the blood returning to the patient's body.

### 9.6.3 Enzyme reaction kinetics

Our goal now is to develop relationships that can be used to describe the rates or kinetics of chemical reactions that are catalyzed by enzymes. A description of the enzyme reaction kinetics will allow us to develop mathematical models for immobilized enzyme reactors that can be used to analyze experimental data, provide information for scale-up of our devices, and explore the effects of operating conditions on device performance. The heparinase reactor described previously will be used as a model reaction system for these discussions.

The successful development of an immobilized enzyme reactor requires knowledge of the enzyme kinetics, an understanding of the effects on the observed reaction rate of reactant or substrate diffusion, and a design equation for the specific reactor that is used (Fogler, 2005). Each of these aspects is discussed in greater detail in the following discussion.

First, we need to define the kinetics or rate of the enzyme reaction and how it depends on the concentration of the substrate (reactant). This usually entails defining the free enzyme kinetics (enzyme in solution and not on a solid support) and the kinetics after the enzyme has been immobilized on the support material. In some cases, immobilization has no effect on the intrinsic activity of the enzyme, i.e., relative to its rate in solution. However, in most cases, the immobilization of the enzyme can significantly alter the kinetics of the conversion process.

Generally, the kinetics of enzyme reactions are described by the Michaelis-Menten equation. The Michaelis-Menten equation can be derived by assuming that the conversion of substrate to product occurs in two steps, i.e.,



In the first step, the substrate (S) combines with the enzyme (E) to form an enzyme-substrate complex ( $E^*S$ ). In the second step, the enzyme-substrate complex ( $E^*S$ ) is converted into product (P) and free enzyme (E), which is then available to recombine with substrate.

The rate-controlling step in this reaction process is assumed to be the conversion of the enzyme-substrate complex to product as given by step 2 in [Equation 9.65](#). Accordingly, it is therefore assumed that the reaction forming the enzyme-substrate complex, i.e., step 1 in [Equation 9.65](#), is at equilibrium. The rate of the enzyme reaction is then given by

$$r_S = -\frac{dS}{dt} = \frac{dP}{dt} = k_{cat}E^*S \quad (9.66)$$

where  $k_{cat}$  is a first order rate constant that relates the reaction rate ( $r_S$ ) to the concentration of the enzyme-substrate complex, i.e.,  $E^*S$ . S and P are the respective concentrations of the substrate and the product.

From step 1 of [Equation 9.65](#), we can define the enzyme-substrate dissociation constant (reciprocal of the equilibrium constant) as  $K_m = SE/E^*S$  and then  $E^*S = SE/K_m$  with the result that [Equation 9.66](#) becomes

$$r_S = -\frac{dS}{dt} = \frac{dP}{dt} = k_{cat} \frac{SE}{K_m} \quad (9.67)$$

Letting  $E_0$  represent the total concentration of the enzyme, then  $E_0$  must equal the sum of the free enzyme concentration, i.e., E, and the amount of enzyme bound to substrate, i.e.,  $E^*S$ . Hence, we can write that  $E_0 = E + E^*S$ . Since  $E^*S = SE/K_m$ , we then have that  $E = K_m E_0 / (K_m + S)$ . Substituting this result into [Equation 9.67](#) then gives us an expression for the rate of the enzyme reaction as

$$r_S = \frac{k_{cat}E_0S}{K_m + S} = \frac{V_{max}S}{K_m + S} \quad (9.68)$$

where the reaction rate,  $r_S$ , has units of moles or mass/((reaction volume)time). S represents the substrate or reactant concentration in units of moles or mass per volume.  $V_{max}$  represents the maximum reaction rate for a given total enzyme concentration  $E_0$  in Units/(reaction volume); hence, we see that  $V_{max} = k_{cat}E_0$ , and  $k_{cat}$  is the reaction rate constant in moles or mass/Units time.

Enzyme activity is commonly expressed in terms of *Units* (U), and for heparinase, a unit of activity is defined as the amount of enzyme required to degrade 1 mg of heparin  $h^{-1}$ . The actual amount or mass of enzyme needed is dependent on the enzyme purity and is usually reported as so many units of activity per milligram of enzyme.  $K_m$  is the Michaelis constant and is equal to the substrate concentration at which the reaction rate is equal to one-half the maximum rate ( $V_{max}$ ).

It is important to note that at a high substrate concentration, the reaction rate saturates at  $V_{\max}$  because in total there are not enough available free enzyme molecules for the substrate reaction. The reaction rate is then independent of the substrate concentration and is therefore said to be zero order in the substrate concentration, i.e.,  $r_s = V_{\max}S^0$ . At low substrate concentrations ( $S \ll K_m$ ), the reaction rate is linearly proportional to the substrate concentration and is therefore said to be first order in the substrate concentration, i.e.,  $r_s = V_{\max} S^1$ .

### Example 9.8

The following table of data was obtained (Bernstein et al., 1987b) for the kinetics of heparin degradation by heparinase in solution at 37°C and a pH of 7.4. From these data, determine the values of  $K_m$  and  $k_{cat}$ .

Heparin Degradation Kinetics

Enzyme Loading, U mL <sup>-1</sup>	Heparin Concentration, mg mL <sup>-1</sup>	Reaction Rate, mg mL <sup>-1</sup> h <sup>-1</sup>	Normalized Reaction Rate, mg U <sup>-1</sup> h <sup>-1</sup>
24	1	20.83	0.868
	0.5	18.18	0.758
	0.25	13.70	0.571
	0.1	11.11	0.463
	0.05	7.58	0.316
43	1	38.46	0.894
	0.5	32.26	0.750
	0.25	30.30	0.705
	0.1	23.81	0.554
	0.05	16.67	0.388
57	1	50	0.877
	0.5	40	0.702
	0.25	38.46	0.675
	0.1	26.32	0.462
67	1	55.56	0.829
	0.5	52.63	0.786
	0.25	50	0.746
	0.1	35.71	0.533

Source: Bernstein, H. et al., *Biotechnol. Bioeng.*, 30, 239, 1987b.

### Solution

Note that it is convenient for this type of analysis to divide the enzyme reaction rate by the corresponding enzyme concentration, thus expressing the rate on a per unit amount of enzyme that is present in the reactor. One unit of heparinase (1 U) is defined as the amount of enzyme required to degrade 1 mg heparin h<sup>-1</sup>. Hence, we can rewrite [Equation 9.68](#) as

$$R = \frac{r_s}{E_0} = \frac{k_{cat}S}{K_m + S}$$

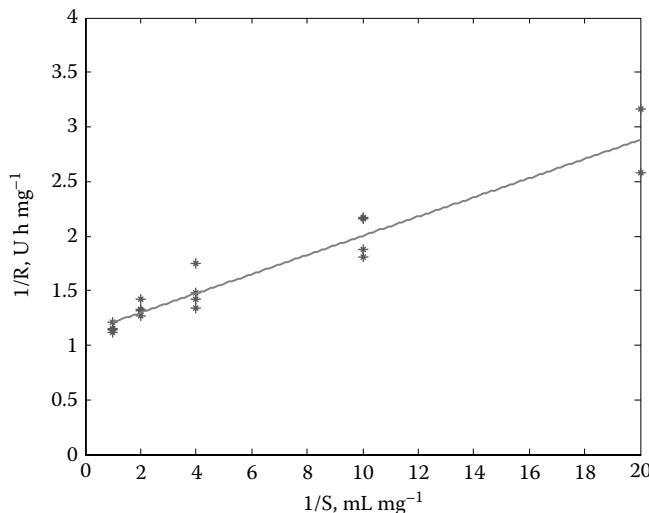


Figure 9.10 Lineweaver-Burk plot.

and this equation can then be inverted and rearranged to give

$$\frac{1}{R} = \left( \frac{K_m}{k_{cat}} \right) \frac{1}{S} + \frac{1}{k_{cat}}$$

This equation shows that if we plot the data in the table as  $1/R$  versus  $1/S$ , the plot should be linear with an intercept equal to  $1/k_{cat}$  and a slope equal to  $K_m/k_{cat}$ . This is called the *Lineweaver-Burk method* for analyzing enzyme reaction data. Using this method on the data in the table for heparin degradation by heparinase, we find that  $K_m = 0.078 \text{ mg mL}^{-1}$  and  $k_{cat} = 0.891 \text{ mg U}^{-1} \text{ h}^{-1}$ . As shown in Figure 9.10, we find that the Michaelis-Menten model provides an excellent representation of the heparin degradation kinetics.

#### 9.6.4 Reaction and diffusion in immobilized enzyme systems

When an enzyme is immobilized within a supporting structure, the substrate has to diffuse into the material in order to come into contact with the immobilized enzyme. Because the substrate diffuses and then reacts within the support structure, a concentration gradient is established within the support structure, and the reaction rate depends on location. A reaction-diffusion model is therefore needed to describe how the substrate diffuses through the porous support particle and reacts through the action of the immobilized enzyme. The description of the reaction and diffusion process is also dependent on the geometry of the supporting structure for the enzyme, and here we will assume it is spherical. Extensions to other support geometries are straightforward once a given geometry has been examined in detail (Aris, 1957).

Diffusion through the support material also requires that we know the substrate diffusivity ( $D_{AB}$ ) in the bulk or free solution, which is contained within the porous structure of the immobilized enzyme particle. We also need to know how the solute diffusivity is affected by the properties of the support

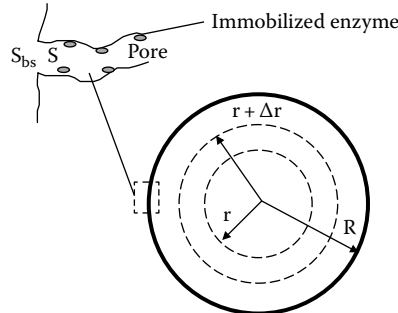


Figure 9.11 Shell balance on a spherical immobilized enzyme particle.

itself, specifically the porosity, pore size, and tortuosity. For substrates that have molecular dimensions that are comparable to the pore size, we will also need to include the effects of steric exclusion and hindered diffusion as discussed earlier in [Chapter 6](#). These factors combine to define the effective diffusivity ( $D_e$ ) of the substrate in the support particle, as given by

$$D_e = \frac{\varepsilon D_{AB}}{\tau} \Omega_r \quad (9.69)$$

In this equation,  $\varepsilon$  represents the porosity of the support,  $\tau$  is the tortuosity of the pores, and  $\Omega_r$  represents the reduction of the substrate diffusivity due to the proximity of the pore wall as given by [Equation 6.13](#).

[Figure 9.11](#) illustrates a spherical immobilized enzyme particle. Within this porous spherical particle, we define a shell volume of thickness  $\Delta r$ , which contains a uniformly distributed immobilized enzyme. We can write the following steady-state shell balance on the substrate:

$$4\pi r^2 D_e \frac{dS}{dr} \Big|_{r+\Delta r} - 4\pi r^2 D_e \frac{dS}{dr} \Big|_r = 4\pi r^2 \Delta r \left( \frac{V_{max} S}{K_m + S} \right) \quad (9.70)$$

In [Equation 9.70](#),  $S$  is the concentration of the substrate within the fluid-filled pores of the enzyme particle. Also, the enzyme reaction rate is defined in terms of the total volume of the enzyme particle. This equation states that the amount of substrate reacted within the shell volume is equal to the difference in the amount of substrate entering and leaving the shell volume by diffusion. After dividing by  $4\pi\Delta r$  and taking the limit as  $\Delta r$  approaches zero, we obtain the reaction-diffusion equation for the substrate in the spherical enzyme particle:

$$D_e \frac{d^2 S}{dr^2} + \frac{2D_e}{r} \frac{dS}{dr} = \frac{V_{max} S}{K_m + S} \quad (9.71)$$

The boundary conditions (BCs) are

$$\begin{aligned} BC1 : \quad r = 0, \quad \frac{dS}{dr} &= 0 \\ BC2 : \quad r = R, \quad S &= K S_{bs} \end{aligned} \quad (9.72)$$

In BC2 of [Equation 9.72](#),  $K$  represents the substrate partition coefficient, which may include effects other than simple steric exclusion, e.g., electrostatic attraction or repulsion due to the presence of surface charges on the substrate and the particle. The partition coefficient is defined as the ratio of the substrate concentration on the pore side of the support surface ( $S$ ) to that on the surface on the bulk side ( $S_{bs}$ ) as shown in [Figure 9.11](#). The substrate concentration at the surface of the support ( $S_{bs}$ ) may also differ from the bulk substrate concentration ( $S_b$ ) because of external mass transfer effects. This is discussed later.

The solution of [Equations 9.71](#) and [9.72](#) is facilitated through the definition of the following dimensionless variables:  $s' = S/KS_{bs}$  and  $r' = r/R$ . On substitution of this dimensionless substrate concentration and radial dimension, we obtain

$$\frac{d^2 s'}{dr'^2} + \frac{2}{r'} \frac{ds'}{dr'} = 9\phi^2 \frac{s'}{1+\beta s'} \quad (9.73)$$

The dimensionless boundary conditions are given by

$$\begin{aligned} BC1: \quad r' = 0, \quad \frac{ds'}{dr} = 0 \\ BC2: \quad r' = 1 \quad s' = 1 \end{aligned} \quad (9.74)$$

Two additional parameters,  $\phi$  and  $\beta$ , also result:

$$\begin{aligned} \phi &= \frac{R}{3} \left[ \frac{V_{max}}{K_m D_e} \right]^{1/2} \\ \beta &= \frac{S_{bs} K}{K_m} \end{aligned} \quad (9.75)$$

The quantity  $\phi$  is especially important in reaction-diffusion problems and is known as the *Thiele modulus*. The square of this quantity represents the ratio of the substrate reaction rate to its diffusion rate. Its magnitude allows one to determine whether the overall reaction rate is *reaction limited* (small  $\phi$ , minimal intraparticle substrate concentration gradient) or *diffusion limited* (large  $\phi$ , significant intraparticle substrate concentration gradient).  $\beta$  is a dimensionless Michaelis constant. Large values of  $\beta$  indicate a zero order reaction, whereas  $\beta \rightarrow 0$  indicates a first order reaction.

The factor  $R/3$  is the ratio of the support volume ( $V_p$ ) to its external surface area ( $A_x$ ). For irregularly shaped particle geometries, we can replace  $R/3$  with this ratio for the particle, i.e.,  $V_p/A_x$ . Aris (1957) has shown that if  $V_p/A_x$  is used as the characteristic dimension for irregularly shaped particles, then the solutions describing the reaction and diffusion in these particles are, for the most part, independent of the particle shape.

## 9.6.5 Solving the immobilized enzyme reaction-diffusion model

The solution to [Equation 9.73](#) for the dimensionless substrate concentration profile in the immobilized enzyme support is usually defined in terms of the effectiveness factor represented by the symbol  $\eta$ . Because of substrate reaction and diffusional effects, the substrate concentration will

generally decrease in the radial direction as one enters the support. This radial decrease in substrate concentration in the support will result in a decrease in the volume-averaged reaction rate for the support in comparison to the reaction rate that would be possible if the substrate concentration was uniform throughout the support and equal to its surface concentration at the pore mouth. The effectiveness factor is used to describe this decrease in the observed reaction rate and is defined by the following expression:

$$\eta = \frac{\text{Observed reaction rate}}{\text{Reaction rate without internal diffusion effects}} = \frac{\frac{4\pi R^2 D_e}{3} \left. \frac{dS}{dr} \right|_{r=R}}{\frac{4}{3} \pi R^3 \left( \frac{V_{max} S|_{r=R}}{K_m + S|_{r=R}} \right)} = \frac{(1+\beta) \left. \frac{ds'}{dr'} \right|_{r'=1}}{3\phi^2} \quad (9.76)$$

It is also important to point out that  $\eta$ , which depends on  $S_{bs}$ , will generally depend on position within the reactor due to consumption of the substrate as it flows through the reactor. Hence, the solution for  $\eta$  will be dependent on the local value of  $S_{bs}$ , which is found by the solution of the reactor design equation for the type of reactor being used. For the special case of a well-mixed reactor, also known as a continuous stirred tank reactor, the substrate concentration is uniform throughout the reactor volume, so there will only be one value of the effectiveness factor, which will depend on  $S_{bs}$ .

The effectiveness factor ( $\eta$ ) varies from zero, i.e., diffusion limited, with a steep intraparticle concentration gradient, to one, i.e., reaction limited, with little change in the intraparticle concentration. The determination of the effectiveness factor using the nonlinear Michaelis-Menten rate equation requires a numerical solution of Equations 9.73 and 9.74 for a given value of  $\beta$ .

An approximate solution for the effectiveness factor in a spherical enzyme particle for Michaelis-Menten kinetics has been obtained using a new approach known as the homotopy perturbation method, in which Ananthaswamy and Subha (2014) showed that the effectiveness factor in a spherical immobilized enzyme particle exhibiting Michaelis-Menten kinetics can be approximated by

$$\eta = \frac{1+\beta}{\phi} \left[ \frac{1}{\sqrt{1+\beta} \tanh\left(\frac{3\phi}{\sqrt{1+\beta}}\right)} - \frac{1}{3\phi} \right] \quad (9.77)$$

Ananthaswamy and Subha (2014) also showed that the intraparticle concentration profile is approximately given by

$$s' = \frac{\sinh\left(\frac{3\phi r'}{\sqrt{1+\beta}}\right)}{r' \sinh\left(\frac{3\phi}{\sqrt{1+\beta}}\right)} \quad (9.78)$$

**Example 9.9**

Estimate the effectiveness factor for the case where the Thiele modulus ( $\phi$ ) is 6 and the dimensionless Michaelis constant ( $\beta$ ) is 4. Assume the particle is spherical and the kinetics are described by the Michaelis-Menten model.

**Solution**

We can use [Equation 9.77](#) to estimate the effectiveness factor for these conditions:

$$\eta = \frac{1+\beta}{\phi} \left[ \frac{1}{\sqrt{1+\beta} \tanh\left(\frac{3\phi}{\sqrt{1+\beta}}\right)} - \frac{1}{3\phi} \right] = \frac{1+4}{6} \left[ \frac{1}{\sqrt{1+4} \tanh\left(\frac{3\times 6}{\sqrt{1+4}}\right)} - \frac{1}{3\times 6} \right] = 0.326$$

The numerical solution presented graphically by Ananthaswamy and Subha (2014) gives a value of  $\eta \approx 0.33$ .

## 9.6.6 Special case of a first order reaction

If  $K_m > KS_{bs}$  or  $\beta = 0$ , then the Michaelis-Menten kinetic model becomes that of a first order reaction. For a first order reaction, we replace  $V_{max}/K_m$  in the definition of the Thiele modulus with the first order rate constant, i.e.,  $k$ . Note that for a first order reaction, the effectiveness factor is independent of the particle surface concentration and hence position in the reactor.

**9.6.6.1 Spherical enzyme particle** Equations [9.73](#) and [9.74](#) can be solved analytically when  $\beta = 0$ , resulting in the following relationship between  $\eta$  and  $\phi$ . Note that the same result is also obtained from [Equation 9.77](#) by setting  $\beta = 0$ :

$$\eta = \frac{1}{\phi} \left( \frac{1}{\tanh 3\phi} - \frac{1}{3\phi} \right) \quad (9.79)$$

where

$$\phi = \frac{R}{3} \sqrt{\frac{k}{D_e}} \quad (9.80)$$

This relationship between the effectiveness factor and the Thiele modulus for a first order reaction is also shown in [Figure 9.12](#).

**9.6.6.2 Cylindrical enzyme particle** For a cylindrically shaped enzyme particle, where the length of the particle is much bigger than the radius, we have for the effectiveness factor (Aris, 1957)

$$\eta = \frac{I_1(2\phi)}{\phi I_0(2\phi)} \quad (9.81)$$

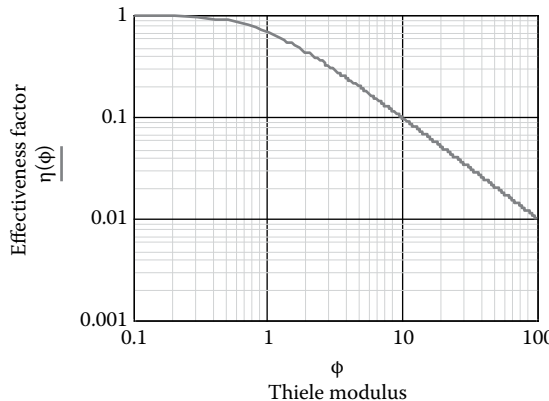


Figure 9.12 Effectiveness factor for a first order reaction.

and the Thiele modulus is defined as

$$\phi = \frac{R}{2} \left( \frac{k}{D_e} \right)^{1/2} \quad (9.82)$$

where  $k = V_{\max}/K_m$ . In [Equation 9.81](#),  $I_0$  and  $I_1$  are modified Bessel functions of the first kind, of zero order and first order, respectively.

**9.6.6.3 Flat plate enzyme particle** For a large thin slab of total thickness  $2L$ , we have for the effectiveness factor (Aris, 1957)

$$\eta = \frac{\tanh(\phi)}{\phi} \quad (9.83)$$

and the Thiele modulus is defined as

$$\phi = L \left( \frac{k}{D_e} \right)^{1/2} \quad (9.84)$$

where  $k = V_{\max}/K_m$ .

### Example 9.10

For the conditions in [Example 9.9](#), calculate the effectiveness factor assuming the enzyme reaction described by Michaelis-Menten kinetics can be approximated as a first order reaction. Do this for spherical, cylindrical, and slab geometries.

### Solution

The Thiele modulus is equal to 6, and since we assume the reaction is first order,  $\beta = 0$ . From [Figure 9.12](#), we see that the effectiveness factor is about 0.16. From [Equations 9.79](#), [9.81](#), and [9.83](#), we can calculate the values of the effectiveness factor for the sphere, the cylinder, and the slab.

As shown in the table, all three values of the effectiveness factor are basically the same, which shows that for these common shapes, and for a first order reaction, the effectiveness factor has the same dependence on the Thiele modulus when the Thiele modulus is defined with a characteristic length of  $V_p/A_x$ ; hence,  $\phi = V_p / A_x \sqrt{k / D_e}$ .

Enzyme Particle Geometry	Effectiveness Factor, $\eta$
Sphere	0.1574
Cylinder	0.16
Slab	0.167

We also see from Equations 9.79, 9.81, and 9.83 that for large values of  $\phi$ , the value of  $\eta$  approaches  $1/\phi$ , which in this case for a  $\phi = 6$  gives an asymptotic  $\eta \approx 0.167$ .

### 9.6.7 Observed reaction rate

With the effectiveness factor known, we can write the observed reaction rate for the immobilized enzyme as follows:

$$r_s = \eta \frac{V_{max} K S_{bs}}{K_m + K S_{bs}} \quad (9.85)$$

where

$S_{bs}$  is the substrate concentration at the support surface

$\eta$  accounts for the reduction in the reaction rate due to the internal substrate concentration gradient

### 9.6.8 External mass transfer resistance

The flow of blood or other fluids around the immobilized enzyme support results in the formation of a thin boundary layer of fluid along the surface of the enzyme particle. This boundary layer provides an additional resistance for mass transfer that must be accounted for. An external mass transfer coefficient ( $k_m$ ) is defined to account for this flow-induced external mass transfer resistance.

Conservation of mass requires, for a given particle, that the following steady-state relationship hold between the external mass transfer rate and the reaction rate within the support:

$$4\pi R^2 k_m (S_b - S_{bs}) = \frac{4}{3} \pi R^3 \eta \left( \frac{V_{max} K S_{bs}}{K_m + K S_{bs}} \right) \quad (9.86)$$

This equation can be solved for the substrate concentration on the surface of the particle ( $S_{bs}$ ) in terms of the bulk substrate concentration ( $S_b$ ). Recall it is this surface concentration that is used in the calculation of the effectiveness factor, as discussed earlier.

From Table 5.1, the following equation describes the external mass transfer coefficient in packed beds containing immobilized enzyme particles:

$$\frac{k_m}{V_0} = 1.17 \left( \frac{\rho d_{particle} V_0}{\mu} \right)^{-0.42} \left( \frac{\mu}{\rho D_{AB}} \right)^{-0.67} \quad (9.87)$$

This equation is also equivalent to  $Sh = 1.17 Re^{0.58} Sc^{0.33}$ , where  $Sh = k_m d_{\text{particle}} / D_{AB}$ ,  $Re = \rho d_{\text{particle}} V_0 / \mu$ ,  $Sc = \mu / \rho D_{AB}$ , and  $d_{\text{particle}}$  is the particle diameter. In [Equation 9.87](#),  $V_0$  is the superficial velocity of the fluid, i.e., the volumetric flow rate of the fluid divided by the cross-sectional area of the vessel that contains the enzyme particles. Generally, one will want to operate the reactor in such a manner that the external mass transfer resistance is negligible; hence, in many cases  $S_{bs} = S_b$ . This can be accomplished by high bulk flow rates in the case of a plug flow reactor or intense mixing in a well-mixed reactor.

**9.6.8.1 External mass transfer resistance for a first order reaction** Now, we will consider the special case of a first order reaction occurring in an immobilized enzyme particle with external mass transfer resistance and internal diffusion limitations (Aris, 1957). We can write for a given enzyme particle of volume ( $V_p$ ) and external area ( $A_x$ ) the steady-state reaction rate per volume of particle as

$$\dot{r}_S = \frac{k_m A_x (S_b - S_{bs})}{V_p} = \eta \left( \frac{V_{max}}{K_m} \right) K S_{bs} = \eta k K S_{bs} \quad (9.88)$$

Solving for  $S_{bs}$ , we obtain

$$S_{bs} = \frac{S_b}{\eta \left( \frac{1}{\eta} + \frac{k K V_p}{k_m A_x} \right)} \quad (9.89)$$

The substrate reaction rate can then be written in terms of just the bulk substrate concentration:

$$\dot{r}_S = \frac{k K S_b}{\frac{1}{\eta} + \frac{k K V_p}{k_m A_x}} = E k K S_b \quad (9.90)$$

where  $E$  is defined as the overall effectiveness factor and accounts for both internal and external diffusion limitations and is given by

$$\frac{1}{E} = \frac{1}{\eta} + \frac{k K V_p}{k_m A_x} \quad (9.91)$$

## 9.6.9 Reactor design equations

Finally, we need a reactor design equation that, in concert with the earlier information on the enzyme kinetics and diffusional effects, provides a relationship as to how the substrate concentration varies within the reaction volume. One usually assumes that either the reaction mixture flows through the reactor packed with the enzyme particles in plug flow (uniform velocity profile in the direction normal to the flow), leading to a change in substrate concentration in the direction of flow, or that the reaction volume is well mixed, resulting in a uniform substrate concentration throughout the reaction volume.

**9.6.9.1 Packed bed reactor** Figure 9.13 shows a packed bed immobilized enzyme reactor. The entering flow rate of the fluid is  $Q_b$ , which in biomedical applications can be, e.g., blood or plasma. The bulk substrate concentration entering the reactor is represented by  $S_b^{in}$ . A steady-state shell balance can also be performed on a section of the reactor volume ( $A_{xs} \Delta x$ ), where  $A_{xs}$  is the cross-sectional area of the reactor. It is assumed that the fluid flows through the reactor in plug flow; hence, the velocity does not change with radial position:

$$Q_b S_b|_x - Q_b S_b|_{x+\Delta x} = (1 - \varepsilon_R) \Delta x A_{xs} \eta \left( \frac{V_{max} K S_{bs}}{K_m + K S_{bs}} \right) \quad (9.92)$$

In this equation,  $\varepsilon_R$  represents the void volume in the reactor, i.e., the volume of the reactor not occupied by the immobilized enzyme particles. Dividing by  $\Delta x$  and taking the limit as  $\Delta x \rightarrow 0$ , results in the following differential equation:

$$Q_b \frac{dS_b}{dx} = -(1 - \varepsilon_R) A_{xs} \eta \left( \frac{V_{max} K S_{bs}}{K_m + K S_{bs}} \right) \quad (9.93)$$

BC1:  $x = 0, S_b = S_b^{in}$

This equation can be solved numerically along with Equation 9.86, which provides the relationship between  $S_b$  and  $S_{bs}$  due to the effects of external mass transfer resistance. Since  $\beta$  depends on  $S_{bs}$  (see Equation 9.75), which also depends on  $x$ , we will need to evaluate the value of  $\eta$  as a function of  $x$ .

For the special case where one can assume that  $\eta$  is approximately constant and external mass transfer effects are negligible, i.e.,  $S_{bs} = S_b$ , Equation 9.93 can be integrated analytically for a reactor of length  $L$  to give the following result:

$$K_m \ln \left( \frac{S_b^{out}}{S_b^{in}} \right) + K (S_b^{out} - S_b^{in}) = - \frac{(1 - \varepsilon_R) A_{xs} L K V_{max} \eta}{Q_b} \quad (9.94)$$

Oftentimes, the operation of a chemical reactor is defined in terms of the residence time ( $\tau$ ), i.e., the time the reacting fluid spends in the reactor. For a packed bed plug flow reactor, the residence time defined in terms of the reactor void volume is given by

$$\tau = \frac{A_{xs} L \varepsilon_R}{Q_b} \quad (9.95)$$

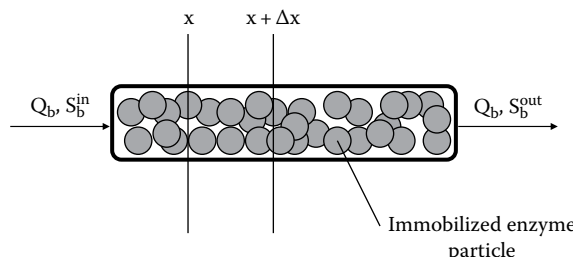


Figure 9.13 Shell balance for a packed bed immobilized enzyme reactor.

In addition, we can define the conversion of the substrate, i.e.,  $X_S \equiv 1 - \left( S_b^{out} / S_b^{in} \right)$ . With these additional definitions, [Equation 9.94](#) can be written as

$$K_m \ln(1 - X_S) - K S_b^{in} X_S = -\frac{(1 - \varepsilon_R) K V_{max} \eta}{\varepsilon_R} \tau \quad (9.96)$$

For given values of the enzyme kinetics and either the size of the reactor or residence time, [Equations 9.94](#) and [9.96](#) can be solved for the exiting substrate concentration and the substrate conversion.

**9.6.9.2 Packed bed reactor with first-order kinetics and internal and external diffusion limitations** For the special case of a first order reaction and both internal and external diffusion limitations, our steady-state substrate balance from  $x$  to  $x + \Delta x$  referring to [Figure 9.13](#) can be written as

$$Q_b S_b|_x - Q_b S_b|_{x+\Delta x} = (1 - \varepsilon_R) \Delta x A_{xs} E k K S_b \quad (9.97)$$

where  $E$  is the overall effectiveness factor given by [Equation 9.91](#). Dividing by  $\Delta x$  and taking the limit as  $\Delta x \rightarrow 0$  gives

$$Q_b \frac{dS_b}{dx} = -(1 - \varepsilon_R) A_{xs} E k K S_b \quad (9.98)$$

BC1:  $x = 0, S_b = S_b^{in}$

[Equation 9.98](#) can be integrated to give

$$S_b^{out} = S_b^{in} \exp \left[ -\frac{(1 - \varepsilon_R) A_{xs} L E k K}{Q_b} \right] \quad (9.99)$$

**9.6.9.3 Well-mixed reactor** The other type of commonly used immobilized enzyme reactor is the well-mixed reactor shown in [Figure 9.14](#). Perfect mixing results in a uniform substrate concentration throughout the reactor volume. The exiting concentration of the substrate is also the same as that within the reactor; hence, the concentration throughout the bulk fluid of the reactor is  $S_b^{out}$ .

A steady-state substrate mass balance provides the following equation that can be solved for the exiting substrate concentration:

$$Q_b S_b^{in} = (1 - \varepsilon_R) V_{reactor} \eta \left( \frac{V_{max} K S_b^{out}}{K_m + K S_b^{out}} \right) + Q_b S_b^{out} \quad (9.100)$$

In [Equation 9.100](#)

$V_{reactor}$  is the total reaction volume

$(1 - \varepsilon_R)$  is the fraction of this volume consisting of the immobilized enzyme particles

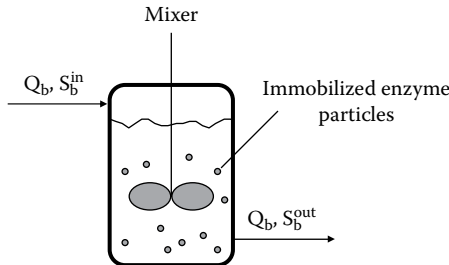


Figure 9.14 A well-mixed immobilized enzyme reactor.

[Equation 9.100](#) can be solved, along with [Equation 9.86](#), and a value of the effectiveness factor evaluated at  $S_{bs}^{out}$ , to determine the exiting substrate concentration  $S_b^{out}$ .

In the absence of external mass transfer effects, i.e.,  $S_{bs}^{out} = S_b^{out}$ , [Equation 9.100](#) simplifies to

$$S_b^{in} = \frac{(1 - \varepsilon_R)}{\varepsilon_R} \eta \left( \frac{V_{max} K S_b^{out}}{K_m + K S_b^{out}} \right) \tau + S_b^{out} \quad (9.101)$$

which can be solved for the value of  $S_b^{out}$ , which will require iteration since  $\eta$  also depends on the value of  $S_b^{out}$ . Once again, we have also defined the residence time, i.e.,  $\tau$ , as given by [Equation 9.95](#), with  $A_{xs} L$  now equal to  $V_{reactor}$ .

**9.6.9.4 Well-mixed reactor with first-order kinetics and internal and external diffusion limitations** For the special case of a first order reaction and both internal and external diffusion limitations, our steady-state substrate balance for the well-mixed reactor becomes

$$Q_b S_b^{in} = (1 - \varepsilon_R) V_{reactor} E k K S_b^{out} + Q_b S_b^{out} \quad (9.102)$$

[Equation 9.102](#) can then be solved to obtain the substrate concentration exiting the reactor:

$$S_b^{out} = \frac{Q_b S_b^{in}}{(1 - \varepsilon_R) V_{reactor} E k K + Q_b} \quad (9.103)$$

### Example 9.11

In one set of data obtained in an immobilized heparinase reactor, the observed heparin conversion was found to be 0.63 for an inlet heparin concentration of  $0.2 \text{ mg mL}^{-1}$  (Bernstein et al., 1987b). The heparinase was immobilized on a cross-linked agarose support, and the flow pattern in the reactor was well mixed. The total volume of the enzyme particles, i.e.,  $(1 - \varepsilon_R) V_{reactor}$ , in the reactor was  $90 \text{ mL}$ , and the enzyme loading per enzyme particle was  $130 \text{ U mL}^{-1}$ . The diffusivity of heparin was found to be  $1.2 \times 10^{-6} \text{ cm}^2 \text{ s}^{-1}$ . The porosity of the immobilized enzyme particle was 0.92 and the tortuosity was unity. The radius of a heparin molecule is  $1.5 \text{ nm}$ , and the pores in the enzyme particle have a radius of  $35 \text{ nm}$ . The partition

coefficient,  $K$ , was found from experiments to be equal to 0.36. The enzyme particle had a radius of 0.0112 cm. The flow rate through the reactor was  $120 \text{ mL min}^{-1} = 2 \text{ mL s}^{-1}$ . The external mass transfer coefficient was estimated to be  $0.154 \text{ cm min}^{-1} = 0.0026 \text{ cm s}^{-1}$ . From these data, calculate the heparin conversion assuming the heparin reaction rate is first order. Include both internal and external diffusion limitations. Use the kinetic parameters for heparinase obtained in [Example 9.8](#), i.e.,  $k_{\text{cat}} = 0.891 \text{ mg U}^{-1} \text{ h}^{-1}$  and  $K_m = 0.078 \text{ mg mL}^{-1}$ , which gives a  $V_{\text{max}} = k_{\text{cat}} E_0 = 115.83 \text{ mg mL}^{-1} \text{ h}^{-1}$ .

### Solution

We can calculate the exiting heparin concentration from the reactor using [Equation 9.103](#), which also serves as a guide to our solution strategy. The effective diffusivity of heparin within the enzyme particle is first calculated by [Equation 9.69](#), where the value of  $\lambda$  is equal to  $1.5 \text{ nm}/35 \text{ nm} = 0.043$ , and from [Equation 6.13](#), we obtain an  $\omega_r = 0.91$ . Hence,

$$D_e = \frac{\varepsilon D_{AB}}{\tau} \omega_r = \frac{0.92 \times 1.2 \times 10^{-6} \text{ cm}^2 \text{ s}^{-1}}{1} \times 0.91 = 1.005 \times 10^{-6} \text{ cm}^2 \text{ s}^{-1}$$

Next, we calculate the first order rate constant, which is given by

$$k = \frac{V_{\text{max}}}{K_m} = \frac{115.83 \text{ mg mL}^{-1} \text{ h}^{-1}}{0.078 \text{ mg mL}^{-1}} \times \frac{1 \text{ h}}{3600 \text{ s}} = 0.413 \text{ s}^{-1}$$

With  $D_e$  and  $k$  determined, we calculate the Thiele modulus as

$$\phi = \frac{R}{3} \sqrt{\frac{k}{D_e}} = \frac{0.0112 \text{ cm}}{3} \sqrt{\frac{0.413 \text{ cm s}^{-1}}{1.005 \times 10^{-6} \text{ cm}^2 \text{ s}^{-1}}} = 2.393$$

From this value of  $\phi$ , we can calculate the effectiveness factor from [Equation 9.79](#) and obtain  $\eta = 0.36$ . Next, we calculate from [Equation 9.91](#) the overall effectiveness factor, which includes internal and external diffusion limitations:

$$E = \frac{1}{\frac{1}{\eta} + \frac{kKV_p}{k_m A_x}} = \frac{1}{\frac{1}{0.36} + \frac{0.413 \text{ s}^{-1} \times 0.36 \times 0.0112 \text{ cm}}{3 \times 0.0026 \text{ cm s}^{-1}}} = 0.334$$

We can now calculate from [Equation 9.103](#) the exiting substrate concentration:

$$S_b^{\text{out}} = \frac{Q_b S_b^{\text{in}}}{(1 - \varepsilon_R) V_{\text{reactor}} E k K + Q_b}$$

$$S_b^{\text{out}} = \frac{2 \text{ mL s}^{-1} \times 0.2 \text{ mg mL}^{-1}}{90 \text{ mL} \times 0.334 \times 0.413 \text{ s}^{-1} \times 0.36 + 2 \text{ mL s}^{-1}} = 0.062 \text{ mg mL}^{-1}$$

Next, we calculate the predicted heparin conversion:

$$X_{\text{heparin}}^{\text{predicted}} = 1 - \frac{S_b^{\text{out}}}{S_b^{\text{in}}} = 1 - \frac{0.062 \text{ mg mL}^{-1}}{0.2 \text{ mg mL}^{-1}} = 0.69$$

The actual heparin conversion was found to be 0.63. The error is therefore 9.52%. The predicted heparin conversion is higher than the observed value. This is most likely due to the use of the soluble heparinase kinetics found in [Example 9.8](#). The immobilization of the heparinase will most likely lead to a modest reduction in  $k_{\text{cat}}$ .

## 9.7 Affinity adsorption

Adsorption is the process where a solute in a solution literally sticks to the surface of a solid surface. Adsorption creates an adsorbed layer of the solute on the solid surface. Adsorption is not the same as absorption. In absorption, the solute goes into the interior of another substance, which can be a solid or another liquid.

There are two types of adsorption known as either physical or chemical adsorption. In physical adsorption, the solute binds to the solid surface through relatively weak physical interactions between the substance and the solid. The adsorbed substance retains its chemical structure. In chemical adsorption, chemical bonds are actually formed between the adsorbed substance and the solid material.

Adsorption processes can be very selective in terms of the interaction between the solid surface and the solutes found in the solution. For example, in *affinity adsorption*, another substance known as a *ligand* is attached to the surface of a solid material by chemical means. The ligand has a very specific binding site for a substance that is found in the solution, as shown in [Figure 9.15](#). Examples of various ligands and the substances they act on that are used in biomedical applications are summarized in [Table 9.8](#).

The application of affinity adsorption as a blood cleanser for the treatment of systemic blood infections, i.e., sepsis, has also been described (Yung et al., 2009; Kang et al., 2014; Didar et al., 2015).

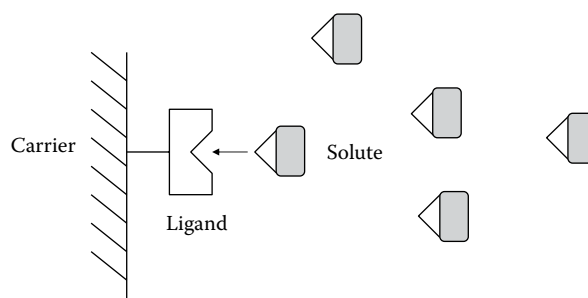


Figure 9.15 Ligand and solute binding.

Table 9.8 Examples of Ligands and the Substances They Bind With

Ligand	Substance That Binds with the Ligand
Enzyme inhibitor	Enzyme
Antigen	Antibodies
Complementary nucleotide sequence	Nucleic acids
Cellular receptors	Hormones
Carrier protein	Vitamin

### 9.7.1 Affinity adsorption of preformed antibodies

An interesting example of the use of affinity adsorption is described in Karoor et al. (2003). As mentioned in their paper, there is great interest in using animal organs as a means to address the shortage of human donor organs. This use of animal organs is also known as *xenotransplantation*, and pigs are receiving the most attention because of their adequate supply and the size of their organs is comparable to those in humans.

However, the transplantation of animal organs into humans leads to a severe antibody-mediated reaction to the foreign tissue, the first phase of which is known as *hyperacute rejection*.\* For this discussion, antibodies are proteins produced by certain cells of the immune system that bind with high specificity to molecules known as *antigens*. An antigen is just a chemical entity found in the foreign tissue that the immune system's antibodies recognize and then bind to.

These antibodies, also known as *preformed natural antibodies*, are found in the recipient of a xenotransplant, and they bind to the endothelial cells that line the blood vessels of the xenograft. These antibodies that bind to the endothelial cells then activate the complement system, which destroys the transplanted organ within several hours of the transplant.

The hyperacute rejection process for the most part involves a particular type of antibody, known as IgM. A few percent of the patient's IgM antibody population consists of xenoreactive IgM antibodies that bind with high specificity to  $\alpha$ -galactosyl structures (sugar-like molecules) that are expressed by nonprimate mammalian and New World monkey cells. The selective removal of these  $\alpha$ -galactosyl-specific IgM antibodies from the patient prior to a xenotransplantation could eliminate the hyperacute rejection of the transplanted organs.

**Figure 9.16** illustrates an affinity adsorption system for removing  $\alpha$ -galactosyl-reactive IgM antibodies (Karoor et al., 2003). Blood either from the body or from a reservoir, in the case of in vitro experiments, flows through a microfiltration hollow fiber membrane cartridge. As the blood flows through the inside of the hollow fibers, plasma is filtered across the hollow fiber membrane wall as a result of the transmembrane pressure difference. Recall that this filtration of blood is also known as plasmapheresis. The exiting blood and the plasma filtrate are then returned to the body or the reservoir.

\* A brief discussion on the immune system can be found in [Section 10.2](#).

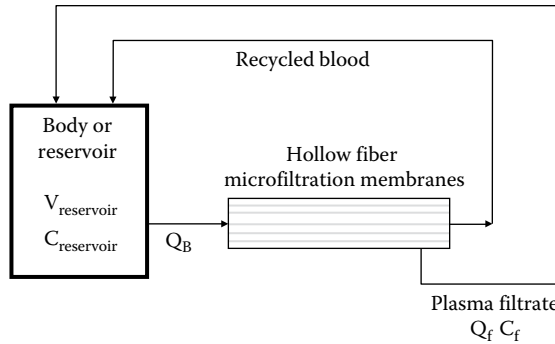


Figure 9.16 Affinity adsorption system.

The pores of these hollow fiber membranes have diameters in the range from 0.2 to 0.5  $\mu\text{m}$ . The diameters of these pores are many times larger than the IgM molecule. The ligand, which in this case is  $\alpha$ -galactosyl, was immobilized on all accessible surfaces of the hollow fiber microfiltration membrane, i.e., the inner, outer, and internal surfaces. As the blood and filtered plasma flow through the hollow fiber membranes, the reactive IgM antibodies bind with the  $\alpha$ -galactosyl ligands that are bound to the membrane surfaces as shown in [Figure 9.15](#).

### 9.7.2 Analysis of an affinity adsorption system to remove preformed antibodies

We can use a simple, well-mixed single-compartment model to describe how the concentration of reactive IgM changes with time in the body or the reservoir (Karoor et al., 2003). Letting  $V_{\text{reservoir}}$  denote the reservoir volume or the IgM distribution volume in the body and  $C_{\text{reservoir}}$  the IgM concentration, we can write the following mass balance on IgM, which expresses the fact that the rate of change of IgM in the body or reservoir must equal the rate at which IgM is being removed from the plasma filtrate flow ( $Q_f$ ) that contacts the  $\alpha$ -galactosyl ligand immobilized within the hollow fiber membrane:

$$V_{\text{reservoir}} \frac{dC_{\text{reservoir}}}{dt} = -Q_f (C_{\text{reservoir}} - C_f) \quad (9.104)$$

For the case where all of the IgM is bound to the  $\alpha$ -galactosyl ligand as it passes through the hollow fiber membranes,  $C_f = 0$  and the [Equation 9.104](#) can be integrated to give the relative concentration of IgM (given by  $\chi$ ) in the reservoir as a function of time:

$$\chi = \frac{C_{\text{reservoir}}}{C_{\text{reservoir}}^0} = e^{-\frac{Q_f t}{V_{\text{reservoir}}}} \quad (9.105)$$

where  $C_{\text{reservoir}}^0$  is the initial concentration of IgM.

The filtration flow or plasmapheresis, i.e.,  $Q_f$ , can be estimated from the following equation (Zydney and Colton, 1986, also see Problem 6.8 for its derivation):

$$\frac{Q_f}{Q_b^{\text{in}}} = 1 - \exp \left[ -0.90\beta \ln \left( \frac{C_w}{C_b^{\text{in}}} \right) \right] \quad (9.106)$$

where

$$\beta = \frac{2}{3} \left( \frac{a^2 L}{R^3} \right)^{2/3}$$

$Q_b^{\text{in}}$  is the inlet blood flow rate

$C_b^{\text{in}}$  is the bulk fluid red blood cell volume fraction at the inlet (0.40)

$C_w$  is the red blood cell volume fraction at the membrane surface (0.95)

$a$  is the red blood cell radius (4  $\mu\text{m}$ )

$L$  is the length of the hollow fibers

$R$  is the inside radius of the hollow fibers

The characteristic time for the IgM adsorption process is defined as  $\tau_s \equiv V_{\text{reservoir}}/Q_f$ ; therefore, the number of reservoir volumes that have been filtered (i.e., RF) in a period of time ( $t$ ) through the affinity adsorption membrane system is given by

$$RF = \text{Reservoir volumes filtered} = \frac{Q_f t}{V_{\text{reservoir}}} \quad (9.107)$$

Hence, we can write [Equation 9.105](#) as

$$\chi = e^{-RF} \quad (9.108)$$

Results of the studies by Karoor et al. (2003) show that greater than 90% removal of the IgM antibodies, i.e.,  $C_{\text{reservoir}}/C_{\text{reservoir}}^0 < 0.10$ , can be obtained after three volumes of the plasma have been filtered through the affinity adsorption system.

In designing an affinity adsorption system, one must be certain that the amount of ligand or solute to be removed, i.e.,  $V_{\text{reservoir}} C_{\text{reservoir}}^0$ , is less than the maximum adsorbed solute capacity that is possible for the membrane system. For a human-scale device to remove xenoreactive IgM antibodies, the reservoir or IgM distribution volume would approximate the volume of plasma in the body, which is 3000 mL. The IgM concentration is about 0.033 mg  $\text{mL}^{-1}$ , so the total amount of IgM to be removed is on the order of 100 mg. IgM binding capacities for the systems studied by Karoor et al. (2003) had total binding capacities on the order of several hundred mg of IgM.

### Example 9.12

Karoor et al. (2003) obtained the data shown in the following table for the relative concentration of IgM as a function of the reservoir volumes filtered. Six hundred nylon hollow fiber membranes having inner and outer diameters of 330 and 550  $\mu\text{m}$ , respectively, were used. The active length of the hollow fibers was 10.2 cm, and the total luminal surface area was 718  $\text{cm}^2$ . The filtration flow rate ( $Q_f$ ) was 50  $\text{mL min}^{-1}$ , and the reservoir volume was 1200 mL. The initial IgM concentration was 0.019 mg  $\text{mL}^{-1}$ . Compare the model

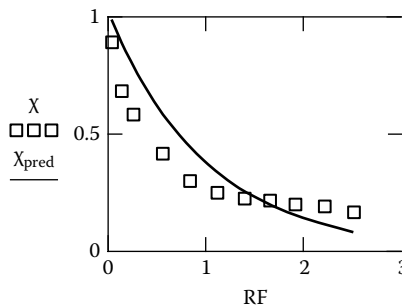


Figure 9.17 Relative reservoir concentration as a function of reservoir volumes filtered.

developed previously for an affinity adsorption system to the results obtained by Karoor et al. (2003). Also, calculate the predicted fractional filtrate yield, i.e.,  $Q_f/Q_b^{\text{in}}$ .

Reservoir Volumes Filtered (RF), $\frac{Q_f t}{V_{\text{reservoir}}}$	Relative Concentration ( $X$ ), $\frac{C_{\text{reservoir}}}{C_{\text{reservoir}}^0}$
0.025	0.89
0.13	0.68
0.25	0.58
0.55	0.41
0.83	0.30
1.1	0.25
1.38	0.22
1.63	0.21
1.9	0.20
2.20	0.19
2.5	0.16

### Solution

From [Equation 9.106](#), we calculate that the fractional filtrate yield, i.e.,  $Q_f/Q_b^{\text{in}}$ , is equal to 0.23. From [Equation 9.105](#), we can calculate the relative concentration of the IgM antibody in the reservoir. [Figure 9.17](#) shows a comparison between the affinity adsorption model developed above and the results from the above table. The comparison between the model and the data is quite good.

## Problems

- 9.1** Estimate the clearance and fractional % removal of urea from a flat plate dialyzer for both cocurrent and countercurrent flow under the following conditions:

$$\text{Urea diffusivity} = 2 \times 10^{-5} \text{ cm}^2 \text{ s}^{-1}$$

Four flat plate membranes each with the following dimensions:

Dialyzer length = 85 cm

Dialyzer width = 15 cm

Blood flow rate = 200 mL min<sup>-1</sup> (total)

Dialyzer flow rate = 500 mL min<sup>-1</sup> (total)

Mass transfer resistances

Membrane = 25 min cm<sup>-1</sup>

Blood side = 8 min cm<sup>-1</sup>

Dialysate side = 35 min cm<sup>-1</sup>

- 9.2** Estimate the urea flux  $[(\text{NH}_2)_2\text{CO}] (\text{g m}^{-2} \text{ h}^{-1})$  through a cellulosic membrane that is 0.001 in. in thickness. The blood at the membrane surface has a urea concentration of 1 mg mL<sup>-1</sup>. Assume the dialysis fluid on the other side of the membrane surface is free of urea. The void volume of the cellulosic membrane is 0.40, and the membrane tortuosity is 2.0. The pores in the membrane have a diameter such that they exclude all molecules larger than a molecular weight of 20,000.
- 9.3** The following data for the antibiotic imipenem were obtained from six patients suffering multiorgan failure (Hashimoto et al., 1997, see also Problem 8.10). All patients were anuric because of complete renal failure and were on continuous venovenous hemodialysis. The antibiotic was first delivered by an intravenous infusion pump for 30 min, resulting in an initial plasma concentration of 32.37  $\mu\text{g mL}^{-1}$ . Following the infusion, blood samples were taken over the next 12 h. In addition to the blood samples, drug concentrations in the blood exiting the hemodialysis unit were also taken. The dialysate entering the hemodialyzer was free of drug, and the concentration of the drug in the dialysate leaving the dialyzer was also measured. The blood flow rate through the hemodialyzer was set at 60 mL min<sup>-1</sup> and the dialysate flow was set at 20 mL min<sup>-1</sup>. The hemodialyzer had a total surface area of 0.5 m<sup>2</sup>. Using this data, develop a model that describes the drug removal process from the patient's body by the hemodialyzer. Carefully state all of your assumptions. Determine key parameters such as the total body clearance, the dialyzer clearance, and the overall mass transfer coefficient for the dialyzer. Compare your model to the actual data. The table below summarizes the drug concentrations in the blood entering the dialyzer, the blood leaving the dialyzer, and the exiting dialysate.

Time, min	Blood Drug Concentration Entering the Dialyzer, $\mu\text{g mL}^{-1}$	Blood Drug Concentration Leaving the Dialyzer, $\mu\text{g mL}^{-1}$	Drug Concentration in Dialysate Leaving the Dialyzer, $\mu\text{g mL}^{-1}$
0	32.47	23	21
30	24	20.5	14
60	18.5	16	12
120	13	11	8.8
180	10	8	6.4
360	4.6	3.8	2
540	2	1.6	1.4
720	1.12	0.9	0.6

- 9.4** At the start of CAPD using a 2.5 wt.% glucose solution, the filtration rate of water from the plasma was determined to be about  $6 \text{ mL min}^{-1}$ . Estimate the hydraulic conductance ( $L_p$  in  $\text{mL h}^{-1} \text{ m}^{-2} \text{ mmHg}^{-1}$ ) of the peritoneal membrane.
- 9.5** The following data were presented by Lysaght and Farrell (1989) for urea (molecular weight 60) and inulin (molecular weight 5200) transport during CAPD. The initial glucose concentration in the dialysate solution was equal to 1.5 wt.%. Assuming a constant peritoneal fluid volume of 2.4 L, estimate the permeability of the peritoneal membrane for each solute. What thickness of a stagnant film of water is required to give an equivalent permeability for urea and inulin? Explain the difference in the observed peritoneal membrane permeabilities based on your understanding of solute diffusion through hydrogels.

Time, min	Ratio of Dialysate to Plasma Concentration for Urea	Ratio of Dialysate to Plasma Concentration for Inulin
0	0.03	0
50	0.33	0.085
100	0.57	0.16
150	0.69	0.21
200	0.77	0.27
300	0.91	0.36
400	0.96	0.42

- 9.6** The following data were presented by Lysaght and Farrell (1989) for urea (molecular weight 60) transport during CAPD. The urea concentration in blood was  $100 \text{ mg (100 mL)}^{-1}$ . From this data, estimate the urea permeability of the peritoneal membrane.

Time, min	Peritoneal Volume, mL	Dialysate Urea Concentration, mg (100 mL) $^{-1}$
0	1983	10
15	2304	30
30	2543	42
45	2938	55
60	3146	62

- 9.7** Analyze the performance of an oxygenator that uses an ultrathin ( $25 \mu\text{m}$ ) membrane made of polyalkylsulfone cast on microporous polypropylene. The oxygen permeability of this membrane is reported (Gray, 1981) to be  $1100 \text{ mL(STP) min}^{-1} \text{ m}^{-2} \text{ atm}^{-1}$  and that for carbon dioxide is reported to be  $4600 \text{ mL(STP) min}^{-1} \text{ m}^{-2} \text{ atm}^{-1}$ . What membrane area is needed to deliver  $250 \text{ mL min}^{-1}$  of oxygen and remove  $200 \text{ mL min}^{-1}$  of carbon dioxide? Carefully state your assumptions.
- 9.8** Vaslef et al. (1994) measured the oxygen transport rate in a Sarns SMO1 oxygenator as a function of the blood flow rate. The oxygenator contained hollow fibers with an outer diameter of  $290 \mu\text{m}$ . The blood flowed external and perpendicular to the hollow fibers. The blood was obtained from cows, and the properties of the blood were

$C_{\text{Sat}}' = 7800 \mu\text{M}$ ,  $n = 2.85$ ,  $P_{50} = 29.1 \text{ mmHg}$ , and  $H = 37\%$ . The blood entering the oxygenator had an oxygen saturation of 38%. Pure oxygen at a  $\text{pO}_2$  of 760 mmHg flowed within the hollow fibers. The total surface area of the hollow fibers available for oxygen transport was  $1.87 \text{ m}^2$ , and the void space, i.e.,  $\varepsilon_{\text{module}}$ , within the oxygenator module was 0.576. The frontal area ( $A_f$ ) normal to the blood flow was  $36.88 \text{ cm}^2$ , and the blood flow path was 9.5 cm in length. Calculate the oxygen transport rate for blood flow rates of  $1.41$ ,  $3.19$ , and  $4.86 \text{ L min}^{-1}$ . The measured oxygen transport rates for these blood flows are  $161$ ,  $305$ , and  $370 \text{ mL min}^{-1}$  (BTP), respectively. Use the mass transfer correlation they developed using water, which says that  $\text{Sh} = 0.136 \text{ Re}^{0.832} \text{ Sc}^{1/3}$ .

- 9.9** Yang and Cussler (1986) considered the design of a human gill using hollow fibers. To support a human, they assumed the artificial gill will have to provide up to  $2500 \text{ mL min}^{-1}$  of oxygen at 1 atm and  $37^\circ\text{C}$  for moderate levels of activity. Develop your design for the human gill and determine the hollow fiber membrane area that is required. How big is your human gill? What other issues need to be considered for the design of the human gill?
- 9.10** Calculate the effectiveness factor for an enzyme reaction that follows Michaelis-Menten kinetics. Assume the Thiele modulus is 4 and  $\beta = 2$ . Compare your result to the value obtained assuming the reaction is first order.
- 9.11** The following kinetic data (Sung et al., 1986) were obtained for the enzyme bilirubin oxidase at a pH of 7.4 and a temperature of  $37^\circ\text{C}$ . The substrate was bilirubin. The enzyme loading in the reactor was equivalent to  $0.15 \text{ U L}^{-1}$ , where a “Unit” of enzyme activity is defined as the amount of enzyme that catalyzes the conversion of  $1 \mu\text{mol min}^{-1}$  of bilirubin. Assuming the data follows the Michaelis-Menten rate law, determine the values of  $V_{\text{max}}$ ,  $K_m$ , and  $k_{\text{cat}}$ .

Bilirubin Concentration, $\mu\text{M}$	Reaction Rate, $\mu\text{M Bilirubin min}^{-1}$
1	0.015
5	0.055
10	0.089
15	0.130
25	0.185
40	0.230
50	0.244

- 9.12** Suppose the bilirubin oxidase from [Problem 9.11](#) is immobilized within an agarose gel (Sung et al., 1986). The enzyme loading in the gel equals  $10 \text{ U mL}^{-1}$  of wet gel. Calculate the conversion of bilirubin in a well-mixed reactor containing a total gel volume of 15 mL. The void fraction in the reactor is 70%. Assume the flow rate through the reactor is equal to  $1.2 \text{ mL min}^{-1}$  and that the entering serum bilirubin concentration is  $200 \mu\text{M}$ . The value of  $k_{\text{cat}}$  for these conditions is equal to  $4.67 \times 10^{-4} \mu\text{mol min}^{-1} \text{ U}^{-1}$ . Assume the value of  $K_m$  is unaffected by immobilization or other substances found in serum.
- 9.13** Fukui et al. (1994) measured the in vitro oxygen transfer rates using an intravascular lung assist device, or ILAD. The membrane oxygenator consisted of microporous polypropylene hollow fibers that were placed within a flexible polyvinyl chloride (PVC) tube. The PVC tube was 30 cm in length with a 20 mm inside diameter. The total surface area of the hollow fibers was  $0.3 \text{ m}^2$ . The blood flows along a straight path outside of the fibers, and the gas flows within

the hollow fibers. For blood flow rates of 1, 2, and 3 L min<sup>-1</sup>, the oxygen transfer rates (BTP) were 60, 120, and 140 mL min<sup>-1</sup>, respectively. Estimate the number and the diameter of hollow fibers needed to reproduce their results.

- 9.14** A series of experiments was performed using various sizes of particles containing an immobilized enzyme in order to determine the importance of diffusion within the particles. The substrate concentration is much less than the value of  $K_m$ , so the reaction may be assumed to be first order. In addition, the bulk solution was well mixed and the concentration of the substrate at the surface of the particles is  $2 \times 10^{-4}$  mol cm<sup>-3</sup>. The partition coefficient was also found to be  $K = 1$ . The table below summarizes the data that was obtained:

Diameter of the Particle, cm	Observed Reaction Rate, mol h <sup>-1</sup> cm <sup>-3</sup>
0.050	0.22
0.010	0.98
0.005	1.60
0.001	2.40
0.0005	2.40

From the data in the above table, determine values of the first order rate constant ( $k$ ) and the effective diffusivity of the substrate within the particle ( $D_e$ ). To assess the validity of the assumptions you make to find  $k$  and  $D_e$ , also calculate the effectiveness factor ( $\eta$ ), the Thiele modulus ( $\phi$ ), and the predicted reaction rate for each particle size. Make a graph that compares the predicted reaction rate to the observed reaction rate for each particle size. How does it look?

- 9.15** A biotech company is designing an immobilized enzyme reactor for the removal of a toxin from blood. The device will be connected to the patient by an arteriovenous shunt. Blood will flow over a packed bed of particles (100 µm in diameter) containing the immobilized enzyme. The following data has been obtained for the toxin enzyme kinetics:

$$K = 1$$

$$V_{\max} = 1 \times 10^{-9} \text{ mol cm}^{-3} \text{ s}^{-1}$$

$$K_m = 1 \times 10^{-9} \text{ mol cm}^{-3}$$

$$D_e = 5 \times 10^{-7} \text{ cm}^2 \text{ s}^{-1}$$

The maximum concentration of the toxin entering the reactor is estimated to be  $1 \times 10^{-11}$  mol cm<sup>-3</sup>. Estimate the blood residence time within the reactor to obtain a 60% per pass conversion of the toxin in the blood.

- 9.16** Design a packed bed heparinase reactor to achieve a 70% conversion of heparin. Assume an enzyme loading of 120 U mL<sup>-1</sup> of immobilized enzyme and a feed substrate concentration of 0.2 mg mL<sup>-1</sup>. The flow rate of plasma to your reactor is 120 mL min<sup>-1</sup>. Use the heparinase kinetics from [Example 9.8](#), and assume a first order reaction.
- 9.17** Derive the performance equation shown in [Table 9.4](#) for a countercurrent hemodialyzer.

- 9.18** Design an aquapheresis cartridge that can remove up to  $500 \text{ mL h}^{-1}$  of fluid from the body. Specify the membrane properties such as total membrane area, NMWCO, membrane thickness, and membrane porosity that you recommend. How many hollow fibers are required and what are their dimensions in terms of length and diameter? What are the operating pressures for your system and the effective pressure drop across the cartridge?
- 9.19** Starting with [Equation 9.78](#) show that [Equation 9.77](#) is the effectiveness factor for a spherical enzyme particle for Michaelis-Menten kinetics.
- 9.20** In one set of data obtained in an immobilized heparinase reactor, the observed heparin conversion was found to be 0.54 for an inlet heparin concentration of  $0.5 \text{ mg mL}^{-1}$  (Bernstein et al., 1987b). The heparinase was immobilized on a cross-linked agarose support, and the flow pattern in the reactor was well mixed. The total volume of the enzyme particles, i.e.,  $(1 - \varepsilon_R) V_{\text{reactor}}$ , in the reactor was 80 mL, and the enzyme loading per enzyme particle was  $100 \text{ U mL}^{-1}$ . The diffusivity of heparin was found to be  $1.2 \times 10^{-6} \text{ cm}^2 \text{ s}^{-1}$ . The porosity of the immobilized enzyme particle was 0.92, and the tortuosity was unity. The radius of a heparin molecule is 1.5 nm, and the pores in the enzyme particle have a radius of 35 nm. The partition coefficient, K, was found from experiments to be equal to 0.36. The enzyme particle had a radius of 0.0112 cm. The flow rate through the reactor was  $120 \text{ mL min}^{-1} = 2 \text{ mL s}^{-1}$ . The external mass transfer coefficient was estimated to be  $0.154 \text{ cm min}^{-1} = 0.0026 \text{ cm s}^{-1}$ . From these data, calculate the heparin conversion assuming the heparin reaction rate is first order. Include both internal and external diffusion limitations. Use the kinetic parameters obtained in [Example 9.8](#), i.e.,  $k_{\text{cat}} = 0.891 \text{ mg U}^{-1} \text{ h}^{-1}$  and  $K_m = 0.078 \text{ mg mL}^{-1}$ .
- 9.21** Design a hollow fiber membrane hemodialysis module for daily home use. Assume the patient is connected to the hemodialyzer for only an hour or so each day.
- 9.22** A “biospleen” is being developed to remove endotoxins from blood. Endotoxins are lipopolysaccharides (LPS) that are a major component of the outer membranes of pathogenic Gram-negative bacteria. These substances are released as a result of the death of the bacteria during antibiotic treatment, and when present in the blood, they evoke a strong immune response that can lead to septic shock and death. It is proposed to capture these endotoxins by immobilizing mannose-binding lectins (MBLs) on the internal surface of hollow fibers. The endotoxins in the blood flowing through the hollow fibers will be adsorbed from the blood by the MBLs. The proposed flow rate of the blood to the “biospleen” is  $50 \text{ mL min}^{-1}$ , and there are 5000 hollow fibers in the device. The inside diameter of the hollow fibers is 200  $\mu\text{m}$ . During the early period of time after the device has been in contact with the blood, the MBLs have a very large capacity for the adsorption of endotoxins that are present in the blood. The binding of the LPS with the MBLs is also assumed to happen very fast relative to the diffusion of the large LPS molecules from the bulk blood to the surface of the hollow fiber where the MBLs are. Hence, it is reasonable to assume that the concentration of the endotoxin is zero at the inside surface of the hollow fibers. The LPS endotoxin diffusivity in blood is estimated to be about  $5 \times 10^{-7} \text{ cm}^2 \text{ s}^{-1}$ . If the length of the hollow fibers in the biospleen is 30 cm, estimate the fractional removal of the LPS endotoxin, i.e.,  $1 - C_{\text{out}}/C_{\text{in}}$ , where  $C_{\text{in}}$  and  $C_{\text{out}}$  are the concentrations of LPS in blood entering and exiting the “biospleen.” Assume the density of the blood is  $1.06 \text{ g cm}^{-3}$  and that the apparent viscosity of the blood in these hollow fibers is 2.9 cP.

# Chapter 10 Tissue engineering and regenerative medicine

## 10.1 Introduction

Over eight million surgical procedures are performed each year in the United States for the treatment of organ failure or the loss of tissue function as a result of disease or injury (Holder et al., 1997). Organ transplantation has also become a routine and successful treatment method for the replacement of a failed organ. Organs routinely transplanted include the kidneys, heart, lungs, liver, intestines, and pancreas. Part of this success is due to better therapies to prevent rejection episodes, as well as improved techniques for the procurement and storage of whole organs prior to transplant.

Organ transplantation has saved and improved the quality of many lives; however, its widespread application is severely limited by a shortage of whole organ donors. In the United States, only a few thousand organ donors are available each year. Yet, over 100,000 people in the United States are on waiting lists for an organ transplant, and over 20 per day of these will die waiting for an organ (Wiles et al., 2016). Certainly, extracorporeal devices such as the hemodialyzer, bioartificial liver (to be discussed in [Chapter 11](#)), and the artificial heart (Jarvik, 1981; Spotnitz, 1987; Rosenberg, 1995) and left ventricular assist devices (Griffith et al., 2001) can be used until an organ is available. These devices therefore serve as a *bridge* to a transplant. The continued development and improvement of these devices will help alleviate the pain and suffering while awaiting an organ transplant. However, these devices come with many limitations and, by themselves, are still not a perfect solution.

Many diseases do not involve an entire organ but only certain tissues or cell types lose their function or are damaged, e.g., in osteoarthritis or in a damaged heart valve. In these cases, it may be simpler to restore or regenerate the lost function of the specific tissue or cells than to replace an entire organ.

## 10.2 Background

The transplantation of the cells necessary to replace the lost function of a tissue or an organ is receiving considerable attention and is the basis of tissue engineering and regenerative medicine (Cima et al., 1991a,b; Langer and Vacanti, 1993; Brown et al., 2000; Ma and Choi, 2001; Palsson and Bhatia, 2004; van Blitterswijk et al., 2008; Harrison et al., 2014; Wobma and Vunjak-Novakovic, 2016). This approach is also known as TERM, which is an acronym for tissue engineering and regenerative medicine. TERM is being considered for the treatment of a variety of diseases and medical problems, some of which are outlined in [Table 10.1](#).

TERM is a rapidly developing multidisciplinary field that utilizes life science and engineering principles to construct biological substitutes containing viable and functioning cells for the restoration, maintenance, replacement, or improvement of a tissue function, or even a whole organ (Langer and Vacanti, 1993). The realm of TERM has also been extended in recent years to include the use of

Table 10.1 Opportunities for TERM

Liver diabetes	Dental plastic/reconstructive surgery
Parkinson's disease	Nerve regeneration
Kidney	Site-specific delivery of growth factors
Chronic pain	Cornea
Esophagus	Skin
Ureter	Intestine
Bladder	Trachea
Cartilage	Bone
Muscle regeneration	Blood
Artificial blood vessels	In vitro models for cancer
	Stem cells
Gene therapy	Parathyroid
Cell production	In vitro hematopoiesis
Alzheimer's disease	Neurological diseases
Heart valves	Lymphocytes
Spine	Intervertebral disks
Retina	
Whole organs	
In vitro drug screening	

tissue engineered structures as an in vitro platform for the evaluation and testing of new drugs and as models of diseases such as cancer (Neiman et al., 2014; Beauchamp et al., 2015; Bray et al., 2015; Wobma and Vunjak-Novakovic, 2016).

### 10.2.1 Cells for TERM

The cells that are used in TERM can be harvested from a variety of sources. For example, the cells can be obtained from a human donor (*allograft*), animals (*xenograft*), the patient themselves (*autograft*), or from a genetically engineered cell line (Morgan et al., 1994; Chang, 1997; Zalzman et al., 2003).

*Stem cells* have the potential of being a rich source of cellular material for TERM applications, and there is much interest in the use of both adult and embryonic stem cells. Adult stem cells are found within a variety of tissues in the adult body, and they are the precursor cells that are needed for repairing or rebuilding tissue as a result of injury, disease, or aging (Pittenger et al., 1999).

Embryonic stem cells, however, are isolated from what is known as the *inner cell mass* of the *blastocyst* that later forms the embryo. The isolation of the inner cell mass from a developing embryo for tissue engineering applications, and for the treatment of disease, results in the death of the embryo, and in the case of a human embryo, this has raised ethical issues. For example, is the development from conception to birth the *development TO a human being* or the *development OF a human being* (van Blitterswijk, 2008)? This has created a moral dilemma in the sense of whether it is morally justifiable to use embryonic stem cells from human embryos to treat human diseases.

Stem cells possess the unique property of *pluripotency*, which is not found in most other terminally differentiated cells. This means that stem cells readily replicate and they have the potential to

differentiate under the right conditions into other cell types that are found in the body. For example, adult bone marrow has many types of stem cells that can be coaxed to differentiate into about every type of cell found in the body.

In addition to stem cells, there are also what are known as *progenitor cells*, which are further along in the differentiation process than a stem cell. Progenitor cells reside in all kinds of tissues found in the body. Under the right conditions, progenitor cells can differentiate into a more specific cell type; however, they cannot replicate indefinitely like a stem cell. When presented with the proper signals, progenitor cells can therefore replace those cells that are lost as a result of injury or through normal attrition.

A particular type of stem cell found both in embryos and in adults is the *mesenchymal stem cell*. A mesenchymal stem cell can differentiate to form cartilage, bone, tendons, ligaments, muscle, marrow stroma, and connective tissue (Caplan, 1991; Pittenger et al., 1999). Mesenchymal stem cells are receiving considerable attention because of their potential to provide a cell source for a variety of tissue engineered constructs that can be used in a variety of TERM applications, especially for bone and cartilage repair (Madry et al., 2014; Im, 2016). In many cases, the patient's own mesenchymal stem cells can be harvested from their own bone marrow and used for these applications (Sart et al., 2014).

Another promising stem cell type (Kuroda et al., 2014; Yu et al., 2016) are known as *adult human circulating/peripheral blood CD34<sup>+</sup> cells*. This class of stem cell also includes circulating endothelial progenitor cells and hematopoietic stem/progenitor cells. This type of stem cell has been shown to promote bone regeneration and tissue neovascularization and has potential applications in the treatment of myocardial infarction and various disorders of the liver.

A recent promising discovery are the so-called *induced pluripotent stem cells*, or iPSCs, that can be made by genetically reprogramming adult somatic cells to become pluripotent stem cells (Takahashi and Yamanaka, 2006; Harrison et al., 2014; Beauchamp et al., 2015). iPSCs have properties that are similar to those of embryonic stem cells. Hence, iPSCs also have the potential to overcome the ethical issues associated with the use of tissue derived from human embryos since the pluripotent cells needed for TERM can be obtained from the patient.

### 10.2.2 The tissue engineering process

Transplanted cells have the potential to grow and form larger tissue structures when implanted in the vicinity of existing mature tissue. However, a potential problem is the loose association of the transplanted cells that provides no guide for attachment, restructuring, and the formation of larger 3D cellular aggregates and tissue structures. Additionally, the transplanted cells cannot survive if they do not have an adequate supply of blood to provide oxygen, nutrients, and a means for waste product removal. Furthermore, any therapeutic product released by the transplanted cells needs to have access to the host's vasculature in order for it to be effective. This requires that each transplanted cell be within a hundred microns or so of a capillary. Initially, the existing capillary supply in the tissue surrounding the cellular transplant may not be optimal for the sustained growth of the transplanted cells. This severely limits the size of the cellular aggregates that can form, unless a means is provided for the formation of a vascular capillary bed (angiogenesis) within the transplanted cells. The goal of tissue engineering is therefore to develop methods and techniques that can enhance the success of cellular transplants.

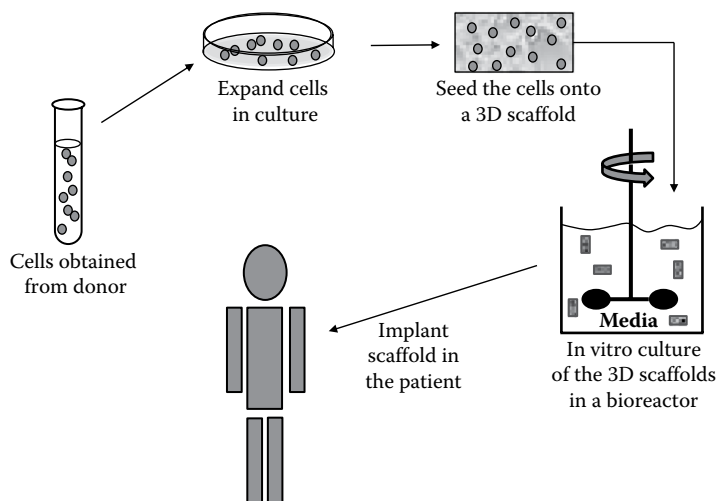


Figure 10.1 The tissue engineering process.

**Figure 10.1** illustrates the basic steps of the tissue engineering process. This process consists of several steps and includes developing a source for the required cells, expanding these cells through in vitro tissue culture, seeding the cells into a scaffold material with the appropriate extracellular matrix (ECM) materials, and providing the resulting constructs with any required mechanical stimulus or molecular signaling molecules to ensure proper differentiation of the resulting tissue. Once these steps have been completed, the tissue engineered construct can be implanted into a patient.

**10.2.2.1 Immunoprotection of the transplanted cells** In some cases, the transplanted cells in the tissue engineered construct need to be protected from the host's immune system. This can be a result of the use of foreign cells or the need to protect the cells from an autoimmune response, which occurs in the process leading to insulin-dependent diabetes. This *immunoprotection* of the transplanted cells from the host's immune system can be accomplished through the use of an *immunoisolation membrane* (Colton, 1995).

The immunoprotection concept is illustrated in **Figure 10.2**. The immunoisolation membrane used to provide immune protection to the transplanted cells is permeable to small molecules, such as required nutrients and the therapeutic agent released by the cells, but impermeable to the larger molecules (antibodies and complement) and cells of the host's immune system. Immunoprotection of the transplanted cells therefore does not require the use of immunosuppressive drugs or *immunomodification* (Lanza and Chick, 1994b) of the cells prior to transplant. Because of this immunoprotection, there is the potential to use cells and tissues from animals (xenografts) or genetically engineered cell lines, which vastly increases the availability of donor tissue. For example, in the development of a bioartificial pancreas for the treatment of insulin-dependent diabetes, immunoprotected islets of Langerhans from rats were transplanted into diabetic mini pigs and successfully restored normal blood glucose levels (Neufeld et al., 2013). Several examples of this immunoprotection approach to create what are known as bioartificial organs will be examined in greater detail in **Chapter 11**.

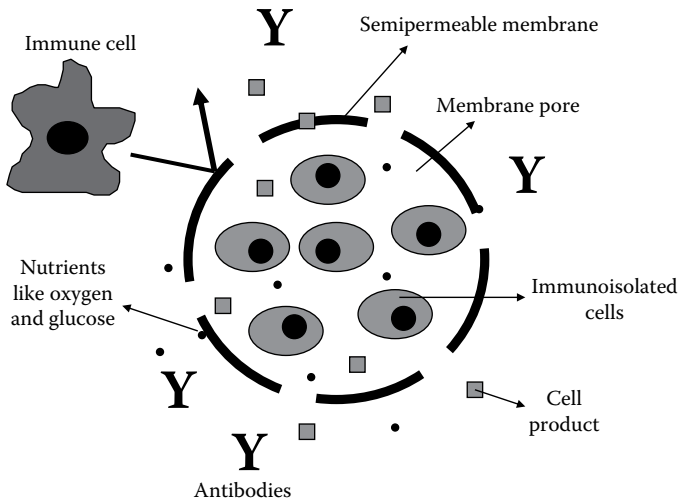


Figure 10.2 Concept of immunoisolation.

### 10.3 The extracellular matrix

Most of the efforts in tissue engineering is now focusing on the use of polymeric support structures or scaffolds for guiding the growth and organization of the transplanted cells into the desired 3D shape (Cima et al., 1991a,b; Goldstein et al., 1999; Oerther et al., 1999; Petersen et al., 2002; Leach et al., 2003; Radisic et al., 2003; Palsson and Bhatia, 2004; Pratt et al., 2004; van Blitterswijk, 2008). These scaffolds can be made from synthetic or naturally occurring polymeric materials. Tissues and even whole organs can also be treated with special chemicals and made acellular leaving behind a natural scaffold for the seeding of new cells (Price et al., 2015).

These materials used as scaffolds are either biodegradable or nonbiodegradable and can be formed into a variety of shapes with mechanical properties similar to the tissue they are replacing. However, to better understand how polymeric support structures can enhance the growth of transplanted cells, it is necessary to first examine how cells organize themselves within natural tissue structures.

Tissues are not only made up entirely of cells but also consist of an extracellular gel-like fluid containing a variety of macromolecules collectively referred to as the ECM (Alberts et al., 1989; Anderson, 1994; Rubin and Farber, 1994; Long, 1995; Naughton et al., 1995; Hubbell, 1997; Parsons-Wingerter and Sage, 1997; Dee et al., 2002). The major components of the ECM are the glycosaminoglycans (GAGs), proteoglycans, collagens, elastic fibers, structural glycoproteins, and the basement membrane.

The ECM macromolecules are secreted locally for the most part by specialized cells called *fibroblasts*. Several of the most important types of macromolecules found within the ECM are summarized in [Table 10.2](#). These materials that comprise the ECM form a unique composition for each type of tissue. These ECM materials are in intimate contact with the cells and hold them together, forming an organized 3D cross-linked mesh-like structure. The ECM gives the tissue its mechanical strength and serves as a pipeline for intercellular signaling.

Table 10.2 Major Macromolecules of the Extracellular Matrix

<i>Glycosaminoglycans (GAGs)</i>	—forms the ECM gel
<i>Collagen</i>	—provides strength and organization to the ECM
<i>Elastin</i>	—provides resilience or elasticity
<i>Fibronectin</i>	—adhesion of fibroblasts and other cells
<i>Laminin</i>	—adhesion of cells to the basal lamina
<i>Aggrecan</i>	—resists compressive loads

The ECM therefore plays an active role in organizing the tissue since it not only serves to provide for the 3D organization of cells and adjacent layers of tissue but also provides a mechanism for intercellular communication and controls cellular processes such as proliferation, cell migration, attachment, differentiation, and repair.

Most mammalian cells are anchorage dependent and possess cell-surface receptors for a variety of these ECM macromolecules. Hence, some of these ECM macromolecules possess so-called *attachment factors* that are responsible for the development, growth, and metabolic functions of cells. The ECM itself has also been used, because of these properties, as a scaffold for tissue engineering applications.

This tissue organizing principle of the ECM is shown in [Figure 10.3](#) for the case of *epithelial cells* that are supported by a layer of *connective tissue*. Connective tissues (also called the *stroma*) provide the framework for the formation and organization of most of the larger structures found within the body. The specific functional cells that define a tissue, e.g., the hepatocytes found in the liver, or the islets of Langerhans in the pancreas, are called *parenchymal cells*.

Using [Figure 10.3](#) as our guide, the following discussion will focus on a description of the major constituents of the ECM, i.e., the GAGs, collagens, elastin, fibronectin, and aggrecan.

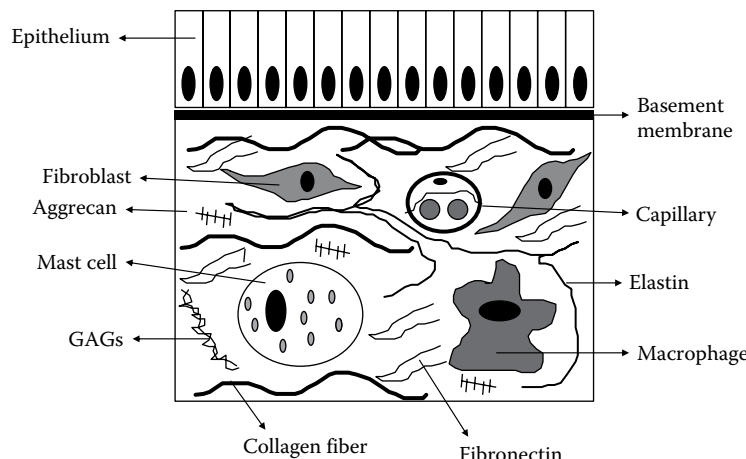


Figure 10.3 Connective tissue.

### 10.3.1 Glycosaminoglycans

*GAGs* form from long linear polymers consisting of a repeating disaccharide unit. Molecular weights range from several thousand to over a million. GAGs tend to have a large number of negative charges because of the presence of carboxyl and sulfate groups. They are highly extended forming random coil-like structures. Because they are also hydrophilic, they form in combination with the interstitial fluid the hydrated gel-like material throughout which the other macromolecules of the ECM are found. In addition, GAGs bind with growth factors and intercellular messenger molecules known as *cytokines*.

There are four types of GAGs depending on what types of sugars they are made from. They are *hyaluronic acid*, *chondroitin sulfate* and *dermatan sulfate*, *heparan sulfate* and *heparin*, and *keratan sulfate*. With the exception of hyaluronic acid, they also form what are called *proteoglycans* through covalent bonds with proteins.

### 10.3.2 Collagens

*Collagens* are fibrous proteins that are made from three polypeptide chains that form the tough, triple-stranded helical structure of the collagen molecule. The tensile strength of tissues is provided by collagen. Collagens are also the most prevalent protein material found within the ECM, and they have several unique functions.

Although more than twenty types of collagen molecules have been identified, there are four that are most important. These are the *fibrillar collagens* (type I, type II, and type III) and type IV collagen. The first three types of collagen molecules assemble themselves into much larger structures called collagen fibrils that aggregate further to form collagen fibers. Type I collagen makes up about 90% of the collagen found in the body. It is found mostly in the skin, tendons, ligaments, various internal organs, and bone. Type II collagen is primarily found in cartilage, and type III collagen is found in blood vessels, as well as the skin. Type IV collagen organizes itself to form sheets within the basal lamina of the basement membrane. Fibroblasts have the ability to organize the collagen fibrils they secrete forming sheets or rope-like structures; therefore, they can affect the spatial organization of the matrix they produce.

### 10.3.3 Elastin

*Elastin* is a hydrophobic glycoprotein molecule that through cross-links with other elastin molecules can form a network of sheets and filaments with the unique property of being elastic, allowing for recoil after periods of stretch. The elasticity is a result of the random coil-like structure of the elastin molecule. The elastic nature of elastin is important in blood vessels, the skin, lungs, and uterus. Inelastic collagen fibrils are interwoven with elastin to limit and control the degree of stretching.

### 10.3.4 Fibronectin

*Fibronectin* is the principal adhesive glycoprotein found within the ECM. Next to collagen, it is the second most prevalent macromolecule found in the ECM. Fibronectin binds to other ECM molecules, such as collagen, and to cell-surface receptors. It therefore has a principal role in the attachment of cells to the ECM. Fibronectin is a dimer made up of two subunit chains that are bound together at one end by a pair of disulfide bonds. Along the length of the chains are a series of functional domains that can bind to specific types of molecules (e.g., collagen or heparin) or cell-surface

receptors. The cell-binding domain has a specific tripeptide sequence consisting of the amino acids: arginine (R), glycine (G), and aspartic acid (D), often referred to as the *RGD sequence*. Peptides containing this sequence will inhibit the attachment of cells to fibronectin through their competition for the RGD binding site on the cell surface.

In addition to fibronectin, there are several other ECM adhesion proteins that express the RGD sequence. These include *vitronectin* found primarily in blood cells. *Thrombospondin* is secreted by a variety of cells involved in the development of the ECM. It serves to bind together other components of the ECM like fibronectin. *Von Willebrand factor* is made by megakaryocytes (platelet-generating cells found in the bone marrow). It is stored in circulating platelets. Von Willebrand factor is released by platelets as a result of injury to blood vessels, and this factor then binds to collagen. The platelets then bind to the von Willebrand factor that is also bound to collagen. Fibrinogen is another of the clotting proteins found in the blood. During blood clot formation, fibrinogen is converted to fibrin that forms a mesh-like structure that traps red blood cells and platelets.

### 10.3.5 Aggrecan

Aggrecan is a chondroitin and keratan sulfate proteoglycan that is a key component of the ECM in cartilaginous tissues. It provides cartilage, as well as the intervertebral disk, the ability to withstand compressive loads.

### 10.3.6 Basement membrane

The *basal lamina* is a continuous mat-like structure of ECM materials that separates specific cells, such as epithelial, endothelial, or muscle, from the underlying layer of connective tissue. The basal lamina consists of two distinct layers, the *lamina rara*\* directly beneath the basal membrane of the specific cells above and the *lamina densa*<sup>†</sup> just below the lamina rara. Found below the two layers of the basal lamina is the collagen-containing *lamina reticularis* that connects the basal lamina to the connective tissue that lies below it. All three of these layers together constitute what is known as the *basement membrane* (see [Figure 10.3](#)). The basal lamina consists primarily of type IV collagen, proteoglycans, such as those formed from heparan sulfate, and the glycoprotein *laminin*.

Laminin is an extremely large protein with a molecular weight of 850,000 made from three long polypeptide chains that form the shape of a cross. It also contains a number of functional domains throughout its structure with sites for binding to type IV collagen, heparan sulfate, and laminin cell-surface receptors. Laminin has a major role in the formation and maintenance of blood vessels.

## 10.4 Cellular interactions

There are three types of interactions involving cells. These interactions may be classified as cell-ECM, cell-cell, and cell-growth factor (Long, 1995). [Figure 10.4](#) illustrates the various interactions of cells with their surrounding environment. Cells interact with other cells, the ECM, and growth factors through cell-surface receptor proteins that are an integral part of the cell membrane. Binding of cell-surface

---

\* Under the electron microscope, this layer is translucent to electrons.

<sup>†</sup> Under the electron microscope, this layer is somewhat opaque to electrons.

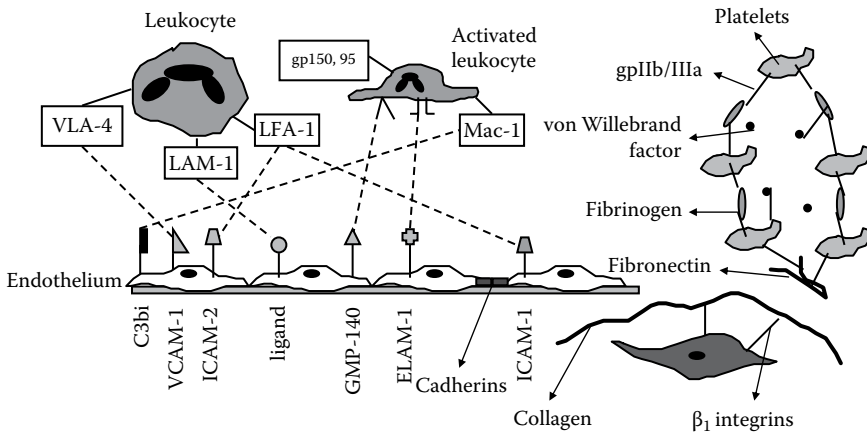


Figure 10.4 Cellular interactions.

receptors to surrounding ECM components such as collagen, fibronectin, and laminin enables the cell to link up to the surrounding matrix. Binding of cell-surface receptors between cells allows them to organize into larger structures such as tissues and organs. Cell-surface receptor interactions with growth factors provide control over a variety of cellular functions through the control of gene expression.

There are four types of cell adhesion receptors (Hubbell, 1997). Three of these receptors are mainly involved in cell-cell interactions, and the fourth is involved in both cell-cell and cell-ECM interactions. The adhesion receptors used in cell-cell interactions include the *cadherins*, the *selectins*, and the *cell adhesion molecules* (CAMs). The receptors involved in cell-ECM interactions belong to a general family of adhesion receptors known as *integrins* (Horwitz, 1997).

#### 10.4.1 Cadherins

Cadherins take part in what is known as homophilic binding, i.e., the binding of a cadherin molecule on one cell with an identical cadherin on another cell of the same type. They do not bind with ECM components. The cadherin molecule binding is strongly dependent on the presence of extracellular  $\text{Ca}^{++}$ .

#### 10.4.2 Selectins

The selectins are a family of CAMs that are found on the surfaces of endothelial cells, leukocytes, and platelets. They exhibit heterophilic binding between the blood cells and the endothelial cells that line the blood vessels. They are important in the localization of leukocytes to sites of inflammation and tissue injury. The three most important selectins are called GMP-140, endothelial leukocyte adhesion molecule-1, and leukocyte adhesion molecule-1. Like the cadherins, their activity is dependent on the presence of extracellular calcium.

#### 10.4.3 Cell adhesion molecules

The CAMs are members of the immunoglobulin gene superfamily. These receptors bind independently of extracellular calcium levels. CAMs are involved in recognition of antigens (foreign agents) and cell-cell interactions. Antigen recognition involves both the T-lymphocyte receptor and

two special antigen-presenting molecules called major histocompatibility complex classes I and II (MHC I and MHC II). These specialized CAMs will be discussed further in [Chapter 11](#) in the section on immunology.

Two other CAMs are important factors in localizing leukocytes to regions of tissue injury. For example, intercellular adhesion molecule (ICAM)-1 is found on the surfaces of both endothelial cells and leukocytes and binds to the integrin called leukocyte function antigen-1 (LFA-1) that is found on macrophages and neutrophils. ICAM-2, found on endothelial cells, also binds to LFA-1 and helps to localize neutrophils to sites of injured tissue. Vascular cell adhesion molecule (VCAM)-1 is expressed by endothelial cells as a response to injury or inflammation and also promotes adherence of leukocytes to endothelial cells.

#### 10.4.4 Integrins

The integrins (Horwitz, 1997) are a family of adhesion molecules that are involved in both cell-cell interactions and binding with molecules found in the ECM. Integrin molecules are heterodimers consisting of two protein subunits, the  $\alpha$  chain and the  $\beta$  chain. There are at least 15 variants of the  $\alpha$  subunit and 8 variants of the  $\beta$  subunit. Overall, there are at least 20 different heterodimer  $\alpha\beta$  integrins. The  $\beta$  subunits provide the functional aspects of the dimeric integrin molecule; hence, integrins are classified according to the type of their  $\beta$  chain. The subclasses having the  $\beta_1$ ,  $\beta_2$ , and  $\beta_3$  chains are the most common. The  $\beta_1$  and  $\beta_3$  subclasses are primarily involved in interactions between the cell and the ECM. The  $\beta_2$  subclass involves mostly cell-cell interactions involving leukocytes.

$\beta_1$  integrins are also referred to as *very late after* (VLA) antigens (Margiotta et al., 1994). VLA antigens are numbered according to the number of the  $\alpha$  subunit that forms the heterodimer with the  $\beta_1$  subunit. These subclasses bind with a variety of ECM proteins such as collagen, fibronectin, and laminin. The primary recognition site for  $\beta_1$  integrins is the RGD sequence described earlier. Therefore, this group of integrins is important for the overall organization and function of a variety of cell types. VLA-4 is also a receptor found on leukocytes for VCAM-1 expressed by endothelial cells.

Cell-cell interactions, mainly leukocyte to leukocyte, involve mostly the  $\beta_2$  group of integrins. Hence this subclass is known as the “leukocyte” integrins. The common  $\beta_2$  subunit is also known as cluster designation (CD)18, a protein with a molecular weight of 95,000. The most important  $\alpha$  subunits, in combination with  $\beta_2$ , form the leukocyte integrins known as LFA-1, Mac-1 (macrophage antigen-1), and gp150,95 (a glycoprotein with an  $\alpha$  subunit of molecular weight 150,000 along with the  $\beta_2$  subunit protein with a molecular weight of 95,000). These  $\alpha$  subunits are also respectively known by the cluster designations CD11a, CD11b, and CD11c. The expression of these integrins on leukocytes is particularly important for defense against bacterial infections.

The  $\beta_3$  integrins comprise the platelet glycoprotein receptor, known as gpIIb/IIIa, and the vitronectin receptor. Both of these receptors also recognize the RGD sequence of ECM proteins such as vitronectin, fibronectin, thrombospondin, fibrinogen, and von Willebrand factor. The aggregation of platelets is enhanced by the release of von Willebrand factor. gpIIb/IIIa is calcium dependent and found on the surface of activated platelets. This integrin is important for platelet aggregation and adherence of platelets to the subendothelium. This occurs through binding of this receptor to fibrinogen, fibronectin, vitronectin, and von Willebrand factor.

### 10.4.5 Cytokines and growth factors

A variety of cells also secrete soluble proteins known as *cytokines*. Cytokines serve as intercellular chemical messengers. Many of these proteins are required for the normal development, growth, and proliferation of cells. They are also involved in processes such as inflammation and wound healing and the varied responses of the immune system. Many are *mitogens*, i.e., they stimulate the proliferation of specific types of cells. They are then referred to as *growth factors*.

Growth factors bind to specific receptors on the surface of their target cell and have the ability to induce or direct the action of specific genes in the targeted cell. A variety of growth factors have been identified, and some of the more important of these for TERM applications are summarized in **Table 10.3**. All of these growth factors also play a key role during the wound healing process, and many are involved in the growth of new blood vessels. Many of these growth factors can also be used to stimulate and accelerate the growth and differentiation of stem cells used in polymeric scaffolds for tissue engineering applications (Babensee et al., 2000).

Since many growth factors have short biological half-lives, e.g., the half-life of transforming growth factor- $\beta$  (TGF- $\beta$ ) is less than 30 min, techniques are being developed for the controlled release of growth factors to maintain a critical level of the growth factor within the tissue engineered construct (Babensee et al., 2000; Spicer and Mikos, 2010; Madry et al., 2014). Growth factors are very potent and their concentrations tend to be very small. For example, Madry et al. (2014) states that for the chondrogenic differentiation of mesenchymal stem cells (MSCs), the critical concentration of the growth factor TGF- $\beta$  is about 10 ng mL $^{-1}$ .

Platelet-derived growth factor (PDGF) is a mitogen for cells such as smooth muscle, fibroblasts, and neuroglial. PDGF is stored in platelets and is released after platelet aggregation at the site of injury

Table 10.3 Growth Factors

Growth Factor	Property
Platelet-derived growth factor (PDGF)	Mitogen for smooth muscle cells, fibroblasts, and neuroglial cells; chemotactic signal for immune system cells
Epidermal growth factor	Mitogen for a variety of cell types, accelerates wound healing
Fibroblast growth factors (aFGF and bFGF) and vascular endothelial cell growth factor (VEGF)	Stimulates growth of blood vessels; mitogen for endothelial cells, fibroblasts, smooth muscle cells
Tumor necrosis factor (TNF)	Stimulates growth of blood vessels
Bone morphogenetic protein (BMP)	Induce the formation of bone and cartilage
Osteogenic protein (OP)	Induce the formation of bone
Insulin-like growth factor (INF-I)	Stimulates growth of blood vessels
Transforming growth factor (TGF- $\beta$ )	Controls cellular response to other growth factors, stimulates chondrogenesis
Nerve growth factor (NGF)	Stimulates axon growth
Stromal cell-derived growth factor (SDF-1)	Stimulates growth of blood vessels
Keratinocyte-derived growth factor (KGF)	Involved in wound healing
Epithelial cell growth factor (EGF)	Important in wound healing
Hepatocyte growth factor (HGF)	Important in organ regeneration and wound healing
Interleukin-2 (IL-2)	Stimulates proliferation of T-lymphocytes
Interleukin-6 (IL-6)	Stimulates proliferation and differentiation of B-lymphocytes

to blood vessels. Damaged endothelial and smooth muscle cells also secrete PDGF. PDGF is also a chemotactic signal for inflammatory cells such as macrophages and neutrophils.

Epidermal growth factor (EGF) stimulates the growth of a variety of cell types. EGF accelerates the healing of many wounds and stimulates fibroblasts to deposit collagen.

Fibroblast growth factor (FGF) comes in two forms, acidic (aFGF) and basic (bFGF). bFGF is an order of magnitude more potent than aFGF. FGF and vascular endothelial cell growth factor (VEGF) stimulate the growth of capillaries, a process called angiogenesis (Folkman, 1985; Folkman and Klagsbrun, 1987). FGF also promotes the growth of fibroblasts, endothelial cells, and smooth muscle cells. These processes affected by FGF also accelerate wound healing.

Another angiogenic growth factor is tumor necrosis factor- $\alpha$  (TNF- $\alpha$ ), which is secreted by activated macrophages during the initial stages of inflammation. Insulin-like growth factor-1 (IGF-1) not only plays a major role in growth but also stimulates angiogenesis.

TGF- $\beta$  can either promote or inhibit the growth of cells by controlling their response to other growth factors. TGF- $\beta$  has also been shown to be important for the growth and differentiation of MSCs for the repair of damaged articular cartilage (Madry et al., 2014; Kim et al., 2015).

Several other important growth factors include nerve growth factor (NGF) that enhances the function of neurons and stimulates axon growth, interleukin-2 (IL-2) that stimulates the proliferation of T-lymphocytes, and interleukin-6 (IL-6) that stimulates the proliferation of B-lymphocytes and their differentiation to antibody-secreting plasma cells. There are also several hematopoietic\* growth factors that are specific to the development and differentiation of blood cells.

Other growth factors of interest to tissue engineering include stromal cell-derived growth factor (SDF-1), epithelial cell growth factor (EGF), and keratinocyte-derived growth factor (KGF). These three growth factors are important in wound healing and angiogenesis. Hepatocyte growth factor (HGF) plays an important role in organ regeneration and wound healing, and bone morphogenetic protein (BMP) and osteogenic protein (OP) stimulate the formation of bone and cartilage.

A cocktail of growth factors can also be used to enhance the growth and differentiation of the cells within a tissue engineered scaffold. For example, for MSC differentiation and maturation to form cartilage, a combination of IGF, TGF, FGF, and BMP can be used (Shimomura et al., 2014).

### 10.5 Support structures for tissue engineering applications

With this background on how cells organize themselves within the body, we can now address the properties required for a support structure for transplanted cells. **Table 10.4** summarizes some of the characteristics that are important to consider in selecting materials to serve as support structures for transplanted cells. A variety of biological and synthetic polymers can be used as biomaterials, and many of these can be used to provide the support structure for transplanted cells. **Table 10.5** summarizes some of the materials that are being used or being considered for use as support structures in tissue engineering.

---

\* Hematopoiesis is the process of blood cell development and differentiation.

---

Table 10.4 Desirable Properties of Scaffold Structures for TERM

---

Biocompatible
Nonimmunogenic
Negligible toxicity
Locally and systemically
The polymer and any of its degradation products
Chemically and mechanically stable
Processable into a variety of shapes
Hollow tubes, sheets, arbitrary 3D shapes
Open foam or sponges
Woven or nonwoven mesh-like structures
High porosity
High internal surface area to volume ratio
Controllable pore size
Promotes cell attachment
Promotes angiogenesis
Favorable interaction/mobilization of host cells
Ability to release active compounds such as growth factors
Ability of the cells and ECM materials to interact with the support structure
Ability to obtain the desired cellular response

---

### 10.5.1 Biomaterials

The biomaterials listed in [Table 10.5](#) are grouped as to whether or not they are biodegradable. Long-term implantation of nonbiodegradable biomaterials poses the risk of localized infection, chronic inflammation, and the development of fibrous encapsulation of the implant. This can compromise the proper functioning of transplanted cells if they were to reside within the porous structure of these materials. Nonbiodegradable materials, such as polytetrafluoroethylene (PTFE), PU, and Dacron, are preferred for those applications where their structural integrity is more important than the requirement for them to serve as scaffolds for transplanted cells, e.g., as vascular grafts or structural components of artificial organs. These materials can also be made into a variety of 3D configurations. Other materials such as agarose gel are nonbiodegradable materials that have found widespread use in cell encapsulation and have been proposed as scaffolds in tissue engineering (Park et al., 2010).

Biodegradable materials are now attracting significant interest for tissue engineering applications. Biodegradable materials allow the transplanted cells sufficient time to organize the desired 3D structure and develop their own blood supply. The biodegradable polymers are easily hydrolyzed by the body's fluids and slowly disappear without leaving behind any foreign residues. Examples of biologically derived biodegradable polymers include collagen, GAGs, fibrin gels, chitosan, and small intestinal submucosa (SIS). Collagen is one of the ECM materials and can be prepared as fibers (Cavallaro et al., 1994) or as a gel. Collagen is being used in applications such as tissue repair and artificial skin (Morgan and Yarmush, 1997). SIS has many interesting properties and is widely used as a bioscaffold and for the repair of tissues (Le Visage et al., 2006). SIS is harvested from the small

## Basic Transport Phenomena in Biomedical Engineering

---

Table 10.5 Materials for TERM

<b>Nonbiodegradable</b>	<b>Applications</b>
Alginates	Food additives, cell encapsulation
Agarose	Cell culture and cell encapsulation, scaffold
Cellulose	Bone tissue engineering
Polydimethylsiloxane or silicone (PDMS)	Breast, penile, testicular prostheses, catheters, drug delivery, heart valves, membrane oxygenators, shunts, tubing, orthopedics
Silk fibroin	Stem cell applications for cartilage and bone
Ceramics and bioactive glass	Bone repair
Polyurethanes	Artificial hearts and ventricular assist devices, catheters, intra-aortic balloons, wound dressings
Polytetrafluoroethylene (PTFE)	Heart valves, vascular grafts, reconstruction, shunts, membrane oxygenators, catheters, sutures, coatings
Polyethylene (PE)	Artificial hips, catheters, shunts, syringes, tubing
Polysulfone	Heart valves, penile prostheses, artificial heart
Polycarbonate	Hard contact lenses
Poly(methyl methacrylate) (PMMA)	Bone cement, fracture fixation, intraocular lenses, dentures, plasmapheresis membranes
Poly(2-hydroxyethylmethacrylate) (PHEMA)	Controlled drug release, contact lenses, catheters, coatings, artificial organs
Polyacrylonitrile (PAN)	Hemodialysis membranes
Polymides (nylon)	Hemodialysis membranes, sutures
Polyethylene terephthalate (Dacron)	Vascular grafts, tissue patches, shunts
Polypropylene (PP)	Valve structures, plasmapheresis membranes, sutures
Polyvinyl chloride (PVC)	Tubing, plasmapheresis membranes, blood bags
Poly(ethylene-co-vinyl acetate)	Drug delivery devices
Polystyrene (PS)	Tissue culture flasks
Poly(vinyl pyrrolidone) (PVP)	Blood plasma extender
Polyvinyl alcohol (PVA)	Dental, tissue repair, scaffolds for bioartificial organs
<b>Biodegradable</b>	<b>Applications</b>
Poly(L-lactic acid) (PLA), poly(glycolic acid) (PGA), and poly(lactide-co-glycolide) (PLGA)	Controlled release drug delivery devices, sutures, scaffolds for cell transplantation and tissue engineering
Collagen	Artificial skin, hemostasis, tissue regeneration scaffold
GAGs (hyaluronan)	Tissue repair, viscoelastic, wound care
Small intestinal submucosa (SIS)	Bioscaffolds and tissue repair
Chitosan	Scaffolds for tissue engineering, inhibitors of blood coagulation, cell encapsulation, membrane barriers, contact lens materials
Polyhydroxyalkanoates (PHA)	Controlled drug release, sutures, artificial skin
Poly( $\epsilon$ -caprolactone) (PCL)	Implantable contraceptive devices, controlled drug release, surgical staples, scaffolds for cell transplantation and tissue engineering
Polyphosphoesters (PPE)	Cartilage and bone, nerve and organ regeneration

(Continued)

Table 10.5 (Continued) Materials for TERM

Biodegradable	Applications
Polyphosphazenes (PPA)	Bone and nerve regeneration
Polyanhydrides (PA)	Bone
Starch	Thermoplastic starches (TPS) for use as scaffolds

Sources: Friedman, D.W. et al., Biomaterials: An historical perspective, in *Implantation Biology*, Chapter 1, Greco, R.S. (ed.), CRC Press, Inc., Boca Raton, FL, 1994; Marchant, R.E. and Wang, I.W., Physical and chemical aspects of biomaterials used in humans, in *Implantation Biology*, Greco, R.S. (ed.), CRC Press, Inc., Boca Raton, FL, 1994, pp. 13–38; Saltzman, W.M., Cell interactions with polymers, in *Principles of Tissue Engineering*, Lanza, R.P., Langer, R., and Chick, W.L. (eds.), R.G. Landes Co., Boulder, CO, 1997, pp. 225–246; Pachence, J.M. and Kohn, J., Biodegradable polymers for tissue engineering, in *Principles of Tissue Engineering*, Lanza, R.P., Langer, R., and Chick, W.L. (eds.), R.G. Landes Co., Boulder, CO, 1997, pp. 273–293; Van Blitterswijk, C., *Tissue Engineering*, Elsevier, London, U.K., 2008.

intestine of pigs and consists of a rather loose scaffold of ECM materials. This scaffold of ECM materials comprises oriented collagen fibers, GAGs, and attached growth factors such as bFGF, VEGF, and TGF- $\beta$ .

PLA, poly(glycolic acid) (PGA), and poly(lactide-co-glycolide) (PLGA) are naturally occurring hydroxy acids. They are biodegradable and have been approved for use by the Food and Drug Administration (FDA) for use in sutures, controlled drug release, and surgical support fabrics (Cima et al., 1991a,b). A great deal of effort is focusing on these materials for tissue engineering applications (Mooney et al., 1994, 1995a,b, 1996; Holder et al., 1997; Kaufmann et al., 1997; Blitterswijk, 2008). They degrade by hydrolysis and form natural by-products. Their absorption rate can also be controlled from months to years (Mooney et al., 1994, 1995a,b; Agrawal et al., 1995). The degradation rate of these materials is dependent on their initial molecular weight, the surface area that is exposed, degree of crystallinity, and, for the case of copolymer blends, the ratio of the hydroxy acid monomers used (Pachence and Kohn, 1997).

The resulting structure formed from a biomaterial must be mechanically strong enough to support the growth of the transplanted cells and chemically compatible with the intended duration of use. For example, cells secrete a variety of enzymes that may degrade the polymer used. For a biodegradable material, this cell-induced degradation rate must be considered during formulation of the biomaterial to achieve the desired degradation rate. In the case of nonbiodegradable materials, they must withstand the cellular attack and not form by-products that are inflammatory or immunogenic and therefore capable of compromising the function of the implant.

The material used to form the support structure will also generally be in direct contact with the host's immune system and connective tissue such as fibroblasts. For any biomaterial, activation of the host's immune system (Wiles et al., 2016), as well as a fibrotic connective tissue response, will tend to wall off and isolate the transplanted support structure blocking its intended function. The host's reaction and formation of a fibrotic capsule around the implant is a function not only of the materials used but also depends on the shape and microstructure of the implant.

Unlike in vitro tissue culture of cells wherein the cells are usually grown in only two dimensions, the transplanted support structure containing the cells needs to be three dimensional. Furthermore, the

resulting 3D polymer scaffold must in general have high porosity, significant internal surface area, and a controlled pore size distribution. All of these properties must not compromise the structural strength of the material.

### 10.5.2 Techniques for making polymeric scaffolds

Polymer scaffolds used in tissue engineering applications must be processable into whatever 3D shape is required for the implant. A variety of techniques may be used to process polymer scaffolds. These include methods such as fiber bonding, solvent casting, particulate salt-leaching, membrane lamination, melt molding, polymer/ceramic fiber composite foams, phase separation, and in situ polymerization (Lu and Mikos, 1996; Thomson et al., 1997; Ma and Choi, 2001).

Another popular approach is electrospinning (Teo and Ramakrishna, 2006; Nam et al., 2007, 2008, 2009), which has the ability to easily produce porous structures that are highly interconnected and similar to that found in tissue and the ECM. The pore sizes of these scaffolds can be controlled by adjusting the electrospinning operating conditions such as the voltage, the distance between the spinneret and the grounded collection plate, and the solution viscosity. In addition, the macroscopic porosity can be controlled by combining electrospinning with the salt-leaching technique.

**Figure 10.5** shows microphotographs of a biodegradable open sponge-like scaffold and a mesh-like structure. Both of these scaffolds exhibit high porosity (>80%) and large pores. The poly(DTE carbonate) shown on the left in **Figure 10.5** was prepared by the salt-leaching technique. The resulting structure has pores in the range 200–500 µm and has been considered for bone regeneration. The PGA nonwoven mesh on the right has fibers 10–50 µm in diameter and has been considered for use in organ regeneration. These materials were shown to interact favorably with the surrounding tissue allowing for ingrowth of tissue and the formation of a vascular network throughout the support structure.

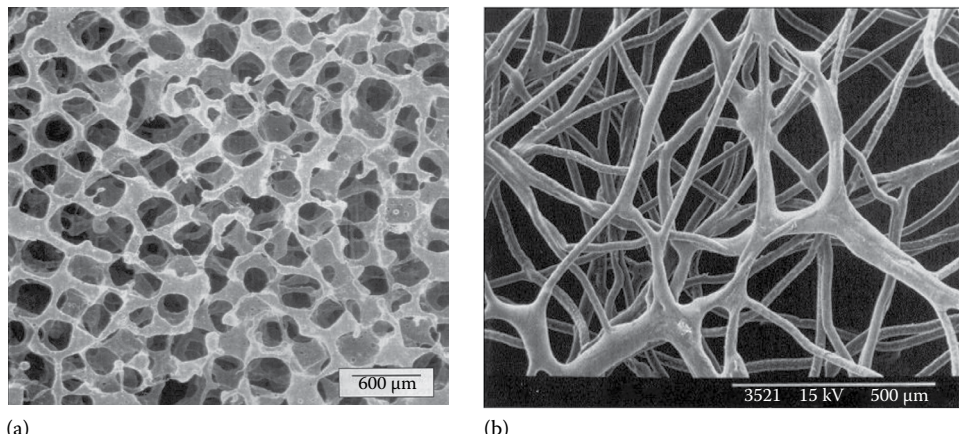


Figure 10.5 Scanning electron micrographs of polymeric scaffolds for tissue engineering.  
 (a) Poly(desaminotyrosyl-tyrosin ethyl ester carbonate) polymer scaffold (b) bonded poly(glycolic acid) nonwoven fiber mesh. (From James, K. and Kohn, J., *MRS Bull.*, 21, 22, 1996; Lu, L. and Mikos, A.G., *MRS Bull.*, 21, 28, 1996. With permission.)

The high porosity of the structures shown in [Figure 10.5](#) is also important for nutrient and product transport. To avoid the presence of nonvascular regions and to optimize implant size, it is important to be able to control the pore size distribution. A high internal-surface-area-to-volume ratio will also provide numerous sites for cell adhesion to the polymer support structure. A high internal surface area also allows for surface treatment of the polymer structure with ECM materials and/or growth factors in order to enhance interaction of the support with the transplanted cells and promote their proliferation and differentiation.

The ECM can also be designed using macromolecular analogues with specific properties that enhance the scaffold's use in tissue engineering applications (Welsh and Tirrell, 2000). In addition, synthetic hydrogels have been proposed that have *biomimetic properties*\* in the sense that these materials have the ability to communicate with cells through the presentation of bound adhesion and growth factors, and they can be remodeled through the action of cellular proteases (Pratt et al., 2004).

All of these traditional techniques for making scaffolds for TERM applications have been found to have some limitations, in particular, not being able to form the complex internal architecture found in tissues and organs. This has led to the development of newer techniques for making scaffolds popularly known as 3D printing and bioprinting.

**10.5.2.1 3D printing** 3D printing of tissue engineering scaffolds is a new approach that is very promising and is therefore receiving considerable attention for a variety of applications in TERM (Derby, 2012; Blakely et al., 2015; Holmes et al., 2015; Sears et al., 2016). These TERM applications of 3D printing build on the significant advances that have been made in the field of rapid prototyping. 3D printing allows for the fabrication of scaffolds with complex shapes and internal architecture that can mimic closely an actual biological tissue or anatomical structure. In addition, during the scaffold design phase, a variety of scaffolds with varying internal architecture can easily be designed and printed allowing for the optimization of the scaffold design for each specific application.

In a typical *acellular* 3D process, the scaffold is made before the cells are added to the construct. The desired scaffold structures are designed using computer-aided design (CAD) software, which then translates the complex geometrical scaffold shape and internal architecture into a file that is then read by the 3D printer. The file format sent to the 3D printer is usually a \*.stl, where *stl* is short for stereolithography, or a \*.amf, where *amf* means additive manufacturing file. A special software in the 3D printer then reads these files and guides the printer to make the scaffold, layer by layer, in what is also known as an *additive manufacturing* process.

There are many types of 3D printers and they generally fall into the following three categories (Sears et al., 2016) that are known as *stereolithography* (SLA), *solid free-form fabrication* (SFF), and *powder-fusion printing* (PFP).

SLA uses a laser beam to photopolymerize a liquid resin material contained within a reservoir. The reservoir containing the resin material is lowered as each successive layer of the resin material at the surface is polymerized and hardened to form the desired shape of the scaffold material. SLA is a very promising approach for the 3D printing of scaffolds because there are many biocompatible photopolymers and the technique has a very high spatial resolution, with

---

\* Meaning to imitate a biological function or structure.

the thickness of each layer printed on the order of 20  $\mu\text{m}$ . As an example, Neiman et al. (2014) describe the use of SLA to make open channel hydrogel scaffolds for the *in vitro* 3D perfusion of hepatocytes. The hepatocytes showed enhanced production of albumin in comparison to the same cells in 2D culture.

SFF builds a polymeric scaffold layer by layer by extruding filaments or granules of a polymeric material through a heated nozzle onto a build platform where the extruded material hardens (Lee et al., 2010). SFF printers typically use polymers that can be melted and extruded through a nozzle at temperatures of about 200°C. Some common polymers that are being used include polycarbonate, acrylonitrile butadiene styrene, and polylactic acid (PLA).

For TERM applications of SFF, there are also many biodegradable polymers and hydrogels (Hong et al., 2015) that can be used, and most of these melt at much lower temperatures. For example, polycaprolactone (PCL), which melts at 65°C, has been successfully extruded at a temperature of 125°C to form scaffolds with a honeycomb-like network of regularly sized pores (Zein et al., 2002; Sears et al., 2016).

Hong et al. (2015) 3D printed a variety of hydrogel scaffold shapes using a mixture of sodium alginate and poly(ethylene glycol) (PEG). The resulting hydrogel scaffolds that were printed using SFF were described as being tough and biocompatible. Hong et al. (2015) state that successful printing of 3D scaffolds using hydrogels is highly dependent on the viscosity of the pre-gel solution. The pre-gel solution should be *pseudoplastic* having a low viscosity at high shear rates, so it can easily pass through the printer nozzle and then have a higher viscosity at low shear rates so that the printed part can hold its shape.

A technique similar to SFF, known as *precision extrusion deposition* (PED), has also been used to make polymeric scaffolds with a controlled 3D architecture consisting of interconnected pores with a uniform pore size distribution (Yildirim et al., 2008). PED builds the scaffold through layer-by-layer extrusion of the polymer based on a predefined geometry controlled by a CAD program. By giving the PED scaffolds made from polycaprolactone (PCL) an oxygen-based plasma treatment, it was found that cell adhesion was enhanced and cell proliferation increased. PCL has been shown to be particularly suited for bone tissue engineering applications because of its mechanical properties, good biocompatibility, and ability to biodegrade (Yildirim et al., 2010).

PFP forms a thin layer of fine granular particles comprised of plastic or metal, which are fused together through the heating action of a laser. The layer is then recoated with more particles, and the sintering process is repeated until the desired shape has been made. In some cases, rather than using a laser, the particles can be fused together using special solvents and adhesives. One advantage of PFP is that the granular particles can be a mixture of different materials. In addition, this technique can use metallic particles of just about any composition to make shapes that have superior strength properties. Hence, there is much interest in this approach for making rigid structures such as bone.

Once the scaffold has been 3D printed by one of these methods, it is then seeded with cells and cultured *in vitro* prior to implantation. In some cases, the scaffold may be implanted right after it is printed, and the patient's cells in the implant site will infiltrate and take up residence within the scaffold and form new tissue.

A particularly exciting clinical example of 3D printing is the bioresorbable airway splint (Zopf et al., 2013) used to treat a life-threatening condition in newborns known as *tracheobronchomalacia*,

which causes collapse of the airway. A bioresorbable tracheal splint customized specifically to the anatomy of the patient was designed based on a computed tomographic image of the patient's airway. A CAD based on the patient's airway anatomy was then used to 3D print an airway splint from the biomaterial polycaprolactone (PCL). The institutional review board where this work was performed obtained an emergency-use exemption from the FDA so that this airway splint could be used to save a 2-month-old infant's life.

**10.5.2.2 Bioprinting** The term *bioprinting* is also being used to describe processes that can print in three dimensions all of the components that are found in the tissue (Derby, 2012; Blakely et al., 2015). This means not only the various cell types found in the tissue but also the components of the ECM. In a method analogous to inkjet printers, bioprinting has the capability to strategically place different cell types and ECM materials (*bioink*) in each layer of the construct as it is created. When using stem or progenitor cells, the cells deposited at specific locations can be subsequently induced to differentiate into the desired cell type. With continued advances in this area, it may even be possible to bioprint entire organs.

Bioprinting processes are typically based on the techniques of extrusion printing, laser-assisted bioprinting (LAB), and inkjet printing (Sears et al., 2016). When 3D bioprinting living cells within the scaffold structure, a special consideration needs to be given to ensuring that the cells remain viable during and after the processing steps. Hence, the cell printing needs to be done in an environment that does not overly stress the cells and cause damage to them. Also, there are limitations on the environmental conditions that are used when printing cells. For example, the need for aqueous solutions containing nutrient media and temperatures in the range from ambient temperature to 37°C.

*Extrusion bioprinting* is similar in some respect to SFF and uses a pseudoplastic fluid containing a mixture of the cells, ECM materials, and the scaffold biomaterials. The extrusion and subsequent gelation process to form the cellular scaffold must be done in such a manner that the cells are not harmed. One advantage of this approach is that a high cell density within the scaffold can be achieved accelerating the development of the desired tissue structure. Because the material extruded is usually water based with the consistency of a gel or a paste, this approach seems to be better for applications where the resulting softer scaffold structure can be used.

LAB uses the energy from a pulse laser to precisely deposit the cells from a solution onto the surface of the substrate material. This approach has high precision and resolution, but the laser heating to evaporate the solution from around the cells can damage the cells. In addition, it is not an ideal approach for building large 3D scaffolds; hence, it is better suited as an adjunct to other 3D printing methods.

*Inkjet bioprinting* utilizes the many advances in inkjet printing technology to precisely build up, layer by layer, both cells and other biomaterials to form 3D scaffolds. This technique can deposit with great precision in a predetermined pattern tiny droplets containing the cellular and scaffold materials. The complex 3D structure is then built up layer by layer as material and cells are deposited by the inkjets. The advantages of this approach include its inherent speed and the ability to have multiple inkjet nozzles each dedicated to depositing a particular bioink, i.e., a cell type or a particular biomaterial. Hence, there can be a separate nozzle for each cell type, one or more nozzles for each ECM and scaffold material, and perhaps other nozzles for growth factors. All of these materials can be laid down in whatever pattern is desired for the bioprinted scaffold.

## 10.6 Biocompatibility and the initial response to an implant

In the best of situations, the implanted scaffold structure becomes vascularized by the host during the period of time the transplanted cells are also increasing in number. However, the metabolic demands of the transplanted cells, in some cases, cannot be met by the vasculature that is also developing at the same time within the implant. In these cases, it may be better to first implant the support structure, allowing it to become vascularized, and then to transplant, or seed the cells, at a later point in time (Takeda et al., 1995). This gives the transplanted cells the opportunity to start in a well-vascularized region, thus eliminating any transport limitations due to the metabolic requirements of the transplanted cells.

Prevascularization of the implant can also be enhanced by first seeding the implant with the host's endothelial cells (Holder et al., 1997). The endothelial cell-loaded scaffolds are believed to enhance vascularization by any or all of the following mechanisms. The endothelial cells can form new capillaries, they may provide chemical signals (ECM and growth factors) for growth of blood vessels, and they may merge with the host's own vascular ingrowth. Immobilization of growth factors on the support material, or within controlled release microspheres, can also be used to facilitate vascularization and improve survival of the transplanted cells (Thompson et al., 1988, 1989; Mooney et al., 1996; Madry et al., 2014).

The success of a particular scaffold used in a tissue engineering application will also depend on its biocompatibility, which depends in part on the host's complex immune response (Wiles et al., 2016). The immune system as it pertains to TERM and bioartificial organs will be discussed in more detail in [Chapter 11](#).

The immune response comes from the *innate immune system* and the *adaptive immune system*. The innate immune response to a tissue engineered implant is driven primarily by phagocytic cells such as neutrophils and macrophages that recognize the biomaterials as foreign objects. The adaptive immune response has two components, and these are known as the cell-mediated response and the humoral response. The hallmark of the adaptive immune system is specificity and memory. The cell-mediated response primarily involves activated helper and cytotoxic T-lymphocytes. The helper T-cells secrete cytokines that stimulate macrophages and B-lymphocytes. The humoral response involves these activated B-lymphocytes that secrete antibodies that bind to specific antigens on foreign objects marking them for consumption by phagocytes.

Biocompatibility is the ability of the biomaterial to not provoke the immune system and to be able to withstand whatever the response is from the host's immune system. Because of a material's biocompatibility, it can perform its intended function with little or no harm being done to the surrounding tissues or in a larger sense to the host. Hence, a biomaterial should not release anything that is toxic; not promote a response by the immune system (nonimmunogenic); if in contact with blood, not cause clots to form (nonthrombogenic); and not cause cancer (noncarcinogenic).

How the body responds to a particular biomaterial will also depend on how the biomaterial was processed. For example, the biomaterial's composition and the presence of contaminants and impurities, degree of crystallinity, porosity, surface properties, degradation kinetics, sterility, and wearability all play a role in determining the biocompatibility of a given biomaterial. Biocompatibility, however, is not just intrinsic to the biomaterial being used but also depends to a significant degree on the patient. Hence, it is expected that biocompatibility will vary to some degree among patients as a

result of their general health, age, sex, lifestyle, and sensitivity of their tissues and immune system to the particular biomaterial being used.

### 10.6.1 The body's response to an implant

The first response after implant of a tissue engineering scaffold will be the adsorption of a variety of proteins and macromolecules on the surfaces of the scaffold material. These molecules will initiate a host response that will include both localized inflammatory and immune responses, as well as processes that promote the repair and regeneration of any damaged tissues. In addition, there will also be infiltration of the scaffold by a variety of cell types. All of these processes will determine whether or not the scaffold is successfully incorporated into the host. This process is very similar to what occurs during wound healing and involves three somewhat overlapping phases referred to as *inflammation, proliferation, and maturation* (Arnold and West, 1991; Hammar, 1993).

The *inflammation period* lasts for several days and involves the arrival of *platelets* and *neutrophils*. Activation of the clotting process and release of growth factors (PDGF, EGF, TGF) (Alberts et al., 1982) lead to the formation of a collagen-free fibrin network that serves as a scaffold for the inflammatory cells. The neutrophils release factors that attract *monocytes* and also ingest foreign material by phagocytosis. The monocytes also enter the site and are transformed into *macrophages* and, when fused together, become *foreign body giant cells*. The giant cells continue to clean up the site removing dead tissue and bacteria and walling off large debris.

During the *proliferative phase*, the macrophages release a variety of factors (PDGF, TGF, EGF, and FGF) that activate the migration and proliferation of fibroblasts and endothelial cells. The fibroblasts release a variety of ECM materials and begin to form a collagen network. The generally low oxygen levels within the site will also stimulate the movement and growth of capillary sprouts from the surrounding vasculature. These capillary sprouts are formed from endothelial cells and invade the site of the implant forming a vascular bed. Over a period of weeks, the entire site becomes vascularized and this marks the end of the proliferative phase.

The *maturation phase* involves final remodeling of the site resulting in contraction of the wound and organization of the collagen matrix. This is also a critical time for tissue engineering applications since the reduced oxygen demand of the cells involved in wound healing can result in regression of the vascular supply.

## 10.7 Cell transplantation into scaffolds

Thompson et al. (1988, 1989) in a classic set of experiments were one of the first to show that porous polymeric scaffolds are capable of developing within their confines a neovascularized tissue region that could support the differentiated function of the transplanted cells. They induced the formation of *organoid* neovascular structures in rats using PTFE fibers coated with collagen and the angiogenesis initiator acidic fibroblast growth factor (aFGF). The fibers were about 20 µm in diameter, and a bundle or cotton ball-like mass of these fibers was implanted within the abdominal cavity adjacent to the liver.

To demonstrate the efficacy of a cellular transplant using the vascularized PTFE support structure, they used as a host for the implant the Gunn rat. *Homozygous* Gunn rats lack the liver enzyme needed

for the conjugation of bilirubin. Recall that bilirubin is a product obtained from hemoglobin at the end of a red blood cell's life span. The conjugated form of bilirubin is readily passed from the liver via the bile and then removed from the body through the feces. Since the Gunn rat cannot conjugate bilirubin, its plasma bilirubin levels are increased significantly from the normal level of  $<1 \text{ mg dL}^{-1}$ .

The Wistar rat is genetically identical to the Gunn rat except that it has the ability to conjugate bilirubin. In their initial set of experiments, Thompson et al. obtained hepatocytes from the livers of the syngeneic Wistar rats. These hepatocytes were then seeded onto collagen-coated PTFE fibers that did not contain the angiogenesis promoter aFGF. This structure was then implanted adjacent to the liver of the Gunn rat. Because the Gunn and Wistar rats are genetically the same, there is no need for immunosuppressive agents or immunoisolation of the transplanted cells.

For the first 10 days after implantation, the plasma bilirubin levels remained unchanged as shown in [Figure 10.6a](#). By the 20th day, the plasma bilirubin levels had decreased by about 50%. Shortly

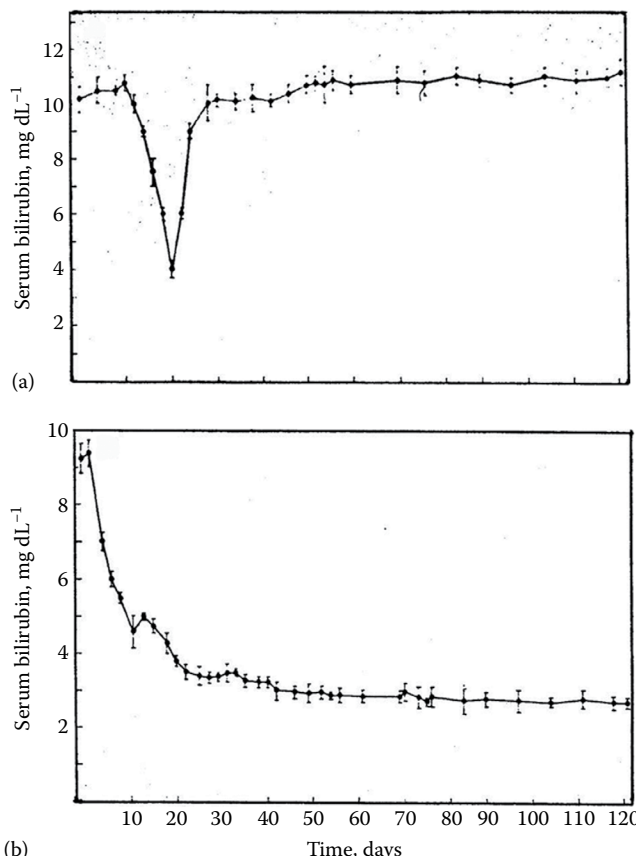


Figure 10.6 Plasma bilirubin levels following transplantation of hepatocytes into Gunn rats.  
 (a) Collagen-coated PTFE support structure with hepatocytes added at time of implantation. (b) Collagen-coated PTFE support structure with aFGF. Hepatocytes added 28 days after implantation.  
 (From Thompson, J.A. et al., *Proc. Natl. Acad. Sci. USA*, 86, 7928, 1989. With permission.)

thereafter, the plasma bilirubin levels returned to their original high levels and remained there for the remaining days of the experiment.

The lack of long-term function of the hepatocytes in these preliminary studies can be attributed to several effects. First, the angiogenesis factor, aFGF, was not used in these first experiments. This resulted in less vascularization of the support structure. Furthermore, the cells were seeded into the support structure at the time of implant. The lack of a good vascular supply at the time of cell seeding is clearly not optimal for cell growth and the transport of nutrients and bilirubin. This accounts for the delayed response with regard to any effect on the plasma bilirubin levels. For the first 10 days, the implant was still in the process of tissue ingrowth and the development of a blood supply that is needed for efficient mass transport. It also allowed for the accumulation of bile acids that led to the death of the cells after about 20 days. Clearly, these results show that seeding the cells at the time the support structure is implanted is not the best approach.

In their second set of experiments, the collagen-coated PTFE fibers containing adsorbed aFGF were first implanted. After 28 days, a suspension of Wistar rat hepatocytes was seeded into the network of the now vascularized fibers. As shown in [Figure 10.6b](#), we see that the plasma bilirubin levels began to decrease within 1 day. After about 10 days, the plasma bilirubin levels had decreased by about 50%, and at the end of the 120-day experiment, this reduction was >60%.

These results strongly suggest that polymeric scaffold structures, through their ability to form their own vascular supply, can be used to sustain the long-term function of transplanted cells. Additionally, it appears from these results to be better to first vascularize the support structure for several weeks before seeding the implant with the transplanted cells. Furthermore, these results demonstrate that transplanted cells carrying a normal gene are able to restore the function lost by the host's own genetically compromised cells.

## 10.8 Bioreactor design for tissue engineering

Critical to the success of tissue engineering for many applications is the in vitro culturing of cells or tissue within the 3D scaffold. In vitro culturing will allow the cells to establish the desired tissue within the scaffold prior to implantation into the patient. This in vitro culture is facilitated through the use of specially designed bioreactors that provide precise control over the environmental conditions that are conducive to the establishment of a viable tissue engineered construct that is ready at the appropriate time for transplantation into the patient (Martin and Vermette, 2005; Mazzei et al., 2010; Schmelzer et al., 2014). The use of these custom-designed bioreactors improves the level of control and facilitates the reproducibility and scalability of the processes used to manufacture a tissue engineered construct. Hence, a bioreactor will provide much better control over the culture conditions than what is achievable in standard 2D tissue culturing techniques. A bioreactor therefore provides an opportunity for the seeded cells to differentiate and populate the construct and create an ECM.

A bioreactor can be designed and customized for the unique 3D shape of a tissue engineered construct and will also provide control of process variables such as temperature, pressure, pH, dissolved oxygen levels, nutrient supply, and waste product removal. In addition, a bioreactor can be designed to provide for mechanical stimulation or conditioning of the construct, which in many cases is crucial for the proper differentiation of the cells (Carver and Heath, 1999; Finlay et al., 2016).

The use of bioreactors also improves control over the manufacturing process, reducing production costs while improving overall product quality. This ensures that the tissue engineered construct meets product specifications and that these products comply with good manufacturing practices and meet the criteria set by regulators such as the FDA.

The design of a bioreactor for a specific tissue engineering application involves the consideration of several key factors. First, we need to address how the cells are seeded or loaded into the polymeric scaffold. Cell seeding can be as simple as pipetting a solution containing the cells onto the surface of the construct allowing capillary action to draw this solution of cells into the scaffold structure. A more efficient method of seeding the cells is to pump or perfuse a solution of cells through the pores of the construct. Perfusion seeding of the cells will give a more uniform initial distribution of cells in the construct.

Once the cells have been distributed into the scaffold, the bioreactor design must be capable of keeping these cells alive. Without the proper distribution\* of key nutrients and oxygen throughout the scaffold, there will be regions near the interior where the cells cannot survive resulting in a nonuniform cell density throughout the scaffold. The deposition of ECM materials like GAGs has also been shown to be dependent on the local oxygen concentration (Obradovic et al., 2000). Oxygen transport therefore is often the limiting nutrient not only for keeping the cells alive but also to ensure that the cells proliferate and establish an ECM. In addition, waste products cannot be allowed to accumulate within the construct since these products can harm the cells.

**Figure 10.7** illustrates the four basic approaches that can be used for the design of a bioreactor. Static culture techniques simply rely on diffusion to distribute key nutrients and oxygen to the cells, and this approach is similar in concept to a multiwell plate. Static culture has significant internal and external diffusion limitations and, in general, cannot be used as a large-scale tissue engineering bioreactor. Another approach is to eliminate external diffusion limitations by inducing fluid motion over the surface of the construct. This can be accomplished by agitation, which causes a flow of media across the surfaces of the construct. A rotating bioreactor can also achieve a flow of

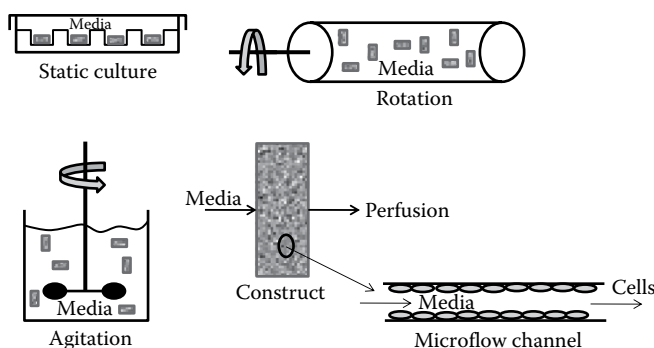


Figure 10.7 Bioreactor configurations.

---

\* The transport of oxygen and key nutrients in a bioreactor can be described using the principles outlined in [Chapters 5 through 7](#). Reactor design principles are discussed in [Section 9.6.9](#).

the media across the surfaces of the construct and eliminates any damage to the constructs by the agitator. Although agitation or rotation can eliminate external diffusion limitations, there can still be significant internal diffusional barriers\* that can affect the viability and the properties of the tissue in the interior regions of the construct.

Hence, bioreactors for tissue engineering applications may need to provide some means of perfusing the innermost regions of the construct with the nutrient media. Perfusion of the construct with the culture medium results in the convective transport of these nutrients into the innermost regions of the construct, which is much more efficient than what can be obtained by diffusion alone. Perfusioning the construct with the culture medium will therefore improve the transport of oxygen and key nutrients (Tilles et al., 2001; Allen and Bhatia, 2003; Kitagawa et al., 2005; Zhao and Ma, 2005; Mehta and Linderman, 2006; Lee et al., 2010; Gardel et al., 2014; Schmelzer et al., 2014).

As shown in [Figure 10.7](#), perfusion bioreactors provide for a convective flow of the nutrient media over the surface of a very thin layer of cells.<sup>†</sup> This involves designing the porous structure of a scaffold with nutrient channels to ensure that the culture media is uniformly distributed to all the regions of the construct (Mehta and Linderman, 2006). These microflow channels can be designed into the porous construct using 3D microfabrication techniques (Lee et al., 2010; Park et al., 2010). This will ensure that key nutrients and oxygen can reach those cells located in the most interior regions of the construct. In addition, the perfusion medium can also be loaded with oxygen carriers such as perfluorocarbons (PFCs) (Radisic et al., 2004, 2005). As discussed in [Section 7.12](#), PFC solutions overcome the low solubility of oxygen in water with the result that significantly more oxygen can be transported.

In many applications, the cells that are loaded into the construct must be exposed to the proper biomechanical environment in order to differentiate properly (Gemmati and Guldberg, 2009; Mathes et al., 2010; Shaikh et al., 2010; Finlay et al., 2016). This is known as mechanical or physical conditioning of the cells as they grow and differentiate in the in vitro environment of the bioreactor. For example, it is well known that cells can respond to a variety of forces that are caused by fluid flow, pressure, and dynamic loading. Hence, cells can respond to forces related to shear, strain, pressure, and mechanical loads. In many cases, it is therefore necessary to incorporate these physiological forces into the operation of the bioreactor so that the cells differentiate into the desired tissue. Examples where mechanical conditioning has been shown to be important include the tissue engineering of blood vessels, heart valves, tendons and ligaments, cartilage, bone, oral tissues, and intervertebral disks.

### Example 10.1

A construct for a tissue engineering application consists of a polymeric scaffold that incorporates cylindrical flow channels so that the culture media can be perfused through the construct during in vitro culture. Each flow channel in the scaffold is 300  $\mu\text{m}$  in diameter, and the length of each flow channel is 25 mm. Surrounding and concentric to each flow channel is a cylindrical volume of tissue whose thickness is 50  $\mu\text{m}$ . The tissue in the construct consumes oxygen at the rate of  $10 \mu\text{M s}^{-1}$  based on the total scaffold volume in the region that contains the tissue.

\* See [Sections 9.6.4](#) through [9.6.8](#) for a discussion on internal diffusion and reaction phenomena in porous materials. In this case, the enzyme kinetics will be replaced by the cellular kinetics for a particular substrate of interest.

<sup>†</sup> See [Sections 7.9.1](#) and [7.9.2](#) for a discussion of oxygen transport in perfusion bioreactors.

The  $pO_2$  of the culture media entering the flow channels is 150 mmHg. Estimate the flow rate of the media per flow channel ( $cm^3 h^{-1}$ ) so that the  $pO_2$  in the tissue region is greater than 20 mmHg. Also calculate the  $pO_2$  of the media leaving the flow channel. Assume that the Henry's constant for the nutrient media is  $0.74 \text{ mmHg } \mu\text{M}^{-1}$  and the oxygen diffusivity in the tissue surrounding the flow channel is  $2.41 \times 10^{-5} \text{ cm}^2 \text{ s}^{-1}$  (Bentley et al., 1993).

### Solution

The cylindrical flow channels within the construct are similar in concept to the Krogh tissue cylinder discussed in [Section 6.4](#). In this case, oxygen is just a dissolved solute in the culture media, so we do not have to take into account the binding of oxygen with hemoglobin as was done when we have blood. We can therefore use [Equation 6.82](#) to describe the oxygen concentration in the tissue region that surrounds each flow channel in the construct.

$$\bar{C}_A(r,z) = C_A^0 - \frac{R_A^{\max}}{V r_c^2} \left[ r_T^2 - (r_c + \bar{L})^2 \right] z - \frac{R_A^{\max}}{2r_c K_O} \left[ r_T^2 - (r_c + \bar{L})^2 \right]$$

$$+ \frac{R_A^{\max}}{4D_T} \left[ r^2 - (r_c + \bar{L})^2 \right] - \frac{R_A^{\max} r_T^2}{2D_T} \ln \left( \frac{r}{r_c + \bar{L}} \right)$$

The critical oxygen level in the tissue is specified as 20 mmHg, and this will occur at the position defined by  $L = 25 \text{ mm}$  and  $r_T = \left( \frac{300 \mu\text{m}}{2} + 50 \mu\text{m} \right) = 200 \mu\text{m}$ , which is also known as the *lethal corner*. Also the flow channel is in intimate contact with the surrounding tissue, so  $\bar{L}$  and  $P_m$  are both equal to zero. The overall mass transfer coefficient ( $K_O$ ) is then equal to the mass transfer coefficient ( $k_m$ ) for the media in the flow channel. Using Henry's law ( $pO_2 = H_{\text{oxygen}} C$ ) to replace the oxygen concentration with the  $pO_2$ , the previous equation becomes

$$pO_2(r_T, L) = pO_2^{\text{in}} - \frac{R_A^{\max} H_{\text{oxygen}}}{V r_c^2} (r_T^2 - r_c^2) L$$

$$- \frac{R_A^{\max} H_{\text{oxygen}}}{2r_c k_m} (r_T^2 - r_c^2) + \frac{R_A^{\max} H_{\text{oxygen}}}{4D_T} (r_T^2 - r_c^2) - \frac{R_A^{\max} H_{\text{oxygen}} r_T^2}{2D_T} \ln \left( \frac{r_T}{r_c} \right)$$

This equation can then be solved for the average velocity of the culture media in a flow channel recognizing that  $k_m$  depends on the unknown value of  $V$ . The value of  $V$  is adjusted until the  $pO_2$  in the lethal corner equals 20 mmHg. The analysis of this problem shows that the flow is laminar and that the concentration profile in the media flowing through the flow channel is not fully developed, so [Equation 5.169](#) is used to calculate the mass transfer coefficient. When [Equation 5.169](#) is used in the previous equation, the required average velocity of the media flowing in the flow channel is found to be  $0.129 \text{ cm s}^{-1}$ , which gives a volumetric flow rate of media per flow channel of  $0.327 \text{ cm}^3 \text{ h}^{-1}$ . From [Equation 6.80](#), the exiting  $pO_2$  of the media can be found as shown below:

$$pO_2^{\text{out}} = 150 \text{ mmHg} - \frac{0.74 \text{ mmHg } \mu\text{M}^{-1} \times 10 \mu\text{M s}^{-1} \times 2.5 \text{ cm}}{0.129 \text{ cm s}^{-1} \times 0.015^2 \text{ cm}^2} (0.02^2 - 0.015^2) \text{ cm}^2$$

$$pO_2^{\text{out}} = 38.5 \text{ mmHg}$$

## Problems

- 10.1** Consider a bioreactor for growing a cornea. Within this bioreactor, glucose diffuses from a well-stirred bulk liquid solution across a thin hydrogel layer and then the glucose diffuses and reacts within a multilayer of epithelium, which lies on top of the hydrogel layer (Perez et al., 1995). The epithelium consists of  $N$  layers of cells, each cell  $h_c$  in thickness. The cells consume glucose at a first order volumetric rate given by  $k_1 C$ , where  $C$  is the local concentration of glucose and  $k_1$  is the first order rate constant. The surface of the cells exposed to the gas phase above is a no flux boundary for glucose, and  $C$  will therefore attain its minimum value at that interface ( $C_{\min}$ ). Calculate the fractional drop  $\left( \frac{C_b}{C_{\min}} \right)$  in the glucose concentration from the bulk liquid medium ( $C_b$ ) to the outermost epithelial surface ( $C_{\min}$ ). Assume there is no mass transfer resistance between the bulk solution and the surface of the hydrogel. Some additional information needed to solve this problem is shown in the table below.

Parameter	Value	Description
$h_c$	15 $\mu\text{m}$	Thickness of single cell layer
$k_1$	$1.5 \times 10^{-3} \text{ s}^{-1}$	Glucose rate constant
$C_b$	3.2 mg mL $^{-1}$	Bulk glucose concentration
$D_G$	$3 \times 10^{-6} \text{ cm}^2 \text{ s}^{-1}$	Diffusivity of glucose in the hydrogel
$K_p$	2	Glucose hydrogel partition coefficient, bulk gel or gel epithelium
$L$	0.05 cm	Hydrogel thickness
$N$	5	Layers of epithelial cells
$D_e$	$6 \times 10^{-6} \text{ cm}^2 \text{ s}^{-1}$	Glucose diffusivity in epithelium

- 10.2** Review the research literature on tissue engineering and write a short paper on an interesting design for a bioreactor. Explain how the proposed bioreactor addresses any transport limitations and provides for mechanical conditioning of the cells in the construct.
- 10.3** Select from [Table 10.1](#) an application for tissue engineering. Prepare a presentation for your class that summarizes recent advancements in the area you selected. Topics covered in your presentation should include a description of the clinical need, the methodology used, results that have been obtained (in vitro, in animals, and the status of any human clinical trials), the potential clinical impact, potential market impact, safety issues, and additional development needs.
- 10.4** Design a tissue engineered system for the delivery to the systemic circulation of human growth hormone (hGH). hGH has a molecular weight of 22,000 g mol $^{-1}$ . Assume that the hGH has an apparent distribution volume in the body of 30 L. Assume that autologous cells were transfected with a recombinant gene for hGH. The production rate of hGH from these cells is about 2500  $\frac{\text{ng}}{10^6 \text{ cells } 24 \text{ h}}$ . The plasma concentration of hGH should be maintained at about 10 ng mL $^{-1}$ . Assume hGH has a half-life in the body of about 2.3 h. Describe your system for delivering hGH and carefully state all assumptions. How many cells will be required for the delivery of the hGH?
- 10.5** Write a paper that addresses some of the ethical issues associated with tissue engineering.

- 10.6** Redo [Example 10.1](#) assuming the scaffold construct is perfused with culture media containing an insoluble PFC material at a volume fraction of 0.60. The PFC material forms an emulsion that has an enhanced solubility for oxygen. The Henry's constant for the PFC material is equal to  $0.04 \text{ mmHg } \mu\text{M}^{-1}$ , where the  $\mu\text{M}$  refers to the volume of the PFC oxygen-carrying material only. The Henry's constant for dissolved oxygen in the aqueous portion of the artificial blood is  $0.85 \text{ mmHg } \mu\text{M}^{-1}$ .
- 10.7** Radisic et al. (2006) measured the oxygen gradients in cultured constructs containing cardiac tissue. The scaffolds were made from collagen sponges that were thin round disks nominally 1.8 mm in radius and 1.8 mm in thickness. In addition to measuring the oxygen gradient within these constructs, they also measured the cell viability, which was found to decrease exponentially with depth ( $z$ ) according to the following equation,  $\delta(z) = ae^{-bz}$ , where  $\delta(z)$  is the live cell density at position  $z$ . Assuming that the oxygen concentration only depends on the scaffold radius and depth, show that the oxygen concentration within the scaffold is given by the following equation:

$$D_{\text{oxygen}} \left( \frac{1}{r} \frac{\partial}{\partial r} \left( r \frac{\partial C}{\partial r} \right) + \frac{\partial^2 C}{\partial z^2} \right) = \frac{V_{\max} \delta(z) C}{K_{\text{oxygen}} + C} = \frac{V_{\max} a e^{-bz} C}{K_{\text{oxygen}} + C}$$

The boundary conditions (BCs) for the above equation are based on known measurements of the oxygen concentration at the top, side, and bottom surfaces of the scaffold and are given by

$$\begin{aligned} \text{BC1: } & C(r,0) = C_{\text{top}} \\ \text{BC2: } & C(r,L) = C_{\text{bottom}} \\ \text{BC3: } & C(R,z) = C_{\text{top}} \\ \text{BC4: } & \left. \frac{\partial C}{\partial r} \right|_{r=0,z} = 0 \end{aligned}$$

Boundary condition 4 expresses the fact that the oxygen concentration is symmetric about the centerline of the scaffold along the  $z$  axis. In the above equation,  $D_{\text{oxygen}}$  is the effective diffusivity of oxygen within the scaffold,  $C$  is the concentration of oxygen, and it was assumed by these researchers that the oxygen consumption can be described by the Michaelis-Menten equation. Hence,  $V_{\max}$  is the maximum oxygen consumption rate per cell.  $K_{\text{oxygen}}$  is the Michaelis constant and is the concentration of oxygen where the oxygen consumption rate is equal to one-half of  $V_{\max}$ . The following table summarizes the values of key parameters that were reported in their study.

Parameter	Value
$R$ and $L$ (construct radius and thickness)	1.8 mm
$V_{\max}$ (maximum $O_2$ consumption rate)	$1.5 \text{ nmol min}^{-1} (10^6 \text{ cells})^{-1}$
$K_{\text{oxygen}}$ (Michaelis constant)	$6.875 \mu\text{M}$
$a$ (pre-exponential factor for cell distribution)	$1.7053 \times 10^8 \text{ cells cm}^{-3}$
$b$ (live cell density exponential decay constant)	$0.0042 \mu\text{M}^{-1}$
$D_{\text{oxygen}}$ ( $O_2$ diffusivity in the tissue)	$2.0 \times 10^{-5} \text{ cm}^2 \text{ s}^{-1}$
$C_{\text{top}}$ ( $O_2$ concentration at the top surface)	$175.6 \mu\text{M}$
$C_{\text{bottom}}$ ( $O_2$ concentration at the bottom surface)	$22.4 \mu\text{M}$

Using the above mathematical model, and the parameters provided in the table, solve the differential equation for the oxygen concentration as a function of  $r$  and  $z$  in the cardiac tissue scaffold. Compare your results for  $C(0, z)$  to the following data that were presented in this paper.

Depth, $\mu\text{m}$	Centerline Oxygen Concentration, $\mu\text{M}$
0	175.6
100	149
200	140
300	130
400	120
500	110
600	105
700	100
800	95
900	85
1000	75
1100	65
1200	60
1300	55
1400	50
1500	45
1600	40
1700	35
1800	22.4

- 10.8** Krewson et al. (1995) presented the steady-state data in the table below for the distribution of NGF in the vicinity of a thin cylindrical controlled drug release device implanted into the brain of a rat. The polymeric disks containing radiolabeled  $\text{I}^{125}\text{-NGF}$  were 2 mm in diameter and 0.8 mm in thickness. NGF has a molecular weight of 28,000 g mol $^{-1}$ . Assume that the NGF is eliminated from the brain tissue by a first order process, i.e., the rate of elimination is proportional to the concentration of NGF, i.e.,  $k_{\text{apparent}} C_{\text{NGF}}$  where  $k_{\text{apparent}}$  is the apparent first order elimination rate constant for NGF and accounts for processes such as metabolism, cellular internalization, or uptake by the brain's systemic circulation. Then develop a steady-state reaction-diffusion model to analyze these data. The boundary conditions, assuming the origin of the Cartesian coordinate system to be the midline of the polymeric disk, are as follows:

$$C_{\text{NGF}} = C_0 \quad \text{at } x = a \quad \text{and} \quad C_{\text{NGF}} = 0 \quad x = \infty$$

where  $a$  is the half-thickness of the polymeric disk. Estimate the value of the Thiele modulus  $\left(a \sqrt{\frac{k_{\text{apparent}}}{D_T}}\right)$  that provides the best estimate of the data.  $D_T$  represents the diffusivity of NGF in the brain tissue, which is estimated to be  $4 \times 10^{-7} \text{ cm}^2 \text{ s}^{-1}$ . Using this value of  $D_T$  for NGF, what is the value of  $k_{\text{apparent}}$ ? Using, [Equation 8.30](#) calculate the half-life of NGF in the brain tissue.

How does this value of the NGF half-life compare to the reported half-life of NGF in brain tissue of about 1 h?

Distance from Polymer/Tissue Interface, mm	NGF Concentration, $\mu\text{g mL}^{-1}$
0	37.0
0.1	31.5
0.2	20.0
0.3	15.0
0.4	10.5
0.5	8.5
0.6	6.5
0.8	3.5
1.0	2.2

# Chapter 11 Bioartificial organs

## 11.1 Background

Tissue engineering and regenerative medicine is a very promising approach for the treatment of a variety of medical conditions. The treatment of a disease or medical problem using this approach requires the availability of the appropriate cells and the creation of an artificial support structure or scaffold to contain them. The cells may be obtained from a variety of sources, e.g., from an expanded population of the host's own cells (perhaps genetically modified), from other compatible human donors, from animal sources, or even from genetically engineered cell lines. The cells to be transplanted are then seeded into a polymeric scaffold or construct. The scaffold can then be placed within a bioreactor and then implanted in the patient at the appropriate time. However, with the exception of *autologous cells*, one of the major obstacles that must be overcome is the rejection of the transplanted cells by the host's immune system. The transplanted cells will be destroyed quickly by the host's immune system unless they are immunologically similar to the host's own cells (Benjamin and Leskowitz, 1991).

Immunosuppressive drugs can be used to suppress the host's immune system and prolong the function of transplanted cells that are a relatively close match to the host. However, immunosuppressive drugs have potent side effects, and in the case, e.g., of transplanting the islets of Langerhans, or their  $\beta$  cells, to treat insulin-dependent diabetes, these drugs may result in a situation where the cure is worse than the disease. Genetically engineered cell lines, in addition to their possibly being rejected by the host's immune system, also pose additional risks that need to be considered. For example, the direct implantation of an immortal (usually of tumor origin) cell line can lead to the unchecked growth of the implanted cells. There is also the risk of these cells moving and proliferating at a site other than the desired site, and they can change to a potentially hazardous form with the loss of their original therapeutic function. In some applications, the full potential of tissue engineering and regenerative medicine will be limited unless techniques can be developed to either restrict the host's immune response or somehow modify the transplanted cells to make them more acceptable to the host's immune system, i.e., *immunomodification* (Lanza and Chick, 1994b).

## 11.2 Some immunology

The immune response to foreign materials (*antigens*) such as transplanted cells is primarily an adaptive response consisting of a *cell-mediated component* and a *humoral component* (Benjamin and Leskowitz, 1991; Gray, 2001). The major cellular components are the *B-lymphocytes* and the *T-lymphocytes*. The B-lymphocytes, or B cells, form in the *bone marrow* and, when properly activated by antigens, form proteins called *antibodies* that comprise the active agents of the humoral component of the immune system. The T-lymphocytes originate in the *thymus* and come in two basic types, the *CD4<sup>+</sup> (helper) T cells* and the *CD8<sup>+</sup> (killer or cytotoxic) T cells*.

The immune system is activated by its intimate contact with foreign molecules called *antigens* (*antibody generating*). Antigens must possess *foreignness*, meaning the antigen is unlike anything the immune system has seen before. Immature B- and T-lymphocytes that react against *self-antigens* (e.g., the body's own proteins) are eliminated during their maturation phase in the bone marrow or the thymus. This is known as the *clonal deletion theory*. Thus, the mature B and T cells are *self-tolerant* and do not normally react against the body's own tissues.

Antigens generally have molecular weights  $>6000 \text{ g mol}^{-1}$  and possess some degree of molecular complexity. In fact, there can be many sites along the surface of such large molecules that are *immunogenic*.<sup>\*</sup> These sites are referred to as *epitopes*. Fortunately, many synthetic polymers used as biomaterials, although of high molecular weight, do not possess a sufficient amount of molecular complexity to provoke an immune response. Lower molecular weight materials, although not immunogenic by themselves, can associate, e.g., with larger carrier molecules, like a protein, to give an immune response directed at the lower molecular weight compound. In this case, the lower molecular weight compound is referred to as a *hapten*.

## 11.2.1 B-Lymphocytes

Each B cell has a unique antibody receptor on its surface that only recognizes a specific antigen. The B cell inventory within an individual is capable of producing as many as 100 million distinct antibodies. This allows the immune system to respond to almost any known or unknown antigen. If a specific B cell comes into contact with its corresponding antigen, it becomes activated through a process that we shall later see also involves the CD4 $^{+}$  or helper T cells. The activated B cell then begins to reproduce, rapidly increasing the number of B cells that are specific for a given antigen. This expanded collection of B-lymphocytes with a given specificity is referred to as a *clone of lymphocytes*. This selection by the antigen of a specific reactive clone of lymphocytes from a large pool of existing lymphocytes, each with their own unique antigen specificity, is called the *clonal selection theory*. These B cells then differentiate to form *plasma cells* that begin to secrete antibodies with the same antigen specificity.

## 11.2.2 Antibodies

*Antibodies* are proteins and are also called *gamma globulins* or *immunoglobulins*. They comprise about 20% of the total amount of protein found in plasma. There are five classes of antibodies that are called IgA, IgD, IgE, IgG, and IgM, where Ig stands for immunoglobulin and the letter designates the antibody class. The basic structure of an antibody molecule consists of a pair of light polypeptide chains and a pair of heavy polypeptide chains held together by disulfide bonds, as shown in Figure 11.1.

Conceptually, the antibody molecule is *Y shaped*, with each light chain paired in the upper branches of the Y with the heavy chains that form the Y structure. The molecule consists of three fragments. Two of these fragments are identical and reside at the top of the Y, and each of these binds with antigen. These fragments are referred to as Fab, for *fragment antigen binding*. The base of the Y is

---

\* An immunogen is a molecule that can induce a specific response of the immune system. An antigen refers to the ability of a given molecule to react with the products of an immune response, e.g., the binding of an antigen to an antibody. In this discussion, we will assume that antigen and immunogen are synonymous.

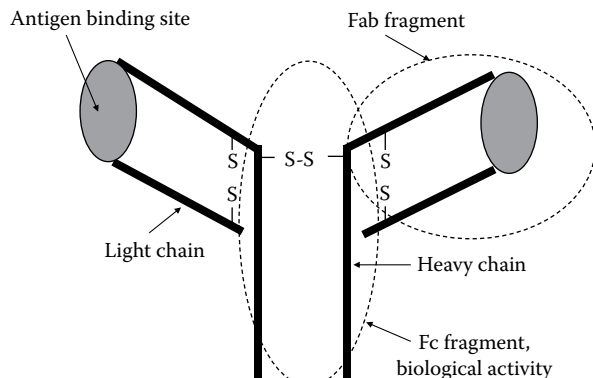


Figure 11.1 Structure of an antibody.

called the *Fc fragment*, for *fragment crystallizable*. The Fc fragment does not bind with antigen but is responsible for the biological activity of the antibody after it binds with antigen. The Fc fragment is referred to as a *constant region* in terms of its amino acid sequence since it is the same for all antibodies within a given class. Since the Fab fragments bind to antigen, their structure is highly *variable* in order to provide the multitudinous shapes or conformations required for antigen specificity and recognition. The specific antigen binding characteristics of the Fab fragments is determined by their unique sequence of amino acids. Although an activated B cell (or plasma cell) makes antibodies with only a single antigen specificity, it can switch to make a different class of antibody, while still retaining the same antigen specificity.

IgG is the major immunoglobulin in the body and is found in all the fluid spaces in the body. It consists of a single Y-shaped molecule with a molecular weight of about  $150,000 \text{ g mol}^{-1}$ . IgG has several important biological properties that are found in some of the other antibody classes as well. Because of its ability to bind two antigens per IgG molecule, IgG can cause the clumping or *agglutination* of particulate antigens such as those of invading microorganisms. These large antibody-antigen complexes are then readily phagocytized by phagocytic cells such as *neutrophils* and *macrophages*. In the case of smaller soluble antigens, this cross-linking of antigen and IgG leads to much larger complexes that become insoluble and *precipitate* out of solution and are then phagocytized.

IgG is also capable of binding to a variety of epitopes found on the surfaces of invading cells. The cell then becomes covered with IgG molecules that have their Fc fragments sticking out. Many phagocytic cells have surface receptors for the IgG Fc fragments allowing the phagocyte to bind to, engulf, and then destroy the invading organism. IgG is therefore an *opsonizing antibody* (*opsonin* is a Greek word that means to prepare for eating) since it facilitates the subsequent “eating” of the invading microorganism or cell by phagocytic cells.

The Fc receptor on an IgG molecule bound by the Fab fragments to a cellular antigen also binds to specific receptors on so-called *natural killer lymphocytes* (*NK cells*). The NK cells will then be attracted to and destroy the invading cell by the release of toxic substances called *perforins* (Ojcius et al., 1998). Perforins form channels in the cell membrane of the target cell, making them leak and resulting in the death of the cell. This process is called *antibody-dependent cell-mediated cytotoxicity*, or ADCC.

IgG is also capable of neutralizing many toxins by binding to their active site. Viruses are also neutralized in a similar manner. In this case, the IgG molecule binds and blocks sites on the virus's surface coat that is used by the virus for attachment to the cells it normally invades. IgG, when bound to antigen, is also capable of activating the *complement system*. The complement system consists of a group of protein enzyme precursors that when activated undergo an amplifying cascade of reactions that generate *cell membrane attack complexes* (MACs) that literally punch holes through the cell membrane. This results in the lysis and death of the targeted cell.

IgA is found primarily in the fluid secretions of the body, e.g., in saliva, tears, mucous, and gastrointestinal fluids. It is found in a dimeric form, i.e., it consists of two Y-shaped antibodies linked at the base of the Y. The molecular weight of this antibody is about  $400,000 \text{ g mol}^{-1}$ . Its primary role is as a defense against local infections where it stops the invading microorganism from penetrating the body's epithelial surfaces that line the respiratory and gastrointestinal tracts. It does not activate the complement system.

IgM forms a planar star-like pentamer and consists of five antibody molecules joined together at the base of the Fc fragments. Its molecular weight is about  $900,000 \text{ g mol}^{-1}$ , and it is found mainly in the intravascular spaces. It has only five antigen binding sites because the restricted pentameric structure does not allow the Fab fragments to be open fully. Therefore, large antigens bound to one Fab will block the adjacent Fab. IgM is a very efficient agglutinating antibody since its large structure provides for binding between epitopes that are widely spaced on the antigen. IgM is also an excellent activator of the complement system. IgM is also found on the surface of mature B-lymphocytes where it serves as the specific antigen receptor.

IgD is also present primarily on the cell surface of the B-lymphocytes and is believed to be involved in the maturation of these cells. It exists as a single antibody molecule and therefore has a molecular weight of about  $150,000 \text{ g mol}^{-1}$ . Not much is really known about this antibody, although, it does seem to play a role in B cell activation and also activates basophils and mast cells stimulating them to make antimicrobial agents.

Finally, IgE also exists as a single antibody molecule and has a molecular weight of about  $200,000 \text{ g mol}^{-1}$ . The Fc fragment of the IgE molecule binds with high affinity to specific receptors found on *mast cells* and *basophils*. Mast cells are found outside of the capillaries within the connective tissue region (see [Figure 10.3](#)). Mast cells are involved in the process of inflammation and are responsible for the secretion of *heparin* into the blood as well as *histamine*, *bradykinin*, and *serotonin*. Basophils are a type of white blood cell or *granulocyte* that mediates the inflammation process through release of these same substances. When antigen binds to two adjacent cell surface-bound IgE molecules, the cell (mast or basophil) becomes activated and releases a host of potent biologically active compounds such as histamine. These agents are responsible for the dilation and increased permeability of the blood vessels. In normal situations, these changes facilitate the movement of the immune system components, such as white blood cells, antibodies, and complement, into localized sites of inflammation and infection. However, in people with allergies, a particular antigen, in this case called an *allergen*, stimulates the IgE on the surface of mast cells and basophils, leading to the unwanted effects of an allergic reaction.

### 11.2.3 T-Lymphocytes

The *T-lymphocytes* are the other major cell type that forms the basis of the cell-mediated immune response. The T cells are characterized by the presence of an antigen-specific *T cell receptor*, or *TcR*.

The TcR consists of an antigen-recognizing molecule called Ti in close association with another polypeptide complex called CD3. The T cells, unlike the B cells, are not, however, activated by free antigen. T cell activation requires that the antigen be *presented* by other cells such as macrophages or other B cells. These cells that present antigen to the T cells are collectively called *accessory cells* or *antigen-presenting cells* (APCs).

The APCs ingest and breakdown the polypeptide antigen into much smaller fragments. These fragments then become associated with special molecules called the *major histocompatibility complex* (MHC). There are two major types of MHC molecules, called *MHC class I* and *MHC class II*. Recall that these molecules belong to the class of cell adhesion molecules (CAMs). The MHC class I molecule is expressed by almost every nucleated cell found in the body. The MHC class II molecule is only found in specialized APCs such as B cells and macrophages. The MHC molecule forms an antigen binding area in the shape of a cleft or pocket. This pocket can accept polypeptide antigens consisting of up to 20 amino acids. The complex of small antigen and MHC is then transported to the surface of the cell where the antigen is presented for recognition by the TcR. The T cell therefore only recognizes antigen in combination with the MHC molecule.

T cell antigen recognition is shown in [Figure 11.2](#). On the left side of this figure, we see a foreign material such as a dead virus, a cancer cell, a microorganism, or a large polypeptide being ingested and broken down by an APC. The antigen, in combination with an MHC class II molecule, is then transported to the cell surface for antigen presentation. On the right side of this figure, we see a live virus infecting the cell. As the virus takes over the operation of the cell to increase the number of viruses, many of the viral peptides that are produced are transported to the cell surface by MHC class I molecules for antigen presentation. The presence of antigen and MHC class I will then be recognized by the T cell.

However, in either case, the TcR by itself has a low affinity for antigen bound to MHC. To facilitate the recognition and binding of the TcR with the antigen/MHC complex, there exist two important *accessory molecules* called *CD4* and *CD8* that also serve to distinguish between the two principal types of T cells.

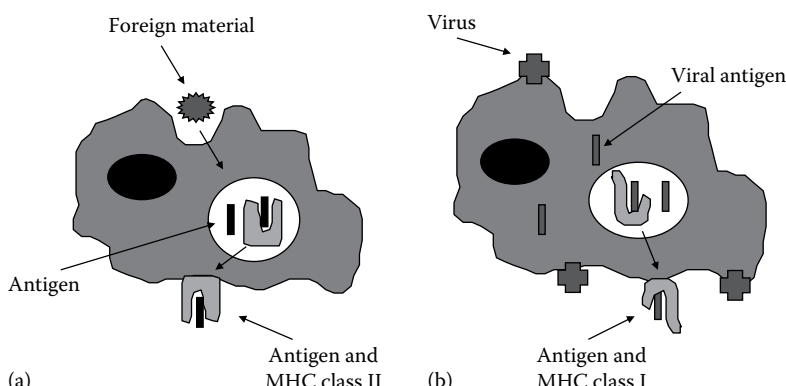


[Figure 11.2](#) Presentation of antigen by MHC class I and II molecules. (a) Antigen-presenting cell and (b) virally infected cell.

T cells that have the *CD4 molecule* are known as *CD4<sup>+</sup>* or *helper T cells*, whereas those that have the *CD8 molecule* are known as *CD8<sup>+</sup>* or *cytotoxic T cells*. *CD4<sup>+</sup>* T cells only recognize antigen that is bound to the MHC class II molecule on the surface of an APC (see [Figure 11.2a](#)). The *CD8<sup>+</sup>* T cell can only recognize antigen that is bound to the MHC class I molecule on the surface of all other nucleated cells found in the body as shown in [Figure 11.2b](#). This is called *MHC restriction*, i.e., the response of *CD4<sup>+</sup>* T cells is restricted to only that antigen bound to MHC class II molecules, whereas the response of *CD8<sup>+</sup>* T cells is restricted to only that antigen bound to MHC class I molecules.

#### [11.2.4 Interaction between APCs, B cells, and T cells](#)

With this background, we can now examine the cooperative relationship that exists between the APCs, B cells, and T cells during the immune response. First, let's consider the interaction between a resting *CD4<sup>+</sup>* T cell, an APC, and a B cell. This is illustrated in [Figure 11.3](#). The first step involves the ingestion by an APC of an antigen that, in this example, contains both a B cell epitope and a T cell epitope. The APC could be a macrophage that engulfs the antigen, or a B cell that internalizes the antibody-antigen complex. The T cell epitope is then expressed on the surface of the APC in combination with an MHC class II molecule. A *CD4<sup>+</sup>* T cell that has a Ti-CD3 receptor that is specific for this particular antigen then binds with the antigen/MHC class II complex. Note that the CD4 molecule stabilizes the binding of the antigen/MHC complex with the TcR.

This binding of the *CD4<sup>+</sup>* T cell and the antigen/MHC class II complex constitutes the first signal for the activation of the *CD4<sup>+</sup>* T cell. This is then followed by the release of a second signal by the APC of a soluble substance called *interleukin-1* (IL-1) that is also essential for T cell activation. IL-1 is a small protein with a molecular weight of 15,000 g mol<sup>-1</sup> that belongs to a class of substances called *lymphokines*. Lymphokines are cellular messengers that have an effect on other lymphocytes and are a subcategory of a broader class of intercellular messengers called *cytokines*. The *CD4<sup>+</sup>* T cell then becomes activated and begins to secrete its own interleukins, specifically IL-2, IL-4, and IL-5.

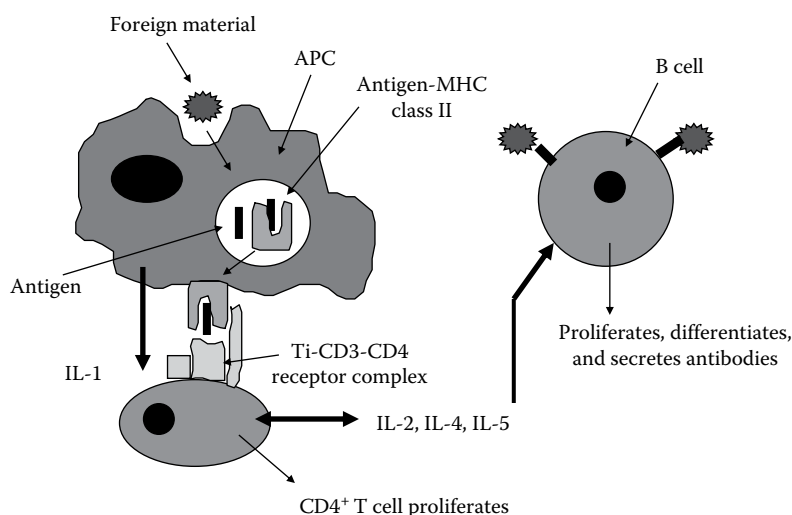


[Figure 11.3 Interaction between APC, CD4<sup>+</sup> T cell, and the B cell.](#)

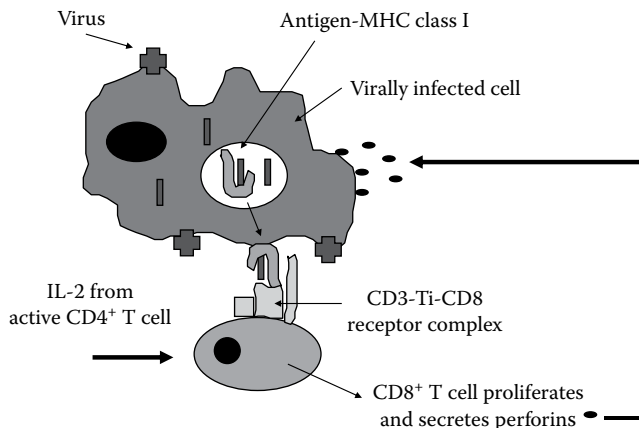


Figure 11.4 Activation of CD8<sup>+</sup> T cells.

IL-2 induces the CD4<sup>+</sup> T cell to proliferate, rapidly forming a clone of CD4<sup>+</sup> T cells that are reactive to the specific antigen presented by the APC. IL-4 then activates the B cells, and IL-5 induces the activated B cells to proliferate in number, forming a clone of B cells.

It is important to note that binding of antigen with the B cell receptor is not sufficient for the B cell to become activated and then differentiate to antibody-secreting plasma cells. The B cell must become activated through the process shown in [Figure 11.3](#), which also involves the CD4<sup>+</sup> T cell. Additionally, the B cell need not bind with the same epitope that activated the T cell. Hence, the activated B cell may release antibodies with a different epitope specificity. Since the CD4<sup>+</sup> T cell is responsible for the activation of the B cell, it is referred to as the *helper* T cell. The activated CD4<sup>+</sup> T cell also secretes other lymphokines, such as *γ-interferon*, that serves to attract and activate macrophages and NK cells and inhibits viral replication.

[Figure 11.4](#) illustrates how the CD8<sup>+</sup> T cell becomes activated. Here, we see that the CD8<sup>+</sup> TcR binds with the antigen/MHC class I complex presented, e.g., by a virally infected cell. Once again, the CD8 molecule stabilizes the interaction between the TcR and the antigen/MHC complex. This binding of TcR and antigen/MHC complex represents the first signal. In order for the CD8<sup>+</sup> T cells to proliferate, i.e., form a clone of CD8<sup>+</sup> T cells and become activated, it also must receive a second signal that is provided by the IL-2 that is released as a result of the activation of the CD4<sup>+</sup> T cell shown in [Figure 11.3](#). The activated CD8<sup>+</sup> T cell will then kill any cell that expresses the appropriate combination of antigen and MHC class I. The activated CD8<sup>+</sup> T cell accomplishes this cellular destruction through the release of special molecules called *perforins* that destroy the cell membranes of the target cell. Because of their role in cell death, the CD8<sup>+</sup> T cells are also known as cytotoxic T cells or killer T cells.

## 11.2.5 The immune system and transplanted cells

The previous discussion illustrates the complexity as well as the coordination that exists between the different components of the immune system. The immune system through an elegant process is capable of recognizing *self* from *non-self*. Our interest here is to prevent or restrict the action of the immune

system toward the transplanted cells. The immune system response to transplanted cells involves a combination of effects resulting from antibodies, complement, macrophages, B cells, and T cells.

Antibodies recognize the foreign antigens presented by the transplanted cells and induce the destruction of the transplanted cells through the activation of the complement system and NK cells by the process of ADCC. The rejection of the transplanted cells also occurs by a T cell response against the MHC molecules that are expressed by the transplanted cells. The transplanted cells contain foreign MHC class I and class II molecules. The foreign MHC class II molecules are present on *passenger leukocytes* and macrophages that are present in the transplanted tissue. The foreign MHC class II molecules are sufficiently similar to the host's own combination of antigen/MHC class II complex to trigger the activation of the CD4<sup>+</sup> T cells. This is also true for the foreign MHC class I molecules, leading to the activation of the host's CD8<sup>+</sup> T cells. The activation of these T cells and the antibody-producing B cells then leads to the destruction of the transplanted cells.

### 11.3 Immunoisolation

A promising method for restricting the host's immune response is to immunoisolate the transplanted cells (Lanza et al., 1995; Zielinski et al., 1997; Gray, 2001; Ludwig et al., 2013; Neufeld et al., 2013). This concept was shown earlier in [Figure 10.2](#). [Figure 11.5](#) presents a more detailed view of *immunoisolation* showing the possible pathways for the rejection of the transplanted cells (Colton, 1995). Immunoisolation can be accomplished through the use of a specially designed polymeric membrane that prevents the passage of the major components of the immune system, i.e., the immune cells, antibodies, and complement.

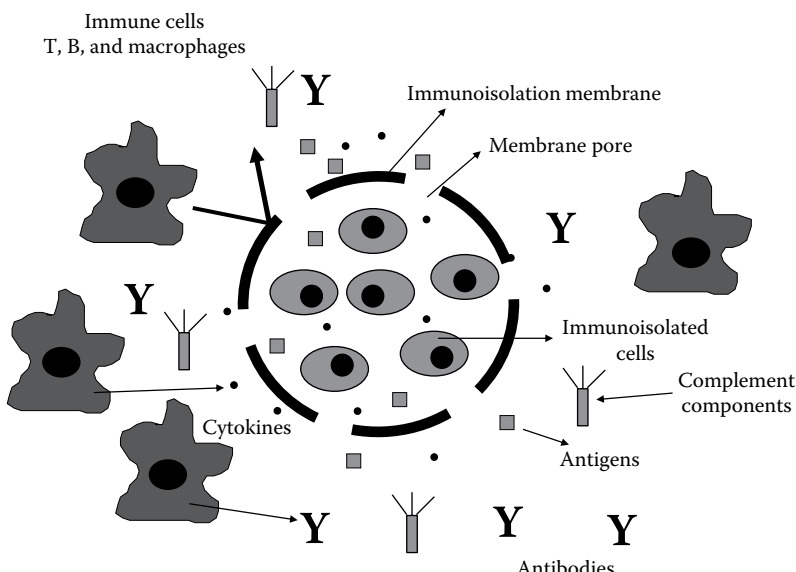


Figure 11.5 Pathways for rejection of immunoisolated cells involve both humoral and cellular components of the immune system.

The immune response occurs as a result of antigens shed by the transplanted cells. These antigens may be products secreted by the functioning cells or materials released by the death of the transplanted cells. These antigens will cross the immunoisolation membrane and, when recognized and presented by the host's immune system, lead to the cellular and humoral immune responses discussed earlier.

To restrict the passage of cells such as lymphocytes and macrophages, the pores or spaces within the immunoisolation membrane must be no larger than a micron or so. Recent evidence indicates that blocking the entry of the cellular component of the immune system is sufficient to prevent the rejection of allografts (Colton, 1995). This is of special interest for applications involving allogeneic cells for gene therapy (Chang et al., 1993; Liu et al., 1993; Hughes et al., 1994; Al-Hendy et al., 1995; Chang, 1997; Zalzman et al., 2003).

However, openings that restrict the entry of immune cells will still allow the passage of antibodies and complement, which must be blocked for the successful use in a bioartificial organ of xenogeneic cells. Therefore, the solute permeability characteristics of the immunoisolation membrane are critical for achieving the successful immunoisolation of xenogeneic transplanted cells. This requires that the membrane have significant permeability to essential small molecular weight solutes such as oxygen, glucose, growth factors, and molecular carriers such as albumin and transferrin.\* The membrane also must be permeable to waste products and to the therapeutic product, e.g., in treatment of diabetes, this would be insulin. On the other hand, the membrane must have negligible permeability to the humoral components of the immune system, i.e., antibodies, complement, and various cytokines and lymphokines.

As we discussed earlier, antibodies have molecular weights ranging from 150,000 to 900,000 g mol<sup>-1</sup>. Naturally occurring antibodies of the IgM class exist in the host and are reactive against the MHC of xenografts. In addition, antibodies produced from autoimmune diseases such as diabetes would be expected to bind to antigens on donor islets of Langerhans.

In the absence of immune cells, antibody binding to antigens on the surface of the transplanted cells is usually not sufficient to damage the cells. However, if both antibodies and complement are present, then the transplanted cells can be destroyed by complement activation and formation of the MAC (Iwata et al., 1996).

The complement system is activated by two different routes called the *classical pathway* and the *alternative pathway*. The classical pathway requires the formation of antigen-antibody complexes for its initiation, whereas the alternative pathway does not. The alternative pathway becomes activated in response to the recognition of large polysaccharide molecules present on the surface of the cell membranes of invading microorganisms. As far as the immunoisolation of transplanted cells is concerned, the classical pathway is of most interest for this discussion.

The activation of the classical pathway involves nine protein components known as C1 through C9. C1 is the first component to become activated and requires the binding with antigen of either two or more adjacent IgG antibodies or a single IgM antibody. C1 consists of three subunits called C1q, C1r, and C1s. Their molecular weights are respectively 400,000, 95,000, and 85,000 g mol<sup>-1</sup>. The C1q subunit is the first subunit activated, and it binds with the Fc fragment of the bound antibodies. Its activation then activates the C1r subunit which then activates the C1s subunit which activates C4 and so on.

\* Albumin carries fatty acids and transferrin carries iron.

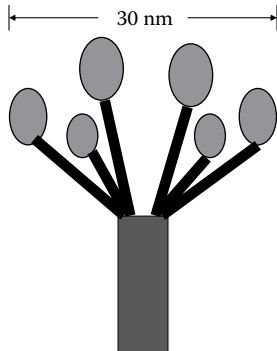


Figure 11.6 Complement C1q molecule.

As we discussed earlier, in the absence of immune cells, the binding of antibody with antigen is not sufficient to damage the transplanted cells. The destruction of the antibody-laden cell will require the presence and activation of complement. Since the C1q subunit must bind with either IgM or several IgG to start the cascade of complement reactions, the immunoisolation membrane must be capable of preventing the passage of the C1q molecule.

C1q has an interesting molecular shape as shown in [Figure 11.6](#). The critical dimension of C1q is the span of the six projections from the cylindrical base, which is about 30 nm. Because of the presence of proteins coating the walls of the pores in the immunoisolation membrane, the maximum pore size allowable for blocking C1q is on the order of 50 nm (Colton and Avgoustiniatos, 1991; Colton, 1995; Zielinski et al., 1997).

Several other issues with regard to immunoisolation also need to be considered. The immunoisolation membrane may be capable of preventing the passage of immune cells and complement C1q. However, the activation of the immune cells by antigens released by the transplanted cells will also result in the release of such lymphokines as IL-1 and other cytotoxic agents such as nitric oxide, peroxides, and free radicals. These substances can be toxic to the transplanted cells. Lymphokines have small molecular weights, typically around  $20,000 \text{ g mol}^{-1}$ , and because of their small size may pass through the immunoisolation membrane. Several studies, however, have shown that immunoisolated cells were not affected by the presence of IL-1 (Zekorn et al., 1990). Substances such as IL-1, and other highly reactive species, may be consumed by other reactions before they can penetrate the immunoisolation membrane to any significant distance (Colton, 1995). In addition, many bioartificial organs operate at very low tissue densities in order to provide for the effective oxygenation of the transplanted cells. The reduced tissue density results in a lower concentration of shed antigens and hence a reduced concentration of humoral agents.

The shed antigens could also cause the host to undergo a life-threatening *anaphylactic reaction*\* or to suffer from *antibody-mediated hypersensitivity reactions*.<sup>†</sup> Lanza et al. (1994) examined these issues by transplanting immunoprotected canine and porcine islets into rats. The islets were encased

\* A result of a significant release of inflammatory mediators such as histamine causing severe hypotension and bronchiolar constriction. Can cause death due to circulatory and respiratory failure.

<sup>†</sup> An inappropriate or exaggerated response of the immune system to an antigen. Binding of antibodies to the antigen starts the process.

within an acrylic hollow fiber membrane with a nominal molecular weight cutoff of about 80,000 g mol<sup>-1</sup>. Their studies showed that the immunoprotected islet xenografts caused the host to generate antibodies to antigens given off by the transplanted islets. However, there was no evidence of any other pathological effects of these antibody-antigen immune complexes. Subsequent studies using immunoprotected human islets in human patients with diabetes (Scharp et al., 1994; Shiroki et al., 1995) have shown that the immunoisolation membrane can protect against not only the allogeneic immune response but also against the autoimmune components responsible for the development of insulin-dependent diabetes mellitus (IDDM).

## 11.4 Permeability of immunoisolation membranes

Figure 11.7 presents permeability data obtained on a hollow fiber immunoisolation membrane for a variety of solutes of different molecular weight (Dionne et al., 1996). This particular membrane was made from a copolymer of acrylonitrile and vinyl chloride. The permselective membrane consists of a thin skin on either side of a much thicker spongy wall region that provides overall structural strength. The thickness of the spongy wall was about 100 µm, and these membranes were similar to those that were successfully used in preliminary tests to immunoisolate human islets in patients with diabetes (Scharp et al., 1994). These membranes had a reported nominal molecular weight cutoff of 65,000 g mol<sup>-1</sup>.

Notice how the permeability of this membrane at first decreases gradually as the solute molecular weight increases. As the solute molecular weight continues to increase, the permeability decreases much more rapidly. This can be explained by recalling our equation for solute permeability given by Equation 6.15. The size of low molecular weight solutes is much smaller than the pores in the membrane. For these solutes, steric exclusion ( $K$ ) and solvent drag ( $\omega_s$ ) effects caused by the pore wall are negligible. The decrease in permeability is therefore directly related to the decrease in solute diffusivity, which according to Equations 5.40 and 5.41, is inversely proportional to the solute radius, or the one-third power of the solute molecular weight. This is also shown as the dashed line in Figure 11.7. As the solute size reaches a critical fraction of the membrane average pore size, steric exclusion and solvent drag become more important, and the solute permeability rapidly decreases with increasing solute molecular weight.

These data also clearly show the problem of defining the *nominal molecular weight cutoff* (NMWCO) for the membrane. There does not exist a molecular weight above which the solute permeability drops to zero. Surprisingly, we see that even very large molecules, here at the extreme represented by a molecular weight of about 440,000 in Figure 11.7, have a measurable permeability. Therefore, a membrane's molecular weight cutoff is very subjective and dependent on the definition that one chooses to apply. For example, some membrane manufacturers define the molecular weight cutoff on the basis of the 90% retention of a given solute after so many hours of dialysis. Others base it on the ultrafiltration of a solution in which a particular solute is 90% retained.

Although the exact nature of the pores or openings within the membrane is not known, descriptions such as those based on the hydrodynamic pore model developed in Chapter 6 (see Equation 6.12) provide a useful framework for understanding the transport of various solutes and also provide a means for correlating data. The data shown in Figure 11.7 can therefore be used to obtain an estimate of the average pore size in the membrane. This is shown in the following example.

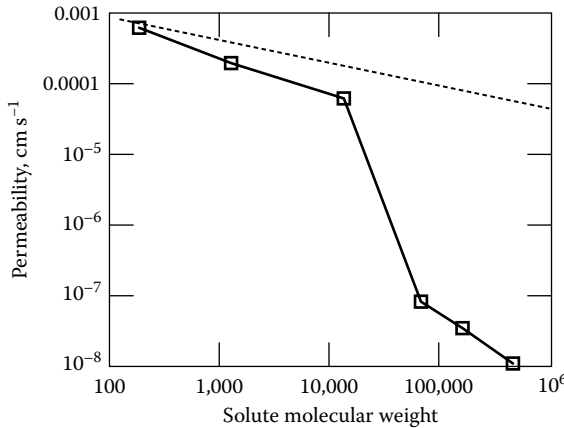


Figure 11.7 Immunoisolation membrane permeability. (Data from Dionne, K.E. et al., *Biomaterials*, 17, 257, 1996.)

### Example 11.1

Using the solute permeability data shown in Figure 11.7, determine the average size of the pores in the membrane. Recall that the membrane is 100  $\mu\text{m}$  thick. The table below summarizes the physical properties of the solutes that were used. Use the hindered diffusion model developed by Bungay and Brenner (1973) to describe the effect of the pore size on the diffusion of the solute. This equation is used, rather than the Renkin model given in Equation 6.12, because the Bungay and Brenner equation is generally valid for the entire range of the ratio of solute to pore size, i.e.,  $0 \leq a/r \leq 1$ . The Renkin equation is only valid for  $a/r < 0.4$  and may not provide a correct description of the diffusion of larger molecules in comparably sized pores. In the Bungay and Brenner model,  $\omega_r = 6\pi/K_t$  in the permeability equation given by Equation 6.15.  $K_t$  is given by the following equation. In this equation,  $a$  is the molecular radius and  $r$  is the pore radius:

$$K_t = \frac{9}{4} \pi^2 \sqrt{2} \left(1 - \frac{a}{r}\right)^{-5/2} \left[ 1 + \sum_{n=1}^2 z_n \left(1 - \frac{a}{r}\right)^n \right] + \sum_{n=0}^4 z_{n+3} \left(\frac{a}{r}\right)^n$$

with  $z_1 = -1.2167$ ,  $z_2 = 1.5336$ ,  $z_3 = -22.5083$ ,  $z_4 = -5.6117$ ,  $z_5 = -0.3363$ ,  $z_6 = 1.216$ , and  $z_7 = 1.647$ .

Solute	Molecular Weight	Stokes-Einstein Radius, nm	$D_{\text{water}} \times 10^6 \text{ cm}^2 \text{ s}^{-1} 37^\circ\text{C}$	$P_m \times 10^8 \text{ cm s}^{-1}$
Glucose	180	0.35	9.24	63,200
Vitamin B12	1,300	0.77	5.00	20,000
Cytochrome C	13,400	1.65	1.78	6,160
Bovine serum albumin (BSA)	67,000	3.61	0.964	7.95
IgG	155,000	5.13	0.629	3.59
Apo ferritin	440,000	5.93	0.611	1.07

Source: Dionne, K.E. et al., *Biomaterials*, 17, 257, 1996.

### Solution

Since the membrane consists of two permselective skins and a much thicker spongy wall region, the observed solute permeabilities must account for the resistances of all three regions. Therefore, the observed permeability is given by the following equation assuming the two skins are equivalent in their resistance to mass transfer:

$$\frac{1}{P_m} = \frac{2}{\frac{\varepsilon_{\text{skin}} D_{AB} K_{\text{tot}}}{\tau_{\text{skin}} \bar{L}_{\text{skin}}} + \frac{1}{\frac{\varepsilon_{\text{sponge}} D_{AB}}{\tau_{\text{sponge}} \bar{L}_{\text{sponge}}}}}$$

The porosity of the sponge is assumed to be about 0.8, and the tortuosity of the sponge is assumed to be unity. The nonlinear regression analysis is based on two variables, the pore radius ( $r$ ) and a parameter  $\alpha$ . The parameter  $\alpha$  accounts for the group  $\frac{\varepsilon_{\text{skin}}}{\tau_{\text{skin}} \bar{L}_{\text{skin}}}$  for which the individual values of the parameters are not known. Since the permeability values vary over several orders of magnitude, it is appropriate to define the objective function for the regression analysis in terms of the natural logarithm of the permeabilities. Hence, we write the sum of the square of the errors for the nonlinear regression analysis as follows for the data points ranging from  $i = 1$  to  $N$ :

$$\text{SSE}(r, \alpha) = \sum_{i=1}^N \left[ \ln(P_{mi}) - \ln(P_{m\text{calc}}(i, r, \alpha)) \right]^2$$

The result of the regression analysis is shown in [Figure 11.8](#) and provides an estimated pore diameter of 14.2 nm.

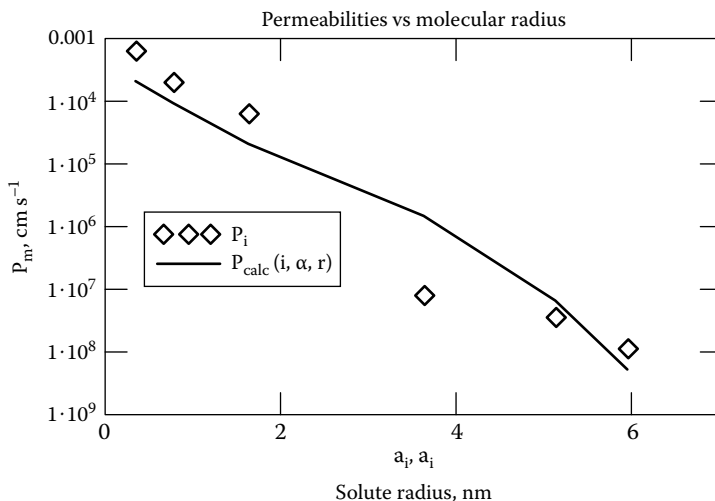


Figure 11.8 Measured and predicted permeabilities in an immunoisolation membrane.

## 11.5 Membrane Sherwood number

The solute permeabilities shown in [Figure 11.7](#) can also be compared to the permeability the solute would have in an aqueous layer that has the same thickness as the membrane itself. Therefore, we can write the following equation that expresses the ratio of these respective permeabilities:

$$\frac{P_m}{P_{\text{aqueous layer}}} = \frac{P_m}{\frac{D_{AB}}{\bar{L}}} = \frac{P_m \bar{L}}{D_{AB}} = \frac{D_e}{D_{AB}} = Sh_m \quad (11.1)$$

We see that this ratio of permeabilities is equivalent to defining a Sherwood number for the membrane, i.e.,  $Sh_m$ , that represents the ratio of the effective diffusivity, i.e.,  $D_e = P_m \bar{L}$ , of the solute through the membrane to that of the aqueous solute diffusivity. This process has the effect of eliminating membrane thickness ( $\bar{L}$ ) as a variable when correlating membrane permeability data.

The data shown in [Figure 11.7](#) are replotted as the membrane Sherwood number versus solute molecular weight in [Figure 11.9](#). We see that for low molecular weight solutes, the membrane Sherwood number is relatively constant. In this example, it is about 0.68. As the solute molecular weight is increased and the solute size becomes comparable to that of the pores, the membrane Sherwood number begins to decrease rapidly.

## 11.6 Examples of bioartificial organs

*Bioartificial organs* contain living tissue or cells that are immunoisolated by polymeric membranes with the properties discussed earlier. These devices are also known as *hybrid artificial organs* since they consist of both artificial materials and living tissue or cells. Bioartificial organs are being considered for the treatment of a variety of diseases, such as diabetes, liver failure, and kidney failure, and neurological disorders such as Parkinson's or Alzheimer's disease; for the control of pain; and for the delivery of a variety of therapeutic products secreted by genetically engineered cell lines.

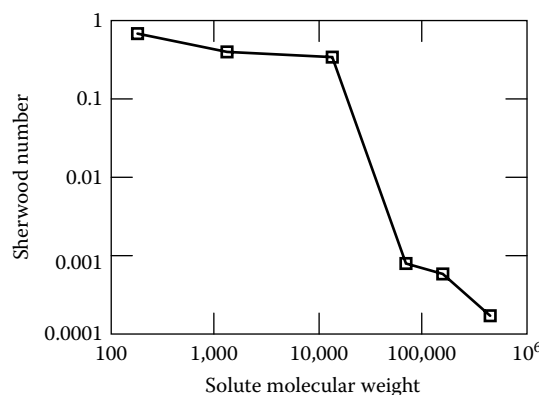


Figure 11.9 Immunoisolation membrane Sherwood number. (Data from Dionne, K.E. et al., *Biomaterials*, 17, 257, 1996.)

For diabetes, the bioartificial organ contains insulin-secreting and glucose-responsive cells that secrete, minute by minute, the appropriate amount of insulin needed to maintain blood glucose levels within a very narrow range (Scharp and Marchetti, 2014; Bartlett et al., 2016). Bioartificial livers and the bioengineered kidney (Attanasio et al., 2016) attempt to replace all of the physiological functions of these complex organs. The treatment of neurological disorders involves the use of specialized genetically engineered cells that secrete neuroprotective and neuroactive products such as dopamine, nerve growth factor, glial cell line-derived neurotrophic factor, or brain-derived neurotrophic factor. Immunoprotected cells that secrete pain-reducing neuroactive compounds such as  $\beta$ -endorphin are being considered for the treatment of pain resulting from cancer. Genetically engineered cell lines can also be used to treat a variety of other diseases. Examples include providing a specific hormone (e.g., growth hormone), replacing missing clotting factors in hemophilia (factor VIII or IX), and providing needed enzymes in such diseases as adenosine deaminase deficiency that results in severe combined immunodeficiency disease. More details about these specific applications of bioartificial organs may be found in the list of references. In the following discussion, we will look at bioartificial organ replacements for the endocrine cells of the pancreas, the liver, and the kidney as representative systems.

### 11.6.1 The bioartificial pancreas

The focus of much of the research and development on bioartificial organs has been on the treatment of IDDM, or type I diabetes, with a *bioartificial pancreas*. This is because IDDM is a chronic disease with many serious complications such as blindness, kidney disease, gangrene, heart disease, and stroke, which lead to a poorer quality of life for those afflicted with this disease. IDDM is caused by an autoimmune process (Notkins, 1979; Atkinson and MacLaren, 1990) that destroys the insulin-secreting  $\beta$  cells found within the *islets of Langerhans*. The islets of Langerhans are scattered throughout the pancreas and represent about 1%–2% of the pancreas mass. Both environmental (viruses or chemicals) and hereditary factors are also involved in the development of type I diabetes. Type I diabetes therefore represents a major health problem in the United States. Over 1.5 million people in the United States have this disease, and an additional 30,000 cases are diagnosed each year in that country alone. The cost of healthcare for patients with IDDM is tens of billions of dollars each year. Although a pancreas transplantation can eliminate the need for exogenous insulin, this approach is limited by the shortage of donor organs and the complications and side effects associated with the required immunosuppressive drugs.

Insulin is a small protein (6000 g mol<sup>-1</sup>) and the key hormone involved in the regulation of the body's blood glucose levels. In diabetes, insulin is no longer produced by the  $\beta$  cells found in the islets of Langerhans. In the absence of insulin, glucose levels in the blood exceed normal values by several times. This is a result of the body's cells not being able to metabolize glucose. Without the ability to use glucose as an energy source, the body responds by metabolizing fats and proteins with a corresponding increase in the body fluids of ketoacids such as acetoacetic acid. This excess acid results in a condition known as *ketoacidosis*, which, if left untreated, can lead to death.

The conventional treatment for IDDM involves the daily administration of exogenous insulin to replace the insulin that is no longer produced by the patient's  $\beta$  cells found within the islets of Langerhans. This results in the almost normal metabolism of carbohydrates, fats, and proteins. However, even with exogenous insulin, the patient's blood glucose levels are not controlled as well

as normal. The healthy islet  $\beta$  cells are able to regulate the release of insulin in such a manner so as to maintain blood glucose levels within a narrow range, about  $80\text{--}120 \text{ mg dL}^{-1}$ . Insulin injections are not capable of providing such close control because of the difficulty of properly timing the injections and the inherent insulin transport delays from the site of injection. The abnormally high blood glucose levels, or *hyperglycemia*, in patients treated with exogenous insulin is now believed to be the primary cause of the long-term complications of diabetes (American Diabetes Association, 1993). These elevated blood glucose levels lead to protein *glycosylation* that damages the microvasculature and other tissues in the body.

Methods have recently been developed that allow for the isolation of mass quantities of the islets of Langerhans from the pancreas of humans and from large mammals such as pigs, thus providing a potentially unlimited supply of donor islet tissue (Ricordi et al., 1988, 1990a,b; Warnock et al., 1988, 1989; Inoue et al., 1992; Ricordi, 1992; Lanza and Chick, 1994a; Lacy, 1995; Lakey et al., 1996; Maki et al., 1996; Cheng et al., 2004; Grundfest-Broniatowski et al., 2009; Ludwig et al., 2013; Neufeld et al., 2013; Scharp and Marchetti, 2014). The use of these allogenic or xenogeneic cells without immunosuppression requires that they be immunoisolated in a device such as a bioartificial organ. Transplanting the donor islets without immunoprotection is only warranted in those cases where the patient is already receiving immunosuppressive therapy, e.g., as a result of a kidney transplant to treat end-stage renal disease. In an otherwise healthy patient with diabetes, immunosuppressive drugs and their attendant problems would not be needed if the islets were immunoisolated. The immunoisolation of the islets would not only protect them from the host's normal response to foreign tissue but also from those agents of the immune system that caused the original autoimmune destruction of the patient's own cells. These immune system *memory cells* are still capable of responding to the antigens that resulted in the original destruction of the patient's own islets and could possibly destroy the donor islets or donor  $\beta$  cells.

Immunoisolation requires the use of an immunoisolatory membrane that has the following properties. First, it must be biocompatible and have a solute permeability profile that allows for the efficient transport of small molecules such as oxygen, key nutrients, and insulin. In addition, the immunoisolation membrane must exclude immune cells and immunoactive molecules. Because of the limitations on oxygen transport, the transplanted cells need to be within a hundred microns or so of the capillaries, which serve as the oxygen source, or there needs to be a means of providing an oxygen source (Ludwig et al., 2013; Neufeld et al., 2013). The insulin-secreting cells and the immunoisolation membrane also need to be easy to assemble and sterilize before implantation in the patient. Since there is the possibility that the device can lose function over time, there either needs to be a means to resupply the device with more insulin-secreting cells or the device needs to be easy to remove from the body so that a new device can be implanted.

The goal of the bioartificial pancreas is therefore to utilize the glucose regulating capability of healthy donor islets to provide improved blood glucose control in patients with type I diabetes. This approach should minimize the complications of the disease and improve the quality of the patient's life. Because of the advances in genetic engineering, there is also the possibility of using genetically engineered  $\beta$  cells (Efrat, 1999; Zalzman et al., 2003; Tatake et al., 2007) instead of the islets of Langerhans. Genetically engineered  $\beta$  cells that can respond to changing glucose levels with the appropriate insulin response will ensure a consistent source of cellular material for use in a bioartificial pancreas.

**11.6.1.1 Bioartificial pancreas approaches** A variety of approaches have been described over the years for the bioartificial pancreas, and most of these have been tested extensively in animals. An excellent review of these devices can be found in the early papers by Colton and Avgoustiniatos (1991), Mikos et al. (1994), Lanza et al. (1995), and Colton (1995), as well as in more recent reviews by Scharp and Marchetti (2014), Song and Roy (2016), and Bartlett et al. (2016). A series of books related to islet transplantation and the bioartificial pancreas have also been published (Ricordi, 1992; Lanza and Chick, 1994c).

These devices can be broadly classified into the following three categories: *intravascular (with and without ultrafiltration)*, *microencapsulation*, and *macroencapsulation*. These approaches are illustrated in Figure 11.10.

Of concern in any of these approaches for a bioartificial pancreas are the ability of the device to be readily fabricated and seeded with islets or cells, their stability and reliability over an extended period of time, and their cost. These issues also relate to the overall biocompatibility of the device. Specifically, device toxicity, immune system response, the potential for fibrotic encapsulation, and for intravascular devices, the potential for thrombosis. Furthermore, the devices must be capable of maintaining the long-term viability of the donor tissue and have the proper mass transfer characteristics to normalize blood glucose control. This requires a proper understanding of the critical role of oxygen transport (Colton, 2014), along with the mass transfer properties of the immunoisolation and the device itself.

**11.6.1.2 Intravascular devices** The intravascular devices (Figure 11.10a and b) (Chick et al., 1977; Moussy et al., 1989; Lepeintre et al., 1990; Sarver and Fournier, 1990; Maki et al., 1991, 1993; Petruzzo et al., 1991; Sullivan et al., 1991; Lanza et al., 1992a,b,c,d,e, 1993) involve a direct

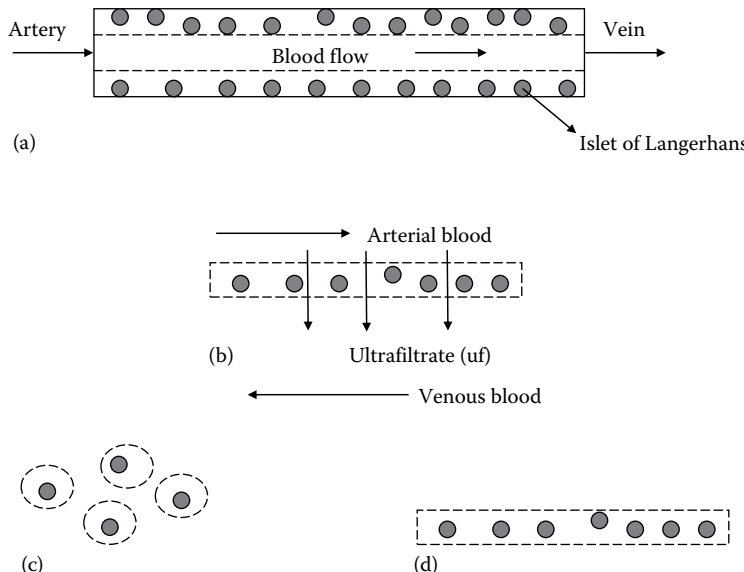


Figure 11.10 Approaches for a bioartificial pancreas: (a) intravascular without UF, (b) intravascular with UF, (c) microencapsulation, and (d) macroencapsulation.

connection to the vascular system of the host via an arteriovenous shunt. Blood flows through the lumen of small polymeric hollow fibers or in the spaces between flat membrane sheets. Adjacent to the blood flow path, and protected by the immunoisolation membrane, are the islets.

An advantage of this type of device is that the convective flow of the blood provides the potential for better mass transfer rates than what can be obtained by simple diffusion from the tissue surrounding the device. The close contact with a sizable flow of blood also offers the potential for good tissue oxygenation.

In some cases, an ultrafiltration flow (UF) of plasma ([Figure 11.10b](#)) from the arterial side can flow through the immunoisolation membrane and enter the region that contains the islets (Reach et al., 1981, 1984). Recent advances in ultrathin silicon nanopore membranes have brought about a renewed interest in the intravascular approach (Fissell et al., 2009; Song et al., 2016). This UF then leaves the islet compartment and reenters the venous blood, much like the Starling flow found in capillaries. The UF has the potential of greatly enhancing the transport of oxygen to the transplanted cells (see [Section 7.9.1](#) and [Example 7.10](#)) as well as improving the glucose-insulin kinetics of the device.

The primary disadvantages of the intravascular approach are the surgical risk associated with device implantation, connection to the host's vascular system, the potential to form blood clots, and the complexity of the surgery needed for device removal at a later time.

One of the first pioneering experiments to demonstrate the feasibility of the intravascular approach for a bioartificial pancreas was performed by Chick et al. (1977). A rat with chemically induced diabetes was connected ex vivo to an intravascular device containing cells obtained from neonatal rats. The device used in these experiments consisted of a bundle of 100 hollow fibers with diameters less than 1 mm and a fiber length of 11 cm. The fibers had a nominal molecular weight cutoff of about 50,000 g mol<sup>-1</sup>.

After connection of the animal to the ex vivo intravascular device, there followed a rapid decrease in blood glucose levels reaching normalized values of 110–130 mg dL<sup>-1</sup> (considered normal for a rat) after about 6 h. After the removal of the device, blood glucose levels rapidly increased and returned to their diabetic levels. These results indicated the feasibility and the potential of the bioartificial pancreas for the treatment of IDDM.

A particularly serious problem with devices that contained numerous hollow fiber membranes was the formation of blood clots in the entrance and exit header regions of the device. These regions of the device, where the bloodstream is either expanding or contracting, tend to form secondary flows or swirls that induce the formation of blood clots.

In an effort to minimize the formation of blood clots, without the use of anticoagulants such as heparin, a device with a single coiled hollow fiber membrane tube was developed by Maki et al. (1991). This device consists of an annular-shaped acrylic chamber 9 cm in diameter and 2 cm thick. The chamber contains a 30–35 cm length of a coiled hollow fiber tube with an inner diameter of 5–6 mm and a wall thickness of 120–140 µm. The hollow fiber tube was connected at each end to polytetrafluoroethylene arterial grafts that provided the connection of the device to the vascular system by an arteriovenous shunt. The larger bore size of the single hollow fiber tube eliminates the thrombosis observed in smaller bore hollow fiber tubes and in the header regions of the device described earlier. Low-dose aspirin therapy was also found to contribute to long-term patency through aspirin's ability to prevent platelet activation.

The hollow fiber membrane had a nominal molecular weight cutoff of about 80,000 g mol<sup>-1</sup>. A cavity surrounded the coiled hollow fiber membrane and provided a 5–6 mL volume for the placement of the islets of Langerhans. This device was evaluated in pancreatectomized dogs using allogeneic canine islets and xenogeneic bovine and porcine islets. The device was implanted within the abdominal cavity and *anastomosed* to the left common iliac artery and the right common iliac vein.

This device was able to demonstrate improved blood glucose control for varying periods of time using both allo- and xenogeneic islets (Lanza et al., 1992a,b,c,d,e). For example, in a dog implanted with a single device containing about 42,000 canine islet equivalents,\* prior to device implantation, this particular dog had a fasting blood glucose level of 230 mg dL<sup>-1</sup> and required about 16 U day<sup>-1</sup> of insulin.<sup>†</sup> After implantation, no exogenous insulin was provided for the 280-day period of the experiment. During the first 140 days, the fasting blood glucose was nearly normal and averaged 116 mg dL<sup>-1</sup>, which compares favorably to the value of 91 mg dL<sup>-1</sup> observed in normal dogs. After 140 days, glucose control began to deteriorate over the rest of the experiment.

Results obtained with xenogeneic implants containing porcine islets in this device were also very encouraging (Maki et al., 1996). Prior to receiving porcine islets, one particular dog had a fasting blood glucose level of 479 mg dL<sup>-1</sup> and required 39 U day<sup>-1</sup> of insulin. After this dog received 216,000 EIN of porcine islets, fasting blood glucose averaged 185 mg dL<sup>-1</sup> and exogenous insulin averaged about 10 U day<sup>-1</sup>. This device failed after 271 days of operation. An analysis of the porcine islets after device removal did not show any evidence of immune cell infiltration. These tests therefore presented clear evidence that xenogeneic porcine islets could be protected from the host's immune system using immunoisolation membranes. The only major complication in the use of these devices in dogs was vascular thrombosis. However, this clotting problem may be unique to dogs because of their known hypercoagulability.

**11.6.1.3 Microencapsulation** The microencapsulation approach (see Figure 11.10c) involves the placement of one or several islets within small polymeric capsules (Sun et al., 1977, 1996; Altman et al., 1986; Gharapetian et al., 1986; Sugamori and Sefton, 1989; Lum et al., 1991; Soon-Shiong et al., 1992a,b, 1993; Lanza et al., 1995; Tun et al., 1996). The microcapsules are then injected within the peritoneal cavity. The diameter of the microcapsule is typically in the range of 300–600 µm. Other microencapsulation approaches include immunoprotective surface or conformal coatings of the islets, which results in a much thinner layer of polymer material that encloses the islets (Pathak et al., 1992).

Microencapsulation provides diffusion distances on the order of 20–200 µm and very high surface areas per volume of islet tissue. Accordingly, the small size of a microcapsule provides good diffusion characteristics for nutrients and oxygen, which improves islet or cell viability. This also provides for a good glucose-insulin response that offers the potential for normalization of blood glucose levels.

The microcapsules usually consist of the islet or cellular aggregates immersed within a hydrogel material with another eggshell-like layer that provides the immunoisolation characteristics and

\* The equivalent islet number (EIN) is defined as the number of islets 150 µm in diameter that are equivalent in volume to a given sample of islets.

† Insulin dose is based on U(nits) of insulin where 1 U of insulin = 34.7 µg of insulin.

mechanical strength. A wide variety of polymer chemistries have been described for the hydrogel and the immunoprotective layer, and some of these are described in the following references: Gharapetian et al. (1986, 1987), Sefton et al. (1987), Douglas and Sefton (1990), Matthew et al. (1993), Lanza et al. (1995), and Sun et al. (1996).

Of particular concern in selecting the microcapsule chemistry is the formation of a fibrotic capsule around the encapsulated islet. Fibrotic capsule formation can severely limit the diffusion of nutrients and oxygen, resulting in the loss of islet or cellular function. The success of the microencapsulation approach is therefore strongly dependent on choosing membrane materials that minimize this fibrotic reaction.

An example of the microencapsulation approach was described by Soon-Shiong (1994) and demonstrated in large animals and several human patients. They used an alginate-poly-L-lysine encapsulation system. Alginates are natural polymers composed of the polysaccharides mannuronic acid and guluronic acid. Soon-Shiong (1994) showed that the high mannuronic acid residues in the alginate are responsible for the fibrotic response. Mannuronic acid was shown to induce the lymphokines IL-1 and tumor necrosis factor, which are known to promote the proliferation of fibroblasts and lead to fibrotic capsule formation. By reducing the alginate's mannuronic acid content and increasing the guluronic acid content (>64%), they were able to minimize the fibrotic response. The higher guluronic acid content also provided another benefit. It was found that alginates with higher guluronic acid contents were mechanically stronger.

These modified alginate microcapsules were evaluated in a series of nine spontaneously diabetic dogs. Three of the dogs received free unencapsulated islets, and the other six dogs received encapsulated islets. The donor islets were obtained from other dogs, and each recipient received their quantity of islets by an intraperitoneal injection. The islets were provided at an average dose of about 20,000 EIN kg<sup>-1</sup> of body weight.

Exogenous insulin was stopped four days prior to islet injection, and the plasma glucose levels at that time averaged 312 mg dL<sup>-1</sup>. The first day after receiving the islets, the blood glucose levels were reduced to an average of 116 mg dL<sup>-1</sup> in those animals that received encapsulated islets and averaged 120 mg dL<sup>-1</sup> in those receiving free islets. The rejection of the unprotected free islets occurred rapidly with hyperglycemia returning in about 6 days. The animals receiving encapsulated islets exhibited normoglycemia for periods of time ranging from 63 to 172 days, for a median period of 105 days. The failure of the encapsulated islets was attributed to membrane failure as a result of the water-soluble nature of the alginate system.

Sun et al. (1996) developed a microencapsulation system for islets using alginate-polylysine-alginate microcapsules. Most microcapsules contained only a single islet and had diameters in the range of 250–350 µm. Preclinical studies were done using microencapsulated porcine islets implanted into spontaneously diabetic cynomolgus monkeys. Seven monkeys receiving an average of 16,100 EIN kg<sup>-1</sup> body weight were insulin independent for an average of 289 days. The shortest duration of control was 120 days and the longest 803 days. Prior to receiving the islets, fasting blood glucose levels averaged 353 mg dL<sup>-1</sup>. Following the transplant, fasting blood glucose levels averaged 112 mg dL<sup>-1</sup>. During the experiments, blood samples from the animals were tested repeatedly for the presence of antiporcine islet antibodies. No antibodies were detected, confirming the presence of an effective immunoisolation of the porcine islets. Diabetic control animals also received unencapsulated islets. However, normal glucose levels were only maintained for

about 9 days after which the islets were destroyed by the host's immune system with a return to pretransplant diabetic levels of the blood glucose.

The results obtained from using the microencapsulation approach are very promising. However, there still are some technical difficulties with this approach that must be overcome. The strength and integrity of the microcapsules needs to be improved to provide long-term functioning and viability of the islets. The aggregation of the microcapsules is also a problem as this affects their mass transfer characteristics and impacts glucose control and islet survival. The total volume for the smaller microcapsules of Sun et al. (1996) is modest. For example, using their monkey results and assuming a 70 kg patient, a total of 1.1 million EIN would be required ( $16,100 \text{ EIN kg}^{-1}$  body weight). With one islet per 300  $\mu\text{m}$  diameter microcapsule, this amounts to a total bead volume of only 16 mL. The loss of islet function with time can be compensated for by the injection of fresh microcapsules. The retrieval of the small microcapsules could be difficult if this should be necessary after their introduction.

**11.6.1.4 Macroencapsulation** Macroencapsulation (see [Figure 11.10d](#)) involves placing numerous islets within the immunoisolation membrane structure. Typical approaches involve the use of hollow fibers that encase the islets (Altman et al., 1986; Lacy et al., 1991; Lanza et al., 1991, 1992b,c,e), a much larger flat bag-like structure (Inoue et al., 1992; Gu et al., 1994; Hayashi et al., 1996), thin polymeric hydrogel sheets (Storrs et al., 2001), or a thin scaffold laminated to a thin immunoisolation membrane (Grundfest-Broniatowski et al., 2009). Their larger size and smaller number also make retrieval less of a problem in comparison to microcapsules.

The major limitation of the macroencapsulation approach is that oxygen needs to diffuse over relatively large distances from the surrounding tissue and then through the layer of islets within the device itself (see [Figure 7.7](#) and [Example 7.6](#)). The design challenge is to provide enough islets in a single device to achieve normoglycemia in the patient while being able to provide sufficient oxygen transport to keep the islets alive (see [Problems 7.29](#) and [7.30](#)). This oxygen diffusion limitation means that the islet volume fraction within the device is rather small. This makes planar designs for these devices rather thin, which provides for better oxygen transport to the islets. However, the device radius can be rather large to provide enough volume to hold the required dose of islets for normoglycemia. This means that several devices may be needed to treat diabetes in humans.

The membranes used for macroencapsulation must not only possess the needed immunoisolation permeability requirements but, because of their larger size, must also provide sufficient mechanical strength to maintain their integrity. This is a difficult objective since the membrane wall must be thin for diffusional purposes, and this may compromise overall strength. In many cases, it has been found that thin-walled hollow fiber membranes were prone to breaking (Lanza et al., 1995). The rupture of the membrane wall will result in the rejection of the islet tissue and loss of function. As is the case for microcapsules, membrane chemistry is an important factor in minimizing the formation of fibrous tissue around the implant.

Most of the early attention given to the macroencapsulation technique has been focused on the use of hollow fibers. A trade-off exists on the selection of the fiber diameter. A large diameter fiber will result in a shorter overall length but can lead to diffusional limitations. The lack of oxygen transport and the accumulation of waste products can therefore result in a central core of necrotic tissue. On the other hand, a small fiber diameter, while improving the mass transport characteristics, can result in an incredibly long fiber length. This longer length increases the probability of breakage and makes the implantation of the fibers more difficult.

An example of the use of hollow fibers as a vehicle for the macroencapsulation of the islets of Langerhans has been reported (Lanza et al., 1991, 1992b,c,e, 1995). This particular system has been studied in some detail in both rats and dogs using a variety of sources for the islets. The islets were enclosed within semipermeable hollow fiber membranes that were 2–3 cm in length and had an internal diameter of 1.8–4.8 mm. The membrane wall thickness ranged from 69 to 105  $\mu\text{m}$ , and the membrane had a nominal molecular weight cutoff of 50,000–80,000 g mol<sup>-1</sup>. Depending on the fiber diameter, approximately 9–50 fibers were implanted within the peritoneal cavity of each rat.

When these fibers contained bovine islets (20,000 EIN) and they were implanted in the peritoneal cavity of rats whose diabetes was induced chemically using the drug *streptozotocin* (*STZ*), the diabetic state was reversed within 24 h after implantation. In some cases, normoglycemia was maintained for 1 year. However, the wider bore membranes (4.5–4.8 mm ID) that were retrieved after several months were found to contain a necrotic core as a result of oxygen transport limitations. Viable islets were only found to exist within a 0.5–1 mm layer along the membrane wall. Some of the late failure of the implants was also attributable to membrane breakage as a result of the thin membrane wall.

Similar results were obtained using canine islets contained within the same hollow fibers and implanted within the peritoneal cavity of diabetic BB/Wor rats (Lanza et al., 1992c). This type of rat develops autoimmune diabetes with a pathology similar to that found in humans. The canine islet xenografts provided normoglycemia in these rats for more than 8 months. This is an important result since it shows that the immunoisolation membrane protected the islet xenografts from the host's normal graft rejection response, as well as from the autoimmune disease process that produced the original diabetes. The protection of the islets from the autoimmune disease process is important in order to successfully treat human patients with diabetes.

The hollow fiber macroencapsulation of islets was also tested in pancreatectomized dogs. Lanza et al. (1992a,b,c,d,e) summarized the results obtained for two dogs that were insulin-free for at least 70 days after receiving islet allografts contained within these fibers. Each dog received between 155 and 248 fibers containing a total of about 300,000 EIN. This equates to a total fiber length of about 500 cm. The dogs had an average weight of about 17 kg, providing an islet loading of nearly 20,000 EIN kg<sup>-1</sup> of body weight. For a 70 kg human, the total number of islets would therefore be about 1.4 million EIN, or a total fiber length on the order of 2100 cm (70 ft).

Storrs et al. (2001) have described a macroencapsulation approach known as the islet sheet. In their approach, a mixture of highly purified alginate with a reinforcing polymeric mesh is sandwiched between acellular alginate layers. The resulting flat sheet construct is then allowed to gel. The ultra-thin acellular alginate layers are highly cross-linked and form the immunoisolation barrier. The thickness of the immunoisolation barrier is about 50–75  $\mu\text{m}$ . The islet sheets are typically 250  $\mu\text{m}$  thick with an active width of 3 cm and a length of 7 cm. The thinness of the islet sheets provides for excellent transport of oxygen and allows for an islet volume fraction of up to 40%. Because of the high tissue density, it is estimated that 10 sheets containing 400,000 islet equivalents would be needed to treat a human with diabetes. In these early studies on the islet sheet, a pancreatectomized beagle dog that received six islet sheets was able to maintain normal fasting glucose levels for 84 days.

Recently, in order to overcome the oxygen transport limitations, investigators have proposed devices with rechargeable internal supplies of oxygen (Ludwig et al., 2013; Neufeld et al., 2013) or a means

such as the electrolysis of water to generate oxygen in situ (Wu et al., 1999). The macroencapsulation approach described in Neufeld et al. (2013) allows for the daily recharging of a central cavity with oxygen. The device they evaluated in minipigs was a round disk 68 mm in diameter with a thickness of 18 mm. Oxygen levels in the gas chamber over a 24 h period varied between 1011 mmHg at the time of charging and decreased to about 300–500 mmHg after 24 h as a result of oxygen consumption by the islets and diffusion into the surrounding tissue. When this device was loaded with rat islets, it restored normoglycemia in chemically induced (STZ) diabetic minipigs during study periods up to 70 days. This result demonstrates that the immunoisolation concept can protect xenogeneic islets and that the periodic supply of oxygen is beneficial to islet function and viability.

In some cases, tissue engineering has been used along with the macroencapsulation approach (Hill et al., 1994; Sarver et al., 1995). Adjacent or integral to the immunoisolation membrane is a thin layer of a porous scaffold material that becomes vascularized by the host after implantation. The use of tissue engineering allows control over the environment adjacent to the immunoisolation membrane. Therefore, any fibrotic response to the implant can be minimized, and through the growth of an adjacent layer of vascular tissue, intimate contact with the host's vasculature can be obtained. This has the potential to improve the viability and long-term functioning of the transplanted tissue.

### Example 11.2

Consider a bioartificial pancreas with an internal gas chamber for the periodic recharging of the device with oxygen. Assume the partial pressure of oxygen in the tissue space surrounding the implanted device, i.e.,  $pO_2^B$ , is 68 mmHg and the partial pressure of oxygen in the gas chamber, i.e.,  $pO_2^{GC}$ , is 500 mmHg. Let the cells within the device be the islets of Langerhans with an oxygen consumption rate of  $25.9 \mu\text{M s}^{-1}$ . The thickness of the islet layer in the region between the gas chamber and the immunoisolation membrane is 200  $\mu\text{m}$ , and the islet cell volume fraction is 0.80. The islets are suspended within a hydrogel for which the effective oxygen diffusivity, i.e.,  $D_T$ , is estimated to be  $1.67 \times 10^{-5} \text{ cm}^2 \text{ s}^{-1}$ . The oxygen permeability of the immunoisolation membrane, i.e.,  $P_m$ , is  $4 \times 10^{-3} \text{ cm s}^{-1}$ . Calculate the  $pO_2$  at the interface between the islet layer and the immunoisolation membrane, i.e., at  $x = \delta$ , where  $\delta$  is the thickness of the cell layer as measured from the interface between the cell layer and the gas chamber. Assume Henry's constant for oxygen is  $0.74 \text{ mmHg } \mu\text{M}^{-1}$ .

### Solution

Equation 7.24 can be used to describe the oxygen transport within the islet layer:

$$D_T \frac{d^2 pO_2}{dx^2} = \Gamma_{\text{oxygen}} H_{\text{oxygen}} \phi \quad (\text{A})$$

The boundary conditions (BCs) are as follows:

$$\text{BC1: } x = 0, \quad pO_2 = pO_2^{GC}$$

$$\text{BC2: } x = \delta, \quad -D_T \frac{dpO_2}{dx} \Big|_{x=\delta} = P_m \left( pO_2 \Big|_{x=\delta} - pO_2^B \right)$$

BC1 states that the oxygen partial pressure at the interface between the gas chamber and the islet layer is equal to the value in the gas chamber. BC2 states that the flux of oxygen leaving the islet layer at  $x = \delta$  must equal the flux of oxygen across the immunoisolation membrane. The solution to [Equation A](#) can be shown to be given by

$$pO_2(x) = \left( \frac{\Gamma_{\text{oxygen}} H_{\text{oxygen}} \phi}{2\delta P_T} \right) x^2 - \left[ \frac{P_m \Gamma_{\text{oxygen}} H_{\text{oxygen}} \phi}{2P_T (P_T + P_m)} + \frac{\Gamma_{\text{oxygen}} H_{\text{oxygen}} \phi}{(P_T + P_m)} + \frac{P_m (pO_2^{\text{GC}} - pO_2^{\text{B}})}{\delta (P_T + P_m)} \right] x + pO_2^{\text{GC}}$$

where the oxygen permeability in the islet layer, i.e.,  $P_T$ , is defined as  $D_T/\delta$ . Solving for the  $pO_2$  at  $x = \delta$  in the previous equation, we obtain  $pO_2(\delta) = 110.9$  mmHg. This example is a rework of [Example 7.6](#) where we found the minimum partial pressure of oxygen in the islet layer to be about 20 mmHg for a cell volume fraction of 0.15. With an *in situ* source of oxygen, we can increase the islet layer cell volume fraction to 0.80 with a minimum oxygen partial pressure of about 111 mmHg. This clearly shows the vast improvement in the oxygen supply that can be gained by providing an *in situ* oxygen source when using the macroencapsulation approach.

### 11.6.2 Number of islets needed

One issue confronting all of the devices discussed thus far concerns the amount of tissue required to achieve normoglycemia in a human patient with diabetes. The previously mentioned studies in rats and dogs have used islet loadings on the order of 20,000 EIN kg<sup>-1</sup> body weight. This is considerably higher than the benchmark study reported by Warnock et al. (1988). They found that the threshold islet loading for treating pancreatectomized dogs corresponded to  $\approx 4.3$   $\mu\text{L}$  of islet tissue kg<sup>-1</sup>. This equates to about 2500 EIN kg<sup>-1</sup>. It is important to point out, however, that these were unencapsulated autologous islets that were implanted within the liver or the spleen. These islets had no artificial mass transfer resistance to overcome and no host immune response that would lead to rejection. This result most likely defines the lower limit on islet loading. Certainly, improvements in the mass transfer characteristics of the devices discussed so far could lead to islet loadings more on the order of 5,000–10,000 EIN kg<sup>-1</sup>. Based on the results presented in diabetic minipigs by Neufeld et al. (2013), they predict that a human device would require 300,000–500,000 islets. These investigators state that this would require the implantation of two devices, each 68 mm in diameter, or a single elliptical device with 500,000 islets (about 7,000 EIN kg<sup>-1</sup>) measuring 110 × 70 × 18 mm.

Overall device size is dependent on the amount of tissue needed, as well as on the device mass transfer characteristics for nutrients, oxygen, waste products, and the therapeutic agent itself. The mass transfer characteristics therefore are a critical factor in defining the islet tissue loading within the device itself.

The results presented so far demonstrate the potential of the bioartificial pancreas as a method for treating diabetes. Long-term islet survival within the device will be the key to the success of the bioartificial pancreas. Islets have the potential to function for many years as evidenced by the fact that, unless they become diseased, they exist for as long as the life span of the animal they are found in. Therefore, islets should be capable of surviving within a bioartificial pancreas for many years.

Islet survival is a function of many variables, including the amount of trauma they experience during their isolation and purification; the device mass transfer characteristics for nutrients, oxygen, and waste products; the integrity of the membrane immunoisolation system; and finally the host's response to the implant. This latter factor determines the nature of the physiological environment in the vicinity of the implant. Certainly, the formation of a region of undervascularized fibrotic tissue will not provide the conditions needed for the long-term functioning and survival of the islets. Because of questions concerning the long-term viability and functioning of the islet tissue, it may be necessary to periodically recharge the patients with islets. A bioartificial pancreas that has the ability to be reseeded would certainly offer an advantage.

### 11.6.3 Islet insulin release model

The design of a bioartificial pancreas also requires an understanding of the insulin release rate from an islet or insulin-producing cells and its dependence on plasma glucose levels. Islets that have been isolated from a pancreas or genetically engineered cells are usually challenged in culture with a step change in the glucose concentration. The glucose challenge is used to assess islet or cell viability, the insulin release rate, and glucose responsiveness. When challenged in this manner, islets or insulin-secreting cells release insulin in a biphasic fashion (Grodsky, 1972).

**Figure 11.11** illustrates the insulin response of rat islets (Nomura et al., 1984) to a rapid ramp increase in the glucose concentration from an initial value of  $80 \text{ mg dL}^{-1}$  to a final value of  $200 \text{ mg dL}^{-1}$ . Initially, the islets respond to the rate of change of the plasma glucose concentration, resulting in a maximum of the first-phase insulin release rate within a few minutes of the glucose challenge. Following this, the second-phase islet insulin release rate is proportional to the difference between the plasma glucose concentration and its fasting value of about  $80 \text{ mg dL}^{-1}$ . We see that this second-phase release rate is relatively constant once the glucose level has achieved a steady-state value.

A mathematical description of the islet insulin release rate during a glucose challenge can be obtained through the application of control theory. Nomura et al. (1984) have shown that the dynamics of the glucose-induced secretion of insulin can be expressed as the sum of the proportional response to

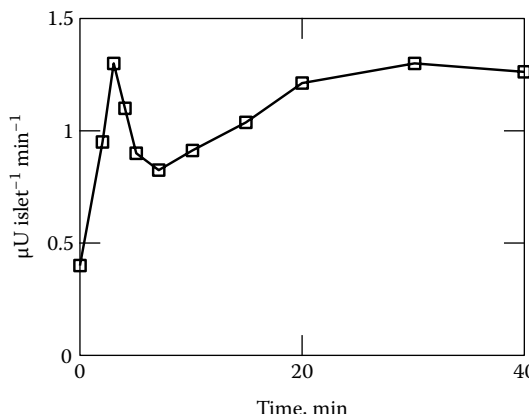


Figure 11.11 Rat islet insulin secretion rate. (Data from Nomura, N. et al., *Comput. Biomed. Res.*, 17, 570, 1984.)

the glucose concentration and a derivative response to the rate of change in the glucose concentration, each with a first order lag time, respectively given by  $T_1$  and  $T_2$ . The Laplace transform of the islet insulin release rate can therefore be expressed as follows:

$$r_{\text{islet}}(s) = \left[ \frac{K_p}{1 + T_1 s} + \frac{T_d s}{1 + T_2 s} \right] C_G(s) \quad (11.2)$$

This equation may be inverted (in the Laplace transform sense) to give [Equation 11.3](#) for the islet insulin release rate in terms of the glucose concentration, i.e.,  $C_G(t)$ , and its rate of change:

$$r_{\text{islet}}(t) = \int_{-\infty}^t C_p C_G(z) e^{-(t-z)/T_1} dz + \int_{-\infty}^t C_d \frac{dC_G(z)}{dz} e^{-(t-z)/T_2} dz \quad (11.3)$$

The parameters in this equation, i.e.,  $C_p (= K_p/T_1)$ ,  $C_d (= T_d/T_2)$ ,  $T_1$ , and  $T_2$ , may be obtained by performing a nonlinear regression analysis of islet or cellular insulin release rate data such as that shown in [Figure 11.11](#). This can be accomplished by first representing the ramp glucose profile as follows:

$$\begin{aligned} C_G(t) &= C_G^0, \quad \text{for } t < 0 \\ C_G(t) &= \left( \frac{C_G^{\text{ss}} - C_G^0}{t_0} \right) t + C_G^0, \quad \text{for } 0 \leq t \leq t_0 \\ C_G(t) &= C_G^{\text{ss}}, \quad \text{for } t \geq t_0 \end{aligned} \quad (11.4)$$

These equations may be substituted into [Equation 11.3](#) to obtain algebraic expressions for the islet insulin release rate for a ramp change in the glucose concentration:

$$\begin{aligned} r_{\text{islet}}(t) &= C_p T_1 C_G^0 e^{-t/T_1} + C_p T_1^2 \left( \frac{C_G^{\text{ss}} - C_G^0}{t_0} \right) \left[ \frac{t}{T_1} - \left( 1 - e^{-t/T_1} \right) \right] \\ &\quad + C_p C_G^0 T_1 \left( 1 - e^{-t/T_1} \right) + C_d T_2 \left( \frac{C_G^{\text{ss}} - C_G^0}{t_0} \right) \left( 1 - e^{-t/T_2} \right), \quad \text{for } 0 \leq t \leq t_0 \end{aligned} \quad (11.5)$$

$$\begin{aligned} r_{\text{islet}}(t) &= C_p C_G^0 T_1 e^{-t/T_1} + C_p T_1^2 \left( \frac{C_G^{\text{ss}} - C_G^0}{t_0} \right) \left[ e^{-(t-t_0)/T_1} \left( \frac{t_0}{T_1} - 1 \right) + e^{-t/T_1} \right] \\ &\quad + C_p C_G^0 T_1 \left[ e^{-(t-t_0)/T_1} - e^{-t/T_1} \right] + C_p C_G^{\text{ss}} T_1 \left( 1 - e^{-(t-t_0)/T_1} \right) \\ &\quad + C_d \left( \frac{C_G^{\text{ss}} - C_G^0}{t_0} \right) T_2 \left[ e^{-(t-t_0)/T_2} - e^{-t/T_2} \right], \quad \text{for } t > t_0 \end{aligned} \quad (11.6)$$

[Example 11.3](#) illustrates how the parameters in the Nomura et al. (1984) islet insulin release model may be determined for rat islets through the use of the previous equations.

### Example 11.3

Determine the constants in the Nomura et al. (1984) insulin release model for the rat islet perfusion data shown in [Figure 11.11](#).

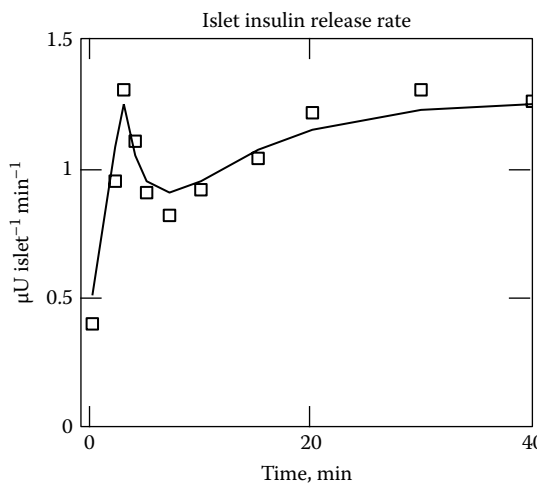


Figure 11.12 Comparison of measured and predicted insulin release rate.

### Solution

A nonlinear regression analysis finds the values of  $T_1 = 10.11$  min,  $T_2 = 1.88$  min,  $C_p = 6.26 \times 10^{-4} \mu\text{U dL mg}^{-1} \text{min}^{-2}$  islet $^{-1}$ , and  $C_d = 0.011 \mu\text{U dL mg}^{-1} \text{min}^{-1}$  islet $^{-1}$  best fit the data shown in Figure 11.11. Figure 11.12 shows that the Nomura model provides an excellent fit to the islet insulin release data.

The actual in vivo response of islets depends not only on glucose levels but also depends in a significant way on the levels of other nutrients such as amino acids and gastrointestinal hormones.\* These latter substances, in the presence of rising glucose levels, can almost double the insulin secretion rate of an islet. However, no quantitative framework is available to describe the effect of these additional secretagogues on the insulin secretion rate.

Under physiological conditions, the variation in plasma glucose levels is less pronounced than a glucose challenge test on islets and the biphasic insulin release pattern is not as evident. In fact, the insulin secretion rate under these conditions displays a strong sigmoidal dependence on the blood glucose levels (Guyton, 1991; Sturis et al., 1991). The insulin secretion rate for the human pancreas saturates at a value of about  $200,000 \mu\text{U min}^{-1}$  when the glucose concentration reaches  $300 \text{ mg dL}^{-1}$ . Since the human pancreas contains about 1 million islets, this saturation insulin release rate is  $0.2 \mu\text{U islet}^{-1} \text{min}^{-1}$ .

Sturis et al. (1991) represented the insulin secretion rate under physiological conditions as a sigmoidal function of the plasma glucose concentration. The following equation proposed by Sturis et al. (1991) can then be used to describe the in vivo insulin response of an islet:

$$r_{\text{islet}} = \frac{0.209}{1 + \exp(-3.33G_B + 6.6)} \quad (11.7)$$

\* Gastrointestinal hormones include gastrin, secretin, cholecystokinin, and gastric inhibitory peptide.

In this equation, the islet insulin release rate is in units of  $\mu\text{U islet}^{-1} \text{ min}^{-1}$  and the glucose concentration ( $G_B$ ) is in  $\text{mg mL}^{-1}$ . For a normal glucose concentration of  $100 \text{ mg dL}^{-1}$ , [Equation 11.7](#) gives a basal insulin release rate of  $0.0077 \mu\text{U islet}^{-1} \text{ min}^{-1}$ . At  $300 \text{ mg dL}^{-1}$ , the islet insulin release rate is  $0.2 \mu\text{U islet}^{-1} \text{ min}^{-1}$ .

#### 11.6.4 Pharmacokinetic modeling of glucose and insulin interactions

Although device testing in experimental diabetic animals provides conclusive proof of a device's efficacy and potential, mathematical models are also useful tools for investigating the myriad parameters that affect device performance. Mathematical models also provide the opportunity to perform scale-up studies. For example, they allow for the critical examination of the results obtained in small laboratory animals and the extrapolation of these results to understand how the device may perform in humans.

Several physiological pharmacokinetic models of glucose and insulin metabolism have been described (Guyton et al., 1978; Sorenson et al., 1982; Berger and Rodbard, 1989; Sturis et al., 1991, 1995; Li et al., 2006; Makroglou et al., 2006; Buchwald, 2011). These models can be combined with an islet glucose-insulin response model, and a device model, to assess quantitatively the level of glucose control that can be achievable (Smith et al., 1991).

The pharmacokinetic model for glucose and insulin metabolism proposed by Sturis et al. (1991, 1995) is particularly attractive because of its relative simplicity and its ability to represent the experimentally observed temporal oscillations of insulin and glucose levels (Kraegen et al., 1972). The secretion of insulin in humans has been found to exhibit two distinct types of periodic oscillations: a rapid oscillation with a period of 10–15 min and a longer or ultradian oscillation with a period of 100–150 min. The rapid oscillations are of small amplitude (insulin  $<1\text{--}2 \mu\text{U mL}^{-1}$  and glucose  $<1 \text{ mg dL}^{-1}$ ) and may be the result of an intrinsic pacemaker in the islets. The ultradian oscillations exhibit a much larger amplitude and are self-sustained when the stimulus is continuously presented, e.g., by a constant infusion of glucose or by continuous enteral glucose feeding. On the other hand, the ultradian oscillations are damped when the glucose stimulus is presented as a discrete event, e.g., by either a meal or ingestion of a fixed quantity of glucose.

[Figure 11.13](#) presents a block diagram of the Sturis et al. (1991) model for describing the interactions between glucose and insulin. This model is based on four negative feedback loops involving interactions between glucose and insulin: (1) elevated glucose levels stimulate the secretion of insulin, and the resulting increase in insulin levels decreases the endogenous production of glucose, which then has the effect of lowering glucose levels; (2) elevated glucose levels stimulate the secretion of insulin, and the resulting increase in insulin levels enhances glucose utilization, which also has the effect of reducing glucose levels; (3) rising levels of glucose inhibit production of glucose; and (4) increasing levels of glucose stimulate its utilization. These four loops control the amount of glucose and insulin in the body. However, because of the nonlinear and dynamic interaction between glucose and insulin, the amounts of these substances in the body are never at a stable equilibrium.

The model also includes two time delays, which are important for describing the observed oscillatory dynamics. The first delay affects the suppression by insulin of glucose production or the recovery of this process when insulin levels decrease. The second delay considers the fact that the biological action of insulin correlates better with the concentration of insulin in an interstitial compartment that equilibrates slowly with the plasma insulin concentration.

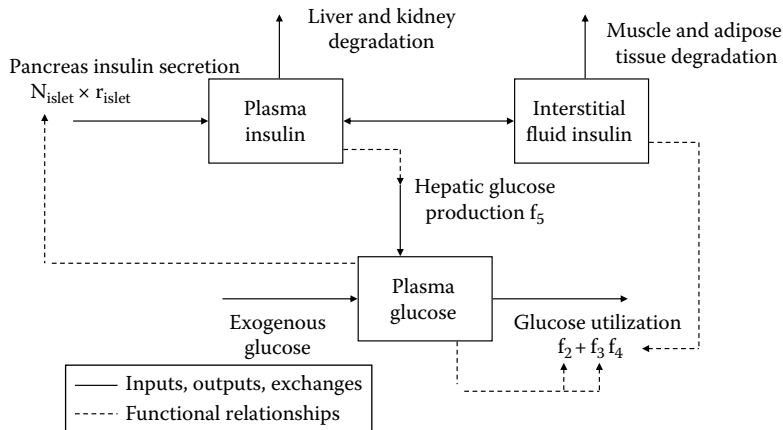


Figure 11.13 Model of glucose and insulin interactions in the body. (After Sturis, J. et al., *Am. J. Physiol.*, 260, E801, 1991.)

The three main variables in the model are the concentration of glucose in the plasma ( $G_B$ , mg mL<sup>-1</sup>), the concentration of insulin in the plasma ( $I_B$ , μU mL<sup>-1</sup>), and the concentration of insulin in the interstitial fluid ( $I_{IF}$ , μU mL<sup>-1</sup>). There are also three additional variables that are introduced to account for the delay between the plasma insulin level and its effect on glucose production ( $x_1$ ,  $x_2$ ,  $x_3$  with time lag  $\tau_d$ ).

A total of six differential equations are needed to describe the state of the system as a function of time (here in minutes). These equations are as follows:

$$\begin{aligned}
 V_{Bi} \frac{dI_B}{dt} &= r_{islet} (G_B) N_{islets} - E(I_B - I_{IF}) - \frac{I_B V_{Bi}}{\tau_p} \\
 \frac{dI_{IF}}{dt} &= E \left( \frac{I_B}{V_{IF}} - \frac{I_{IF}}{V_{IF}} \right) - \frac{I_{IF}}{\tau_i} \\
 V_{Bg} \frac{dG_B}{dt} &= r_{Gin}(t) - f_2(G_B) - f_3(G_B)f_4(I_{IF}) + f_5(x_3) \\
 \frac{dx_1}{dt} &= 3 \frac{I_B V_{Bi} - x_1}{\tau_d}, \quad \frac{dx_2}{dt} = 3 \frac{x_1 - x_2}{\tau_d}, \quad \frac{dx_3}{dt} = 3 \frac{x_2 - x_3}{\tau_d}
 \end{aligned} \tag{11.8}$$

The insulin secretion rate of an islet,  $r_{islet}$ , was given earlier by [Equation 11.7](#) and is multiplied by the number of islets in the pancreas ( $N_{islets}$ ).

The insulin that is released by the islets in the pancreas distributes in the plasma space of volume given by  $V_{Bi}$ , and it also enters the interstitial fluid space represented by the distribution volume  $V_{IF}$ . The insulin transport rate into the interstitial fluid is proportional to the difference in the insulin concentration in the two compartments and is described by a rate constant  $E$ . Insulin is degraded within the plasma space by a first order rate process with a time constant given by  $\tau_p$ . Interstitial insulin enhances glucose utilization as described by the function  $f_4(I_{IF})$ , and interstitial insulin is also degraded with a time constant of  $\tau_i$ .

Glucose is assumed to distribute throughout a single compartment ( $V_{Bg}$ ) and affects its own utilization through the functions  $f_2$  and  $f_3$ . Glucose utilization represented by  $f_2$  is insulin independent, whereas  $f_3$  is multiplied by an additional term  $f_4$  that is dependent on the interstitial insulin concentration. The functions  $f_2$  ( $\text{mg min}^{-1}$ ) and  $f_3 \times f_4$  ( $\text{mg min}^{-1}$ ) are given by the following equations:

$$f_2 = 72[1 - \exp(-6.94G_B)]$$

$$f_3 \times f_4 = 10G_B \times \left[ \frac{90}{1 + \exp\left(-1.772 \ln\left(I_{IF}\left(1 + \frac{V_{IF}}{E\tau_i}\right)\right) + 7.76\right)} + 4 \right] \quad (11.9)$$

Insulin also inhibits the production of glucose by the liver ( $f_5$ ) via a process that is dependent on a time delay ( $\tau_d$ ) between the appearance of insulin in the plasma and its inhibitory effect on glucose production. The function  $f_5$  ( $\text{mg min}^{-1}$ ) is given by the next equation and is dependent on a time-delayed plasma insulin concentration represented by  $x_3$ :

$$f_5 = \frac{180}{1 + \exp\left(\frac{0.29x_3}{V_{Bi}} - 7.5\right)} \quad (11.10)$$

Glucose can enter the body in an arbitrary time-varying fashion as given by the function  $r_{Gin}(t)$  ( $\text{mg min}^{-1}$ ) in [Equation 11.8](#). For example, the glucose input function for a meal, or an *oral glucose tolerance test (OGTT)*, can be described by the following equation that describes the absorption of glucose from the gastrointestinal tract. In this equation,  $D$  ( $\text{mg}$ ) represents the total amount of glucose ingested,  $k_a$  ( $\text{min}^{-1}$ ) is the absorption rate constant, and  $k_e$  ( $\text{min}^{-1}$ ) is the elimination rate constant:

$$r_{Gin}(t) = Dk_e \left( \frac{k_a}{k_a - k_e} \right) (e^{-k_e t} - e^{-k_a t}) \quad (11.11)$$

[Table 11.1](#) summarizes the values of all the parameters used in the model of Sturis et al. (1991). For a given glucose input function, the previous equations can be solved numerically to provide the time course of the plasma glucose and insulin levels.

Table 11.1 Parameter Values for the Sturis et al. Model of Glucose and Insulin Interactions

Parameter	Value
$E$ (rate constant for exchange of insulin between plasma and the interstitial fluid compartment)	$200 \text{ mL min}^{-1}$
$V_{Bi}$ (insulin plasma distribution volume)	$3,000 \text{ mL}$
$V_{IF}$ (insulin interstitial fluid distribution volume)	$11,000 \text{ mL}$
$V_{Bg}$ (glucose plasma distribution volume)	$10,000 \text{ mL}$
$\tau_p$ (time constant for plasma insulin degradation)	$6 \text{ min}$
$\tau_i$ (time constant for interstitial fluid insulin degradation)	$100 \text{ min}$
$\tau_d$ (time delay between plasma insulin and glucose production)	$36 \text{ min}$

Sources: Sturis, J. et al., *Am. J. Physiol.*, 260, E801, 1991; Sturis, J. et al., Phase-locking regions in a forced model of slow insulin and glucose oscillations, in: *Dynamical Disease: Mathematical Analysis of Human Illness*, Belair, J., Glass, L., An der Heiden, U., and Milton, J. (eds.), AIP Press, 1995.

### 11.6.5 Using the pharmacokinetic model to evaluate the performance of a bioartificial pancreas

We can now use the Sturis et al. (1991) pharmacokinetic model outlined in [Section 11.6.4](#), along with an insulin release model for an islet, to explore the level of glucose control that is possible with a bioartificial pancreas. There are two basic types of tests that can be used to measure the level of glucose control. One stringent measure of glucose control that is frequently used is called the k-value. The k-value represents the slope of the least squares fit of the logarithm of the plasma glucose concentration plotted as a function of time for the 50 min following the intravenous administration of a dose of glucose. This glucose dose is typically  $0.5 \text{ g kg}^{-1}$  of body weight and is referred to as an *intravenous glucose tolerance test*, or IVGTT.

Following the glucose dose for the IVGTT, plasma glucose levels rapidly rise within a few minutes to levels exceeding  $300 \text{ mg dL}^{-1}$  from the initial fasting level of around  $80 \text{ mg dL}^{-1}$ . The rate of glucose decay following an IVGTT is indicative of the glucose and insulin responsiveness of the patient's pancreas. The k-value is expressed in units of  $\% \text{ min}^{-1}$ . If the k-value following an IVGTT is less than  $1\% \text{ min}^{-1}$ , then the patient is assumed to have diabetes.

Normal k-values range from about 2 to  $3\% \text{ min}^{-1}$ . A bioartificial pancreas would need to provide a k-value greater than about  $1.5\% \text{ min}^{-1}$  to be considered effective at controlling blood glucose levels in a patient with diabetes. This somewhat lower than normal k-value is acceptable because the IVGTT provides a major glucose challenge that is not normally observed following a meal.

The OGTT involves the oral administration of a beverage containing 50 g of glucose. Glucose levels greater than  $140 \text{ mg dL}^{-1}$  2 h after administration of the glucose may be indicative of diabetes.

The simulation of blood glucose and insulin levels following an IVGTT or an OGTT using the pharmacokinetic model outlined above is straightforward. Assume that the islets are macroencapsulated within a thin sheet and that the immunoisolation membrane of the bioartificial pancreas is the controlling mass transfer resistance for glucose and insulin transport. As shown in [Figure 11.14](#), two well-mixed compartments are used to define the distribution of glucose and insulin within the device and the rest of the body. The distribution of insulin also includes an additional interstitial fluid compartment to account for the delay in its action, as discussed earlier. Unsteady mass balances for glucose and insulin can now be written for each of the compartments.

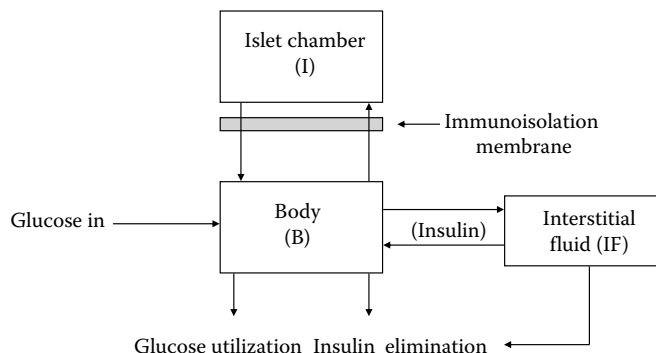


**Figure 11.14** Compartmental model for evaluation of a bioartificial pancreas.

*Islet or cell chamber*

$$\begin{aligned} V_I \frac{dI_I}{dt} &= N_{\text{islets}} r_{\text{islet}} - P_{mI} S_m (I_I - I_B) \\ V_I \frac{dG_I}{dt} &= P_{mG} S_m (G_B - G_I) \end{aligned} \quad (11.12)$$

*Body distribution volume*

$$\begin{aligned} V_{Bi} \frac{dI_B}{dt} &= P_{mI} S_m (I_I - I_B) - E(I_B - I_{IF}) - \frac{I_B V_{Bi}}{\tau_p} \\ V_{Bg} \frac{dG_B}{dt} &= r_{Gin}(t) - P_{mG} S_m (G_B - G_I) - f_2(G_B) - f_3(G_B) f_4(I_{IF}) + f_5(x_3) \end{aligned} \quad (11.13)$$

*Interstitial fluid space for insulin*

$$V_{IF} \frac{dI_{IF}}{dt} = E(I_B - I_{IF}) - \frac{V_{IF} I_{IF}}{\tau_i} \quad (11.14)$$

*Equations for delayed insulin action on glucose production*

$$\frac{dx_1}{dt} = 3 \frac{V_{Bi} I_B - x_1}{\tau_d}, \quad \frac{dx_2}{dt} = 3 \frac{x_1 - x_2}{\tau_d}, \quad \frac{dx_3}{dt} = 3 \frac{x_2 - x_3}{\tau_d} \quad (11.15)$$

For the special case of an IVGTT, the value of  $r_{Gin}(t)$  would be set equal to zero.

The initial conditions for the solution of the above equations for either an IVGTT or an OGTT are based on fasting levels. Fasting plasma glucose levels are typically about 80 mg dL<sup>-1</sup>. Assuming negligible consumption of glucose by the tissue in the bioartificial pancreas, one may reasonably assume that the initial glucose concentration in the bioartificial pancreas is the same as that found in the rest of the body. However, since the IVGTT glucose dose is rapidly distributed throughout the body distribution volume, in comparison to the length of time required for its subsequent removal, we assume that at  $t = 0$  (+), the plasma glucose level is given by the equation below:

$$G_B(t = 0+) = G_B(\text{fasting}) + \frac{500(\text{mg/kg bw}) \times (\text{body weight, kg})}{V_{Bg}} \quad (11.16)$$

Fasting plasma insulin levels are about 10 μU mL<sup>-1</sup>. During the fasting period, we assume that the bioartificial pancreas is at a steady-state equilibrium with the rest of the body as far as insulin is concerned. Accordingly, the islet insulin secretion rate based on the fasting glucose concentration must match the rate of insulin removal from the body. The steady-state solution of the set of

compartmental insulin equations provides the following relationships for the initial insulin concentration in each of the compartments:

$$\begin{aligned} I_B^0 &= \frac{N_{\text{islets}} r_{\text{islet}}^0 (G_B^0) \tau_i}{V_{IF}} \times \frac{1}{\frac{V_{Bi} \tau_i}{V_{IF} \tau_p} - \frac{1}{\frac{V_{IF}}{\tau_i E} + 1}} \\ I_{IF}^0 &= \frac{I_B^0}{\left( \frac{1}{\tau_i E} + \frac{1}{V_{IF}} \right) V_{IF}} \\ I_I^0 &= I_B^0 + \frac{N_{\text{islets}} r_{\text{islet}}^0 (G_B^0)}{P_{ml} S_m} \end{aligned} \quad (11.17)$$

The solution of [Equations 11.12 through 11.17](#) provides the temporal change in the plasma glucose concentration following the administration of either an OGTT or an IVGTT to a patient with a bioartificial pancreas. The above equations can be easily modified to evaluate the glucose control for a variety of bioartificial pancreas approaches. The following example illustrates a prediction of the plasma glucose levels using a bioartificial pancreas following an OGTT.

### Example 11.4

Estimate the glucose concentrations following an OGTT using islets that are macroencapsulated between two immunoisolation membrane disks. A total of 50 g of glucose is taken orally. In [Equation 11.11](#), the glucose absorption rate constant is  $0.042 \text{ min}^{-1}$  and the glucose elimination rate constant is  $0.0083 \text{ min}^{-1}$ . Base the calculation on a 70 kg patient receiving a total of 750,000 EIN. Assume the islet insulin secretion rate is given by [Equation 11.7](#). The half-thickness of the islet chamber is 75  $\mu\text{m}$ . The void volume within the islet chamber must be at least 65% for sufficient oxygen transport. The immunoisolation membrane permeabilities for glucose and insulin are based on the membrane developed by Baker et al. (1997), i.e.,  $4 \times 10^{-4} \text{ cm s}^{-1}$  for glucose and  $8 \times 10^{-5} \text{ cm s}^{-1}$  for insulin.

### Solution

[Figure 11.15](#) provides the solution for the glucose and insulin concentrations as a function of time. Note the damped ultradian oscillations of the glucose and insulin concentrations with time. The bioartificial pancreas provides a glucose and insulin response that is very similar to that observed in normal patients (Kraegen et al., 1972), which shows that the bioartificial pancreas has the potential to restore normoglycemia in patients with diabetes. The size of the device is 18 cm (7 in.) in diameter and only several millimeters in thickness. Rather than one large unit, several smaller units could be implanted. For example, four units each 9 cm (3.5 in.) in diameter would be equivalent. Membranes with better glucose and insulin permeabilities would result in a smaller device.

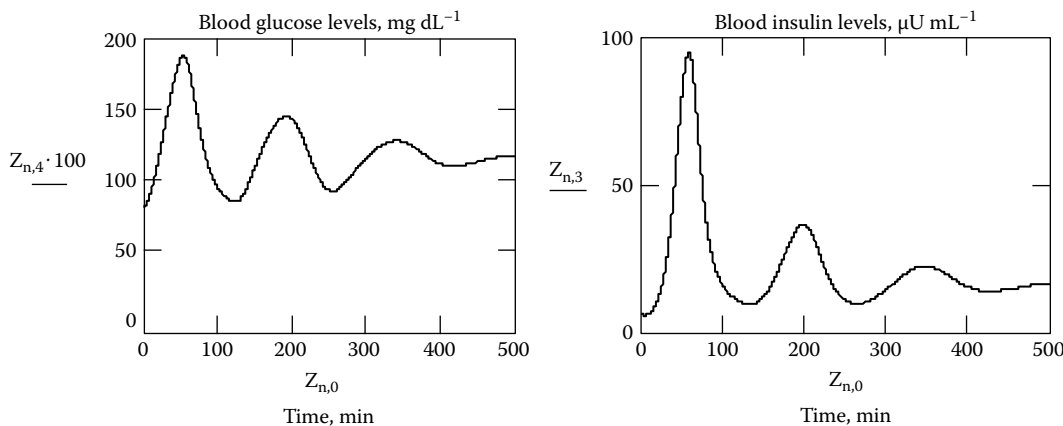


Figure 11.15 Predicted glucose and insulin levels in a bioartificial pancreas following an OGTT.

## 11.7 The bioartificial liver

The liver is a very complex organ that performs a variety of life-sustaining functions (Yarmush et al., 1992; Galletti and Jauregui, 1995; Davidson et al., 2010). These functions include detoxifying the blood, regulating glucose levels, and making a variety of proteins. The human liver weighs about 1500 g and is highly vascularized. From Table 7.3, we see that the liver receives over 25% of the cardiac output. The liver blood supply comes from two major sources. These are the *hepatic artery* and the *portal vein*. The portal vein collects the venous drainage from the spleen, the pancreas, and the intestines. The portal vein input from these regions passes through the liver before entering the rest of the systemic circulation. The liver therefore has the ability to detoxify potentially harmful substances that are absorbed from the gastrointestinal tract.

The basic functional cellular units of the liver are called the *hepatocytes*. Each hepatocyte is about 25  $\mu\text{m}$  in diameter, and there are close to 250 billion of them in the human liver, accounting for 75% of the liver volume. The hepatocytes are metabolically very active and provide an incredible variety of functions. Their role in carbohydrate metabolism includes the storage of excess glucose as *glycogen* and the release of this stored form of glucose (*glycogenolysis*) when blood glucose levels are low. In addition, the liver converts other sugars such as galactose and fructose to glucose. If blood glucose levels are low and the glycogen stores are also depleted, then the liver performs a process known as *gluconeogenesis* wherein glucose is synthesized from amino acids.

The liver also plays a major role in fat metabolism. The liver is principally responsible for the body's ability to derive energy from fats. The liver can also convert excess carbohydrates and proteins into fat, synthesizes cholesterol and phospholipids, and forms the lipoprotein carrier molecules. The lipoproteins are responsible for transporting cholesterol, phospholipids, and fats to other tissues throughout the body. Cholesterol and phospholipids are important components of cellular membranes. The liver has an extremely important role in protein metabolism. These functions include the deamination of amino acids as a prelude to their use as an energy source, or their conversion to carbohydrates or fats. The deamination of amino acids produces large amounts of ammonia. The liver converts the ammonia into urea, which is then excreted by the kidneys. Without this function, ammonia levels in the blood rapidly increase, leading to hepatic coma and death.

With the exception of the gamma globulins (immunoglobulins or antibodies), practically all of the plasma proteins are made in the liver, the most important being *albumin*. The liver also makes most of the substances found in the blood that are responsible for the clotting of blood. These include fibrinogen, prothrombin, and most of the other *clotting factors*. The liver also provides storage for a variety of nutrients such as vitamins and iron, which is stored as a protein complex called *ferritin*. The hepatocytes, because of their high enzyme content, also provide a major role in the detoxification and conjugation of a variety of materials such as drugs, environmental toxins, and hormones that are produced elsewhere in the body. These by-product materials are water soluble and are excreted in the bile or by the kidneys.

The liver has the unique capability of being able to regenerate itself following tissue damage. This is extremely beneficial, considering the role it plays in detoxifying materials from the gastrointestinal tract. However, if the tissue damage rate exceeds the liver's ability to regenerate, then liver failure results, leading to a life-threatening situation. Liver failure accounts for over 60,000 deaths each year in the United States.

There are principally two types of liver failure: *cirrhosis* and *fulminant hepatic failure*. Cirrhosis of the liver accounts for over half of the deaths due to liver disease. In cirrhosis, fibrotic tissue forms in place of the damaged liver tissue severely compromising the liver's ability to regenerate. Common causes of cirrhosis include alcoholism and chronic hepatitis. Fulminant hepatic failure is a rapidly progressing failure of the liver that can lead to death within several weeks of onset. It can be caused by chemical and viral hepatitis.

Liver failure causes a variety of life-threatening abnormalities, including the accumulation of ammonia or bilirubin in the plasma and decreased levels of albumin and clotting factors. There is also a buildup of toxins and overactivity of the hormonal systems that are believed to lead to a condition known as *hepatic encephalopathy* that can cause irreversible brain damage, coma, and death.

The only long-term and relatively successful treatment method for liver failure is transplantation. However, liver transplantation is severely limited by the shortage of donor organs. Many patients therefore die before a liver becomes available, or they succumb shortly after the transplant because of the complications and brain damage associated with liver failure.

### 11.7.1 Artificial liver systems

The treatment of liver failure by artificial means has been the focus of considerable research. **Table 11.2** provides a summary of some of the artificial liver systems that have been evaluated (Yarmush et al., 1992). The primary goal of these artificial liver systems is to provide a means to maintain the patient in a stable state until a liver transplant is possible, or in some cases, artificial

Table 11.2 Artificial Liver Systems

Hemodialysis	Cross circulation
Hemoperfusion	Extracorporeal perfusion
Immobilized enzymes	Cross hemodialysis
Plasma exchange	Hepatocyte hemoperfusion

liver support can provide the liver the chance to regenerate and the patient can return to a normal life without a transplant.

The difficulty in developing an artificial liver is the multitude of functions the liver performs. Initially, it was thought that the best approach is to minimize the buildup of toxins. Accordingly, efforts focused on such approaches as hemodialysis, hemoperfusion, and immobilized enzyme reactors for the removal of these materials.

The *hemodialysis* systems were similar to those used in kidney dialysis, with the exception that they used membranes with a higher molecular weight cutoff to allow the passage of the larger-sized toxic materials. This approach was still not effective at removing large protein-bound toxins. *Hemoperfusion* employed beds of activated carbon that adsorbed the toxic molecules (Ding et al., 2014). A particular problem with this approach is its nonspecificity, removing beneficial substances as well. *Immobilized enzyme reactors* used liver enzymes to provide for a more specific removal of the toxic molecules. The major difficulty is providing a complete set of liver enzymes. These three approaches also suffered from the disadvantage that they do not restore any of the synthetic functions of the liver.

Other approaches that were used attempted to both reduce the level of toxins and restore substances normally synthesized by the liver. These methods included plasma exchange, cross circulation, extracorporeal perfusion, and cross hemodialysis. *Plasma exchange* involves replacing the patient's plasma with donor plasma. Provided the exchange rate is sufficiently high, this approach can replace the lost liver function. However, the major limitation is the large amount of donor plasma needed and the increased risk to the patient of viral infections. *Cross circulation* involved connecting the patient's circulation to that of another human. In this way the healthy liver is shared. However, the risk to the human donor limits the widespread use of this approach. The *extracorporeal perfusion* of the patient's blood through a xenogeneic liver has also been tried. Some success with this approach has been achieved using pig and baboon livers. However, the liver function degrades quickly as a result of the host's immune rejection response. *Cross hemodialysis* attempts to minimize the host's immune response to the donor liver by perfusing the donor liver with a separate supply of blood. This blood is then sent through a hemodialyzer where it is contacted across a dialysis membrane with the patient's own blood. In this way toxins are removed and synthetic substances are added to the patient's blood. The *hemoperfusion of liver tissue* has also been tried. Liver tissue pieces are directly contacted with the patient's blood. Frozen or freeze dried dead tissue was comparable in activity to fresh tissue indicating that only those few layers of cells near the surface of the fresh liver pieces are adequately oxygenated. The dead tissue still contained enzymes with some residual activity.

### 11.7.2 Bioartificial livers

The hemoperfusion of liver tissue pieces is not capable of providing optimal conditions for the long-term function of the liver tissue. In the absence of an intact vasculature, the mass transfer resistances within the liver pieces are just too large for simple diffusion to overcome. Recently, attention has been focused on the development of *bioartificial livers* that are based on the use of isolated hepatocytes (Jauregui et al., 1997; Allen et al., 2001; Legallais et al., 2001; Nose, 2001; Patzer, 2001; Sauer et al., 2001; Kobayashi et al., 2003; Davidson et al., 2010; Lee and Cho, 2012). The use of isolated hepatocytes in a properly designed bioartificial liver has the potential to mimic the synthetic,

metabolic, biliary excretion and detoxifying functions of a normal liver. Isolated hepatocytes are not as severely affected by mass transfer limitations, and furthermore, they can be immunoprotected. The challenge is to design the bioartificial liver so that the isolated hepatocytes can maintain their differentiated functions and continue to detoxify the blood, regulate glucose levels in the body, and synthesize proteins.

Isolated hepatocytes have been proposed for both implantable and extracorporeal systems. Implantable systems are based on the tissue engineering concepts discussed in [Chapter 10](#) and involve the encapsulation of the hepatocytes in a manner similar to the techniques already discussed for islets (Cai et al., 1988; Cima et al., 1991a; Johnson et al., 1994; Yang et al., 1994, Powers et al., 2002).

The hepatocytes can come from primary sources such as from human donors as well as animals like the pig and the rabbit. Alternatively, cell lines based on hepatic tumors and immortalized cells have also been developed. In addition, stem cells and progenitor cells have the potential, given the proper signals, to differentiate into hepatocytes (Lee and Cho, 2012).

The mass of hepatocytes that is needed to treat liver failure is estimated to be on the order of 10%–40% of the original liver mass (Yarmush et al., 1992; Rozga et al., 1994; Davidson et al., 2010). At the low end of this range, this amounts to 25 billion cells or a cellular volume on the order of 200 mL. Attachment to a support structure, or encapsulation of this quantity of cells, while still maintaining a reasonable device volume, is a major obstacle with implantation approaches. For example, for hepatocytes attached to microcarriers,\* the estimated total volume is 500 mL. For microencapsulation within a polymeric capsule, this volume is 2500 mL, whereas macroencapsulation in hollow fibers yields a volume that is estimated to be 1300 mL.

Because of these size constraints, extracorporeal bioartificial livers are an attractive approach for providing temporary liver function until an organ is available for transplantation or the patient's liver can regenerate. The patient's blood or plasma flows through an external circuit that provides contact with the hepatocytes. The hepatocytes can be presented to the patient's blood or plasma in a number of ways. The simplest is as a suspension of cells. However, this provides no immunoprotection, and like most mammalian cells, hepatocytes do better if they are attached to something. In some cases, the suspension of cells can be placed within the shell space of a hemodialyzer and separated from the blood or plasma stream by a dialysis membrane. Although this approach provides immunoprotection, the low molecular weight cutoff of the dialysis membrane severely limits the molecular sizes that can be detoxified or synthesized. Other approaches involve perfusing the patient's blood or plasma through columns packed with microcarrier-attached hepatocytes, or hepatocytes encapsulated within polymeric beads. Hepatocytes attached to microcarriers, however, provide no immunoprotection. Hollow fiber units have also been proposed. In these systems, the hepatocytes are within the shell space and attach themselves to the outer surface of the hollow fibers. Blood or plasma flows through the lumen of the hollow fibers.

One major limitation of the membrane-based approaches discussed so far involves the significant mass transfer resistance created by the presence of the membrane. Solute transport through the membrane and into the space containing the hepatocytes is by diffusion only. This not only limits the supply of

\* A microcarrier is a small particle about 200 µm in diameter, sometimes coated with ECM materials, that provides for cell attachment and formation of a confluent monolayer of cells.

essential nutrients and oxygen to the hepatocytes but also limits the detoxification and biosynthesis rates of the hepatocytes as well. To overcome these membrane diffusional limitations, some bioartificial livers incorporate the perfusion of plasma through the region that contains the hepatocytes.\*

### 11.7.3 Examples of extracorporeal bioartificial livers

**Figure 11.16** illustrates one approach that provides three distinct compartments (Nyberg et al., 1992, 1993a,b). The first compartment consists of a gel-like collagen matrix that traps the hepatocytes within the hollow fiber lumen. The second compartment consists of the space within the lumen of the hollow fiber that results after the contraction of the original collagen suspension containing the hepatocytes. The third compartment is the shell space that surrounds the hollow fibers. The hollow fibers have a nominal molecular weight cutoff of  $100,000 \text{ g mol}^{-1}$  and immunoprotect the hepatocytes from the patient's immune system.

In operation, the patient's blood flows through the shell space. Substances to be detoxified readily diffuse through the hollow fiber membrane and into the collagen gel that contains the hepatocytes. Similarly, substances produced by the hepatocytes diffuse across the membrane and are carried away by the blood to the patient. Of particular note in this system is the presence of the space within the lumen that is formed after the gel contracts. This space provides an additional flow path that allows the simultaneous perfusion of the hepatocytes with specific nutrients, growth factors, and hormones that are needed to maintain their differentiated function and viability. Extracellular matrix (ECM)-type materials can also be incorporated into the gel that contains the hepatocytes. In this way, the hepatocytes can be presented with an optimal culture environment while performing their liver support functions.

In one particular test, this bioartificial liver was evaluated *in vitro* over a period of 7 days. Approximately  $5 \times 10^7$  cells were loaded into the device. Hepatocyte function was evaluated on the basis of albumin production, oxygen consumption, and lidocaine clearance. It is important to point out that unlike the bioartificial pancreas, there is no single measure of differentiated hepatocyte function.

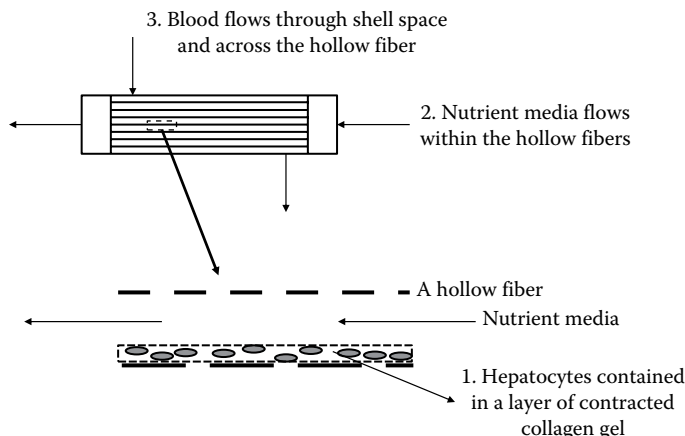


Figure 11.16 A three compartment hollow fiber bioartificial liver. (From Nyberg, S.L. et al., *Biotechnol. Bioeng.*, 41, 194, 1993b.)

\* See [Section 7.9](#) on perfusion bioreactors..

However, albumin was steadily produced during the 7-day period at rates comparable to that seen in static cultures. Furthermore, oxygen consumption remained relatively constant following an initial decline over the first two days of culture. This initial decrease in the oxygen consumption, although possibly being related to cell death, was also considered to be a result of the increased metabolic demands on the hepatocytes as a result of the trauma during their isolation and placement in a new environment.

The cytochrome P-450 system (Hantsen, 1998) is a major pathway for the biotransformation in the liver of many substances and is an important function that must be provided by a bioartificial liver. Lidocaine clearance can be used as a measure of oxidative metabolism provided by the cytochrome P-450 system. Lidocaine clearance in this bioartificial liver was relatively constant, and the presence of lidocaine metabolites demonstrated that lidocaine biotransformation was occurring. Electron micrographs after 7 days of operation showed the presence of differentiated viable hepatocytes.

**Figure 11.17** illustrates an extracorporeal bioartificial liver system known as HepatAssist that consists of several integrated components (Giorgio et al., 1993; Rozga et al., 1993, 1994; Jauregui et al., 1997). A plasmapheresis unit is first used to form a plasma stream from arterial blood. This plasma stream feeds into a high flow plasma recirculation loop that forms the core of the bioartificial liver support system. Within the recirculation loop, plasma first enters a column loaded with activated cellulose-coated charcoal. The activated charcoal column is used to enhance the detoxification capability of the overall system and to protect the hepatocytes from any toxic materials found in the patient's plasma. The detoxified plasma then enters a membrane oxygenator. This ensures an adequate supply of oxygen to maintain the viability and function of the hepatocytes. The oxygenated plasma then flows through the hollow fiber module that contains the hepatocytes. The plasma flows through the hollow fiber lumens, and the hepatocytes are in the shell space that surrounds the hollow fibers. Plasma exiting the hollow fiber cartridge is then recombined with the cellular components of the blood and returned to the patient's body.

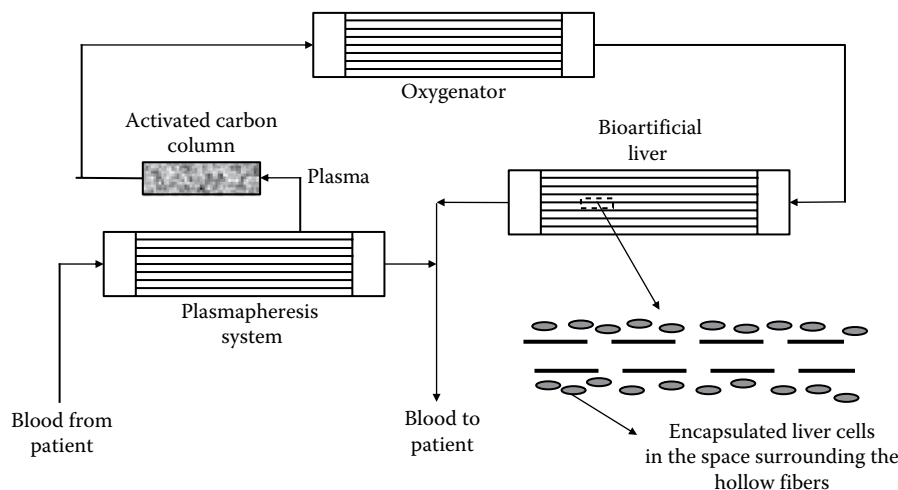


Figure 11.17 Components of the HepatAssist bioartificial liver. (From Jauregui, H.O. et al., Extracorporeal artificial liver support, in: *Principles of Tissue Engineering*, Lanza, R.P., Langer, R., and Chick, W.L. (eds.), R.G. Landes Co., 1997, pp. 463–479.)

The hepatocytes within the bioartificial liver cartridge are attached to collagen-coated microcarrier beads that occupy the shell space. About six billion porcine hepatocytes are used. The hollow fibers have large pore sizes ( $0.2\text{ }\mu\text{m}$ ) that allow for significant fluid convection through the hollow fiber membrane as a result of the transfiber pressure drop. From the fiber entrance to its midpoint, there is a significant flow of plasma out of the hollow fiber and into the shell space that contains the anchored hepatocytes. From the fiber midpoint to the fiber exit, this flow reverses itself and reenters the fiber lumen. This is much like the Starling flow phenomena discussed in [Chapter 3](#) for capillaries. This convective flow into the shell space passes freely between the microcarrier beads that contain the hepatocytes on their surfaces. This convective flow through the shell space provides for very efficient contacting of the plasma solutes and the hepatocytes, and far surpasses what is achievable by diffusion alone.

One limitation of the approach shown in [Figure 11.17](#) is the lack of complete immunoisolation of the xenogeneic porcine hepatocytes. Plasma perfusion eliminates the cellular components of the immune system; however, antibodies and complement will readily flow across the membrane and into the shell space that contains the hepatocytes. However, the treatment time proposed for this device is relatively short, and the patient is immunosuppressed in anticipation of a liver transplant. So the trade-off between a high transmembrane flow resulting in good mass transport and the resultant permeability to the humoral components of the immune system seems appropriate. Certainly, longer-term use of this device will require improved methods of immunoisolation that do not compromise the mass transport properties of the hepatocyte bioreactor.

[Figure 11.18](#) illustrates the extracorporeal liver assist device, or ELAD (Sussman et al., 1992; Kelly and Sussman, 1994). This is a hollow fiber device that uses a cloned human cell line in place of hepatocytes. The cell line is derived from a hepatoblastoma and selected for liver-specific functions.

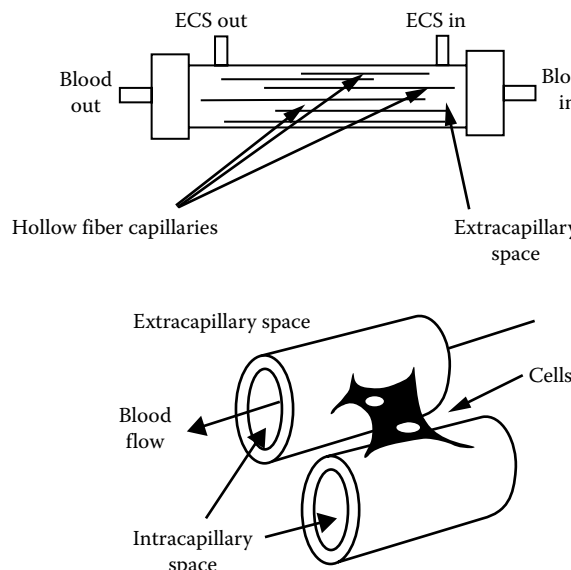


Figure 11.18 The extracorporeal liver assist device (ELAD). (From Sussman, N.L. et al., *Hepatology*, 16, 60, 1992. With permission.)

These cells exhibit the ability to synthesize protein, urea, and glucose and are capable of detoxifying substances via the cytochrome P-450 system. The use of a human cell line provides an unlimited supply of cells and minimizes the immune problems that may result from the use of xenogeneic hepatocytes. The ELAD is seeded with 2 g of cells and is placed in culture until 200 g of cells are obtained. This quantity of cells is capable of producing therapeutic levels of plasma proteins. For example, 5 g of albumin are produced each day, which is about one-half the normal daily production rate of a healthy adult human liver.

Blood flows from the patient's vein through a standard hemodialysis pump. The blood exiting the pump is mixed with heparin to prevent blood clots and then passes through the lumen of the hollow fibers of the ELAD device. A portion of the blood flowing through the hollow fibers forms a plasma ultrafiltrate that perfuses the shell space where it comes into direct contact with the cells. The ultrafiltration of the blood allows the delivery of higher molecular weight solutes at rates significantly higher than that possible by diffusion alone. The ultrafiltrate, then passes through a 0.45  $\mu\text{m}$  filter before it is returned to the patient.

An evaluation of this device in dogs with fulminant hepatic failure provided rapid improvement in blood chemistry. There was also a rapid rise in plasma human albumin and  $\alpha$ -fetoprotein levels following the connection of the device. Factor V-dependent clotting times showed a corresponding rapid decrease. After 48 h of treatment, the dogs with fulminant hepatic failure have sufficiently recovered that they can be disconnected from the device. Compared to control animals that die, the treated animals regenerated their own livers.

To overcome some of the transport limitations of the bioartificial liver devices described above, a novel approach has been developed that uses three separate hollow fiber membrane bundles (Sauer et al., 2001; Schmelzer et al., 2009). As shown in [Figure 11.19](#), the hepatocytes are distributed throughout the complex 3D extracapillary space formed by these three sets of hollow fiber bundles. Two sets of these hollow fiber bundles contain hydrophilic membranes with a NMWCO of about

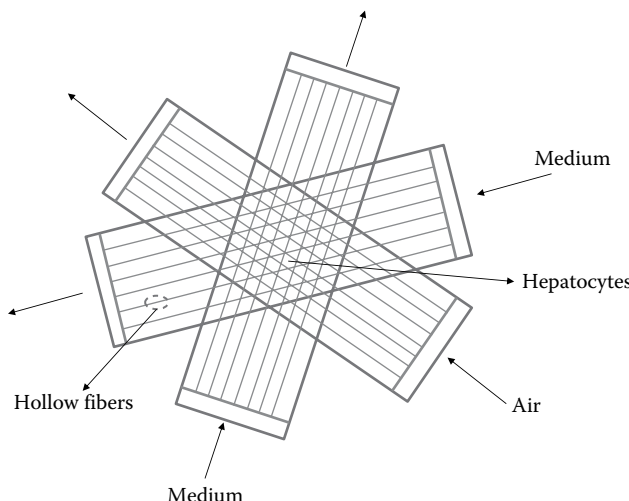


[Figure 11.19](#) A bioartificial liver comprising three bundles of hollow fiber membranes. (From Schmelzer, E. et al., *Biotechnol. Bioeng.*, 103, 817, 2009.)

300,000 g mol<sup>-1</sup>. One end of each bundle is closed off, thus making the plasma that enters the bioreactor in the first hollow fiber bundle flow into the extracapillary space before exiting the bioreactor through the second hollow fiber bundle. The hollow fibers in the third bundle are hydrophobic and are used to supply oxygen and remove carbon dioxide. The unique arrangement of these three hollow fiber bundles provides a means for plasma perfusion of the extracapillary space containing the hepatocytes while also providing for the efficient transport of oxygen. This bioartificial liver containing human hepatocytes has been successfully used as a bridge to transplant in patients suffering from liver failure.

### Example 11.5

As part of the design of a bioartificial liver, there is a hollow fiber membrane cartridge that first treats the plasma with a mix of immobilized enzymes to remove any toxic components that are in the plasma. The plasma to this device comes from a plasmapheresis unit that separates a portion of the plasma from the patient's blood. The immobilized enzyme particles are in the shell space that surrounds the hollow fibers. The plasma therefore flows within the hollow fibers. The plasma flow rate to the device is 250 mL min<sup>-1</sup>, and there are 6500 hollow fibers in the device. The inside diameter of the hollow fibers is 400 µm. These fibers are microporous and have a very high solute permeability. The enzyme loading in the shell space is quite large, and the enzyme reactions may be considered to be very fast in comparison to the mass transfer processes. Hence, it is reasonable to assume that the concentration of any toxic material in the plasma is zero at the inside surface of the hollow fibers. For a target toxin having a molecular weight of 300 g mol<sup>-1</sup>, the diffusivity of this solute in the plasma would be about  $4.6 \times 10^{-6}$  cm<sup>2</sup> s<sup>-1</sup>. If the hollow fibers are 25 cm in length, estimate the fractional removal of this toxin from this device. Assume the density of the plasma is 1.024 g cm<sup>-3</sup> and the viscosity is 1.2 cP.

### Solution

We assume the plasma flow is evenly distributed to the hollow fibers. Also, that the conversion of the toxic material is the same for each fiber. Hence, we can focus on just one hollow fiber. The plasma flow rate for each fiber is therefore equal to  $6.41 \times 10^{-4}$  cm<sup>3</sup> s<sup>-1</sup>. From this value of the flow rate, we find that the average plasma velocity within the hollow fiber is 0.51 cm s<sup>-1</sup>. Using this average velocity, we calculate a Re = 1.74, which means the plasma flow is laminar within the hollow fiber. We also find that the Sc = 2604. We can calculate the change in the toxin concentration within the hollow fiber using [Equation 5.160](#) with C<sub>AS</sub> = 0:

$$\frac{C_A^{\text{out}}}{C_A^{\text{in}}} = \exp\left(-\frac{4 k_m L}{V_{\text{average}} d_{\text{tube}}}\right)$$

Next, we calculate k<sub>m</sub> using [Equation 5.169](#) and obtain Sh = 4.36 and k<sub>m</sub> =  $5.01 \times 10^{-4}$  cm s<sup>-1</sup>. The fractional removal of the toxin is given by

$$\text{Fraction removed} = 1 - \frac{C_A^{\text{out}}}{C_A^{\text{in}}} = 1 - \exp\left(-\frac{4 \times 5.01 \times 10^{-4} \text{ cm s}^{-1} \times 25 \text{ cm}}{0.51 \text{ cm s}^{-1} \times 0.04 \text{ cm}}\right) = 1 - 0.0858$$

$$\text{Fraction removed} = 0.9142$$

## 11.8 The bioartificial kidney

Another potential area for the application of bioartificial organ technology is in the development of a bioartificial kidney also known as renal replacement therapy (Ip and Aebischer, 1989; Cieslinski and Humes, 1994; Humes, 1995, 1997; Fissell et al., 2001, 2009, 2013; Attanasio et al., 2016; Poornajad et al., 2016). Patients with end-stage renal disease can be treated for many years either by hemodialysis or by the newer technique of *continuous ambulatory peritoneal dialysis*. However, these are not permanent solutions, and these patients ultimately require a kidney transplant in order to survive. The mortality on an annualized basis for hemodialysis patients with end-stage renal disease is about 13%, whereas in age-matched patients that receive a kidney transplant, the annual mortality is 4% (Fissell et al., 2001). This data shows that a normal or transplanted kidney provides physiologic functions that are not provided by hemodialysis.

The kidney not only provides a filtration and waste removal function but also provides several other important functions that are important to the metabolic, immune, and endocrine systems of the body. For example, *erythropoietin* is released by specialized cells found in the kidney in response to hypoxia. Erythropoietin is a major stimulus for the production of red blood cells in the bone marrow. Uremic patients therefore suffer from *anemia*. Low blood pressure causes the release of *renin* from the juxtaglomerular cells that are found in the kidney. Renin initiates the formation of *angiotensin II*, a potent vasoconstrictor, that results in an increase in blood pressure. Angiotensin II also acts on the kidneys, decreasing the excretion of both salt and water. This expands the extracellular fluid volume with the result that the blood pressure is increased. The kidneys are also responsible for the conversion of vitamin D into a substance\* that promotes the absorption of calcium from the intestine. Without this substance, the bones become severely weakened because of the loss of calcium. These other very important functions that are performed by the healthy kidney are therefore compromised as a result of kidney failure.

As shown earlier in [Figure 8.3](#), the functional unit of the kidney is called the nephron. Recall that it consists of two major components, the glomerulus and the renal tubule. The glomerulus is responsible primarily for the selective ultrafiltration of waste products from the blood. It must perform this waste removal function and at the same time retain essential blood components such as albumin. The glomerular filtrate that is formed then passes through the various segments of the renal tubule. The specialized segments of the renal tubule regulate the amount of urine that is formed and its final solute composition. The renal tubule cells therefore have the ability to control both the fluid reabsorption rate and the transport rate of an individual solute. This is accomplished in such a manner so as to maintain homeostasis with regard to the body's fluid volume and overall composition. Because of the chemical sensing and selective transport ability of the renal tubule, it is unlikely that this sophisticated function could ever be reproduced artificially. Accordingly, artificial kidneys or hemodialyzers will primarily function at the level of simply removing waste products by dialysis.

A bioartificial kidney has the potential of reproducing many of the homeostatic, regulatory, and endocrine functions that are performed by the healthy kidney. This would far surpass the filtration function of existing dialysis systems and allow blood purification to occur in a more physiologic fashion. A bioartificial kidney consists of two main components, an artificial glomerulus and a bioartificial renal tubule (Ip and Aebischer, 1989; Fissell et al., 2001; Humes et al., 2004). The artificial

\* 1,25-dihydroxycholecalciferol.

glomerulus can be fabricated from polymeric membranes or the newer silicon nanopore membranes that have a high hydraulic conductance (Fissell et al., 2009, 2013). The transmembrane pressure gradient can be controlled to provide the desired bulk flow rate of plasma across the membrane. This bulk flow, or ultrafiltration of the plasma, will also provide for significant convective transport of solutes across the membrane. The convective transport of all solutes will be essentially the same up to the molecular weight cutoff of the membrane. This is especially important for the larger size solutes where much more can be removed by convection than by simple diffusion. The artificial glomerular membranes can be configured as hollow fibers or in the case of silicon nanopore membranes as flat sheets. The major requirement being that the membrane arrangement is conducive to the production of a significant ultrafiltration (UF) flow.

Several problems still need to be addressed with regard to the fabrication of an artificial glomerulus. These include uncontrolled bleeding as a result of anticoagulation, a decreased ultrafiltration rate over time as a result of protein deposition in the membrane, and the challenge of developing a nonthrombogenic membrane. One exciting possibility for overcoming the clotting tendency of most polymeric materials is to cover the blood-contacting surfaces with a monolayer of autologous endothelial cells. Endothelial cells form the blood-contacting lining of the body's blood vessels and in the absence of injury are responsible for preventing the blood from clotting.

The bioartificial renal tubule would consist of viable renal epithelial cells supported within a tubular structure such as a hollow fiber membrane. These renal tubule cells can be obtained from the renal proximal tubule since it is this section of the renal tubule that reclaims the majority of the water, salt, glucose, amino acids, and other species that are filtered from the glomerular capillaries (Fissell et al., 2001).

Another possibility for creating a renal tubule is to use renal tubule stem cells (Cieslinski and Humes, 1994; Humes and Cieslinski, 1992). *Stem cells* are a class of highly proliferative cells that give rise to cells that have a differentiated function. The resulting differentiated cells provide the ultimate physiologic structure and function found in the body's tissues and organs. Perhaps the best-known class of stem cells is the *pluripotent hemopoietic stem cells* (PHSC) (Koller and Palsson, 1993) that are responsible for the formation of all the differentiated cells found in blood. The differentiated cells arising from the PHSC consist of the red blood cells, white blood cells, and platelets. In many cases the terminally differentiated state of the cell is incapable of reproducing. Therefore, the stem cell has the responsibility of producing and replacing those terminally differentiated cells that have become damaged or injured for a variety of reasons. For example, renal tubule stem cells would regenerate renal tubules following their injury. In the presence of the proper growth factors, renal tubule stem cells have the capability to form tubule-like structures in culture. The isolation and culture of human renal tubule stem cells could therefore be an important source of tissue for the formation of bioartificial renal tubules.

Figure 11.20 shows the extracorporeal hemoperfusion system described by Fissell et al. (2001) and Humes et al. (2004). In experiments performed on nephrectomized dogs, venous blood is pumped through a standard hollow fiber dialyzer or hemofilter (artificial glomerulus). The ultrafiltrate that is formed on the shell side of the hemofilter is then pumped through the luminal space of a hollow fiber cartridge (artificial proximal tubule), which they called the renal assist device (RAD). The blood leaving the hemofilter flows through the extracapillary space of the RAD. Proximal tubule cells line the luminal surface of the hollow fibers in the RAD providing for reabsorption into the blood of about

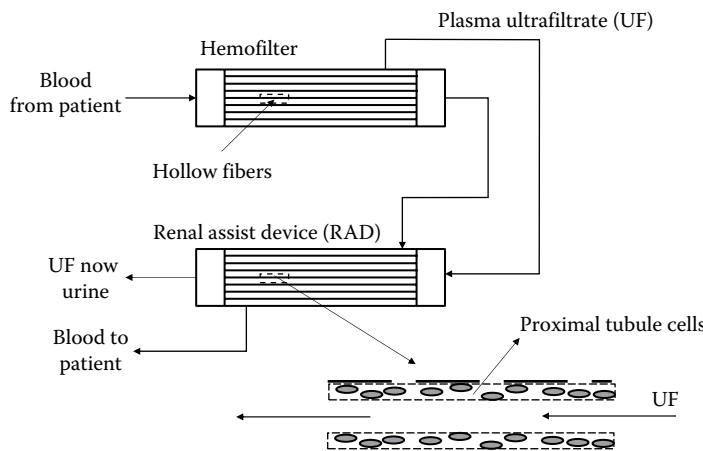


Figure 11.20 A bioartificial kidney. (From Fissell, W.H. et al., *Ann. NY Acad. Sci.*, 944, 284, 2001; Attanasio, C. et al., *Tissue Eng.*, 22, 330, 2016.)

50% of the hemofilter ultrafiltrate. The ultrafiltrate flow to the RAD cartridge is controlled by adjusting the pressure difference between the luminal and extracapillary sides of the RAD cartridge. The luminal effluent from the RAD cartridge is the urine, and the blood leaving the extracapillary space of the RAD cartridge is returned to the body. The system shown in Figure 11.20 is currently being evaluated in clinical trials in humans with acute renal failure and multiorgan failure (Humes et al., 2004).

There is also much interest in the production of whole kidneys using tissue engineering concepts (Attanasio et al., 2016; Poornejad et al., 2016). These approaches use organ-shaped scaffolds that are made from whole kidneys that have been stripped of their cells using special detergents leaving behind a biologically derived scaffold, ECM components, and vasculature that can then be reseeded with the appropriate types of cells. The goal is to bioengineer a functional whole kidney.

## 11.9 Design considerations for bioartificial organs

The design of a bioartificial organ is based on the mass transfer principles outlined in Chapters 5 through 7 as well as the reactor design principles described in Section 9.6. The design of a bioartificial organ must provide sufficient cell mass to effect the desired physiological response in the patient. Furthermore, the proposed design must allow for the efficient transport of key nutrients and the removal of any waste products. In most cases, the limiting nutrient is oxygen and the device design must be capable of transporting oxygen to all of the cells (Davidson et al., 2010).

### Example 11.6

A perfusion bioreactor is being designed to contain hepatocytes for the treatment of liver failure. The bioreactor will consist of thin rectangular microflow channels with the hepatocytes encased within a gel-like material that coats the surfaces of the walls of the microflow channel.

Assume the cell fraction of the hepatocytes in the gel-like layer is 0.65 and that the  $pO_2$  of the perfusion fluid flowing through the microflow channel is 95 mmHg. The gel itself has a negligible effect on the diffusivity of oxygen, and the hepatocytes consume oxygen at the rate of  $35 \mu\text{M s}^{-1}$ . What is the maximum thickness of the gel-like layer of hepatocytes? Assume the value of  $H_{O_2}$  is  $0.74 \text{ mmHg } \mu\text{M}^{-1}$ .

### Solution

The situation that is described is similar to the discussion found in [Section 7.8](#) for oxygen transport in tissue engineered constructs and bioartificial organs. In this case, we can use [Equation 7.26](#) to describe the oxygen profile in the cell containing gel-like material that coats the walls of the flow channel. This equation can be solved for the maximum thickness ( $\delta$ ) assuming the  $pO_2$  is 0 mmHg at the interface between the gel layer and the wall of the flow channel, i.e., at  $x = \delta$ . [Equation 7.26](#) can then be written as shown below:

$$pO_2(\delta) = pO_2^{x=0} + \left[ \frac{\Gamma_{\text{oxygen}} H_{\text{oxygen}} \phi \delta^2}{2 D_T} \right] (-1)$$

Assuming the perfusion fluid has a negligible change in  $pO_2$  and that there is no mass transfer resistance between the flowing perfusion fluid and the surface of the gel-like material, then  $pO_2^{x=0} = 95 \text{ mmHg}$ . The diffusivity of oxygen in the tissue is assumed to be equal to  $2.41 \times 10^{-5} \text{ cm}^2 \text{ s}^{-1}$  (Bentley et al., 1993). Solving the previous equation results in a value of  $\delta = 165 \mu\text{m}$ .

## Problems

- 11.1** Prepare a paper and presentation that describes a specific application of a bioartificial organ. Include a description of the clinical need, the approach used, results that have been obtained (in vitro, in animals, and the status of any clinical trials), the potential clinical impact, the potential market impact, safety issues, and additional development needs.
- 11.2** In [Example 11.1](#), the hindered diffusion model of Bungay and Brenner (1973) was used to estimate the effective pore size of the hollow fiber immunoisolation membrane based on the measured solute permeabilities. This hindered diffusion model provides at best a semiquantitative description of the membrane's solute permeability. Discuss factors that may impact the ability of the hindered diffusion model to describe solute permeability data in immunoisolation membranes.
- 11.3** Baker et al. (1997) developed an immunoisolation membrane by incorporating a high water content polyvinyl alcohol (PVA) hydrogel into a thin disk-shaped microporous polyethersulfone (PES) filter. The PES filter had a thickness of 150  $\mu\text{m}$ , a porosity of 81%, and a mean pore size of 0.2  $\mu\text{m}$ . The hydrogel formed in the pores of the microporous membrane was found to contain 86% water by weight. The 0.2  $\mu\text{m}$  pores of the microporous membrane should block the cellular components of the immune system, and the PVA hydrogel through control of the PVA cross-linking can be tailored to control the passage of high molecular weight solutes. The table below summarizes the physical properties of the solutes that were used and their measured permeability in this composite membrane.

Solute	Molecular Weight	Solute Radius, nm	$D \times 10^6, \text{cm}^2 \text{s}^{-1}, 23^\circ\text{C}$	$P_m \times 10^8, \text{cm s}^{-1}$
Glucose	180	0.36	6.38	40,000
Vitamin B12	1,355	0.75	3.10	16,000
Inulin	5,500	1.41	1.65	8,000
Lysozyme	14,500	1.92	1.22	80
Myoglobin	16,890	1.9	1.21	70
Chymotrypsinogen	25,000	2.24	1.04	60
Ovalbumin	45,000	2.73	0.851	25
Albumin	69,000	3.55	0.655	4
IgG	160,000	5.35	0.434	4.5
Blue dextran	2,000,000	9.26	0.251	0.5

Source: Baker, A.R. et al., *Cell Transplant.*, 6, 585, 1997.

What is the effective pore size of the composite membrane based on the hindered diffusion model? An alternative model for solute diffusion through this composite membrane can be based on the methods outlined in Chapter 6 for gels. In this case, the solute moves through a random fibrous network consisting of the cross-linked polymer chains of the PVA hydrogel. Use Equations 6.47 and 6.48 to describe the solute permeability results.

- 11.4 It is estimated that perhaps as many as 500,000 patients with diabetes could benefit from a bioartificial pancreas. Assuming that each patient needs about 1 million islets and that the islets need to be replaced each year, then about 1000 pancreatic islet isolations need to be performed each day to meet this demand for islets. Prepare a report that describes a process for the massive isolation of islets of Langerhans from the pancreas of a large mammal such as a dog or a pig. Be sure to describe any safety issues. The references should first be consulted for an assessment of the current state of islet isolation methods for a single pancreas.
- 11.5 Derive an expression for the steady-state islet insulin secretion rate based on the Nomura et al. (1984) model.
- 11.6 Derive Equations 11.5 and 11.6 for the islet insulin release rate following a step change in the glucose concentration.
- 11.7 The following perfusion data was obtained by Lakey et al. (1996) for canine islets of Langerhans. The islets were challenged with glucose that was initially at  $50 \text{ mg dL}^{-1}$  followed by a prompt increase to  $500 \text{ mg dL}^{-1}$ . Use the Nomura et al. (1984) islet insulin release model to describe these data.

Time, min	Islet Insulin Release Rate, $\mu\text{U islet}^{-1} \text{min}^{-1}$
0	0.10
5	0.83
8	0.75
28	0.61
50	0.68
60	0.50

- 11.8 Use the Sturis et al. (1991, 1995) pharmacokinetic model for glucose and insulin to describe an OGTT for a normal person. How do the normal person glucose and insulin profiles compare to those obtained in [Example 11.3](#) using a bioartificial pancreas?
- 11.9 Repeat [Example 11.3](#) assuming a 70 kg patient receives an IVGTT. What is the k-value?
- 11.10 Repeat [Example 11.3](#) assuming the islets are macroencapsulated in the hollow fibers described in [Example 11.2](#). These hollow fiber membranes have a nominal external diameter of 950  $\mu\text{m}$ . What is the entire length of fibers needed?
- 11.11 For the device described in [Example 11.3](#), the oxygen permeability of the membrane is estimated to be  $0.001 \text{ cm s}^{-1}$ . Show that the maximum volume fraction of the islets is 0.35.
- 11.12 Repeat [Example 11.3](#) assuming the half-thickness of the device is 350  $\mu\text{m}$ . The membrane oxygen permeability is estimated to be  $0.001 \text{ cm s}^{-1}$ . How are the glucose and insulin profiles affected by a change in device thickness? What volume fraction of islets is allowable based on oxygen transport limitations?

# References

- Abbas, M. and V.P. Tyagi. 1987. Analysis of a hollow fiber artificial kidney performing simultaneous dialysis and ultrafiltration. *Chem. Eng. Sci.*, 42: 133–142.
- Agrawal, C.M., G.G. Niederauer, and K.A. Athanasiou. 1995. Fabrication and characterization of PLA-PGA orthopedic implants. *Tissue Eng.*, 1: 241–252.
- Alberts, B., D. Bray, J. Lewis, M. Raff, K. Roberts, and J.D. Watson. 1989. *Molecular Biology of the Cell*, 2nd ed. New York: Garland Publishing, Inc.
- Al-Hendy, A., G. Hortelano, G.S. Tannenbaum, and P.L. Chang. 1995. Correction of the growth defect in dwarf mice with nonautologous microencapsulated myoblasts—An alternate approach to somatic gene therapy. *Hum. Gene Ther.*, 6: 165–175.
- Allen, J.W. and S.N. Bhatia. 2003. Formation of steady state oxygen gradients in vitro: Application to liver zonation. *Biotechnol. Bioeng.*, 82: 253–262.
- Allen, J.W., T. Hassanein, and S.N. Bhatia. 2001. Advances in bioartificial liver devices. *Hepatology*, 34: 447–455.
- Al-Malah, K.I. 2013. Evaluation of mass transfer coefficient of gas absorption into falling liquid film. *Chem. Eng. Process Technol.*, 1: 1018–1024.
- Altman, J.J., D. Houlbert, P. Callard, P. McMillan, B.A. Solomon, J. Rosen, and P.M. Galletti. 1986. Longterm plasma glucose normalization in experimental diabetic rats with microencapsulated implants of benign human insulinomas. *Diabetes*, 35: 625–633.
- Ameer, G.A., W. Harmon, R. Sasisekharan, and R. Langer. 1999a. Investigation of a whole blood fluidized bed Taylor-Couette flow device for enzymatic heparin neutralization. *Biotechnol. Bioeng.*, 62: 602–608.
- Ameer, G.A., S. Raghavan, R. Sasisekharan, W. Harmon, C.L. Cooney, and R. Langer. 1999b. Regional heparinization via simultaneous separation and reaction in a novel Taylor-Couette flow device. *Biotechnol. Bioeng.*, 63: 618–624.
- American Diabetes Association. 1993. Position Statement. Implications of the diabetes control and complications trial. *Diabetes*, 42: 1555–1558.
- Ananthaswamy, V., R. Shanthakumari, and M. Subha. 2014. Simple analytical expressions of the nonlinear reaction diffusion process in an immobilized biocatalyst particle using the new homotopy perturbation method. *Rev. Bioinformatics Biometrics*, 3: 22–28.
- Anderson, J.M. 1994. The extracellular matrix and biomaterials. In *Implantation Biology*, R.S. Greco (ed.), pp. 113–130. Boca Raton, FL: CRC Press, Inc.
- Anderson, J.L. and J.A. Quinn. 1974. Restricted transport in small pores. *Biophys. J.*, 14: 130–149.
- Aris, R. 1957. On shape factors for irregular particles—I. The steady state problem. Diffusion and reaction. *Chem. Eng. Sci.*, 6: 262–268.
- Armer, T.A. and T.R. Hanley. 1986. Characterization of mass transfer in the hollow fiber artificial kidney. *Chem. Eng. Commun.*, 47: 49–71.
- Arnold, F. and D.C. West. 1991. Angiogenesis in wound healing. *Pharmacol. Therapy*, 52: 407–422.
- Arpaci, V.S. 1966. *Conduction Heat Transfer*. Reading, MA: Addison-Wesley.
- Atkinson, M.A. and N.K. MacLaren. 1990. What causes diabetes? *Sci. Am.*, July: 62–71.
- Attanasio, C., M.T. Latancia, L.E. Otterbein, and P.A. Netti. 2016. Update on renal replacement therapy: Implantable artificial devices and bioengineered organs. *Tissue Eng.*, 22: 330–340.
- Babensee, J.E., L.V. McIntire, and A.G. Mikos. 2000. Growth factor delivery for tissue engineering. *Pharm. Res.*, 17: 497–504.

## References

---

- Bailey, J.E. and D.F. Ollis. 1986. *Biochemical Engineering Fundamentals*, 2nd ed. New York: McGraw-Hill.
- Baker, A.R., R.L. Fournier, J.G. Sarver, J.L. Long, P.J. Goldblatt, J.M. Horner, and S.H. Selman. 1997. Evaluation of an immunoisolation membrane formed by incorporating a polyvinyl alcohol hydrogel within a microporous filter support. *Cell Transplant.*, 6: 585–595.
- Bale, S.S., L. Moore, M. Yarmush, and R. Jindal. 2016. Emerging in vitro liver technologies for drug metabolism and inter-organ interactions. *Tissue Eng.*, 22: 1–12.
- Barbee, J.H. and G.R. Cokelet. 1971a. Prediction of blood flow in tubes with diameters as small as 29 $\mu$ . *Microvasc. Res.*, 3: 17–21.
- Barbee, J.H. and G.R. Cokelet. 1971b. The Fahraeus effect. *Microvasc. Res.*, 3: 6–16.
- Bartlett, S.T., J.F. Markmann, P. Johnson, O. Korsgren, B.J. Hering, D. Scharp, T.W.H. Kay et al. 2016. Report from IPITA-TTS opinion leaders meeting on the future of  $\beta$ -cell replacement. *Transplantation*, 100: S1–S44.
- Bass, L. and S. Keiding. 1988. Physiologically based models and strategic experiments in hepatic pharmacology. *Biochem. Pharmacol.*, 37: 1425–1431.
- Bawa, R., R.A. Siegel, B. Marasca, M. Karel, and R. Langer. 1985. An explanation for the controlled release of macromolecules from polymers. *J. Control. Release*, 1: 259–267.
- Bazilevsky, A.V., K.G. Kornev, A.N. Rozhkov, and A.V. Neimark. 2003. Spontaneous absorption of viscous and viscoelastic fluids by capillaries and porous substrates. *J. Colloid Interface Sci.*, 262: 16–24.
- Beauchamp, P., W. Moritz, J.M. Kelm, N.D. Ullrich, I. Agarkova, B.D. Anson, T.M. Suter, and C. Zuppinger. 2015. Development and characterization of a scaffold-free 3D spheroid model of induced pluripotent stem cell-derived human cardiomyocytes. *Tissue Eng.*, 21: 852–861.
- Beck, R.E. and J.S. Schultz. 1970. Hindered diffusion in microporous membranes with known pore geometry. *Science*, 170: 1302–1305.
- Benjamin, E. and S. Leskowitz. 1991. *Immunology: A Short Course*. New York: Wiley-Liss.
- Bentley, T.B., H. Meng, and R.N. Pittman. 1993. Temperature dependence of oxygen diffusion and consumption in mammalian striated muscle. *Am. J. Physiol.*, 264: H1825–H1830.
- Berger, M. and D. Rodbard. 1989. Computer simulation of plasma and glucose dynamics after subcutaneous insulin injection. *Diabetes Care*, 12: 725–736.
- Bernstein, H., V.C. Yang, and R. Langer. 1987a. Distribution of heparinase covalently immobilized to agarose: Experimental and theoretical studies. *Biotechnol. Bioeng.*, 30: 196–207.
- Bernstein, H., V.C. Yang, and R. Langer. 1987b. Immobilized heparinase: In vitro reactor model. *Biotechnol. Bioeng.*, 30: 239–250.
- Bird, R.B., W.E. Stewart, and E.N. Lightfoot. 2002. *Transport Phenomena*, 2nd ed. New York: John Wiley & Sons.
- Blakely, A.M., K.L. Manning, A. Tripathi, and J.R. Morgan. 2015. Bio-pick, place, and perfuse: A new instrument for three-dimensional tissue engineering. *Tissue Eng.*, 21: 737–746.
- Bray, L.J., M. Binner, A. Holzheu, J. Friedrichs, U. Freudenberg, D.W. Hutmacher, and C. Werner. 2015. Multi-parametric hydrogels support 3D in vitro bioengineered microenvironment models of tumour angiogenesis. *Biomaterials*, 53: 609–620.
- Brinkman, H.C. 1947. A calculation of the viscous force exerted by a flowing fluid on a dense swarm of particles. *Appl. Sci. Res.*, A1: 27–34.
- Brown, A.N., B.-S. Kim, E. Alsberg, and D.J. Mooney. 2000. Combining chondrocytes and smooth muscle cells to engineer hybrid soft tissue constructs. *Tissue Eng.*, 6: 297–305.
- Buchwald, P. 2011. A local glucose- and oxygen concentration-based insulin secretion model for pancreatic islets. *Theor. Biol. Med. Model.*, 8: 20.
- Bungay, P.M. and H. Brenner. 1973. The motion of a closely fitting sphere in a fluid filled tube. *Int. J. Multiphas. Flow*, 1: 25.
- Burton, A.C. 1972. *Physiology and Biophysics of the Circulation*, 2nd ed. Chicago, IL: Year Book Medical Publishers, Inc.
- Bush, M.B., P.E. Petros, and B.R. Barrett-Lennard. 1997. On the flow through the human female urethra. *J. Biomech.*, 30: 967–969.
- Cai, Z., Z. Shi, G.M. O'Shea, and A.M. Sun. 1988. Microencapsulated hepatocytes for bioartificial liver support. *Artif. Organs*, 12: 388–393.
- Caplan, A. 1991. Mesenchymal stem cells. *J. Orthopaedic Res.*, 9: 641–650.
- Cappello, A., F. Grandi, C. Lamberti, and A. Santoro. 1994. Comparative evaluation of different methods to estimate urea distribution volume and generation rate. *Int. J. Artif. Organs*, 17: 322–330.

- Carver, S.E. and C.A. Heath. 1999. Semi-continuous perfusion system for delivering intermittent physiological pressure to regenerating cartilage. *Tissue Eng.*, 5: 1–11.
- Castro, C.I. and J.C. Briceno. 2010. Perfluorocarbon-based oxygen carriers: Review of products and trials. *Artif. Organs*, 34: 622–634.
- Catapano, G., A. Wodetzki, and U. Baurmeister. 1992. Blood flow outside regularly spaced hollowfibers: The future concept of membrane devices? *Int. J. Artif. Organs*, 15: 327–330.
- Cavallaro, J.F., P.D. Kemp, and K.H. Kraus. 1994. Collagen fabrics as biomaterials. *Biotechnol. Bioeng.*, 43: 781–791.
- Chang, P.L. 1997. Nonautologous gene therapy with implantable devices. *IEEE Eng. Med. Biol.*, September/October: 145–150.
- Chang, P.L., N. Shen, and A.J. Wescott. 1993. Delivery of recombinant gene products with microencapsulated cells in vivo. *Hum. Gene Ther.*, 4: 433–440.
- Charm, S.E. and G.S. Kurland. 1974. *Blood Flow and Microcirculation*. New York: John Wiley & Sons.
- Cheng, S.-Y., J. Gross, and A. Sambanis. 2004. Hybrid pancreatic tissue substitute consisting of recombinant insulin-secreting cells and glucose responsive material. *Biotechnol. Bioeng.*, 87: 863–873.
- Chick, W.L., J.J. Perna, V. Lauris, D. Low, P.M. Galletti, G. Panol, A.D. Whittemore, A.A. Like, C.K. Colton, and M.J. Lysaght. 1977. Artificial pancreas using living beta cells: Effects on glucose homeostasis in diabetic rats. *Science*, 197: 780–782.
- Cieslinski, D.A. and H.D. Humes. 1994. Tissue engineering of a bioartificial kidney. *Biotechnol. Bioeng.*, 43: 678–681.
- Cima, L.G., D.E. Ingber, J.P. Vacanti, and R. Langer. 1991a. Hepatocyte culture on biodegradable polymeric substrates. *Biotechnol. Bioeng.*, 38: 145–158.
- Cima, L.G., J.P. Vacanti, C. Vacanti, D. Ingber, D. Mooney, and R. Langer. 1991b. Tissue engineering by cell transplantation using degradable polymer substrates. *J. Biomech. Eng.*, 113: 143–151.
- Clark, W.R. and D. Gao. 2002. Properties of membranes used for hemodialysis therapy. *Semin. Dial.*, 15: 191–195.
- Colton, C.K. 1995. Implantable biohybrid artificial organs. *Cell Transplant.*, 4: 415–436.
- Colton, C.K. 2014. Oxygen supply to encapsulated therapeutic cells. *Adv. Drug Deliv. Rev.*, 67–68: 93–110.
- Colton, C.K. and E.S. Avgoustiniatos. 1991. Bioengineering in development of the hybrid artificial pancreas. *J. Biomech. Eng.*, 113: 152–170.
- Colton, C.K. and E.G. Lowrie. 1981. Hemodialysis: Physical principles and technical considerations. In *The Kidney*, 2nd ed., vol. II, B.M. Brenner and F.C. Rector, Jr. (eds.). Philadelphia, PA: WB Saunders Co.
- Cooney, D.O. 1976. *Biomedical Engineering Principles*. New York: Marcel Dekker, Inc.
- Crank, J. 1975. *The Mathematics of Diffusion*, 2nd ed. London, U.K.: Oxford University Press.
- Curry, F.E. and C.C. Michel. 1980. A fiber matrix model of capillary permeability. *Microvasc. Res.*, 20: 96–99.
- Cussler, E.L. 1984. *Diffusion: Mass Transfer in Fluid Systems*. Cambridge, U.K.: Cambridge University Press.
- Dagan, Z., S. Weinbaum, and R. Pfeffer. 1982. An infinite series solution for the creeping motion through an orifice of finite length. *J. Fluid Mech.*, 115: 505–523.
- Davidson, A.J., M.J. Ellis, and J.B. Chaudhuri. 2010. A theoretical method to improve and optimize the design of bioartificial livers. *Biotechnol. Bioeng.*, 106: 980–988.
- Dee, K.C., D.A. Puleo, and R. Bizios. 2002. *Tissue-Biomaterial Interactions*. Horsoken, NJ: John Wiley & Sons.
- Deen, W.M. 1987. Hindered transport of large molecules in liquid-filled pores. *AIChE J.*, 33: 1409–1425.
- Derby, B. 2012. Printing and prototyping of tissues and scaffolds. *Science*, 338: 921–926.
- Didar, T.F., M.J. Cartwright, M. Rottman, A.R. Graveline, N. Gamini, A.L. Watters, D.C. Leslie et al. 2015. Improved treatment of systemic blood infections using antibiotics with extracorporeal opsonin hemoadsorption. *Biomaterials*, 67: 382–392.
- Ding, W., L. He, G. Zhao, H. Zhang, Z. Shu, and D. Gao. 2004. Double porous media model for mass transfer of hemodialyzers. *Int. J. Heat Mass Trans.*, 47: 4849–4855.
- Ding, W., W. Li, S. Sun, X. Zhou, P.A. Hardy, S. Ahmad, and D. Gao. 2015. Three-dimensional simulation of mass transfer in artificial kidneys. *Artif. Organs*, 39: E79–E89.
- Ding, W., L. Zhou, S. Sun, W. Li, and D. Gao. 2014. A new method to increase the adsorption of protein-bound toxins in artificial liver support systems. *Artif. Organs*, 38: 954–962.
- Dionne, K.E., B.M. Cain, R.H. Li, W.J. Bell, E.J. Doherty, D.H. Rein, M.J. Lysaght, and F.T. Gentile. 1996. Transport characterization of membranes for immunoisolation. *Biomaterials*, 17: 257–266.
- Dionne, K.E., C.K. Colton, and M.L. Yarmush. 1989. Effect of oxygen on isolated pancreatic tissue. *ASAIO Trans.*, 35: 739–741.

## References

---

- Dionne, K.E., C.K. Colton, and M.L. Yarmush. 1991. A microperfusion system with environmental control for studying insulin secretion by pancreatic tissue. *Biotechnol. Prog.*, 7: 359–368.
- Douglas, J.A. and M.V. Sefton. 1990. The permeability of EUDRAGIT RL and HEMA-MMA microcapsules to glucose and inulin. *Biotechnol. Bioeng.*, 36: 653–664.
- Efrat, S. 1999. Genetically engineered pancreatic beta-cell lines for cell therapy of diabetes. *Ann. NY Acad. Sci.*, 875: 286–293.
- Ehsan, S.M. and S.C. George. 2013. Nonsteady state oxygen transport in engineered tissue: Implications for design. *Tissue Eng.*, 19: 1433–1441.
- Einstein, A. 1956. *Investigations on the Theory of the Brownian Movement*. New York: Dover Publications, Inc.
- Federspiel, W.J. and K.A. Henchir. 2004. *Lung, Artificial: Basic Principles and Current Applications. Encyclopedia of Biomaterials and Biomedical Engineering*. New York, NY: Marcel-Dekker.
- Finlay, S., B.B. Seedhom, D.O. Carey, A.J. Bulpitt, D.E. Treanor, and J. Kirkham. 2016. In vitro engineering of high modulus cartilage-like constructs. *Tissue Eng.*, 22: 382–397.
- Fissell, W.H., A. Dubnisheva, A.N. Eldridge, A.J. Fleischman, A.L. Zydny, and S. Roy. 2009. High-performance silicon nanopore hemofiltration membranes. *J. Membr. Sci.*, 326: 58–63.
- Fissell, W.H., J. Kimball, S.M. Mackay, A. Funke, and H.D. Humes. 2001. The role of a bioengineered kidney in renal failure. *Ann. NY Acad. Sci.*, 944: 284–295.
- Fissell, W.H., S. Roy, and A. Davenport. 2013. Achieving more frequent and longer dialysis for the majority: Wearable dialysis and implantable artificial kidney devices. *Kidney Int.*, 84: 256–264.
- Fogler, H.S. 2005. *Elements of Chemical Reaction Engineering*, 4th ed. New York: Prentice-Hall, Inc.
- Folkman, J. 1985. Tumor angiogenesis. *Cancer Res.*, 43: 175–203.
- Folkman, J. and M. Klagsbrun. 1987. Angiogenic factors. *Science*, 235: 442–447.
- Foster, T.H., D.F. Hartley, M.G. Nichols, and R. Hilf. 1993. Fluence rate effects in photodynamic therapy of multicell spheroids. *Cancer Res.*, 53: 1249–1254.
- Freeman, B. 1995. Osmosis. In *Encyclopedia of Applied Physics*, vol. 13, G.L. Trigg (ed.). Berlin, Germany: VCH Publishers.
- Friedman, E.A. 1989. Toward a hybrid bioartificial pancreas. *Diabetes Care*, 12: 415–419.
- Friedman, D.W., P.J. Orland, and R.S. Greco. 1994. Biomaterials: An historical perspective. In *Implantation Biology*, Chapter 1, R.S. Greco (ed.). Boca Raton, FL: CRC Press, Inc.
- Fukui, Y., A. Funakubo, and T. Kawamura. 1994. Development of an intra blood circuit membrane oxygenator. *ASAIO J.*, 40: M732–M734.
- Fung, Y.C. 1993. *Biomechanics: Mechanical Properties of Living Tissues*, 2nd ed. New York: Springer-Verlag.
- Gabriel, J.L., T.F. Miller, M.R. Wolfson, and T.H. Shaffer. 1996. Quantitative structure-activity relationships of perfluorinated hetero-hydrocarbons as a potential respiratory media. *ASAIO J.*, 42: 968–973.
- Gaehtgens, P. 1980. Flow of blood through narrow capillaries: Rheological mechanisms determining capillary hematocrit and apparent viscosity. *Biorheology*, 17: 183–189.
- Galban, C.J. and B.R. Locke. 1997. Analysis of cell growth in a polymer scaffold using a moving boundary approach. *Biotechnol. Bioeng.*, 56: 422–432.
- Galletti, P.M. and C.K. Colton. 1995. Artificial lungs and blood-gas exchange devices. In *The Biomedical Engineering Handbook*, J.D. Bronzino (ed.), pp. 1879–1997. Boca Raton, FL: CRC Press, Inc.
- Galletti, P.M., C.K. Colton, and M.J. Lysaght. 1995. Artificial kidney. In *The Biomedical Engineering Handbook*, J.D. Bronzino (ed.), pp. 1898–1922. Boca Raton, FL: CRC Press, Inc.
- Galletti, P.M. and H.O. Jauregui. 1995. Liver support systems. In *The Biomedical Engineering Handbook*, J.D. Bronzino (ed.), pp. 1952–1966. Boca Raton, FL: CRC Press, Inc.
- Gardel, L.S., L.A. Serra, R.L. Reis, and M.E. Gomes. 2014. Use of perfusion bioreactors and large animal models for long bone tissue engineering. *Tissue Eng.*, 20: 126–146.
- Garred, L.J., B. Canaud, and P.C. Farrell. 1983. A simple kinetic model for assessing peritoneal mass transfer in chronic ambulatory peritoneal dialysis. *ASAIO J.*, 6: 131–137.
- Gemmitti, C.V. and R.E. Goldberg. 2009. Shear stress magnitude and duration modulates matrix composition and tensile mechanical properties in engineered cartilaginous tissue. *Biotechnol. Bioeng.*, 104: 809–820.
- Gharapetian, H., N.A. Davies, and A.M. Sun. 1986. Encapsulation of viable cells within polyacrylate membranes. *Biotechnol. Bioeng.*, 28: 1595–1600.
- Gharapetian, H., M. Maleki, G.M. O’Shea, R.C. Carpenter, and A.M. Sun. 1987. Polyacrylate microcapsules for cell encapsulation: Effects of copolymer structure on membrane properties. *Biotechnol. Bioeng.*, 29: 775–779.

- Gibaldi, M. and D. Perrier. 1982. *Pharmacokinetics*, 2nd ed. New York: Marcel Dekker, Inc.
- Gibbon, J.H. 1954. Application of a mechanical heart and lung apparatus to cardiac surgery. *Minnesota Med.*, 37: 71.
- Giorgio, T.D., A.D. Moscioni, J. Rozga, and A.A. Demetriou. 1993. Mass transfer in a hollow fiber device used as a bioartificial liver. *ASAIO J.*, 39: 886–892.
- Goldstein, A.S., G. Zhu, G.E. Morris, R.K. Meszlenyi, and A.G. Mikos. 1999. Effect of osteoblastic culture conditions on the structure of poly(DL-lactic-co-glycolic acid) foam scaffolds. *Tissue Eng.*, 5: 421–432.
- Goldstick, T.K., V.T. Ciuryla, and L. Zuckerman. 1976. Diffusion of oxygen in plasma and blood. *Adv. Exp. Med. Biol.*, 75: 183–190.
- Goorha, Y.K., P. Deb, T. Chatterjee, P.S. Dhot, and R.S. Prasad. 2003. Review article: Artificial blood. *Med. J. Armed Forces India*, 59: 45–50.
- Gray, D.N. 1981. The status of olefin-SO<sub>2</sub> copolymers as biomaterials. In *Biomedical and Dental Applications of Polymers*, C.G. Gebelein and F.F. Koblitz (eds.), pp. 21–27. New York: Plenum Publishers.
- Gray, D.N. 1984. Polymeric membranes for artificial lungs. In *Polymer Materials and Artificial Organs*, ACS Symposium Series No. 256, C.G. Gebelein (ed.), pp. 151–161. Washington, DC: American Chemical Society.
- Gray, D.W.R. 2001. An overview of the immune system with specific reference to membrane encapsulation and islet transplantation. *Ann. NY Acad. Sci.*, 944: 226–239.
- Griffith, B.P., R.L. Kormos, H.S. Borovetz, K. Litwak, J.F. Antaki, V.L. Poirier, and K.C. Butler. 2001. HeartMate II left ventricular assist system: From concept to first clinical use. *Ann. Thorac. Surg.*, 71: 5116–5120.
- Grodsky, G.M. 1972. A threshold distribution hypothesis for packet storage of insulin and its mathematical modeling. *J. Clin. Investig.*, 51: 2047–2059.
- Grodzinsky, A.J. 2011. *Fields, Forces, and Flows in Biological Systems*. New York: Garland Science.
- Grundfest-Broniatowski, S.F., G. Tellioglu, K.S. Rosenthal, J. Kang, G. Erdodi, B. Yalcin, M. Cakmak et al. 2009. A new bioartificial pancreas utilizing amphiphilic membranes for the immunoisolation of porcine islets. *ASAIO J.*, 55: 400–405.
- Gu, Y.J., K. Inoue, S. Shinohara, R. Doi, M. Kogire, T. Aung, S. Sumi et al. 1994. Xenotransplantation of bioartificial pancreas using a mesh-reinforced polyvinyl alcohol bag. *Cell Transplant.*, 3: S19–S21.
- Guyton, A.C. 1991. *Textbook of Medical Physiology*, 8th ed. Philadelphia, PA: WB Saunders Co.
- Guyton, J.R., R.O. Foster, J.S. Soeldner, M.H. Tan, C.B. Kahn, L. Koncz, and R.E. Gleason. 1978. A model of glucose insulin homeostasis in man that incorporates the heterogeneous fast pool theory of pancreatic insulin release. *Diabetes*, 27: 1027–1042.
- Guzman, A.M., R.A. Escobar, and C.H. Amon. 2005. Methodology for predicting oxygen transport on an intravenous membrane oxygenator combining computational and analytical models. *J. Biomech. Eng.*, 127: 1127–1140.
- Hachiya, H.L., P.A. Halban, and G.L. King. 1988. Intracellular pathways of insulin transport across vascular endothelial cells. *Am. J. Physiol.*, 255 (Cell Physiol. 24): C459–C464.
- Hacker, M., K. Bachmann, and W. Messer. 2009. *Pharmacology: Principles and Practice*. Burlington, MA: Academic Press.
- Hammar, H. 1993. Wound healing. *Int. J. Dermatol.*, 32: 6–15.
- Hantsen, P.D. 1998. Understanding drug-drug interactions. *Sci. Med.*, 5: 16–25.
- Harrison, R.H., J.-P. St-Pierre, and M.M. Stevens. 2014. Tissue engineering and regenerative medicine: A year in review. *Tissue Eng.*, 20: 1–16.
- Hashimoto, S., M. Honda, M. Yamaguchi, M. Sekimoto, and Y. Tanaka. 1997. Pharmacokinetics of imipenem and cilastatin during continuous venovenous hemodialysis in patients who are critically ill. *ASAIO Journal*, 43: 84–88.
- Hayashi, H., K. Inoue, T. Aung, T. Tun, G. Yuanjun, W. Wenjing, S. Shinohara et al. 1996. Application of a novel B cell line MIN6 to a mesh reinforced polyvinyl alcohol hydrogel tube and three layer agarose microcapsules: An in vitro study. *Cell Transplant.*, 5: S65–S69.
- Haynes, R.F. 1960. Physical basis of the dependence of blood viscosity on tube radius. *Am. J. Physiol.*, 198: 1193.
- Henderson, B.W. and T.J. Dougherty. 1992. How does photodynamic therapy work? *Photochem. Photobiol.*, 55: 145–157.
- Hewitt, T.J., B.G. Hattler, and W.J. Federspiel. 1998. A mathematical model of gas exchange in an intravenous membrane oxygenator. *Ann. Biomed. Eng.*, 26: 166–178.
- Heywood, H.K., D.L. Bader, and D.A. Lee. 2006. Rate of oxygen consumption by isolated articular chondrocytes is sensitive to medium glucose concentration. *J. Cell Physiol.*, 206(2): 402–410.

## References

---

- Hill, R.S., L.A. Martinson, S.K. Young, and R.W. Dudek. 1994. Macroporous devices for diabetes correction. In *Immunoisolation of Pancreatic Islets*, Chapter 12, R.P. Lanza and W.L. Chick (eds.). Boulder, CO: RG Landes Co.
- Holder, W.D., H.E. Gruber, W.D. Roland, A.L. Moore, C.R. Culberson, A.B. Loebssack, K.J.L. Burg, and D.J. Mooney. 1997. Increased vascularization and heterogeneity of vascular structures occurring in polyglycolide matrices containing aortic endothelial cells implanted in the rat. *Tissue Eng.*, 3: 149–160.
- Holmes, B., W. Zhu, J. Li, J.D. Lee, and L.G. Zhang. 2015. Development of novel three-dimensional printed scaffolds for osteochondral regeneration. *Tissue Eng.*, 21: 403–415.
- Hong, S., D. Sycks, H.F. Chan, S. Lin, G.P. Lopez, F. Guilak, K.W. Leong, and X. Zhao. 2015. 3D printing of highly stretchable and tough hydrogels into complex, cellularized structures. *Adv. Mater.*, 27: 4035–4040.
- Horwitz, A.F. 1997. Integrins and health. *Sci. Am.*, 276: 68–75.
- Hubbell, J.A. 1997. Matrix effects. In *Principles of Tissue Engineering*, R.P. Lanza, R. Langer, and W.L. Chick (eds.), pp. 247–262. Austin, TX: R.G. Landes Co.
- Hughes, M., A. Vassilakos, D.W. Andrews, G. Hortelano, J. Belmont, and P.L. Chang. 1994. Construction of a secretable adenosine deaminase for a novel approach to somatic gene therapy. *Hum. Gene Ther.*, 5: 1445–1454.
- Humes, H.D. 1995. Tissue engineering of the kidney. In *The Biomedical Engineering Handbook*, J.D. Bronzino (ed.), pp. 1807–1824. Boca Raton, FL: CRC Press, Inc.
- Humes, H.D. 1997. Application of cell and gene therapies in the tissue engineering of renal replacement devices. In *Principles of Tissue Engineering*, R.P. Lanza, R. Langer, and W.L. Chick (eds.), pp. 577–589. Boulder, CO: R.G. Landes Co.
- Humes, H.D. and D.A. Cieslinski. 1992. Interaction between growth factors and retinoic acid in the induction of kidney tubulogenesis. *Exp. Cell Res.*, 201: 8–15.
- Humes, H.D., W.F. Weitzel, R.H. Bartlett, F.C. Swaniker, E.P. Paganini, J.R. Luderer, and J. Sobota. 2004. Initial clinical results of the bioartificial kidney containing human cells in ICU patients with acute renal failure. *Kidney Int.*, 66: 1578–1588.
- Im, G.-I. 2016. Endogenous cartilage repair by recruitment of stem cells. *Tissue Eng.*, 22: 160–171.
- Inoue, K., T. Fujisato, Y.J. Gu, K. Burczak, S. Sumi, M. Kogire, T. Tobe et al. 1992. Experimental hybrid islet transplantation: Application of polyvinyl alcohol membrane for entrapment of islets. *Pancreas*, 7: 562–568.
- Intaglietta, M. 1997. Whitaker Lecture 1996. Microcirculation, biomedical engineering, and artificial blood. *Ann. Biomed. Eng.*, 25: 593–603.
- Intaglietta, M. and R.M. Winslow. 1995. Artificial blood. In *The Biomedical Engineering Handbook*, J.D. Bronzino (ed.), pp. 2011–2024. Boca Raton, FL: CRC Press, Inc.
- Ip, T.K. and P. Aebscher. 1989. Renal epithelial-cell-controlled solute transport across permeable membranes as the foundation for a bioartificial kidney. *Artif. Organs*, 13: 58–65.
- Iwashashi, H., K. Yuri, and Y. Nose. 2004. Development of the oxygenator: Past, present, and future. *J. Artif. Organs*, 7: 111–120.
- Iwata, H., N. Morikawa, and Y. Ikada. 1996. Permeability of filters used for immunoisolation. *Tissue Eng.*, 2: 289–298.
- Jacobs, M.L. et al. 1993. *Diabetes*, 42: 1649–1655.
- James, K. and J. Kohn. 1996. New biomaterials for tissue engineering. *MRS Bull.*, 21: 22–26.
- Jauregui, H.O., C.J.P. Mullon, and B.A. Solomon. 1997. Extracorporeal artificial liver support. In *Principles of Tissue Engineering*, R.P. Lanza, R. Langer, and W.L. Chick (eds.), pp. 463–479. Austin, TX: R.G. Landes Co.
- Jarvik, R.K. 1981. The total artificial heart. *Sci. Am.*, 244: 74–80.
- Johnson, L.B., J. Aiken, D. Mooney, B.L. Schloo, L. Griffith-Cima, R. Langer, and J.P. Vacanti. 1994. The mesentary as a laminated vascular bed for hepatocyte transplantation. *Cell Transplant.*, 3: 273–281.
- Joshi, A. and J. Raje. 2002. Sonicated transdermal drug transport. *J. Control. Release*, 83: 13–22.
- Jurmann, M.J., S. Demertzis, H.-J. Schaeffers, T. Wahlers, and A. Haverich. 1992. Intravascular oxygenation for advanced respiratory therapy. *ASAIO J.*, 38: 120–124.
- Kanani, D.M., W.H. Fissell, S. Roy, A. Dubnisheva, A. Fleischman, and A.L. Zydny. 2010. Permeability-selectivity analysis for ultrafiltration: Effect of pore geometry. *J. Membr. Sci.*, 349: 405–410.
- Kang, J.H., M. Super, C.W. Yung, R.M. Cooper, K. Domansky, A.R. Graveline, T. Mammoto et al. 2014. An extracorporeal blood-cleansing device for sepsis therapy. *Nat. Med.*, 20: 1211–1221.
- Kareiva, P.M. 1983. Local movement in herbivorous insects: Applying a passive diffusion model to mark-recapture field experiments. *Oecologia*, 57: 322–327.

- Karoor, S., J. Molina, C.R. Buchmann, C. Colton, J.S. Logan, and L.W. Henderson. 2003. Immunoaffinity removal of xenoreactive antibodies using modified dialysis or microfiltration membranes. *Biotechnol. Bioeng.*, 81: 134–148.
- Katoh, S. and F. Yoshida. 1972. Rates of absorption of oxygen into blood under turbulent conditions. *Chem. Eng. J.*, 3: 276–285.
- Kaufmann, P.M., S. Heimrath, B.S. Kim, and D.J. Mooney. 1997. Highly porous polymer matrices as a three-dimensional culture system for hepatocytes. *Cell Transplant.*, 6: 463–468.
- Kedem, O. and A. Katchalsky. 1958. Thermodynamic analysis of the permeability of biological membranes to non-electrolytes. *Biochem. Biophys. Acta*, 27: 229.
- Kelly, J.H. and N.L. Sussman. 1994. The Hepatix extracorporeal liver assist device in the treatment of fulminant hepatic failure. *ASAIO J.*, 40: 83–85.
- Kim, I.L., C.G. Pfeifer, M.B. Fisher, V. Saxena, G.R. Meloni, M.Y. Kwon, M. Kim, D.R. Steinberg, R.L. Mauck, and J.A. Burdick. 2015. Fibrous scaffolds with varied fiber chemistry and growth factor delivery promote repair in a porcine cartilage defect model. *Tissue Eng.*, 21: 2680–2690.
- Kitigawa, T., T. Yamaoka, R. Iwase, and A. Murakami. 2005. Three-dimensional cell seeding and growth in radial-flow perfusion bioreactor for in vitro tissue reconstruction. *Biotechnol. Bioeng.*, 93: 947–954.
- Kobayashi, N., T. Okitsu, S. Nakaji, and N. Tanaka. 2003. Hybrid bioartificial liver: Establishing a reversibly immortalized human hepatocyte line and developing a bioartificial liver for practical use. *J. Artif. Organs*, 6: 236–244.
- Kolff, W.J. 1947. *New Ways of Treating Uremia: The Artificial Kidney, Peritoneal Lavage, Intestinal Lavage*. London, U.K.: J.A. Churchill.
- Koller, M.R. and B.O. Palsson. 1993. Tissue engineering: Reconstitution of human hematopoiesis ex vivo. *Biotechnol. Bioeng.*, 42: 909–930.
- Kornev, K.G. and A.V. Neimark. 2001. Spontaneous penetration of liquids into capillaries and porous membranes revisited. *J. Colloid Interface Sci.*, 235: 101–113.
- Koushanpour, E. 1976. *Renal Physiology*. Philadelphia, PA: WB Saunders Co.
- Kraegen, E.W., J.D. Young, E.P. George, and L. Lazarus. 1972. Oscillations in blood glucose and insulin after oral glucose. *Horm. Metab. Res.*, 4: 409–413.
- Krewson, C.E. 1995. et al. *Brain Research*, 680: 196–206.
- Krogh, A. 1919. The number and distribution of capillaries in muscles with calculations of the oxygen pressure head necessary for supplying the tissue. *J. Physiol.*, 52: 409–415.
- Kuroda, R., T. Matsumoto, Y. Kawakami, T. Fukui, Y. Mifune, and M. Kurosaka. 2014. Clinical impact of circulating CD34 positive cells on bone regeneration and healing. *Tissue Eng.*, 20: 190–199.
- Labecki, M., B.D. Bowen, and J.M. Piret. 1996. Two-dimensional analysis of protein transport in the extracapillary space of hollow-fibre bioreactors. *Chem. Eng. Sci.*, 51: 4197–4213.
- Lacy, P.E. 1995. Treating diabetes with transplanted cells. *Sci. Am.*, 273: 501–548.
- Lacy, P.E., O.D. Hegre, A. Gerasimidi-Vazeou, F.T. Gentile, and K.E. Dionne. 1991. Maintenance of normoglycemia in diabetic mice by subcutaneous xenografts of encapsulated islets. *Science*, 254: 1782–1784.
- Lagerlund, T.D. and P.A. Low. 1993. Mathematical modeling of time dependent oxygen transport in rat peripheral nerve. *Comput. Biol. Med.*, 23: 29–47.
- Lakey, J.R.T., G.L. Warnock, Z. Ao, and R.V. Rajotte. 1996. Bulk cryopreservation of isolated islets of Langerhans. *Cell Transplant.*, 5: 395–404.
- Lamb, H. 1932. *Hydrodynamics*. New York: Dover Publications.
- Langer, R. and J.P. Vacanti. 1993. Tissue engineering. *Science*, 260: 920–926.
- Langer, R., J.P. Vacanti, C.A. Vacanti, A. Atala, L.E. Freed, and G. Vunjak-Novakovic. 1995. Tissue engineering: Biomedical applications. *Tissue Eng.*, 1: 151–161.
- Lanza, R.P., A.M. Beyer, and W.L. Chick. 1994. Xenogeneic humoral responses to islets transplanted in biohybrid diffusion chambers. *Transplantation*, 57: 1371–1375.
- Lanza, R.P., A.M. Beyer, J.E. Staruk, and W.L. Chick. 1993. Biohybrid artificial pancreas. *Transplantation*, 56: 1067–1072.
- Lanza, R.P., K.M. Borland, P. Lodge, M. Carretta, S.J. Sullivan, T.E. Muller, B.A. Solomon, T. Maki, A.P. Monaco, and W.L. Chick. 1992a. Treatment of severely diabetic pancreatectomized dogs using a diffusion-based hybrid pancreas. *Diabetes*, 41: 886–889.
- Lanza, R.P., K.M. Borland, J.E. Staruk, M.C. Appel, B.A. Solomon, and W.L. Chick. 1992b. Transplantation of encapsulated canine islets into spontaneously diabetic BB/Wor rats without immunosuppression. *Endocrinology*, 131: 637–642.

## References

---

- Lanza, R.P., D.H. Butler, K.M. Borland, J.M. Harvey, D.L. Faustman, B.A. Solomon, T.E. Muller et al. 1992c. Successful xenotransplantation of a diffusion based biohybrid artificial pancreas: A study using canine, bovine, and porcine islets. *Transplant. Proc.*, 24: 669–671.
- Lanza, R.P., D.H. Butler, K.M. Borland, J.E. Staruk, D.L. Faustman, B.A. Solomon, T.E. Muller et al. 1991. Xenotransplantation of canine, bovine, and porcine islets in diabetic rats without immunosuppression. *Proc. Natl. Acad. Sci. USA*, 88: 11100–11104.
- Lanza, R.P. and W.L. Chick. (eds.). 1994a. *Procurement of Pancreatic Islets*, vol. 1. Boulder, CO: R.G. Landes Co.
- Lanza, R.P. and W.L. Chick. (eds.). 1994b. *Immunoisolation of Pancreatic Islets*, vol. 2. Boulder, CO: R.G. Landes Co.
- Lanza, R.P. and W.L. Chick. (eds.). 1994c. *Immunomodulation of Pancreatic Islets*, vol. 3. Boulder, CO: R.G. Landes Co.
- Lanza, R.P., W.M. Kuhntreiber, and W.L. Chick. 1995. Encapsulation technologies. *Tissue Eng.*, 1: 181–196.
- Lanza, R.P., A.P. Monaco, S.J. Sullivan, and W.L. Chick. 1992d. *Pancreatic Islet Cell Transplantation*, Chapter 22, C. Ricordi (ed.). Boulder, CO: R.G. Landes Co.
- Lanza, R.P., S.J. Sullivan, and W.L. Chick. 1992e. Islet transplantation with immunoisolation. *Diabetes*, 41: 1503–1510.
- Lauffenburger, D.A. and J.J. Linderman. 1993. *Receptors*. New York: Oxford University Press.
- Lavin, A., C. Sung, A.L. Klibanov, and R. Langer. 1985. A potential treatment for neonatal jaundice. *Science*, 230: 543–545.
- Leach, J.B., K.A. Bivens, C.W. Patrick Jr., and C.E. Schmidt. 2003. Photocrosslinked hyaluronic acid hydrogels: Natural, biodegradable tissue engineering scaffolds. *Biotechnol. Bioeng.*, 82: 579–589.
- Lee, C.-J. and Y.-L. Chang. 1988. Theoretical evaluation of the performance characteristics of a combined hemodialysis/hemoperfusion system—I. Single pass flow. *Can. J. Chem. Eng.*, 66: 263–270.
- Lee, C.-J., S.-T. Hsu, and S.-C. Hu. 1989. A one compartment single pore model for extracorporeal hemoperfusion. *Comput. Biol. Med.*, 19: 83–94.
- Lee, J.S. and S.-W. Cho. 2012. Liver tissue engineering: Recent advances in the development of a bio-artificial liver. *Biotechnol. Bioprocess Eng.*, 17: 427–438.
- Lee, T.-W., K.-S. Bae, H.S. Choi, and M.-J. Chern. 2014. Computational simulations of flow and oxygen/drug delivery in a three dimensional capillary network. *ISRN Biomath.*, 2014: 1–11. <http://dx.doi.org/10.1155/2014/359327>.
- Lee, W., V. Lee, S. Pollio, P. Keegan, J.-H. Lee, K. Fischer, J.-K. Park, and S.-S. Yoo. 2010. On-demand three-dimensional freeform fabrication of multi-layered hydrogel scaffold with fluidic channels. *Biotechnol. Bioeng.*, 105: 1178–1186.
- Legallais, C., B. David, and E. Dore. 2001. Bioartificial livers (BAL): Current technological aspects and future developments. *J. Membr. Sci.*, 181: 81–95.
- Lekner, J. 2007. Viscous flow through pipes of various cross-sections. *Eur. J. Phys.*, 28: 521–527.
- Lepeintre, J., H. Briandet, F. Moussy, D. Chicheportiche, S. Darquy, J. Rouchette, P. Imbaud, J.J. Duron, and G. Reach. 1990. Ex vivo evaluation in normal dogs of insulin released by a bioartificial pancreas containing isolated rat islets of Langerhans. *Artif. Organs*, 14: 20–27.
- Levick, J.R. 1991. *An Introduction to Cardiovascular Physiology*. Boston, MA: Butterworths & Co.
- Le Visage, C., S.-H. Yang, L. Kadakia, A.N. Sieber, J.P. Kostuik, and K.W. Leong. 2006. Small intestinal submucosa as a potential bioscaffold for intervertebral disc regeneration. *Spine*, 31: 2423–2430.
- Lewis, R. 1997. New directions in research on blood substitutes. *Genetic Eng. News*, 17: 1.
- Li, C.Y., K.R. Stevens, R.E. Schwartz, B.S. Alejandro, J.H. Huang, and S.N. Bhatia. 2014. Micropatterned cell-cell interactions enable functional encapsulation of primary hepatocytes in hydrogel microtissues. *Tissue Eng.*, 20: 2200–2212.
- Li, J., Y. Kuang, and C.C. Mason. 2006. Modeling the glucose-insulin regulatory system and ultradian insulin secretory oscillations with two explicit time delays. *J. Theor. Biol.*, 242: 722–735.
- Li, Z., T. Yipintsoi, and J.B. Bassingthwaite. 1997. Nonlinear model for capillary-tissue oxygen transport and metabolism. *Ann. Biomed. Eng.*, 25: 604–619.
- Lifson, N., K.G. Kramlinger, R.R. Mayrand, and E.J. Lender. 1980. Blood flow to the rabbit pancreas with special reference to the islets of Langerhans. *Gastroenterology*, 79: 466–473.
- Liu, H., F.A. Ofosu, and P.L. Chang. 1993. Expression of human factor IX by microencapsulated recombinant fibroblasts. *Hum. Gene Ther.*, 4: 291–301.
- Long, M.W. 1995. Tissue microenvironments. In *The Biomedical Engineering Handbook*, J.D. Bronzino (ed.), pp. 1692–1709. Boca Raton, FL: CRC Press, Inc.

- Lu, L. and A.G. Mikos. 1996. The importance of new processing techniques in tissue engineering. *MRS Bull.*, 21: 28–32.
- Ludwig, B., A. Reichel, A. Steffen, B. Zimerman, A.V. Schally, N.L. Block, C.K. Colton et al. 2013. Transplantation of human islets without immunosuppression. *Proc. Natl. Acad. Sci. USA*, 110: 19054–19058.
- Lum, Z.-P., I.T. Tai, M. Krestow, J. Norton, I. Vacek, and A.M. Sun. 1991. Prolonged reversal of diabetic state in NOD mice by xenografts of microencapsulated rat islets. *Diabetes*, 40: 1511–1516.
- Lysaght, M.J. and P.C. Farrell. 1989. Membrane phenomena and mass transfer kinetics in peritoneal dialysis. *J. Membr. Sci.*, 44: 5–33.
- Lysaght, M.J. and J. Moran. 1995. Peritoneal dialysis equipment. In *The Biomedical Engineering Handbook*, J.D. Bronzino (ed.), pp. 1923–1935. Boca Raton, FL: CRC Press, Inc.
- Ma, P.X. and J.-W. Choi. 2001. Biodegradable polymer scaffolds with well-defined interconnected spherical pore network. *Tissue Eng.*, 7: 23–33.
- Madry, H., A. Rey-Rico, J. Venkatesan, B. Johnstone, and M. Cucchiari. 2014. Transforming growth factor beta-releasing scaffolds for cartilage tissue engineering. *Tissue Eng.*, 20: 106–125.
- Maki, T., J.P.A. Lodge, M. Carretta, H. Ohzato, K.M. Borland, S.J. Sullivan, J. Staruk et al. 1993. Treatment of severe diabetes mellitus for more than one year using a vascularized hybrid artificial pancreas. *Transplantation*, 55: 713–718.
- Maki, T., I. Otsu, J.J. O’Neil, K. Dunleavy, C.J.P. Mullon, B.A. Solomon, and A.P. Monaco. 1996. Treatment of diabetes by xenogeneic islets without immunosuppression. *Diabetes*, 45: 342–347.
- Maki, T., C.S. Ubhi, H. Sanchez-Farpon, S.J. Sullivan, K. Borland, T.E. Muller, B.A. Solomon, W.L. Chick, and A.P. Monaco. 1991. Successful treatment of diabetes with the biohybrid artificial pancreas in dogs. *Transplantation*, 51: 43–51.
- Makarewicz, A.J., L.F. Mockros, and R.W. Anderson. 1993. A pumping intravascular lung with active mixing. *ASAIO J.*, 39: M466–M469.
- Makrogloou, A., J. Li, and Y. Kuang. 2006. Mathematical models and software tools for the glucose-insulin regulatory system and diabetes: An overview. *Appl. Num. Math.*, 56: 559–573.
- Malda, J., J. Rouwkema, D.E. Martens, E.P. le Comte, F.K. Kooy, J. Tramper, C.A. van Blitterswijk, and J. Riesle. 2004. Oxygen gradients in tissue engineered PEGT/PBT cartilaginous constructs: Measurement and modeling. *Biotechnol. Bioeng.*, 86: 9–18.
- Mann, G.E., L.H. Smaje, and D.L. Yudilevich. 1979. Permeability of the fenestrated capillaries in the cat submandibular gland to lipid-insoluble molecules. *J. Physiol.*, 297: 335–354.
- Marchant, R.E. and I.-W. Wang. 1994. Physical and chemical aspects of biomaterials used in humans. In *Implantation Biology*, R.S. Greco (ed.), pp. 13–38. Boca Raton, FL: CRC Press, Inc.
- Margiotta, M.S., L.D. Benton, and R.S. Greco. 1994. Integrins, adhesion molecules, and biomaterials. In *Implantation Biology*, R.S. Greco (ed.), pp. 149–163. Boca Raton, FL: CRC Press, Inc.
- Martin, Y. and P. Vermette. 2005. Bioreactors for tissue mass culture: Design, characterization, and recent advances. *Biomaterials*, 26: 7481–7503.
- Mathes, S.H., L. Wohlgemuth, L. Uebersax, R. von Mentlen, D.S. Thoma, R.E. Jung, C. Gorlach, and U. Graf-Hausner. 2010. A bioreactor test system to mimic the biological and mechanical environment of oral soft tissues and to evaluate substitutes for connective tissue grafts. *Biotechnol. Bioeng.*, 107: 1029–1039.
- Matsuda, N. and K. Sakai. 2000. Blood flow and oxygen transfer rate of an outside blood flow membrane oxygenator. *J. Membr. Sci.*, 170: 153–158.
- Matthew, H.W., S.O. Salley, W.D. Peterson, and M.D. Klein. 1993. Complex coacervate microcapsules for mammalian cell culture and artificial organ development. *Biotechnol. Prog.*, 9: 510–519.
- Maxwell, J.C. 1873. *A Treatise on Electricity and Magnetism*, vol. 1. Oxford, U.K.: Clarendon Press.
- Mazzei, D., M.A. Guzzardi, S. Giusti, and A. Ahluwalia. 2010. A low shear stress modular bioreactor for connected cell culture under high flow rates. *Biotechnol. Bioeng.*, 106: 127–137.
- McCabe, W.L., J.C. Smith, and P. Harriott. 1985. *Unit Operations of Chemical Engineering*, 4th ed. New York: McGraw-Hill.
- McMurtrey, R.J. 2016. Analytic models of oxygen and nutrient diffusion, metabolism dynamics, and architecture optimization in three-dimensional tissue constructs with applications and insights in cerebral organoids. *Tissue Eng.*, 22: 1–29.
- McNabb, M.E., R.V. Ebert, and K. McCusker. 1982. Plasma nicotine levels produced by chewing nicotine gum. *JAMA*, 248: 865–868.

## References

---

- Mehta, K. and J.J. Linderman. 2006. Model-based analysis and design of a microchannel reactor for tissue engineering. *Biotechnol. Bioeng.*, 94: 596–609.
- Merrill, E.W., A.M. Benis, E.R. Gilliland, T.K. Sherwood, and E.W. Salzman. 1965. Pressure flow relations of human blood in hollow fibers at low flow rates. *J. Appl. Physiol.*, 20: 954–967.
- Mikos, A.G., M.G. Papadaki, S. Kouvroukoglou, S.L. Ishaug, and R.C. Thomson. 1994. Mini-review: Islet transplantation to create a bioartificial pancreas. *Biotechnol. Bioeng.*, 43: 673–677.
- Mirhashemi, S., K. Messmer, and M. Intaglietta. 1987. Tissue perfusion during normovolemic hemodilution investigated by a hydraulic model of the cardiovascular system. *Int. J. Microcirc. Clin. Exp.*, 6: 123–136.
- Mitragotri, S. 2003. Modeling skin permeability to hydrophilic and hydrophobic solutes based on four permeation pathways. *J. Control. Release*, 86: 69–92.
- Mitragotri, S., Y.G. Anissimov, A.L. Bunge, H.F. Frasch, R.H. Guy, J. Hadgraft, G.B. Kasting, M.E. Lane, and M.S. Roberts. 2011. Mathematical models of skin permeability: An overview. *Int. J. Pharm.*, 418: 115–129.
- Mochizuki, S. and A.L. Zydny. 1992. Effect of protein adsorption on the transport characteristics of asymmetric ultrafiltration membranes. *Biotechnol. Prog.*, 8: 553–561.
- Mooney, D.J., C. Breuer, K. McNamara, J.P. Vacanti, and R. Langer. 1995a. Fabricating tubular devices from polymers of lactic and glycolic acid for tissue engineering. *Tissue Eng.*, 1: 107–117.
- Mooney, D.J., P.M. Kaufmann, K. Sano, S.P. Schwendeman, K. Majahod, B. Schloo, J.P. Vacanti, and R. Langer. 1996. Localized delivery of epidermal growth factor improves the survival of transplanted hepatocytes. *Biotechnol. Bioeng.*, 50: 422–429.
- Mooney, D.J., B.-S. Kim, J.P. Vacanti, R. Langer, and A. Atala. 1997. Tissue engineering: Genitourinary system. In *Principles of Tissue Engineering*, R.P. Lanza, R. Langer, and W.L. Chick (eds.), pp. 591–600. Boulder, CO: R.G. Landes Co.
- Mooney, D.J., G. Organ, J.P. Vacanti, and R. Langer. 1994. Design and fabrication of biodegradable polymer devices to engineer tubular tissues. *Cell Transplant.*, 3: 203–210.
- Mooney, D.J., S. Park, P.M. Kaufmann, K. Sano, K. McNamara, J.P. Vacanti, and R. Langer. 1995b. Biodegradable sponges for hepatocyte transplantation. *J. Biomed. Mater. Res.*, 29: 959–965.
- Morgan, J.R., R.G. Tompkins, and M.L. Yarmush. 1994. Genetic engineering and therapeutics. In *Implantation Biology*, R.S. Greco (ed.), pp. 387–400. Boca Raton, FL: CRC Press, Inc.
- Morgan, J.R. and M.L. Yarmush. 1997. Bioengineered skin substitutes. *Sci. Med.*, 4: 6–15.
- Moss, G.P., S.C. Wilkinson, and Y. Sun. 2012. Mathematical modelling of percutaneous absorption. *Curr. Opin. Colloid Interface Sci.*, 17: 166–172.
- Moussy, F., J. Rouchette, G. Reach, R. Cannon, and M.Y. Jaffrin. 1989. In vitro evaluation of a bioartificial pancreas under various hemodynamic conditions. *Artif. Organs*, 13: 109–115.
- Nachum, Z., A. Shupak, and C.R. Gordon. 2006. Transdermal scopolamine for prevention of motion sickness: Clinical pharmacokinetics and therapeutic applications. *Clin. Pharmacokinet.*, 45: 543–566.
- Nagase, K., F. Kohori, and K. Sakai. 2005. Oxygen transfer of a membrane oxygenator composed of crossed and parallel hollow fibers. *Biochem. Eng. J.*, 24: 105–113.
- Nam, J., Y. Huang, S. Agarwal, and J. Lannutti. 2007. Improved cellular infiltration in electrospun fiber via engineered porosity. *Tissue Eng.*, 13: 2249–2257.
- Nam, J., Y. Huang, S. Agarwal, and J. Lannutti. 2008. Materials selection and residual solvent retention in biodegradable electrospun fibers. *J. Appl. Polym. Sci.*, 107: 1547–1554.
- Nam, J., B. Rath, T.J. Knobloch, J.J. Lannutti, and S. Agarwal. 2009. Novel electrospun scaffolds for the molecular analysis of chondrocytes under dynamic compression. *Tissue Eng.*, 15: 513–523.
- Naughton, G.K., W.R. Tolbert, and T.M. Grillot. 1995. Emerging developments in tissue engineering and cell technology. *Tissue Eng.*, 1: 211–219.
- Neiman, J.A., Shepard, R. Raman, V. Chan, M.G. Rhoads, M.S.B. Raredon, J.J. Velazquez et al. 2014. Photopatterning of hydrogel scaffolds coupled to filter materials using stereolithography for perfused 3D culture of hepatocytes. *Biotechnol. Bioeng.*, 112: 777–787.
- Neufeld, T., B. Ludwig, U. Barkai, G.C. Weir, C.K. Colton, Y. Evron, M. Balyura et al. 2013. The efficacy of an immunoisolating membrane system for islet xenotransplantation in minipigs. *PLoS ONE*, 8: 1–13.
- Niro, R., J.P. Byers, R.L. Fournier, and K. Bachmann. 2003. Application of a convective-dispersion model to predict in vivo hepatic clearance from in vitro measurements using cryopreserved human hepatocytes. *Curr. Drug Metab.*, 4: 357–369.
- Nomura, N., M. Schiiri, R. Kawamori, Y. Yamasaki, N. Iwama, and H. Abe. 1984. A mathematical insulin secretion model and its validation in isolated rat pancreatic islets perfusion. *Comput. Biomed. Res.*, 17: 570–579.

- Nose, Y. 2001. Historical perspectives of hybrid hepatic assist devices. *Ann. NY Acad. Sci.*, 944: 18–34.
- Notari, R.E. 1987. *Biopharmaceutics and Clinical Pharmacokinetics*, 4th ed. New York: Marcel Dekker, Inc.
- Notkins, A.L. 1979. The causes of diabetes. *Sci. Am.*, 241: 62–73.
- Noult, R.A. and D.G. Lealst. 1987. Diffusion coefficient of aqueous benzoic acid at 25°C. *J. Chem. Eng. Data*, 32: 418–420.
- Nugent, L.J. and R.K. Jain. 1984a. Extravascular diffusion in normal and neoplastic tissues. *Cancer Res.*, 44: 238–244.
- Nugent, L.J. and R.K. Jain. 1984b. Pore and fiber-matrix models for diffusive transport in normal and neoplastic tissues. *Microvasc. Res.*, 28: 270–274.
- Nyberg, S.L., H.J. Mann, R.P. Remmel, W.-S. Hu, and F.B. Cerra. 1993a. Pharmacokinetic analysis verifies P450 function during in vitro and in vivo application of a bioartificial liver. *ASAIO J.*, 39: M252–M256.
- Nyberg, S.L., J.L. Platt, K. Shirabe, W.D. Payne, W.-S. Hu, and F.B. Cerra. 1992. Immunoprotection of xenocytes in a hollow fiber bioartificial liver. *ASAIO J.*, 38: M463–M467.
- Nyberg, S.L., R.A. Shatford, M.V. Peshwa, J.G. White, F.B. Cerra, and W.-S. Hu. 1993b. Evaluation of a hepatocyte entrapment hollow fiber bioreactor: A potential bioartificial liver. *Biotechnol. Bioeng.*, 41: 194–203.
- Obradovic, B., J.H. Meldon, L.E. Freed, and G. Vunjak-Novakovic. 2000. Glycosaminoglycan deposition in engineered cartilage: Experiments and mathematical model. *AICHE J.*, 46: 1860–1871.
- Oerther, S., H. LeGall, E. Payan, F. Lapicque, N. Presle, P. Hubert, J. Dexheimer, P. Netter, and F. Lapicque. 1999. Hyaluronate-alginate gel as a novel biomaterial: Mechanical properties and formation mechanism. *Biotechnol. Bioeng.*, 63: 206–215.
- Ogston, A.G. 1958. The spaces in a uniform random suspension of fibers. *Trans. Faraday Soc.*, 54: 1754–1757.
- Oie, S. and T.N. Tozer. 1979. Effect of altered plasma protein binding on apparent volume of distribution. *J. Pharm. Sci.*, 68: 1203–1205.
- Ojcius, D.M., C.-C. Liu, and J.D. Young. 1998. Pore-forming proteins. *Sci. Med.*, 5: 44–53.
- Opong, W.S. and A.L. Zydny. 1991. Diffusive and convective protein transport through asymmetric membranes. *AICHE J.*, 37: 1497–1510.
- Owen, D.H., J.J. Peters, and D.F. Katz. 2000. Rheological properties of contraceptive gels. *Contraception*, 62: 321–326.
- Pachence, J.M. and J. Kohn. 1997. Biodegradable polymers for tissue engineering. In *Principles of Tissue Engineering*, R.P. Lanza, R. Langer, and W.L. Chick (eds.), pp. 273–293. Austin, TX: R.G. Landes Co.
- Palsson, B.O. and S. Bhatia. 2004. *Tissue Engineering*. Upper Saddle River, NJ: Pearson Prentice Hall.
- Panchagnula, R. 1997. Transdermal delivery of drugs. *Indian J. Pharmacol.*, 29: 140–156.
- Park, J.H., B.G. Chung, W.G. Lee, J. Kim, M.D. Brigham, J. Shim, S. Lee et al. 2010. Microporous cell-laden hydrogels for engineered tissue constructs. *Biotechnol. Bioeng.*, 106: 138–148.
- Parsons-Wingerter, P. and E.H. Sage. 1997. Regulation of cell behavior by extracellular proteins. In *Principles of Tissue Engineering*, R.P. Lanza, R. Langer, and W.L. Chick (eds.), pp. 111–131. Austin, TX: R.G. Landes Co.
- Pathak, C.P., A.S. Sawhney, and J.A. Hubbell. 1992. Rapid photopolymerization of immunoprotective gels in contact with cells and tissues. *J. Am. Chem. Soc.*, 114: 8311–8312.
- Patzer, J.F. 2001. Advances in bioartificial liver assist devices. *Ann. NY Acad. Sci.*, 944: 320–333.
- Petley, A. et al. 1995. *Diabetes*, 44: 152–155.
- Perez, E.P., E.W. Merrill, D. Miller, and L.G. Cima. 1995. Corneal epithelial wound healing on bilayer composite hydrogels. *Tissue Eng.*, 1: 263–277.
- Petersen, E.F., R.G.S. Spencer, and E.W. McFarland. 2002. Microengineering neocartilage scaffolds. *Biotechnol. Bioeng.*, 78: 802–805.
- Petruzzo, P., L. Pibirri, M.A. DeGiudici, G. Basta, R. Calafiore, A. Falorni, P. Brunetti, and G. Brotzu. 1991. Xenotransplantation of microencapsulated pancreatic islets contained in a vascular prosthesis: Preliminary results. *Transplant Int.*, 4: 200–204.
- Phillips, G.D., R.A. Whitehead, and D.R. Knighton. 1991. Initiation and pattern of angiogenesis in wound healing in the rat. *Am. J. Anat.*, 192: 257–262.
- Phillips, R., J. Kondev, J. Theriot, and H.G. Garcia. 2013. *Physical Biology of the Cell*, 2nd ed. London, U.K.: Garland Science.
- Pittenger, M.F., A.M. Mackay, S.C. Beck, R.K. Jaiswal, R. Douglas, J.D. Mosca, M.A. Moorman, D.W. Simonetti, S. Craig, and D.R. Marshak. 1999. Multilineage potential of adult human mesenchymal stem cells. *Science*, 284: 143–147.
- Poling, B.E., J.M. Prausnitz, and J.P. O'Connell. 2001. *The Properties of Gases and Liquids*, 5th ed. New York: McGraw-Hill.

## References

---

- Poornejad, N., L.B. Schaumann, E.M. Buckmiller, B.L. Roeder, and A.D. Cook. 2016. Current cell-based strategies for whole kidney regeneration. *Tissue Eng.*, 22: 358–370.
- Potts, R.O. and R.H. Guy. 1992. Predicting skin permeability. *Pharm. Res.*, 9: 663–669.
- Powers, M.J., K. Domansky, M.R. Kaazempur-Mofrad, A. Kalezi, A. Capitano, A. Upadhyaya, P. Kurzawski et al. 2002. A microfabricated array bioreactor for perfused 3D liver culture. *Biotechnol. Bioeng.*, 78: 257–269.
- Pratt, A.B., F.E. Weber, H.G. Schmoekel, R. Muller, and J.A. Hubbell. 2004. Synthetic extracellular matrices for in situ tissue engineering. *Biotechnol. Bioeng.*, 86: 27–36.
- Prausnitz, J.M., R.N. Lichtenthaler, and E.G. de Azevedo. 1986. *Molecular Thermodynamics of Fluid-Phase Equilibria*, 2nd ed. Englewood Cliffs, NJ: Prentice-Hall, Inc.
- Prausnitz, J.M. and F.H. Shair. 1961. A thermodynamic correlation of gas solubilities. *AIChE J.*, 7: 682.
- Price, A.P., L.M. Godin, A. Domek, T. Cotter, J. D'Cunha, D.A. Taylor, and A. Panoskaltsis-Mortari. 2015. Automated decellularization of intact, human-sized lungs for tissue engineering. *Tissue Eng.*, 21: 94–103.
- Pries, A.R., T.W. Secomb, and P. Gaehtgens. 1996. Biophysical aspects of blood flow in the microvasculature. *Cardiovasc. Res.*, 32: 654–667.
- Putcha, L., N.M. Cintron, J. Tsui, J.M. Vanderploeg, and W.G. Kramer. 1989. Pharmacokinetics and oral bioavailability of scopolamine in normal subjects. *Pharm. Res.*, 6: 481–485.
- Qiao, J., L. Qi, X. Mu, and Y. Chen. 2011. Monolith and coating enzymatic microreactors of L-asparaginase: Kinetics study by MCE-LIF for potential application in acute lymphoblastic leukemia (ALL) treatment. *Analyst*, 136: 2077–2083.
- Radisic, M., W. Deen, R. Langer, and G. Vunjak-Novakovic. 2005. Mathematical model of oxygen distribution in engineered cardiac tissue with parallel channel array perfused with culture medium containing oxygen carriers. *Am. J. Physiol. Heart Circ. Physiol.*, 288: H1278–H1289.
- Radisic, M., M. Euloth, L. Yang, R. Langer, L. Freed, and G. Vunjak-Novakovic. 2003. High density seeding of myocyte cells in cardiac tissue engineering. *Biotechnol. Bioeng.*, 82: 403–414.
- Radisic, M., J. Malda, E. Epping, W. Geng, R. Langer, and G. Vunjak-Novakovic. 2006. Oxygen gradients correlate with cell density and cell viability in engineered cardiac tissue. *Biotechnol. Bioeng.*, 93: 332–342.
- Radisic, M., L. Yang, J. Boublik, R.J. Cohen, R. Langer, L.E. Freed, and G. Vunjak-Novakovic. 2004. Medium perfusion enables engineering of compact and contractile cardiac tissue. *Am. J. Physiol. Heart Circ. Physiol.*, 286: H507–H516.
- Ramachandran, P.A. and R.A. Mashelkar. 1980. Lumped parameter model for hemodialyzer with application to simulation of patient-artificial kidney system. *Med. Biol. Eng. Comput.*, 18: 179–188.
- Reach, G., M.Y. Jaffrin, and J.F. Desjeux. 1984. A U-shaped bioartificial pancreas with rapid glucose-insulin kinetics. In vitro evaluation and kinetic modelling. *Diabetes*, 33: 752–761.
- Reach, G., P. Poussier, A. Sausse, R. Assan, M. Itoh, and J.E. Gerich. 1981. Functional evaluation of a bioartificial pancreas using isolated islets perfused with blood ultrafiltrate. *Diabetes*, 30: 296–301.
- Reid, R.C., J.M. Prausnitz, and T.K. Sherwood. 1977. *The Properties of Gases and Liquids*, 3rd ed. New York: McGraw-Hill.
- Renkin, E.M. 1954. Filtration, diffusion, and molecular sieving through porous cellulose membranes. *J. Gen. Physiol.*, 38: 225.
- Renkin, E.M. 1977. Multiple pathways of capillary permeability. *Circ. Res.*, 41: 735–743.
- Renkin, E.M. and F.E. Curry. 1979. Transport of water and solutes across capillary endothelium. In *Membrane Transport in Biology*, vol. 4, Chapter 1, G. Giebisch and D.C. Tosteson (eds.). New York: Springer-Verlag.
- Richardson, P.D. 1987. Artificial lungs and oxygenation devices. In *Handbook of Bioengineering*, Chapter 27, R. Skalak and S. Chien (eds.). New York: McGraw-Hill Co.
- Ricordi, C. 1992. *Pancreatic Islet Cell Transplantation*. Boulder, CO: RG Landes Co.
- Ricordi, C., P.E. Lacy, E.H. Finke, B.J. Olack, and D.W. Scharp. 1988. Automated method for isolation of human pancreatic islets. *Diabetes*, 37: 413–420.
- Ricordi, C., C. Soccia, A. Davalli, C. Staudacher, A. Vertova, P. Baro, M. Freschi et al. 1990a. Swine islet isolation and transplantation. *Horm. Metabol. Res.*, 25: 26–30.
- Ricordi, C., C. Soccia, A. Davalli, A. Vertova, P. Baro, I. Sassi, S. Braghi, N. Giuzzi, G. Pozza, and V. DiCarlo. 1990b. Application of the automated method to islet isolation in swine. *Transplant. Proc.*, 22: 784–785.
- Riley, M.R., H.M. Buettner, F.J. Muzzio, and S.C. Reyes. 1995a. Monte Carlo simulation of diffusion and reaction in two dimensional cell structures. *Biophys. J.*, 68: 1716–1726.
- Riley, M.R., F.J. Muzzio, and H.M. Buettner. 1995b. The effect of structure on diffusion and reaction in immobilized cell systems. *Chem. Eng. Sci.*, 50: 3357–3367.

- Riley, M.R., F.J. Muzzio, H.M. Buettner, and S.C. Reyes. 1994. Monte Carlo calculation of effective diffusivities in two- and three-dimensional heterogeneous materials of variable structure. *Phys. Rev. E*, 49: 3500–3503.
- Riley, M.R., F.J. Muzzio, H.M. Buettner, and S.C. Reyes. 1995c. Diffusion in heterogeneous media: Application to immobilized cell systems. *AICHE J.*, 41: 691–700.
- Riley, M.R., F.J. Muzzio, H.M. Buettner, and S.C. Reyes. 1996. A simple correlation for predicting effective diffusivities in immobilized cell systems. *Biotechnol. Bioeng.*, 49: 223–227.
- Ritger, P.L. and N.A. Peppas. 1987. A simple equation for description of solute release I. Fickian and non-Fickian release from non-swelling devices in the form of slabs, spheres, cylinders or discs. *J. Control. Release*, 5: 23–36.
- Robertson, B.C. and A.L. Zydny. 1990a. Hindered protein diffusion in asymmetric ultrafiltration membranes with highly constricted pores. *J. Membr. Sci.*, 49: 287–303.
- Robertson, B.C. and A.L. Zydny. 1990b. Protein adsorption in asymmetric ultrafiltration membranes with highly constricted pores. *J. Colloid Interface Sci.*, 134: 563–575.
- Rochow, N., A. Manan, W.-I. Wu, G. Fusch, S. Monkman, J. Leung, E. Chan et al. 2014. An integrated array of microfluidic oxygenators as a neonatal lung assist device: In vitro characterization and in vivo demonstration. *Artif. Organs*, 38: 856–866.
- Rosen, S.L. 1993. *Fundamental Principles of Polymeric Materials*, 2nd ed. New York: John Wiley & Sons.
- Rosenberg, G. 1995. Artificial heart and circulatory assist devices. In *The Biomedical Engineering Handbook*, J.D. Bronzino (ed.), pp. 1839–1846. Boca Raton, FL: CRC Press, Inc.
- Rowland, M. and T.N. Tozer. 1995. *Clinical Pharmacokinetics: Concepts and Applications*. Philadelphia, PA: Lippincott, Williams, & Wilkins.
- Rozga, J., E. Morsiani, E. LePage, A.D. Moscioni, T. Giorgio, and A.A. Demetriou. 1994. Isolated hepatocytes in a bioartificial liver: A single group view and experience. *Biotechnol. Bioeng.*, 43: 645–653.
- Rozga, J., F. Williams, M.-S. Ro, D.F. Neuzil, T.D. Giorgio, G. Backfisch, A.D. Moscioni, R. Hakim, and A.A. Demetriou. 1993. Development of a bioartificial liver: Properties and function of a hollow fiber module inoculated with liver cells. *Hepatology*, 17: 258–265.
- Rubin, E. and J.L. Farber. 1994. *Pathology*, 2nd ed. Philadelphia, PA: J.B. Lippincott Co.
- Saltzman, W.M. 1997. Cell interactions with polymers. In *Principles of Tissue Engineering*, R.P. Lanza, R. Langer, and W.L. Chick (eds.), pp. 225–246. Boulder, CO: R.G. Landes Co.
- Sandler, S.I. 1989. *Chemical Engineering Thermodynamics*, 2nd ed. New York: John Wiley & Sons.
- Sart, S., A.-C. Tsai, Y. Li, and T. Ma. 2014. Three-dimensional aggregates of mesenchymal stem cells: Cellular mechanisms, biological properties, and applications. *Tissue Eng.*, 20: 365–380.
- Sarver, J.G. 1994. Development of a tracer technique that utilizes a physiological pharmacokinetic model to quantitatively assess the change in mass transfer rates associated with vascular growth and the application of this technique to the evaluation of a novel bioartificial organoid. PhD dissertation. The University of Toledo, Toledo, OH.
- Sarver, J.G. and R.L. Fournier. 1990. Numerical investigation of a novel spiral wound membrane sandwich design for an implantable bioartificial pancreas. *Comput. Biol. Med.*, 20: 105–119.
- Sarver, J.G., R.L. Fournier, P.J. Goldblatt, T.L. Phares, S.E. Mertz, A.R. Baker, R.J. Mellon, J.M. Horner, and S.H. Selman. 1995. Tracer technique to measure in vivo chemical transport rates within an implantable cell transplantation device. *Cell Transplant.*, 4: 201–217.
- Sauer, I.M., N. Obermeyer, D. Kardassis, T. Theruvath, and J.C. Gerlach. 2001. Development of a hybrid liver support system. *Ann. NY Acad. Sci.*, 944: 308–319.
- Scharp, D.W. and P. Marchetti. 2014. Encapsulated islets for diabetes therapy: History, current progress, and critical issues requiring solution. *Adv. Drug Deliv.*, 67–68: 35–73.
- Scharp, D.W., C.J. Swanson, B.J. Olack, P.P. Latta, O.D. Hegre, E.J. Doherty, F.T. Gentile, K.S. Flavin, M.F. Ansara, and P.E. Lacy. 1994. Protection of encapsulated human islets implanted without immunosuppression in patients with type I or type II diabetes and in nondiabetic control subjects. *Diabetes*, 43: 1167–1170.
- Schlichting, H. 1979. *Boundary Layer Theory*. New York: McGraw-Hill.
- Schmelzer, E., A. Finoli, I. Nettleship, and J.C. Gerlach. 2014. Long-term three-dimensional perfusion culture of human adult bone marrow mononuclear cells in bioreactors. *Biotechnol. Bioeng.*, 112: 801–810.
- Schmelzer, E., K. Mutig, P. Schrade, S. Bachmann, J.C. Gerlach, and K. Zeilinger. 2009. Effect of human patient plasma ex vivo treatment of gene expression and progenitor cell activation of primary human liver cells in multi-compartment 3D perfusion bioreactors for extra-corporeal liver support. *Biotechnol. Bioeng.*, 103: 817–827.

## References

---

- Schrezenmeir, J., J. Kirchgessner, L. Gero, L.A. Kunz, J. Beyer, and W. Mueller-Klieser. 1994. Effect of microencapsulation on oxygen distribution in islets organs. *Transplantation*, 57: 1308–1314.
- Scott, M.D., K.L. Murad, F. Koumpouras, M. Talbot, and J.W. Eaton. 1997. Chemical camouflage of antigenic determinants: Stealth erythrocytes. *Proc. Natl. Acad. Sci. USA*, 94: 7566–7571.
- Sears, N.A., D.R. Seshadri, P.S. Dhavalikar, and E. Cosgriff-Hernandez. 2016. A review of three-dimensional printing in tissue engineering. *Tissue Eng.*, 22: 1–13.
- Secomb, T.W., R. Hsu, M.W. Dewhirst, B. Klitzman, and J.F. Gross. 1993. Analysis of oxygen transport to tumor tissue by microvascular networks. *Int. J. Radiation Oncol. Biol. Phys.*, 25: 481–489.
- Sefton, M.V., R.M. Dawson, R.L. Broughton, J. Blysniuk, and M.E. Sugamori. 1987. Microencapsulation of mammalian cells in a water insoluble polyacrylate by coextrusion and interfacial precipitation. *Biotechnol. Bioeng.*, 29: 135–143.
- Serra L., J. Doménech, and N.A. Peppas. 2006. Drug transport mechanisms and release kinetics from molecularly designed poly(acrylic acid-g-ethylene glycol) hydrogels. *Biomaterials*, 27: 5440–5451.
- Shah, N. and A. Mehra. 1996. Modeling of oxygen uptake in perfluorocarbon emulsions. *ASAIO J.*, 42: 181–189.
- Shaikh, F.M., T.P. O'Brien, A. Callanan, E.G. Kavanagh, P.E. Burke, P.A. Grace, and T.M. McGloughlin. 2010. New pulsatile hydrostatic pressure bioreactor for vascular tissue-engineered constructs. *Artif. Organs*, 34: 153–158.
- Shaoting, W., Z. Fengbao, M. Tengxiang, and G. Hanqing. 1990. Investigation on patient-artificial kidney system using compartment models. *Chem. Eng. Sci.*, 45: 2943–2948.
- Shi, C., G.J. Wright, C.L. Ex-Lubeskie, A.D. Bradshaw, and H. Yao. 2013. Relationship between anisotropic diffusion properties and tissue morphology in porcine TMJ disc. *Osteoarthr. Cartilage*, 21: 625–633.
- Shimomura, K., Y. Moriguchi, C.D. Murawski, H. Yoshikawa, and N. Nakamura. 2014. Osteochondral tissue engineering with biphasic scaffold: Current strategies and techniques. *Tissue Eng.*, 20: 468–476.
- Shiroki, R., T. Mohanakumar, and D.W. Scharp. 1995. Analysis of the serological and cellular sensitization induced by encapsulated human islets transplantation in type I and type II diabetes patients. *Cell Transplant.*, 4: 535–538.
- Shuler, M. and F. Kargi. 2001. *Bioprocess Engineering: Basic Concepts*, 2nd ed. Upper Saddle River, NJ: Prentice Hall, Inc.
- Smith, B., J.G. Sarver, and R.L. Fournier. 1991. A comparison of islet transplantation and subcutaneous insulin injections for the treatment of diabetes mellitus. *Comput. Biol. Med.*, 21: 417–427.
- Song, S., G. Faleo, R. Yeung, R. Kant, A.M. Posselt, T.A. Desai, Q. Tang, and S. Roy. 2016. Silicon nanopore membrane (SNM) for islet encapsulation and immunoisolation under convective transport. *Sci. Rep.*, 6: 23679.
- Song, S. and S. Roy. 2016. Progress and challenges in macroencapsulation approaches for type 1 diabetes (T1D) treatment: Cells, biomaterials, and devices. *Biotechnol. Bioeng.*, 113: 1381–1402.
- Soon-Shiong, P. 1994. Encapsulated islet transplantation: Pathway to human clinical trials. In *Immunoisolation of Pancreatic Islets*, vol. 3, Chapter 6, R.P. Lanza and W.L. Chick (eds.). Boulder, CO: R.G. Landes Co.
- Soon-Shiong, P., E. Feldman, R. Nelson, R. Heintz, N. Merideth, P. Sandford, T. Zheng, and J. Komtebedde. 1992a. Long-term reversal of diabetes in the large animal model by encapsulated islet transplantation. *Trans. Proc.*, 24: 2946–2947.
- Soon-Shiong, P., E. Feldman, R. Nelson, R. Heintz, Q. Yao, O. Smidsrod, and P. Sandford. 1993. Longterm reversal of diabetes by the injection of immunoprotected islets. *Proc. Natl. Acad. Sci. USA*, 90: 5843–5847.
- Soon-Shiong, P., E. Feldman, R. Nelson, J. Komtebedde, O. Smidsrod, G. Skjak-Braek, T. Espvik, R. Heintz, and M. Lee. 1992b. Successful reversal of spontaneous diabetes in dogs by intraperitoneal microencapsulated islets. *Transplantation*, 54: 769–774.
- Sorenson, J.T., C.K. Colton, R.S. Hillman, and J.S. Soeldner. 1982. Use of a pharmacokinetic model of glucose homeostasis for assessment of performance requirements for improved insulin therapies. *Diabetes Care*, 5: 148–157.
- Spicer, P.P. and A.G. Mikos. 2010. Fibrin glue as a drug delivery system. *J. Control. Release*, 148: 49–55.
- Spotnitz, H.M. 1987. Circulatory assist devices. In *Handbook of Bioengineering*, R. Skalak and S. Chien (eds.), pp. 38.1–38.18. New York, NY: McGraw-Hill, Inc.
- Staverman, A.J. 1948. Non-equilibrium thermodynamics of membrane processes. *Trans. Faraday Soc.*, 48: 176–185.
- Storrs, R., R. Dorian, S.R. King, J. Lakey, and H. Rilo. 2001. Preclinical development of the islet sheet. *Ann. NY Acad. Sci.*, 944: 252–266.
- Stryer, L. 1988. *Biochemistry*. New York: W.H. Freeman and Company.

- Sturis, J., C. Knudsen, N.M. O'Meara, J.S. Thomsen, E. Mosekilde, E. Van Cauter, and K.S. Polonsky. 1995. Phase-locking regions in a forced model of slow insulin and glucose oscillations. In *Dynamical Disease: Mathematical Analysis of Human Illness*, J. Belair, L. Glass, U. An der Heiden, and J. Milton (eds.). New York, NY: AIP Press.
- Sturis, J., K.S. Polonsky, E. Mosekilde, and E. Van Cauter. 1991. Computer model for mechanisms underlying ultradian oscillations of insulin and glucose. *Am. J. Physiol.*, 260: E801–E809.
- Sugamori, M.E. and M.V. Sefton. 1989. Microencapsulation of pancreatic islets in a water insoluble polyacrylate. *Trans. Am. Soc. Artif. Organs*, 35: 791–799.
- Sullivan, S.J., T. Maki, K.M. Borland, M.D. Mahoney, B.A. Solomon, T.E. Muller, A.P. Monaco, and W.L. Chick. 1991. Biohybrid artificial pancreas: Longterm implantation studies in diabetic, pancreatectomized dogs. *Science*, 252: 718–721.
- Sun, A.M., W. Parisius, G.M. Healy, I. Vacek, and H.G. Macmorine. 1977. The use, in diabetic rats and monkeys, of artificial capillary units containing cultured islets of Langerhans. *Diabetes*, 26: 1136–1139.
- Sun, Y., X. Ma, D. Zhou, I. Vacek, and A.M. Sun. 1996. Normalization of diabetes in spontaneously diabetic cynomolgus monkeys by xenografts of microencapsulated porcine islets without immunosuppression. *J. Clin. Invest.*, 98: 1417–1422.
- Sung, C., A. Lavin, A.M. Klibanov, and R. Langer. 1986. An immobilized enzyme reactor for the detoxification of bilirubin. *Biotechnol. Bioeng.*, 28: 1531–1539.
- Sussman, N.L., M.G. Chong, T. Koussayer, D. He, T.A. Shang, H.H. Whisenand, and J.H. Kelly. 1992. Reversal of fulminant hepatic failure using an extracorporeal liver assist device. *Hepatology*, 16: 60–65.
- Takahashi, K. and S. Yamanaka. 2006. Induction of pluripotent stem cells from mouse embryonic and adult fibroblast cultures by defined factors. *Cell*, 126: 663–676.
- Takeda, T., S. Murphy, S. Uyama, G.M. Organ, B.L. Schloo, and J.P. Vacanti. 1995. Hepatocyte transplantation in swine using prevascularized polyvinyl alcohol sponges. *Tissue Eng.*, 1: 253–262.
- Tao, J.C., E.L. Cussler, and D.F. Evans. 1974. Accelerating gallstone dissolution. *Proc. Natl. Acad. Sci. USA*, 71: 3917–3921.
- Tatake, R.J., M.M. O'Neill, C.A. Kennedy, V.D. Reale, J.D. Runyan, K.-A.D. Monaco, K. Yu, W.R. Osborne, R.W. Barton, and R.D. Schneiderman. 2007. Glucose-regulated insulin production from genetically engineered human non-beta cells. *Life Sci.*, 81: 1346–1354.
- Teo, W.E. and S. Ramakrishna. 2006. A review on electrospinning design and nanofibre assemblies. *Nanotechnology*, 17: R89–R106.
- Thomas, H.W. 1962. The wall effect in capillary instruments: An improved analysis suitable for application to blood and other particulate suspensions. *Biorheology*, 1: 41–56.
- Thomas, L.C. 1992. *Heat Transfer*. New York: Prentice-Hall.
- Thompson, J.A., K.D. Anderson, J.M. DiPietro, J.A. Zwiebel, M. Zametta, W.F. Anderson, and T. Maciag. 1988. Site-directed neovessel formation in vivo. *Science*, 241: 1349–1352.
- Thompson, J.A., C.C. Haudenschild, K.D. Anderson, J.M. DiPietro, W.F. Anderson, and T. Maciag. 1989. Heparin-binding growth factor 1 induces the formation of organoid neovascular structures in vivo. *Proc. Natl. Acad. Sci. USA*, 86: 7928–7932.
- Thomson, R.C., M.J. Yaszemski, and A.G. Mikos. 1997. Polymer scaffold processing. In *Principles of Tissue Engineering*, R.P. Lanza, R. Langer, and W.L. Chick (eds.), pp. 263–272. Austin, TX: R.G. Landes Co.
- Tilles, A.W., H. Baskaaran, P. Roy, M.L. Yarmush, and M. Toner. 2001. Effects of oxygenation and flow on the viability and function of rat hepatocytes cocultured in a microchannel flat-plate bioreactor. *Biotechnol. Bioeng.*, 74: 379–389.
- Tinoco, I., K. Sauer, J.C. Wang, and J.D. Puglisi. 2001. *Physical Chemistry: Principles and Applications in Biological Sciences*, 4th ed. New York: Prentice-Hall, Inc.
- Todo, H., T. Oshizaka, W.R. Kadhum, and K. Sugibayashi. 2013. Mathematical model to predict skin concentration after topical application of drugs. *Pharmaceutics*, 5: 634–651.
- Tong, J. and J.L. Anderson. 1996. Partitioning and diffusion of proteins and linear polymers in polyacrylamide gels. *Biophys. J.*, 70: 1505–1513.
- Tozer, T.N. and M. Rowland. 2006. *Introduction to Pharmacokinetics and Pharmacodynamics*. Baltimore, MD: Lippincott, Williams & Wilkins.
- Tsai, A.G., K.-E. Arfors, and M. Intaglietta. 1990. Analysis of oxygen transport to tissue during extreme hemodilution. *Adv. Exp. Med. Biol.*, 277: 881–887.

## References

---

- Tun, T., H. Hayashi, T. Aung, Y.-J. Gu, R. Doi, H. Kaji, Y. Echigo et al. 1996. A newly developed three layer agarose microcapsule for a promising biohybrid artificial pancreas: Rat to mouse xenotransplantation. *Cell Transplant.*, 5: S59–S63.
- Tyn, M.T. and T.W. Gusek. 1990. Prediction of diffusion coefficients of proteins. *Biotechnol. Bioeng.*, 35: 327–338.
- Vadapalli, A., D. Goldman, and A.S. Popel. 2002. Calculations of oxygen transport by red blood cells and hemoglobin solutions in capillaries. *Artif. Cells Blood Substit. Immobil. Biotechnol.*, 30: 157–188.
- Van Blitterswijk, C. (ed.). 2008. *Tissue Engineering*. London, U.K.: Elsevier.
- Van de Pas, N.C.A., R.A. Woutersen, B. van Ommen, I.M.C.M. Rietjens, and A.A. de Graaf. 2012. A physiologically based in silico kinetic model predicting plasma cholesterol concentrations in humans. *J. Lipid Res.*, 53: 2734–2746.
- Vaslef, S.N., L.F. Mockros, and R.W. Anderson. 1989. Development of an intravascular lung assist device. *ASAIO Trans.*, 35: 660–664.
- Vaslef, S.N., L.F. Mockros, R.W. Anderson, and R.J. Leonard. 1994. Use of a mathematical model to predict oxygen transfer rates in hollow fiber membrane oxygenators. *ASAIO J.*, 40: 990–996.
- Verma, R.K., D. Murali Krishna, and S. Garg. 2002. Formulation aspects in the development of osmotically controlled oral drug delivery systems. *J. Control. Release*, 79: 7–27.
- Vilker, V.L., C.K. Colton, and K.A. Smith. 1981. The osmotic pressure of concentrated protein solutions: Effect of concentration and pH in saline solutions of bovine serum albumin. *J. Colloid Interface Sci.*, 79: 548–566.
- Wake, M.C., C.W. Patrick Jr., and A.G. Mikos. 1994. Pore morphology effects on the fibrovascular tissue growth in porous polymer substrates. *Cell Transplant.*, 3: 339–343.
- Wang, T., D. Miller, F. Burczynski, and X. Gu. 2014. Evaluation of percutaneous permeation of repellent DEET and sunscreen oxybenzone from emulsion-based formulations in artificial membrane and human skin. *Acta Pharm. Sin. B*, 4: 43–51.
- Warnock, W.L., D.K. Ellis, M. Cattral, D. Untch, N.M. Kneteman, and R.V. Rajotte. 1989. Viable purified islets of Langerhans from collagenase perfused human pancreas. *Diabetes*, 38: 136–139.
- Warnock, W.L., D. Ellis, R.V. Rajotte, I. Dawidson, S. Baekkeskov, and J. Egebjerg. 1988. Studies of the isolation and viability of human islets of Langerhans. *Transplantation*, 45: 957–963.
- Warnock, W.L. and R.V. Rajotte. 1988. Critical mass of purified islets that induce normoglycemia after implantation into dogs. *Diabetes*, 37: 467–470.
- Welling, P.G. 1986. *Pharmacokinetics: Processes and Mathematics*. ACS monograph 185. Washington, DC: American Chemical Society.
- Welsh, E.R. and D.A. Tirrell. 2000. Engineering the extracellular matrix: A novel approach to polymeric biomaterials. I. Control of the physical properties of artificial protein matrices designed to support adhesion of vascular endothelial cells. *Biomacromolecules*, 1: 23–30.
- Wenzl, R., A. van Beek, P. Schnabel, and J. Huber. 1998. Pharmacokinetics of etonogestrel released from the contraceptive implant Implanon®. *Contraception*, 58: 283–288.
- Wickramasinghe, S.R., J.D. Garcia, and B. Han. 2002a. Mass and momentum transfer in hollow fiber blood oxygenators. *J. Membr. Sci.*, 208: 247–256.
- Wickramasinghe, S.R., B. Han, J.D. Garcia, and P. Specht. 2005. Microporous membrane blood oxygenators. *AIChE J.*, 51: 656–670.
- Wickramasinghe, S.R. and B. Han. 2005. Designing microporous hollow fibre blood oxygenators. *Trans. IChemE Part A*, 83: 256–267.
- Wickramasinghe, S.R., C.M. Kahr, and B. Han. 2002b. Mass transfer in blood oxygenators using blood analogue fluids. *Biotechnol. Prog.*, 18: 867–873.
- Wiles, K., J.M. Fishman, P. De Coppi, and M.A. Birchall. 2016. The host immune response to tissue-engineered organs: Current problems and future directions. *Tissue Eng.*, 22: 208–219.
- Winslow, R.M. 1997. Blood substitutes. *Sci. Med.*, 4: 54–63.
- Wobma, H. and G. Vunjak-Novakovic. 2016. Tissue engineering and regenerative medicine 2015: A year in review. *Tissue Eng.*, 22: 101–113.
- Wright, J.C., S.T. Leonard, C.L. Stevenson, J.C. Beck, G. Chen, R.M. Jao, P.A. Johnson, J. Leonard, and R.J. Skowronski. 2001. An in vivo/in vitro comparison with a leuprolide somotic implant for the treatment of prostate cancer. *J. Control. Release*, 75: 1–10.

- Wu, H., E.S. Avgoustiniatos, L. Swette, S. Bonner-Weir, G.C. Weir, and C.K. Colton. 1999. In situ electrochemical oxygen generation with an immunoisolated device. *Ann. NY Acad. Sci.*, 875: 105–125.
- Yang, M.B., J.P. Vacanti, and D.E. Ingber. 1994. Hollow fibers for hepatocyte encapsulation and transplantation: Studies of survival and function in rats. *Cell Transplant.*, 3: 373–385.
- Yang, M.-C. and E.L. Cussler. 1986. Designing hollow-fiber contactors. *AIChE J.*, 32: 1910–1916.
- Yarmush, M.L., J.C.Y. Dunn, and R.G. Tompkins. 1992. Assessment of artificial liver support technology. *Cell Transplant.*, 1: 323–341.
- Yildirim, E.D., R. Besunder, S. Guceri, F. Allen, and W. Sun. 2008. Fabrication and plasma treatment of 3D polycaprolactone tissue scaffolds for enhanced cellular function. *Virtual Phys. Prototyp.*, 3: 199–207.
- Yildirim, E.D., R. Besunder, D. Pappas, F. Allen, S. Guceri, and W. Sun. 2010. Accelerated differentiation of osteoblast cells on polycaprolactone scaffolds driven by a combined effect of protein coating and plasma modification. *Biofabrication*, 2: 1–12.
- Young, M.E., P.A. Carroad, and R.L. Bell. 1980. Estimation of diffusion coefficients of proteins. *Biotechnol. Bioeng.*, 22: 947–955.
- Yoshida, F. and N. Ohshima. 1966. Diffusivity of oxygen in blood serum. *J. Appl. Physiol.*, 21: 915–919.
- Yu, K.-R., H. Natanson, and C.E. Dunbar. 2016. Gene editing of human hematopoietic stem and progenitor cells: Promise and potential hurdles. *Human Gene Therapy*, 27: 729–740.
- Yung, C.W., J. Fiering, A.J. Mueller, and D.E. Ingber. 2009. Micromagnetic-microfluidic blood cleansing device. *Lab Chip*, 9: 1171–1177.
- Zalzman, M., S. Gupta, R.K. Giri, I. Berkovich, B.S. Sappal, O. Karniel, M.A. Zern, N. Fleischer, and S. Efrat. 2003. Reversal of hyperglycemia in mice by using human expandable insulin-producing cells differentiated from fetal liver progenitor cells. *Proc. Natl. Acad. Sci. USA*, 100: 7253–7258.
- Zekorn, T., U. Siebers, R.G. Bretzel, M. Renardy, H. Planck, P. Zschocke, and K. Federlin. 1990. Protection of islets of Langerhans from interleukin-1 toxicity by artificial membranes. *Transplantation*, 50: 391–394.
- Zelman, A. 1987. The artificial kidney. In *Handbook of Bioengineering*, Chapter 39, R. Skalak and S. Chien (eds.). New York: McGraw-Hill Co.
- Zhao, F. and T. Ma. 2005. Perfusion bioreactor system for human mesenchymal stem cell tissue engineering: Dynamic cell seeding and construct development. *Biotechnol. Bioeng.*, 91: 482–493.
- Zhmud, B.V., F. Tiberg, and K. Hallstensson. 2000. Dynamics of capillary rise. *J. Colloid Interface Sci.*, 228: 263–269.
- Zielinski, B.A., M.B. Goddard, and M.J. Lysaght. 1997. Immunoisolation. In *Principles of Tissue Engineering*, R.P. Lanza, R. Langer, and W.L. Chick (eds.), pp. 323–332. Austin, TX: R.G. Landes Co.
- Zein, I., D.W. Hutmacher, K.C. Tan, and S.H. Teoh. 2002. Fused deposition modeling of novel scaffold architectures for tissue engineering applications. *Biomaterials*, 23: 1169–1185.
- Zopf, D.A., S.J. Hollister, M.E. Nelson, R.G. Ohye, and G.E. Green. 2013. Bioresorbable airway splint created with a three-dimensional printer. *N. Engl. J. Med.*, 368: 2043–2045.
- Zydny, A.L. 1995. Therapeutic apheresis and blood fractionation. In *The Biomedical Engineering Handbook*, J.D. Bronzino (ed.), pp. 1936–1951. Boca Raton, FL: CRC Press, Inc.
- Zydny, A.L. and C.K. Colton. 1986. A concentration polarization model for the filtrate flux in cross-flow microfiltration of particulate suspensions. *Chem. Eng. Commun.*, 47: 1–21.



Taylor & Francis

Taylor & Francis Group

<http://taylorandfrancis.com>

# Index

## A

Absolute pressure, 6  
Absolute temperature, 4–5  
Accumulation, 9  
Acidic fibroblast growth factor (aFGF), 535–536  
Acidosis, 456  
Active transport, 146–147  
Activity coefficient, 63–66  
Adaptive immune system, 534  
Adenosine triphosphate (ATP), 146  
Adsorption, distribution, metabolism, excretion, and toxicity (ADMET), 399  
Affinity adsorption  
    chemical adsorption, 505  
    ligand and solute binding, 505–506  
    physical adsorption, 505  
    of preformed antibodies  
        affinity adsorption membrane system, 508  
        characteristic time, IgM adsorption process, 508  
         $\alpha$ -galactosyl-reactive IgM antibodies removal, 506–507  
        hyperacute rejection, 506  
        plasmapheresis, 506, 508  
        preformed natural antibodies, 506  
        xenotransplantation, 506  
    relative reservoir concentration, 509  
    reservoir volumes filtered, 509  
Affinity columns, 451  
aFGF, *see* Acidic fibroblast growth factor  
Aggrecan, 522  
Aggregates, 153  
Albumin, 153  
Aldosterone, 410  
Alpha globulins, 153  
Anemia, 456  
Angiotensin II, 587  
Antidiuretic hormone, 410  
Antigen-presenting cells (APCs), 549–551  
Antigens, 506

Apparent distribution volumes, drug, 403  
    biological half-life, 413  
    Oie-Tozer equation, 404–407  
    plasma clearance, 412  
    renal clearance, 410–411  
    total plasma concentration, 404  
Apparent viscosity, 157, 166  
Aquapheresis, 451, 470  
Area test, 64  
Artificial blood  
    blood transfusion, 387  
    hemoglobin-based oxygen carriers, 388  
    oxygenated blood carries, 389  
    oxygen therapeutics, 388  
    oxygen transport rate, 390–391  
    PFCs, 388–390  
    RBCs, 388–389  
    volume expanders, 387  
Artificial liver systems, 579–580  
Atmospheric pressure, 6  
ATP, *see* Adenosine triphosphate  
Automated peritoneal dialysis (APD), 467  
Avogadro's number, 5

## B

Barometer, 6  
Barometric pressure, 6  
Basal lamina, 522  
Bernoulli equation, 188–189, 191–200  
Beta globulins, 153  
Biconcave discoid, 153  
Binary systems, 48–49  
Bingham plastic, 158  
Bioartificial organs  
    design of, 589–590  
    examples of, 558–559  
    immunoisolation  
        albumin and transferrin, 553  
        anaphylactic reaction, 554–555  
        complement system, 553–554

- lymphocytes and macrophages, 553  
lymphokines, 554  
pathways, 552  
permeability, 555–557
- immunology  
  antibodies, 546–548  
  APCs, 550–551  
  B-lymphocytes, 546, 550–551  
  cell-mediated component and humoral component, 545  
  T-lymphocytes, 548–551
- immunosuppressive drugs, 545
- kidney, 587–589
- liver  
  carbohydrate metabolism, 578  
  cirrhosis, 579  
  cross circulation, 579–580  
  development, 580–581  
  extracorporeal bioartificial livers, 582–586  
  fat metabolism, 578  
  fulminant hepatic failure, 579  
  gamma globulins, 579  
  hemodialysis, 579–580  
  hepatic artery, 578  
  hepatocytes, 578, 581  
  implantable and extracorporeal systems, 581  
  membrane-based approaches, 581–582  
  portal vein, 578
- membrane Sherwood number, 558
- pancreas  
  approaches, 561  
  glucose and insulin interactions, 572–574  
  intravascular devices, 561–563  
  islet insulin release model, 569–572  
  IVGTT, 575–578  
  macroencapsulation, 565–568  
  microencapsulation, 563–565  
  number of islets needed, 568–569  
  OGTT, 575–578
- Blood  
  alpha and beta globulins, 153  
  boundary layer theory  
    flow near a wall set in motion, 177–182  
    laminar flow of fluid along flat plate, 183–187  
  capillary action, 202–205  
  capillary viscometer and laminar flow, tubes  
    Hagen–Poiseuille equation, 159–163  
    Rabinowitsch equation, 163–164  
    viscosity, 158  
  wall shear stress, 159, 164
- Casson equation  
  experimental data, 167–168  
  low shear rates, 170  
  reduced average velocity *vs.* wall shear stress, 168–169  
  shear stress, 167  
  velocity profile, 168–169
- cellular component, 153–155
- equilibrium capillary rise, 200–202
- gamma globulins, 153
- key flow equations, 164–165
- mechanical energy balance equation  
  Bernoulli equation, 188–189, 191–200  
  Fanning friction factor, 190  
  frictional effects, 190  
  gravitational acceleration, 189  
  hydraulic diameter, 191  
  mass conservation, 189  
  sudden contractions and expansions, 190–191  
  units, 189
- Rabinowitsch equation, 163–164
- rheology  
  Bingham plastic and Casson fluid, 158  
  dilatant fluid, 157  
  laminar flow, 155–156  
  shear stress-shear rate relationship, 157  
  velocity profile development, 155–156
- tube diameter effect  
  Fahraeus effect, 170–171  
  Fahraeus–Lindqvist effect, 171–173  
  marginal zone theory, 173–176
- Blood oxygenators, 451  
  background, 470–471  
  carbon dioxide transfer, 482–484  
  hollow fiber membrane calculations, 484–488  
  operational characteristics, 471–472  
  oxygen transfer  
    blood-side equation, 476–477  
    blood-side mass transfer coefficient, 479–481  
    blood-side mass transfer resistance, 476  
    blood-side membrane area, 477  
    constant oxygen partial pressure, 478–479  
    gas-side equation, 477  
    mass balance model, 475  
    mass transfer coefficient, 476  
    shell balance, 475  
  types, 472–474

- Body fluids, 125–126  
 capillary endothelium, 139–140  
 capillary plasma protein retention, 127–129  
 compositions, 126–127  
 extracellular fluid, 125  
 filtration flow  
     capillary membrane, 133  
     hydraulic conductance, 133–135  
     hydrodynamic and osmotic pressures, 132  
     volumetric fluid transfer rate, 132  
 hematocrit, 125  
 intracellular fluid, 125–126  
 lymphatic system, 139  
 net capillary filtration rate  
     blood flow, 138–139  
     capillary characteristics, 136  
     continuous capillaries, 136  
     discontinuous capillaries, 136  
     electrical properties, 137  
     fenestrated capillaries, 136  
     Starling flow, 137  
 osmotic pressure  
     calculation, 130–131  
     factors, 131–132  
     osmolarity, 129–130  
 transcellular fluid, 125  
 Bohr effect, 359  
 Bosanquet equation, 203  
 Boundary conditions  
     chemical reaction, 226–228  
     concentration, 225–226  
     convective transport, 226  
     initial condition, 225  
     zero solute flux, 226  
 Boundary layer theory  
     flow near a wall set in motion  
         boundary layer thickness, 178, 182  
         complementary error function, 181  
         error function, 181  
         kinematic viscosity, 179  
         Laplace transforms, 179–181  
         partial differential equation, 178  
         semi-infinite quantity, 177  
         velocity profile, 178  
     laminar flow of fluid along flat plate  
         boundary conditions, 184–185  
         boundary layer thickness, 183, 185  
         friction factor, 187  
         Leibnitz's rule, 184  
         Newtonian fluid, 184  
         power, 186  
 laminar flow number, 185  
 Reynolds number, 185  
 steady-state mass balance, 183  
 von Karman momentum balance equation, 184  
 Bubble oxygenators, 472–473  
 Bubble point temperature, 88–89
- C**
- CAD software, *see* Computer-aided design software  
 Capillary action, 202–205  
 Capillary endothelium, 139–140  
 Capillary force, 202  
 Capillary rise, 200–202  
 Capillary viscometer and laminar flow  
     Hagen–Poiseuille equation, 159–163  
     Rabinowitsch equation, 163–164  
     viscosity, 158  
     wall shear stress, 159, 164  
 Carbaminohemoglobin, 359  
 Carrier proteins, 142  
 Casson equation  
     experimental data, 167–168  
     low shear rates, 170  
     reduced average velocity vs. wall shear stress, 168–169  
     shear stress, 167  
     velocity profile, 168–169  
 Casson fluid, 158, 168–169  
 Cell adhesion molecules (CAMs), 523–524  
 Cell membrane  
     action potentials, 144–146  
     carrier proteins and channel proteins, 142  
     coupled transport, 142  
     electrochemical gradient, 142  
     enzymes, 141  
     ion pumps, 146–147  
     lipid bilayer, 141  
     Nernst equilibrium membrane potential, 143  
     net driving force, 143–144  
     phospholipids, cholesterol, and glycolipids, 141  
     structure, 141  
     transmembrane proteins, 141  
 Channel proteins, 142  
 Chemical potential, 47  
 CHF, *see* Congestive heart failure  
 Cirrhosis, 579  
 Clausius–Clapeyron equation, 61  
 Clonal deletion theory, 546  
 Closed system, 35–36  
 Collagens, 521

- Colloid osmotic pressure, *see* Osmotic pressure  
Combination of variables, 271  
Complementary error function, 181  
Compressibility factor ( $Z$ ), 53–55  
Computer-aided design (CAD) software, 531–533  
Congestive heart failure (CHF), 470  
Connective tissues, 520  
Conservation of mass  
    chemical reactions, 11–12  
    extent of reaction, 13–15  
    law of conservation, 9–11  
    material balances, 15–18  
Contact angle, 201  
Continuous ambulatory peritoneal dialysis (CAPD), 587  
    APD, 467  
    average mass removal rate of a particular solute, 467  
    constant volume model, 468–469  
    mass transfer characteristics, 467  
    mathematical models, 468  
    peritoneum, 466–467  
    solute transport rate, 468  
    transport properties, 468  
    with ultrafiltration, 469  
Continuous capillary, 136  
Continuous infusion  
    controlled release drug delivery systems, 415  
    drug concentration vs. time, 415  
    implantable devices, 427–429  
    inulin infusion, 416–418  
    osmotic pump drug delivery system, 418–420  
    single-compartment model, 415  
    steady-state plasma drug concentration, 416  
    transdermal patches, 420–427  
Controlled release drug delivery systems, 415  
    from implantable devices, 427–429  
    by osmotic pump, 418–420  
    transdermal patches  
        drug permeability, 421  
        plasma drug concentration, 422  
        rate-limiting membrane, 422–423  
        skin permeability, 423–424  
        stratum corneum permeability, 420–421, 424–427  
        unsteady mass balance, 422  
Convection, 221  
    cylindrical tube and fluid flow  
        average Sherwood number, 272–273  
        bulk flow, 269–270  
        dimensionless quantities, 268–269  
        dimensionless variables, 270–271  
        gamma function, 271–272  
        mass balance, 273–275  
        partial differential equation, 269  
dimensionless quantities, 268–269  
dimensionless variables, 270–271  
gamma function, 271–272  
mass balance, 273–275  
partial differential equation, 269  
similarity transform technique/combination of variables, 271  
volumetric flow rate ( $Q$ ), 272  
disk rotation  
    axial velocity, 258–259  
    dimensionless distance, 257–258, 260–262  
    gamma function property, 259  
    3D flow, 256–257  
laminar flow  
    average mass transfer coefficient, 266–267  
    boundary layer thickness, 264–265  
    Fick's first law, 263–264  
    length averaged mass transfer coefficient, 266  
    polymeric material, 267–268  
    Schmidt number, 265–266  
    semi-infinite flat plate, 262–263  
    steady-state solute balance, 263  
short contact time solution  
    liquid film, 248–256  
    mass transfer coefficient, 250–251  
    Peclét number, 249  
    penetration distance, 248  
Critical point (C), 59  
Cytokines, 550–551

## D

- Damköhler number (Da), 374, 378  
Danckwerts' boundary conditions, 374  
Darcy's law, 309  
Degrees of freedom, 15  
Derived dimensional quantities  
    equations of state, 7–8  
    pressure, 6–7  
    SI units, 3, 5  
    volume, 7  
Diffusion, 221  
    cylindrical tube and fluid flow  
        average Sherwood number, 272–273  
        bulk flow, 269–270  
        dimensionless quantities, 268–269  
        dimensionless variables, 270–271  
        gamma function, 271–272  
        mass balance, 273–275  
        partial differential equation, 269

- similarity transform technique/combination of variables, 271  
 volumetric flow rate ( $Q$ ), 272
- disk rotation  
 axial velocity, 258–259  
 dimensionless distance, 257–258, 260–262  
 gamma function property, 259  
 3D flow, 256–257
- laminar flow  
 average mass transfer coefficient, 266–267  
 boundary layer thickness, 264–265  
 Fick's first law, 263–264  
 length averaged mass transfer coefficient, 266  
 polymeric material, 267–268  
 Schmidt number, 265–266  
 semi-infinite flat plate, 262–263  
 steady-state solute balance, 263
- semi-infinite stagnant medium, 241–243
- short contact time solution  
 liquid film, 248–256  
 mass transfer coefficient, 250–251  
 Peclet number, 249  
 penetration distance, 248
- Diffusion limited, 276
- Dilatant fluid, 157
- Dimensional equation, 8–9
- Dimensions, 1
- 2,3-Diphosphoglycerate (DPG), 359
- Discontinuous capillary, 136
- Donnan potential, 108–109
- Drag coefficient, 187
- Drug clearance  
 area under the curve, 413  
 biological half-life, 413  
 plasma clearance, 412–413  
 renal clearance, 410–412  
 urine, accumulation in, 413–414
- Drug distribution  
 apparent distribution volumes, 403  
 biological half-life, 413  
 Oie-Tozer equation, 404–407  
 plasma clearance, 412  
 renal clearance, 410–411  
 total plasma concentration, 404
- diffusion rate limited, 403
- drug metabolism, 407–408
- perfusion rate limited, 403
- renal excretion, 408–410
- true distribution volumes, 403
- E**
- Edema, 456
- Elastin, 521
- Embryonic stem cells, 516
- Endocytosis, 140
- Engineering problems, 16, 18–19
- Entropy, 38
- Entropy change, 41–42
- Epidermal growth factor (EGF), 526
- Equation of state, 7–8
- Equilibrium capillary rise, 200–202
- Equivalent islet number (EIN), 563–565
- Error function, 181
- Erythrocytes, 153
- Erythropoietin, 456
- Exact differentials, 44–46
- Exocytosis, 140
- Extent of reaction, 13–15, 110–111
- Extracellular matrix (ECM)  
 aggrecan, 522  
 basement membrane, 522  
 collagens, 521  
 connective tissues, 520  
 elastin, 521  
 fibroblasts, 519  
 fibronectin, 521–522  
 glycosaminoglycans, 521  
 macromolecules, 519–520
- Extracorporeal devices  
 affinity adsorption  
 chemical adsorption, 505  
 ligand and solute binding, 505–506  
 physical adsorption, 505  
 of preformed antibodies, 506–508  
 relative reservoir concentration, 509  
 reservoir volumes filtered, 509
- applications, 451
- blood oxygenators  
 background, 470–471  
 carbon dioxide transfer, 482–484  
 hollow fiber membrane, 484–488  
 operational characteristics, 471–472  
 oxygen transfer, 475–482  
 types, 472–474
- contacting schemes, 451–453
- hemodialysis  
 aquapheresis, 470  
 background, 456–457  
 clearance and dialysance, 459–460  
 dialysate composition, 457–458

- peritoneal dialysis, 466–469  
single compartment model, urea hemodialysis, 464–466  
solute transfer, 460–464  
ultrafiltration, 458–459
- immobilized enzyme reactors  
background, 488–489  
design equations, 500–505  
enzyme reaction kinetics, 490–493  
external mass transfer resistance, 499–500  
first order reaction, 497–499  
medical application, 489–490  
observed reaction rate, 499  
reaction-diffusion model, 493–497
- solute transport  
mass transfer coefficients, 453–454  
solute diffusivity in blood, 454–456
- Extracorporeal hemoperfusion system, 588–589  
Extracorporeal liver assist device (ELAD), 584–585  
Extracorporeal perfusion, 580  
Extrusion bioprinting, 533
- F**
- Fab, *see* Fragment antigen binding  
Fahraeus effect, 170–171  
Fahraeus–Lindqvist effect, 171–173  
Fanning friction factor, 190  
Fc, *see* Fragment crystallizable  
Fenestrated capillary, 136  
Fibrin, 153  
Fibrinogen, 153  
Fibroblast growth factor (FGF), 526  
Fibronectin, 521–522  
Fick’s first law  
Cartesian coordinates, 223  
diffusivity of solute A, 223  
dilute solution, 225  
equimolar counterdiffusion, 225  
forced convection, 224  
stagnant/quiescent fluid, 224  
Fick’s second law  
constant surface concentration, 232–233  
infinite planar stagnant medium, 238–240  
infinite stagnant medium, 236–238  
Laplacian operator, 233–234  
semi-infinite stagnant medium, 234–236  
Film oxygenators, 473  
Film theory, 242–243  
Filtration flow, 308  
Fire triangle, 92
- First law of thermodynamics  
closed system, 35–36  
isolated system, 35  
steady flow process, 36–37
- First-order drug absorption and elimination  
mass balance, 429–430  
nonlinear regression analysis, 431  
peak time concentration, 430  
plasma concentration levels, 431–433  
plasma drug concentration, 429, 431  
single-compartment model, 429
- Flammability limits  
benzene, 93  
combustion engines, furnaces, and incinerators, 91  
fire triangle, 92  
flammable mixtures, 93–94  
lower and upper flammability limits, 92
- Flow limited, 276
- Fluid superficial velocity, 373
- Fragment antigen binding (Fab), 546  
Fragment crystallizable (Fc), 547  
Friction factor, 187  
Fulminant hepatic failure, 579  
Fundamental dimensions  
mass, 3  
mole, 5  
SI units, 1, 3  
temperature, 4–5  
weight, 3
- Fundamental property relations  
exact differentials, 44–46  
reversible process, 44  
single fluid phase, 43–44
- G**
- Gamma function, 259, 271–272  
Gamma globulins, 153, 546  
Gauge pressures, 6  
Gibbs-Donnan effect  
NaCl concentration, 103–105, 107–108  
osmotic pressure, 105–107  
semipermeable membrane, 102–103  
Gibbs-Duhem equation, 48  
Gibbs free energy (G), 43  
Glomerular filtrate, 408–409  
Glomerular filtration rate (GFR), 409, 412  
Glomerulus, 587  
Glycosaminoglycans (GAGs), 521  
Gram mole, 5  
Gravitational force, 202

**H**

Hagen-Poiseuille equation  
 cylindrical tube, 159–162  
 noncircular cross section, 162–163

Haldane effect, 359

Heat capacity, 40–41

Helmholtz free energy (A), 43

Hematocrit (Hct), 125

Hemodialysis  
 aquapheresis, 470  
 background, 456–457  
 CAPD  
   APD, 467  
   average mass removal rate of a particular solute, 467  
   constant volume model, 468–469  
   mass transfer characteristics, 467  
   mathematical models, 468  
   peritoneum, 466–467  
   solute transport rate, 468  
   transport properties, 468  
   with ultrafiltration, 469  
 clearance, 459–460  
 dialysance, 460  
 dialysate composition, 457–458  
 single compartment model, urea hemodialysis, 464–466  
 solute transfer  
   blood concentration, 461  
   cocurrent pattern, 460  
   extraction ratio, 461  
   mass transfer in hollow fiber membrane, 463–464  
   number of transfer units, 461  
   performance equation, 461–462  
   shell mass balance, 461  
   urea clearance, 462–463  
 systems, 580  
 ultrafiltration, 458–459

Hemoglobin, 349  
 allosteric protein, 355  
 heme group, 354–355  
 oxygen binding capacity, 354  
 polypeptide chains, 354  
 prosthetic group, 354  
 protoporphyrin, 355  
 structure, 354

Hemoperfusion, 451

Hemostasis, 153

Henderson-Hasselbalch equation, 114

Henle's loop, 408–409

Henry's constant (H), 77–78

Henry's law, 346, 352, 355

HepatAssist bioartificial liver, 583

Hill equation, 356–358

Homozygous, 535–536

Hydraulic conductance, 133–135

Hydraulic diameter, 280

Hyperacute rejection, 506

**I**

Ideal solution model, 56–58

Immobilized enzyme reactors, 451, 580  
 background, 488–489  
 design equations  
   heparin conversion, 502–505  
   packed bed reactor, 501–502  
   substrate concentration, 500  
   well-mixed reactor, 502–503

enzyme reaction kinetics  
 conversion process, 490  
 enzyme-substrate dissociation constant, 491  
 free enzyme kinetics, 490  
 heparin degradation, 492  
 Lineweaver-Burke plot, 493  
 Michaelis-Menten equation, 491  
 rate of enzyme reaction, 491  
 substrate concentration, 491–492  
 external mass transfer resistance, 499–500

first order reaction  
 cylindrical enzyme particle, 497–499  
 flat plate enzyme particle, 499  
 spherical enzyme particle, 497–499  
 Thiele modulus, 498–499

medical application, 489–490  
 observed reaction rate, 499

reaction-diffusion model  
 boundary conditions, 494–495  
 dimensionless variables, 495  
 effective diffusivity, 494  
 effectiveness factor, 495–497  
 intraparticle concentration profile, 496  
 solute diffusivity, 493  
 spherical immobilized enzyme particle, 494  
 steady-state shell balance, 494  
 substrate diffusivity, 493–494  
 Thiele modulus, 495

Immunoglobulin A (IgA), 548

Immunoglobulin D (IgD), 548

- Immunoglobulin E (IgE), 548  
Immunoglobulin G (IgG), 547–548  
Immunoglobulin M (IgM), 548  
Immunoisolation  
    albumin and transferrin, 553  
    anaphylactic reaction, 554–555  
    complement system, 553–554  
    lymphocytes and macrophages, 553  
    lymphokines, 554  
    membrane, 518–519  
    pathways, 552  
    permeability, 555–557  
Immunology  
    antibodies, 546–548  
    APCs, 550–551  
    B-lymphocytes, 546, 550–551  
    cell-mediated component and humoral component, 545  
    T-lymphocytes, 548–551  
Immunoprotection, 518–519  
Induced pluripotent stem cells (iPSCs), 517  
Inertial force, 202–203  
Infinite quiescent medium  
    drug particles, 244–247  
    solute concentration ( $C_A$ ), 243–244  
    sphere and fluid, 247  
Inflammation period, 535  
Initial condition, 225  
Inkjet bioprinting, 533  
Innate immune system, 534  
Insulin-dependent diabetes mellitus (IDDM), 555  
Interleukin-1 (IL-1), 550–551  
Internal energy (U), 35–36  
Intravascular devices, 561–563  
Intravenous glucose tolerance test (IVGTT), 575–578  
Intravenous (IV) injection, 414–415  
Irreversible processes, 38  
Irreversible thermodynamics, membrane transport  
    cross coefficients, 308  
    Darcy's law, 309  
    driving forces, 307–308  
    filtration flow, 308  
    linear combination, 308  
     $L_p$ ,  $P_m$ , and  $\sigma$  parameters, 310–312  
    multicomponent membrane transport, 312  
    Peclet number (Pe), 312–313  
    reflection coefficient, 309  
    total mass transfer rate, 309–310  
    ultrafiltration, 308  
Isentropic process, 42  
Islet insulin release model, 569–572  
Islet of Langerhans, 361–362  
Isolated system, 35
- K**
- Kelvin equation, 96  
Kidney, bioartificial  
    angiotensin II, 587  
    clinical trials, 589  
    continuous ambulatory peritoneal dialysis, 587  
    glomerulus, 587–588  
    PHSC, 588  
    RAD, 588–589  
    renal tubule, 587–588  
Kinematic viscosity, 179  
Kinetic energy ( $E_K$ ), 35–36  
Krogh tissue cylinder model  
    capillary bed, 318  
    cell-free plasma layer, 319–320  
    convection vs. diffusion effects, 323–325  
    critical radius, 321–322  
    cylindrical layer of tissue, 318  
    effective diffusivity, 318  
    glucose concentration, 322–323  
    in hollow fiber, 318  
    maximum reaction rate, 319  
    Michaelis-Menten equation, 318  
    oxygen transport  
        approximate solution, 384–387  
        capillary oxygenated hemoglobin mass balance, 381  
        capillary unbound oxygen mass balance, 381–383  
        tissue oxygen mass balance, 383–384  
    solute concentration, 320–321  
    steady-state shell balance, 320
- L**
- Laminar flow  
    average mass transfer coefficient, 266–267  
    boundary layer thickness, 264–265  
    Fick's first law, 263–264  
    length averaged mass transfer coefficient, 266  
    polymeric material, 267–268  
    Schmidt number, 265–266  
    semi-infinite flat plate, 262–263  
    steady-state solute balance, 263  
Laminin, 127, 522  
Laplace transform technique, 179–181

- Laplace-Young equation, 95  
 Laplacian operator, 233–234  
 Laser-assisted bioprinting (LAB), 533  
 Law of conservation, 9–11  
 Leibnitz's rule, 184  
 Lewis-Randall rule, 57  
 LFL, *see* Lower flammability limit  
 Linear regression, 20, 22–26  
 Lineweaver-Burke method, 493  
 Lipid bilayer, 141  
 Liver, bioartificial  
     carbohydrate metabolism, 578  
     cirrhosis, 579  
     cross circulation, 579–580  
     development, 580–581  
     extracorporeal bioartificial livers  
         albumin production, 582–583  
         compartment hollow fiber, 582  
         cytochrome P-450 system, 583  
         ELAD, 584–585  
         HepatAssist, 583  
         hollow fiber bundles, 585–586  
         lidocaine clearance, 582  
         limitation, 584  
         oxygen consumption, 582  
     fat metabolism, 578  
     fulminant hepatic failure, 579  
     gamma globulins, 579  
     hemodialysis, 579–580  
     hepatic artery, 578  
     hepatocytes, 578, 581  
     implantable and extracorporeal systems, 581  
     membrane-based approaches, 581–582  
     portal vein, 578  
 Liver tissue, hemoperfusion of, 580  
 Log mean concentration difference, 276–277  
 Lower flammability limit (LFL), 92  
 Lucas–Washburn equation, 204  
 Lymphatic system, 139  
 Lymphokines, 550–551
- M**
- Macroencapsulation, 565–568  
 MACs, *see* Membrane attack complexes  
 Major histocompatibility complex (MHC), 549  
 Marginal zone theory, 173–176  
 Mass, 3  
 Mass average velocity, 221  
 Mass average velocity vector, 221–222  
 Mass balance, 273–275
- Mass concentration, 221  
 Mass transfer  
     binary diffusion, 223  
     boundary conditions, 225–228  
     concentration, 221  
     convection, 221  
         cylindrical tube and fluid, 268–275  
         disk rotation, 256–262  
         laminar flow, 262–268  
         short contact time solution, 248–256  
     cylindrical tube, 278–282  
 diffusion, 221  
     cylindrical tube and fluid, 268–275  
     disk rotation, 256–262  
     laminar flow, 262–268  
     semi-infinite stagnant medium, 241–243  
     short contact time solution, 248–256
- diffusivity  
     Chapman-Enskog theory, 228  
     experimental data, 228  
     Stokes-Einstein equation, 229–232  
     in water, 229
- Fick's first law  
     Cartesian coordinates, 223  
     diffusivity of solute A, 223  
     dilute solution, 225  
     equimolar counterdiffusion, 225  
     forced convection, 224  
     stagnant/quiescent fluid, 224
- Fick's second law  
     constant surface concentration, 232–233  
     infinite planar stagnant medium, 238–240  
     infinite stagnant medium, 236–238  
     Laplacian operator, 233–234  
     semi-infinite stagnant medium, 234–236
- flowing fluid  
     arbitrary cross section, 277–278  
     concentration profile, 275  
     log mean concentration difference, 276–277
- infinite quiescent medium  
     drug particles, 244–247  
     solute concentration ( $C_A$ ), 243–244  
     sphere and fluid, 247
- mass average velocity, 221  
 mass average velocity vector, 221–222  
 mass transfer coefficient  $k_m$ , 240–241  
 molar average velocity, 221  
 molar average velocity vector, 222  
 molar flux of species, 222  
 velocity, 222

- Mass transfer coefficient  $k_m$ , 226, 240–241  
Mass transfer controlling, 228  
Mass transfer, heterogeneous materials  
    irreversible thermodynamics, membrane transport  
        cross coefficients, 308  
        Darcy's law, 309  
        driving forces, 307–308  
        filtration flow, 308  
        linear combination, 308  
         $L_p$ ,  $P_m$ , and  $\sigma$  parameters, 310–312  
        multicomponent membrane transport, 312  
        Peclet number (Pe), 312–313  
        reflection coefficient, 309  
        total mass transfer rate, 309–310  
        ultrafiltration, 308  
    solute diffusion/transport  
        across a thin porous membranes, 292–293  
        across gel membranes, 306–307  
        from blood, 289–290  
        in blood and tissue, 304–306  
        between a capillary and surrounding tissue space, 317–329  
        by filtration and diffusion across capillary wall, 313–317  
        by filtration flow across a membrane, 329–339  
        membrane permeability, 295–298  
        porosity, 289  
        within a porous polymeric material, 298–304  
Renkin equation, mica membranes, 293–294  
restricted/hindered diffusion, 291  
steric exclusion, 290–291  
tortuosity, 290  
Material balances, 15–18  
Maturation phase, 535  
Maxwell equations, 45–46  
Membrane attack complexes (MACs), 548  
Membrane oxygenators, 473–474  
    carbon dioxide transfer, 482–484  
    hollow fiber membrane calculations, 484–488  
    oxygen transfer  
        blood-side equation, 476–477  
        blood-side mass transfer coefficient, 479–481  
        blood-side mass transfer resistance, 476  
        blood-side membrane area, 477  
        constant oxygen partial pressure, 478–479  
        gas-side equation, 477  
    mass balance model, 475  
    mass transfer coefficient, 476  
    shell balance, 475  
Mesenchymal stem cell (MSC), 517  
MHC, *see* Major histocompatibility complex  
Michaelis constant, 319  
Michaelis-Menten equation, 318, 490  
Michaelis-Menten rate model, 408  
Microchannel perfusion bioreactor, oxygen transport  
    average oxygen concentration, 378  
    boundary conditions, 377–378  
    convective-diffusion equation, 377  
    Damkohler number, 378  
    dimensionless oxygen concentration profile, 378  
    dimensionless variables, 377  
    oxygen concentration control, 376  
    parallel-plate microchannel bioreactor, 376  
    Peclet number, 377–378  
    pO<sub>2</sub> levels, 379–380  
    steady-state shell balance, 376  
Microencapsulation, 563–565  
Molar average velocity, 221  
Molar average velocity vector, 222  
Molar concentration, 221  
Molecular weight, 5
- ## N
- Nephron structure, 408–409  
Nernst equation, 109  
Nernst equilibrium membrane potential, 143  
Nerve growth factor (NGF), 526  
Newtonian liquid, 159–163  
Newton's method, 71  
Newton's second law, 203  
Nominal molecular weight cutoff (NMWCO), 555  
Nonlinear regression, 20, 26–28  
Non-Newtonian liquid, 163–164  
Normal boiling point ( $T_{BP}$ ), 60  
Numerical methods  
    first order differential equation, 29–30  
    integration, 28–29  
    linear regression, 20, 22–26  
    nonlinear regression, 20, 26–28  
    root finder, 32–33  
    second order differential equation, 30–31  
    shear stress *vs.* shear rate, 19–21  
    variable of interest, 32–33
- ## O
- Oie-Tozer equation, 404–407  
Oral glucose tolerance test (OGTT), 574–578  
Osmosis, 78–79

- Osmotic pressure, 78–81  
 calculation, 130–131  
 factors, 131–132  
 osmolarity, 129–130
- Oxygen diffusion, multicellular systems  
 Brockman bodies, 349–350, 352–354  
 capillaries, 349  
 hemoglobin, 349  
   allosteric protein, 355  
   heme group, 354–355  
   oxygen binding capacity, 354  
   polypeptide chains, 354  
   prosthetic group, 354  
   protoporphyrin, 355  
   structure, 354  
 Henry's constant, 349–350  
 Hill equation, 356–358  
 hypoxia, 349  
 necrosis, 349  
 oxygen-hemoglobin dissociation curve  
   allosteric interactions, 358  
   Bohr effect, 359  
   carbaminohemoglobin, 359  
   dissolved oxygen concentration, 355  
   DPG, 359  
   equilibrium partial pressure of oxygen, 355  
   Haldane effect, 359  
   shifts, 358  
 oxygen levels, 356  
 oxygen partial pressure, 349  
 pO<sub>2</sub> profiles, 349–350  
 spherical volume of cells  
   diffusional oxygen transport rate, 351  
   oxygen consumption rate, 350–354  
   oxygen mass balance, 351  
 tissue oxygenation  
   change in blood oxygenation, 361–362  
   steady-state oxygen mass balances, 359–360  
   tissue oxygen consumption rate, 359–361
- Oxygen-hemoglobin dissociation curve  
 allosteric interactions, 358  
 Bohr effect, 359  
 carbaminohemoglobin, 359  
 dissolved oxygen concentration, 355  
 DPG, 359  
 equilibrium partial pressure of oxygen, 355  
 Haldane effect, 359  
 shifts, 358
- Oxygen transport  
 in Krogh tissue cylinder approach  
   approximate solution, 384–387
- capillary oxygenated hemoglobin mass balance, 381  
 capillary unbound oxygen mass balance, 381–383  
 tissue oxygen mass balance, 383–384
- oxygen mass balance, blood oxygenator, 363–364
- in perfusion bioreactors  
 convective and diffusive transport of oxygen, 373–376  
 microchannel perfusion bioreactor, 376–380  
 planar cellular construct, 372–373
- in planar bioartificial organs  
 boundary conditions, 365  
 conceptual model, 364–365  
 oxygen concentration, 365  
 oxygen profile, 365–367  
 steady-state shell balance, 364
- in planar tissue engineered constructs  
 average partial pressure of oxygen, 367–368  
 in vitro culture, 368–370  
 maximum thickness, 370–372  
 polymeric scaffold, 367
- P**
- Pancreas, bioartificial approaches, 561  
 glucose and insulin interactions, 572–574  
 intravascular devices, 561–563  
 islet insulin release model, 569–572  
 IVGTT, 575–578  
 macroencapsulation, 565–568  
 microencapsulation, 563–565  
 number of islets needed, 568–569  
 OGTT, 575–578
- Partial differential equation, 269
- Partial molar property  
 binary systems, 48–49  
 chemical potential, 47  
 Gibbs-Duhem equation, 48  
 Gibbs free energy, 51–52  
 ideal gas, 49–51  
 property change of mixing, 49  
 pure component value, 48
- Partial pressure (P<sub>i</sub>), 49–50
- PCL, *see* Polycaprolactone
- PDGF, *see* Platelet-derived growth factor
- Peclet number (Pe), 249, 312–313, 374, 377–378
- PED, *see* Precision extrusion deposition
- Perfect vacuum, 6

- Perfluorocarbons (PFCs), 539  
Perforins, 547  
*Peritoneal dialysis, see Continuous ambulatory peritoneal dialysis*  
Pharmaceutics, 399  
Pharmacodynamics, 399  
Pharmacokinetics (PK)  
    ADMET, 399  
    bioartificial pancreas  
        glucose and insulin interactions, 572–574  
        IVGTT, 575–578  
        OGTT, 575–578  
    compartmental PK models, 401–402  
    continuous infusion  
        controlled release drug delivery systems, 415  
        drug concentration *vs.* time, 415  
        implantable devices, 427–429  
        inulin infusion, 416–418  
        osmotic pump drug delivery system, 418–420  
        single-compartment model, 415  
        steady-state plasma drug concentration, 416  
        transdermal patches, 420–427  
    drug clearance  
        area under the curve, 413  
        biological half-life, 413  
        plasma clearance, 412–413  
        renal clearance, 410–412  
        urine, accumulation in, 413–414  
    drug distribution, factors affecting  
        apparent distribution volumes, 403–407  
        diffusion rate limited, 403  
        drug metabolism, 407–408  
        perfusion rate limited, 403  
        renal excretion, 408–410  
        true distribution volumes, 403  
entry routes, drugs  
    enteral route, 399  
    parenteral routes, 399–401  
first-order drug absorption and elimination  
    mass balance, 429–430  
    nonlinear regression analysis, 431  
    peak time concentration, 430  
    plasma concentration levels, 431–433  
    plasma drug concentration, 429, 431  
        single-compartment model, 429  
intravenous injection, 414–415  
model independent PK models, 402  
physiological PK models, 402  
physiological response to drug, 401  
two-compartment models, 433–434  
    with drug absorption from implantable device, 440  
    with drug absorption from transdermal patch, 440  
    first order absorption, 437–440  
    IV injection, 434–437  
Pharmacology, 399  
Phase equilibrium  
    chemical equilibrium, 109–114  
    distribution of a solute, two liquid phases, 81–83  
    Donnan potential, 108–109  
    equilibrium dialysis, 97–103  
    excess property ( $M^E$ )  
        activity coefficient, 63–66  
        residual properties, 62–63  
    flammability limits  
        benzene, 93  
        combustion engines, furnaces, and incinerators, 91  
        fire triangle, 92  
        flammable mixtures, 93–94  
        lower and upper flammability limits, 92  
    freezing point depression, 71–73  
    gas solubility, 74–78  
    Gibbs-Donnan effect  
        NaCl concentration, 103–105, 107–108  
        osmotic pressure, 105–107  
        semipermeable membrane, 102–103  
    multistage solute extraction, 84–87  
    osmotic pressure, 78–81  
pure component  
    Clausius-Clapeyron equation, 61  
    compressed liquid, 62  
    critical point, 59  
    enthalpy of melting, 61  
    enthalpy of sublimation, 61  
    heat of vaporization, 61  
    saturated liquid and saturated vapor states, 59–62  
semipermeable rigid barrier/membrane, 58  
single-stage solute extraction, 83–84  
solid-gas equilibrium, 73–74  
solubility of a solid, liquid solvent  
    enthalpy of fusion, 68  
    infinite dilution activity coefficient, 69  
    Newton's method, 71  
    pure phase, 66–67  
Scatchard-Hildebrand equation, 69  
solubility parameters, 69–71  
triple point ( $T_{tp}$ ), 67–68

- thermodynamics of surfaces, 94–97  
 vapor-liquid equilibrium  
     boiling temperature, 88–91  
     bubble point temperature, 87–91  
     dew point temperature, 87, 89–91  
     equilibrium distribution of N, 87  
     fugacity of component i, 87–88  
     Raoult's law, 88  
 Pinocytosis, 140  
 Pitot tube, 194–195  
 Plasma drug concentration, 400–401  
 Plasmapheresis, 138, 451, 506, 508  
 Platelet-derived growth factor (PDGF), 525–526  
 Platelets, 153  
 Pluripotential hemopoietic stem cells (PHSC), 588  
 Polycaprolactone (PCL), 532  
 Polytetrafluoroethylene (PTFE), 527  
 Potential energy ( $E_p$ ), 35–36  
 Pound force, 3  
 Pound mass, 3–4  
 Pound mole, 5  
 Powder-fusion printing (PFP), 531–532  
 Poynting factor, 62  
 Precision extrusion deposition (PED), 532  
 Preformed natural antibodies, 506  
 Progenitor cells, 517  
 Proliferative phase, 535  
 Property change of mixing, 49  
 Pseudoplastic fluid, 158  
 PTFE, *see* Polytetrafluoroethylene  
 Pure component fugacity ( $f_i$ )  
     experimental PVT data/equation of state, 53–55  
     real gas, 52  
     residual property, 52–53
- Q**  
 Quenching distance, 94
- R**  
 Rabinowitsch equation, 163–164  
 Raoult's law, 88  
 Reaction controlling, 227  
 Receptor-mediated transcytosis, 140  
 Red blood cells (RBCs), 153  
     axial accumulation, 171  
     biconcave discoid, 153  
     dimensions of, 153, 155
- Reflection coefficient, 309  
 Renal assist device (RAD), 588–589  
 Renal excretion, drug, 408–410  
 Renal tubule, 587  
 Renkin-Crone equation  
     diffusion limited, 325  
     flow limited, 325  
     solute concentration, 324–325  
     solute extraction, 325  
     solute's permeability, 326–327  
 Renkin equation, mica membranes, 293–294  
 Residual property, 52–53  
 Reverse osmosis, 80  
 Reversible process, 38–39  
 Reynolds number, 185  
 Rheology  
     Bingham plastic and Casson fluid, 158  
     Casson equation, 167–170  
     dilatant fluid, 157  
     laminar flow, 155–156  
     shear stress-shear rate relationship, 157  
     velocity profile development, 155–156  
 Rouleaux, 153
- S**  
 Saturated liquid, 59–62  
 Saturated vapor, 59–62  
 Saturation pressure, 59–60  
 Scatchard equation, 99, 101  
 Scatchard-Hildebrand equation, 69  
 Schmidt number (Sc), 247, 265–266  
 Second law of thermodynamics, 37–38  
 SFF, *see* Solid free-form fabrication  
 Shaft work ( $W_s$ ), 36–37  
 Sherwood number (Sh), 241  
 Short contact time solution  
     liquid film, 248–256  
     mass transfer coefficient, 250–251  
     Peclet number, 249  
     penetration distance, 248  
 Similarity transform technique, 271  
 Single phase open system  
     fugacity of component i, 55–56  
     ideal solution model, 56–58  
     partial molar property  
         binary systems, 48–49  
         chemical potential, 47  
         Gibbs-Duhem equation, 48  
         Gibbs free energy, 51–52  
         ideal gas, 49–51

- property change of mixing, 49  
pure component value, 48  
pure component fugacity ( $f_i$ )  
experimental PVT data/equation of state, 53–55  
real gas, 52  
residual property, 52–53  
total differential of nM, 46  
**SIS, see Small intestinal submucosa**  
Small intestinal submucosa (SIS), 527, 529  
Sodium-potassium pump, 146–147  
Solid free-form fabrication (SFF), 532  
Solute diffusion/transport  
across a thin porous membranes, 292–293  
across gel membranes, 306–307  
from blood, 289–290  
in blood and tissue  
effective diffusivity, 304  
interstitial fluid and other gel-like materials, 305–306  
Monte Carlo simulations, 305  
between a capillary and surrounding tissue space, 317–318  
Krogh tissue cylinder model, 318–324  
Renkin-Crone equation, 324–327  
in vascular beds, 328–329  
by filtration and diffusion across capillary wall  
capillary, characteristics of, 313  
diffusivity of glucose, 313–314  
diffusivity of oxygen, 314  
oxygen transport rate, 314–316  
protein transport rate, 316–317  
solute categories, 313  
solute transport rates, 313–314  
by filtration flow across a membrane  
bulk concentration, hollow fiber, 334–339  
bulk flow, hollow fiber, 333–334  
concentration polarization, 330–331  
plasmapheresis, 329  
sieving coefficient, 330–333  
membrane permeability  
capillary wall, 295–296  
microporous membranes, 295  
and overall mass transfer coefficient, 296–298  
partition coefficient, 291  
porosity, 289  
within a porous polymeric material  
concentration distribution, 300–301  
drug concentration, 298  
eigenvalues and eigenfunctions, 299  
microporous polymeric disk, 298–299  
separation of variables technique, 299  
solution valid for long contact times, 304  
solution valid for short contact times, 301–302  
Renkin equation, mica membranes, 293–294  
restricted/hindered diffusion, 291  
in single pore of thin planar membrane, 291–292  
steric exclusion, 290–291  
tortuosity, 290  
Solute membrane permeability, 295  
Specific volume, 7  
Square of the error (SSE), 22  
Standard atmosphere, 7  
Starling flow, 137  
Steady-state problem, 9  
Stereolithography (SLA), 531–532  
Stoichiometric coefficients, 12  
Stokes-Einstein equation, 229–232  
Stokes-Einstein radius, 231  
Surface energy, 94  
Surface tension, 94

## T

- Temperature, 4–5  
Thermodynamics  
entropy change, 41–42  
first law  
closed system, 35–36  
isolated system, 35  
steady flow process, 36–37  
fundamental property relations  
exact differentials, 44–46  
single fluid phase, 43–44  
Gibbs free energy (G), 43  
heat capacity, 40–41  
Helmholtz free energy (A), 43  
phase equilibrium  
chemical equilibrium, 109–114  
distribution of a solute, two liquid phases, 81–83  
Donnan potential, 108–109  
equilibrium dialysis, 97–103  
excess property ( $M^E$ ), 62–66  
flammability limits, 91–94  
freezing point depression, 71–73

- gas solubility, 74–78  
 Gibbs-Donnan effect, 102–108  
 multistage solute extraction, 84–87  
 osmotic pressure, 78–81  
 pure component, 59–62  
 semipermeable rigid barrier/membrane, 58  
 single-stage solute extraction, 83–84  
 solid-gas equilibrium, 73–74  
 solubility of a solid, liquid solvent, 66–71  
 thermodynamics of surfaces, 94–97  
 vapor-liquid equilibrium, 87–91
- second law, 38–39  
 single phase open system  
 fugacity of component i, 55–56  
 ideal solution model, 56–58  
 partial molar property, 47–52  
 pure component fugacity, 52–55  
 total differential of nM, 46
- Thiele modulus, 495
- Third law of thermodynamics, 38
- Tissue engineering and regenerative medicine (TERM)  
 biocompatibility, 534–535  
 biomaterials, 527–530  
 bioreactor design, 537–539  
 cell transplantation, 535–537  
 cellular interactions, 522  
 cadherins, 523  
 CAMs, 523–524  
 cytokines, 525–526  
 ECM components, 522–523  
 growth factors, 525–526  
 integrins, 524  
 selectins, 523  
 definition, 515–516  
 desirable properties, 526–527
- ECM  
 aggrecan, 522  
 basement membrane, 522  
 collagens, 521  
 connective tissues, 520  
 elastin, 521  
 fibroblasts, 519  
 fibronectin, 521–522  
 glycosaminoglycans, 521  
 macromolecules, 519–520
- immunoprotection, 518–519  
 initial response, 534–535  
 opportunities, 515–516  
 organ transplantation, 515
- polymer scaffolds  
 bioprinting, 533  
 ECM, 530  
 electrospinning, 530  
 methods, 530  
 scanning electron micrographs, 530  
 3D printing, 531–533  
 stem cells, 516–517
- Tissue oxygenation  
 change in blood oxygenation, 361–362  
 steady-state oxygen mass balances, 359–360  
 tissue oxygen consumption rate, 359–361
- T-lymphocytes, 548–551
- Torricelli equation, 192
- Triple point ( $T_{tp}$ ), 67
- Tube diameter effect  
 Fahraeus effect, 170–171  
 Fahraeus–Lindqvist effect, 171–173  
 marginal zone theory, 173–176
- Two-compartment models, 433–434  
 drug absorption  
 first order absorption, 437–440  
 from implantable device, 440  
 from transdermal patch, 440
- IV injection  
 apparent distribution volume, 435–436  
 first order rate constants, 435  
 pharmacokinetic parameters, 436–437  
 unsteady mass balance equation, 434–435  
 rate constants, 434
- U**
- Ultrafiltration, 308  
 UNIFAC model, 64–66  
 Units, 1–2  
 Universal gas constant, 7  
 Unsteady problem, 9  
 Upper flammability limit (UFL), 92  
 Uremia, 456  
 Uremic coma, 456
- V**
- van't Hoff's law, 80  
 Vapor-liquid equilibrium  
 boiling temperature, 88–91  
 bubble point temperature, 87–91

dew point temperature, 87, 89–91  
equilibrium distribution of N, 87  
fugacity of component i, 87–88  
Raoult’s law, 88  
Vapor pressure, 59–60  
Very late after (VLA) antigens, 524  
Viscous force, 202–203  
Volume, 7  
von Karman momentum balance equation, 184

**W**

Wall shear stress, 159, 163–164, 203  
Weight, 3  
White blood cells (WBCs), 153

**X**

Xenotransplantation, 506